THE UNIVERSITY *of* EDINBURGH

This thesis has been submitted in fulfilment of the requirements for a postgraduate degree (e. g. PhD, MPhil, DClinPsychol) at the University of Edinburgh. Please note the following terms and conditions of use:

- This work is protected by copyright and other intellectual property rights, which are retained by the thesis author, unless otherwise stated.
- A copy can be downloaded for personal non-commercial research or study, without prior permission or charge.
- This thesis cannot be reproduced or quoted extensively from without first obtaining permission in writing from the author.
- The content must not be changed in any way or sold commercially in any format or medium without the formal permission of the author.
- When referring to this work, full bibliographic details including the author, title, awarding institution and date of the thesis must be given.

Aluminium/Boron Exchange Reactions for Catalysis

THE UNIVERSITY *of* EDINBURGH

Alexander F. Beaton Garcia

A Thesis Submitted for the Degree of Doctor of Philosophy

2023

Declaration

I certify:

a) that the thesis has been composed by myself, and

b) either that the work is my own, or, where I have been a member of a research group, that I have made a substantial contribution to the work, such contribution being clearly indicated, and

c) that the work has not been submitted for any other degree or professional qualification except as specified, and

d) that any included publications are my own work, except where indicated throughout the thesis and summarised and clearly identified on the declarations page of the thesis.

Alexander F. Beaton Garcia

Abstract

The multi-trillion-dollar chemical industry is reliant on catalysts to efficiently transform bulk materials into higher value chemicals. However, the most commonly used catalysts are made from precious heavy metals which are expensive, scarce and toxic. The need to switch to more Earth-abundant elements is becoming increasingly important for sustainability and economic reasons. Aluminium is the third most abundant element in the Earth's crust – it is cheap, readily available and recyclable. Yet, the use of aluminium in catalysis is still currently limited as it is less thoroughly developed than transition metal-based systems.

Recently, aluminium catalysts have found applications in the borylation of unsaturated substrates. In these reactions, exchange of substituents between aluminium and boron is hypothesised to be a key step. Despite this, there is limited detailed insight into the processes that underpin these transformations and this hinders the development of the next generation of improved aluminium catalysts. In this thesis, I set out to gain detailed insight into this key Al/B exchange, providing useful applications as a result of these revelations. Chapter 1 gives context to the rest of the thesis by providing an overview of relevant stoichiometric and catalytic reactivity at aluminium.

In Chapter 2, aluminium catalysts that mediate alkene hydroboration with pinacolborane under mild conditions are developed. A surprising link between catalyst size and catalyst performance is revealed.

In Chapter 3, the mechanism of this protocol is examined in depth. A synergistic effect between aluminium and boron is discovered, which explains the dependence on catalyst size with the observed catalytic performance.

In Chapter 4, the potential of a favourable Al-C(sp^3)/B-H exchange step is highlighted by switching to a borane with diminished Lewis acidity. This enables the first example of alkene hydroboration with HBdan. The mechanism is distinct to the analogous reaction with pinacolborane.

Finally, in Chapter 5, Al/B exchange is progressed beyond hydridoboranes. Compatible exchange pathways at aluminium with silylboranes are discovered, which enables convenient access to silylalanes. The properties of these silylalanes are investigated, and promising catalytically relevant reactivity is uncovered.

Lay Summary

In some ways, a catalyst is like a chemical satnav, guiding reactions along efficient routes towards a given product. By avoiding “wrong turns”, catalysts provide savings in time, energy and resources. And much like a satnav, a catalyst is not consumed by this process and so can be reused multiple times.

Catalysis is integral to the modern world; its use is estimated to be involved in the production of around 90% of the world’s chemicals, including the manufacture of agrochemicals, pharmaceuticals and materials. This means it is directly linked to the food we eat, the healthcare we depend on, and the technology that makes modern life comfortable. As the world continues to use up its resources, catalysis becomes increasingly important in the pursuit of a sustainable world.

The most widely used catalysts in industry contain precious metals, such as platinum, palladium and ruthenium. Although the chemistries of these transition metals are well-established, their increasing scarcity makes their use expensive, particularly in large scale processes. Additionally, the extracting and refining processes for these metals can have significant environmental impacts. As a widely recycled and abundant element, aluminium is an outstanding candidate to replace these metals, at least from an economic and sustainability perspective. But why is it not more widely used for this purpose?

The answer is because the chemistry of aluminium is markedly different to that of transition metals. Returning to the satnav analogy; think of aluminium as being unable to communicate with the well-established satellite infrastructure that has been built over many years for transition metals. A separate infrastructure must be built for aluminium before it can be more widely used to guide reactions to their target destinations.

This work aims to address the “lack of infrastructure” currently available for aluminium catalysts. A promising development in recent years is the recognition that aluminium can instruct the addition of a boron group across simple molecules to generate key chemical building blocks. In these processes, a proposed key feature involves the swapping of groups between aluminium and boron – much like the switching of partners in a ceilidh dance. It is this partner switching between aluminium and boron that this thesis focuses on. Key questions answered in this work include: which partners (substituents) can be swapped with which? Can the best dancers

(catalysts) be predicted? And which dances (protocols) can be performed using this partner (substituent) switching routine?

Acknowledgements

My PhD experience certainly would not have been the same without the great fortune of meeting and working with the many fantastic people encountered on this journey.

Firstly, I'd like to thank my supervisors Dr Michael Cowley and Prof. Stephen Thomas for your continual support, advice and for fostering a wonderful working environment. I hope you have enjoyed discussing my chemistry as much I have enjoyed discussing it with both of you. Thank you for providing me with the freedom to explore my curiosity, and especially for steering that curiosity in the right direction, allowing me to write a body work that somewhat resembles a thesis. A paragraph will never be enough to describe how thankful I am, but I want you both to know that I thoroughly enjoyed my PhD experience.

This work would not have been possible without the technical staff at the University of Edinburgh. To the NMR staff, Juraj Bella and Dr Lorna Murray – thank you for your time, patience and willingness to help with even the most challenging of requests. To Dr Gary Nichol, thank you for running and solving my crystallography samples, even when the quality was sometimes dubious. To Dr Logan Mackay, Alan Taylor and Dr Faye Cruickshank; thank you for running the mass spectrometry on my samples, even when those sensitive aluminium compounds threatened to clog up your machines.

Being involved in two groups, I could really write another entire chapter thanking everyone, but instead I'll try to keep it brief. Thank you to the past and current members of the Cowley group for being excellent lab mates: Abi, Ella, Peter, Clement, Rosie, Dan, Ryan, Vesela, Jordann, Malavika, Ben, Crystal, Sandro and Justyna. Thanks for showing me how to expertly manipulate air-sensitive samples, for the general camaraderie and for putting up with my Eurolab playlist. I know you all secretly enjoyed it. Thank you also to Lindsay, Konrad and Hongyi for being such enthusiastic students to supervise.

Although I didn't get the chance to work in the Thomas group labs during my PhD, I always very much felt like I belonged to the group. Thanks for allowing me to steal your chemicals, time on the autocolumn and your brains during group meetings. To all past and present members – Jamie, Andrew, Dom, Kieran, Liam, Joanne, Jingying, Adrián, Milan, Rory, Nojus, Joe, Julie – thanks for a great time. Thanks also

to the many undergraduates and visiting students – you have truly enriched our experience with your presence and I've made some lifelong friends from your visits.

I owe special thanks to Jordann, Malavika, Dom and Luke (in addition to Mike and Steve) for proofreading this thesis. I can't imagine how difficult and painful reading through those first drafts were. In particular, thank you Jordann for submitting and solving a key crystal structure in my absence. The result gave me great joy. Also, to Dom; thank you not only for being a terrific colleague, but also an amazing flatmate. I will cherish those discussions about chemistry, financial strategies and life in general.

Football has played a big role in providing me with another creative and physical outlet during my PhD. I would like to thank the entire football crew for allowing me to show you how the beautiful game should be played; in particular, thanks to Kieran, Luke and Sam for organising this.

To my parents, you have supported me in everything I have done in life and I could not be more thankful. Thank you especially for providing me with shelter and food whilst I have been locked away writing this thesis. It would not have been possibly to complete this PhD if it were not for your support.

Finally, I would like to give a special thanks to my partner, Kiani. You have truly enriched my PhD experience; thank you for all the love, support and laughs you have provided. Thanks in particular for providing me with unrealistic expectations for how quickly it was possible to write a thesis.

Contents

Declaration i

Abstract ii

Lay Summary iii

Acknowledgements v

Abbreviations xi

Chapter 1: Introduction 1

1.1 Aluminium 2

1.2 Organoaluminium 3

1.2.1 Direct synthesis 3

1.2.2 Structure 5

1.2.3 Exchange 6

1.2.4 Addition reactions 9

1.2.5 Deprotonation 12

1.3 Recent applications of aluminium in catalysis 13

1.4 Aluminium-catalysed hydroboration 16

1.4.1 Exchange at Al–O 19

1.4.2 Exchange at Al–N 22

1.4.3 Exchange at Al–C 25

1.5 Aluminium-catalysed dehydrocoupling 31

1.6 General aims 33

Chapter 2: Aluminium-catalysed alkene hydroboration with HBpin: Development and scope 34

2.1 Introduction 35

2.2 Aims 40

2.3 Results and Discussion 42

2.3.1 Synthesis of m-terphenyl alanes 42

2.3.2 Stoichiometric experiments 44

2.3.3 Catalytic studies 48

2.4 Conclusions and future outlook 57

Chapter 3: Aluminium-catalysed alkene hydroboration with HBpin: Mechanistic insight 59

3.1 Introduction 60

3.2 Aims 61

3.3 Results and discussion 62

3.3.1 Does RBpin play an additional role? 62

3.3.2 Is BH_3 involved? 65

3.3.3 How do sterics affect the species involved in catalysis? 67

3.3.4 ^{Mes}TerAl catalysis: what species are involved? 71

3.3.5 Does aluminium mediate exchange with HBpin? 78

3.3.6 Single-turnover studies 79

3.3.7 What mediates hydroelementation? 81

3.3.8 How does BH_3 impact catalysis? 85

3.3.9 What role does the Lewis base play? 87

3.3.10 What is the rate dependence in catalysis? 88

3.3.11 Mechanistic proposal 89

3.3.12 Why is the $^{p\text{-}Tol}$TerAl system not catalytically active? 91

3.4 Conclusions and future outlook 93

Chapter 4: Aluminium-catalysed alkene hydroboration with HBdan 95

4.1 Introduction 96

4.1.1 Stability of Bdan 96

4.1.2 Reactivity of Bdan 98

4.1.3 Modification of diaminonaphthalene backbone 101

4.1.4 Strategies for installing Bdan 103

4.2 Aims and objectives 110

4.3 Results and discussion 111

4.3.1 Stoichiometric reactivity 111

4.3.2 Catalytic hydroboration - optimisation 113

4.3.3 Catalytic hydroboration - scope 116

4.3.4 Derivatisations 118

4.3.5 Mechanistic insights 121

4.4 Conclusions and future outlook 127

Chapter 5: Access to silylalanes by σ-bond metathesis 128

5.1 Introduction 129

5.2 Aims 135

5.3 Results and discussion 136

5.3.1 Which m-terphenyl alanes react with silylboranes? 136

5.3.2 Isolation of silylalanes 140

5.3.3 How are the disilylalanes formed? 142

5.3.4 Can disilylalanes be made by salt metathesis? 146

5.3.5 Photolysis of disilylalane ^{Mes}TerAl(Si)$_2$ 146

5.3.6 How might 5-A and 5-B be formed? 153

5.4 Conclusions and future outlook 155

Chapter 6: Overall conclusions and future outlook 158

Chapter 7: Experimental 163

7.1 General considerations 164

7.2 Synthesis of *m*-terphenyl alanes 167

7.3 Experimental details for Chapter 2 188

7.3.1 Catalysis Optimisation 188

7.3.2 Synthesis of pinacolboronic esters from terminal alkene substrates 188

7.3.3 Stoichiometric hydroalumination of alkenes 202

7.3.4 Single-turnover experiments 204

7.3.5 Catalytic hydroboration of alkenes 210

7.4 Experimental details for Chapter 3 215

7.4.1 Assessing influence of boronic esters on hydroalumination 215

7.4.2 Interaction between ^{Ar}TerAlH$_2$ and RBpin 217

7.4.3 Monitoring hidden BH$_3$ catalysis 222

7.4.4 Influence of sterics on formation of boron-containing species in catalysis. 225

7.4.5 Identifying species in catalysis (p-Tol and Tipp) 228

7.4.6 Identifying Al–H–B species in catalysis (Mes) 232

7.4.7 Probing effect of aluminium on exchange reactions with HBpin 245

7.4.8 Single turnover experiments *250*

7.4.9 Nature of hydroelementation *254*

7.4.10 Influence of BH_3 on catalysis *256*

7.4.11 VTNA *259*

7.5 Experimental details for Chapter 4 263

7.5.1 Optimisation of diazaborinine synthesis *263*

7.5.2 Synthesis of diazaborinines *266*

7.5.3 Alkyl Bdan derivatisations *285*

7.5.4 Stoichiometric experiments *289*

7.5.5 Mechanistic insights *291*

7.6 Experimental details for Chapter 5 294

7.6.1 Screening compatible reagents for Al–X/Si–B σ-bond metathesis *294*

7.6.2 Attempted synthesis of disilylalane using salt metathesis (ABG-0702) . *299*

7.6.3 Synthesis of disilylalane *301*

7.6.4 Photolysis of disilylalane *308*

7.7 Analysis of ^{11}B NMR spectroscopy as a quantitative technique 315

7.8 Crystallographic Data 319

References 328

Abbreviations

AIE	aggregate induced emission
Ar	aryl
^{Ar}Ter	*m*-terphenyl; 2,6-$Ar_2C_6H_3$
BBN	9-Borabicyclo[3.3.1]nonane
Bu	butyl
cat.	catalytic
Cy	cyclohexyl
DABCO	1,4-diazabicyclo[2.2.2]octane
Dipp	2,6-diisopropylphenyl
EI	electron ionisation
equiv.	equivalents
Et	ethyl
EXSY	exchange spectroscopy
HBcat	catecholborane
HBdan	1,8-diaminonaphthalatoborane
HBpin	pinacolborane
Hex	hexyl
HMBC	heteronuclear multiple bond correlation
HMDS	hexamethyldisilazide
HMDSO	hexamethyldisiloxane
HMQC	heteronuclear multiple quantum coherence
HOMO	highest occupied molecular orbital
HRMS	high-resolution mass spectrometry
HSQC	heteronuclear single quantum coherence
i	iso
IR	infrared

J	coupling constant
LB	Lewis base
LG	leaving group
Me	methyl
Mes	mesityl; 2,4,6-trimethylphenyl
MPV	Meerwein–Ponndorf–Verley
NHC	*N*-heterocyclic carbene
NMR	nuclear magnetic resonance
Oct	octyl
ORTEP	oak ridge thermal-ellipsoid plot program
Ph	phenyl
ppb	parts per billion
ppm	parts per million
Pr	propyl
p-Tol	*p*-tolyl; 4-methylphenyl
SADI	same difference
stoich.	stoichiometric
t	tertiary
THF	tetrahydrofuran
Tipp	2,4,6-triisopropylphenyl
TMEDA	*N,N,N′,N′*-tetramethylethylenediamine
TNT	2,4,6-trinitrotoluene
TS	transition-state
UV-vis	Ultraviolet-visible spectroscopy
XRD	X-ray diffraction
δ	chemical shift (ppm)

Chapter 1:

Introduction

Catalysis has revolutionised synthetic chemistry, offering efficient transformations of feedstock materials to key chemical building blocks and elegant routes to increasingly challenging synthetic targets. As one of the twelve key principles of green chemistry,[1] catalysis has found particular importance in industrial applications due to the increased savings from energy, waste and time that are particularly apparent in high-throughput, large scale processes.[2]

Catalytic processes in industry are dominated by the use of precious metals due to their more established reactivity.[3–8] These metals, however, are expensive, scarce, and can impose significant environmental costs during their production.[9] For this reason, sustainable Earth-abundant transition metal catalysts have been developed.[10–13] In recent years, increasing examples of main group-catalysis have emerged, offering complementary reactivity and sustainable alternatives to transition metal-catalysis.[14–20]

1.1 Aluminium

As the third most abundant element in the Earth's crust, aluminium has the potential to mitigate many of the issues associated with precious metals. However, unlike transition metals, aluminium does not have ready access to multiple oxidation states. Although there have been some preliminary investigations into the redox capabilities of aluminium,[21–24] catalytic applications involving redox processes have yet to be realised. Catalysis at aluminium is therefore dominated by redox-neutral pathways that exploit the intrinsic properties of aluminium in its most stable +3 oxidation state.

Lewis acidity is one of the fundamental properties of aluminium(III) compounds. This arises from the vacant *p*-orbital possessed by trivalent aluminium compounds, resulting in an electron-deficient aluminium centre. To obtain a stable octet configuration, the vacant *p*-orbital can accept a lone pair of electrons from a Lewis base to form a Lewis acid-base adduct (**Scheme 1-1.i**). Consequentially, aluminium has a strong affinity to heteroatoms, and in particular oxygen.

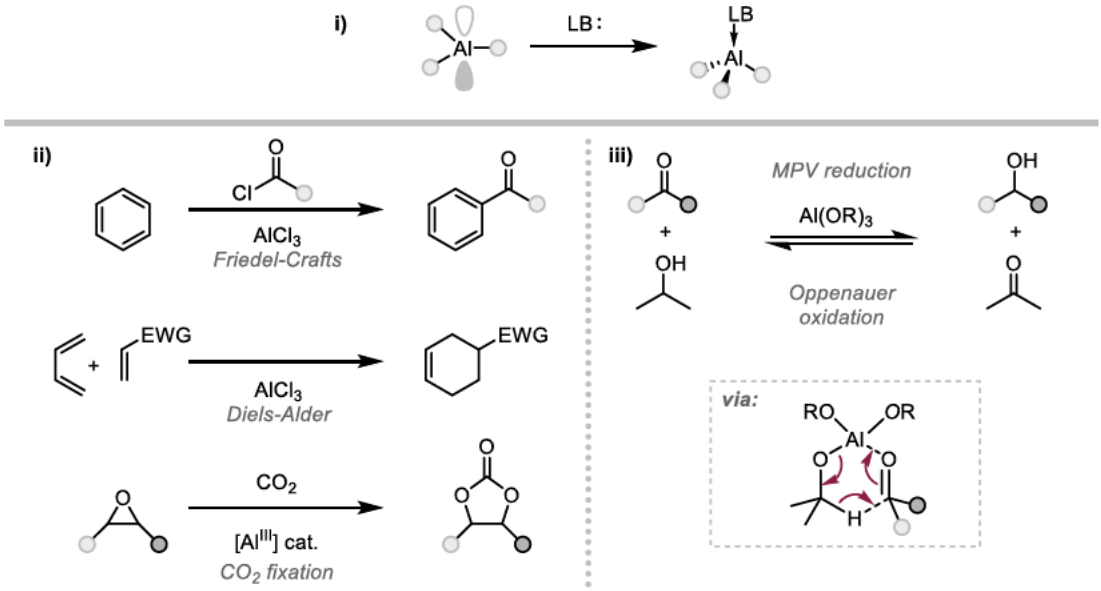

Scheme 1-1. i) Pictorial representation of trivalent aluminium behaving as a Lewis acid; LB = Lewis base. ii) Examples of Lewis acid applications of aluminium in catalysis. iii) Aluminium mediating hydride transfer reactions.

This Lewis acidity is the predominant feature of aluminium in catalysis (**Scheme 1-1.ii**). Examples of applications include Friedel-Crafts reactions,[25] cycloaddition reactions[26,27] and CO_2 fixation into epoxides.[28] Additionally, the coordinating capabilities of aluminium can mediate hydride transfer reactions between carbonyls, resulting in Meerwein-Pondorf-Verley (MPV) reductions[29–31] or Oppenauer oxidations,[32,33] depending on the reaction conditions (**Scheme 1-1.iii**).

Although aluminium(III) reagents were almost exclusively employed as Lewis acids in early synthetic applications, Karl Ziegler's pioneering research in the early 1950's demonstrated more versatile roles for aluminium reagents in synthesis than previously understood. His revolutionary work inspired intense research on organoalanes over the forthcoming decades.[34–36] The fundamental understanding of organoalanes accumulated by this work laid the foundations for subsequent advances in aluminium catalysis that have emerged in recent decades.

1.2 Organoaluminium

1.2.1 Direct synthesis

Ziegler discovered that trialkyl alanes could be generated in a "direct synthesis" pathway from the reaction of metallic aluminium with alkenes in the presence of dihydrogen (**Scheme 1-2.i**).[37] The reaction proceeds by alkene hydroalumination from aluminium hydride species generated *in situ*; when aluminium metal reacts with dihydrogen in the presence of a Lewis base instead of an alkene, LB•AlH_3 is formed

(**Scheme 1-2.ii**).[38] Alternatively, alkali metal aluminium hydrides, $MAlH_4$, can be generated in the presence of an alkali metal (M) in place of a Lewis base or alkene (**Scheme 1-2.iii**).[39]

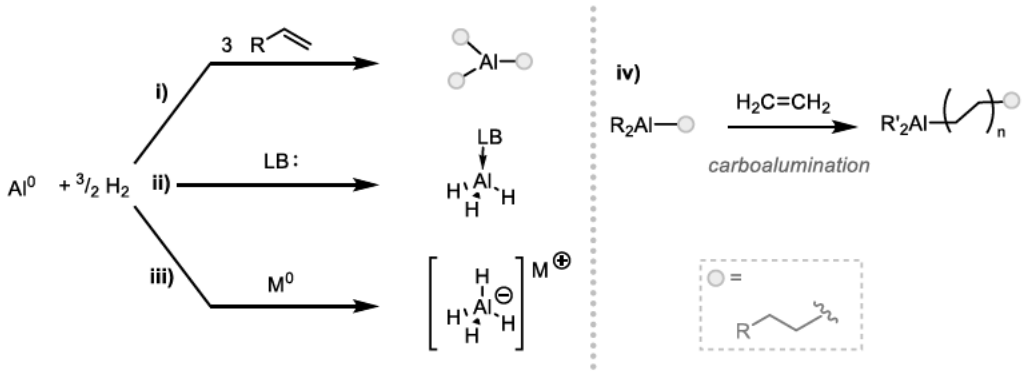

Scheme 1-2. Direct synthesis of i) trialkyl alanes; ii) LB•AlH_3; iii) $MAlH_4$. iv) Ethene can insert into Al–alkyl bonds, leading to polymerisation.

Direct synthesis of $(i\text{Bu})_3\text{Al}$, from isobutene, aluminium and dihydrogen, proceeds smoothly,[40] but is a more challenging pathway for the synthesis of Et_3Al.[41] Instead, ethene would insert into the Al–C bonds, resulting in a chain lengthening process (**Scheme 1-2.iv**).[42] This reactivity would become known as carboalumination (discussed in **Section 1.2.4**) and is a key component of Ziegler-Natta catalysis for the polymerisation of ethylene.[43] This process was, and continues to be, crucial for the production of high-density polyethylene and earned Karl Ziegler and Giulio Natta the 1963 Nobel Prize in Chemistry.[44]

Alkene insertion into Al–C and Al–H bonds is more difficult with bulkier alkenes. When 1,2-disubstituted alkenes are used, only di-*sec*-alkyl aluminium hydrides are formed (**Scheme 1-3.i**).[35] The reason for this is two-fold: firstly, steric hindrance between the bulky aluminium hydride and alkene prevents facile insertion. Secondly, dehydroalumination – β-hydride elimination of an alkene from an alkyl alane – is more prevalent in bulkier systems. Thus, even if the tri-substituted alane is formed momentarily, rapid dehydroalumination prevents it from accumulating. Dehydroalumination is used to conveniently prepare the commonly used $(i\text{Bu})_2\text{AlH}$ (DIBAL–H) from $(i\text{Bu})_3\text{Al}$ at high temperatures (**Scheme 1-3.ii**).[41,45]

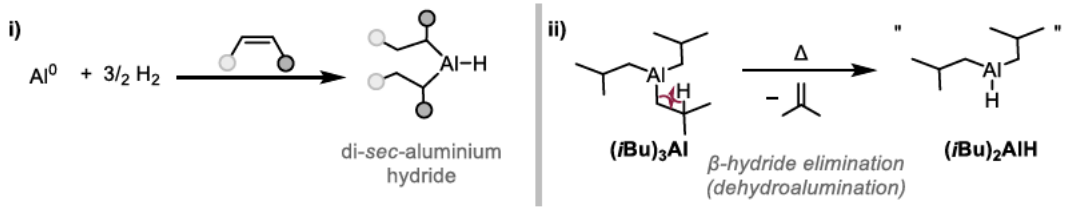

Scheme 1-3. i) Direct synthesis using 1,2-disubstituted alkenes leads to di-sec-aluminium hydrides; ii) Dehydroalumination of (iBu)$_3$Al at high temperatures leads to formation of (iBu)$_2$AlH.

1.2.2 Structure

Much of the reactivity of organoalanes can be explained or influenced by the structures present under reaction conditions. For this reason, significant efforts have been taken to understand this structure/activity relationship.

Aluminium compounds strive to achieve a stable octet configuration. This means that in the absence of a Lewis base, electronic saturation of aluminium can be achieved by bridging with electron-deficient bonds. Thus, trialkyl alanes typically form associated dimeric structures with bridging alkyl groups (**Scheme 1-4.i**). These dimeric structures are considered sp^3-hydridised at aluminium and contain 3-centre-2-electron (3c-2e) bonds,[46] like those found in diborane (**Scheme 1-4.ii**).[47,48] However, trialkyl boranes contrast with their aluminium counterparts in that they are monomeric at room temperature.[49,50] This difference can be explained by the more Lewis acidic aluminium centre and the greater polarisation of the Al–C bonds in comparison with boron.

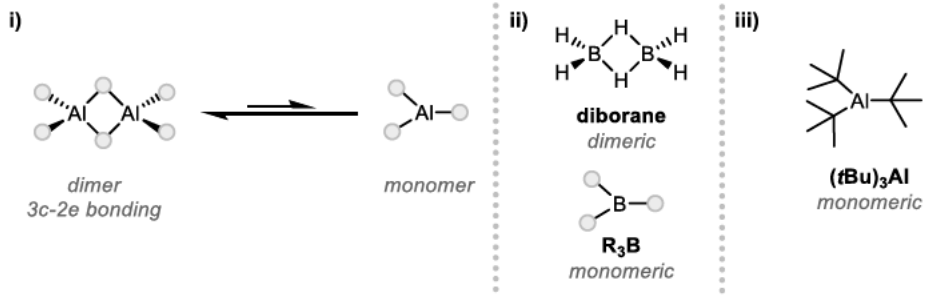

Scheme 1-4. i) Al(alkyl)$_3$ can exist in equilibrium between dimeric and monomeric species; ii) Comparison of structure with diborane and B(alkyl)$_3$; iii) tBu$_3$Al is monomeric.

These electron-deficient bridged associated species typically exist in equilibrium with the dissociated monomeric unit (**Scheme 1-4.i**). The substituents at aluminium therefore greatly influence the position of this equilibrium; increasing the steric bulk of these alkyl substituents kinetically stabilises monomeric alanes. While smaller alanes, such as Me$_3$Al and Et$_3$Al, are predominantly found as dimers,[51–54] neat (iBu)$_3$Al is only 39.4% associated at 10 °C[55] and the even more sterically encumbered (tBu)$_3$Al is entirely monomeric (**Scheme 1-4.iii**).[56,57]

Hydrides and unsaturated aliphatic groups are better bridging ligands than alkyl groups. Thus, $(i\text{Bu})_2\text{AlH}$ contains bridging hydrides instead of bridging alkyl groups (**Scheme 1-5**).[53,58] In a similar manner $(\text{alkyl})_2\text{Al(alkynyl)}$ contains only alkyne bridging, regardless of the alkyl groups present.[35,59,60] In alane (AlH_3), all hydrides are capable of bridging and this results in a polymeric structure,[61,62] contrasting with BH_3 which is dimeric (**Scheme 1-4.ii**).[47,48]

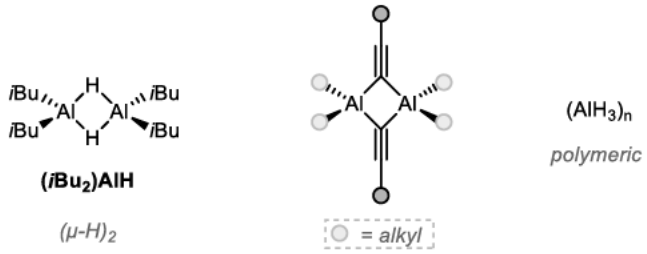

Scheme 1-5. Examples of different aluminium compounds to highlight bridging capabilities of substituents.

1.2.3 Exchange

A consequence of reversible dimer formation is substituent redistribution at aluminium, which is thought to proceed by formation of an associative complex (**Scheme 1-6.i**). Generally, redistribution maximises the formation of dimers containing the best bridging groups possible. This is exemplified by the reaction of excess $(i\text{Bu})_3\text{Al}$ with Me_3Al; the resulting dimer is only bridged with methyl groups (**Scheme 1-6.ii**).[35] Similarly, smaller primary alanes redistribute to make secondary alanes and AlH_3 (polymeric).[63,64] When all substituents have similar bridging capabilities, exchange is entropy driven and a statistical mixture is formed.[35]

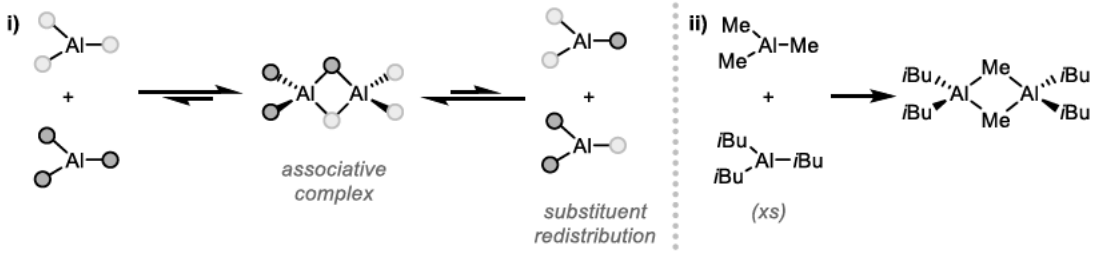

Scheme 1-6. i) Redistribution of organoalanes. ii) Reaction of Me_3Al with excess $(i\text{Bu})_3\text{Al}$.

If there is no reversible monomer/dimer equilibrium at a given temperature, then redistribution does not occur. For example, dialkyl vinyl alanes do not dissociate below 100 °C due to strong vinyl-group bridging and therefore do not redistribute at lower temperatures.[35,59] On the other end of the scale, trialkylboranes do not undergo redistribution in the absence of a catalyst as they are monomeric (**Scheme 1-7.i**).[65]

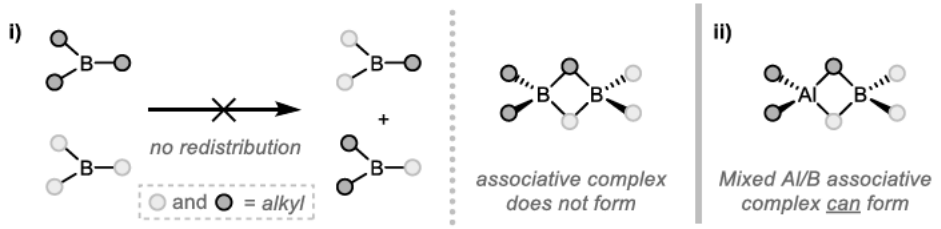

Scheme 1-7. i) Trialkylboranes do not redistribute as they are monomeric and do not form associative complexes; ii) Associative complexes between trialkylalanes and trialkylboranes can form.

However, rapid redistribution *is* observed between triorganoboranes and trialkyl alanes.[65] This implies the formation of intermediate associative complexes between these two species (**Scheme 1-7.ii**). If trialkyl alanes are regenerated in this process, only catalytic quantities are required to redistribute the substituents at boron (**Scheme 1-8.i**). This exchange can also be exploited to generate alanes with frameworks that are more readily accessible for boron, such as 5- and 6-membered group 13-heterocycles (**Scheme 1-8.ii**).[66] It has also been used to prepare $Al(C_6F_5)_3$ from the reaction between Et_3Al and $B(C_6F_5)_3$ (**Scheme 1-8.iii**).[67,68]

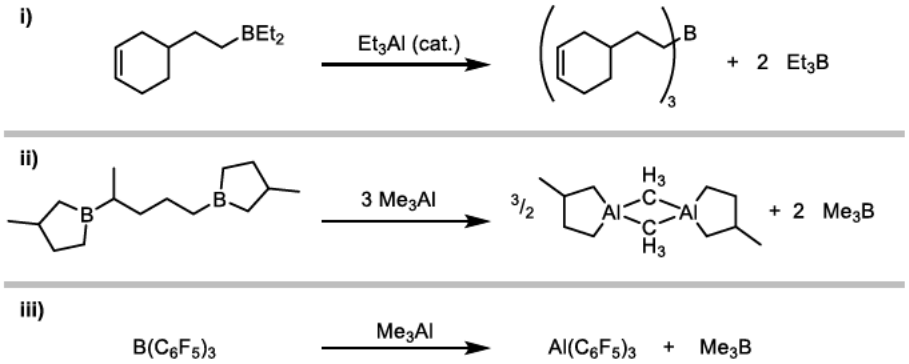

Scheme 1-8. i) Organoalanes can catalyse the redistribution of organoboranes; Substituent redistribution between boron and aluminium can be used to make ii) aluminium heterocycles and iii) $Al(C_6F_5)_3$.

The associative complexes that aluminium reagents form are reminiscent of the transition-state structures for σ-bond metathesis processes (**Scheme 1-9**). A σ-bond metathesis reaction is defined as a [2σ + 2σ] cycloaddition in which substituents are exchanged between two element centres in a concerted process.[69] Since it proceeds through a tightly ordered transition-state structure, these reactions are typically characterised by a large negative entropy of activation. As a redox-neutral process, σ-bond metathesis has emerged as an important turnover pathway for d^0 metals (particularly lanthanides)[69,70] and *p*-block elements,[14–20] which do not readily participate in redox chemistry. In this work, *redistribution* – which proceeds similarly – will be used primarily to refer to exchange processes at the same element centre.

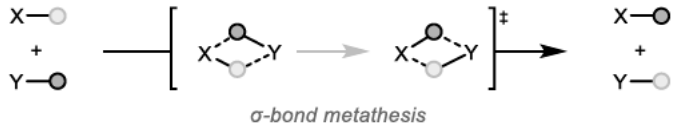

Scheme 1-9. Pictorial representation of a σ-bond metathesis process.

Exchange of non-carbon-based substituents between boron and aluminium is also possible (**Scheme 1-10**). Typically, the stronger heterophilicity of aluminium in comparison to boron drives these reactions. This effect is especially profound when a strong B–C bond is formed from a relatively weak Al–C bond. Consequently, Al–C exchange has been observed with various B–X bonds, including, but not necessarily limited to X = O,[71–75] F,[71,76] Cl,[77–79] Br,[78] I,[78,80] H[81] and Se[82].

Scheme 1-10. Pictorial representation of Al–R/B–X σ-bond metathesis.

Hydride transfer from aluminium to boron represents another common exchange pathway. The reaction of aluminium hydrides with boronic esters (B–O)[83–86] and organotrifluoroborates (B–F)[87] is an important method for accessing monoalkyl boranes and boronates. These are challenging to synthesise by olefin hydroboration due to the susceptibility of all B–H bonds to add across olefins in most cases. Alternatively, the resulting aluminium product can serve as the target species; Al–H/B–C exchange of vinyl boranes with (iBu)$_2$AlH yields vinyl alanes, which can be functionalised in distinct ways to vinyl boranes (**Scheme 1-11**).[88]

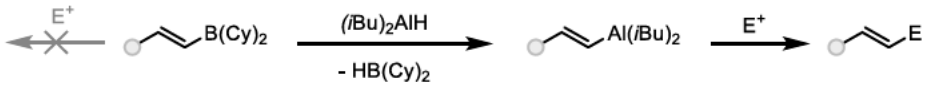

Scheme 1-11. Vinyl boranes can react with aluminium hydrides to make vinyl alanes.

Hydride transfer in the reverse direction, i.e. from boron to aluminium, has been observed or implied at several different Al–X bonds (C, N, O, S, Se) as a key catalytic step for the regeneration of an aluminium hydride catalyst,[89,90] a topic that will be discussed later (**Sections 1.3** to **1.5**).

Building on the exchange processes of aliphatic substituents at aluminium with boron, the heterophilicity of aluminium enables organoalanes to engage in substituent exchange at other element centres too. Thus, driven by the formation of Al–X bonds (X = heteroatom), alkyl alanes are practical alkylating reagents for other *p*-block

elements containing E–X bonds (E = *p*-block element; **Scheme 1-12.i**).[91] In a similar manner, organoalanes can transmetallate with transition metals; accordingly, these reagents can be used as coupling partners in transition metal-catalysed procedures (**Scheme 1-12.ii**).[92–94]

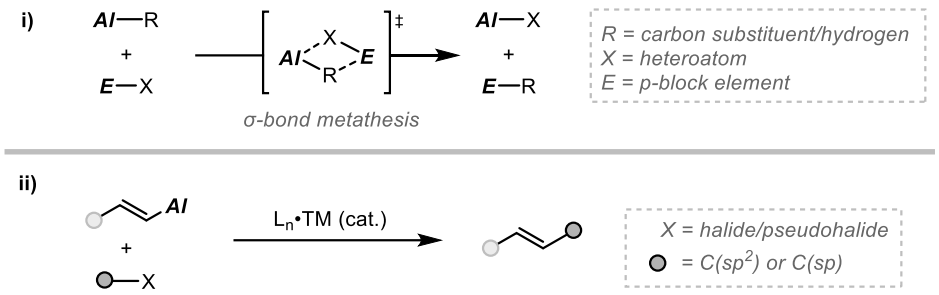

Scheme 1-12. Aluminium can also exchange substituents with: i) other *p*-block elements; ii) transition metals, allowing applications in cross-coupling reactions.

In addition to these processes, Al–X formation also drives the direct reaction of organoalanes with electrophiles, such as halides, allyl halides and unsaturated substrates.[34] Notably, the related organoboranes do not exhibit the same reactivity and this can be explained by the more polarised and weaker Al–C bond in comparison to B–C bonds.

The Lewis acidity at three-coordinate aluminium and the weak Al–C bonds also make organoalanes prone to facile oxidation.[95,96] Thus, O_2 can insert into the Al–C bonds to initially form short-lived peroxide intermediates before collapsing to aluminium alkoxides. Although this property generally makes organoalanes air-sensitive, it also makes them useful precursors for the synthesis of alcohols, which form after the aluminium alkoxide is quenched with water. Four-coordinate aluminate species, such as $LiAlH_4$, which do not have a readily accessible vacant *p*-orbital at aluminium, are more stable to oxygen and can be handled in air on the bench.[97]

The unique reactivity of organoalanes renders them valuable synthetic intermediates. In the following section, the preparation of organoalanes by hydroalumination and carboalumination will be explored.

1.2.4 Addition reactions

Addition across olefins

The simple preparation of $(i\text{Bu})_2\text{AlH}$ by dehydroalumination of $(i\text{Bu})_3\text{Al}$ has led to its widespread application for the synthesis of organoalanes from olefin hydroalumination. Olefin hydroalumination is proposed to proceed by an interaction of the olefin π-system with the vacant *p*-orbital at monomeric aluminium (**Scheme**

1-13).[58] A 4-membered transition-state follows,[98] usually resulting in anti-Markovnikov *syn*-addition across the olefin, in a similar manner to olefin hydroboration.[99]

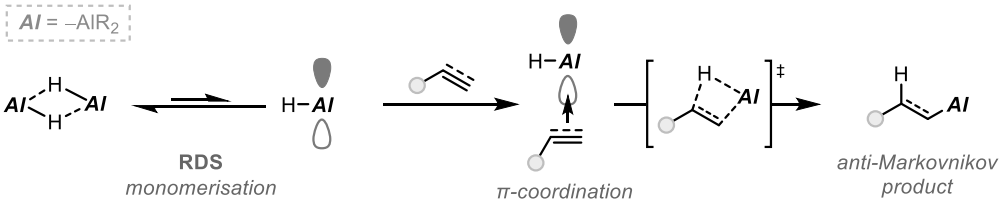

Scheme 1-13. Mechanism of olefin hydroalumination.

The rate-limiting step for this process is monomerisation of the aluminium hydride reagent,[58] which typically exist as hydride-bridged associated species. Therefore, uncatalysed reactions – in particular, those involving $(i\text{Bu})_2\text{AlH}$ – are usually performed at elevated temperatures to facilitate oligomer dissociation.[35] More forcing temperatures (>100 °C) are generally avoided to limit selectivity issues associated with dehydroalumination and/or carboalumination. Oligomer dissociation can also be enhanced by increasing the steric bulk at aluminium, and this leads to faster hydroalumination at lower temperatures. Indeed, Power showed that bulky *m*-terphenyl ($2,6\text{-Ar}_2\text{C}_6\text{H}_3$) alanes could react with olefins at room temperature. The rate of addition correlated with the steric bulk at aluminium.[64]

In a similar manner, carboalumination proceeds by olefin coordination to a monomeric triorganolane species.[100,101] However, unlike hydroalumination, the rate-limiting step is not monomerisation; it is instead proposed to be the electrophilic attack of aluminium to the alkyne from the π-coordination complex (**Scheme 1-14**).[102] This results in a 4-membered transition-state[103] which usually leads to the formation of the anti-Markovnikov products by *syn*-addition of Al–C across the olefin.

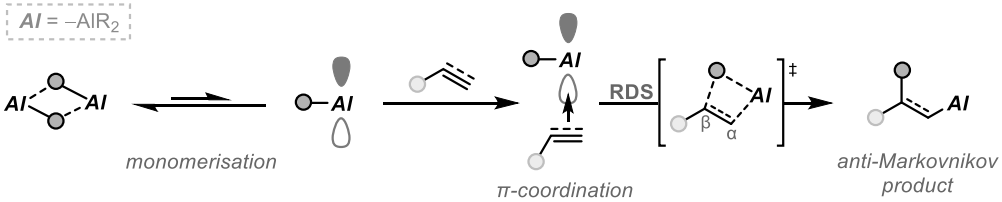

Scheme 1-14. Mechanism of olefin carboalumination.

Reaction conditions required for carboalumination are typically more forcing than for hydroalumination. Normally, elevated temperatures (> 100 °C) and/or high olefin pressures are required,[37] unless the olefin is strained.[104–106] That hydroalumination is more facile than carboalumination can be attributed to the enhanced bridging capabilities of hydride in comparison to alkyl groups [36] A better

bridging group can more effectively stabilise the 4-membered transition state, which has to bridge between two different electron-deficient centres: the β-carbon and aluminium. This also explains why the reactivity of Al–C towards olefins is faster with increased unsaturation at the C–substituent, with Al–alkynyl being the fastest and Al–alkyl being the slowest.[36]

Both uncatalysed hydro- and carboalumination suffer from several drawbacks, such as low reactivity under ambient conditions, inflexible regio- and stereoselectivity and often other selectivity issues arising from dehydroalumination and/or unwanted carboalumination. To circumvent these issues, transition metal-catalysed protocols have been developed using various metal sources.[107–110] Details for these processes will not be elaborated here, but important elements that mediate these transformations include nickel[111] and especially the early transition metals, titanium and zirconium.[107,112,113] It is worth noting that organoboranes, such as Et_3B and $PhB(OH)_2$, can also catalyse alkene hydroalumination with *in situ*-generated Cl_2AlH.[114] This mechanism has yet to be fully understood but is expected to proceed by hydride transfer from aluminium to boron to generate catalytically active B–H species.[115]

Addition across polarised unsaturated substrates

Another key property of aluminium compounds is “latent nucleophilicity”.[34] This describes the enhanced nucleophilic character of the substituents at aluminium upon formation of an electronically saturated 4-coordinate aluminate species. This means that although aluminium compounds are polarised due to the low electronegativity of aluminium (χ = 1.61; the lowest in the *p*-block), it retains its Lewis acidic properties until it has been coordinated. For this reason, trivalent organoalanes and aluminium hydrides can be used to selectively add across unsaturated bonds containing heteroatoms. This latent nucleophilicity property is perhaps best exemplified by the sequential Beckmann rearrangement[116,117]/ alkylation / reduction sequence mediated by organoalanes (**Scheme 1-15**).[118]

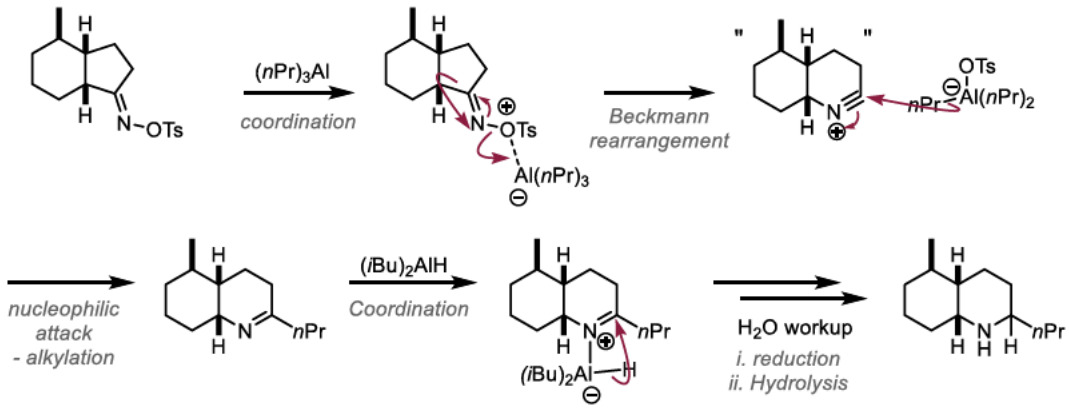

Scheme 1-15. Example of organoaluminium behaving as a Lewis acid, nucleophile and hydride source depending on coordination number.

When aluminium is already coordinatively saturated, pre-coordination of a Lewis base is not required to make the substituents at aluminium more nucleophilic. In this regard, anionic four-coordinate aluminium hydrides – in particular $LiAlH_4$ – have gained an important status as strong and versatile reducing agents for the reduction of polarised unsaturated substrates.[119–121]

1.2.5 Deprotonation

A potential by-product from the attempted addition of Al–H or Al–C across terminal alkynes are alkynyl alanes, which arise from deprotonation of the terminal C–H proton. This becomes more prevalent as the acidity of the alkyne C–H bond increases and/or when smaller alkyl substituents at aluminium are used.[122] The presence of a Lewis base can make deprotoalumination of the C–H bond selective against addition across the alkyne (**Scheme 1-16**).[123,124] This prevents π-coordination of the alkyne substrate to the aluminium centre and also increases the basicity of the substituents at aluminium.

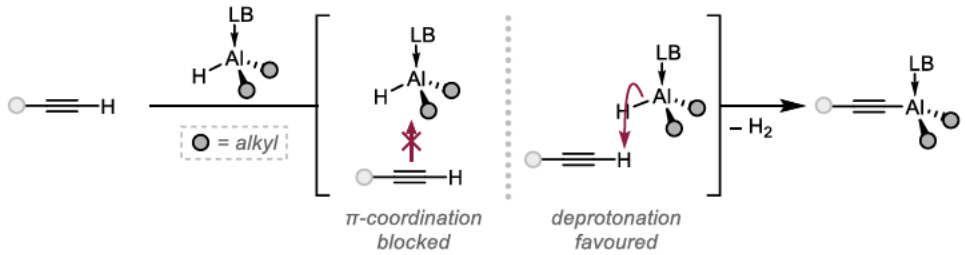

Scheme 1-16. Deprotoalumination of alkynes can be facilitated with a Lewis base.

While four-coordinate alanes are more basic than their trivalent counterparts, deprotonation of E–H bonds (E = heteroatom such O, N, S, P) can still readily occur using trivalent alanes. These reactions take advantage of the "latent nucleophilicity" properties of organoalanes; reactions proceed by initial coordination of the

heteroatom to aluminium to form the more basic aluminate complex *in situ*, resulting in deprotonation (**Scheme 1-17**).[35] This is an important and facile synthetic route to generate Al–E containing compounds.

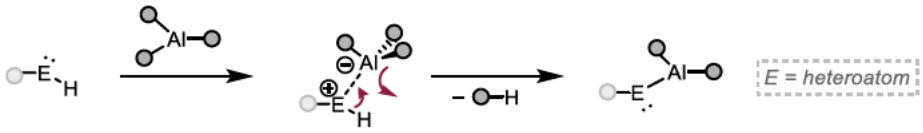

Scheme 1-17. Deprotonation of E–H bonds with trivalent organoaluminium.

This property is also synthetically valuable in organic applications. Aluminium can function as the coordinating site, allowing selective deprotonation at nearby acidic protons. For example, aluminium amides have been used to synthesise allylic alcohols from epoxides by selective deprotonation at the α-position (**Scheme 1-18.i**).[125,126] Alternatively, the resulting Al–E bonds that arise from E–H deprotonation can be used as a nucleophilic source of E. The Woodward group reported an application of this for preparing the β-lactam ring in cephalosporin C (**Scheme 1-18.ii**).[127]

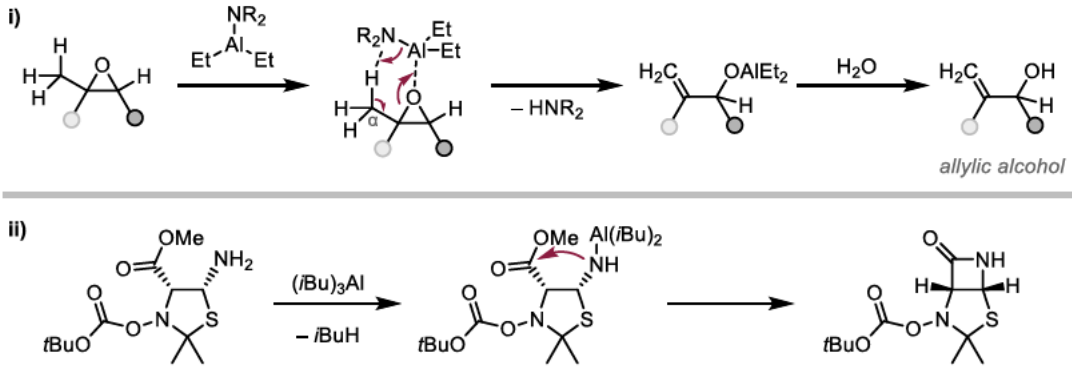

Scheme 1-18. i) Aluminium amides can selectively deprotonate epoxides to give allylic alcohols; ii) Synthesis of β-lactam ring in cephalosporin C from nucleophilic attack of an ester from an aluminium amide.

1.3 Recent applications of aluminium in catalysis

Thus far, three key features of organoaluminium reactivity have been described: *exchange* (σ-bond metathesis), *addition* (hydroalumination/insertion), and *deprotonation* (protonolysis). The reactivities of each of these processes can be understood by the structural features of the respective organoalanes. Applications of aluminium in catalysis beyond Lewis acid catalysis over the past two decades have largely focused on combining two of these three key features (**Scheme 1-19**). These include:

a) *Hydroelementation* reactions with protic sources, which have been achieved by combining *addition* of Al–E across olefins, followed by *deprotonation* of the stochiometric protic source, E–H, with the resulting Al–C bond (**Scheme 1-19.a**).
b) *Hydroelementation* reactions with hydride sources, which leverage Al–H *addition* across unsaturated bonds with *exchange* reactions at aluminium using a stoichiometric hydride source, M–H (**Scheme 1-19.b**).
c) *Dehydrocoupling* reactions, which take advantage of the basicity of Al–C and Al–H bonds to *deprotonate* E–H bonds and combines this with the capacity for the resulting Al–E bond to *exchange* with a stoichiometric hydride source, M–H (**Scheme 1-19.c**).

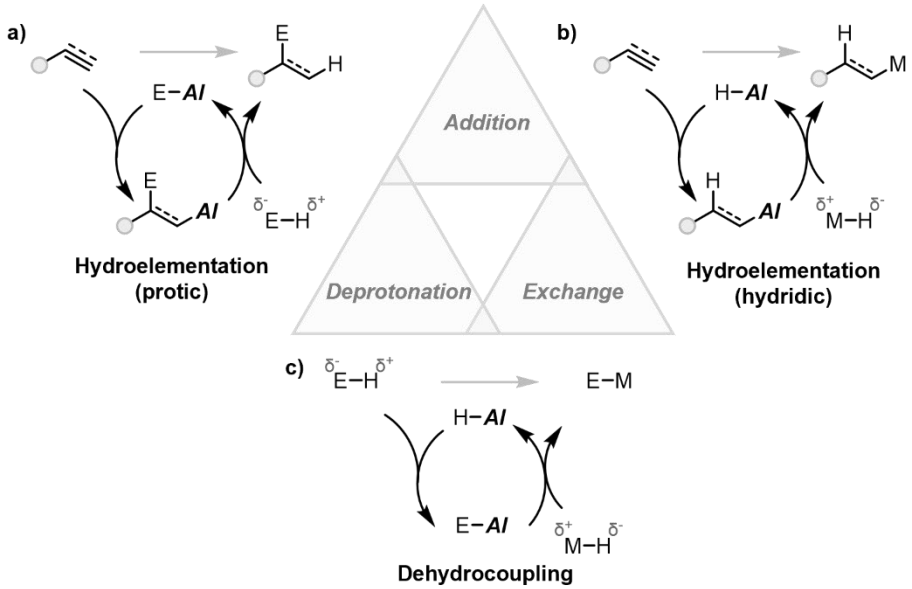

Scheme 1-19. Three key features of organoaluminium chemistry: addition, deprotonation and exchange. A combination of these processes can result in catalysis. General mechanisms provided for aluminium-catalysed a) hydroelementation with a protic source; b) hydroelementation with a hydridic source; c) dehydrocoupling.

Catalysis proceeding by the deprotonation/exchange pathway outlined in **Scheme 1-19.a** has been used for intramolecular hydroamination reactions with amino alkenes to generate cyclic amines (**Scheme 1-20.i**).[128,129] It has also been used to mediate hydrophosphination reactions of alkenes, alkynes and carbodiimides with diphenylphosphine (**Scheme 1-20.ii**).[130] Imine[131–137] and alkene[138] hydrogenation with dihydrogen (**Scheme 1-20.iii**) can also be catalysed with aluminium hydrides and are expected to proceed by similar mechanisms. As these reactions don't proceed by Al/B exchange, they will not be further discussed.

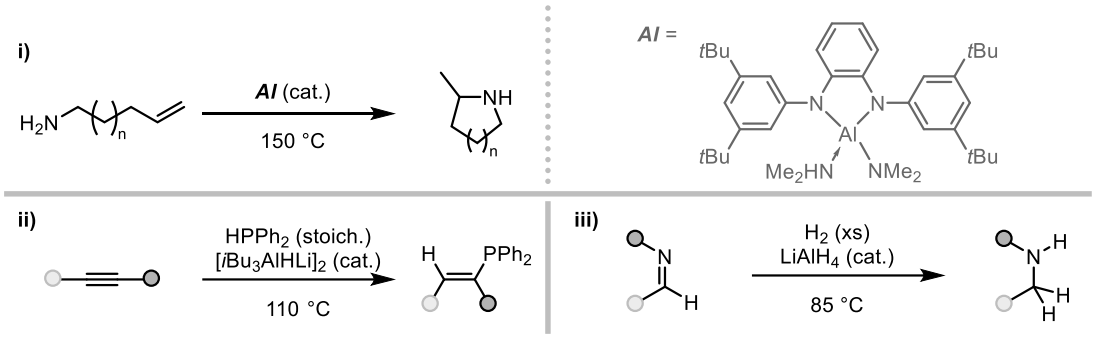

Scheme 1-20. Aluminium-catalysed i) alkene hydroamination;[129] ii) alkyne hydrphosphination;[130] iii) imine hydrogenation.[135]

The pathways outlined in **Scheme 1-19.b** and **Scheme 1-19.c** make use of the capacity for aluminium to exchange substituents with a suitable stoichiometric hydride source to regenerate the aluminium hydride catalyst. The use of milder hydride sources as a turnover reagent means that highly reactive aluminium hydride species do not need to be used stoichiometrically. Ultimately, this leads to more controlled reactions, with beneficial safety profiles and potentially improved chemo-selectivity.

The stoichiometric hydride source commonly used in these applications is pinacolborane (HBpin). It is *usually* considered inert towards substrates in the absence of a catalyst and so it has been used to test the catalytic capabilities of new aluminium hydride compounds. Furthermore, its products – pinacolboronic esters and heteroatom derivatives – are versatile synthetic building blocks.[139–143] In principle, silanes could also function as a viable hydride source for these applications. Indeed, several examples of aluminium-catalysed hydrosilylation reactions do exist.[144–150] However, these are thought to proceed by Lewis acid catalysis so will not be discussed.

Thus, aluminium hydride catalysts have most commonly been applied in hydroboration and dehydrocoupling reactions with HBpin. These applications are herein explored.

1.4 Aluminium-catalysed hydroboration

The first example of an aluminium-catalysed hydroboration reaction was reported in 2015 by Roesky, Yang and Parameswaran.[151] They discovered that a β-diketiminate-supported aluminium hydride complex containing a triflate substituent **1-I(OTf)** would catalyse the hydroboration of carbonyls with HBpin at room temperature (**Scheme 1-21**). A mechanism was proposed that follows the insertion/σ-bond metathesis (Al–O/B–H) pathway (**Scheme 1-19.b**). Calculations suggested that Al–H insertion across the carbonyl π-system represented the rate-limiting step.

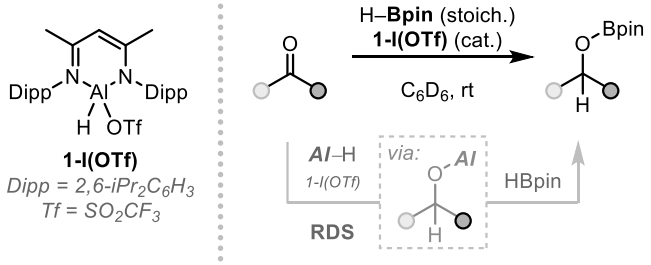

Scheme 1-21. First example of aluminium-catalysed hydroboration with proposed pathway.

This seminal report inspired a rapid development of aluminium-catalysed hydroboration protocols over the proceeding years. A wide variety of different aluminium structures have shown catalytic activity across a wide range of both polarised and unpolarised unsaturated substrates. These include aldehydes and ketones,[81,152,161–165,153–160] esters,[81,166,167] carbonates,[167] carboxylic acids,[167] CO_2,[167–171] imines,[157,172] nitriles,[81,173–176] isonitriles,[176] heteroallenes (such as carbodiimides, isocyanates etc),[174,177,178] pyridine,[176] alkenes[81,179–182] and alkynes.[60,152,184,185,157–159,172,179,181–183] Ring-opening of cyclic ethers, such as epoxides,[167] THF and THP[186] have also been achieved.

Most of these examples report the same proposed insertion/σ-bond metathesis pathway. However, in most cases, other pathways were not considered, and control reactions were not performed to rule out other mechanisms. In recent years, the constitution of the "true" catalyst and the generality of an insertion/σ-bond metathesis mechanism have been called into question.

The viability of an Al–O/B–H σ-bond metathesis process, proposed in Roesky, Yang and Parameswaran's report[151] as a key step for regenerating the aluminium hydride catalyst **1-I(OTf)**, was scrutinised by Aldridge and co-workers.[187] A similar β-diketiminate aluminium hydride complex **1-I(R)** was found to react stoichiometrically with CO_2 (**Scheme 1-22**). However, when attempts were made to react the resulting aluminium κ^1-formate complex **1-I(R,CO$_2$)** with a hydridoborane (HBpin, H-*B*-9-BBN or catecholborane; HBcat), regeneration of the aluminium hydride **1-I(R)** was not observed in any case. Only with $Me_2S{\bullet}BH_3$ would trace quantities of aluminium hydride **1-I(R,BH$_3$)** be formed, and this could only be explained by the formation of a stable tetrahydroborate complex. The report argued that Al–O/B–H metathesis is thermodynamically unfavourable, due to the comparatively stronger bond strengths in the starting materials in comparison to the products ($\Delta H° > 120$ kJ mol^{-1}). Indeed, exchange in the opposite direction, i.e. Al–H/B–O exchange, has been used stoichiometrically to synthesise boron hydrides from boronic esters using aluminium hydrides.[83–86]

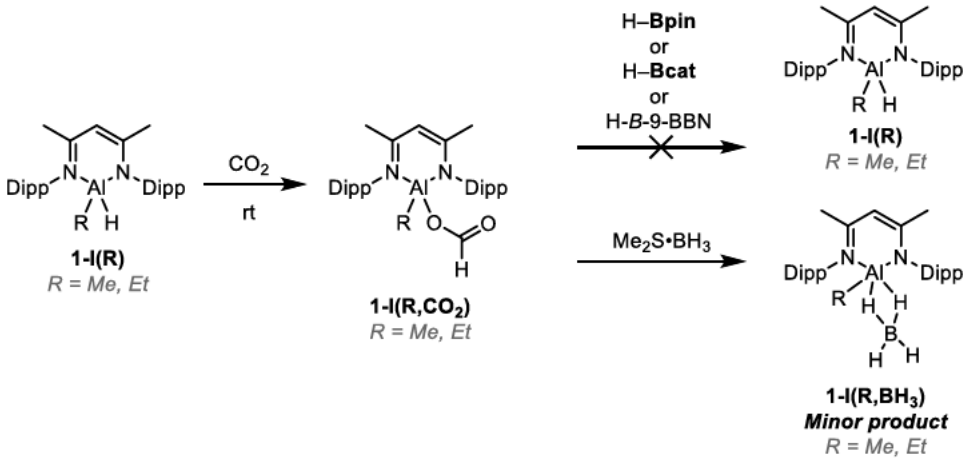

Scheme 1-22. Single-turnover experiments to demonstrate the challenging Al–O/B–H σ-bond metathesis step for CO_2 hydroboration.

Thomas later demonstrated that pinacolborane (HBpin) was not immune to decomposition in catalysis; in the presence of certain nucleophiles, including aluminium hydrides, it would form catalytically active BH_3 and borohydride species (**Scheme 1-23.i**).[188,189] These boranes have been shown to catalyse the hydroboration of a range of substrates with HBpin (**Scheme 1-23.ii**).[190] These include carbonyls,[191] carboxylic acids,[192] esters,[193] carbonates,[193] olefins,[194] nitriles[195] and *N*-heteroarenes.[196–198] Often, these reactions can proceed under relatively mild conditions (rt – 60°C) and within reasonable timeframes. As a result, these *in situ*-generated boranes can be responsible for the catalytic activity observed for many reported "catalysts" across the periodic table,[188,189] almost certainly including

aluminium. This phenomenon has been termed "hidden boron catalysis".[188] Although this understanding is still relatively new for HBpin, it has long been known that HBcat, a less stable dioxaborolane, could readily decompose under catalytic conditions. In 1992, Burgess, Baker and Marder reported the formation of BH_3 species in the presence of rhodium catalysts.[199] Later, Harder reported similar observations with a calcium hydride pre-catalyst.[200]

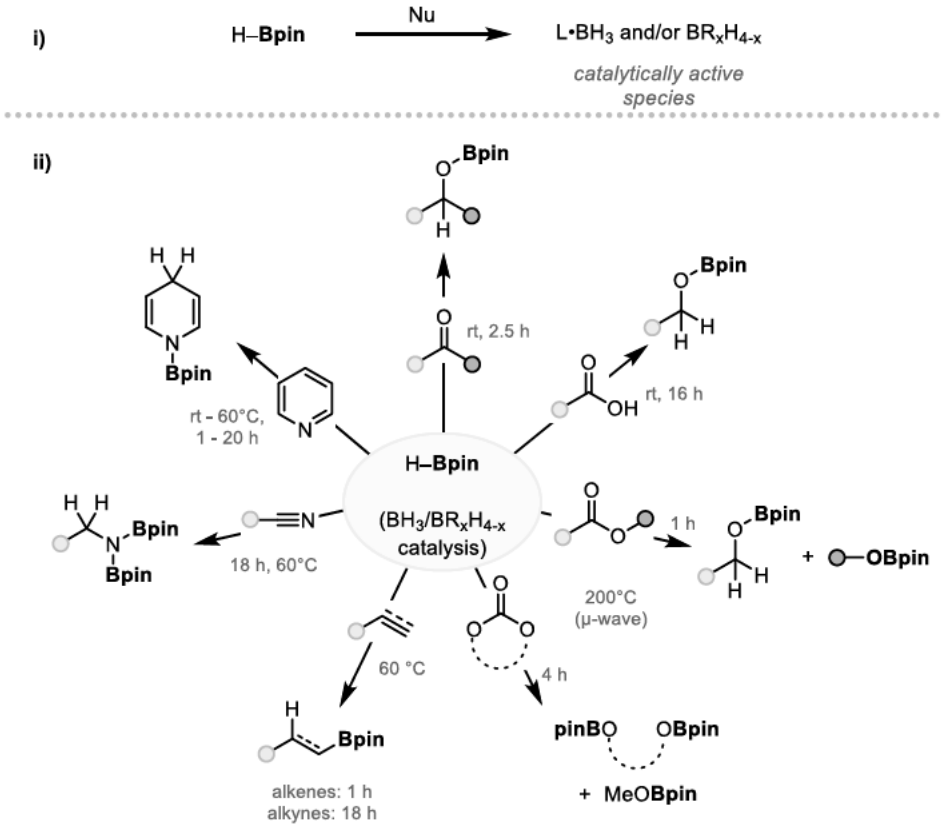

Scheme 1-23. i) In the presence of a nucleophile, HBpin can decompose to different borane species that can be catalytically active; ii) Examples of borane catalysis with representative reaction conditions for each transformation.

Perhaps hidden boron catalysis can largely explain the initial rapid development of aluminium hydride "catalysts" for hydroboration; in many cases, reaction conditions and reaction selectivity offered little, if no, improvements over the capabilities offered by borane catalysts. Furthermore, since the concept of hidden boron catalysis was introduced in 2020, development in aluminium-catalysed hydroboration reactions appears to have slowed. For example, a Reaxys document search for "aluminium catalysed hydroboration" (April 2023) recorded 23 results for 2019; since 2020, no more than 13 results per year have been recorded.

Future development of aluminium catalysts, for applications in hydroboration reactions or other protocols, requires careful experimental insight to understand the

exact role of the aluminium catalyst. Thus, the viability of the proposed steps should be examined, and control experiments should be performed to rule out other possible pathways.

Here, select examples of aluminium-catalysed hydroboration are discussed. These examples have been chosen based on the inclusion of control experiments, from the novelty of their transformations (in comparison to boron-catalysed procedures) or from other interesting points of discussion.

1.4.1 Exchange at Al–O

Among the many examples of aluminium-catalysed carbonyl reduction with HBpin, few have commented on how the structure of the aluminium catalyst may impact its reactivity. In this regard, Mulvey sought to compare the catalytic activity of neutral alanes in comparison with bimetallic aluminate complexes.[157] Enhanced catalytic activity for the reduction of polarised substrates, such as carbonyls and imines, was observed for bimetallic aluminate complexes. Thus, it was proposed that the greater polarity, induced by the bimetallic complexes, in the reactive intermediates enhanced both the insertion and σ-bond metathesis steps in the mechanism. The metal cation may also play a key role in coordinating to the substrate, a hypothesis testified by the diminished reactivity observed when the cation is coordinated by donor ligands.[159]

Scheme 1-24. Comparison of catalytic activity for neutral vs anionic aluminium hydrides on ketone hydroboration with HBpin.

This work was carried out prior to widespread awareness of hidden boron catalysis. Thus, control reactions for this alternative pathway were not performed. Although hidden boron catalysis can therefore not be ruled out for this protocol, it does suggest that metal cations can impact this process, regardless of whether hidden boron catalysis is operating or not. If, however, it was operating, the enhanced catalytic activity for bimetallic systems may also be explained by enhanced HBpin decomposition with a more nucleophilic pre-catalyst.

In the same year, Singh showed that cationic aluminium complexes with a bis(phosphinimino)amine ligand **1-II(H)** could effectively reduce aldehydes and ketones with HBcat (**Scheme 1-25**).[160] Single-turnover reactions were used to show the plausibility of the insertion/σ-bond metathesis pathway. Remarkably, the

Al–O/B–H metathesis of the inserted product **1-II(OR)** with HBcat was shown to proceed smoothly at room temperature. This contrasts drastically with the unfavourable exchange process described by Aldridge in their neutral aluminium formate complex **1-I(CO_2)**. Thus, it is possible that cationic alanes might favour exchange reactions in comparison to their neutral counterparts.

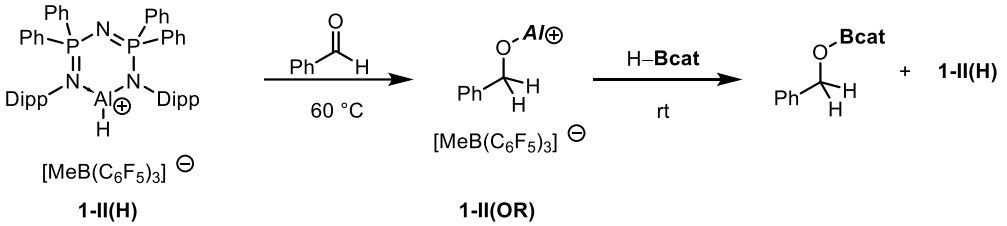

Scheme 1-25. Single-turnover experiments to demonstrate plausibility of aldehyde hydroboration with HBcat using cationic complex X-H.

The notion that it can be advantageous for aluminium to be cationic for Al–O/B–H metathesis was later backed up by Mézailles and So.[169] It was reported that a Zwitterionic (cationic at aluminium) bis(phosphoranyl)methanido aluminium hydride complex **1-III(H)** would reduce CO_2 with both HBpin and $Me_2S{\bullet}BH_3$, again contrasting with Aldridge's neutral aluminium hydride **1-I(H)**.[187] Importantly, no BH_3 was formed in the reaction between the aluminium hydride catalyst and HBpin in the absence of substrate. A stoichiometric reaction showed that aluminium hydride **1-III(H)** reacts with CO_2 at room temperature within 15 minutes (**Scheme 1-26**). The resulting κ^1-formate complex **1-III(CO_2)** was also capable of catalysing the reduction of CO_2 with HBpin, suggesting its involvement in the mechanism. A reaction between formate complex **1-III(CO_2)** with $Me_2S{\bullet}BH_3$ at 110 °C overnight showed that aluminium hydride **1-III(H)** was regenerated, implying that Al–O/B–H metathesis was possible at this temperature. Tracking the reaction by high-resolution mass spectrometry indicated that the reaction likely proceeded through several intermediates in which BH_3 first inserts into the formate substituent.

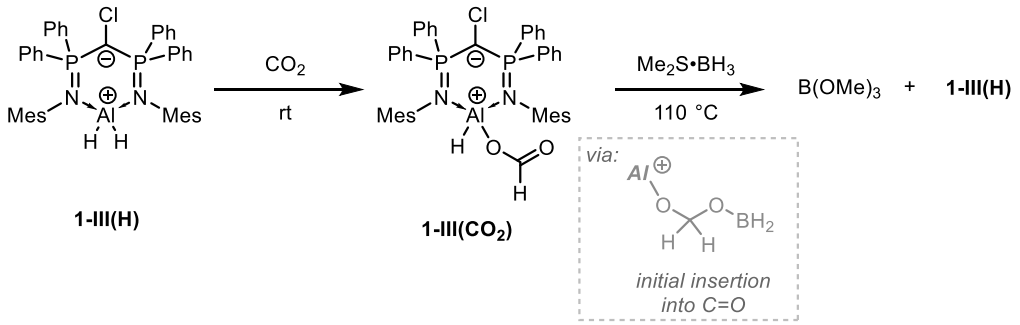

Scheme 1-26. Single-turnover experiments to demonstrate plausibility of CO_2 hydroboration with $Me_2S{\bullet}BH_3$ using cationic complex 1-III(H).

The same catalyst **1-III(H)** was used to mediate aldehyde and ketone hydroboration with HBpin.[169] Higher temperatures, of at least 60 °C, were required, in contrast to the milder conditions reported for other aluminium hydrides and nucleophilic initiators. In combination with the lack of BH_3 observed under catalytic conditions, the higher temperatures required can likely be explained by the challenging Al–O/B–H metathesis in a true insertion/metathesis pathway mediated by aluminium.

Careful choice of substrate may also enhance Al–O/B–H σ-bond metathesis. Rueping reported the asymmetric hydroboration of heteroaryl ketones with HBpin using an aluminium catalyst with an enantioenriched biphenol ligand (**Scheme 1-27.i**).[156] Conveniently, the catalyst could be generated *in situ* using equimolar Me_3Al and diol ligand precursor. Excellent yields and enantiomeric excess (up to 99% yield and 99% *ee*) were observed across a range of 2-heteroaryl ketones within two hours at room temperature. The pendent heteroaryl in proximity to the ketone was key to the success of the reaction and served to closely bind the aluminium centre by chelation (**Scheme 1-27.ii**). This facilitated hydride attack at one face of the ketone and possibly also facilitated the σ-bond metathesis process with HBpin by stabilising the aluminium centre in both the transition-state structure and product.

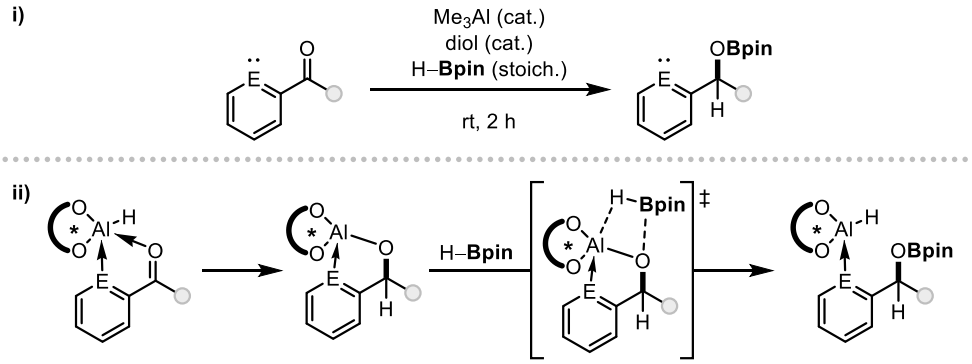

Scheme 1-27. i) Aluminium-catalysed enantioselective hydroboration of heteroaryl ketones using an enantioenriched diol ligand; ii) pathway of insertion/exchange outlined.

An alternative approach to aluminium-catalysed enantioselective ketone reduction with HBpin was recently reported by Kästner and Peters.[161] Rather than using an aluminium hydride reagent as the active catalyst, this approach used an enantioenriched salen-aluminium complex **1-IV**, which contained a pendent ammonium salt on the ligand (**Scheme 1-28.i**). The aluminium centre was used to coordinate the ketone substrate, while the pendent ammonium salt directed and activated HBpin towards nucleophilic attack at one face of the substrate (**Scheme 1-28.ii**). While not an example of catalysis that proceeds by Al/B exchange, it is an

important example of cooperative catalysis between aluminium and a non-innocent ligand and offers an alternative strategy for aluminium-catalysed hydroboration.

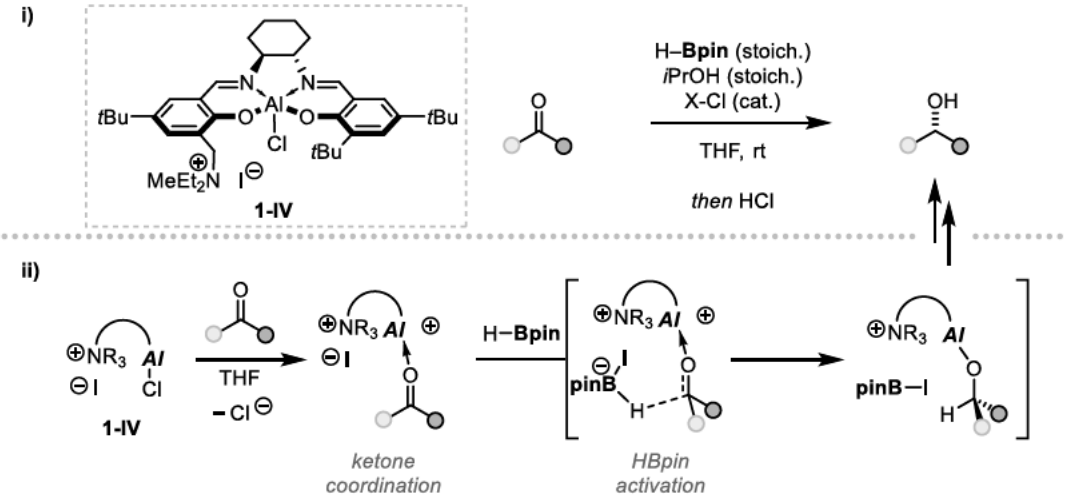

Scheme 1-28. i) Alternative approach to aluminium-catalysed enantioselective ketone reduction with HBpin using an enantioenriched salen-aluminium complex with a pendent ammonium salt; ii) outline of proposed key steps in mechanism.

1.4.2 Exchange at Al–N

Evidence for exchange at Al–N bonds with boron is slightly more conclusive. Roesky, Yang and Ma explored carbodiimide hydroboration with HBpin using β-diketiminate aluminium catalyst **1-V(H)** (**Scheme 1-29.i**).[178] The reaction was selective for the monohydroboration product under the conditions used (70 to 80 °C; 2 to 60 h). Single-turnover experiments were performed to show that aluminium hydride **1-V(H)** would insert into the carbodiimide substrate, and that the resulting Al–N intermediate **1-V(NR$_2$)** would react with HBpin to generate the corresponding borylated product. Notably, however, resonances for aluminium hydride **1-V(H)** were not observed in the corresponding spectrum following this reaction, but this was not explained by the authors.

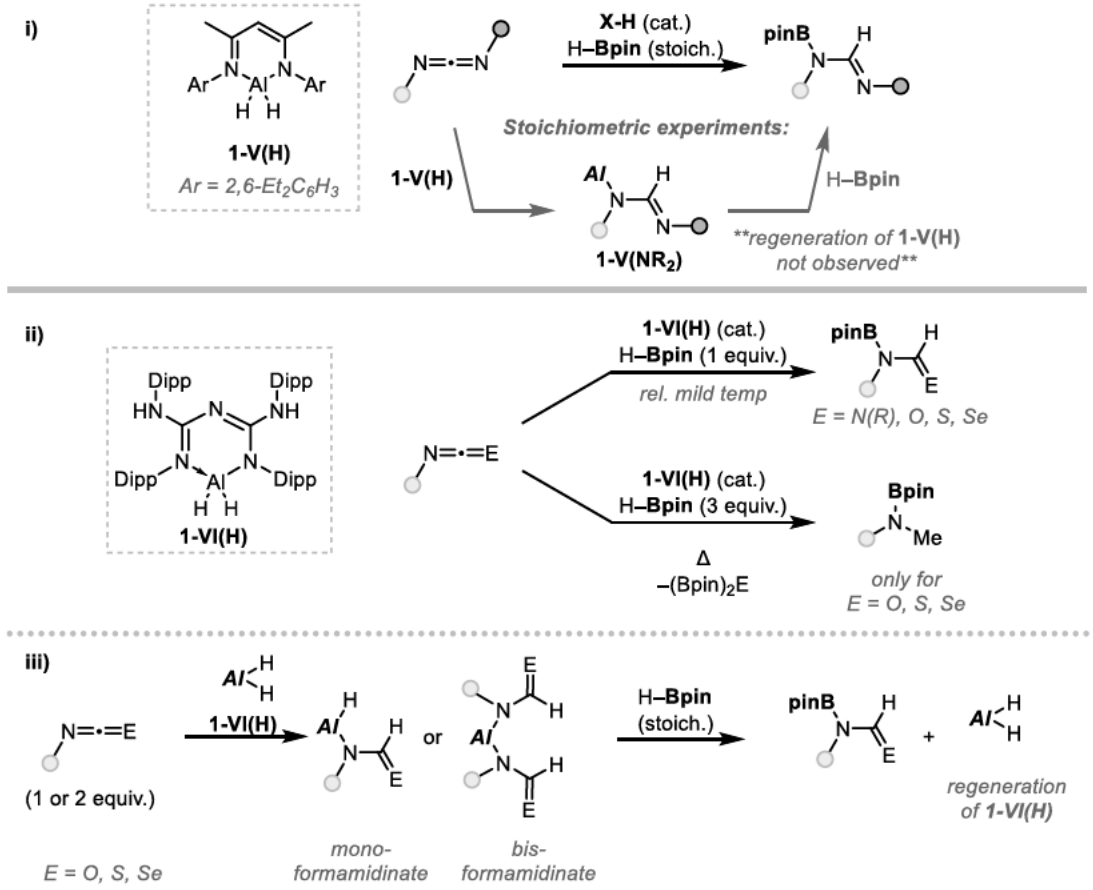

Scheme 1-29. i) Aluminium-catalysed monohydroboration of carbodiimide using X-H. Single-turnover experiments demonstrate plausibility of insertion/exchange pathway; ii) Aluminium-catalysed mono- and trihydroboration of hetereoallenes using X-H; iii) Single-turnover experiments demonstrate plausibility of insertion/exchange pathway for X-H.

Using a bis-guanidate-supported aluminium hydride complex **1-VI(H)**, Nembenna extended the scope to heteroallenes, which included carbodiimides but also isocyanates, isothiocyanates and isoselenocyanates (**Scheme 1-29.ii**).[177] Like in the previous example, selective monohydroboration was observed for carbodiimides. More interesting however, was the reactivity with isocyanate derivatives. By using relatively mild conditions (which varied depending on substrate), selective monohydroboration could be achieved, delivering *N*-borylated amide derivatives. Under more forceful conditions, "triple" hydroboration occurred, which resulted in cleavage of the C=X bond (X = O, S, Se) and gave borylated amines instead. A series of single-turnover experiments were performed to show that aluminium hydride **1-VI(H)** would insert into either one or two equivalents of the heteroallene substrate, and that the resulting mono- or bis(formamidinate) alane would react stoichiometrically with HBpin to give the resulting borylated product (**Scheme 1-29.iii**). This time, regeneration of the aluminium hydride **1-VI(H)** was observed, maintaining the integrity of the proposed Al–N/B–H metathesis pathway.

Aluminium hydrides can also catalyse nitrile hydroboration. Direct evidence for Al–N/B–H metathesis for this process is less clear. However, Panda reported no observable decomposition of HBpin under reaction conditions using aluminium methyl pre-catalysts supported by N-P-Se ligands, **1-VII(Me)** and **1-VIII(Me)** (**Scheme 1-30.i**).[173,182] Notably, nitrile reduction with HBpin using catalyst **1-VIII(Me)** showed good functional group tolerance towards esters (**Scheme 1-30.ii**). Nitrile hydroboration with HBpin using catalyst **1-VIII(Me)** was found to be first order in each of the catalyst, nitrile and HBpin. Ultimately, the mechanism was proposed to follow the insertion/σ-bond metathesis model with a rate-limiting Al–N/B–H exchange step. This was based on an unsupported claim which stated that this exchange step was much slower than nitrile hydroalumination with **1-VIII(Me)**.

Exchange of Al–N bonds with HBpin does not always give rise to the expected *N*-borylated product. Mulvey demonstrated that the reaction between dialkylaluminium amide **1-IX** with HBpin resulted in the formation of the HBpin ring-opened product **1-X** instead (**Scheme 1-30.iii**).[201] Thus, in certain circumstances, particularly when the substituents at the amide are bulky, Al–N/B–O metathesis is favoured over Al–N/B–H metathesis. Although the product **1-X** retains a B–H bond, limited catalytic activity for ketone reduction was observed, indicating that ring-opening of HBpin constitutes a possible decomposition pathway.

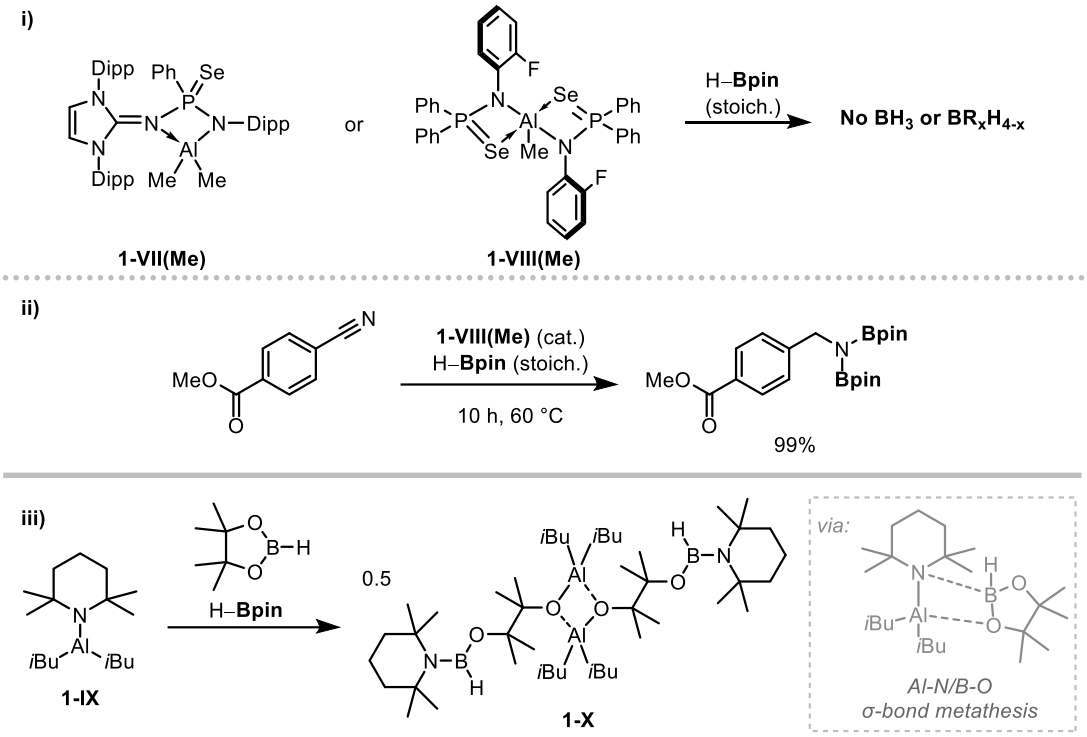

Scheme 1-30. i) Catalysts for nitrile hydroboration, X-Me and Y-Me, do not decompose HBpin; ii) demonstration of ester group tolerance for nitrile hydroboration with Y-Me; iii) Ring-opening of HBpin with an aluminium amide by Al–N/B–O σ-bond metathesis.

1.4.3 Exchange at Al–C

Catalysis

Aluminium-catalysed hydroboration of alkynes has been proposed to proceed through two different possible mechanisms: a pathway that proceeds by alkyne deprotonation (protonolysis; **Scheme 1-31.i**) or through a pathway that proceeds by an hydroalumination/σ-bond metathesis pathway (**Scheme 1-31.ii**).

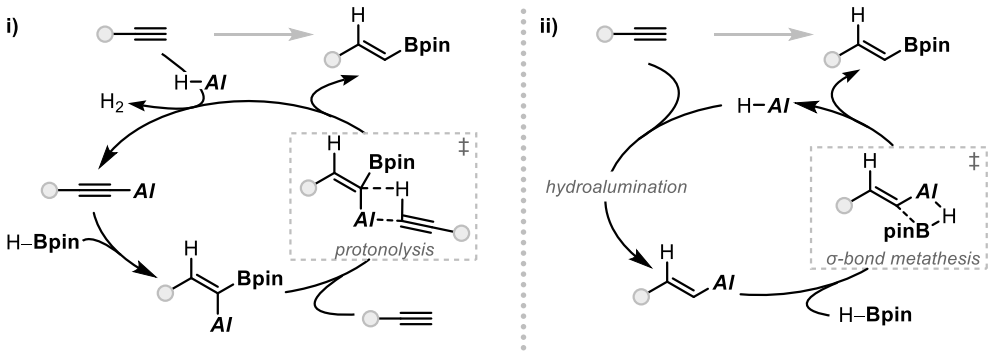

Scheme 1-31. Two proposed mechanisms for aluminium-catalysed alkyne hydroboration: i) a pathway that proceeds by deprotonation and direct hydroboration; ii) a pathway that proceeds by hydroalumination and σ-bond metathesis.

The deprotonation pathway was originally proposed by Roesky, Parameswaran and Yang on the basis that the β-diketiminate-supported aluminium dihydride catalyst **1-V(H)** reacted stoichiometrically with phenylacetylene to generate the corresponding aluminium acetylide **1-V(C*sp*)**.[183] Using calculations, it was proposed that the resulting aluminium acetylide **1-V(C*sp*)** could be activated towards hydroboration by HBpin, generating a geminal borylalane **1-V(Bpin)** (**Scheme 1-32.i**). Protonolysis of **1-V(Bpin)** with the alkyne, i.e. Al–C/C–H metathesis, would then deliver the vinyl boronic ester product and regenerate the aluminium acetylide catalyst, **1-V(C*sp*)**. This pathway has also been proposed to explain the catalytic behaviour of other aluminium catalysts.[152,159,172,176]

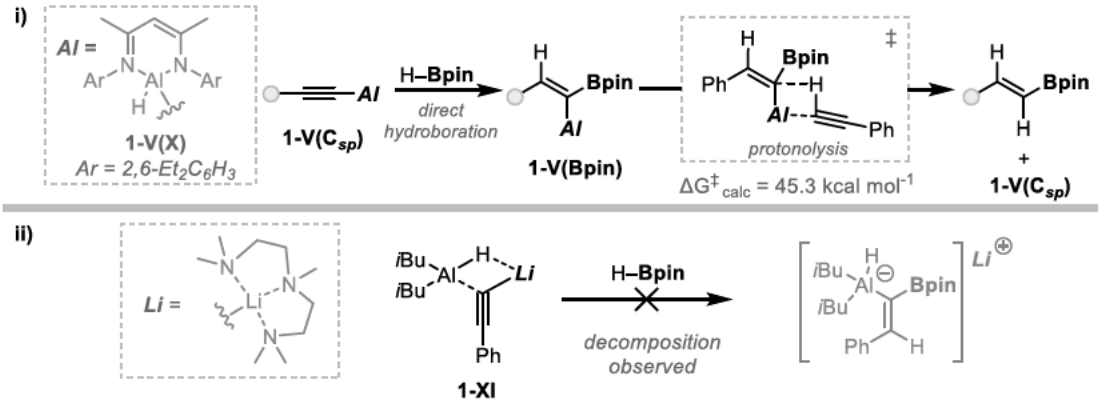

Scheme 1-32. i) The barrier for the protonolysis step in the *deprotonation* pathway; ii) The reaction of aluminium acetylide Y with HBpin leads to decomposition.

However, this proposed pathway has proven controversial. In a review of aluminium catalysis for reduction chemistry,[18] Nikonov highlighted that the calculated barrier for the protonolysis step ($\Delta G^{\ddagger}$ = 45.3 kcal mol^{-1}) was unrealistically high for a reaction that proceeds at room temperature (**Scheme 1-32.i**). Decomposition of aluminium hydride **1-V(H)** with HBpin was also discovered in an NMR spectrum in the supplementary information of Roesky's original publication, even though the caption mentioned that "no noticeable reaction was observed".[183] Mulvey and Okuda later demonstrated that the reaction of an aluminium acetylide **1-XI** with HBpin led to NMR spectra that were "broadly uninterpretable and indicative of decomposition of the reaction mixtures in stoichiometric regimes" (**Scheme 1-32.ii**), casting doubt on the direct hydroboration step.[159] Taken together, these clues indicated that an alternative mechanism was likely operating.

Thomas and Cowley described an alternative pathway for aluminium-catalysed hydroboration of alkynes that proceeded by the insertion/exchange pathway for Et_3Al•DABCO (DABCO = 1,4-diazabicyclo[2.2.2]octane) and $(iBu)_2AlH$ catalysts.[60]

Stoichiometric experiments were performed to show that vinyl alane **1-XII**, generated from alkyne hydroalumination, would react with HBpin to give the vinyl boronic ester product **1-XIII** (**Scheme 1-33.i**). In further support of this mechanism over the deprotonation pathway, no evidence of dihydrogen evolution was observed (**Scheme 1-33.ii**). In addition, the substrate scope was extended to internal alkynes which do not have an acidic terminal C–H.

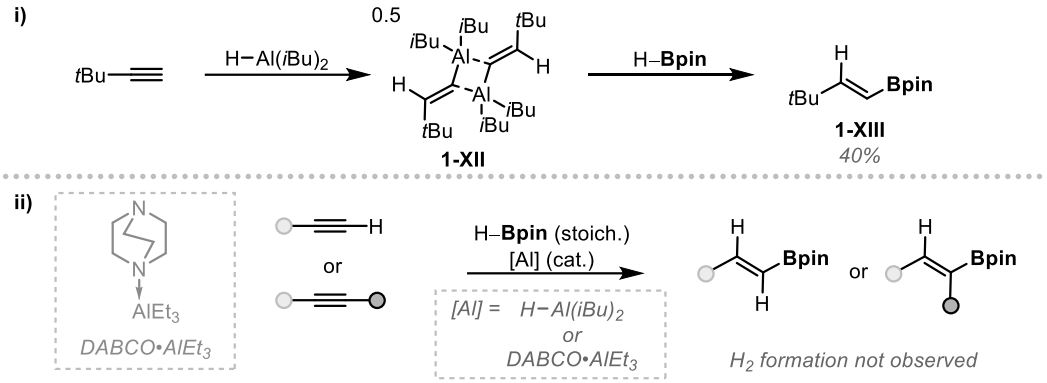

Scheme 1-33. i) Single-turnover experiments used to demonstrate the viability of an insertion/exchange pathway for aluminium-catalysed alkyne hydroboration with HBpin; ii) Evidence against the *deprotonation* pathway for DABCO•$AlEt_3$- and $(iBu)_2AlH$-catalysed alkyne hydroboration with HBpin.

Bakewell found that the mechanism for aluminium amidinate-catalysed alkyne hydroboration with HBpin depended on the structure, size and stability of the catalyst.[185] The smallest catalyst in the series **1-XIV(H)** resulted in decomposition of HBpin to BH_3 by Al–H/B–O metathesis, which also generated the corresponding aluminium pinacolate species (**1-XIV(pin)**; **Scheme 1-34**). In this case, at least some of the catalytic activity could be explained by the formation of hidden borane species. However, bulkier systems, such as **1-XV(H)**, did not decompose HBpin to BH_3 under catalytic conditions. Instead, formation of an HBpin adduct of the catalyst **1-XV(Bpin)** was observed. Curiously, this adduct was found to be essential for the reactivity of the aluminium amidinate with alkyne; the absence of HBpin led to no observed reactivity with aluminium hydride **1-XIV(H)** or **1-XV(H)**, either by hydroalumination or by deprotonation. To explain the observed catalytic activity for **1-XV(H)**, it was proposed that HBpin facilitated partial de-ligation of the amidinate ligand, thus opened up a free coordination space for the alkyne. The results highlight that the mechanism for hydroboration can be more nuanced than previously thought.

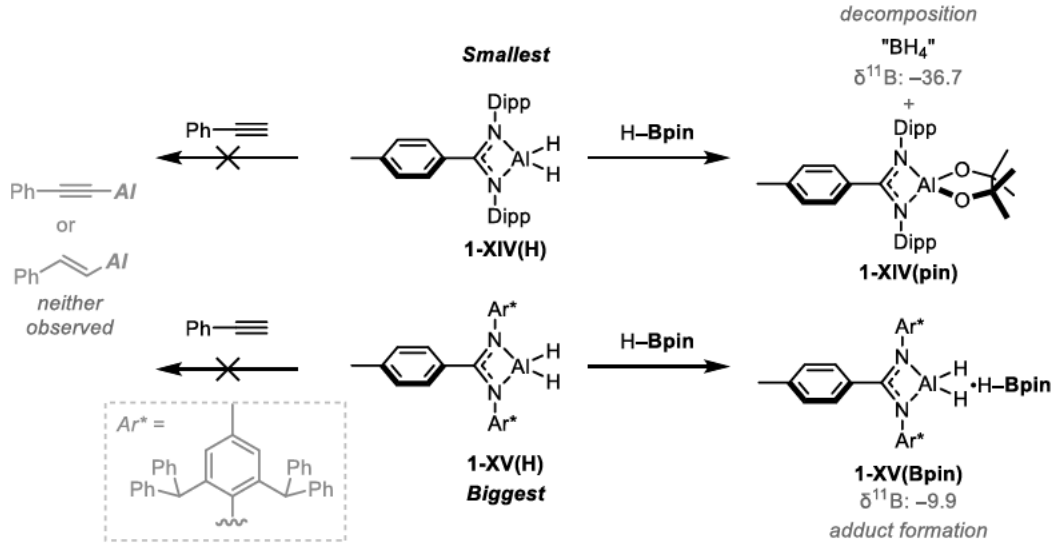

Scheme 1-34. The reactivity of aluminium amidinates with HBpin depend on ligand size; neither complex reacts with phenylacetylene.

In all reported cases of aluminium-catalysed alkene hydroboration, an insertion/exchange pathway (**Scheme 1-19.b**) has been proposed. However, direct experimental evidence for this pathway using reported catalysts is lacking. Bismuto demonstrated the plausibility of this pathway through stoichiometric experiments, using $(i\text{Bu})_2\text{AlH}$ as a soluble aluminium hydride surrogate in place of optimal catalyst, LiAlH_4. An alkyl alane, generated by alkene hydroalumination with $(i\text{Bu})_2\text{AlH}$, could react with HBpin to generate the corresponding alkyl boronic ester (**Scheme 1-35.i**).[81]

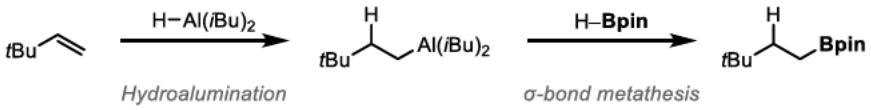

Scheme 1-35. i) Single-turnover experiments used to demonstrate the viability of an insertion/exchange pathway for aluminium-catalysed alkene hydroboration with HBpin.

Control reactions for hidden boron catalysis in aluminium-catalysed alkene hydroboration with HBpin are rare, with only one report noted. Panda and Chandrasekhar showed that HBpin did not decompose to BH_3 in the presence of an *N*,*N*-chelated aluminium methyl pre-catalyst **1-VII-Me**, where MeBpin was the only observable boron-containing product from the reaction (**Scheme 1-36.i**).[182] Panda had earlier demonstrated that a different *N*,*N*-chelated aluminium methyl pre-catalyst **1-XVI(Me)** could efficiently catalyse alkene hydroboration with HBpin at room temperature (**Scheme 1-36.ii**).[179] Although control experiments were not performed in this case, BH_3 is very unlikely to be responsible for this catalytic activity as it does not effectively catalyse alkene hydroboration with HBpin at this temperature.[194]

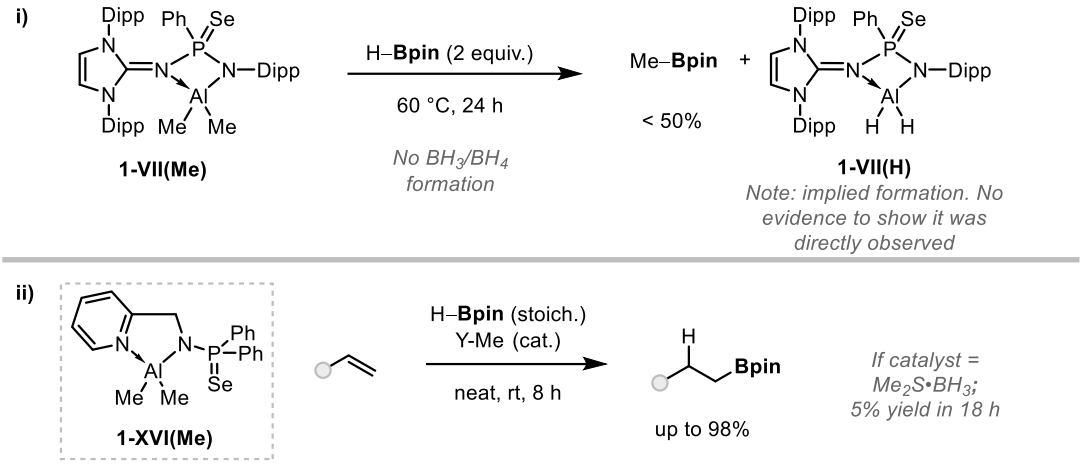

Scheme 1-36. i) Aluminium dimethyl pre-catalyst X-Me, active in alkene hydroboration, did not decompose HBpin under reaction conditions; ii) Aluminium dimethyl pre-catalyst X-Me can catalyse alkene hydroboration at room temperature.

Substituent effects on Al–C/B–H exchange

Based on various examples of stoichiometric Al–C/B–H exchange with HBpin, a picture can be built up on the effect of substituents at aluminium on this process. When aluminium is substituted only with carbon substituents, exchange proceeds "immediately" at room temperature (**Scheme 1-37.i**).[81] In contrast, the *N*,*N*-chelated aluminium dimethyl complex **1-VII(Me)** reacted only slowly with HBpin (**Scheme 1-37.ii**). Even after 24 hours at 60 °C, less than 50% conversion of HBpin to MeBpin was observed.[182] Further heteroatom substitution at aluminium results in even less reactivity; a terpyridine-supported dialkyl alane complex **1-XVII** did not react with HBpin at the Al–alkyl site (**Scheme 1-37.iii**).[158] Thus, the degree of coordinative and/or electronic saturation at aluminium likely dictates the capacity of the corresponding alkyl alane to undergo Al–C/B–H exchange with HBpin.

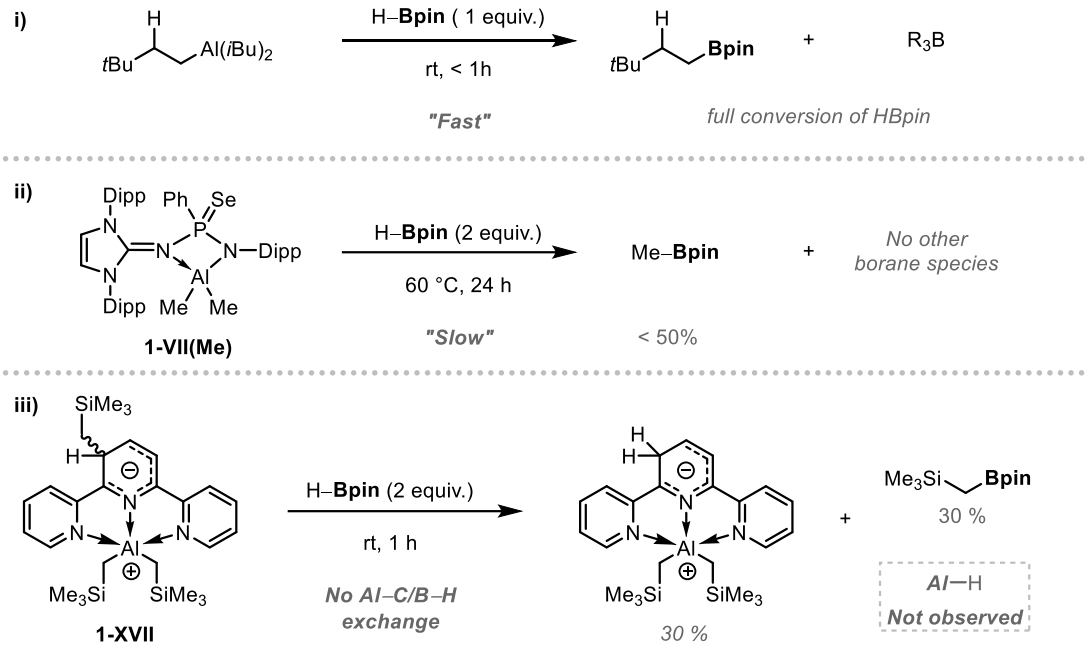

Scheme 1-37. Comparison of Al–C(sp^3)/B–H σ-bond metathesis reactions at different catalytically active alkyl alanes.

To support this idea, alkynyl boronic esters were not generated when an acetylide-substituted aluminate **1-XI** reacted with HBpin (**Scheme 1-32.ii**).[159] In addition, alkynyl boronic esters were not formed when alkynes reacted with HBpin in the presence of a β-diketiminate substituted aluminium hydride catalyst, even though the corresponding aluminium acetylide **1-V(C_{sp})** is proposed to be formed (**Scheme 1-32.ii**).[183] Aluminium acetylides, however, can undergo Al–C/B–H exchange with HBpin when aluminium is not substituted by heteroatoms (**1-XIX(C_{sp})**; **Scheme 1-40.i**).[202]

These observations may be explained by the requirement to form associative complexes in the transition-state structure of a σ-bond metathesis pathway (**Scheme 1-38.i**). Aluminium compounds form associative complexes to stabilise coordinative and electronic unsaturation. Therefore, the ease of which associative complexes can form is diminished as aluminium becomes more coordinatively and electronically saturated. It has also been suggested that σ-complexes could form prior to the formation of associative complexes (**Scheme 1-38.ii**).[69] For Al–C/B–H exchange with HBpin, this would involve an interaction between the H–B bond (highest occupied molecular orbital (HOMO) of HBpin)[203] and the vacant *p*-orbital at aluminium. In both cases, an unsaturated aluminium centre would lead to enhanced reactivity.

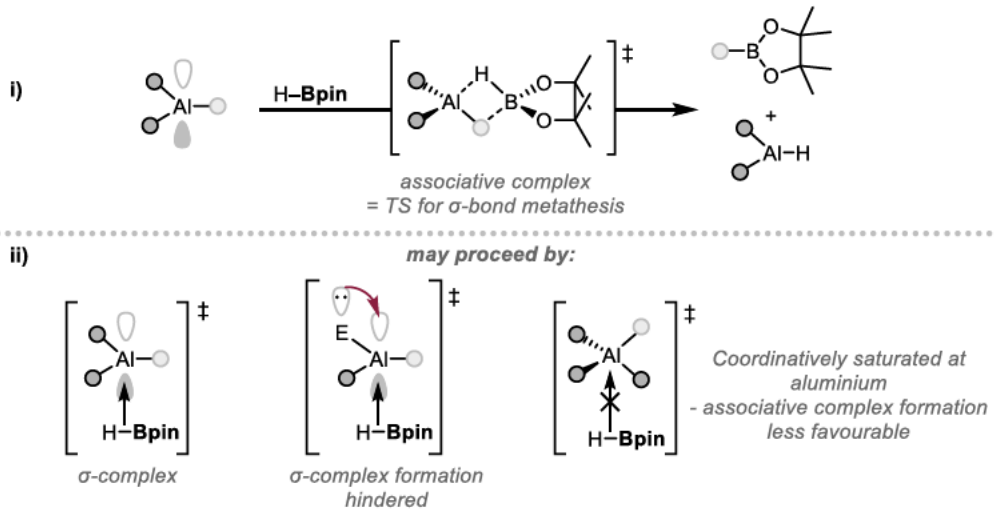

Scheme 1-38. Explanation for favourable Al–C/B–H σ-bond metathesis at electronically and coordinatively unsaturated alkyl alanes; i) transition-state (TS) for σ-bond metathesis is an associative complex; ii) Possible formation of σ-complexes prior to associative complex formation.

1.5 Aluminium-catalysed dehydrocoupling

Aluminium has been used to catalyse dehydrocoupling reactions between E–H (E = heteroatom) and B–H containing compounds (**Scheme 1-39.i**) through a deprotonation/exchange pathway (**Scheme 1-19.c**). Roesky, Yang and Parameswaran reported that β-diketiminate substituted aluminium dihydride **1-V(H)** would catalyse the dehydrocoupling of alcohols, thiols and amines with HBpin and H-*B*-9-BBN at room temperature.[183] Computational analysis predicted that the reaction proceeded by the deprotonation/exchange pathway, with a rate-limiting substrate deprotonation by the catalyst.

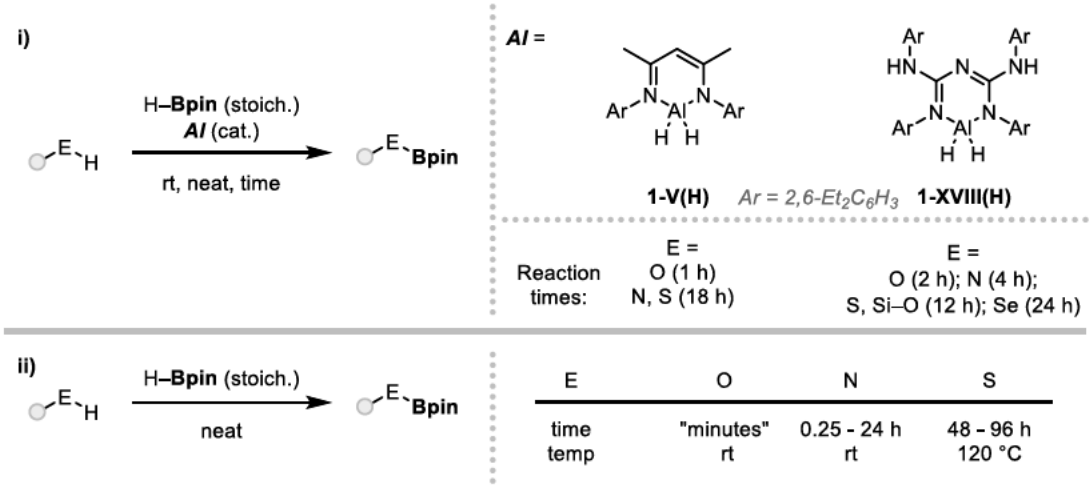

Scheme 1-39. i) Comparison of dehydrocoupling conditions for aluminium hydride catalysts X-H and Y-H; ii) Conditions for uncatalysed dehydrocoupling with HBpin.

Nembenna used a bis-guanidate-supported aluminium dihydride catalyst 1**-XVIII(H)** to extend the scope of aluminium-catalysed dehydrocoupling reactions with HBpin to include selenols and silanols, in addition to the alcohols, thiols and amines previously reported (**Scheme 1-39.i**).[154] In this example, stoichiometric experiments were used to show the plausibility of the deprotonation/exchange pathway for amine dehydrocoupling. However, it should also be noted that although the catalytic reaction proceeded at room temperature, the stoichiometric control reactions were heated to 70 °C and 80 °C respectively. Similarly, selenol dehydrocoupling proceeded at room temperature under catalysis, but the stoichiometric deprotonation of the selenol with the aluminium dihydride catalyst required heating to 70 °C. More experiments would therefore be required to rule out other possible mechanisms.

It is important to note that neither of these publications performed control reactions to determine the background reactivity of the substrate with HBpin. This could potentially be misleading, as the dehydrocoupling of amines, alcohols and thiols with HBpin has also been reported in the absence of a catalyst (**Scheme 1-39.ii**).[204] This background reaction is especially prevalent when the reaction is performed neat. At room temperature, alcohols can be dehydrocoupled within just minutes; amines can be fully reacted within a matter of hours.[204] Dehydrocoupling of thiols with HBpin is more challenging, however, requiring extended reaction times (2 to 3 days) and high temperatures (120 °C).[204] Based on this background reactivity, perhaps only the dehydrocoupling of thiols can qualify as true aluminium-catalysed dehydrocoupling.

Dehydrocoupling of terminal alkynes with HBpin does not, however, proceed in the absence of a catalyst. Cowley and Thomas used a tethered amino-alane catalyst **1-XIX(H)** to mediate this reaction (**Scheme 1-40.i**).[202] The structure of this catalyst was key to this transformation; the pendent amine made alkyne deprotonation more favourable over alkyne hydroalumination, presumably by blocking π-coordination of the alkyne to aluminium (**Scheme 1-40.ii**). The resulting aluminium acetylide **1-XIX(C_{sp})** reacted with HBpin to regenerate the aluminium hydride catalyst **1-XIX(H)** and give the alkynyl boronic ester product (**Scheme 1-40.i**). Kinetic studies suggested that deprotonation was the rate-limiting step and was mediated by a dimeric aluminium hydride complex.

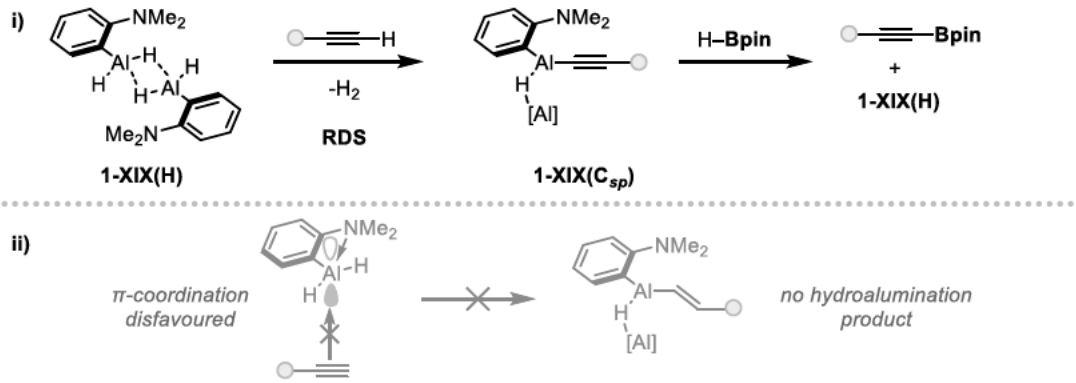

Scheme 1-40. i) Pathway for C-H borylation of terminal alkynes with HBpin using aluminium hydride catalyst X-H; ii) Explanation for selectivity observed.

1.6 General aims

Exchange of substituents between aluminium and boron (by σ-bond metathesis) has been used extensively for aluminium-catalysed hydroboration protocols. Yet despite this, many protocols lack the deeper molecular-level understanding required to further develop aluminium catalysis in this domain. With the increasing awareness of hidden boron catalysis, the role of aluminium in some of these transformations has been questioned.

This thesis aims to establish the behaviour of aluminium in hydroboration catalysis. Using the knowledge acquired from these investigations, the development of new protocols that leverage the potential of aluminium/boron exchange are explored.

Chapter 2:

Aluminium-catalysed alkene hydroboration with HBpin: Development and scope

2.1 Introduction

Organoboranes are highly reactive, versatile reagents but their air- and moisture-sensitivity make them challenging to handle. In contrast, pinacolboronic esters (RBpin) are usually bench-stable and can often be purified by column chromatography.[205] Additionally, their capacity to undergo a wide range of stereospecific transformations[141] makes them excellent chemical building blocks.

An atom-efficient route towards alkyl boron reagents is by alkene hydroboration (**Scheme 2-1.i**). Like alkene hydroalumination, this is thought to proceed by interaction of the alkene π-orbital with the vacant *p*-orbital at boron.[206,207] Unstabilised boranes, like H-*B*-9-BBN or BH_3, readily engage in uncatalysed alkene hydroboration;[208,209] in contrast, pinacolborane (HBpin), the precursor towards pinacolboronic esters, does not.[13,194,210] The Lewis acidity at boron in Bpin reagents is tempered by the donation of the lone pair of electrons from the adjacent oxygen atoms into the vacant *p*-orbital at boron (**Scheme 2-1.ii**). Olefins therefore do not readily react with HBpin in the absence of a catalyst.[13,194,210] The stability of pinacolboronic esters in air and moisture can ultimately be attributed to this *p*-orbital stabilisation.[205,211]

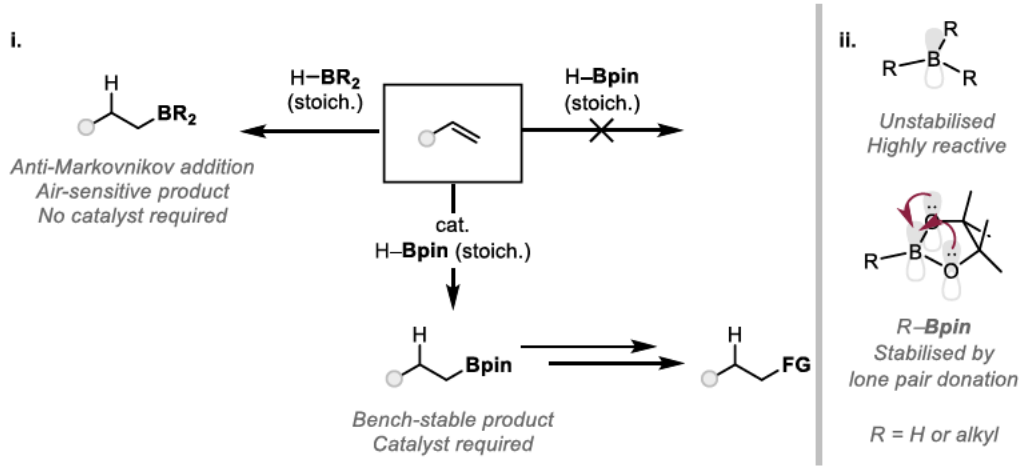

Scheme 2-1. i) Explanation for stability of RBpin compared to unstabilised organoboranes; ii) Comparison of reactivity between HBpin and unstabilised hydroboranes. RBpin is readily functionalised.

Catalysed alkene hydroboration with stabilised boranes, such as HBpin or HBcat, can be advantageous in comparison to uncatalysed hydroboration with more reactive boranes. Control over chemo-, regio- and stereo-selectivity is possible using catalysis and more challenging without (**Scheme 2-2.i**).[212,213] These transformations are most commonly catalysed by a transition metal complex and typically proceed by oxidative addition of the B–H bond into the catalyst. The alkene would then coordinate to the resultant complex prior to migratory insertion into the M–H bond. Finally,

reductive elimination leads to the formation of the hydroboration product (**Scheme 2-2.ii**).[212] Early examples of catalysed alkene hydroboration used precious transition metal catalysts[212–215] (most notably rhodium[213,215]), but the desire to move away from these elements led to the development of first-row transition metal catalysts[216] as cheaper, less toxic and more abundant substitutes.

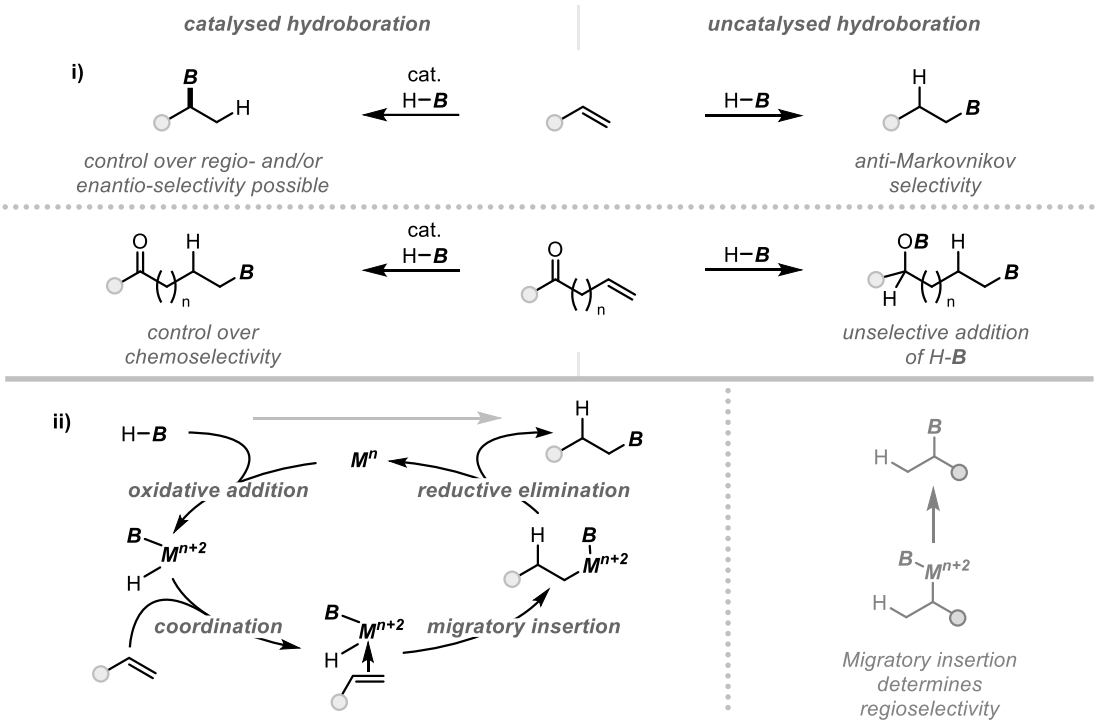

Scheme 2-2. i) Catalysed vs uncatalysed alkene hydroboration; ii) typical mechanism for transition metal-catalysed alkene hydroboration.

Early main group elements offer a sustainable alternative and orthogonal reactivity, but do not readily engage in the redox chemistry that governs transition metal catalysis. Historically, this has largely limited their use to simple stoichiometric processes or Lewis acid catalysis. However, the development of σ-bond metathesis as a redox neutral pathway for catalyst regeneration has led to an exponential growth in the field of main group catalysis.[14–20]

Alkenes are considered challenging substrates as they are unpolarised and contain a lower-lying HOMO in comparison to the similarly unpolarised alkynes. This has resulted in relatively few examples of main group-catalysed alkene hydroboration with HBpin in comparison to other unsaturated substrates.[217] Of the main group elements, those in group 13, predominantly boron and aluminium, have thus far been most effective for catalysing this transformation.[189,190,217,218]

Aided by the availability and practicality of ^{11}B NMR spectroscopy, boron-catalysed alkene hydroboration with HBpin is best understood.[194,219,220] These reactions proceed by alkene hydroboration with a hydridoborane catalyst, followed by transborylation (commonly by σ-bond metathesis) of the resulting alkylborane with HBpin. This final step delivers the alkylBpin product and regenerates the hydridoborane catalyst (**Scheme 2-3.i**). The activation parameters of B–C(sp^3)/B–H exchange between gem-diboryl alkane **2-I** with HBpin have been experimentally determined (**Scheme 2-3.ii**).[219] The free energy value obtained ($\Delta G^{\ddagger}_{exp}$ = 28(3) kcal mol^{-1}) was significantly greater than that observed for B–C(sp^2)/B–H exchange ($\Delta G^{\ddagger}_{exp}$ = 20.3 kcal mol^{-1}).[210] The strongly negative $\Delta S^{\ddagger}_{exp}$ value obtained (–36(8) eu) is indicative of an ordered transition state, which can be used to support the existence of the proposed σ-bond metathesis process.[69]

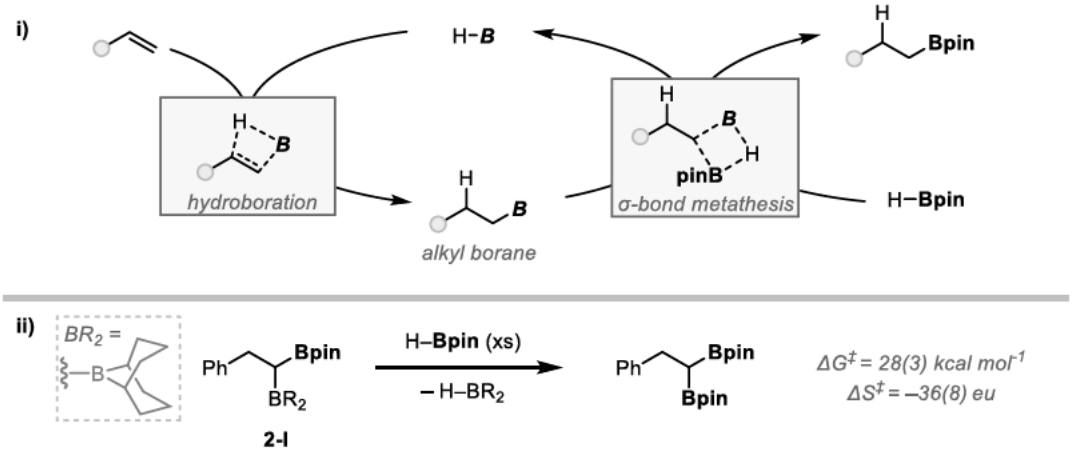

Scheme 2-3. i) Mechanism for boron-catalysed alkene hydroboration; ii) Outcome and thermodynamic parameters for B–C(sp^3)/B–H exchange of 2-I with HBpin.

The related boron-catalysed alkyne hydroboration with HBpin, originally discovered by Arase and Hoshi,[221] has been studied in extensive depth by Thomas and Lloyd-Jones.[210] The use of single-turnover labelled experiments ($^2H/^{10}B$) gave evidence of a stereo-selective σ-bond metathesis pathway and ruled out other possible mechanisms for turnover, such as alkoxy ligand metathesis or dehydroboration (**Scheme 2-4**). Identification of species present under catalysis also revealed mechanisms for catalyst deactivation, such as Markovnikov addition of the catalyst across the alkyne or over-addition of the catalyst to the vinylBpin product.

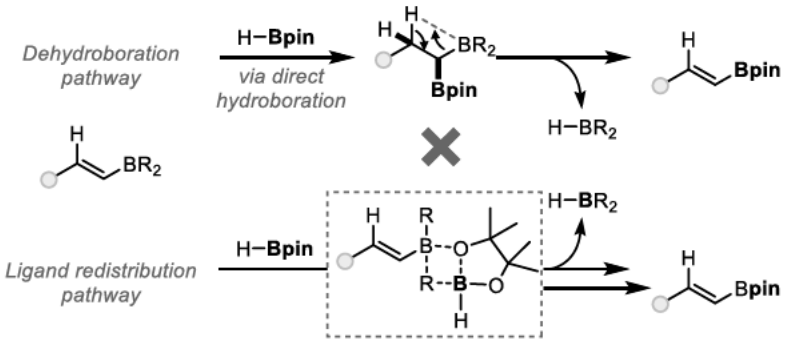

Scheme 2-4. Alternative turnover pathways shown – these have been ruled out by experimental investigations.

Despite a detailed mechanistic understanding, boron-catalysed alkene hydroboration has encountered some limitations. The availability of enantioenriched boranes[222–225] for stoichiometric alkene hydroboration should be readily exploitable for asymmetric catalysis. However, extensive studies by the Thomas group into transborylation have found C(sp^3)–B/B–H exchange to be especially challenging, particularly when HBpin or pro-chiral alkenes are used (unpublished work – from theses).[226–228] Boron-catalysed alkene hydroboration with HBpin therefore requires conditions that are not amenable to asymmetric catalysis, such as high temperatures (**Scheme 2-5**).

Switching to an aluminium catalyst could circumvent this issue, as the exchange of alkyl substituents between boron and aluminium has long been established.[65] For Al–C(sp^3)/B–H metathesis, the exchange of a weak Al–C bond (ΔHf_{298K} ≈ 255 kJ mol^{-1}) to a much stronger B–C bond (ΔHf_{298K} ≈ 448(29) kJ/mol) should lead to favourable exchange thermodynamics ($\Delta H°$ ≈ 148 kJ mol^{-1}). In contrast, based on ΔHf_{298K} values, there would not be any enthalpic gain for a B–C(sp^3)/B–H σ-bond metathesis reaction, ($\Delta H°$ = 0 kJ mol^{-1}). The longer Al–C bond in comparison to a B–C bond may also lower the kinetic barrier to exchange by diminishing steric clash between the substituents on aluminium and the approaching HBpin.

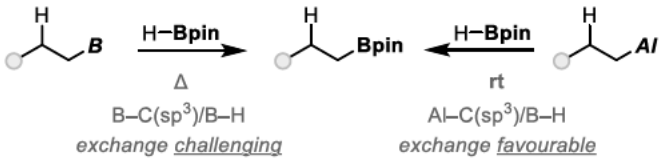

Scheme 2-5. Comparison between aluminium- and boron-catalysed alkene hydroboration with HBpin.

There is some experimental evidence that Al–C(sp^3)/B–H exchange is indeed favourable; Bismuto *et al.* demonstrated that trialkyl alanes react with HBpin to give the corresponding alkylBpin product at room temperature (**Scheme 2-5**).[81] As

stoichiometric alkene hydroalumination is already well-established,[35,58,229] this reaction has ultimately formed the basis for all the aluminium-catalysed alkene hydroboration protocols reported to date.[81,179–182] Akin to the borane-catalysed protocols, each example was proposed to follow the same general mechanism that proceeds by alkene hydroalumination with the aluminium hydride catalyst, followed by σ-bond metathesis of the resulting alkyl alane with HBpin. This key turnover step would deliver the pinacolboronic ester product and regenerate the aluminium hydride catalyst (**Scheme 2-6.i**). Although this mechanism is generally agreed and widely invoked, direct evidence for this pathway using the reported catalysts (**2-II** to **2-VI**; **Scheme 2-6.ii**) is lacking.

With the recent understanding that *hidden boron catalysis*[188,189] can mediate alkene hydroboration with HBpin, it is especially important to establish the role of the aluminium catalyst. The exact species and processes involved in catalysis remain unknown, and thus it is difficult to know how catalyst performance can be improved or applied in other systems. Ultimately, the limited mechanistic insight into this procedure impedes the development of aluminium-catalysed hydroboration.

i)

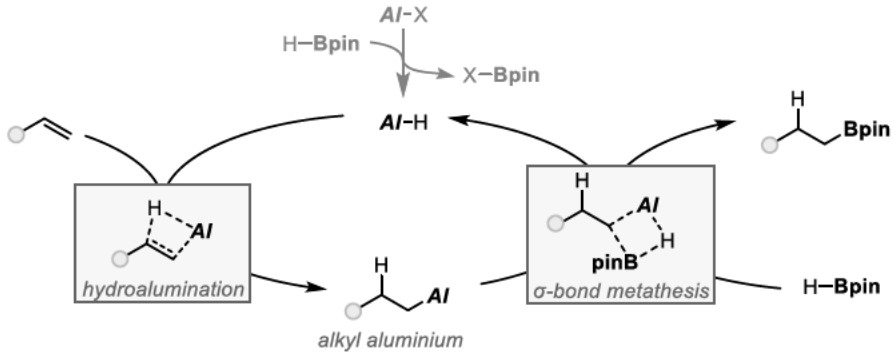

ii)

	Bismuto *et. al.*, *2018*	Shi *et. al.*, *2019*	An *et. al.*, *2019*	Panda *et. al.*, *2019*	Panda *et. al.*, *2023*
Pre-catalyst	$LiAlH_4$	$AlEt_3$	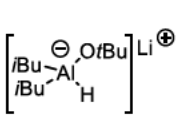	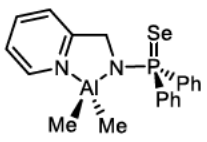	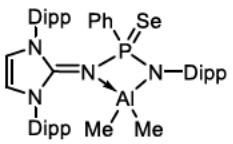
	2-II	**2-III**	**2-IV**	**2-V**	**2-VI**
Conditions	(10 mol%) 110 °C, 4 h	(10 mol%) 100 °C, 24 h	(5 mol%) 110 °C, 2 h	(3 mol%) 30 °C, 8 h	(2 mol%) 60 °C, 12 h

Scheme 2-6. i) Generally agreed mechanism for the aluminium-catalysed alkene hydroboration with HBpin; ii) List of previously used aluminium catalysts for alkene hydroboration with HBpin.

2.2 Aims

With most examples of aluminium-catalysed alkene hydroboration requiring high temperatures (**Scheme 2-6.ii**), this work set out to understand how to more efficiently mediate alkene hydroboration with HBpin using aluminium catalysts. Without additional insight, an insertion/exchange pathway was assumed. Based on the stoichiometric experiments described by Bismuto (**Scheme 2-5**; see also **Scheme 1-37.i**, Chapter 1), it is most likely that the alkene hydroalumination step is slow relative to the Al–C(sp^3)/B–H σ-bond metathesis step. This may be specific to cases where aluminium is not coordinatively or electronically saturated, as this has been noted to slow down the σ-bond metathesis step (see **Scheme 1-37**, Chapter 1). It was therefore hypothesised that an efficient aluminium hydride catalyst for alkene hydroboration should readily react with alkenes under mild conditions and also be electronically unsaturated.

With these criteria in mind, *m*-terphenyl (2,6-$Ar_2C_6H_3$; Ar = aryl) substituted aluminium hydrides stood out as obvious candidates for potentially effective catalysts for this purpose. These aluminium hydrides have been shown by Power to react with alkenes at room temperature.[64] The steric bulk provided by the *m*-terphenyl substituents was thought to enhance the formation of reactive monomeric species in solution through kinetic stabilisation (**Scheme 2-7**). Indeed, the rate of alkene hydroalumination was found to correlate with the steric bulk at aluminium. Moreover, the bulky framework stabilised these primary alanes from redistribution[64] – which should be important under catalysis to avoid catalyst decomposition.

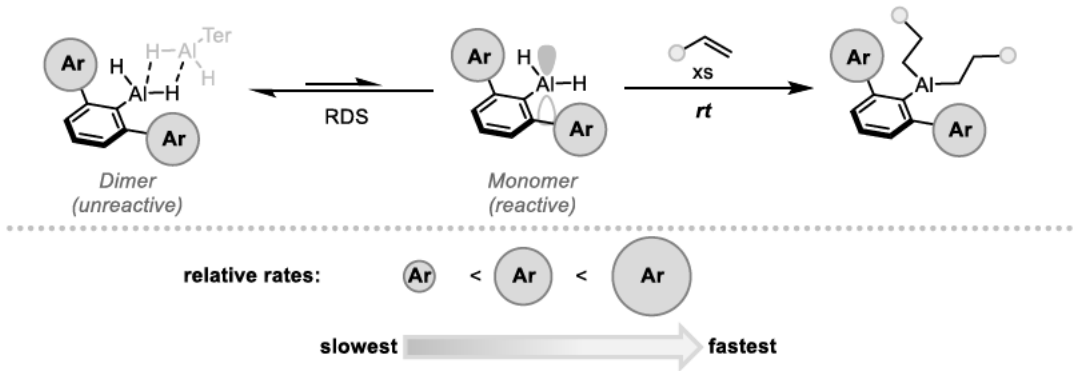

Scheme 2-7. *m*-Terphenyl alanes react with alkenes at room temperature and rates are correlated with steric bulk.

Less certain, however, would be the capacity of the resulting alkyl alanes to engage in Al–C(sp^3)/B–H σ-bond metathesis with HBpin due to the steric bulk surrounding aluminium. Consequently, it was anticipated that any potential catalytic activity would be sensitive to the steric crowding at aluminium.

The overarching aim of this project, therefore, was to assess the capabilities of *m*-terphenyl alanes to catalyse alkene hydroboration with HBpin and to examine the influence of steric bulk on potential catalytic activity. By performing mechanistic experiments, it was anticipated that the influence of steric bulk could be understood in relation to the proposed mechanistic steps – alkene hydroalumination and Al–C(sp^3)/B–H σ-bond metathesis. Furthermore, a comparison with the more widely established boron-catalysed hydroboration procedures would be made.

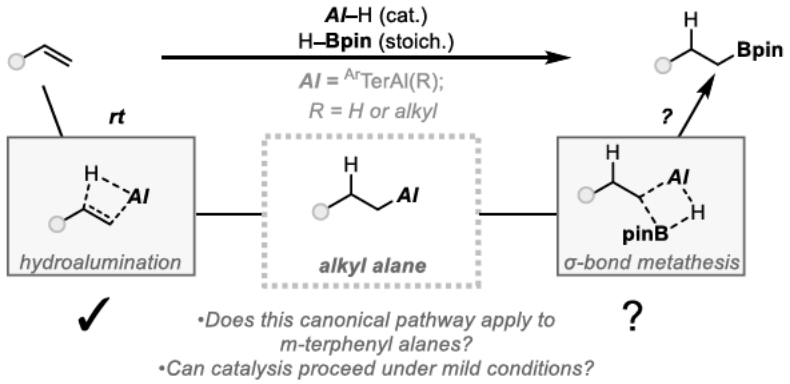

Scheme 2-8. Aims for Chapter 2.

2.3 Results and Discussion

2.3.1 Synthesis of *m*-terphenyl alanes

The project began by preparing a series of *m*-terphenyl-(2,6-$Ar_2C_6H_3$; ^{Ar}Ter) substituted aluminium hydrides (^{Ar}TerAlH_2) and alkyls (^{Ar}TerAlR_2). The steric bulk at aluminium was manipulated by varying the size of the flanking aryl substituents (Ar) of the *m*-terphenyl unit (^{Ar}Ter). To facilitate reaction monitoring by ^{1}H NMR spectroscopy, aryl substituents (Ar) were chosen based on the presence of simple spectroscopic handles. With this in mind, three flanking aryl groups were chosen: 4-methylphenyl (*p*-Tol), 2,4,6-trimethylphenyl (Mes) and 2,4,6-triisopropylphenyl (Tipp). Each of these aryl groups have characteristic sets of ^{1}H NMR alkyl resonances that will be referred to throughout this thesis. A general description of these resonances is presented in **Scheme 2-9**.

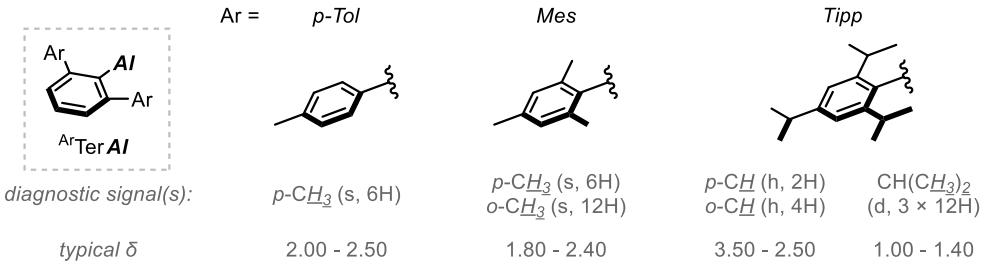

Scheme 2-9. The series of *m*-terphenyl alanes prepared, with the diagnostic alkyl signals noted. ***Al*** = AlX_2, where X= H and/or alkyl.

The precursor to the target *m*-terphenyl alanes (^{Ar}Ter***Al***) are the *m*-terphenyl iodides (^{Ar}TerI). These were prepared according to Hart's reported route[230] (later optimised by Figueroa)[231] from 1,3-dichlorobenzene, *n*BuLi, aryl magnesium bromide and iodine (**Scheme 2-10.i**). Lithium/halogen exchange of ^{Ar}TerI with *n*BuLi gave the lithiated arene (^{Ar}TerLi; **Scheme 2-10.ii**).[232] Reaction of ^{Ar}TerLi with dialkyl aluminium chlorides (R = Me, Et, *i*Bu) in hexane at –78 °C followed by warming to room temperature overnight yielded the dialkyl-substituted *m*-terphenyl alanes (^{Ar}TerAlR_2, **Scheme 2-10.ii**).[233] The aluminium dihydrides (^{Ar}TerAlH_2) were synthesised, according to Power,[234] by the reaction of ^{Ar}TerLi with Me_3N•AlH_3 in Et_2O/alkanes, followed by hydride abstraction of the resulting aluminate (^{Ar}TerAlH_3•Li) with Me_3SiCl (1 equiv.; **Scheme 2-10.iii**).[234] Again, the reaction pathway was general for each Ar group.

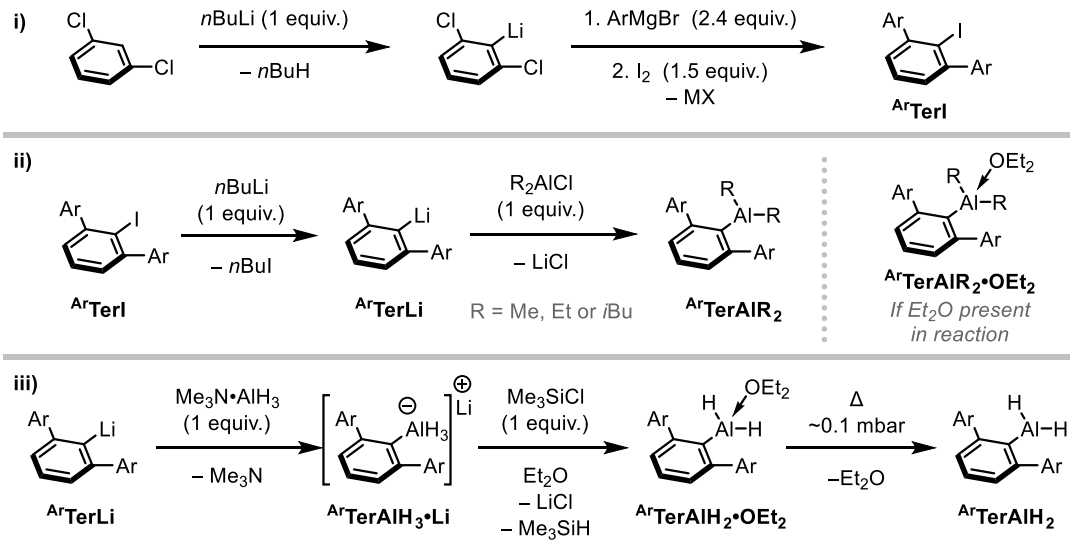

Scheme 2-10. i) Synthetic route towards *m*-terphenyl iodides; ii) synthetic route towards *m*-terphenyl-substituted dialkyl alanes; iii) synthetic route towards *m*-terphenyl-substituted primary alanes.

When Et_2O was present during synthesis, either as the solvent or when carried through from the aryl lithium reagent ($^{Ar}TerLi•Et_2O$), the alane•Et_2O adducts ($^{Ar}TerAlH_2•Et_2O$ or $^{Ar}TerAlR_2•Et_2O$) resulted. Avoiding Et_2O and other coordinating solvents enabled the direct synthesis of donor-free dialkyl alanes ($^{Ar}TerAlR_2$), which were prepared by reacting ether-free $^{Ar}TerLi$ with dialkyl aluminium chlorides in pentane or hexane. In contrast, Et_2O could not be avoided in the synthetic route towards *m*-terphenyl-substituted primary alanes ($^{Ar}TerAlH_2$) due to the insolubility of $Me_3N•AlH_3$ in alkanes. Donor-free primary alanes ($^{Ar}TerAlH_2$) were instead prepared by heating the corresponding diethyl ether adduct ($^{Ar}TerAlH_2•OEt_2$) under vacuum (c.a. 100 °C; 0.1 mbar) for 30-60 minutes (**Scheme 2-10.iii**).

In the absence of Lewis base donors, *m*-terphenyl-substituted primary alanes ($^{Ar}TerAlH_2$) form hydride-bridged dimers featuring three-centre two-electron bonding (3c-2e).[234] Although $AlMe_3$ is dimeric and also uses this bonding pattern,[51,235,236] the related *m*-terphenyl-substituted dimethyl alanes ($^{Ar}TerAlMe_2$) do not – the dialkyl alane compounds of the form $^{Ar}TerAlR_2$ are monomeric.[64,233,237] When $^{Mes}TerAlEt_2$ was reacted with $^{Mes}TerAlH_2$ in toluene or CH_2Cl_2 at room temperature, the formation of secondary alane, $^{Mes}TerAl(H)Et$, resulted (**Scheme 2-11.i**). Like the *m*-terphenyl-substituted primary alanes ($^{Ar}TerAlH_2$), this secondary alane ($^{Mes}TerAl(H)Et$) is also a hydride-bridged dimer (**Scheme 2-11.ii**). For clarity of viewing and understanding

stoichiometries, the monomeric units are drawn in each scheme (with the exception of **Scheme 2-11**).

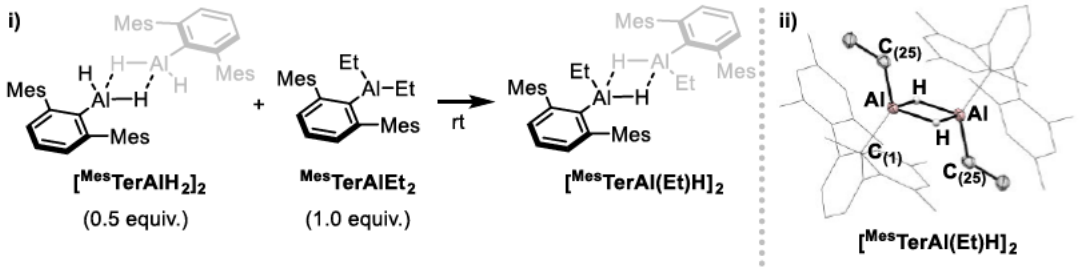

Scheme 2-11. i) Synthetic route towards *m*-terphenyl-substituted monoalkyl alanes; ii) ORTEP representation of ^{Mes}TerAl(Et)H (50% probability ellipsoids). For clarity, the ^{Mes}Ter-substituent is displayed in wireframe and the hydrogen atoms have been removed, except for the bridging hydrides. Selected bond lengths (A) and angles (°): Al–H 1.68(2), Al•••Al 2.634(1), Al–$C_{(1)}$ 1.971(2), Al–$C_{(25)}$ 1.947(2), $C_{(1)}$–Al–H 108.0(7), $C_{(1)}$–Al–Al 115.03(7), $C_{(25)}$–Al–Al 114.13(8).

The solubilities of these primary (^{Ar}TerAlH_2), secondary (^{Ar}TerAl(R)H) and tertiary alanes (^{Ar}TerAlR_2) in non-coordinating solvents apparently relate to their aggregation state. The monomeric tertiary alanes (^{Ar}TerAlR_2) are very soluble in alkane solvents, while the dimeric primary (^{Ar}TerAlH_2) and secondary alanes (^{Ar}TerAl(R)H) are mostly insoluble in alkanes and only sparingly soluble in CH_2Cl_2 or toluene. Notably, the Et_2O adduct of primary alanes (^{Ar}TerAlH_2•Et_2O) exhibited greatly improved solubility in CH_2Cl_2 or toluene in comparison to donor-free primary alanes (^{Ar}TerAlH_2).

2.3.2 Stoichiometric experiments

With the target alanes prepared, the plausibility of the generally accepted mechanism for aluminium-catalysed alkene hydroboration was assessed. This involved the detailed examination of the individual steps – alkene hydroalumination and Al–C(sp^3)/B–H σ-bond metathesis. Thus, the potential for *m*-terphenyl alanes to catalyse alkene hydroboration by this mechanism would be better understood. Moreover, it would be possible to establish the relationship between these key mechanistic steps and the steric hindrance at aluminium. Understanding the potential rate-limiting step under catalysis should allow rational design of a better catalyst.

Hydroalumination

The relative rates of alkene hydroalumination for ^{Ar}TerAlH_2 (Ar = *p*-Tol, Mes, Tipp) under catalytically relevant conditions (75 mM in CD_2Cl_2, rt; **Scheme 2-12**) were investigated, using 1-octene (1 equiv.) as the model substrate. ^{1}H NMR spectroscopy was used to monitor the reaction progression, which was estimated by tracking the

consumption of 1-octene. The intention behind this was to determine which of the *m*-terphenyl alanes were fastest for alkene hydroalumination, without attempting to draw any conclusions regarding mechanistic insight for this process. For comparison purposes, the initial rates were calculated using the integrated rate law for a first order reaction (Equation 1) using the first five data points. The half-life ($t_{1/2}$) of the reaction was calculated according to Equation 2.

Equation 1:
$$ln[1\text{-octene}]_t = -kt + ln[1\text{-}octene]_0;$$

Plotting ***ln[1-octene]$_t$*** *vs* ***t*** *gives the gradient as* ***–k***

Equation 2:
$$t_{1/2} = \frac{\ln(2)}{k}$$

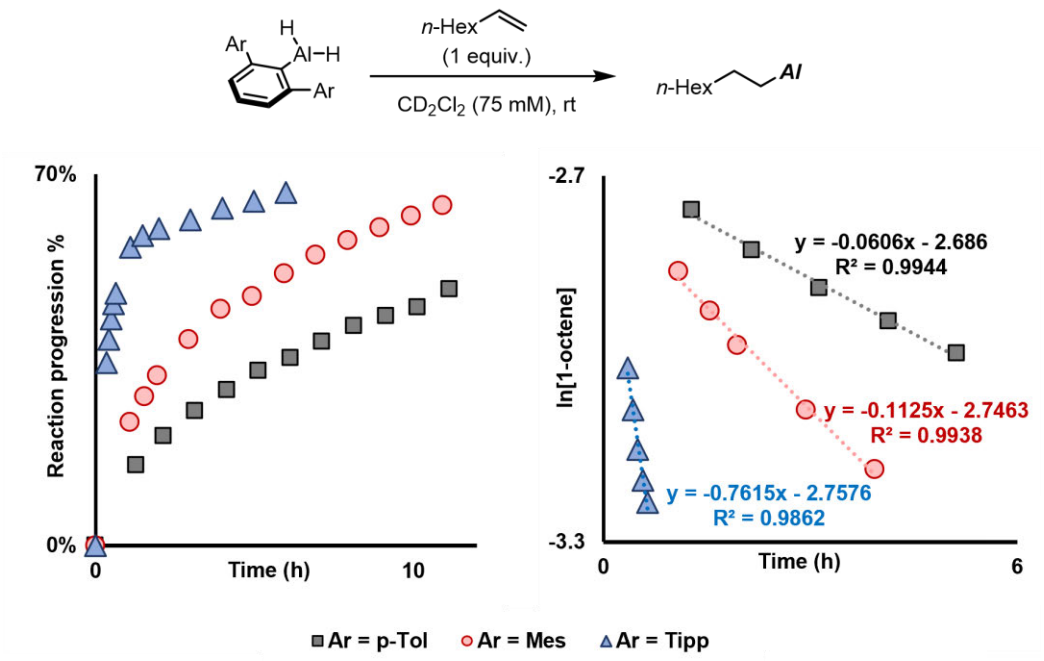

Scheme 2-12: Comparison of alkene hydroalumination reaction rates for different sized alanes. LEFT: reaction progression for each alane; RIGHT: log plot for the concentration of 1-octene against time, used for the calculation of 1st order reaction rates.

The bulkiest primary alane, ^{Tipp}TerAlH$_2$ ($t_{1/2}$ = 0.9 hours), was found to react with 1-octene an order of magnitude faster than ^{Mes}TerAlH$_2$ ($t_{1/2}$ = 6.2 hours) and $^{p\text{-Tol}}$TerAlH$_2$ ($t_{1/2}$ = 11.4 hours) under these conditions. These observations are consistent with Power's results,[64] whereby the rate of alkene hydroalumination is proportional to the steric bulk at aluminium. This holds true despite the diminished solubility of ^{Tipp}TerAlH$_2$ at this concentration (75 mM) in CH_2Cl_2. This poor solubility can explain the significant deceleration of reaction rate after approximately one hour.

At this point, the rate of solubilisation/diffusion of ^{Tipp}TerAlH$_2$ presumably became the limiting factor.

Al(sp^3)–C/B–H exchange – Turnover

Next, the reaction of the resulting alkyl alanes with HBpin was investigated. Our group has previously established that B–C(sp^3)/B–H exchange proceeds only sluggishly at room temperature and is rate determining for boron-catalysed hydroboration protocols.[219,226–228] Indeed, Et_3B does not appreciably react with excess HBpin at room temperature in CH_2Cl_2 over 16 hours (**Scheme 2-13.i**). Thus, it was especially intriguing to determine how Al–C(sp^3)/B–H exchange would compare.

The reaction between ^{Ar}TerAl(octyl)$_2$ (Ar = *p*-Tol, Mes, Tipp; prepared *in situ* from ^{Ar}TerAlH$_2$ and 1-octene (2 equiv.)) with HBpin (5 equiv.) in C_6D_6 at room temperature was monitored by ^{1}H and ^{11}B NMR spectroscopy (**Scheme 2-13.ii**). Despite the steric bulk surrounding aluminium, the reaction proceeded smoothly and rapidly in each case. Within 30 minutes, full consumption of the alkyl alane was observed (as determined by the disappearance of the diagnostic AlC*H*$_2$R resonances by ^{1}H NMR spectroscopy; typically multiplets around δ 0) alongside the formation of octylBpin (δ^{1}H: 0.87; t, *J* = 7.0 Hz, 2H; BC*H*$_2$R). Notably, this was true even for the most sterically demanding alane (^{Tipp}TerAl(octyl)$_2$). Importantly, the Al–C/B–H exchange also appeared to be selective for the alkyl groups over the bulky aryl substituent, as inferred by the lack of Ar*B*pin ^{11}B signal at δ 30-31.[238] This selectivity would be crucial for catalyst regeneration and was attributed to the robustness of the bulky *m*-terphenyl substituent, which presumably raises the kinetic barrier of C(sp^2)–Al/B–H exchange relative to C(sp^3)–Al/B–H exchange.

The observation of selective Al–C/B–H exchange for the alkyl groups in ^{Ar}TerAl(octyl)$_2$ (Ar = *p*-Tol, Mes, Tipp) with HBpin implied the regeneration of ^{Ar}TerAlH$_2$. However, it is important to highlight that the resonances associated with these primary alanes were not detected in these reactions. Instead, intractable ^{1}H NMR spectra were observed, featuring what appears to be multiple different *m*-terphenyl species based on the diagnostic alkyl resonances depicted in **Scheme 2-9**. At this stage, these observations were ascribed to the sensitivity of the Lewis acidic aluminium centre towards other coordinating groups, which in this instance could be the oxygen atoms in RBpin. A comprehensive analysis is provided in **Chapter 3**.

To determine the activation parameters for the Al–C(sp^3)/B–H exchange reaction, attempts were made to construct an Eyring plot by obtaining rate data at different temperatures.[239] In particular, the proposed σ-bond metathesis mechanism should be associated with a strongly negative $\Delta S^{\ddagger}$ value.[69] To facilitate this, ^{Mes}TerAlEt$_2$ and ^{Mes}TerAl(*i*Bu)$_2$ – proxies for ethene and isobutene hydroalumination – were used as convenient sources of dialkyl alane. These can be prepared in one step from the corresponding *m*-terphenyl lithium (^{Mes}TerLi) through the salt metathesis route outlined in **Scheme 2-10.ii**. This contrasts with ^{Mes}Ter(octyl)$_2$, which requires an extra two steps for its preparation.

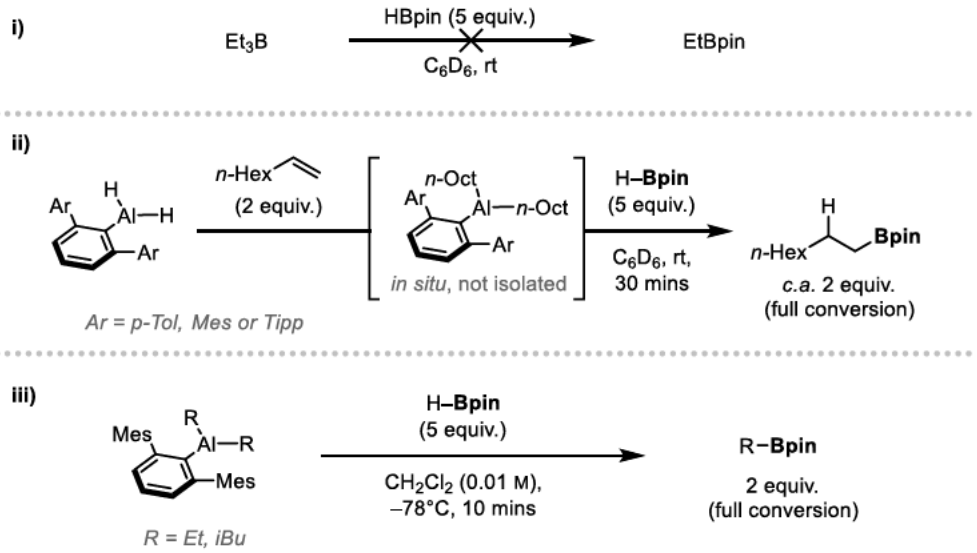

Scheme 2-13. i) Reaction of HBpin (5 equiv.) with Et_3B; ii) single-turnover experiments showing feasibility of hydroalumination/σ-bond metathesis pathway for aluminium-catalysed hydroboration; iii) attempted monitoring of Al-C(sp^3)/B-H exchange at low temperature.

However, these investigations were complicated by the extremely rapid reaction between ^{Mes}TerAlR$_2$ (R = Et or *i*Bu) and HBpin (5 equiv.), which made it impractical to obtain usable data to determine the activation parameters. In CH_2Cl_2, even at very low temperatures (–78 °C) and concentrations (0.1 M), formation of the corresponding alkylBpin product was observed within ten minutes (**Scheme 2-13.iii**). This result is particularly striking when compared with the non-reactivity of Et_3B with HBpin at room temperature, thereby indicating that Al–C(sp^3)/B–H exchange is significantly more favourable than B–C(sp^3)/B–H exchange.

These results highlight the promising future for aluminium catalysts in the realm of enantioselective alkene hydroboration. Given that ^{Mes}TerAl(*i*Bu)$_2$ is the product of isobutene hydroalumination, the results suggest that Al–C(sp^3)/B–H exchange is sufficiently favourable to allow catalytic compatibility with pro-chiral 1,1-disubstituted

alkenes. These substrates are especially challenging for boron-catalysed alkene hydroboration as the corresponding alkyl boranes do not readily react with HBpin, even at elevated temperatures.

To summarise, Al–C(sp^3)/B–H exchange was found to be rapid (–78 °C, minutes), and alkene hydroalumination to be comparably much slower (room temperature, hours). That both steps proceed, regardless of the steric bulk at aluminium, suggests that each *m*-terphenyl alane should be catalytically active, based on the canonical mechanism. Since the bulkiest alane, ^{Tipp}TerAlH$_2$, is fastest for the slow alkene hydroalumination step, it follows that it should also be the fastest performing catalyst for alkene hydroboration with HBpin – if the reaction indeed proceeds by the reported mechanism (**Scheme 2-14**).

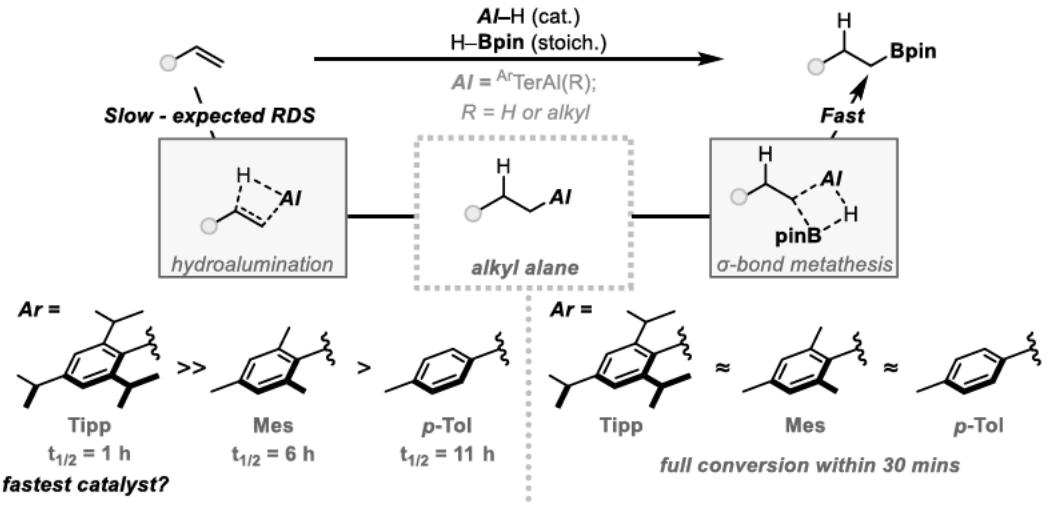

Scheme 2-14: Comparison of hydroalumination rates versus σ-bond metathesis.

2.3.3 Catalytic studies

Evaluating influence of X group (^{Mes}TerAlX$_2$)

Before proceeding with catalytic studies, it was important to avoid the solubility issues that were encountered whilst investigating alkene hydroalumination using the primary alanes (^{Ar}TerAlH$_2$). Given that alkyl alanes (^{Ar}TerAlR$_2$) readily reacted with HBpin, it was envisioned that the more soluble and more conveniently prepared dimethyl alanes (^{Ar}TerAlMe$_2$; one step from ^{Ar}TerLi vs two steps for ^{Ar}TerAlH$_2$) could be used as pre-catalysts. Indeed, each ^{Ar}TerAlMe$_2$ (Ar = *p*-Tol, Mes, Tipp) reacted with excess HBpin (12 equiv.) in CH_2Cl_2 at room temperature to give 2 equiv. MeBpin (**Scheme 2-16**), implying the formation of aluminium hydride, ***Al***–H.

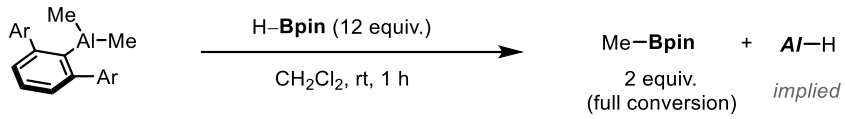

Scheme 2-15. Reaction of *m*-terphenyl-substituted dimethyl alanes with HBpin (12 equiv.).

The impact on catalytic activity of switching to a dimethyl alane (^{Ar}TerAlMe$_2$) pre-catalyst from a primary alane (^{Ar}TerAlH$_2$) was determined. The catalytic activity of different ^{Mes}Ter***Al*** catalysts (***Al*** = AlH$_2$, AlMe$_2$, AlMe$_2$•OEt$_2$; 10 mol%) for the hydroboration of 1-octene with HBpin (12 equiv.) at room temperature in CH_2Cl_2 was compared. The reaction progress was estimated by tracking the formation of octylBpin by ^{1}H NMR spectroscopy (δ 0.73; t, *J* = 7.7 Hz, 2H; BC*H$_2$*R) using the integration of the aromatic *m*-terphenyl resonances as an internal standard (which were assumed to remain constant throughout the reaction).[240] The initial rates were calculated with the integrated rate law for a zero-order reaction (Equation 3) using the first six data points. The corresponding $t_{1/2}$ values were calculated according to Equation 4. It should be noted that these data were intended only for comparison purposes and not to make any conclusions regarding the mechanism.

Equation 3: $$[octylBpin]_t = kt + [octylBpin]_0$$

*Plotting **[octylBpin]** vs **t** gives **k** as the gradient.*

Equation 4 $$t_{1/2} = \frac{[\mathrm{octylBpin}]_\infty}{2k}$$

Where [octylBpin]$_\infty$ = 0.75 M

Similar reaction rates were observed for alkene hydroboration catalysed by ^{Mes}TerAlH$_2$ ($t_{1/2}$ = 4.5 h) or ^{Mes}TerAlMe$_2$ ($t_{1/2}$ = 4.0 h), while the Et$_2$O adduct, ^{Mes}TerAlMe$_2$•OEt$_2$, gave a slightly improved performance ($t_{1/2}$ = 3.2 h) (**Scheme 2-16**). The similar performance between ^{Mes}TerAlH$_2$ and ^{Mes}TerAlMe$_2$ suggested that dimethyl alanes could reasonably be used to analyse the impact of the *m*-terphenyl substituents on catalysis. The effect of Et$_2$O on the reaction will be discussed in **Chapter 3**.

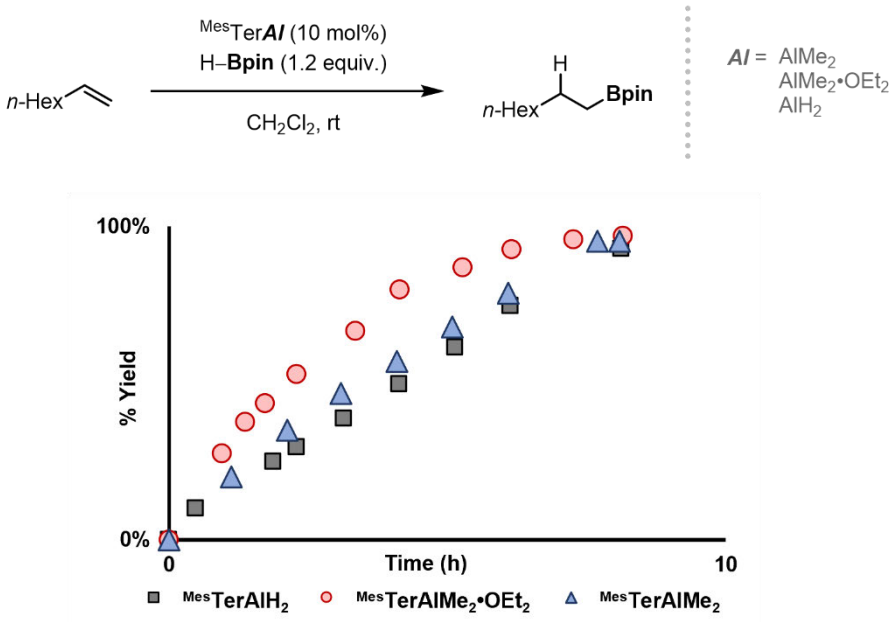

Scheme 2-16. Comparison of rates for alkene hydroboration with HBpin catalysed by different ^{Mes}Terphenyl alanes. Yield of octylBpin presented.

In contrast, it could be argued that using Et_2O adducts for this purpose might not accurately reflect the impact of the *m*-terphenyl substituents on catalysis due to the slightly improved catalyst performance of $^{Mes}TerAlMe_2•OEt_2$ in comparison to $^{Mes}TerAlMe_2$ and $^{Mes}TerAlH_2$. However, using the Et_2O adduct was found to be essential for solubilising the $^{Tipp}Ter\boldsymbol{Al}$ system. When donor-free $^{Tipp}TerAlMe_2$ was used to catalyse the hydroboration of 1-octene with HBpin in CH_2Cl_2 (0.75 M), the precipitation of crystalline $[^{Tipp}TerAl(H)Me]_2$ was observed, which was characterised by X-ray crystallography (see appendix). Clearly, the precipitation of catalyst would impact the catalytic activity observed. To ensure that the influence of the *m*-terphenyl substituent on catalysis could be fairly compared, the most soluble catalyst systems – $^{Ar}TerAlMe_2•OEt_2$ (Ar = *p*-Tol, Mes, Tipp) – were employed.

Evaluating influence of the *m*-terphenyl substituent on catalysis

The performance of the *m*-terphenyl-substituted alanes were evaluated for their catalytic capabilities in alkene hydroboration with HBpin. Using ^{1}H NMR spectroscopy to monitor the reaction progress, 1-octene (1 equiv.) was reacted with HBpin (1.2 equiv.) in the presence of $^{Ar}TerAlMe_2•OEt_2$ (10 mol%) in CH_2Cl_2 at room temperature (**Scheme 2-17**). The reaction progression was estimated analogously to that described for the experiments shown on **Scheme 2-16**, while the reaction rates and $t_{1/2}$ were calculated according to Equation 3 and Equation 4 respectively.

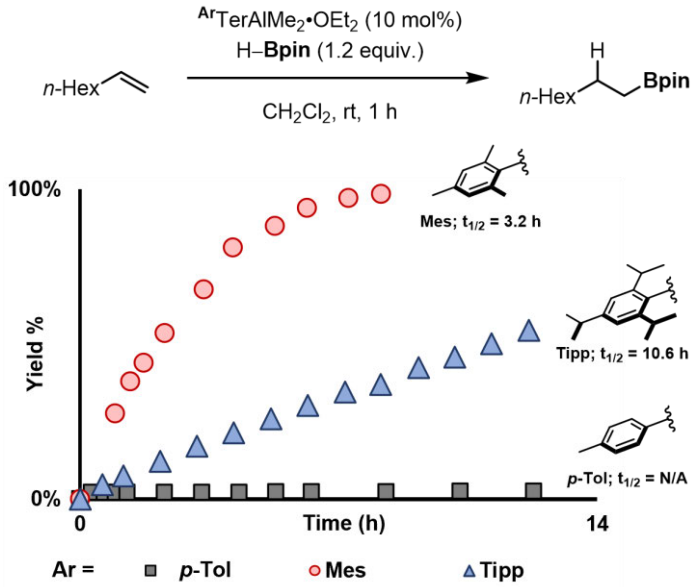

Scheme 2-17. Comparison of rates for alkene hydroboration with HBpin catalysed by *m*-terphenyl alanes of varying degrees of steric bulk.

The obtained results were both unexpected and striking. The mid-sized ^{Mes}TerAlMe$_2$•OEt$_2$ catalyst demonstrated the fastest activity under catalytic conditions ($t_{1/2}$ ~ 3.2 hours), whereas the larger ^{Tipp}TerAlMe$_2$•OEt$_2$ catalyst was significantly slower ($t_{1/2}$ ~ 10.6 hours; k_{rel} = 0.30). Interestingly, the smallest alane, $^{p\text{-Tol}}$TerAlMe$_2$•OEt$_2$ was not catalytically active at all, despite the capability of the corresponding primary alane ($^{p\text{-Tol}}$TerAlH$_2$) to react with alkenes, and for the resulting alkyl alanes ($^{p\text{-Tol}}$TerAlR$_2$; R = Me, octyl) to react with HBpin. These results are remarkable because the observed catalytic activities do not align with the relative rates noted for the ostensibly "slow" hydroalumination step. Although the ^{Tipp}Ter***Al*** system was fastest for alkene hydroboration, it was not the fastest catalyst. The general mechanism of hydroalumination/σ-bond metathesis therefore fails to account for the observations under catalysis – we have labelled this disconnect the "*rate problem*".

The origin of this *rate problem* is convoluted and will be investigated in **Chapter 3.** The rest of the chapter will focus on the optimisation and scope of the reaction in order to assess any limitations and fulfil the potential of this protocol.

Optimisation

Using ^{Mes}TerAlMe$_2$ (10 mol%) and 1-octene (1 equiv.) with HBpin (2 equiv.) as model reagents, optimisation studies began by screening a range of solvents (**Table 2-1**). Over 16 hours, the reaction performed best in CH_2Cl_2 (>95% **Table 2-1**, entry 1), but catalytic activity was also observed in the other non-coordinating solvents used, toluene (73%; **Table 2-1,** entry 3) and hexane (39%; **Table 2-1,** entry 2). Catalysis did not proceed well in coordinating solvents: limited activity was detected in Et_2O (14%; **Table 2-1**, entry 4), while catalysis was completely diminished in THF (<5%; **Table 2-1**, entry 5). The results point to the importance of an available *p*-orbital for catalytic activity.

Table 2-1. Solvent screening

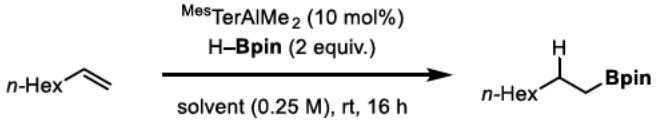

Entry	Solvent	Conc. (M)	Yield (%)
1	DCM	0.25	>95
2	hexane	0.25	39
3	toluene	0.25	73
4	Et_2O	0.25	14
5	THF	0.25	3

Following this, a concentration screen was performed in CH_2Cl_2 (**Table 2-2**, entries 1-5), using a shorter reaction time of 4 hours. A direct correlation between the reaction concentration and the yield of octylBpin was noted, with the reaction performing best under neat conditions (neat: >95% yield; 1 M: 75%; 0.25 M: 46%).

The stoichiometries of catalyst and HBpin were also assessed. Good catalytic activity could be achieved down to a catalyst loading of 5 mol%, but at the expense of a slower reaction rate (85%; **Table 2-2**, entry 6). Thus, a catalyst loading of 10 mol% was maintained. The number of equivalents of HBpin could be lowered to 1.2 equiv. without affecting yield (>95%; **Table 2-2**, entry 7).

Table 2-2. Optimisation of conditions

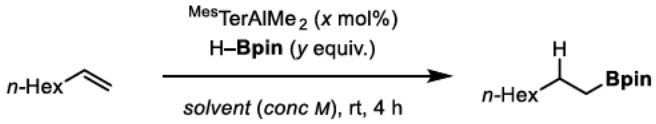

Entry	Solvent	Conc. (M)	Cat. Loading (mol%)	Equiv. HBpin	Yield (%)
1	DCM	2.5	10	2	>95
2	DCM	1	10	2	78
3	DCM	0.5	10	2	67
4	DCM	0.25	10	2	46
5	neat	~3	10	2	>95
6	neat	~3	5	2	85
7	neat	~3	10	1.2	>95

The optimised conditions established for the ^{Mes}TerAlMe$_2$ catalyst were then applied to other catalysts (**Table 2-3**). The relative reactivity of each different sized catalyst (after 2 hours: $^{p\text{-Tol}}$TerAlMe$_2$ = 12%; ^{Mes}TerAlMe$_2$ = 74%; ^{Tipp}TerAlMe$_2$ = 41%) mirrored the trends observed under NMR conditions. It was noted that the primary alane, ^{Mes}TerAlH$_2$, appeared to react more slowly (62%; **Table 2-3,** entry 4) than ^{Mes}TerAlMe$_2$, but this could possibly be attributed to solubility issues. In practical terms, ^{Mes}TerAlH$_2$ was comparably effective to ^{Mes}TerAlMe$_2$. An attempt was made at developing a bench-stable system using [^{Mes}TerAlH$_3$]Li•OEt$_2$ as a more stable pre-catalyst, with Me$_3$SiCl as an "activator" to generate the primary alane catalyst (^{Mes}TerAlH$_2$) *in situ*. However, this approach resulted in significantly lower yields (20%; **Table 2-3,** entry 5).

Table 2-3. Catalyst screening

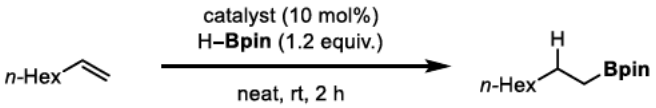

Entry	Catalyst	Yield (%)
1	^{Mes}TerAlMe$_2$	74
2	$^{p\text{-Tol}}$TerAlMe$_2$	12
3	^{Tipp}TerAlMe$_2$	41
4	^{Mes}TerAlH$_2$	62
5	[^{Mes}TerAlH$_3$]Li•OEt$_2$ + Me$_3$SiCl (1:1)	20

Scope

To understand the limitations of the *m*-terphenyl alane-catalysed alkene hydroboration, a substrate scope was performed, initially of monosubstituted alkenes (**Table 2-4**). Although the optimised conditions led to the full conversion of 1-octene within 4 hours, it was later discovered that styrenes reacted more slowly. Thus, to enable a more general procedure for each alkene, substrates were reacted for 18 hours. Crucially, the linear boronic ester product was selectively obtained in all cases.

Aliphatic alkenes substituted with 1°, 2° and 3° alkyl groups – 1-octene (>95%; **2-1a**), cyclohexyl ethylene (>95%; **2-1b**) and *t*Bu-ethylene (>95%; **2-1c**) – all proceeded to full conversion. The reaction also worked well for 5-bromopentene (>95%; **2-1d**), despite the potential for cyclisation from the polarised Al–C bond in the expected alkyl alane intermediate. Allyl trimethylsilane also gave excellent yields (>95%; **2-1e**), however allyl Bpin did not (32%; **2-1f**). This can possibly be explained by the close proximity of the oxygen atoms (in Bpin) to aluminium in the corresponding alkyl alane intermediate, which could interfere with catalytic processes.

Styrene reacted smoothly under the reaction conditions to give the corresponding pinacolboronic ester (**2-1i**) in a 72% yield. Generally, electron-rich styrenes gave better yields: 4-Me-styrene (86%; **2-1j**), 4-*t*Bu-styrene (91%; **2-1m**) and ibuprofen derivative 4-*i*Bu-styrene (68%; **2-1n**) all proceeded efficiently. Mono *ortho*-substitution with a methyl group was well-tolerated (**2-1k**; >95%), but substitution at both *ortho*-positions completely shut down catalysis (**2-1l**). Although this was not further investigated, this could be explained by the extra steric bulk preventing either alkene hydroalumination or the approach of HBpin to the reactive Al–C(sp^3) position.

Para-substitution of styrene with Lewis basic groups did not lead to catalyst inhibition as observed in **Table 2-1**, as 4-dimethylamino-styrene (75%; **2-1p**) and 4-methoxy-styrene (88%; **2-1o**) gave good to excellent yields. However, *ortho*-substitution with methoxy (**2-2f; Scheme 2-18**) did not yield any product, even though *ortho*-substitution was permitted with methyl groups. This further alluded to the inhibition of catalysis when Lewis basic functionality is located in close proximity to the aluminium centre in the alkyl alane intermediate.

Table 2-4. Substrate scope of monosubstituted alkenes

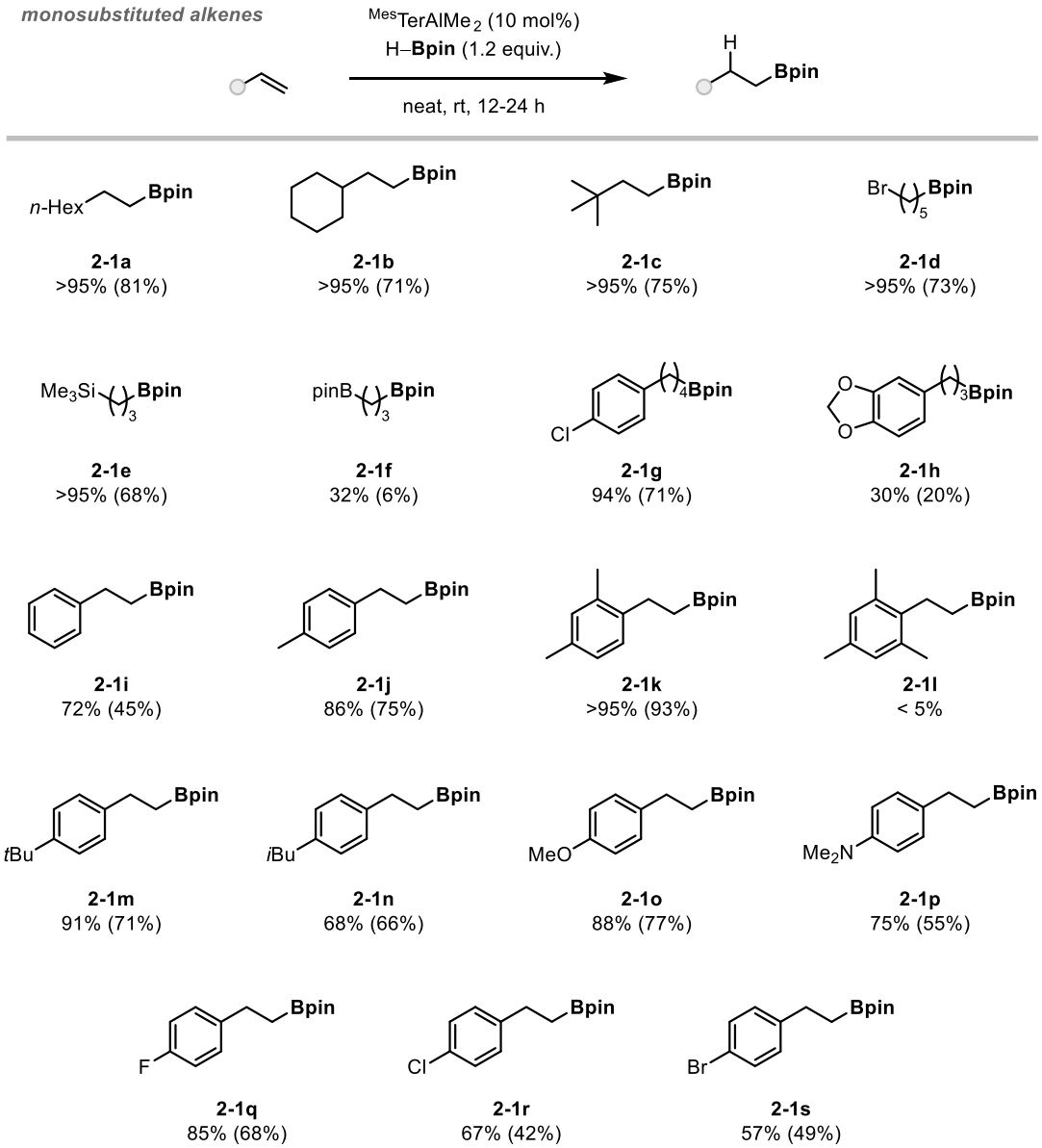

NMR yields provided (isolated yields in parentheses).

Electron deficient alkenes – styrenes containing halides in the *para*-position – gave good to moderate yields of the corresponding boronic esters (4-F: 85%, **2-1q**; 4-Cl: 67%, **2-1r**; 4-Br: 57%, **2-1s**) and were well-tolerated by the aluminium catalyst. Notably, if the alkene is situated in a distal location to the electron withdrawing group (**2-1g**), better yields are obtained (94%). This suggests that electronics of the alkene, rather than the substituents themselves, play a crucial role in determining how well the reaction proceeds.

Substrates containing reducible functional groups were not well-tolerated under the reaction conditions (**Scheme 2-18.i**). Ester **2-2a**, amide **2-2b**, aldehyde **2-2c**, sulphonamide **2-2d** and tosyl-protected alcohol **2-2e** all led to catalyst decomposition – unsurprising given the hydridic nature of the catalyst. The methylenedioxy-functionality present in safrole was, however, somewhat permitted (30%; **2-1h, Table 2-4**).

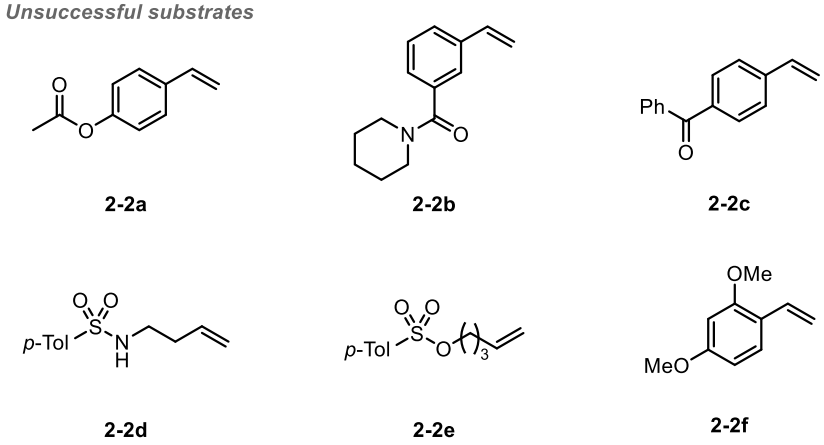

Scheme 2-18. Unsuccessful monosubstituted substrates.

The capability of ^{Mes}TerAl(*i*Bu)$_2$ to react smoothly with HBpin to yield (*i*Bu)Bpin gave promise for expanding the scope to the more challenging 1,1-disubstituted alkenes (**Table 2-5**). Indeed, 2-methylpentene gave the respective alkyl boronic ester in a good yield (63%; **2-1t**) but required longer reaction times (48 h) than the monosubstituted alkenes (18 h; **Table 2-4**). Since Al–C(sp^3)/B–H exchange for ^{Mes}TerAl(*i*Bu)$_2$ with HBpin was rapid, a slower formation of the alkyl alane, presumably by alkene hydroalumination, can possibly explain the longer times required. Thus, all 1,1-disubstituted alkenes were reacted for 48 hours. Importantly, terpenes were well-tolerated, even for substrates with highly substituted alkyl fragments: limonene (68%; **2-1u**), β-pinene (52%; **2-1v**) and (+)-valencene (68%; **2-1w**) all gave good yields.

Table 2-5. Substrate scope of 1,1-disubstituted alkenes

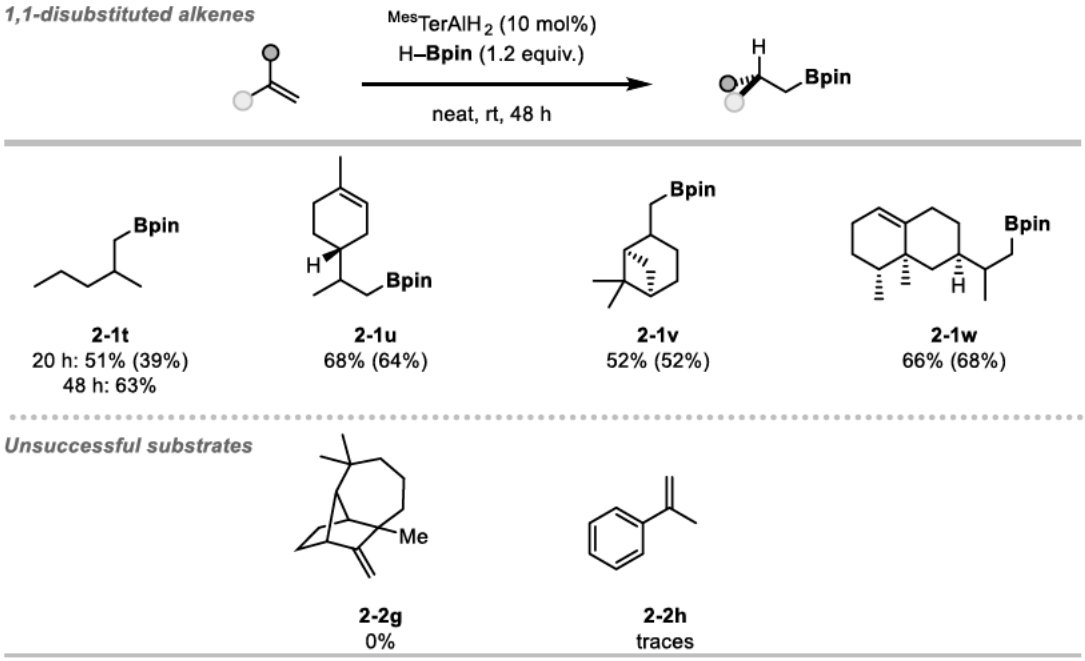

NMR yields provided (isolated yields in parentheses).

Since these alkenes are pro-chiral, and all proceeded at room temperature, there is potential for this protocol to be adapted to give enantioenriched boronic esters. Longifolene (**2-2g**), with two tertiary carbons attached to the alkene, did not react under the reaction conditions as this was presumably too bulky. No reaction was also observed for α-methyl-styrene (**2-2h**). The similar steric demands of limonene compared to α-methyl-styrene suggests an electronic argument for explaining this lack of reactivity.

2.4 Conclusions and future outlook

Bulky *m*-terphenyl alanes are capable of catalysing alkene hydroboration with HBpin at room temperature, for both monosubstituted and 1,1-disubstituted alkenes. The rates for the slow alkene hydroalumination step are proportional to the steric bulk at aluminium, but the relative rates under catalysis do not follow this. Thus, the generally agreed mechanism described for Al-catalysed hydroboration – consisting of alkene hydroalumination followed by Al–C(sp^3)/B–H exchange with HBpin – cannot explain the relative rates observed for these catalysts (**Scheme 2-19**). This disconnect has been labelled as the *rate problem*. The mechanism for this reaction is investigated in **Chapter 3.**

However, it was shown that Al–C(sp^3)/B–H exchange is extremely favourable and is key to the formation of boronic esters at room temperature; B–C(sp^3)/B–H exchange requires higher temperatures. Thus, aluminium has the potential to enable catalysis beyond what is capable for boron. In **Chapter 4**, this favourable exchange is exploited for the synthesis of alkyl diazaborinines from alkenes with HBdan – a borane with extremely diminished Lewis acidity.

In the future, the favourable Al–C(sp^3)/B–H exchange suggests that alane catalysts have potential in asymmetric catalysis. Other substrates should also be investigated, such as alkynes or other reducible functional groups. Moreover, Al–C(sp^3)/Si–H exchange should be explored, as this could open up the possibility for aluminium-catalysed hydrosilylation procedures.

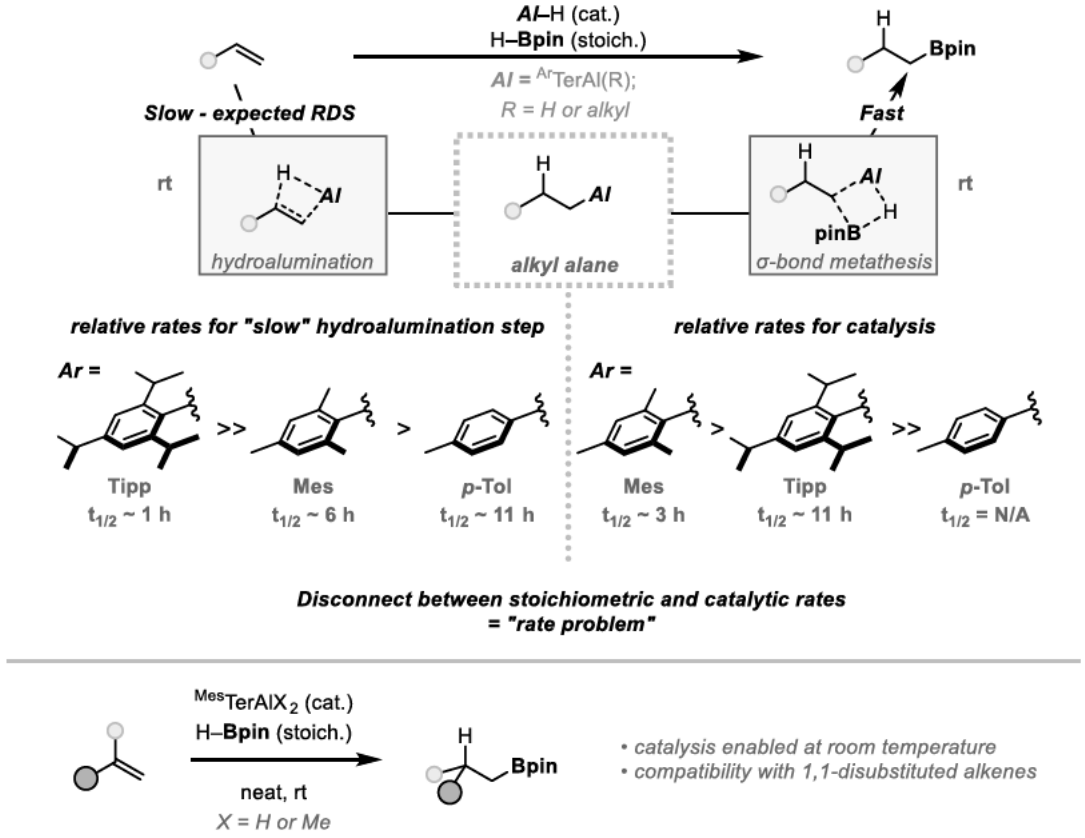

Scheme 2-19. Summary of findings from Chapter 2.

Chapter 3:

Aluminium-catalysed alkene hydroboration with HBpin: Mechanistic insight

3.1 Introduction

It has been widely proposed that aluminium-catalysed alkene hydroboration with HBpin proceeds in two steps: 1. Alkene hydroalumination; 2. Al–C(sp^3)/B–H σ-bond metathesis.[81,179–181] The *rate problem* (see **Chapter 2**) describes the disconnect between the observed rates for these processes under stoichiometric conditions with the rates observed under catalysis (for *m*-terphenyl alanes). Importantly, it indicates the possibility that the reported mechanism cannot be generally applied across all aluminium catalysts for this transformation.

An alternative explanation is required to reveal the reasons for this *rate problem*. There are some hints that the proposed two-step mechanism is an over-simplification; several reports have implied or shown the existence of a catalyst•HBpin adduct in main group-catalysed hydroboration with HBpin.[185,202,241–243] In particular, Bakewell revealed that aluminium amidinates do not react with alkynes in the absence of HBpin, showing that $LAlH_2$•HBpin adduct formation is important to mediate alkyne hydroboration with HBpin.[185] In the case of a less stable aluminium amidinate catalyst, partial decomposition of HBpin to BH_3 led to the reaction being mediated by hidden boron catalysis.[188,189]

Hidden boron catalysis can also explain the catalytic behaviour of many other main group-catalysed alkene hydroboration protocols with HBpin.[188,189] Often, these protocols lack control experiments for hidden boron catalysis which can result in misleading mechanistic proposals. Although these procedures often use inexpensive and convenient pre-catalyst sources (such as NaOH[244] or K_2CO_3[245]), the catalytic capabilities are limited to that of BH_3. Sometimes BH_3 is formed under catalysis but cannot fully explain the observed reactivity/rates, such as in the case of $LiAlH_4$.[81] In these cases, it would be useful to identify the role of the co-catalyst in the reaction to develop better procedures. In other instances, background BH_3 formation from off-cycle processes can cause deleterious effects, leading to issues of chemo-, regio- and stereoselectivity.[189,199] Understanding and controlling background BH_3 formation is important, and has led to improved selectivity in aluminium-catalysed C–H borylation of alkynes.[202] In addition, hidden boron catalysis has been used in tandem with zinc catalysis to mediate the triborylation of alkynes with HBpin.[246] Thus, enhanced mechanistic knowledge ultimately leads to improved catalytic protocols.

3.2 Aims

We aimed to investigate the mechanism for the *m*-terphenyl alane-catalysed alkene hydroboration with HBpin (**Scheme 3-1**) and solve the *rate problem* on a molecular level. This *rate problem*, alongside findings reported in the literature, prompted several key questions about our system:

- Does RBpin play an additional role in the catalytic cycle?
- Is BH_3 generated under catalysis, and does it contribute to the mechanism?
- What is the role of aluminium?
- How do sterics influence the mechanistic processes?

By answering these questions, we hoped to understand the root causes of the *rate problem* and gain useful insight to improve aluminium-catalysed protocols.

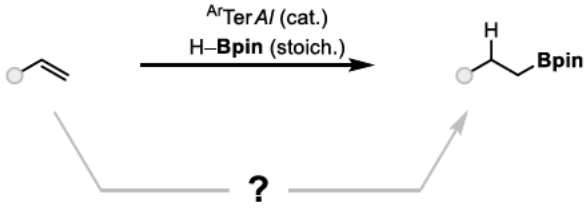

Scheme 3-1. The mechanism for *m*-terphenyl alane-catalysed alkene hydroboration with HBpin will be investigated.

3.3 Results and discussion

3.3.1 Does RBpin play an additional role?

To explain the *rate problem*, it was first hypothesised that RBpin (R = H, alkyl) could perturb the monomer/dimer equilibrium of the primary alanes (^{Ar}TerAlH$_2$), thereby impacting the relative rates of alkene hydroalumination for each catalyst. This hypothesis was based on the findings that LAlH$_2$•HBpin adducts are involved in aluminium amidinate-catalysed alkyne hydroboration,[185] and of the observation that [^{Ar}TerAlH$_2$]$_2$ was not generated in solution when ^{Ar}TerAlR$_2$ reacted with excess HBpin. This was despite full conversion of the dialkyl alane to RBpin by Al–H/B–C(sp^3) exchange (see **Chapter 2**, **section 2.3.2**).

To test this hypothesis, the reaction of ^{Ar}TerAlH$_2$ (Ar = Mes and Tipp) and 1-octene (1 equiv.; rt, CH_2Cl_2 (0.1 M)) in the presence and absence of MeBpin (1 equiv.) was monitored by ^{1}H NMR spectroscopy (**Scheme 3-2**). The reaction progress was tracked by monitoring the consumption of 1-octene, using the aromatic protons on the *m*-terphenyl backbone as an internal standard. The initial rates were calculated from the first eleven minutes of the reaction using **Equation 3**. The half-life was approximated from these rates by using the zero-order integrated rate law (**Equation** 4) to provide a useful comparison between reactions. MeBpin was chosen instead of HBpin to avoid turnover. A low concentration (0.1 M) was also used to avoid the insolubility issues previously encountered (see **Chapter 2**, **section 2.3.2**), where higher concentrations were used to reflect catalytic conditions.

The lower concentration did not impact the relative rate of alkene hydroalumination; in the absence of MeBpin, 1-octene reacted with the smaller alane, ^{Mes}TerAlH$_2$ ($t_{1/2}$ = 3.8 h; k_{rel} = 1), much slower than the larger alane, ^{Tipp}TerAlH$_2$ ($t_{1/2}$ = 0.8 h; k_{rel} = 5.1). In the presence of MeBpin, the rate of alkene consumption was enhanced almost ten-fold for ^{Mes}TerAlH$_2$ ($t_{1/2}$ = 0.5 h; k_{rel} = 8.9); in contrast, no rate-enhancement was observed for ^{Tipp}TerAlH$_2$ ($t_{1/2}$ = 0.8 h; k_{rel} = 5.1). Notably, the presence of MeBpin rendered alkene hydroalumination much faster for ^{Mes}TerAlH$_2$ than for ^{Tipp}TerAlH$_2$, mirroring the relative order of reactivity observed under catalysis. These findings represented the first observations where an external reagent affected reaction rates differently depending on the structure of the aluminium catalyst.

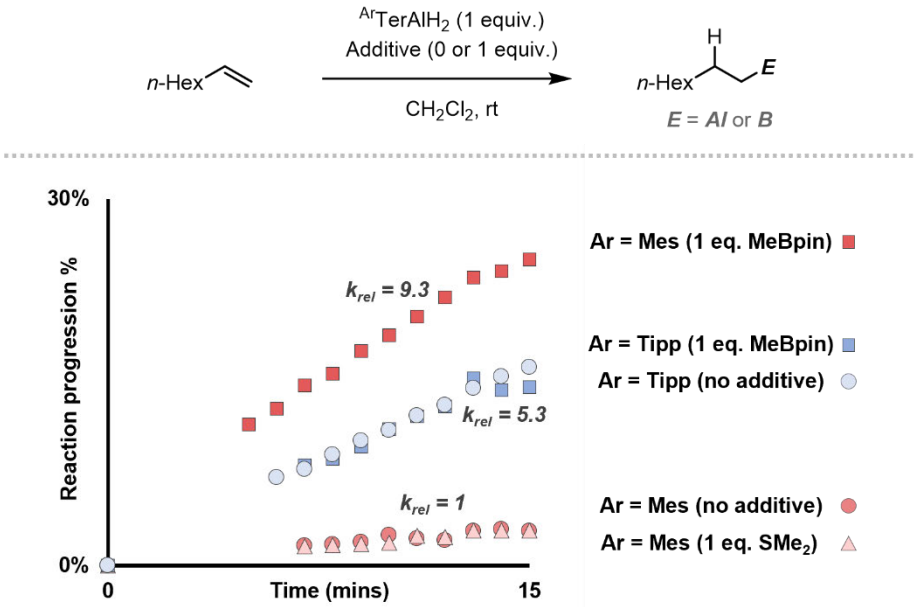

Scheme 3-2. Comparing the initial reactivity of $^{Ar}TerAlH_2$ (Ar = Mes or Tipp) with 1-octene in the presence or absence of MeBpin.

To assess whether this rate-enhancement with MeBpin can be explained by a Lewis base effect, the rate of 1-octene hydroalumination with $^{Mes}TerAlH_2$ was monitored in the presence of SMe_2 (1 equiv.). However, the rate of 1-octene consumption in the presence of SMe_2 was unchanged in comparison to without SMe_2, thereby ruling out this hypothesis.

To gain insight into an alternative role for MeBpin, the ^1H NMR spectra of $^{Mes}TerAlH_2$ and $^{Tipp}TerAlH_2$ in the presence of MeBpin (1 equiv.) were compared (CH_2Cl_2, room temperature). Little interaction was observed between $^{Tipp}TerAlH_2$ and MeBpin within 10 minutes (**Scheme 3-3.i**). In contrast, new resonances were observed in the reaction containing $^{Mes}TerAlH_2$, indicating the formation of several new species. These observations are consistent with a change in rate for alkene consumption in the presence of MeBpin for $^{Mes}TerAlH_2$ but not for $^{Tipp}TerAlH_2$. Understanding the new species generated may explain the rate-enhancement effect.

It was noted that a set of resonances that appeared in the reaction between $^{Mes}TerAlH_2$ and MeBpin – assumed to arise from a single common species – were also formed when MeBpin was replaced with other RBpin compounds (R = octyl, *t*$BuCH_2CH_2$- and H; (**Scheme 3-3.ii**)). Bakewell reported the formation of an aluminium pinacolate species when aluminium amidinates were reacted with HBpin,[185] and it was suspected that a similar species may have been formed in this example. To test this idea, $^{Mes}TerAlH_2$ was reacted with pinacol in C_6D_6 at room temperature and the reaction indeed gave resonances that matched those observed

in the presence of RBpin (**Scheme 3-3.iii**). Specifically, each of these reactions resulted in singlets at δ 2.31 (12H; *p*-Mes-CH_3), δ 1.85 (24H, *o*-Mes-CH_3) and δ 0.40 (12H, pinacolate-C$\underline{H_3}$). These resonances were ascribed to the formation of a 2:1 *m*-terphenyl alane-pinacolate complex. However, as this species was only formed in small quantities, it could not be isolated or identified. This unknown product will hitherto be referred to as ***Al*–pin.** This species would be distinct in structure to the 1:1 aluminium pinacolate complex observed by Bakewell.[185] The analogous 1:1 *m*-terphenyl alane-pinacolate complex, [^{Mes}TerAl(pin)]$_2$, was obtained as the major product from the reaction between ^{Mes}TerAlH_2 and pinacol, and was characterised by XRD. However, the ^{1}H resonances attributed to this product were not observed when RBpin was used. Although ***Al*–pin** appears to lack any catalytically relevant features, it may play an important non-innocent role under catalysis (see **section 3.3.9**).

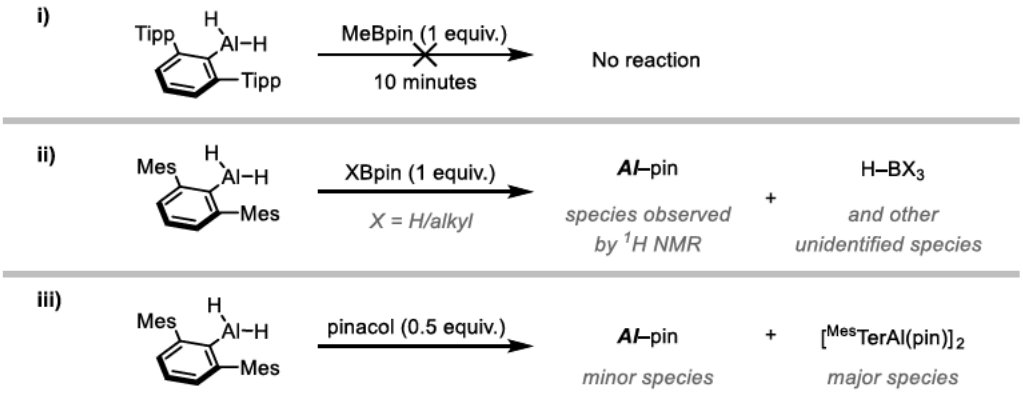

Scheme 3-3. i) The reaction of ^{Tipp}TerAlH_2 with MeBpin (1 equiv.); ii) The reaction of ^{Mes}TerAlH_2 with XBpin (X = H/alkyl/aryl; 1 equiv.); iii) The reaction of ^{Mes}TerAlH_2 with pinacol (0.5 equiv.).

The transfer of pinacol from boron to aluminium implies the transfer of hydrides from aluminium to boron. Indeed, ^{1}H-^{11}B HMQC revealed the formation of several 4-coordinate H–BX_3 species (see **section 7.4.2**). The presence of these B–H species therefore might explain this observed rate-enhancement for stoichiometric alkene hydroalumination and thus for catalytic hydroboration with ^{Mes}TerAlH_2. Incidentally, Yamamoto revealed that organoboranes can catalyse alkene hydroalumination, although this mechanism has never been identified.[114]

3.3.2 Is BH_3 involved?

Given that B–H species were formed when ^{Ar}TerAlH$_2$ reacted with RBpin, it was essential to probe the formation of BH_3 under catalytic conditions and to exclude hidden boron catalysis. The formation of BH_3 for each ^{Ar}TerAlH$_2$ catalyst was quantified using the TMEDA (*N,N,N′,N′*-tetramethylethylenediamine) quenching procedure as described by Bage *et al.*[188] This method conveniently quantifies BH_3 formation under reaction conditions by generating an air- and moisture-stable TMEDA•BH_3 adduct, which is readily characterised by its distinctive ^{11}B signal (δ –10.6, q, $^1J_{B\text{-}H}$ = 98.4 Hz). Thus, ^{Ar}TerAlH$_2$ (Ar = *p*-Tol, Mes, Tipp) was reacted neat with HBpin (12 equiv.) at room temperature for 1 hour in the absence of alkene (to avoid BH_3 consumption) and the reaction was quenched with TMEDA (20 equiv.; **Scheme 3-4.i**). It was found that the largest primary alane, ^{Tipp}TerAlH$_2$, generated significantly lower quantities of BH_3 (1.6 mol%) in comparison to ^{Mes}TerAlH$_2$ (8.3 mol%) and $^{p\text{-}Tol}$TerAlH$_2$ (9.0 mol%). Apparently, the size of the primary alane correlated with the amount of BH_3 generated under reaction conditions. This suggested that the steric bulk in ^{Tipp}TerAlH$_2$ can largely prevent the decomposition of HBpin.

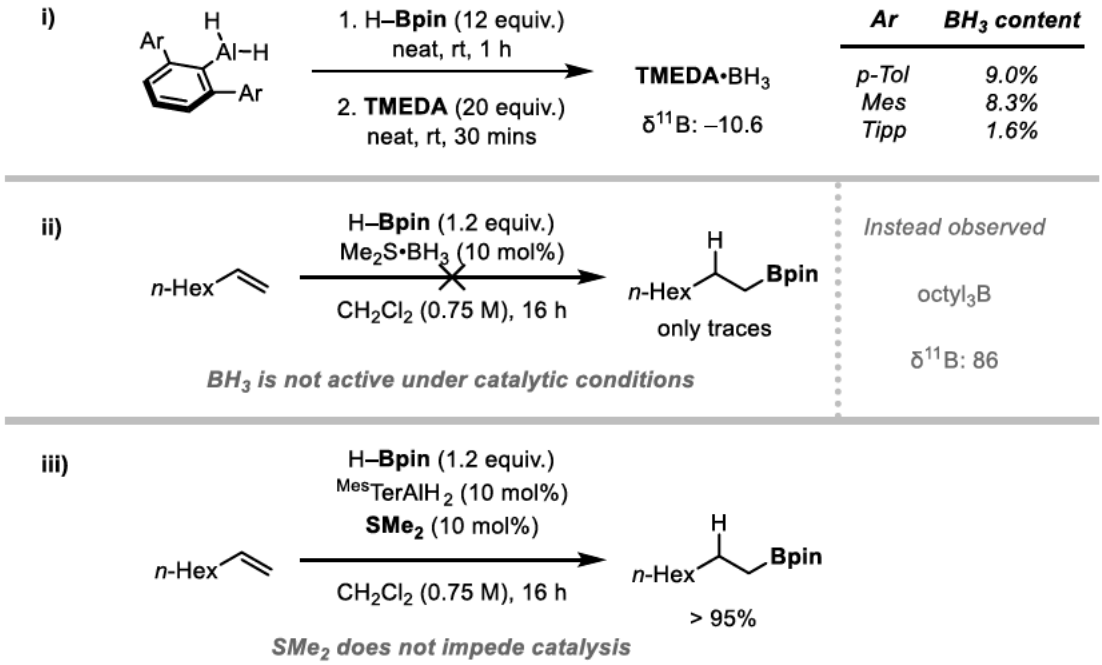

Scheme 3-4. i) TMEDA quenching reactions quantify BH_3 formation under catalysis; ii) Me_2S•BH_3 does not catalyse alkene hydroboration with HBpin at room temperature; iii) The presence of SMe_2 does not shut down catalysis in the ^{Mes}Ter*Al* system.

The formation of BH_3 cannot itself explain the catalytic activity of *m*-terphenyl alanes – the $^{p\text{-}Tol}$Ter*Al* system was catalytically inactive despite significant quantities of BH_3 being formed when $^{p\text{-}Tol}$TerAlH$_2$ reacted with HBpin. As further evidence of the notion that BH_3 alone is not the active catalyst, Me_2S•BH_3 did not catalyse alkene

hydroboration with HBpin under the same conditions (CH_2Cl_2, rt; **Scheme 3-4.ii**). This observation could not be attributed to catalyst inhibition by SMe_2, as SMe_2 did not inhibit catalysis for $^{Mes}TerAlH_2$ (**Scheme 3-4.iii**). The lack of catalytic activity for BH_3 can be explained by unfavourable B–C(sp^3)/B–H exchange under the conditions used;[219] Et_3B did not react with HBpin at room temperature (**Scheme 3-5.a**).

Despite evidence that BH_3 alone does not catalyse alkene hydroboration under these conditions, this does not fully preclude a role for BH_3 under catalysis. It is well established that BH_3, and other hydridoboranes, readily engage in alkene hydroboration under mild conditions to make alkyl boranes.[208,209] It follows that alkyl boranes should also form in the $^{Mes}TerAl$ and $^{p\text{-}Tol}TerAl$ systems from the BH_3 species generated by HBpin decomposition. The formation of hydridoboranes might therefore explain the enhanced rate of alkene consumption for $^{Mes}TerAlH_2$ in the presence of MeBpin.

With this in mind, it was hypothesised that hidden boranes could mediate alkene hydroelementation in the catalytic cycle. If alkyl groups could transfer from boron to aluminium, this would allow alkyl alanes to be formed by circumventing a slow hydroalumination step. Given that Al–C(sp^3)/B–H exchange of $^{Mes}TerAlR_2$ with HBpin was found to be rapid (see **Chapter 2, section 2.3.2**), aluminium could play a key role in the turnover step to generate the boronic ester products (RBpin). To test this, Et_3B was reacted with HBpin (5 equiv.) in the presence of $^{Mes}TerAlH_2$ (1 equiv.; CH_2Cl_2, rt). This time, the smooth formation of EtBpin was observed (**Scheme 3-5.b**), contrasting the lack of reactivity of Et_3B with HBpin in the absence of $^{Mes}TerAlH_2$ (**Scheme 3-5.a**). In other words, aluminium has mediated the exchange of Et_3B with HBpin.

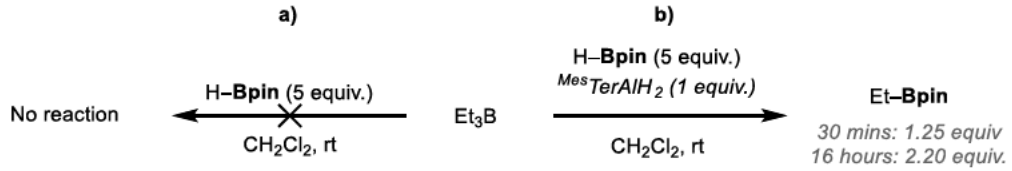

Scheme 3-5. a) Reaction of Et_3B with HBpin in the absence of $^{Mes}TerAlH_2$; b) reaction of Et_3B with HBpin in the presence of $^{Mes}TerAlH_2$.

Thus, it appears that both boron and aluminium species may play a key role in the catalytic cycle. The divergent reactivity of each *m*-terphenyl alane under catalytic conditions suggests that sterics impact the formation and reactivity of these species, leading to changes in mechanism.

3.3.3 How do sterics affect the species involved in catalysis?

To better understand how steric bulk at aluminium influences the formation of different boron-containing species under catalysis, catalytic reactions were monitored by ^{11}B NMR spectroscopy. Each ^{Ar}TerAlMe$_2$ (Ar = *p*-Tol, Mes, Tipp) catalyst was first reacted with HBpin (12 equiv.) in the absence of alkene (**Scheme 3-6**; CH_2Cl_2, rt). In each case, MeBpin (*ca.* 2 equiv.) was formed, alongside $B(OR)_3$ species (*ca.* δ 20 - 22), which arose from the decomposition of HBpin. In the case of the ^{Mes}Ter*Al* and $^{p\text{-Tol}}$Ter*Al* systems, an ^{11}B signal was also observed at *ca.* δ –35 (unresolved pentet), indicating the formation of a borohydride (BH_4) species. In contrast, the ^{Tipp}Ter*Al* system resulted in the formation of a species at δ –9, comparable to that observed for the LAlH$_2$•HBpin adduct in Bakewell's aluminium amidinate system.[185] As both the ^{Mes}Ter*Al* and $^{p\text{-Tol}}$Ter*Al* systems generated BH_3 under catalytic conditions, the species observed at *ca.* δ –35 was thought to arise from the formation of a BH_3 adduct of an aluminium hydride; *i.e.* an aluminium tetrahydroborate complex.[247–250]

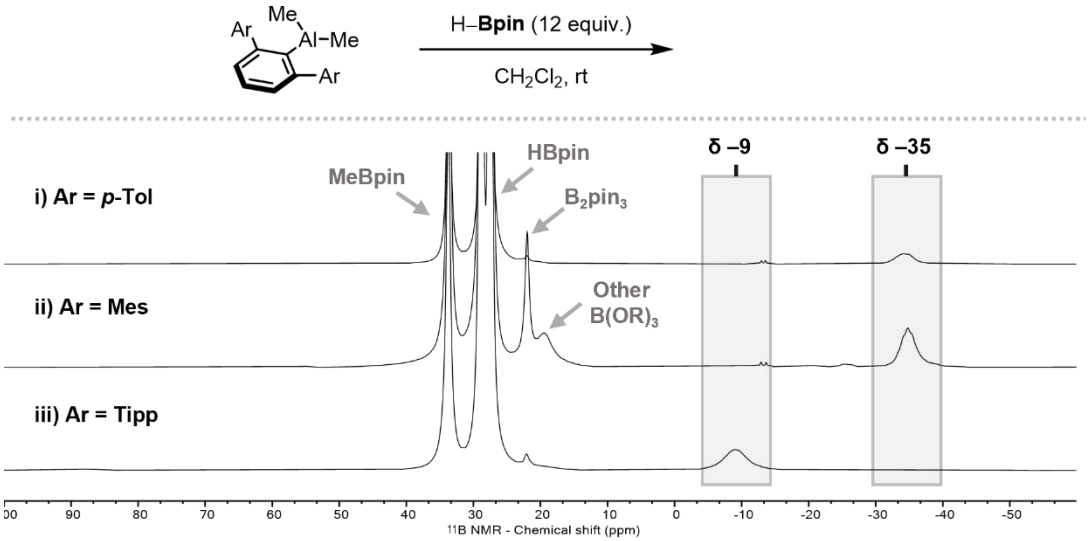

Scheme 3-6. Stacked ^{11}B NMR spectra (CH_2Cl_2) for the reaction of ^{Ar}TerAlMe$_2$ with HBpin (12 equiv.). **i**) Ar = *p*-Tol; **ii**) Ar = Mes; **iii**) Ar = Tipp.

The independent synthesis of the ^{Mes}TerAl(BH$_4$)$_2$ complex, **3-Mes-1**, by the reaction of ^{Mes}TerAlH$_2$ with Me$_2$S•BH$_3$ (2 equiv.) in CH_2Cl_2, was consistent with this idea (**Scheme 3-7.i**), with **3-Mes-1** displaying the same ^{11}B resonance at δ –34.8 (p, $^1J_{B\text{-}H}$ = 86 Hz) as observed in catalysis. From this synthetic route, **3-Mes-1** was isolated in a 71% yield and was fully characterised. Several tetrahydroborate complexes of aluminium are known,[247–253] although none have yet been implicated in aluminium-catalysed hydroboration with HBpin.

Crystals suitable for X-ray diffraction were obtained by the slow evaporation of a pentane solution containing **3-Mes-1**. For the tetrahydroborate ligand, the H-atoms were located on the Fourier difference map and their positions refined using two separate SADI (same distance) restraints for the B–H bond distances of the two bridging hydrides and the two remaining hydrides. Crystallographic analysis revealed the formation of a 5-coordinate aluminium centre featuring coordination to two κ^2-$[BH_4]^-$ substituents, presumably *via* 3c-2e bonding (**Scheme 3-7.ii**). Geometrically, **3-Mes-1** is a basally-distorted square pyramid (τ_5 = 0.029) at aluminium and tetrahedral at boron. The $AlCB_2$ framework itself is trigonal-planar, with a C–Al–B bond angle of 124.50(4)° and a B–Al–B bond angle of 111.01(8)°. The Al•••B distance is 2.1772(13) Å, which is just slightly longer than the sum of the covalent radii (1.21(4) Å + 0.84(3) Å = 2.05(7) Å)[254] and lies in a similar range to other aluminium tetrahydroborate complexes.[247–249,253,255] The different hydride environments are apparent by IR spectroscopy, with bands at 2534 cm^{-1} and 2465 cm^{-1} representing the terminal B–H stretches, and bands at 2026 cm^{-1} and 1447 cm^{-1} characteristic for Al–H–B stretching modes.[256] Conversely, ^{1}H NMR spectroscopy displayed magnetically equivalent hydrides, with a broad quartet observed between δ 0.60 and –0.33 as a result of coupling to the spin-$^3/_2$ ^{11}B nucleus. This degeneracy can be attributed to the rapid exchange of bridging and terminal hydrides on the NMR time scale.[257] As is common with other aluminium tetrahydroborate complexes, coupling to the spin-$^5/_2$ ^{27}Al nucleus was not observed by ^{1}H or ^{11}B NMR spectroscopy, but it likely explains the line broadening observed in the ^{11}B NMR spectrum.[257]

i)

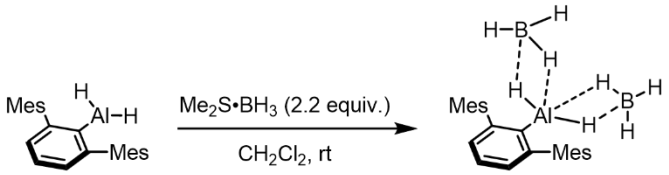

3-Mes-1
(δ^{11}B: –34.8)

ii)

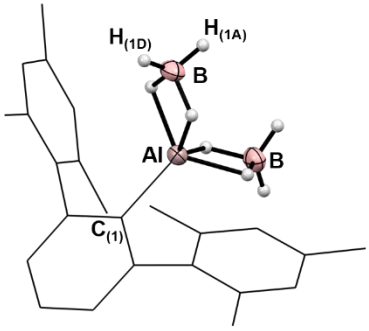

3-Mes-1

Parameter	Measurement
Al•••B	2.1772(13) Å
Al–*H*–B	1.66(2) Å
Al–*H*–*B* (average)	1.178(3) Å
B–$H_{(1A)}$ (terminal)	0.949(18) Å
B–$H_{(1D)}$ (terminal)	0.904(18) Å
Al–C	1.9308(14) Å
C–Al–B	124.50(4) °
B–Al–B	111.01(8) °

Scheme 3-7. i) Synthesis of 3-Mes-1 by the reaction of ^{Mes}TerAlH$_2$ with Me$_2$S•BH$_3$ (2 equiv.); ii) ORTEP representation of 3-Mes-1 (50% probability ellipsoids). For clarity, the ^{Mes}Ter-substituent is displayed in wireframe and the hydrogen atoms have been removed, except for the bridging and terminal hydrides. Chosen parameters are provided in a table.

In the $^{p\text{-Tol}}$Ter*Al* system, the formation of the related bis(tetrahydroborate) alane, **3-*p*-Tol-1**, under catalysis reaction conditions was confirmed by the clean formation of the same diagnostic ^{11}B resonance at δ –34.3 (p, $^1J_{B\text{-}H}$ = 86 Hz) for the reaction between $^{p\text{-Tol}}$TerAlH$_2$ and Me$_2$S•BH$_3$ (2 equiv.) in CH$_2$Cl$_2$ (**Scheme 3-8.i**). The structure was corroborated by the formation of the characteristic broad quartet in ^{1}H NMR spectroscopy for the B*H*$_4$ unit between δ 0.80 and –0.09.

^{Tipp}TerAlH$_2$ also reacted with Me$_2$S•BH$_3$ (2 equiv.) to give a product consistent with the formation of a tetrahydroborate species, **3-Tipp-1** (δ^{11}B: –33.5; **Scheme 3-8.i**). However, the absence of this product in catalysis confirmed that **3-Tipp-1** was not formed under catalysis reaction conditions. Rather, the ^{11}B signal at δ –9.1 observed under catalysis could be replicated by the reaction of ^{Tipp}TerAlH$_2$ with HBpin (1 equiv; **Scheme 3-8.ii.a**), further alluding to the formation of a ^{Tipp}TerAlH$_2$•HBpin adduct (**3-Tipp-A**). Attempts to isolate **3-Tipp-A** failed but analysis of the reaction mixture by ^{1}H NMR spectroscopy revealed that the *m*-terphenyl environment retained the same symmetry, while the methyl protons of the pinacolate group were split into four distinct resonances, suggesting hindered rotation of this group. In the presence of THF (50 equiv.), the ^{11}B signal for **3-Tipp-A** (δ –9.1) disappeared (**Scheme 3-8.ii.b**). This was attributed to a reversible adduct formation, allowing THF to coordinate with aluminium and liberate HBpin. Some concomitant decomposition of HBpin was also observed, as inferred by the formation of B(OR)$_3$ (δ 20 to 22) and of

several BH_4 species (δ –33 to –40), which could have been instigated by the probable formation of THF•***Al***–H.

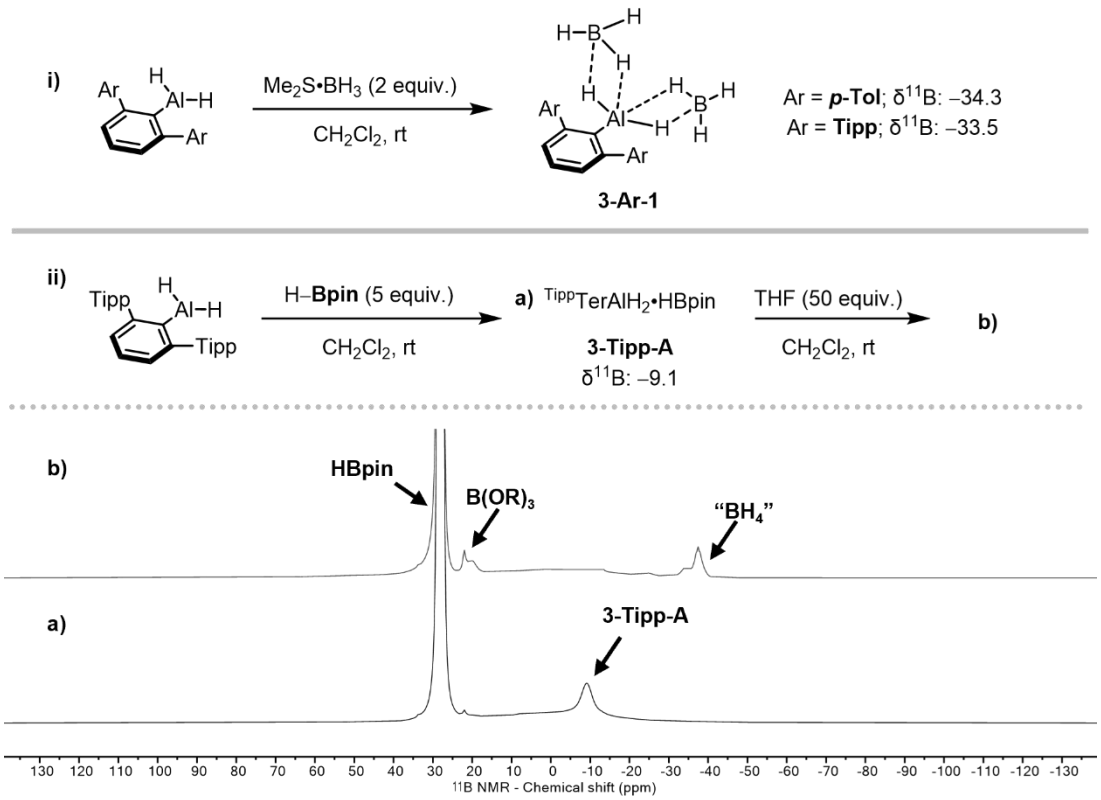

Scheme 3-8. i) The reaction of ^{Ar}TerAlH$_2$ with Me_2S•BH_3 (2 equiv.) generates **3-Ar-1**; ii) Stacked ^{11}B NMR spectra (CH_2Cl_2) for a) the reaction of ^{Tipp}TerAlH$_2$ with HBpin (1 equiv.); b) following the addition of THF (50 equiv.).

The $^{p\text{-Tol}}$Ter*Al* system behaved similarly to the ^{Mes}Ter*Al* system in the absence of alkene; similar quantities of BH_3 were formed which led to the formation of the tetrahydroborate complexes, **3-Mes-1** and **3-*p*-Tol-1**. However, when 1-octene (10 equiv.) was added to the reaction mixture formed from ^{Ar}TerAlMe$_2$ and HBpin (12 equiv.), different behaviours were observed:

- In the ^{Mes}Ter*Al* system (**Scheme 3-9.i**), **3-Mes-1** was consumed with concomitant generation of several new boron-containing species (approx. ^{11}B signals: δ 87 (octyl$_3$B), 4, –14 and –28), including the octylBpin product (δ 33.2). Traces of an L•BH_3 species were observed, with the distinctive ^{11}B signal at *ca.* δ –13 (q, $^1J_{B\text{-}H}$ = 97.4 Hz) overlapped by the broad ^{11}B resonance at δ –14.
- In the $^{p\text{-Tol}}$Ter*Al* system (**Scheme 3-9.ii**), **3-*p*-Tol-1** was mostly unconsumed. The resonances observed in the ^{Mes}Ter*Al* system were not observed in this system, apart from octyl$_3$B and the aforementioned L•BH_3

species. A small quantity of a new boron-containing species was also observed at δ –41. OctylBpin was *not* formed.

- In the ^{Tipp}Ter*Al* system (**Scheme 3-9.iii**), the resonance attributed to adduct **3-Tipp-A** at δ –9.1 did not disappear but octylBpin was formed. No other 4-coordinate boron species were observed.

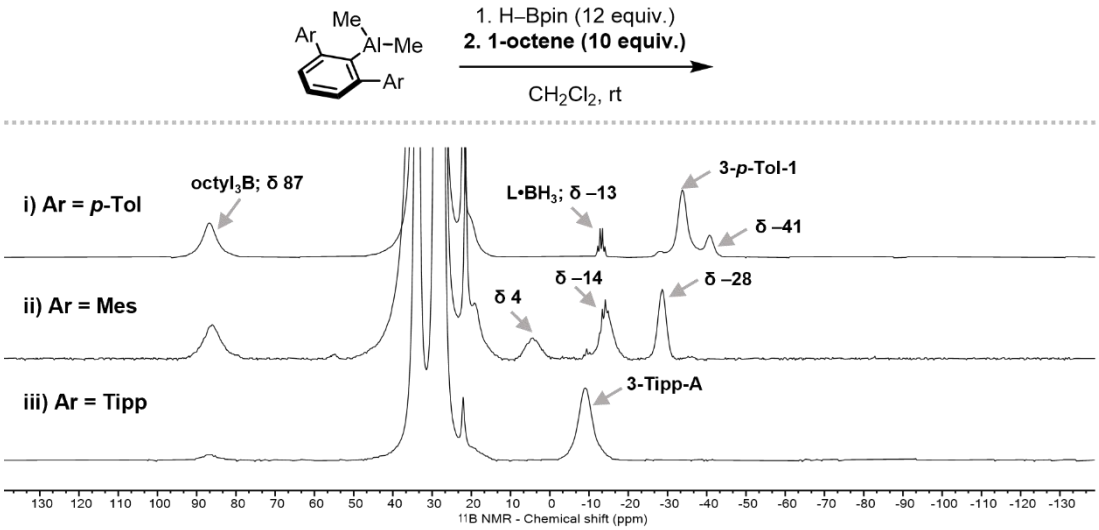

Scheme 3-9. Stacked ^{11}B NMR spectra displaying the boron-containing species under catalysis in the presence of 1-octene for i) the $^{p\text{-Tol}}$TerAl system; ii) the ^{Mes}TerAl system; iii) the ^{Tipp}TerAl system.

These observations reveal that each system behaves differently under catalytic conditions, resulting in vastly different reaction pathways. The absence of BH_3 formation in the ^{Tipp}Ter*Al* system suggests that this mechanism likely follows true, distinct aluminium catalysis. Meanwhile, the formation of new boron-containing species in the ^{Mes}Ter*Al* system can likely explain its catalytic behaviour. The absence of some of these species in the $^{p\text{-Tol}}$Ter*Al* system therefore may explain why this system is not catalytically active.

3.3.4 ^{Mes}Ter*Al* catalysis: what species are involved?

The appearance of the 4-coordinate boron species at *ca.* δ –14 and –28 in the ^{Mes}Ter*Al* system coincided with the consumption of tetrahydroborate alane **3-Mes-1** when 1-octene was introduced. This observation suggested that these intermediates could be Al–H–B species containing alkyl substituents. To identify these species, and to better understand how alkyl substitution at boron or aluminium influences the ^{11}B chemical shift, a systematic evaluation of the reactions between ^{Mes}TerAl(H)$_x$R$_{(2-x)}$ and BH$_x$R$_{(3-x)}$ in CH_2Cl_2 were conducted by ^{11}B NMR spectroscopy (**Scheme 3-10**).

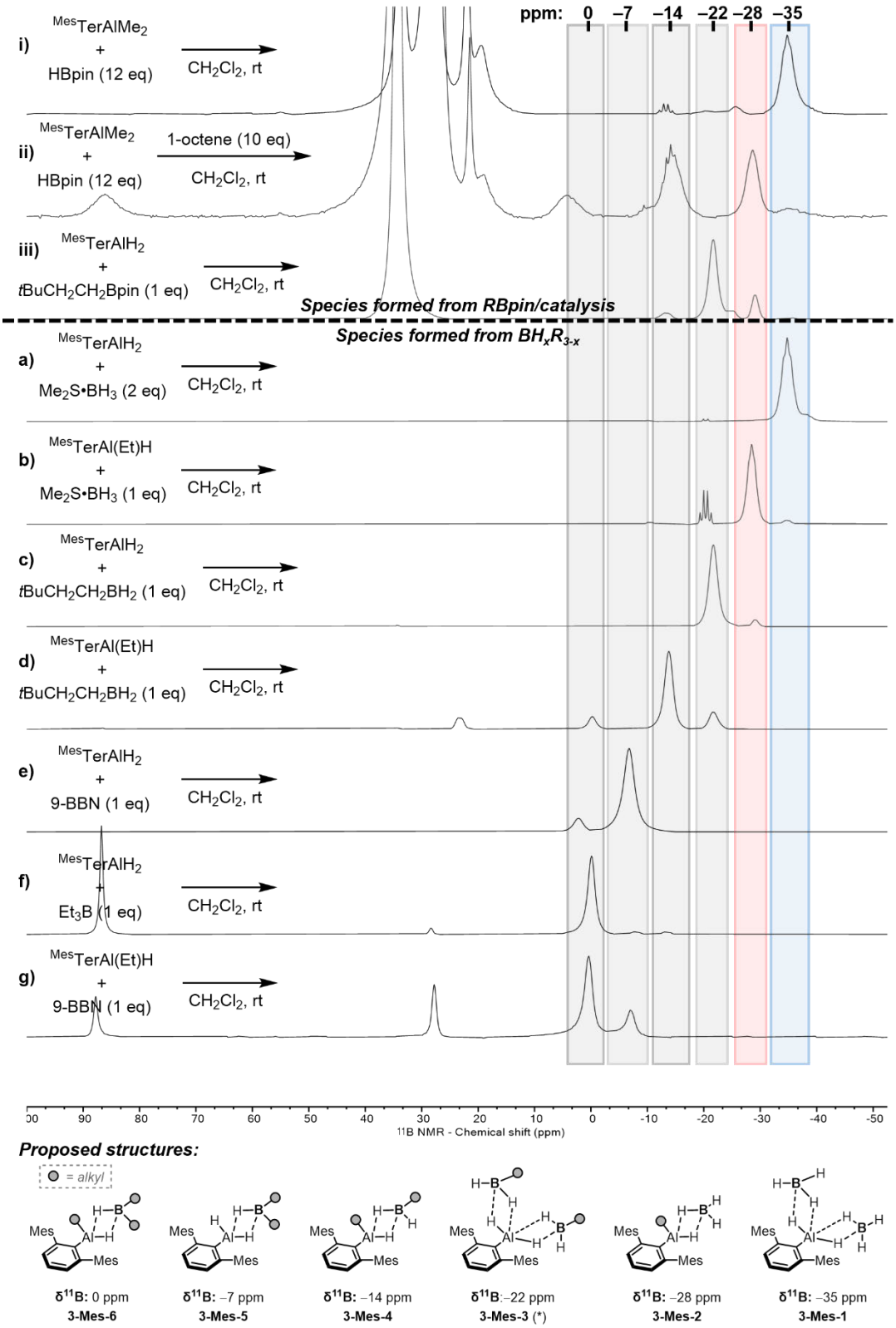

Scheme 3-10. Stacked ^{11}B NMR spectra for the reaction of a series of ^{Mes}TerAl(H)$_x$R$_{(2-x)}$ with BH$_x$R$_{(3-x)}$; **i-iii)** arise from catalytic reactions or with RBpin; **a- g)** arise from stoichiometric reactions with R$_x$BH$_{3-x}$. Alkyl substitution at aluminium and boron correlates with the ^{11}B chemical shift.

The reaction between ^{Mes}TerAl(Et)H and $Me_2S{\bullet}BH_3$ (1 equiv.) resulted in the appearance of a broadened pentet in the ^{11}B NMR spectrum at δ –28.2 (**Scheme 3-10.b**), which was proposed to be that of ^{Mes}TerAl(Et)H•BH_3, **3-Mes-2^{Et}** (**Scheme 3-11**). Analysis of the crude reaction mixture by ^{1}H NMR spectroscopy corroborated the formation of the tetrahydroborate fragment (broad quartet between δ 0.43 and –0.17) and the presence of the alkyl alane (*AlC<u>H₂</u>*CH_3: δ –0.24; q, $^3J_{H\text{-}H}$ = 8.1 Hz). The ^{11}B signal attributed to **3-Mes-2^{Et}** (δ –28.2) was similar to the signal observed under catalysis (*ca.* δ –28) when 1-octene was present. It follows that **3-Mes-2** could be a key catalytic intermediate species. Unfortunately, attempts to isolate **3-Mes-2^{Et}** were hampered by its instability in solution (CH_2Cl_2); after 3 days, the ^{1}H and ^{11}B resonances attributed to **3-Mes-2^{Et}** had mostly disappeared, resulting in an indecipherable mixture by ^{1}H NMR spectroscopy, while ^{11}B NMR spectroscopy revealed the regeneration of $Me_2S{\bullet}BH_3$ and the conversion of **3-Mes-2^{Et}** to a new unknown species at δ –37.2.

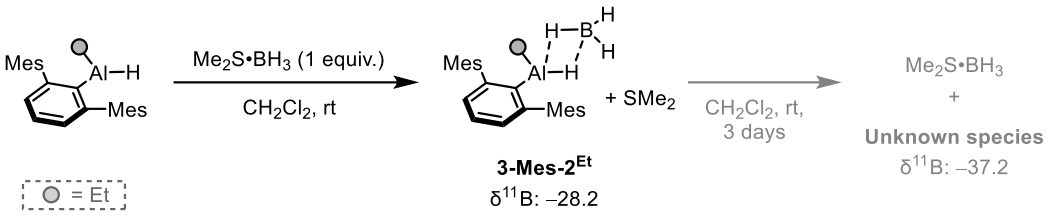

Scheme 3-11. Formation of 3-Mes-2 *in situ*

The reaction between ^{Mes}TerAlH_2 and monoalkylborane RBH_2 (R = $–CH_2CH_2t$Bu; 1 equiv.) resulted in the appearance of a broad singlet in the ^{11}B NMR spectrum at δ –21.7 (**Scheme 3-10.c**), which was attributed to the possible formation of ^{Mes}TerAlH_2•$(H_2BR)_2$, **3-Mes-3^{R}** (**Scheme 3-12.i**). This species was also formed when RBpin (1 equiv.) was reacted with ^{Mes}TerAlH_2 (**Scheme 3-10.iii**). Species similar to **3-Mes-3^{R}**, e.g. **3-Mes-3^{Me}**, can therefore possibly explain the enhanced reactivity of ^{Mes}TerAlH_2 with alkenes in the presence of MeBpin. **3-Mes-3^{R}** was not isolated, but the related **3-Mes-3^{Mes}** could be prepared in a 51% yield from the reaction of ^{Mes}TerAlH_2 with MesBH_2 (2.1 equiv.) in toluene at room temperature (**Scheme 3-12.ii**). Structural insight was provided by single crystal X-ray diffraction following successful recrystallisation of **3-Mes-3^{Mes}** from a super saturated solution of hexane. The H-atoms for the MesBH_3 substituent were located on the Fourier difference map and their positions refined using two separate SADI restraints for the B-H bond distances of the two bridging hydrides and the one remaining hydride. A similar structure to **3-Mes-1** was revealed, featuring a pentacoordinate aluminium complex

with 3c-2e hydride-bridging between aluminium and two mesityl borane fragments **(Scheme 3-12.iii)**.

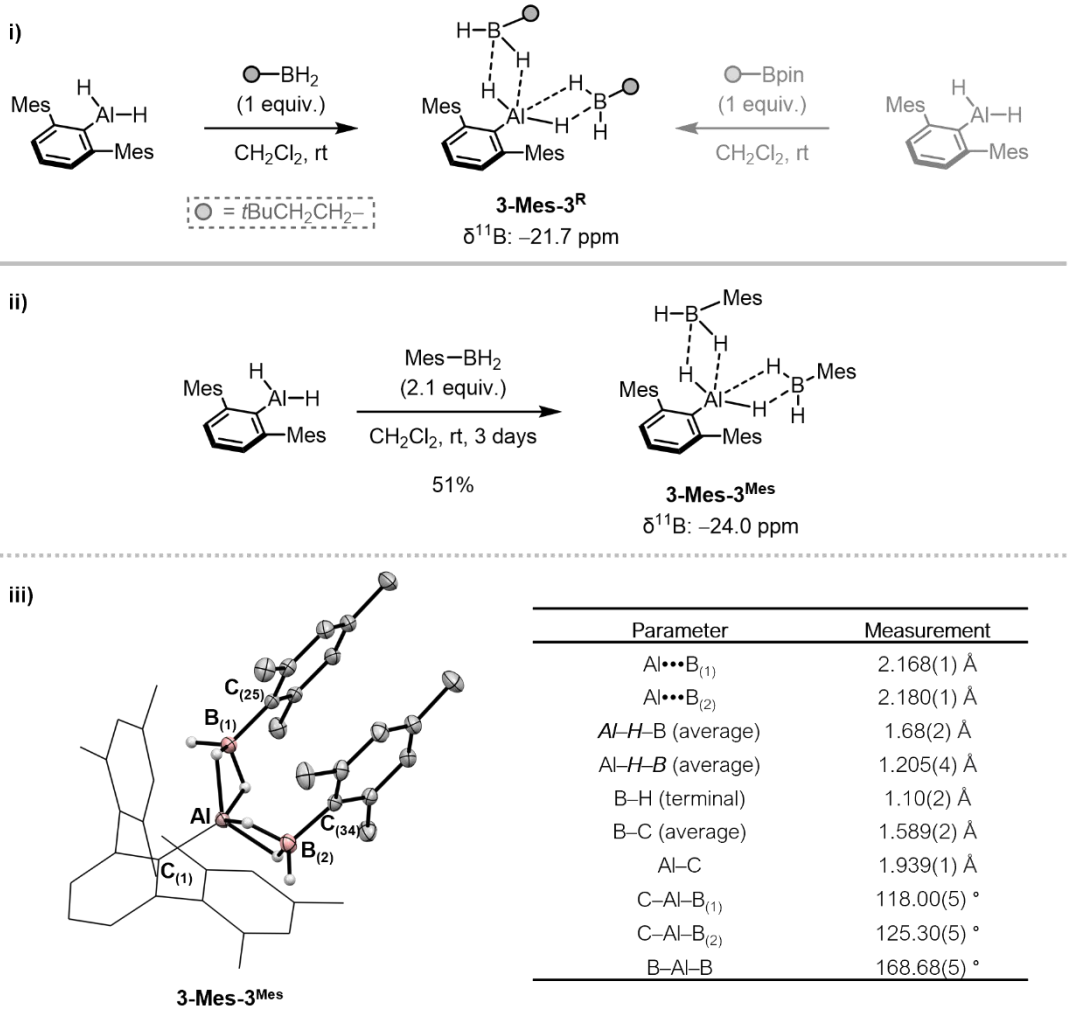

Parameter	Measurement
Al•••$B_{(1)}$	2.168(1) Å
Al•••$B_{(2)}$	2.180(1) Å
Al–H–B (average)	1.68(2) Å
Al–*H–B* (average)	1.205(4) Å
B–H (terminal)	1.10(2) Å
B–C (average)	1.589(2) Å
Al–C	1.939(1) Å
C–Al–$B_{(1)}$	118.00(5) °
C–Al–$B_{(2)}$	125.30(5) °
B–Al–B	168.68(5) °

Scheme 3-12. i) Formation of 3-Mes-3 *in situ*; ii) Synthesis of 3-Mes-3^{Mes}; iii) Crystal structure of 3-Mes-3^{Mes} with chosen parameters.

As observed for **3-Mes-1**, the geometry at aluminium is a basally-distorted square pyramid (τ = 0.010) and tetrahedral at boron. The $AlCB_2$ framework is also trigonal-planar, but the added steric bulk from the Mes-groups at boron led to distorted angles for C–Al–$B_{(1)}$ (118.0 °) vs C–Al–$B_{(2)}$ (125.3 °). This corresponded to different Al•••B distances for Al–$B_{(1)}$ (2.168(1) Å) in comparison to Al–$B_{(2)}$ (2.180(1) Å), although both distances remain comparable to that found in **3-Mes-1** (2.1772(13) Å). The different stretches observed in IR spectroscopy reflected the different environments for the terminal (2428 cm^{-1}) and bridging hydrides (2029 cm^{-1} and 1943 cm^{-1}). Despite this, the ^{1}H NMR spectrum again displayed magnetically equivalent hydrides, with a broad singlet observed at δ 1.77 ($w_{1/2}$ ≈ 260 Hz). The lack of distinct ^{11}B coupling in the ^{1}H NMR spectrum corresponded with the lack of ^{1}H coupling in the ^{11}B NMR spectrum; **3-Mes-3^{Mes}** displayed a broad singlet at δ –24.0 and this can likely

be explained by the line broadening effects that arise from coupling to the spin-$^5/_2$ ^{27}Al nucleus.[257] The upfield chemical shift of **3-Mes-3^{Mes}** in comparison to **3-Mes-3^{R}** presumably results from shielding by the bulky Mes group at boron.

The reaction between ^{Mes}TerAl(Et)H and monolalkylborane RBH_2 (R = $–CH_2CH_2tBu$; 1 equiv.) resulted in the appearance of a broad singlet in the ^{11}B NMR spectrum at δ –13.8 (**Scheme 3-10.d**), which was attributed to the formation of ^{Mes}TerAl(Et)H•H_2BR, **3-Mes-4^{Et,R}**, as the major product (**Scheme 3-13**). A similar signal was observed under catalysis (*ca.* δ –14) when 1-octene was introduced, indicating that **3-Mes-4** could also be a key catalytic intermediate. Analysis of the crude reaction mixture containing **3-Mes-4^{Et,R}** by ^{1}H NMR spectroscopy supported the presence of the ethyl alane functionality (*Al*C*H*$_2$CH$_3$), which was inferred by the formation of a new quartet at δ –0.23 ($^3J_{H-H}$ = 8.2 Hz, 2H). The hydride resonances could not be located, presumably due to overlapping alkyl proton resonances. When the reaction mixture was left for several days, the resonances for *Al*C*H*$_2$CH$_3$ were overlapped by new *Al*C*H*$_2$R signals, which inferred alkyl exchange between boron and aluminium. In addition, the ^{11}B NMR spectrum suggested that **3-Mes-4^{Et,R}** might exist in equilibrium with **3-Mes-3** and other Al–H–B species (**3-Mes-5** and **3-Mes-6**; see below for details of their possible structures). Combined, these processes ultimately hampered attempts to isolate **3-Mes-4^{Et,R}**.

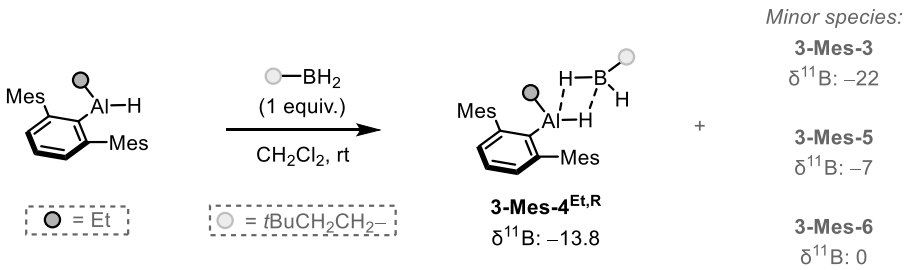

Scheme 3-13. Formation of 3-Mes-4 *in situ.*

The reaction between ^{Mes}TerAlH$_2$ and dialkylborane H-*B*-9-BBN (1 equiv.) resulted in the appearance of a broad singlet in the ^{11}B NMR spectrum at δ –6.8 (**Scheme 3-10.e**), which was attributed to ^{Mes}TerAlH$_2$•(H-*B*-9-BBN), **3-Mes-5^{BBN}** (**Scheme 3-14.i**). When Et_2BH was used in place of H-*B*-9-BBN, **3-Mes-5^{Et}** was initially formed (δ –8.1), but alkyl transfer from boron to aluminium was observed over time and resulted in the formation of **3-Mes-4^{Et}** (**Scheme 3-14.ii**). Redistribution of the alkyl fragment also led to the formation of Et_3B, **3-Mes-3^{Et}** and **3-Mes-6^{Et}** (see **Scheme 3-15** for details related to **3-Mes-6**). The lack of alkyl redistribution with H-*B*-9-BBN was attributed to the chelating framework around boron. The ^{1}H NMR spectrum of the crude reaction mixture containing **3-Mes-5^{BBN}** was complicated by

the presence of at least two distinct *m*-terphenyl products, as judged by the aromatic proton signals. This also corresponded to the formation of two distinct broad singlets at δ 4.18 and at δ 3.37, which were attributed to Al–*H* resonances. This implied that **3-Mes-5^{BBN}** could be a 1:1 complex between aluminium and boron. Reversible dissociation under mild conditions of the H-*B*-9-BBN fragment from an Al–H–B species has been reported,[249] but the presence of free H-*B*-9-BBN was not observed by ^{11}B NMR spectroscopy. Instead, different coordination modes of H-*B*-9-BBN to *Al*–H, as judged by the appearance of a minor ^{11}B resonance at δ 2.2 (**Scheme 3-10.e**), might explain the observation of two distinct species.

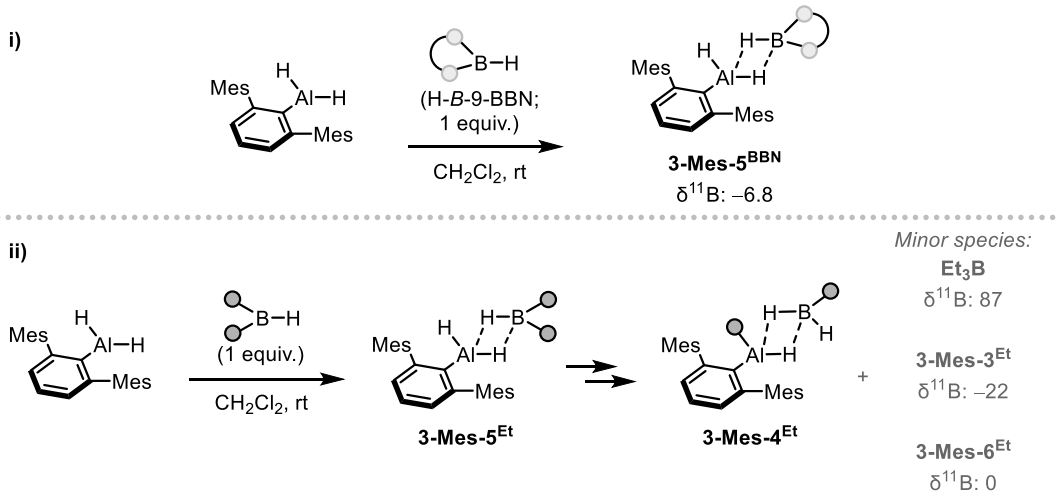

Scheme 3-14. i) Formation of 3-Mes-5 *in situ* with H-*B*-9-BBN; ii) Formation of 3-Mes-5 with Et_2BH leads to alkyl transfer.

The reaction between ^{Mes}TerAl(Et)H and dialkylborane H-*B*-9-BBN (1 equiv.) resulted in the appearance of a broad singlet in the ^{11}B NMR spectrum at δ 0.4 (**Scheme 3-10.g**), which was attributed to ^{Mes}TerAl(Et)H•(H-*B*-9-BBN), **3-Mes-6^{Et,BBN}** (**Scheme 3-15.i**). A ^{11}B resonance in a similar region (δ –0.1, **Scheme 3-10.f**) was also formed when ^{Mes}TerAlH_2 reacted with trialkylborane BEt_3 (1 equiv.; **Scheme 3-15.ii**), with distinct signals characteristic to that of *Al*C*H*$_2$CH$_3$ observed by ^{1}H NMR spectroscopy (δ –0.17, q, *J* = 8.1 Hz). This gave further support for alkyl transfer from boron to aluminium *via* Al–H/B–C(sp^3) exchange, resulting in the formation of **3-Mes-6^{Et}**.

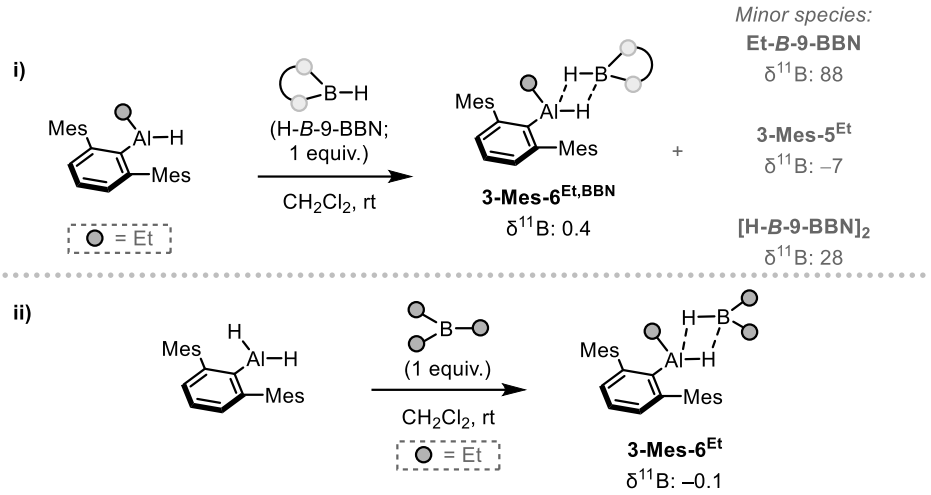

Scheme 3-15. i) Formation of 3-Mes-6 *in situ* with H-*B*-9-BBN; ii) Formation of 3-Mes-6 by boron to aluminium alkyl transfer.

The species detected during catalysis with a ^{11}B chemical shift of δ 4.1 was not observed in any of the reactions between ^{Mes}TerAl(H)$_x$R$_{(2-x)}$ and BH$_x$R$_{(3-x)}$ and therefore is unlikely to be related to an Al–H–B species. Instead, this signal may be attributed to alkoxy tri- or dialkylboron-ate species, e.g. [(R'O)BR$_3$]$^-$ or [(R'O)$_2$BR$_2$]$^-$. These species typically exhibit a ^{11}B chemical shift in the range of δ 0 to 10.[258–260] As this ^{11}B signal was not observed in the absence of alkene, it was unlikely to be related to a trialkoxyborohydride species (possibly of the form [R'O(H)Bpin]$^-$), which also displays ^{11}B signals in this region.[191]

The boron-containing species present under the catalytic conditions for the ^{Mes}Ter*Al* system have been identified, shedding light on the key intermediates involved in the process. The formation of R$_3$B, [(R'O)$_{4-x}$•BR$_x$]$^-$ (x = 2 or 3), and alkyl alane species **3-Mes-2** and **3-Mes-4** was observed in the presence of alkene. In contrast, the catalytically inactive $^{p\text{-Tol}}$Ter*Al* system did not generate any related alkyl alane species. This absence strongly supports the notion that **3-Mes-2** and **3-Mes-4** play a crucial role as catalytic intermediates in the ^{Mes}Ter*Al* system. These findings provide insight into the underlying catalytic mechanism and also emphasise the importance of understanding the roles of different species in the overall process.

3.3.5 Does aluminium mediate exchange with HBpin?

The transfer of alkyl group from boron to aluminium by Al–H/B–C(sp^3) exchange was identified as a possible pathway to generate alkyl alanes (**Scheme 3-16.i**). It should be noted that this exchange is remarkably rare – no examples were found on Reaxys or Sci-finder for this transformation as of March 2023. Only one example of "carbon" transfer from a boron centre to an aluminium hydride was found, which was of an Al–H/B–C(sp^2) exchange of alkenyl boranes with DIBAL-H to generate alkenyl alanes (**Scheme 3-16.ii**).[88] This pathway may explain Yamamoto's organoborane-catalysed alkene hydroalumination (**Scheme 3-16.iii**), the mechanism of which has remained unknown since its discovery in the 1980's.[114]

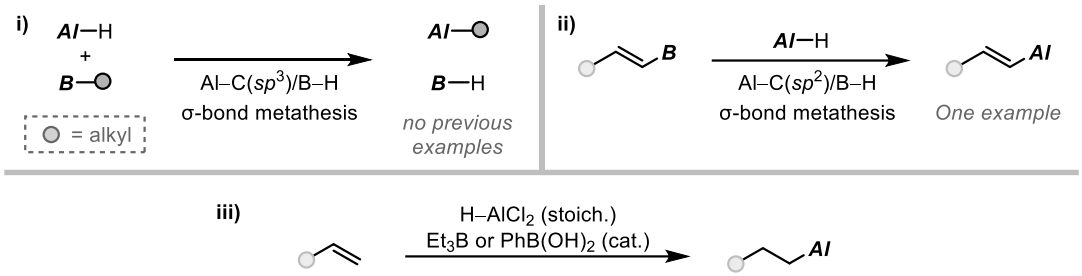

Scheme 3-16. i) Pictorial representation of Al–H/B–C(sp^3) σ-bond metathesis; ii) alkenyl boranes react with Al–H by Al–H/B–C(sp^2) σ-bond metathesis; iii) organoborane-catalysed hydroalumination of alkenes with $HAlCl_2$

The formation of alkyl alanes may explain the reactivity of Et_3B with HBpin in the presence of $^{Mes}TerAlH_2$ (**Scheme 3-5**), as dialkylborohydride alkyl alane **3-Mes-6^{Et}** was observed from the reaction between Et_3B and $^{Mes}TerAlH_2$ (1 equiv.; CH_2Cl_2, rt). The reaction of HBpin with **3-Mes-6^{Et}** (obtained from this reaction mixture) was monitored by ^{11}B NMR spectroscopy. It was found that **3-Mes-6^{Et}** was rapidly consumed to give dialkylborohydride aluminium hydride **3-Mes-5^{Et}** and EtBpin (**Scheme 3-17.i**), suggesting that exchange occurred at the Al–C position. It could also be argued that the alkylborohydride substituents in Al–H–B species might also be capable at participating in exchange reactions with HBpin at the B–C position (due to the enhanced nucleophilicity at carbon in 4-coordinate boron-ate complexes in comparison to 3-coordinate alkyl boranes).[261] However, alkylborohydride alane **3-Mes-3^{R}** (R = $–CH_2CH_2tBu$) did not react with HBpin to give RBpin under standard conditions (room temperature, CH_2Cl_2; **Scheme 3-17.ii**).

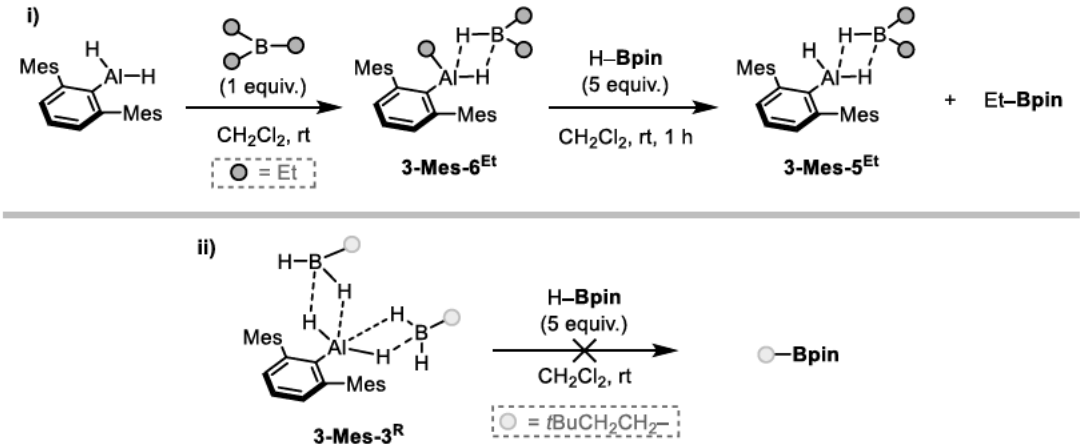

Scheme 3-17. i) 3-Mes-6 reacts with HBpin at the Al–alkyl position; ii) 3-Mes-3 does not react with HBpin.

Although these results gave some useful insight and clearly show that alkyl alane formation is crucial for turnover with HBpin, it prompted further questions, specifically:

- How exactly are the alkyl alanes, **3-Mes-2** and **3-Mes-4**, formed under catalysis in the ^{Mes}Ter*Al* system?
- Why are alkyl alanes formed in the ^{Mes}Ter*Al* system but not the $^{p\text{-Tol}}$Ter*Al* system?

3.3.6 Single-turnover studies

To better understand how alkyl alanes **3-Mes-2** and **3-Mes-4** were formed under catalysis, and to confirm their catalytic relevance, single-turnover experiments were undertaken (**Scheme 3-18**). ^{11}B NMR spectroscopy was used to monitor the reaction between **3-Mes-1** (prepared *in situ* from the reaction between ^{Mes}TerAlH$_2$ + Me$_2$S•BH$_3$ (2 equiv.)) and 1-octene (1 equiv.) in CD_2Cl_2 at room temperature. The formation of **3-Mes-2^{octyl}** was observed alongside *ca.* one equivalent of Me$_2$S•BH$_3$ at δ –20, providing further evidence that **3-Mes-2^{octyl}** contains only one tetrahydroborate substituent at aluminium. The addition of HBpin (1 equiv.) to the reaction mixture resulted in the formation of octylBpin and the regeneration of **3-Mes-1**, thus potentially closing a catalytic cycle. This also coincided with the consumption of Me$_2$S•BH$_3$, which was used to form the second tetrahydroborate ligand in **3-Mes-1**.

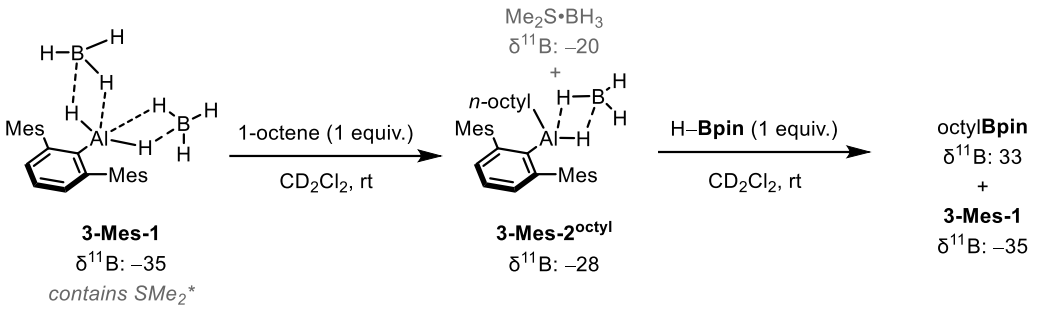

Scheme 3-18. The reaction of 3-Mes-1 with 1-octene gives 3-Mes-2, which in turn reacts with HBpin to regenerate 3-Mes-1 and deliver octylBpin.

The formation of alkylborohydride alkyl alane **3-Mes-4** was next investigated. It was anticipated that further reaction of tetrahydroborate alkyl alane **3-Mes-2** with alkene would lead to the formation of **3-Mes-4**. However, reaction of **3-Mes-2^{Et}** (generated *in situ* from the reaction between ^{Mes}TerAl(Et)H with $Me_2S{\bullet}BH_3$ (1 equiv.)) with 1-octene (2 equiv.) did not form **3-Mes-4^{Et,octyl}** as anticipated (**Scheme 3-19.i**). This is consistent with a strongly bound tetrahydroborate ligand on alkyl alanes, as noted by Aldridge,[249] which would prevent BH_3 dissociating and consequently participating in hydroboration. Aldridge proposed that σ-electron-donating groups at aluminium hydrides increase the polarity of the Al–H bond, which in turn makes the hydride group a better donor and explains the increased strength of binding to BH_3.[249]

It was therefore deduced that **3-Mes-4** must be generated in catalysis by an alternative pathway. One possibility is by the reaction of alkyl boranes with aluminium hydrides. This could be through direct coordination of a monoalkyl borane with ^{Mes}TerAl(R)H (**Scheme 3-19.ii**) or it could be through alkyl transfer from boron to aluminium by the reaction of ^{Mes}TerAlH_2 with a dialkyl borane (which proceeds *via* formation of **3-Mes-3**, such as in the case with Et_2BH; **Scheme 3-19.iii**). Alternatively, the reaction of alkyl alanes with BH_3 might also generate **3-Mes-4**; **3-Mes-4^{Me}** was observed as a minor product in the reaction between ^{Mes}TerAlMe_2 and $Me_2S{\bullet}BH_3$ (0.5 to 2 equiv.; **Scheme 3-19.iv**). This further highlights that alkyl transfer can proceed in both directions between aluminium and boron. A possible driving force for this exchange pathway is the formation of 3c-2e bonds between boron and aluminium.[187] This limits the presence of coordinatively unsaturated monomeric aluminium and boron species that possess vacant *p*-orbitals.

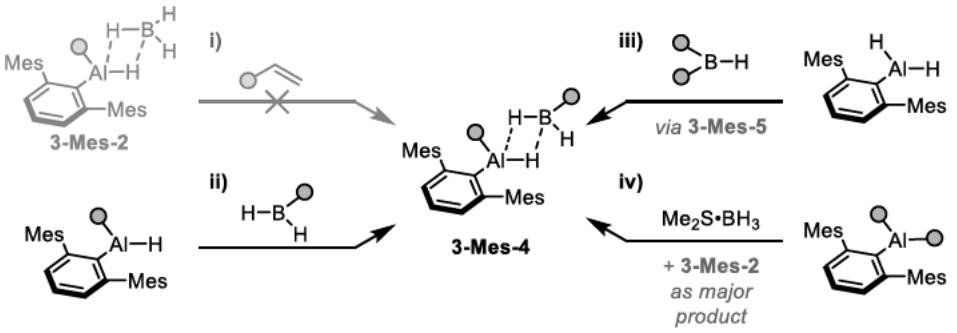

Scheme 3-19. Different pathways towards the formation of 3-Mes-4.

As **3-Mes-4** can be generated through a variety of different routes, catalytic studies were simplified by focusing on the pathway that proceeds by **3-Mes-2.** The findings from this system would also likely apply to **3-Mes-4.**

3.3.7 What mediates hydroelementation?

Early investigations into the reactivity of $Al(BH_4)_3$ with alkenes[262] – pre-dating the discovery of alkene hydroboration[208] – showed that hydroelementation proceeded by a rate-limiting dissociation of BH_3 to give the active $HAl(BH_4)_2$ and BH_3 species *in situ* (**Scheme 3-20**).[262] Later, investigations into the reactivity of independently prepared $HAl(BH_4)_2$ with ethene confirmed that both $RAl(BH_4)_2$ and R_3B had been formed.[263] The formation of both alkyl alanes and alkyl boranes were used to suggest that both hydroalumination and hydroboration were simultaneously occurring, but the possibility of alkyl transfer from boron to aluminium was not considered.

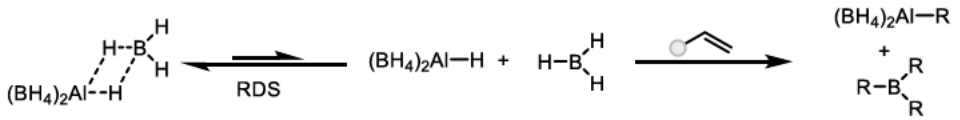

Scheme 3-20. The reaction of $Al(BH_4)_3$ with alkenes proceeds by a rate-determining dissociation of BH_3. Alkyl alanes and alkyl boranes are formed.

The direct formation of tetrahydroborate alkyl alane **3-Mes-2** by the reaction of bis(tetrahydroborate) alane **3-Mes-1** with alkene appears to suggest that the alkyl alane functionality is generated through hydroalumination. However, it was also found that alkyl alanes **3-Mes-6** and **3-Mes-4** can be generated by the reaction of $^{Mes}TerAlH_2$ with R_3B and R_2BH respectively, *i.e.,* by alkyl transfer from boron to aluminium. Thus, two mechanisms can be proposed (**Scheme 3-21**): *Pathway a)*, that proceeds by alkene hydroalumination followed by coordination with BH_3; and *Pathway b)*, that proceeds by alkene hydroboration followed by alkyl transfer from boron to aluminium.

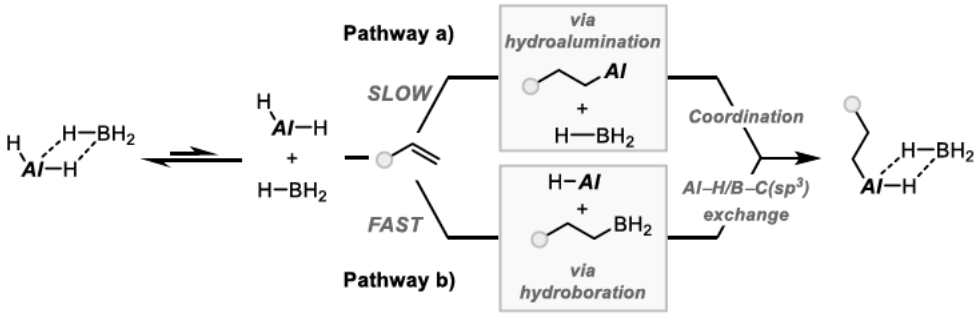

Scheme 3-21. Two possible pathways to generate alkyl alane tetrahydroborates. Pathway a) that proceeds by alkene hydroalumination, and Pathway b) that proceeds by alkene hydroboration. *Al* represents AlR_{3-n}, where n is the number of substituents drawn at aluminium with solid bonds.

Credibility to *Pathway a)* was provided by the reaction between ^{Mes}TerAl(octyl)H (generated *in situ* from the reaction between ^{Mes}TerAlH$_2$ with 1-octene (1 equiv.)) and $Me_2S{\bullet}BH_3$ (1 equiv.)) which gave **3-Mes-2^{octyl}** (**Scheme 3-22**). **3-Mes-2^{octyl}** was not isolated, but the crude reaction mixture allowed analysis of the compound by ^{1}H and ^{11}B NMR spectroscopy, providing valuable diagnostic resonances which were used to track in catalytic studies. Similar characteristic resonances to **3-Mes-2^{Et}** were observed.

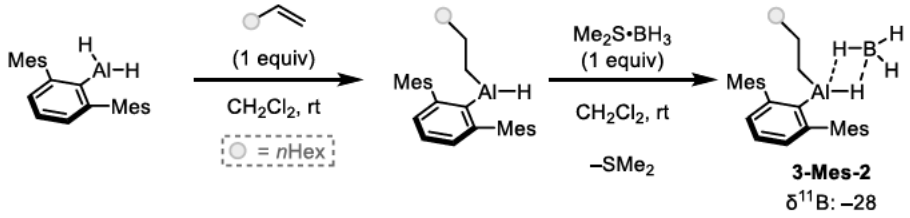

Scheme 3-22. Formation of 3-Mes-2 by a hydroalumination pathway

To assess whether *Pathway b)* was possible, it was necessary to investigate whether alkyl alane **3-Mes-2** could be generated from an alkyl borane (**Scheme 3-23**). Although alkylborohydride alane **3-Mes-3^R** resulted as the major product when ^{Mes}TerAlH$_2$ reacted with RBH_2 (R = –CH_2CH_2tBu; 0.25 to 2 equiv.), small quantities of alkyl alane **3-Mes2^R** were also formed. The selectivity of **3-Mes-2^R** formation in comparison to **3-Mes-3^R** was increased with fewer equivalents of RBH_2. This could possibly be explained by the requirement of a terminal aluminium hydride to mediate this transformation; higher concentrations of RBH_2 would lead to quicker formation of a more stable bis(alkylborohydride) alane **3-Mes-3** species and inhibit the alkyl transfer process. It was speculated that in catalysis, low concentrations of monoalkyl borane would be maintained as its formation would be dependent on the dissociation of BH_3 from **3-Mes-1**. Monoalkyl boranes would also be quickly consumed by the

aluminium hydride upon formation. Accordingly, it was proposed that *Pathway b)* was also a viable route to alkyl alane **3-Mes-2**.

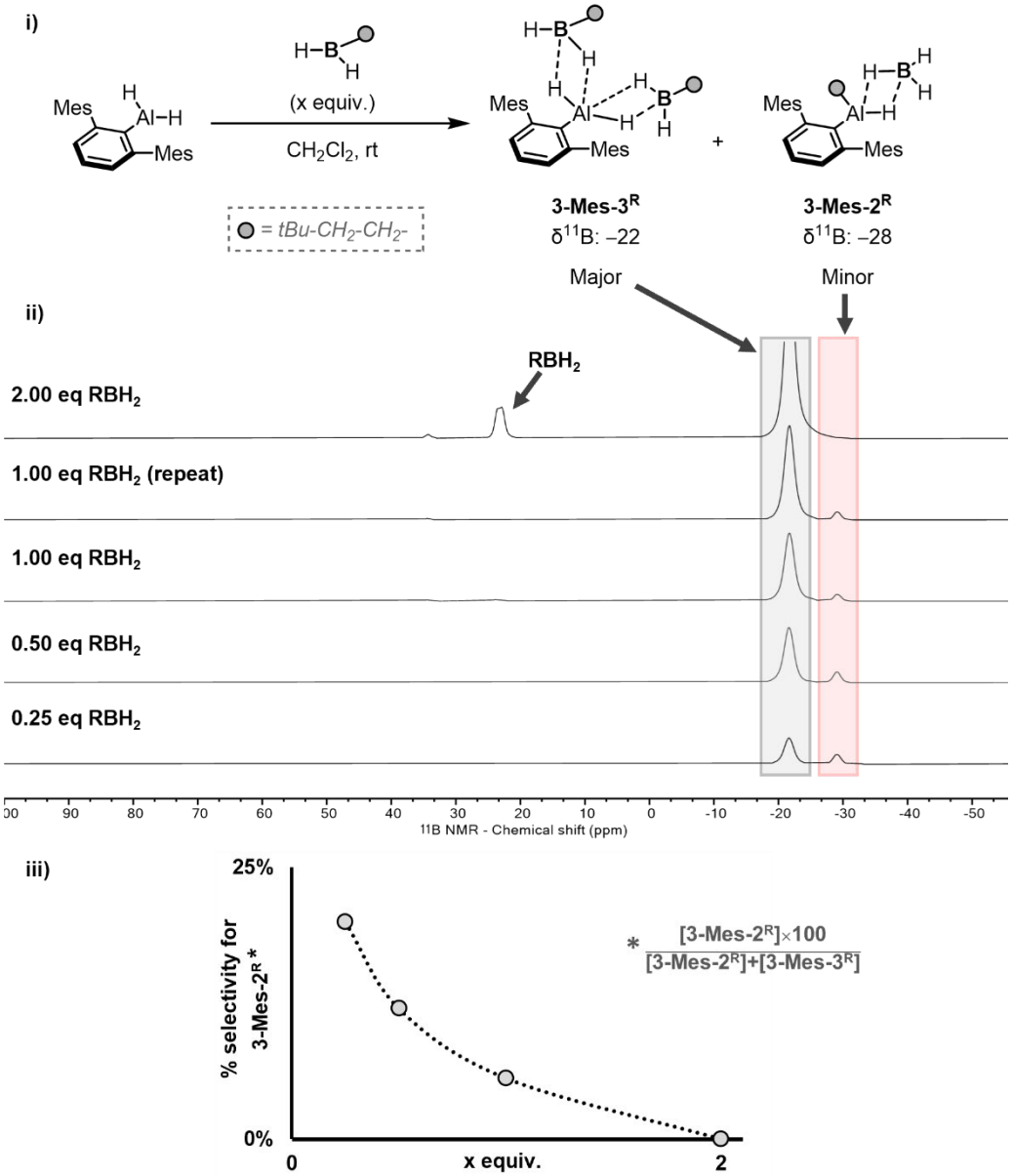

Scheme 3-23. Assessing capacity of monoalkylboranes to transfer alkyl group to aluminium. i) RBH_2 reacts with $^{Mes}TerAlH_2$ to give both coordination and alkyl transfer products; ii) Stacked ^{11}B NMR spectra (CH_2Cl_2) for this reaction; iii) Plotting percentage selectivity of 3-Mes-2^R formation against stoichiometry of RBH_2 used.

In the case of *Pathway b)*, a rapid alkyl transfer from boron to aluminium might explain the direct formation of alkyl alane **3-Mes-2** from bis(tetrahydroborate) alane **3-Mes-1** in the presence of alkene without observing any alkyl borane intermediates. It was hypothesised that a borane substituted with a sterically demanding group may slow the alkyl transfer step from boron to aluminium, enabling the observation of alkyl borane intermediates. Thus, the reaction of (Mes)borohydride alane **3-Mes-3^{Mes}** with

1-octene (1 equiv.) in CH_2Cl_2 at room temperature was probed using ^{11}B NMR spectroscopy (**Scheme 3-24**). The initial formation of alkyl(Mes)borohydride alane **3-Mes-5^{Mes,octyl}** (δ –10.6) was observed, suggesting that the reaction proceeded by *Pathway b).* Conversely, a reaction proceeding by *Pathway a)* would have instead resulted in the initial formation of (Mes)borohydride alkyl alane **3-Mes-4^{Mes,octyl}**. As the reaction proceeded, alkyl(Mes)borohydride alane **3-Mes-5^{Mes,octyl}** was consumed with concomitant formation of (Mes)borohydride alkyl alane **3-Mes-4^{Mes,octyl}** (δ –17.5) over several hours. This showed that alkyl transfer from boron to aluminium was still possible in this system, but that it was substantially slowed due to the bulky Mes-substituent at boron. Throughout this reaction, the formation of alkyl(Mes)borohydride alkyl alane **3-Mes-6^{Mes,octyl}** was also observed (δ –4.8). As **3-Mes-6** can be generated from the reaction of ^{Mes}TerAlH$_2$ with R_3B, **3-Mes-6^{Mes,octyl}** may have been generated *via* formation of MesB(octyl)$_2$, which could have been formed by sequential hydroboration of 1-octene with MesBH$_2$.

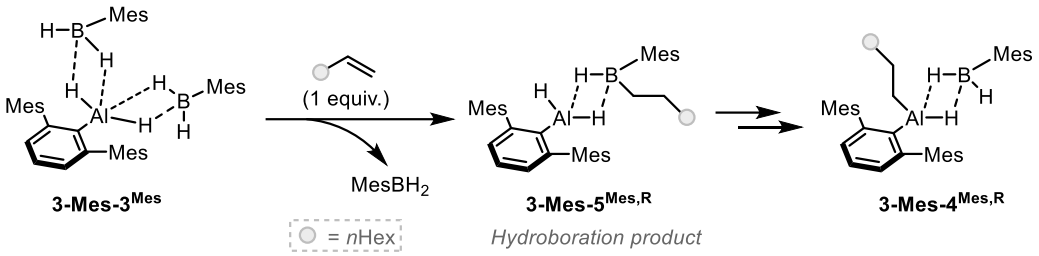

Scheme 3-24. Reaction of 3-Mes-3^{Mes} with 1-octene (1 equiv.)

The results suggest that both hydroalumination and hydroboration pathways likely contribute in some extent towards the formation of the catalytically relevant intermediates. However, there are three main factors that we believe point in favour towards the hydroboration pathway dominating the hydroelementation step:

- The formation of monomeric aluminium hydride is a pre-requisite for alkene hydroalumination. The ready formation of bis(tetrahydroborate) alane **3-Mes-1** from [^{Mes}TerAlH$_2$]$_2$ in the presence of BH_3 suggests that **3-Mes-1** is a thermodynamically more stable species, making the formation of monomeric aluminium hydride even less favourable for **3-Mes-1** than for [^{Mes}TerAlH$_2$]$_2$.
- Alkene hydroboration is generally much more favourable than alkene hydroalumination.[58,264]
- The direct observation of alkyl borane species when alkyl transfer from boron to aluminium is slowed (*i.e.,* in the case of alkylborohydride alane **3-Mes-3^{Mes}**).

3.3.8 How does BH_3 impact catalysis?

If BH_3 indeed functions as a co-catalyst in the ^{Mes}Ter*Al* catalytic system, a change in catalytic rate might be expected if the concentration of BH_3 were to be manipulated. To test this, catalytic reactions were doped with $Me_2S{\bullet}BH_3$ and compared to the background reaction which contained equimolar SMe_2. To carefully control the formation of BH_3 under catalysis, and to simplify analysis of the reaction intermediates, pre-isolated **3-Mes-1** was used as catalyst. Thus, the reaction of 1-octene with HBpin (1.2 equiv.) catalysed by **3-Mes-1** (5 mol%) was monitored by ^{1}H and ^{11}B NMR spectroscopy in the presence of SMe_2 (10 mol%; **a**; **Scheme 3-25.i**) or $Me_2S{\bullet}BH_3$ (10 mol%; **b**; **Scheme 3-25.i**). Curiously, the presence of BH_3 did not impact the reaction rate at all; octylBpin formation was identical in both reactions (**a** and **b**) during the initial phase. However, this was attributed to the rapid consumption of BH_3 by hydroboration of 1-octene, which hampered attempts to monitor its influence. The only discernible difference was that lower yields of octylBpin were obtained for the reaction containing $Me_2S{\bullet}BH_3$, which arose from the aforementioned consumption of 1-octene (**Scheme 3-25.ii**). The comparable rates with diminished quantities of 1-octene hinted that the reaction may be zero-order in alkene.

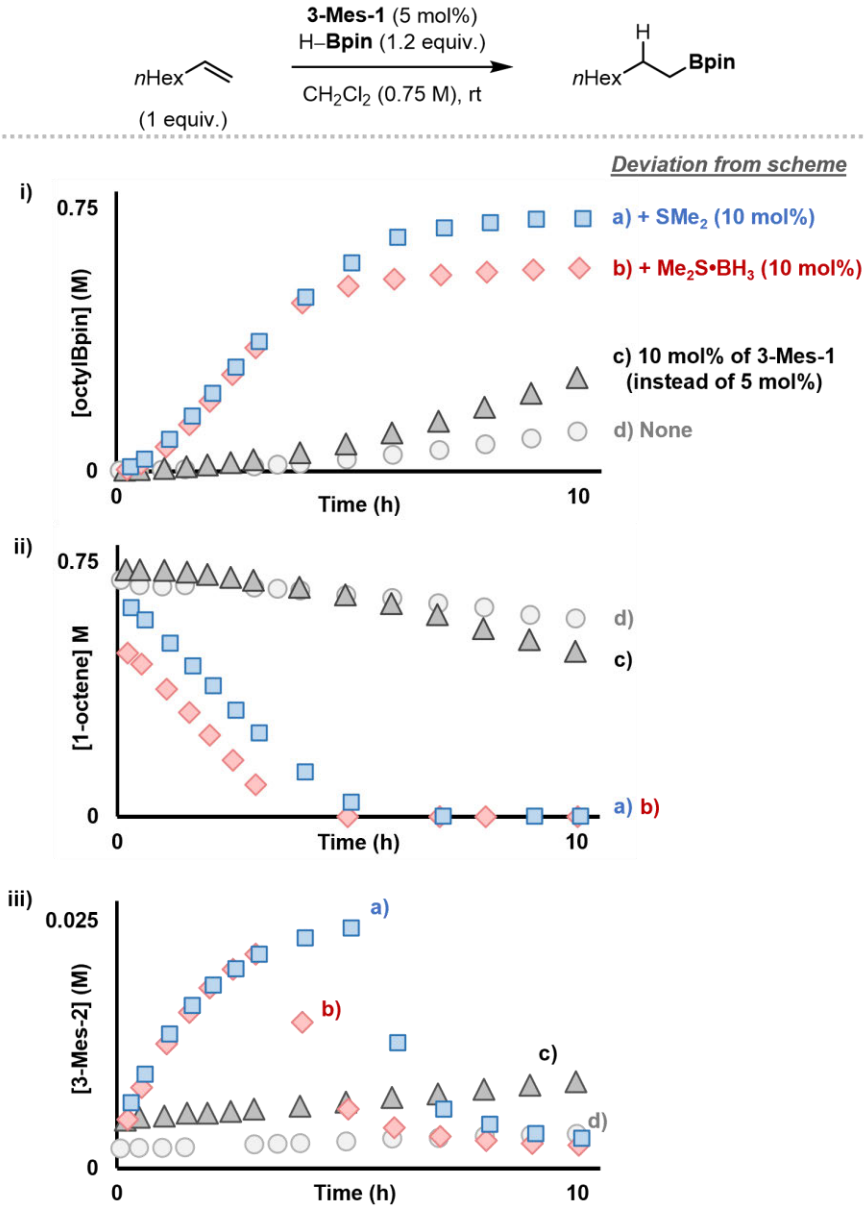

Scheme 3-25. Tracking the concentration of different species i). [octylBpin]; ii) [1-octene]; iii) [3-Mes-2]) in the 3-Mes-1-catalysed 1-octene hydroboration with HBpin in different conditions: a) + SMe_2 (10 mol%); b)+ $Me_2S•BH_3$ (10 mol%); c) catalyst loading of 10 mol%; d) No deviation from scheme.

Rather, it was the presence of Lewis base, SMe_2, that had the greatest impact on catalysis; the absence of SMe_2 resulted in a much slower reaction rate (compare profiles **c** and **d** with **a** and **b; Scheme 3-25.i**). By avoiding the formation of decomposition products such as ***Al*–pin**, it was expected that using pre-isolated **3-Mes-1** in place of ^{Mes}TerAlMe$_2$ or ^{Mes}TerAlH$_2$ would lead to faster catalysis. However, this was only the case when SMe_2 was present, otherwise using ^{Mes}TerAlMe$_2$ or ^{Mes}TerAlH$_2$ pre-catalysts resulted in much faster reactivity (see **Chapter 2**; **section 2.3.3**). Either this meant that **3-Mes-1** was not actually a true catalytic intermediate in the ^{Mes}Ter*Al* system, or it suggested a crucial role for a Lewis

base (and thus a crucial role for ***Al*–pin** as the Lewis base in the absence of SMe_2). An important role for a Lewis base in this system might also explain the slightly faster catalytic rate for alkene hydroboration in the presence of $^{Mes}TerAlMe_2$•OEt_2 in comparison to $^{Mes}TerAlMe_2$ or $^{Mes}TerAlH_2$ (see **Chapter 2**; **section 2.3.2**).

To summarise, a direct effect of BH_3 concentration on catalysis could not be identified. In contrast, a dramatic, and unexpected, role for a Lewis base species in catalysis was found instead. Thus, the role of the Lewis base was investigated.

3.3.9 What role does the Lewis base play?

For the initial alkene hydroelementation step, it was proposed that dissociation of BH_3 from **3-Mes-1** was required, in accordance with BH_3 dissociation being rate-limiting for the reaction between $Al(BH_4)_3$ with alkenes.[262] The Lewis base may therefore act to coordinate BH_3 in **3-Mes-1** and allow dissociation of LB•BH_3. To test this, **3-Mes-1** was titrated against SMe_2 (1 – 55 equiv.) in CH_2Cl_2 at room temperature and monitored by ^{11}B NMR spectroscopy (**Scheme 3-26**). The formation of Me_2S•BH_3 was observed alongside consumption of **3-Mes-1**, which coincided with the formation of a new borohydride species at δ –38.8 (pentet, $^1J_{B–H}$ = 84 Hz). As this species was also formed when $^{Mes}TerAlH_2$ reacted with fewer than two equivalents of Me_2S•BH_3 (0.5 and 1 equiv.), it was assigned as $^{Mes}TerAl(BH_4)H$, **3-Mes-7**. The observations directly show that Lewis bases allow dissociation of BH_3 from **3-Mes-1**.

It was hypothesised that facilitating the dissociation of BH_3 using a Lewis base would accelerate the formation of **3-Mes-2** under catalysis. Returning to the catalytic examples employing **3-Mes-1** as catalyst, the formation of **3-Mes-2^{octyl}** in the presence and absence of SMe_2 was investigated by ^1H NMR spectroscopy (**Scheme 3-25.iii**). In the presence of SMe_2, rapid formation of **3-Mes-2^{octyl}** was initially observed, followed by a sharp drop in its presence once 1-octene had been fully consumed. In contrast, the absence of SMe_2 led to the slow progressive build-up of **3-Mes-2^{octyl}** which coincided with the reaction rate increasing. This implied an order dependence of **3-Mes-2** on catalysis. Importantly, it also showed that the dissociation of BH_3 in **3-Mes-1** with a Lewis base is a crucial component of the catalytic reaction.

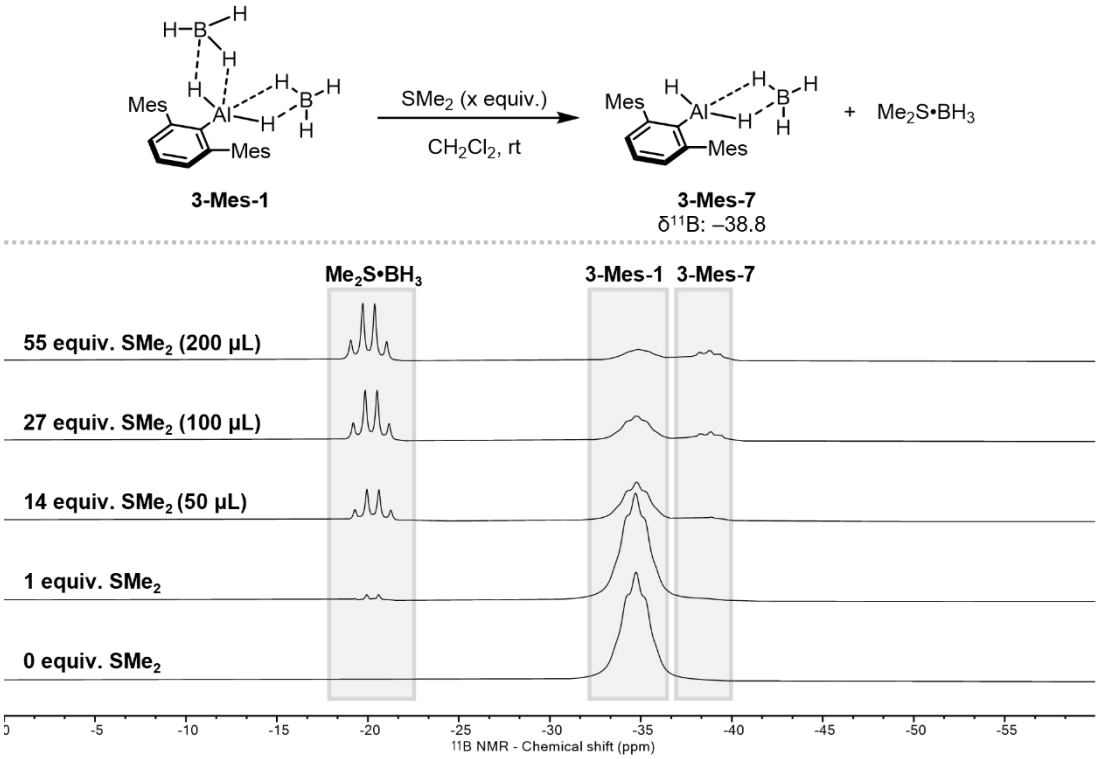

Scheme 3-26. Stacked ^{11}B NMR spectra (CH_2Cl_2) for the reaction of 3-Mes-1 with different quantities of SMe_2.

3.3.10 What is the rate dependence in catalysis?

To shed further light on the reaction mechanism and to better understand the rate-limiting step, variable time normalised analysis (VTNA) was used (**Scheme 3-27**). VTNA, developed by Burés,[265] is a graphical analysis method that works by comparing reaction profiles over variably normalised time scales, allowing simple extraction of reaction orders and k_{obs} from experiments derived from catalytically relevant conditions. This was especially important in this instance, given the numerous processes potentially involved in the reaction. Thus, the formation of 4-*t*Bu-phenethylBpin from the reaction of 4-*t*Bu-styrene with HBpin in the presence of **3-Mes-1**, conveniently generated *in situ* from ^{Mes}TerAlH_2 and Me_2S•BH_3, was tracked by ^1H NMR spectroscopy, with varied initial concentrations of each starting material. **3-Mes-1** was deliberately generated in this way since the absence of SMe_2 as the Lewis base resulted in a completely distinct reaction profile. This is because **3-Mes-1** does not generate ***Al–pin*** in the presence of HBpin, which is the implied intrinsic source of Lewis base in catalytic reactions involving ^{Mes}TerAlMe_2 and ^{Mes}TerAlH_2.

i) Standard conditions:

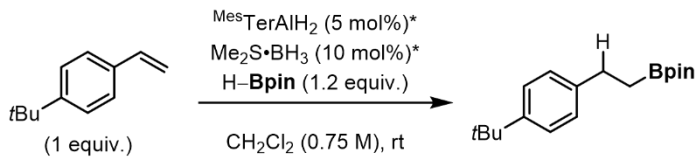

** Combined to make **3-Mes-1** ("cat."; 5 mol%) and SMe_2 (10 mol%) in situ*

ii)

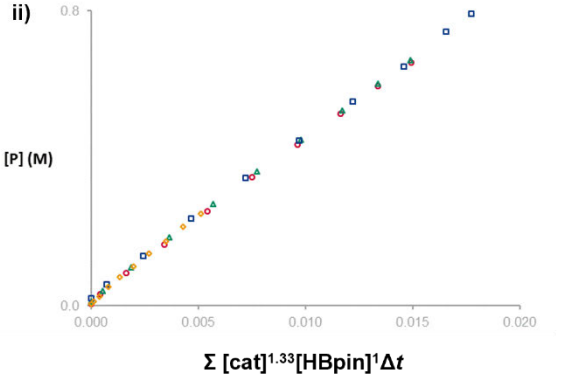

iii)

Entry	Catalyst (Equiv.)	Alkene (Equiv.)	HBpin (Equiv.)
1	0.05	1**	1.2
2	0.025	1	1.2
3	0.05	1.25	1.2
4	0.05	1	1.5

***1 equiv. = 0.75 M*

Scheme 3-27. VTNA studies for the 3-Mes-1 catalysed 1-octene hydroboration with HBpin; i) standard reaction conditions; ii) overlay of reaction profiles corresponding to orders of reagents; iii) Series of experiments used for VTNA analysis

Remarkably, the reaction was found to be zero-order in 4-*t*Bu-styrene, showing that alkene hydroelementation is not rate-limiting (contrasting the implications of the stoichiometric experiments described in Chapter 2). Instead, it was found that the reaction was first order in HBpin and $^4/_3$ order in **3-Mes-2**, indicating that both species are involved in the rate-limiting step. The fractional rate order for **3-Mes-2** is indicative of other complex processes and that its rate dependence changes at different stages of the reaction; the sharp drop in [**3-Mes-2**] when alkene is consumed in catalysis possibly explains this. The results suggest that σ-bond metathesis between **3-Mes-2** and HBpin is rate-limiting, which would explain the build-up of **3-Mes-2**, as observed in catalysis. Given that the monomeric dialkyl alanes ($^{Mes}TerAlR_2$) reacted rapidly with HBpin even at low temperatures, it is likely that this process requires the partial dissociation of BH_3 from **3-Mes-2** to proceed.

3.3.11 Mechanistic proposal

From the experiments performed, a detailed mechanistic picture for the ^{Mes}Ter*Al* system was obtained (**Scheme 3-28**). The reaction begins by the partial decomposition of HBpin with the $^{Mes}TerAlMe_2$ and $^{Mes}TerAlH_2$ pre-catalysts to give **3-Mes-1** and ***Al*-pin** (in the case of $^{Mes}TerAlMe_2$, MeBpin is also formed by Al–C(sp^3)/B–H σ-bond metathesis with HBpin). The formation of ***Al*–pin** is not insignificant; it likely plays a crucial role as a Lewis base to dissociate BH_3 from

3-Mes-1 to presumably give **3-Mes-7**. From here, it was proposed that L•BH_3 reacts with the alkene to give RBH_2, which can transfer the *B*-alkyl group to **3-Mes-7** by Al–H/B–C(sp^3) exchange to give **3-Mes-2** and regenerate BH_3. This key boron to aluminium alkyl transfer circumvents the need to generate alkyl alanes through a slow alkene hydroalumination step. This step is followed by a rate-limiting Al–C/B–H exchange between **3-Mes-2** and HBpin, which likely requires at least partial dissociation of BH_3 in **3-Mes-2** to proceed. This results in the formation of the pinacolboronic ester product and regeneration of **3-Mes-1**.

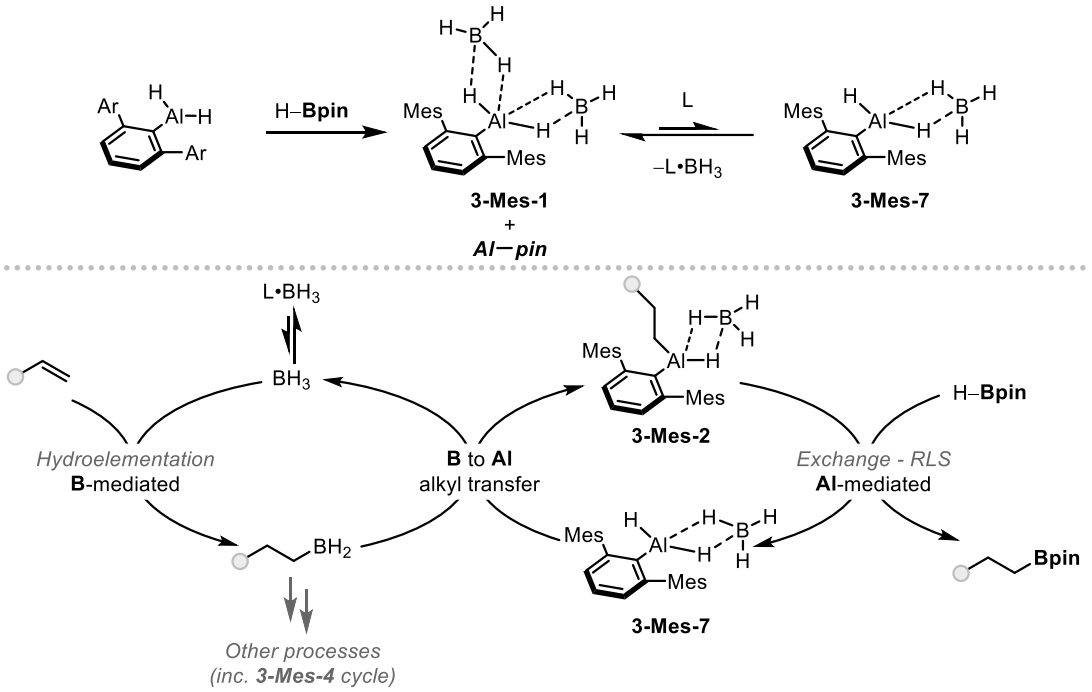

Scheme 3-28. Proposed mechanism for alkene hydroboration when catalysed by a ^{Mes}Ter*Al* system. RLS = rate-limiting step.

It is important to note that if alkyl transfer from boron to aluminium is slower than hydroboration, formation of secondary and tertiary boranes result. In the presence of $^{Mes}TerAlH_2$, alkyl transfer from secondary boranes to aluminium results in the formation of **3-Mes-4**, which was also observed in catalysis. This would lead to an alternative, but similar, catalytic cycle involving Al–C(sp^3)/B–H exchange as the turnover step.

3.3.12 Why is the *p*-TolTer*Al* system not catalytically active?

Alkyl alane formation from the transfer of alkyl groups from boron to aluminium is a critical component of the MesTer*Al* catalytic system. When this alkyl transfer step does not happen, catalysis does not proceed. This is one possible explanation for the lack of catalytic activity in the *p*-TolTer*Al* system; the build-up of trialkyl borane is observed instead of alkyl alane formation (**Scheme 3-29.i**; see also **Scheme 3-9.ii**).

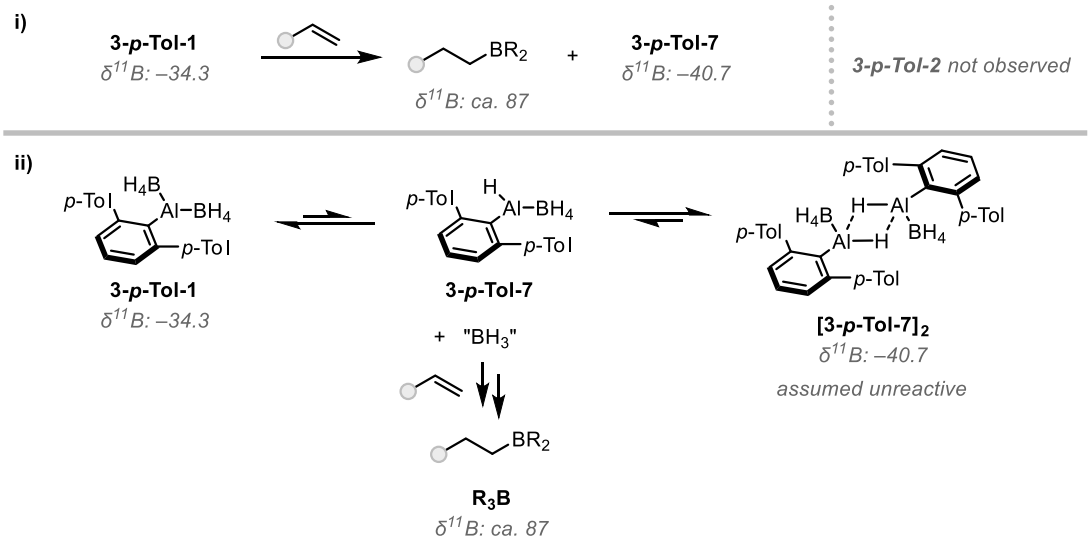

Scheme 3-29. Explanation for catalytic inactivity of *p*-TolTer*Al* system. i) in the presence of alkene, 3-*p*-Tol-1 does not generate alkyl alanes; ii) rapid dimerisation of 3-*p*-Tol-1 is proposed to be the reason why alkyl groups are not transferred to aluminium.

This may arise from the lack of steric bulk around aluminium causing the formation of catalytically inactive species. Assuming BH_3 dissociates from **3-*p*-Tol-1**, **3-*p*-Tol-7** would form (**Scheme 3-29.ii**). In the presence of alkene, BH_3 will undergo hydroboration to give alkyl boranes that could in principle react with **3-*p*-Tol-7** to give **3-*p*-Tol-2**. However, the lack of steric protection at aluminium in **3-*p*-Tol-7** could also lead to formation of the dimer, [**3-*p*-Tol-7**]$_2$, which may be unreactive towards alkyl boranes. This would explain the appearance of the resonance at δ –40.7 in the ^{11}B NMR spectrum under catalysis (**Scheme 3-9.ii**). A dimeric structure might also explain the upfield resonance in comparison to **3-Mes-7** (δ^{11}B: –38.8), which could be monomeric, particularly in the presence of SMe_2 or other Lewis base.

Other forms of catalyst deactivation are also possible. Smaller primary alanes have the tendency to redistribute substituents, giving rise to secondary alanes and AlH_3.[63,64] Redistribution reactions are also observed for triorganoalanes.[35] In the case of *p*-TolTerAlMe_2, redistribution of the *m*-terphenyl fragment was observed in the presence of MeBpin in C_6D_6 to give *p*-TolTer_2AlMe (**Scheme 3-29.iii**). This assignment was based on the integral ratio of the AlC$\underline{H_3}$ resonance (δ –1.66, 3H = 1 × AlC$\underline{H_3}$)

with the methyl resonance on the *p*-Tol group (δ 1.99, 12H = 4 × C*H*$_3$ = 2 × $^{p\text{-Tol}}$Ter groups) by ^{1}H NMR spectroscopy. This was accompanied by the formation of Me_3B (δ^{11}B: 86.4), implying the transfer of pinacol from boron to aluminium to give another unknown aluminium pinacolate species. It should be noted that although $^{p\text{-Tol}}Ter_2AlMe$ was not observed in catalysis, it highlights that sufficient steric protection at aluminium is required to prevent decomposition by substituent redistribution.

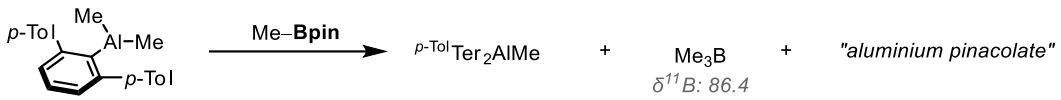

Scheme 3-30. Redistribution of $^{p\text{-Tol}}TerAlMe_2$ in the presence of MeBpin.

3.4 Conclusions and future outlook

The *rate problem* arises from the different behaviour of each ^{Ar}Ter*Al* system under catalytic conditions. Specifically, the formation and reactivity of boranes determine the catalytic activity observed in these systems (**Scheme 3-31**).

HBpin was found to be most stable in the larger ^{Tipp}Ter*Al* system, in which little BH_3 formation was observed. This indicated that catalysis likely proceeds by the widely-reported two-step mechanism of alkene hydroalumination and Al–C(sp^3)/B–H exchange. The formation of an adduct with HBpin, **3-Tipp-A**, was implied and likely represents the resting state species of the catalytic cycle.

In the smaller $^{p\text{-Tol}}$Ter*Al* and ^{Mes}Ter*Al* systems, HBpin is less stable and results in BH_3 formation. In catalysis, this leads to the formation of the aluminium tetrahydroborate species, **3-*p*-Tol-1** and **3-Mes-1**. For the ^{Mes}Ter*Al* system, this results in *hidden cooperative catalysis*, whereby BH_3 mediates the alkene hydroelementation step. Alkyl transfer from boron to aluminium generates alkyl alanes, bypassing the slow alkene hydroalumination pathway. This explains why the ^{Mes}Ter*Al* system is faster than the ^{Tipp}Ter*Al* system in catalysis despite the slower stoichiometric hydroalumination observed in **Chapter 2**. Onwards reactivity of the alkyl alane with HBpin gives the pinacolboronic ester product and regenerates the aluminium hydride functionality.

In contrast, the formation of boranes in the $^{p\text{-Tol}}$Ter*Al* system ultimately diminishes catalytic activity. It is likely that aggregates, such as tetrahydroborate-substituted aluminium hydride dimer [**3-*p*-Tol-7**]$_2$, readily form and this means that alkyl boranes do not readily transfer the alkyl group to aluminium under catalytic conditions. As alkyl alane formation is essential to generate the pinacolboronic ester products with HBpin, the $^{p\text{-Tol}}$Ter*Al* system is not capable of catalysing alkene hydroboration. The presence of boranes may also lead to other pathways for decomposition, such as substituent redistribution. Thus, lack of steric protection at aluminium leads to catalyst decomposition.

The results provide added nuance to the already reported mechanisms for alkene hydroboration by aluminium or *hidden boron* catalysis. It highlights the involvement of tetrahydroborate species, which have previously been overlooked in main group-catalysed hydroboration protocols with HBpin. The awareness of these species may shed light on the observed reactivity in other protocols. In addition, the potential of using cooperative main group catalysis is highlighted; by leveraging the

strengths of different elements, it may be possible to access protocols that would otherwise be inaccessible through individual elements alone. In particular, the combination of chiral boranes (of which, many are easily accessible) with alanes should be explored in the quest to mediate enantioselective alkene hydroboration with HBpin **(Scheme 3-31)**.

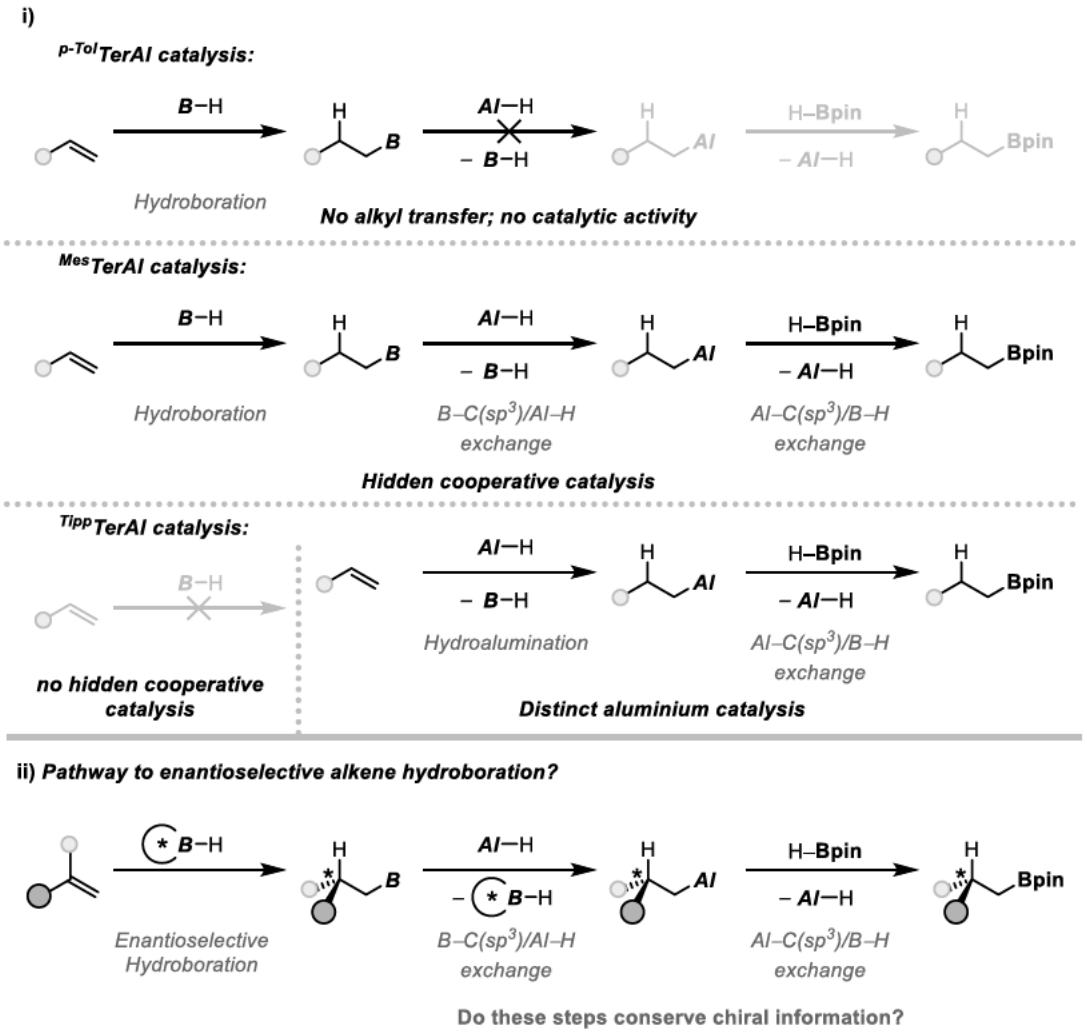

Scheme 3-31. i) Summary of catalytic reactivity observed for each ^{Ar}Ter*Al* system; ii) suggestion for future work in enantioselective alkene hydroboration.

Chapter 4:

Aluminium-catalysed alkene hydroboration with HBdan

4.1 Introduction

As discussed in previous chapters, pinacolboronic esters (RBpin; **Figure 4-1.i**) are usually air- and moisture stable and this has led to their widespread use in organic synthesis. However, there are some situations where the pinacolate fragment (pin) fails to provide sufficient protection for the boron functionality. To address this, alternative boron-protecting groups have been developed, most notably the MIDA-protected boronates (MIDA = *N*-methyliminodiacetic acid; **Figure 4-1.ii**).[266]

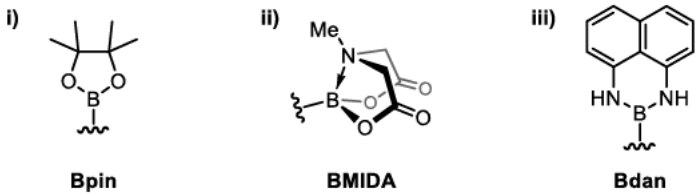

Figure 4-1. Commonly used boron-protecting groups.

In recent years, there has been a resurgence in the application of 1,8-diaminonaphthyl("dan")-protected boranes in synthesis (Bdan; **Figure 4-1.iii**), despite their discovery in the early 1960s.[267] This renewed interest stems from the growing recognition of the advantages offered by Bdan in terms of stability and compatibility. The stability of these compounds can be attributed to the donation of electron-density into the boron atom from the adjacent nitrogen atoms. Structurally, Bdan compounds feature an N–B–N fragment arranged in a 6-membered ring, classifying them as 1,3,2-diazaborinines. Additionally, compounds featuring a 1,3,2-diazaborinine core have demonstrated intriguing materials properties.[268–274] Therefore, the preparation of these reagents is of great interest.

Here, an overview of the reactivity, properties and synthesis of Bdan compounds is provided.

4.1.1 Stability of Bdan

In some circumstances where a pinacolboronic ester is unstable to air or moisture, replacing Bpin with the more robust Bdan unit can enable the isolation of the borylated compound under ambient conditions. This strategy was effective for the isolation of 4-borylated isochromenes,[275] which would otherwise undergo decomposition. Additionally, the synthetically useful silylboranes can be rendered air-stable using the Bdan group ($PhMe_2SiBdan$).[276] In contrast, the more commonly used pinacolboronic ester derivative ($PhMe_2SiBpin$) decomposes in air within several hours.[276]

The Bdan group is also resistant to hydrolysis[277] and has shown excellent stability in the presence of alcohols, Lewis bases and anions such as hydroxide, alkoxides and even fluoride (**Scheme 4-1.i**).[278,279] The outstanding stability of Bdan under conditions in which other air-stable boranes (like the commonly used pinacolboronic esters) are not, has made Bdan the boron-protecting group of choice in many applications.

One example where this characteristic is useful is for the generation of boryl benzynes.[279] In organic synthesis, benzynes are commonly generated by the reaction of *ortho*-trimethylsilylphenyl triflates (*o*-TT) with a fluoride source. However, the fluorophilicity of boron makes the preparation of boryl benzynes challenging; in most examples of borylated *o*-TT (**4-I**), the fluoride anion would preferentially attack the boron fragment over the $–SiMe_3$ group, even in the presence of a MIDA-protected boronate.[279] However, this issue can be addressed by using Bdan, which is more stable towards fluoride anions. In this example, the resulting borylated benzynes (**4-II**) were trapped with an amine to generate *ortho*-substituted boryl anilines (**4-III**; **Scheme 4-1.ii**).[279]

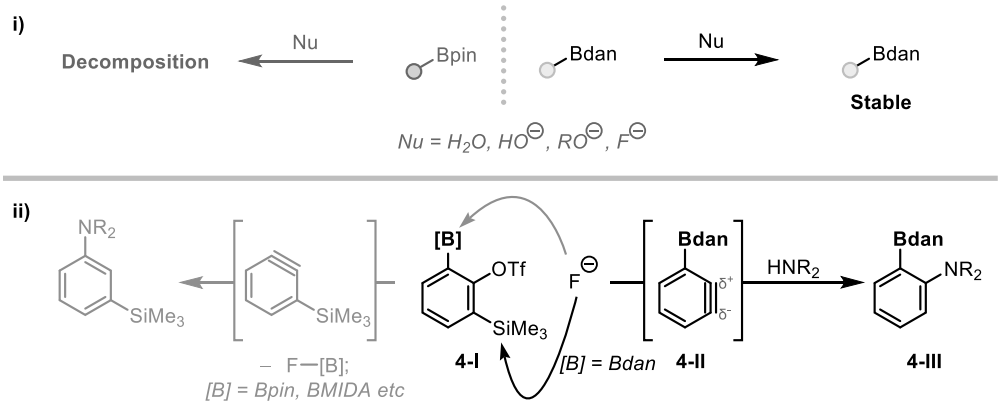

Scheme 4-1. i) Stability of RBdan vs RBpin with nucleophiles; ii) selective benzyne formation using borylated o-TT in the presence of fluoride.

Bdan can also be used as an effective protecting group for boron in Suzuki-Miyaura cross-coupling reactions (SMC).[280–286] Typically, SMC involves the palladium-catalysed coupling of aryl (pseudo)halides and aryl organoboron reagents through a sequence of steps: oxidative addition of aryl halide to Pd; transmetallation of the aryl borane with Pd; reductive elimination of the two aryl fragments from Pd. In the transmetallation step, the formation of a 4-coordinate boron-ate complex, usually with a base, is crucial. However, due to the remarkable stability of Bdan towards nucleophiles and bases, the boron-ate complex formation is hindered, resulting in inhibition of the transmetallation step at the Bdan position. Consequently, in the presence of both C(sp^2)–Bpin and C(sp^2)–Bdan functionalities, the cross-coupling

reaction selectively occurs at the C(sp^2)–Bpin position. Importantly, Bdan exhibits excellent tolerance towards a wide range of bases, including NaOH,[286] even though this can deprotect the commonly used MIDA-protected boronate.[266] Although stable under basic conditions, deprotection of Bdan to the boronic acid can proceed smoothly under aqueous acidic conditions. This orthogonal reactivity has been exploited for iterative SMC (**Scheme 4-2**).[285]

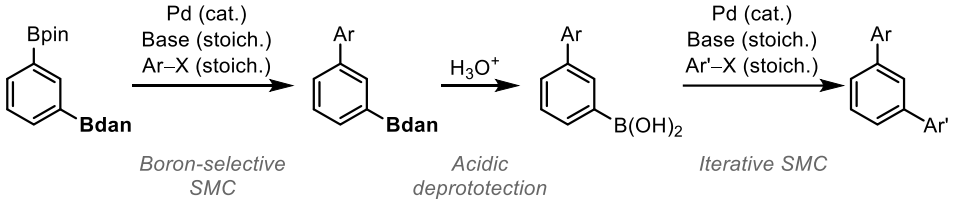

Scheme 4-2. Boron-selective and iterative Suzuki-Miyaura coupling (SMC), exploiting the stability of Bdan followed by deprotection in acidic conditions.

4.1.2 Reactivity of Bdan

Deprotection

Protection of the boron fragment with Bdan early in the synthetic route can be a useful strategy when the target product or a late-stage intermediate contains a boronic acid functionality. This approach has been used for the synthesis of ^{10}B-enriched *p*-borono-*L*-phenylalanine (**Scheme 4-3.i**), which has applications in boron neutron capture therapy for the treatment of cancer.[287]

In cases where revealing the boronic acid leads to intramolecular reactivity, formation of *B*-heterocycles can result. Using Bdan for this is especially advantageous as the target molecular framework for the *B*-heterocycle can be readily prepared by a series of boron-selective SMC. This approach has been applied for the synthesis of bioactive dibenzoxaborins (**Scheme 4-3.ii**).[288] The BN analogue of a dibenzoperylene was also prepared in a similar way (**Scheme 4-3.iii**), and this has potential applications in optoelectronic and semiconductor materials due to its absorbance and fluorescence properties.[289]

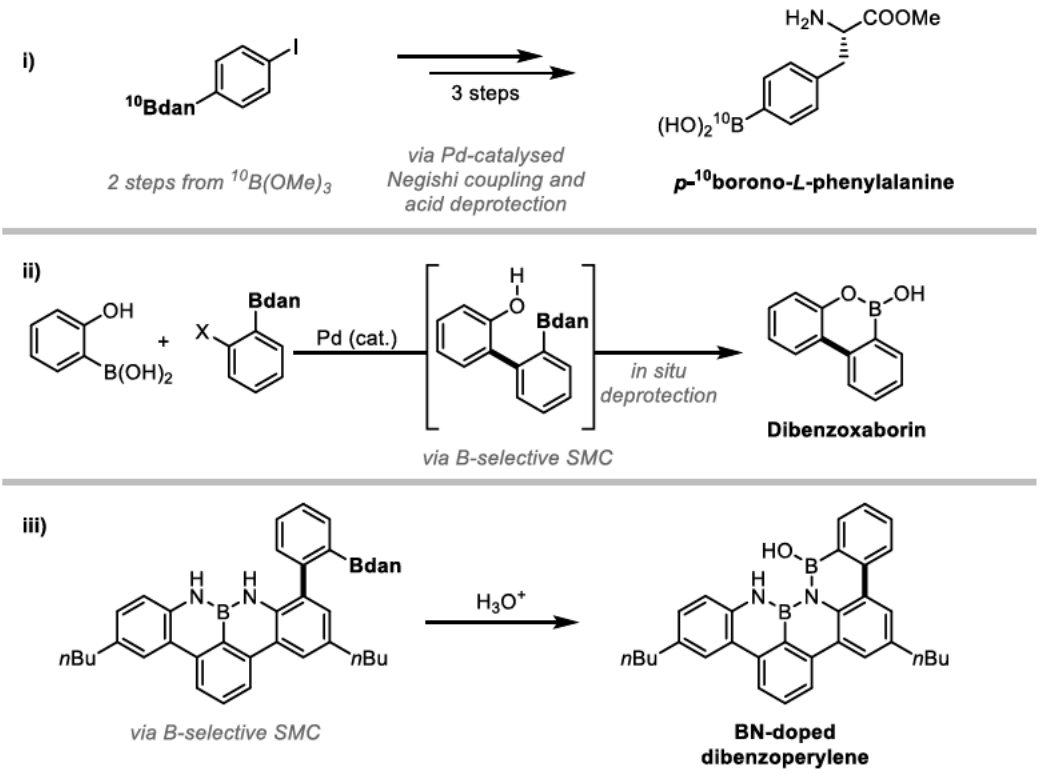

Scheme 4-3. i) Bdan allows early installation of ^{10}B, enabling straightforward synthesis of *p*-borono-l-phenylalanine. Acid deprotection of Bdan allows access to ii) dibenzoxaborins and iii) *BN*-doped dibenzoperylenes.

Bdan as the reactive group

The stability of Bdan towards nucleophiles is now well established, but more recent examples are emerging that employ Bdan as the reactive site. Although commonly used bases, such as NaOH, LiO*t*Bu and K_2CO_3 etc., do not form boron-ate complexes with ArBdan compounds,[290] KO*t*Bu does. This means that KO*t*Bu enables ArBdan to transmetallate onto palladium catalysts, allowing it to participate in SMC directly at the Bdan position (**Scheme 4-4**).[290,291]

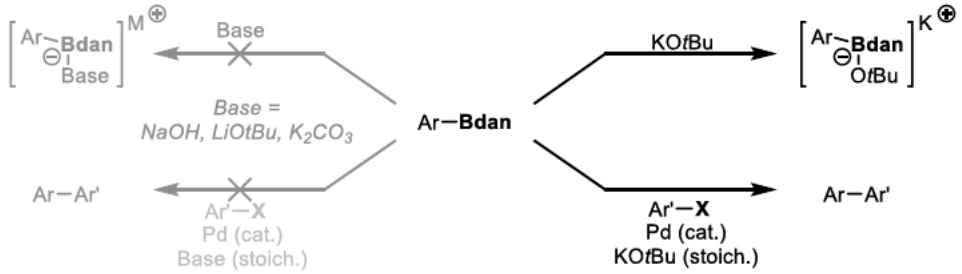

Scheme 4-4. KO*t*Bu enables SMC of ArBdan due to formation of boron-ate species; other bases do not.

Although ArBdan species require the strong nucleophilicity of KO*t*Bu for SMC, alkynylBdan compounds can undergo SMC under milder conditions: K_2CO_3 was

found to be sufficiently basic to mediate the palladium-catalysed cross-coupling between alkynylBdan compounds and aryl/alkenyl halides, allylic carbonates and acyl chlorides.[292] Earlier organotin studies suggested that alkynyl–M transmetallation to Pd(II) is more facile than for aryl–M, with transmetallation rates up to 46 times faster for $PhCCSnMe_3$ in comparison to $PhSnMe_3$.[293] These observations may explain the reactivity trend above.

Oxidative addition into Si–B bonds has been proposed and observed as a key step for platinum- and palladium-catalysed Si–B addition to olefins.[294–296] Although *Si*–Bpin coupling partners have typically been used for these processes, the application of $PhMe_2SiBdan$ for the silaboration of alkynes suggests that the diminished Lewis acidity of $PhMe_2SiBdan$ does not impede the crucial oxidative addition step (**Scheme 4-5**).[276] As an added benefit, alkynes containing Lewis basic groups are tolerated as $PhMe_2SiBdan$ is stable to nucleophiles, whereas $PhMe_2SiBpin$ is not.[276]

$PhMe_2SiBdan$ has also been used in the copper-catalysed hydrosilylation of alkynes. The reaction was proposed to proceed by a B–Si/Cu–O σ-bond metathesis to generate the active copper silyl reagent and give MeOBdan as the by-product. Sila-cupration of the alkyne was then followed by protonolysis with MeOH to complete the catalytic cycle (Scheme 4-5). σ-Bond metathesis for a Bdan-containing compound has also been reported for B–Cl/P–Si exchange in the synthesis of borylphosphines.[297]

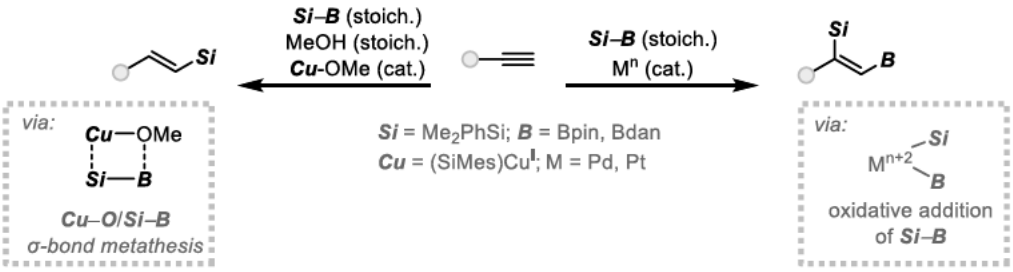

Scheme 4-5. *Si*-Bdan reagents engage in σ-bond metathesis with Cu-O catalysts, or oxidative addition into Pd and Pt catalysts. These processes are key steps in alkyne hydrosilylation or alkyne silaborylation respectively.

In a B–C(sp^2)/B–B transborylation strategy, alkenyl boranes can exchange boron groups with diboranes, although computational studies indicate that this process does not proceed through σ-bond metathesis.[298] Instead, activation of the diborane with a methoxide anion generates a nucleophilic boron species **4-IV** capable of attacking the electrophilic alkenyl borane. This leads to the formation of a quaternised alkenyl boron-ate species **4-V** and alkoxyborane, MeOBdan (**Scheme**

4-6). The transborylation step proceeds by a 1,2-alkenyl shift to give **4-VI.** Subsequent reaction of **4-VI** with alkoxyborane MeOBdan gives the transborylated alkenyl borane product. It could be anticipated that the greater electrophilicity of Bpin in comparison to Bdan would lead to selective boron-ate formation at the Bpin position when pinBBdan reacts with methoxide. This would result in the transfer of the Bdan moiety to the alkenylborane. However, this transfer does not occur, and computation studies suggest that this transfer would be energetically unfavourable. Consequently, the kinetically accessible alkenylBpin product is formed instead.

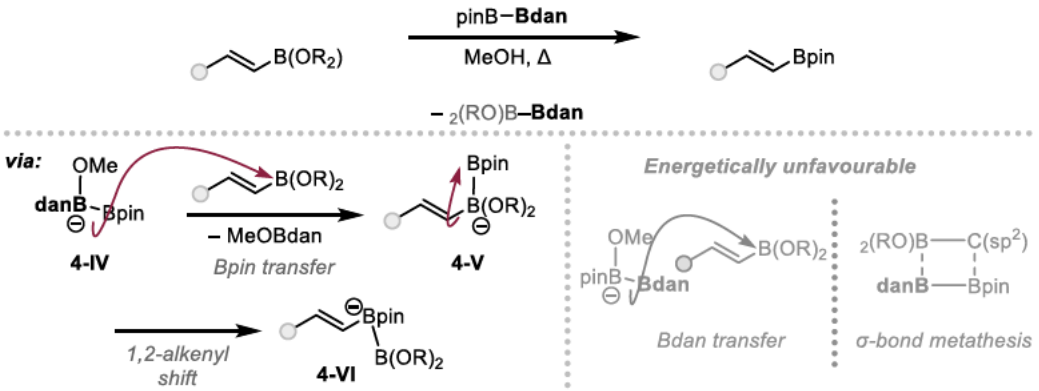

Scheme 4-6. MeOH-promoted transborylation of alkenyl boranes with diboranes.

Despite the diminished Lewis acidity at boron, allyl Bdan reagents (**4-VII**) can be used for the allylation of aldehydes when activated with $Et_2O{\bullet}BF_3$ (**Scheme 4-7**).[299] BF_3 is proposed to coordinate to the nitrogen lone pair, rendering the allyl borane reagent more electrophilic. The high diastereoselectivity of the resulting alkenes (**4-VIII**) is suggestive of a closed transition-state structure. The allyl Bdan reagents (**4-VII**) applied in this reaction also contain Bpin at the homo-allylic position. The resulting products therefore become allyl boronic esters (**4-VIII**), which can undergo further allylation reactivity. These compounds (**4-VII**) can therefore be used as synthetically valuable double allylation reagents.

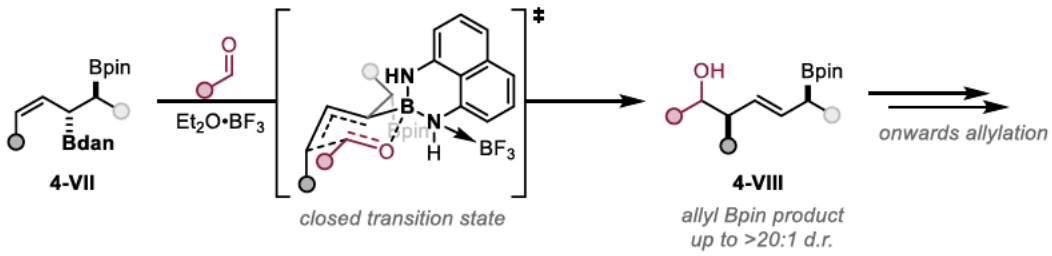

Scheme 4-7. BF_3-promoted allylation of aldehydes using allyl Bdan reagents.

4.1.3 Modification of *diaminonaphthalene* backbone

Modification of the diaminonapthalene fragment is also possible and this can be useful for modulating the photophysical properties of 1,3,2-diazaborinines. Insertion into the N–H bond of Bdan was achieved using a palladium-catalysed

Larock-type cyclisation; hexagonal ring-fused NBN phenalenes (**4-IX**) were prepared from *ortho*-bromo aryl Bdan compounds with alkynes in this way (**Scheme 4-8**).[300] This approach provides a convenient route to a diverse library of substitution patterns on the phenalene ring, which can allow fine-tuning of the photophysical properties.

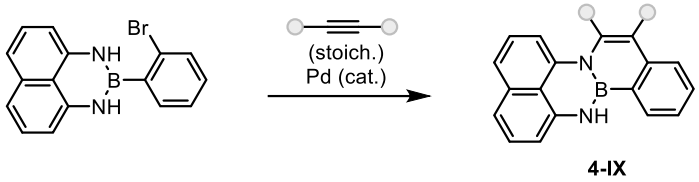

4-IX

Scheme 4-8. Pd-catalysed Larock-type cyclisation of o-bromo aryl Bdan reagents with alkynes.

Friedel-Crafts acylation on the aryl backbone of Bdan can also be used to modulate the photophysical properties of Bdan-containing compounds. PhBdan reacts under Sugasawa conditions (BCl_3, $AlCl_3$, MeCN),[301] or with trifluoracetic anhydride with base to give *ortho*-substituted $–CH_3$ (**4-X**) or $–CF_3$ (**4-XI**) ketones, respectively (**Scheme 4-9.i**).[269] *para*-Substituted ketones (**4-XIII**) could be prepared by using the Sugasawa conditions on 1,8-diaminonaphthalene, prior to installing the boron fragment through a condensation with a boronic acid (**Scheme 4-9.ii**). Ketone substitution on the diaminonaphthalene backbone leads to decreased HOMO-LUMO gaps and significantly stronger fluorescence in comparison with PhBdan. These properties make diamine **4-XII** an ideal chemosensor for boronic acids – widely used in the pharmaceutical industry in SMC reactions,[302] yet are suspected to be hazardous to health.[303] The ability to detect boronic acids is therefore crucial, and it was shown that diamine **4-XII** can detect trace quantities (1-20 ppm) of $PhB(OH)_2$; a concentration that would be challenging using alternative spectroscopic techniques.

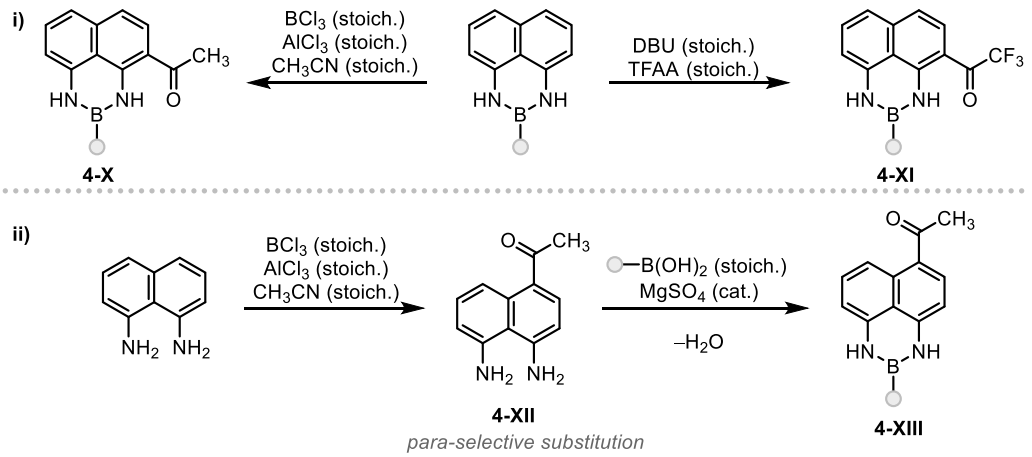

Scheme 4-9. i) Friedel-Crafts acylation of arylBdan results in o-substituted products; ii) Friedel-Crafts acylation of 1,8-diaminonaphthalene results in p-substituted products.

The quantum yield of Bdan-containing compounds is known to increase upon aggregation in what is termed Aggregate Induced Emission (AIE).[269,272,273] Restricted intramolecular rotation in the solid-state prevents the excited state from decaying by non-radiative pathways (**Scheme 4-10**), giving rise to this phenomenon.[268] This property has potential for use in anti-counterfeiting ink[272] and for the sensitive detection of explosives (at ppb concentration), such as 2,4,6-trinitrotoluene (TNT), which quench the fluorescence as a result of hydrogen bond interactions.[273] Applications of Bdan-containing molecules as fluorescent probes also include fluoride[270] and Cr^{3+}/Fe^{3+} ion detection.[271]

Scheme 4-10. Rotational freedom in solution state vs solid-state.

4.1.4 Strategies for installing Bdan

Commonly, Bdan-containing compounds are synthesised through the condensation of the corresponding boronic acid with 1,8-diaminonaphthalene (**Scheme 4-11.i**).[285,304] Alternatively, pinacolboronic esters can undergo transesterification with 1,8-diaminonaphthalene in the presence of $FeCl_3$ and imidazole ($C_3N_2H_4$; **Scheme 4-11.ii**).[305] Although these strategies are reliable and high-yielding, they require the boron functionality to be pre-installed in the starting material.

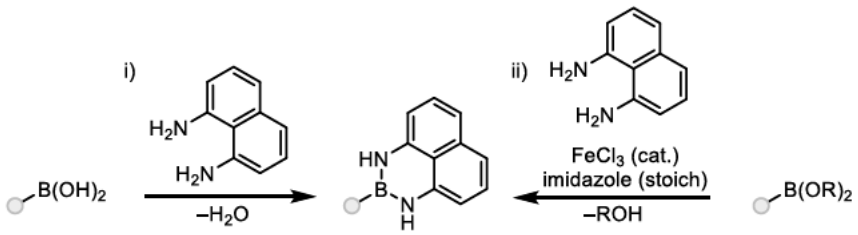

Scheme 4-11. Synthesis of RBdan through i) condensation or ii) transesterification.

Olefins are an abundant chemical feedstock, making them cheaper and more widely available than compounds already containing boron functionality. It is therefore important to develop protocols that directly transform olefins into value added products. In this regard, copper(I)–boryls have emerged as exceptional catalysts for

olefin borylation reactions, as borylcupration readily proceeds with a range of olefins.[306]

Since copper(I)–boryls are conveniently prepared through a Cu–O/B–B σ-bond metathesis pathway (**Scheme 4-12.i**), diboranes have gained traction as valuable boron-installing starting materials in combination with a copper alkoxide catalyst. To generate Cu–Bdan, pinBBdan is used. The selectivity in the formation of Cu–Bdan over Cu–Bpin can be explained by the diminished Lewis acidity of the Bdan fragment, rendering Bpin more susceptible to attack by the alkoxide, thereby generating alkoxyBpin as the by-product.[307,308] The regioselectivity for borylcupration is governed by the Lewis acidity at boron: for more Lewis acidic boranes such as Bpin, borylcupration proceeds with anti-Markovnikov selectivity to give linear borylated products; for less Lewis acidic boranes such as Bdan, the branched product is formed instead (**Scheme 4-12.ii**).[309]

Turnover of the organocopper intermediate is often achieved using electrophiles with oxygen-containing leaving groups (**Scheme 4-12.ii**), which leads to regeneration of the Cu–O bond. These turnover reagents have included: methanol, resulting in protoborylation;[310] hydroxylamines, leading to aminoboration;[308] alkoxystannanes, inducing borylstannation[311] and allylic phosphates, giving rise to borylallylation.[312] Alternatively, transmetallation of the organocopper intermediate with Pd(II) enables cross-coupling with aryl halides (**Scheme 4-12.iii**).[313]

In certain substrates, borylcupration results in the copper centre being located at the β-position to a leaving group (LG). β-Elimination of Cu–LG delivers the unsaturated product and provides catalyst turnover (**Scheme 4-12.iv**). This approach has been used to transform allylic phosphates into allylic Bdan products,[310] and to generate allenyl Bdan species from propargylic alcohols (in the presence of $Ti(O\textit{i}Pr)_4$)[314] or from propargyl-gem dichlorides.[315]

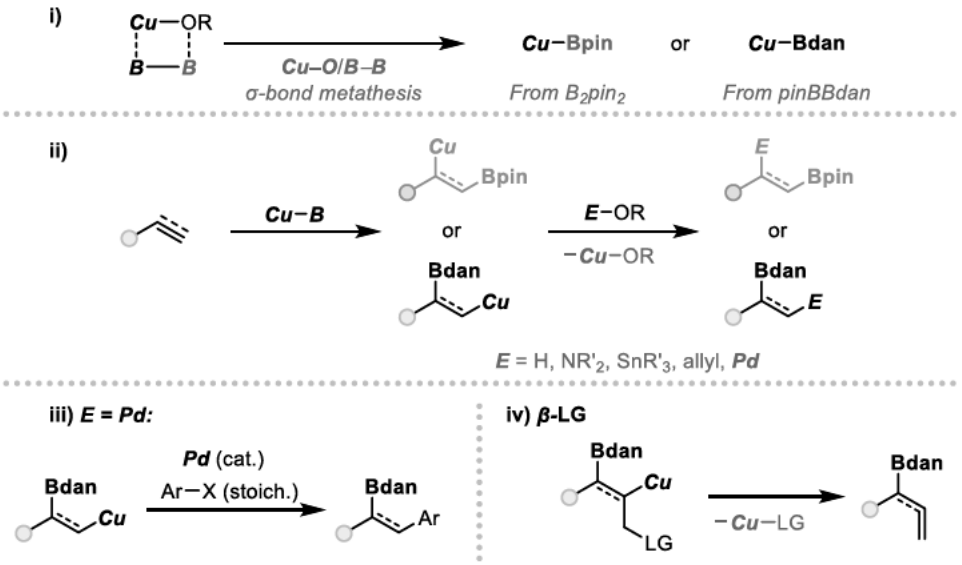

Scheme 4-12. i) σ-bond metathesis between Cu-OR and diboranes generate Cu-boryls. ii) Selectivity of Cu-boryl addition across olefins depends on electronics at boron; resulting organocopper reagents can react with electrophiles. iii) Transmetallation with a Pd-catalyst enables cross-coupling with aryl halides. iv) β-elimination of Cu–LG generates unsaturated products.

Although copper catalysis dominates for the introduction of Bdan into a molecule using pinBBdan, other transition metals have also been used. In these cases, a transition metal-boryl complex is also thought to be involved. In the cobalt-catalysed 1,1-diborylation of alkynes with pinBBdan, the reaction proceeds by Co–C(*sp*)/B–B exchange (**Scheme 4-13.i**).[316] Meanwhile, the palladium-catalysed borylation of aryl halides with pinBBdan is thought to proceed by Pd–O/B–B exchange from the L_n•Pd(Ar)–OAc intermediate (**Scheme 4-13.ii**).[317]

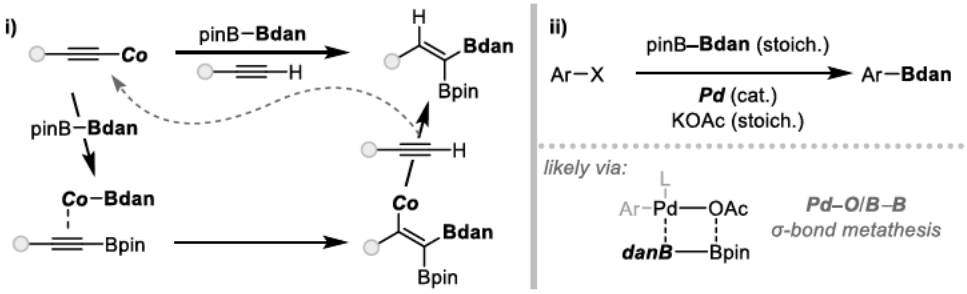

Scheme 4-13: i) Co-catalysed 1,1-diborylation of alkynes with diboranes. ii) Pd-catalysed borylation of ArX with diboranes.

Various transition metal-free approaches have also been reported for the borylation of substrates with pinBBdan. Pioneered by the Fernández group, alkoxide activation of pinBBdan generates a nucleophilic Bdan moiety (**4-XIV**) that can react at electrophilic sites, such as α-β-unsaturated ketones,[318] alkenes,[319] alkynes[320] or diaryliodonium salts[321] to give β-borylketones, 1,2-diboryl alkanes, 1,2-diborylalkenes or borylated arenes respectively (**Scheme 4-14.i**). Substrate activation of pinBBdan

is also possible (**Scheme 4-14.ii**). Examples include: alkynyl esters, to give 1,1-diboryl alkenyl esters;[322] alkynamides, which give *trans*-1,2-diboryl alkenamides;[323] and diazoalkanes, to give 1,1-diborylalkanes.[324] A Sandmeyer-type reaction has also been used to convert anilines directly into arylBdan compounds using pinBBdan (**Scheme 4-14.iii**).[325]

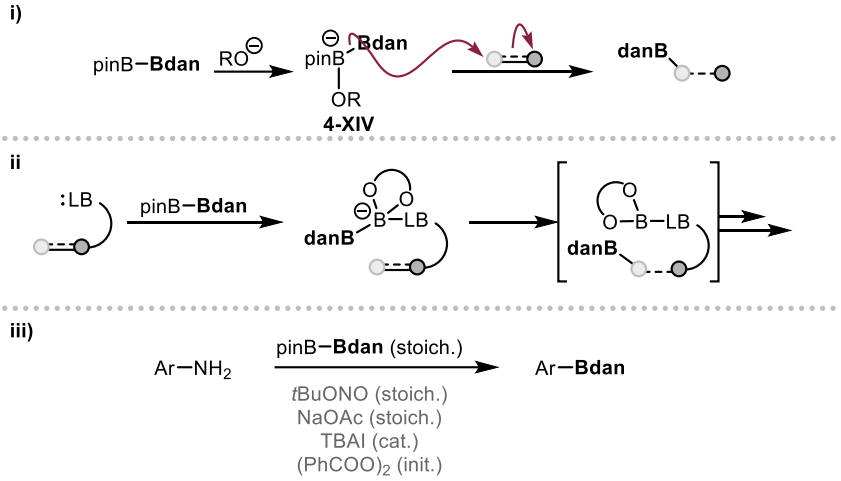

Scheme 4-14. i) Alkoxide activation of pinBBdan. ii) Substrate activation of pinBBdan. iii) Sandmeyer-type reaction to generate arylBdan from anilines.

Evidently, pinBBdan is a versatile reagent for the installation of Bdan into a variety of substrates. However, the loss of the Bpin moiety (if it is not present in the final product) accounts for a significant loss of atom economy. Where only the Bdan component is desired in the product, use of HBdan instead would give a more atom efficient process. Despite this, there are significantly fewer examples of HBdan being used in synthesis.

The diminished reactivity of HBdan typically requires the use of a transition metal catalyst to induce reactivity. C–H borylations of arenes,[326] alkenes[327] and alkynes[328] with HBdan have been achieved using iridium, rhodium and zinc catalysis respectively, leaving H_2 as the only by-product.

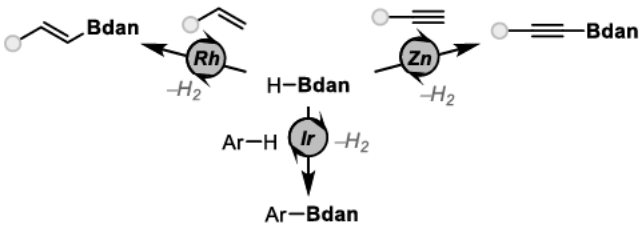

Scheme 4-15. Dehydroborylation of alkenes, olefins and arenes using catalysis.

Only two examples of olefin hydroboration with HBdan have been reported – in both cases, alkynes were used. The copper hydride-catalysed *cis*-hydroboration of alkynes with HBdan proceeds by hydrocupration of the alkyne, followed by σ-bond metathesis of the resulting alkenyl cuprate with HBdan to deliver the alkenylBdan product and regenerate the Cu–H catalyst (**Scheme 4-16.i**).[329] In contrast, the ruthenium-catalysed *trans*-hydroboration of alkynes with HBdan proceeds through the addition of a Ru–Bdan complex across the alkyne (**Scheme 4-16.ii**). Although boryl-metallation initially forms the *cis*-product, steric repulsion between the bulky NHC ligand on ruthenium with the Bdan moiety causes rapid isomerisation to the *trans*-product, either *via* Ojima's proposed Zwitterion[330] (**4-XV**) or Crabtree's proposed metallacyclopropane.[331] Turnover is again achieved through σ-bond metathesis with HBdan, delivering the (*Z*)-alkenyl diazaborinine product and regenerating the Ru–Bdan catalyst.[332]

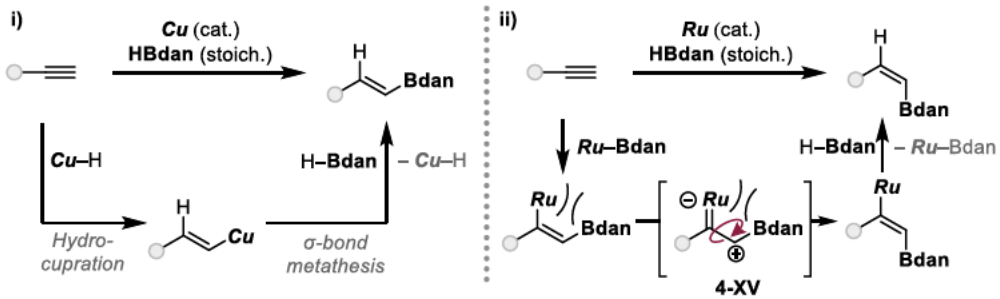

Scheme 4-16. i) Cu-catalysed cis-hydroboration of alkynes with HBdan; ii) Ru-catalysed trans-hydroboration of alkynes with HBdan.

It is worth noting that no examples of alkene hydroboration with HBdan could be identified (**Scheme 4-17.i**). Only two examples of formal alkene hydroboration to make alkylBdan have been reported, but these instead use the diboranes pinBBdan[333] or B_2dan_2[334] as the boron source. In the example with pinBBdan (**Scheme 4-17.ii**),[333] a copper photocatalyst (Cu-PC) is thought to generate a reactive boryl radical (•Bdan) from pinBBdan. The alkene then intercepts the boryl radical (•Bdan) to give an alkyl radical, which subsequently reacts with H_2O to give the alkylBdan product.[333] In the example with B_2dan_2 (**Scheme 4-17.iii**),[334] a boron-ate

species is generated with KO*t*Bu. This boron-ate species undergoes transmetallation onto a copper alkoxide catalyst, forming a Cu(I)–Bdan species, which can add across styrenes. The resulting η^3-benzylcopper species **4-XVI** is then protonated with HO*t*Bu to give the alkylBdan product and regenerate the copper alkoxide catalyst.[334]

Most synthetic approaches towards alkylBdan compounds instead rely on addition across alkenylBdan species (**Scheme 4-17.iv**). Enantioselective reduction of alkenylBdans to alkylBdans was achieved using cobalt catalysis with H_2,[335] or with copper catalysis, combining ROH with $R_3Si–H$ to formally hydrogenate the double bond.[336] Hydrometallation of alkenylBdan substrates has the added benefit of allowing the resulting alkyl copper intermediate to react with suitable electrophiles (**Scheme 4-17.iv**), such as Michael acceptors,[337] or undergo transmetallation with a palladium catalyst to enable onwards cross-coupling with aryl halides.[313]

The stability of Bdan compounds towards nucleophiles allows for compatibility with organometallic reagents. Alkyl (and aryl) Bdan species could be synthesised by the direct reaction of Grignard reagents with HBdan (**Scheme 4-17-v**).[338] Enantioenriched 3,3-borylalkyl esters and thioesters were generated by enantioselective conjugate addition of organocuprates to β-borylated α,β-unsaturated esters and thioesters (**Scheme 4-17-vi**).[339] The enhanced stability of Bdan towards alcoholysis compared to Bpin also allows alkylBdan to be synthesised from 1,2-diborylalkanes by selective protodeborylation of the Bpin moiety in the presence of base and refluxing methanol (**Scheme 4-17-vii**).[319]

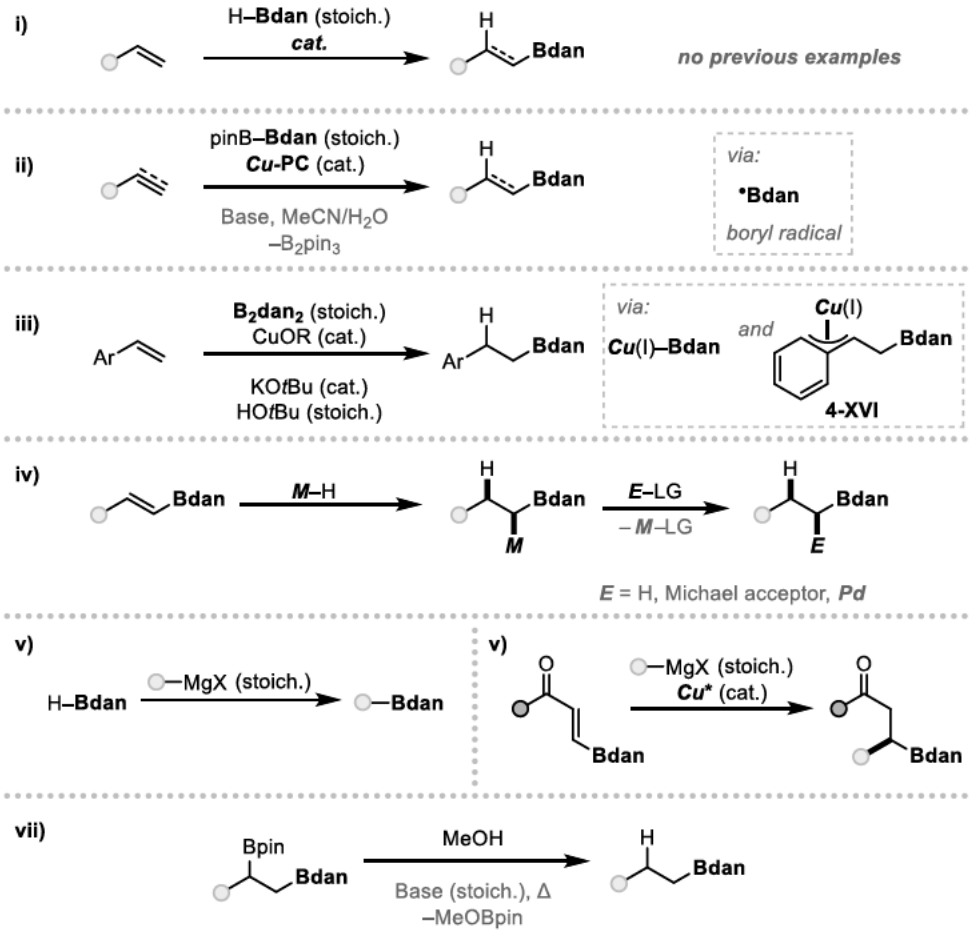

Scheme 4-17. Strategies for synthesising alkylBdan: i) No examples of alkene hydroboration with HBdan. ii) Formal hydroboration of olefins using pinBBdan and H_2O, mediated by a Cu-photocatalyst. iii) Metal hydride-catalysed hydrofunctionalisation of alkenylBdan. iv) Stoichiometric reaction of aryl and alkyl Grignards with HBdan. v) Cu-catalysed asymmetric addition of Grignard reagents to β-borylated α,β-unsaturated esters and thioesters. vi) Selective proto-deborylation at the Bpin site gives access to alkylBdan.

4.2 Aims and objectives

We aimed to address the absence of alkene hydroboration with HBdan in the literature. Although 1,8-diaminonaphthalene is an exceptional protecting group for boron, we wished to probe the limits of Al–C/B–H σ-bond metathesis by using HBdan in place of HBpin. The enhanced stability of HBdan towards nucleophiles compared with HBpin may also lead to a change in mechanism, particularly if HBdan does not decompose to BH_3 under the reaction conditions as observed for HBpin (see **Chapter 3**). The scope and limitations of the protocol would be examined and we wished to demonstrate the synthetic utility of alkylBdan compounds.

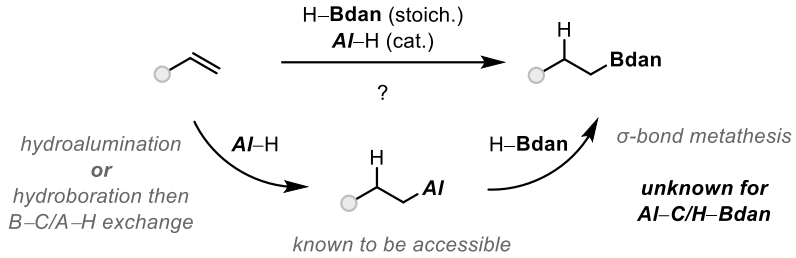

Scheme 4-18. Potential mechanistic pathway for aluminium hydride-catalysed alkene hydroboration with HBdan.

4.3 Results and discussion

In Chapters 2 and 3, the capacity of alkyl alanes to react with HBpin under mild conditions by Al–C(sp^3)/B–H σ-bond metathesis was demonstrated **(Scheme 4-19.i**). Extending this reactivity for the less Lewis acidic and less reactive HBdan (**Scheme 4-19.ii**) would further highlight the capability for Al–C(sp^3) species to engage in σ-bond metathesis with H–B compounds, and provide a new atom-economic platform to generate alkylBdan compounds from alkenes.

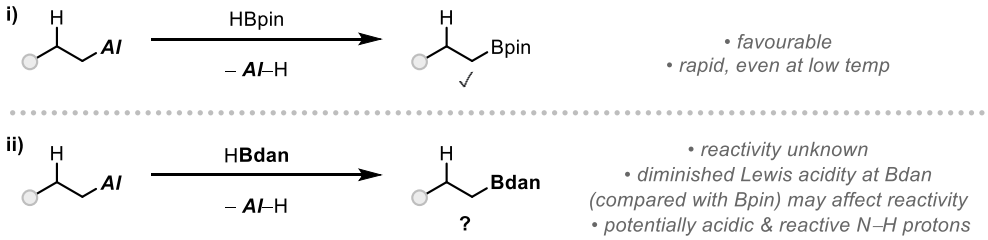

Scheme 4-19. i) Al-C(sp^3)/B-H exchange with HBpin is favourable. ii) Al-C(sp^3)/B-H exchange with HBdan is unknown. Challenges presented.

4.3.1 Stoichiometric reactivity

The study began by probing the stoichiometric reactivity between HBdan and ^{Mes}TerAlEt$_2$ (**Scheme 4-20.i**). Using ^{11}B NMR spectroscopy to monitor the formation of new boron species, ^{Mes}TerAlEt$_2$ was reacted with excess HBdan (5 equiv.) at room temperature for 16 hours. Although ^{Mes}TerAlEt$_2$ reacted rapidly with HBpin at room temperature (full conversion within 30 mins), the reaction with HBdan was much slower, giving only a 26% yield of EtBdan after 16 hours. Presumably the diminished Lewis acidity of HBdan in comparison to HBpin renders it less reactive towards alkyl alanes. However, the formation of the new alkylBdan species remained encouraging, and raising the temperature to 80 °C led to an 86% yield of EtBdan over the same time. Notably, no *m*-terphenylBdan products were observed, indicating that the σ-bond metathesis pathway was selective for the alkyl group over the bulky aryl group, even at the elevated temperatures.

Al–C(sp^3)/B–H σ-bond metathesis with HBdan was not specific only to *m*-terphenyl-substituted alanes; Et$_3$Al also reacted with HBdan (5 equiv.) in toluene to give EtBdan, albeit with reduced yields (24% at rt or 35% at 80 °C; **Scheme 4-20.ii**). Et$_3$B was also generated as a by-product (0.47 equiv. at 80 °C), which was notably absent for ^{Mes}TerAlEt$_2$. This inferred that the bulky *m*-terphenyl group could help prevent decomposition pathways (for example, “dan” transfer from B to Al).

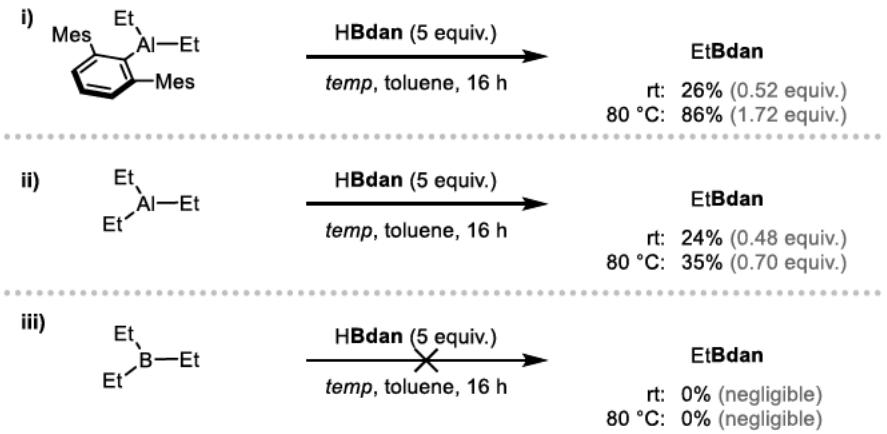

Scheme 4-20. Reactivity of HBdan with i) ^{Mes}TerAlEt$_2$; ii) AlEt$_3$; iii) BEt$_3$

The reaction between Et_3B and HBdan (5 equiv.) in toluene led to no observable formation of EtBdan, even at 80 °C (**Scheme 4-20.iii**). This further demonstrated that exchange between B–H reagents with alkyl alanes is significantly more favourable than for alkyl boranes. Presumably, the thermodynamic driving force for the formation of a stronger B–C bond from a weaker, longer and more polarised Al–C(sp^3) bond can explain this enhanced reactivity. Like the analogous transformation with HBpin, this experiment also strengthens the argument that alkyl alanes, rather than alkyl boranes, are key intermediates for t he synthesis of alkylBdan.

With the knowledge that alkyl alanes can react with HBdan to generate alkylBdan products under stoichiometric conditions, the potential application of this stoichiometric reactivity in catalysis was investigated.

4.3.2 Catalytic hydroboration - optimisation

A series of aluminium compounds were evaluated for their catalytic capabilities for alkene hydroboration with HBdan, using 4-*t*Bu-styrene as a model substrate (**Table 4-1**). Most of the catalysts screened under the given conditions (toluene, 80 °C, 16 h) exhibited little or no reactivity (**Table 4-1**; entries 4-8, 10-11). Although the stoichiometric reaction of $AlEt_3$ with HBdan gave EtBdan, $AlMe_3$ showed no catalytic activity (**Table 4-1**; entry 8). This disparity may be attributed to unselective ligand exchange, giving ***Al–dan*** species and trialkylboranes. Smaller alanes, such as $Me_3N{\bullet}AlH_3$ (**Table 4-1**; entry 6) and $LiAlH_4$ (**Table 4-1**; entry 4), were not catalytically active at all, despite $LiAlH_4$ being utilised as a catalyst for alkene hydroboration with HBpin.[81] This observation can be attributed to the enhanced stability of HBdan towards nucleophiles compared to HBpin. Furthermore, $Me_2S{\bullet}BH_3$ did not give any product (**Table 4-1**; entry 5), consistent with the lack of reactivity between trialkylborane and HBdan under the specified conditions.

While $AlCl_3$ (**Table 4-1**; entry 10) and $(i\text{Bu})_2AlH$ (**Table 4-1**; entry 7) alone did not exhibit catalytic activity for the hydroboration of 4-*t*Bu-styrene with HBdan, combining the two reagents in a 2:1 ratio resulted in a 45% yield of the product (entry 12). Furthermore, Et_2AlCl also showed hints of reactivity (23% using 1.5 equiv. HBdan; **Table 4-1**; entry 9). These results imply that monochloroalanes, generated *in situ*, could be used as effective catalysts for this transformation. However, both of these approaches also produced other alkylBdan compounds (EtBdan or *i*BuBdan), which would pose challenges in the purification of the target alkylBdan compound. An attempt to generate chloroalane without alkyl groups by combining $AlCl_3$ and $LiAlH_4$ in a 2:1 ratio was found to be ineffective for catalysis (**Table 4-1**; entry 11).

Among the *m*-terphenyl-substituted alanes, only the smallest $^{p\text{-Tol}}TerAlH_2$ (**Table 4-1**; entry 1) did not give the product in greater than stoichiometric quantities with respect to the catalyst. In contrast, the larger $^{Mes}TerAlH_2$ (**Table 4-1**; entry 2) and $^{Tipp}TerAlH_2$ (**Table 4-1**; entry 3) catalysts gave full conversion to the alkylBdan product. In both cases, the reaction demonstrated regioselectivity for the linear product, as no branched product was observed in the crude ^1H NMR spectra. $^{Mes}TerAlH_2$ was eventually chosen for further optimisation due to its slightly enhanced performance at 10 mol% catalyst loading (47%, **Table 4-2**; entry 1) in comparison to $^{Tipp}TerAlH_2$ (34%, **Table 4-2**; entry 5).

Table 4-1. Evaluation of catalysts

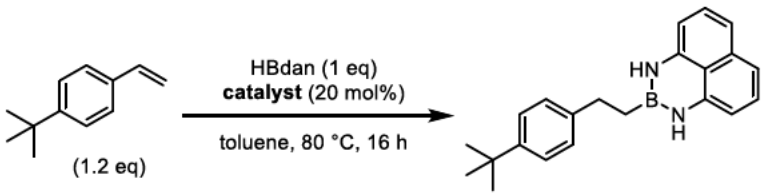

Entry	Catalyst	Yield
1	$^{p\text{-Tol}}$TerAlH$_2$	18%
2	^{Mes}TerAlH$_2$	>95%
3	^{Tipp}TerAlH$_2$	>95%
4	LiAlH$_4$	0%
5	Me$_2$S•BH$_3$	0%
6	Me$_3$N•AlH$_3$	0%
7	(*i*Bu)$_2$AlH	4%
8	AlMe$_3$	8%
9	AlEt$_2$Cl (1.5 equiv. HBdan)	23%
10	AlCl$_3$	0%
11	AlCl$_3$ (20 mol%) + LiAlH$_4$ (10 mol%)	< 2%
12	AlCl$_3$ (10 mol%) + (*i*Bu)$_2$AlH (20 mol%)	45% (HBdan consumed)*

*Stoichiometric formation of *i*BuBdan also formed, insinuating that chloroalanes might be catalytically active.

Efforts were made to reduce the catalyst loading from 20 mol%. In Chapter 3, a rate-enhancement effect of boranes paired with a Lewis base was found to enhance the ^{Mes}TerAlH$_2$-catalysed hydroboration of alkenes with HBpin in comparison to ^{Tipp}TerAlH$_2$ catalysis. Therefore, a range of additives were screened with the anticipation that the catalytic activity could similarly be enhanced for the synthesis of diazaborinines with HBdan. However, none of the screened additives delivered more product; rather, catalysis was diminished in each case (**Table 4-2**; entries 7–13). Catalyst poisoning was especially pronounced in the presence of THF (**Table 4-2**; entry 9), presumably due to the formation of a strong adduct with the alane catalyst This adduct likely hindered the aluminium catalyst from participating in the key hypothesised steps of alkene hydroalumination and σ-bond metathesis.

Table 4-2. Evaluation of conditions

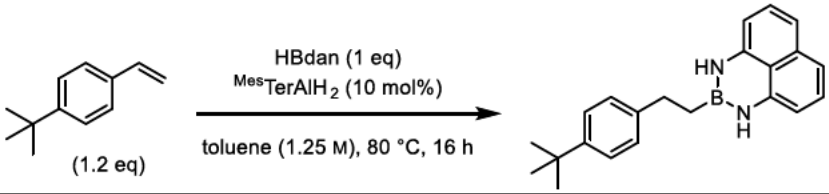

Entry	Deviation from standard conditions	Yield
1	none	47%
2	20 mol%	> 95%
3	5 mol%	13%
4	^{Tipp}TerAlH$_2$ instead of ^{Mes}TerAlH$_2$; 20 mol%	>95%
5	^{Tipp}TerAlH$_2$ instead of ^{Mes}TerAlH$_2$; 10 mol%	34%
6	^{Tipp}TerAlH$_2$ instead of ^{Mes}TerAlH$_2$; 5 mol%	13%
7	+ 20 mol% $Me_2S{\bullet}BH_3$	33%
8	+ 20 mol% SMe_2	20%
9	+ 20 mol% THF	5%
10	+ 20 mol% Et_2O	28%
11	+ 20 mol% Cy_2BH	45%
12	+ 20 mol% MeBpin	10%
13	+ 20 mol% HBpin	37%
14	**110 °C** instead of 80 °C	59%
15	**110 °C;** 1.1 eq. alkene instead of 1.2 equiv.	61%
16	**110 °C; 1.0 eq. alkene** instead of 1.2 equiv.	68%
17	**110 °C; 1.0 eq. alkene**; 1.2 eq. HBdan instead of 1.0 eq.	61%
18	**110 °C; 1.0 eq. alkene;** 2.5 M instead of 1.25 M	68%
19	**110 °C; 1.0 eq. alkene;** *neat* instead of 1.25 M	15%
20	**110 °C; 1.0 eq. alkene; 24 h** instead of 16 h	91%

The yield of the product could be enhanced by elevating the reaction temperature from 80 °C (47%, **Table 4-2**; entry 1) to 110 °C (59%, **Table 4-2**; entry 14). Adjusting the stoichiometry of the alkene from 1.2 equivalents to 1.0 equivalents (68%, **Table 4-2**; entry 16) yielded further improvements. Interestingly, increasing the stoichiometry of HBdan to 1.2 equivalents led to lower yields (61%, **Table 4-2**; entry 17). Increasing the concentration of the reaction to 2.5 M did not improve catalysis (68%, **Table 4-2**; entry 18). Running the reaction neat led to significantly lower yields (15%, **Table 4-2**; entry 19) despite the full consumption of alkene and HBdan. Instead, the reaction resulted in the formation of insoluble material, which was presumed to be polymeric. Finally, extending the reaction time to 24 hours (from 16 hours) gave the product in a satisfactory 91% yield (**Table 4-2**; entry 20).

4.3.3 Catalytic hydroboration - scope

Following optimisation of the reaction conditions, the scope and limitations of the protocol were assessed (Table 4-3). Styrenes substituted with inductively donating groups, 4-*t*Bu-styrene (**4-1b**; 91%) and 4-*i*Bu-styrene (**4-1c**; 78%), gave excellent to good yields under the optimised conditions, while unsubstituted styrene required a longer reaction time (48 h) to reach 82% yield (**4-1a**). Some steric bulk was tolerated at the *ortho*-position, with 2,4-dimethylstyrene giving an excellent yield (**4-1d**; 85%); however, no product was formed with the bis *ortho*-substituted 2,4,6-trimethylstyrene (**4-2b**). Presumably, the added steric bulk hinders the approach of HBdan towards the alkyl alane intermediate. Mono-substituted aliphatic alkenes, 1-octene (**4-1i**; 93%) and vinylcyclohexane (**4-1j**; 85%) proceeded smoothly, meanwhile vinyl norbornene gave slightly lower, yet still good yield (**4-1k**; 63%).

The tolerance of the hydroboration reaction to different functional groups was then tested. Alkenes containing arenes substituted with Lewis basic groups did not lead to (significant) inhibition of reactivity (**Table 4-2**) with good tolerance of methoxy (**4-1e**; 85%) and thioether (**4-1m**; 71%) substrates. *para*-Substituted halostyrene derivatives also reacted smoothly to give moderate to good yields (X = F, **4-1f**: 63%; X = Cl, **4-1g**: 42%; X = Br, **4-1h**: 78%). Tri*iso*propylsilyl protected 5-pentenol gave the diazaborinine **4-1l** in good yield (74%). 5-Bromo-1-pentene eventually gave moderate yields of diazaborinine **4-1n** but the reaction temperature had to be lowered to 45 °C to prevent side reactions with the alkyl bromide, presumably such as *N*-alkylation or catalyst decomposition by ***Al***–Br formation. Attempts to react ester **4-2a** led to no product formation, likely as a result of catalyst decomposition by preferential reduction of the ester rather than reactivity at the alkene. The resulting aluminium alkoxide might not react with HBdan due to the strength of the Al–O bond.[187]

It is perhaps interesting to point out that, although Bdan compounds have demonstrated extreme robustness under a variety of conditions, many of these alkylBdan compounds exhibited a degree of air-sensitivity which has not previously been mentioned in the literature. If these compounds have been left in air at room temperature, a purple hue is developed over the course of several hours or days, which possibly arises from slow oxidation of the 1,8-diaminonaphthyl moiety.[340] When these oxidised compounds were analysed by ^{11}B NMR spectroscopy, the same characteristic ^{11}B signal at *ca*. δ 32 was retained, suggesting that the boron centre remained unperturbed. Decomposition in this way may explain the significant reduction in yields for some isolated compounds in comparison to their NMR yields.

Table 4-3. Substrate scope.

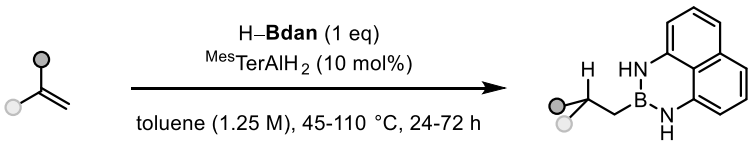

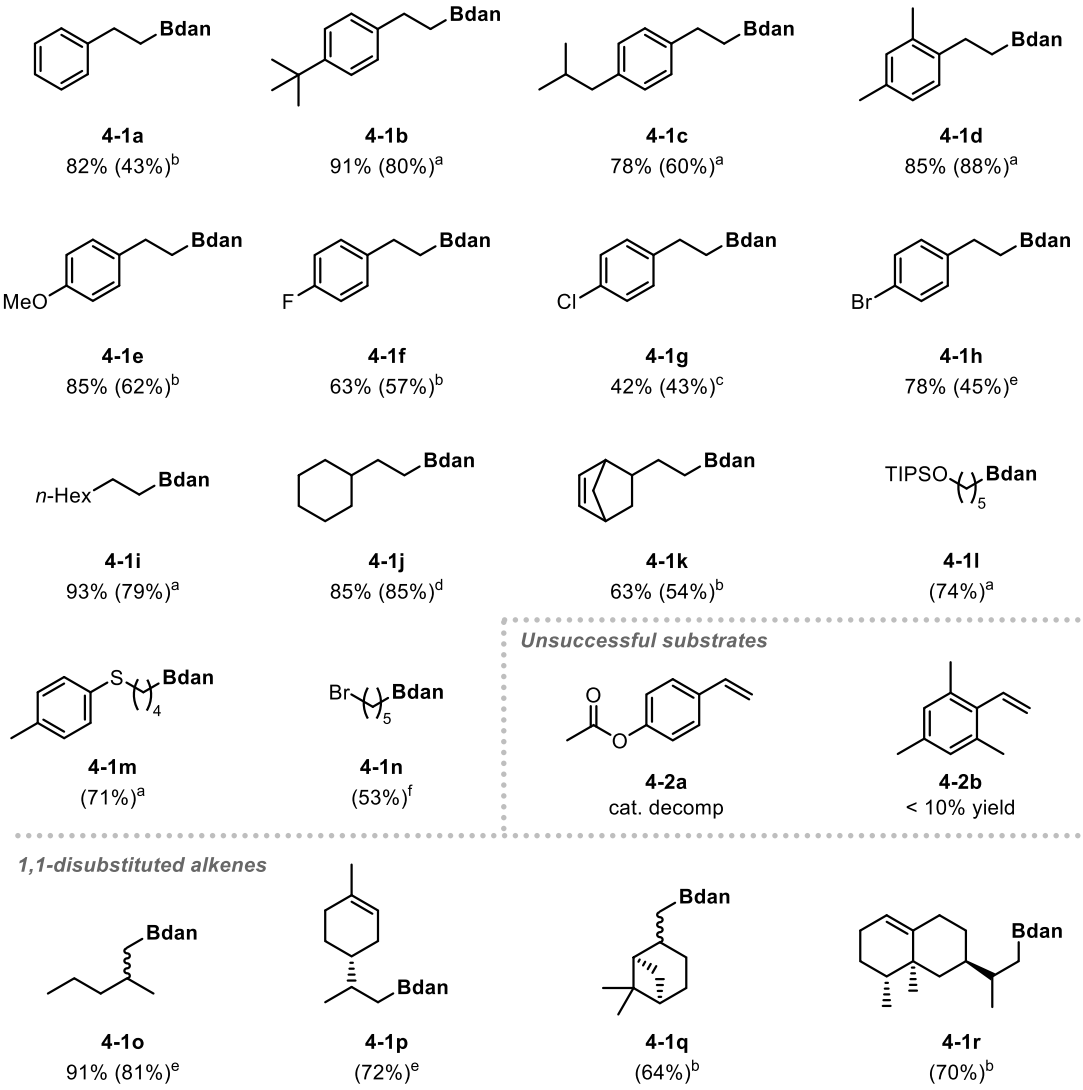

NMR yields provided where possible (isolated yields in parentheses). [a]Reaction performed at 110 °C for 24 h; [b]Reaction performed at 110 °C for 48 h; [c]Reaction performed at 110 °C for 72 h; [d]Reaction performed at 80 °C for 16 h, 20 mol% catalyst, 1.2 equiv. alkene; [e]Reaction performed at 110 °C for 24 h with 20 mol% catalyst; [f]Reaction performed at 45°C for 72 h.

Given that mono-substituted aliphatic alkenes reacted so efficiently under these conditions, it was questioned whether the scope could be extended towards the use of the more challenging and hindered 1,1-disubstituted alkenes. Indeed, the reaction proceeded smoothly for this substrate class, even for highly substituted alkyl fragments. The simplest alkene of this class, 2-methyl-1-pentene gave the corresponding product **4-1o** in excellent yield (91%). Terpenes, which are considerably bulkier and more complex in comparison, were also well tolerated. Limonene gave good yield of the corresponding diazaborinine (**4-1p**; 72%), as did valencene (**4-1r**; 70%) and the more sterically congested β-pinene (**4-1q**; 64%). This reactivity is promising, as the compatibility of prochiral substrates implies that enantioselective catalysis may be possible with the right, enantioenriched ligand system.

4.3.4 Derivatisations

With a variety of alkylBdan compounds prepared, synthetic applications of these compounds were investigated. As Bdan has been shown to be an effective protecting group for boron, alkylBdan was specifically applied under conditions that would not be tolerated for alkylBpin.

The fluorophilicity of boron means that the protodeborylation of boronic esters can generally be carried out using fluoride sources, such as CsF or *n*Bu_4NF, in the presence of H_2O.[341] However, arylBdan compounds have been reported to exhibit stability to fluoride anions.[278,279] To determine whether alkylBdan compounds would also demonstrate this stability, the deprotection of the siloxy-substituted pentylBdan **4-1l** with a fluoride source was attempted. **4-1l** was treated with excess *n*Bu_4NF (2 equiv.) in THF at room temperature for 16 hours and then quenched with brine. This resulted in the smooth formation of the corresponding alcohol **4-3a** (82%; **Scheme 4-21**), further establishing “dan” as a remarkable protecting group for boron towards fluoride anions.

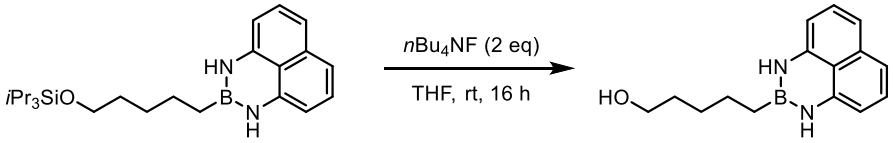

4-1l **4-3a**
82% (76% isolated)

Scheme 4-21. Tri*iso*propylsilylether (TIPS)-deprotection using *n*Bu_4NF in the presence of Bdan.

Next, functionalisation of the nitrogen atoms in Bdan was attempted. Hints of unwanted *N*-alkylation during the synthesis of Bdan alkyl bromide **4-1n** had already been observed. Under strongly basic conditions, the nitrogen atoms of the Bdan unit may be liable to selective deprotonation, leading to selective functionalisation. It was reasoned that this would also be a good experiment to test the stability of the Bdan protecting group towards strong bases. LiHMDS was selected as a strong, bulky and non-coordinating base. Thus, alkyl bromide **4-1n** was reacted with LiHMDS (1.5 equiv.) in THF at –78 °C and slowly warmed to room temperature overnight (**Scheme 4-22**). Analysis of the crude reaction mixture by ^{1}H NMR spectroscopy revealed the formation of the alkylated product **4-3b**, a 7-membered BN ring, in a 47% yield. The ^{1}H NMR spectrum also displayed resonances at δ 5.85 (ddt) and δ 5.02 (m) (**Figure 4-2**), suggesting that a new alkene species had formed, which was tentatively assigned as the E2-product, **4-3c**. For intermolecular alkylation, it would therefore be recommended to add the alkyl halide following complete deprotonation of the NH moiety.

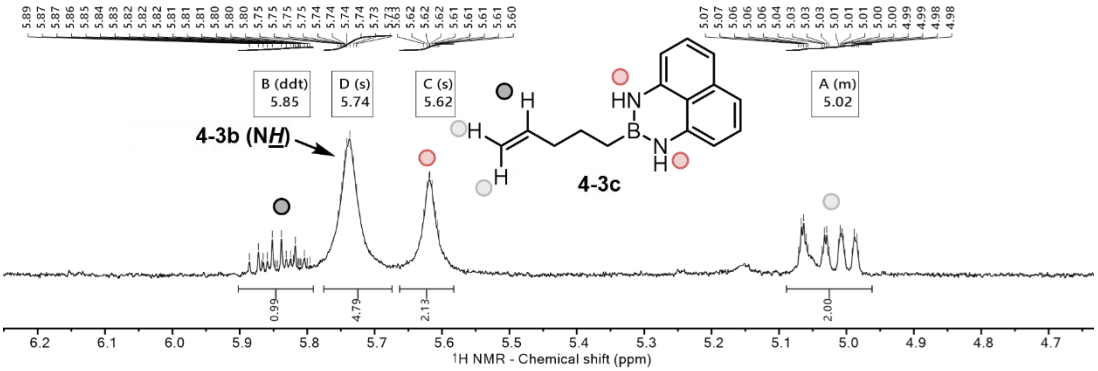

Figure 4-2. ^{1}H NMR spectrum ($CDCl_3$) of the crude mixture obtained following the reaction between alkyl bromide 4-1n and LiHMDS. The spectrum is zoomed in to highlight the formation of alkene resonances.

In a previous attempt to isolate *BN*-heterocycle **4-3b**, co-elution of the alkene **4-3c** in column chromatography resulted in contaminated product. Having previously isolated alcohol **4-3a** from the *i*Pr$_3$SiO-deprotection reaction with *n*Bu$_4$NF, it was known that transformation of alkene **4-3c** to the more polar alcohol **4-3a**, by hydroboration/oxidation, would lead to a more facile isolation of *BN*-heterocycle **4-3b** by column chromatography. It was also reasoned that this would be a good approach to test the stability of the Bdan moiety under oxidative conditions. Thus, a THF solution of the crude reaction mixture containing *BN*-heterocycle **4-3b** and alkene **4-3c** was treated with THF•BH_3 (0.8 equiv. with respect to **4-3c**) for 1 hour (rt), followed by sodium perborate (2 equiv. with respect to **4-3c**) for 2 hours (rt). The alkene **4-3c** was fully converted to the corresponding alcohol **4-3a**, allowing *BN*-heterocycle **4-3b** to be cleanly isolated following column chromatography in a

42% yield. This corresponded to an 89% recovery of the *BN*-heterocycle **4-3b** present in the crude material, showing that alkylBdan is largely stable to sodium perborate, even though this reagent is regularly used to oxidise pinacolboronic esters and other organoboranes.[342,343]

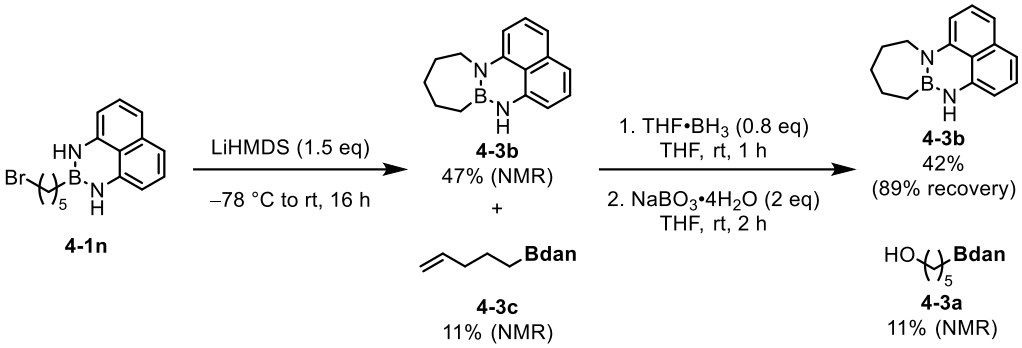

Scheme 4-22. N–H deprotonation with LiHMDS followed by cyclisation, and compatibility with $NaBO_3•4H_2O$.

The compatibility of alkylBdan with other oxidising agents was next explored. Initially, oxidation of the sulfide **4-1m** to the sulfoxide **4-3d** was attempted using *m*-CPBA in CH_2Cl_2, but this led to the immediate formation of a dark purple solution (Table 4-4; entry 1), reminiscent of the colour that alkylBdan compounds formed after exposure to air (O_2) for several days. This decomposition product has not been identified, but it was suspected that this could be caused by electrophilic oxidation on the 1,8-diaminonaphthyl group.[340] Electrophilic acylation of arylBdan has been reported on the *ortho*-position of the "dan" fragment (**Scheme 4-9.i**); a consequence of the HOMO lying on the "dan" backbone (as opposed to the B–aryl group).[269]

To overcome this issue, the oxidation was attempted with a less electrophilic reagent than *m*-CPBA. Thus, H_2O_2 (1 equiv.) was reacted with the sulfide **4-1m** in a solution of EtOH at room temperature over 48 hours and the sulfoxide **4-3d** was obtained in a 42% yield (**Table 4-4**; entry 2). The moderate yield can perhaps be explained by the low solubility of the sulfide **4-1m** in EtOH which resulted in longer reaction times and a darkening of the solution over time, implying unselective oxidation. Other solvent systems involving THF were also attempted, and while this helped with solubility, this did not improve yields (**Table 4-4**; entry 4). Although some compatibility with H_2O_2 was observed, these attempts demonstrated that alkylBdan is much more stable towards nucleophilic oxidation reagents, such as sodium perborate.

Table 4-4. Optimisation for sulfide oxidation in the presence of Bdan.

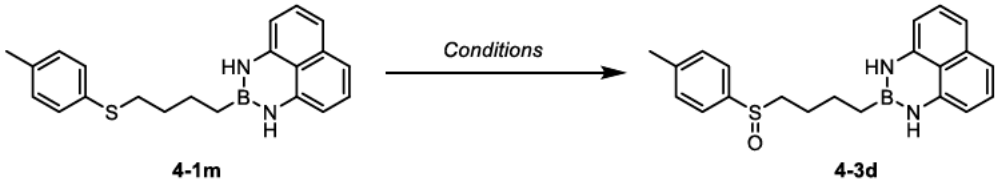

Entry	Conditions	Yield
1	*m*-CPBA (1.05 equiv.); CH_2Cl_2, –78°C to rt, 16 h	Decomp
2	H_2O_2 (1 equiv.); EtOH, rt, 48 h	42% (33% isolated)
3	H_2O_2 (3.5 equiv.); EtOH, rt, 48 h	17%
4	H_2O_2 (3.5 equiv.); THF, rt, 48 h	25%

4.3.5 Mechanistic insights

Having previously unravelled the mechanism for *m*-terphenyl alane-catalysed alkene hydroboration with HBpin (see **Chapter 3**), we were curious to determine to what extent the enhanced stability of HBdan in comparison to HBpin would impact the mechanism. In both these protocols, it has been established that the reactions must proceed through alkyl alane intermediates (**Scheme 4-23**). These react with the hydridoborane by an Al–C(sp^3)/B–H exchange to generate the alkyl–Bpin or –Bdan products. Although hidden boron catalysis can explain the reactivity of other systems,[188,189] alkyl boranes did not appreciably react with HBpin or HBdan under the reaction conditions, so this pathway can be excluded.

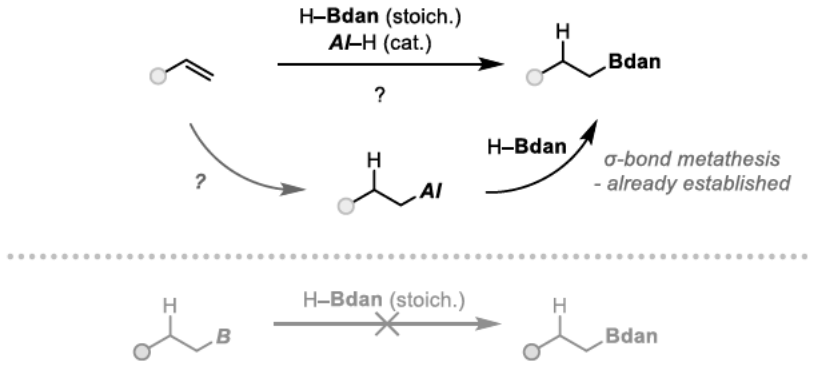

Scheme 4-23. Summary of known features about the mechanism.

Firstly, the formation of the alkyl alane intermediate in the Bdan system was investigated. It is well established that alkyl alanes can be made through alkene hydroalumination.[344] However, **Chapter 3** revealed the possibility of an alternative pathway for alkyl alane formation when BH_3 is formed under reaction conditions. This

pathway instead proceeds by alkene hydroboration with BH_3 to give alkyl boranes, which react with aluminium hydrides by Al–H/B–C(sp^3) exchange to give the alkyl alanes. While this route efficiently generates alkyl alanes and enhances catalytic rates (see **Chapter 3**), the formation of BH_3 can pose challenges in situations where stereocontrol or functional group tolerance is important.

The formation of BH_3 under catalysis reaction conditions was probed using the TMEDA-quenching experiment described by Bage *et. al.*[188] (see **Chapter 3, section 3.3.2** for details). Thus, the reaction between ^{Mes}TerAlH_2 and HBdan (10 equiv.) in toluene at 110 °C (standard catalytic conditions without the substrate) was quenched with TMEDA (50 equiv.) after 16 hours. Analysis of the reaction mixture by ^{11}B NMR spectroscopy revealed the absence of TMEDA•BH_3, suggesting that BH_3 was not formed under the reaction conditions (**Scheme 4-24.i**). Instead, the only observable boron species was HBdan. This showed that HBdan is considerably more stable to the aluminium hydride catalyst than HBpin, and suggests that the alkyl alane intermediate is formed by alkene hydroalumination rather than *helper borane catalysis* (see Chapter 3).

To gain further insight into the species formed under catalysis, the reaction between ^{Mes}TerAlH_2 and HBdan (5 equiv.) in C_6D_6 was monitored by ^{11}B NMR spectroscopy (**Scheme 4-24.ii**). At room temperature, the formation of a broad singlet at δ –5 was observed in addition to the ^{11}B signal for HBdan (**Scheme 4-24.ii.a**). The ^{11}B resonance at δ –5 was tentatively attributed to the formation of a ^{Mes}TerAlH_2•HBdan adduct, possibly featuring bridging hydrides between aluminium and boron. The chemical shift was upfield compared to another known 4-coordinate Bdan structure in the literature ([*t*BuO•PhBdan]K: δ^{11}B = –1).[290] The formation of an adduct, rather than of $[H_2Bdan]^-[\boldsymbol{Al}]^+$, was corroborated by the disappearance of the ^{11}B signal at δ –5 when THF (25 equiv.) was added (**Scheme 4-24.ii.b.i**). This can be explained by preferential coordination of THF to the aluminium centre, resulting in HBdan being liberated.

When 4-*t*Bu-styrene (5 equiv.) was added to the reaction mixture containing the ^{Mes}TerAlH_2•HBdan adduct instead of THF, trace quantities of the corresponding alkylBdan product (δ^{11}B: 31) began to slowly form at room temperature (**Scheme 4-24.ii.b.ii**). In addition to this, the ^{11}B resonance at δ –5 remained, although the ^{1}H NMR spectrum displayed new resonances, which indicated that a new adduct had formed (**Scheme 4-25**; discussed below).

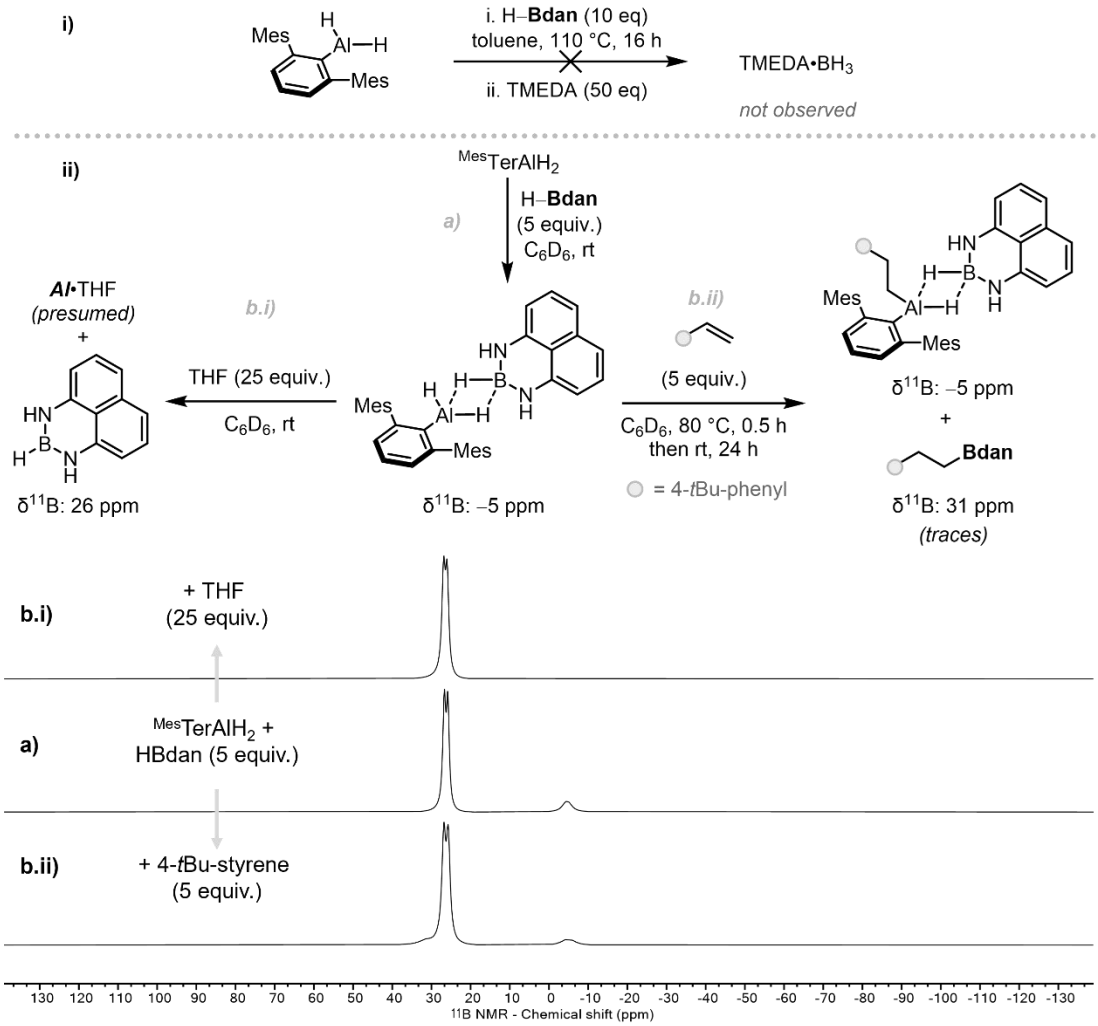

Scheme 4-24. i) TMEDA-quenching study. ii) Stacked ^{11}B NMR spectra (C_6D_6) of a) the reaction between ^{Mes}TerAlH$_2$ + HBdan (5 equiv.); b.i) following the addition of THF (25 equiv.) *or* b.ii) following the addition of 4-*t*Bu-styrene (5 equiv.)

The ^{1}H NMR spectrum for the reaction between ^{Mes}TerAlH$_2$ and HBdan (5 equiv.) further alluded to the formation of a ^{Mes}TerAlH$_2$•HBdan adduct (**Scheme 4-25.ii;** blue resonances). The resonances associated with [^{Mes}TerAlH$_2$]$_2$ (**Scheme 4-25.i**) disappeared in the presence of HBdan, giving rise to new signals for the *m*-terphenyl backbone (see resonances labelled as [Ar', *p*-H]; [Mes-H]; [Ar', *o*-H] and [Mes, CH_3]) alongside new signals attributed to a new *Bdan* fragment (see resonances labelled as *Al*•Bdan). In the presence of 4-*t*Bu-styrene (5 equiv.), similar but distinct signals were observed (**Scheme 4-25.iii;** red) alongside a resonance that was characteristic for the formation of AlC*H*$_2$R (δ^{1}H: –0.15, m, 2H), implying that alkene hydroalumination had occurred. In both cases, the integrations of the new *m*-terphenyl and Bdan signals suggested the formation of a 1:1 complex between aluminium and boron.

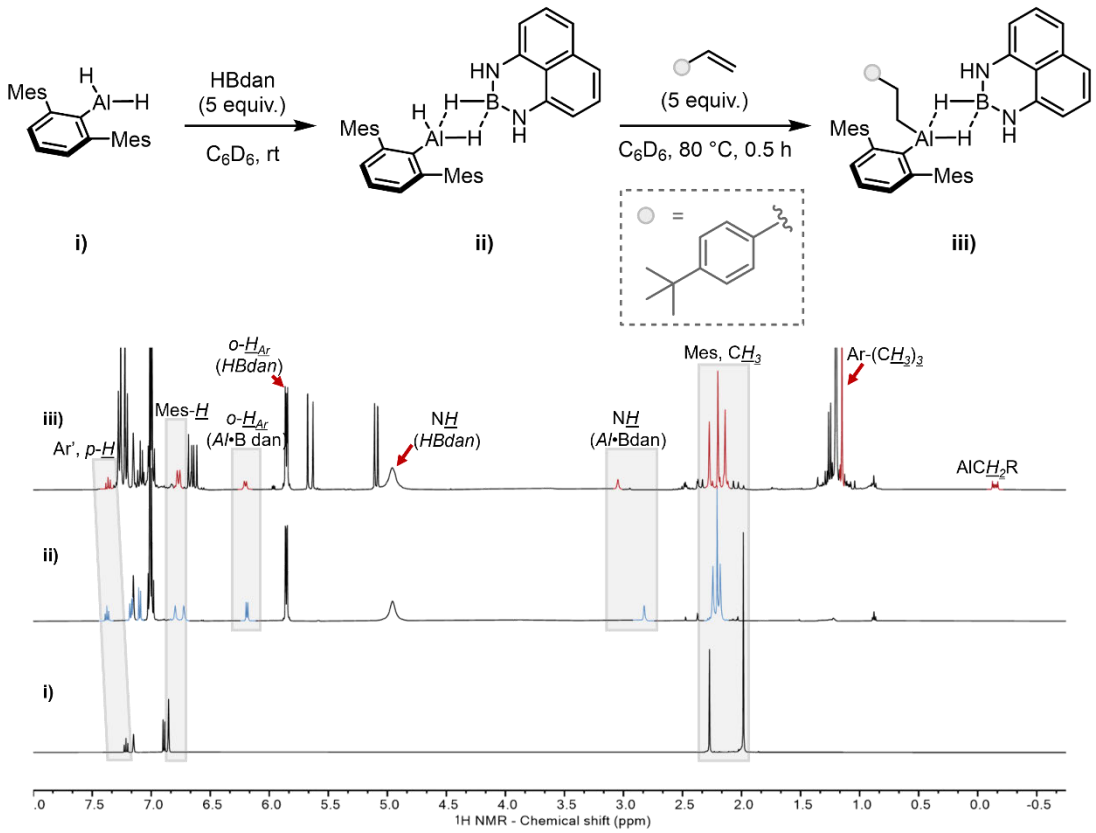

Scheme 4-25. Stacked ^{1}H NMR spectra (C_6D_6) of i) ^{Mes}TerAlH$_2$; ii) ^{Mes}TerAlH$_2$ + HBdan (5 equiv.); iii) ^{Mes}TerAlH$_2$ + HBdan (5 equiv.) + 4-*t*Bu-styrene (5 equiv.). Resonances attributed to ^{Mes}TerAlH$_2$•HBdan (blue) and ^{Mes}TerAl(R)H•HBdan (red) that are not overlapped by other signals are highlighted. Diagnostic resonances are labelled. *Al*•Bdan refers to the Bdan unit of the Al/B adduct.

Two possible coordination modes for ^{Mes}TerAlH$_2$•HBdan (and its alkyl derivative) were hypothesised: (***μ-H***)$_2$, with two bridging hydrides, or ***μ-H-μ-N***, featuring a bridging hydride and nitrogen (**Scheme 4-26.i**). The different coordinating modes would be readily distinguished by analysing the symmetry of the Bdan unit: a (***μ-H***)$_2$ structure would be C_2-symmetric, while a ***μ-H-μ-N*** structure would not. In particular, the N*H* resonances of the Bdan unit would help reveal this information. The N*H* resonance for ^{Mes}TerAlH$_2$•HBdan was identified using ^{1}H-^{15}N HMBC (δ^{1}H: 2.82; 2H). The large change in chemical shift between this species and the N*H* of HBdan (δ^{1}H: 4.96; 2H) makes the N*H* resonance a valuable diagnostic signal for identifying adduct formation and a change of environment at HBdan. In the presence of 4-*t*Bu-styrene, the N*H* resonance became slightly deshielded (δ^{1}H: 3.05; 2H). In both cases, the single N*H* environment observed by ^{1}H NMR spectroscopy was suggestive of a symmetrical Bdan environment, indicating that the (***μ-H***)$_2$ bonding mode was present. Although the Bdan environment was symmetrical in both adducts, it is noteworthy to point out that the protons associated with the flanking Mes group (*m*-H

and *o*-CH_3) on the *m*-terphenyl backbone became inequivalent due to hindered rotation.

Attempts to isolate the ^{Mes}TerAlH$_2$•HBdan complex were unsuccessful, and it was suspected that a reversible adduct formation impeded these attempts. To gain further information on the possibility of chemical exchange between ^{Mes}TerAlH$_2$ and HBdan, ^{1}H EXSY NMR was used (**Scheme 4-26.ii**). Indeed, a cross-peak attributed to chemical exchange was observed between the N*H* of HBdan (δ 4.95) and the N*H* of the adduct (δ 2.82) at room temperature with a mixing time of 200 ms. Reversible adduct formation is concordant with the disappearance of the adduct in the presence of THF as monitored by ^{11}B NMR spectroscopy (**Scheme 4-24.ii-b**). In the presence of alkenes, hydroalumination might proceed by initial dissociation of HBdan to generate the required monomeric ^{Mes}TerAlH$_2$.

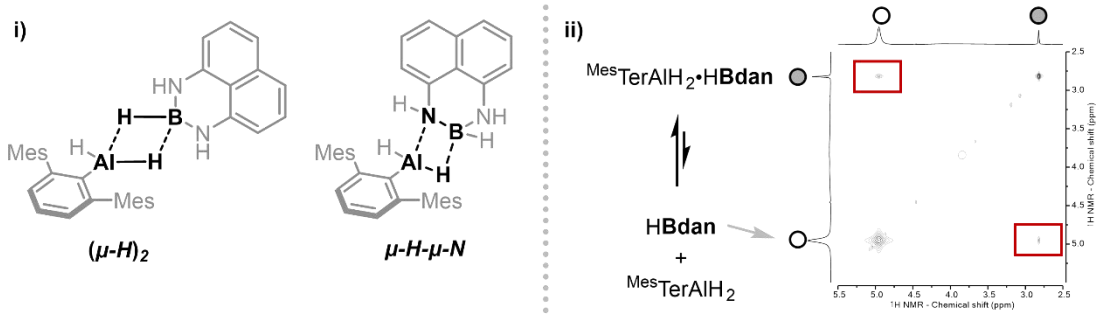

Scheme 4-26. i) Different possible coordination modes of ^{Mes}TerAlH$_2$•HBdan. ii) ^{1}H EXSY NMR spectrum of the reaction mixture containing ^{Mes}TerAlH$_2$•HBdan and HBdan

Although acidic N–H protons were present alongside aluminium hydrides, H_2 was not formed at room temperature. At catalytically relevant temperatures (>80 °C), however, evidence of dehydrocoupling between ^{Mes}TerAlH$_2$ and HBdan *was* observed (formation of H_2, desymmetrisation of the Bdan resonances, see **Appendix**), which likely led to the formation of aluminium amides. Although this is largely suppressed in the presence of alkenes – alkyl alanes can instead react with HBdan by σ-bond metathesis – these observations hinted at a potential pathway for catalyst decomposition.

Mechanistically, the ^{Mes}TerAlH$_2$-catalysed alkene hydroboration with HBdan is proposed to proceed in a distinct pathway to the analogous procedure with HBpin (**Scheme 4-27**). The enhanced stability of HBdan towards the catalyst in comparison to HBpin leads to the initial formation of a ^{Mes}TerAlH$_2$•HBdan adduct by (***μ-H***)$_2$ coordination, instead of the tetrahydroborate complex **3-Mes-1** observed when using HBpin (which arises from aluminium hydride mediated decomposition of HBpin to

BH_3). Dissociation of HBdan from ^{Mes}TerAlH_2•HBdan would generate the reactive monomeric aluminium hydride that can react with alkenes by hydroalumination. The alkyl alane was observed to exist as the HBdan adduct in its resting state. It is proposed that HBdan likely dissociates from this adduct before the resulting monomeric alkyl alane reacts with HBdan by Al-C(sp^3)/B-H exchange to deliver the alkylBdan products and regenerate the aluminium hydride catalyst.

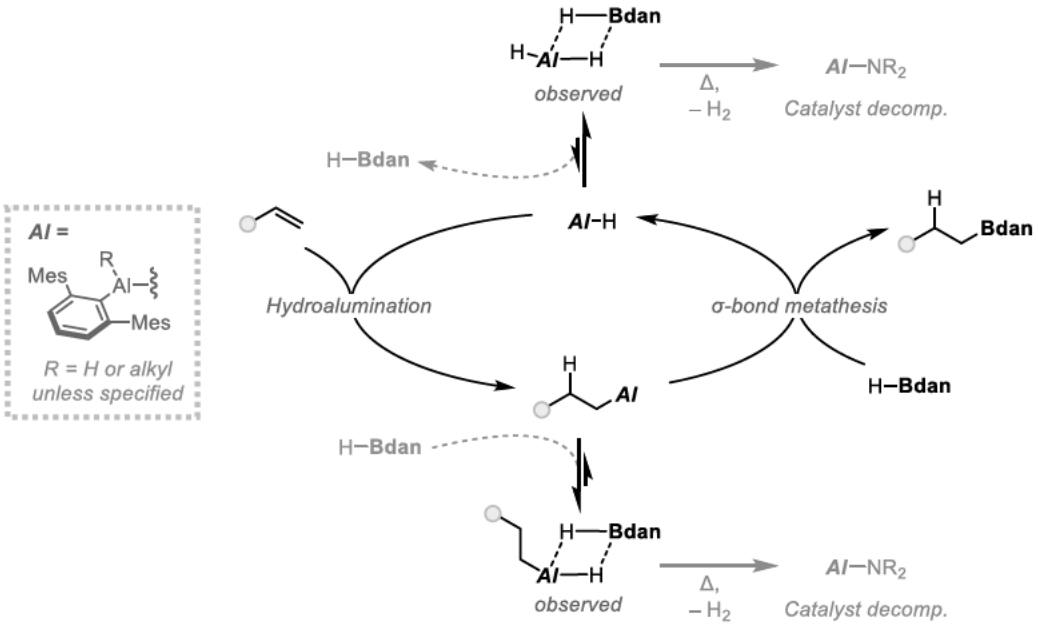

Scheme 4-27. Proposed mechanism for the ^{Mes}TerAlH_2-catalysed alkene hydroboration with HBdan.

4.4 Conclusions and future outlook

Here, the potential of a highly favourable Al–C/B–H exchange pathway has been highlighted by enabling alkene hydroboration with HBdan – a borane of diminished Lewis acidity – using aluminium catalysis. The reaction represents an atom efficient route towards alkyl diazaborinines from an abundant feedstock, avoiding the use of pinBBdan or other stoichiometric organometallic reagents.

The enhanced stability of Bdan towards nucleophiles enables alkylBdan compounds to be used under reaction conditions that pinacolboronic esters and other more reactive boranes would not tolerate, further cementing the status of “dan” as a useful protecting group for boron. Moreover, the stability of Bdan under catalytic conditions in comparison to Bpin precludes the formation of BH_3 in catalysis, which may be favourable in situations where the presence of BH_3 might be detrimental (e.g. for reasons of chemo- or stereo-selectivity). The protocol is an example of distinct, true aluminium catalysis.

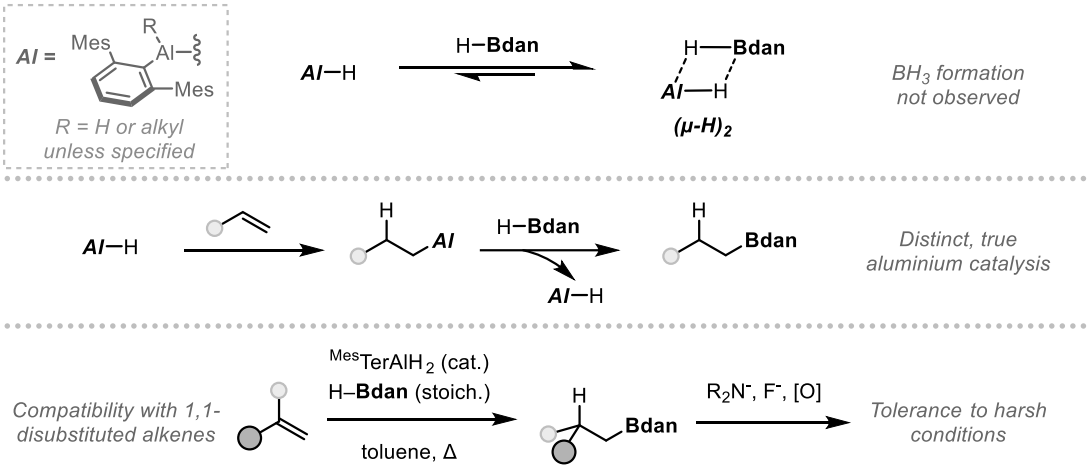

Scheme 4-28. Summary of Chapter 4.

Chapter 5:

Access to silylalanes by σ-bond metathesis

5.1 Introduction

The previous chapters of this thesis focused on investigating Al–C(sp^3)/B–H exchange as a catalyst turnover pathway. This led to the development of aluminium hydride catalysts for alkene hydroboration using HBpin and HBdan (**Scheme 5-1.i**). Exchange of Al–X (X = N, O, S, Se) with HBpin has also been reported to be involved in other examples of aluminium hydride-catalysed hydroboration protocols (**Scheme 5-1.ii**; see also **Chapter 1**). In this chapter, I explore the potential of an alternative turnover pathway by changing the substituent at boron to generate Al–E compounds by Al–R/B–E exchange (**Scheme 5-1.ii;** E = element other H). This could offer unique reactivities in comparison to the aluminium hydride catalysts currently developed.

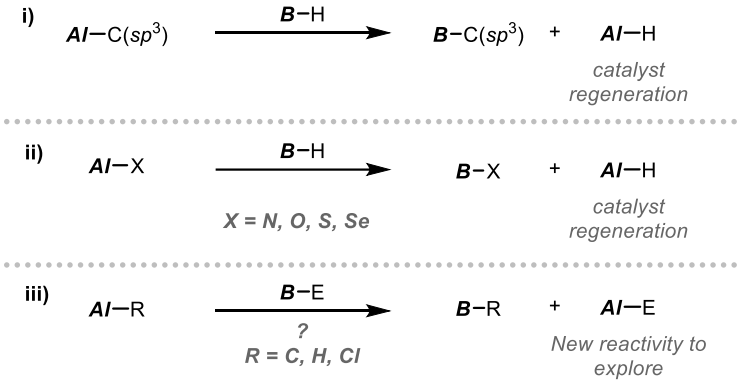

Scheme 5-1. Overview of Al/B exchange explored in i) this thesis so far; ii) the literature; iii) this chapter. *B* = Bpin

Examples of E–B exchange at main group-centres remain scarce. The Hill group have been at the forefront of this space, exploring Mg–C exchange with diboranes (**Scheme 5-2.i**)[345–351] and silylboranes (**Scheme 5-2.ii**)[352–355] to access magnesium boryl and magnesium silyl compounds respectively. These reagents serve as nucleophilic sources of boron[346,348,351] and silicon,[353–355] yet have found interesting applications beyond reacting with simple electrophiles. The magnesium boryl species generated in this way have been used to synthesise unsymmetrical diboranes (**Scheme 5-2.iii**) and triboranes (**Scheme 5-2.iv**) using a variety of borane sources.[345–347,349] Meanwhile, the magnesium silyl species (***Mg–Si***) have found applications in catalytic desilacoupling of amines using $PhMe_2SiBpin$[352] (**Scheme 5-2.v**) and stoichiometric deoxygenation of isocyanates (**Scheme 5-2.vi**).[354] Crimmin has also reported on the stoichiometric defluorosilylation of fluoroolefins using the same magnesium silyl reagent, ***Mg–Si*** (**Scheme 5-2.vii**).[356]

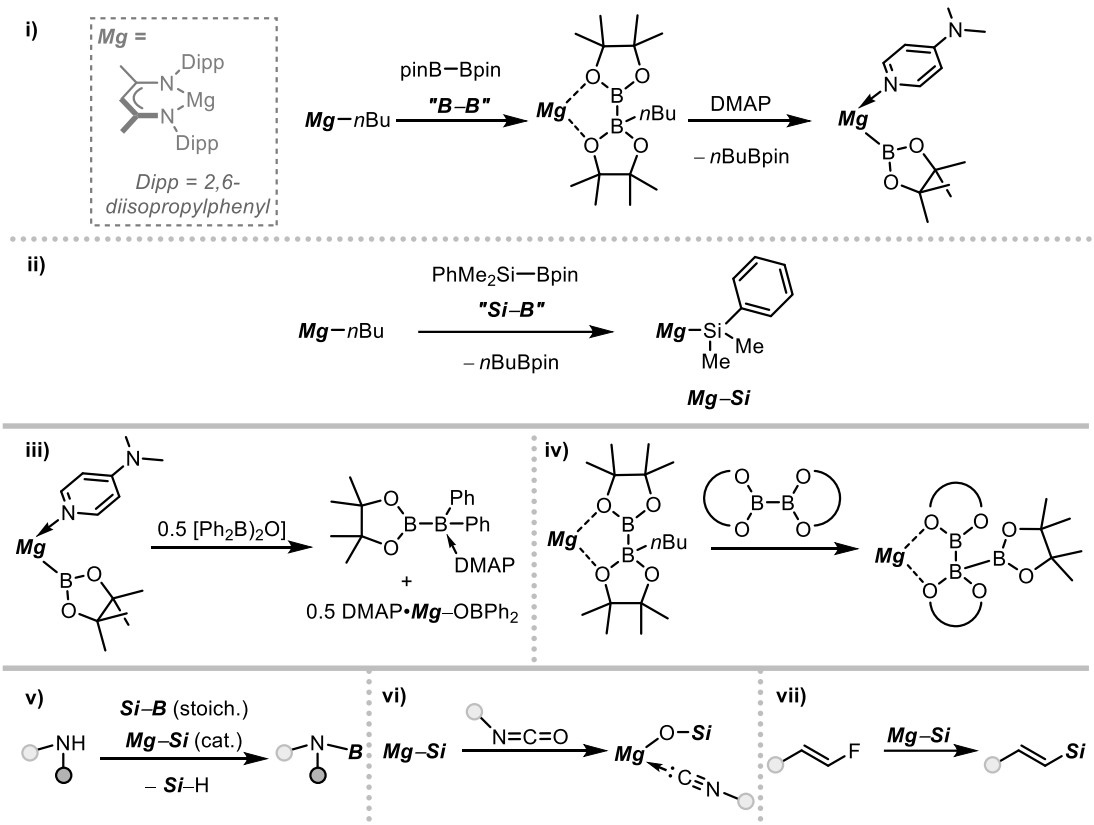

Scheme 5-2. i) formation of magnesium boryl from Mg–C/B–B exchange; ii) formation of magnesium silyl from Mg–Si/B–B exchange; iii) example of unsymmetrical diborane synthesis mediated by a magnesium boryl; iv) example of triborane generation mediated by magnesium; v) desilaboration of amines mediated by a magnesium silyl catalyst; vi) Deoxygenation of isocyanates by *Mg–Si*; vii) defluorosilylation mediated by *Mg–Si*. *Si* = $SiMe_2Ph$; *B* = Bpin.

Similarly, the potential of diboranes and silylboranes to engage in exchange reactions with zinc has also been explored.[357,358] Takita and Uchiyama showed that borylzincates could be generated *in situ* from diethyl zinc, B_2pin_2 and NaO*t*Bu (**Scheme 5-3.i**).[357] This system was applied in the borylation of aryl halides using catalytic zinc, *via* a pathway involving halogen-zinc exchange (**Scheme 5-3.ii**). Additionally, borylzincates were used for the borylzincation of alkynes and benzynes under stoichiometric conditions.[357] Uchiyama later demonstrated that silylzinc reagents could be generated *in situ* from dimethyl zinc and $PhMe_2SiBpin$ in the presence of R_3P (R = *n*Bu or Ph) as a Lewis base.[358] The silylzinc reagents predominantly reacted with alkynes by 1,2-silylzincation (**Scheme 5-3.iii**). The resulting products were quenched with common electrophiles, such as H_2O, allyl bromide, methyl iodide or *N*-iodosuccinimide to give the corresponding alkenyl silanes. Alternatively, turnover was achieved with $PhMe_2SiBpin$, resulting in a catalytic platform that generated the corresponding silaboration products (**Scheme 5-3.iv**).

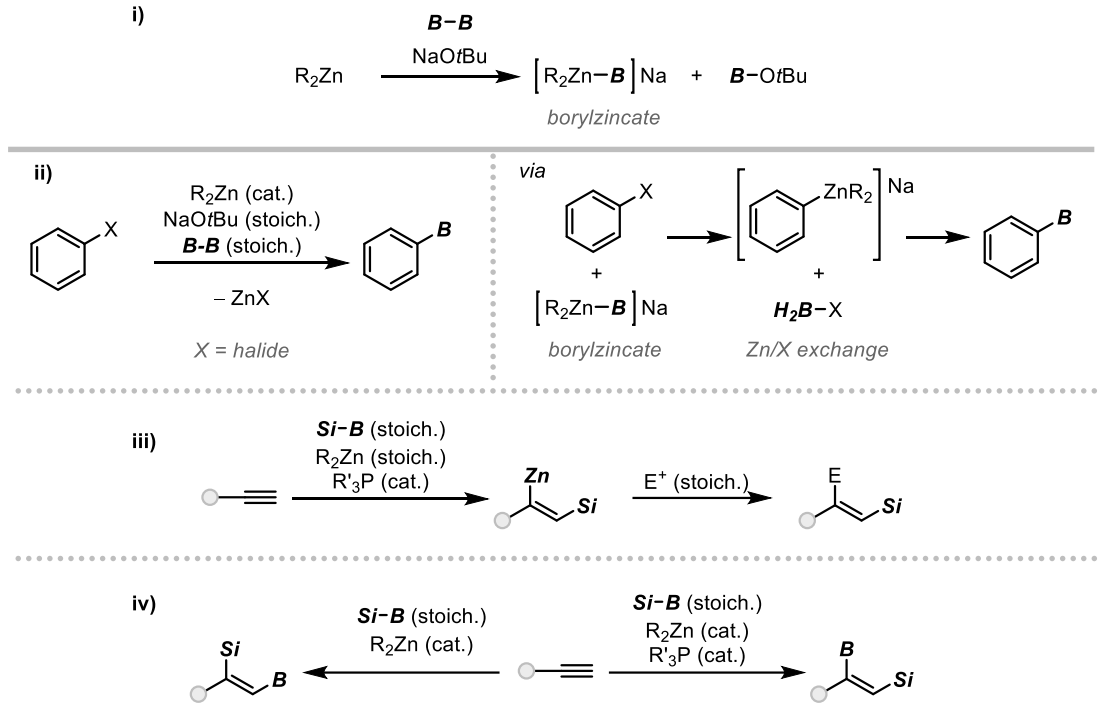

Scheme 5-3. i) Formation of silyl zinc by Zn–C/Si–B exchange; ii) zinc-catalysed borylation of aryl halides with proposed pathway; iii) stochiometric silyl zincation of alkynes leads to vinyl silanes; iv) regio-divergent Zn-catalysed silylboration of alkynes. *Si* = $SiMe_2Ph$; *B* = Bpin.

The potential to access silyl- or borylalanes through the simple redox-neutral pathway involving Al–X/Si–B σ-bond metathesis is intriguing, as the conditions would potentially be mild enough to be applicable in catalysis. This would contrast with current routes towards silyl- and borylalanes, which require highly reactive reagents. For example, syntheses of silylalanes are currently limited to the salt metathesis of silyl anions with aluminium halides,[359,360] transmetallation reactions involving organomercury reagents[361,362] or oxidative addition of Si–H to aluminium(I) species (**Scheme 5-4.i)**.[22,363,364] Borylalanes are currently accessed using synthetically challenging starting materials such as aluminium(I) reagents[22,365–369] or boryl[370–373] and aluminyl[374–376] anions **Scheme 5-4.ii**). More recently, a reductive coupling route between aluminium and boron on a naphthyl backbone (**5-I**) to give the corresponding borylalane (**5-II**) was reported (**Scheme 5-4.iii**).[377]

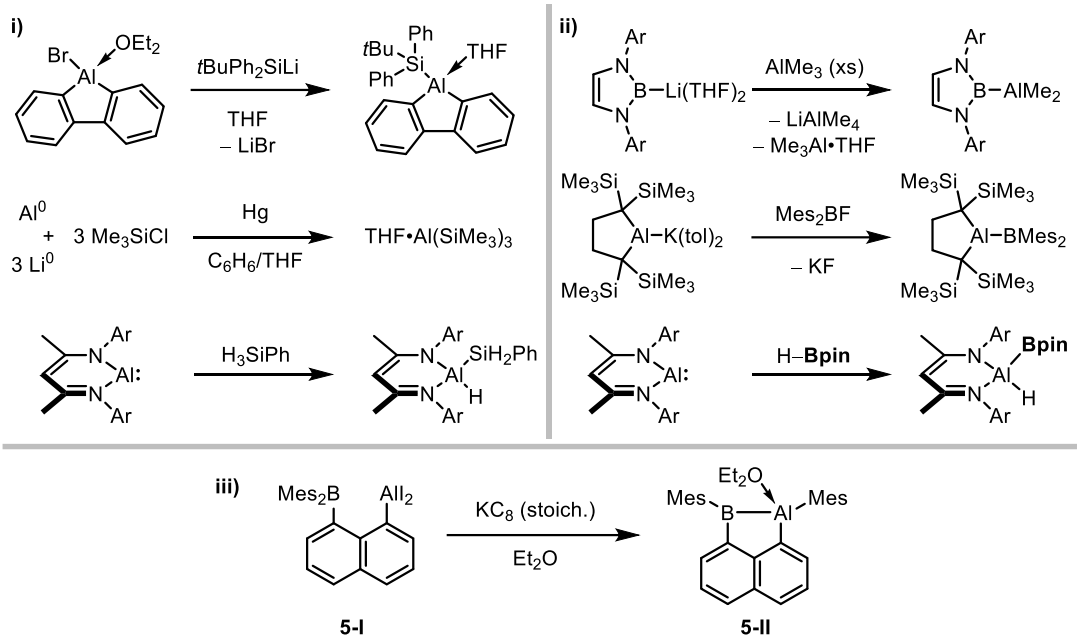

Scheme 5-4. i) Selected examples of routes to silylalanes; ii) selected examples of routes to borylalanes; iii) route to borylalanes by reductive coupling. Ar = 2,6-diisopropylphenyl.

The lack of facile routes towards silyl- and borylalanes has hindered the synthetic applications of these compounds, despite demonstrating some promising reactivities. Unlike alkyl alanes or aluminium hydrides which typically undergo 1,2-addition across unsaturated bonds, borylalanes exhibit unique activation of polarised multiple bonds, often leading to substrate fragmentation and heteroatom insertion into the Al–B bond (**Scheme 5-5.i)**.[376,377] Meanwhile, silylalanes have primarily been employed as nucleophilic sources of silicon in transition metal-catalysed transformations with unsaturated and/or polarised substrates (**Scheme 5-5.ii**).[378–380] Silylalanes have also been used as a stoichiometric reagent to deoxygenate epoxides to give the corresponding alkenes (**Scheme 5-5.iii**).[381] Additionally, silylalanes can undergo uncatalysed 1,2-addition across alkynes (**Scheme 5-5.iv)**,[382] contrasting the apparent lack of reactivity towards olefins by boryl alanes.[377] Addition of silylalanes across alkynes would generate an Al–C bond – therefore, if Al–C/Si–B exchange is feasible, it may be possible to develop a catalytic application featuring this stoichiometric reactivity.

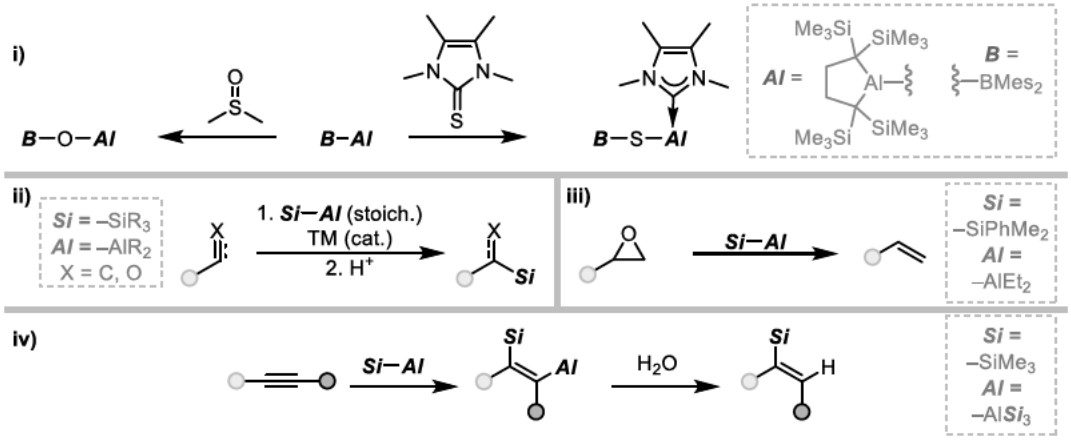

Scheme 5-5. i) examples of heteroatom insertion into borylalanes; ii) transition metal-catalysed silylalumination; iii) stoichiometric epoxide deoxygenation mediated by silylalane; iv) catalyst-free addition of Si–Al across an alkyne.

Access to disilylalanes by this route might potentially lead to intriguing redox-active reactivities at aluminium. Previous studies have demonstrated that the reductive elimination of disilanes at Si(IV)[383] (**5-III**) and B(III)[384] (**5-VII**) centres, initiated by photolysis, would yield the corresponding low-valent Si(II) (**5-IV;** silylene) and B(I) (**5-VIII**; borylene) compounds *in situ* (**Scheme 5-6**). Both silylene **5-IV** and borylene **5-VIII** were isolated in a matrix at low temperatures. Upon warming, silylene **5-IV** would dimerise to give disilene **5-V**,[383] meanwhile borylene **5-VIII** would insert into the C–O bond of the THF solvent to give alkoxy-borane **5-IX**.[384] Alternatively, these low-valent species were reacted with a trapping reagent; silylene **5-IV** was shown to insert into the Si–H bond of Et_3SiH to generate disilane **5-VI**,[383] whilst borylene **5-VIII** engaged in a [2+1] cycloaddition reaction with alkynes to give boracyclopropene **5-X**.[384]

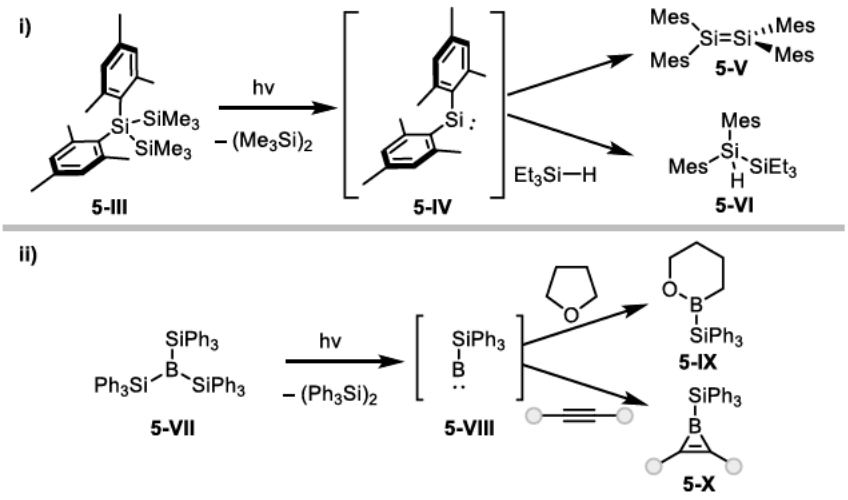

Scheme 5-6. i) formation of a Si(II) species by disilane elimination mediated by irradiation with examples of reactivity; ii) formation of a B(I) species by disilane elimination mediated by irradiation with examples of reactivity.

There is some precedent to photochemical-mediated generation of low-valent aluminium species; Eisch demonstrated that $(Ph_3Al)_2$ would photolyse under irradiation to give biphenyl, aluminium metal and unidentified organoaluminium hydrides (likely $Ph_xAlH_{(3-x)}$).[385] When the same reaction was performed in the presence of excess diphenylacetylene as a trapping reagent, the formation of the [2+1] cycloaddition product, aluminacyclopropene **5-XII** was implied by the formation of *cis*-stilbene **5-XIII** following deuterolysis (**Scheme 5-7**).[385] Eisch proposed that a bridged aluminium(I) species **5-XI** may have been generated as the reactive intermediate *in situ*, although the precise species remains uncertain.

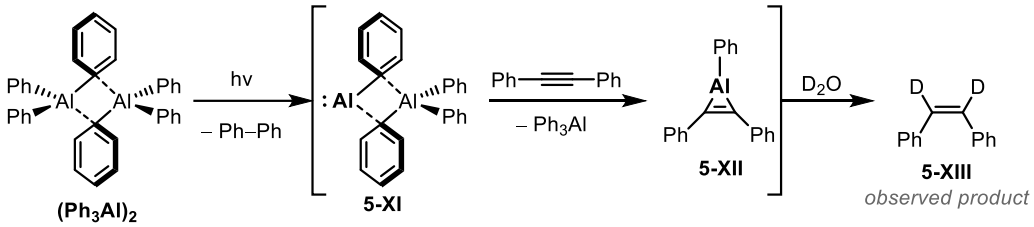

Scheme 5-7. Photolysis of $(Ph_3Al)_2$, with trapping of the presumed sub-valent aluminium species.

5.2 Aims

We aimed to explore the reactivity of silylboranes with *m*-terphenyl alanes with the objective of synthesising silylalanes. The study would focus on identifying appropriate substituents at the aluminium centre to enable Al–X/Si–B exchange and examine the influence of steric bulk on this process. If successful, a comparison would be made to the more commonly used salt metathesis route. Furthermore, the silylalanes would be fully characterised and their initial reactivity would be probed.

In particular, the preparation of disilylalanes were targeted. On the basis that disilanes could be eliminated under irradiation from boron(III) and silicon(IV) centres, it was anticipated that similar reactivity may be possible at an aluminium(III) centre. This could enable the formation of an aluminium(I) species under milder conditions than currently reported, which predominantly rely on the use of strong reducing agents.[21] Since *m*-terphenyl ligands have previously been used to support aluminium(I) centres,[386] it was anticipated that the reactivity of any resulting sub-valent aluminium species could be tempered, and therefore engage in selective oxidative addition with suitable substrates. This would represent an important step in the quest to achieve redox-active catalysis at an aluminium centre. Accordingly, the photochemical reactivity of any prepared disilylalanes would be explored.

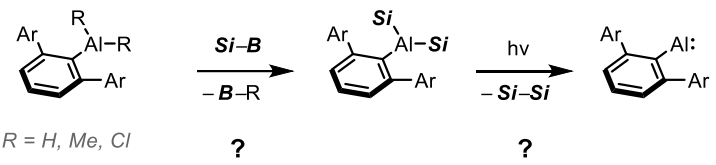

Scheme 5-8. The potential for Al–R/B–Si exchange will be investigated. The photochemical reactivity of any disilylalanes will be explored.

5.3 Results and discussion

5.3.1 Which *m*-terphenyl alanes react with silylboranes?

To investigate the feasibility of generating silylalanes from silylboranes, the reactivity of $PhMe_2SiBpin$ with *m*-terphenyl alanes ($^{Ar}TerAlR_2$; Ar = *p*-Tol, Mes, Tipp) containing different substituents at aluminium (R = H, Me, Cl) was examined in C_6D_6 (**Scheme 5-9**). To conveniently screen for the possibility of Al–R/Si–B exchange with $PhMe_2SiBpin$, the consumption of $PhMe_2Si\underline{B}pin$ (δ 34.9) and formation of R–Bpin species were probed using ^{11}B NMR spectroscopy. The formation of R–Bpin species would imply the formation of silylalanes in the reaction.

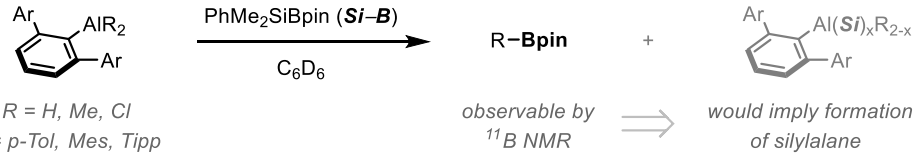

Scheme 5-9. Screening of compatible reagents for Al–R/Si–B exchange with $PhMe_2SiBpin$. *Si* = $SiMe_2Ph$; *B* = Bpin.

The results indicated that Al–C/Si–B exchange was the most promising route to generate silylalanes among the different combinations tested. Each dimethyl alane, $^{Ar}TerAlMe_2$ (Ar = *p*-Tol, Mes, Tipp), reacted with $PhMe_2SiBpin$ in C_6D_6 at room temperature, leading to the formation of MeBpin, as inferred by the formation of the ^{11}B resonance at δ 34.0. Although an Al–Si bond (ΔHf_{298K} = 251(3) kJ mol^{-1}) is weaker than a B–Si bond (ΔHf_{298K} = 289(29) kJ mol^{-1}), the formation of a strong B–C bond (ΔHf_{298K} = 448(29) kJ mol^{-1}) from a weak Al–C bond (ΔHf_{298K} = 255 kJ mol^{-1}) continues to function as a strong thermodynamic driving force for Al/B exchange (ΔH° for Al–C/B–Si exchange ≈ 155 kJ mol^{-1}, based on bond dissociation energies at 298 K, ΔHf_{298}).[387]

In contrast, the aluminium chlorides and aluminium hydrides that were tested proved to be unsuitable for Al–R/B–Si exchange. Dichloroalane $^{Mes}TerAlCl_2{\cdot}OEt_2$ did not exhibit any reactivity with $PhMe_2SiBpin$ at room temperature (**Scheme 5-10.i**), which was attributed to the strength of the Al–Cl bond (ΔHf_{298K} = 408(8) kJ mol^{-1}).[387] Meanwhile, the aluminium dihydrides, $^{Mes}TerAlH_2$ and $^{Tipp}TerAlH_2$, demonstrated unselective exchange with $PhMe_2SiBpin$. Although trace quantities (~2%) of HBpin (δ 28.4; d, $^1J_{B\text{-}H}$ = 176.4 Hz) were initially observed for $^{Mes}TerAlH_2$, greater quantities (~10%) of the presumed Al–H–B adduct, $^{Mes}TerAlH_2{\bullet}(H_2BSiPhMe_2)_n$ ($\delta^{11}B$: –22.9; **3-Mes-3^{Si}**) were formed instead, likely through Al–H/B–O exchange (**Scheme 5-10.ii**). The larger alane, $^{Tipp}TerAlH_2$, displayed minimal reactivity with $PhMe_2SiBpin$

at room temperature, generating only trace quantities (<10%) of a possible adduct (^{Tipp}TerAlH$_2$•B(pin)SiMe$_2$Ph; δ^{11}B: –7.8; **5-Tipp-A**; **Scheme 5-10.iii**). In an attempt to promote the desired Al–H/Si–B exchange, the reaction was heated to 70 °C for 16 hours. However, PhMe$_2$SiBpin remained mostly unreacted (~70%). The other boron-containing species included B(OR)$_3$ (δ^{11}B: 20.2) and a "BH$_4$" species (^{11}B: δ –37.6). Interestingly, a ^{11}B signal at δ 31.3 was also observed, consistent with the formation of PhBpin.[388] These products likely arose from the initial formation of HBpin through the desired Al–H/B–Si exchange pathway, followed by subsequent undesired exchange pathways, including Al–H/B–O and presumably Si–C/B–H σ-bond metatheses.

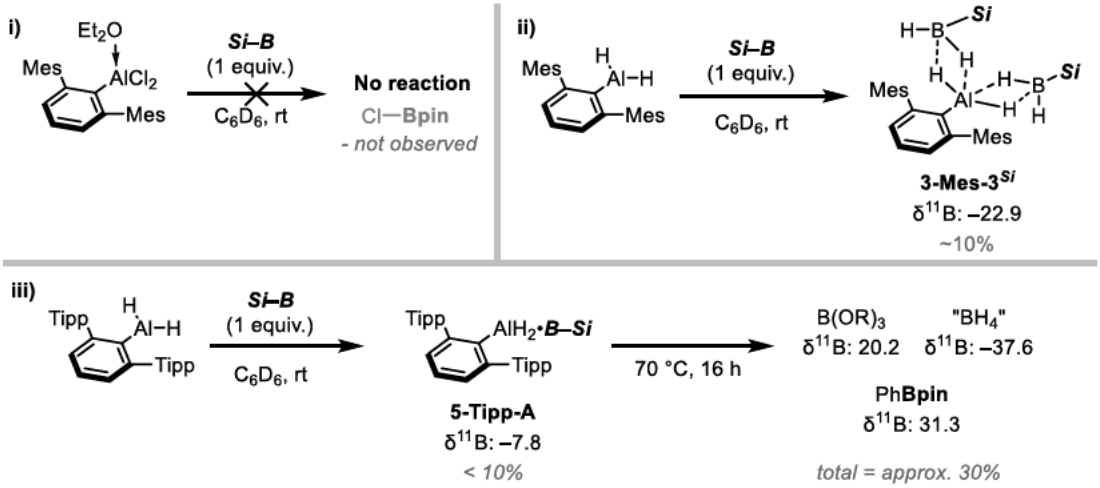

Scheme 5-10. Reaction of PhMe$_2$SiBpin with i) ^{Mes}TerAlCl$_2$•OEt$_2$; ii) ^{Mes}TerAlH$_2$; iii) ^{Tipp}TerAlH$_2$. *Si* = SiMe$_2$Ph; *B* = Bpin.

The reactivity of the dimethyl alanes (^{Ar}TerAlMe$_2$) with PhMe$_2$SiBpin was examined in more depth. ^{Mes}TerAlMe$_2$ was initially observed to react quickly with PhMe$_2$SiBpin (1 equiv.) at room temperature – *ca.* 50% conversion of the silylborane to MeBpin was observed within 30 mins (based on approximate integrals of the ^{11}B resonances; **Scheme 5-11**). Thereafter, the reaction proceeded more slowly and small quantities of PhMe$_2$SiBpin (*ca.* 22%) remained detectable after 1 week.

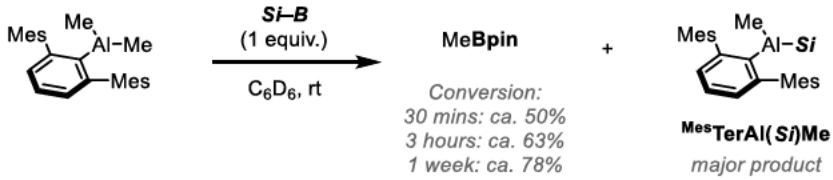

Scheme 5-11. Reaction of ^{Mes}TerAlMe$_2$ with PhMe$_2$SiBpin (1 equiv.). *Si* = SiMe$_2$Ph; *B* = Bpin. Conversions were estimated based on the ratio of MeBpin:PhMe$_2$SiBpin according to ^{11}B NMR integrals.

The observable formation of MeBpin from this reaction strongly suggested the formation of methyl silylalane ^{Mes}TerAl(SiPhMe$_2$)Me (= ^{Mes}TerAl(***Si***)Me), which was corroborated by ^{1}H NMR spectroscopy. The reaction yielded one dominant ^{Mes}Ter environment, as evidenced by the formation of a singular set of MesC$\underline{H_3}$ protons at δ 2.11 and 2.12 (*ortho*- and *para*-CH$_3$). The detection of the SiC$\underline{H_3}$ resonances on the SiMe$_2$Ph fragment (s, δ 0.20) were facilitated by the presence of ^{29}Si satellites ($^2J_{Si–H}$ = 6.1 Hz). Relative to the ^{Mes}Ter resonances, the integral of this SiC$\underline{H_3}$ resonance (6H), was consistent with the presence of a single -SiMe$_2$Ph group in the molecule. ^{1}H-^{29}Si HMQC displayed a cross-peak between this ^{1}H resonance at δ 0.20 and a ^{29}Si resonance at δ –26.8. The chemical shift of this ^{29}Si signal was in the same region as another (arylmethyl)silylalane (Ar$_2$Me$\underline{Si}$AlMe$_2$; δ –31.4).[389] A second, less intense cross-peak for this ^{29}Si resonance at δ –26.8 was also observed with another ^{1}H signal at δ –0.60 (s). The relative integral for the ^{1}H signal at δ –0.60 corresponded to three protons, and therefore consistent with the AlC$\underline{H_3}$ functionality. Other minor unidentified resonances were also present but overall, the NMR spectroscopic data was consistent with the formation of methyl silylalane ^{Mes}TerAl(***Si***)Me as the major product.

To investigate whether both Al–Me substituents could be exchanged to generate the disilylalane (^{Mes}TerAl(SiPhMe$_2$)Me = ^{Mes}TerAl(***Si***)$_2$), ^{Mes}TerAlMe$_2$ was treated with two equivalents of PhMe$_2$SiBpin in C$_6$D$_6$, initially at room temperature. However, only one equivalent was consumed even when the reaction was heated to 80 °C for 20 hours (**Scheme 5-12**). This indicated that steric congestion at ^{Mes}TerAl(***Si***)Me may prevent further reactivity with PhMe$_2$SiBpin.

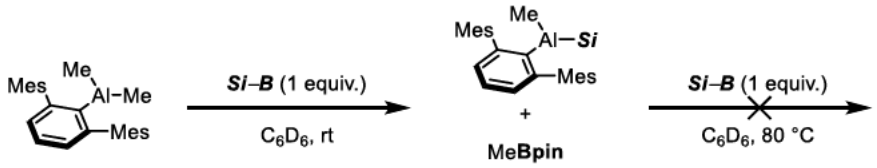

Scheme 5-12. Only one methyl group was exchanged between ^{Mes}TerAlMe$_2$ and PhMe$_2$SiBpin. *Si* = SiMe$_2$Ph; *B* = Bpin.

The effect of steric bulk at aluminium on Al–C/Si–B exchange was next investigated. The reaction of PhMe$_2$SiBpin (1 equiv.) with the bulkier dimethyl alane, ^{Tipp}TerAlMe$_2$, led to a much slower reaction, with only trace quantities of MeBpin formation after 24 hours (**Scheme 5-13.i**). Even after heating to 80 °C for a further 24 hours, less than 50% conversion of PhMe$_2$SiBpin was observed.

When the smaller dimethyl alane, $^{p\text{-Tol}}$TerAlMe$_2$, was used, slow formation of MeBpin was also observed, even when treated with excess PhMe$_2$SiBpin (2.5 equiv.). This was accompanied by the consistent presence of Me$_3$B in small quantities. To investigate this unexpectedly slow reactivity, the reaction was probed by ^{1}H NMR spectroscopy. The ^{1}H NMR spectrum (**Scheme 5-13.ii**, "24 h (rt)") initially displayed peaks with relative integrals consistent with the formation of methyl silylalane, $^{p\text{-Tol}}$TerAl(***Si***)Me, as the major species (δ 2.05 (s, 6H; *p*-Tol, C*H*$_3$), 0.10 (s, 6H; SiC*H*$_3$), -0.44 (s, 3H; AlC*H*$_3$)). Under excess PhMe$_2$SiBpin, it might be expected that further exchange would lead to the corresponding disilylalane, $^{p\text{-Tol}}$TerAl(***Si***)$_2$. However, like in the ^{Mes}Ter*Al* system, no more than one equivalent of PhMe$_2$SiBpin was consumed, even after heating at 70 °C for six hours. Instead, the reaction appeared to equilibrate to a mixture of $^{p\text{-Tol}}$Ter$_2$AlMe (see **Chapter 3**, **section 3.3.12**) and $^{p\text{-Tol}}$TerAl(***Si***)Me (~35:65 before heating to ~50:50 after heating; **Scheme 5-13.ii**). This observation is reminiscent of the redistribution of substituents observed for $^{p\text{-Tol}}$TerAlMe$_2$ in the presence of MeBpin in **Chapter 3**. These results highlight the importance of fine-tuning the steric properties at the aluminium centre. It is necessary to provide sufficient space for interaction with the PhMe$_2$SiBpin reagent to enable exchange, while ensuring sufficient steric protection at aluminium to avoid uncontrolled rearrangements.

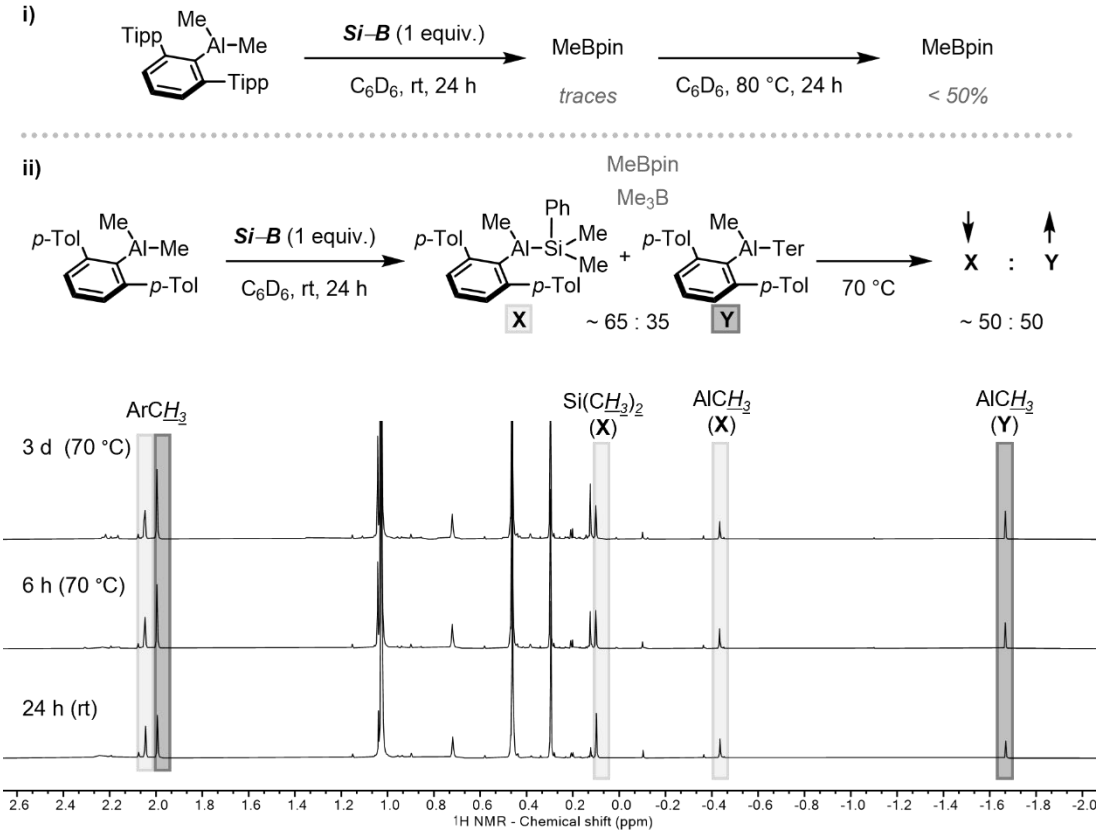

Scheme 5-13. i) Reaction between ^{Tipp}TerAlMe$_2$ with PhMe$_2$SiBpin; ii) Stacked ^{1}H NMR spectra (C_6D_6) tracking the reaction between $^{p\text{-Tol}}$TerAlMe$_2$ with PhMe$_2$SiBpin. Redistribution of substituents is observed. Signals associated with X are highlighted in light grey; . Signals associated with Y are highlighted in dark grey. ***Si*** = SiMe$_2$Ph; ***B*** = Bpin.

5.3.2 Isolation of silylalanes

With a suitable synthetic route identified for the preparation of a silylalane, efforts were made to isolate ^{Mes}TerAl(***Si***)Me. Thus, a scaled-up reaction (1 mmol scale) of ^{Mes}TerAlMe$_2$ with PhMe$_2$SiBpin (1 equiv.) in pentane was performed. The reaction was stirred for four days at room temperature which resulted in the full consumption of the starting materials, as evidenced by ^{1}H NMR spectroscopy. The ^{1}H NMR spectrum of the crude reaction mixture displayed the diagnostic signals for ^{Mes}TerAl(***Si***)Me along with another unidentified *m*-terphenyl-containing species in minor quantities. The volatiles were removed *in vacuo* and the crude reaction mixture was redissolved in the minimum volume of pentane and stored at –30 °C overnight, resulting in the formation of faint-yellow crystals suitable for analysis by X-ray diffraction.

Unexpectedly, the crystalline material obtained was not that of methyl silylalane ^{Mes}TerAl(***Si***)Me, but of disilylalane ^{Mes}TerAl(***Si***)$_2$ instead (**Figure 5-1**). The X-ray crystal structure revealed a monomeric alane with a CAlSi$_2$ trigonal planar core. The

$C_{(1)}$–Al–Si bond angles were 123.59(2)° and 125.75(2)°, while the $Si_{(1)}$–Al–$Si_{(2)}$ bond angle was relatively more contracted at 110.36(1)°. The Al–Si bond lengths were 2.4712(3) Å and 2.4832(4) Å, slightly shorter in comparison to those in $Al(Si(MetBu_2)_3)_3$ (2.5038(10)).[390] Curiously, the Al–Si bond lengths are more comparable with silylalanes that are four-coordinate at aluminium.[360,361,363,391,392] Notably, π-stacking is absent at the phenyl groups on silicon; a gauche arrangement is observed instead to avoid steric clash, exhibiting a torsion angle of 74.82(1)° for [$C_{(27)}$–$Si_{(1)}$–$Si_{(2)}$ –$C_{(35)}$].

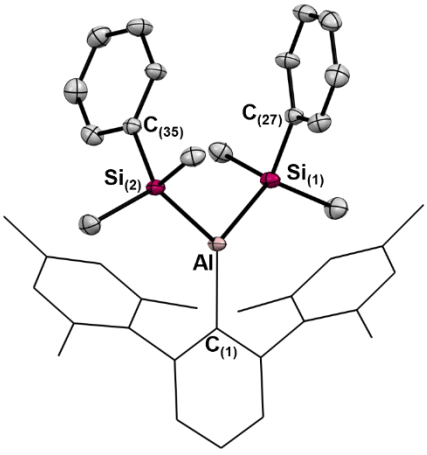

$^{Mes}TerAl(\boldsymbol{Si})_2$

Parameter	Measurement
Al–$Si_{(1)}$	2.4832(4) Å
Al–$Si_{(2)}$	2.4712(3) Å
Al–$C_{(1)}$	1.9728(8) Å
$Si_{(1)}$–Al–$Si_{(2)}$	110.36(1) °
$C_{(1)}$–Al–$Si_{(1)}$	125.75(2) °
$C_{(1)}$–Al–$Si_{(2)}$	123.59(2) °
χ[$C_{(27)}$–$Si_{(1)}$–$Si_{(2)}$ –$C_{(35)}$]	74.82(1) °

Figure 5-1. ORTEP representation of $^{Mes}TerAl(\boldsymbol{Si})_2$ (50% probability ellipsoids). For clarity, hydrogen atoms have been removed and the ^{Mes}Ter-substituent is displayed in wireframe. A table of selected parameters is included.

The remaining crystalline material was isolated by filtration to give disilylalane $^{Mes}TerAl(\boldsymbol{Si})_2$ in a low yield of 5%. The compound was fully characterised by standard spectroscopic techniques. The ^{1}H NMR spectrum indicated a C_2-symmetry of $^{Mes}TerAl(\boldsymbol{Si})_2$ in solution, with a single set of aryl–*H* and aryl–C*H*$_3$ protons for the *m*-terphenyl substituent in addition to a single SiC*H*$_3$ ^{1}H resonance at δ 0.08 (s, 12H). The ^{29}Si chemical shift of δ –25.3 is comparable to that of $^{Mes}TerAl(\boldsymbol{Si})Me$. Analysis of $^{Mes}TerAl(\boldsymbol{Si})_2$ by UV/vis spectroscopy revealed a moderate absorption at 368 nm (ε = 443 $M^{-1}cm^{-1}$), which indicated the potential to engage in photochemistry at this wavelength. Characterisation of $^{Mes}TerAl(\boldsymbol{Si})_2$ allowed assignment of the minor unidentified resonances that were consistently present from the reaction between $^{Mes}TerAlMe_2$ and $PhMe_2SiBpin$ (1 equiv.).

From the same reaction, $^{Mes}TerAl(\boldsymbol{Si})Me$ was eventually obtained in a low yield (8%) as colourless crystalline material from the concentrated mother liquor following storage at –30 °C for 2 days. Due to time constraints, this product was not analysed

by X-ray crystallography but was fully characterised by ^{1}H, ^{13}C and ^{29}Si NMR spectroscopy, high-resolution mass spectrometry (electron ionisation) and IR spectroscopy. All data were consistent with the formation of ^{Mes}TerAl(***Si***)Me. In contrast to ^{Mes}TerAl(***Si***)$_2$, ^{Mes}TerAl(***Si***)Me did not give a strong absorption at 368 nm under UV/vis spectroscopy (**Figure 5-2**). Absorption bands were only visible at shorter wavelengths (< 320 nm) but these can likely be attributed to the aryl substituents of the *m*-terphenyl group.[393]

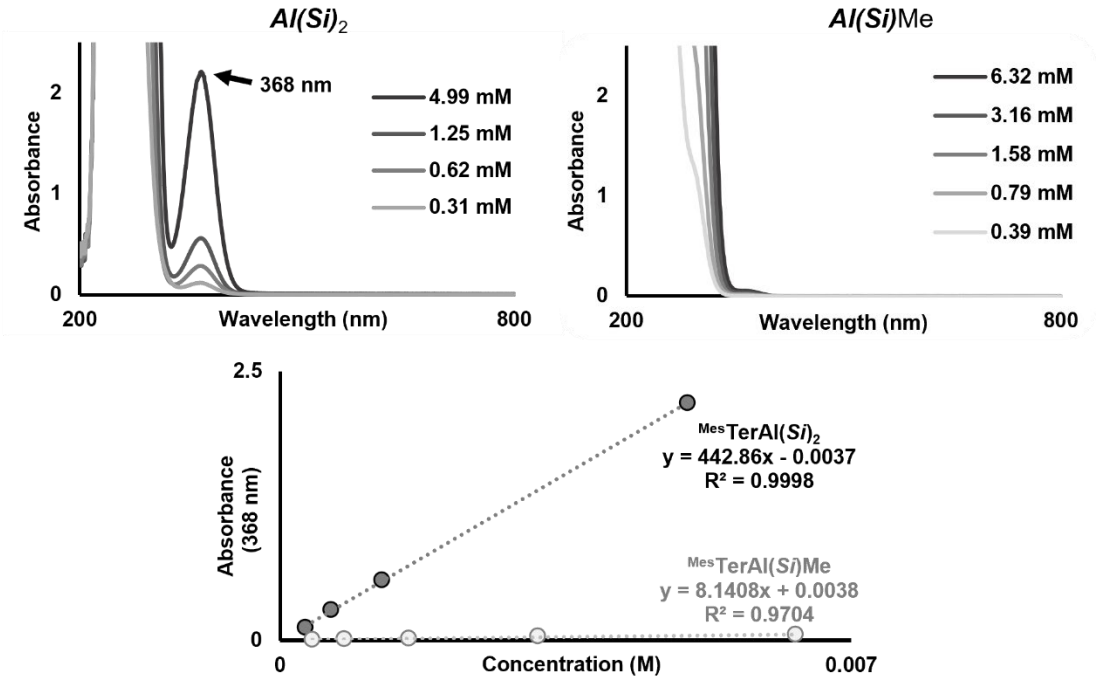

Figure 5-2. UV-vis data spectra for ^{Mes}TerAl(*Si*)$_2$ and ^{Mes}TerAl(*Si*)Me with absorbance vs concentration plot used for calculating ε; ***Al*** = ^{Mes}TerAl; ***Si*** = SiMe$_2$Ph

5.3.3 How are the disilylalanes formed?

The mechanism of generating ^{Mes}TerAl(***Si***)$_2$ was particularly intriguing as ^{Mes}TerAl(***Si***)Me did not seem to react with additional equivalents of PhMe$_2$SiBpin. Considering the promising photochemical properties of ^{Mes}TerAl(***Si***)$_2$, efforts were made to better understand the mechanism of its formation with the overall goal of improving its yield to explore its photochemical behaviour. Accordingly, several hypotheses were formulated to explain the formation of the disilylalane, ^{Mes}TerAl(***Si***)$_2$:

Hypothesis 1: Equilibrium with MeBpin (**Scheme 5-14.i**)

It was hypothesised that ^{Mes}TerAl(***Si***)$_2$ *could* be generated directly from the reaction of ^{Mes}TerAl(***Si***)Me with PhMe$_2$SiBpin, contrary to previous experimental observations. However, in the presence of MeBpin, ^{Mes}TerAl(***Si***)$_2$ would exist in equilibrium with ^{Mes}TerAl(***Si***)Me. As ^{Mes}TerAl(***Si***)Me is observed as the major product in the solution-

state, the equilibrium would lie almost exclusively in favour of this species. In this hypothesis, the formation of crystalline ^{Mes}TerAl(***Si***)$_2$ when the reaction mixture was maintained at –30 °C would be explained by a kinetically disfavoured reaction between ^{Mes}TerAl(***Si***)$_2$ and MeBpin at this low temperature. Moreover, the precipitation of ^{Mes}TerAl(***Si***)$_2$ would drive the equilibrium towards this product.

Hypothesis 2: Redistribution (**Scheme 5-14.ii**)

It was also hypothesised that ^{Mes}TerAl(***Si***)$_2$ could be generated by the redistribution of ^{Mes}TerAl(***Si***)Me. Notably, the by-product of this reaction would be ^{Mes}TerAlMe$_2$, which would further react with PhMe$_2$SiBpin to generate more ^{Mes}TerAl(***Si***)Me.

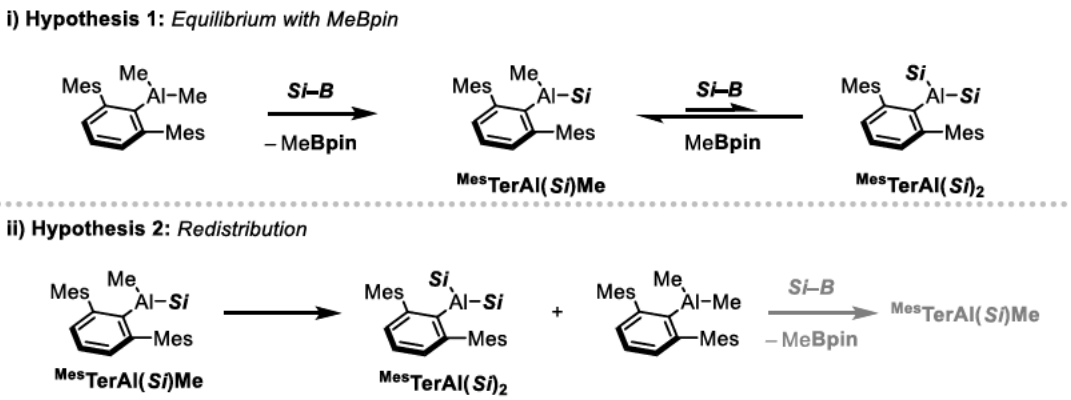

Scheme 5-14. Different hypotheses for the formation of ^{Mes}TerAl(Si)$_2$. *Si* = SiMe$_2$Ph; *B* = Bpin.

To test the plausibility of *hypothesis 1*, ^{Mes}TerAl(***Si***)$_2$ was reacted with MeBpin in C_6D_6 at room temperature. If this hypothesis was viable, the reaction would immediately form ^{Mes}TerAl(***Si***)Me and PhMe$_2$SiBpin. However, resonances attributed to these species were not observed by ^{1}H or ^{11}B NMR spectroscopy, even when the reaction was heated to 80 °C for four hours (**Scheme 5-15**). Accordingly, the hypothesis was discarded.

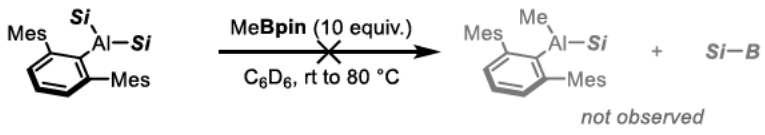

Scheme 5-15. ^{Mes}TerAl(*Si*)$_2$ does not appear to react with MeBpin. *Si* = SiMe$_2$Ph; *B* = Bpin.

To test the plausibility of *hypothesis 2*, the possible redistribution of ^{Mes}TerAl(***Si***)Me was tracked by ^{1}H NMR spectroscopy over time. Any redistribution would lead to the formation of ^{Mes}TerAl(***Si***)$_2$ and ^{Mes}TerAlMe$_2$. However, no such redistribution was observed when ^{Mes}TerAl(***Si***)Me was kept at room temperature for

16 hours or when heated to 80 °C for 84 hours (**Scheme 5-16**). Accordingly, this hypothesis was also ruled out.

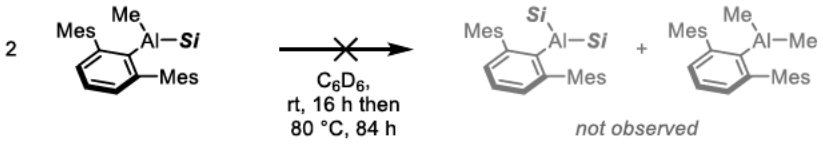

Scheme 5-16. Redistribution of substituents at ^{Mes}TerAl(*Si*)Me likely does not explain formation of ^{Mes}TerAl(*Si*)$_2$.

The formation of ^{Mes}TerAl(***Si***)$_2$ therefore required another explanation. A third hypothesis was that alkyl boranes with less steric hindrance than PhMe$_2$SiBpin, such as PhMe$_2$SiBMe$_2$, could mediate the exchange of the methyl group at the sterically congested ^{Mes}TerAl(***Si***)Me (**Scheme 5-17**). This was based on the initial formation and subsequent consumption of trace quantities of a potential silylorganoborane,[394] PhMe$_2$SiBMe$_2$, inferred by the trace ^{11}B resonance at δ 104.9 initially observed during the reaction between ^{Mes}TerAlMe$_2$ and PhMe$_2$SiBpin.

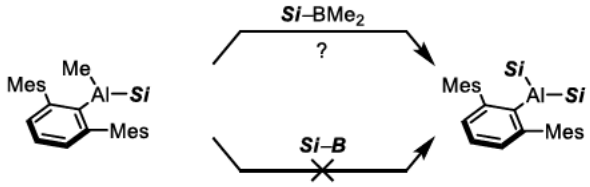

Scheme 5-17. ^{Mes}TerAl(*Si*)$_2$ is not made by exchange between ^{Mes}TerAl(*Si*)$_2$.and PhMe2SiBpin. But could it be made by exchange of an organosilylborane? ***Si*** = SiMe$_2$Ph; ***B*** = Bpin.

To test this, it was necessary to observe the effects of PhMe$_2$SiBMe$_2$ on the reaction. To avoid the need to isolate PhMe$_2$SiBMe$_2$, it was decided to generate PhMe$_2$SiBMe$_2$ *in situ* from PhMe$_2$SiBpin to facilitate proceedings. AlMe$_3$ was found to be an effective reagent for swapping the pinacol group at boron in PhMe$_2$SiBpin with methyl groups. This was evidenced by the immediate precipitation of a white solid, assumed to be an aluminium pinacolate species, upon the reaction of AlMe$_3$ with PhMe$_2$SiBpin at room temperature. Additionally, the ^{11}B NMR spectrum displayed highly deshielded resonances between δ 95–110, suggesting that organosilylboranes had been formed.[394]

Thus, the effect of adding $AlMe_3$ to the reaction mixture containing $^{Mes}TerAlMe_2$ and $PhMe_2SiBpin$ was investigated by ^1H NMR spectroscopy (**Scheme 5-18**). After 40 hours of the reaction between $^{Mes}TerAlMe_2$ and $PhMe_2SiBpin$ in neat conditions at room temperature, the NMR yield (based on conversion from starting material to products) of $^{Mes}TerAl(\boldsymbol{Si})Me$ was 60% and of $^{Mes}TerAl(\boldsymbol{Si})_2$ was 31%. At this point, 0.5 equivalents of $AlMe_3$ in hexane was added to the frozen reaction mixture at –85 °C and the reaction was allowed to thaw. After stirring for 16 hours, more $^{Mes}TerAl(\boldsymbol{Si})Me$ (47%; –13%) had converted to $^{Mes}TerAl(\boldsymbol{Si})_2$ (46%; +15%). Finally, an additional 1.5 equivalents of $AlMe_3$ was added under the same conditions and the reaction was stirred for a further 16 hours, resulting in yet more conversion of $^{Mes}TerAl(\boldsymbol{Si})Me$ (34%; –13%) to $^{Mes}TerAl(\boldsymbol{Si})_2$ (60%; +14%). These observations therefore indicated that $^{Mes}TerAl(\boldsymbol{Si})_2$ was likely formed by the reaction of $^{Mes}TerAl(\boldsymbol{Si})Me$ with $PhMe_2SiBMe_2$, and that adding $AlMe_3$ to the reaction mixture would enhance this process.

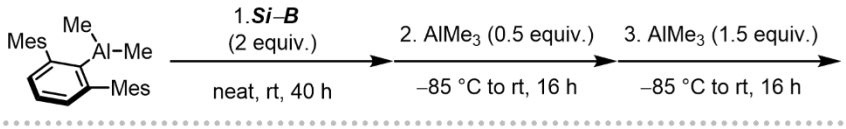

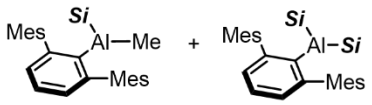

Step	$^{Mes}TerAl(Si)Me$	$^{Mes}TerAl(Si)_2$
1	60%	31%
2	47%	46%
3	34%	60%

Scheme 5-18. Composition of $^{Mes}TerAl(Si)_2$ and $^{Mes}TerAl(Si)Me$ compared following sequential addition of $AlMe_3$ to the reaction between $^{Mes}TerAl(Si)Me$ and $PhMe_2SiBpin$. *Si* = $SiMe_2Ph$; *B* = Bpin.

After removing the volatile components *in vacuo*, $^{Mes}TerAl(\boldsymbol{Si})_2$ was isolated in a 26% yield by fractional recrystallisation from cold pentane. The low yield was attributed to the high solubility of $^{Mes}TerAl(\boldsymbol{Si})_2$ in apolar solvents and the presence of $^{Mes}TerAl(\boldsymbol{Si})Me$, therefore necessitating crystallisation as a means to isolate the target disilylalane. It was hoped that the reaction could be simplified by adding $AlMe_3$ at the start of the reaction between $^{Mes}TerAlMe_2$ and $PhMe_2SiBpin$, but this completely prevented the formation of $^{Mes}TerAl(\boldsymbol{Si})_2$ altogether. This suggested that it is important to generate $^{Mes}TerAl(\boldsymbol{Si})Me$ first before adding $AlMe_3$, however further optimisation is required to improve the yield of $^{Mes}TerAl(\boldsymbol{Si})_2$.

5.3.4 Can disilylalanes be made by salt metathesis?

Salt metathesis between ^{Mes}TerAlCl$_2$•OEt$_2$ and PhMe$_2$SiLi (2 equiv.) in THF was also explored in an effort to access greater yields of ^{Mes}TerAl(***Si***)$_2$. When the deep red THF solution of PhMe$_2$SiLi was added to a solution of ^{Mes}TerAlCl$_2$•OEt$_2$ in THF at room temperature, the colour gradually faded over a period of 40 minutes. However, rather than forming the target disilylalane, ^{Mes}TerAl(***Si***)$_2$, the ^{1}H NMR spectrum of the reaction mixture revealed only the formation of ^{Mes}TerAlCl$_2$•THF. This was indicated by the distinctive ^{1}H resonances at δ 3.34 and δ 0.78 for the formation of an *Al•THF* adduct and lack of observable SiC*H$_3$* protons in the ^{1}H NMR spectrum. A second attempt was made, with a longer reaction time of 3 days. Although the ^{1}H NMR spectrum showed that ^{Mes}TerAlCl$_2$•THF had fully reacted this time, a complex spectrum resulted involving the formation of several different *m*-terphenyl and silicon-containing species. Furthermore, the reaction produced a viscous oil that could not be precipitated, despite several attempts involving different solvent systems, and this made purification of the reaction products challenging. These observations highlight the benefits of using PhMe$_2$SiBpin as the nucleophilic silicon source in place of PhMe$_2$SiLi, as in some cases, PhMe$_2$SiBpin can be more selective. Additionally, it can be used in apolar solvents, whereas PhMe$_2$SiLi cannot due to solubility issues.

5.3.5 Photolysis of disilylalane ^{Mes}TerAl(*Si*)$_2$

With a restricted time-frame and limited quantities of ^{Mes}TerAl(***Si***)$_2$ and ^{Mes}TerAl(***Si***)Me on hand, it was necessary to be selective when investigating the reactivity of these silylalanes. The possibility of generating an aluminium(I) species under photolysis was especially appealing, and so the behaviour of these silylalanes under irradiation was investigated. Thus, the reactivity of ^{Mes}TerAl(***Si***)$_2$ and ^{Mes}TerAl(***Si***)Me following irradiation at 365 nm in C_6D_6 at room temperature was compared (**Scheme 5-19**). Immediately noticeable was the lack of colour change observed for the sample containing ^{Mes}TerAl(***Si***)Me in comparison with ^{Mes}TerAl(***Si***)$_2$, which became progressively more orange over the course of an hour.

The formation of only trace new ^{1}H signals after one hour indicated that only minimal reactivity had occurred for ^{Mes}TerAl(***Si***)Me. This corresponded with the lack of absorbance at 365 nm by UV/vis spectroscopy. In contrast, the ^{1}H NMR spectrum for the solution originally containing ^{Mes}TerAl(***Si***)$_2$ showed that it had been completely consumed. The SiC*H$_3$* ^{1}H resonance at δ 0.08 for ^{Mes}TerAl(***Si***)$_2$ gave way to a new major ^{1}H resonance at δ 0.30 with similar intensity. The ^{1}H–^{29}Si HMBC spectrum (taken after 6 minutes of irradiation) displayed a cross-peak between this ^{1}H signal at

δ 0.30 with a ^{29}Si signal at δ –22.1. This ^{29}Si chemical shift was consistent with the formation of the disilane, $(PhMe_2Si)_2$.[395] Confusingly, the ^{1}H NMR resonances for this product did not match the reported data for $(PhMe_2Si)_2$ in C_6D_6.[395] However, this was attributed to an error in the reported ^{1}H chemical shifts, as the ^{13}C chemical shifts were later revealed to exactly match the reported signals for $(PhMe_2Si)_2$.

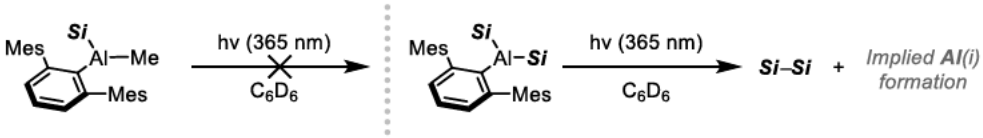

Scheme 5-19. Comparison of reactivity observed for ^{Mes}TerAl(*Si*)Me and ^{Mes}TerAl(*Si*)$_2$ following irradiation at 365 nm in C_6D_6. ***Si*** = $SiMe_2Ph$.

The formation of disilane $(PhMe_2Si)_2$ indicated successful cleavage of the Al–Si bonds under irradiation (*i.e.*, potential reductive elimination) and implied that aluminium(I) might have been formed *in situ*. However, the fate of the aluminium species was unclear, with only trace resonances observed in the aryl C*H* and Mes–C*H*$_3$ regions that would normally be expected for the *m*-terphenyl substituent. This was likely attributed to the unselective reaction with the benzene solvent, which can react with low-valent aluminium species.[24,396,397] Moreover, since deuterated benzene was used, the resonances of any newly formed species would not be readily observable by ^{1}H NMR spectroscopy.

To test whether cleavage of the Al–Si bonds is a concerted or stepwise process (**Scheme 5-20.i**), ^{Mes}TerAl(***Si***)$_2$ was irradiated at 365 nm in CH_2Cl_2 (**Scheme 5-20.ii**), which was used as a radical trap. The use of protonated solvent was also expected to facilitate the observation of new *m*-terphenyl products by avoiding the formation of deuterated products. Similar to the reaction performed in C_6D_6, the colourless solution became progressively more orange as the reaction proceeded. Analysis of the reaction mixture by ^{1}H NMR spectroscopy (CH_2Cl_2) revealed that ^{Mes}TerAl(***Si***)$_2$ had been mostly consumed after 15 minutes, giving rise to a new major SiC*H*$_3$ ^{1}H signal at δ 0.70, and a trace SiC*H*$_3$ ^{1}H signal at δ 0.33. The ^{1}H-^{29}Si HMBC spectrum displayed a cross-peak between the major ^{1}H signal at 0.70 with a ^{29}Si signal at δ 20.4, consistent with the formation of $PhMe_2SiCl$.[398] Meanwhile the trace ^{1}H signal at δ 0.33 displayed a cross-peak with a ^{29}Si signal at δ –22.1, consistent with that of disilane $(PhMe_2Si)_2$. As the results showed that only minor quantities of the disilane $(PhMe_2Si)_2$ had been generated, this indicated that Al–Si cleavage likely proceeded in a stepwise manner, whereby silyl radical formation would lead to chloride atom abstraction from CH_2Cl_2 (**Scheme 5-20.iii**). The result does not, however, rule out

initial formation and subsequent cleavage by photolysis of disilane $(PhMe_2Si)_2$ under reaction conditions, which may also explain the formation of $PhMe_2SiCl$.

Although the ^1H resonances attributed to the *m*-terphenyl backbone were more clearly visible than when C_6D_6 was used, it remained challenging to determine the products that had been formed. The presence of six new major resonances in the Mes–C*H*$_3$ region between δ 1.5 and δ 2.5 indicated that at least three different *m*-terphenyl containing species were formed (accounting for *o*- and *p*-C*H*$_3$). These species likely arose from multiple different forms of radical recombination from a sub-valent aluminium species, such as chloride or proton abstraction from the solvent molecule.

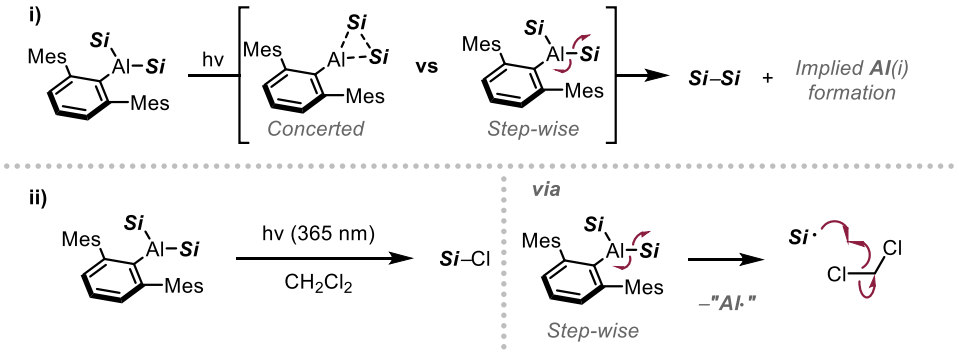

Scheme 5-20. i) Possible Al–Si fragmentation pathways; ii) reactivity of ^{Mes}TerAl(*Si*)$_2$ under photolysis in CH_2Cl_2 with an explanation for the observed reactivity. ***Si*** = $SiMe_2Ph$.

These observations demonstrated that highly reactive low-valent aluminium species are likely formed by photolysis. However, the high reactivity of these species led to unselective reactivity with non-innocent solvents and precluded detailed analysis of the aluminium products.

To better understand the reactivity at aluminium, photolysis of ^{Mes}TerAl(***Si***)$_2$ at 365 nm was performed in the presence of excess bis(trimethylsilyl)acetylene **5-1** (10 equiv.) in cyclohexane. Alkyne **5-1** is a common trapping reagent for highly reactive low-valent species, and typically results in the formation of the [2+1] cycloaddition product, **5-2**. For example, a β-diketiminate-supported aluminium(I) reagent was found to react with alkyne **5-1** to give the corresponding aluminacyclopropene product.[399] The cyclohexane solvent was chosen with expectations that it would be mostly inert under reaction conditions, but it was also found to be more solubilising than acyclic alkanes, such as pentane or hexane. Furthermore, the single proton environment greatly facilitated reaction monitoring by ^1H NMR spectroscopy (**Scheme 5-21**).

A snapshot of the reaction mixture was taken by ^{1}H NMR spectroscopy prior to irradiation to verify that no reaction had taken place between ^{Mes}TerAl(***Si***)$_2$ and alkyne **5-1** under ambient light (**Scheme 5-21 –** "before hv"). Following irradiation for 45 minutes at room temperature, the formation of a single set of new *m*-terphenyl resonances appeared (approximately 17% conversion, based on relative integration with the starting material), alongside the formation of two new SiC*H*$_3$ resonances of approximately equal intensity (see resonances labelled "c"). After irradiation for five hours, this new species and ^{Mes}TerAl(***Si***)$_2$ had been completely consumed. In its place, two new *m*-terphenyl products had formed, while the SiC*H*$_3$ region displayed three new signals: one major singlet ("a") and two smaller singlets ("b") of equal intensity.

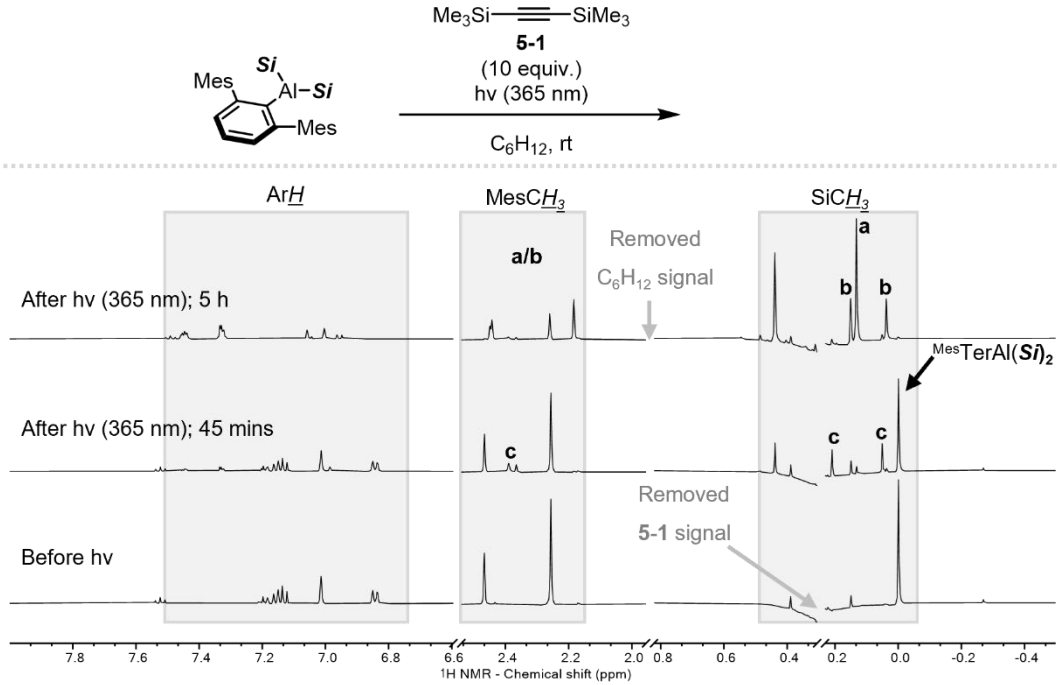

Scheme 5-21. Stacked ^{1}H NMR spectra (cyclohexane) monitoring the reaction between ^{Mes}TerAl(*Si*)$_2$ and alkyne **5-1** in cyclohexane at 365 nm. Formation of relevant new species are labelled "a", "b" and "c". Only areas of interest are included. *The large C$_6$H$_{12}$ solvent peak (δ 2.0 – 0.8) and the bis(trimethylsilyl)acetylene (5-1) reagent peak (δ 0.30 – 0.20) have been omitted for clarity.* ***Si*** = SiMe$_2$Ph.

The volatile components were removed *in vacuo* and the reaction mixture was redissolved in C_6D_6. The resulting spectrum (**Figure 5-3.i**) displayed the same ^{1}H resonances, attributed to those of disilane $(PhMe_2Si)_2$, that were observed when ^{Mes}TerAl(***Si***)$_2$ was irradiated in C_6D_6 in the absence of alkyne **5-1**. This time, the formation of $(PhMe_2Si)_2$ was confirmed by ^{13}C and ^{29}Si (^{1}H-^{n}X HMBC; **Figure 5-3.ii-iii**) NMR spectroscopy. The remaining reaction mixture consisted of the excess alkyne **5-1**, and two new *m*-terphenyl species, **5-A** (resonances labelled "a") and **5-B** (resonances labelled "b"). Attempted crystallisation of the crude mixture using a

combination of hexamethyldisiloxane (HMDSO) and pentane at –30 °C precipitated a white amorphous solid. This contained a mixture of **5-A** and **5-B** in an approximate 58:42 ratio, with only minor quantities of $(PhMe_2Si)_2$ and alkyne **5-1**. Unfortunately, repeated attempts to isolate these species by recrystallisation failed due to the small scale used and lack of available time.

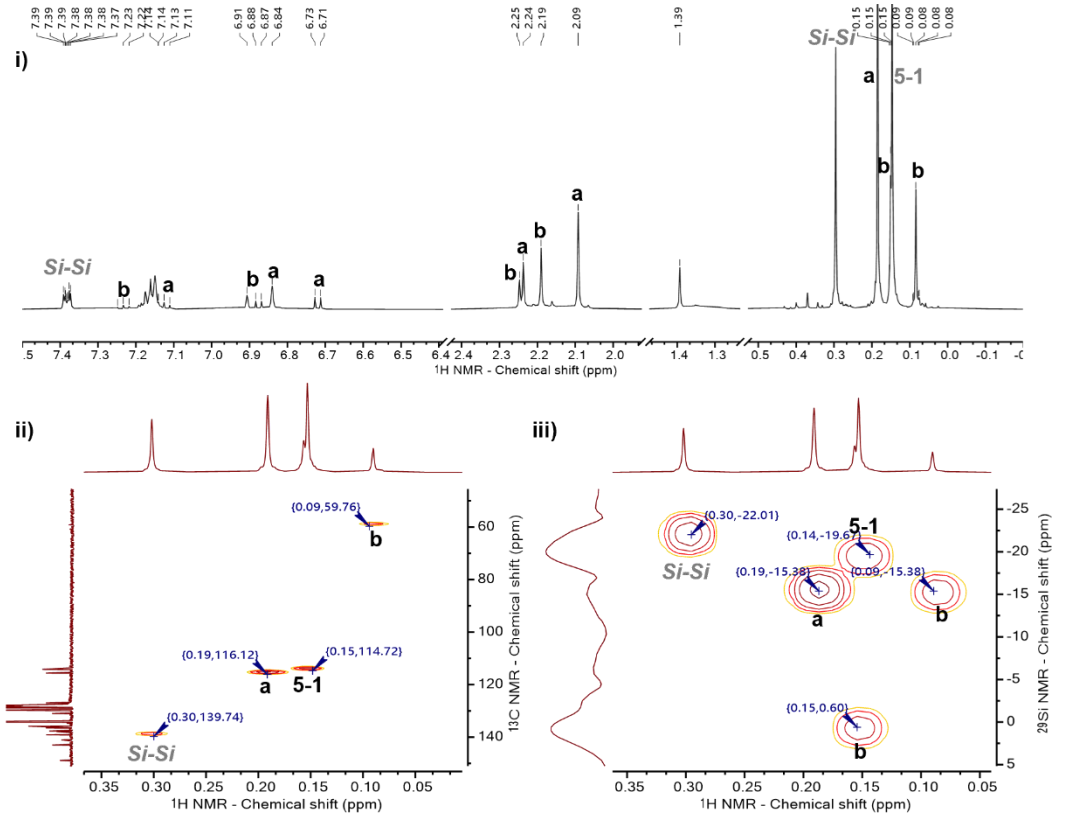

Figure 5-3. Crude NMR spectra (C_6D_6) obtained for the reaction between ^{Mes}TerAl(*Si*)$_2$ and alkyne **5-1** in cyclohexane at 365 nm. Relevant signals are labelled. **i)** ^{1}H NMR spectrum; **ii)** ^{1}H-^{13}C HMBC spectrum; **iii)** ^{1}H-^{29}Si HMBC spectrum. ***Si*** = $SiPhMe_2$; ***Si–Si*** = $(SiPhMe_2)_2$.

Based on the relative integrations of the *m*-terphenyl resonances in **5-A** and **5-B** in comparison with the newly formed SiC*H*$_3$ resonances from several fractions, it was inferred that **5-A** and **5-B** each contained four trimethylsilyl groups. This ruled out aluminacyclopropene derivative **5-C** as a possible product, even though aluminium(I) species have previously been observed to undergo [2+1] cycloaddition with the same alkyne, **5-1**.[399–401] However, initial formation of aluminacyclopropene derivative **5-C** might explain the intermediate formed after irradiation for 45 minutes. Presuming that the aluminium centre had indeed reacted at the alkyne position, and that the trimethylsilyl groups had not migrated, the 4:1 ratio of trimethylsilyl groups with respect to the *m*-terphenyl ligand suggested that both **5-A** and **5-B** possibly contained a 5-membered *Al*[$C_4(SiMe_3)_4$] core. Several structural isomers of ***E***[C_4R_4] are known or thought to exist (***E*** = R–element; **Figure 5-4**):

Figure 5-4. Comparison between the different possible geometric isomers of *E*[C_4R_4]; E = R-heteroatom (except for V, in which case it is just "heteroatom").

Cyclopentadiene derivative **I** is the most common. When E = Al–R, these species are called alumoles, of which several have been reported.[402–404] Bicyclic alkene isomer **II,** termed "housene" in reference to its appearance as a two-dimensional structure, has previously been reported when E = P–Cl.[405] Pyramidal structure **III** is called "pyramidane", and several of these have been reported for when E = Si,[406] Ge,[407] Sn,[407] Pb,[408] B–R (R = Cl[409] or C_6F_5[410]) and P^+.[405] A pentagermapyramidane (Ge_5R_4) has also been reported.[411] Tricyclic isomer **IV** has been theorised[412–414] but never isolated. The high ring strain associated with the bis-cyclopropane fragment likely corresponds to a highly strained system. Spiropentadiene isomer **V** has been isolated as an all-silicon system (Si_5R_4).[415] Since structures **I** to **III** are most commonly observed and structures **IV** and **V** exhibit high ring strain, only structures **I** to **III** were considered as possible geometries for **5-A** and **5-B**.

In **5-A**, the four trimethylsilyl groups displayed a single ^{1}H resonance at δ 0.19 which corresponded to 36 protons and indicated a highly symmetrical environment (assuming that a dynamic process was not occurring). From the structures previously discussed, this could only be possible in pyramidane structure **III**. The ^{13}C chemical shift of the skeletal carbon in pyramidines is particularly diagnostic for this structure. For pyramidanes with the E[$C_4(SiMe_3)_4$] core, ^{13}C signals are found in the region around δ 110 (see **Table 5-1**). To obtain the ^{13}C chemical shift associated with species **5-A**, ^{1}H-^{13}C HMBC was used to analyse the correlation with the SiC*H*$_3$ ^{1}H resonance at δ 0.19 (**Figure 5-3.ii)**. A cross-peak was observed with a ^{13}C signal at δ 116.1, which is consistent with the chemical shift reported for the other reported pyramidanes (**Table 5-1**). The ^{29}Si chemical shift of the trimethylsilyl group, obtained by ^{1}H-^{29}Si HMBC, was observed at δ –15.4 (**Figure 5-3.iii)**, which is also in the same region as those previously reported (**Table 5-1**). Combined, these results aligned with the assignment of a possible pyramidane structure for **5-A (Figure 5-5.ii)**.

Table 5-1. Comparison of ^{13}C chemical shifts for the skeletal carbon in pyramidanes containing an $E[C_4(SiMe_3)_4]$ core. A comparison with the lithium and magnesium cyclobutadiene salts are made. The colon (:) denotes a lone pair.

E	Si:[406]	Ge:[407]	Sn:[407]	Pb:[408]	B-Cl[409]	P^+[405]	5-A	Li[416]	Mg[417]
$\delta^{13}C$ (skeletal C)	101.0	102.9	106.5	114.8	101.8	114.9	116.1	104.1	109.2
$\delta^{29}Si$ ($-SiMe_3$)	-12.3	-12.6	-14.2	-18	-11	-3.9	-15.4	-23.7	-24.7

In contrast to **5-A**, the trimethylsilyl groups in **5-B** are inequivalent, with ^1H resonances at δ 0.16 and 0.09 corresponding to 18 protons each. This indicated that there are two trimethylsilyl groups at each of the two different chemical environments and suggested that the structure could either be alumole **I** or housene **II**. These structures can be readily distinguished by the ^{13}C chemical shift of the skeletal carbons.

The ^{13}C resonances for the skeletal carbons in alumole **5-3** (**Figure 5-5.i**),[402] have been located at δ 144.0 for Al*C*=C, and at δ 156.4 for AlC=*C*. Meanwhile, the ^{13}C resonances for phosphahousene **5-4 (Figure 5-5.ii)** have been calculated to be at δ 57.7 for sp^3-*C* and at δ 179.2 for sp^2-*C*.[405] However, due to rapid exchange of the P–Cl fragment across the C_4-base in comparison to the NMR timescale, **5-4** instead displays an averaged ^{13}C chemical shift at δ 111.8, which is close to the calculated average of δ 118.4. It could be argued that phosphorus is a very different element to aluminium, and therefore cannot be reasonably compared. However, to the best of my knowledge, this is the only reported example of a housene structure. In addition, the ^{13}C NMR chemical shift of the corresponding phosphapyramidane, $P^+[C_4(SiMe_3)_4]$ (δ114.9),[405] is similar to that observed for the proposed aluminapyramidane, **5-A** (δ116.1). Therefore, the comparison used may not be as unreasonable as first anticipated.

To obtain the ^{13}C chemical shift of the skeletal carbons in **5-B**, ^1H-^{13}C HMBC was used (**Figure 5-3.ii)**. Unfortunately, the cross-peak for the ^1H signal at δ 0.16 could not be found, perhaps due to a low signal-to-noise ratio at this region arising from the overlapping signals of residual alkyne **5-1**. However, the ^1H resonance at δ 0.09 displayed a cross-peak with the ^{13}C signal at δ 59.8, which is similar to the calculated chemical shift of the sp^3-*C* in phosphahousene **5-4**.[405] Notably, this signal appeared to be "silent" on the one-dimensional ^{13}C NMR spectrum. This could be explained by the line broadening effects that arise from coupling to the quadrupolar ^{27}Al nucleus. This observation suggested that the sp^3–C was attached to aluminium,

as would be expected in a housene structure. The ^{29}Si chemical shifts for the trimethylsilyl groups, obtained by ^{1}H-^{29}Si HMBC, were found at δ 0.6 and δ –15.4 (**Figure 5-3.iii)**. The average of these chemical shifts (δ –7.4) is consistent with the ^{29}Si chemical shift observed in phosphahousene **5-4** (δ –8.9), which itself is averaged due to the aforementioned hopping of the P–Cl fragment. Thus, the chemical shifts obtained for **5-B** are consistent with the formation of an aluminahousene structure (**Figure 5-5.ii**).

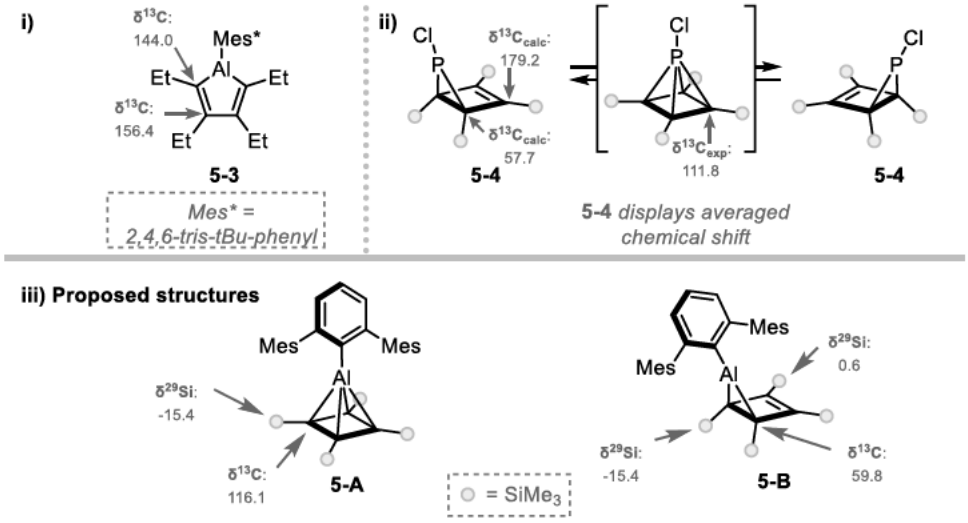

Figure 5-5. ^{13}C chemical shifts for relevant i) alumole or ii) housene reported structures; iii) Proposed structures for 5-A and 5-B.

5.3.6 How might 5-A and 5-B be formed?

The plausible formation of **5-A** and **5-B** from the irradiation of ^{Mes}TerAl(***Si***)$_2$ in the presence of alkyne **5-1** raises an intriguing question regarding their mechanism of formation. The formation of disilane (PhMe$_2$Si)$_2$ under these conditions suggested the generation of an aluminium(I) intermediate following stepwise cleavage of the Al–Si bonds. Based on the reported activity of aluminium(I) compounds with alkyne **5-1**, and of the observation of a short-lived unidentified species during the course of the reaction, it was possible that aluminacyclopropene derivative **5-C** was formed as an intermediate (**Scheme 5-22.i**). Aluminacyclopropenes have been proposed to react with alkynes by a [2+3] cycloaddition to give alumoles,[418] which in this case would generate alumole **5-D**. In a related boron analogue, borole **5-5** can be irradiated to generate borapyramidine **5-7** (**Scheme 5-22.ii**).[410] This reaction has been calculated to proceed by the borahousene intermediate **5-6**, presumably by a photochemically-mediated [2π+2π] electrocyclisation. A similar mechanism may explain the formation of pyramidane **5-A** from aluminacyclopropene **5-C** *via* housene **5-B (Scheme 5-22.i)**.

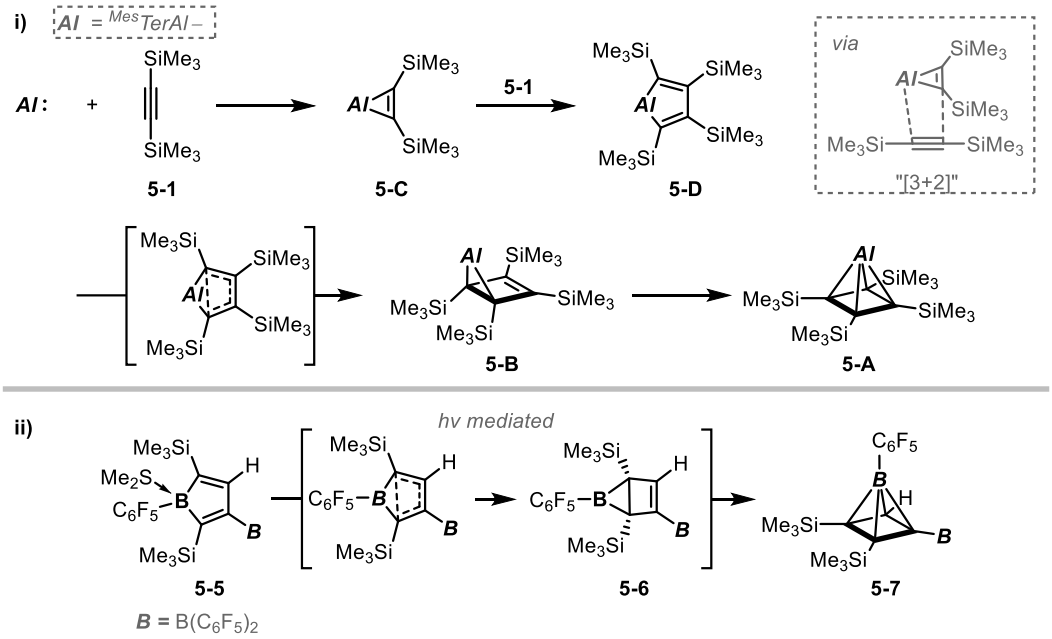

Scheme 5-22. i) Possible pathway for the generation of 5-A and 5-B inspired by reported pathways for the other *E*[C_4R_4] structures. ii) Formation of a borahousene 5-7 from borole 5-5 via borahousene 5-6.

The formation of borapyramidine **5-7** from borahousene **5-6** is calculated to be highly exergonic ($\Delta G° = -25.9$ kcal mol^{-1}) and almost barrierless ($\Delta G^{‡} = 0.6$ kcal mol^{-1}).[410] While the housene structure in this case represents a transition-state, changing the apex element from boron to aluminium has been calculated to greatly stabilise the housene isomer and can result in this structure being the energy minima.[419] This stabilisation possibly explains the formation of aluminahousene **5-B** in addition to aluminapyramidine **5-A**. When the apex consists of Al–Cl, a low barrier is calculated for the migration of aluminium around the C_4-base in housenes (*via* pyramidanes).[419] Presumably, the bulky *m*-terphenyl backbone in our system sufficiently impeded rapid migration of aluminium, allowing both isomers to be observed by NMR spectroscopy.

An alternative mechanism that proceeds without formation of alumole **5-D** could also be considered. In principle, aluminacyclopropene **5-C** could undergo a photochemically-mediated [2+2] cycloaddition with alkyne **5-1** to directly yield aluminahousene **5-B** (**Scheme 5-23**). This pathway would bypass a challenging insertion of alkyne **5-1** into the Al–C bonds of sterically congested aluminacyclopropene **5-C**. Again, interconversion of aluminahousene **5-B** would give aluminapyramidine **5-A**.

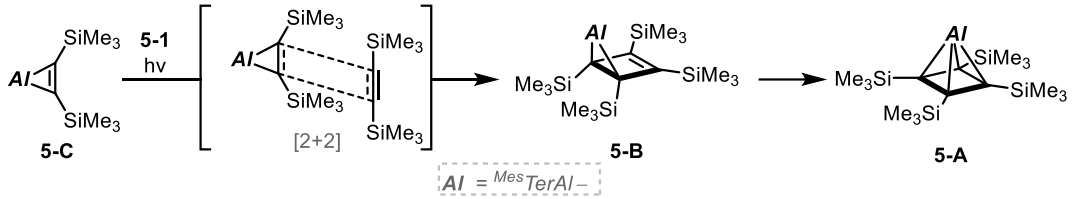

Scheme 5-23. Another possible route to 5-A and 5-B *via* [2+2] cycloaddition of 5-1 with 5-C.

To better understand the mechanism of formation of **5-A** and **5-B**, it would be useful to identify the unknown intermediate (proposed to be **5-C**) that originally forms in this reaction. Monitoring the relative formation of **5-A** and **5-B** over time might also provide clues to this and may enable the selective preparation of one isomer over the other.

5.4 Conclusions and future outlook

Silylboranes react with *m*-terphenyl-substituted alkyl alanes by Al–C/B–Si exchange to give access to silylalanes, with formation of C–B bonds as a strong driving force. Use of aluminium hydrides led predominantly to unselective exchange at the B–O position, while aluminium chlorides were unreactive (**Scheme 5-24.i**). A goldilocks zone was established whereby sufficient steric bulk at aluminium was required to avoid redistribution of substituents, while it was important to allow sufficient space at aluminium to allow interaction with the $PhMe_2SiBpin$ reagent (**Scheme 5-24.ii**).

The first Al–C/B–Si exchange at $^{Mes}TerAlMe_2$ involves $PhMe_2SiBpin$, while the second exchange at the resulting $^{Mes}TerAl(\boldsymbol{Si})Me$ intermediate requires the less sterically encumbered $PhMe_2SiBMe_2$ (**Scheme 5-24.ii**). This process can be enhanced by doping the reaction with $AlMe_3$, which most likely works by generating $PhMe_2SiBMe_2$ from $PhMe_2SiBpin$ by Al–C/B–O metathesis.

The photochemical properties and reactivity of $^{Mes}TerAl(\boldsymbol{Si})Me$ and $^{Mes}TerAl(\boldsymbol{Si})_2$ were probed (**Scheme 5-24.iii**). $^{Mes}TerAl(\boldsymbol{Si})Me$ did not absorb light at 365 nm, and this corresponded with a lack of reactivity under irradiation at this wavelength. In contrast, $^{Mes}TerAl(\boldsymbol{Si})_2$ absorbs moderately in this region, and this led to successful cleavage of the Al–Si bonds when irradiated, as evidenced by the formation of disilane $(PhMe_2Si)_2$ in C_6D_6 and cyclohexane. Cleavage of the Al–Si bonds may proceed in a stepwise manner, as suggested by the formation of $PhMe_2SiCl$ when $^{Mes}TerAl(\boldsymbol{Si})_2$ was irradiated in CH_2Cl_2, which functioned as a radical trap. These observations suggested that low-valent aluminium(I) species were likely generated *in situ* by photolysis, importantly negating the need to use reducing agents.

When ^{Mes}TerAl(*Si*)$_2$ was irradiated at 365 nm in the presence of bis(trimethylsilyl)acetylene **5-1**, the formation of two major products were observed, in addition to the disilane (PhMe$_2$Si)$_2$ by-product. By comparing the chemical shifts of these species with known structures, these products were postulated to be aluminapyramidane **5-A** and aluminahousene **5-B** (**Scheme 5-24.iv**). Further efforts are required to isolate these species in order to verify these proposed structures, but if this can be fulfilled, they would represent the first aluminium-containing compounds of these geometrical isomers.

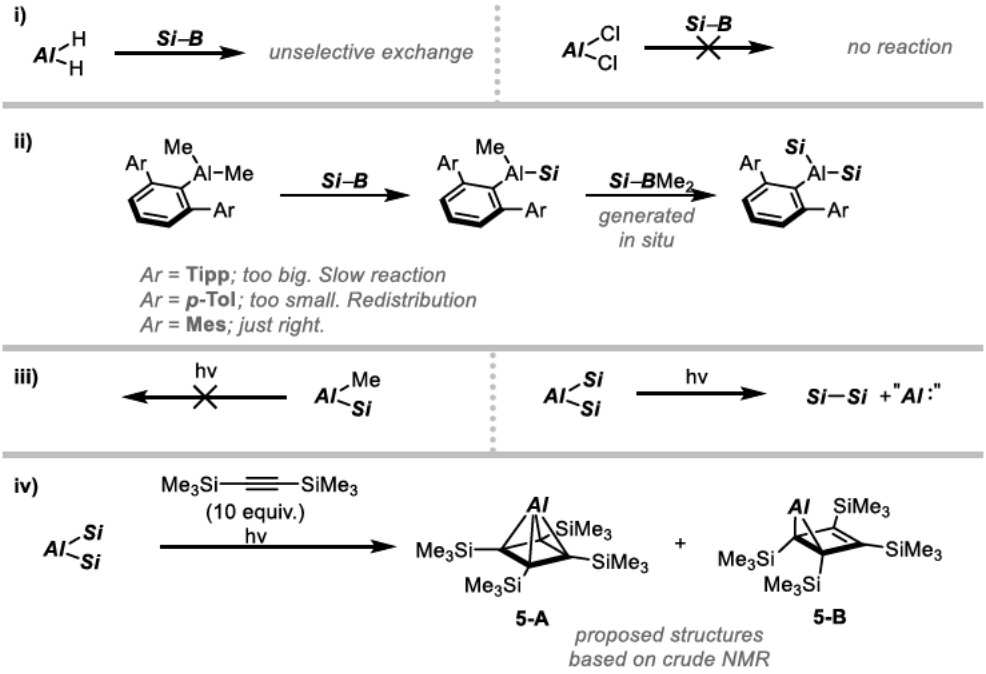

Scheme 5-24. Summary of Chapter 5: i) Al–H/B–Si exchange is unselective, Al–Cl/B–Si exchange does not proceed; ii) Al–*C*/*B*–*Si* exchange with *Si*-*B* is feasible for ^{Mes}TerAlMe$_2$ but not for ^{Mes}TerAl(*Si*)Me. Formation of ^{Mes}TerAl(Si)$_2$ likely requires Si–BMe$_2$; iii) Comparison of *Al*(*Si*)Me and Al(*Si*)$_2$ reactivity under irradiation; iv) possible formation of aluminapyramidane 5-A and aluminahousene 5-B structures following reactivity of *Al*(*Si*)$_2$ with bis(trimethylsilyl)acetylene under irradiation. *Al* = ^{Mes}TerAl-; *Si* = SiMe$_2$Ph; *B* = Bpin.

Future work should focus on several key areas:

- The reactivity of silylalanes with unsaturated substrates should be investigated, with the possibility of regenerating silylalanes using PhMe$_2$SiBpin in mind (**Scheme 5-25.i**). This would lead to a redox-neutral pathway that would avoid using hydrides as a turnover reagent.
- The possible isolation of the *in situ* generated aluminium(I) species should also be explored. As it can likely be generated from photolysis, isolation of an aluminium(I) species in a matrix may be possible (for example, in frozen cyclohexane).

- Given that an aluminium(I) species would formed be from the cleavage of an Al–Si bond rather than by reduction, the possibility of generating a rare example of a triplet aluminium(I) species should be examined. This may result in unique reactivity in comparison to singlet aluminium(I) examples. This could be conveniently studied from irradiating ^{Mes}TerAl(***Si***)$_2$ in the presence of relevant substrates.
- Finally, if ^{Mes}TerAl(***Si***)$_2$ can be regenerated using PhMe$_2$SiBpin from any intermediate, this would potentially unlock access to a redox-active catalytic pathway using photolysis to instigate “reductive elimination” at aluminium (**Scheme 5-25.ii**).

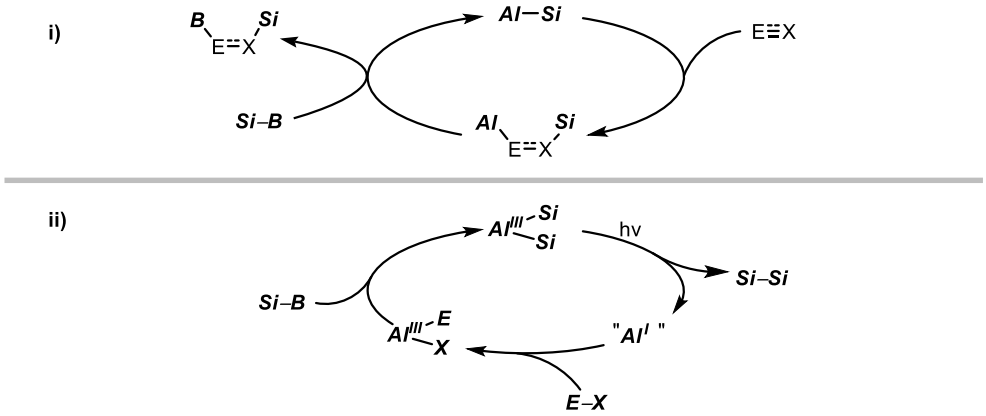

Scheme 5-25. Future work: Application of silylalanes in i) redox-neutral catalysis and ii) redox-active catalysis.

Chapter 6:

Overall conclusions and future outlook

At the outset of this work, aluminium/boron exchange had been proposed as a key process in aluminium-catalysed hydroboration reactions with HBpin. However, this process had not been comprehensively studied, particularly for alkene hydroboration. Moreover, the influence of catalyst structure had not been considered for this protocol. This work aimed to address this knowledge gap.

The catalytic activity of *m*-terphenyl alanes for alkene hydroboration with HBpin was initially investigated, with a view to understanding the impact on catalysis of steric bulk at aluminium. Catalysis proceeds at room temperature for the larger *m*-terphenyl alane catalysts (**Scheme 6-1**). Notably, 1,1-disubsituted alkenes are compatible under mild conditions. These are typically challenging substrates for the more established boron-catalysed procedures.

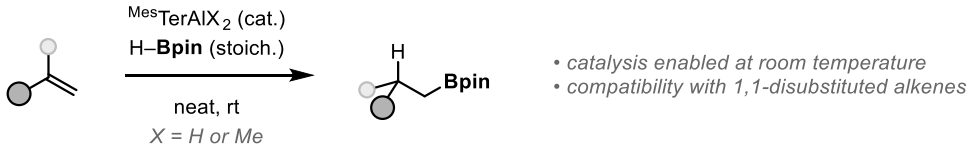

Scheme 6-1. *m*-Terphenyl alanes catalyse alkene hydroboration with HBpin under mild conditions.

However, the observed dependence on steric bulk at aluminium for catalysis is not consistent with the expected trend based on the commonly accepted and widely invoked pathway that proceeds by alkene hydroalumination and Al–C(sp^3)/B–H σ-bond metathesis. The fastest alane for the slow hydroalumination step (^{Tipp}Ter*Al*) is not the fastest catalyst (^{Mes}Ter*Al*). Moreover, the smallest system ($^{p\text{-}Tol}$Ter*Al*) is not catalytically active despite being capable of participating in the stoichiometric steps. This discrepancy is referred to as *the rate problem*.

The rate problem can be explained by examining how steric bulk impacts aluminium/boron exchange. Generally, Al–C(sp^3)/B–H exchange is extremely favourable for *m*-terphenyl alkyl alanes, proceeding rapidly and with selective exchange of the alkyl group – regardless of the steric bulk at aluminium. However, only the largest *m*-terphenyl alane (^{Tipp}Ter*Al*) can mitigate Al–H/B–O exchange; this means that the smaller systems (^{Mes}Ter*Al* and $^{p\text{-}Tol}$Ter*Al*) generate BH_3 *in situ* (**Scheme 6-2**). As a result, the secondary effects of BH_3 formation had to be considered when analysing the catalytic behaviour of these systems.

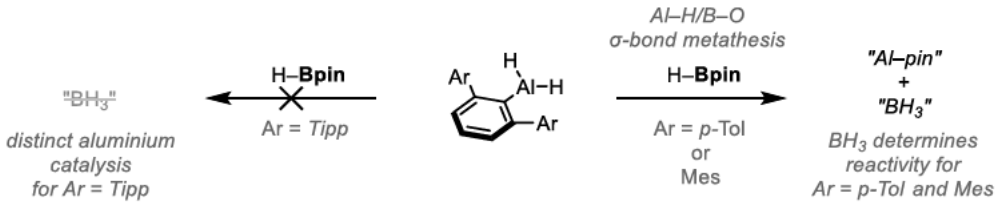

Scheme 6-2. Lack of steric bulk at aluminium leads to decomposition of HBpin to BH_3 by Al–H/B-O σ-bond metathesis.

BH_3 alone does not catalyse alkene hydroboration under the mild conditions used; however, the results presented in this thesis strongly indicate that it may function as a co-catalyst in the ^{Mes}Ter*Al* system. The formation of alkyl alanes – crucial intermediates for alkene hydroboration with HBpin – is likely mediated by an alkene hydroboration/ boron-to-aluminium alkyl transfer sequence. This mechanism bypasses a slow alkene hydroalumination step and can explain why the ^{Mes}Ter*Al* system is faster than the ^{Tipp}Ter*Al* system in catalysis. This has been termed *hidden cooperative catalysis* (**Scheme 6-3**). Key to the alkyl transfer step (B–C(sp^3)/Al–H exchange) is the formation of coordinatively saturated Al–H–B bridged species, which overcomes the thermodynamic challenge of converting strong B–C bonds to weak Al–C bonds.

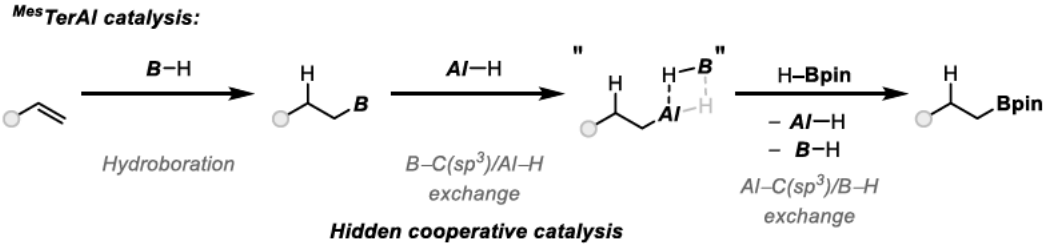

Scheme 6-3. Pictorial explanation of *hidden cooperative catalysis*.

Insufficient steric bulk at aluminium in the $^{p\text{-Tol}}$Ter*Al* system most likely means that the boron-to-aluminium alkyl transfer step is slower than the formation of stable Al–H–B aggregates. The absence of alkyl alane formation can likely account for the lack of catalytic activity in this system. Furthermore, insufficient steric bulk makes the alane susceptible to catalyst deactivation through redistribution processes.

The favourable Al–C(sp^3)/B–H exchange step was demonstrated by using HBdan, a hydridoborane with extremely diminished Lewis acidity, as the stoichiometric hydride source (**Scheme 6-4.i**). This breakthrough led to the development of aluminium catalysts for alkene hydroboration with HBdan (**Scheme 6-4.ii**); the first example of this transformation. The stability of HBdan precludes the formation of BH_3 under catalysis, meaning that the catalytic pathway proceeds by

distinct aluminium catalysis. The stability of Bdan was further established by performing transformations of alkylBdan compounds – with preservation of the 1,3,2-diazaborninine core – under oxidative conditions, or with anions such as fluoride and LiHMDS (**Scheme 6-4.iii**).

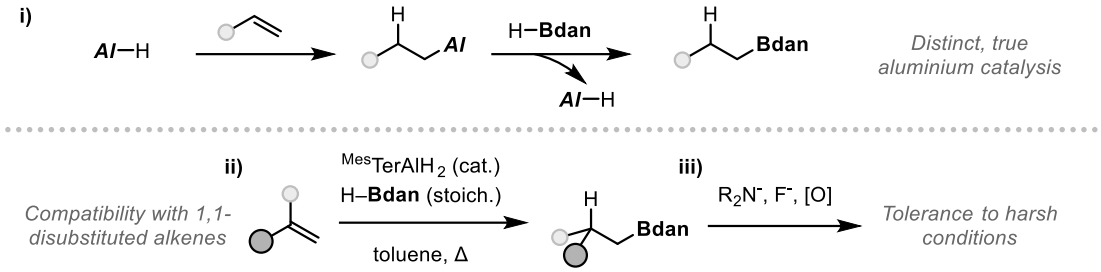

Scheme 6-4. i) HBdan reacts with alkyl alanes by Al–C(sp^3)/B–H σ-bond metathesis; ii) This allows *m*-terphenyl alanes to catalyse alkene hydroboration with HBdan. The stability of the Bdan products were demonstrated.

In addition to hydridoboranes, silylboranes ($PhMe_2SiBpin$) can also undergo aluminium/boron exchange with alkyl alanes, resulting in the formation of silylalanes, $^{Mes}TerAl(SiMe_2Ph)Me$ and $^{Mes}TerAl(SiMe_2Ph)_2$ (**Scheme 6-5.i**). Notably, disilylalane $^{Mes}TerAl(SiMe_2Ph)_2$ displays interesting photochemical behaviour; irradiation at 365 nm leads to cleavage of the Al–Si bonds, generating a disilane ($(SiMe_2Ph)_2$), implying that a potential reductive elimination process has occurred (**Scheme 6-5.ii**). Attempts to capture the proposed low oxidation-state aluminium species with bis(trimethylsilyl)acetylene led to the formation of two main compounds, which were tentatively assigned as pyramidane and housene structures (**Scheme 6-5.iii**). Further investigations would be required to verify their existence, but if confirmed, these would represent the first examples of such geometrical isomers involving aluminium.

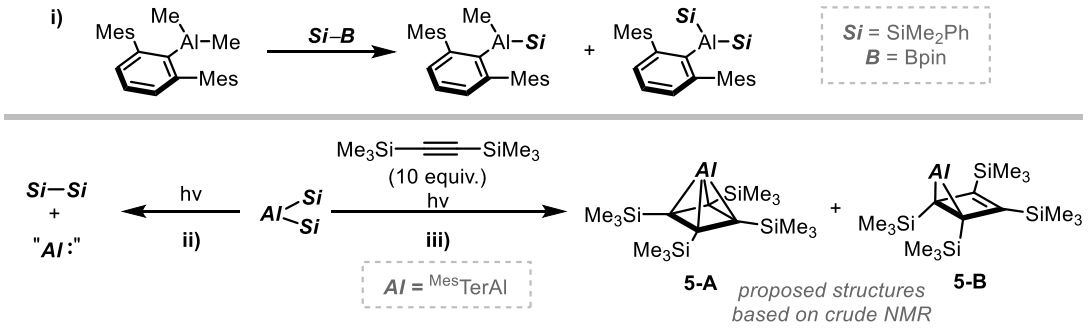

Scheme 6-5. i) Al–C(sp^3)/Si–B σ-bond metathesis generates silylalanes; ii) disilylalanes photolyse under irradiation; iii) in the presence of bis(trimethylsilyl)acetylene, pyramidanes and/or housenes may be formed.

Future research should explore the potential of combining enantioenriched boranes with aluminium hydrides as a synergistic approach for catalysing asymmetric alkene hydroboration with hydridoboranes. By avoiding background BH_3 formation –

using bulkier alanes or more stable hydridoboranes (such as HBdan) – it may be possible to achieve good enantioselectivity. Other stoichiometric hydride sources may also be considered. For example, the application of silanes might enable hydrosilylation reactions.

Additionally, the potential of silylalanes to mediate catalysis should be investigated. This could be achieved by exploring the stoichiometric reactivity of silylalanes with unsaturated substrates. If silylboranes can regenerate silylalanes by this route, this could unlock aluminium-catalysed silylboration reactions. Finally, the promising photochemical reactivity of disilylalanes should be further explored with the ultimate goal of achieving redox-active catalysis at an aluminium centre.

Chapter 7:

Experimental

7.1 General considerations

Reaction Setup: All reactions were performed in oven (110 °C) and/or flamed-dried glassware under an atmosphere of anhydrous and O_2-free nitrogen or argon, unless otherwise indicated. All air- and moisture sensitive reactions were carried out using standard vacuum line and Schlenk techniques, or in a glovebox with a purified argon atmosphere. All glassware was cleaned using base (KOH, *i*PrOH) and acid (HCl_{aq}) baths and rinsed 3 × with water. All reported reaction temperatures correspond to external bath temperatures. Room temperature (rt) was approximately 22 °C.

NMR Spectroscopy: ^{1}H, ^{11}B, ^{13}C, ^{19}F and ^{29}Si NMR spectra were recorded on Bruker Avance III 400 and 500 MHz; Bruker AVI 400 MHz; Bruker Avance I 600 MHz spectrometers and performed at 298 K using glass NMR tubes. Chemical shifts are reported in parts per million (ppm; δ). ^{1}H NMR spectra were referenced to the residual protonated solvent peak ($CHCl_3$: δ 7.26; C_6D_5H: δ 7.15; $CDHCl_2$: δ 5.32). ^{13}C NMR spectra were referenced to the deuterated solvent peak ($CDCl_3$, δ 77.16; C_6D_6: δ 128.06; CD_2Cl_2: δ 53.84).[420] ^{11}B NMR spectra were referenced externally to $Et_2O{\bullet}BF_3$ (δ 0.0). "Presat" refers to pre-saturation of the largest resonances (i.e. protonated solvent peaks) in the NMR spectrum. Multiplicities are indicated by app. (apparent), br. (broad), s (singlet), d (doublet), t (triplet), q (quartet), quin. (quintet), sext. (sextet), sept. (septet), non. (nonet). Coupling constants, *J*, are reported in Hertz and rounded to the nearest 0.1 Hz. Integration is provided and assignments are indicated.

Background suppression was applied to ^{11}B NMR spectra using the standard zgbs_bb pulse program. ^{11}B NMR spectra were then processed by manual phase correction followed by baseline correction using Whittaker Smoother (manually adjusted to avoid removing broad signals attributed to boron-containing compounds) – see section 7.7 for details.

Infrared Spectroscopy: Infra-red (IR) spectra of the compounds (neat) were recorded on a Shimadzu IRAffinity-1 spectrometer (serial no. A213749) spectrometer using ATR. Relevant peaks are reported in cm^{-1}.

Mass Spectrometry: Mass spectrometry (MS) was performed by the University of Edinburgh, School of Chemistry, Mass Spectrometry Laboratory. High resolution mass spectra were recorded on a VG autospec, or Thermo/Finnigan MAT 900, mass spectrometer. Electron Impact (EI^+) spectra were performed at 70 eV using methane as the carrier gas, with either a double focusing sector field (DFSF) or time-of-flight

(TOF) mass analyzer. Chemical Ionization (CI^+) spectra were performed with methane reagent gas, with either a double focusing sector field (DFSF) or time-of-flight (TOF) mass analyzer. Electrospray Ionization (ESI^+) spectra were performed using a time-of-flight (TOF) mass analyzer. Data are reported in the form of *m/z*.

Melting Points: Melting points (m.p.) were determined on a Stuart Scientific SMP10, or Griffin Gallankamp, melting point apparatus in capillary tubes and are uncorrected.

Chromatography: Analytical thin-layer chromatography was performed on aluminium-backed silica plates (Merck 60 F_{254}). Pet. eth. refers to petroleum ether 40-60. Product spots were visualised by UV light at 254 nm, and subsequently developed using potassium permanganate solution or by heating the TLC plate with a heat gun (to reveal diazaborinines). Flash column chromatography was performed on the Teledyne ISCO CombiFlash NextGen 300+ using RediSep Rf normal phase silica flash columns (12, 25, 40, or 80 g; 20-40 microns). Substrates were purified using 40/60 petroleum ether and EtOAc on a gradient of 100:0 to 0:100 with flow rates of 10-110 mL min-1 depending on the size of column and ΔRf.

Solvents: Anhydrous C_6D_6 was distilled from potassium. CD_2Cl_2 was dried by percolation through a plug of neutral alumina under a positive pressure of argon. Both C_6D_6 and CD_2Cl_2 were degassed using three cycles of free/pump/thaw. Protonated reaction solvents (CH_2Cl_2, THF, Et_2O, toluene, pentane, hexane) were obtained from an inert purification system (*Inert: PureSolv MD5)*. All dry solvents were stored over 4 Å molecular sieves and kept under an argon atmosphere. Solvents for filtration, transfers, chromatography, and recrystallization were dichloromethane (CH_2Cl_2) (ACS grade, amylene stabilized), ether (Et_2O) (Fisher, BHT stabilized ACS grade), ethyl acetate (EtOAc) (Fisher, ACS grade), hexane (Optima), methanol (MeOH) (ACS grade), pentane (ACS grade), and petroleum ether (40–60°C, ACS grade).

Chemicals: All reagents were purchased from Merck, Alfa Aesar, Acros organics, Tokyo Chemical Industries UK, Fluorochem and Apollo Scientific or synthesised within the laboratory. $AlMe_2Cl$ (1.0 M in hexanes), $AlEt_2Cl$ (1 M in hexanes) and *n*BuLi (2.5 M in hexanes) were transferred into an airtight J. Young's tap ampoule and then used as supplied. HBpin was distilled and stored in a glovebox freezer (–30 °C) and thawed before use. Alkenes were passed through a small plug of alumina and sparged with a stream of nitrogen. $LiAlH_4$ was purified by extraction with Et_2O to afford a white solid after removal of solvent *in vacuo*, and stored under an inert atmosphere. MesI,[421] TippI,[421] $Me_3N{\bullet}AlH_3$[422], HBdan[292], MesBpin,[423] $MesBH_2$,[424] *t*$BuCH_2CH_2$Bpin[81]

were synthesised according to previously reported procedures. All other reagents were used as supplied unless indicated otherwise.

Note: in most cases, the experiment code has been provided as a reference to group members.

7.2 Synthesis of *m*-terphenyl alanes

General procedure A: preparation of m-terphenyl iodides

By modification of the method of Figueroa.[231]

An aryl Grignard solution was freshly prepared prior to synthesis of the *m*-terphenyl iodide as follows:

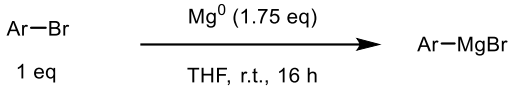

A solution of aryl bromide (120 mmol) in THF (150 mL) was added dropwise to a suspension of magnesium turnings (5.10 g, 210 mmol) in THF (150 mL) at a rate such that the suspension did not reflux. The suspension was stirred at room temperature for 16 hours to give a dark solution. After allowing the solids to settle, the solution was transferred *via* cannula directly into a dropping funnel when required in the next step.

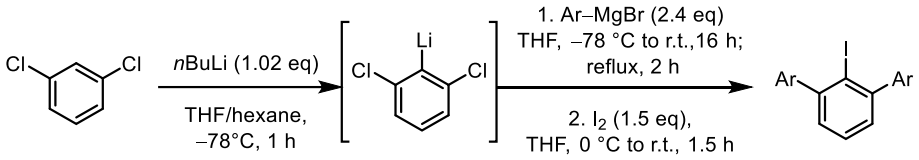

n-Butyl lithium (2.5 M solution in hexanes, 20.5 mL, 51.2 mmol, 1.02 equiv.) was added dropwise over 30 minutes to a solution of 1,3-dichlorobenzene (5.85 mL, 50.2 mmol, 1 equiv.) in THF (100 mL) at −78 °C, resulting in the formation of a white suspension. The suspension was stirred at this temperature for a further 1 hour, then treated with the freshly prepared aryl magnesium bromide solution (0.4 M in THF, 300 mL, 120 mmol, 2.4 equiv.), which was added dropwise over 2 hours. *Note: during these 3 hours of nBuLi and ArMgBr addition, the reaction temperature was maintained at –78 °C to avoid exothermic decomposition, which is thought to occur above –50 °C for 2,6-dichlorophenyl lithium.*[425] The resulting light-brown solution was slowly warmed to room temperature over 16 hours, then heated under reflux for 2 hours. The solution was cooled to 0 °C and iodine (19.1 g, 75.3 mmol, 1.5 equiv.) was added as a solid in one portion. The cold bath was removed and the solution was stirred at room temperature for 1.5 hours. Excess iodine in the solution was quenched with a saturated aqueous solution of Na_2SO_3 (*ca.* 100 mL) and the resulting thick white aqueous phase was separated from the organic phase. The aqueous phase was extracted with Et_2O (3 × 150 mL) and the combined organic phases were washed once with brine (*ca.* 20 mL), dried ($MgSO_4$), filtered and concentrated *in vacuo* to give a semi-solid. The crude product was then purified as specified.

$^{p\text{-Tol}}$TerI (ABG-0115)

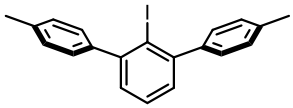

According to general procedure A, 4-bromotoluene (20.9 g, 120 mmol), magnesium turnings (5.10 g, 210 mmol), *n*-butyl lithium (2.5 M solution in hexanes, 20.5 mL, 51.2 mmol), 1,3-dichlorobenzene (5.85 mL, 50.2 mmol) and iodine (19.1 g, 75.3 mmol) were reacted. The product was washed with hexanes (4 × 10 mL), suspended in EtOH (150 mL) then heated to reflux for 2 hours. The white amorphous solid was cooled to 0°C, filtered cold then washed with cold MeOH (2 × 3 mL) and cold pentane (2 × 15 mL). The product was dried under high vacuum (0.01-0.001 mbar) for 2 hours to give $^{p\text{-Tol}}$TerI as an amorphous white solid (12.5 g, 65%).

^{1}H NMR (500 MHz, Chloroform-*d*) δ 7.39 (app. dd, *J* = 7.9, 7.1 Hz, 1H; Ar', *p*-*H*), 7.32 – 7.24 (m, 10H; Ar' and *p*-Tol, 10 × Ar*H*), 2.45 (s, 6H; *p*-Tol, 2 × C*H*$_3$).

^{13}C {^{1}H} NMR (126 MHz, Chloroform-*d*) δ 147.8, 142.7, 137.0, 129.1, 128.4, 128.3, 127.3, 104.0, 21.1.

Data were in accordance with those previously reported.[426]

$^{p\text{-Tol}}$TerLi (ABG-0212)

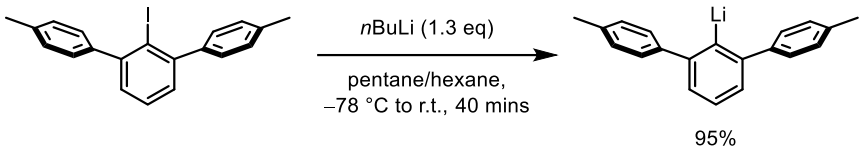

95%

By modification of the method of Parkin,[427] $^{p\text{-Tol}}$TerI (3.84 g, 10 mmol, 1 equiv.) was suspended in pentane (40 mL) and cooled to –78 °C. *n*-Butyl lithium (2.5 M solution in hexanes, 5.2 mL, 13 mmol, 1.3 equiv.) was added dropwise and the cold bath was removed. The solution was stirred for 40 minutes as it warmed to room temperature and the white suspension was filtered on a frit. The solid was washed with pentane (2 × 10 mL) and dried *in vacuo* to give the $^{p\text{-Tol}}$TerLi as an amorphous white solid (2.51 g, 95%).

^{1}H NMR (500 MHz, Benzene-d_6) δ 7.42 (d, *J* = 7.5 Hz, 2H; Ar', 2 × *m*-*H*), 7.33 (d, *J* = 7.7 Hz, 4H; *p*-Tol, 4 × Ar*H*), 7.30 (t, *J* = 7.5 Hz, 1H; Ar', *p*-*H*), 6.77 (d, *J* = 7.5 Hz, 4H; *p*-Tol, 4 × Ar*H*), 2.03 (s, 6H; *p*-Tol, 2 × CH_3).

^{13}C {^{1}H} NMR (126 MHz, Benzene-d_6) δ 151.7, 144.3, 136.0, 130.6, 126.5, 126.1, 124.0, 20.5. (*C*-Li not observed, presumably due to quadrupolar line broadening from ^{7}Li)

^{7}Li NMR (194 MHz, Benzene-d_6) δ 2.17.

Data were in accordance with those previously reported.[427]

$^{p\text{-Tol}}$TerAlH$_3$Li•(OEt$_2$)$_{0.5}$ (ABG-0215)

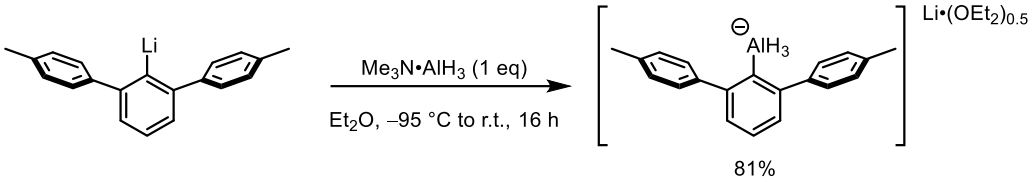

A solution of $H_3Al•NMe_3$ (847 mg, 9.5 mmol) in Et_2O (40 mL) was added dropwise to a cold solution of $^{p\text{-Tol}}$TerLi (2.51 g, 9.5 mmol) in Et_2O (20 mL) at −95 °C. The reaction was stirred for 16 hours and allowed to slowly warm to room temperature. The solvent was removed *in vacuo* and pumped for *ca.* 2 hours at 40 °C to give a foam. The foam was dissolved in Et_2O (10 mL) and hexane (50 mL) and the solution was concentrated *in vacuo* to *ca*. 10 mL to give an amorphous white solid and a white gel-like substance. The mixture washed with pentane (2 × 10 mL) and dried *in vacuo* to give $^{p\text{-Tol}}$TerAlH$_3$Li•(OEt$_2$)$_{0.5}$ as a free flowing white amorphous solid (2.56 g, 81%).

^{1}H NMR (500 MHz, Benzene-d_6) δ 7.45 (d, *J* = 7.5 Hz, 4H; *p*-Tol, 4 × Ar*H*), 7.36 (d, *J* = 7.9 Hz, 2H; Ar', 2 × *m*-*H*), 7.30 (app. dd, *J* = 8.4, 6.6 Hz, 1H; Ar', *p*-*H*), 7.01 – 6.95 (m, 4H; *p*-Tol, 4 × Ar*H*), 3.15 (q, *J* = 7.0 Hz, 2H; OC*H*$_2$CH$_3$, 2.15 (s, 6H; *p*-Tol, 2 × C*H*$_3$), 0.97 (t, *J* = 7.0 Hz, 3H; OCH$_2$C*H*$_3$).

^{13}C {^{1}H} NMR (126 MHz, Benzene-d_6) δ 152.4, 145.6, 136.4, 130.2, 129.6, 129.3, 127.0, 65.9, 21.1, 15.2. (*C*-Al carbon not observed, presumably due to quadrupolar line broadening from ^{27}Al).

^{7}Li NMR (194 MHz, Benzene-d_6) δ -2.61.

IR (neat) 3038*w*, 2976w, 2920w, 1757*m* (broad), 1513*m*, 1434*m*

MS HRMS-EI (m/z): found 286.1294; $[M-H]^{\bullet+}$ ($C_{20}H_{19}Al$), requires 286.1297

$^{p\text{-Tol}}$TerAlH$_2$ (ABG-0218)

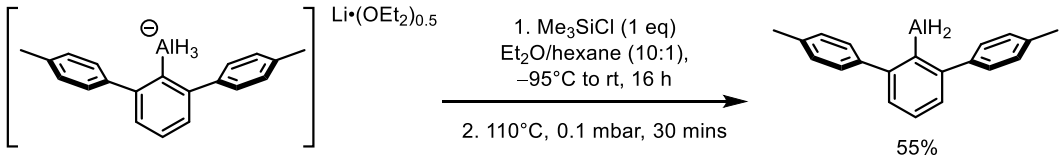

Me_3SiCl (933 µL, 7.35 mmol, 1 equiv.) was added dropwise to a suspension of $^{p\text{-Tol}}$TerAlH$_3$Li•(OEt$_2$)$_{0.5}$ (2.43 g, 7.35 mmol, 1 equiv.) in Et$_2$O/*n*-hexane (10:1, 60 mL) at −95 °C. The reaction was stirred for 16 hours with slow warming to room temperature. The precipitated salts were separated by filtration and the colourless filtrate was diluted with hexane (*ca.* 60 mL). The solution was concentrated *in vacuo* to *ca.* 15 mL and stored at −20 °C over 3 days to precipitate an amorphous white powder. The solid was filtered and then washed with pentane (2 × 5 mL). Volatiles were removed *in vacuo*, firstly at room temperature and then heated at 110 °C (*ca.* 0.1 mbar) for 30 minutes to give $^{p\text{-Tol}}$TerAlH$_2$ as an amorphous white powder (1.16 g, 55% yield).

^{1}H NMR (500 MHz, Benzene-d_6) δ 7.32 – 7.16 (m, 7H; 7 × Ar*H*), 6.94 (d, *J* = 7.7 Hz, 4H; 4 × Ar*H*), 3.61 (br s, 2H; Al*H*$_2$), 2.17 (s, 6H; *p*-Tol, 2 × C*H*$_3$).

IR (CH_2Cl_2) 2978*w*, 1869*w* (br, Al-H), 1360*s*, 1306*s*

EA Multiple attempts to obtain elemental analysis (EA) failed.

MS HRMS-EI (m/z): found 567.2187; [M_2-5H (decomp)] ($C_{40}H_{33}Al_2$), requires 567.2208*

The resulting compound gave a poor ^{13}C NMR spectra in the absence of added THF (*ca.* 5 equiv.) due to low solubility.

$^{p\text{-Tol}}$TerAlH$_2$•THF

^{1}H NMR (500 MHz, Benzene-d_6, THF) δ 7.75 – 7.69 (m, 4H; *p*-Tol, 4 × Ar*H*), 7.51 (d, *J* = 7.6 Hz, 2H; Ar', 2 × *m*-*H*), 7.40 (app. dd, *J* = 8.1, 7.0 Hz, 1H; Ar', *p*-*H*), 7.09 (d, *J* = 7.7 Hz, 4H; *p*-Tol, 4 × Ar*H*), 4.28 (s, 2H; Al*H*$_2$), 2.12 (s, 6H; *p*-Tol, C*H*$_3$).

^{13}C {^{1}H} NMR (126 MHz, Benzene-d_6, THF) δ 152.7, 144.9, 136.1, 129.5, 129.1, 128.2, 126.9, 21.0. (*C*-Al not observed, presumably due to quadrupolar line broadening from ^{27}Al)

*Although only the decomposition product could be observed by mass spectrometry, the primary alane was crystallised as the DMAP-adduct to confirm the aluminium dihydride functionality:

$^{p\text{-Tol}}$TerAlH$_2$•DMAP (ABG-0549)

C_6D_6 (0.6 mL) was added to a mixture of $^{p\text{-Tol}}$TerAlH$_2$ (28.6 mg, 0.1 mmol) and DMAP (12.2 mg, 0.1 mmol, 1 equiv.) in an NMR tube at room temperature. The mixture was shaken vigorously and the resulting colourless solution was analysed by NMR spectroscopy after *ca.* 10 minutes, which revealed the clean formation of $^{p\text{-Tol}}$TerAlH$_2$•DMAP. The solvent was removed *in vacuo* and the crude reaction mixture was recrystallised from toluene/hexane (70:30, 0.7 mL) with slow cooling to give $^{p\text{-Tol}}$TerAlH$_2$•DMAP as colourless block crystals.

^{1}H NMR (601 MHz, Benzene-d_6) δ 7.77 (d, J = 7.8 Hz, 4H; *p*-Tol, 4 × Ar*H*), 7.56 (d, J = 7.6 Hz, 2H; Ar', 2 × *m*-*H*), 7.43 (t, J = 7.6 Hz, 1H; Ar', *p*-*H*), 7.38 (app br s, $w_{1/2}$ ~ 14 Hz, 2H; DMAP, 2 × Ar*H*), 7.01 (d, J = 7.7 Hz, 4H; *p*-Tol, 4 × Ar*H*), 5.22 (d, J = 7.0 Hz, 2H; DMAP, 2 × Ar*H*), 4.81 (br s, $w_{1/2}$ ~ 87 Hz, 2H; Al*H$_2$*), 2.10 (s, 6H; *p*-Tol, 2 × C*H$_3$*), 1.83 (s, 6H; DMAP, 2 × C*H$_3$*).

^{13}C {^{1}H} NMR (151 MHz, Benzene-d_6) δ 154.5 (DMAP, *C*NR$_2$, 153.4 (Ar, *o*-C$_{Ar}$), 150.0 (observed by HMBC; Ar', *ipso*-*C$_{Ar}$*Al), 146.9 (DMAP, *C$_{Ar}$*H), 145.3 (*p*-Tol, *ipso*-*C$_{Ar}$*), 135.4 (*p*-Tol, *C$_{Ar}$*CH$_3$), 129.5 (*p*-Tol, *C$_{Ar}$*H), 129.2 (*p*-Tol, *C$_{Ar}$*H), 127.7 (Ar, *p*-*C$_{Ar}$*H, 126.9 (Ar, *m*-*C$_{Ar}$*H), 105.6 (DMAP, *C$_{Ar}$*H, 38.0 (DMAP, *C*H$_3$, 21.1 (*p*-Tol, *C*H$_3$).

XRD See **section 7.8**

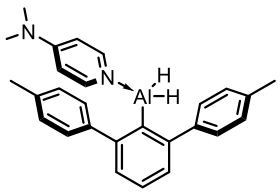

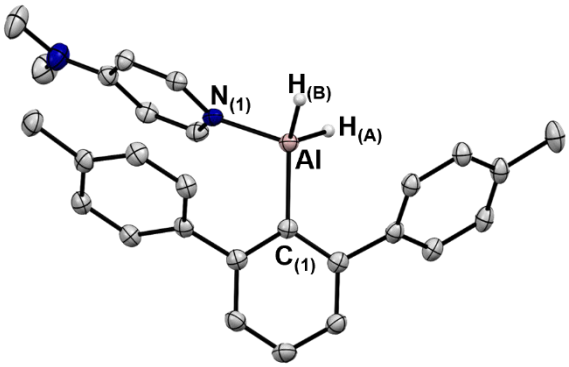

$^{p\text{-Tol}}$TerAlMe$_2$ (ABG-0137)

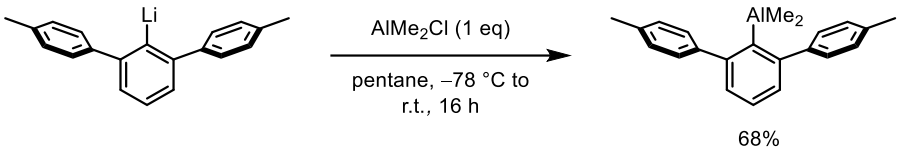

$AlMe_2Cl$ (1 M in hexanes, 5 mL, 5 mmol) was added dropwise to a suspension of $^{p\text{-Tol}}$TerLi (1.32 g, 5 mmol) in pentane (20 mL) at −78 °C. The solution was stirred for 16 hours and allowed to warm to room temperature. The precipitated salts were separated by filtration and the colourless filtrate was concentrated *in vacuo* to *ca*. 10 mL. The solution was placed in a −20 °C freezer yielding $^{p\text{-Tol}}$TerAlMe$_2$ as colourless needles over several days. Concentration of the mother liquor yielded a second crop of colourless needles (combined yield: 1.07 g, 68% yield).

^{1}H NMR (500 MHz, Benzene-d_6) δ 7.48 – 7.45 (m, 2H; Ar', 2 × *m*-*H*), 7.41 – 7.38 (m, 4H; *p*-Tol, 4 × Ar*H*), 7.38 – 7.35 (app. dd, *J* = 8.1, 7.0, Hz 1H; Ar', *p*-*H*), 7.00 (d, *J* = 7.7 Hz, 4H; *p*-Tol, 4 × Ar*H*), 2.05 (s, 6H; *p*-Tol, 2 × C*H*$_3$), -0.53 (s, 6H; 2 × Al-C*H*$_3$).

^{13}C {^{1}H} NMR (126 MHz, Benzene-d_6) δ 150.1, 145.8, 137.5, 131.8, 129.3, 126.3, 125.0, 20.9, -7.1. (*C*-Al not observed, presumably due to quadrupolar line broadening from ^{27}Al).

IR (neat) 2920*w*, 1512*m*, 1442*m*, 1179*s*, 1104*s*

m.p. (*n*-pentane) 114-115°C

EA Calculated for $C_{22}H_{23}Al$: C, 84.04; H, 7.37. Found: C, 83.75; H, 7.38

^{Mes}TerI (ABG-0221)

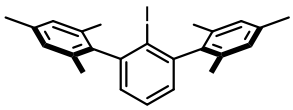

According to general procedure A, mesityl bromide (18.7 mL, 120 mmol), magnesium turnings (5.10 g, 210 mmol), *n*-butyl lithium (2.5 M solution in hexanes, 20.5 mL, 51.2 mmol), 1,3-dichlorobenzene (5.85 mL, 50.2 mmol) and iodine (19.1 g, 75.3 mmol) were reacted. The product was distilled under high vacuum (0.01 mbar) at 130 °C to remove mesityl iodide and residual solvents. The light-yellow solid was suspended in EtOH (200 mL), heated to reflux for 2 h and then slowly cooled to room temperature. The off-white solid was filtered from the yellow solution, then recrystallised (hot toluene/MeOH) to give ^{Mes}TerI as colourless needles (13.9 g, 63%).

^{1}H NMR (500 MHz, Chloroform-*d*) δ 7.46 (t, *J* = 7.5 Hz, 1H; Ar', *p*-H), 7.08 (d, *J* = 7.4 Hz, 2H; Ar', 2 × *m*-H), 6.96 (s, 4H; Mes, 4 × *m*-H), 2.35 (s, 6H; Mes, 2 × *p*-CH_3), 1.98 (s, 12H; Mes, 4 × *o*-CH_3).

^{13}C {^{1}H} NMR (126 MHz, Chloroform-*d*) δ 147.1, 142.1, 137.2, 135.4, 128.8, 128.1, 127.8, 107.6, 21.2, 20.2.

Data were in accordance with those previously reported.[428]

^{Mes}TerLi (ABG-0230)

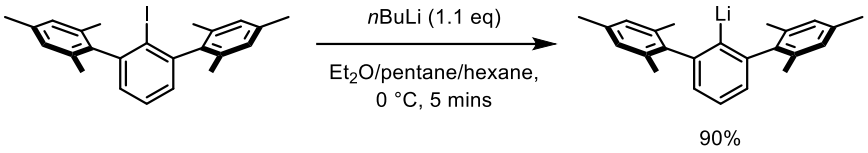

^{Mes}TerI (4.41 g, 10 mmol, 1 equiv.) was suspended in Et_2O/pentane (1:1, 40 mL) and cooled to 0 °C. *n*-Butyl lithium (2.5 M solution in hexanes, 4.4 mL, 11 mmol, 1.1 equiv.) was added dropwise over 2 minutes to give a pale-yellow solution. The solution was stirred at this temperature for 5 minutes and the solvent was removed *in vacuo* in the ice bath. The white solid was washed with pentane (2 × 10 mL) and dried *in vacuo* for 1 hour to give ^{Mes}TerLi as a free flowing, white amorphous solid (2.88 g, 90%)

^{1}H NMR (500 MHz, Benzene-d_6) δ 7.22 (t, *J* = 7.5 Hz, 1H; Ar', *p*-*H*), 6.83 (q, *J* = 7.4 Hz, 6H; Ar', 2 × *m*-H overlapped with Mes, 4 × *m*-*H*), 2.17 (s, 6H; Mes, 2 × *p*-C*H*$_3$), 1.82 (s, 12H; Mes, 4 × *o*-C*H*$_3$).

^{13}C {^{1}H} NMR (126 MHz, Benzene-d_6) δ 151.5, 143.0, 136.0, 136.0, 135.4, 129.4, 123.4, 21.2, 20.8. (*C*-Li not observed, presumably due to quadrupolar line broadening from ^{7}Li)

^{7}Li NMR (194 MHz, Benzene-d_6) δ 1.53.

Data were in accordance with those previously reported.[429]

^{Mes}TerAlH$_3$•Li (ABG-0231)

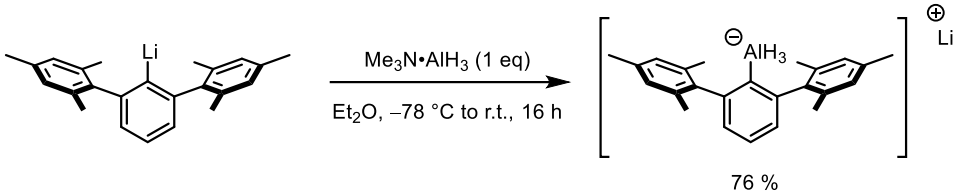

By modification of the method of Power,[234] a solution of $Me_3N•AlH_3$ (308 mg, 3.46 mmol) in Et_2O (20 mL) was added dropwise to a cold solution of ^{Mes}TerLi (1.11 g, 3.46 mmol) in Et_2O (20 mL) at −78 °C. The reaction was stirred for 16 hours and allowed to slowly warm to room temperature. The solvent was removed *in vacuo* and stirred *in vacuo* for *ca.* 2 hours. The white solid was washed with hexanes (2 × 5 mL) and dried *in vacuo* for 1.5 hours to give ^{Mes}TerAlH$_3$•Li as an amorphous white solid (923 mg, 76%).

^{1}H NMR (500 MHz, Benzene-d_6) δ 7.34 (t, *J* = 7.5 Hz, 1H; Ar', *p*-*H*), 6.97 (s, 4H; Mes, 4 × *m*-*H*), 6.95 (d, *J* = 7.5 Hz, 2H; Ar', 2 × *m*-*H*), 2.24 (s, 6H; Mes, 2 × *p*-C*H*$_3$), 2.10 (s, 12H; Mes, 4 × *o*-C*H*$_3$).

^{13}C {^{1}H} NMR (126 MHz, Benzene-d_6, THF) δ 151.5, 145.1, 136.7, 134.5, 127.9, 127.6, 126.0, 21.7, 21.3. (*C*-Al not observed, presumably due to quadrupolar line broadening from ^{27}Al)

^{7}Li NMR (194 MHz, Benzene-d_6) δ -3.52.

Data were in accordance with those previously reported**.**[234]

^{Mes}TerAlH$_2$ (ABG-0233)

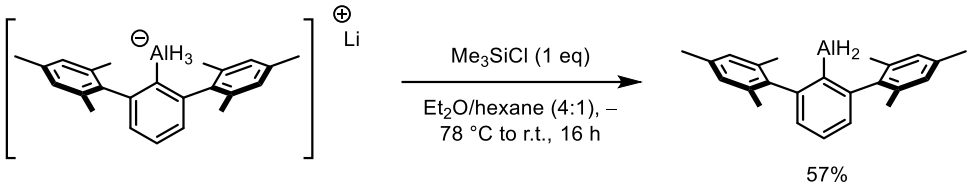

By modification of the method of Power,[234] Me_3SiCl (435 µL, 3.43 mmol) was added dropwise to a suspension of ^{Mes}TerAlH$_3$•Li (1.20 g, 3.43 mmol) in Et_2O/*n*-hexane (4:1, 22 mL) at −78 °C. The reaction was stirred for 16 hours and slowly warmed to room temperature. The precipitated salts were separated by filtration and the volatiles from the filtrate were removed *in vacuo*. The white solid was washed with pentane (2 × 10 mL) then dried *in vacuo* for 1 hour to yield ^{Mes}TerAlH$_2$ as an amorphous white solid (580 mg, 51%). More product was obtained by concentrating the mother liquor to *ca.* 15 ml, followed by slow cooling to −20 °C to yield colourless needles of ^{Mes}TerAlH$_2$ (combined yield: 666 mg, 57%).

^{1}H NMR (500 MHz, Benzene-d_6) δ 7.21 (t, *J* = 7.6 Hz, 1H; Ar', *p*-*H*), 6.89 (d, *J* = 7.6 Hz, 2H; Ar', 2 × *m*-*H*), 6.85 (s, 4H; Mes, 4 × *m*-*H*), 3.45 (s, 2H; Al*H*$_2$), 2.27 (s, 6H; Mes, 2 × *p*-C*H*$_3$), 1.99 (s, 12H; Mes, 4 × *o*-C*H*$_3$).

^{13}C {^{1}H} NMR (126 MHz, Benzene-d_6) δ 151.1, 141.3, 136.7, 136.0, 130.3, 128.9, 126.3, 21.4, 20.9. (*C*-Al not observed, presumably due to quadrupolar line broadening from ^{27}Al)

Data were in accordance with those previously reported.[234]

^{Mes}TerAlMe$_2$ (ABG-0144)

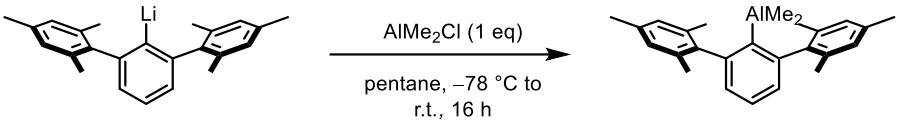

63%

By modification of the method of Power,[237] $AlMe_2Cl$ (1 M in hexanes, 4.52 mL, 4.52 mmol) was added dropwise to a suspension of ^{Mes}TerLi (1.45 g, 4.52 mmol) in *n*-hexane (20 mL) at −78 °C. The solution was stirred for 16 hours and allowed to warm to room temperature. The precipitated salts were separated by filtration and the colourless filtrate was dried *in vacuo* to give ^{Mes}TerAlMe$_2$ as an amorphous white solid (1.06 g, 63% yield).

^{1}H NMR (500 MHz, Benzene-d_6) δ 7.34 (t, *J* = 7.6 Hz, 1H; Ar', *p*-H), 7.02 (d, *J* = 7.6z Hz, 2H; Ar', 2 × *m*-H), 6.83 (s, 4H; Mes, 4 × *m*-H), 2.14 (s, 12H; Mes, 4 × *o*-CH_3), 2.10 (s, 6H; Mes, 2 × *p*-CH_3), -0.70 (s, 6H; Al(CH_3)$_2$).

^{1}H NMR (400 MHz, Methylene chloride-d_2) δ 7.44 (t, *J* = 7.5 Hz, 1H; Ar', *p*-H), 7.05 (d, *J* = 7.6 Hz, 2H; Ar', 2 × *m*-H), 6.96 (s, 4H; Mes, 4 × *m*-H), 2.32 (s, 6H; Mes, 2 × *p*-CH_3), 2.05 (s, 12H; Mes, 4 × *o*-CH_3), -1.02 (s, 6H; Al(CH_3)$_2$).

^{13}C {^{1}H} NMR (151 MHz, Benzene-d_6) δ 148.8, 141.3, 137.4, 136.4, 129.4, 129.1, 125.4, 21.1, 21.1, -7.1. (C-Al not observed, presumably due to quadrupolar line broadening from ^{27}Al)

Data were in accordance with those previously reported.[237]

^{Mes}TerAlEt$_2$ (ABG-0193)

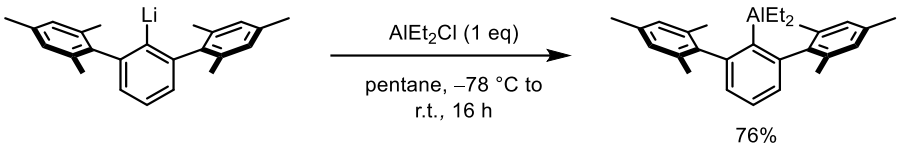

$AlEt_2Cl$ (1 M in hexanes, 2.15 mL, 2.15 mmol) was added dropwise to a suspension of ^{Mes}TerLi (727 mg, 2.27 mmol) in pentane (20 mL) at −78 °C. The solution was stirred for 16 hours and allowed to warm to room temperature. The precipitated salts were separated by filtration. The volatiles from the colourless filtrate were removed *in vacuo* to give ^{Mes}TerAlEt$_2$ as an amorphous white solid (656 mg, 76% yield).

^{1}H NMR (500 MHz, Benzene-d_6) δ 7.32 (t, *J* = 7.6 Hz, 1H; Ar', *p*-*H*), 7.02 (d, *J* = 7.6 Hz, 2H; Ar', 2 × *m*-*H*), 6.84 (s, 4H; Mes, 4 × *m*-C*H*$_3$), 2.15 (s, 12H; Mes, 4 × *o*-CH_3), 2.11 (s, 6H; Mes, 2 × *p*-C*H*$_3$), 0.87 (t, *J* = 8.2 Hz, 6H; 2 × Al-CH_2-C*H*$_3$), -0.04 (q, *J* = 8.2 Hz, 4H; 2 × AlC*H*$_2$$CH_3$).

^{13}C {^{1}H} NMR (126 MHz, Benzene-d_6) δ 152.1 (*C*–Al; identified by HMBC), 148.8, 141.5, 137.4, 136.3, 129.2, 129.2, 125.5, 21.1, 21.1, 8.1, 2.9.

IR (neat) 2897*m*, 2860*m*, 1448*m*, 1377*m*, 1100*m*, 852*m*, 805*m*

EA Calculated for $C_{28}H_{35}Al$: C, 84.38; H, 8.85; Found: C, 84.37; H, 8.85

^{Mes}TerAl(*i*Bu)$_2$ (ABG-0338)

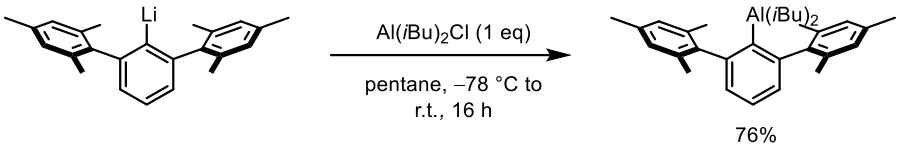

(*i*Bu)$_2$AlCl (0.8 M in heptane, 2.4 mL, 1.92 mmol) was added dropwise to a suspension of ^{Mes}TerLi (615 mg, 1.92 mmol) in pentane (19 mL, 0.1 M) at −78 °C. The solution was stirred for 16 hours and allowed to warm to room temperature. The precipitated salts were separated by filtration. The volatiles from the colourless filtrate were removed *in vacuo* to give ^{Mes}TerAl(*i*Bu)$_2$ as an amorphous white solid (735 mg, 84% yield).

^{1}H NMR (500 MHz, Benzene-d$_6$) δ 7.31 (t, J = 7.6 Hz, 1H; Ar', *p*-*H*), 6.98 (d, J = 7.6 Hz, 2H; Ar', 2 × *m*-*H*), 6.83 (s, 4H; Mes, 4 × *m*-*H*), 2.16 (s, 12H; Mes, 4 × *o*-C*H*$_3$), 2.13 (s, 6H; Mes, 2 × *p*-C*H*$_3$), 1.86 – 1.72 (m, 2H; *i*Bu, 2 × C*H*, 0.78 (d, J = 6.5 Hz, 12H; *i*Bu, 4 × C*H*$_3$), 0.16 (d, J = 7.5 Hz, 4H; 2 × AlC*H*$_2$R).

^{13}C {^{1}H} NMR (126 MHz, Benzene-*d*$_6$) δ 151.2 (Ar, *ipso*-*C*-Al), 148.9 (Ar, *o*-*C*-Mes), 141.3 (Mes, *ipso*-*C*-Ar), 137.4 (Mes, *p*-*C*-CH$_3$), 136.6 (Mes, *o*-*C*-CH$_3$), 129.3 (Ar, *p*-*C*-H), 129.2 (Mes, *m*-*C*-H), 125.7 (Ar, *m*-*C*-H), 28.2 (*i*Bu, RCH(*C*H$_3$)$_2$), 26.2 (*i*Bu, R*C*H(CH$_3$)$_2$), 25.8 (*i*Bu, Al*C*H$_2$R), 21.3 (Mes, *o*-*C*H$_3$), 21.1 (Mes, *p*-*C*H$_3$).

IR (neat) 2944*m*, 2859*m*, 1449*m*, 1377*m*, 677*s*

m.p. 98-100°C (pentane)

MS HRMS-EI (m/z): found 454.3179; [M] (C$_{32}$H$_{43}$Al), requires 454.3175

^{Mes}TerAl(Et)H (ABG-0239)

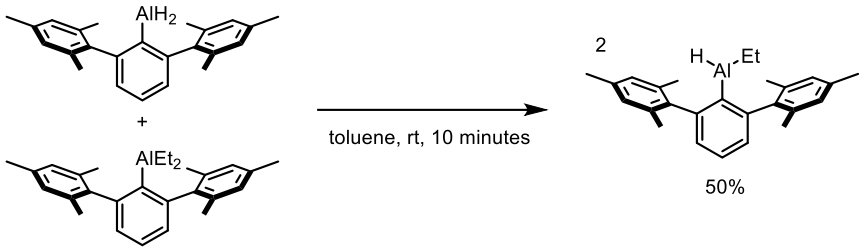

A solution of ^{Mes}TerAlEt$_2$ (80 mg, 0.2 mmol) in toluene (0.5 mL) was added to a solution of ^{Mes}TerAlH$_2$ (68 mg, 0.2 mmol) in toluene (0.5 mL) at room temperature. The resultant suspension was dissolved with gentle warming and slowly cooled to room temperature to precipitate colourless needles. The solid was filtered, washed with pentane (2 × 0.5 mL) and then dried *in vacuo* to give ^{Mes}TerAl(Et)H as colourless needles (74 mg, 50%).

^{1}H NMR (500 MHz, Benzene-d_6) δ 7.21 (t, *J* = 7.6 Hz, 1H; Ar', *p*-*H*), 6.91 (m, 6H: most likely singlet (4H; Mes, 4 × *m*-*H*) with overlapping doublet (2H; Ar', 2 × *m*-H)), 2.69 (br s, 1H; Al*H*), 2.35 (s, 6H; Mes, *p*-C*H*$_3$), 2.01 (s, 12H; Mes, *o*-C*H*$_3$), 0.83 (t, *J* = 8.1 Hz, 3H; AlCH$_2$C*H*$_3$), -0.29 (q, *J* = 8.1 Hz, 2H; AlC*H*$_2$CH$_3$).

^{13}C {^{1}H} NMR (126 MHz, Benzene-d_6) δ 150.3, 141.2, 135.9, 135.8, 129.1, 128.6, 126.7, 21.1, 20.9, 9.7, -0.1 (*C*-Al not observed, presumably due to quadrupolar line broadening from ^{27}Al).

IR (neat) 2916*m*, 2867*m*, 1373*m* (br, Al-H$_{bridging}$), 1326*m* (br, Al-H$_{bridging}$), 850*s*, 814*s*, 801*s*

m.p. (CH_2Cl_2) 262-264 °C

MS HRMS-EI (m/z): found 370.2239; [M] ($C_{26}H_{31}Al$), requires 370.2236

Crystals suitable for X-ray crystallography were originally grown using the following preparation:

C_6D_6 (0.6 mL) was added to a mixture of ^{Mes}TerAlEt$_2$ (19.9 mg, 0.05 mmol) and ^{Mes}TerAlH$_2$ (17.1 mg, 0.05 mmol). The solution spontaneously crashed out a white precipitate over ten minutes, which was dissolved upon gentle warming with a heat gun. Slow cooling to room temperature yielded colourless cubes of sufficient quality for X-ray crystallography.

^{Tipp}TerI (ABG-0010)

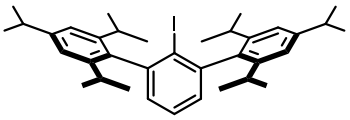

According to general procedure A, 1-bromo-2,4,6-triisopropylbenzene (29.7 mL, 120 mmol), magnesium turnings (5.10 g, 210 mmol), *n*-butyl lithium (2.5 M solution in hexanes, 20.5 mL, 51.2 mmol), 1,3-dichlorobenzene (5.85 mL, 50.2 mmol) and iodine (19.1 g, 75.3 mmol) were reacted. The product was distilled under high vacuum (0.01 mbar) at 180 °C to remove any ^{Tipp}TerI and residual solvents. The solid was suspended in EtOH (200 mL), heated to reflux for 16 h and then slowly cooled to room temperature. The off-white solid was filtered from the yellow solution, then recrystallised from hot toluene/MeOH to give ^{Tipp}TerI as colourless needles (19.7 g, 65%).

^{1}H NMR (500 MHz, Chloroform-*d*) δ 7.39 (t, *J* = 7.5 Hz, 1H; Ar', *p*-*H*), 7.14 (d, *J* = 7.4 Hz, 2H; Ar', *m*-*H*), 7.05 (s, 4H; Tipp, *m*-*H*), 2.95 (hept, *J* = 6.9 Hz, 2H; Tipp, 2 × *p*-C*H*$(CH_3)_2$), 2.52 (hept, *J* = 6.9 Hz, 4H; Tipp, 4 × *o*-C*H*$(CH_3)_2$)), 1.31 (d, *J* = 6.9 Hz, 12H; Tipp, 2 × CH(C*H*$_3)_2$)), 1.21 (d, *J* = 6.9 Hz, 12H; Tipp, 2 × CH(C*H*$_3)_2$)), 1.08 (d, *J* = 6.8 Hz, 12H; Tipp, 2 × CH(C*H*$_3)_2$)).

^{13}C {^{1}H} NMR (126 MHz, Chloroform-*d*) δ 148.4, 146.7, 145.6, 140.3, 128.2, 127.3, 120.7, 111.0, 34.2, 30.9, 24.9, 24.1, 23.3.

Data were in accordance with those previously reported.[430]

^{Tipp}TerLi•OEt$_2$ (ABG-0113)

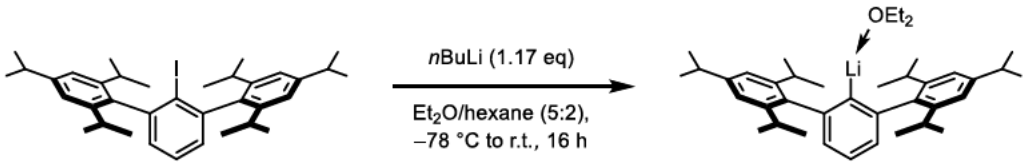

63%

^{Tipp}TerI (3.65 g, 6 mmol, 1 equiv.) was dissolved in Et$_2$O/*n*-hexane (5:2, 70 mL) and cooled to −78°C. *n*-Butyl lithium (2.5 M solution in hexanes, 2.4 mL, 6 mmol) was added dropwise and the reaction was allowed to slowly warm to room temperature over 16 hours with stirring. The clear solution was concentrated to *ca*. 40 mL and the precipitated amorphous solid was filtered. More solid was precipitated from the filtrate, which was re-dissolved under gentle warming. Slow cooling to room temperature resulted in the formation of colourless needles. The mixture was cooled to −20 °C for 16 h to induce further crystallisation. The large colourless needles were filtered and dried *in vacuo* to yield ^{Tipp}TerLi•OEt$_2$ (2.12 g, 63%).

^{1}H NMR (500 MHz, Benzene-d_6) δ 7.39 (app. dd, *J* = 7.8, 6.9 Hz, 1H; Ar', *p*-H), 7.27 (d, *J* = 7.4 Hz, 2H; Ar', 2 × *m*-H), 7.15 (s, 4H; Tipp, 4 × *m*-H), 3.50 (hept, *J* = 6.9 Hz, 4H; Tipp, 4 × *o*-CH(CH$_3$)$_2$), 2.89 (hept, *J* = 6.9 Hz, 2H; Tipp, 2 × CH(CH$_3$)$_2$), 2.69 (q, *J* = 7.1 Hz, 4H; 2 × OCH$_2$CH$_3$), 1.31 (d, *J* = 6.9 Hz, 12H; Tipp, 2 × CH(CH$_3$)$_2$), 1.28 (d, *J* = 6.9 Hz, 12H; Tipp, 2 × CH(CH$_3$)$_2$), 1.21 (d, *J* = 6.9 Hz, 12H; Tipp, 2 × CH(CH$_3$)$_2$), 0.50 (t, *J* = 7.1 Hz, 6H; 2 × OCH$_2$CH$_3$).

^{13}C {^{1}H} NMR (126 MHz, Benzene-d_6) δ 150.6, 147.7, 146.9, 145.9, 123.5, 123.0, 120.3, 66.2, 34.9, 30.2, 24.9, 24.7, 24.6, 14.2. (C-Li not observed, presumably due to quadrupolar line broadening from ^{7}Li)

^{7}Li NMR (156 MHz, Benzene-d_6) δ 1.18.

Data were in accordance with those previously reported.[430]

^{Tipp}TerAlH$_3$•Li(OEt$_2$)$_{0.67}$(NMe$_3$)$_{0.33}$ (ABG-0120)

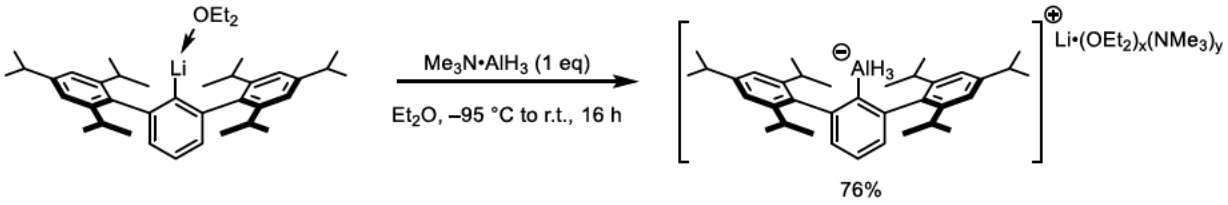

By modification of the method of Power,[234] a solution of $H_3Al•NMe_3$ (602 mg, 6.75 mmol) in Et_2O (30 mL) was added dropwise to a cold solution of ^{Tipp}TerLi•OEt_2 (3.60 g, 6.75 mmol) in Et_2O (30 mL) at −95 °C. The reaction was stirred overnight and allowed to slowly warm to room temperature. The solvent was removed *in vacuo* and the resulting white foam was washed with pentane (2 × 5 mL). The solid was dried *in vacuo* for 1.5 hours to give ^{Tipp}TerAlH$_3$•Li as an amorphous white solid as a mixture of the trimethylamine and diethyletherate adduct (3.02 g, 76%).

The resulting compound gave a poor ^{13}C NMR spectra in the absence of added THF (ca. 8 equiv.) due to low solubility.

^{1}H NMR (500 MHz, Benzene-d_6) δ 7.32 (t, J = 7.6 Hz, 1H; Ar', *p*-H), 7.21 (s, 4H, Tipp, 4 × *m*-H), 7.19 (d, J = 7.4 Hz, 2H; Ar', 2 × *m*-H), 3.38 (hept, J = 6.9 Hz, 4H; Tipp, 4 × *o*-CH(CH$_3$)$_2$), 3.26 (q, J = 7.0 Hz, approx. 2.7 H; $^4/_3$ × OCH$_2$CH$_3$), 2.91 (hept, J = 6.9 Hz, 2H; Tipp, 2 × *p*-CH(CH$_3$)$_2$), 2.09 (s, 3H, NCH$_3$), 1.50 (d, J = 6.9 Hz, 12H; Tipp, 2 × CH(CH$_3$)$_2$), 1.32 (d, J = 6.9 Hz, 12H; Tipp, 2 × CH(CH$_3$)$_2$), 1.28 (d, J = 6.9 Hz, 12H; Tipp, 2 × CH(CH$_3$)$_2$), 1.10 (t, J = 7.0 Hz, 4H; $^4/_3$ × OCH$_2$CH$_3$).

^{13}C {^{1}H} NMR (126 MHz, Benzene-d_6 + THF) δ 150.3, 147.1, 146.3, 143.5, 127.2, 125.7, 120.0, 34.8, 30.9, 25.8, 24.6, 23.9, 14.3. (C-Al not observed, presumably due to quadrupolar line broadening from ^{27}Al)

^{7}Li NMR (194 MHz, Benzene-d_6) δ 0.28.

^{27}Al NMR (130 MHz, Benzene-d_6) δ 112.34.

Data were in accordance with those previously reported.[234]

^{Tipp}TerAlH$_2$ (ABG-0478)

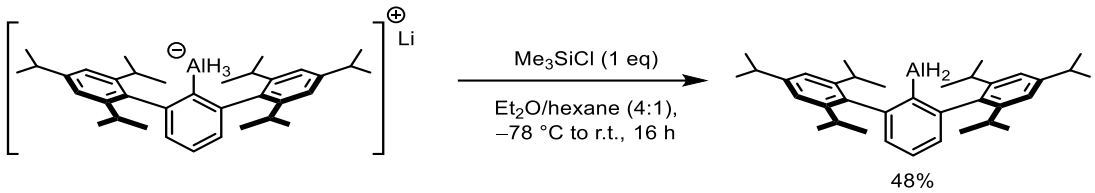

By modification of the method of Power,[234] Me_3SiCl (595 µL, 4.69 mmol, 1 equiv.) was added dropwise to a suspension of ^{Tipp}TerAlH$_3$•Li(OEt$_2$) (2.78 g, 4.69 mmol, 1 equiv.) in Et_2O/hexane (4:1, 30 mL) at –95 °C. The cold bath was removed following 10 minutes of stirring, and the reaction was allowed to warm to room temperature over 16 hours. The precipitated salts were allowed to settle and then separated by filtration to give a colourless filtrate. The volatiles from the filtrate were removed *in vacuo* to give an amorphous white powder, which was then heated to 110 °C for 30 minutes under dynamic vacuum (*ca.* 1 × 10^{-2} mbar) to remove the diethyl ether adduct. The amorphous white powder was washed with toluene (50 mL) and then pentane (10 mL). Although the product appeared clean by NMR spectroscopy, NMR silent impurities affected further reactivity and so the white powder was extracted with CH_2Cl_2 (3 × 100 mL) and the solvent was removed *in vacuo* to give ^{Tipp}TerAlH$_2$ as an amorphous white solid (1.14 g, 48%).

^{1}H NMR (500 MHz, Benzene-d_6) δ 7.14 (s, 4H; Tipp, 4 × *m*-H), 7.11 (app. dd, *J* = 8.1, 7.1 Hz, 1H; Ar', *o*-H), 6.99 (d, *J* = 7.6 Hz, 2H; Ar', 2 × *m*-H), 3.29 (s, 2H; AlH$_2$), 2.96 (h, *J* = 6.7 Hz, 2H; Tipp, 2 × *p*-CH(CH$_3$)$_2$), 2.85 (h, *J* = 6.9 Hz, 4H; Tipp, 4 × *o*-CH(CH$_3$)$_2$), 1.38 (d, *J* = 6.9 Hz, 12H; Tipp, 2 × CH(CH$_3$)$_2$), 1.16 (d, *J* = 6.9 Hz, 12H; Tipp, 2 × CH(CH$_3$)$_2$), 1.06 (d, *J* = 6.8 Hz, 12H; Tipp, 2 × CH(CH$_3$)$_2$).

^{13}C {^{1}H} NMR (126 MHz, Benzene-d_6) δ 150.3, 148.5, 146.8, 141.9, 139.6, 121.4, 34.7, 30.8, 26.0, 24.4, 23.9. (C-Al not observed, presumably due to quadrupolar line broadening from ^{27}Al)

Data were in accordance with those previously reported.[234]

^{Tipp}TerAlMe$_2$ and ^{Tipp}TerAlMe$_2$•OEt$_2$ (ABG-0074/0428)

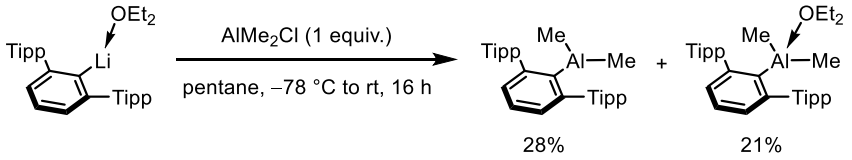

$AlMe_2Cl$ (1 M in hexanes, 4.3 mL, 4.3 mmol) was added dropwise to a suspension of ^{Tipp}TerLi•OEt_2 (2.40 g, 4.26 mmol) in *n*-pentane (20 mL) at −78 °C. and the reaction was stirred for 16 hours with slow warming to room temperature. The precipitated salts were separated by filtration and then further extracted with *n*-hexane (2 × 5 mL). The volatiles from the combined filtrates were removed *in vacuo* and the resultant amorphous white solid was re-dissolved in hot *n*-hexane (15 mL). The clear solution was slowly cooled to room temperature in the cooling oil bath, yielding ^{Tipp}TerAlMe$_2$ as colourless cubes over 3 days (653 mg, 1.21 mmol, 28% yield). The supernatant was filtered and stored in the fridge (2 °C) over 2 days to give ^{Tipp}TerAlMe$_2$•OEt_2 as colourless needles (552 mg, 0.90 mmol, 21% yield).

^{Tipp}TerAlMe$_2$:

^{1}H NMR (500 MHz, Benzene-d_6) δ 7.36 – 7.26 (m, 3H; Ar', *p*-H and 2 × *m*-H), 7.20 (s, 4H; Tipp, 4 × *m*-H), 3.15 (hept, J = 6.8 Hz, 4H; Tipp, 4 × *o*-C*H*$(CH_3)_2$), 2.82 (hept, J = 6.9 Hz, 2H; Tipp, 2 × *p*-C*H*$(CH_3)_2$), 1.30 (d, J = 6.9 Hz, 12H; Tipp, 2 × CH(C*H*$_3)_2$), 1.23 (d, J = 6.9 Hz, 12H; Tipp, 2 × CH(C*H*$_3)_2$), 1.12 (d, J = 6.8 Hz, 12H; Tipp, 2 × CH(C*H*$_3)_2$), -0.80 (s, 6H; 2 × Al-C*H*$_3$).

^{13}C {^{1}H} NMR (126 MHz, Benzene-d_6) δ 153.2, 149.3, 147.8, 147.2, 140.1, 128.1 (overlapped by C_6D_6, identified by COSY), 127.2, 121.5, 34.9, 30.7, 26.4, 24.4, 22.7, -5.8.

m.p. (hexane) 217-220°C

IR (neat) 2955*s*, 2866*m*, 1459*m*, 1362*m*

MS HRMS-EI (m/z): found 538.4123; [M] ($C_{38}H_{55}Al$), requires 538.4114

^{Tipp}TerAlMe$_2$•OEt$_2$:

^{1}H NMR (500 MHz, Benzene-d_6) δ 7.31 – 7.24 (m, 3H; Ar*H*), 7.20 (s, 4H; Tipp, 4 × *m*-*H*), 3.22 (br s, 4H; 2 × OC*H*$_2$CH$_3$), 3.17 (hept, *J* = 6.8 Hz, 4H; Tipp, 4 × *o*-C*H*(CH$_3$)$_2$), 2.85 (hept, *J* = 6.9 Hz, 2H; Tipp, 2 × *p*-C*H*(CH$_3$)$_2$), 1.34 (d, *J* = 6.9 Hz, 12H; Tipp, 2 × CH(C*H*$_3$)$_2$), 1.26 (d, *J* = 7.0 Hz, 12H; Tipp, 2 × CH(C*H*$_3$)$_2$), 1.14 (d, *J* = 6.6 Hz, 12H; Tipp, 2 × CH(C*H*$_3$)$_2$), 0.89 (br s, 6H; 2 × OCH$_2$C*H*$_3$), -0.85 (s, 6H; Al(C*H*$_3$)$_2$).

^{13}C {^{1}H} NMR (126 MHz, Benzene-d_6) δ 152.9 (Ar, *ipso*-*C*-Al), 148.6 (Tipp, *p*-*C*-*i*Pr), 148.4 (Ar, *o*-*C*-Ar'), 147.1 (Tipp, *o*-*C*-*i*Pr), 141.1 (Tipp, *ipso*-*C*-Ar), 128.2 (Ar, *m*-*C*H), 126.9 (Ar, *p*-*C*H), 121.2 (Tipp, *m*-*C*-H), 66.9 (O*C*H$_2$CH$_3$), 34.9 (*p*-*i*Pr, *C*H), 30.8 (*o*-*i*Pr, *C*H), 26.4 (*o*-*i*Pr, *C*H$_3$), 24.4 (*p*-*i*Pr, *C*H$_3$), 22.9 (*o*-*i*Pr, *C*H$_3$), 14.8 (OCH$_2$*C*H$_3$), -5.7 (Al*C*H$_3$).

m.p. (hexane) 214-219 °C

IR (neat) 2957*s*, 2867*m*, 1458*m*, 1361*m*

7.3 Experimental details for Chapter 2

7.3.1 Catalysis Optimisation

Procedure for the optimisation tables in Chapter 2:

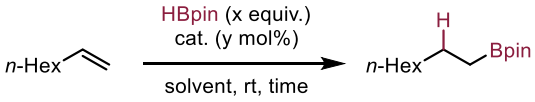

1-octene (40 µL, 0.25 mmol, 1 equiv.) and HBpin (x equiv.) were sequentially added to a solution of catalyst (y mol%) in solvent. The reaction was stirred for the noted length of time then quenched by exposure to O_2 (air). The yield was determined by ^{1}H NMR spectroscopy, using 1,3,5-trimethoxybenzene as internal standard.

7.3.2 Synthesis of pinacolboronic esters from terminal alkene substrates

General procedure B (mono-substituted alkenes):

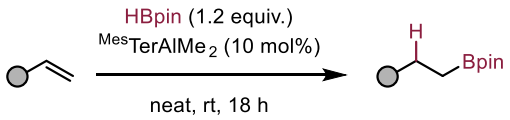

A vial was charged with ^{Mes}TerAlMe$_2$ (0.05 mmol. 18.5 mg) in the glovebox and capped with a lid bearing a PTFE/rubber septum. The tube was removed from the glovebox and charged with alkene (0.5 mmol) and then HBpin (87 µL, 0.6 mmol). The reaction was stirred at room temperature for 18 hours and then quenched by exposure to air. After bubbling ceased, mesitylene (50 µL) was added as an internal standard and diluted with $CDCl_3$. An aliquot was taken to determine the NMR yield. The product was purified by flash column chromatography (12 g silica), eluting from 100% petroleum ether to 90/10 petroleum ether/ethyl acetate.

General procedure C (1,1-disubstituted alkenes):

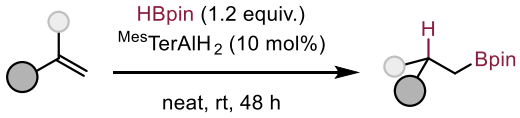

HBpin (87 µL, 0.6 mmol, 1.2 equiv.) was added to a suspension of ^{Mes}TerAlH$_2$ (17.1 mg, 0.05 mmol, 10 mol%) in neat alkene (0.5 mmol, 1 equiv.). The reaction was stirred at room temperature for 48 hours before quenching with air (O_2), adding mesitylene as internal standard (50 µL) and diluting with $CHCl_3$. The product was purified with column chromatography (12 g SiO_2, eluting with 40/60 petroleum ether:ethyl acetate (99:1 to 95:5)) to give the pure boronic ester.

2-1a; 4,4,5,5-tetramethyl-2-octyl-1,3,2-dioxaborolane (ABG-0195)

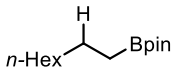

According to general procedure B, 1-octene (80 µL, 0.5 mmol) was reacted with HBpin (87 µL, 0.6 mmol) in the presence of $^{Mes}TerAlMe_2$ (18.5 mg, 0.05 mmol) to give the product as a colourless oil (98 mg, 81% yield).

^{1}H NMR (500 MHz, Chloroform-*d*) δ 1.41 (m, 2H), 1.34 – 1.26 (m, 10H), 1.24 (s, 12H), 0.95 – 0.87 (m, *J* = 7.0 Hz, 3H), 0.79 (t, *J* = 7.8 Hz, 2H).

^{13}C {^{1}H} NMR (126 MHz, Chloroform-*d*) δ 83.0, 32.6, 32.1, 29.5, 29.4, 25.0, 24.2, 22.8, 14.3. (*C*-B not observed, presumably due to quadrupolar line broadening from ^{11}B)

^{11}B NMR (160 MHz, Chloroform-*d*) δ 34.1.

Data were in accordance with those previously reported.[179]

2-1b; 2-cyclohexyl-1-(4,4,5,5-tetramethyl-1,3,2-dioxaborolan-2-yl)ethane (ABG-0334)

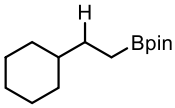

According to general procedure B, vinyl cyclohexane (70 µL, 0.5 mmol) was reacted with HBpin (87 µL, 0.6 mmol) in the presence of $^{Mes}TerAlMe_2$ (18.5 mg, 0.05 mmol) to give the product as a colourless oil (85 mg, 71% yield).

^{1}H NMR (500 MHz, Chloroform-*d*) δ 1.78 – 1.58 (m, 5H), 1.33 – 1.26 (m, 2H), 1.24 (s, 12H), 1.22 – 1.06 (m, 4H), 0.90 – 0.79 (m, 2H), 0.78 – 0.71 (m, 2H).

^{13}C {^{1}H} NMR (126 MHz, Chloroform-*d*) δ 83.0, 40.1, 33.1, 31.5, 26.9, 26.6, 25.0. (*C*-B not observed, presumably due to quadrupolar line broadening from ^{11}B)

^{11}B NMR (160 MHz, Chloroform-*d*) δ 34.3.

Data were in accordance with those previously reported.[431]

2-1c; 2-(3,3-dimethylbutyl)-4,4,5,5-tetramethyl-1,3,2-dioxaborolane (ABG-0301-A)

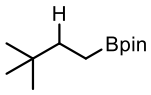

According to general procedure B, *t*Bu-ethylene (66 µL, 0.5 mmol) was reacted with HBpin (87 µL, 0.6 mmol) in the presence of $^{Mes}TerAlMe_2$ (0.05 mmol, 18.5 mg) to give the product as a colourless oil (80 mg, 75% yield).

^{1}H NMR (500 MHz, Chloroform-*d*) δ 1.33 – 1.28 (m, 2H), 1.25 (s, 12H), 0.85 (s, 9H), 0.75 – 0.68 (m, 2H).

^{13}C {^{1}H} NMR (126 MHz, Chloroform-*d*) δ 83.0, 37.9, 31.0, 29.0, 25.0, 5.9.

^{11}B NMR (160 MHz, Chloroform-*d*) δ 34.4.

Data were in accordance with those previously reported.[431]

2-1d; 2-(5-bromopentyl)-4,4,5,5-tetramethyl-1,3,2-dioxaborolane (ABG-0324)

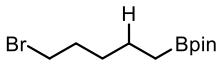

According to general procedure B, 5-bromo-1-pentene (63 µL, 0.5 mmol) was reacted with HBpin (87 µL, 0.6 mmol) in the presence of $^{Mes}TerAlMe_2$ (0.05 mmol, 18.5 mg) to give the product as a colourless oil (101 mg, 73% yield).

^{1}H NMR (500 MHz, Chloroform-*d*) δ 3.40 (t, *J* = 6.9 Hz, 2H), 1.94 – 1.79 (m, 2H), 1.48 – 1.39 (m, 4H), 1.24 (s, 12H), 0.79 (t, *J* = 7.3 Hz, 2H).

^{13}C {^{1}H} NMR (126 MHz, Chloroform-*d*) δ 83.1, 34.1, 32.8, 31.0, 25.0, 23.3. (*C*-B not observed, presumably due to quadrupolar line broadening from ^{11}B)

^{11}B NMR (160 MHz, Chloroform-*d*) δ 34.0

Data were in accordance with those previously reported.[179]

2-1e; Trimethyl(3-(4,4,5,5-tetramethyl-1,3,2-dioxaborolan-2-yl)propyl)silane (ABG-0350/0197-B)

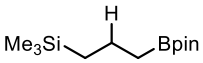

According to general procedure B, allyl trimethylsilane (81 µL, 0.5 mmol) was reacted with HBpin (87 µL, 0.6 mmol) in the presence of $^{Mes}TerAlH_2$ (0.05 mmol, 17.1 mg) to give the product as a colourless oil (84 mg, 68% yield).

^{1}H NMR (500 MHz, Chloroform-*d*) δ 1.50 – 1.41 (m, 2H), 1.27 (s, 12H), 0.85 (t, *J* = 7.7 Hz, 2H), 0.59 – 0.50 (m, 2H), -0.01 (s, 9H).

^{13}C {^{1}H} NMR (126 MHz, Chloroform-*d*) δ 83.0, 25.0, 20.3, 18.7, -1.5. (*C*-B not observed, presumably due to quadrupolar line broadening from ^{11}B)

^{11}B NMR (160 MHz, Chloroform-*d*) δ 34.0.

^{29}Si NMR (99 MHz, Chloroform-*d*) δ 0.72.

Data were in accordance with those previously reported.[431]

2-1f; 1,3-bis(4,4,5,5-tetramethyl-1,2-oxaborolan-2-yl)propane (ABG-0197-A)

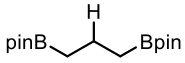

According to general procedure B, allyl Bpin (95 µL, 0.5 mmol) was reacted with HBpin (87 µL, 0.6 mmol) in the presence of $^{Mes}TerAlMe_2$ (0.05 mmol, 18.5 mg) to give the product as a colourless oil (4.3 mg, 6% yield).

^{1}H NMR (500 MHz, Chloroform-*d*) δ 1.55 – 1.51 (m, 2H), 1.23 (s, 24H), 0.81 (t, *J* = 7.9 Hz, 4H).

^{13}C {^{1}H} NMR (126 MHz, Chloroform-*d*) δ 82.9, 25.0, 18.7. (*C*-B not observed, presumably due to quadrupolar line broadening from ^{11}B)

^{11}B NMR (160 MHz, Chloroform-*d*) δ 34.1.

Data were in accordance with those previously reported.[432]

2-1g; 2-(4-(4-chlorophenyl)butyl)-4,4,5,5-tetramethyl-1,3,2-dioxaborolane (ABG-0332)

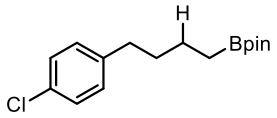

According to general procedure B, 4-(p-chlorophenyl)-1-butene (70 mg, 0.42 mmol) was reacted with HBpin (87 µL, 0.6 mmol) in the presence of ^{Mes}TerAlMe$_2$ (0.05 mmol, 18.5 mg) to give the product as a colourless oil (92 mg, 71% yield).

^{1}H NMR (500 MHz, Chloroform-*d*) δ 7.25 – 7.18 (m, 2H), 7.13 – 7.07 (m, 2H), 2.66 – 2.49 (m, 2H), 1.64 – 1.54 (m, 3H), 1.45 (dt, *J* = 15.3, 7.6 Hz, 2H), 1.24 (s, 12H), 0.80 (t, *J* = 7.8 Hz, 2H).

^{13}C {^{1}H} NMR (126 MHz, Chloroform-*d*) δ 141.5, 131.3, 129.9, 128.4, 83.1, 35.2, 34.2, 25.0, 23.8. (*C*-B not observed, presumably due to quadrupolar line broadening from ^{11}B)

^{11}B NMR (160 MHz, Chloroform-*d*) δ 34.0.

Data were in accordance with those previously reported.[433]

2-1h; 2-(3-(Benzo[d][1,3]dioxol-5-yl)propyl)-4,4,5,5-tetramethyl-1,3,2-dioxaborolane (ABG-0368)

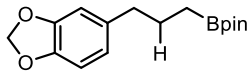

According to general procedure B, safrole (76 µL, 0.5 mmol) was reacted with HBpin (87 µL, 0.6 mmol) in the presence of ^{Mes}TerAlMe$_2$ (0.05 mmol, 18.5 mg) to give the product as a colourless oil (29 mg, 20% yield).

^{1}H NMR (500 MHz, Chloroform-*d*) δ 6.73 – 6.66 (m, 2H), 6.64 – 6.58 (m, 1H), 5.90 (s, 2H), 2.56 – 2.46 (m, 2H), 1.74 – 1.61 (m, 2H), 1.24 (s, 12H), 0.86 – 0.75 (m, 2H).

^{13}C {^{1}H} NMR (126 MHz, Chloroform-*d*) δ 147.6, 145.6, 136.8, 121.4, 109.2, 108.1, 100.8, 83.1, 38.4, 26.5, 25.0.

^{11}B NMR (160 MHz, Chloroform-*d*) δ 34.0.

Data were in accordance with those previously reported.[434]

2-1i; 4,4,5,5-tetramethyl-2-phenethyl-1,3,2-dioxaborolane (ABG-0301-B)

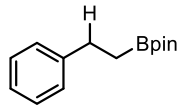

According to general procedure B, styrene (58 µL, 0.5 mmol) was reacted with HBpin (87 µL, 0.6 mmol) in the presence of $^{Mes}TerAlMe_2$ (0.05 mmol, 18.5 mg) to give the product as a colourless oil (53 mg, 45% yield).

^{1}H NMR (500 MHz, Chloroform-*d*) δ 7.28 – 7.20 (m, 4H), 7.18 – 7.11 (m, 1H), 2.79 – 2.69 (m, 2H), 1.22 (s, 12H), 1.18 – 1.10 (m, 2H).

^{13}C {^{1}H} NMR (126 MHz, Chloroform-*d*) δ 144.6, 128.3, 128.2, 125.6, 83.2, 30.1, 25.0. (*C*-B not observed, presumably due to quadrupolar line broadening from ^{11}B)

^{11}B NMR (160 MHz, Chloroform-*d*) δ 33.9.

Data were in accordance with those previously reported.[431]

2-1j; 4,4,5,5-tetramethyl-2-(4-methylphenethyl)-1,3,2-dioxaborolane (ABG-0210-C)

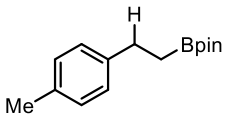

According to general procedure B, 4-Me-styrene (67 µL, 0.5 mmol) was reacted with HBpin (87 µL, 0.6 mmol) in the presence of $^{Mes}TerAlMe_2$ (0.05 mmol, 18.5 mg) to give the product as a colourless oil (92.1 mg, 75% yield).

^{1}H NMR (500 MHz, Chloroform-*d*) δ 7.13 – 7.04 (m, 4H), 2.74 – 2.67 (m, 2H), 2.30 (s, 3H), 1.23 (s, 12H), 1.14 – 1.08 (m, 2H).

^{13}C {^{1}H} NMR (126 MHz, Chloroform-*d*) δ 141.4, 134.9, 128.9, 127.9, 83.1, 29.5, 24.8, 21.0. (*C*-B not observed, presumably due to quadrupolar line broadening from ^{11}B)

^{11}B NMR (160 MHz, Chloroform-*d*) δ 33.8.

Data were in accordance with those previously reported.[431]

2-1k; 2-(2,4-dimethylphenethyl)-4,4,5,5-tetramethyl-1,3,2-dioxaborolane (ABG-0210-D)

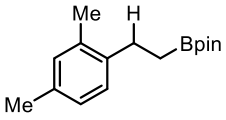

According to general procedure B, 2,4-dimethylstyrene (75 µL, 0.5 mmol) was reacted with HBpin (87 µL, 0.6 mmol) in the presence of $^{Mes}TerAlMe_2$ (0.05 mmol, 18.5 mg) to give the product as a colourless amorphous solid (120.5 mg, 93% yield).

^{1}H NMR (500 MHz, Chloroform-*d*) δ 7.07 (d, *J* = 7.5 Hz, 1H), 6.93 (d, *J* = 7.9 Hz, 2H), 2.72 – 2.60 (m, 2H), 2.27 (s, 6H), 1.24 (s, 12H), 1.13 – 1.02 (m, 2H).

^{13}C {^{1}H} NMR (126 MHz, Chloroform-*d*) δ 139.7, 135.7, 135.1, 131.0, 128.2, 126.6, 83.2, 26.9, 25.0, 21.0, 19.3.

^{11}B NMR (160 MHz, Chloroform-*d*) δ 33.9.

Data were in accordance with those previously reported.[435]

2-1m; 4,4,5,5-tetramethyl-2-(4-*tert*-butylphenyl-1-ethyl)-1,3,2-dioxaborolane (ABG-0217-D)

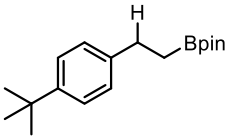

According to general procedure B, 4-*t*Bu-styrene (99 µL, 0.5 mmol) was reacted with HBpin (87 µL, 0.6 mmol) in the presence of $^{Mes}TerAlMe_2$ (0.05 mmol, 18.5 mg) to give the product as a colourless solid (102 mg, 71% yield).

^{1}H NMR (500 MHz, Chloroform-*d*) δ 7.30 – 7.27 (m, 2H), 7.17 – 7.13 (m, 2H), 2.74 – 2.68 (m, 2H), 1.30 (s, 9H), 1.22 (s, 12H), 1.17 – 1.09 (m, 2H).

^{13}C {^{1}H} NMR (126 MHz, Chloroform-*d*) δ 148.3, 141.4, 127.6, 125.1, 83.1, 34.3, 31.41, 29.4, 24.8.

^{11}B NMR (160 MHz, Chloroform-*d*) δ 33.9.

Data were in accordance with those previously reported.[179]

2-1n; 4,4,5,5-tetramethyl-2-(4-*iso*-butylphenyl-1-ethyl)-1,3,2-dioxaborolane (ABG-0333)

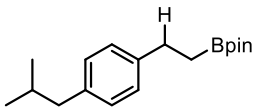

According to general procedure B, 4-*i*Bu-styrene (91 µL, 0.5 mmol) was reacted with HBpin (87 µL, 0.6 mmol) in the presence of ^{Mes}TerAlMe$_2$ (0.05 mmol, 18.5 mg) to give the product as a colourless oil (96 mg, 66% yield).

^{1}H NMR (500 MHz, Chloroform-*d*) δ 7.11 (d, *J* = 8.1 Hz, 2H), 7.03 (d, *J* = 8.1 Hz, 2H), 2.76 – 2.61 (m, 2H), 2.42 (d, *J* = 7.2 Hz, 2H), 1.83 (dp, *J* = 13.6, 6.8 Hz, 1H), 1.21 (s, 12H), 1.17 – 1.09 (m, 2H), 0.89 (d, *J* = 6.6 Hz, 6H).

^{13}C {^{1}H} NMR (126 MHz, Chloroform-*d*) δ 141.7, 138.9, 129.1, 127.8, 83.2, 45.2, 30.4, 29.7, 25.0, 22.5.

^{11}B NMR (160 MHz, Chloroform-*d*) δ 33.8.

IR 2973*m*, 2957*m*, 2926*m*, 2865*w*, 1372*s*, 1318*s*, 1143*s*, 968*m*, 842*m*

MS HRMS-EI (m/z): found 288.2260; ($C_{18}H_{29}BO_2$) requires 288.2261

2-1o; 2-(4-methoxyphenethyl)-4,4,5,5-tetramethyl-1,3,2-dioxaborolane (ABG-0363-P)

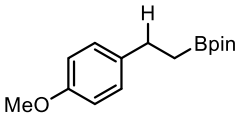

According to general procedure B, 4-methoxystyrene (70 µL, 0.5 mmol) was reacted with HBpin (87 µL, 0.6 mmol) in the presence of ^{Mes}TerAlMe$_2$ (0.05 mmol, 18.5 mg) to give the product as a colourless oil (101 mg, 77% yield).

^{1}H NMR (500 MHz, Chloroform-*d*) δ 7.17 – 7.10 (m, 2H), 6.85 – 6.77 (m, 2H), 3.78 (s, 3H), 2.74 – 2.58 (m, 2H), 1.22 (s, 12H), 1.16 – 1.00 (m, 2H).

^{13}C {^{1}H} NMR (126 MHz, Chloroform-*d*) δ 157.7, 136.7, 129.0, 113.8, 83.2, 77.4, 77.2, 76.9, 55.4, 29.2, 25.0.

^{11}B NMR (160 MHz, Chloroform-*d*) δ 33.8.

Data were in accordance with those previously reported.[431]

2-1p; *N,N*-dimethyl-4-(2-(4,4,5,5-tetramethyl-1,3,2-dioxaborolan-2-yl)ethyl)aniline (ABG-0297)

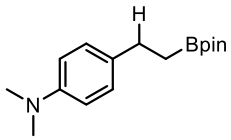

According to general procedure B, *N,N*-dimethyl-4-vinylaniline (74 mg, 0.5 mmol) was reacted with HBpin (87 µL, 0.6 mmol) in the presence of ^{Mes}TerAlMe$_2$ (0.05 mmol, 18.5 mg) to give the product as a colourless oil (76 mg, 55% yield).

^{1}H NMR (500 MHz, Chloroform-*d*) δ 7.09 (d, *J* = 8.7 Hz, 2H), 6.75 – 6.65 (m, 2H), 2.89 (s, 6H), 2.72 – 2.59 (m, 2H), 1.23 (s, 12H), 1.17 – 1.00 (m, 2H).

^{13}C {^{1}H} NMR (126 MHz, Chloroform-*d*) δ 149.1, 133.1, 128.7, 113.3, 83.2, 41.2, 29.053890, 25.0.

^{11}B NMR (160 MHz, Chloroform-*d*) δ 34.0.

Data were in accordance with those previously reported.[436]

2-1q; 2-(4-fluorophenethyl)-4,4,5,5-tetramethyl-1,3,2-dioxaborolane (ABG-0209-A)

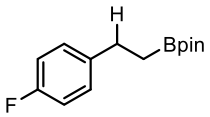

According to general procedure B, 4-fluoro-styrene (60 µL, 0.5 mmol) was reacted with HBpin (87 µL, 0.6 mmol) in the presence of ^{Mes}TerAlMe$_2$ (0.05 mmol, 18.5 mg) to give the product as a colourless oil (86 mg, 68% yield).

^{1}H NMR (500 MHz, Chloroform-*d*) δ 7.19 – 7.13 (m, 2H), 6.97 – 6.89 (m, 2H), 2.71 (t, *J* = 8.1 Hz, 2H), 1.21 (s, 12H), 1.15 – 1.08 (m, 2H).

^{13}C {^{1}H} NMR (126 MHz, Chloroform-*d*) δ 162.2, 140.1, 129.4 (d, *J* = 7.6 Hz), 114.9 (d, *J* = 21.0 Hz), 83.3, 29.3, 25.0. (*C*-B not observed, presumably due to quadrupolar line broadening from ^{11}B)

^{11}B NMR (160 MHz, Chloroform-*d*) δ 33.9.

^{19}F NMR (471 MHz, Chloroform-*d*) δ -118.45 (d, *J* = 9.5 Hz).

Data were in accordance with those previously reported.[431]

2-1r; 2-(4-chlorophenyl)ethyl)-4,4,5,5-tetramethyl-[1,3,2]-dioxaborolane (ABG-0322)

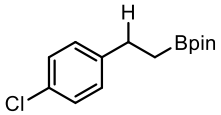

According to general procedure B, 4-chloro-styrene (60 µL, 0.5 mmol) was reacted with HBpin (87 µL, 0.6 mmol) in the presence of ^{Mes}TerAlMe$_2$ (0.05 mmol, 18.5 mg) to give the product as a colourless oil (54 mg, 42% yield).

^{1}H NMR (500 MHz, Chloroform-*d*) δ 7.25 – 7.18 (m, 2H), 7.17 – 7.12 (m, 2H), 2.78 – 2.60 (m, 2H), 1.21 (s, 12H), 1.15 – 1.07 (m, 2H).

^{13}C {^{1}H} NMR (126 MHz, Chloroform-*d*) δ 143.0, 131.3, 129.5, 128.4, 83.3, 29.5, 25.0. (*C*-B not observed, presumably due to quadrupolar line broadening from ^{11}B)

^{11}B NMR (160 MHz, Chloroform-*d*) δ 33.8.

Data were in accordance with those previously reported [437]

2-1s; 2-(4-bromophenyl)ethyl)-4,4,5,5-tetramethyl-[1,3,2]-dioxaborolane (ABG-0293, 0273, 0210, 0364)

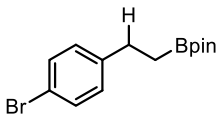

According to general procedure B, 4-bromo-styrene (67 µL, 0.5 mmol) was reacted with HBpin (87 µL, 0.6 mmol) in the presence of ^{Mes}TerAlMe$_2$ (0.05 mmol, 18.5 mg) to give the product as an amorphous white solid (76 mg, 49% yield).

^{1}H NMR (500 MHz, Chloroform-*d*) δ 7.39 – 7.34 (m, 2H), 7.12 – 7.06 (m, 2H), 2.77 – 2.62 (m, 2H), 1.22 (s, 12H), 1.15 – 1.05 (m, 2H).

^{13}C {^{1}H} NMR (126 MHz, Chloroform-*d*) δ 143.5, 131.3, 130.0, 119.3, 83.3, 29.5, 25.0. (*C*-B not observed, presumably due to quadrupolar line broadening from ^{11}B)

^{11}B NMR (160 MHz, Chloroform-*d*) δ 33.8.

Data were in accordance with those previously reported.[437]

2-1t; 4,4,5,5-tetramethyl-2-(2-methyl-pentyl)-[1,3,2]dioxaborolane (ABG-0335)

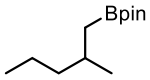

According to general procedure C, 2-methyl-1-pentene (76 µL, 0.5 mmol) was reacted with HBpin (87 µL, 0.6 mmol) in the presence of ^{Mes}TerAlH$_2$ (0.05 mmol, 17.1 mg) for 16 hours to give the product as a colourless oil (41 mg, 39% yield).

^{1}H NMR (500 MHz, Chloroform-*d*) δ 1.76 – 1.63 (m, 1H), 1.40 – 1.09 (m, 4H), 1.25 (s, 12H), 0.90 (d, *J* = 6.6 Hz, 3H), 0.87 (t, *J* = 7.2 Hz, 3H), 0.85 – 0.79 (m, 1H), 0.67 – 0.60 (m, 1H).

^{13}C {^{1}H} NMR (126 MHz, Chloroform-*d*) δ 82.9, 42.2, 29.4, 25.0, 25.0, 22.5, 20.5, 14.5.

^{11}B NMR (160 MHz, Chloroform-*d*) δ 33.9.

Data were in accordance with those previously reported.[431]

2-1u; (±)2-(2-(4-methylcyclohex-3-en-1-yl)propyl)-4,4,5,5-tetramethyl-1,3,2-dioxaborolane (ABG-0343)

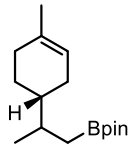

According to general procedure C, (*R*)-(+)-limonene (85 µL, 0.5 mmol) was reacted with HBpin (87 µL, 0.6 mmol) in the presence of $^{Mes}TerAlH_2$ (0.05 mmol, 17.1 mg) to give the product as a colourless oil (85 mg, 64% yield - mixture of diastereomers).

^{1}H NMR (500 MHz, Chloroform-*d*) δ 5.38 – 5.35 (m, 1H), 2.06 – 1.88z (m, 3H), 1.77 – 1.60 (m, 3H), 1.63 (s, 3H), 1.37 – 1.25 (m, 1H), 1.25 (s, 6H), 1.24 (s, 6H), 1.22 – 1.11 (m, 1H), 0.92 – 0.87 (m, 3H), 0.64 (dd, *J* = 15.3, 9.9 Hz, 1H).

^{13}C {^{1}H} NMR (126 MHz, Chloroform-*d*) – both diastereomers present: δ 134.1, 134.0, 121.3, 121.2, 83.0, 40.8, 40.7, 34.0, 33.9, 31.1, 31.1, 29.3, 28.6, 27.0, 26.1, 25.1, 25.1, 24.9, 23.6, 19.5, 19.2.

^{11}B NMR (160 MHz, Chloroform-*d*) δ 34.2.

Data were in accordance with those previously reported.[433]

2-1v; 2-(((1S,5S)-6,6-dimethylbicyclo[3.1.1]heptan-2-yl)methyl)-4,4,5,5-tetramethyl-1,3,2-dioxaborolane (ABG-0344)

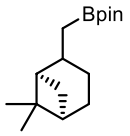

According to general procedure C, (–)-β-pinene (79 µL, 0.5 mmol) was reacted with HBpin (87 µL, 0.6 mmol) in the presence of ^{Mes}TerAlH$_2$ (0.05 mmol, 17.1 mg) to give the product as an amorphous white solid (68 mg, 52% yield - mixture of diastereomers).

^{1}H NMR (500 MHz, Chloroform-*d*) δ 2.35 – 2.20 (m, 2H), 2.03 (dtd, *J* = 14.8, 10.5, 2.7 Hz, 1H), 1.96 – 1.86 (m, 1H), 1.89 – 1.74 (m, 3H), 1.46 – 1.34 (m, 1H), 1.24 (d, *J* = 1.5 Hz, 12H), 1.17 (s, 3H), 1.02 (s, 3H), 1.03 – 0.86 (m, 3H).

^{13}C {^{1}H} NMR (126 MHz, Chloroform-*d*) δ 83.0, 49.0, 41.5, 39.0, 37.5, 34.1, 28.5, 26.8, 25.1, 24.9, 24.5, 23.3, 20.9.

^{11}B NMR (160 MHz, Chloroform-*d*) δ 33.9.

Data were in accordance with those previously reported.[438, 439]

2-1w; 2-((R)-2-((2R,8R,8aS)-8,8a-dimethyl-1,2,3,4,6,7,8,8a-octahydronaphthalen-2-yl)propyl)-4,4,5,5-tetramethyl-1,3,2-dioxaborolane (ABG-0362)

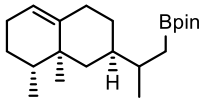

According to general procedure C, (+)-valencene (159 µL, 0.5 mmol (70% purity)) was reacted with HBpin (87 µL, 0.6 mmol) in the presence of ^{Mes}TerAlMe$_2$ (0.05 mmol, 18.5 mg) to give the product as a colourless oil (113 mg, 68% yield - mixture of diastereomers).

^{1}H NMR (500 MHz, Chloroform-*d*) δ 5.30 – 5.28 (m, 1H), 2.28 – 2.15 (m, 1H), 2.09 – 1.96 (m, 2H), 1.96 – 1.87 (m, 1H), 1.83 – 1.76 (m, 1H), 1.76 – 1.64 (m, 1H), 1.64 – 1.54 (m, 1H), 1.51 – 1.42 (m, 1H), 1.42 – 1.28 (m, 3H), 1.25 – 1.24 (m, 12H), 1.13 – 0.80 (m, 11H), 0.80 – 0.58 (m, 2H).

^{13}C {^{1}H} NMR (126 MHz, Chloroform-*d*) δ 144.2, 119.6, 119.6, 83.0, 44.1, 42.6, 41.3, 41.3, 40.0, 38.0, 38.0, 37.3, 34.5, 34.4, 33.1, 33.0, 31.5, 30.2, 27.4, 27.4, 26.1, 25.1, 25.1, 25.0, 24.9, 19.5, 18.9, 18.8, 18.7, 15.9.

^{11}B NMR (160 MHz, Chloroform-*d*) δ 34.1.

Data were in accordance with those previously reported.[438, 440]

7.3.3 Stoichiometric hydroalumination of alkenes

Assessing influence of *m*-terphenyl size (ABG-0238a-c)

The procedure to compare the rates of hydroalumination presented in Scheme 2-12 in Chapter 2 are as follows:

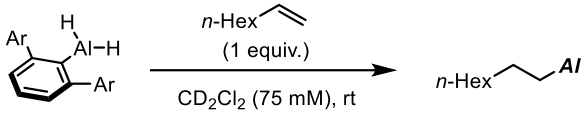

Over a flow of argon, 1-octene (8 µL, 0.05 mmol, 1 equiv.) was added to an NMR tube containing a solution/suspension of $^{Ar}TerAlH_2$ (0.05 mmol, 1 equiv.) in CD_2Cl_2 (total volume = 0.67 mL, 0.075 M w.r.t. 1-octene) at room temperature and shaken vigorously. The reaction progress was monitored by tracking the consumption of 1-octene (δ 5.83, ddt, *J* = 16.9, 10.2, 6.7 Hz, 1H; RC*H*=CH_2) at room temperature with ^1H NMR spectroscopy, using the total integration of aromatic protons as an internal standard (assumed to have remained constant).[240]

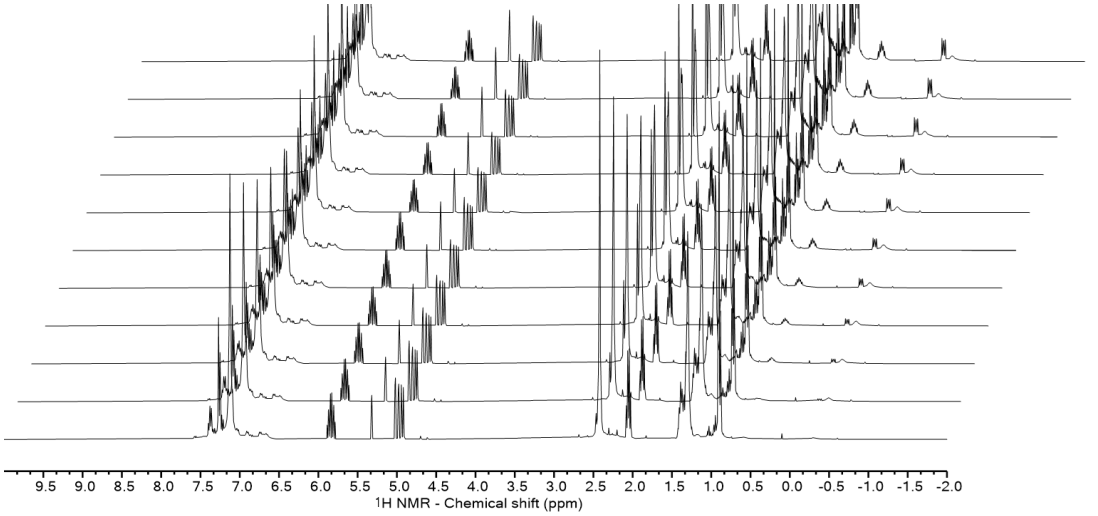

Figure 7-1. ^1H NMR spectra (CD_2Cl_2) for the reaction of 1-octene with $^{p\text{-Tol}}TerAlH_2$ against time.

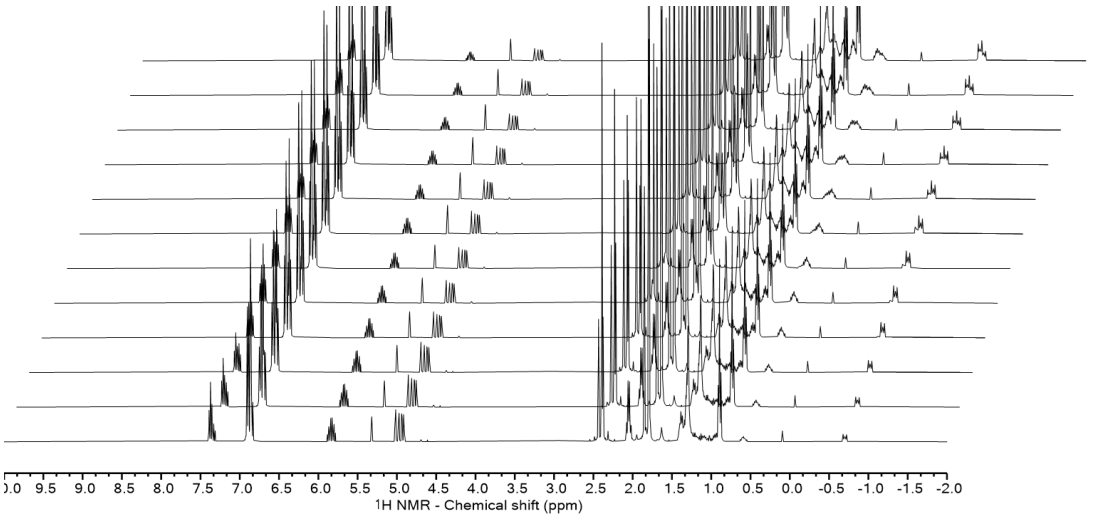

Figure 7-2. ^1H NMR spectra (CD_2Cl_2) for the reaction of 1-octene with $^{Mes}TerAlH_2$ against time.

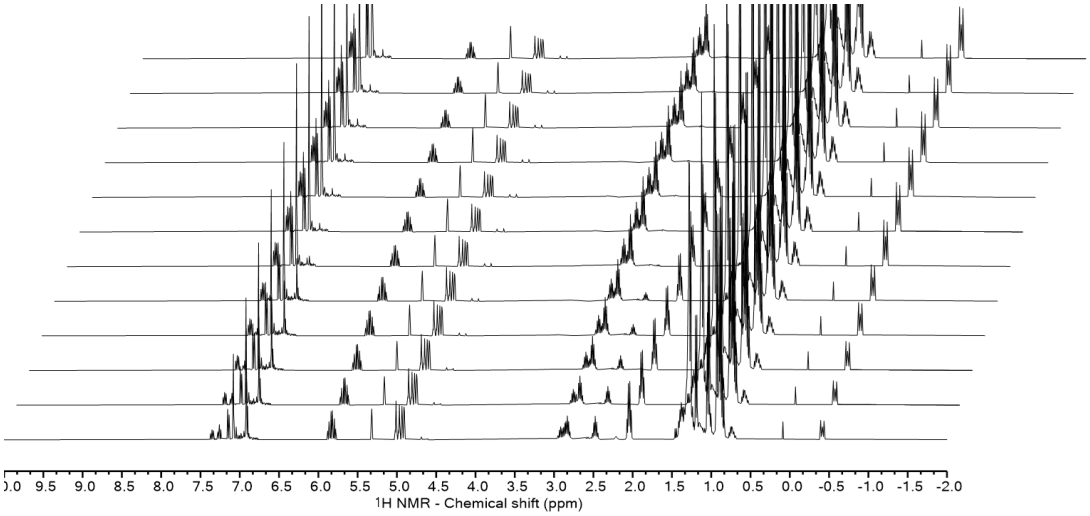

Figure 7-3. ^{1}H NMR spectra (CD_2Cl_2) for the reaction of 1-octene with ^{Tipp}TerAlH$_2$ against time.

The reaction progression was calculated as:

$$\left(1 - \frac{[1-octene]_t}{[1-octene]_0}\right) \times 100$$

Calculation of relative rates:

The first 5 data points were taken to analyse the initial reaction rates (reaction rates drop off for ^{Tipp}TerAlH$_2$ after this due to insolubility issues).

First-order kinetics were assumed, thus:

(Eq. 1): $\ln[1\text{-octene}]_t = -kt + \ln[1\text{-octene}]_0$

Plotting **$\ln[1\text{-octene}]_t$** vs **t** gives the gradient as ***–k***

(Eq. 2): $t_{1/2} = \ln(2)/k$

Ar	*k* (mol L^{-1} h^{-1})	$t_{1/2}$ (h)
p-Tol	0.0606	11.4
Mes	0.1125	6.2
Tipp	0.7615	0.9

7.3.4 Single-turnover experiments

The procedures to monitor the single-turnover experiments, presented in Scheme 2-13, Chapter 2, are as follows:

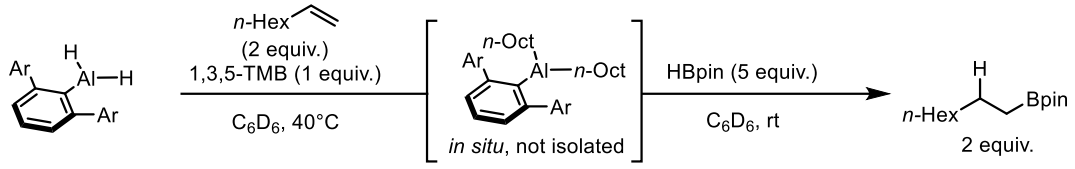

1,3,5-TMB = 1,3,5-trimethoxybenzene

1. Alkene hydroalumination:

Stock solutions of ^{Ar}TerAlH$_2$ (0.05 M in C_6D_6), 1,3,5-trimethoxybenzene (0.5 M in C_6D_6) and 1-octene (0.5 M in C_6D_6) were prepared in advance.

1-octene (40 µL, 0.5 M in C_6D_6, 0.02 mmol, 2 equiv.) was added to a solution of ^{Ar}TerAlH$_2$ (200 µL, 0.05 M in C_6D_6, 0.01 mmol, 1 equiv.) and 1,3,5-trimethoxybenzene (20 µL, 0.5 M in C_6D_6, 0.01 mmol, 1 equiv.) in an NMR tube and topped up with C_6D_6 (340 µL) to make a total volume of 600 µL. Although the reaction proceeds at room temperature (*see Section 7.3.3*), for convenience, the reaction was heated at 40 °C and the conversion was monitored periodically by ^{1}H NMR spectroscopy.

^{Mes}TerAl(octyl)$_2$ (1,3,5 trimethoxybenzene; ABG-0125-B):

^{1}H NMR (400 MHz, Benzene-d_6) δ 7.33 (t, J = 7.6 Hz, 1H; Ar', p-H), 7.01 (d, J = 7.6 Hz, 2H; Ar', 2 × m-H), 6.88 (s, 4H; Mes, 4 × m-H), 3.31 (s, 12H; Mes, 4 × o-CH$_3$), 2.18 (s, 6H; ; Mes, 2 × p-CH$_3$), 1.41 – 0.83 (m, 30H; H$_{alkyl}$), 0.16 – 0.04 (m, 4H; AlCH$_2$R).

^{Tipp}TerAl(octyl)$_2$ (1,3,5 trimethoxybenzene; ABG-0126-B):

^{1}H NMR (400 MHz, Benzene-d_6) δ 7.35 – 7.25 (m, 3H; ArH), 7.23 (s, 4H; Tipp, m-H), 3.16 (hept, J = 6.8 Hz, 4H; Tipp, 4 × o-CH(CH$_3$)$_3$), 2.87 (hept, J = 6.9 Hz, 2H; Tipp, 2 × p-CH(CH$_3$)$_3$), 1.60 – 1.02 (m, 23H; H$_{alkyl}$) (overlapped by (CH$_3$)$_2$CHAr doublets), 1.38 (d, J = 6.9 Hz, 12H; Tipp, CH(CH$_3$)$_3$), 1.29 (d, J = 6.9 Hz, 12H; Tipp, CH(CH$_3$)$_3$), 1.13 (d, J = 6.8 Hz, 12H; Tipp, CH(CH$_3$)$_3$), 0.94 – 0.82 (m, 7H; H$_{alkyl}$), 0.15 – -0.13 (m, 4H; AlCH$_2$R).

$^{p\text{-Tol}}$TerAl(octyl)$_2$ (1,3,5 trimethoxybenzene) (ABG-0670)

^{1}H NMR (500 MHz, Benzene-d_6) δ 7.46 (m, 5H; Ar*H*), 7.38 – 7.32 (m, 1H; Ar*H*), 7.30 (d, *J* = 7.9 Hz, 1H; Ar*H*), 7.11 (d, *J* = 7.5 Hz, 3H; Ar*H*), 6.94 (d, *J* = 7.7 Hz, 1H; Ar*H*), 2.12 (s, 6H; *p*-Tol, C*H*$_3$), 1.34 – 1.13 (m, 24H; *H*$_{alkyl}$), 0.94 – 0.83 (m, 6H; *H*$_{alkyl}$) 0.15 (t, *J* = 7.5 Hz, 4H; AlC*H*$_2$R).

For $^{p\text{-Tol}}$TerAlH$_2$, 1-octene was not fully consumed. Although the target bis-alkyl species was the major product, we also observed resonances attributed to other unidentified $^{p\text{-Tol}}$Ter*Al* containing species. To generate $^{p\text{-Tol}}$TerAl(alkyl)$_2$ more cleanly, we opted to use an excess of a more volatile alkene (*t*-butylethylene), that would allow the full conversion to the target compound and to conveniently remove the excess alkene afterwards:

$^{p\text{-Tol}}$TerAl(CH$_2$CH$_2$*t*Bu)$_2$ (ABG-0515)

*t*Bu-ethylene (66 µL, 0.5 mmol, 10 equiv.) was added to a suspension of $^{p\text{-Tol}}$TerAlH$_2$ (14.3 mg, 0.05 mmol, 1 equiv.) in C_6D_6 (0.6 mL) in an NMR tube. The reaction was mixed through continuous inversion for 24 hours at room temperature, before being heated in an oil bath at 80 °C for 1 hour. The volatiles were removed *in vacuo* and re-dissolved in C_6D_6 to give the target compound deemed sufficiently clean for single-turnover experiments.

^{1}H NMR (500 MHz, Benzene-d_6) δ 7.46 (d, *J* = 7.5 Hz, 2H; 2 × Ar, *m*-*H*), 7.43 – 7.37 (m, 4H; *p*-Tol, Ar*H*), 7.34 (app. dd, *J* = 8.1, 7.0 Hz, 1H; Ar', *p*-*H*), 7.05 (d, *J* = 7.7 Hz, 4H; *p*-Tol, Ar*H*), 2.10 (s, 6H; *p*-Tol, C*H*$_3$), 1.03 – 0.94 (m, 4H; 2 × AlCH$_2$C*H*$_2$R), 0.81 (s, 18H; 2 × (C*H*$_3$)$_3$), 0.10 – -0.07 (m, 4H; 2 × AlC*H*$_2$R).

2. Al–C(sp^3)/B–H σ-bond metathesis with HBpin

Once the dialkyl alanes had formed, HBpin (7.3 µL, 0.05 mmol, 5 equiv.) was added and the reaction was monitored by NMR spectroscopy. In all cases, the complete consumption of AlC*H*$_2$R and formation of product B*pin* resonances were observed within 30 minutes.

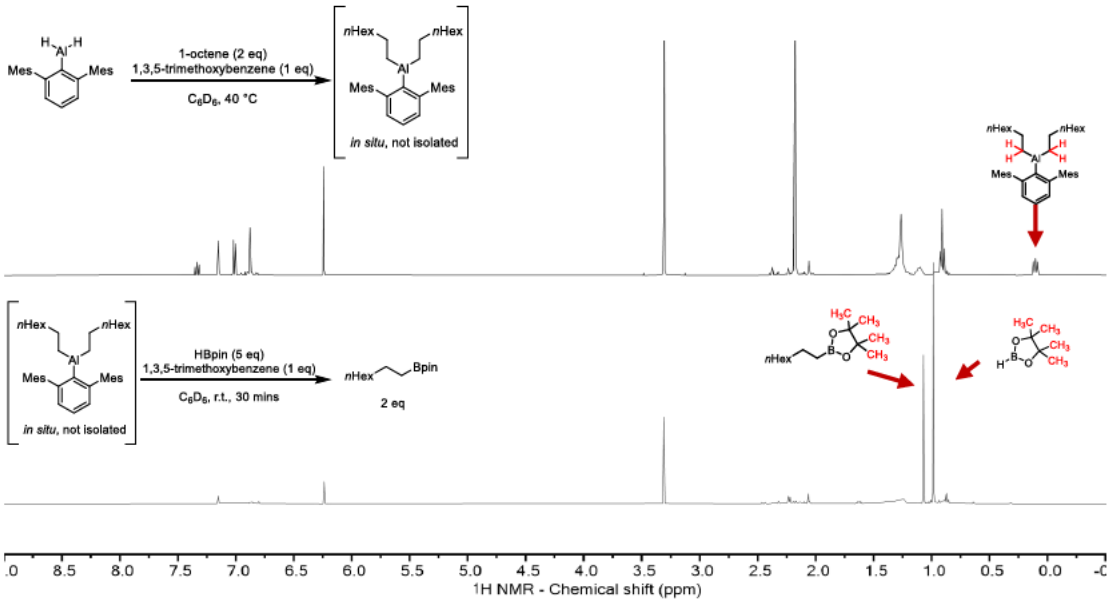

Figure 7-4. Stacked ^{1}H NMR (C_6D_6) spectra showing single turnover experiments for $^{Mes}TerAlH_2$. Starred is trimethoxybenzene internal standard. (ABG-0125-B)

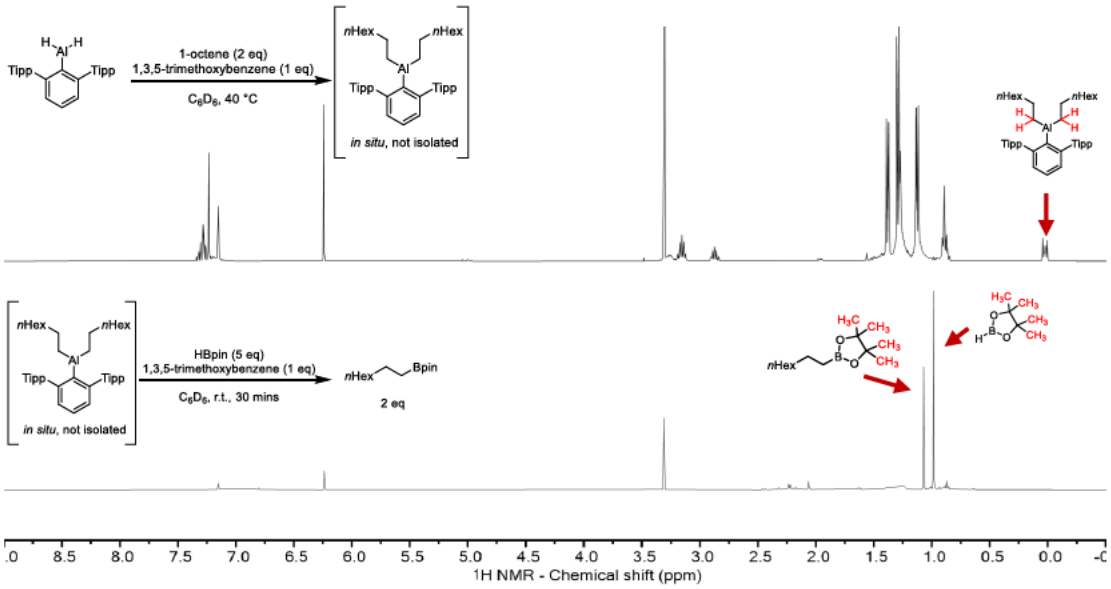

Figure 7-5. Stacked ^{1}H NMR (C_6D_6) spectra showing single turnover experiments for $^{Tipp}TerAlH_2$. Starred is trimethoxybenzene internal standard. (ABG-0126-B)

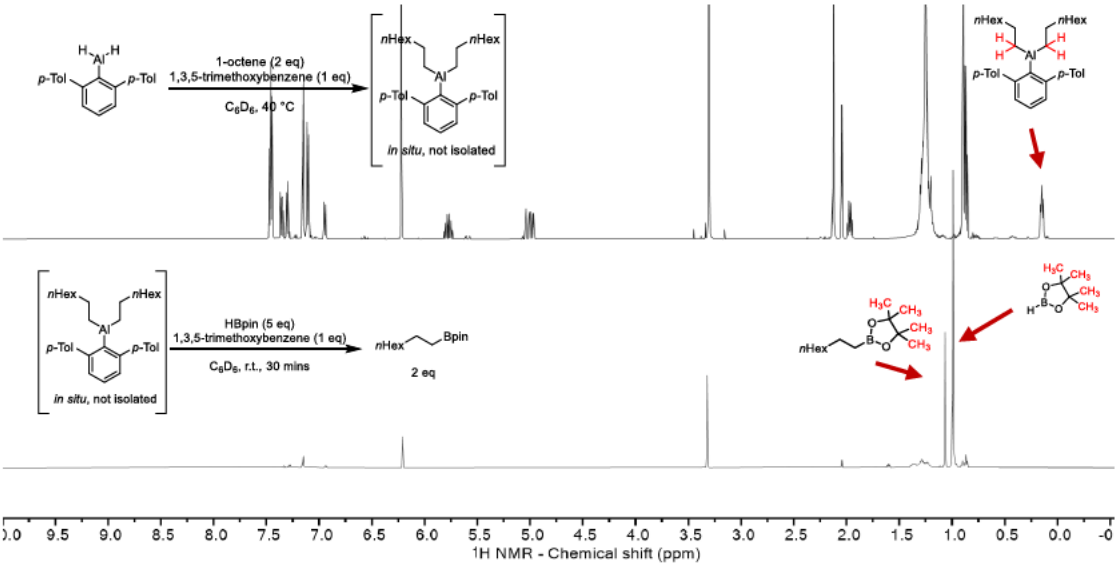

Figure 7-6. Stacked ^{1}H NMR (C_6D_6) spectra showing single turnover experiments for $^{p\text{-Tol}}TerAlH_2$ using 1-octene as the alkene. Starred is trimethoxybenzene internal standard. Circled is unreacted 1-octene. (ABG-0670)

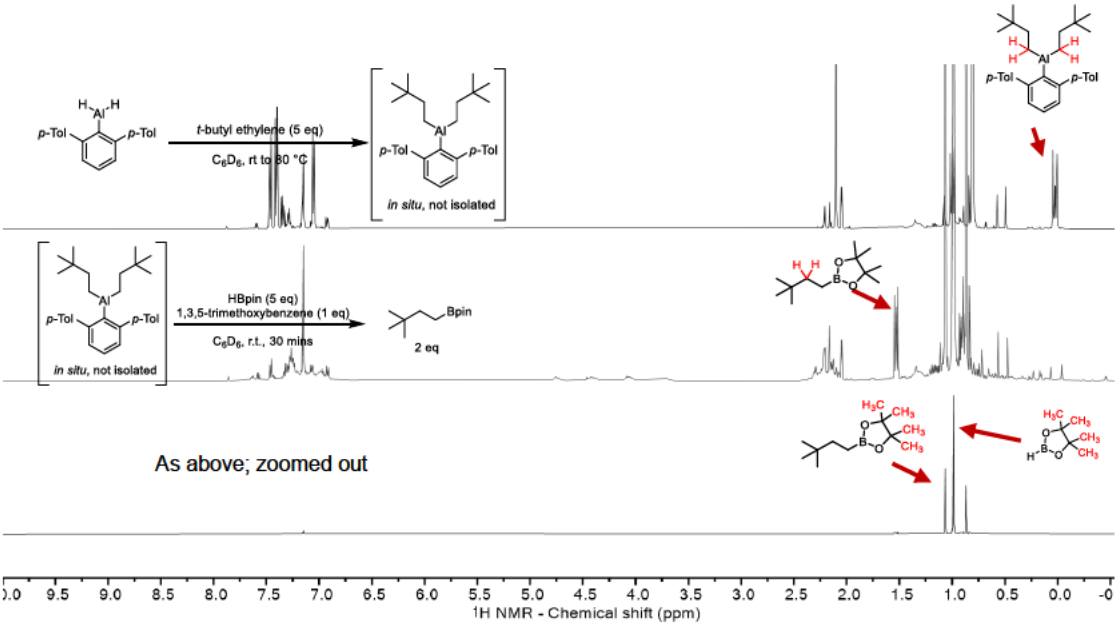

Figure 7-7. Stacked ^{1}H NMR (C_6D_6) spectra showing single turnover experiments for $^{p\text{-Tol}}TerAlH_2$ using *tert*-butyl ethylene as the alkene. (ABG-0515)

Attempted monitoring of Al–C(sp^3)/B–H exchange at low temperature

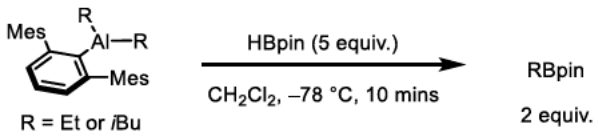

HBpin (7.3 µL, 0.05 mmol, 5 equiv.) was added to a stock solution of ^{Mes}TerAl(alkyl)$_2$ (alkyl = Et or *i*Bu) (1 mL, 0.01 M in CH_2Cl_2, 0.01 mmol, 1 equiv.) at –78 °C in a screw capped vial equipped with a septum. The reaction was quenched after 10 minutes by bubbling through air (O_2) for 30 seconds with a bleed needle at –78 °C. The reaction was analysed by ^{11}B NMR spectroscopy.

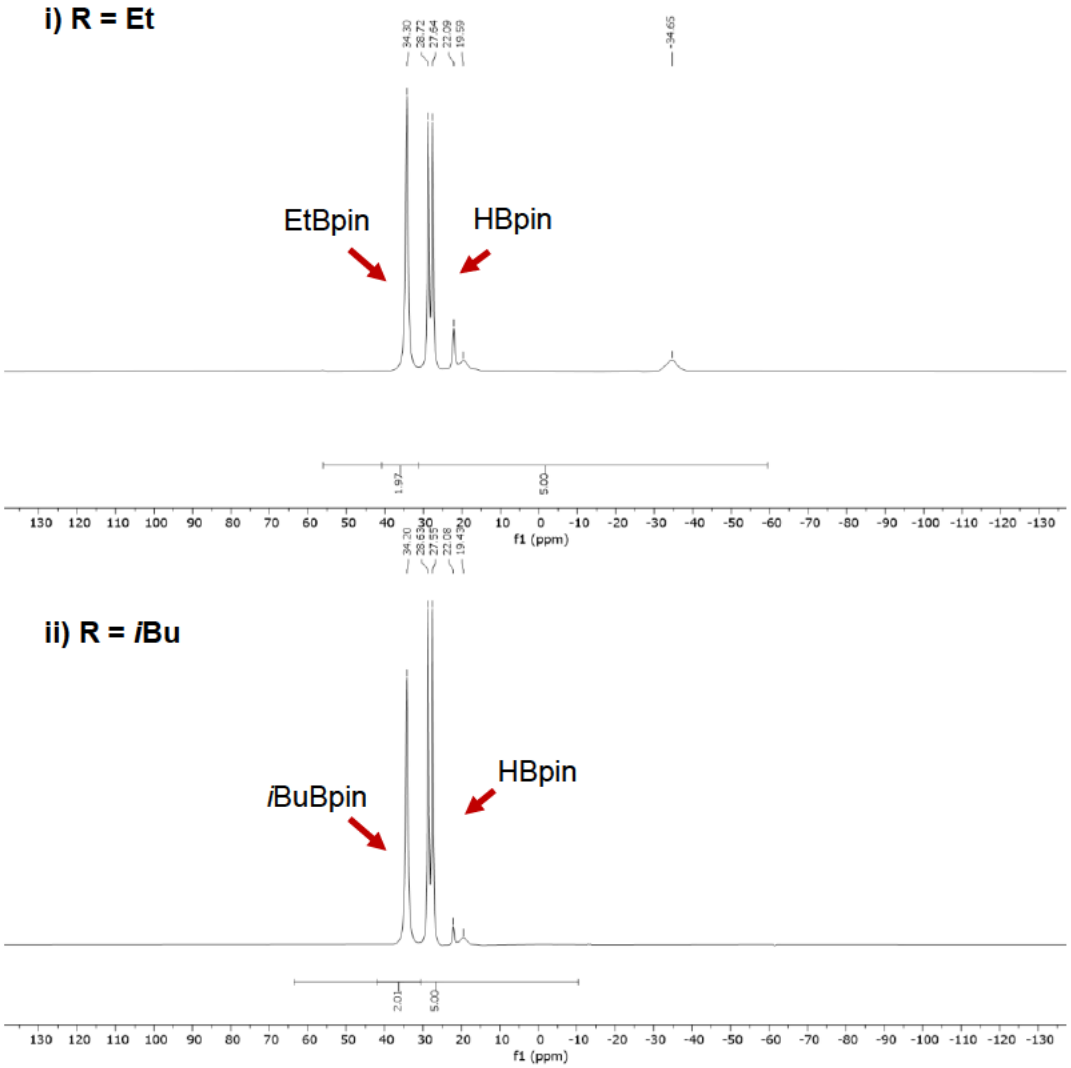

Figure 7-8. Stacked ^{11}B NMR (CH_2Cl_2) of 5 eq HBpin + i) ^{Mes}TerAlEt$_2$ (ABG-0347); ii) ^{Mes}TerAl*i*Bu$_2$ (ABG-0347)

^{Ar}TerAlMe$_2$ with HBpin

The procedure to monitor the reaction between ^{Ar}TerAlMe$_2$ with HBpin, presented in Scheme 2-13 in Chapter 2, is as follows:

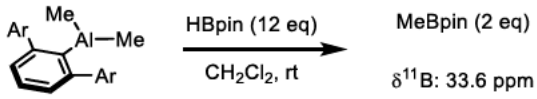

HBpin (87 µL, 0.6 mmol, 12 equiv.) was added to a solution of ^{Ar}TerAlMe$_2$ (0.05 mmol) in CD_2Cl_2 (580 µL; total volume = 667 µL) in an NMR tube and shaken vigorously. The sample was run within 1 hour of HBpin addition.

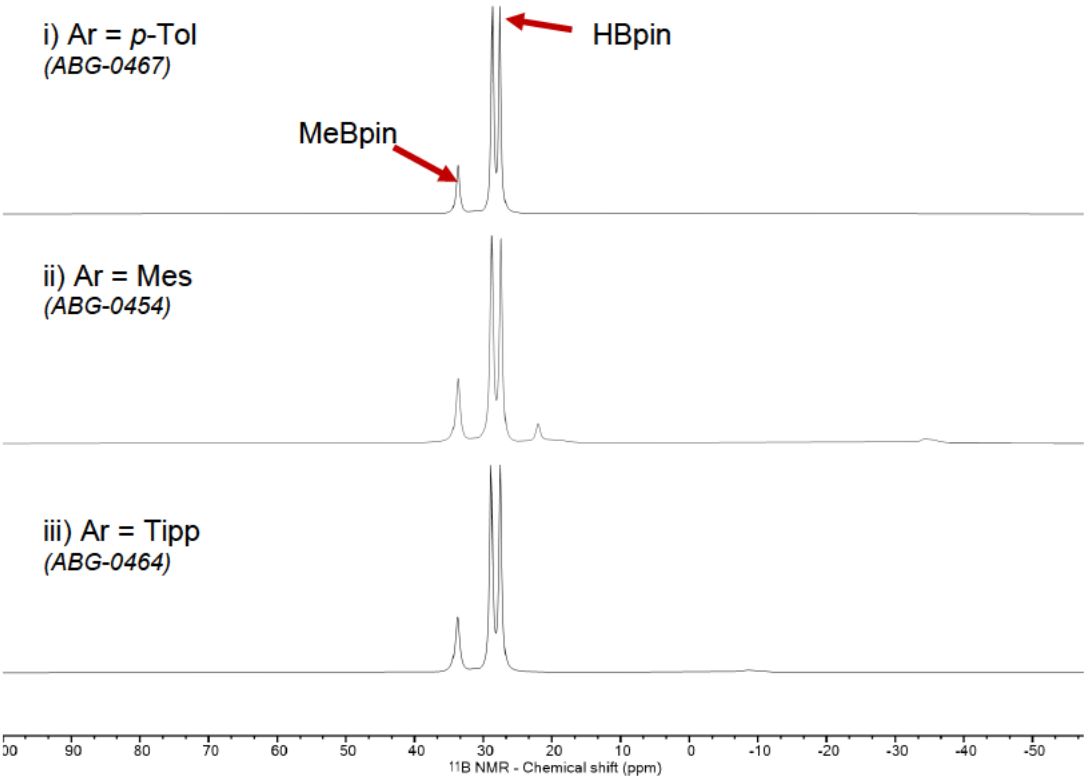

Figure 7-9. Stacked ^{11}B NMR spectra (CH_2Cl_2) of the reaction between dimethyl alanes of varying steric bulk and HBpin.

7.3.5 Catalytic hydroboration of alkenes

During initial monitoring of alkene hydroboration by NMR spectroscopy, we observed that using the diethyl ether adduct of the ^{Tipp}TerAlMe$_2$ catalyst precursor lead to improved solubilities for the catalyst. To ensure that a fair comparison was made across the different sizes of alanes, the diethyl ether adduct for $^{p\text{-Tol}}$TerAlMe$_2$ and ^{Mes}TerAlMe$_2$ were also prepared prior to monitoring by NMR. These could be conveniently synthesised by dissolving the compound in Et$_2$O, followed by removal of the *volatiles in vacuo* at room temperature.

Preparation of ^{Ar}TerAlMe$_2$•OEt$_2$ adducts

$^{p\text{-Tol}}$TerAlMe$_2$•OEt$_2$ (ABG-0291)

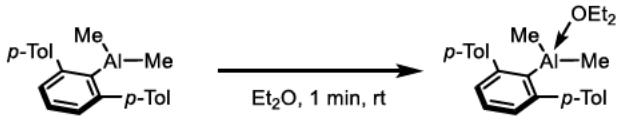

$^{p\text{-Tol}}$TerAlMe$_2$ (75 mg, 0.24 mmol) was dissolved in Et$_2$O (0.3 mL). The solvent was removed *in vacuo* to yield $^{p\text{-Tol}}$TerAlMe$_2$•OEt$_2$ as a colourless foam. (87 mg, 93%).

^{1}H NMR (500 MHz, Benzene-d_6) δ 7.65 – 7.59 (m, 4H; *p*-Tol, 4 × Ar*H*), 7.48 – 7.43 (m, 2H; Ar', 2 × *m*-*H*), 7.36 (app. dd, *J* = 8.0, 7.0 Hz, 1H; Ar', *p*-*H*), 7.11 – 7.07 (m, 4H; *p*-Tol, Ar*H*), 2.91 (q, *J* = 7.1 Hz, 4H; 2 × OC*H*$_2$CH$_3$), 2.16 (s, 6H; *p*-Tol, 2 × C*H*$_3$), 0.49 (t, *J* = 7.1 Hz, 6H; 2 × OCH$_2$C*H*$_3$), -0.62 (s, 6H; Al(C*H*$_3$)$_2$).

^{13}C {^{1}H} NMR (126 MHz, Benzene-d_6) δ 152.6, 145.5, 136.2, 129.5 (*p*-Tol *m*-Ar and *o*-Ar), 127.7, 127.1, 66.5, 21.1, 13.8, -5.3. (*C*-Al not observed, presumably due to quadrupolar line broadening from ^{27}Al)

IR (neat) 2920*w*, 1512*m*, 1434*m*

^{Mes}TerAlMe$_2$•OEt$_2$ (ABG-0519)

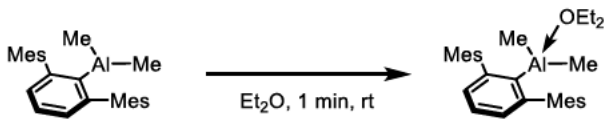

^{Mes}TerAlMe$_2$ (100 mg, 0.27 mmol) was dissolved in Et$_2$O (5 mL) and then the volatiles were removed *in vacuo*. The white solid was dissolved in hexane (*ca.* 5 mL) which grew colourless cubes of ^{Mes}TerAlMe$_2$•OEt$_2$ after storage at –20 °C overnight (69 mg, 57%).

^{1}H NMR (500 MHz, Benzene-d_6) δ 7.32 (t, *J* = 7.5 Hz, 1H; Ar', *p*-*H*), 6.98 (d, *J* = 7.5 Hz, 2H; Ar', *o*-*H*), 6.88 (s, 4H; Mes, *m*-*H*), 3.09 (q, *J* = 7.0 Hz, 4H; 2 × OC*H*$_2$CH$_3$), 2.22 (s, 6H; Mes, *p*-C*H*$_3$), 2.21 (s, 12H; Mes, *o*-C*H*$_3$), 0.64 (t, *J* = 7.1 Hz, 6H; 2 × OCH$_2$C*H*$_3$), -0.87 (s, 6H; Al(C*H*$_3$)$_2$).

^{13}C {^{1}H} NMR (126 MHz, Benzene-d_6) δ 151.2, 151.0, 144.0, 143.3, 136.5, 135.8, 128.5, 127.3, 67.6, 21.8, 21.2, 14.1, -5.8.

IR (neat) 2917*w*, 1609*w*, 1548*w*, 1441*m*, 1189*m*

m.p. (*n*-hexane) 123-127 °C

For ^{Tipp}TerAlMe$_2$•OEt$_2$, see ***section 7.2***.

Comparison of rate between ^{Mes}Terphenyl aluminium derivatives: (ABG-254/270)

The procedure to compare the catalytic activity of reaction of different ^{Mes}Ter***Al*** catalysts (***Al*** = –$AlMe_2$, –$AlMe_2$•OEt_2, –AlH_2) for 1-octene hydroboration with HBpin, presented in **Scheme 2-16.ii** in **Chapter 2**, is as follows:

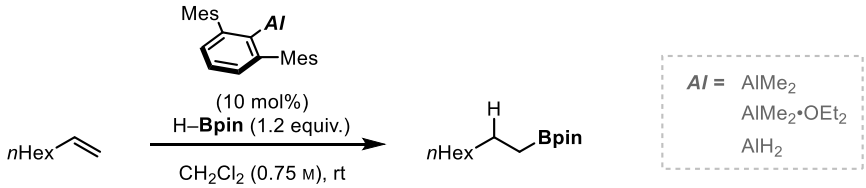

Over a flow of argon, HBpin (87 µL, 0.6 mmol) was added to an NMR tube containing a solution of *m*-terphenyl aluminium (0.05 mmol, 10 mol%) and 1-octene (80 µL, 0.5 mmol) in CD_2Cl_2 (total volume = 667 µL, 0.75 M w.r.t. alkene). The formation of octylBpin (δ 0.73; t, *J* = 7.7 Hz, 2H; BC*H*$_2$R) was followed by ^{1}H NMR spectroscopy, using the total integration of aromatic protons as an internal standard (assumed to have remained constant).[240]

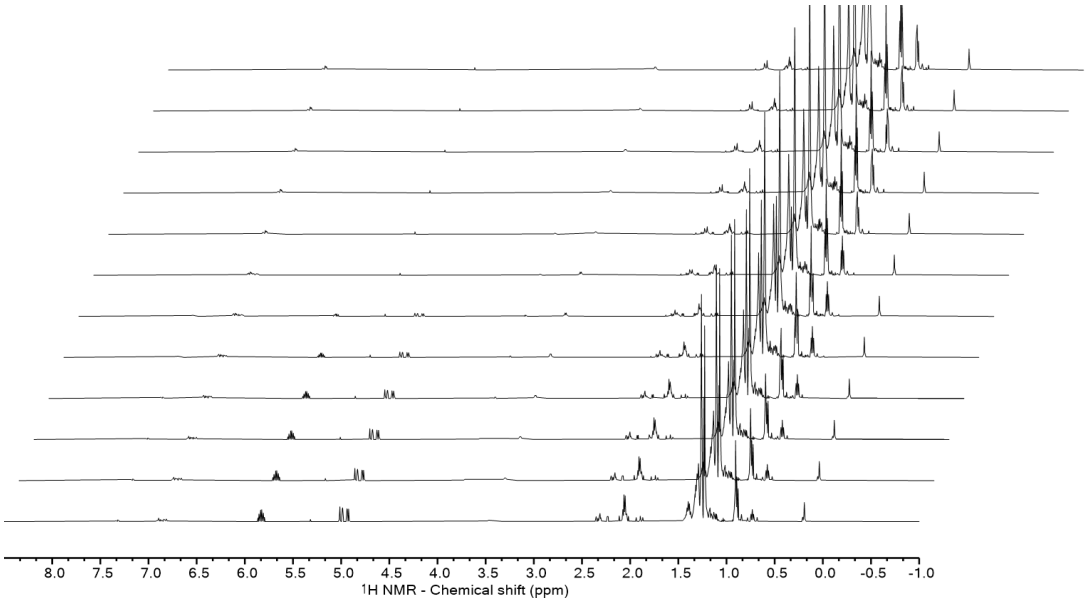

Figure 7-10. ^{1}H NMR spectra (CD_2Cl_2) against time for the reaction of 1-octene with HBpin catalysed by ^{Mes}Ter$AlMe_2$•OEt_2.

Initial rates were calculated from the first six data points. The data best fit zero-order kinetics.

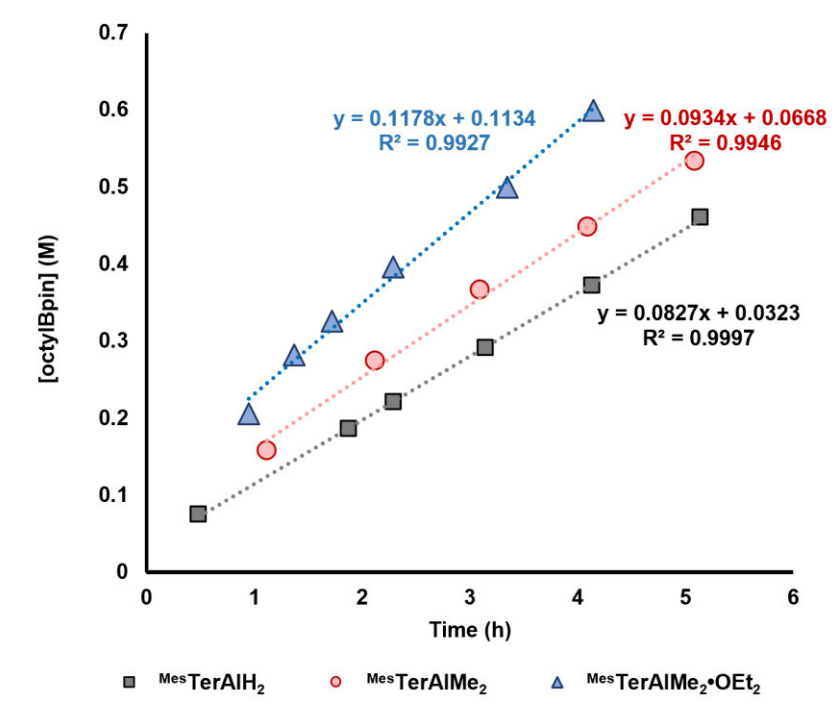

Figure 7-11: Calculation of rates for alkene hydroboration with HBpin catalysed by different ^{Mes}Ter*Al* derivatives.

Equations 3 and 4 were used to calculate *k* and $t_{1/2}$ respectively for each of these systems.

Eq. (3):

$$[octylBpin]_t = kt + [octylBpin]_0$$

*Plotting **[octylBpin]** vs **t** gives **k** as the gradient.*

Eq. (4):

$$t_{1/2} = \frac{[\text{octylBpin}]_\infty}{2k}$$

Where $[octylBpin]_\infty$ = 0.75 M

Catalyst	*k* (mol L^{-1} h^{-1})	$t_{1/2}$ (h)
^{Mes}TerAlH$_2$	0.083	4.53
^{Mes}TerAlMe$_2$	0.093	4.02
^{Mes}TerAlMe$_2$•OEt$_2$	0.118	3.18

Comparison of rates for varying *m*-terphenyl bulk

The procedure to compare the catalytic activity of different ^{Ar}TerAlMe$_2$•OEt$_2$ catalysts (Ar = *p*-Tol (ABG-0294), Mes (ABG-0270), Tipp (ABG-0194)) for 1-octene hydroboration with HBpin, presented in **Scheme 2-17** in **Chapter 2**, is as follows:

General procedure for monitoring hydroboration by NMR spectroscopy:

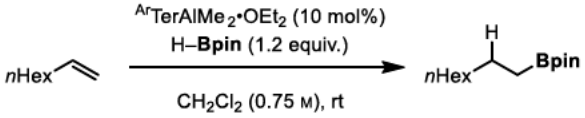

Over a flow of argon, HBpin (87 µL, 0.6 mmol) was added to an NMR tube containing a solution of ^{Ar}TerAlMe$_2$•OEt$_2$ (0.05 mmol, 10 mol%; Ar = *p*-Tol, Mes, Tipp) and 1-octene (80 µL, 0.5 mmol) in CD_2Cl_2 (total volume = 667 µL, 0.75 M w.r.t. alkene). The formation of octylBpin (δ 0.73; t, J = 7.7 Hz, 2H; BC$\underline{H_2}$R) was followed by ^{1}H NMR spectroscopy, using the total integration of aromatic protons as an internal standard (assumed to have remained constant).

Calculation of relative rates

Initial rate was estimated from the first 5 hours of data. The data fitted best with zero order kinetics. Thus Equations 3 and 4 were used to calculate k and $t_{1/2}$ respectively for each of these systems.

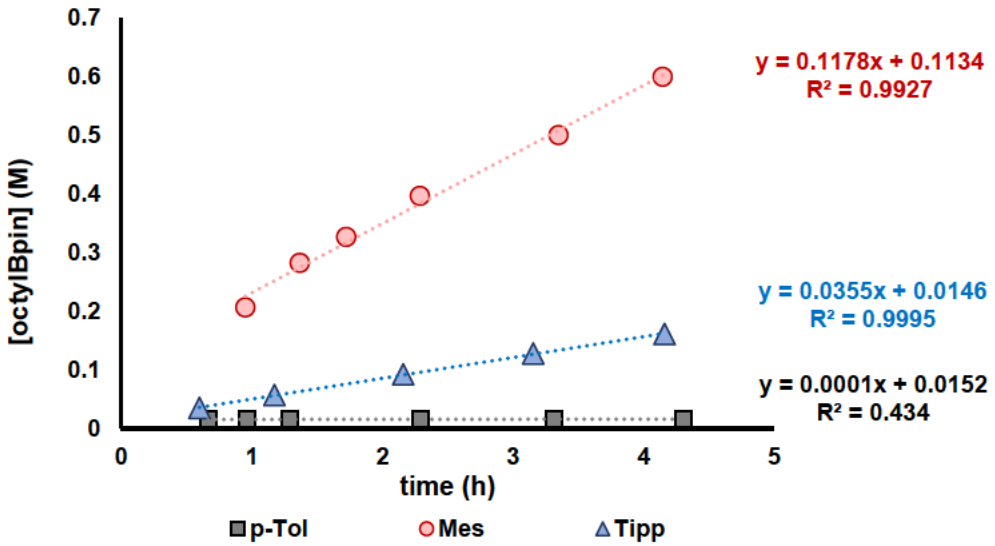

Ar =	k (mol L^{-1} h^{-1})	k_{rel}	$t_{1/2}$
p-Tol	0.0001	0.001	N/A*
Mes	0.118	1.000	3.2
Tipp	0.036	0.301	10.6

* The reaction rate is negligible, rendering the $t_{1/2}$ value meaningless.

7.4 Experimental details for Chapter 3

7.4.1 Assessing influence of boronic esters on hydroalumination

The procedure to compare the influence of boronic esters on stoichiometric 1-octene hydroalumination with $^{Ar}TerAlH_2$ (Ar = Mes, Tipp), presented in **Scheme 3-2** in **Chapter 3**, is as follows (ABG-0394-0396):

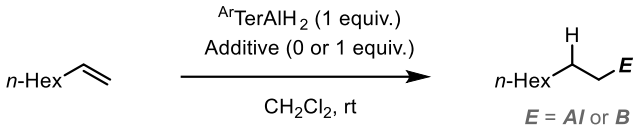

1-octene (0.1 M in CD_2Cl_2, 100 µL, 0.01 mmol, 1 equiv.) was added to an NMR tube equipped with a rubber septum containing a solution of $TerAlH_2$ (0.01 mmol, 1 equiv.) and additive (0.01 mmol, 1 equiv.) in CD_2Cl_2 (total volume = 0.87 mL, 11.5 mM w.r.t. 1-octene) and shaken vigorously. The reaction progression at room temperature was monitored by tracking the consumption of 1-octene (δ 5.83, ddt, *J* = 16.9, 10.2, 6.7 Hz, 1H; RC*H*=CH_2) with ^1H NMR spectroscopy, using the total integration of aromatic protons as an internal standard (assumed to have remained constant).[240]

The reaction progression was calculated using the equation:

$$\left(1 - \frac{[1-octene]_t}{[1-octene]_0}\right) \times 100$$

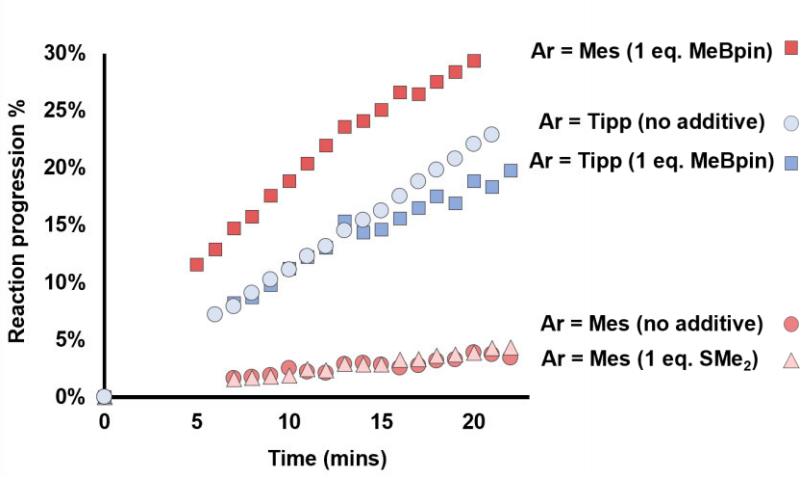

Figure 7-12. Comparing the effect of additives on the hydroalumination of 1-octene (11.5 mM).

The concentration of products, i.e. octyl alanes and alkyl boranes, [octyl*E*], was assumed to correlate with the consumption of 1-octene; i.e.:

$$[octylE] = reaction\ progression \times [1-octene]_0$$

The initial rate for the formation of [octylE] was taken from the first 11 minutes and calculated using zero-order rates analogously to equation 3. The approximate half-life for the reaction was calculated analogously to equation 4.

Where $[1\text{-octene}]_0$ = 11.5 mM

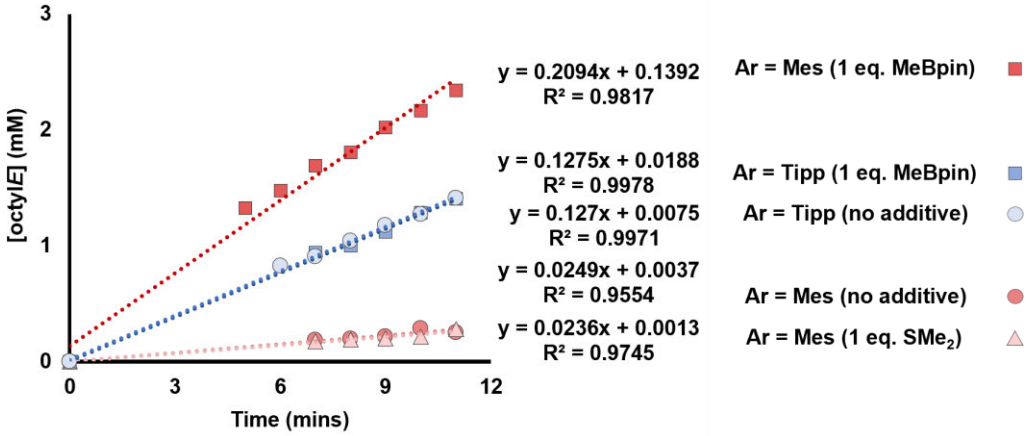

Figure 7-13. Data points used to calculate initial rates of hydroelementation.

Table S2. Comparison of relative rates for 1-octene hydroelementation with the combination of different aluminium dihydrides and additives.

Entry	Ar	Additive (1 equiv.)	k ($mmol^{-1}$ min^{-1})	$t_{1/2}$ (h)	k_{rel} – to Ar = Mes (no additive)	k_{rel} – to Ar = Tipp (no additive)
1	Mes	No additive	0.025	3.8	1.0	0.2
2	Mes	SMe_2	0.024	4.1	0.9	0.2
3	Mes	MeBpin	0.209	0.5	8.9	1.6
4	Tipp	No additive	0.127	0.8	5.4	1.0
5	Tipp	MeBpin	0.128	0.8	5.4	1.0

7.4.2 Interaction between ^{Ar}TerAlH$_2$ and RBpin

On **Scheme 3-3** in **Chapter 3**, the interaction between ^{Ar}TerAlH$_2$ with RBpin was analysed as followed:

MeBpin

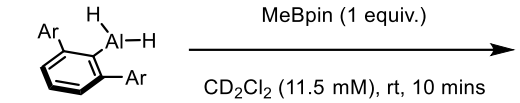

Ar = Mes or Tipp

MeBpin (1.9 µL, 0.01 mmol, 1 equiv.) was added to an NMR tube equipped with a rubber septum containing a solution of ^{Ar}TerAlH$_2$ (0.01 mmol, 1 equiv.; Ar = Mes, Tipp) in CD_2Cl_2 (total volume = 0.87 mL, 11.5 mM) and shaken vigorously. The ^{1}H NMR spectra were obtained within ten minutes of adding MeBpin.

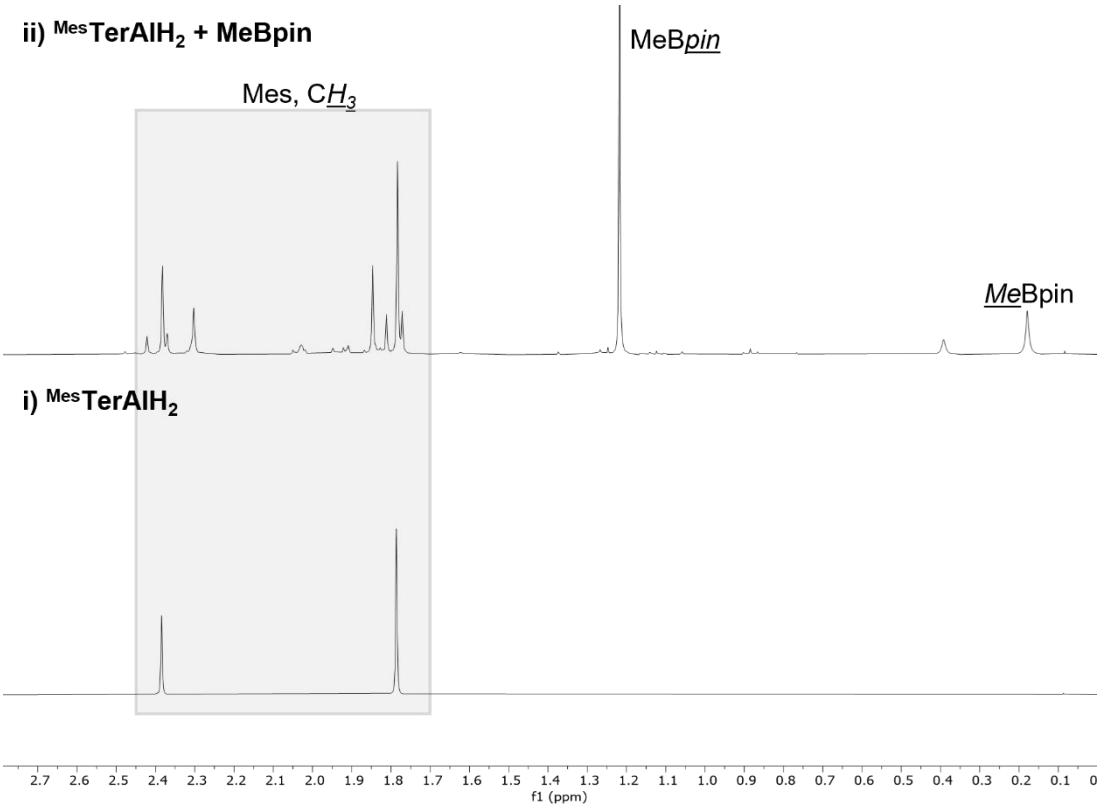

Figure 7-14. Stacked ^{1}H NMR spectra (CD_2Cl_2) of i) ^{Mes}TerAlH$_2$ and ii) ^{Mes}TerAlH$_2$ + MeBpin (1 equiv.; ABG-0395-B)

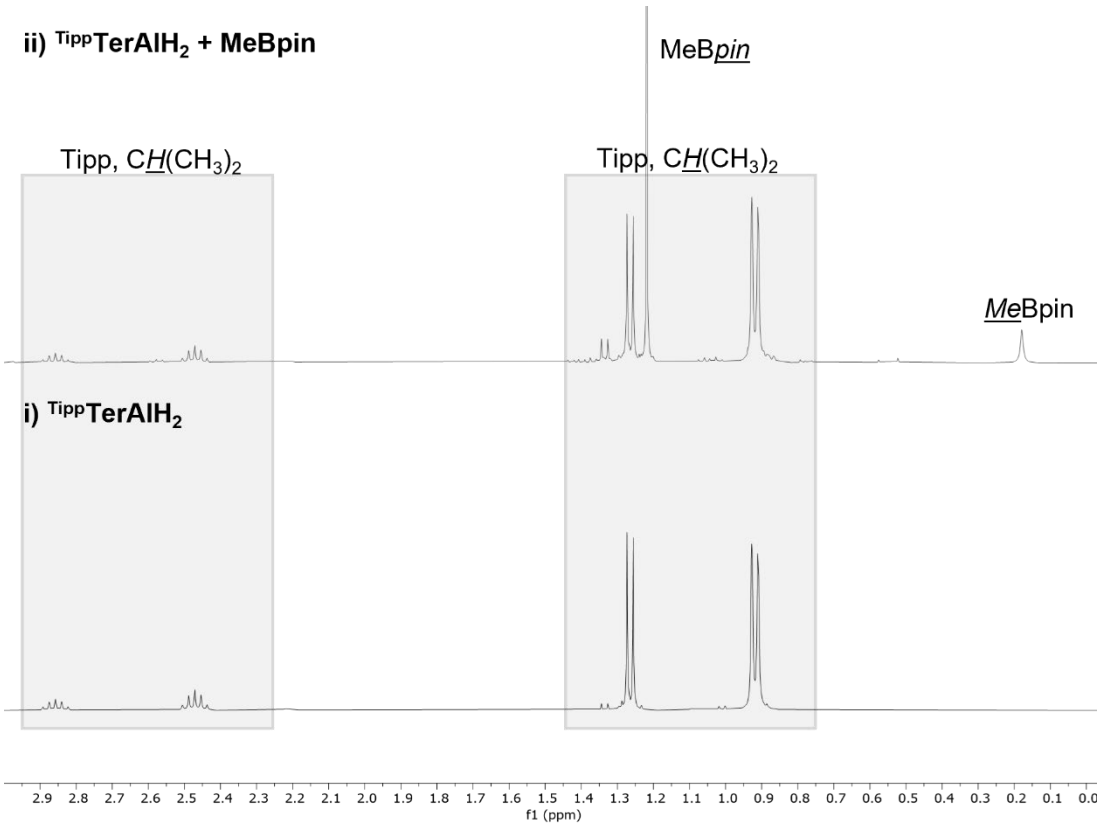

Figure 7-15. Stacked ^{1}H NMR spectra (CD_2Cl_2) of i) $^{Tipp}TerAlH_2$ and ii) $^{Tipp}TerAlH_2$ + MeBpin (1 equiv.; ABG-0396-B)

Other RBpin:

Where Ar = Mes, it was found that similar resonances would form, regardless of the group attached to Bpin:

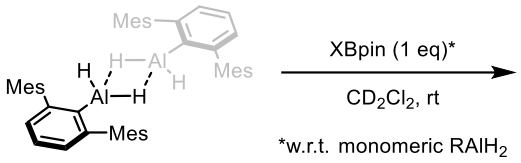

RBpin (0.05 mmol, 1 equiv.; R = H–, Me–, *n*-octyl–, *t*BuCH$_2$CH$_2$–) was added to an NMR tube equipped with a rubber septum containing a solution of ^{Mes}TerAlH$_2$ (17.1 mg, 0.05 mmol, 1 equiv.) in CD_2Cl_2 (total volume = 0.67 mL) and shaken vigorously. The ^{1}H NMR spectra were obtained within one hour of adding RBpin.

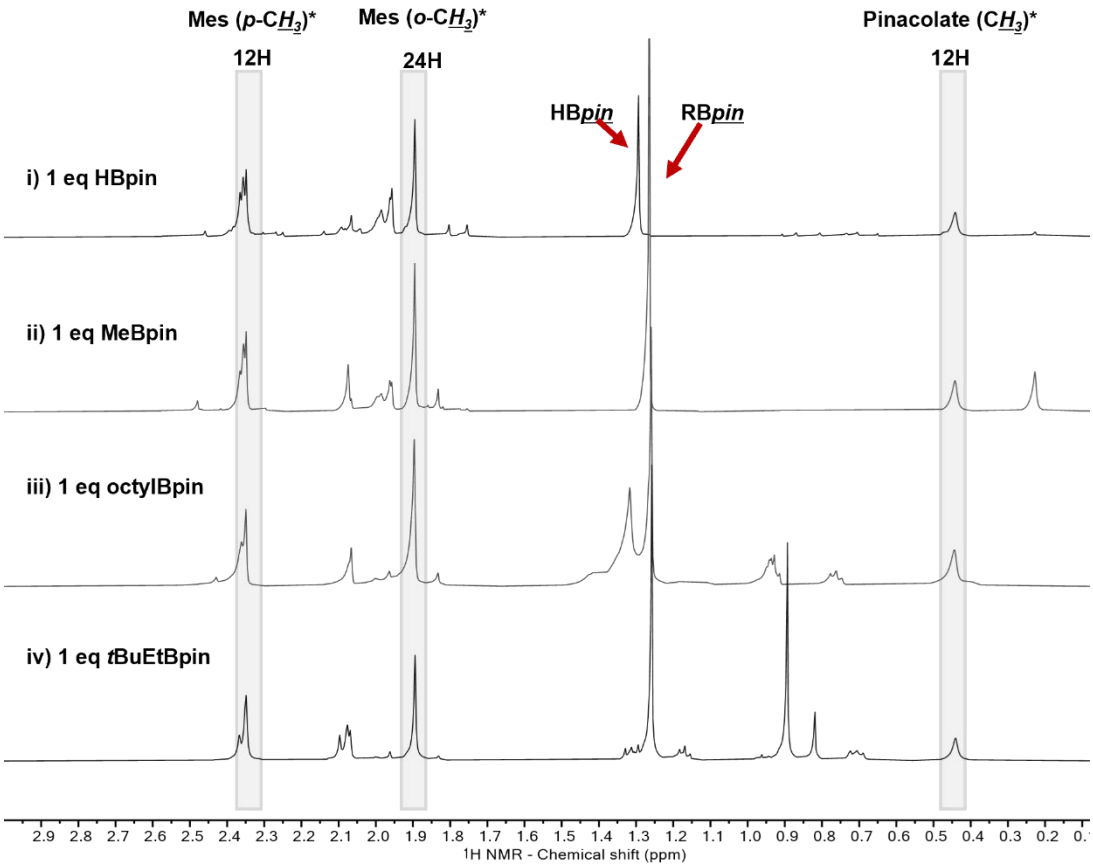

Figure 7-16. Stacked ^{1}H NMR (CD_2Cl_2) spectra of ^{Mes}TerAlH$_2$ in the presence of: i) HBpin (1 equiv.; ABG-0236-A); ii) MeBpin (1 equiv.; ABG-0236-B); iii) OctylBpin (1 equiv.; ABG-0236-C); iv) *t*BuCH$_2$CH$_2$Bpin (1 equiv.; ABG-0408). *The resonances of the newly formed major species are highlighted.

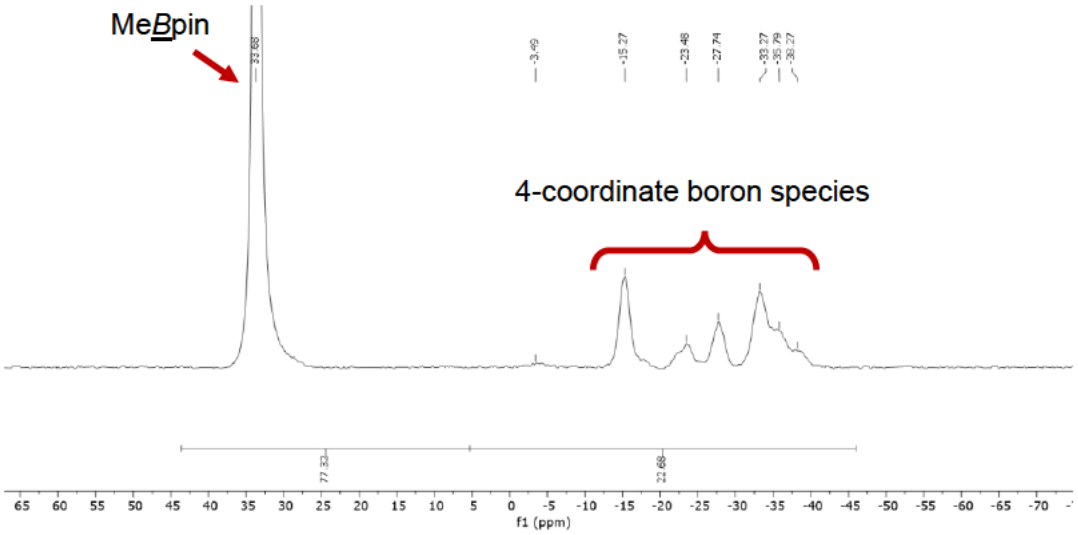

Figure 7-17. ^{11}B NMR spectrum (CD_2Cl_2) for the reaction between $^{Mes}TerAlH_2$ and MeBpin (ABG-0236-B).

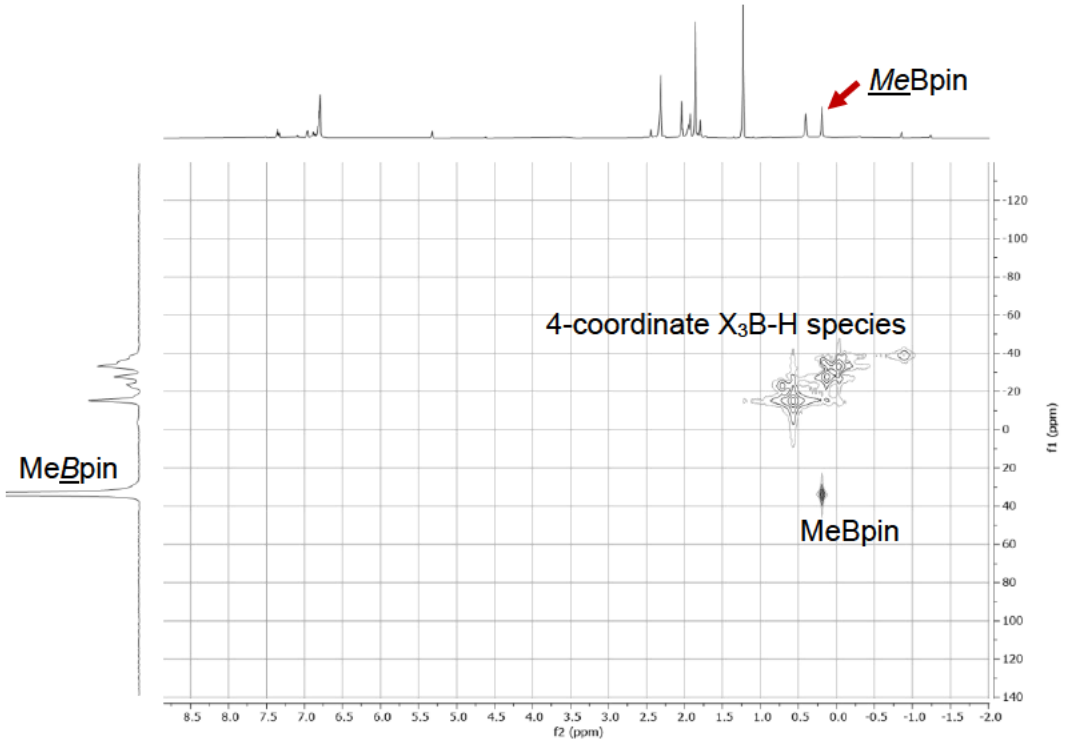

Figure 7-18 . ^{1}H-^{11}B HMQC (CD_2Cl_2) for the reaction between $^{Mes}TerAlH_2$ and MeBpin (ABG-0236-B).

On **Scheme 3-3** in **Chapter 3**, pinacol transfer from Bpin to aluminium was shown. To determine this:

Pinacol (6.0 mg, 0.025 mmol, 0.5 equiv.) was added to a solution of $^{Mes}TerAlH_2$ (17.1 mg, 0.05 mmol, 1 equiv.) in C_6D_6 (total volume = 0.67 mL) and shaken vigorously. The ^{1}H NMR spectra was obtained within one hour of adding pinacol.

The spectrum was compared to an analogous solution containing MeBpin (9.6 µL, 0.05 mmol, 1 equiv.) in place of pinacol. Both spectra were compared to an NMR sample containing only $^{Mes}TerAlH_2$ in C_6D_6.

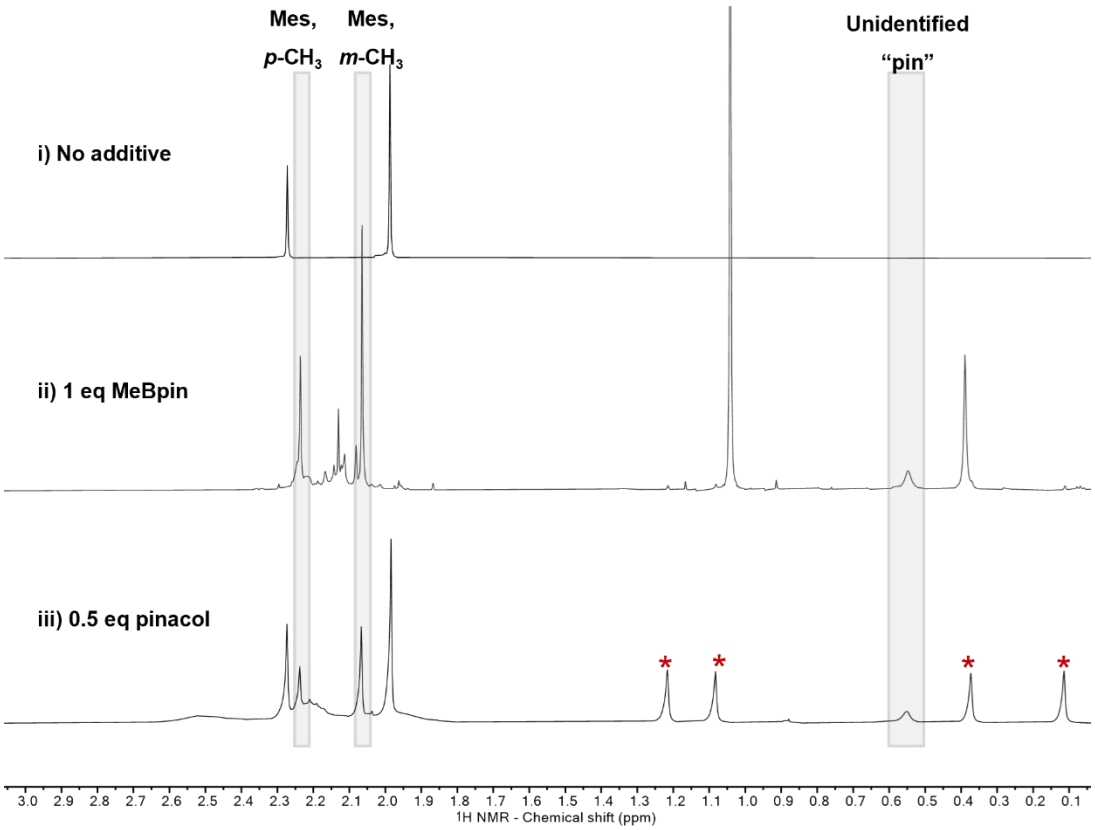

Figure 7-19. Stacked ^1H NMR (C_6D_6) spectra of $^{Mes}TerAlH_2$ in the presence of: i) no additive (ABG-0299-A); ii) MeBpin (1 equiv.; ABG-0299-C); iii) pinacol (0.5 equiv.; ABG-0442). Starred resonances are the inequivalent pinacolate methyl peaks of the major species, $[^{Mes}TerAl(pin)_2]_2$. Highlighted (grey box) are the resonances of the unidentified pinacol transfer species.

^{Mes}TerAl(pin) (ABG-0431):

^{1}H NMR: (500 MHz, C_6D_6) δ 7.21 (t, *J* = 7.6 Hz, 1H; Ar', *p*-H), 6.98 – 6.56 (m, 6H; Ar' and Mes, 6 × *m*-H), 2.50 (br s, $w_{1/2}$ ~ 77 Hz, 6H; Mes, 2 × CH_3), 2.21 (br s, $w_{1/2}$ ~ 52 Hz, 6H; Mes, 2 × CH_3), 1.95 (br s, $w_{1/2}$ ~ 77 Hz, 6H; Mes, 2 × CH_3), 1.22 (s, 3H; pin, CH_3), 1.08 (s, 3H; pin, CH_3), 0.37 (s, 3H; pin, CH_3), 0.11 (s, 3H; pin, CH_3).

***Al–pin* (ABG-0442):**

^{1}H NMR (601 MHz, C_6D_6) δ 7.24 (t, *J* = 7.6 Hz, 2H; Ar', 2 × *p*-H), 6.87 (d, *J* = 7.5 Hz, 4H; Ar', 4 × *m*-H), 6.80 (s, 8H; Mes, 8 × *m*-H), 2.24 (s, 12H; Mes, *p*-CH_3), 2.07 (s, 24H; Mes, *o*-CH_3), 0.55 (s, 12H; pin, CH_3).

7.4.3 Monitoring hidden BH_3 catalysis

In section 3.3.2 in Chapter 3, control reactions to test for hidden boron catalysis were undertaken. The procedures for these experiments are as follows:

Identifying BH_3 concentration through TMEDA quenching (ABG-0672-674)

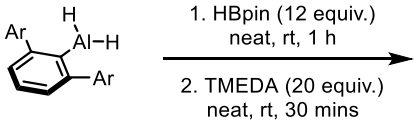

Ar	*BH_3 content*
p-Tol	*9.0%*
Mes	*8.3%*
Tipp	*1.6%*

HBpin (87 µL, 0.6 mmol, 12 equiv.) was added neat to $^{Ar}TerAlH_2$ (0.05 mmol; Ar = *p*-Tol, Mes or Tipp) and stirred for 1 hour at room temperature. At this point, TMEDA (150 µL, 1 mmol, 20 equiv.) was added, stirred for 30 minutes and then exposed to air. An aliquot was taken for ^{11}B NMR analysis in $CDCl_3$.

To quantify the formation of TMEDA•BH_3 in ^{11}B NMR spectroscopy, the full spectrum was integrated to 120 (for 12 equiv. of borane w.r.t. catalyst). The integral for TMEDA•BH_3 (^{11}B NMR: δ –9.75 (q)) therefore relates to the % composition of TMEDA•BH_3 formed in the reaction, and therefore the % of BH_3 formed under catalysis before quenching with TMEDA.

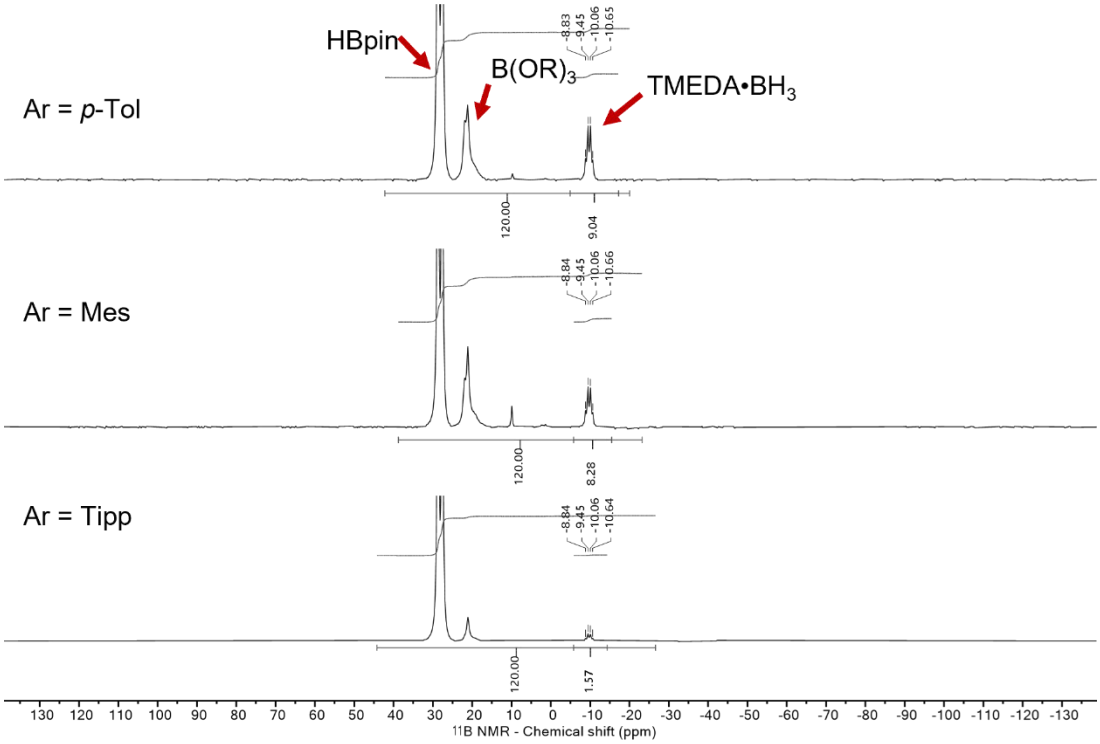

Figure 7-20. Stacked ^{11}B NMR spectra (CH_2Cl_2) of the reaction between $^{Ar}TerAlH2$ with HBpin under catalytic conditions, but in the absence of alkene and quenched with TMEDA.

Assessing background catalysis by BH_3 (ABG-0706)

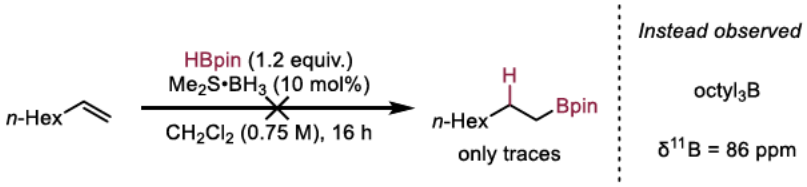

HBpin (87 µL, 0.60 mmol, 1.2 equiv.) was added to a solution of 1-octene (80 µL, 0.50 mmol, 1.0 equiv.), $Me_2S•BH_3$ (4.8 µL, 0.05 mmol, 10 mol%) and 1,3,5-trimethoxybenzene (0.5 M in C_6D_6, 100µL, 0.05 mmol, 0.1 equiv.) in CH_2Cl_2 at room temperature in an NMR tube. The reaction was shaken and then left for 16 hours before being analysed by NMR spectroscopy.

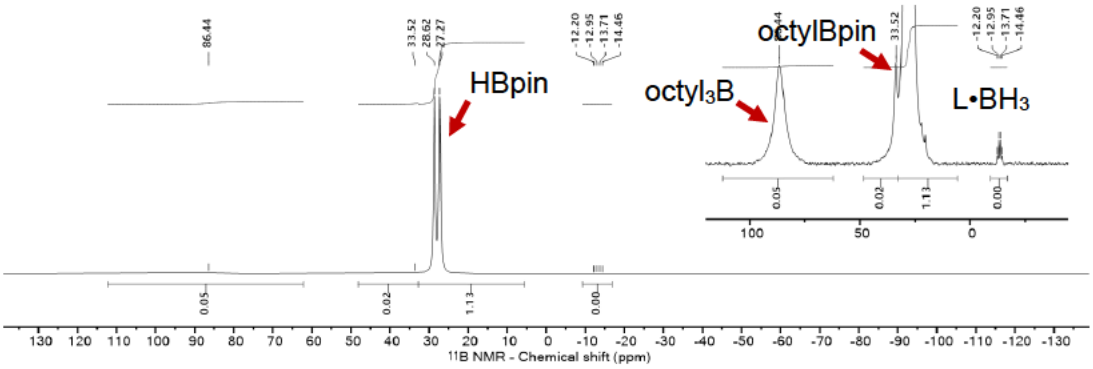

Figure 7-21. ^{11}B NMR spectrum (CH_2Cl_2) of the attempted hydroboration of 1-octene with HBpin using $Me_2S•BH_3$ as catalyst (spectrum integrated to 1.2 equiv. of boron).

Assessing possible suppression of catalysis by SMe_2 (ABG-0266)

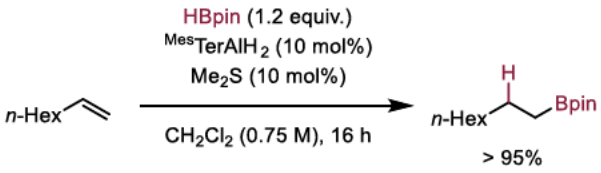

HBpin (87 µL, 0.60 mmol, 1.2 equiv.) was added to a solution of 1-octene (80 µL, 0.50 mmol, 1.0 equiv.), $^{Mes}TerAlH_2$ (17.1 mg, 0.05 mmol, 10 mol%) and SMe_2 (3.7 µL, 0.05 mmol, 0.1 equiv.) in CH_2Cl_2 at room temperature in an NMR tube. The reaction was shaken and then left for 16 hours before being analysed by NMR spectroscopy.

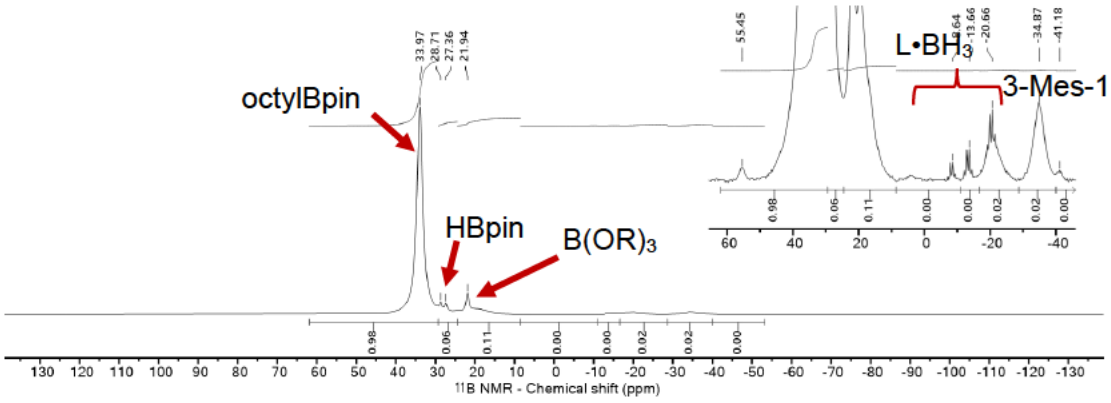

Figure 7-22. ^{11}B NMR spectrum (CH_2Cl_2) of the hydroboration of 1-octene with HBpin using $^{Mes}TerAlH_2$ as catalyst in the presence of SMe_2 (spectrum integrated to 1.2 equiv. of boron).

On scheme 3-5, the reaction of Et_3B with HBpin (in the presence and absence of $^{Mes}TerAlH_2$) was shown. For experimental details, see section 7.4.7.

7.4.4 Influence of sterics on formation of boron-containing species in catalysis.

In Section 3.3.3 in Chapter 3, the boron-containing species present under catalysis for each *m*-terphenyl alane catalyst were compared. The procedure is as follows:

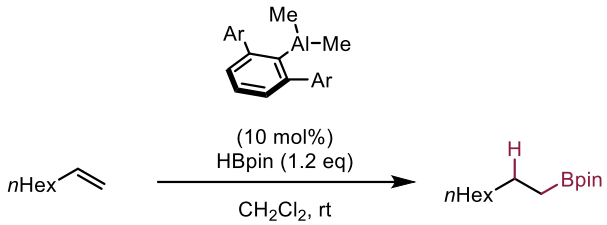

HBpin (87 µL, 0.60 mmol, 1.2 equiv.) was added to a solution $^{Ar}TerAlMe_2$ (0.05 mmol, 10 mol%) in CH_2Cl_2 at room temperature. The mixture was shaken vigorously and the ^{11}B NMR spectra were recorded within 1 hour. 1-octene (80 µL, 0.50 mmol, 1.0 equiv.) was then added, the NMR tube was shaken vigorously, and the reaction was monitored by ^{11}B NMR spectroscopy over time.

Ar = Mes (ABG-0454)

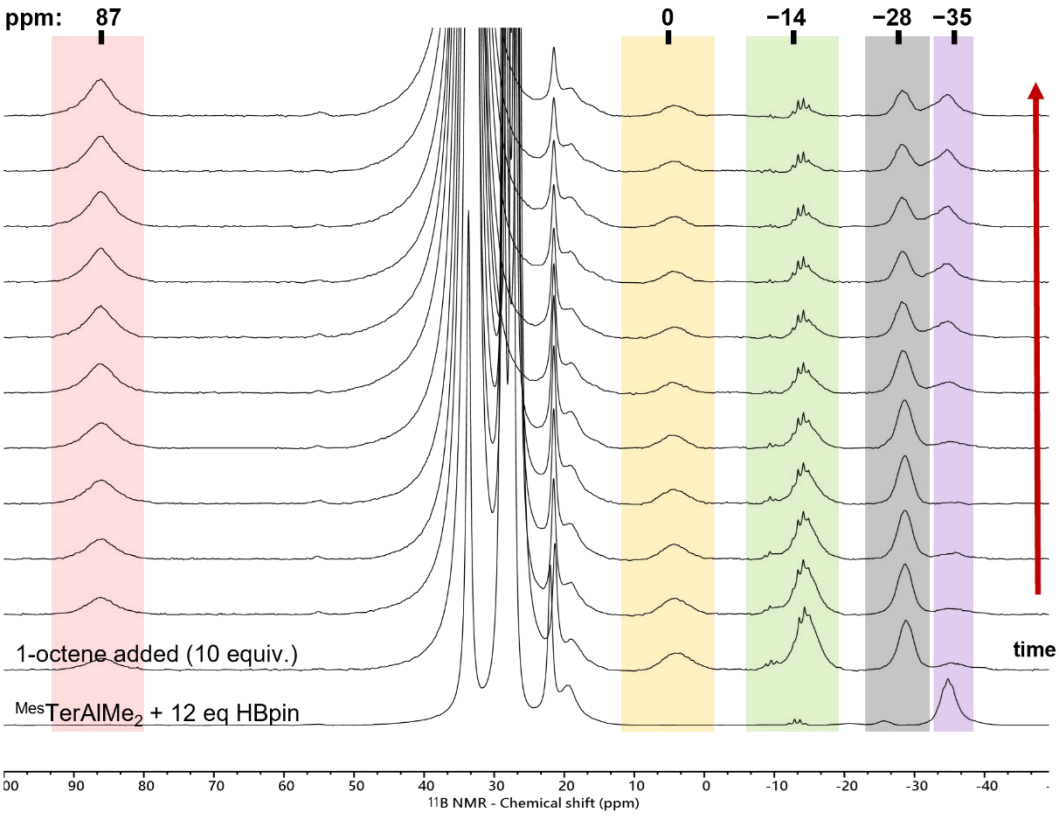

Figure 7-23. Stacked ^{11}B NMR spectra of the $^{Ar}TerAlMe_2$ catalysed hydroboration of 1-octene with HBpin (Ar = Mes).

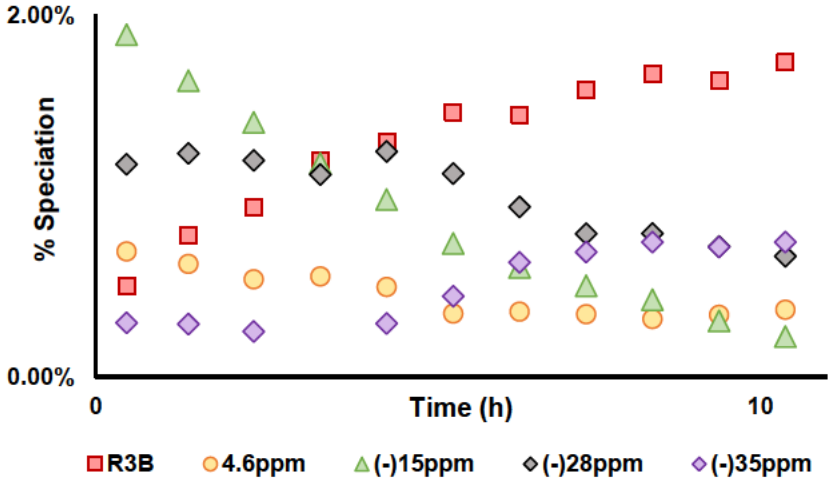

Figure 7-24. The speciation of the observed boron-containing species over time under catalytic conditions (excluding XBpin species).

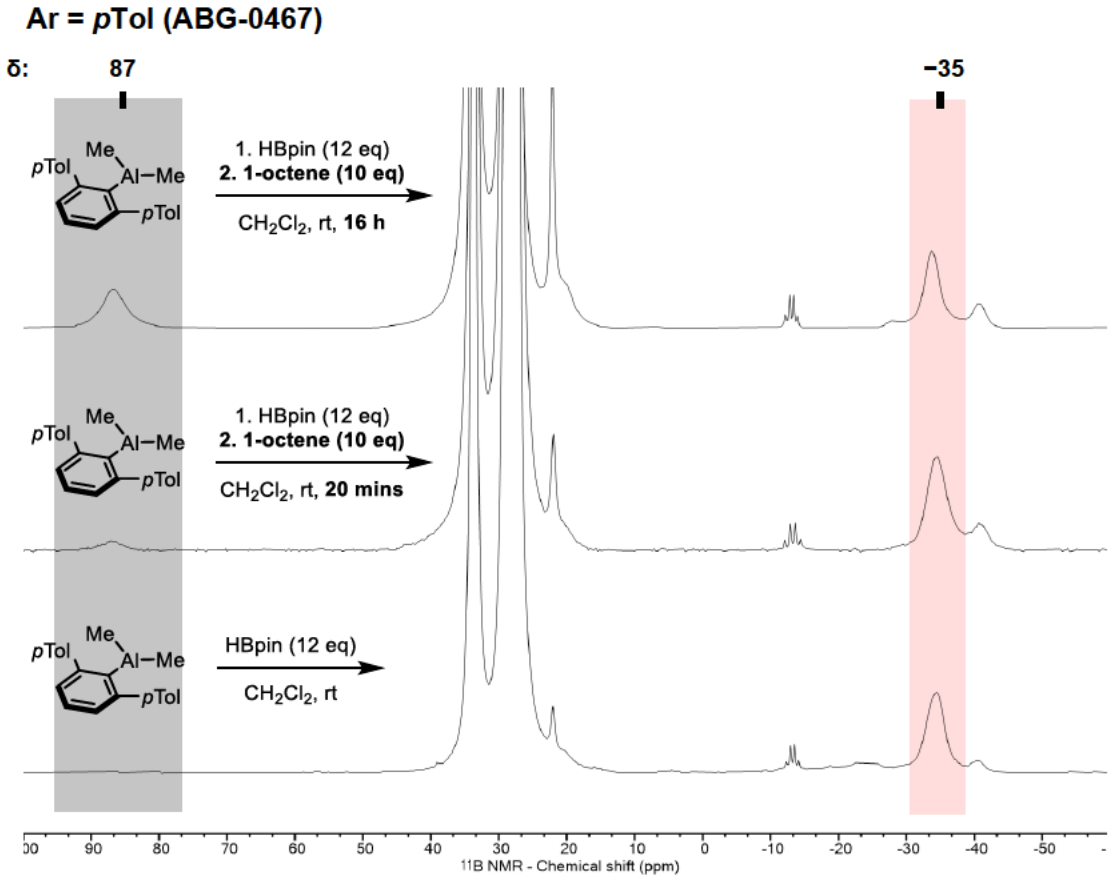

Figure 7-25. Stacked ^{11}B NMR spectra of the $^{Ar}TerAlMe_2$ catalysed hydroboration of 1-octene with HBpin (Ar = *p*Tol).

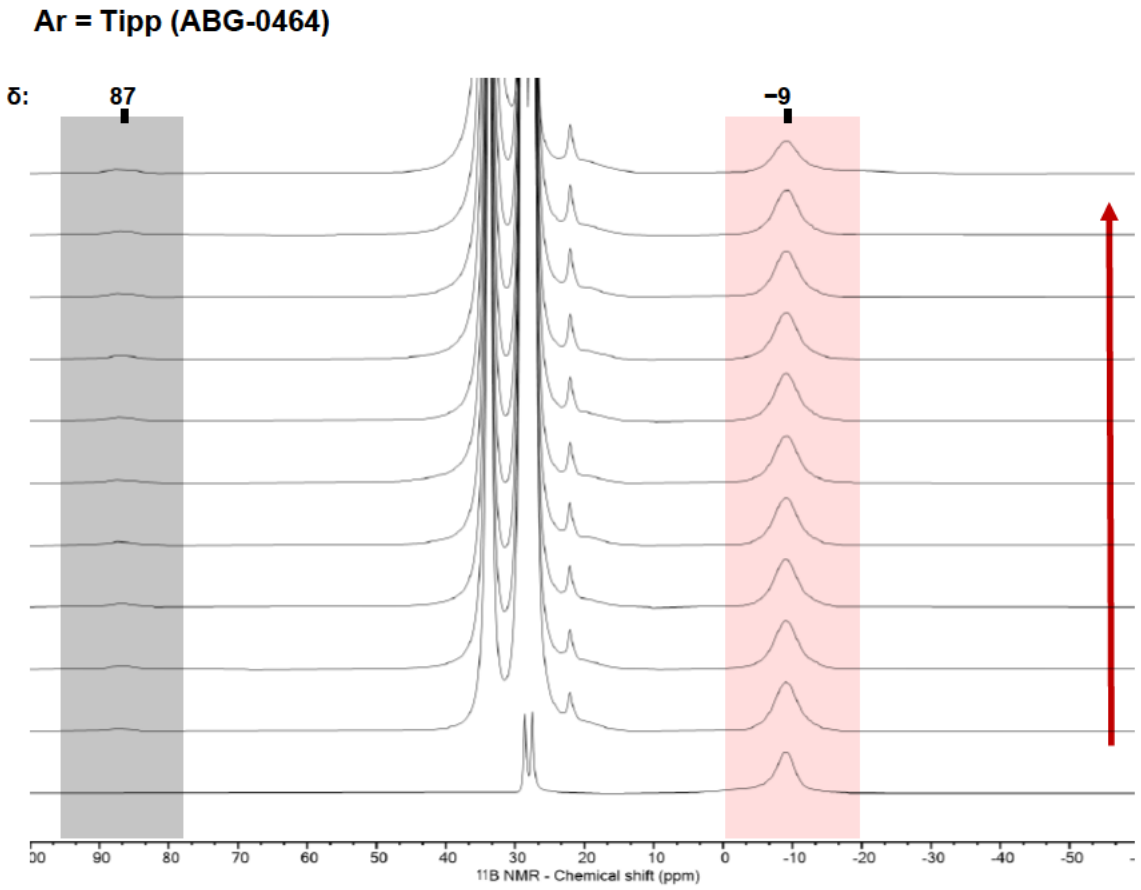

Figure 7-26. i) Stacked ^{11}B NMR spectra of the $^{Ar}TerAlMe_2$ catalysed hydroboration of 1-octene with HBpin (Ar = Tipp) with comparison to ii) the reaction of $^{Tipp}TerAlH_2$ with HBpin.

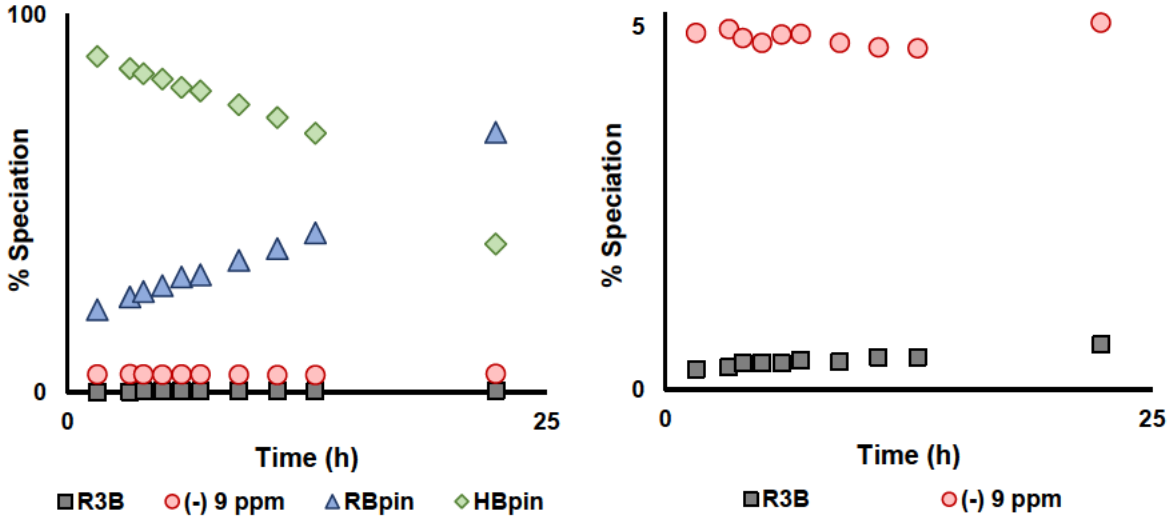

Figure 7-27. i) % speciation of boron species in the $^{Ar}TerAlMe_2$ catalysed hydroboration of 1-octene with HBpin (Ar = Tipp). ii) zoom in of non-Bpin species

7.4.5 Identifying species in catalysis (*p*-Tol and Tipp)

p-Tol

3-p-Tol-1 (ABG-0468)

$Me_2S•BH_3$ (9.5 µL, 0.1 mmol, 2 equiv.) was added to a solution of $^{p\text{-Tol}}$TerAlH$_2$ (14.3 mg, 0.05 mmol, 1 equiv.) in CH_2Cl_2 (0.65 mL). The reaction was vigorously shaken and then analysed by NMR spectroscopy. The ^{11}B NMR resonance matched what was observed under catalytic conditions.

^{1}H NMR (500 MHz, CH_2Cl_2) δ 7.51 (t, *J* = 7.6 Hz, 1H; Ar', *p*-*H*), 7.38 (app. t, *J* = 5.7 Hz, 5H; Ar*H*), 7.31 (app. d, *J* = 7.7 Hz, 3H; Ar*H*), 7.07 (app. dd, *J* = 18.2, 7.7 Hz, 1H; Ar*H*), 2.42 (s, 6H; *p*-Tol, 2 × CH_3), 0.77 – 0.05 (br q, $w_{1/2}$ ~ 237 Hz, 8H; 2 × B*H*$_4$).

^{11}B NMR (160 MHz, CH_2Cl_2) δ -34.35 (p, *J* = 90.9 Hz).

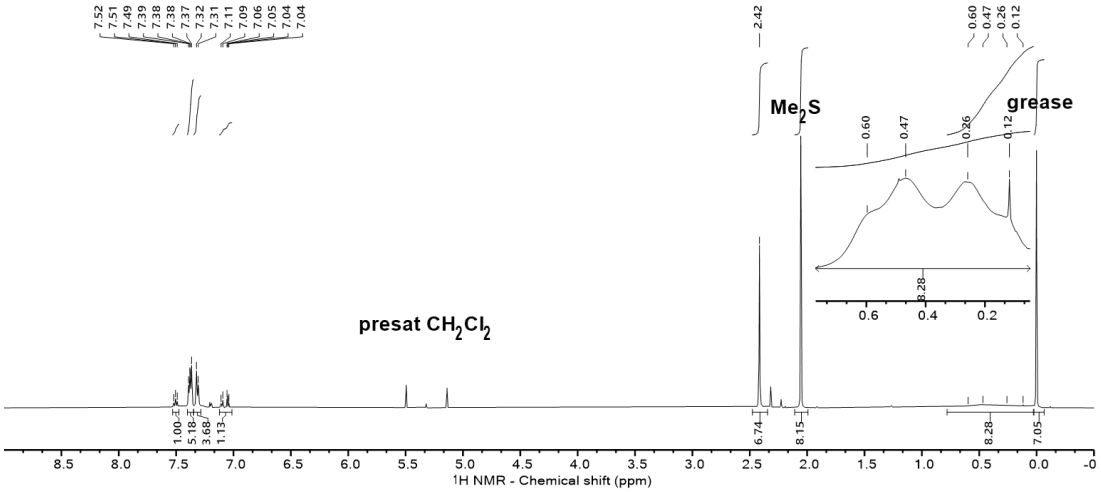

Figure 7-28. ^{1}H NMR spectrum (CH_2Cl_2) for the reaction between $^{p\text{-Tol}}$TerAlH$_2$ with $Me_2S•BH_3$ (2 equiv.).

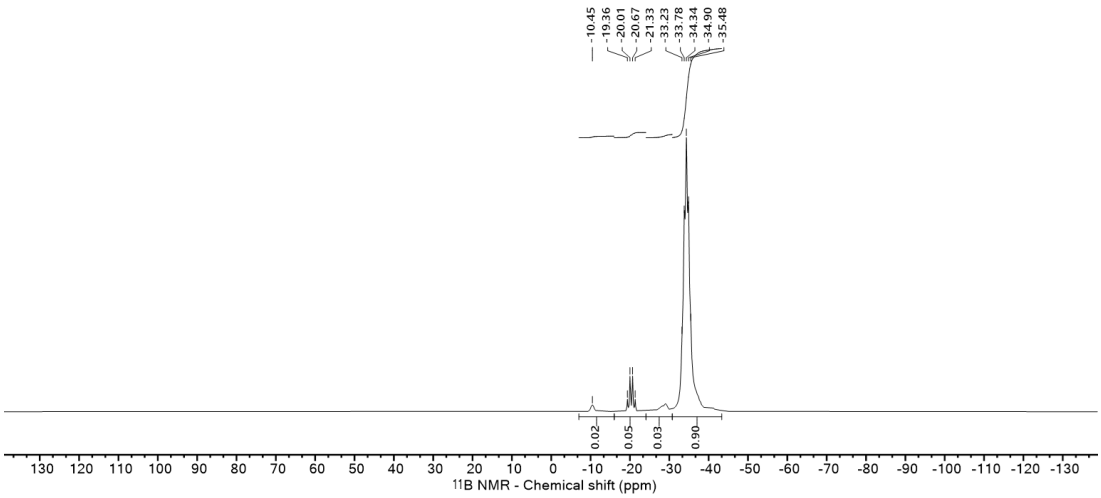

Figure 7-29. ^{11}B NMR spectrum (CH_2Cl_2) for the reaction between $^{p\text{-Tol}}$TerAlH$_2$ with $Me_2S•BH_3$ (2 equiv.).

Redistribution in the presence of MeBpin (ABG-0415)

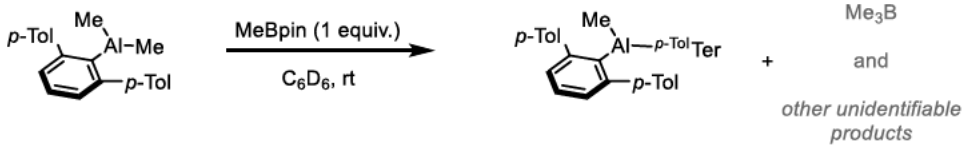

MeBpin (9.6 µL, 0.05 mmol, 1 equiv.) was added to a solution of $^{p\text{-Tol}}$TerAlMe$_2$ (15.7mg, 0.05 mmol, 1 equiv.) in C_6D_6 (0.65 mL). The reaction was vigorously shaken and then analysed by NMR spectroscopy. The ^{1}H spectrum displayed resonances that point to the tentative formation of $^{p\text{-Tol}}$Ter$_2$AlMe.

^{1}H NMR (500 MHz, Benzene-d_6) δ 1.99 (s, 12H; p-Tol, 4 × C$\underline{H}_3$), -1.66 (s, 3H; AlC$\underline{H}_3$). (aromatic signals not assigned due to overlapping peaks):

This corresponded with the formation of Me_3B:

^{11}B NMR (160 MHz, Benzene-d_6) δ 86.4.

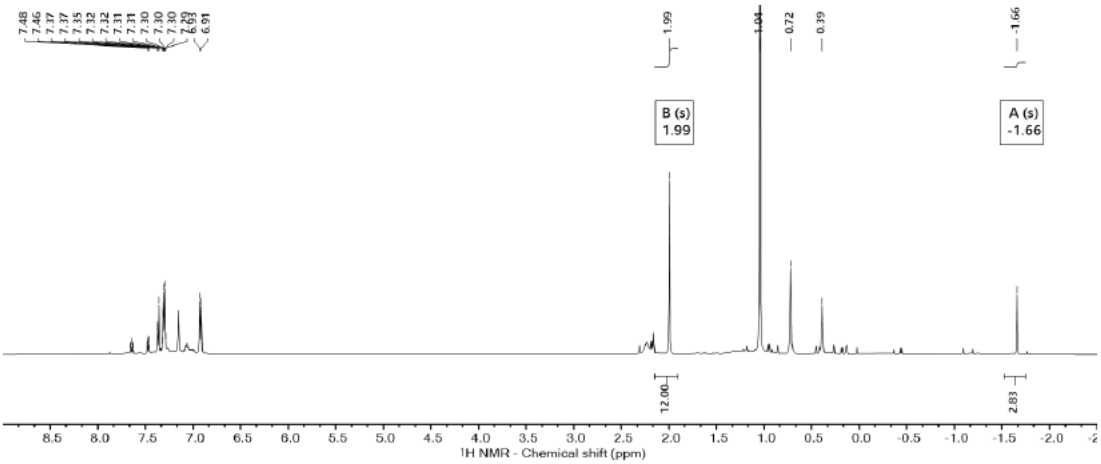

Figure 7-30. ^{1}H NMR spectrum (C_6D_6) for the reaction between $^{p\text{-Tol}}$TerAlMe$_2$ with MeBpin (1 equiv.). Starred (*) = MeBpin.

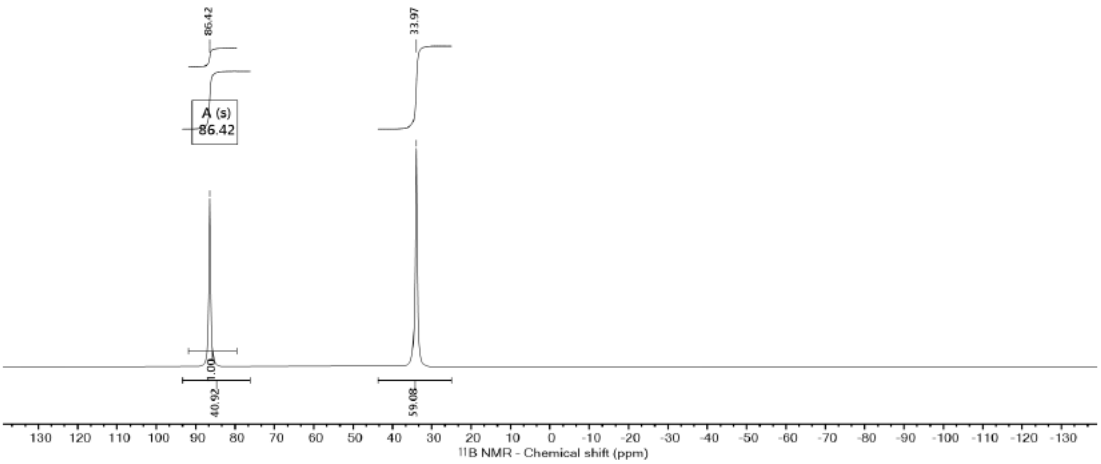

Figure 7-31. ^{11}B NMR spectrum (C_6D_6) for the reaction between $^{p\text{-Tol}}$TerAlMe$_2$ with MeBpin (1 equiv.).

Tipp

3-Tipp-1 (ABG-0469)

$Me_2S{\bullet}BH_3$ (4.7 µL, 0.05 mmol, 2 equiv.) was added to a solution of $^{Tipp}TerAlH_2$ (12.8 mg, 0.025 mmol, 1 equiv.) in CH_2Cl_2 (0.65 mL). The reaction was vigorously shaken and then analysed by NMR spectroscopy. The ^{11}B NMR resonance did not match what was observed under catalytic conditions.

^{1}H NMR (500 MHz, CH_2Cl_2) δ 7.50 (t, *J* = 7.6 Hz, 1H; Ar', *p*-*H*), 7.27 (d, *J* = 7.6 Hz, 2H; Ar', 2 × *m*-*H*), 7.09 (s, 4H; Tipp, 4 × *m*-*H*), 2.92 (hept, *J* = 6.8 Hz, 2H; Tipp, 2 × *p*-C*H*$(CH_3)_2$), 2.67 (hept, *J* = 6.8 Hz, 4H; Tipp, 4 × *o*-C*H*$(CH_3)_2$), 1.26 (d, *J* = 7.0 Hz, 12H; Tipp, 2 × CH(C*H*$_3)_2$), 1.20 (d, *J* = 6.9 Hz, 12H; Tipp, 2 × CH(C*H*$_3)_2$), 1.03 (d, *J* = 6.8 Hz, 12H; Tipp, 2 × CH(C*H*$_3)_2$), 0.53 – -0.40 (br q, 8H; B*H*$_4$).

^{11}B NMR (160 MHz, CH_2Cl_2) δ -33.5 (p, *J* = 85.5 Hz).

3-Tipp-A (ABG-0466)

HBpin (3.6 µL, 0.025 mmol, 1 equiv.) was added to a solution of $^{Tipp}TerAlH_2$ (12.8 mg, 0.025 mmol, 1 equiv.) in CH_2Cl_2 (0.65 mL). The reaction was vigorously shaken and then analysed by NMR spectroscopy. The ^{11}B NMR resonance matched what was observed under catalytic conditions.

^{1}H NMR (400 MHz, CH_2Cl_2) δ 7.45 (t, *J* = 7.6 Hz, 1H; Ar', *p*-*H*), 7.18 (d, *J* = 7.5 Hz, 2H; Ar', *m*-*H*), 7.05 (s, 4H; Tipp, 4 × *m*-*H*), 2.89 (hept, *J* = 6.9 Hz, 2H; Tipp, 2 × *p*-C*H*$(CH_3)_2$), 2.70 (hept, *J* = 6.8 Hz, 4H; Tipp, 2 × *o*-C*H*$(CH_3)_2$), 1.24 (d, *J* = 6.9 Hz, 12H; Tipp, 2 × CH(C*H*$_3)_2$), 1.20 (d, *J* = 6.9 Hz, 12H; Tipp, 2 × CH(C*H*$_3)_2$), 1.03 (d, *J* = 6.8 Hz, 12H; Tipp, 2 × CH(C*H*$_3)_2$), 0.91 (app. d, *J* = 6.7 Hz, 6H; Bpin, 2 × C*H*$_3$), 0.78 (s, 3H; Bpin, C*H*$_3$), 0.57 (s, 3H; Bpin, C*H*$_3$).

^{11}B NMR (160 MHz, CH_2Cl_2) δ -9.0.

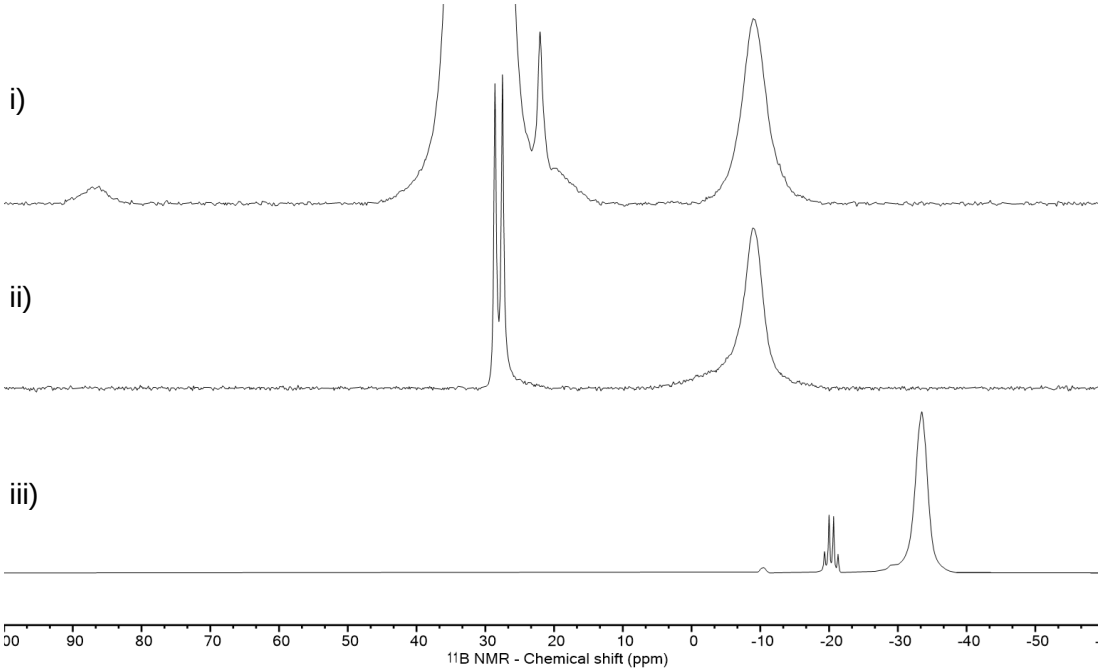

Figure 7-32. Stacked ^{11}B NMR (CH_2Cl_2) spectra of i) $^{Tipp}TerAlMe_2$ catalysed hydroboration of 1-octene with HBpin; ii) $^{Tipp}TerAlH_2$ + HBpin (1 equiv.); iii) $^{Tipp}TerAlH_2$ + $Me_2S{\bullet}BH_3$ (2 equiv.)

Reversibility of 3-Tipp-A formation (ABG-0710)

On Scheme 3-8.ii) on Chapter 3, the stability of **3-Tipp-A** in THF was probed accordingly:

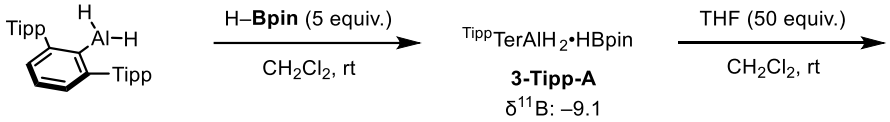

HBpin (18.1 µL, 0.125 mmol, 5 equiv.) was added to a solution of $^{Tipp}TerAlH_2$ (12.8 mg, 0.025 mmol, 1 equiv.) in CH_2Cl_2 (0.65 mL). The reaction was vigorously shaken and then analysed by NMR spectroscopy. The ^{11}B NMR resonance confirmed that **3-Tipp-A** had been formed. THF (0.1 mL, 0.75 mmol, 50 equiv.) was added by syringe, the reaction was vigorously shaken and then analysed again by NMR spectroscopy. The consumption of **3-Tipp-A** was observed.

7.4.6 Identifying Al–H–B species in catalysis (Mes)

In **Section 3.3.4**, the plausible identity of different Al–H–B containing species were identified using stoichiometric experiments between *m*-terphenyl alanes and boranes containing different levels of alkyl substitution.

3-Mes-1:

^{Mes}TerAl(BH$_4$)$_2$ (ABG-0492/ABG-0683)

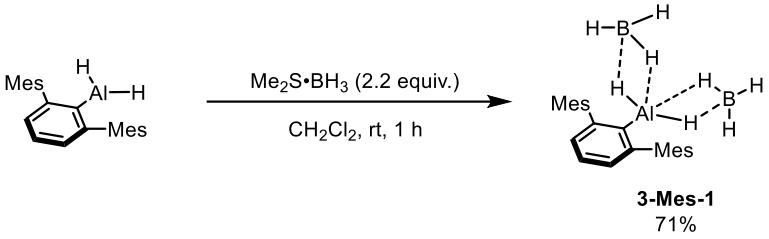

3-Mes-1
71%

$Me_2S•BH_3$ (105 µL, 1.1 mmol) was added to a solution of $^{Mes}TerAlH_2$ (171 mg, 0.5 mmol) in CH_2Cl_2 (10 mL, 0.05 M) at room temperature. The reaction was stirred for 1 hour and then the solvent and excess $Me_2S•BH_3$ was removed *in vacuo* with extended pumping for *ca*. 2 hours to give the product as an amorphous white solid (131 mg, 71%). Crystalline solid was grown from slow evaporation of a pentane solution.

^{1}H NMR (500 MHz, CH_2Cl_2) δ 7.57 (t, *J* = 7.6 Hz, 1H; Ar', *p*-*H*), 7.12 (d, *J* = 7.6 Hz, 2H; Ar', 2 × *m*-*H*), 6.95 (s, 4H; Mes, 4 × *m*-*H*), 2.31 (s, 6H; Mes, 2 × *p*-C*H*$_3$), 2.01 (s, 12H; Mes, 4 × *o*-C*H*$_3$), 0.60 – -0.33 (br q, $w_{1/2}$ ~ 260 Hz; 8H; 2 × B*H*$_4$).

^{13}C {^{1}H} NMR (126 MHz, CH_2Cl_2) δ 149.2, 138.9, 137.4, 135.6, 130.4, 127.8, 125.3, 20.0, 19.7.

^{11}B NMR (128 MHz, CH_2Cl_2) δ -34.8 (p, *J* = 86.9, 85.8 Hz).

^{27}Al NMR (130 MHz, CH_2Cl_2) No signal observed.

IR 2917*w* (C-H), 2534*w* (B-$H_{terminal}$), 2465*w* (B-$H_{terminal}$), 2026*m* (B-$H_{bridging}$), 1447*m*

MS HRMS-EI (m/z): found 370.2570; [M] ($C_{24}H_{33}AlB_2$), requires 370.2578

3-Mes-2

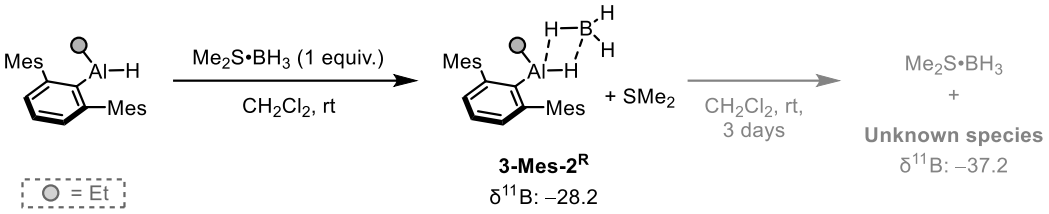

3-Mes-2^{Et} (ABG-0457)

$Me_2S•BH_3$ (1.4 µL, 0.015 mmol, 1 equiv.) was added to a solution of MesTerAl(Et)H (5.6 mg, 0.015 mmol, 1 equiv.) in CH_2Cl_2 (0.6 mL). The mixture was vigorously shaken and analysed by NMR spectroscopy within one hour. **3-Mes-2^{Et}** was obtained as the major species but not isolated.

^{1}H NMR (500 MHz, CH_2Cl_2) δ 7.49 (t, *J* = 7.6 Hz, 1H; Ar', *p*-*H*), 7.07 (d, *J* = 7.6 Hz, 2H; Ar', 2 × *m*-*H*), 6.95 (s, 4H; Mes, 4 × *m*-*H*), 2.30 (s, 6H; Mes, 2 × *p*-C*H*$_3$), 2.02 (s, 12H; Mes, 4 × *o*-C*H*$_3$), 0.60 (t, *J* = 8.1 Hz, 3H; AlCH$_2$C*H*$_3$), 0.13 (br q, 4H; B*H*$_4$), -0.24 (q, *J* = 8.1 Hz, 2H; AlC*H*$_2$CH$_3$).

^{11}B NMR (160 MHz, CH_2Cl_2) δ -28.47 (*br* p, *J* ~ 85.1 Hz).

The solution was left to sit for 3 days and then analysed again by NMR spectroscopy. All resonances attributed to **3-Mes-2^{Et}** had disappeared, indicating decomposition.

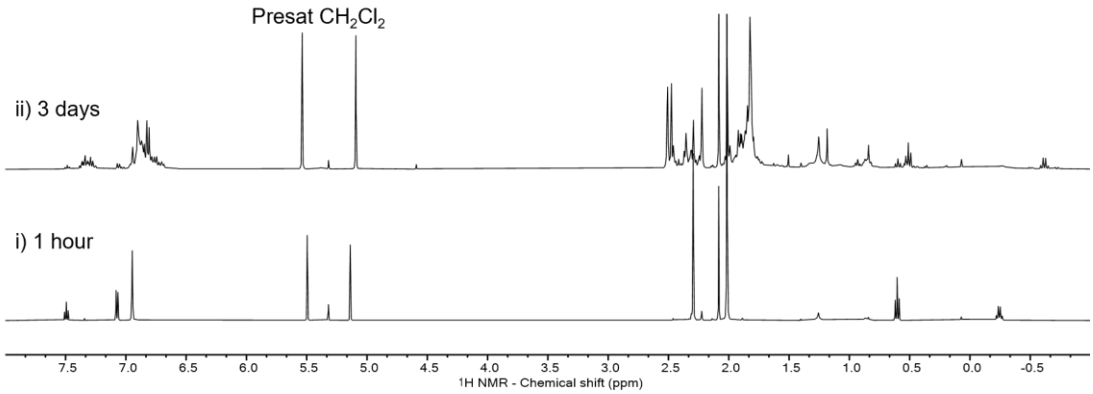

Figure 7-33. Stacked ^{1}H NMR spectra (CH_2Cl_2) of the reaction between ^{Mes}TerAl(Et)H with $Me_2S•BH_3$ after i) 1 hour; ii) 3 days.

3-Mes-2^{octyl} (ABG-0711)

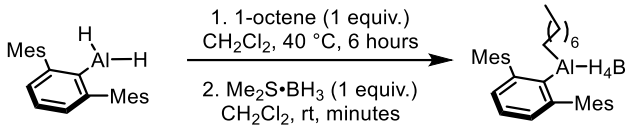

1-octene (8 µL, 0.05 mmol, 1 equiv.) was added to a solution of ^{Mes}TerAlH$_2$ (17.1 mg, 0.05 mmol, 1 equiv.) in CH_2Cl_2. The NMR tube was vigorously shaken and then heated at 40 °C. The reaction was monitored by ^{1}H NMR spectroscopy and the consumption of 1-octene was observed after 6 hours. At this point, $Me_2S•BH_3$ (4.75 µL, 0.05 mmol, 1 equiv.) was added and the NMR tube was vigorously shaken. Analysis by ^{1}H and ^{11}B NMR spectroscopy showed that the product was obtained as a mixture containing unreacted $Me_2S•BH_3$ and trace quantities of octyl$_3$B. Regardless, the reaction provides spectroscopic handles for this compound, used to monitor the behaviour of the catalyst under catalysis.

^{1}H NMR (500 MHz, CH_2Cl_2) δ 7.49 (t, *J* = 7.6 Hz, 1H; Ar', *p*-*H*), 7.06 (d, *J* = 7.6 Hz, 2H; Ar', 2 × *m*-*H*), 6.94 (s, 4H; Mes, 4× *m*-*H*), 2.30 (s, 6H; Mes, 2 × *p*-C*H*$_3$), 2.02 (s, 12H; Mes, 4 × *o*-C*H*$_3$), 1.37 – 0.92 (m, 15H; octyl, C*H*), 0.16 (br q, 4H; B*H*$_4$), -0.11 – -0.25 (m, 2H; AlC*H*$_2$R).

^{13}C {1H} NMR (126 MHz, CH_2Cl_2) δ 149.4, 140.4, 137.7, 136.3, 130.0, 128.7, 125.7, 34.8, 32.0, 29.3, 29.2, 24.1, 22.7, 20.9, 20.6, 13.9, 9.4 (Al-*C*H$_2$-R).

^{11}B NMR (160 MHz, CH_2Cl_2) δ -28.2 (*br* p)

3-Mes-3

3-Mes-3^{CH_2CH_2tBu} (ABG-0481)

A solution of *t*BuCH$_2$CH$_2$BH$_2$ (9.8 mg, 0.1 mmol, 2 equiv.) in CH$_2$Cl$_2$ (0.2 mL) was added to a suspension of ^{Mes}TerAlH$_2$ (17.1 mg, 0.05 mmol, 1 equiv.) in CH$_2$Cl$_2$ (0.5 mL). The mixture was vigorously shaken and then analysed by NMR spectroscopy within 1 hour at room temperature.

^{1}H NMR (500 MHz, CH$_2$Cl$_2$) δ 7.54 (t, *J* = 7.6 Hz, 1H; Ar', *p*-*H*), 7.11 (d, *J* = 7.6 Hz, 2H; Ar', 2 × *o*-*H*), 6.94 (s, 4H; Mes, 4 × *m*-*H*), 2.32 (s, 6H; Mes; 2 × *p*-CH$_3$), 2.02 (s, 12H; Mes; 4 × *o*-C*H*$_3$), 0.94 – 0.88 (m, 4H; 2 × BCH$_2$C*H*$_2$R), 0.77 (s, 18H; 2 × (C*H*$_3$)$_3$), 0.34 – 0.22 (m, 4H; 2 × BC*H*$_2$CH$_2$R).

Signals attributed to RB*H*$_3$ *were located at ca. δ 0.7 but were broad and overlapped by other residual signals.*

^{11}B NMR (160 MHz, CH$_2$Cl$_2$) δ -21.7.

Notes:

- The reaction was also performed using 1 equiv. of *t*BuCH$_2$CH$_2$BH$_2$ and resulted in the same product being formed (likely alongside 1:1 adduct).
- The same product was also generated using *t*BuCH$_2$CH$_2$Bpin (1 equiv.) in place of *t*BuCH$_2$CH$_2$BH$_2$.

^{Mes}TerAlH$_2$•(MesBH$_2$)$_2$; 3-Mes-3^{Mes} (ABG-0450/0531)

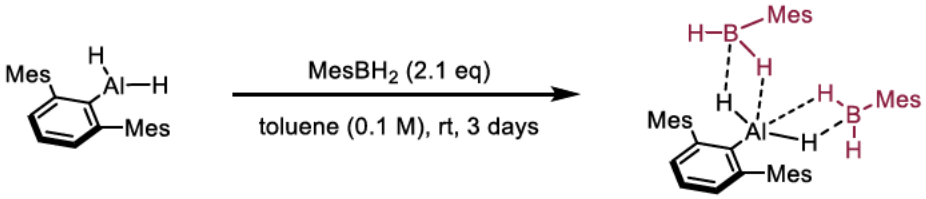

Toluene (10 mL) was added to a mixture of ^{Mes}TerAlH$_2$ (342 mg, 1.0 mmol, 1 equiv.) and MesBH$_2$ (277 mg, 2.1 mmol, 2.1 equiv.). The clear solution was stirred for 3 days at room temperature (although it later became apparent that the reaction is completed within < 1 hour) and then the solvent was removed *in vacuo* over a warm water bath (~40 °C) to give a colourless amorphous solid. The solid dissolved in hot hexane (25 mL, 60 °C), filtered into a pre-warmed Schlenk flask (60 °C) and allowed to slowly cool to room temperature overnight to give the product as colourless needles, which were filtered and washed with cold pentane (1 mL). The filtrate was slowly cooled to –25°C overnight to yield a second crop of colourless needles (combined yield: 307 mg, 0.51 mmol, 51% yield).

^{1}H NMR (500 MHz, Benzene-d_6) δ 7.33 (t, J = 7.6 Hz, 1H; Ar', p-H), 7.02 (d, J = 7.6 Hz, 2H; Ar', 2 × m-H), 6.87 (s, 4H; Mes, 4 × m-H), 6.51 (s, 4H; Mes, 4 × m-H), 2.19 (s, 12H; Mes, 4 × o-CH$_3$), 2.18 (s, 6H; Mes, 2 × p-CH$_3$), 2.09 (s, 6H; Mes, 2 × p-CH$_3$), 1.90 (s, 12H; Mes, 4 × o-CH$_3$), 1.77 (s, broad, $w_{1/2}$ ≈ 260 Hz, 6H; 2 × Mes-BH$_3$)

^{13}C {^{1}H} NMR (126 MHz, Benzene-d_6) δ 150.4, 140.5, 140.3, 137.9, 136.6, 135.2, 131.0, 129.0, 127.2, 125.8, 22.9, 20.8, 20.8, 20.7. (C-Al and C-B resonances not observed due to quadrupolar line broadening.)

^{11}B NMR (160 MHz, Benzene-d_6) δ -24.0 (app. s)

^{27}Al NMR (130 MHz, Benzene-d_6) No signal observed

IR 2914m, 2428m (B-H$_{terminal}$), 2029m (B-H$_{bridging}$), 1943w (B-H$_{bridging}$), 1609m, 1554m, 1440s

MS HRMS-EI (m/z): found 606.4160; [M] (C$_{42}$H$_{53}$AlB$_2$), requires 606.4143

mp 192 – 194 °C (hexane)

3-Mes-4

3-Mes-4^{CH_2CH_2tBu,Et} (ABG-0506)

A solution of *t*Bu$CH_2CH_2BH_2$ (4.9 mg, 0.05 mmol, 1 equiv.) in CH_2Cl_2 (0.2 mL) was added to a suspension of ^{Mes}TerAl(Et)H (18.5 mg, 0.05 mmol, 1 equiv.) in CH_2Cl_2 (0.5 mL). The mixture was vigorously shaken, left for 6 hours and then analysed by NMR spectroscopy. As shown in Scheme 3.10.e. in Chapter 3, 3-Mes-4^{CH_2CH_2tBu} is obtained as the major product in a mixture of other Al–H–B species.

^{1}H NMR (500 MHz, CH_2Cl_2) δ 7.49 (t, *J* = 7.6 Hz, 1H; Ar', *p*-*H*), 7.08 (d, *J* = 7.5 Hz, 2H; Ar', 2 × *m*-*H*), 6.95 (s, 4H; Mes, 4 × *m*-*H*), 2.30 (s, 6H; Mes, 2 × *p*-C*H*$_3$), 2.03 (d, *J* = 1.8 Hz, 12H; Mes, 4 × *o*-C*H*$_3$), 0.95 – 0.80 (m, 2H; *B*CH_2C*H*$_2$R), 0.76 (s, 9H; (C*H*$_3$)$_3$), 0.62 (t, *J* = 8.0 Hz, 3H; *Al*CH_2C*H*$_3$), 0.35 – 0.14 (m, 2H; *B*C*H*$_2$$CH_2$*t*Bu), -0.23 (q, *J* = 7.2 Hz, 2H; *Al*C*H*$_2$$CH_3$).

Signals attributed to Al–H–B were broad and overlapped by other resonances.

^{11}B NMR (160 MHz, CH_2Cl_2) δ -13.8.

3-Mes-5

3-Mes-5^{BBN} (ABG-0436)

H-*B*-9-BBN (6.1 mg, 0.05 mmol, 1 equiv.) was added to a solution of ^{Mes}TerAlH$_2$ (18.5 mg, 0.05 mmol, 1 equiv.) in CH_2Cl_2 (0.7 mL). The mixture was vigorously shaken, left for 1 hour and then analysed by NMR spectroscopy. As shown in Scheme 3.10.f. in Chapter 3, 3-Mes-4^{BBN} is obtained as the major product in a mixture of other species.

^{11}B NMR (160 MHz, Benzene-d_6) δ 27.9 (H-*B*-9-BBN; 42%*), 2.3 (unknown, 10%*), -6.8 (3-Mes-5^{BBN}, 48%*). **approximated based on ^{11}B NMR integrations.*

^{1}H NMR spectroscopy reveals a complex mixture containing at least 2 × major *m*-terphenyl resonances. In lieu of clear resonances, the ^{1}H NMR spectrum has been provided:

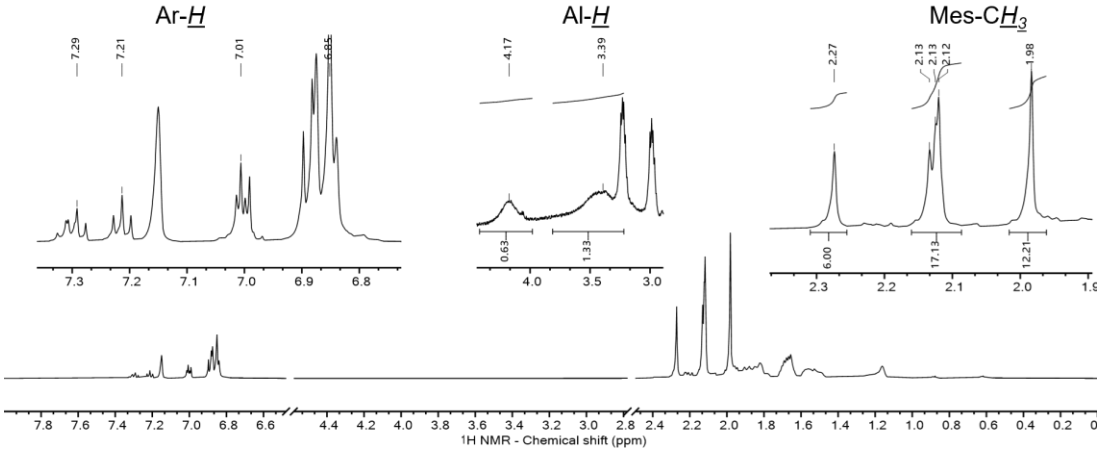

Figure 7-34. ^{1}H NMR spectrum (CH_2Cl_2) for the reaction between ^{Mes}TerAlH$_2$ with H-*B*-9-BBN.

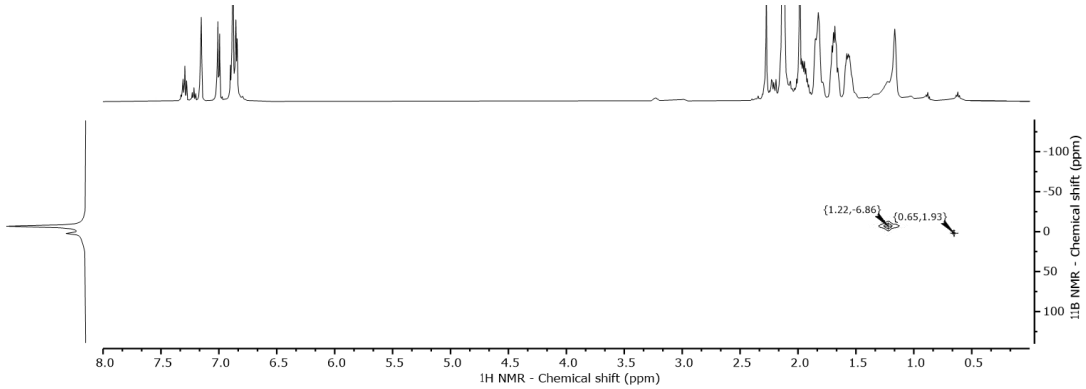

Figure 7-35. ^{1}H-^{11}B HMQC (CH_2Cl_2) for the reaction between ^{Mes}TerAlH$_2$ with H-*B*-9-BBN.

3-Mes-5^{Et} (ABG-0474)

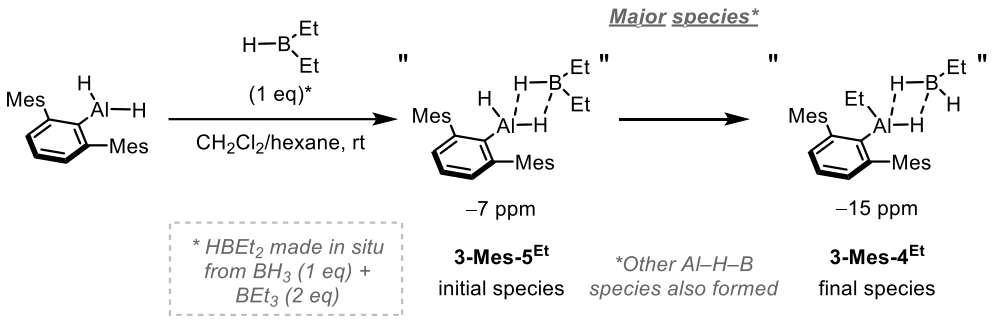

A solution of Et_2BH (1.64 M in hexane, 30 µL, 0.05 mmol, 1 equiv.) was added to a solution of $^{Mes}TerAlH_2$ (17.1 mg, 0.05 mmol, 1 equiv.) in CH_2Cl_2 (0.6 mL). The reaction was monitored by ^{11}B NMR spectroscopy.

^{11}B NMR (160 MHz, CH_2Cl_2) δ 0.4.

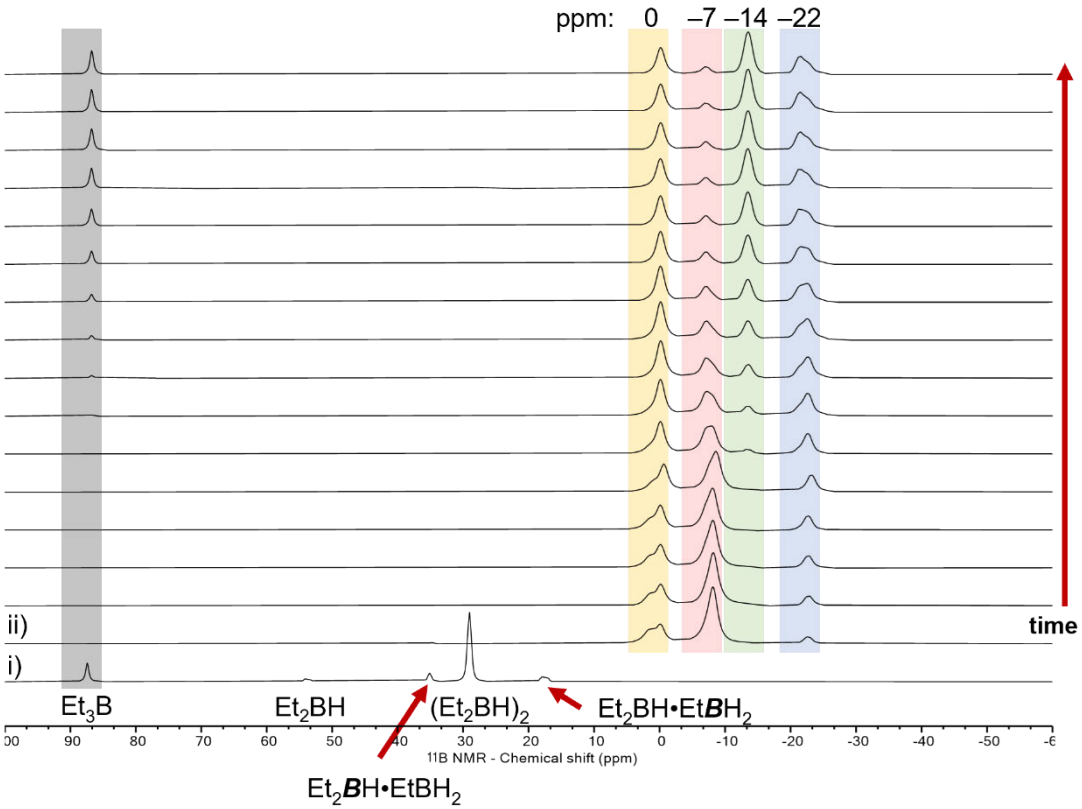

Figure 7-36. Stacked ^{11}B spectrum (CH_2Cl_2) of i) *in situ* generated Et_2BH (approx. 74% conversion to Et_2BH); ii) following the addition of $^{Mes}TerAlH_2$ to this reaction mixture and monitoring over time.

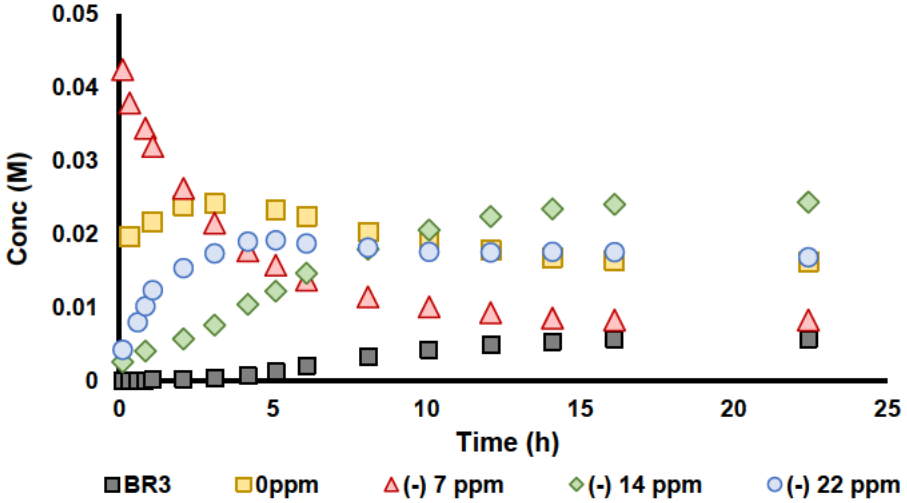

Figure 7-37. Speciation of different boron-containing species against time for the reaction of Et_2BH with $^{Mes}TerAlH_2$

3-Mes-6

3-Mes-6^{BBN,Et} (ABG-0459)

H-*B*-9-BBN (1.8 mg, 0.015 mmol, 1 equiv.) was added to a solution of ^{Mes}TerAl(Et)H (5.6 mg, 0.015 mmol, 1 equiv.) in CH_2Cl_2 (0.65 mL). The reaction was analysed by NMR spectroscopy. **3-Mes-6^{BBN,Et}** was obtained as the major product (~56%) in a mixture also containing **3-Mes-5^{BBN}** (~18%), H-*B*-9-BBN (~16%) and Et-*B*-9-BBN (~13%) (yields approximated based on integrations by ^{11}B NMR spectroscopy). The alkyl region corresponding to the protons on the borabicyclo[3.3.1]nonane fragment could not be distinguished between each species and was simply assigned as a multiplet.

^{1}H NMR (500 MHz, CH_2Cl_2) δ 7.48 (t, *J* = 7.6 Hz, 1H; Ar', *p*-*H*), 7.09 (d, *J* = 7.6 Hz, 2H; Ar', 2 × *m*-*H*), 6.95 (s, 4H; Mes, 4 × *m*-*H*), 2.29 (s, 6H; Mes, 2 × *p*-C*H*$_3$), 2.03 (s, 12H; Mes, 4 × *o*-C*H*$_3$), 1.90 – 0.77 (m, 14H; 9-BBN, alkyl-*H*), 0.58 (t, *J* = 8.1 Hz, 3H; AlCH$_2$C*H*$_3$), -0.17 (q, *J* = 8.1 Hz, 2H; AlC*H*$_2$CH$_3$). *Resonances attributed to the bridging hydrides (Al–H–B) were likely overlapped by other signals and could not be readily located.*

^{11}B NMR (160 MHz, CH_2Cl_2) δ 0.42.

3-Mes-6^{Et} (ABG-0409)

Et_3B (1 M in hexanes, 50 µL, 0.05 mmol, 1 equiv.) was added to a solution of ^{Mes}TerAlH_2 (17.1 mg, 0.05 mmol, 1 equiv.) in CD_2Cl_2 (0.65 mL). The reaction was analysed by NMR spectroscopy.

^{1}H NMR (500 MHz, CD_2Cl_2) δ 7.49 (t, *J* = 7.6 Hz, 1H; Ar', *p*-*H*), 7.11 (d, *J* = 7.6 Hz, 2H; Ar', 2 × *m*-*H*), 6.95 (s, 4H; Mes, 4 × *m*-*H*), 2.30 (s, 6H; Mes, 2 × *p*-C*H*$_3$), 2.06 (s, 12H; Mes, 4 × *o*-C*H*$_3$), 0.63 (t, *J* = 8.1 Hz, 3H; AlCH$_2$C*H*$_3$), 0.61 (t, *J* = 7.5 Hz, 6H; 2 × BCH$_2$C*H*$_3$), 0.31 (m, 4H; 2 × BC*H*$_2$CH$_3$), -0.14 (q, *J* = 8.1 Hz, 2H; AlC*H*$_2$CH$_3$). *Resonances attributed to the bridging hydrides (Al–H–B) were likely overlapped by other signals and could not be readily located.*

^{11}B NMR (160 MHz, CD_2Cl_2) -0.1.

3-Mes-7

^{Mes}TerAl(H)(BH$_4$) (ABG-0259)

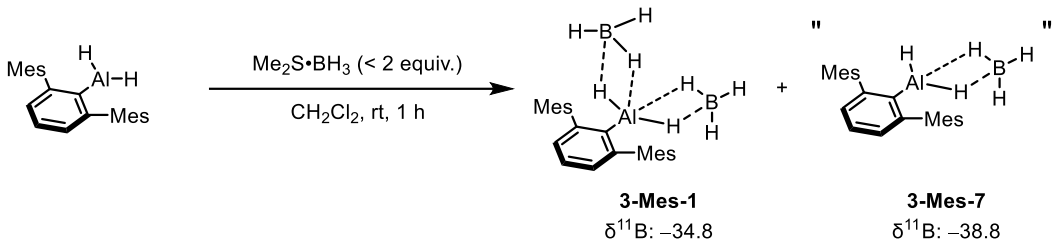

3-Mes-1 δ^{11}B: –34.8 **3-Mes-7** δ^{11}B: –38.8

$Me_2S•BH_3$ (0.025 to 0.1 mmol, 0.5 to 2.0 equiv.) was added to a solution of $^{Mes}TerAlH_2$ (17.1 mg, 0.05 mmol, 1 equiv.) in CH_2Cl_2 (0.67 mL). The mixture was vigorously shaken and analysed by ^{11}B NMR spectroscopy within one hour. A mixture of **3-Mes-1** and **3-Mes-7** was obtained.

3-Mes-7:

^{1}H NMR (500 MHz, CD_2Cl_2) δ 7.46 (t, *J* = 7.6 Hz, 1H; Ar', *p*-*H*), 6.96 (s, 4H; Mes, 4 × *m*-*H*), 6.92 (d, *J* = 15.6 Hz, 2H; Ar', 2 × *m*-*H*), 3.13 (br s, $w_{1/2}$ ~ 325 Hz, 1H; Al*H*), 2.38 (s, 6H; Al•S*Me*$_2$), 2.07 (s, 6H; Mes, 2 × *p*-C*H*$_3$), 1.99 (s, 12H; Mes, 4 × *o*-C*H*$_3$), 0.15 (br q, $w_{1/2}$ ~ 265 Hz, 4H; B*H*$_4$).

^{11}B NMR (160 MHz, CD_2Cl_2) δ -38.8 (p, *J* ~ 85 Hz).

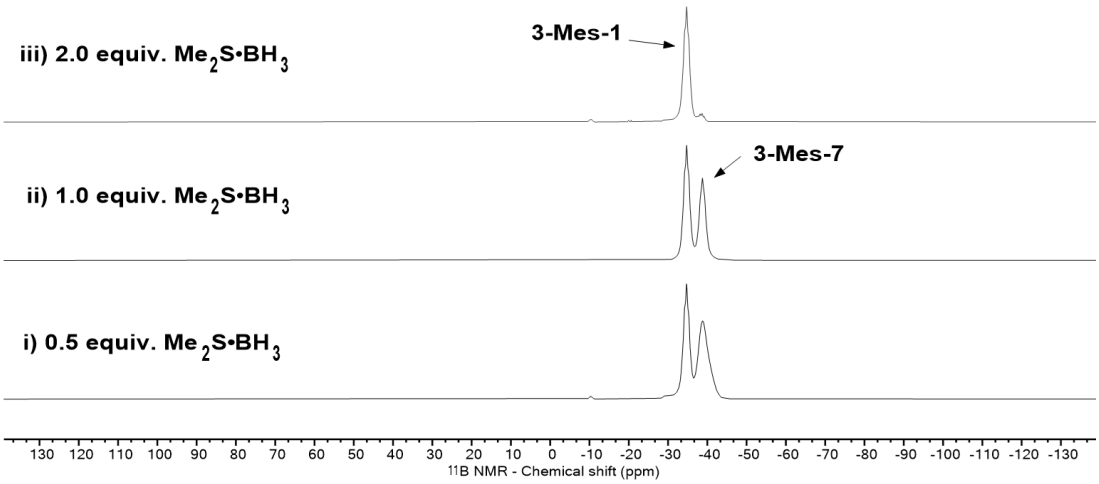

Figure 7-38. Stacked ^{11}B NMR spectra (CH_2Cl_2) of the reaction between $^{Mes}TerAlH_2$ and different quantities of $Me_2S•BH_3$.

Synthesis of boranes used to identify Al–H–B species

tBuCH$_2$H$_2$BH$_2$ (ABG-0479)

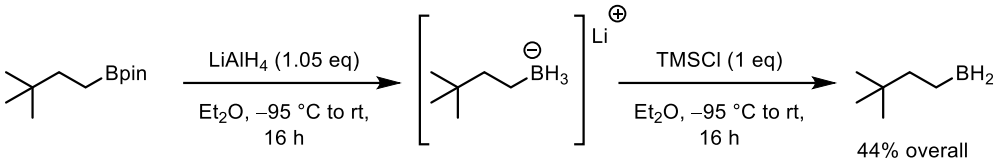

$LiAlH_4$ (319 mg, 8.4 mmol, 1.05 equiv.) in Et_2O (16 mL, 0.5 M) was added dropwise to a solution of *t*$BuCH_2CH_2Bpin$ (1.7 g, 8.0 mmol, 1 equiv.) in Et_2O (32 mL, 0.25 M) at −95 °C. The white precipitate was slowly warmed to room temperature and stirred for 16 hours. The resulting white precipitate was separated by filtration and further extracted with Et_2O (2 × 10 mL). An aliquot analysed by ^{11}B NMR confirmed the consumption of RBpin and the formation of the boron-ate species (^{11}B; 160 MHz, Benzene-d_6; δ -26.09 (q, *J* = 74.0, 73.6 Hz)). The solution was cooled to −95 °C and Me_3SiCl (1 mL, 8 mmol, 1 equiv.) was added dropwise to the resulting white suspension. The suspension was stirred over 16 hours with slow warming to room temperature. The precipitated salts were separated by filtration to give a colourless solution. The solvent was removed *in vacuo* to give a white gum. The product was collected using bulb-to-bulb distillation (*ca.* 1 mbar, 85 °C) as a colourless oil (345 mg, 3.52 mmol, 44% yield).

2 different aggregation states/environments formed (approx. ratio = 2:1)

Major:

^{1}H NMR (500 MHz, Benzene-d_6) δ 4.19 (q, *br*, 1H; B$\underline{H}_{terminal}$), 1.29 – 1.24 (m, 2H; $BCH_2C\underline{H_2}R$), 0.91 (s, 9H; $(C\underline{H_3})_3$), 0.88 – 0.85 (m, 2H *overlapped by tert-butyl peaks, confirmed by COSY, HSQC and HMBC;* $BC\underline{H_2}CH_2R$), 0.29 (s, br, 1H; B$\underline{H}_{bridging}$).

^{13}C {^{1}H} NMR **(**126 MHz, Benzene-d_6) δ 42.1, 31.1, 29.2, 11.5.

^{11}B NMR (160 MHz, Benzene-d_6) δ 22.9.

Minor:

^{1}H NMR (500 MHz, Benzene-d_6) δ 4.19 (q, *br*, 1H; B$\underline{H}_{terminal}$), 1.23 – 1.16 (m, 2H; $BCH_2C\underline{H_2}R$), 0.90 (s, 9H; $(C\underline{H_3})_3$), 0.87 (d, *J* = 7.5 Hz, 2H, *overlapped by tert-butyl peaks, confirmed by COSY, HSQC and HMBC;* $B\underline{CH_2}CH_2R$), 0.29 (s, br, 1H; B$\underline{H}_{bridging}$).

^{13}C {^{1}H} NMR (126 MHz, Benzene-d_6) δ 42.0, 31.1, 29.2, 9.5.

^{11}B NMR (160 MHz, Benzene-d_6) δ 22.9.

Bulk

IR 2953*m*, 2507*m* (B-$H_{terminal}$), 1578*s* (B-$H_{bridging}$)

Note: The ^{11}B NMR spectrum also displays a low intensity signal at δ 34.6 (~1%), which could potentially be attributed to the monomer.

Et_2BH (ABG-0470)

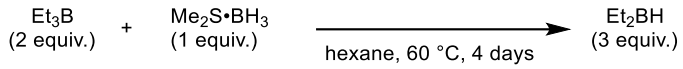

Me_2S•BH_3 (28.5 µL, 0.3 mmol, 0.5 equiv.) was added to BEt_3 (1 M in hexane, 0.6 mL, 0.6 mmol, 1 equiv.) in an NMR tube fitted with a septum. The reaction was vigorously shaken and then monitored periodically by ^{11}B NMR spectroscopy. Although it was originally left at room temperature for 18 hours, it required further heating at 60 °C for 4 days. Et_2BH was formed as the major product in an equilibrium also containing Et_3B and Et_2BH•H_2BEt. Approximately 78% of the total composition was Et_2BH.

^{11}B NMR (160 MHz, C_6H_{14}) δ 87.4 ($Et_3\underline{B}$), 53.8 (d, J = 101.9 Hz; $Et_2\underline{B}H$), 35.0 (t, J = 44.2 Hz; $Et_2\underline{B}H$•H_2BEt), 29.0 (br s, $w_{1/2}$ ~ 120 Hz, $(Et_2\underline{B}H)_2$), 17.6 (dt, J = 126.4, 47.2 Hz; Et_2BH•$H_2\underline{B}Et$).

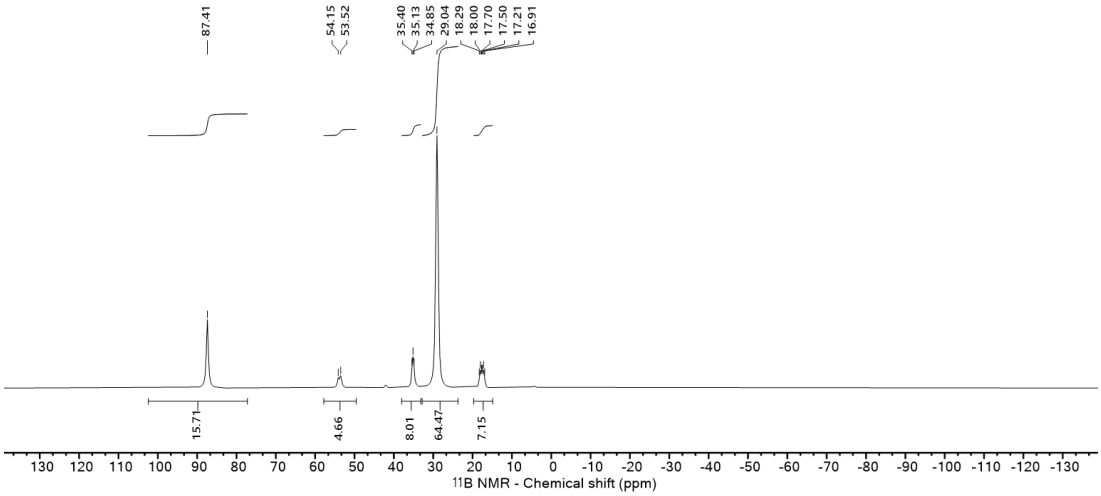

Figure 7-39. ^{11}B NMR spectrum (C_6H_{14}) for the reaction between Me_2S•BH_3 and BEt_3 (2 equiv.)

7.4.7 Probing effect of aluminium on exchange reactions with HBpin

Trialkylboranes (ABG-0446)

HBpin (36.3 µL, 0.25 mmol, 5 equiv.) was added to a solution of Et_3B (1 M in hexane, 50 µL, 0.05 mmol, 1 equiv.) in CH_2Cl_2 (0.65 mL) containing either zero or 1 equiv. of $^{Mes}TerAlH_2$ (17.1 mg, 0.05 mmol). The reaction was monitored periodically by ^{11}B NMR spectroscopy.

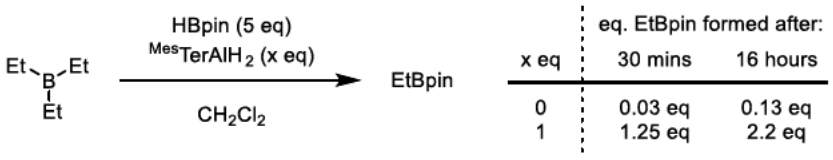

x eq	eq. EtBpin formed after: 30 mins	16 hours
0	0.03 eq	0.13 eq
1	1.25 eq	2.2 eq

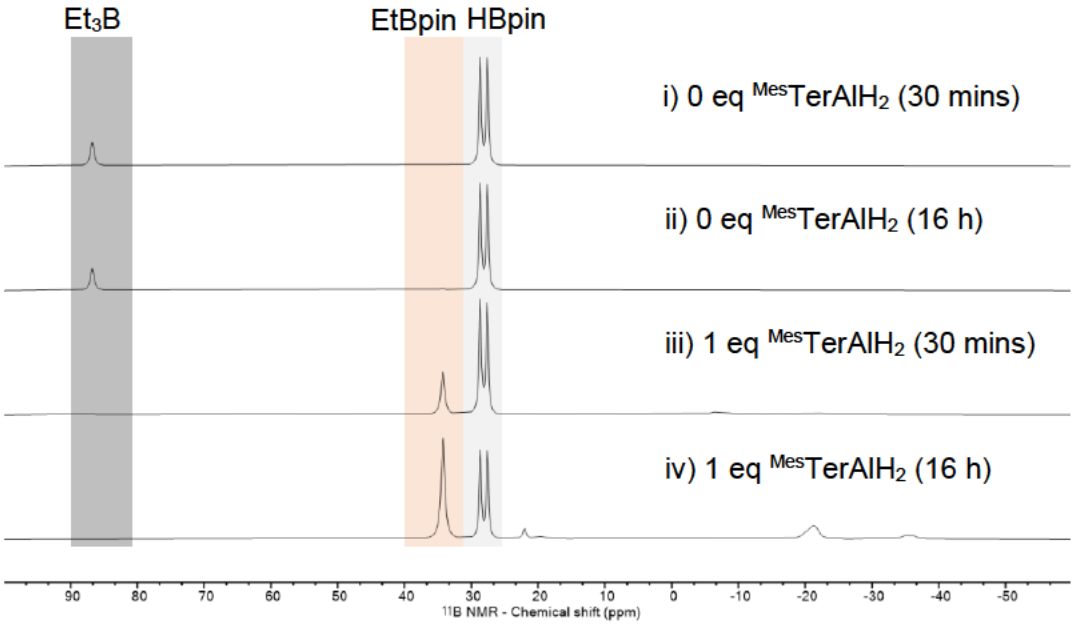

Figure 7-40. Reaction of Et_3B and HBpin with and without the presence of $^{Mes}TerAlH_2$.

Analysing the corresponding borane/alane adducts (ABG-0463)

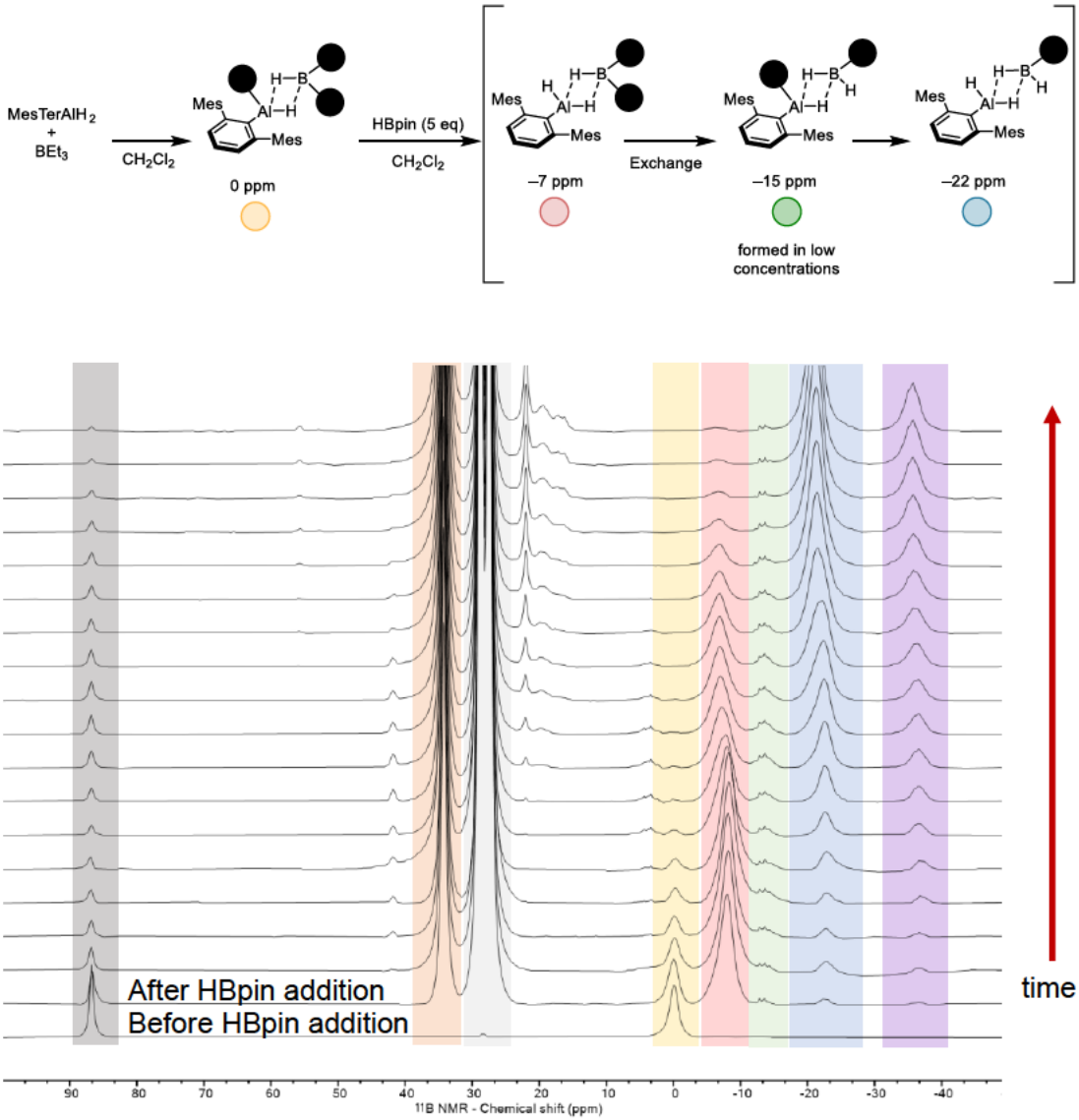

Figure 7-41. Stacked ^{11}B NMR spectra (CH_2Cl_2) of the $^{Mes}TerAlH_2$ promoted exchange of alkyl groups from Et_3B to EtBpin with HBpin.

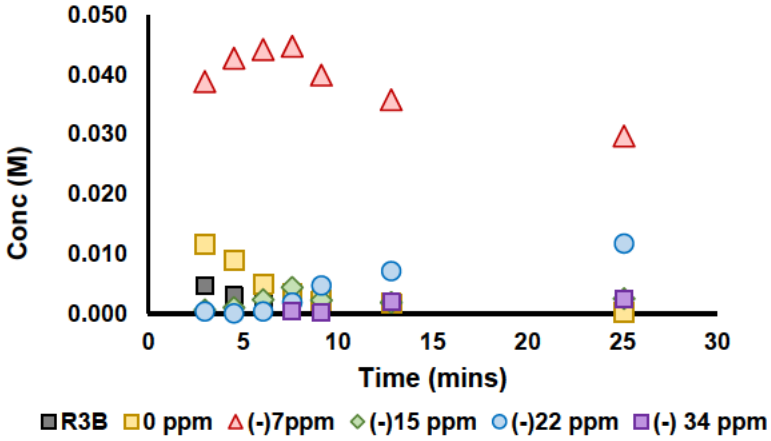

Figure 7-42. Speciation of borane species over time for the ^{Mes}TerAlH$_2$ promoted exchange of alkyl groups from Et$_3$B to EtBpin with HBpin (*first 30 minutes* – excluding HBpin and EtBpin).

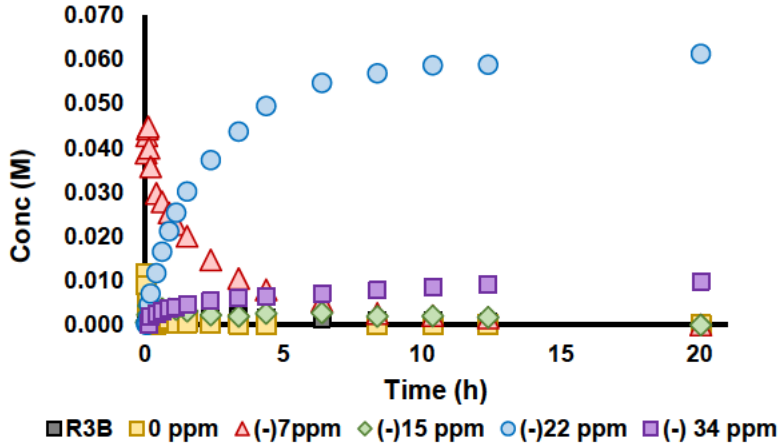

Figure 7-43. Speciation of borane species over time for the ^{Mes}TerAlH$_2$ promoted exchange of alkyl groups from Et$_3$B to EtBpin with HBpin (*first 20 hours* – excluding HBpin and EtBpin).

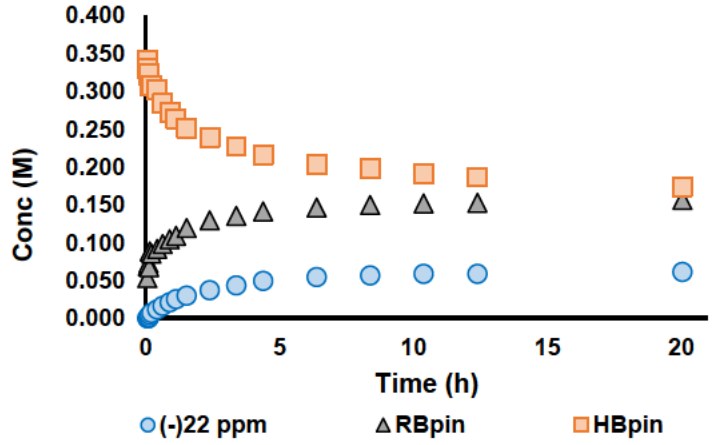

Figure 7-44. Speciation of major boron species over time for the ^{Mes}TerAlH$_2$ promoted exchange of alkyl groups from Et$_3$B to EtBpin with HBpin (first 20 hours – *including* HBpin and EtBpin).

Monoalkyl boranes (ABG-0485-C-2)

On **Figure 7-41**, the formation of **3-Mes-1** was observed, indicating that another exchange from ^{Mes}TerAlH$_2$•H$_2$BEt may be possible (i.e. an exchange of alkyl group from boron) with HBpin.

To test this, 3-Mes-3^{CH_2CH_2tBu} was generated *in situ* by reacting ^{Mes}TerAlH$_2$ (17.1 mg, 0.05 mmol, 1 equiv.) with *t*BuCH$_2$CH$_2$BH$_2$ (4.9 mg, 0.05 mmol, 1 equiv.) in CH$_2$Cl$_2$ (0.65 mL). HBpin (7.3 µL, 0.05 mmol, 1 equiv.) was then added, the reaction was vigorously shaken and then monitored by ^{11}B NMR spectroscopy.

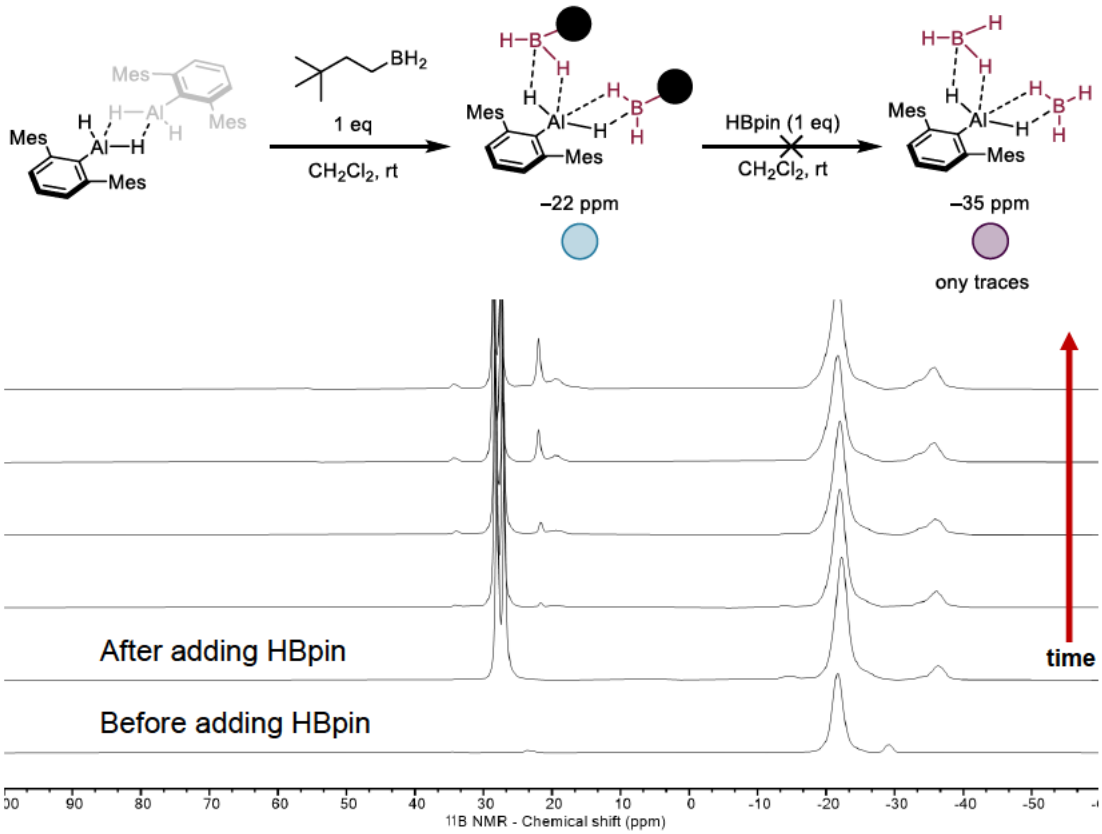

Figure 7-45. Stacked ^{11}B NMR spectra (CH$_2$Cl$_2$) of the reaction between ^{Mes}TerAlH$_2$•(*t*BuEtBH$_2$)$_2$ and HBpin and monitored over time.

Analysis

The formation of the resonance at δ –35 (^{Mes}TerAlH$_2$•B$_2$H$_6$) is suggestive of a hydride/alkyl exchange between HBpin and ^{Mes}TerAlH$_2$•(*t*BuEtBH$_2$)$_2$. However, this did not correspond to an equivalent of RBpin (δ ~34) being formed.

Thus, we probed the formation of ^{Mes}TerAlH$_2$•B$_2$H$_6$ (δ –35) from ^{Mes}TerAlH$_2$•(*t*BuEtBH$_2$)$_2$ (δ –22) with BH$_3$ (ABG-0484):

3-Mes-3^{CH_2CH_2tBu} was generated *in situ* by reacting ^{Mes}TerAlH$_2$ (17.1 mg, 0.05 mmol, 1 equiv.) with *t*BuCH$_2$CH$_2$BH$_2$ (4.9 mg, 0.05 mmol, 1 equiv.) in CH$_2$Cl$_2$ (0.65 mL). Me$_2$S•BH$_3$ (4.7 µL, 0.05 mmol, 1 equiv.) was then added, the reaction was vigorously shaken and then monitored by ^{11}B NMR spectroscopy.

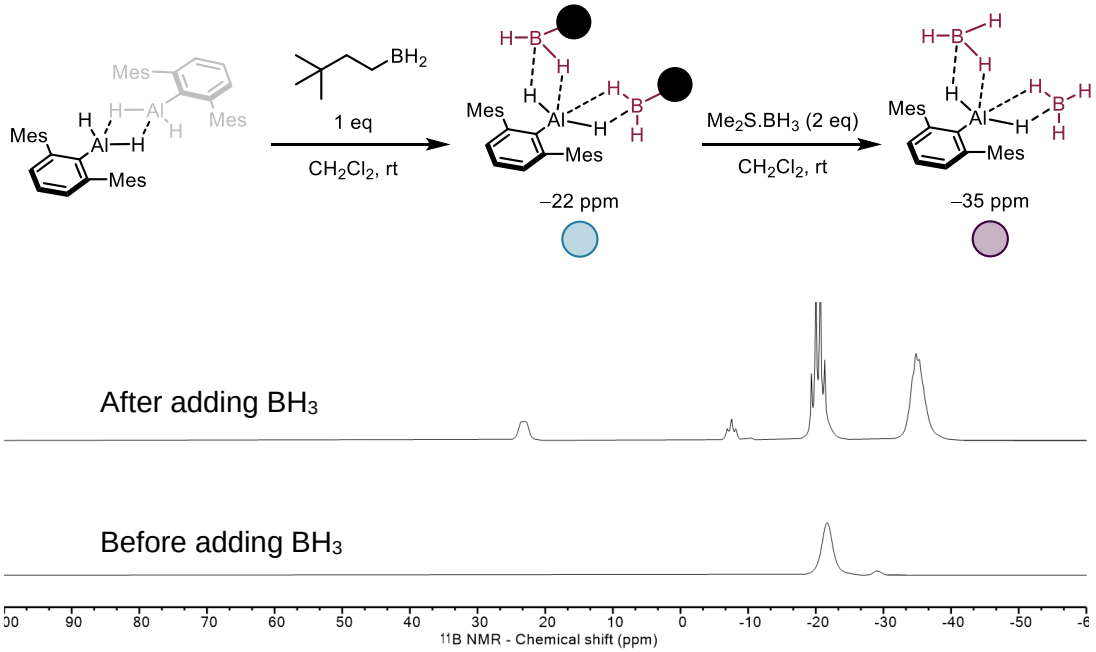

Figure 7-46. Stacked ^{11}B NMR spectra (CH$_2$Cl$_2$) of the reaction between ^{Mes}TerAlH$_2$•(*t*BuEtBH$_2$)$_2$ and HBpin.

Analysis

Indeed, ^{Mes}TerAlH$_2$•B$_2$H$_6$ (δ –35) is formed in the presence of BH$_3$. The results thus point to the alkyl exchange step with HBpin requiring an alkyl aluminium species. Alkyl borane species are largely unreactive with HBpin at room temperature.

7.4.8 Single turnover experiments

$Me_2S•BH_3$ (9.5 µL, 0.1 mmol, 2 equiv.) was added to a solution of $^{Mes}TerAlH_2$ (17.1 mg, 0.05 mmol, 1 equiv.) in CH_2Cl_2 (0.65 mL). The formation of 3-Mes-1 was confirmed by NMR spectroscopy. 1-octene (8.0 µL, 0.05 mmol, 1 equiv.) was added to the reaction mixture through a septum and the reaction was monitored by ^{11}B NMR spectroscopy at room temperature. Once the reaction had reached equilibrium, HBpin (7.3 µL, 0.05 mmol, 1 equiv.) was added through the septum and monitored by ^{11}B NMR spectroscopy.

Hydroelementation (ABG-0460)

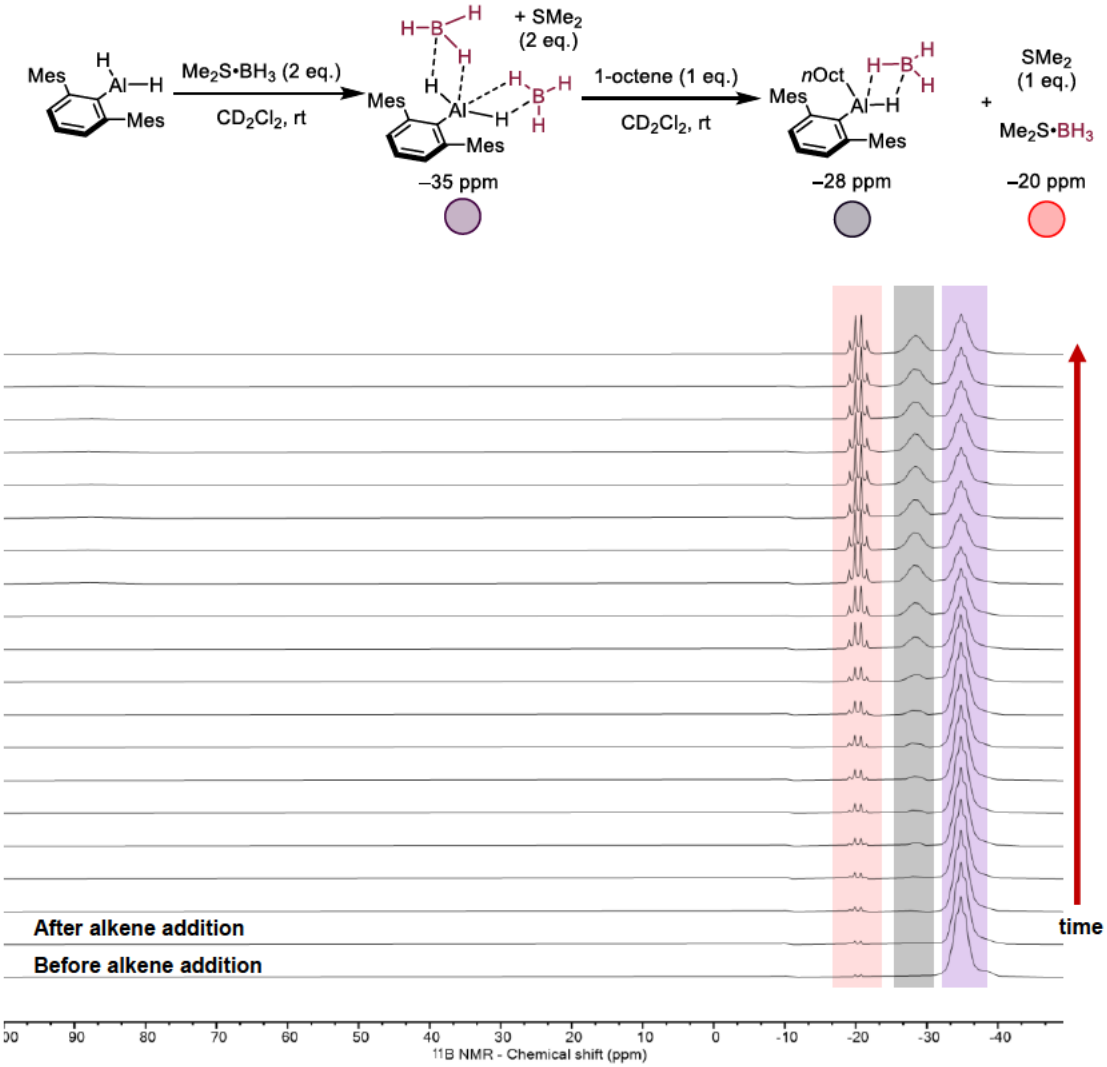

Figure 7-47. Stacked ^{11}B NMR spectrum (CH_2Cl_2) showing the progress over time of the hydroelementation of 1-octene from $^{Mes}TerAlH_2•(BH_3)_2$ (generated *in situ*)

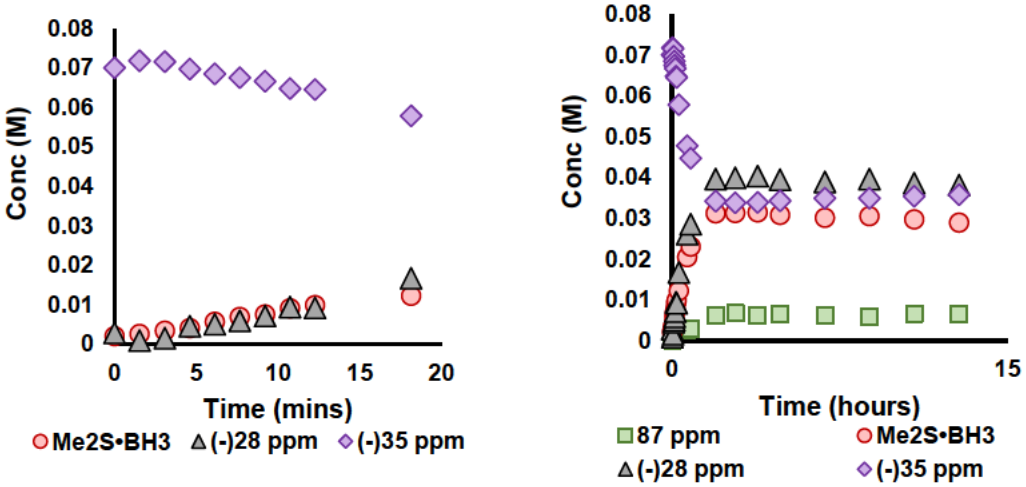

Figure 7-48. The speciation of boron containing compounds in the hydroelementation of 1-octene over i) 20 minutes and ii) 15 hours.

Exchange with HBpin

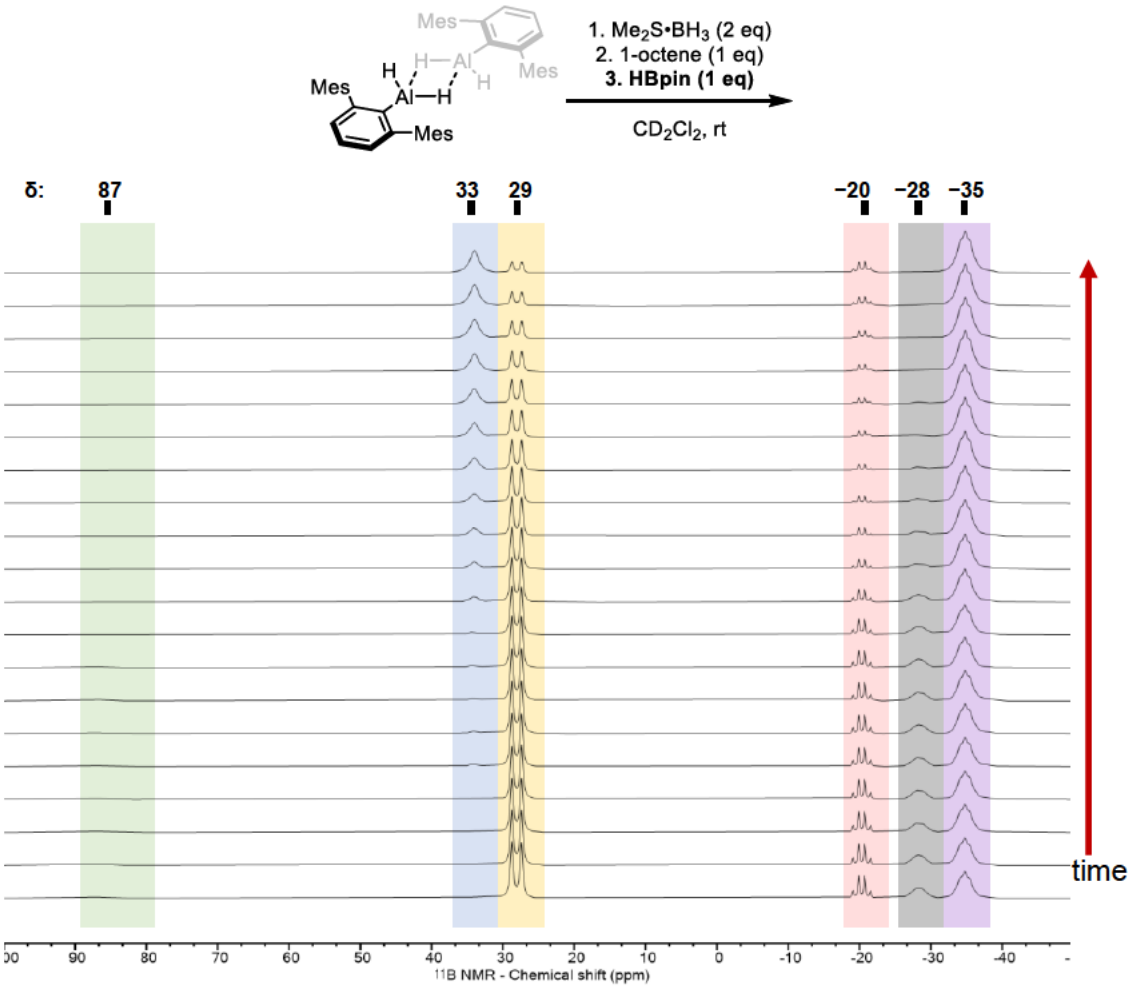

Figure 7-49. Stacked ^{11}B NMR spectra (CH_2Cl_2) of exchange of alkyl aluminium with HBpin.

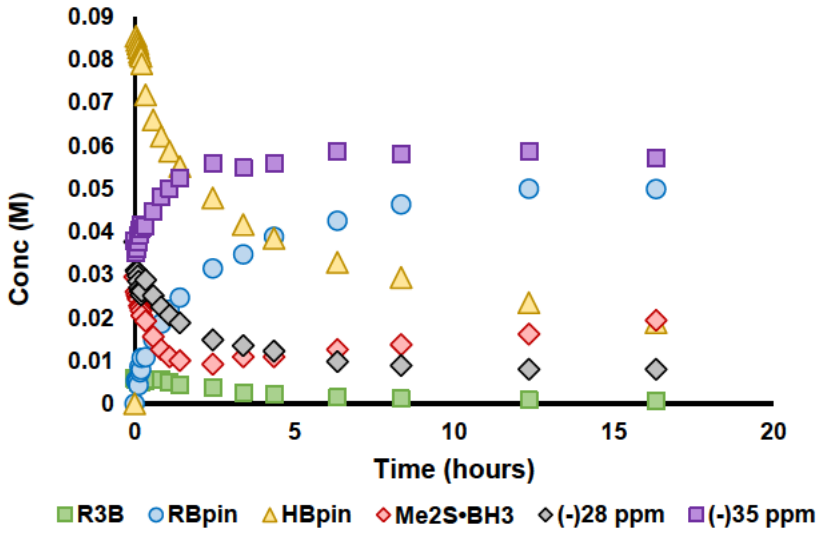

Figure 7-50. Speciation of boron-containing compounds in the exchange reaction with HBpin.

Formation of species at $\delta^{11}B = \delta -14$

Under catalytic conditions (see section 7.4.4) a resonance at δ ~ –14 was observed by ^{11}B NMR spectroscopy, corresponding to the formation of a ^{Mes}TerAl(alkyl)H•RBH_2 type species, **3-Mes-4**:

A similar species can also form in CH_2Cl_2 (0.65 mL) at room temperature by the reaction of ^{Mes}TerAlMe_2 (0.05 mmol, 1 equiv.) with Me_2S•BH_3 (0.025 mmol, 0.5 equiv.) or by the reaction of ^{Mes}TerAl(Et)H (0.05 mol, 1 equiv.) with *t*Bu$CH_2CH_2BH_2$ (4.9 mg, 0.05 mmol, 1 equiv.).

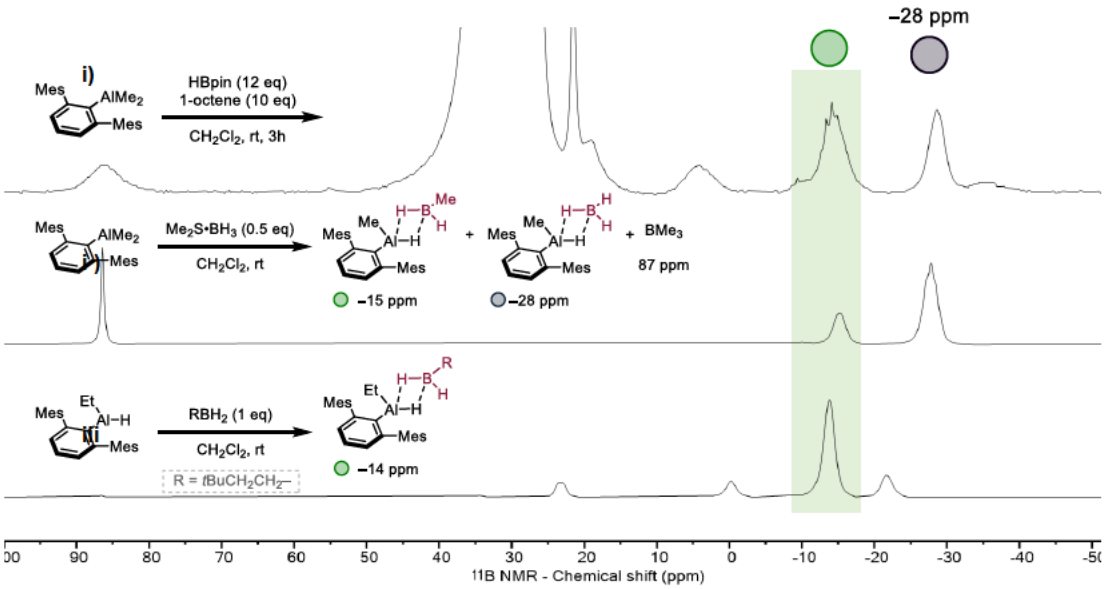

Figure 7-51. Stacked ^{11}B NMR spectra (CH_2Cl_2) for the i) ^{Mes}TerAlMe_2-catalysed hydroboration of 1-octene with HBpin (ABG-0454); ii) reaction of ^{Mes}TerAlMe_2 with Me_2S•BH_3 (0.5 equiv.; ABG-0265); iii) reaction of ^{Mes}TerAl(Et)H with *t*Bu$CH_2CH_2BH_2$ (1 equiv.; ABG-0506).

We reasoned that under catalytic conditions, ^{Mes}TerAl(alkyl)H•RBH$_2$ type species could also be generated by the reaction of ^{Mes}TerAl(alkyl)H•BH$_3$ with alkene. To test this, 1-octene (16 µL, 0.1 mmol, 2 equiv.) was added to a solution of **3-Mes-2^{Et}** (0.05 mmol, 1 equiv.; see section **7.4.5** for preparation) in CH_2Cl_2 (0.65 mL) at room temperature and the reaction was monitored by ^{11}B NMR spectroscopy. After 2 days, *t*BuCH$_2$CH$_2$BH$_2$ (4.9 mg, 0.05 mmol, 1 equiv.) was added, the solution was shaken vigorously and then analysed by ^{11}B NMR spectroscopy.

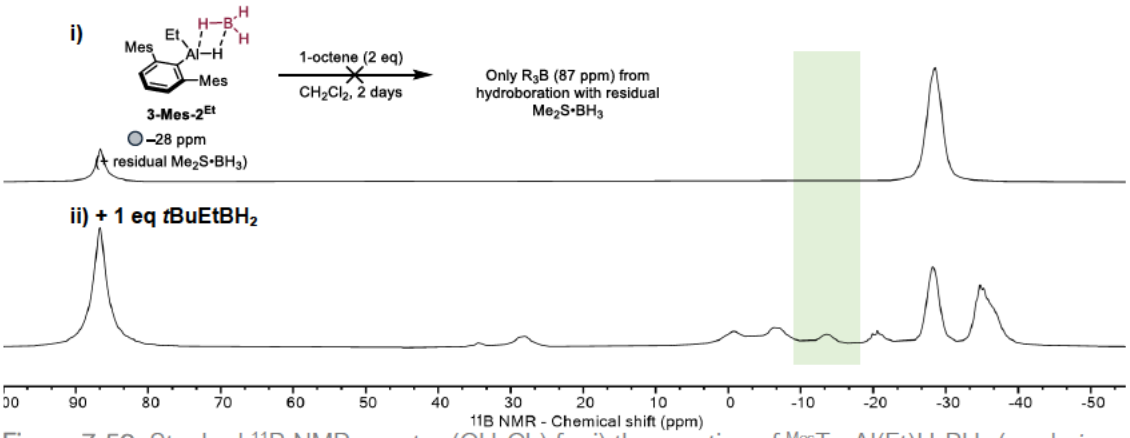

Figure 7-52. Stacked ^{11}B NMR spectra (CH_2Cl_2) for i) the reaction of ^{Mes}TerAl(Et)H•BH$_3$ (made *in situ* from ^{Mes}TerAl(Et)H + Me$_2$S•BH$_3$) with 1-octene (2 equiv.); ii) the addition of *t*BuEtBH$_2$ to this reaction mixture. (ABG-0488).

7.4.9 Nature of hydroelementation

Alkyl transfer from monoalkylborane to aluminium hydride (ABG-0485)

Details for alkyl transfer from monoalkylborane to aluminium dihydride displayed on Scheme 3-23:

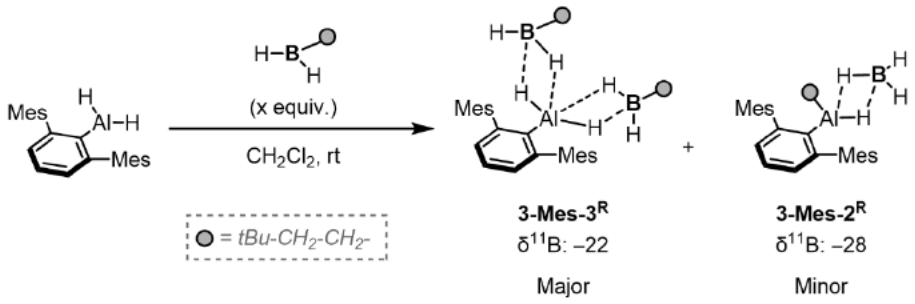

*t*BuCH$_2$CH$_2$BH$_2$ (0.25 M in CH_2Cl_2, 50-400 µL, 0.25 – 2.0 equiv.) was added to a suspension of ^{Mes}TerAlH$_2$ (17.1 mg, 0.05 mmol, 1 equiv.) in CH_2Cl_2 (total volume = 0.67 mL, 0.75 M) at room temperature. The reaction was analysed by ^{11}B NMR spectroscopy.

Reaction of alkene with 3-Mes-3^{Mes} (ABG-0456)

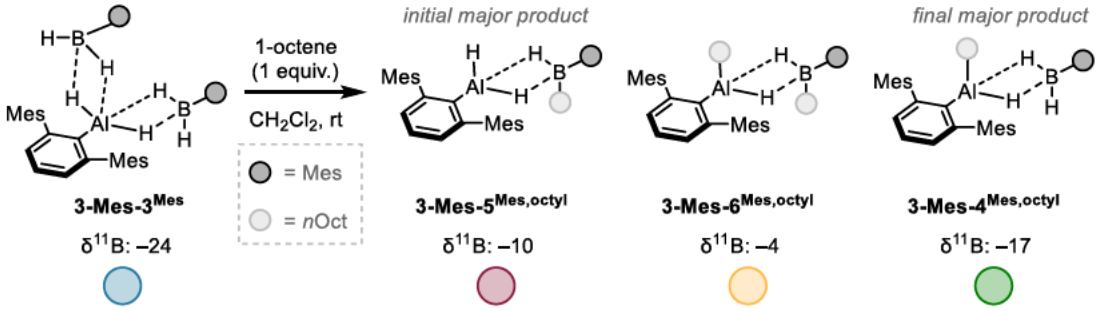

3-Mes-3^{Mes} was made *in situ* by reaction of ^{Mes}TerAlH$_2$ (17.1 mg, 0.05 mmol, 1 equiv.) with MesBH$_2$ (6.6 mg, 0.05 mmol, 1 equiv.) in CH_2Cl_2 (0.75 mL). The formation of 3-Mes-3^{Mes} was confirmed by ^{11}B NMR spectroscopy. 1-octene (8 µL, 0.05 mmol, 1 equiv.) was then added, the reaction was shaken vigorously and then monitored at room temperature by ^{11}B NMR spectroscopy.

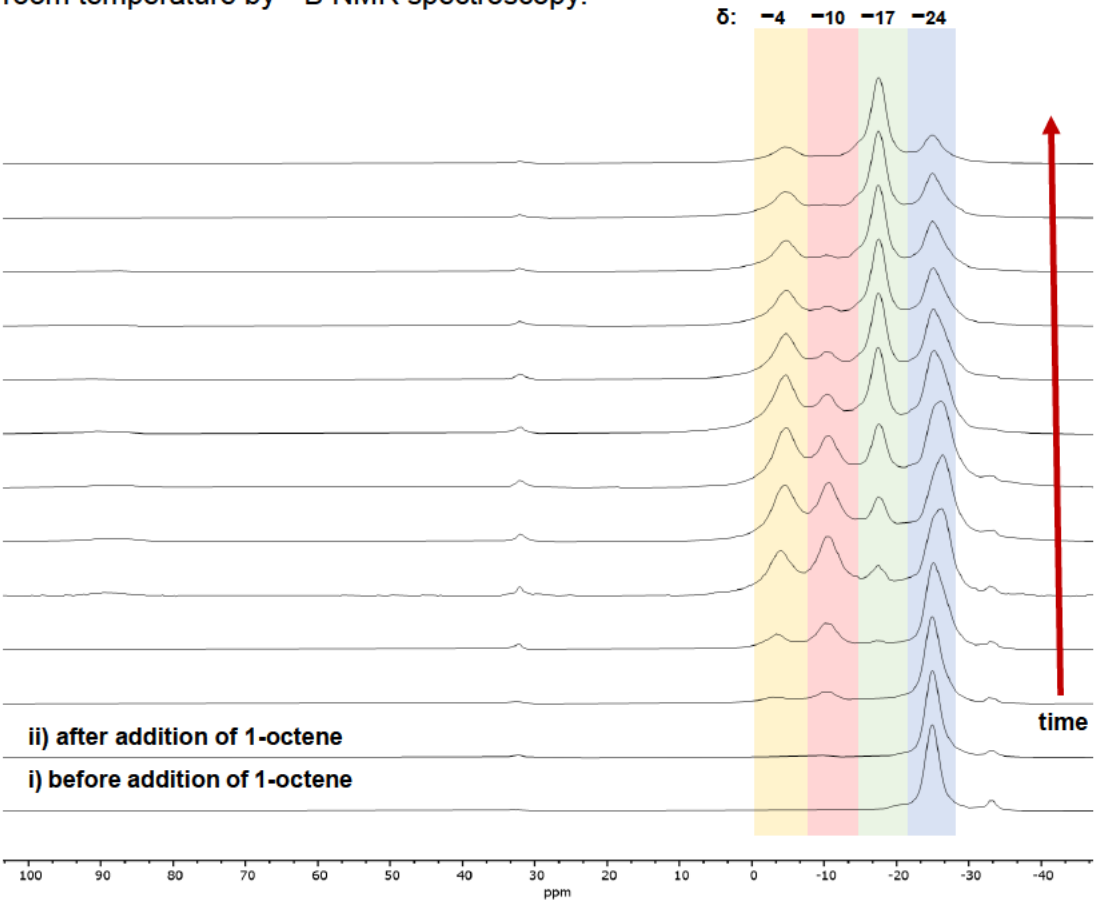

Figure 7-53. Stacked ^{11}B NMR spectra (CH_2Cl_2) of i) the reaction between ^{Mes}TerAlH$_2$ + MesBH$_2$; ii) the addition of 1-octene to this reaction and monitored over time.

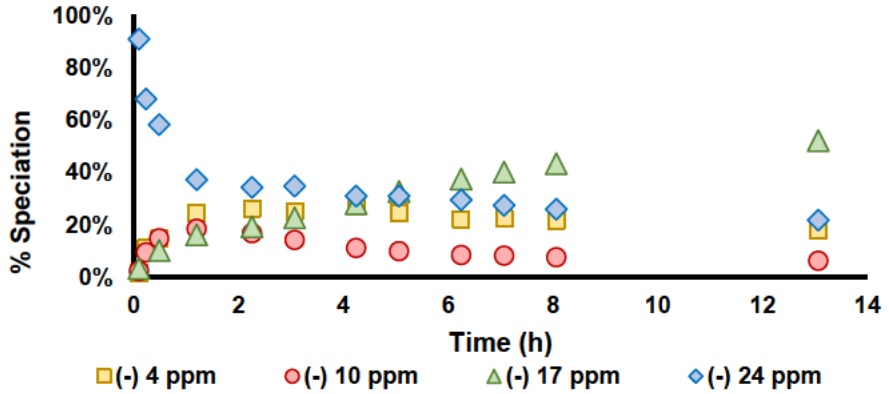

Figure 7-54. The speciation of boron containing compounds in the hydroelementation reaction of 1-octene with ^{Mes}TerAlH$_2$•H$_2$BMes

7.4.10 Influence of BH_3 on catalysis

(ABG-0497)

In **Scheme 3-25** in Chapter 3, the influence of BH_3 on catalysis was probed:

1-octene (80 µL, 0.5 mmol, 1 equiv.) was added to a solution containing HBpin (87 µL, 0.6 mmol, 1.2 equiv.) and the specified amount of **3-Mes-1**, SMe_2 and Me_2S•BH_3 in CH_2Cl_2 (0.6 mL). The reaction was vigorously shaken and the concentration of different species (see below) were monitored periodically by NMR spectroscopy using the aromatic signals as an internal reference (assumed to remain constant throughout the reaction).[240]

Quantities used:

- 3-Mes-1 (9.3 mg, 0.025 mmol, 5 mol%) or (18.5 mg, 0.05 mmol, 10 mol%)
- Me_2S•BH_3 (4.7 µL, 0.05 mmol, 10 mol%)
- SMe_2 (3.7 µL, 0.05 mmol, 10 mol%)

Reaction	3-Mes-1	Me_2S•BH_3	SMe_2
1	5 mol%	-	-
2	10 mol%	-	-
3	10 mol%	10 mol%	-
4	10 mol%	-	10 mol%

Species tracked and diagnostic signals used:

- octylBpin (δ 0.73, t, *J* = 7.7 Hz, 2H; BC*H*$_2$R)
- 1-octene (δ 5.83, ddt, *J* = 16.9, 10.2, 6.7 Hz, 1H; RC*H*=CH$_2$)
- 3-Mes-1 (δ 7.57, t, *J* = 7.6 Hz, 1H; Ar', *p*-*H*)
- 3-Mes-2^{octyl} (δ 7.49 t, *J* = 7.6 Hz, 1H; Ar', *p*-*H*)

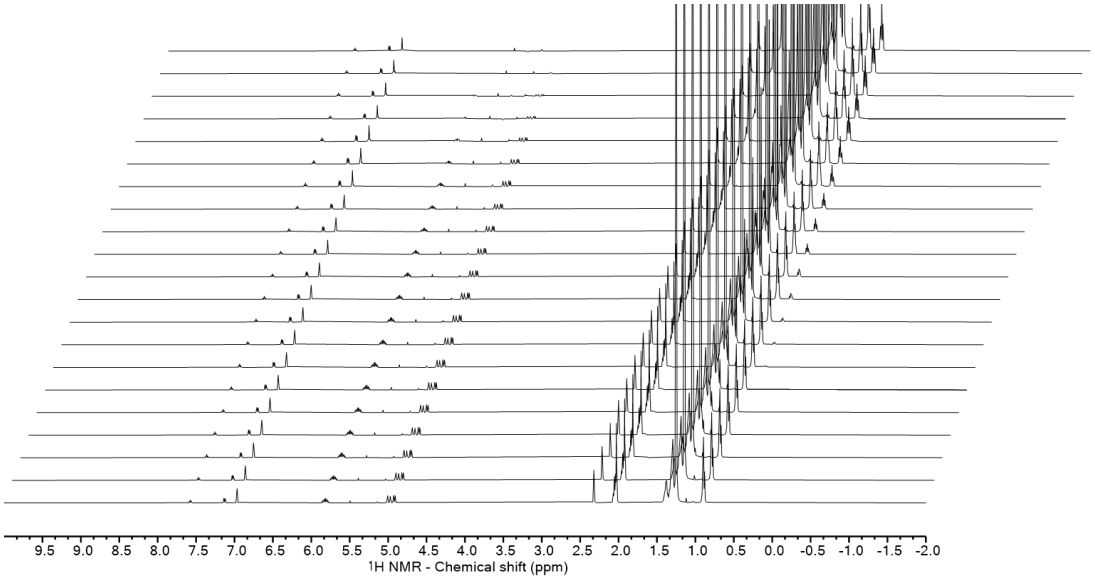

Figure 7-55. ^{1}H NMR spectra (CD_2Cl_2) for "reaction 2" (no additive) against time.

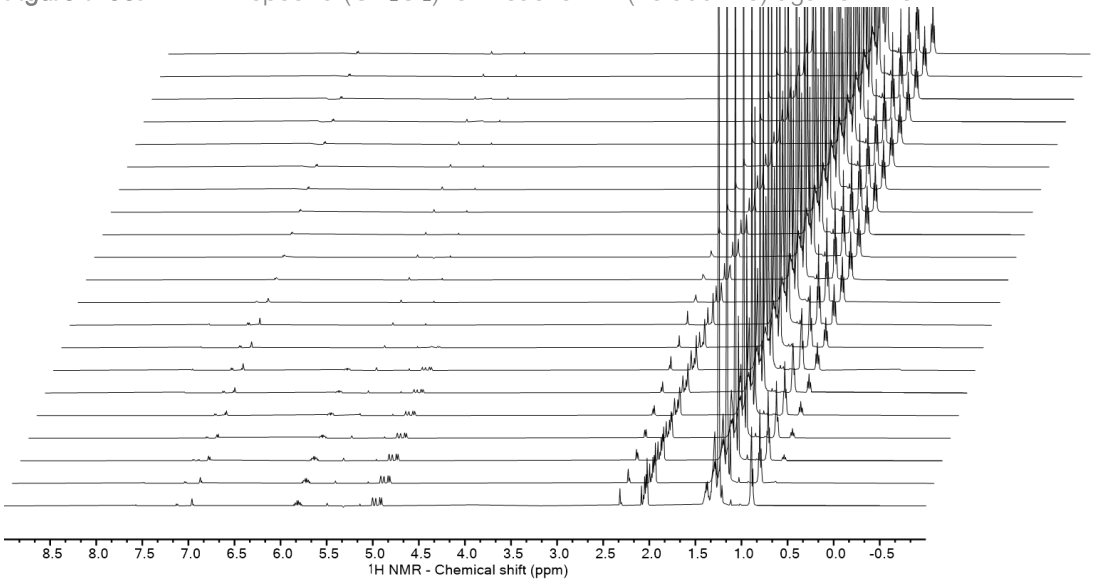

Figure 7-56. ^{1}H NMR spectra (CD_2Cl_2) for "reaction 4" (with SMe_2) against time.

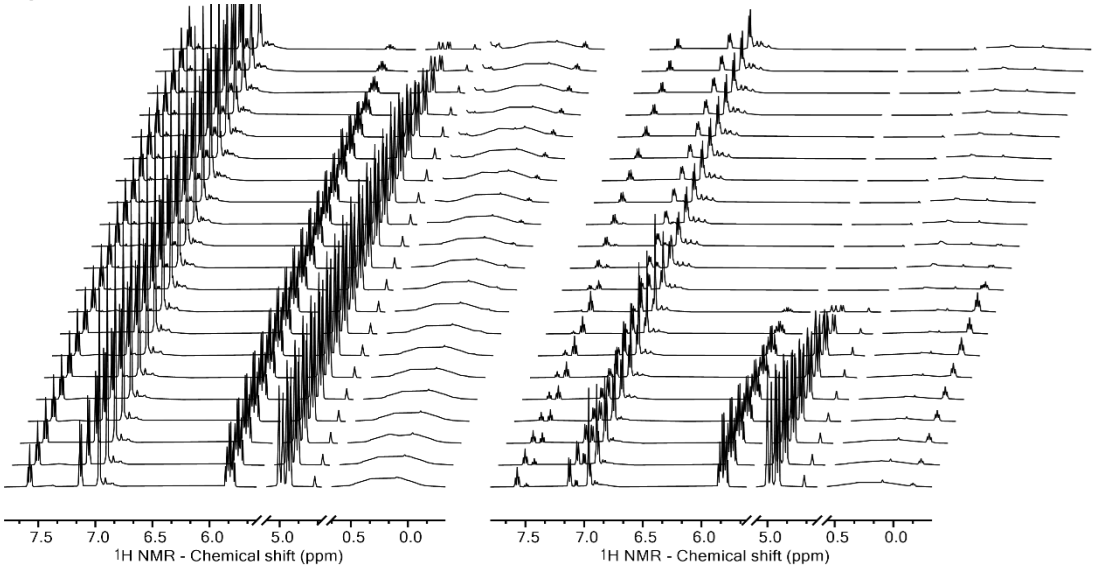

Figure 7-57. ^{1}H NMR spectra (CD_2Cl_2) comparing the aromatic, vinyl and AlC$\underline{H_2}$R resonances for "reaction 2" (left; no additive) vs "reaction 4" (right; with SMe_2) against time.

Role of Lewis base (ABG-0686)

In **Scheme 3-26** in Chapter 3, the effect of adding a Lewis base, using SMe_2 as a probe, on **3-Mes-1** was analysed:

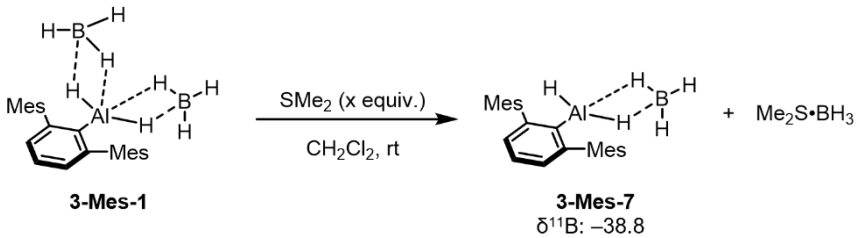

3-Mes-1 **3-Mes-7**
$\delta^{11}B$: –38.8

SMe_2 (1 – 55 equiv.) was added to a solution of 3-Mes-1 (18.5 mg, 0.05 mmol, 10 mol%) in CH_2Cl_2 (0.5 mL). The solution was vigorously shaken and analysed by ^{11}B NMR spectroscopy.

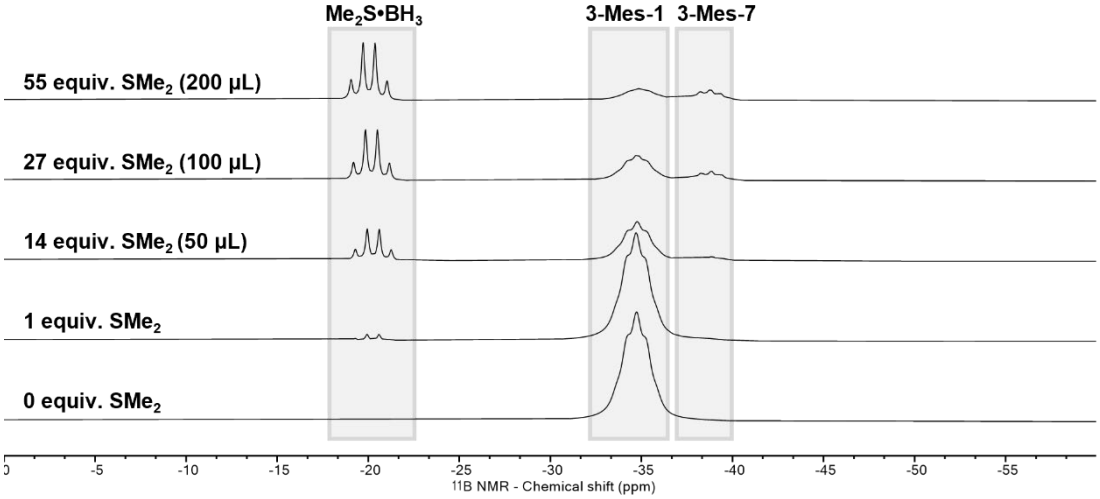

Figure 7-58. Stacked ^{11}B NMR spectra (CH_2Cl_2) for the reaction of 3-Mes-1 with different quantities of SMe_2.

7.4.11 VTNA

(ABG-0509)

A stock solution of **3-Mes-1** (0.125 M in CH_2Cl_2) was prepared by mixing $^{Mes}TerAlH_2$ (119.7 mg, 0.35 mmol) with $Me_2S{\bullet}BH_3$ (66.4 µL, 0.7 mmol) in CH_2Cl_2 (2.8 mL) in a vial. The solution was shaken until dissolved.

The quantities of each reagent were adjusted accordingly. A representative reaction is as follows (reference experiment):

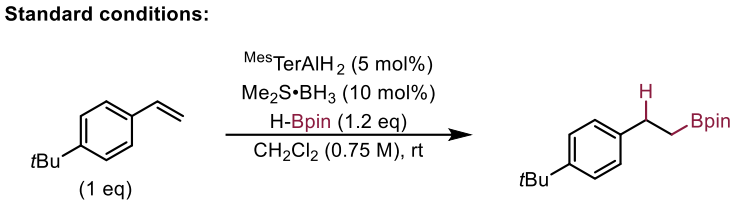

4-*t*Bu-styrene (99 µL, 0.5 mmol, 1 equiv.) was added to a solution of **3-Mes-1** (0.125 M in CH_2Cl_2, 400 µL, 0.05 mmol, 10 mol%) and HBpin (87 µL, 0.6 mmol, 1.2 equiv.) in CH_2Cl_2 (diluted to make a 0.746 M solution). The formation of *t*Bu-phenylethylBpin (δ 1.14; t, *J* = 8.1 Hz, 2H; BC*H*$_2$R) was tracked by ^{1}H NMR spectroscopy using the aromatic signals as an internal reference (assumed to remain constant throughout the reaction).[240]

		Equivalents		
Entry	Experiment	catalyst	alkene	HBpin
1	reference	0.05	1	1.2
2	catalyst*	**0.025**	1	1.2
3	alkene	0.05	**1.25**	1.2
4	HBpin	0.05	1	**1.5**

		Concentration (M)		
Entry	Experiment	catalyst	alkene	HBpin
1	reference	0.037	0.746	0.896
2	catalyst*	0.019	0.746	0.896
3	alkene	0.037	0.933	0.896
4	HBpin	0.037	0.746	1.119

* catalyst refers to **3-Mes-1**, which is made *in situ* from $^{Mes}TerAlH_2$ + $Me_2S{\bullet}BH_3$ (1:2 ratio). Concentrations of "catalyst" in the reaction refer to the sum of [**3-Mes-1**] + [**3-Mes-2^{octyl}**], which are the major observable catalytic species.

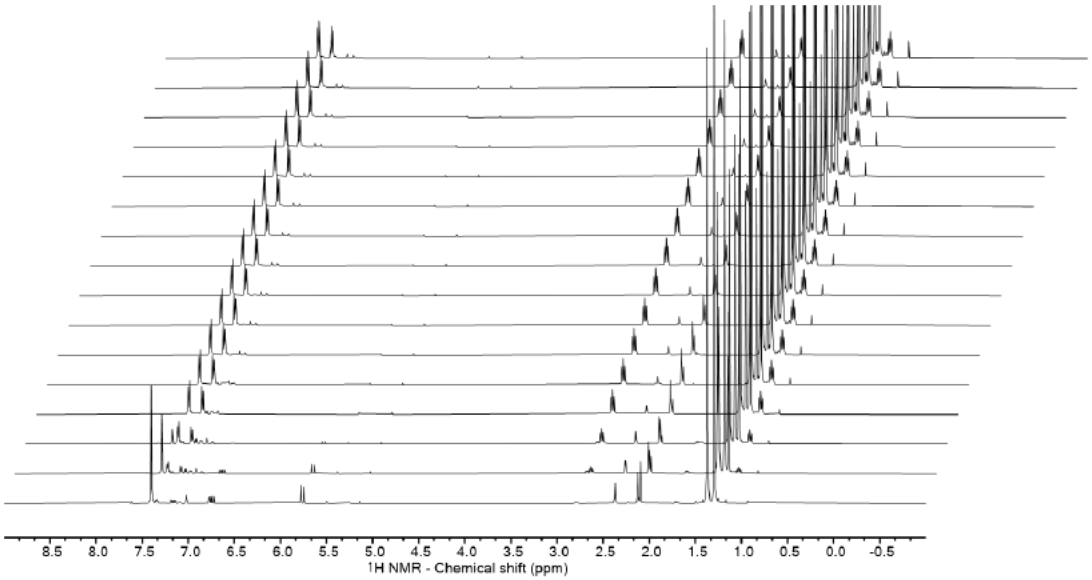

Figure 7-59. ^{1}H NMR spectra (CH_2Cl_2) against time for the "reference" reaction.

Order in catalyst

Order = 1

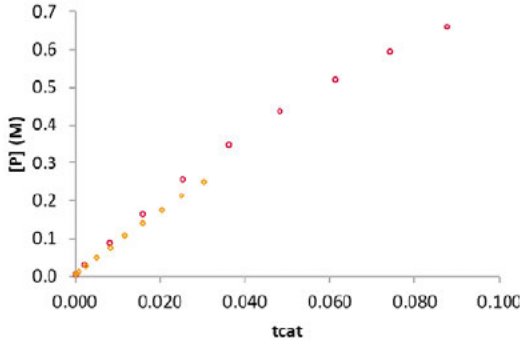

Order = 1.5

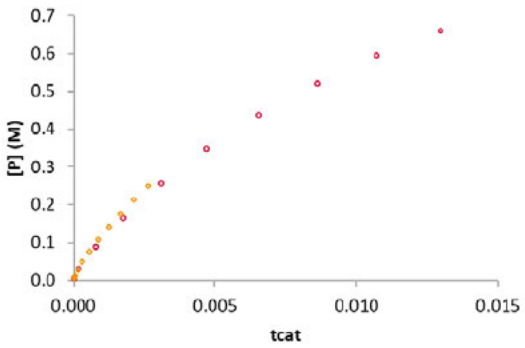

Order = 1.33

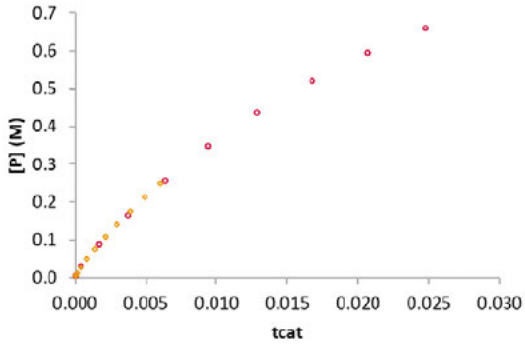

Order in 4-*t*Bu-styrene

Order = -0.5

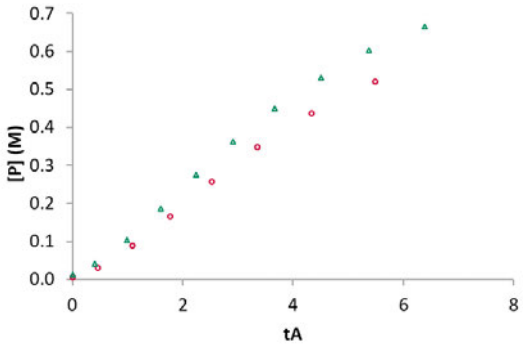

Order = 0.5

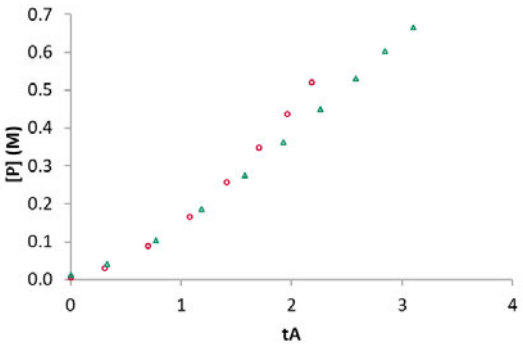

Order = 0

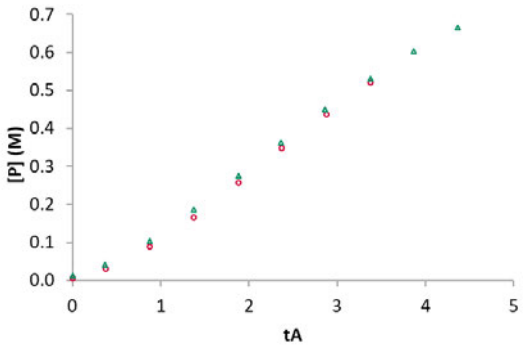

Order in HBpin

Order = 0.5

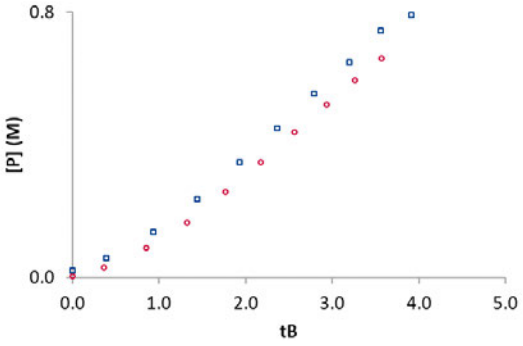

Order = 1.5

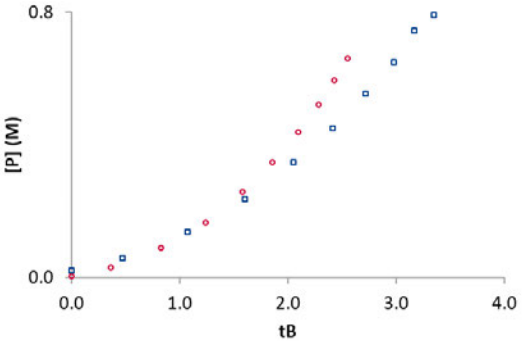

Order = 1

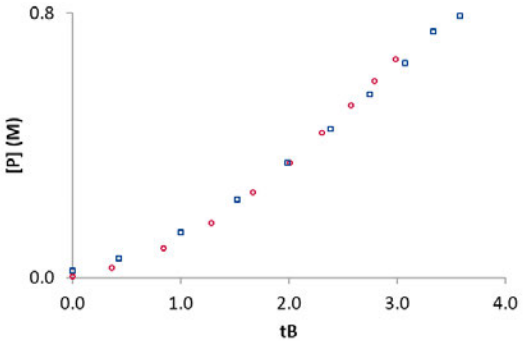

k_{obs}:

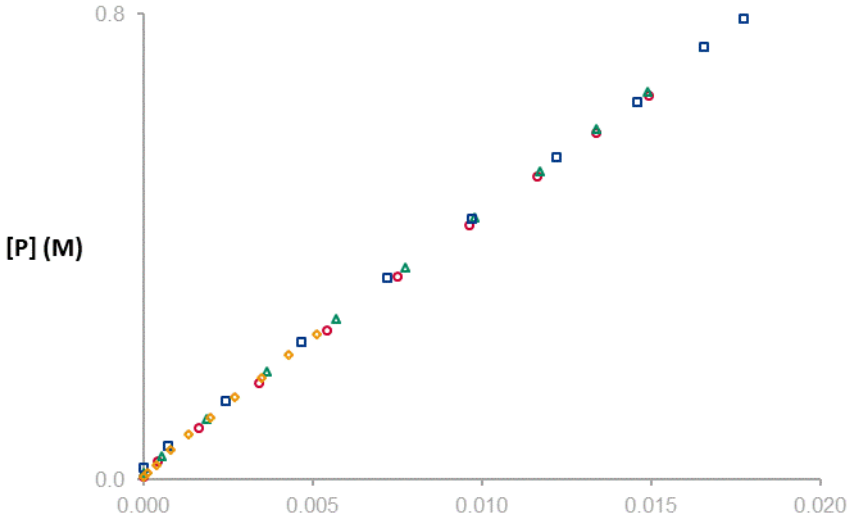

$\Sigma [cat]^{1.33}[HBpin]^{1}\Delta t$

Slope = k_{obs} = 43.7 (R^2 = 0.999)

7.5 Experimental details for Chapter 4

7.5.1 Optimisation of diazaborinine synthesis

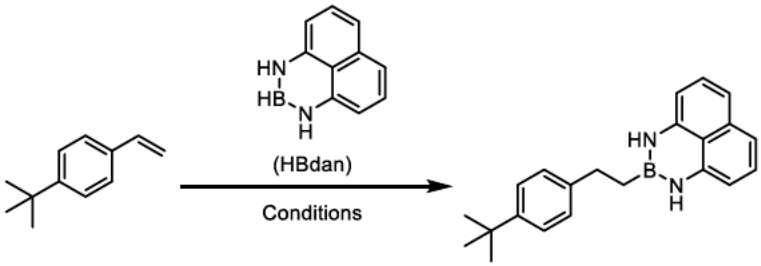

General procedure D: A vial was charged with catalyst (x mol%), HBdan (45.5 mg, 0.25 mmol) and stir bar in the glovebox and sealed with a PTFE/rubber septum cap. The vial was removed from the glovebox and the specified solvent was added. 4-*t*Bu-styrene (59 µL, 0.30 mmol, 1.2 equiv.) was added to the mixture and the reaction vessel was placed in a pre-heated oil bath at the specified temperature. The reaction was stirred at this temperature for the specified time and then removed from the oil bath. Upon cooling to room temperature, 1,3,5-trimethoxybenzene (1 mmol, 1 mL, 1 M in Et_2O) was added. The reaction was shaken and an aliquot (*ca.* 0.1 mL) was taken into an NMR tube. The solvent was removed *in vacuo* and the NMR sample was dissolved in $CDCl_3$. A ^1H NMR was taken with 1 scan and a relaxation delay of 30 seconds. Following phase and baseline correction, the product yield was determined by integrating the characteristic product peak (δ^1H NMR ($CDCl_3$): 2.78 (t, J = 8.1 Hz, 2H)) against the internal standard (1,3,5-trimethoxybenzene; Ar-H (δ^1H NMR ($CDCl_3$): 6.11 (s, 3H))).

Evaluation of catalysts (ABG-0524/0534)

Entry	Catalyst	Yield
1	$^{p\text{-Tol}}$TerAlH$_2$	18%
2	^{Mes}TerAlH$_2$	>95%
3	^{Tipp}TerAlH$_2$	>95%
4	$LiAlH_4$	0%
5	$Me_2S{\bullet}BH_3$	0%
6	$Me_3N{\bullet}AlH_3$	0%
7	DIBAL-H	4%
8	$AlMe_3$	8%

9	$AlEt_2Cl$ (1.5 equiv. HBdan)	23%
10	$AlCl_3$	0%
11	$AlCl_3$ (20 mol%) + $LiAlH_4$ (10 mol%)	< 2%
12	$AlCl_3$ (20 mol%) + $LiAlH_4$ (10 mol%) + Et_2O (20 mol%)	< 2%
13	$AlCl_3$ (10 mol%) + DIBAL-H (20 mol%)	45% (HBdan consumed)*

*Stoichiometric formation of *i*BuBdan also formed, insinuating that chloroalanes might be catalytically active.

Evaluation of catalyst loading (ABG-0527)

Entry	Catalyst loading	Yield $^{Mes}TerAlH_2$	Yield $^{Tipp}TerAlH_2$
1	20 mol%	>95%	>95%
2	10 mol%	47%	34%
3	5 mol%	13%	13%

Evaluation of additives (ABG-0528)

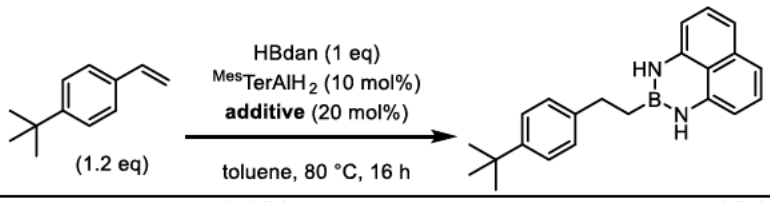

Entry	Additive	Yield
1	none	47%
2	$Me_2S{\bullet}BH_3$	33%
3	SMe_2	20%
4	THF	5%
5	Et_2O	28%
6	Cy_2BH	45%
7	MeBpin	10%
8	HBpin	37%

Evaluation of temperature (ABG-0530)

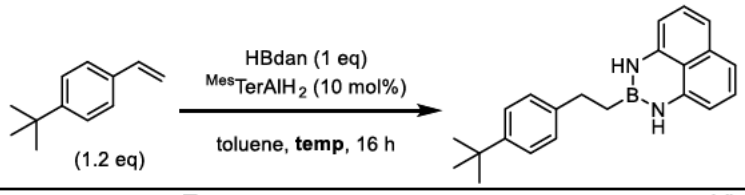

Entry	Temperature	Yield
1	110 °C	59%
2	80 °C	47%

Evaluation of stoichiometry (ABG-0538)

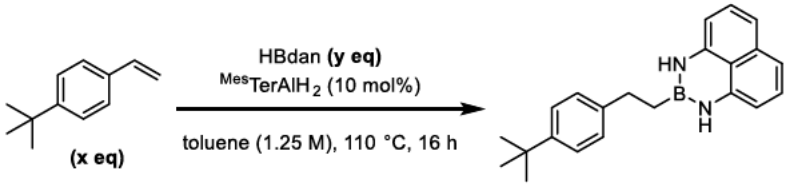

Entry	Substrate equiv.	HBdan equiv.	Yield
1	1.2	1.0	59%
2	1.1	1.0	61%
3	1.0	1.0	68%
4	1.0	1.2	61%

Evaluation of concentration (ABG-0539)

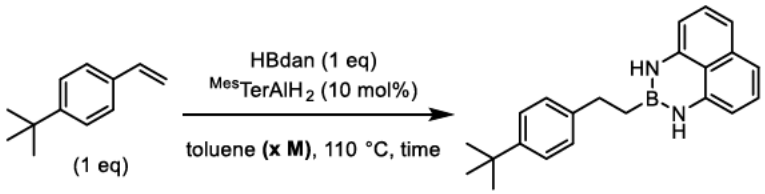

Entry	Concentration (M)	Yield
1	1.25	68%
2	2.5	68%
3	neat	15%*

*full consumption of HBdan and alkene – insoluble solid formed.

Evaluation of reaction time (ABG-0539 vs 0538)

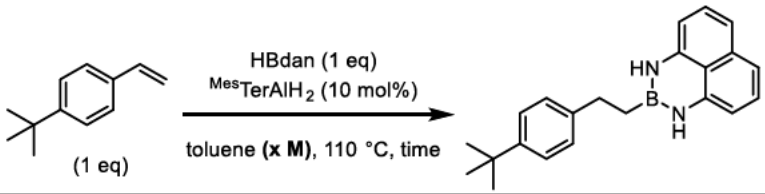

Entry	Concentration (M)	Time	Yield
1	1.25	16 h	68%
2	1.25	24 h	91%

7.5.2 Synthesis of diazaborinines

General procedure E:

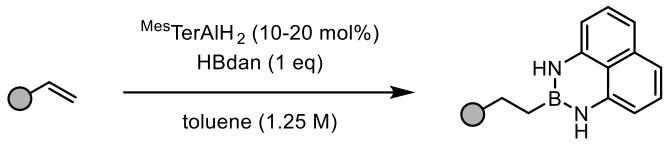

Alkene (0.25 mmol, 1.0 equiv.) was added neat to a mixture of ^{Mes}TerAlH$_2$ (17.1 mg, 0.05 mmol, 20 mol%; ***or*** 8.6 mg, 0.025 mmol, 10 mol%) and HBdan (45.5 mg, 0.25 mmol, 1.0 equiv.) in an NMR tube. The mixture was dissolved in toluene (0.2 mL, 1.25 M) and the solution was reacted at the specified temperature and time. The reaction was followed by ^{11}B NMR spectroscopy. Upon completion, the reaction was cooled to room temperature and quenched by exposure to O_2 (air). Mesitylene (50 µL) was added and the solution was diluted with toluene (0.2 mL). An aliquot (*ca*. 20 µL) was taken for NMR analysis and the remainder was purified by column chromatography (4 g SiO_2, eluting with pet. ether:ethyl acetate (99:1 to 95:5)) to give the pure diazaborinine.

Notes:

- For more volatile substrates, it was beneficial to add an excess of alkene (1.2 equiv.) and to lower the reaction temperature (see procedures for details).
- Diazaborinines appeared to slowly decompose on silica. Therefore, it was beneficial to perform column chromatography quickly, with products removed from the column within *ca.* 7 minutes.
- Diazaborinines slowly oxidised to form purple compounds and thus should be stored under argon. Diazaborinines that are contaminated in this way can be re-purified by dissolving in Et_2O:pet. ether (2:1) and passing quickly through a plug of alumina followed by removal of solvent.
- On the other hand, this oxidation means that diazaborinines can be revealed on the TLC plate by simply applying heat with a heat gun.

4-1a; 2-(phenethyl)-2,3-dihydro-1*H*-naphtho[1,8-*de*][1,3,2]diazaborinine (ABG-0550)

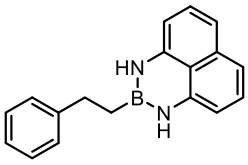

According to general procedure E, styrene (29 µL, 0.25 mmol) was reacted with HBdan (45.5 mg, 0.25 mmol) in the presence of $^{Mes}TerAlH_2$ (8.6 mg, 0.025 mmol) for 48 hours at 110 °C to give the product as an amorphous white solid (29.5 mg, 43% yield).

^{1}H NMR (500 MHz, Chloroform-*d*) δ 7.34 – 7.27 (m, 2H), 7.26 – 7.23 (m, 2H – overlapped by solvent), 7.23 – 7.17 (m, 1H), 7.08 (dd, *J* = 8.3, 7.3 Hz, 2H), 7.00 (dd, *J* = 8.3, 1.0 Hz, 2H), 6.25 (dd, *J* = 7.3, 1.0 Hz, 2H), 5.56 (s, 2H), 2.80 (t, *J* = 8.1 Hz, 2H), 1.25 (t, *J* = 8.1 Hz, 2H).

^{13}C {^{1}H} NMR (126 MHz, Chloroform-*d*) δ 144.0, 141.2, 136.4, 128.6, 128.1, 127.7, 126.0, 119.7, 117.6, 105.7, 31.0, 16.7 (B<u>*C*</u>H_2R - identified by HSQC).

^{11}B NMR (160 MHz, Chloroform-*d*) δ 31.9.

IR(ν_{max}) 3406 (w), 1628 (w), 1598 (s)

MS HRMS-EI (m/z):Found 272.1485, [M•+] ($C_{18}H_{17}BN_2$) requires 272.1479

m.p. 82-84 °C (hexane/Et_2O)

Data were in accordance with those previously reported.[328]

4-1b; 2-(4-(tert-butyl)phenethyl)-2,3-dihydro-1*H*-naphtho[1,8-*de*] [1,3,2]diazaborinine (ABG-0384)

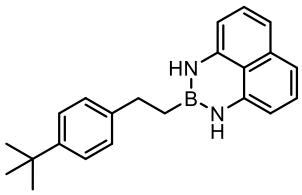

According to general procedure E, 4-*t*Bu-styrene (59 µL, 0.3 mmol) was reacted with HBdan (45.5 mg, 0.25 mmol) in the presence of $^{Mes}TerAlH_2$ (8.6 mg, 0.025 mmol) for 24 hours at 110 °C to give the product as an amorphous white solid (66 mg, 80% yield).

^{1}H NMR (500 MHz, Chloroform-*d*) δ 7.36 – 7.30 (m, 2H), 7.22 – 7.15 (m, 2H), 7.08 (dd, *J* = 8.3, 7.3 Hz, 2H), 6.99 (dd, *J* = 8.3, 0.8 Hz, 2H), 6.25 (dd, *J* = 7.3, 0.9 Hz, 2H), 5.56 (s, 2H), 2.78 (t, *J* = 8.1 Hz, 2H), 1.32 (s, 9H), 1.25 (t, *J* = 8.1 Hz, 2H).

^{13}C {^{1}H} NMR (126 MHz, Chloroform-*d*) δ 148.9, 141.2, 140.9, 136.5, 127.8, 127.7, 125.5, 119.7, 117.6, 105.6, 34.5, 31.6, 30.3, 16.6 (B<u>*C*</u>H_2R - identified by HSQC).

^{11}B NMR (160 MHz, Chloroform-*d*) δ 31.8.

IR(ν_{max}) (neat) 3426.8, 3399.5, 3051.8, 2962.4, 2866.5, 1625.8, 1598.5, 1508.3, 1411.0, 1369.3, 1337.6, 1140.9, 818.4, 760.5, 642.0, 625.5, 599.9.

MS HRMS-EI (m/z): Found 328.2111, [M•+] ($C_{22}H_{25}BN_2$) requires 328.2105

m.p. 106-107 °C (hexane)

Data were in accordance with those previously reported.[334]

4-1c; 2-(4-isobutylphenethyl)-2,3-dihydro-1*H*-naphtho[1,8-*de*][1,3,2]diazaborinine (ABG-0557)

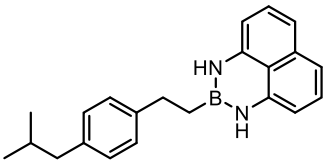

According to general procedure E, 4-*i*Bu-styrene (45 µL, 0.25 mmol) was reacted with HBdan (45.5 mg, 0.25 mmol) in the presence of ^{Mes}TerAlH$_2$ (8.6 mg, 0.025 mmol) for 24 hours at 110 °C to give the product as a colourless oil (49 mg, 60% yield).

^{1}H NMR (500 MHz, Chloroform-*d*) δ 7.19 – 7.13 (m, 2H), 7.12 – 7.05 (m, 4H), 7.00 (dd, *J* = 8.3, 1.0 Hz, 2H), 6.28 – 6.19 (m, 2H), 5.55 (s, 2H), 2.77 (t, *J* = 8.1 Hz, 2H), 2.46 (t, *J* = 7.2 Hz, 2H), 1.85 (dh, *J* = 13.5, 6.8 Hz, 1H), 1.24 (t, *J* = 8.1 Hz, 2H), 0.92 (s, 3H), 0.91 (s, 3H).

^{13}C {^{1}H} NMR (126 MHz, Chloroform-*d*) δ 141.2, 141.1, 139.4, 136.4, 129.4, 127.8, 127.7, 119.7, 117.6, 105.6, 45.2, 30.5, 30.4, 22.5, 16.7 (B*C*H$_2$R - identified by HSQC).

^{11}B NMR (160 MHz, Chloroform-*d*) δ 31.9.

IR(ν_{max}) 3416 (w), 2953 (w), 1628 (w), 1600 (s)

MS HRMS-EI (m/z): Found 328.2104, [M•+] ($C_{22}H_{25}BN_2$) requires 328.2105

4-1d; 2-(2,4-dimethylphenethyl)-2,3-dihydro-1*H*-naphtho[1,8-*de*] [1,3,2]diazaborinine (ABG-0568)

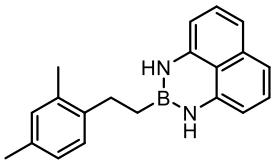

According to general procedure E 2,4-dimethylstyrene (38 µL, 0.25 mmol) was reacted with HBdan (45.5 mg, 0.25 mmol) in the presence of $^{Mes}TerAlH_2$ (8.6 mg, 0.025 mmol) for 24 hours at 110 °C to give the product as an amorphous white solid (66 mg, 88% yield).

^{1}H NMR (500 MHz, Chloroform-*d*) δ 7.14 – 7.06 (m, 3H), 7.04 – 6.90 (m, 4H), 6.27 (dd, *J* = 7.3, 1.0 Hz, 2H), 5.58 (s, 2H), 2.72 (t, *J* = 8.3 Hz, 2H), 2.31 (s, 3H), 2.30 (s, 3H), 1.18 (t, *J* = 8.3 Hz, 2H).

^{13}C {^{1}H} NMR (126 MHz, Chloroform-*d*) δ 141.2, 139.0, 136.5, 135.6, 135.5, 131.2, 128.2, 127.7, 126.9, 119.7, 117.6, 105.7, 27.8, 21.0, 19.4, 15.8 (B*C*H$_2$R - identified by HSQC).

^{11}B NMR (160 MHz, Chloroform-*d*) δ 32.2.

IR(ν_{max}) 3402 (w), 2918 (w), 2863 (w), 1629 (w), 1597 (s)

MS HRMS-EI (m/z): Found 300.1795, [M•+] ($C_{20}H_{21}BN_2$) requires 300.1792

4-1e; 2-(4-methoxyphenethyl)-2,3-dihydro-1*H*-naphtho[1,8-*de*][1,3,2]diazaborinine (ABG-0373)

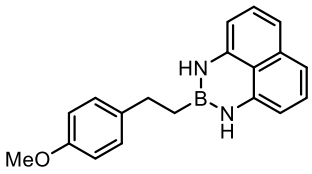

According to general procedure E, 4-methoxy-styrene (42 µL, 0.3 mmol) was reacted with HBdan (45.5 mg, 0.25 mmol) in the presence of $^{Mes}TerAlH_2$ (0.05 mmol, 17.1 mg) for 16 hours to give the product as an amorphous white solid (61 mg, 80% yield).

^{1}H NMR (500 MHz, Chloroform-*d*) δ 7.20 – 7.13 (m, 2H), 7.08 (dd, *J* = 8.3, 7.3 Hz, 2H), 7.00 (dd, *J* = 8.3, 1.0 Hz, 2H), 6.89 – 6.82 (m, 2H), 6.25 (dd, *J* = 7.3, 1.0 Hz, 2H), 5.56 (s, 2H), 3.80 (s, 3H), 2.74 (t, *J* = 8.1 Hz, 2H), 1.22 (t, *J* = 8.1 Hz, 2H).

^{13}C {^{1}H} NMR (126 MHz, Chloroform-*d*) δ 158.0, 141.2, 136.4, 136.0, 129.0, 127.7, 119.7, 117.6, 114.1, 105.6, 55.4, 30.0, 16.8 (B<u>*C*</u>H_2R - identified by HSQC).

^{11}B NMR (160 MHz, Chloroform-*d*) δ 31.94.

IR(ν_{max}) 3393 (m), 3383 (m), 1630 (w), 1600 (s)

MS HRMS-EI (m/z): Found 302.1590, [M•+] ($C_{19}H_{19}BN_2O$) requires 302.1585

m.p. 125-128°C (pet. eth.)

Data were in accordance with those previously reported.[334]

4-1f; 2-(4-fluorophenethyl)-2,3-dihydro-1*H*-naphtho[1,8-*de*][1,3,2]diazaborinine (ABG-0566)

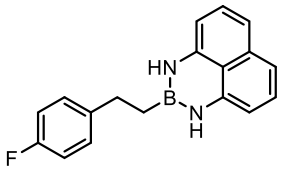

According to general procedure E, 4-fluoro-styrene (30 µL, 0.25 mmol) was reacted with HBdan (45.5 mg, 0.25 mmol) in the presence of ^{Mes}TerAlH$_2$ (8.6 µL, 0.025 mmol) for 48 hours at 110 °C to give the product as an amorphous white solid (41 mg, 57% yield).

^{1}H NMR (500 MHz, Chloroform-*d*) δ 7.23 – 7.16 (m, 2H), 7.09 (dd, *J* = 8.3, 7.3 Hz, 2H), 7.04 – 6.94 (m, 4H), 6.27 (dd, *J* = 7.3, 1.0 Hz, 2H), 5.55 (s, 2H), 2.77 (t, *J* = 8.2 Hz, 2H), 1.22 (t, *J* = 8.2 Hz, 2H).

^{13}C {^{1}H} NMR (126 MHz, Chloroform-*d*) δ 161.4 (d, *J* = 243.5 Hz), 141.1, 139.6 (d, *J* = 3.2 Hz), 136.4, 129.4 (d, *J* = 7.7 Hz), 127.7, 119.7, 117.7, 115.3 (d, *J* = 21.1 Hz), 105.7, 30.2, 17.2 (B*C*H$_2$R - identified by HSQC)

^{11}B NMR (160 MHz, Chloroform-*d*) δ 31.8.

^{19}F NMR (471 MHz, Chloroform-*d*) δ -117.7 (tt, *J* = 8.8, 5.4 Hz).

IR(ν_{max}) 3435 (m), 3052 (w), 2924 (w), 1632 (w), 1597 (s)

MS HRMS-EI (m/z): Found 290.1388, [M•+] ($C_{18}H_{16}BFN_2$) requires 290.1385

m.p. 96-98 °C (pet. eth)

4-1g; 2-(4-chlorophenethyl)-2,3-dihydro-1*H*-naphtho[1,8-*de*][1,3,2]diazaborinine (ABG-0542)

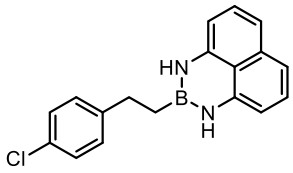

According to general procedure E, 4-chloro-styrene (30 µL, 0.25 mmol) was reacted with HBdan (45.5 mg, 0.25 mmol) in the presence of $^{Mes}TerAlH_2$ (8.6 mg, 0.025 mmol) at 110 °C for 72 hours to give the product as an amorphous white solid (33 mg, 43% yield).

^{1}H NMR (500 MHz, Chloroform-*d*) δ 7.27 (m, 2H), 7.20 – 7.13 (m, 2H), 7.09 (dd, *J* = 8.3, 7.3 Hz, 2H), 7.01 (dd, *J* = 8.4, 1.0 Hz, 2H), 6.27 (dd, *J* = 7.3, 1.0 Hz, 2H), 5.56 (s, 2H), 2.76 (t, *J* = 8.2 Hz, 2H), 1.21 (t, *J* = 8.2 Hz, 2H).

^{13}C {^{1}H} NMR (126 MHz, Chloroform-*d*) δ 142.4, 141.1, 136.4, 131.7, 129.4, 128.7, 127.7, 119.7, 117.8, 105.7, 30.4, 16.9 (B<u>*C*</u>H_2R - identified by HSQC)

^{11}B NMR (160 MHz, Chloroform-*d*) δ 31.9.

IR(ν_{max}) 3420 (w), 1628 (w), 1599 (s)

MS HRMS-ESI (m/z): Found 307.1176, [M+H] ($C_{18}H_{17}BClN_2$) requires 307.1168

m.p. 121-123 °C (pet. eth)

Data were in accordance with those previously reported.[334]

4-1h; 2-(4-bromophenethyl)-2,3-dihydro-1*H*-naphtho[1,8-*de*] [1,3,2]diazaborinine (ABG-0544)

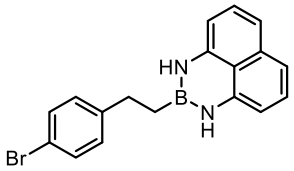

According to general procedure E, 4-bromo-styrene (33 µL, 0.25 mmol) was reacted with HBdan (45.5 mg, 0.25 mmol) in the presence of ^{Mes}TerAlH$_2$ (17.1 mg, 0.05 mmol) for 24 hours at 110 °C to give the product as an amorphous white solid (40 mg, 45% yield).

^{1}H NMR (500 MHz, Chloroform-*d*) δ 7.44 – 7.38 (m, 2H), 7.14 – 7.05 (m, 4H), 7.01 (dd, *J* = 8.3, 1.0 Hz, 2H), 6.27 (dd, *J* = 7.3, 1.1 Hz, 2H), 5.56 (s, 2H), 2.74 (t, *J* = 8.2 Hz, 2H), 1.21 (t, *J* = 8.2 Hz, 2H).

^{13}C {^{1}H} NMR (126 MHz, Chloroform-*d*) δ 142.9, 141.0, 136.4, 131.7, 129.9, 127.7, 119.7, 119.7, 117.8, 105.7, 30.5, 16.8 (B<u>*C*</u>H$_2$R, identified by HSQC).

^{11}B NMR (160 MHz, Chloroform-*d*) δ 31.9.

IR(ν_{max}) 3419 (w), 3393 (w), 1625 (w), 1595 (m)

MS HRMS-ESI (m/z): Found 351.0664, [M+H] ($C_{18}H_{17}BBrN_2$) requires 351.0663

m.p. 140-141 °C (pet. eth)

Data were in accordance with those previously reported.[334]

4-1i; 2-octyl-2,3-dihydro-1*H*-naphtho[1,8-*de*][1,3,2]diazaborinine (ABG-0352/0540)

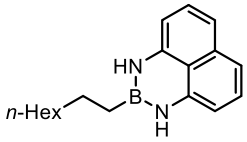

According to general procedure E, 1-octene (48 µL, 0.25 mmol) was reacted with HBdan (45.5 mg, 0.25 mmol) in the presence of $^{Mes}TerAlH_2$ (0.025 mmol, 8.6 mg) for 24 hours at 110 °C to give the product as a colourless oil that solidifies over several days at room temperature (55 mg, 79% yield).

^{1}H NMR (500 MHz, Chloroform-*d*) δ 7.09 (dd, *J* = 8.3, 7.3 Hz, 2H), 6.99 (dd, *J* = 8.3, 1.0 Hz, 2H), 6.29 (dd, *J* = 7.3, 1.0 Hz, 2H), 5.60 (s, 2H), 1.48 – 1.38 (m, 2H), 1.37 – 1.24 (m, 10H), 0.94 – 0.84 (m, 5H).

^{13}C {^{1}H} NMR (126 MHz, Chloroform-*d*) δ 141.4, 136.4 (identified by HMBC) 127.7, 119.5 (identified by HMBC), 117.5, 105.5, 32.7, 32.1, 29.7, 29.4, 25.0, 22.8, 14.3.

^{11}B NMR (160 MHz, Chloroform-*d*) δ 32.0

IR (neat) 3435, 3429, 3053, 2959, 2948, 2920, 2853, 1627, 1598, 1507, 1412, 1369, 1332, 1315, 1131, 817, 758, 724, 607.

MS HRMS-EI (m/z): Found 280.2099, [M•+] ($C_{18}H_{25}BN_2$) requires 280.2105

m.p. 29-30 °C (pentane)

All data were in accordance with those previously reported.[441]

4-1j; 2-(2-cyclohexylethyl)-2,3-dihydro-1*H*-naphtho[1,8-*de*][1,3,2]diazaborinine (ABG-0371)

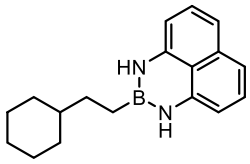

According to general procedure E vinyl cyclohexane (42 µL, 0.3 mmol) was reacted with HBdan (45.5 mg, 0.25 mmol) in the presence of $^{Mes}TerAlH_2$ (0.05 mmol, 17.1 mg) for 16 hours at 80 °C to give the product as an amorphous white solid (59 mg, 85% yield; NMR yield: 85%).

^{1}H NMR (500 MHz, Chloroform-*d*) δ 7.03 (dd, *J* = 8.3, 7.3 Hz, 2H), 6.94 (dd, *J* = 8.3, 1.0 Hz, 2H), 6.24 (dd, *J* = 7.3, 1.0 Hz, 2H), 1.75 – 1.62 (m, 3H), 1.64 – 1.56 (m, 1H), 1.30 – 1.22 (m, 2H), 1.23 – 1.03 (m, 4H), 0.90 – 0.76 (m, 5H).

^{13}C {^{1}H} NMR (126 MHz, Chloroform-*d*) δ 141.4, 136.5, 127.7, 119.7, 117.5, 105.5, 40.0, 33.4, 32.5, 26.9, 26.6, 12.5.

^{11}B NMR (160 MHz, Chloroform-*d*) δ 32.3.

IR(ν_{max}) 3425 (m), 2918 (m), 2918 (m), 2846 (m), 1628 (w), 1596 (s)

MS HRMS-EI (m/z): Found 278.1951, [M•+] ($C_{18}H_{23}BN_2$) requires 278.1949

m.p. 101-103 °C (hexane/Et_2O)

4-1k; 2-(2-(bicyclo[2.2.1]hept-5-en-2-yl)ethyl)-2,3-dihydro-1*H*-naphtho[1,8-*de*][1,3,2]diazaborinine (ABG-0565)

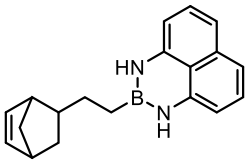

According to general procedure E, 5-vinyl-2-norbornene (mixture of *endo* and *exo*; 37.6 µL, 0.25 mmol) was reacted with HBdan (45.5 mg, 0.25 mmol) in the presence of ^{Mes}TerAlH$_2$ (8.6 mg, 0.025 mmol) for 48 hours to give the product as a colourless oil (39 mg, 54% yield).

Isolated as a mixture of endo-and exo-isomers, reflected in NMR spectra.

^{1}H NMR (500 MHz, Chloroform-*d*) δ 7.14 – 7.06 (m, 2H), 7.02 – 6.97 (m, 2H), 6.30 (ddd, *J* = 7.3, 3.8, 1.0 Hz, 2H), 6.18 – 5.93 (m, 2H), 5.60 and 5.58 (overlapping s, 2H; N*H* for *endo*- and *exo*- isomer), 2.86 – 2.54 (m, 2H), 2.04 – 1.96 (m, 1H), 1.88 (ddd, *J* = 11.2, 8.9, 3.9 Hz, 1H), 1.41 (dq, *J* = 8.0, 2.1 Hz, 1H), 1.39 – 1.27 (m, 1H), 1.27 – 1.17 (m, 2H), 0.91 – 0.78 (m, 2H), 0.54 (ddd, *J* = 11.3, 4.4, 2.6 Hz, 1H).

^{13}C {^{1}H} NMR (126 MHz, Chloroform-*d; major isomer only*) δ 141.3, 137.4, 136.5, 132.4, 127.7, 119.7, 117.5, 105.5, 49.8, 45.4, 42.7, 41.5, 32.6, 29.8, 14.1 (B*C*H$_2$R - identified by HSQC).

^{11}B NMR (160 MHz, Chloroform-*d*) δ 32.1.

IR(ν_{max}) 3404 (w), 2962 (w), 2932 (w), 2863 (w), 1628 (w), 1596 (s)

MS HRMS-ESI (m/z): Found 289.1876, [M+H] ($C_{19}H_{22}BN_2$) requires 289.1871

4-1l; 2-5-((triisopropylsilyl)oxy)pentyl)-2,3-dihydro-1*H*-naphtho[1,8-*de*][1,3,2]diazaborinine (ABG-0589)

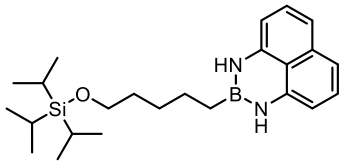

According to general procedure E, triisopropyl(pent-4-en-1-yloxy)silane (60.6 mg, 0.25 mmol) was reacted with HBdan (45.5 mg, 0.25 mmol) in the presence of $^{Mes}TerAlH_2$ (17.1 mg, 0.05 mmol) for 24 hours at 110 °C to give the product as a colourless oil (76.4 mg, 75% yield).

^{1}H NMR (500 MHz, Chloroform-*d*) δ 7.09 (dd, *J* = 8.3, 7.3 Hz, 2H), 7.00 (dd, *J* = 8.3, 1.0 Hz, 2H), 6.29 (dd, *J* = 7.3, 1.0 Hz, 2H), 5.60 (s, 2H), 3.70 (t, *J* = 6.6 Hz, 2H), 1.59 (app. p, *J* = 6.8 Hz, 2H), 1.51 – 1.38 (m, 4H), 1.14 – 0.99 (m, 21H), 0.88 (t, *J* = 7.8 Hz, 2H).

^{13}C {^{1}H} NMR (126 MHz, Chloroform-*d*) δ 141.4, 136.5, 127.7, 119.7, 117.5, 105.5, 63.6, 33.1, 28.9, 24.9, 18.2, 15.4 (B*C*H$_2$R, identified by HSQC), 12.2.

^{11}B NMR (160 MHz, Chloroform-*d*) δ 32.1.

^{29}Si NMR (99 MHz, Chloroform-*d*) δ 12.1.

IR(ν_{max}) 3441 (w), 3406 (w), 2938 (m), 2890 (m) 2864 (m), 1628 (w), 1601 (s)

MS HRMS-EI (m/z): Found 410.2924, [M•+] ($C_{24}H_{39}BN_2OSi$) requires 410.2919

4-1m; 2-(4-(*p*-tolylthio)butyl)-2,3-dihydro-1*H*-naphtho[1,8-*de*][1,3,2]diazaborinine (ABG-0590)

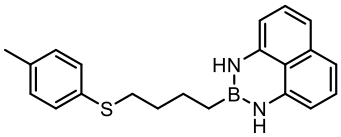

According to general procedure E, but-3-en-1-yl(p-tolyl)sulfane (44.6 mg, 0.25 mmol) was reacted with HBdan (45.5 mg, 0.25 mmol) in the presence of $^{Mes}TerAlH_2$ (17.1 mg, 0.05 mmol) for 24 hours at 110 °C to give the product as an amorphous white solid (61 mg, 71% yield).

^{1}H NMR (500 MHz, Chloroform-*d*) δ 7.28 – 7.24 (m, 2H), 7.13 – 7.06 (m, 4H), 7.00 (dd, *J* = 8.3, 1.0 Hz, 2H), 6.28 (dd, *J* = 7.3, 1.0 Hz, 2H), 5.58 (s, 2H), 2.92 (t, *J* = 7.1 Hz, 2H), 2.31 (s, 3H), 1.74 – 1.65 (m, 2H), 1.63 – 1.53 (m, 2H), 0.87 (t, *J* = 8.1 Hz, 2H).

^{13}C {^{1}H} NMR (126 MHz, Chloroform-*d*) δ 141.2, 136.5, 136.2, 133.0, 130.1, 129.8, 127.7, 119.7, 117.6, 105.6, 34.4, 31.9, 23.9, 21.1, 14.8 (B<u>C</u>H_2R, identified by HSQC).

^{11}B NMR (160 MHz, Chloroform-*d*) δ 32.1.

IR(ν_{max}) 3403 (w), 2921 (w), 1628 (w), 1597 (s)

MS HRMS-EI (m/z): Found 346.1673, [M•+] ($C_{21}H_{23}BN_2S$) requires 346.1670

4-1n; 2-(4-bromophenethyl)-2,3-dihydro-1*H*-naphtho[1,8-*de*] [1,3,2]diazaborinine (ABG-0594)

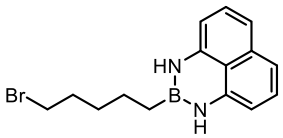

According to general procedure E, 5-bromopent-1-ene (31 µL, 0.25 mmol) was reacted with HBdan (45.5 mg, 0.25 mmol) in the presence of $^{Mes}TerAlH_2$ (17.1 mg, 0.05 mmol) for 72 hours at 45 °C to give the product as an amorphous white solid (42 mg, 53% yield).

^{1}H NMR (500 MHz, Chloroform-*d*) δ 7.09 (dd, *J* = 8.3, 7.3 Hz, 2H), 7.00 (dd, *J* = 8.3, 1.0 Hz, 2H), 6.30 (dd, *J* = 7.3, 1.1 Hz, 2H), 5.60 (s, 2H), 3.44 (t, *J* = 6.8 Hz, 2H), 1.95 – 1.86 (m, 2H), 1.56 – 1.43 (m, 4H), 0.99 – 0 .80 (m, 2H).

^{13}C {^{1}H} NMR (126 MHz, Chloroform-*d*) δ 141.2, 136.5, 127.7, 119.7, 117.6, 105.6, 34.0, 32.7, 31.0, 24.1, 15.2 (B<u>*C*</u>H_2R, identified by HSQC).

^{11}B NMR (160 MHz, Chloroform-*d*) δ 32.0.

IR(ν_{max}) 3406 (m), 2923 (m), 1628 (m), 1597 (s)

MS HRMS-EI (m/z): Found 316.0741, [M•+] ($C_{15}H_{18}BBrN_2$) requires 316.0744

m.p. 67-68°C (EtOAc/pet. ether)

4-1o; 2-(2-methylpentyl)-2,3-dihydro-1*H*-naphtho[1,8-*de*][1,3,2]diazaborinine (ABG-0389)

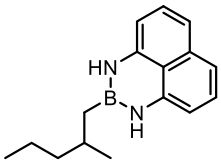

According to general procedure E, 2-methyl-1-pentene (38 µL, 0.3 mmol) was reacted with HBdan (45.5 mg, 0.25 mmol) in the presence of ^{Mes}TerAlH$_2$ (0.05 mmol, 17.1 mg) at 110 °C for 16 hours to give the product as a colourless oil (51 mg, 81% yield).

^{1}H NMR (500 MHz, Chloroform-*d*) δ 7.10 (dd, *J* = 8.3, 7.3 Hz, 2H), 7.00 (dd, *J* = 8.3, 1.0 Hz, 2H), 6.30 (dd, *J* = 7.3, 1.0 Hz, 2H), 5.60 (s, 2H), 1.73 – 1.59 (m, 1H), 1.45 – 1.25 (m, 3H), 1.25 – 1.15 (m, 1H), 0.96 (d, *J* = 6.6 Hz, 3H), 0.95 – 0.87 (m, 4H), 0.69 (dd, *J* = 14.9, 8.4 Hz, 1H).

^{13}C {^{1}H} NMR (126 MHz, Chloroform-*d*) δ 141.4, 136.5, 127.7, 119.7, 117.5, 105.5, 42.3, 30.2, 22.6, 20.6, 14.5. (B<u>*C*</u>H$_2$R resonances not observed, presumably due to quadrupolar line broadening from boron atom).

^{11}B NMR (160 MHz, Chloroform-*d*) δ 31.92.

IR(ν_{max}) 3404 (w), 2953 (w), 2969 (w), 1628 (w), 1597 (s)

MS HRMS-EI (m/z): Found 252.1790, [M•+] ($C_{16}H_{21}BN_2$) requires 252.1792

4-1p; 2-(2-(4-methylcyclohex-3-en-1-yl)propyl)-2,3-dihydro-1*H*-naphtho[1,8-*de*][1,3,2]diazaborinine (ABG-0554)

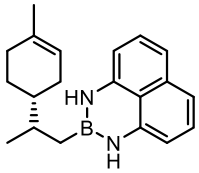

According to general procedure E, (R)-(+)-limonene (43 µL, 0.25 mmol) was reacted with HBdan (45.5 mg, 0.25 mmol) in the presence of $^{Mes}TerAlH_2$ (17.1 mg, 0.05 mmol) for 48 hours at 110 °C to give the product as a colourless oil (54 mg, 72%% yield).

Isolated as mixture of diastereomers, reflected in the NMR.

^{1}H NMR (500 MHz, Chloroform-*d*) δ 7.09 (dd, *J* = 8.2, 7.3 Hz, 2H), 7.00 (dd, *J* = 8.3, 1.0 Hz, 2H), 6.30 (app. dt, *J* = 7.3, 1.0 Hz, 2H), 5.61 (s, 2H), 5.39 (app. s, 1H), 2.03 – 1.91 (m, 2H), 1.85 – 1.71 (m, 2H), 1.65 (s, 3H), 1.63 – 1.55 (m, 1H), 1.45 – 1.35 (m, 1H), 1.34 – 1.20 (m, 1H), 1.04 (dt, *J* = 15.0, 5.6 Hz, 1H; *C*H$_2$*B*), 0.95 (app. t, *J* = 6.4 Hz, 3H), 0.72 – 0.58 (m, 1H; *C*H$_2$*B*).

^{13}C {^{1}H} NMR (126 MHz, Chloroform-*d*) δ 141.4, 136.5, 134.2, 127.7, 121.1, 119.7, 117.5, 105.6, 40.8, 40.7, 34.9, 34.6, 31.1, 31.0, 29.5, 28.4, 27.2, 26.1, 23.6, 21.2 (B*C*H$_2$R - identified by HSQC), 20.9 (B*C*H$_2$R - identified by HSQC), 19.6, 19.1.

^{11}B NMR (160 MHz, Chloroform-*d*) δ 32.3.

IR(ν_{max}) 3409 (w) 2956 (w), 2909 (w), 1628 (w), 1601 (s)

MS HRMS-EI (m/z): Found 304.2112, [M•+] ($C_{20}H_{25}BN_2$) requires 304.2105

4-1q; 2-(((1*R*,5*R*)-6,6-dimethylbicyclo[3.1.1]heptan-2-yl)methyl)-2,3-dihydro-1*H*-naphtho[1,8-*de*][1,3,2]diazaborinine (ABG-0562)

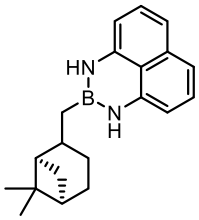

According to general procedure E, (−)-β-pinene (40 µL, 0.25 mmol) was reacted with HBdan (45.5 mg, 0.25 mmol) in the presence of ^{Mes}TerAlH$_2$ (17.1 mg, 0.05 mmol) for 48 hours at 110 °C to give the product as a colourless oil (49 mg, 64% yield).

Isolated as mixture of diastereomers, reflected in the NMR.

^{1}H NMR (500 MHz, Chloroform-*d*) δ 7.09 (dd, *J* = 8.3, 7.3 Hz, 2H), 7.00 (dd, *J* = 8.3, 1.0 Hz, 2H), 6.29 (dt, *J* = 7.3, 1.1 Hz, 2H), 5.60 (s, 2H) (mixture of diastereomers renders remaining aliphatic protons difficult to identify.

^{13}C {^{1}H} NMR (126 MHz, Chloroform-*d*) δ 141.4, 136.5, 127.7, 119.7, 117.5, 105.5, 48.8, 48.5, 41.5, 40.9, 39.8, 39.0, 38.4, 34.3, 32.1, 28.5, 27.0, 26.8, 25.0, 24.9, 24.8, 23.6, 23.3, 20.3. (B<u>*C*</u>H$_2$R resonances not observed, presumably due to quadrupolar line broadening from boron atom).

^{11}B NMR (160 MHz, Chloroform-*d*) δ 31.8.

IR(ν_{max}) 3404 (w), 2976 (w), 2898 (m), 2865 (m), 1628 (w), 1596 (s)

MS HRMS-ESI (m/z): Found 305.2190, [M+H] ($C_{20}H_{26}BN_2$) requires 305.2184

4-1r; 2-((*S*)-2-methyl-4-((1*S*,6*R*)-1,2,6-trimethylcyclohex-2-en-1-yl)butyl)-2,3-dihydro-1*H*-naphtho[1,8-*de*][1,3,2]diazaborinine (ABG-0563)

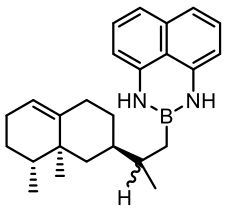

According to general procedure E, (+)-valencene (79 µL, 0.25 mmol, 70% purity) was reacted with HBdan (45.5 mg, 0.25 mmol) in the presence of $^{Mes}TerAlH_2$ (17.1 mg, 0.05 mmol) for 48 hours at 110 °C to give the product as a colourless oil (65 mg, 70% yield).

Product was isolated as a mixture of diastereomers, and is reflected in the NMR spectra:

^{1}H NMR (500 MHz, Chloroform-*d*) δ 7.10 (dd, *J* = 8.3, 7.3 Hz, 2H), 7.00 (dd, *J* = 8.3, 1.0 Hz, 2H), 6.29 (dd, *J* = 7.3, 1.0 Hz, 2H), 5.60 (s, 2H), 5.32 (dt, *J* = 4.6, 2.1 Hz, 1H), 2.26 (tdq, *J* = 12.9, 5.0, 2.5 Hz, 1H), 2.13 – 1.98 (m, 2H), 1.98 – 1.89 (m, 1H), 1.83 (dq, *J* = 12.5, 2.8 Hz, 1H), 1.73 (dddt, *J* = 12.5, 9.9, 4.8, 2.5 Hz, 1H), 1.68 – 1.57 (m, 1H: diastereomer A), 1.57 – 1.47 (m, 2H), 1.45 – 1.37 (m, 3H), 1.37 – 1.08 (m, 1H: diastereomer B), 1.08 – 0.94 (m, 2H), 0.94 – 0.87 (m, 6H), 0.87 – 0.75 (m, 2H), 0.64 (ddd, *J* = 17.7, 14.9, 9.8 Hz, 1H).

^{13}C {^{1}H} NMR (126 MHz, Chloroform-*d*) δ 144.0, 141.4, 136.5, 127.7, 119.9, 119.9, 119.7, 117.5, 105.5, 43.9, 42.6, 41.3, 41.3, 40.2, 40.1, 38.0, 37.9, 35.3, 35.3, 33.0, 33.0, 31.7, 30.5, 27.4, 27.3, 26.1, 19.4, 19.0, 18.8, 18.8, 15.9, 15.8.

(B<u>*C*</u>H_2R resonances not observed, presumably due to quadrupolar line broadening from boron atom; mixture of diastereomers explains extra resonances).

^{11}B NMR (160 MHz, Chloroform-*d*) δ 32.2.

IR(ν_{max}) 3404 (w), 2964 (w), 2914 (m), 1628 (w), 1599 (s)

MS HRMS-ESI (m/z): Found 373.2813, [M+H] ($C_{25}H_{34}BN_2$) requires 373.2810

7.5.3 Alkyl Bdan derivatisations

4-3a; 5-(1*H*-naphtho[1,8-*de*][1,3,2]diazaborinin-2(3*H*)-yl)pentan-1-ol (ABG-0592)

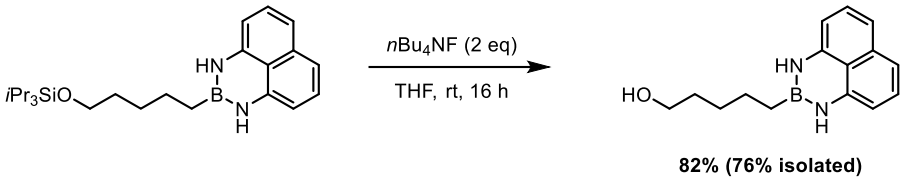

82% (76% isolated)

Tetrabutylammonium fluoride (1 M in THF, 0.28 mL, 0.28 mmol, 2 equiv.) was added to a solution of silylether **4-1l** (57.5 mg, 0.14 mmol) in THF (0.7 mL) at room temperature. The reaction stirred for 16 hours then diluted with Et_2O (3 mL) to give a white precipitate. The organic phase was washed with brine (2 × 3 mL), dried with $MgSO_4$, filtered and volatiles removed *in vacuo*. Mesitylene (20 µL) was added as an internal standard and the crude was analysed by ^{1}H NMR spectroscopy (82% NMR yield). The product was purified with column chromatography (90:10 → 0:100 petroleum ether (40/60):EtOAc) to give the product as an amorphous white solid (27 mg, 76% yield).

^{1}H NMR (500 MHz, Chloroform-*d*) δ 7.09 (dd, *J* = 8.3, 7.3 Hz, 2H), 7.00 (dd, *J* = 8.3, 1.0 Hz, 2H), 6.30 (dd, *J* = 7.3, 1.0 Hz, 2H), 5.62 (s, 2H), 3.67 (t, *J* = 6.6 Hz, 2H), 1.62 (p, *J* = 6.8 Hz, 2H), 1.53 – 1.38 (m, 4H), 1.24 (s, 1H), 0.89 (t, *J* = 7.7 Hz, 2H).

^{13}C {^{1}H} NMR (126 MHz, Chloroform-*d*) δ 141.3, 136.5, 127.7, 119.7, 117.5, 105.6, 63.1, 32.7, 28.7, 24.7, 15.3 (B<u>*C*</u>H_2R, identified by HSQC).

^{11}B NMR (160 MHz, Chloroform-*d*) δ 32.0.

IR(ν_{max}) 3572 (w, *br*), 3399 (w), 3337 (w, *br*), 2923 (w), 2853 (w), 1627 (w), 1595 (s)

MS HRMS-EI (m/z): Found 254.1587, [M•+] ($C_{15}H_{19}BN_2O$) requires 254.1585

4-3b; 10,11,12,13-tetrahydro-7*H*,9*H*-naphtho[1',8':4,5,6][1,3,2]diazaborinino[1,2-*a*][1,2]azaborepine (ABG-0598-A)

Procedure X:

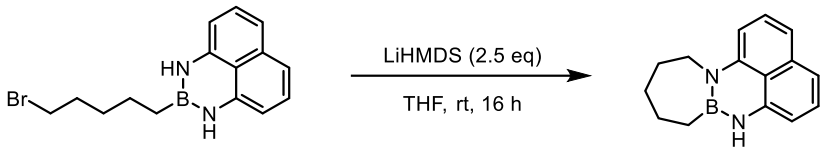

42% (34% isolated)

LiHMDS (1 M in THF, 0.1 mL, 0.01 mmol, 2.5 equiv.) was added to a solution of alkyl bromide **4-1n** (12.6 mg, 0.04 mmol) in THF (0.5 mL) at room temperature. The solution was left for 16 hours, then diluted with Et_2O (1 mL) and quenched with sat. aqueous NH_4Cl. The phases were separated and the aqueous phase was extracted with Et_2O (3 × 1 mL). The combined organic phases were dried with $MgSO_4$, filtered and volatiles removed *in vacuo*. Mesitylene (10 µL) was added as internal standard and the crude was analysed by ^{1}H NMR (42% NMR yield; alkene by-product was also observed – 8% NMR yield). The crude product was purified by flash chromatography (99:1 → 95:5 petroleum ether (40/60):EtOAc) to give the product as an amorphous white solid (3.2 mg, 34% yield).

^{1}H NMR (500 MHz, Chloroform-*d*) δ 7.18 (app. t, *J* = 8.0 Hz, 1H), 7.10 (dd, *J* = 8.2, 7.3 Hz, 1H), 7.01 (ddd, *J* = 8.3, 4.3, 1.0 Hz, 2H), 6.48 (d, *J* = 7.8 Hz, 1H), 6.38 – 6.19 (m, 1H), 5.72 (s, 1H), 3.61 (dd, *J* = 6.4, 2.9 Hz, 2H), 1.74 (qt, *J* = 4.4, 3.2, 2.7 Hz, 4H), 1.71 – 1.64 (m, 2H), 1.16 – 1.01 (m, 2H).

^{13}C {^{1}H} NMR (126 MHz, Chloroform-*d*) δ 143.7, 140.8, 136.7, 127.8, 127.3, 120.5, 117.5, 117.2, 105.5, 102.4, 46.2, 30.9, 28.5, 23.5, 16.0 (B<u>*C*</u>H_2R, identified by HSQC).

^{11}B NMR (160 MHz, Chloroform-*d*) δ 33.4.

IR(ν_{max}) 3404 (w), 2917 (w), 1624 (m), 1590 (s)

MS HRMS-EI (m/z): Found 236.1479, [M•+] ($C_{15}H_{17}BN_2$) requires 236.1479

m.p. 105-106 °C (hexane/Et_2O)

Procedure Y:

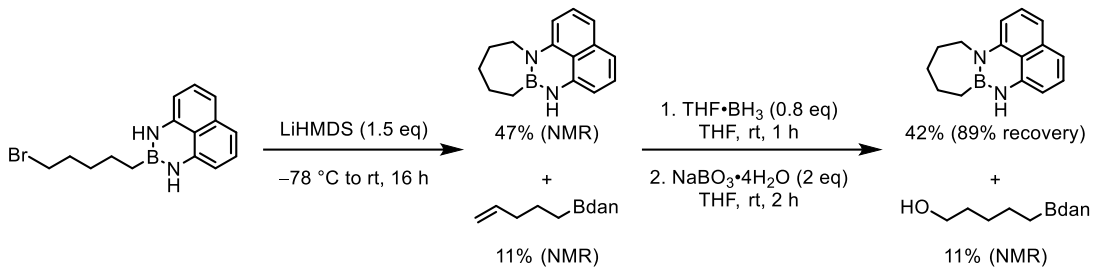

LiHMDS (1 M in THF, 0.2 mL, 0.02 mmol, 1.5 equiv.) was added to a solution of alkyl bromide **4-1n** (42.4 mg, 0.134 mmol) in THF (2.7 mL) at –78 °C. The reaction was slowly warmed over 16 hours and then quenched with aq. sat. NH_4Cl solution and diluted with Et_2O (10 mL). The phases were separated and the aqueous phase was extracted with Et_2O (3 × 5 mL) and the combined organic phases were washed with brine and then dried over $MgSO_4$, filtered and volatiles removed *in vacuo*. Mesitylene (20 µL) was added as internal standard and the crude was analysed by ^1H NMR spectroscopy. The crude was redissolved in THF (0.25 mL) and then THF•BH_3 (1 M in THF, 0.8 equiv. 0.1 mL) was added at room temperature. The solution was stirred for 1 hour and then $NaBO_3$•$4H_2O$ (43.0 mg, 0.268 mmol, 2 equiv.) was added in one portion, followed by the dropwise addition of H_2O (0.3 mL) – *caution: H_2 evolved*. The biphasic solution was vigorously stirred at room temperature for 2 hours and then diluted with Et_2O (3 mL) and quenched with sat. aq. Na_2SO_3 solution. The phases were separated and the aqueous phase was extracted with Et_2O (3 × 2 ml). The combined organic phases were dried with $MgSO_4$, filtered and the solvent removed *in vacuo* to give the crude product. The product was purified by flash chromatography (99:1 → 0:100 petroleum ether (40/60):EtOAc) to give the product as an amorphous white solid (13.2 mg, 42% yield).

4-3d; 2-(4-(*p*-tolylsulfinyl)butyl)-2,3-dihydro-1*H*-naphtho[1,8-*de*][1,3,2]diazaborinine (ABG-0601-A)

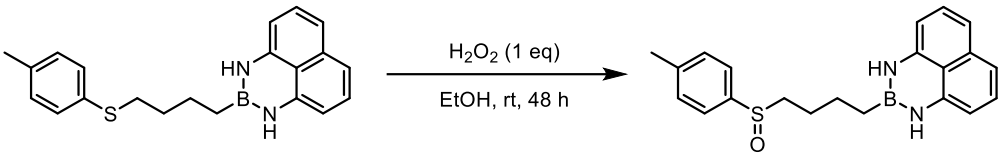

42% (33% isolated)

H_2O_2 (30% w/w in H_2O, 3 µL, 0.03 mmol, 1 equiv.) was added to a suspension of sulfide **4-1m** (10.4 mg, 0.03 mmol) in EtOH (0.4 mL). The suspension was stirred for 72 hours at room temperature, then the volatiles were removed over a flow of N_2. The crude was dissolved in Et_2O (1 mL) and quenched with sat. aqueous Na_2SO_3 solution. The organic phase was separated and the aqueous phase was extracted with Et_2O (3 × 1 mL). The combined organic phases were dried with $MgSO_4$, filtered and volatiles removed *in vacuo*. Mesitylene (10 µL) was added and the crude was analysed by ^{1}H NMR spectroscopy (42% NMR yield). The product was purified by column chromatography (99:1 → 0:100 petroleum ether (40/60):EtOAc) to give the product as a colourless oil (4.8 mg, 33% yield).

^{1}H NMR (500 MHz, Chloroform-*d*) δ 7.56 – 7.42 (m, 2H), 7.30 (d, *J* = 8.0 Hz, 2H), 7.09 (dd, *J* = 8.3, 7.3 Hz, 2H), 7.04 – 6.96 (m, 2H), 6.30 (dd, *J* = 7.3, 0.9 Hz, 2H), 5.68 (s, 2H), 2.82 (t, *J* = 7.3 Hz, 2H), 2.39 (s, 3H), 1.89 – 1.75 (m, *J* = 1H), 1.75 – 1.50 (m, 3H), 0.88 (t, *J* = 7.8 Hz, 2H).

^{13}C {^{1}H} NMR (126 MHz, Chloroform-*d*) δ 141.6, 141.2, 140.9, 136.4, 130.1, 127.7, 124.2, 119.7, 117.6, 105.7, 57.0, 24.9, 24.1, 21.5, 15.0 (B<u>*C*</u>H_2R, identified by HSQC).

^{11}B NMR (160 MHz, Chloroform-*d*) δ 31.8.

IR(ν_{max}) 3405 (w), 3309 (w), 2924 (w), 1628 (m), 1598 (s)

MS HRMS-EI (m/z): Found 362.1619, [M•+] ($C_{21}H_{23}BN_2OS$) requires 362.1619

7.5.4 Stoichiometric experiments

Toluene (0.65 mL) was added to an NMR tube containing the corresponding alkyl alane or (0.05 mmol, 1 equiv.) and HBdan (45.5 mg, 0.25 mmol, 5 equiv.). The mixture was vigorously shaken until dissolution. The resulting solution was left at the specified temperature for 16 hours before analysis by ^{11}B NMR spectroscopy.

Reaction of ^{Mes}TerAlEt$_2$ with HBdan

Room temperature (ABG-0596)

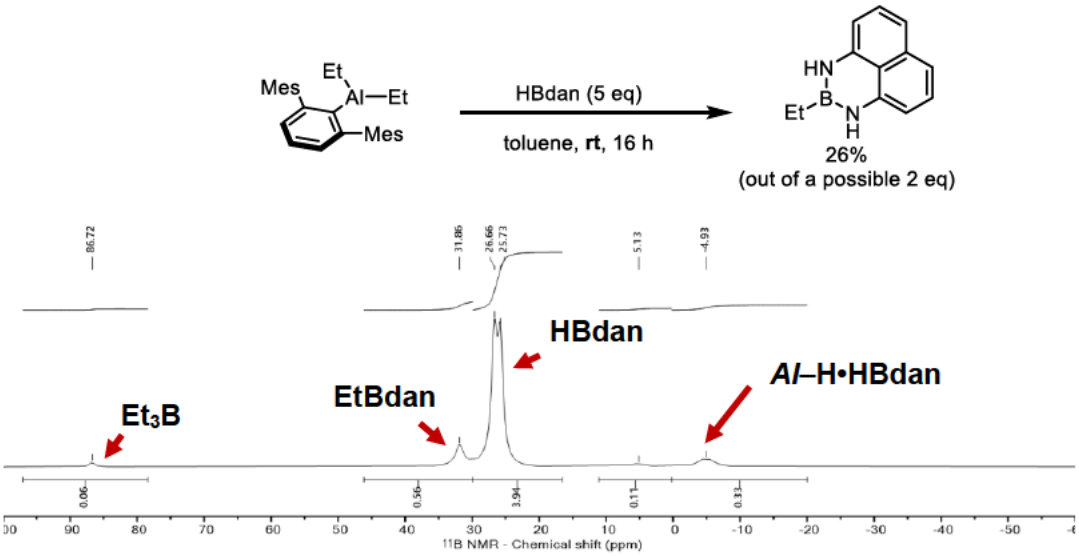

Figure 7-60. ^{11}B NMR spectrum (toluene-*H*8) of ^{Mes}TerAlEt$_2$ + HBdan at rt. (integrated to a total of 5).

80 °C (ABG-0452)

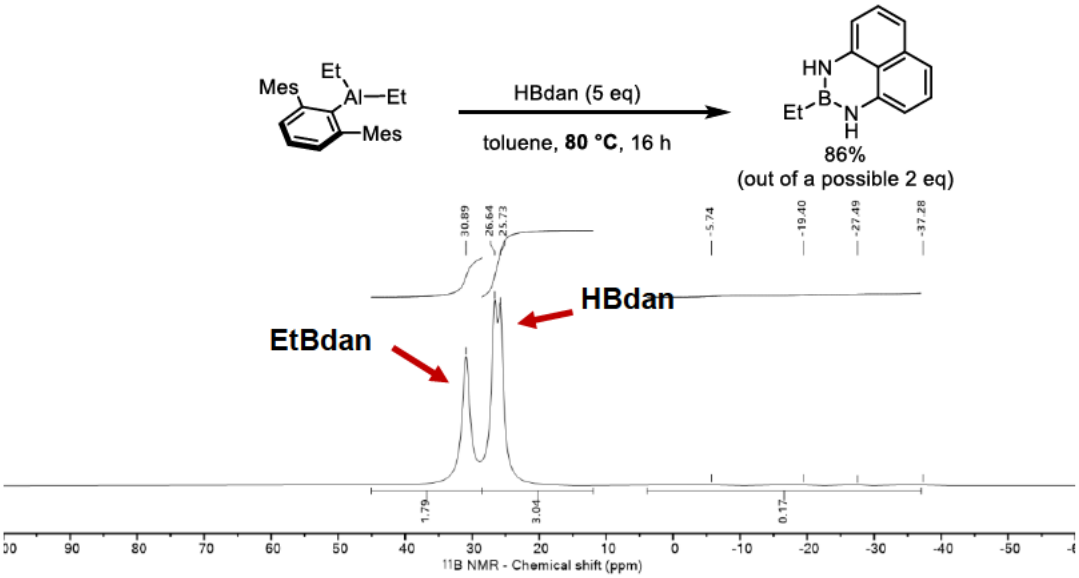

Figure 7-61. ^{11}B NMR spectrum (toluene-*H*-8) of ^{Mes}TerAlEt$_2$ + HBdan at 80 °C (integrated to a total of 5).

Reaction of Et_3Al with HBdan (ABG-0606)

Room temperature

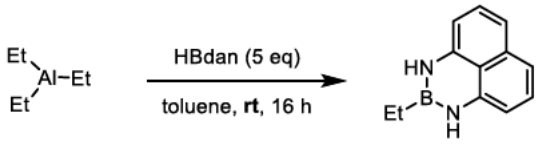

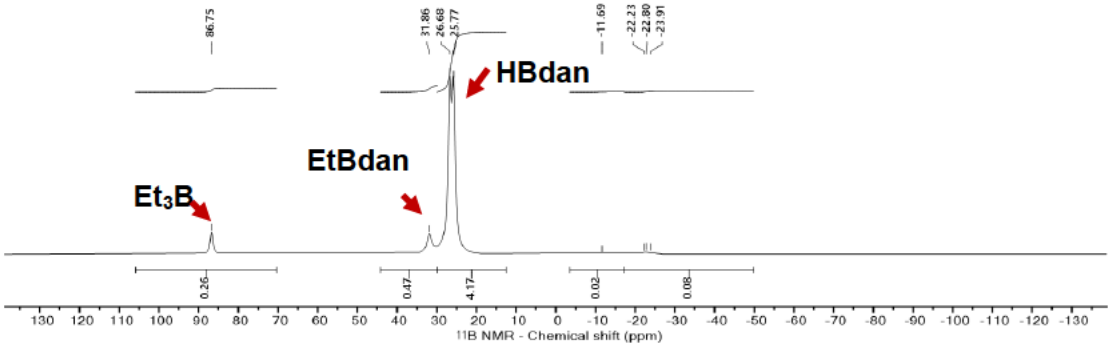

Figure 7-62. ^{11}B NMR spectrum (toluene-*H8*) of Et_3Al + HBdan at rt. (integrated to a total of 5).

80 °C

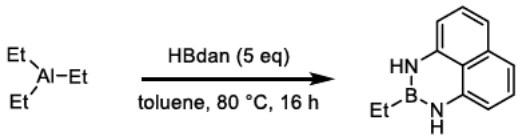

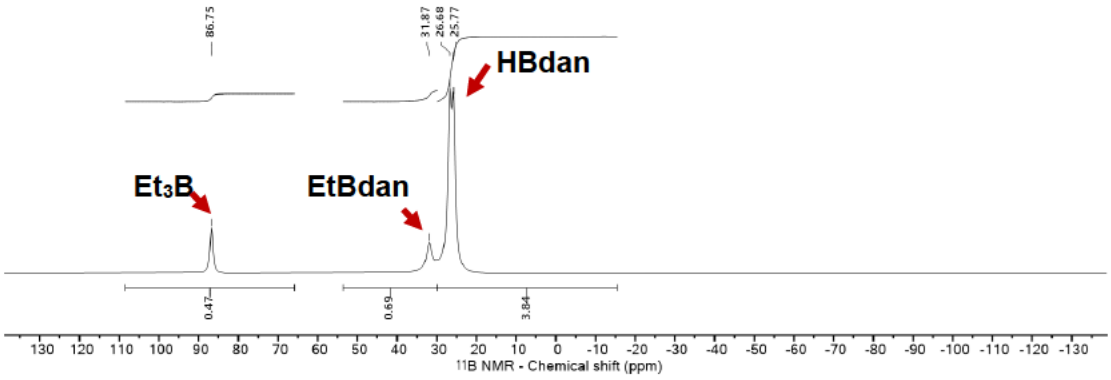

Figure 7-63. ^{11}B NMR spectrum (toluene-*H8*) of Et_3Al + HBdan at 80 °C. (integrated to a total of 5).

Reaction of Et_3B with HBdan (ABG-0453)

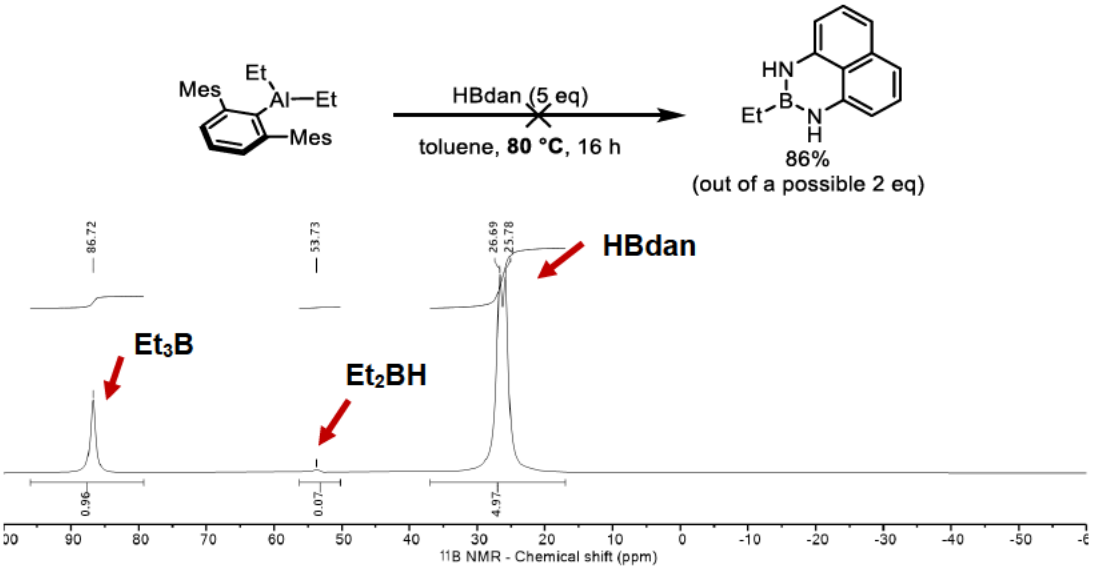

Figure 7-64. ^{11}B NMR spectrum (toluene *H*-8) of the reaction between Et_3B and HBdan (integrated to a total of 6).

7.5.5 Mechanistic insights

Quantifying BH_3 formation under catalytic conditions (ABG-0605)

A mixture of $^{Mes}TerAlH_2$ (8.6 mg, 0.025 mmol, 1 equiv.) and HBdan (45.5 mg, 0.25 mmol, 10 equiv.) was dissolved in toluene (0.2 mL, 1.25 M) and the solution was reacted at 110 °C for 16 hours. The reaction was cooled to room temperature and then *N,N,N′,N′*-tetramethylethylenediamine (TMEDA; 187 µL, 1.25 mmol, 50 equiv.) was added. An aliquot (*ca.* 20 µL) was diluted in $CDCl_3$ and analysed by ^{11}B NMR.

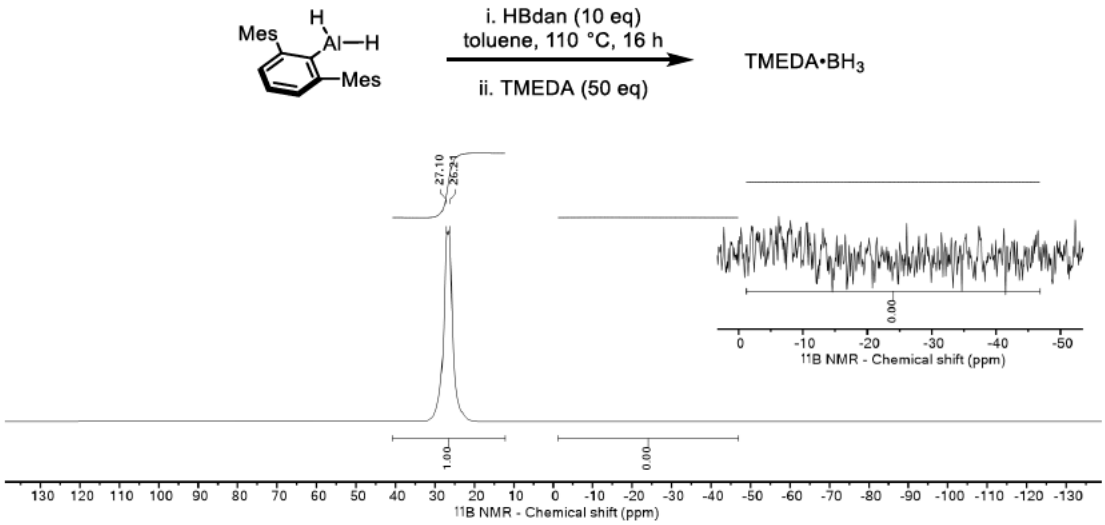

Figure 7-65. ^{11}B NMR spectrum ($CDCl_3$) for the quantification of BH_3 under catalytic conditions using TMEDA quenching[188] *(No TMEDA•BH_3 adduct observed – 4-coordinate boron region highlighted)*

Catalyst + HBdan (ABG-0709)

On Scheme 4.26 and 4.27, the species formed under catalytic conditions were examined accordingly:

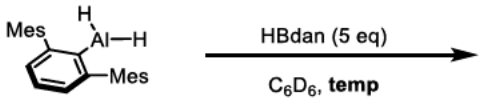

C_6D_6 (0.65 mL) was added to an NMR tube containing ^{Mes}TerAlH$_2$ (8.6 mg, 0.025 mmol, 1 equiv.) and HBdan (45.5 mg, 0.25 mmol, 5 equiv.). The mixture was vigorously shaken until dissolution. The resulting solution was left at the specified temperature and time and analysed by ^{1}H and ^{11}B NMR spectroscopy.

^{1}H-^{15}N HMBC

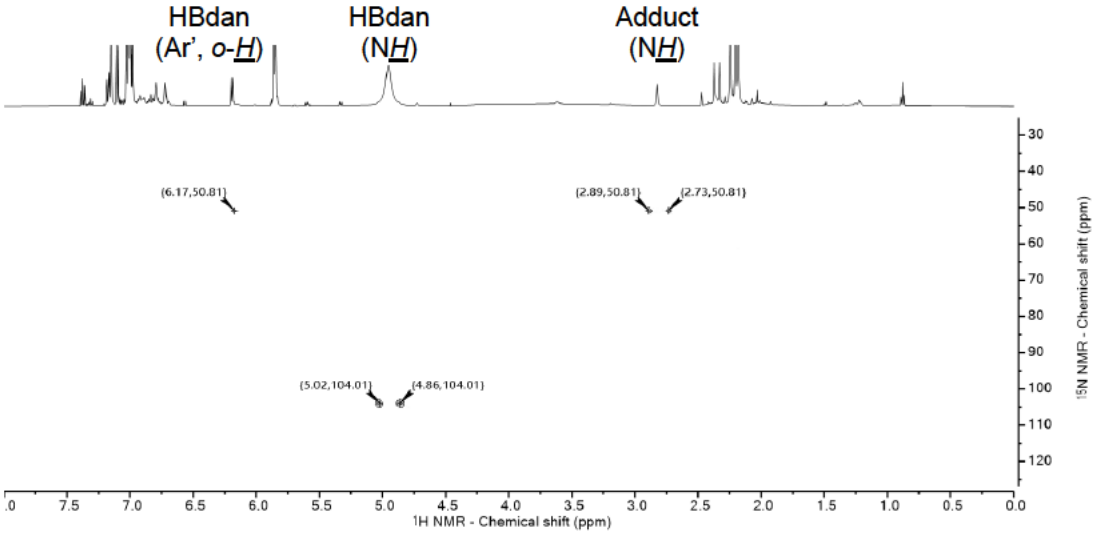

Figure 7-66. ^{1}H-^{15}N HMBC spectrum of the reaction between ^{Mes}TerAlH$_2$ + HBdan (5 equiv.) at rt

Spectral data for ^{Mes}TerAlH$_2$•HBdan:

^{1}H NMR (500 MHz, Benzene-d_6) δ 7.38 (t, J = 7.5 Hz, 1H; Ar', p-H), 7.17 (d, J = 8.2 Hz, 2H; Bdan, 2 × ArH), 7.10 (d, J = 7.5 Hz, 2H; Ar', 2 × m-H), 7.01 – 6.96 (m, 2H; Bdan, 2 × ArH – overlapped with HBdan), 6.76 (app. d, J = 36.3 Hz, 4H; Mes, 4 × m-H), 6.19 (d, J = 7.2 Hz, 2H; Bdan, 2 × ArH), 4.42 – 2.98 (*br* m, 3H; AlH and BH), 2.82 (s, 2H; 2 × NH), 2.24 (s, 6H; Mes, 2 × CH$_3$), 2.21 (s, 6H; Mes, 2 × CH$_3$), 2.18 (s, 6H; Mes, 2 × CH$_3$).

^{11}B NMR (160 MHz, Benzene-d_6) δ -4.61.

^{15}N NMR (51 MHz, Benzene-d_6) δ 50.8

At this point, either:

- THF (0.1 mL, 1.25 mmol, 25 equiv.) was added through a septum at room temperature and the reaction was monitored by ^{11}B NMR spectroscopy (ABG-0709-B-THF)

or

- 4-*t*Bu-styrene (49.2 µL, 0.25 mmol, 5 equiv.) was added through a septum and the reaction was heated at 80°C for 30 minutes and then cooled to room temperature before analysis by NMR spectroscopy.

Diagnostic resonances for ^{Mes}TerAl(R)H•HBdan (ABG-0715):
(i.e. those which are not overlapped by other resonances; R = 4-tBu-phenethyl)

^{1}H NMR (400 MHz, Benzene-d_6) δ 7.40 – 7.34 (t, *J* = 7.5 Hz, 1H; Ar', *p*-H), 6.77 (*app.* d, *J* = 8.5 Hz, 4H; Mes, *m*-H), 6.20 (d, *J* = 7.1 Hz, 2H; Bdan, Ar'H), 3.05 (s, 2H; N*H*), 2.27 (s, 6H; Mes, C*H*$_3$), 2.20 (s, 6H; Mes, C*H*$_3$), 2.14 (s, 6H; Mes, C*H*$_3$), 1.15 (s, 9H; (C*H*$_3$)$_3$), 0.03 – -0.40 (m, 2H; *Al*C*H*$_2$R).

^{11}B NMR (128 MHz, Benzene-d_6) δ -4.8.

7.6 Experimental details for Chapter 5

7.6.1 Screening compatible reagents for Al–X/Si–B σ-bond metathesis

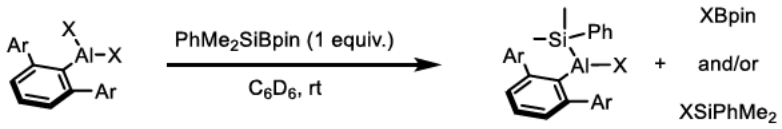

$PhMe_2SiBpin$ (17.5 µL, 0.05 mmol, 1 equiv.) was added to a solution of $^{Ar}TerAlX_2$ (0.05 mmol, 1 equiv.) in C_6D_6 (0.6 mL) at room temperature and monitored by ^1H and ^{11}B NMR spectroscopy over time. In the majority of cases, the reaction is most conveniently tracked by ^{11}B NMR to show if the $PhMe_2SiBpin$ reagent is reacting (and this is provided below).

$^{Ar}TerAlCl_2$ with $PhMe_2SiBpin$

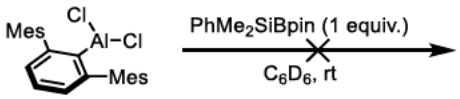

Ar = Mes *(ABG-0640)*

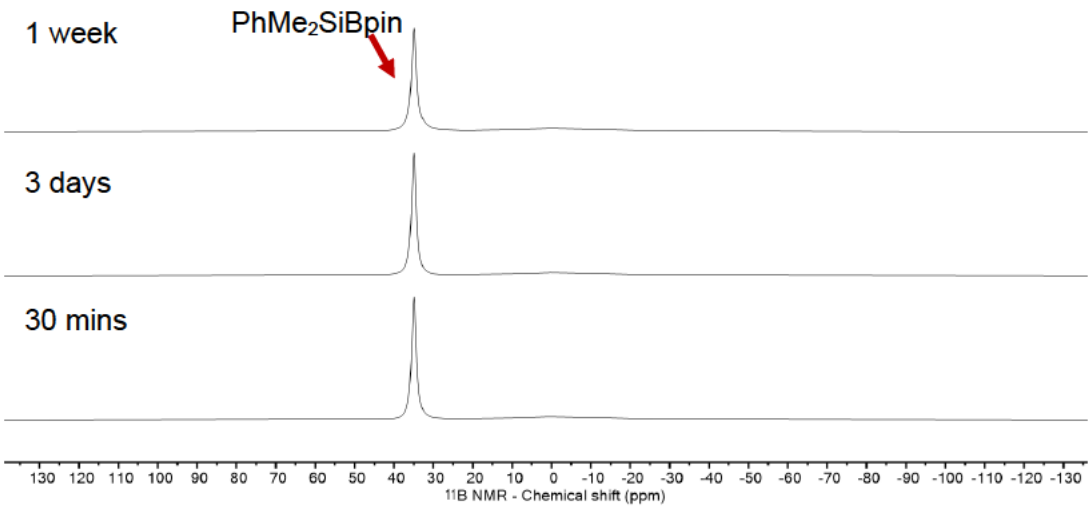

Figure 7-67. Stacked ^{11}B NMR spectra (C_6D_6) of the reaction between $^{Mes}TerAlCl_2$ with $PhMe_2SiBpin$ and monitored over time.

$^{Ar}TerAlH_2$ with $PhMe_2SiBpin$

Ar = Mes *(ABG-0638)*

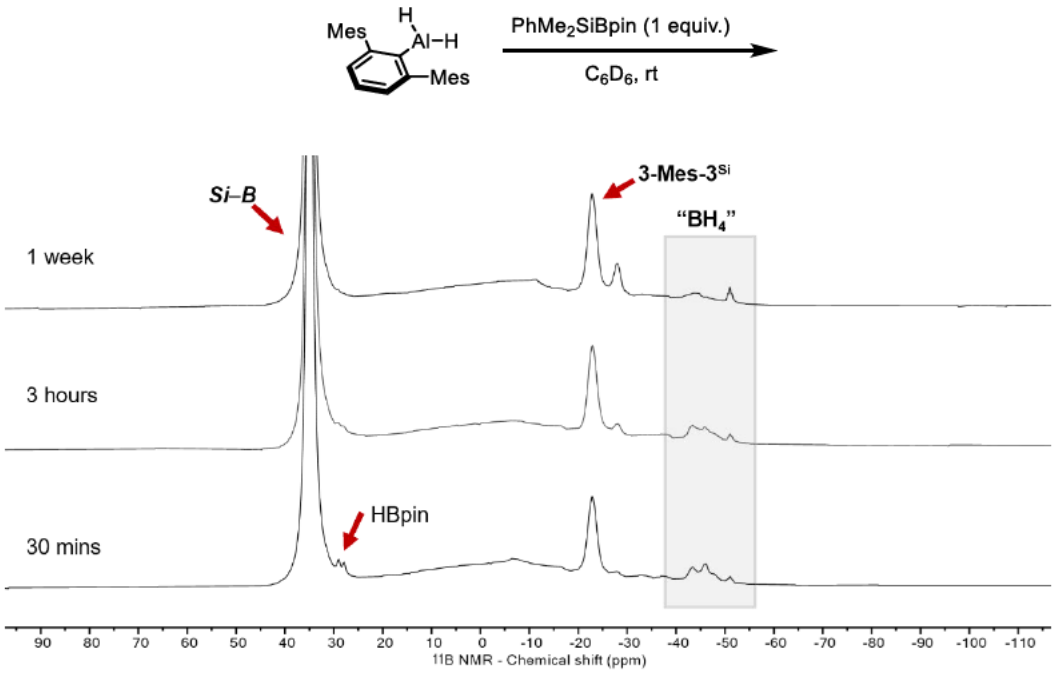

Figure 7-68. Stacked ^{11}B NMR spectra (C_6D_6) of the reaction between $^{Mes}TerAlH_2$ with $PhMe_2SiBpin$ and monitored over time.

Ar = Tipp *(ABG-0649)*

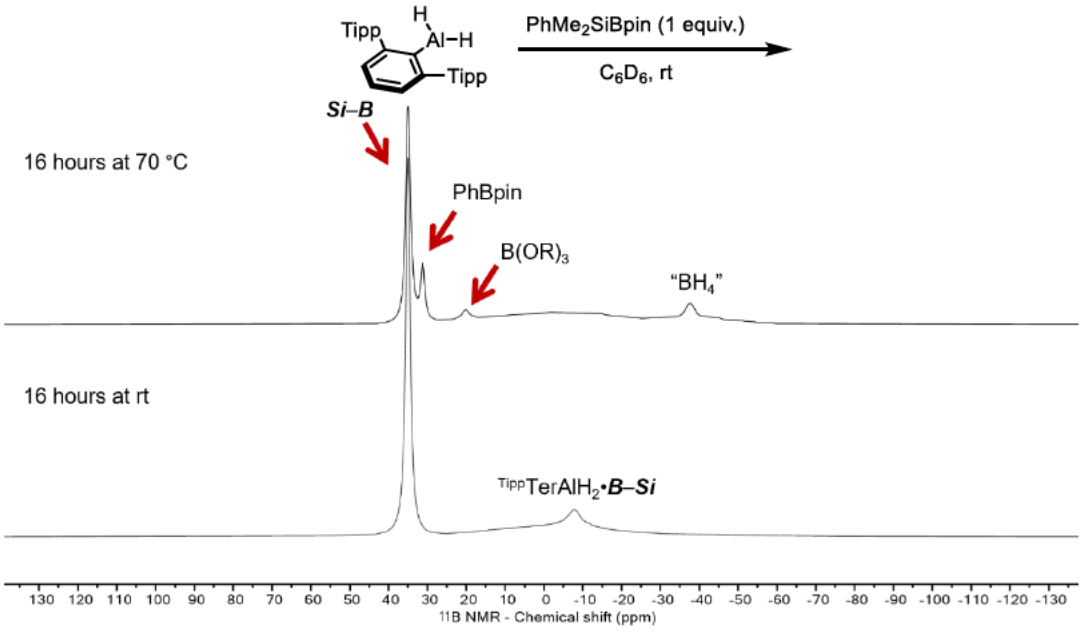

Figure 7-69. Stacked ^{11}B NMR spectra (C_6D_6) of the reaction between $^{Tipp}TerAlH_2$ with $PhMe_2SiBpin$ and monitored over time.

$^{Ar}TerAlMe_2$ with $PhMe_2SiBpin$

Ar = Mes *(ABG-0639)*

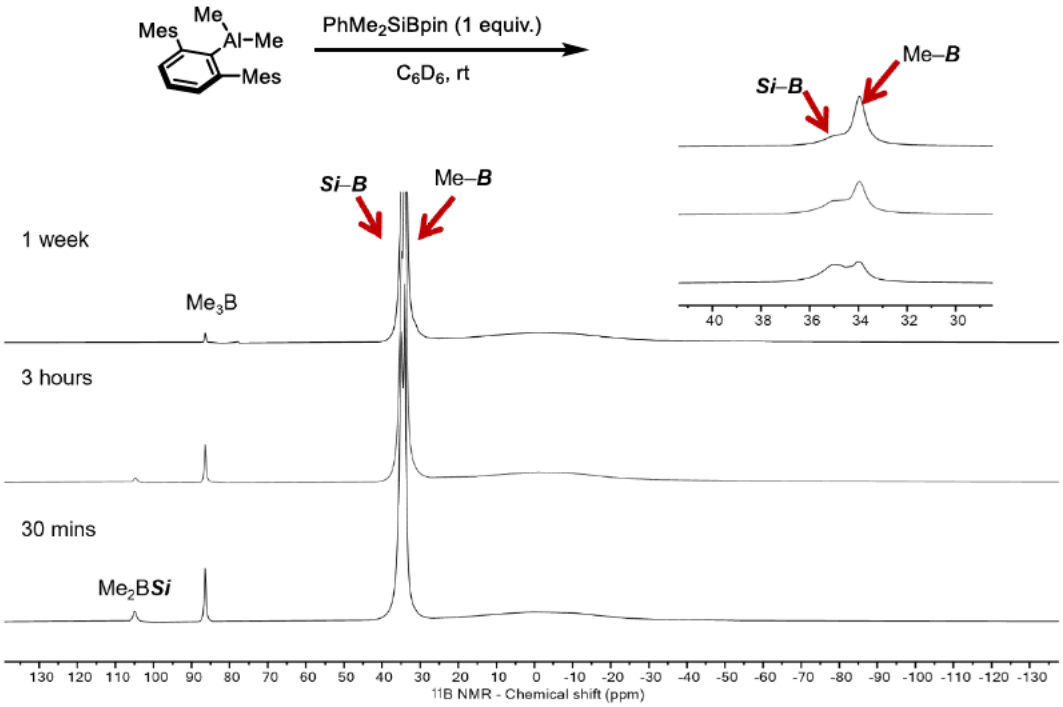

Figure 7-70. Stacked ^{11}B NMR spectra (C_6D_6) of the reaction between $^{Mes}TerAlMe_2$ with $PhMe_2SiBpin$ and monitored over time.

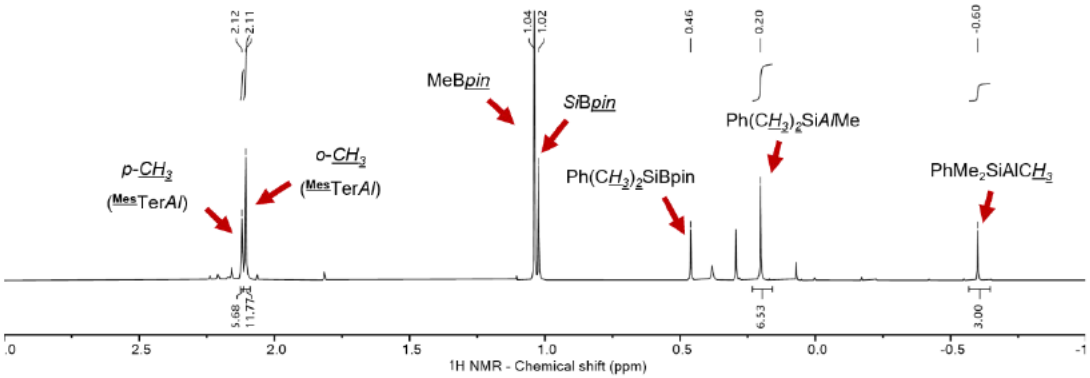

Figure 7-71. ^1H NMR (C_6D_6) of the reaction between $^{Mes}TerAlMe_2$ with HBpin (1 week, crude).

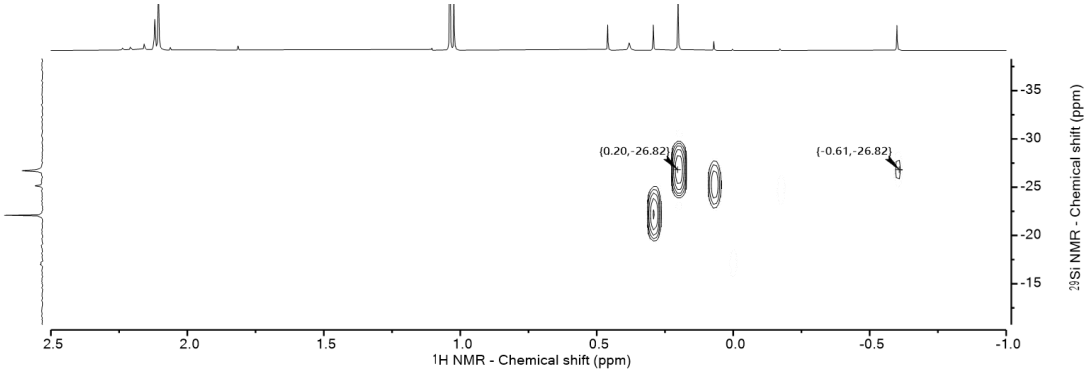

Figure 7-72. ^{1}H-^{29}Si HMQC (C_6D_6) of the reaction between $^{Mes}TerAlMe_2$ with $PhMe_2SiBpin$ (1 week, crude).

Ar = Tipp *(ABG-0675)*

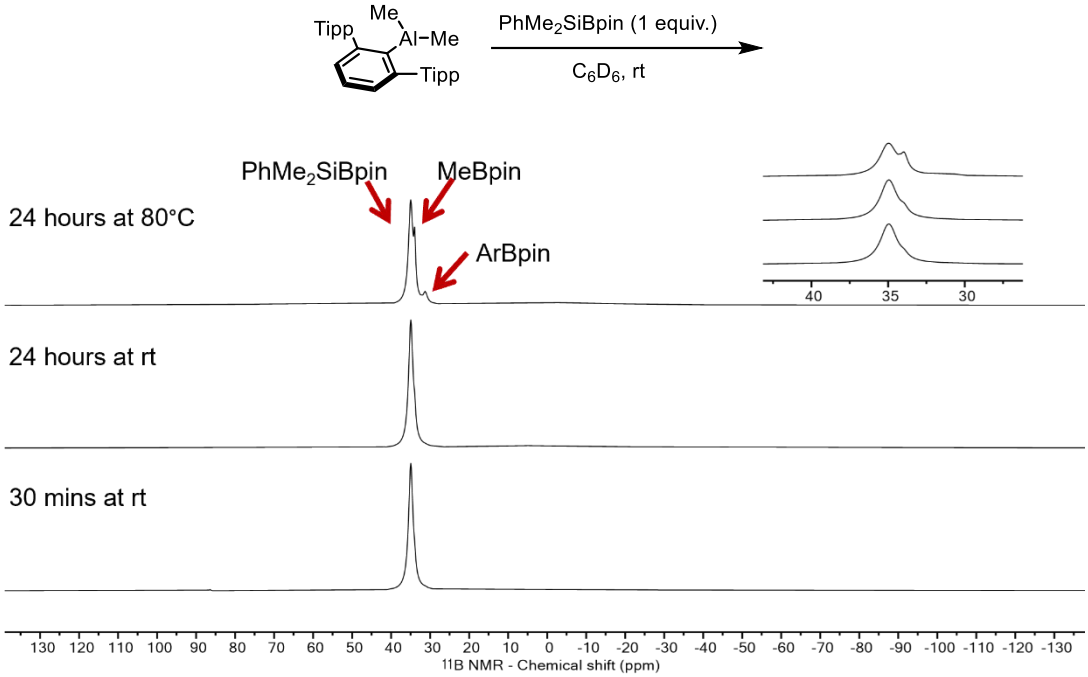

Figure 7-73. Stacked ^{11}B NMR spectra (C_6D_6) of the reaction between $^{Tipp}TerAlH_2$ with $PhMe_2SiBpin$ and monitored over time.

Ar = p-Tol *(ABG-0644)*

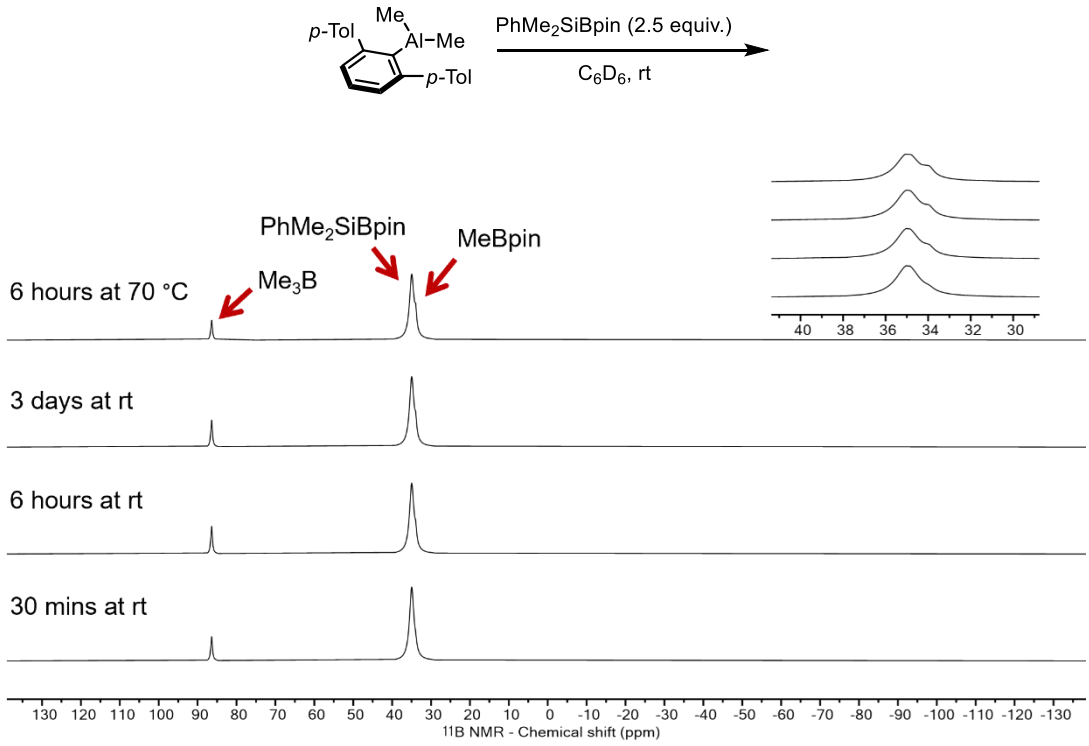

Figure 7-74. Stacked ^{11}B NMR spectra (C_6D_6) of the reaction between $^{p\text{-Tol}}$TerAlMe$_2$ with PhMe$_2$SiBpin (2.5 equiv.) and monitored over time.

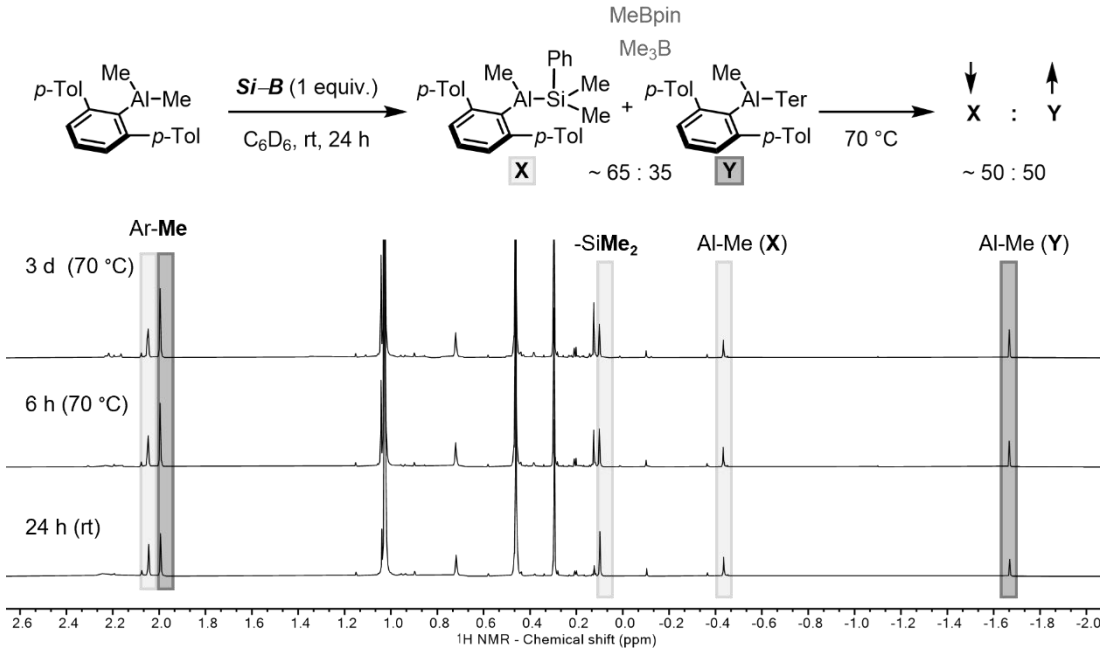

Figure 7-75. Stacked 1H NMR spectra (C_6D_6) of the reaction between $^{p\text{-Tol}}$TerAlMe$_2$ with PhMe$_2$SiBpin (2.5 equiv.) and monitored over time. The formation of X (light grey) and Y (dark grey) are highlighted.

7.6.2 Attempted synthesis of disilylalane using salt metathesis (ABG-0702)

$PhMe_2SiLi$ (1 M in THF, 1.05 mL, 1.05 mmol, 2.1 equiv.) was added dropwise to a solution of $^{Mes}TerAlCl_2 \bullet Et_2O$ (205.7 mg, 0.5 mmol, 1 equiv.) in toluene (5 mL) at room temperature and stirred for 45 minutes. The red/brown mixture turned into a light yellow solution over the course of the 45 minutes. The volatiles were then removed *in vacuo*. The oily residue was extracted with hexane (2 × 10 mL) and the volatiles were removed *in vacuo* to leave an off-white gum, which was subsequently washed with pentane (1 mL) to leave a colourless solid. An NMR was taken which showed the formation only of $^{Mes}TerAlCl_2 \bullet THF$.

^{1}H NMR (500 MHz, Benzene-d_6) δ 7.30 (t, J = 7.6 Hz, 1H; Ar', *p*-H), 6.94 (d, J = 7.6 Hz, 2H; Ar', *m*-H), 6.83 (s, 4H; Mes, *m*-H), 3.48 – 3.17 (m, 4H; 2 × OCH_2CH_2R), 2.27 (s, 12H; Mes, 4 × *o*-CH_3), 2.14 (s, 6H; Mes, 2 × *p*-CH_3), 0.83 – 0.69 (m, 4H; 2 × OCH_2CH_2R).

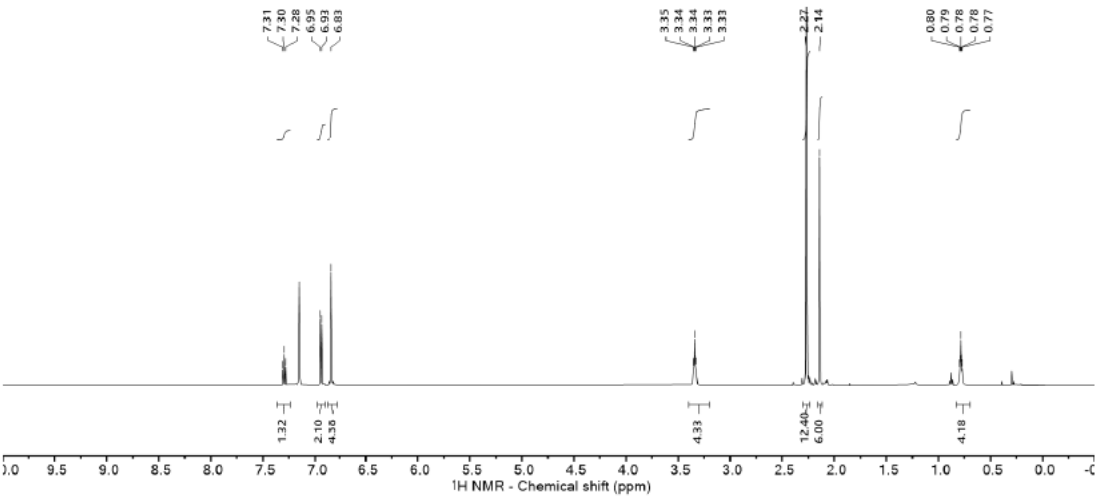

Figure 7-76. ^{1}H NMR spectrum (C_6D_6) of the product obtained from the reaction between $^{Mes}TerAlCl_2 \bullet THF$ and $PhMe_2SiLi$ after 45 minutes at room temperature.

When the reaction was allowed to react longer (3 days rt), $^{Mes}TerAlCl_2$•THF was fully consumed but led to an intractable ^1H NMR spectrum containing at least three different *m*-terphenyl containing products instead. No species could be isolated.

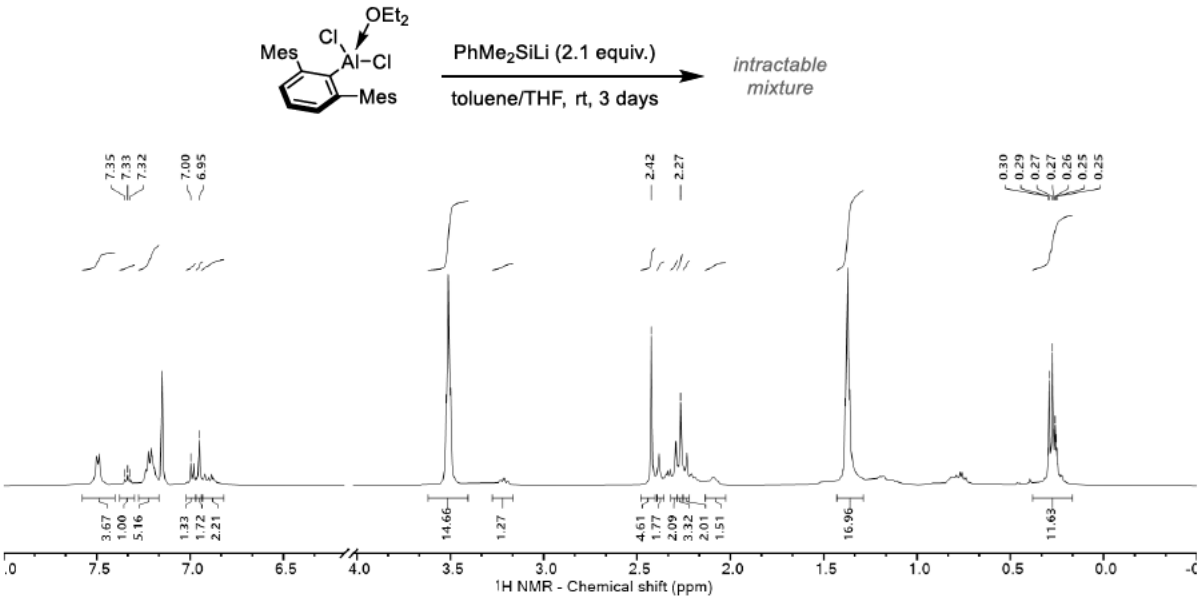

Figure 7-77. ^1H NMR spectrum (C_6D_6) of the mixture obtained from the reaction between $^{Mes}TerAlCl_2$•THF and $PhMe_2SiLi$ after 3 days at room temperature.

7.6.3 Synthesis of disilylalane

Initial isolation of disilylalane (*ABG-0671)*

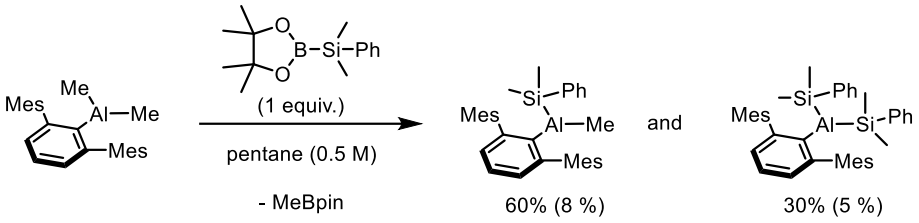

$PhMe_2SiBpin$ (350 µL, 1 mmol, 1 equiv.) was added to a solution of $^{Mes}TerAlMe_2$ (370 mg, 1 mmol, 1 equiv.) in pentane (2 mL, 0.5 M). The reaction was stirred for 4 days at room temperature and then the solvent was removed *in vacuo* to give a white opaque oil. An aliquot was taken for NMR analysis. Upon initial addition of pentane to the crude mixture, white solid precipitated but then re-dissolved upon further addition of pentane (4 mL). The solution was stored at –30 °C for 2 days to give $^{Mes}TerAl(SiMe_2Ph)_2$ as faint yellow crystals (30 mg, 5%). The mother liquor was concentrated to *ca*. 2 mL and stored at –30 °C for 2 days to give $^{Mes}TerAl(Me)SiMe_2Ph$ as colourless crystals (40 mg, 8%).

$^{Mes}TerAl(SiMe_2Ph)_2$ (ABG-0671-FC)

^{1}H NMR (500 MHz, Benzene-d_6) δ 7.32 (t, *J* = 7.5 Hz, 1H; Ar', *p*-*H*), 7.19 – 7.10 (m, 6H; overlapped by benzene; ***Si***, Ar*H*), 6.98 (d, *J* = 7.5 Hz, 2H; 2 × Ar, *o*-*H*), 6.97 – 6.91 (m, 4H; ***Si***, Ar*H*), 6.82 (s, 4H; Mes, 4 × *m*-*H*), 2.21 (s, 6H; Mes, 2 × *p*-C*H*$_3$), 2.17 (s, 12H; Mes, 4 × *o*-C*H*$_3$), 0.08 (s, 12H; 2 × Si(C*H*$_3$)$_2$).

^{13}C {^{1}H} NMR (126 MHz, Benzene-d_6) δ 152.0, 148.7, 142.7, 140.4, 137.7, 136.2, 134.7, 129.7 (identified by HMBC), 129.2 (identified by HMBC), 128.0, 127.8, 126.1, 21.8, 21.2, -0.3.

^{29}Si NMR (99 MHz, Benzene-d_6) δ -25.3

m.p. 175 - 177 °C (pentane)

MS HRMS-EI (m/z): found 610.3019; [M] ($C_{40}H_{47}AlSi_2$), requires 610.3026

IR 3047*w*, 2944*w*, 2919*w*, 2886*w*, 1611*w*, 1447*m*, 1424*m*, 1375*m*, 1238*m*, 1176*m*, 1101*m*, 831*m*, 798*s*, 729*s*, 697*s*, 469*m*, 453*m*

^{Mes}TerAl(Me)SiMe$_2$Ph (ABG-0671-F4)

^{1}H NMR (500 MHz, Benzene-d_6) δ 7.32 (t, *J* = 7.6 Hz, 1H; Ar', *p*-*H*), 7.15 (m, 5H; overlapped by benzene), 7.00 (d, *J* = 7.5 Hz, 2H; Ar', *m*-*H*), 6.76 (s, 4H; Mes, *m*-*H*), 2.12 (s, 6H; Mes, *p*-C*H*$_3$), 2.11 (s, 12H; Mes, *o*-C*H*$_3$), 0.21 (s, 6H; (SiC*H*$_3$)$_2$), -0.59 (s, 3H; AlC*H*$_3$).

^{13}C {^{1}H} NMR (126 MHz, Benzene-d_6) δ 152.5 (identified by HMBC), 148.7, 142.6, 140.8, 137.4, 136.1, 134.2, 129.4, 129.3, 128.4 (identified by HMBC), 125.6, 21.3, 21.1, -1.1, -4.4 (Al*C*H$_3$, identified by HSQC). *Missing a single C peak (Si*Ph*), likely hidden below C_6D_6.*

^{29}Si NMR (99 MHz, Benzene-d6) δ -26.8

m.p. 87-89 °C (pentane)

MS HRMS-EI (m/z): found 490.2642; [M] ($C_{33}H_{39}AlSi$), requires 490.2631

IR 3047*w*, 2946*w*, 2915*w*, 1611*w*, 1551*w*, 1449*m*, 1424*m*, 1376*m*, 1101*m*, 831*m*, 800*s*, 731*s*, 629*s*, 469*m*, 443*m*

Screening conditions for synthesis of disilylalane

2 equiv. $PhMe_2SiBpin$ (ABG-0684)

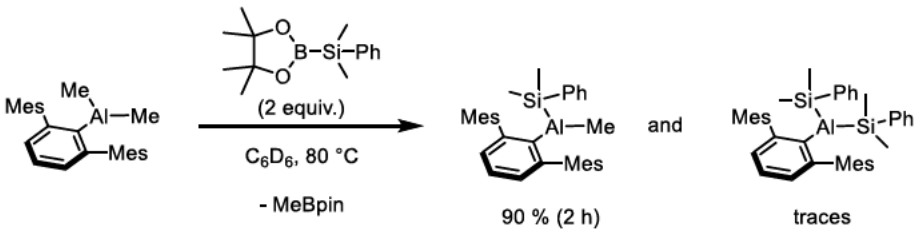

$PhMe_2SiBpin$ (70 µL, 0.2 mmol, 2 equiv.) was added to a solution of $^{Mes}TerAlMe_2$ (37 mg, 0.1 mmol, 1 equiv.) in C_6D_6 (0.65 mL). The reaction was heated at 80 °C and the reaction progress was monitored after 2 hours and 20 hours by ^{11}B NMR spectroscopy.

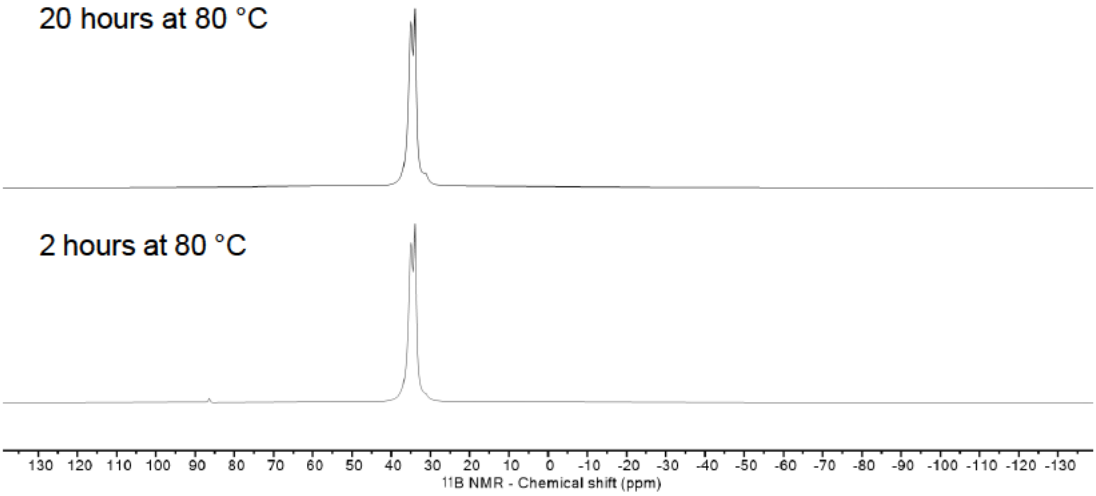

Figure 7-78. Stacked ^{11}B NMR spectra (C_6D_6) of the reaction between $^{Mes}TerAlMe_2$ with $PhMe_2SiBpin$ (2 equiv.) at 80 °C and monitored over time.

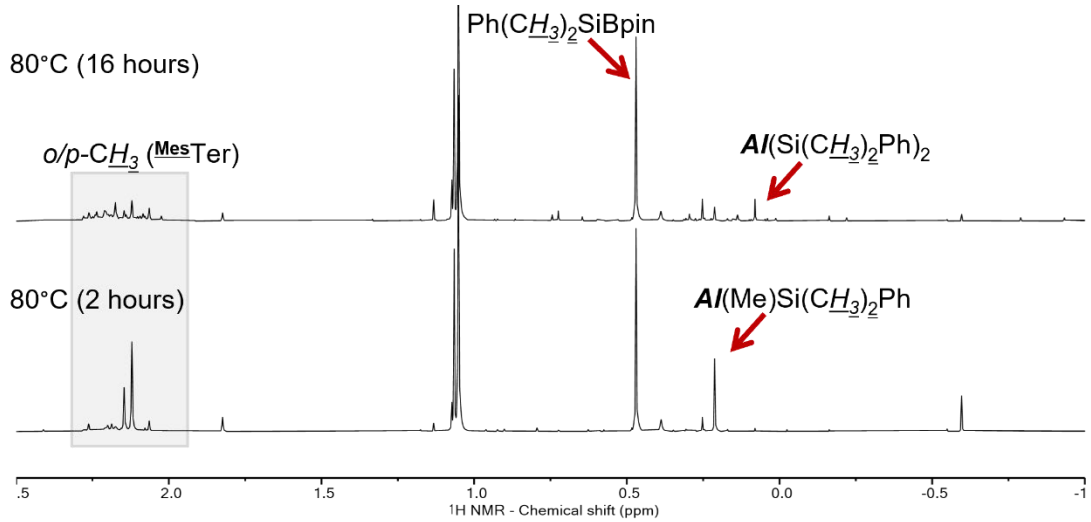

Figure 7-79. Stacked ^{1}H NMR spectra (C_6D_6) of the reaction between $^{Mes}TerAlMe_2$ with $PhMe_2SiBpin$ (2 equiv.) at 80 °C and monitored over time. (zoomed in on area of interest)

Theory #1: Reversible reaction with MeBpin (ABG-0685)

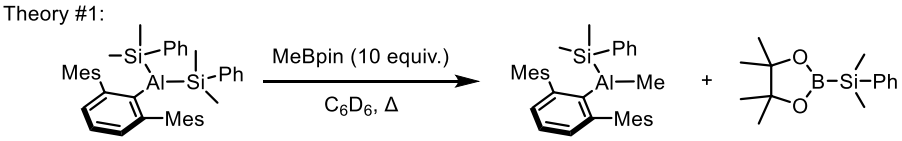

MeBpin (48 µL, 0.25 mmol, 10 equiv.) was added to a solution of $^{Mes}TerAl(SiMe_2Ph)_2$ (15.3 mg, 0.025 mmol, 1 equiv.) in C_6D_6 (0.65 mL) at room temperature. The reaction was shaken vigorously shaken and monitored periodically by ^{1}H NMR spectroscopy. After 24 hours at room temperature, the reaction was heated to 80 °C for 4 hours.

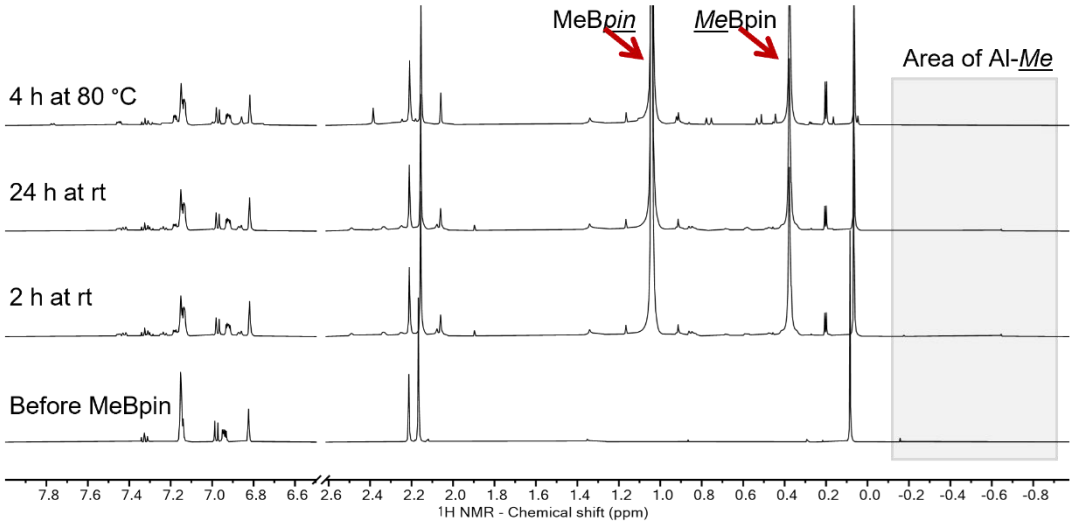

Figure 7-80. Stacked ^{1}H NMR spectra (C_6D_6) of the reaction between $^{Mes}TerAl(SiPhMe_2)_2$ with MeBpin (10 equiv.) monitored over time and at different temperatures (zoomed in on area of interest).

Theory #2: Redistribution of substituents on aluminium (ABG-0671-F4-80C)

Theory #2:

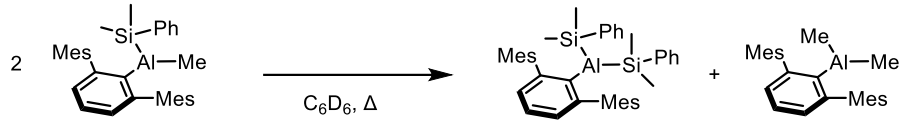

^{Mes}TerAl(SiMe$_2$Ph)Me (12.3 mg, 0.025 mmol) was dissolved in C_6D_6 and left at room temperature for 16 hours. The reaction was then heated to 80 °C for 84 hours. The reaction was monitored periodically but no redistribution was observed.

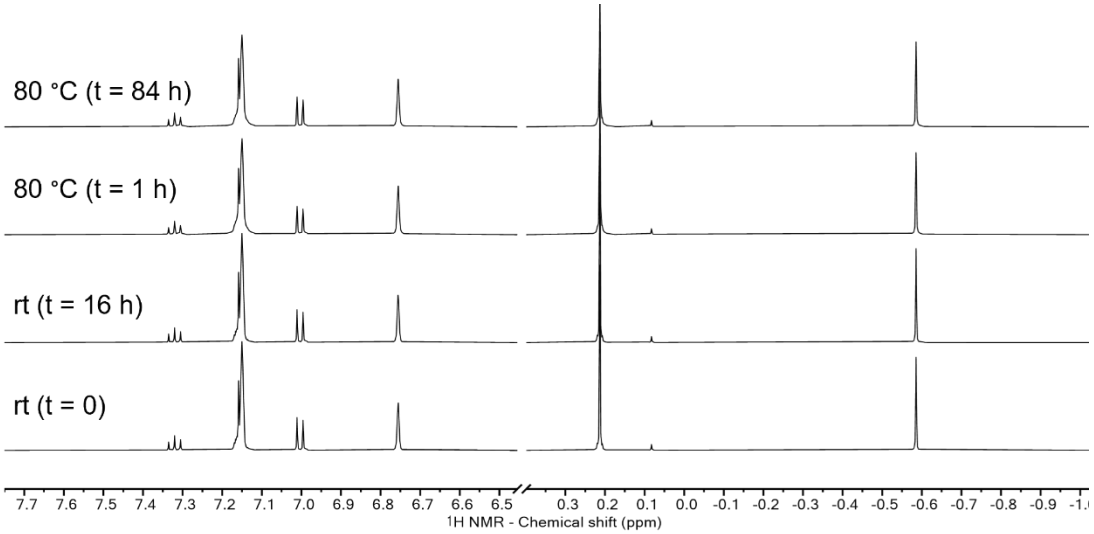

Figure 7-81. Stacked ^{1}H NMR spectra (C_6D_6) of ^{Mes}TerAl(Me)SiPhMe$_2$ over time at different temperatures (zoomed in on area of interest). *Residual trace ^{Mes}TerAl(SiPhMe$_2$)$_2$ – does not grow over time.

Theory #3: Alkyl boranes are responsible for second Al-Me/Si-B exchange

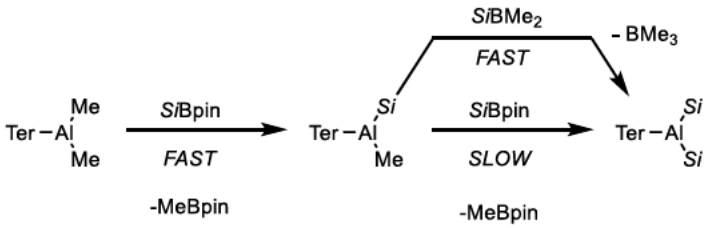

$AlMe_3$ as an alkylating agent (ABG-0698)

To test whether $AlMe_3$ could generate dialkyl silylboranes from $PhMe_2SiBpin$, $AlMe_3$ (2 M in toluene, 25 µL, 0.05 mmol, 1 equiv.) was added to a solution of $PhMe_2SiBpin$ (17.5 µL, 0.05 mmol, 1 equiv.) in *n*-hexane (0.6 mL). The immediate precipitation of an amorphous white solid was observed. The reaction was shaken vigorously and analysed by ^{11}B NMR spectroscopy.

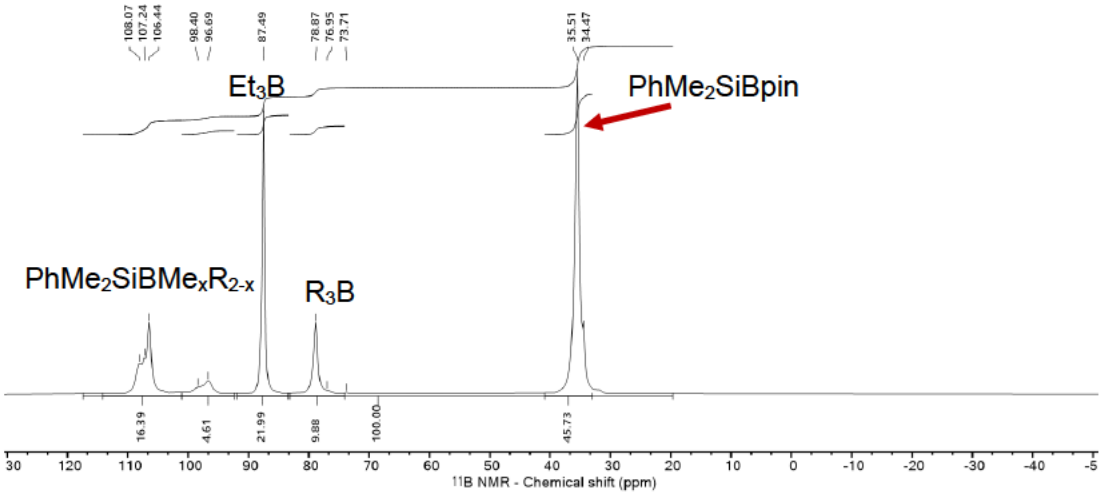

Figure 7-82. ^{11}B NMR spectrum (*n*-hexane) for the reaction between $PhMe_2SiBpin$ and $AlMe_3$ (1 equiv.); R = unknown substituent.

$AlMe_3$ as an additive (ABG-0687)

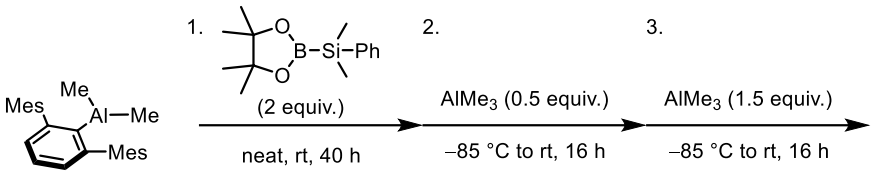

Step	NMR Yield	NMR Yield
1	60%	31%
2	47%	46%
3	34%	60%

$PhMe_2SiBpin$ (350 µL, 1 mmol, 1 equiv.) was added to a solution of $^{Mes}TerAlMe_2$ (370 mg, 1 mmol, 1 equiv.) in toluene (1 mL, 1 M). The reaction was stirred for 1 hour at room temperature and then the volatiles (including toluene and MeBpin) were removed *in vacuo* at 50 °C to give a light-yellow viscous oil. The reaction was stirred neat and monitored by NMR spectroscopy (Step 1).

After 40 hours of stirring neat at room temperature, pentane (8 mL) was added to give a yellow solution with small quantities of an amorphous white precipitate. The reaction was cooled to –95 °C and $AlMe_3$ (2 M in hexane, 0.25 mL, 0.5 mmol, 0.5 equiv.) was added. The reaction was slowly warmed to room temperature overnight to give a yellow solution with increased quantities of an amorphous white precipitate. The suspension was filtered and the volatiles were removed *in vacuo* from the filtrate to give a yellow oil. An aliquot was analysed by NMR spectroscopy (Step 2).

The oil was redissolved in pentane (8 mL), cooled to –95 °C and $AlMe_3$ (2 M in hexane, 0.75 mL, 1.5 mmol, 1.5 equiv.) was added. The formation of a white precipitate was observed within several minutes. The reaction was slowly warmed to room temperature and stirred for 3 days to give a yellow solution with a white precipitate. The volatiles were removed *in vacuo* and the yellow oil was extracted with pentane (3 × 7 mL). The volatiles were removed *in vacuo* and an aliquot was analysed by NMR spectroscopy (Step 3).

Fractional recrystallisation of the yellow oil in cold pentane (–30 °C) yielded $^{Mes}TerAl(SiPhMe_2)_2$ as a light yellow crystalline solid (160 mg, 0.26 mmol, 26 % yield).

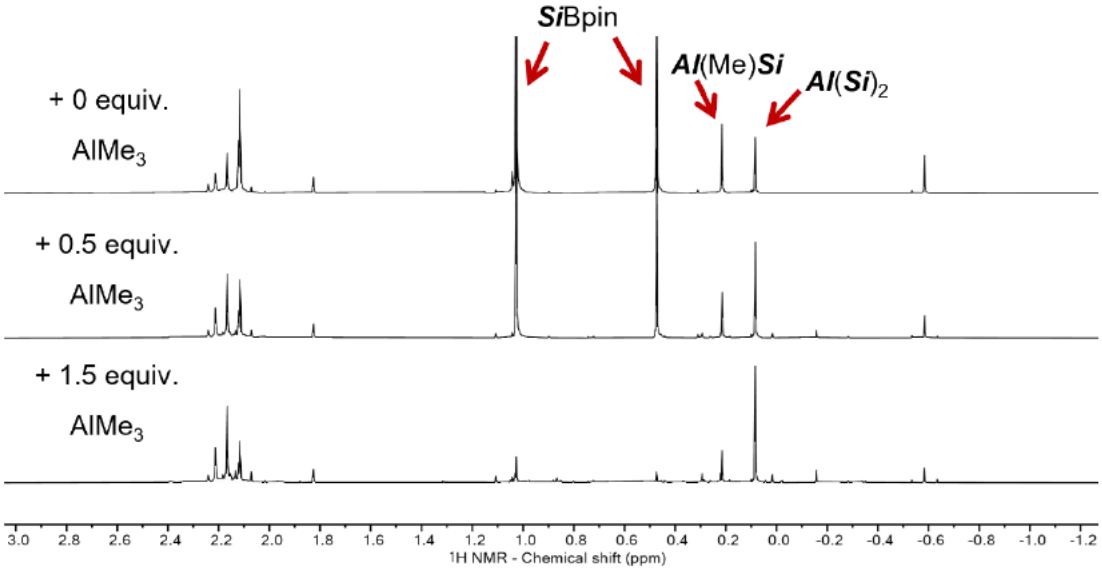

Figure 7-83. Stacked ^{1}H NMR spectra (C_6D_6) of the reaction between ^{Mes}TerAlMe$_2$ and PhMe$_2$SiBpin (2 equiv.) following the addition of different quantities of AlMe$_3$.

7.6.4 Photolysis of disilylalane

C_6D_6

In an NMR tube, ^{Mes}TerAl(SiPhMe$_2$)$_2$ (6.1 mg, 0.01 mmol) was dissolved in C_6D_6 (0.65 mL) to give a clear solution. A snapshot of the sample was analysed by NMR spectroscopy. The sample was irradiated at 365 nm for 1 hour, resulting in the solution becoming yellow. The sample was analysed by NMR spectroscopy.

^{Mes}TerAl(Si)$_2$ (ABG-0671-UV)

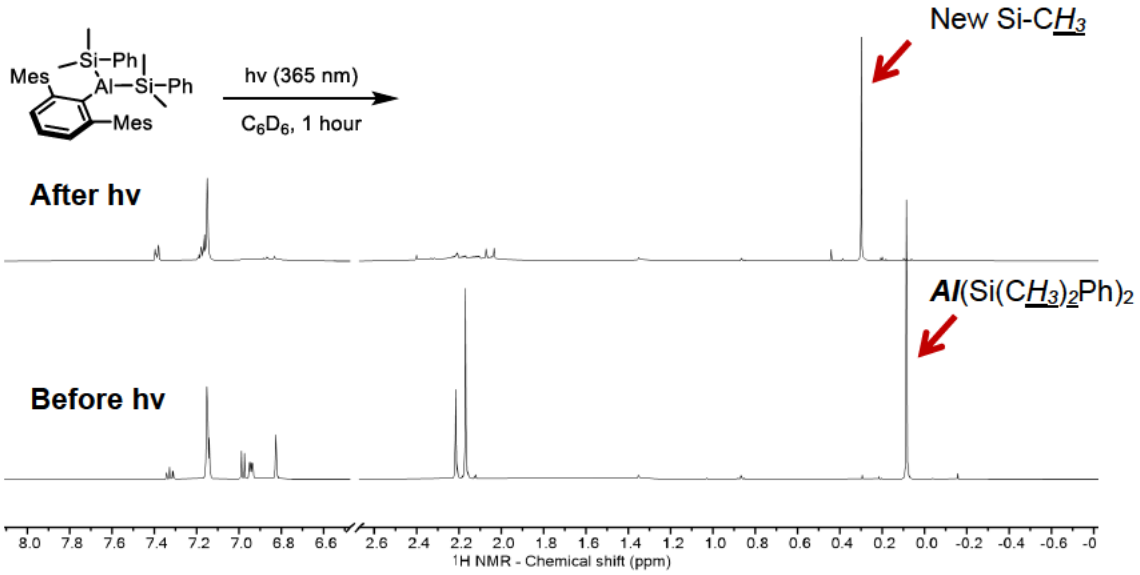

Figure 7-84. Stacked ^{1}H NMR spectra (C_6D_6) of ^{Mes}TerAl(SiMe$_2$Ph)$_2$ before and after irradiation at 365 nm in C_6D_6 for 1 hour.

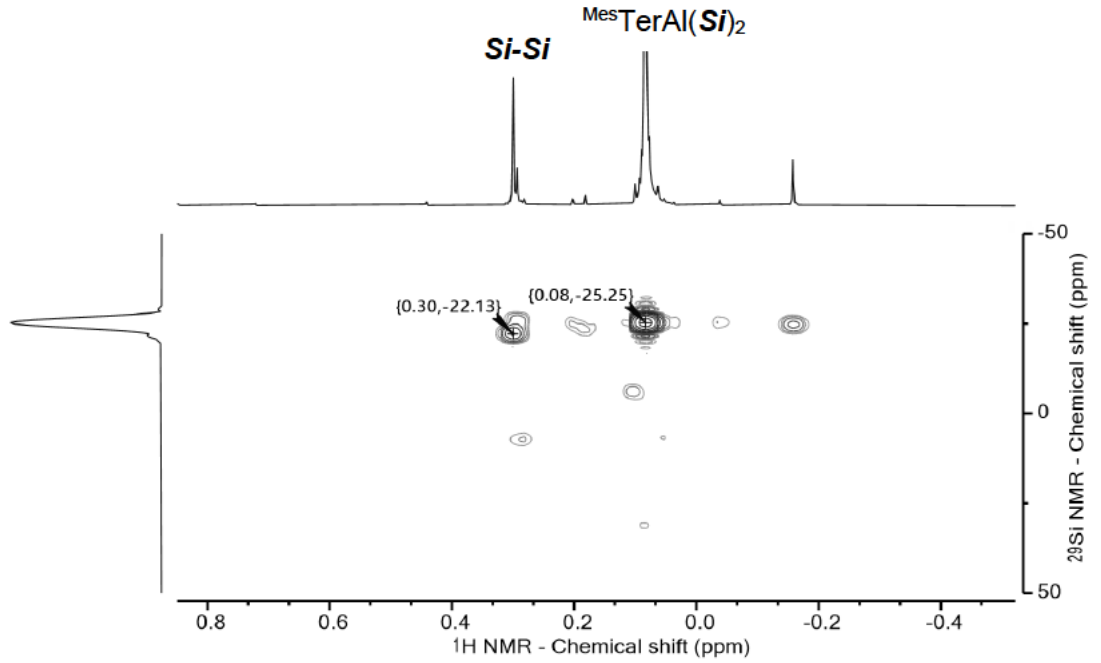

Figure 7-85. ^{1}H-^{29}Si HMBC NMR spectrum (C_6D_6) of $^{Mes}TerAl(SiMe_2Ph)_2$ following irradiation at 365 nm for 6 minutes.

^{Mes}TerAl(Si)Me (ABG-0671-F4-UV)

In an NMR tube, $^{Mes}TerAl(SiPhMe_2)Me$ (4.9 mg, 0.01 mmol) was dissolved in C_6D_6 (0.65 mL) to give a clear solution. A snapshot of the sample was analysed by NMR spectroscopy. The sample was irradiated at 365 nm for 1 hour, resulting in the solution becoming yellow. The sample was analysed again by NMR spectroscopy.

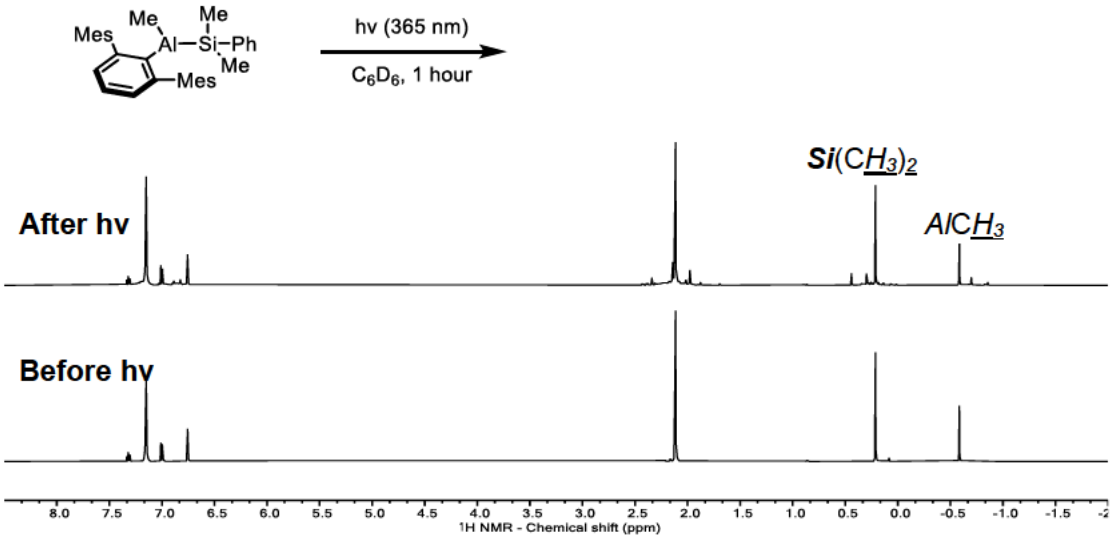

Figure 7-86. Stacked ^{1}H NMR spectra (C_6D_6) of $^{Mes}TerAl(SiMe_2Ph)Me$ before and after irradiation at 365 nm in C_6D_6 for 1 hour.

In CH_2Cl_2 (ABG-0687-F2-UV)

In an NMR tube, ^{Mes}TerAl(SiPhMe$_2$)$_2$ (6.1 mg, 0.01 mmol) was dissolved in CH_2Cl_2 (0.65 mL) to give a clear solution. A snapshot of the sample was analysed by NMR spectroscopy. The sample was irradiated at 365 nm and monitored periodically by NMR spectroscopy. The solution became increasingly yellow as the reaction progressed.

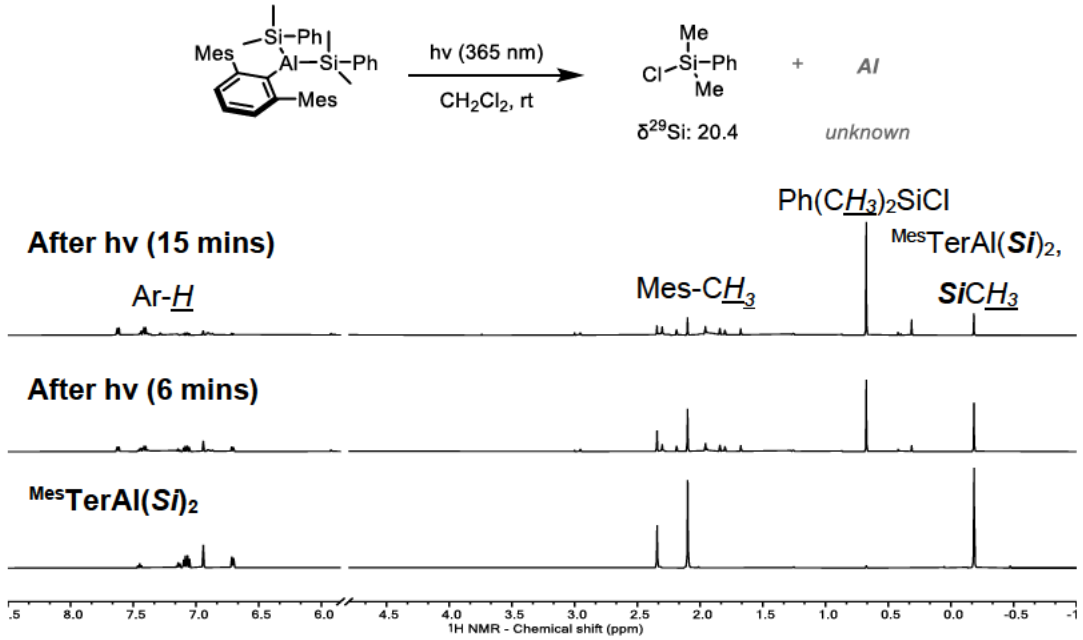

Figure 7-87. Stacked ^{1}H NMR spectra (CH_2Cl_2) of ^{Mes}TerAl(SiMe$_2$Ph)$_2$ before and after irradiation at 365 nm in CH_2Cl_2 for 6 and 15 minutes.

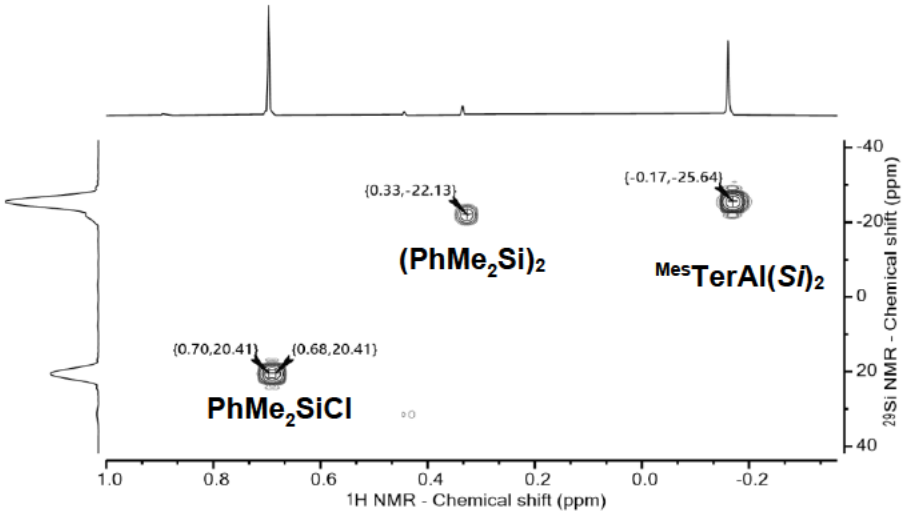

Figure 7-88. ^{1}H-^{29}Si HMBC spectrum (CH_2Cl_2) of ^{Mes}TerAl(SiMe$_2$Ph)$_2$ following irradiation at 365 nm for 6 minutes.

In the presence of $Me_3Si–CC–SiMe_3$ (ABG-0705)

^{Mes}TerAl($SiMe_2Ph$)$_2$ (15.27 mg, 0.025 mmol) was dissolved in cyclohexane (0.6 mL) *via* sonication for 1 minute. Bistrimethylsilyl acetylene (57 µL, 0.25 mmol) was then added to the solution and a baseline NMR spectrum was recorded to confirm that no reaction had taken place. The reaction mixture was then irradiated at 365 nm and the reaction progress was monitored by NMR spectroscopy. Based on the disappearance of the Si–C*H*$_3$ protons associated with ^{Mes}TerAl($SiMe_2Ph$)$_2$, the reaction was judged to have been complete after 5 hours. This was accompanied by a colour change from very pale yellow to orange. The volatiles were removed *in vacuo* and an aliquot of the resulting orange oil analysed by ^{1}H NMR spectroscopy in C_6D_6 (checkpoint 1). The remaining crude mixture was redissolved in pentane/hexamethyldisiloxane (HMDSO) (total volume = *ca.* 0.5 mL) and stored at –30 °C. After *ca.* one month, an amorphous white solid had precipitated, which was separated by filtration and washed with HMDSO. A small sample was taken for analysis by NMR spectroscopy (checkpoint 2). The remainder was redissolved in pentane/HMDSO (total volume = *ca.* 0.2 mL) but no further crystallisation was observed.

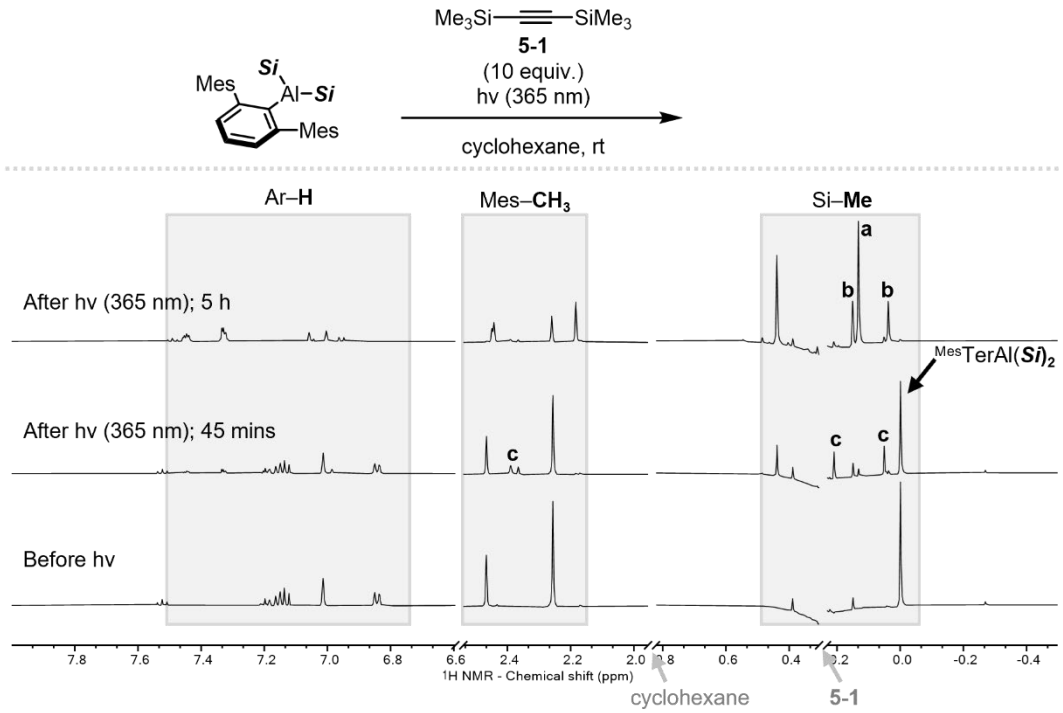

Figure 7-89. Stacked ^{1}H NMR spectra (cyclohexane) tracking the consumption of ^{Mes}TerAl(Si)$_2$ and formation of new species over time.

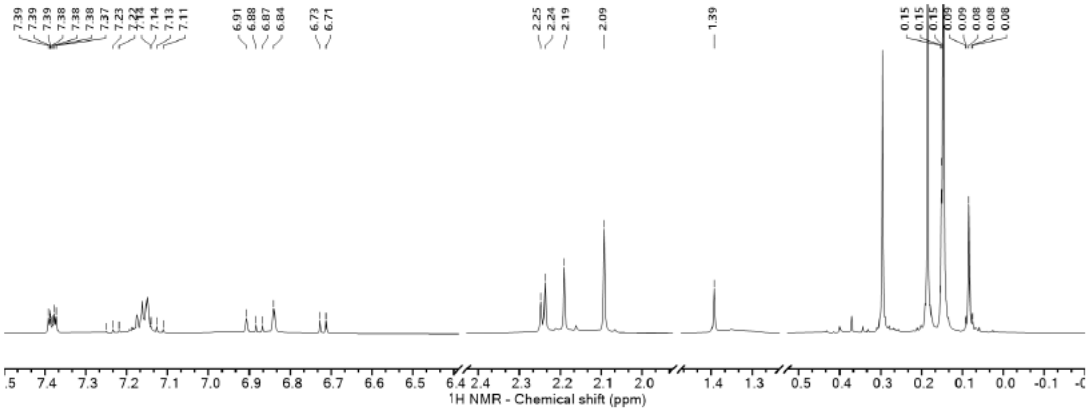

Figure 7-90. ^{1}H NMR spectrum (C_6D_6) of the crude mixture obtained at checkpoint 1.

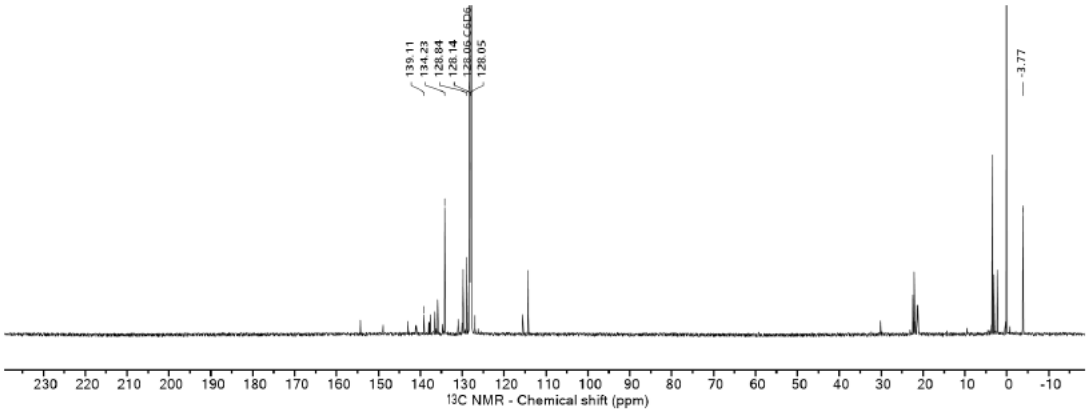

Figure 7-91. ^{13}C {^{1}H} NMR spectrum (C_6D_6) of the crude mixture obtained at checkpoint 1. The peaks labelled are consistent with the formation of the disilane $(PhMe_2Si)_2$.

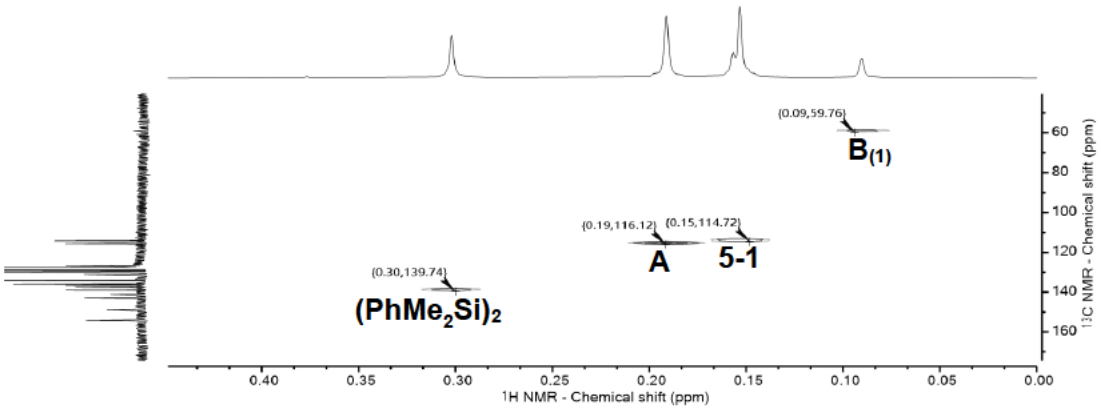

Figure 7-92. ^{1}H-^{13}C HMBC spectrum (C_6D_6) of the mixture obtained at checkpoint 1. This was used to identify the ^{13}C chemical shift for the Me_3Si–C carbon atoms of the different species present.

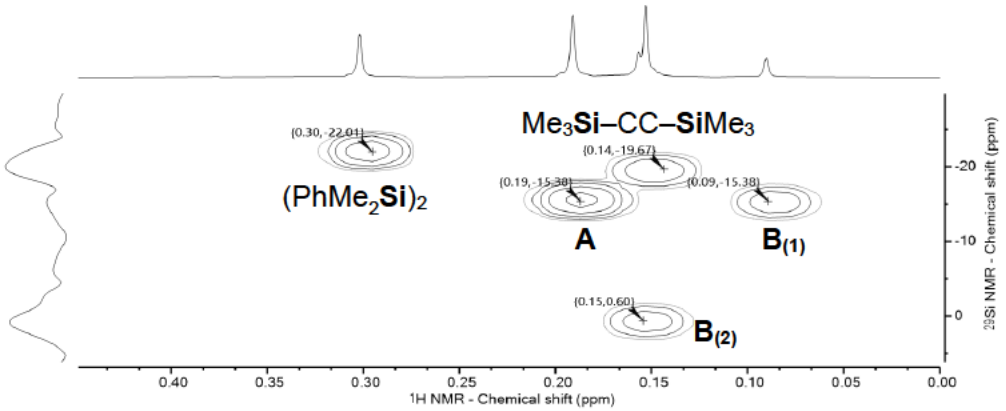

Figure 7-93. ^{1}H-^{29}Si HMBC spectrum (C_6D_6) of the mixture obtained at checkpoint 1. This was used to identify the ^{29}Si chemical shifts for the different silicon environments present.

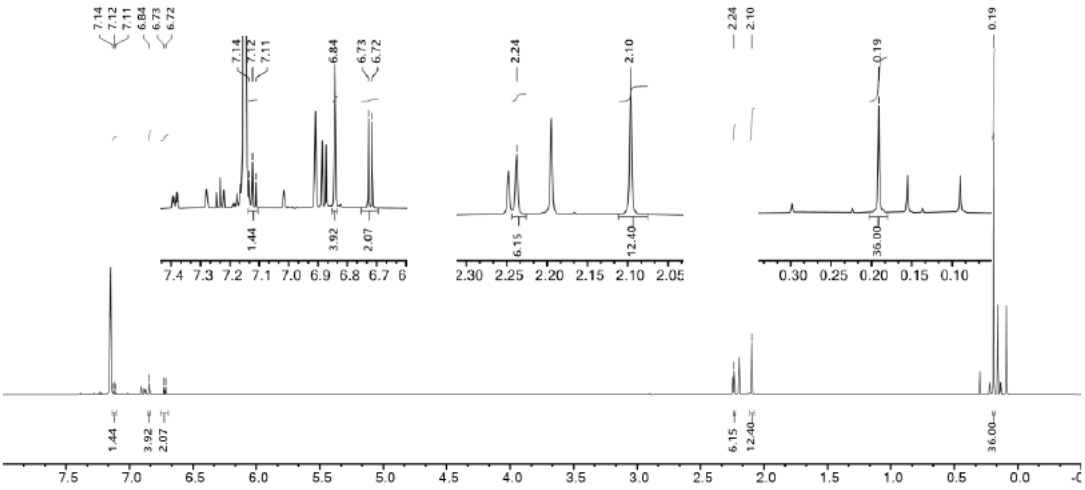

Figure 7-94. ^{1}H NMR spectrum (C_6D_6) of the mixture obtained at checkpoint 2. The resonances of major species A are peak-picked and integrated.

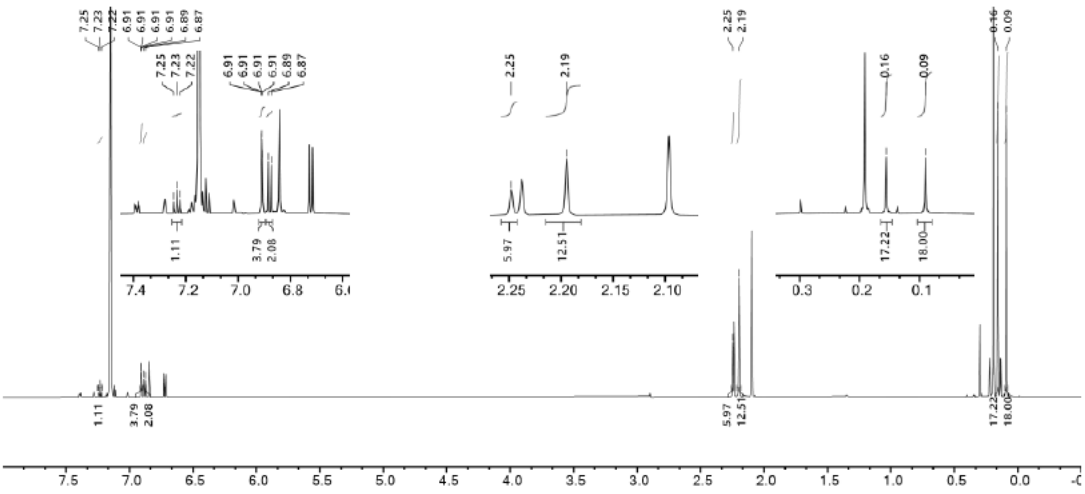

Figure 7-95. ^{1}H NMR spectrum (C_6D_6) of the mixture obtained at checkpoint 2. The resonances of minor species B are peak-picked and integrated.

Approximate ratio of A:B = 58:42

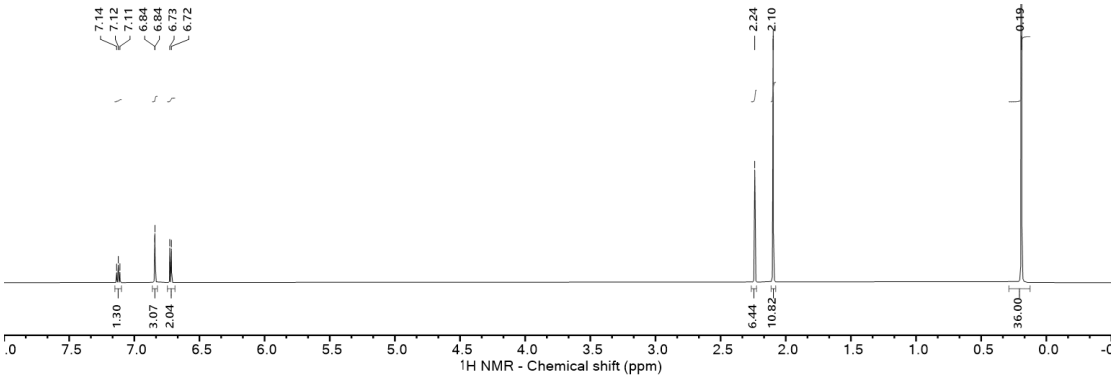

Figure 7-96. Synthetic ^{1}H NMR spectrum (C_6D_6) of major species A

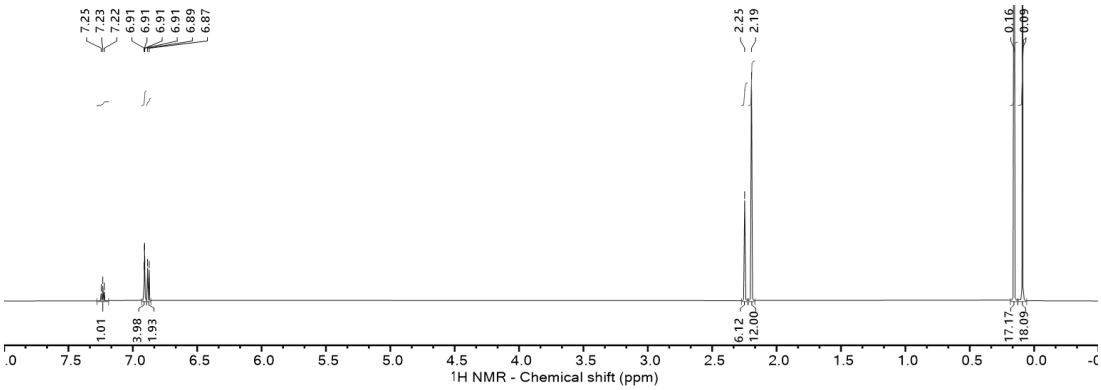

Figure 7-97. Synthetic ^{1}H NMR spectrum (C_6D_6) of minor species B

Major species A

^{1}H NMR (601 MHz, Benzene-d_6) δ 7.12 (t, J = 7.6 Hz, 1H; Ar', p-H), 6.84 (s, 4H; Mes, 4 × m-H), 6.72 (d, J = 7.6 Hz, 2H; Ar', 2 × m-H), 2.24 (s, 6H; Mes, 2 × p-CH_3), 2.10 (s, 12H; Mes, 4 × o-CH_3), 0.19 (s, 36H; 4 × Si(CH_3)$_3$).

^{13}C {^{1}H} NMR (126 MHz, Benzene-d_6) δ 116.1 (C_4 ring)

^{29}Si NMR (99 MHz, Benzene-d_6) δ -15.4

Minor species B

^{1}H NMR (601 MHz, Benzene-d_6) δ 7.23 (t, J = 7.5 Hz, 1H; Ar', p-H), 6.91 (s, 4H; 4 × Mes, m-H), 6.88 (d, J = 7.6 Hz, 2H; Ar', 2 × m-H), 2.25 (s, 6H; Mes, 2 × p-CH_3), 2.19 (s, 12H; Mes, 4 × o-CH_3), 0.16 (s, 18H; 2 × Si(CH_3)$_3$), 0.09 (s, 18H; 2 × Si(CH_3)$_3$).

^{13}C {^{1}H} NMR (126 MHz, Benzene-d_6) δ 59.8 (Al–$C(sp^3)$-C(sp^2))

^{29}Si NMR (99 MHz, Benzene-d_6) δ 0.6, -15.4

7.7 Analysis of ^{11}B NMR spectroscopy as a quantitative technique

The following is a guide for how the ^{11}B NMR spectra was processed, and a comparison to the concentrations calculated by ^{1}H NMR spectroscopy.

Model mixture (ABG-0703):

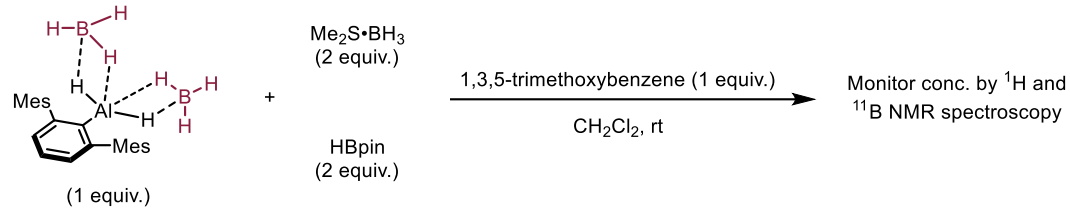

$Me_2S{\bullet}BH_3$ (9.5 µL, 0.1 mmol, 2 equiv.), HBpin (14.5 µL, 0.1 mmol, 2 equiv.) and 1,3,5-trimethoxybenzene (0.5 M in C_6D_6, 100 µL, 0.05 mmol, 1 equiv.) were added to a solution of $^{Mes}TerAlH_2{\bullet}(BH_3)_2$ (18.5 mg, 0.05 mmol, 1 equiv.) in CH_2Cl_2 (0.55 mL) in a small vial. The reaction mixture was thoroughly shaken before being transferred to an NMR tube. NMR spectroscopic analysis was carried out as followed.

Note: we did not observe any noticeable reaction between each of the reagents used above (with the exception of some trace new species) that might affect quantitative analysis.

Processing ^{11}B NMR spectra

1. Unprocessed ^{11}B NMR spectrum

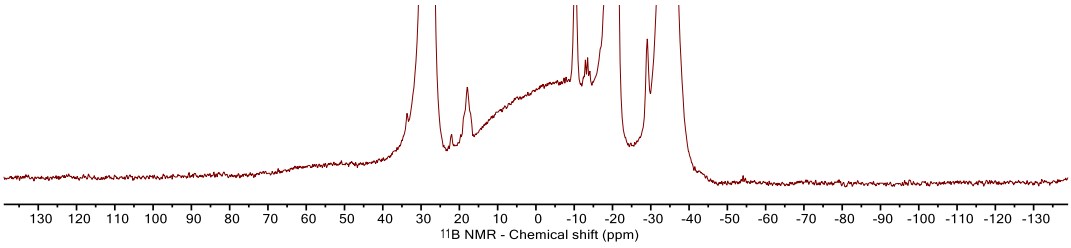

2. Following manual phase correction
3. Manual baseline correction using Whittaker Smoother

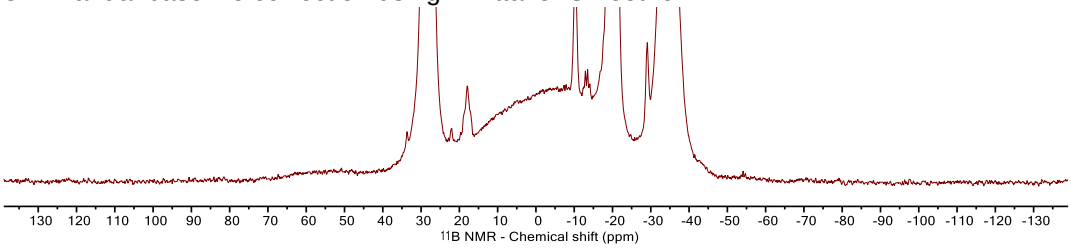

- Uncheck *Autodetect* on the *Filter* parameter
- Drag the slider until the background is correctly suppressed (be wary of broad peaks)

- Press *Ok*

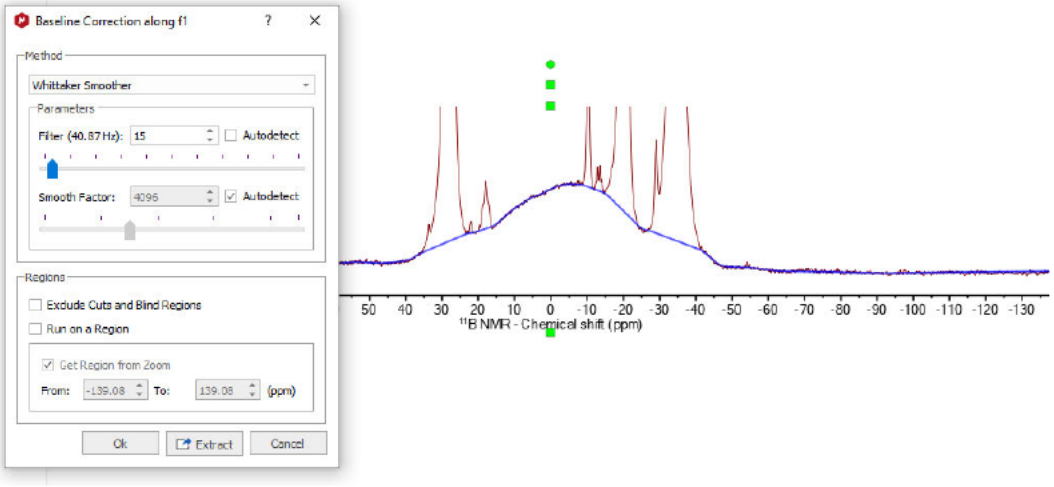

4. Processed spectrum following phase and baseline correction

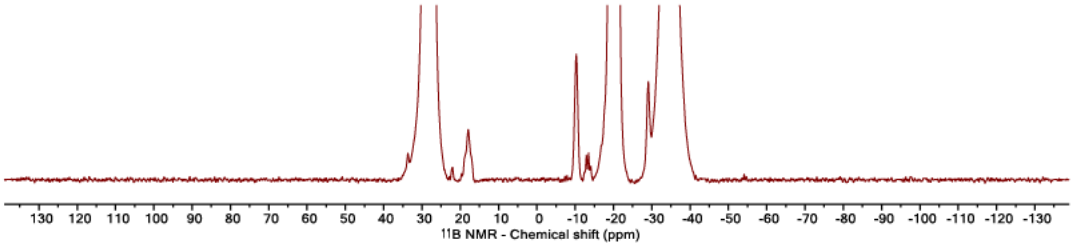

5. Entire NMR region of interest integrated to 1. The peaks are then integrated, giving the resultant integral as a percentage of the total boron content in the reaction.

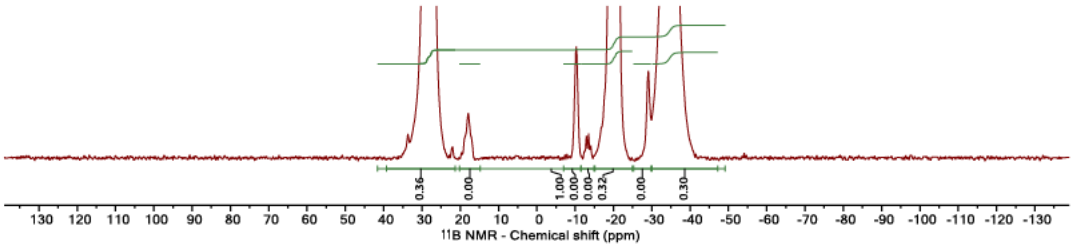

6. How the processed spectrum looks like zoomed out.

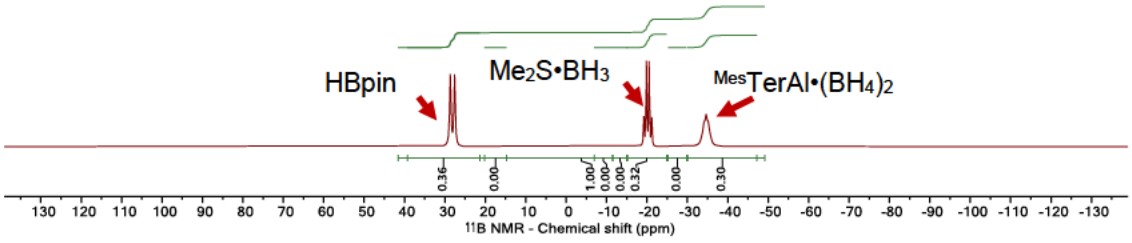

The concentration of each boron containing compound is calculated based on the initial known concentration of boron species in solution (e.g. in this case, 0.45 M)

Total mmol boron	= 0.3 mmol
Volume	= 0.67 mL
Conc (total boron)	= 0.45 M

Table 3. Calculating the concentration of each boron containing species using ^{11}B NMR spectroscopy

Species	#B atoms in species	integration	normalised	Conc.
HBpin	1	0.36	0.36	0.1612 M
$Me_2S•BH_3$	1	0.32	0.32	0.1433 M
$^{Mes}TerAlH_2•(BH_3)_2$	2	0.3	0.15	0.0672 M

Comparison to ^{1}H NMR spectroscopy

An NMR sample was run in the presence of an internal standard (trimethoxybenzene, *ca.* 1 equiv. = 0.075 M). As the reactions were performed in protonated DCM (CH_2Cl_2), a single presat experiment was used.

The following modifications were made to the NMR parameters:

Relaxation time: 30 seconds
Number of scans: 1

The singlet at δ 3.81 (trimethoxybenzene, -O**Me**, 9H) was integrated to 9 and the concentration of the other species were calculated accordingly.

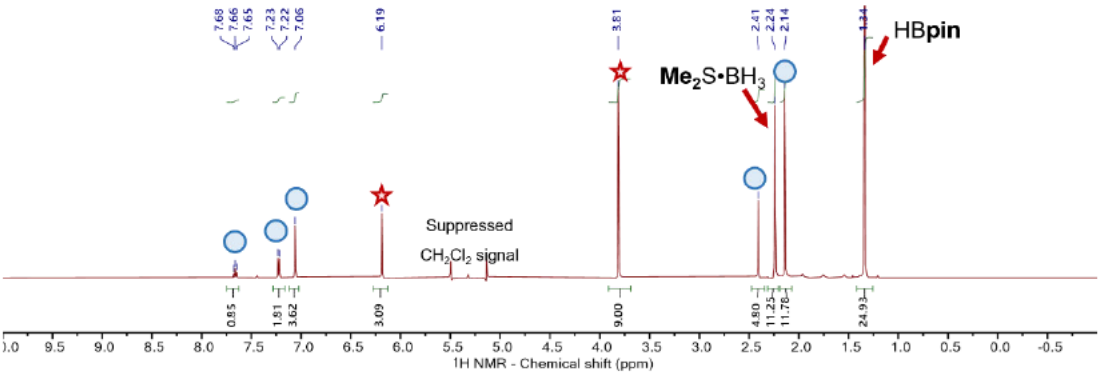

○ = $^{Mes}TerAlH_2•(BH_3)_2$ ☆ = 1,3,5-trimethoxybenzene

Table 4. Comparing the concentration of each boron containing species using ^{1}H and ^{11}B NMR spectroscopy

Species	Conc. (M) (^{1}H NMR)	Conc. (M) (^{11}B NMR)	% difference	Conc. (M) (expected)	% difference (exp. Vs NMR**)
HBpin	0.1550	0.1612	4%	0.1481	6%
$Me_2S•BH_3$	0.1399	0.1433	2%	0.1481	5%
3-Mes-1	0.0663*	0.0672	1%	0.0741	11%

* calculated from the average of all available ^{1}H NMR resonances
** calculated from the average of ^{1}H and ^{11}B concentrations

Analysis

Monitoring reactions by ^{11}B NMR is within <5% margin of error compared to ^{1}H NMR spectroscopy, but allows protonated solvent sources to be used, without the use of solvent suppression techniques. Moreover, the fast relaxation time of ^{11}B compared to ^{1}H (particularly in anaerobic environments) facilitates monitoring of air-sensitive reactions.

The differences between the expected concentrations of each reagent with the concentrations obtained by ^{1}H and ^{11}B NMR can be attributed to experimental error, and are greater than the difference in error between ^{1}H and ^{11}B NMR spectroscopy.

7.8 Crystallographic Data

Unless specified, crystallography was performed and solved by Dr Gary Nichol at the University of Edinburgh.

Full crystallographic data is available at the end of the section.

p-Tol**TerAlH$_2$•DMAP (ABG-0549)**

Experimental

Single colourless block-shaped crystals of ***p*-Tol**TerAlH$_2$•DMAP** were recrystallised from a mixture of toluene and hexane by slow cooling. A suitable crystal with dimensions 0.43 × 0.25 × 0.17 mm^3 was selected and mounted on a MITIGEN holder in Paratone oil on a Rigaku Oxford Diffraction SuperNova diffractometer. The crystal was kept at a steady T = 120.01(10) K during data collection. The structure was solved with the **ShelXT** 2018/2 (Sheldrick, 2018) solution program using dual methods and by using **Olex2** 1.5-beta (Dolomanov et al., 2009) as the graphical interface. The model was refined with **ShelXL** 2018/3 (Sheldrick, 2015) using full matrix least squares minimisation on F^2.

Crystal data

$C_{27}H_{29}AlN_2$, M_r = 408.50, orthorhombic, $Pca2_1$ (No. 29), a = 13.85276(5) Å, b = 27.33166(10) Å, c = 12.39473(4) Å, $\alpha = \beta = \gamma = 90^\circ$, V = 4692.88(3) Å^3, T = 120.01(10) K, Z = 8, Z' = 2, μ(Cu K$_\alpha$) = 0.854, 77255 reflections measured, 9526 unique (R_{int} = 0.0692) which were used in all calculations. The final wR_2 was 0.1136 (all data) and R_1 was 0.0436 (I≥2 σ(I)).

Plot

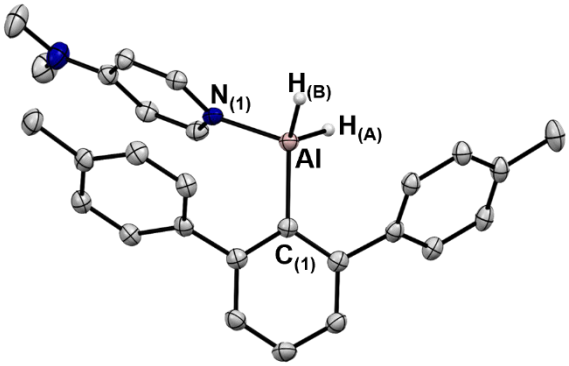

Hydrogen atoms (other than Al–H) omitted for clarity. Thermal ellipsoids set to 50% probability.

^{Mes}TerAl(Et)H (ABG-0239)

Experimental

Single colourless block crystals of **^{Mes}TerAl(Et)H** were recrystallised from d_6-benzene by slow cooling. A suitable crystal with dimensions 0.48 × 0.13 × 0.12 mm^3 was selected and mounted on a MITIGEN holder in Paratone oil on a Rigaku Oxford Diffraction XCalibur diffractometer. The crystal was kept at a steady T = 119.99(15) K during data collection. The structure was solved with the ShelXT 2018/2 (Sheldrick, 2018) solution program using dual methods and by using Olex2 (Dolomanov et al., 2009) as the graphical interface. The model was refined with ShelXL 2018/3 (Sheldrick, 2015) using full matrix least squares minimisation on $\boldsymbol{F^2}$.

Crystal data

$C_{52}H_{62}Al_2$, M_r = 740.97, monoclinic, $P2_1/c$ (No. 14), a = 22.9256(8) Å, b = 9.1694(2) Å, c = 23.7595(8) Å, β = 116.513(4)°, α = γ = 90°, V = 4469.3(3) Å^3, T = 119.99(15) K, Z = 4, Z' = 1, μ(Mo K$_\alpha$) = 0.098, 86296 reflections measured, 8800 unique (R_{int} = 0.0628) which were used in all calculations. The final wR_2 was 0.1299 (all data) and R_1 was 0.0573 (I≥2 σ(I)).

Plot

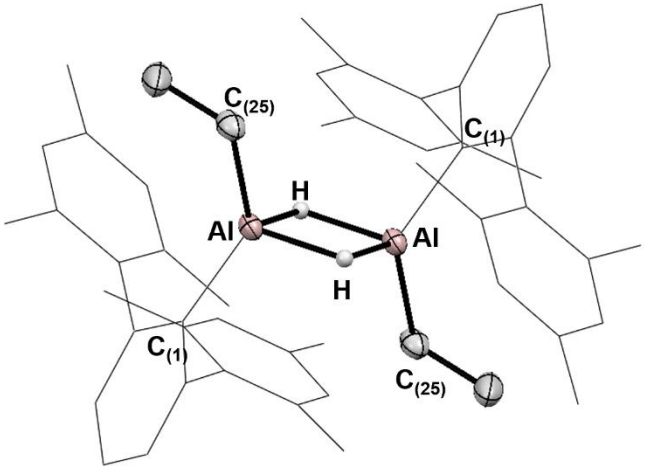

Hydrogen atoms (other than Al–H) omitted and ^{Mes}Ter-substituent displayed in wireframe for clarity. Thermal ellipsoids set to 50% probability.

^{Tipp}TerAl(Me)H (ABG-0438)

Experimental

Single colourless block crystals of **^{Tipp}TerAl(Me)H** were formed spontaneously over 48 hours at room temperature in d_2-dichloromethane (0.67 mL) by the reaction of ^{Tipp}TerAlMe$_2$ (26.9 mg, 0.05 mmol, 10 mol%) with HBpin (87 µL, 0.6 mmol, 1.2 equiv.) in the presence of 1-octene (80 µL, 0.5 mmol, 1.0 equiv.). A suitable crystal with dimensions 0.32 × 0.30 × 0.16 mm^3 was selected and mounted on a MITIGEN holder in Paratone oil on a Bruker D8 VENTURE diffractometer. The crystal was kept at a steady T = 100.0 K during data collection. The structure was solved with the ShelXT 2018/2 (Sheldrick, 2018) solution program using dual methods and by using Olex2 (Dolomanov et al., 2009) as the graphical interface. The model was refined with ShelXL 2018/3 (Sheldrick, 2015) using full matrix least squares minimisation on F^2.

Crystal data

$C_{76}H_{106}Al_2Cl_4D_4$, M_r = 1223.42, monoclinic, $P2_1/c$ (No. 14), a = 13.2338(13) Å, b = 16.0297(14) Å, c = 17.3617(19) Å, β = 105.344(4)°, $\alpha = \gamma$ = 90°, V = 3551.7(6) Å^3, T = 100.0 K, Z = 2, Z' = 0.5, μ(MoK$_\alpha$) = 0.232, 99101 reflections measured, 8798 unique (R_{int} = 0.0477) which were used in all calculations. The final wR_2 was 0.1174 (all data) and R_1 was 0.0424 (I≥2 σ(I)).

Plot

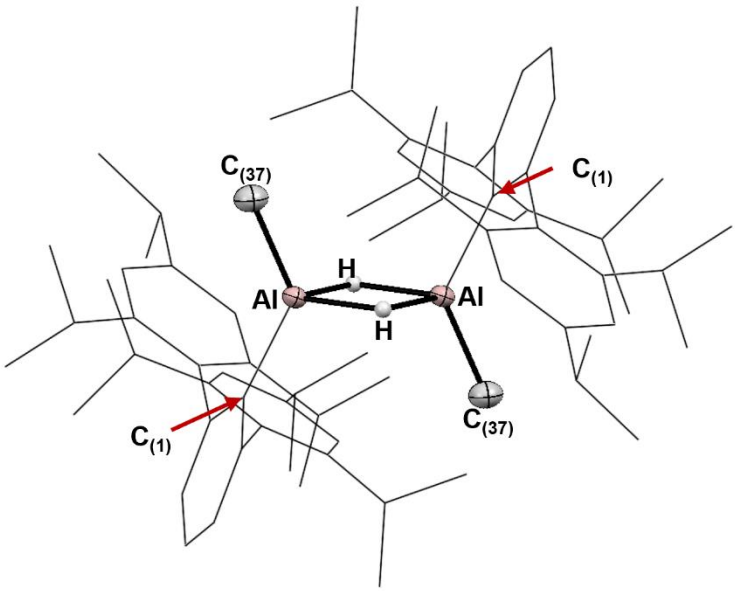

Hydrogen atoms (other than Al–H) omitted and ^{Tipp}Ter-substituent displayed in wireframe for clarity. Thermal ellipsoids set to 50% probability.

[^{Mes}TerAl(pin)]$_2$ (ABG-0431)

Experimental

Single colourless block crystals of **[^{Mes}TerAl(pin)]$_2$** were recrystallised from pentane by slow evaporation. A suitable crystal with dimensions 0.44 × 0.44 × 0.37 mm^3 was selected and mounted on a MITIGEN holder in Paratone oil on a Bruker D8 VENTURE diffractometer. The crystal was kept at a steady T = 100.0 K during data collection. The structure was solved with the ShelXT 2018/2 (Sheldrick, 2018) solution program using dual methods and by using Olex2 (Dolomanov et al., 2009) as the graphical interface. The model was refined with ShelXL 2018/3 (Sheldrick, 2015) using full matrix least squares minimisation on F^2.

Crystal data

$C_{60}H_{74}Al_2O_4$, M_r = 913.15, orthorhombic, $Pna2_1$ (No. 33), a = 21.776(2) Å, b = 12.9998(13) Å, c = 18.2027(17) Å, $\alpha = \beta = \gamma = 90^{\circ}$, V = 5152.9(8) Å^3, T = 100.0 K, Z = 4, Z' = 1, μ(MoK$_\alpha$) = 0.103, 165986 reflections measured, 15701 unique (R_{int} = 0.0412) which were used in all calculations. The final wR_2 was 0.0697 (all data) and R_1 was 0.0258 (I≥2 σ(I)).

Plot

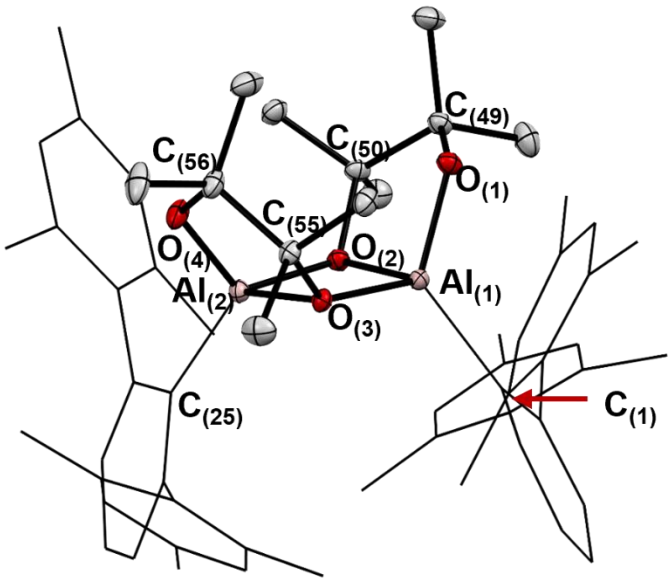

Hydrogen atoms omitted and ^{Mes}Ter-substituent displayed in wireframe for clarity. Thermal ellipsoids set to 50% probability.

Bis(tetrahydroborate) alane 3-Mes-1 (ABG-0683)

Experimental

Single colourless block-shaped crystals of **3-Mes-1** were recrystallised from pentane by slow evaporation. A suitable crystal with dimensions 0.52 × 0.25 × 0.20 mm^3 was selected and mounted on a MITIGEN holder in Paratone oil on a Bruker APEX-II CCD diffractometer. The crystal was kept at a steady T = 100.00 K during data collection. The structure was solved by Dr Jordann Wells with the **ShelXT** (Sheldrick, 2018) solution program using direct methods and by using **Olex2** 1.5 (Dolomanov et al., 2009) as the graphical interface. The model was refined with **ShelXL** 2018/3 (Sheldrick et al., 2015) using full matrix least squares minimisation on F^2.

Crystal data

$C_{40}H_{47}AlSi_2$, M_r = 370.10, monoclinic, $C2/c$ (No. 15), a = 15.2933(16) Å, b = 10.0128(12) Å, c = 17.019(3) Å, β = 115. 393(3)°, $\alpha = \gamma = 90°$, V = 2354.3(5) $Å^3$, T = 100.00 K, Z = 4, Z' = 0.5, μ(Mo K_α) = 0.09, 31802 reflections measured, 3582 unique (R_{int} = 0.031) which were used in all calculations. The final wR_2 was 0.1216 (all data) and R_1 was 0.0517 (I≥2 σ(I)).

Plot

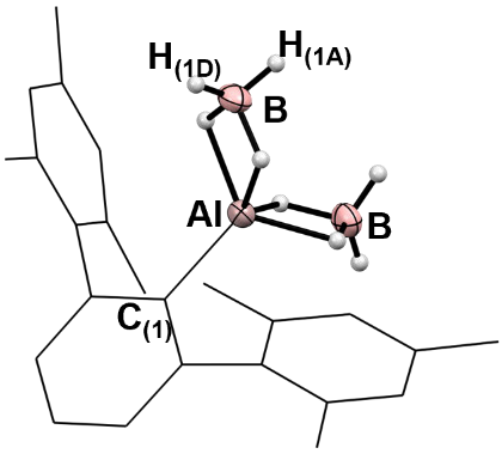

Hydrogen atoms (other than Al–H and B–H) omitted and ^{Mes}Ter-substituent displayed in wireframe for clarity. Thermal ellipsoids set to 50% probability.

Bis(arylborohydride) alane 3-Mes-3^{Mes} (ABG-0450)

Experimental

Single colourless block-shaped crystals of **3-Mes-3^{Mes}** were recrystallised from hexane by slow cooling. A suitable crystal with dimensions 0.31 × 0.31 × 0.23 mm^3 was selected and mounted on a MITIGEN holder in Paratone oil on a Bruker D8 Venture diffractometer. The crystal was kept at a steady T = 100.0 K during data collection. The structure was solved with the **ShelXT** 2018/2 (Sheldrick, 2018) solution program using dual methods and by using **Olex2** 1.3 (Dolomanov et al., 2009) as the graphical interface. The model was refined with **ShelXL** 2018/3 (Sheldrick, 2015) using full matrix least squares minimisation on $\boldsymbol{F^2}$.

Crystal data

$C_{168}H_{212}Al_4B_8$, M_r = 2425.76, triclinic, P-1 (No. 2), a = 9.3191(9) Å, b = 17.9862(16) Å, c = 23.336(2) Å, α = 73.958(2)°, β = 78.896(2)°, γ = 89.569(2)°, V = 3684.4(6) Å^3, T = 100.0 K, Z = 1, Z' = 0.5, μ(MoK_α) = 0.082, 187187 reflections measured, 22498 unique (R_{int} = 0.0386) which were used in all calculations. The final wR_2 was 0.1168 (all data) and R_1 was 0.0416 (I≥2 σ(I)).

Plot

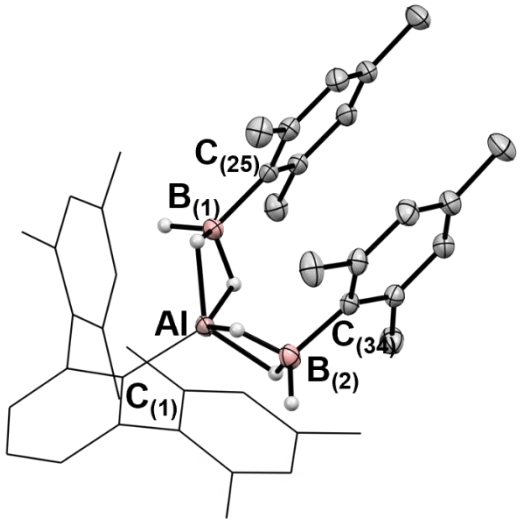

Hydrogen atoms (other than Al–H and B–H) omitted and ^{Mes}Ter-substituent displayed in wireframe for clarity. Thermal ellipsoids set to 50% probability.

Silylalane ^{Mes}TerAl(*Si*)$_2$ (ABG-0671)

Experimental

Single colourless block-shaped crystals of ^{Mes}**TerAl(*Si*)$_2$** were recrystallised from pentane by slow cooling. A suitable crystal with dimensions 0.58 × 0.25 × 0.19 mm^3 was selected and mounted on a MITIGEN holder in Paratone oil on a Bruker APEX-II CCD diffractometer. The crystal was kept at a steady T = 100.00 K during data collection. The structure was solved with the **ShelXS** (Sheldrick, 2008) solution program using direct methods and by using **Olex2** 1.5-beta (Dolomanov et al., 2009) as the graphical interface. The model was refined with **olex2.refine** 1.5-beta (Bourhis et al., 2015) using full matrix least squares minimisation on F^2.

Crystal data

$C_{40}H_{47}AlSi_2$, M_r = 610.971, orthorhombic, $P2_12_12_1$ (No. 19), a = 17.0806(12) Å, b = 19.4168(14) Å, c = 21.6320(15) Å, $\alpha = \beta = \gamma = 90^\circ$, V = 7174.3(9) Å^3, T = 100.00 K, Z = 8, Z' = 2, μ(Mo K$_\alpha$) = 0.149, 177148 reflections measured, 21876 unique (R_{int} = 0.0588) which were used in all calculations. The final wR_2 was 0.0348 (all data) and R_1 was 0.0237 (I≥2 σ(I)).

Plot

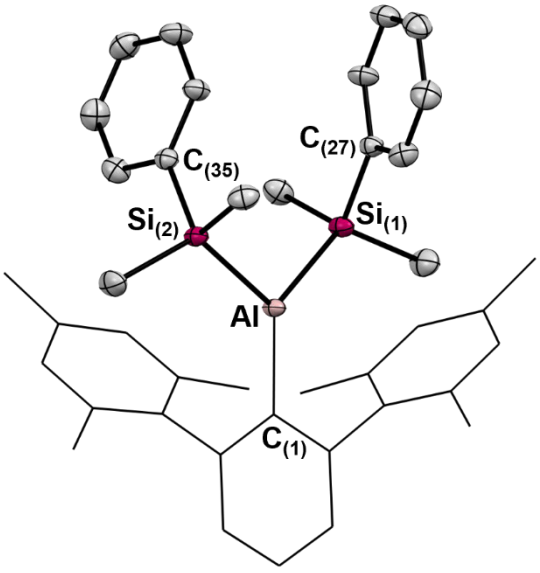

Hydrogen atoms omitted and ^{Mes}Ter-substituent displayed in wireframe for clarity. Thermal ellipsoids set to 50% probability.

Full crystallographic data for all compounds

Compound	$^{p\text{-Tol}}$TerAlH$_2$•DMAP	^{Mes}TerAl(Et)H	^{Tipp}TerAl(Me)H
Formula	$C_{27}H_{29}AlN_2$	$C_{52}H_{62}Al_2$	$C_{76}H_{106}Al_2Cl_4D_4$
$D_{calc.}$/ g cm^{-3}	1.156	1.101	1.144
m/mm^{-1}	0.854	0.098	0.232
Formula Weight	408.5	740.97	1223.42
Colour	colourless	colourless	colourless
Shape	block	block	block
Size/mm^3	0.43×0.25×0.17	0.48×0.13×0.12	0.32×0.30×0.16
T/K	120.01(10)	119.99(15)	100
Crystal System	orthorhombic	monoclinic	monoclinic
Space Group	$Pca2_1$	$P2_1/c$	$P2_1/c$
a/Å	13.85276(5)	22.9256(8)	13.2338(13)
b/Å	27.33166(10)	9.1694(2)	16.0297(14)
c/Å	12.39473(4)	23.7595(8)	17.3617(19)
a/°	90	90	90
b/°	90	116.513(4)	105.344(4)
g/°	90	90	90
V/Å^3	4692.88(3)	4469.3(3)	3551.7(6)
Z	8	4	2
Z'	2	1	0.5
Wavelength/Å	1.54184	0.71073	0.71073
Radiation type	CuK_a	MoK_a	MoK_a
Q_{min}/°	3.577	3.319	2.148
Q_{max}/°	76.021	26.022	28.287
Measured Refl's.	77255	86296	99101
Indep't Refl's	9526	8800	8798
Refl's I≥2 s(I)	9419	7069	7626
R_{int}	0.0692	0.0628	0.0477
Parameters	565	509	520
Restraints	1	0	310
Largest Peak	0.279	0.346	0.588
Deepest Hole	-0.441	-0.251	-0.578
GooF	1.045	1.086	1.048
wR_2 (all data)	0.1136	0.1299	0.1174
wR_2	0.113	0.1214	0.1111
R_1 (all data)	0.0439	0.0764	0.0506
R_1	0.0436	0.0573	0.0424

Compound	[^{Mes}TerAl(pin)]$_2$	3-Mes-1	3-Mes-3	^{Mes}TerAl(*Si*)$_2$
Formula	$C_{60}H_{74}Al_2O_4$	$C_{24}H_{33}AlB_2$	$C_{168}H_{212}Al_4B_8$	$C_{40}H_{47}AlSi_2$
$D_{calc.}$/ g cm^{-3}	1.177	1.044	1.093	1.131
m/mm^{-1}	0.103	0.09	0.082	0.149
Formula Weight	913.15	370.1	2425.76	610.971
Colour	colourless	colourless	colourless	colourless
Shape	block	block	block	block
Size/mm^3	0.44×0.44×0.37	0.52×0.25×0.20	0.31×0.31×0.23	0.58×0.25×0.19
T/K	100	100	100	100
Crystal System	orthorhombic	monoclinic	triclinic	orthorhombic
Space Group	*Pna*2$_1$	*C*2/c	*P*-1	*P*2$_1$2$_1$2$_1$
a/Å	21.776(2)	15.2933(16)	9.3191(9)	17.0806(12)
b/Å	12.9998(13)	10.0128(12)	17.9862(16)	19.4168(14)
c/Å	18.2027(17)	17.019(3)	23.336(2)	21.6320(15)
a/°	90	90	73.958(2)	90
b/°	90	115.393(3)	78.896(2)	90
g/°	90	90	89.569(2)	90
V/Å^3	5152.9(8)	2354.3(5)	3684.4(6)	7174.3(9)
Z	4	4	1	8
Z'	1	0.5	0.5	2
Wavelength/Å	0.71073	0.71073	0.71073	0.71073
Radiation type	Mo*K*$_a$	Mo*K*$_a$	Mo*K*$_a$	Mo*K*$_a$
Q_{min}/°	2.888	2.51	2.23	2.16
Q_{max}/°	30.524	30.27	30.565	30.53
Measured Refl's.	165986	31802	187187	177148
Indep't Refl's	15701	3582	22498	21876
Refl's I≥2 *s*(I)	15194	3003	18528	19441
R_{int}	0.0412	0.031	0.0386	0.0588
Parameters	891	175	883	1621
Restraints	1	2	0	0
Largest Peak	0.275	0.3	0.325	0.1999
Deepest Hole	-0.175	-0.31	-0.293	-0.2353
GooF	1.049	1.052	1.03	1.0754
wR_2 (all data)	0.0697	0.1216	0.1168	0.0348
wR_2	0.0683	0.1142	0.1079	0.0322
R_1 (all data)	0.0274	0.0517	0.0542	0.0338
R_1	0.0258	0.0427	0.0416	0.0237

References

1 P. T. Anastas and J. C. Warner, *Green Chemistry: Theory and Practice*, Oxford University Press, New York, 1998.

2 C. A. Busacca, D. R. Fandrick, J. J. Song and C. H. Senanayake, *Adv. Synth. Catal.*, 2011, **353**, 1825–1864.

3 C. C. C. Johansson Seechurn, M. O. Kitching, T. J. Colacot and V. Snieckus, *Angew. Chemie - Int. Ed.*, 2012, **51**, 5062–5085.

4 C. Liu, C. F. Bender, X. Han and R. A. Widenhoefer, *Chem. Commun.*, 2007, 3607–3618.

5 K. Fagnou and M. Lautens, *Chem. Rev.*, 2003, **103**, 169–196.

6 J. Magano and J. R. Dunetz, *Chem. Rev.*, 2011, **111**, 2177–2250.

7 I. A. I. Mkhalid, J. H. Barnard, T. B. Marder, J. M. Murphy and J. F. Hartwig, *Chem. Rev.*, 2010, **110**, 890–931.

8 L. Ackermann, *Chem. Rev.*, 2011, **111**, 1315–1345.

9 J. D. Hayler, D. K. Leahy and E. M. Simmons, *Organometallics*, 2019, **38**, 36–46.

10 S. W. M. Crossley, C. Obradors, R. M. Martinez and R. A. Shenvi, *Chem. Rev.*, 2016, **116**, 8912–9000.

11 G. Cahiez and A. Moyeux, *Chem. Rev.*, 2010, **110**, 1435–1462.

12 S. K. Gurung, S. Thapa, A. Kafle, D. A. Dickie and R. Giri, *Org. Lett.*, 2014, **16**, 1264–1267.

13 J. V. Obligacion and P. J. Chirik, *Nat. Rev. Chem.*, 2018, **2**, 15–34.

14 H. Bauer and S. Harder, *Early Main Gr. Met. Catal.*, 2020, 175–199.

15 F. Buch, J. Brettar and S. Harder, *Angew. Chemie - Int. Ed.*, 2006, **45**, 2741–2745.

16 S. Harder, *Chem. Rev.*, 2010, **110**, 3852–3876.

17 M. S. Hill, D. J. Liptrot and C. Weetman, *Chem. Soc. Rev.*, 2016, **45**, 972–988.

18 G. I. Nikonov, *ACS Catal.*, 2017, **7**, 7257–7266.

19 K. Revunova and G. I. Nikonov, *Dalt. Trans.*, 2015, **44**, 840–866.

20 R. Rochat, M. J. Lopez, H. Tsurugi and K. Mashima, *ChemCatChem*, 2016, **8**, 10–20.

21 K. Hobson, C. J. Carmalt and C. Bakewell, *Chem. Sci.*, 2020, **11**, 6942–6956.

22 T. Chu, I. Korobkov and G. I. Nikonov, *J. Am. Chem. Soc.*, 2014, **136**, 9195–9202.

23 T. Chu, Y. Boyko, I. Korobkov and G. I. Nikonov, *Organometallics*, 2015, **34**, 5363–5365.

24 J. Hicks, P. Vasko, J. M. Goicoechea and S. Aldridge, *J. Am. Chem. Soc.*, 2019, **141**, 11000–11003.

25 N. O. Calloway, *Chem. Rev.*, 1935, **17**, 327–392.

26 T. Inukai and M. Kasai, *J. Org. Chem.*, 1965, **30**, 3567–3569.

27 P. Yates and P. Eaton, *J. Am. Chem. Soc.*, 1960, **82**, 4436–4437.

28 C. J. Whiteoak, N. Kielland, V. Laserna, E. C. Escudero-Adán, E. Martin and A. W. Kleij, *J. Am. Chem. Soc.*, 2013, **135**, 1228–1231.

29 R. Cohen, C. R. Graves, S. T. Nguyen, J. M. L. Martin and M. A. Ratner, *J. Am. Chem. Soc.*, 2004, **126**, 14796–14803.

30 H. Meerwein and R. Schmidt, *Justus Liebig's Ann. der Chemie*, 1925, **444**, 221–238.

31 W. Ponndorf, *Zeitschrift für Angew. Chemie*, 1926, **39**, 138–143.

32 R. V. Oppenauer, *Recl. des Trav. Chim. des Pays-Bas*, 1937, **56**, 137–144.

33 L. Mandell, *J. Am. Chem. Soc.*, 1956, **78**, 3199–3201.

34 K. Maruoka and H. Yamamoto, *Tetrahedron*, 1988, **44**, 5001–5032.

35 R. Köster and P. Binger, 1965, vol. 7, pp. 263–348.

36 J. J. Eisch, in *Comprehensive Organometallic Chemistry II Volume 11*, eds. E. W. Abel, G. Wilkinson and F. G. A. Stone, Elsevier: Oxford, 1995, pp. 277–311.

37 K. Ziegler, *Angew. Chemie*, 1952, **64**, 323–329.

38 E. C. Ashby, *J. Am. Chem. Soc.*, 1964, **86**, 1882–1883.

39 E. C. Ashby, G. J. Brendel and H. E. Redman, *Inorg. Chem.*, 1963, **2**, 499–504.

40 K. Ziegler, H. Gellert, H. Martin, K. Nagel and J. Schneider, *Justus Liebigs Ann. Chem.*, 1954, **589**, 91–121.

41 K. Ziegler, H.-G. Gellert, H. Lehmkuhl, W. Pfohl and K. Zosel, *Justus Liebigs Ann. Chem.*, 1960, **629**, 1–13.

42 K. Ziegler, E. Holzkamp, H. Breil and H. Martin, *Angew. Chemie*, 1955, **67**, 426–426.

43 L. L. Böhm, *Angew. Chemie Int. Ed.*, 2003, **42**, 5010–5030.

44 The Nobel Prize in Chemistry 1963, https://www.nobelprize.org/prizes/chemistry/1963/summary/, (accessed 24 March 2023).

45 J. J. Eisch, *Organometallic Syntheses Volume 2*, Elsevier, 1981.

46 H.-G. Stammler, S. Blomeyer, R. J. F. Berger and N. W. Mitzel, *Angew. Chemie Int. Ed.*, 2015, **54**, 13816–13820.

47 P. Laszlo, *Angew. Chemie Int. Ed.*, 2000, **39**, 2071–2072.

48 H. C. Longuet-Higgins and R. P. Bell, *J. Chem. Soc.*, 1943, 250.

49 L. S. Bartell and B. L. Carroll, *J. Chem. Phys.*, 1965, **42**, 3076–3078.

50 R. Boese, A. J. Downs, T. M. Greene, A. W. Hall, C. A. Morrison and S. Parsons, *Organometallics*, 2003, **22**, 2450–2457.

51 A. Almenningen, S. Halvorsen, A. Haaland, K. Pihlaja, K. Schaumburg and L. Ehrenberg, *Acta Chem. Scand.*, 1971, **25**, 1937–1945.

52 R. G. Vranka and E. L. Amma, *J. Am. Chem. Soc.*, 1967, **89**, 3121–3126.

53 E. G. Hoffmann, *Justus Liebigs Ann. Chem.*, 1960, **629**, 104–121.

54 J. N. Hay, P. G. Hooper and J. C. Robb, *J. Organomet. Chem.*, 1971, **28**, 193–204.

55 M. B. Smith, *J. Organomet. Chem.*, 1970, **22**, 273–281.

56 A. Keys, P. T. Brain, C. A. Morrison, R. L. Callender, B. A. Smart, D. A. Wann, H. E. Robertson, D. W. H. Rankin and A. R. Barron, *Dalt. Trans.*, 2008, **3**, 404–410.

57 A. R. Cowley, A. J. Downs, S. Marchant, V. A. Macrae, R. A. Taylor and S. Parsons, *Organometallics*, 2005, **24**, 5702–5709.

58 J. N. Hay, G. R. Jones and J. C. Robb, *J. Organomet. Chem.*, 1968, **15**, 295–299.

59 G. Wilke and H. Müller, *Justus Liebigs Ann. Chem.*, 1960, **629**, 222–240.

60 A. Bismuto, S. P. Thomas and M. J. Cowley, *Angew. Chemie - Int. Ed.*, 2016, **55**, 15356–15359.

61 F. M. Brower, N. E. Matzek, P. F. Reigler, H. W. Rinn, C. B. Roberts, D. L. Schmidt, J. A. Snover and K. Terada, *J. Am. Chem. Soc.*, 1976, **98**, 2450–2453.

62 J. W. Turley and H. W. Rinn, *Inorg. Chem.*, 1969, **8**, 18–22.

63 T. Mole and E. A. Jeffery, *Organoaluminium Compounds*, Elsevier: New York, 1972.

64 J. C. Fettinger, P. A. Gray, C. E. Melton and P. P. Power, *Organometallics*, 2014, **33**, 6232–6240.

65 R. Köster and G. Bruno, *Justus Liebigs Ann. Chem.*, 1960, **629**, 89–103.

66 R. Köster and G. Benedikt, *Angew. Chemie*, 1962, **74**, 589–589.

67 J. Klosin, G. R. Roof, E. Y. X. Chen and K. A. Abboud, *Organometallics*, 2000, **19**, 4684–4686.

68 C. H. Lee, S. J. Lee, J. W. Park, K. H. Kim, B. Y. Lee and J. S. Oh, *J. Mol. Catal. A Chem.*, 1998, **132**, 231–239.

69 R. Waterman, *Organometallics*, 2013, **32**, 7249–7263.

70 K. N. Harrison and T. J. Marks, *J. Am. Chem. Soc.*, 1992, **114**, 9220–9221.

71 R. Köster, *Justus Liebigs Ann. Chem.*, 1958, **618**, 31–43.

72 H. Berger, H. Nöth, G. Rub and B. Wrackmeyer, *Chem. Ber.*, 1980, **113**, 1235–1244.

73 H. C. Brown and S. K. Gupta, *J. Am. Chem. Soc.*, 1971, **93**, 1818–1819.

74 O. Zhurakovskyi, R. M. P. Dias, A. Noble and V. K. Aggarwal, *Org. Lett.*, 2018, **20**, 3136–3139.

75 L. Jin, P. Zhang, Y. Li, X. Yu and B. Shi, *J. Am. Chem. Soc.*, 2021, **143**, 12335–12344.

76 M. Kubo, 1959, **82**, 6218–6223.

77 H. Schulz, T. Deforth and W. Siebert, *Zeitschrift für Naturforsch. B*, 1993, **48**, 68–71.

78 H. Nöth and W. Storch, *Synth. React. Inorg. Met. Chem.*, 1971, **1**, 197–205.

79 Y. Ishikawa, K. Suzuki, K. Hayashi, S. Y. Nema and M. Yamashita, *Org. Lett.*, 2019, **21**, 1722–1725.

80 J.-K. Uhm, H. Römich, H. Wadepohl and W. Siebert, *Zeitschrift für Naturforsch. B*, 1988, **43**, 306–308.

81 A. Bismuto, M. J. Cowley and S. P. Thomas, *ACS Catal.*, 2018, **8**, 2001–2005.

82 R. Köster, G. Seidel and M. Yalpani, *Chem. Ber.*, 1989, **122**, 1815–1824.

83 Ö. Seven, M. Bolte, H. Lerner and M. Wagner, *Organometallics*, 2014, **33**, 1291–1299.

84 H. C. Brown, B. Singaram and T. E. Cole, *J. Am. Chem. Soc.*, 1985, **107**, 460–464.

85 B. Singaram, T. E. Cole and H. C. Brown, *Organometallics*, 1984, **3**, 774–777.

86 H. C. Brown and I. Gupta, *J. Organomet. Chem.*, 1971, **32**, 4062–4063.

87 C. M. Bateman, H. Beal, J. E. Barker, B. L. Thompson, D. Donovan, B. J. Grant, J. Shooter, J. H. Arakawa, S. Johnson, C. J. Allen, J. L. Yates, R. Kato, C. W. K. Tinsley, L. N. Zakharov and E. R. Abbey, *Org. Lett.*, 2018, **20**, 3784–3787.

88 M. Hoshi and K. Shirakawa, *Chem. Commun.*, 2002, 2146–2147.

89 D. R. Willcox and S. P. Thomas, *Beilstein J. Org. Chem.*, 2023, **19**, 325–348.

90 A. Das, S. Rej and T. K. Panda, *Dalt. Trans.*, 2022, **51**, 3027–3040.

91 K. Ziegler, *Organometallic Chemistry*, Reinhold Publishing Corporation, 1960.

92 S. Baba and E. Negishi, *J. Am. Chem. Soc.*, 1976, **98**, 6729–6731.

93 E. Negishi and S. Baba, *J. Chem. Soc., Chem. Commun.*, 1976, 596b-597b.

94 H. Ogawa, Z. Yang, H. Minami, K. Kojima, T. Saito, C. Wang and M. Uchiyama, *ACS Catal.*, 2017, **7**, 3988–3994.

95 K. Ziegler, F. Krupp and K. Zosel, *Angew. Chemie*, 1955, **67**, 425–426.

96 K. Ziegler, F. Krupp and K. Zosel, *Justus Liebigs Ann. Chem.*, 1960, **629**, 241–250.

97 A. E. Finholt, A. C. Bond and H. I. Schlesinger, *J. Am. Chem. Soc.*, 1947, **69**, 1199–

1203.

98 J. W. Bundens and M. M. Francl, *Organometallics*, 1993, **12**, 1608–1615.

99 H. Brown and B. C. Rao, *J. Org. Chem.*, 1957, **22**, 1136–1137.

100 J. N. Hay, P. G. Hooper and J. C. Robb, *Trans. Faraday Soc.*, 1970, **66**, 2800–2804.

101 P. E. M. Allen, J. N. Hay, G. R. Jones and J. C. Robb, *Trans. Faraday Soc.*, 1967, **63**, 1636–1646.

102 J. J. Eisch and C. K. Hordis, *J. Am. Chem. Soc.*, 1971, **93**, 4496–4502.

103 J. W. Bundens, J. Yudenfreund and M. M. Francl, *Organometallics*, 1999, **18**, 3913–3920.

104 P. Binger and H. Schäfer, *Tetrahedron Lett.*, 1975, **16**, 4673–4676.

105 M. A. Greene, Y. Liu, J. R. Sanzone and K. A. Woerpel, *Org. Lett.*, 2020, **22**, 7518–7521.

106 J. J. Eisch and N. E. Burlinson, *J. Am. Chem. Soc.*, 1976, **98**, 753–761.

107 E. C. Ashby and S. A. Noding, *J. Org. Chem.*, 1979, **44**, 4364–4371.

108 T. Yoshida and E. ichi Negishi, *J. Am. Chem. Soc.*, 1981, **103**, 4985–4987.

109 M. Dahlmann and M. Lautens, *Catal. Heterofunctionalization*, 2001, **4**, 47–72.

110 F. Sato, in *Fundamental Research in Homogeneous Catalysis*, Springer US, Boston, MA, 1978, pp. 81–92.

111 J. J. Eisch, X. Ma, M. Singh and G. Wilke, *J. Organomet. Chem.*, 1997, **527**, 301–304.

112 E. ichi Negishi and T. Yoshida, *Tetrahedron Lett.*, 1980, **21**, 1501–1504.

113 F. Sato, S. Sato and M. Sato, *J. Organomet. Chem.*, 1976, **122**, C25–C27.

114 K. Maruoka, H. Sano, K. Shinoda, S. Nakai and H. Yamamoto, *J. Am. Chem. Soc.*, 1986, **108**, 6036–6038.

115 K. Maruoka, H. Sano, K. Shinoda and H. Yamamoto, *Chem. Lett.*, 1987, **16**, 73–76.

116 A. H. Blatt, *Chem. Rev.*, 1933, **12**, 215–260.

117 E. Beckmann, *Berichte der Dtsch. Chem. Gesellschaft*, 1886, **19**, 988–993.

118 K. Maruoka, T. Miyazaki, M. Ando, Y. Matsumura, S. Sakane, K. Hattori and H. Yamamoto, *J. Am. Chem. Soc.*, 1983, **105**, 2831–2843.

119 R. F. Nystrom and W. G. Brown, *J. Am. Chem. Soc.*, 1947, **69**, 2548–2549.

120 R. F. Nystrom and W. G. Brown, *J. Am. Chem. Soc.*, 1947, **69**, 1197–1199.

121 R. F. Nystrom and W. G. Brown, *J. Am. Chem. Soc.*, 1947, **69**, 1197–1199.

122 T. Mole and J. R. Surtees, in *Chemistry and industry.*, Society of Chemical Industry, London, 1963, pp. 1727–1728.

123 P. Binger, *Angew. Chemie Int. Ed. English*, 1963, **2**, 686–686.

124 Y. Chen, W. Jiang, B. Li, G. Fu, S. Chen and H. Zhu, *Dalt. Trans.*, 2019, **48**, 9152–9160.

125 A. Yasuda, S. Tanaka, K. Oshima, H. Yamamoto and H. Nozaki, *J. Am. Chem. Soc.*, 1974, **96**, 6513–6514.

126 A. Yasuda, H. Yamamoto and H. Nozaki, *Bull. Chem. Soc. Jpn.*, 1979, **52**, 1705–1708.

127 R. B. Woodward, K. Heusler, J. Gosteli, P. Naegeli, W. Oppolzer, R. Ramage, S. Ranganathan and H. Vorbrüggen, *J. Am. Chem. Soc.*, 1966, **88**, 852–853.

128 J. Koller and R. G. Bergman, *Organometallics*, 2010, **29**, 3350–3356.

129 J. Koller and R. G. Bergman, *Chem. Commun.*, 2010, **46**, 4577.

130 V. A. Pollard, A. Young, R. McLellan, A. R. Kennedy, T. Tuttle and R. E. Mulvey, *Angew. Chemie - Int. Ed.*, 2019, **58**, 12291–12296.

131 H. Elsen, J. Langer, M. Wiesinger and S. Harder, *Organometallics*, 2020, **39**, 4238–4246.

132 J. Pölker, D. Schaarschmidt, J. Bernauer, M. Villa and A. Jacobi von Wangelin, *ChemCatChem*, , DOI:10.1002/cctc.202200144.

133 J. A. Hatnean, J. W. Thomson, P. A. Chase and D. W. Stephan, *Chem. Commun.*, 2014, **50**, 301–303.

134 Z. W. Qu, H. Zhu and S. Grimme, *ChemCatChem*, 2021, **13**, 3401–3404.

135 H. Elsen, C. Färber, G. Ballmann and S. Harder, *Angew. Chemie - Int. Ed.*, 2018, **57**, 7156–7160.

136 A. Friedrich, J. Eyselein, H. Elsen, J. Langer, J. Pahl, M. Wiesinger and S. Harder, *Chem. - A Eur. J.*, 2021, **27**, 7756–7763.

137 H. Elsen, J. Langer, G. Ballmann, M. Wiesinger and S. Harder, *Chem. - A Eur. J.*, 2021, **27**, 401–411.

138 L. H. Slaugh, *Tetrahedron*, 1966, **22**, 1741–1746.

139 T. Ishiyama, T. A. Ahiko and N. Miyaura, *J. Am. Chem. Soc.*, 2002, **124**, 12414–12415.

140 V. K. Aggarwal, J. R. Suárez, S. P. Thomas, M. Althaus and A. Mahmood, *J. Am. Chem. Soc.*, 2010, **132**, 4025–4028.

141 C. Sandford and V. K. Aggarwal, *Chem. Commun.*, 2017, **53**, 5481–5494.

142 C. Solé and E. Fernández, *Angew. Chemie Int. Ed.*, 2013, **52**, 11351–11355.

143 M. G. Civit, X. Sanz, C. M. Vogels, C. Bo, S. A. Westcott and E. Fernández, *Adv. Synth. Catal.*, 2015, **357**, 3098–3103.

144 M. Khandelwal and R. J. Wehmschulte, *Angew. Chemie - Int. Ed.*, 2012, **51**, 7323–7326.

145 J. Chen and E. Y. X. Chen, *Angew. Chemie - Int. Ed.*, 2015, **54**, 6842–6846.

146 K. Jakobsson, T. Chu and G. I. Nikonov, *ACS Catal.*, 2016, **6**, 7350–7356.

147 M. Saleh, D. R. Powell and R. J. Wehmschulte, *Organometallics*, 2017, **36**, 4810–4815.

148 R. Kannan, R. Chambenahalli, S. Kumar, A. Krishna, A. P. Andrews, E. D. Jemmis and A. Venugopal, *Chem. Commun.*, 2019, **55**, 14629–14632.

149 C. P. Hsu, C. A. Liu, C. C. Wen, Y. H. Liu, Y. F. Lin and C. W. Chiu, *ChemCatChem*, , DOI:10.1002/cctc.202101715.

150 N. Sarkar, R. K. Sahoo, S. Mukhopadhyay and S. Nembenna, *Eur. J. Inorg. Chem.*, , DOI:10.1002/ejic.202101030.

151 Z. Yang, M. Zhong, X. Ma, S. De, C. Anusha, P. Parameswaran and H. W. Roesky, *Angew. Chemie - Int. Ed.*, 2015, **54**, 10225–10229.

152 D. Franz, L. Sirtl, A. Pöthig and S. Inoue, *Zeitschrift fur Anorg. und Allg. Chemie*, 2016, **642**, 1245–1250.

153 V. K. Jakhar, M. K. Barman and S. Nembenna, *Org. Lett.*, 2016, **18**, 4710–4713.

154 N. Sarkar, R. K. Sahoo, A. G. Patro and S. Nembenna, *Polyhedron*, 2022, **222**, 115902.

155 Z. Yang, M. Zhong, X. Ma, S. De, C. Anusha, P. Parameswaran and H. W. Roesky, *Angew. Chemie - Int. Ed.*, 2015, **54**, 10225–10229.

156 Y. Lebedev, I. Polishchuk, B. Maity, M. Dinis Veloso Guerreiro, L. Cavallo and M. Rueping, *J. Am. Chem. Soc.*, 2019, **141**, 19415–19423.

157 V. A. Pollard, M. Á. Fuentes, A. R. Kennedy, R. McLellan and R. E. Mulvey, *Angew. Chemie Int. Ed.*, 2018, **57**, 10651–10655.

158 G. Zhang, J. Wu, H. Zeng, M. C. Neary, M. Devany, S. Zheng and P. A. Dub, *ACS Catal.*, 2019, **9**, 874–884.

159 L. E. Lemmerz, R. McLellan, N. R. Judge, A. R. Kennedy, S. A. Orr, M. Uzelac, E. Hevia, S. D. Robertson, J. Okuda and R. E. Mulvey, *Chem. - A Eur. J.*, 2018, **24**, 9940–9948.

160 B. Prashanth, M. Bhandari, S. Ravi, K. R. Shamasundar and S. Singh, *Chem. - A Eur. J.*, 2018, **24**, 4794–4799.

161 M. Titze, J. Heitkämper, T. Junge, J. Kästner and R. Peters, *Angew. Chemie - Int. Ed.*, 2021, **60**, 5544–5553.

162 V. A. Pollard, S. A. Orr, R. McLellan, A. R. Kennedy, E. Hevia and R. E. Mulvey, *Chem. Commun.*, 2018, **54**, 1233–1236.

163 T. Peddarao, N. Sarkar and S. Nembenna, *Inorg. Chem.*, 2020, **59**, 4693–4702.

164 D. Jin, X. Ma, Y. Liu, J. Peng and Z. Yang, *Appl. Organomet. Chem.*, 2019, **33**, 1–10.

165 C. Ni, Z. Pang, Y. Qiao, P. Guo, X. Ma and Z. Yang, *Inorganica Chim. Acta*, 2022, **543**, 121199.

166 N. Sarkar, R. Kumar Sahoo and S. Nembenna, *Chem. - A Eur. J.*, , DOI:10.1002/chem.202203023.

167 B. Yan, S. Dutta, X. Ma, C. Ni, D. Koley, Z. Yang and H. W. Roesky, *Dalt. Trans.*, 2022, **51**, 6756–6765.

168 M. A. Courtemanche, J. Larouche, M. A. Légaré, W. Bi, L. Maron and F. G. Fontaine, *Organometallics*, 2013, **32**, 6804–6811.

169 C. C. Chia, Y. C. Teo, N. Cham, S. Y. F. Ho, Z. H. Ng, H. M. Toh, N. Mézailles and C. W. So, *Inorg. Chem.*, 2021, **60**, 4569–4577.

170 C. L. Shaves, N. Villegas-Escobar, E. R. Clark and I. M. Riddlestone, *Chem. - A Eur. J.*, , DOI:10.1002/chem.202203806.

171 C.-Q. Li, G. Leng and W. Li, *Catal. Sci. Technol.*, 2022, **12**, 6129–6141.

172 A. K. Jaladi, H. Kim, J. H. Lee, W. K. Shin, H. Hwang and D. K. An, *New J. Chem.*, 2019, **43**, 16524–16529.

173 A. Harinath, J. Bhattacharjee and T. K. Panda, *Adv. Synth. Catal.*, 2019, **361**, 850–857.

174 Y. Ding, X. Ma, Y. Liu, W. Liu, Z. Yang and H. W. Roesky, *Organometallics*, 2019, **38**, 3092–3097.

175 W. Liu, Y. Ding, D. Jin, Q. Shen, B. Yan, X. Ma and Z. Yang, *Green Chem.*, 2019, **21**, 3812–3815.

176 N. Sarkar, S. Bera and S. Nembenna, *J. Org. Chem.*, 2020, **85**, 4999–5009.

177 N. Sarkar, R. K. Sahoo and S. Nembenna, *European J. Org. Chem.*, , DOI:10.1002/ejoc.202200941.

178 Q. Shen, X. Ma, W. Li, W. Liu, Y. Ding, Z. Yang and H. W. Roesky, *Chem. – A Eur. J.*, 2019, **25**, 11918–11923.

179 A. Harinath, I. Banerjee, J. Bhattacharjee and T. K. Panda, *New J. Chem.*, 2019, **43**, 10531–10536.

180 A. K. Jaladi, W. K. Shin and D. K. An, *RSC Adv.*, 2019, **9**, 26483–26486.

181 F. Li, X. Bai, Y. Cai, H. Li, S. Zhang, F. Liu, X. Hong, Y. Xu and S. Shi, *Org. Process Res. Dev.*, 2019, **23**, 1703–1708.

182 H. Karmakar, R. Kumar, J. Sharma, J. Bag, K. Pal, T. K. Panda and V. Chandrasekhar,

Dalt. Trans., 2023, 4481–4493.

183 Z. Yang, M. Zhong, X. Ma, K. Nijesh, S. De, P. Parameswaran and H. W. Roesky, *J. Am. Chem. Soc.*, 2016, **138**, 2548–2551.

184 Y. Ding, X. Liu, X. Ma, Y. Liu, M. Zhong, W. Li, Z. Yang and Y. Yang, *J. Organomet. Chem.*, 2018, **868**, 55–60.

185 K. Hobson, C. J. Carmalt and C. Bakewell, *Inorg. Chem.*, 2021, **60**, 10958–10969.

186 D. Mukherjee, H. Osseili, K. N. Truong, T. P. Spaniol and J. Okuda, *Chem. Commun.*, 2017, **53**, 3493–3496.

187 A. Caise, D. Jones, E. L. Kolychev, J. Hicks, J. M. Goicoechea and S. Aldridge, *Chem. - A Eur. J.*, 2018, **24**, 13624–13635.

188 A. D. Bage, T. A. Hunt and S. P. Thomas, *Org. Lett.*, 2020, **22**, 4107–4112.

189 A. D. Bage, K. Nicholson, T. Langer and S. P. Thomas, *ACS Catal.*, 2020, **10**, 13479–13486.

190 A. D. Bage, K. Nicholson, T. A. Hunt, T. Langer and S. P. Thomas, *Synthesis (Stuttg).*, 2023, **55**, 62–74.

191 I. P. Query, P. A. Squier, E. M. Larson, N. A. Isley and T. B. Clark, *J. Org. Chem.*, 2011, **76**, 6452–6456.

192 D. Lunic, N. Sanosa, I. Funes-Ardoiz and C. J. Teskey, *Angew. Chemie Int. Ed.*, , DOI:10.1002/anie.202207647.

193 J. Légaré Lavergne, H.-M. To and F.-G. Fontaine, *RSC Adv.*, 2021, **11**, 31941–31949.

194 N. Ang, C. Buettner, S. Docherty, A. Bismuto, J. Carney, J. Docherty, M. Cowley and S. Thomas, *Synthesis (Stuttg).*, 2018, **50**, 803–808.

195 F. Meger, A. C. W. Kwok, F. Gilch, D. R. Willcox, A. J. Hendy, K. Nicholson, A. D. Bage, T. Langer, T. A. Hunt and S. P. Thomas, *Beilstein J. Org. Chem.*, 2022, **18**, 1332–1337.

196 E. Jeong, J. Heo, S. Park and S. Chang, *Chem. - A Eur. J.*, 2019, **25**, 6320–6325.

197 Y. Zou, B. Zhang, L. Wang and H. Zhang, *Org. Lett.*, 2021, **23**, 2821–2825.

198 A. Jayaraman, H. Powell-Davies and F. G. Fontaine, *Tetrahedron*, 2019, **75**, 2118–2127.

199 K. Burgess, W. A. van der Donk, S. A. Westcott, T. B. Marder, R. T. Baker and J. C. Calabrese, *J. Am. Chem. Soc.*, 1992, **114**, 9350–9359.

200 S. Harder and J. Spielmann, *J. Organomet. Chem.*, 2012, **698**, 7–14.

201 V. A. Pollard, A. R. Kennedy, R. McLellan, D. Ross, T. Tuttle and R. E. Mulvey, *Eur. J. Inorg. Chem.*, 2021, **2021**, 50–53.

202 D. R. Willcox, D. M. De Rosa, J. Howley, A. Levy, A. Steven, G. S. Nichol, C. A. Morrison, M. J. Cowley and S. P. Thomas, *Angew. Chemie - Int. Ed.*, 2021, **60**, 20672–20677.

203 Q. Zhu, P. Wang, J. Zhu, C. Zhu and G. Zeng, *Inorg. Chem.*, 2020, **59**, 15636–15645.

204 E. A. Romero, J. L. Peltier, R. Jazzar and G. Bertrand, *Chem. Commun.*, 2016, **52**, 10563–10565.

205 C. E. Tucker, J. Davidson and P. Knochel, *J. Org. Chem.*, 1992, **57**, 3482–3485.

206 D. J. Nelson and P. J. Cooper, *Tetrahedron Lett.*, 1986, **27**, 4693–4696.

207 H. C. Brown, J. Chandrasekharan and K. K. Wang, *Pure Appl. Chem.*, 1983, **55**, 1387–1414.

208 H. C. Brown and B. C. S. Rao, *J. Am. Chem. Soc.*, 1956, **78**, 5694–5695.

209 H. C. Brown and J. Chen, *J. Org. Chem.*, 1981, **46**, 3978–3988.

210 E. Nieto-Sepulveda, A. D. Bage, L. A. Evans, T. A. Hunt, A. G. Leach, S. P. Thomas and G. C. Lloyd-Jones, *J. Am. Chem. Soc.*, 2019, **141**, 18600–18611.

211 A. J. J. Lennox and G. C. Lloyd-Jones, *Chem. Soc. Rev.*, 2014, **43**, 412–443.

212 C. M. Crudden and D. Edwards, *European J. Org. Chem.*, 2003, **2003**, 4695–4712.

213 A.-M. Carroll, T. P. O'Sullivan and P. J. Guiry, *Adv. Synth. Catal.*, 2005, **347**, 609–631.

214 I. Beletskaya and A. Pelter, *Tetrahedron*, 1997, **53**, 4957–5026.

215 D. Männig and H. Nöth, *Angew. Chemie Int. Ed. English*, 1985, **24**, 878–879.

216 S. K. Bose, L. Mao, L. Kuehn, U. Radius, J. Nekvinda, W. L. Santos, S. A. Westcott, P. G. Steel and T. B. Marder, *Chem. Rev.*, 2021, **121**, 13238–13341.

217 M. Magre, M. Szewczyk and M. Rueping, *Chem. Rev.*, , DOI:10.1021/acs.chemrev.1c00641.

218 C. Ni, X. Ma, Z. Yang and H. W. Roesky, *Eur. J. Inorg. Chem.*, , DOI:10.1002/ejic.202100929.

219 J. H. Docherty, K. Nicholson, A. P. Dominey and S. P. Thomas, *ACS Catal.*, 2020, **10**, 4686–4691.

220 Q. Yin, S. Kemper, H. F. T. Klare and M. Oestreich, *Chem. - A Eur. J.*, 2016, **22**, 13840–13844.

221 K. Shirakawa, A. Arase and M. Hoshi, *Synthesis (Stuttg).*, 2004, **2004**, 1814–1820.

222 H. C. Brown, N. R. Ayyangar and G. Zweifel, *J. Am. Chem. Soc.*, 1964, **86**, 397–403.

223 S. Masamune, B. M. Kim, J. S. Petersen, T. Sato, S. J. Veenstra and T. Imai, *J. Am. Chem. Soc.*, 1985, **107**, 4549–4551.

224 H. C. Brown and G. Zweifel, *J. Am. Chem. Soc.*, 1961, **83**, 486–487.

225 A. Z. Gonzalez, J. G. Román, E. Gonzalez, J. Martinez, J. R. Medina, K. Matos and J. A. Soderquist, *J. Am. Chem. Soc.*, 2008, **130**, 9218–9219.

226 J. Dunne, University of Edinburgh, 2020.

227 A. D. Bage, University of Edinburgh, 2021.

228 D. R. Willcox, University of Edinburgh, 2022.

229 J. J. Eisch and K. C. Fichter, *J. Organomet. Chem.*, 1983, **250**, 63–81.

230 A. Saednya and H. Hart, *Synthesis (Stuttg).*, 1996, **1996**, 1455–1458.

231 B. R. Barnett, C. C. Mokhtarzadeh, J. S. Figueroa, P. Lummis, S. Wang, J. D. Queen, J. Gavenonis, N. Schüwer, T. D. Tilley, J. N. Boynton, P. P. Power, T. B. Ditri, N. Weidemann, B. R. Barnett, D. W. Agnew, J. S. Figueroa, P. W. Smith, T. B. Ditri, B. R. Barnett, A. E. Carpenter, C. C. Mokhtarzadeh, D. W. Agnew, J. S. Figueroa, P. W. Smith, J. K. Pratt, P. P. Power, N. D. Mendelson, J. S. Figueroa, J. D. Queen, P. P. Power, D. W. Agnew, A. E. Carpenter and J. S. Figueroa, in *Inorganic Syntheses*, 2018, vol. 37, pp. 85–122.

232 K. Ruhlandt-Senge, J. J. Ellison, R. J. Wehmschulte, F. Pauer and P. P. Power, *J. Am. Chem. Soc.*, 1993, **115**, 11353–11357.

233 T. Klis, D. R. Powell, L. Wojtas and R. J. Wehmschulte, *Organometallics*, 2011, **30**, 2563–2570.

234 R. J. Wehmschulte, W. J. Grigsby, B. Schiemenz, R. A. Bartlett and P. P. Power, *Inorg. Chem.*, 1996, **35**, 6694–6702.

235 D. Berthomieu, Y. Bacquet, L. Pedocchi and A. Goursot, *J. Phys. Chem. A*, 1998, **102**, 7821–7827.

236 A. W. Laubengayer and W. F. Gilliam, *J. Am. Chem. Soc.*, 1941, **63**, 477–479.

237 J. D. Erickson, J. C. Fettinger and P. P. Power, *Inorg. Chem.*, 2015, **54**, 1940–1948.

238 L. P. Press, A. J. Kosanovich, B. J. McCulloch and O. V. Ozerov, *J. Am. Chem. Soc.*, 2016, **138**, 9487–9497.

239 M. G. Evans and M. Polanyi, *Trans. Faraday Soc.*, 1935, **31**, 875.

240 J. H. Docherty, J. Peng, A. P. Dominey and S. P. Thomas, *Nat. Chem.*, 2017, **9**, 595–600.

241 F. Li, X. Bai, Y. Cai, H. Li, S.-Q. Zhang, F.-H. Liu, X. Hong, Y. Xu and S.-L. Shi, *Org. Process Res. Dev.*, 2019, **23**, 1703–1708.

242 M. Magre, B. Maity, A. Falconnet, L. Cavallo and M. Rueping, *Angew. Chemie - Int. Ed.*, 2019, **58**, 7025–7029.

243 V. Vasilenko, C. K. Blasius, H. Wadepohl and L. H. Gade, *Chem. Commun.*, 2020, **56**, 1203–1206.

244 Y. Wu, C. Shan, J. Ying, J. Su, J. Zhu, L. L. Liu and Y. Zhao, *Green Chem.*, 2017, **19**, 4169–4175.

245 D. H. Ma, A. K. Jaladi, J. H. Lee, T. S. Kim, W. K. Shin, H. Hwang and D. K. An, *ACS Omega*, 2019, **4**, 15893–15903.

246 M. Uzelac, K. Yuan and M. J. Ingleson, *Organometallics*, 2020, **39**, 1332–1338.

247 S. Harder and J. Spielmann, *Chem. Commun.*, 2011, **47**, 11945.

248 D. Franz, E. Irran and S. Inoue, *Dalt. Trans.*, 2014, **43**, 4451–4461.

249 A. Caise, E. L. Kolychev, J. Hicks, M. Á. Fuentes, J. M. Goicoechea and S. Aldridge, *Dalt. Trans.*, 2019, **48**, 10845–10852.

250 P. R. Oddy and M. G. H. Wallbridge, *J. Chem. Soc. Dalt. Trans.*, 1976, 869.

251 H. I. Schlesinger, R. T. Sanderson and A. B. Burg, *J. Am. Chem. Soc.*, 1940, **62**, 3421–3425.

252 M. T. Barlow, A. J. Downs, P. D. P. Thomas and D. W. H. Rankin, *J. Chem. Soc. Dalt. Trans.*, 1979, 1793.

253 P. Bissinger, P. Mikulcik, J. Riede, A. Schier and H. Schmidbaur, *J. Organomet. Chem.*, 1993, **446**, 37–43.

254 B. Cordero, V. Gómez, A. E. Platero-Prats, M. Revés, J. Echeverría, E. Cremades, F. Barragán and S. Alvarez, *Dalt. Trans.*, 2008, 2832.

255 S. Aldridge, A. J. Blake, A. J. Downs, R. O. Gould, S. Parsons and C. R. Pulham, *J. Chem. Soc. Dalt. Trans.*, 1997, 1007–1012.

256 W. C. Price, *J. Chem. Phys.*, 1949, **17**, 1044–1052.

257 P. C. Lauterbur, R. C. Hopkins, R. W. King, O. V. Ziebarth and C. W. Heitsch, *Inorg. Chem.*, 1968, **7**, 1025–1027.

258 S. Sakuragi, T. Akiba, T. Tanahashi and T. Fujihara, *Angew. Chemie - Int. Ed.*, , DOI:10.1002/anie.202202226.

259 R. van Putten, G. A. Filonenko, A. M. Krieger, M. Lutz and E. A. Pidko, *Organometallics*, 2021, **40**, 674–681.

260 D. Peng, M. Zhang and Z. Huang, *Chem. - A Eur. J.*, 2015, **21**, 14737–14741.

261 R. Larouche-Gauthier, T. G. Elford and V. K. Aggarwal, *J. Am. Chem. Soc.*, 2011, **133**, 16794–16797.

262 R. S. Brokaw and R. N. Pease, *J. Am. Chem. Soc.*, 1950, **72**, 3237–3241.

263 A. J. Downs and L. A. Jones, *Polyhedron*, 1994, **13**, 2401–2415.

264 H. C. Brown and B. C. S. Rao, *J. Am. Chem. Soc.*, 1959, **81**, 6423–6428.

265 J. Burés, *Angew. Chemie Int. Ed.*, 2016, **55**, 16084–16087.

266 E. P. Gillis and M. D. Burke, *J. Am. Chem. Soc.*, 2007, **129**, 6716–6717.

267 F. Caserio, Jr., J. Cavallo and R. Wagner, *J. Org. Chem.*, 1961, **26**, 2157–2158.

268 J. Chen and B. Z. Tang, in *Aggregation-Induced Emission: Fundamentals*, John Wiley and Sons Ltd, Chichester, United Kingdom, 2013, vol. 1–2, pp. 307–322.

269 H. E. Hackney, M. Paladino, H. Fu and D. G. Hall, *Chem. – A Eur. J.*, 2020, **26**, 14324–14329.

270 H. Xiao, T. Li, X.-L. Sun, W.-M. Wan, H. Bao, Q. Qian and Q. Chen, *Molecules*, 2022, **27**, 327.

271 T. Li, Y. Sheng, X. Sun, W. Wan, Y. Liu, Q. Qian and Q. Chen, *Polymers (Basel).*, 2022, **14**, 2025.

272 X. Shi, X. Yang, L. Gai, Z. Zhou and H. Lu, *J. Photochem. Photobiol. A Chem.*, 2021, **412**, 113206.

273 W. Wan, D. Tian, Y. Jing, X. Zhang, W. Wu, H. Ren and H. Bao, *Angew. Chemie Int. Ed.*, 2018, **57**, 15510–15516.

274 S. Maruyama and Y. Kawanishi, *J. Mater. Chem.*, 2002, **12**, 2245–2249.

275 K. N. Tu, C. Gao and S. A. Blum, *J. Org. Chem.*, 2018, **83**, 11204–11217.

276 H. Yoshida, Y. Izumi, Y. Hiraoka, K. Nakanishi, M. Nakamoto, S. Hatano and M. Abe, *Dalt. Trans.*, 2022, **51**, 6543–6546.

277 T. Okuyama, K. Takimoto and T. Fueno, *J. Org. Chem.*, 1977, **42**, 3545–3549.

278 Q. I. Churches, J. F. Hooper and C. A. Hutton, *J. Org. Chem.*, 2015, **80**, 5428–5435.

279 A. Takagi, T. Ikawa, K. Saito, S. Masuda, T. Ito and S. Akai, *Org. Biomol. Chem.*, 2013, **11**, 8145.

280 E. J. Wren, X. Wang, A. Farlow, S.-C. Lo, P. L. Burn and P. Meredith, *Org. Lett.*, 2010, **12**, 4338–4340.

281 J. Yin, P. H. Jacobse, D. Pyle, Z. Wang, M. F. Crommie and G. Dong, *J. Am. Chem. Soc.*, 2022, **144**, 16012–16019.

282 T. Tani, N. Takahashi, Y. Sawatsugawa, M. Osano and T. Tsuchimoto, *Adv. Synth. Catal.*, 2021, **363**, 2427–2442.

283 J. C. H. Lee, H.-Y. Sun and D. G. Hall, *J. Org. Chem.*, 2015, **80**, 7134–7143.

284 J. Fyfe and A. Watson, *Synlett*, 2015, **26**, 1139–1144.

285 H. Noguchi, K. Hojo and M. Suginome, *J. Am. Chem. Soc.*, 2007, **129**, 758–759.

286 H. Noguchi, T. Shioda, C.-M. Chou and M. Suginome, *Org. Lett.*, 2008, **10**, 377–380.

287 Y. Hattori, T. Asano, M. Kirihata, Y. Yamaguchi and T. Wakamiya, *Tetrahedron Lett.*, 2008, **49**, 4977–4980.

288 Y. Sumida, R. Harada, T. Kato-Sumida, K. Johmoto, H. Uekusa and T. Hosoya, *Org. Lett.*, 2014, **16**, 6240–6243.

289 M. Fingerle, S. Stocker and H. F. Bettinger, *Synthesis (Stuttg).*, 2019, **51**, 4147–4152.

290 H. Yoshida, M. Seki, S. Kamio, H. Tanaka, Y. Izumi, J. Li, I. Osaka, M. Abe, H. Andoh, T. Yajima, T. Tani and T. Tsuchimoto, *ACS Catal.*, 2020, **10**, 346–351.

291 Y. Mutoh, K. Yamamoto and S. Saito, *ACS Catal.*, 2020, **10**, 352–357.

292 T. Tani, Y. Sawatsugawa, Y. Sano, Y. Hirataka, N. Takahashi, S. Hashimoto, T. Sugiura and T. Tsuchimoto, *Adv. Synth. Catal.*, 2019, **361**, 1815–1834.

293 J. W. Labadie and J. K. Stille, *J. Am. Chem. Soc.*, 1983, **105**, 6129–6137.

294 G. Durieux, M. Gerdin, C. Moberg and A. Jutand, *Eur. J. Inorg. Chem.*, 2008, **2008**, 4236–4241.

295 M. Suginome, H. Nakamura and Y. Ito, *Angew. Chemie Int. Ed. English*, 1997, **36**, 2516–2518.

296 M. Suginome, H. Nakamura and Y. Ito, *Chem. Commun.*, 1996, **11**, 2777.

297 J. A. Bailey, M. Ploeger and P. G. Pringle, *Inorg. Chem.*, 2014, **53**, 7763–7769.

298 P. Dominguez-Molano, G. Bru, O. Salvado, R. J. Maza, J. J. Carbó and E. Fernández, *Chem. Commun.*, 2021, **57**, 13361–13364.

299 S. K. Dorn, A. E. Tharp and M. K. Brown, *Angew. Chemie Int. Ed.*, 2021, **60**, 16027–16034.

300 C.-W. Ju, B. Li, L. Li, W. Yan, C. Cui, X. Ma and D. Zhao, *J. Am. Chem. Soc.*, 2021, **143**, 5903–5916.

301 T. Sugasawa, T. Toyoda, M. Adachi and K. Sasakura, *J. Am. Chem. Soc.*, 1978, **100**, 4842–4852.

302 J. Boström, D. G. Brown, R. J. Young and G. M. Keserü, *Nat. Rev. Drug Discov.*, 2018, **17**, 709–727.

303 M. R. O'Donovan, C. D. Mee, S. Fenner, A. Teasdale and D. H. Phillips, *Mutat. Res. Toxicol. Environ. Mutagen.*, 2011, **724**, 1–6.

304 G. Kaupp, M. R. Naimi-Jamal and V. Stepanenko, *Chem. - A Eur. J.*, 2003, **9**, 4156–4161.

305 J. Wood, L. Marciasini, M. Vaultier and M. Pucheault, *Synlett*, 2014, **25**, 551–555.

306 D. Hemming, R. Fritzemeier, S. A. Westcott, W. L. Santos and P. G. Steel, *Chem. Soc. Rev.*, 2018, **47**, 7477–7494.

307 H. Yoshida, Y. Takemoto and K. Takaki, *Chem. Commun.*, 2014, **50**, 8299–8302.

308 R. Sakae, K. Hirano and M. Miura, *J. Am. Chem. Soc.*, 2015, **137**, 6460–6463.

309 T. Tsushima, H. Tanaka, K. Nakanishi, M. Nakamoto and H. Yoshida, *ACS Catal.*, 2021, **11**, 14381–14387.

310 H. Yoshida, Y. Murashige and I. Osaka, *Adv. Synth. Catal.*, 2019, **361**, 2286–2290.

311 H. Yoshida, Y. Takemoto and K. Takaki, *Chem. Commun.*, 2015, **51**, 6297–6300.

312 S. Radomkit, Z. Liu, A. Closs, M. S. Mikus and A. H. Hoveyda, *Tetrahedron*, 2017, **73**, 5011–5017.

313 H. Lee, S. Lee and J. Yun, *ACS Catal.*, 2020, **10**, 2069–2073.

314 L. Mao, C. Li, L. Xiang, D. Fu, W. Ma and Q. Ye, *J. Org. Chem.*, 2020, **85**, 2823–2831.

315 K.-F. Wu, D.-T. Dai, X.-Y. Sun and Y.-H. Xu, *Org. Lett.*, 2022, **24**, 2660–2664.

316 S. Krautwald, M. J. Bezdek and P. J. Chirik, *J. Am. Chem. Soc.*, 2017, **139**, 3868–3875.

317 L. Xu and P. Li, *Chem. Commun.*, 2015, **51**, 5656–5659.

318 J. Cid, J. J. Carbó and E. Fernández, *Chem. - A Eur. J.*, 2014, **20**, 3616–3620.

319 N. Miralles, J. Cid, A. B. Cuenca, J. J. Carbó and E. Fernández, *Chem. Commun.*, 2015, **51**, 1693–1696.

320 S. Peng, G. Liu and Z. Huang, *Org. Lett.*, 2018, **20**, 7363–7366.

321 N. Miralles, R. M. Romero, E. Fernández and K. Muñiz, *Chem. Commun.*, 2015, **51**, 14068–14071.

322 X. Liu, W. Ming, X. Luo, A. Friedrich, J. Maier, U. Radius, W. L. Santos and T. B. Marder, *European J. Org. Chem.*, 2020, **2020**, 1941–1946.

323 A. Verma, R. F. Snead, Y. Dai, C. Slebodnick, Y. Yang, H. Yu, F. Yao and W. L. Santos, *Angew. Chemie Int. Ed.*, 2017, **56**, 5111–5115.

324 A. B. Cuenca, J. Cid, D. García-López, J. J. Carbó and E. Fernández, *Org. Biomol. Chem.*, 2015, **13**, 9659–9664.

325 S. Ding, Q. Ma, M. Zhu, H. Ren, S. Tian, Y. Zhao and Z. Miao, *Molecules*, 2019, **24**, 377.

326 N. Iwadate and M. Suginome, *J. Organomet. Chem.*, 2009, **694**, 1713–1717.

327 N. Iwadate and M. Suginome, *Chem. Lett.*, 2010, **39**, 558–560.

328 T. Tsuchimoto, H. Utsugi, T. Sugiura and S. Horio, *Adv. Synth. Catal.*, 2015, **357**, 77–82.

329 W. J. Jang, B.-N. Kang, J. H. Lee, Y. M. Choi, C.-H. Kim and J. Yun, *Org. Biomol. Chem.*, 2019, **17**, 5249–5252.

330 I. Ojima, N. Clos, R. J. Donovan and P. Ingallina, *Organometallics*, 1990, **9**, 3127–3133.

331 R. S. Tanke and R. H. Crabtree, *J. Am. Chem. Soc.*, 1990, **112**, 7984–7989.

332 K. Yamamoto, Y. Mohara, Y. Mutoh and S. Saito, *J. Am. Chem. Soc.*, 2019, **141**, 17042–17047.

333 M. Zhong, Y. Gagné, T. O. Hope, X. Pannecoucke, M. Frenette, P. Jubault and T. Poisson, *Angew. Chemie Int. Ed.*, 2021, **60**, 14498–14503.

334 T. Yasuda, Y. Yoshigoe and S. Saito, *Org. Lett.*, 2023, **25**, 2093–2097.

335 P. Viereck, S. Krautwald, T. P. Pabst and P. J. Chirik, *J. Am. Chem. Soc.*, 2020, **142**, 3923–3930.

336 Y. Park and J. Yun, *Org. Lett.*, 2019, **21**, 8779–8782.

337 W. J. Jang, J. Woo and J. Yun, *Angew. Chemie Int. Ed.*, 2021, **60**, 4614–4618.

338 J. Li, M. Seki, S. Kamio and H. Yoshida, *Chem. Commun.*, 2020, **56**, 6388–6391.

339 J. C. H. Lee and D. G. Hall, *J. Am. Chem. Soc.*, 2010, **132**, 11386–11386.

340 R. Davis and N. Tamaoki, *Org. Lett.*, 2005, **7**, 1461–1464.

341 S. Nave, R. P. Sonawane, T. G. Elford and V. K. Aggarwal, *J. Am. Chem. Soc.*, 2010, **132**, 17096–17098.

342 P. Fontani, B. Carboni, M. Vaultier and G. Maas, *Synthesis (Stuttg).*, 1991, **1991**, 605–609.

343 G. W. Kabalka, P. P. Wadgaonkar and T. M. Shoup, *Tetrahedron Lett.*, 1989, **30**, 5103–5104.

344 A. C. M. Baroni, C. C. P. Arruda and D. B. Carvalho, in *PATAI'S Chemistry of Functional Groups*, John Wiley & Sons, Ltd, Chichester, UK, 2017, pp. 1–24.

345 A. Pécharman, M. S. Hill and M. F. Mahon, *Angew. Chemie Int. Ed.*, 2018, **57**, 10688–10691.

346 A. F. Pécharman, A. L. Colebatch, M. S. Hill, C. L. McMullin, M. F. Mahon and C. Weetman, *Nat. Commun.*, 2017, **8**, 1–7.

347 A.-F. Pécharman, M. S. Hill, C. L. McMullin and M. F. Mahon, *Angew. Chemie Int. Ed.*, 2017, **56**, 16363–16366.

348 A.-F. Pécharman, M. S. Hill, G. McMullon, C. L. McMullin and M. F. Mahon, *Chem. Sci.*, 2019, **10**, 6672–6682.

349 A.-F. Pécharman, M. S. Hill and M. F. Mahon, *Dalt. Trans.*, 2018, **47**, 7300–7305.

350 A.-F. Pécharman, N. A. Rajabi, M. S. Hill, C. L. McMullin and M. F. Mahon, *Chem. Commun.*, 2019, **55**, 9035–9038.

351 A.-F. Pécharman, M. S. Hill, C. L. McMullin and M. F. Mahon, *Organometallics*, 2018, **37**, 4457–4464.

352 D. J. Liptrot, M. Arrowsmith, A. L. Colebatch, T. J. Hadlington, M. S. Hill, G. Kociok-Köhn and M. F. Mahon, *Angew. Chemie Int. Ed.*, 2015, **54**, 15280–15283.

353 B. Okokhere-Edeghoghon, M. Dehmel, M. S. Hill, R. Kretschmer, M. F. Mahon, C. L. McMullin, L. J. Morris and N. A. Rajabi, *Inorg. Chem.*, 2020, **59**, 13679–13689.

354 B. Okokhere-Edeghoghon, S. E. Neale, M. S. Hill, M. F. Mahon and C. L. McMullin, *Dalt. Trans.*, 2022, **51**, 136–144.

355 B. Okokhere-Edeghoghon, M. S. Hill, M. F. Mahon and C. L. McMullin, *Chem. Commun.*, 2022, **58**, 10711–10714.

356 G. Coates, H. Y. Tan, C. Kalff, A. J. P. White and M. R. Crimmin, *Angew. Chemie - Int. Ed.*, 2019, **58**, 12514–12518.

357 Y. Nagashima, R. Takita, K. Yoshida, K. Hirano and M. Uchiyama, *J. Am. Chem. Soc.*, 2013, **135**, 18730–18733.

358 Y. Nagashima, D. Yukimori, C. Wang and M. Uchiyama, *Angew. Chemie Int. Ed.*, 2018, **57**, 8053–8057.

359 R. Drescher, L. Wüst, C. Mihm, I. Krummenacher, A. Hofmann, J. Goettel and H. Braunschweig, *Dalt. Trans.*, 2021, **50**, 10400–10404.

360 J. D. Farwell, P. B. Hitchcock and M. F. Lappert, *J. Organomet. Chem.*, 2007, **692**, 5492–5494.

361 D. W. Goebel, J. L. Hencher and J. P. Oliver, *Organometallics*, 1983, **2**, 746–750.

362 L. Rösch and G. Altnau, *J. Organomet. Chem.*, 1980, **195**, 47–53.

363 G. M. Ballmann, M. J. Evans, T. X. Gentner, A. R. Kennedy, J. R. Fulton, M. P. Coles and R. E. Mulvey, *Inorg. Chem.*, 2022, **61**, 19838–19846.

364 M. J. Evans, M. D. Anker and M. P. Coles, *Inorg. Chem.*, 2021, **60**, 4772–4778.

365 J. D. Gorden, A. Voigt, C. L. B. Macdonald, J. S. Silverman and A. H. Cowley, *J. Am. Chem. Soc.*, 2000, **122**, 950–951.

366 A. Hofmann, M. A. Légaré, L. Wüst and H. Braunschweig, *Angew. Chemie - Int. Ed.*, 2019, **58**, 9776–9781.

367 P. E. Romero, W. E. Piers, S. A. Decker, D. Chau, T. K. Woo and M. Parvez, *Organometallics*, 2003, **22**, 1266–1274.

368 Z. Yang, X. Ma, R. B. Oswald, H. W. Roesky, H. Zhu, C. Schulzke, K. Starke, M. Baldus, H. G. Schmidt and M. Noltemeyer, *Angew. Chemie - Int. Ed.*, 2005, **44**, 7072–7074.

369 A. Hofmann, C. Pranckevicius, T. Tröster and H. Braunschweig, *Angew. Chemie - Int. Ed.*, 2019, **58**, 3625–3629.

370 N. Dettenrieder, C. Schädle, C. Maichle-Mössmer and R. Anwander, *Dalt. Trans.*, 2014, **43**, 15760–15770.

371 N. Dettenrieder, H. M. Dietrich, C. Schädle, C. Maichle-Mössmer, K. W. Törnroos and R. Anwander, *Angew. Chemie - Int. Ed.*, 2012, **51**, 4461–4465.

372 W. Lu, H. Hu, Y. Li, R. Ganguly and R. Kinjo, *J. Am. Chem. Soc.*, 2016, **138**, 6650–6661.

373 B. M. Mikhailov and T. V. Potapova, *Bull. Acad. Sci. USSR Div. Chem. Sci.*, 1968, **17**, 1105–1105.

374 K. Koshino and R. Kinjo, *J. Am. Chem. Soc.*, 2020, **142**, 9057–9062.

375 R. J. Schwamm, M. S. Hill, H. Y. Liu, M. F. Mahon, C. L. McMullin and N. A. Rajabi, *Chem. - A Eur. J.*, 2021, **27**, 14971–14980.

376 S. Kurumada and M. Yamashita, *J. Am. Chem. Soc.*, 2022, **144**, 4327–4332.

377 Z. Güven, L. Denker, D. Wullschläger, J. Pablo Martínez, B. Trzaskowski and R. Frank, *Angew. Chemie Int. Ed.*, , DOI:10.1002/anie.202209502.

378 B. M. Trost and J. ichi Yoshida, *Tetrahedron Lett.*, 1983, **24**, 4895–4898.

379 H. Hayami, M. Sato, S. Kanemoto, Y. Morizawa, K. Oshima and H. Nozaki, *J. Am. Chem. Soc.*, 1983, **105**, 4491–4492.

380 K. Wakamatsu, T. Nonaka, Y. Okuda, W. Tückmantel, K. Oshima, K. Utimoto and H. Nozaki, *Tetrahedron*, 1986, **42**, 4427–4436.

381 S. Matsubara, T. Nonaka, Y. Okuda, S. Kanemoto, K. Oshima and H. Nozaki, *Bull. Chem. Soc. Jpn.*, 1985, **58**, 1480–1483.

382 G. Altnau, L. Rösch, F. Bohlmann and M. Lonitz, *Tetrahedron Lett.*, 1980, **21**, 4069–4072.

383 R. West, M. J. Fink and J. Michl, *Science*, 1981, **214**, 1343–1344.

384 B. Pachaly and R. West, *Angew. Chemie Int. Ed. English*, 1984, **23**, 454–455.

385 J. J. Eisch and J. L. Considine, *J. Am. Chem. Soc.*, 1968, **90**, 6257–6259.

386 J. D. Queen, A. Lehmann, J. C. Fettinger, H. M. Tuononen and P. P. Power, *J. Am. Chem. Soc.*, 2020, **142**, 20554–20559.

387 J. A. Dean, in *Lange's Handbook of Chemistry*, ed. J. A. Dean, McGraw-Hill Professional Publishing, 1998, The University of Virginia, 16th edn., 1998, pp. 4.41-4.52.

388 T. Komuro, D. Mochizuki, H. Hashimoto and H. Tobita, *Dalt. Trans.*, 2022, **51**, 9983–9987.

389 J. Belzner, V. Ronneberger, D. Schär, C. Brönnecke, R. Herbst-Irmer and M. Noltemeyer, *J. Organomet. Chem.*, 1999, **577**, 330–336.

390 M. Nakamoto, T. Yamasaki and A. Sekiguchi, *J. Am. Chem. Soc.*, 2005, **127**, 6954–6955.

391 L. Rösch, G. Altenau, C. Krüger and Y.-H. Tsay, *Zeitschrift für Naturforsch. B*, 1983, **38B**, 34–41.

392 M. Fan, E. N. Duesler, H. Nöth and R. T. Paine, *Inorg. Chem.*, 2010, **49**, 2983–2989.

393 NIST Chemistry WebBook, https://webbook.nist.gov/cgi/cbook.cgi?Source=1966TIM%2FPERd10%2F80&Mask=400, (accessed 11 April 2023).

394 J. Carlos Araujo Da Silva, M. Birot, J.-P. Pillot and M. Pétraud, *J. Organomet. Chem.*, 2002, **646**, 179–190.

395 M. Linnemannstöns, J. Schwabedissen, B. Neumann, H. Stammler, R. J. F. Berger and N. W. Mitzel, *Chem. – A Eur. J.*, 2020, **26**, 2169–2173.

396 T. Agou, K. Nagata and N. Tokitoh, *Angew. Chemie - Int. Ed.*, 2013, **52**, 10818–10821.

397 R. J. Wright, A. D. Phillips and P. P. Power, *J. Am. Chem. Soc.*, 2003, **125**, 10784–10785.

398 M. Joost, P. Gualco, Y. Coppel, K. Miqueu, C. E. Kefalidis, L. Maron, A. Amgoune and D. Bourissou, *Angew. Chemie Int. Ed.*, 2014, **53**, 747–751.

399 H. Zhu, R. B. Oswald, H. Fan, H. W. Roesky, Q. Ma, Z. Yang, H. G. Schmidt, M. Noltemeyer, K. Starke and N. S. Hosmane, *J. Am. Chem. Soc.*, 2006, **128**, 5100–5108.

400 H. Zhu, J. Chai, H. Fan, H. W. Roesky, C. He, V. Jancik, H.-G. Schmidt, M. Noltemeyer, W. A. Merrill and P. P. Power, *Angew. Chemie*, 2005, **117**, 5220–5223.

401 C. Cui, S. Köpke, R. Herbst-Irmer, H. W. Roesky, M. Noltemeyer, H. G. Schmidt and B. Wrackmeyer, *J. Am. Chem. Soc.*, 2001, **123**, 9091–9098.

402 T. Agou, T. Wasano, P. Jin, S. Nagase and N. Tokitoh, *Angew. Chemie - Int. Ed.*, 2013, **52**, 10031–10034.

403 C. Krüger, J. C. Sekutowski, H. Hoberg and R. Krause-Göing, *J. Organomet. Chem.*, 1977, **141**, 141–148.

404 H. Hoberg and R. Krause-Göing, *J. Organomet. Chem.*, 1977, **127**, C29–C31.

405 V. Y. Lee, H. Sugasawa, O. A. Gapurenko, R. M. Minyaev, V. I. Minkin, H. Gornitzka and A. Sekiguchi, *Chem. - A Eur. J.*, 2016, **22**, 17585–17589.

406 T. Imagawa, L. Giarrana, D. M. Andrada, B. Morgenstern, M. Nakamoto and D. Scheschkewitz, *J. Am. Chem. Soc.*, 2023, **145**, 4757–4764.

407 V. Y. Lee, Y. Ito, A. Sekiguchi, H. Gornitzka, O. A. Gapurenko, V. I. Minkin and R. M. Minyaev, *J. Am. Chem. Soc.*, 2013, **135**, 8794–8797.

408 V. Y. Lee, O. A. Gapurenko, Y. Ito, T. Meguro, H. Sugasawa, A. Sekiguchi, R. M. Minyaev, V. I. Minkin, R. H. Herber and H. Gornitzka, *Organometallics*, 2016, **35**, 346–356.

409 V. Y. Lee, H. Sugasawa, O. A. Gapurenko, R. M. Minyaev, V. I. Minkin, H. Gornitzka and A. Sekiguchi, *J. Am. Chem. Soc.*, 2018, **140**, 6053–6056.

410 Q. Sun, C. G. Daniliuc, X. Yu, C. Mück-Lichtenfeld, G. Kehr and G. Erker, *J. Am. Chem. Soc.*, 2022, **144**, 7815–7821.

411 V. Y. Lee, Y. Ito, O. A. Gapurenko, A. Sekiguchi, V. I. Minkin, R. M. Minyaev and H. Gornitzka, *Angew. Chemie Int. Ed.*, 2015, **54**, 5654–5657.

412 W. D. Stohrer and R. Hoffmann, *J. Am. Chem. Soc.*, 1972, **94**, 1661–1668.

413 E. Lewars, *J. Mol. Struct. THEOCHEM*, 1998, **423**, 173–188.

414 V. Balaji and J. Michl, *Pure Appl. Chem.*, 1988, **60**, 189–194.

415 T. Iwamoto, M. Tamura, C. Kabuto and M. Kira, *Science*, 2000, **290**, 504–506.

416 A. Sekiguchi, T. Matsuo and H. Watanabe, *J. Am. Chem. Soc.*, 2000, **122**, 5652–5653.

417 K. Takanashi, A. Inatomi, V. Y. Lee, M. Nakamoto, M. Ichinohe and A. Sekiguchi, *Eur. J. Inorg. Chem.*, 2008, **2008**, 1752–1755.

418 T. Agou, K. Nagata, T. Sasamori and N. Tokitoh, *Chem. - An Asian J.*, 2014, **9**, 3099–3101.

419 O. A. Gapurenko, V. Y. Lee, R. M. Minyaev and V. I. Minkin, *Heteroat. Chem.*, 2019, **2019**, 1–6.

420 G. R. Fulmer, A. J. M. Miller, N. H. Sherden, H. E. Gottlieb, A. Nudelman, B. M. Stoltz, J. E. Bercaw and K. I. Goldberg, *Organometallics*, 2010, **29**, 2176–2179.

421 B. Andersh, D. L. Murphy and R. J. Olson, *Synth. Commun.*, 2000, **30**, 2091–2098.

422 R. J. Jouet, A. D. Warren, D. M. Rosenberg and V. J. Bellitto, *MRS Proc.*, 2003, **800**, AA2.4.

423 D. C. Grenz, M. Schmidt, D. Kratzert and B. Esser, *J. Org. Chem.*, 2018, **83**, 656–663.

424 K. Yuan, X. Wang and S. Wang, *Org. Lett.*, 2018, **20**, 1617–1620.

425 T. H. Kress and M. R. Leanna, *Synthesis (Stuttg).*, 1988, **1988**, 803–805.

426 S. Krieck, H. Görls and M. Westerhausen, *J. Am. Chem. Soc.*, 2010, **132**, 12492–12501.

427 A. Sattler and G. Parkin, *J. Am. Chem. Soc.*, 2012, **134**, 2355–2366.

428 C. Gerdes, W. Saak, D. Haase and T. Müller, *J. Am. Chem. Soc.*, 2013, **135**, 10353–10361.

429 J. E. Borger, A. W. Ehlers, M. Lutz, J. C. Slootweg and K. Lammertsma, *Angew. Chemie Int. Ed.*, 2014, **53**, 12836–12839.

430 B. Schiemenz and P. P. Power, *Organometallics*, 1996, **15**, 958–964.

431 L. Zhang, D. Peng, X. Leng and Z. Huang, *Angew. Chemie - Int. Ed.*, 2013, **52**, 3676–3680.

432 H. Ito and K. Kubota, *Org. Lett.*, 2012, **14**, 890–893.

433 M. D. Greenhalgh and S. P. Thomas, *Chem. Commun.*, 2013, **49**, 11230.

434 J. Zheng, J.-B. Sortais and C. Darcel, *ChemCatChem*, 2014, **6**, 763–766.

435 M. K. Bisai, S. Yadav, T. Das, K. Vanka and S. S. Sen, *Chem. Commun.*, 2019, **55**, 11711–11714.

436 Y. Liu, Y. Zhou, H. Wang and J. Qu, *RSC Adv.*, 2015, **5**, 73705–73713.

437 L. Zhang, Z. Zuo, X. Leng and Z. Huang, *Angew. Chemie - Int. Ed.*, 2014, **53**, 2696–2700.

438 W. J. Jang, S. M. Song, J. H. Moon, J. Y. Lee and J. Yun, *J. Am. Chem. Soc.*, 2017, **139**, 13660–13663.

439 J. V. Obligacion and P. J. Chirik, *J. Am. Chem. Soc.*, 2013, **135**, 19107–19110.

440 M. Espinal-Viguri, C. R. Woof and R. L. Webster, *Chem. - A Eur. J.*, 2016, **22**, 11605–11608.

441 JP20140046888 20140310, 2015.

Appendix (NMR data) for:

Aluminium/boron exchange reactions for catalysis

A thesis submitted for the Degree of Doctor of Philosophy

Alexander F. Beaton Garcia,[a] + Prof. Stephen P. Thomas,*[a] Dr. Michael J. Cowley*[a]

[a] EaStCHEM School of Chemistry, University of Edinburgh, Joseph Black Building, David Brewster Road, Edinburgh EH9 3FJ, United Kingdom

Contents

1. *m*-Terphenyl alanes 2
2. Al–H–B species 19
3. Boronic esters 37
4. RBdan 72
5. Silylalanes 114

1. *m*-Terphenyl alanes

$^{p\text{-Tol}}$TerAlH$_3$Li•(OEt$_2$)$_{0.5}$

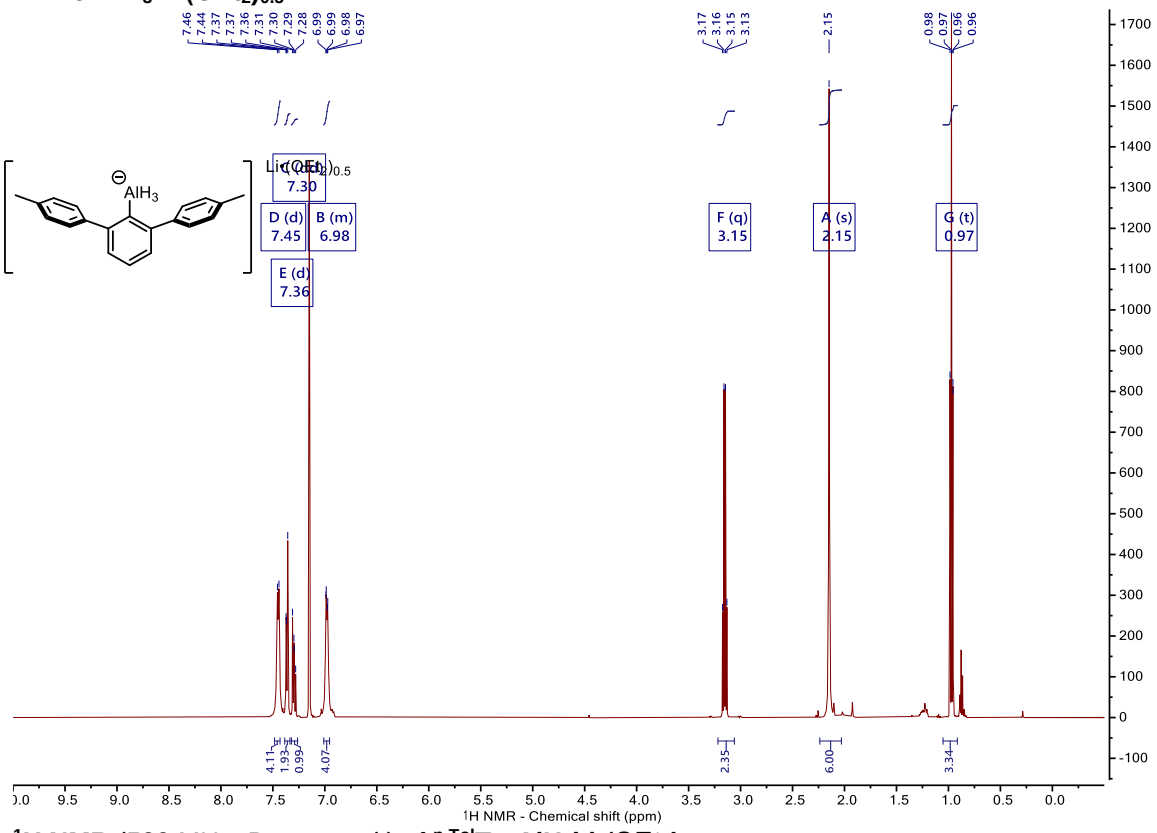

^{1}H NMR (500 MHz, Benzene-d_6) of **$^{p\text{-Tol}}$TerAlH$_3$Li•(OEt$_2$)$_{0.5}$**

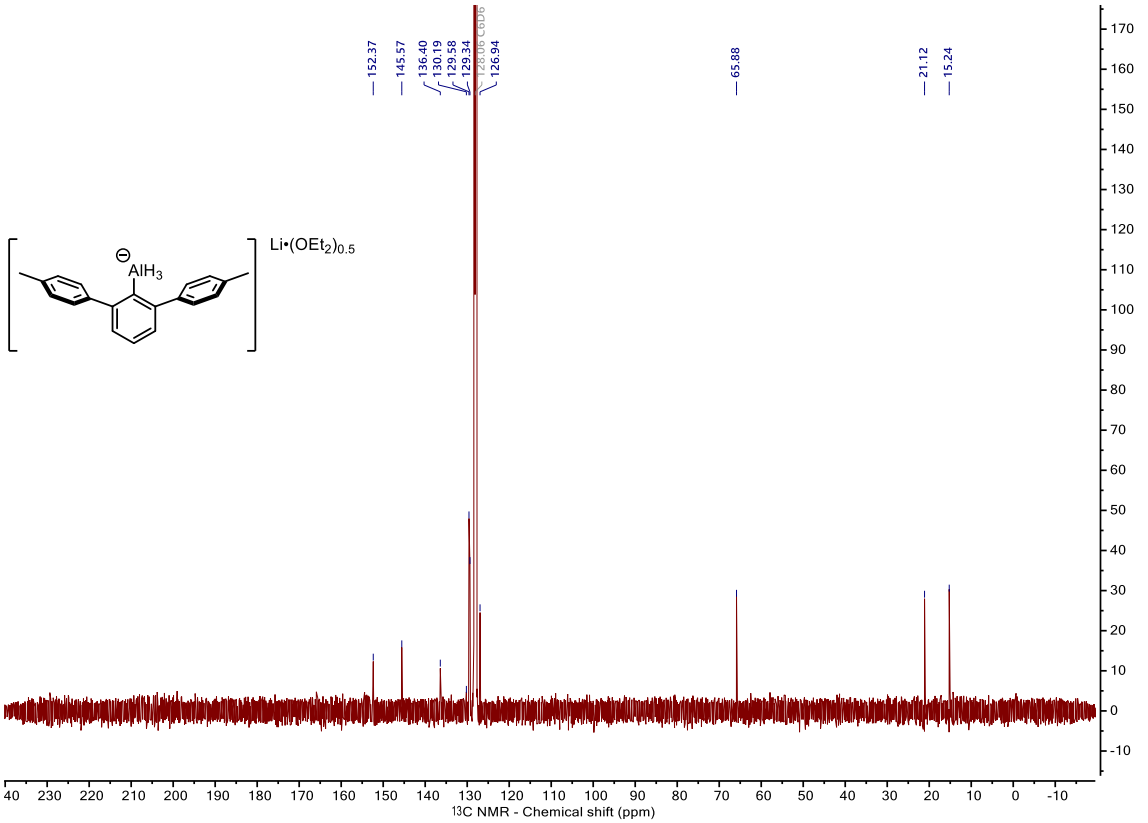

^{13}C {^{1}H} NMR (126 MHz, Benzene-d_6) of **$^{p\text{-Tol}}$TerAlH$_3$Li•(OEt$_2$)$_{0.5}$**

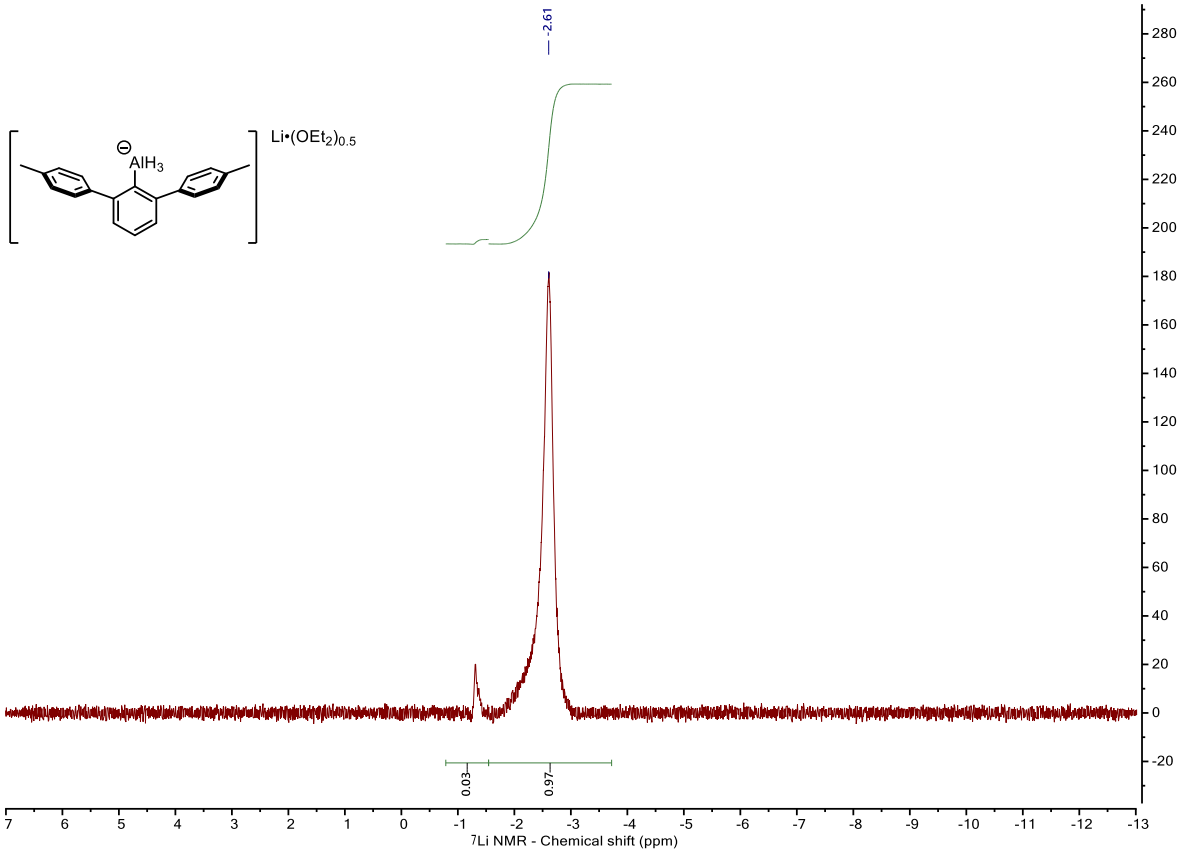

^{7}Li NMR (194 MHz, Benzene-d_6) of **$^{p\text{-Tol}}$TerAlH$_3$Li•(OEt$_2$)$_{0.5}$**

$^{p\text{-Tol}}$TerAlH$_2$

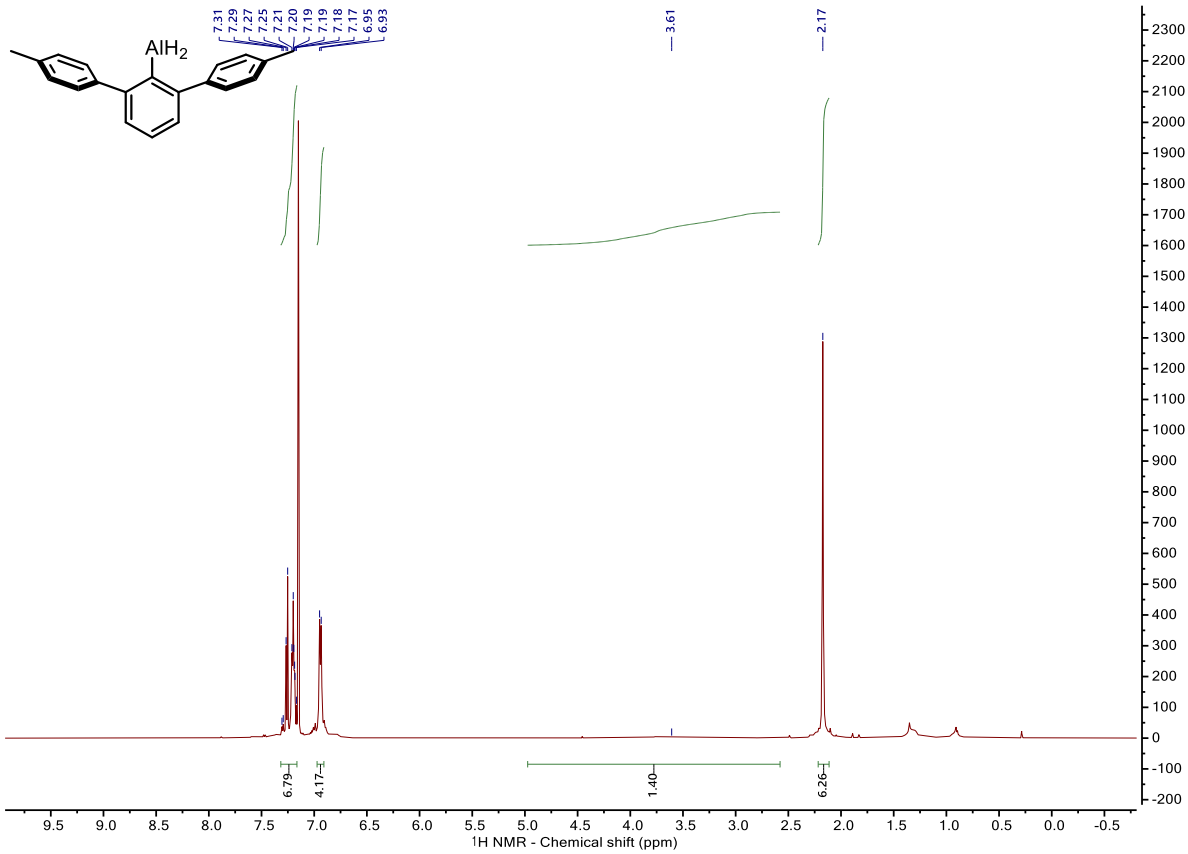

^{1}H NMR (500 MHz, Benzene-d_6) of **$^{p\text{-Tol}}$TerAlH$_2$**

$^{p\text{-Tol}}$TerAlH$_2$•THF

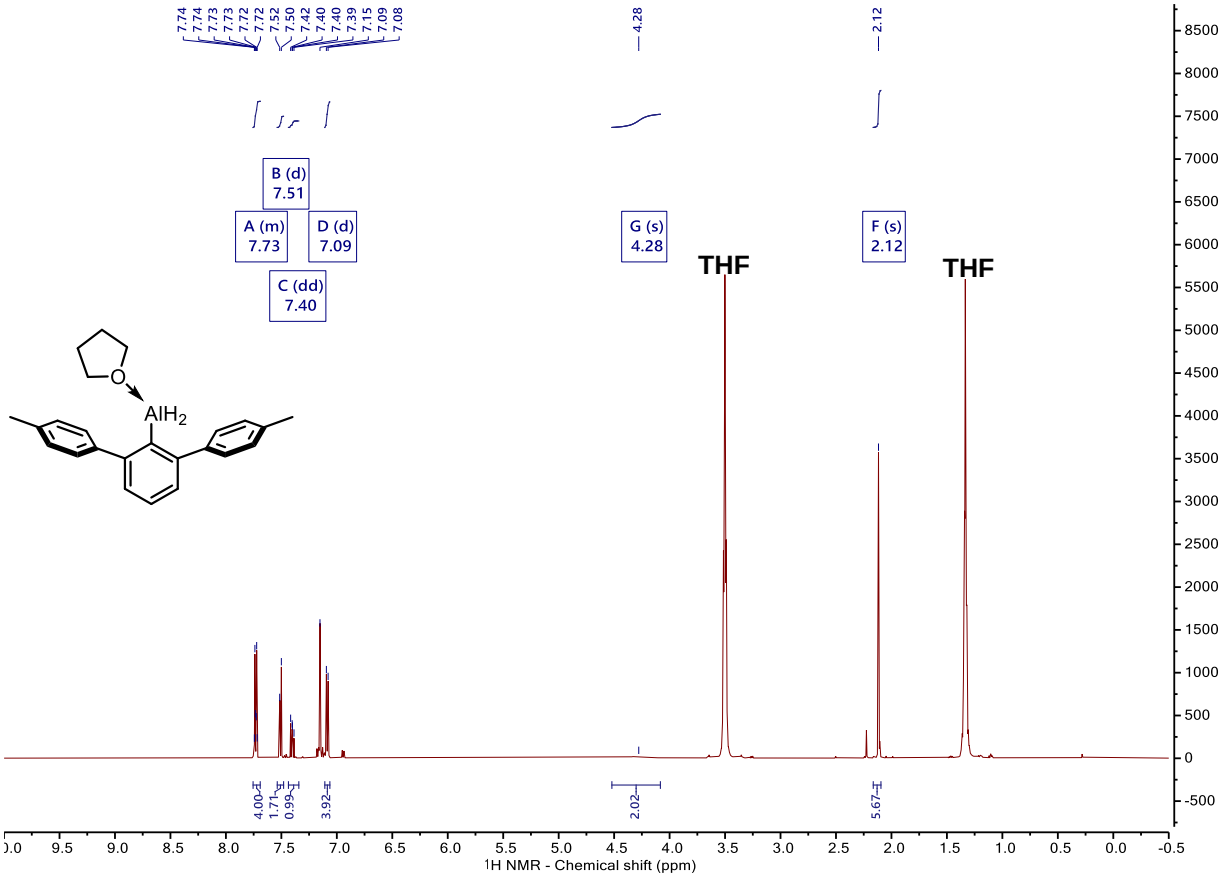

^{1}H NMR (500 MHz, Benzene-d_6, THF) of **$^{p\text{-Tol}}$TerAlH$_2$•THF**

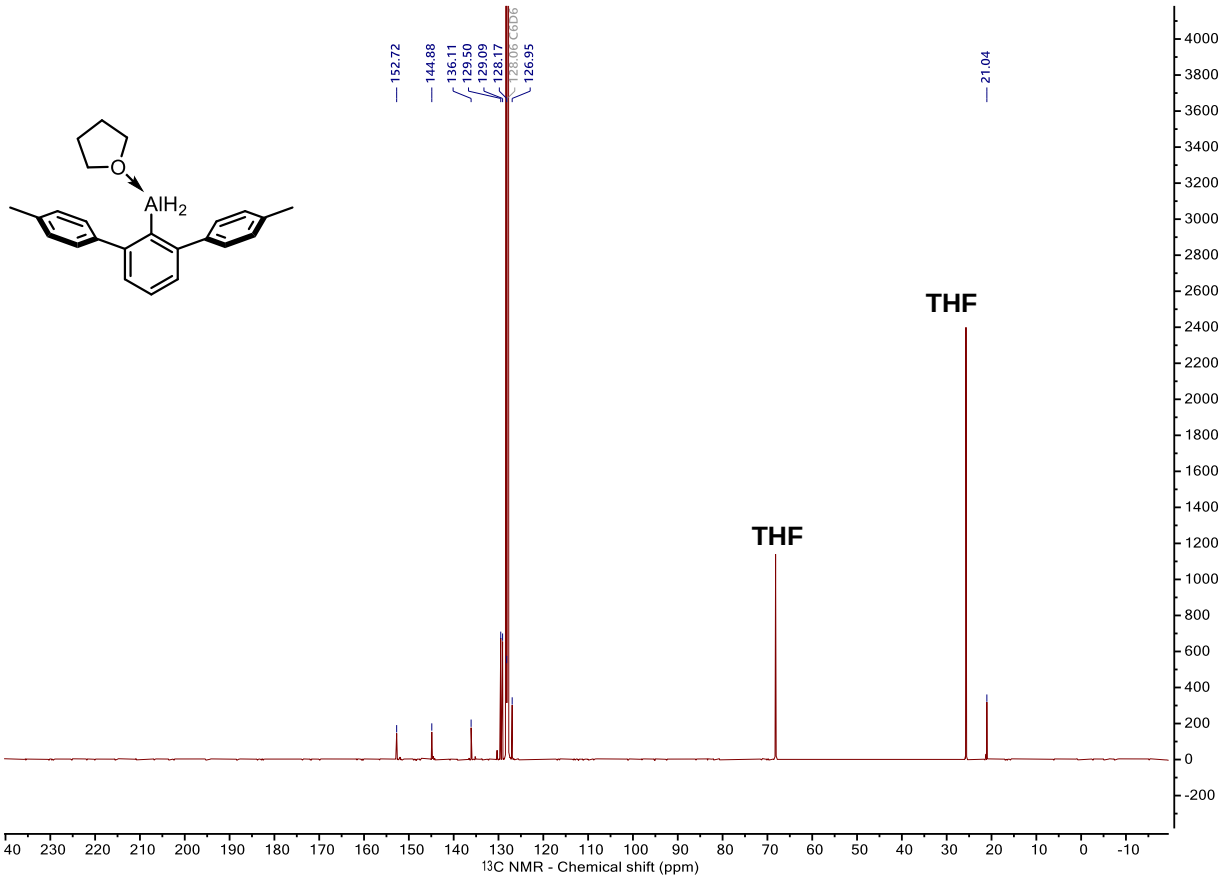

^{13}C {^{1}H} NMR (126 MHz, Benzene-d_6, THF) of **$^{p\text{-Tol}}$TerAlH$_2$•THF**

***p*-Tol**TerAlH$_2$•DMAP

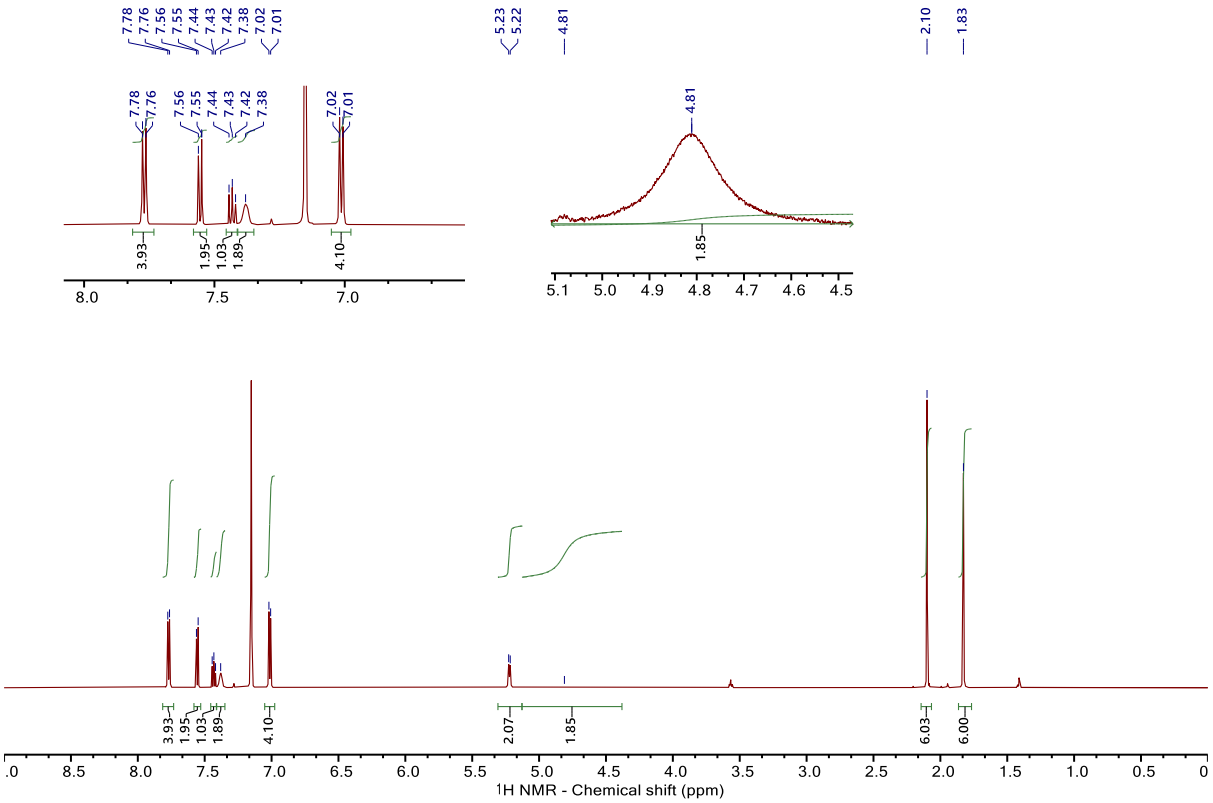

^{1}H NMR (601 MHz, Benzene-d_6) of ***p*-Tol**TerAlH$_2$•DMAP

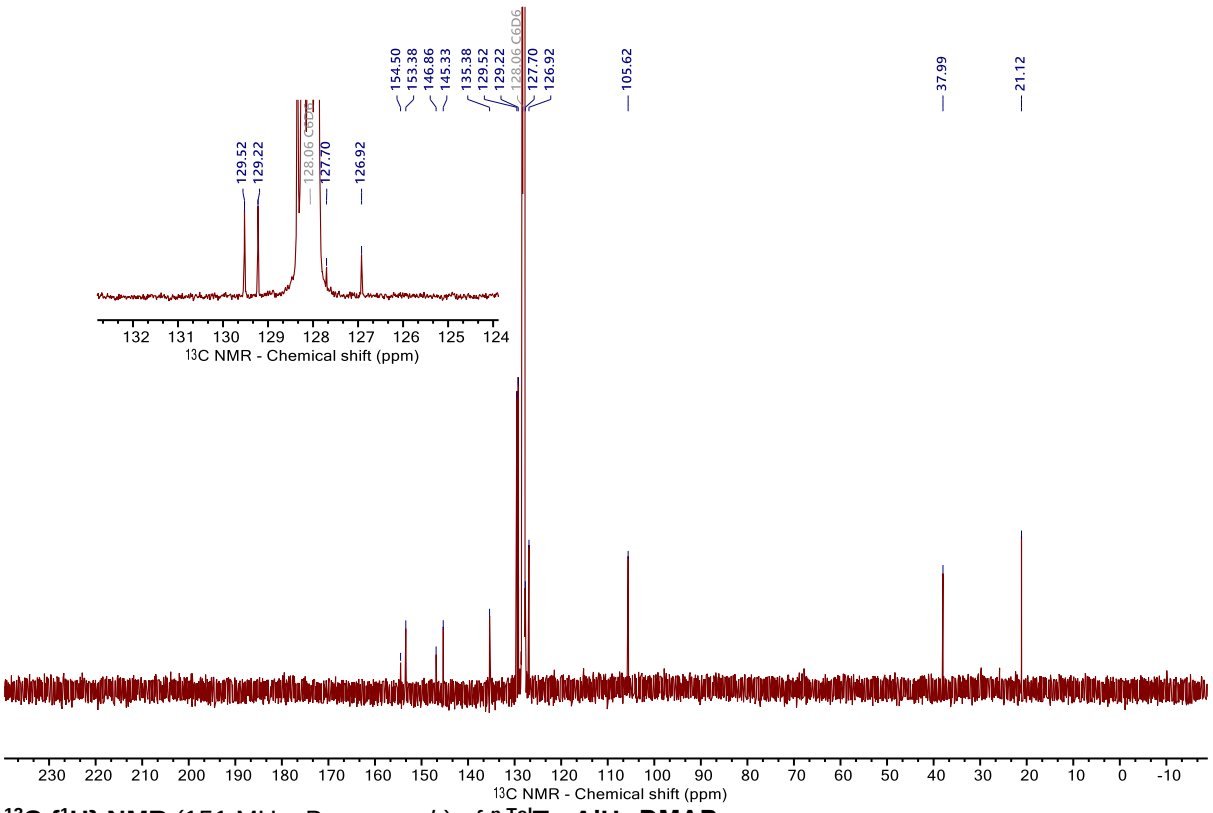

^{13}C {^{1}H} NMR (151 MHz, Benzene-d_6) of ***p*-Tol**TerAlH$_2$•DMAP

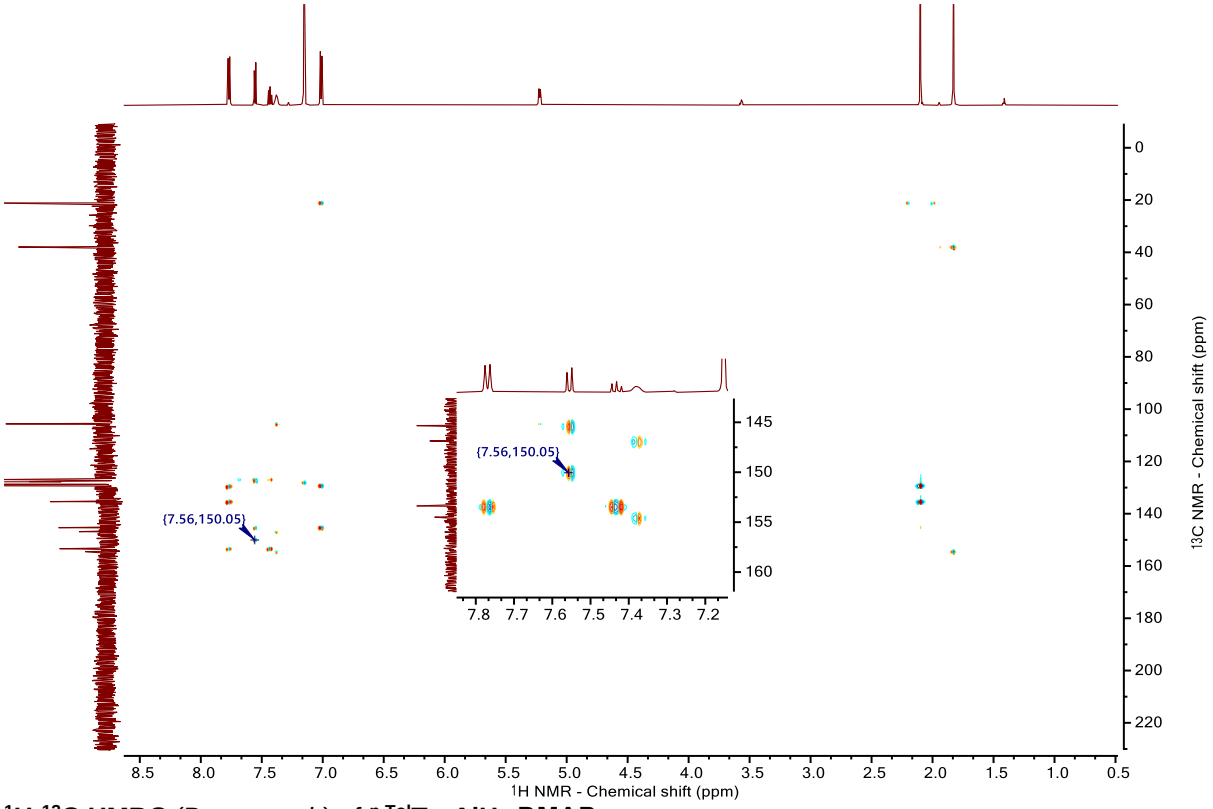

^{1}H-^{13}C HMBC (Benzene-d_6) of **$^{p\text{-Tol}}$TerAlH$_2$•DMAP**

$^{p\text{-Tol}}$TerAlMe$_2$

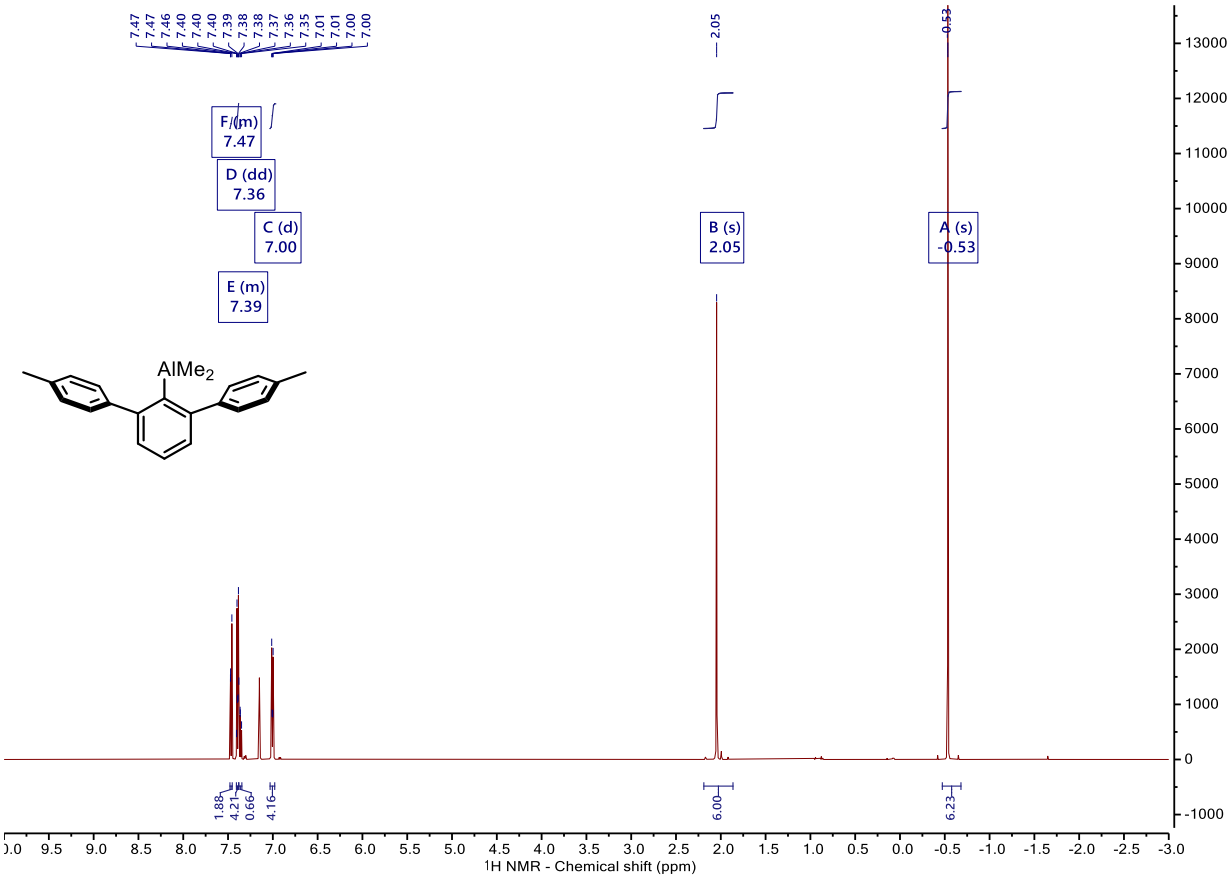

^{1}H NMR (500 MHz, Benzene-d_6) of **$^{p\text{-Tol}}$TerAlMe$_2$**

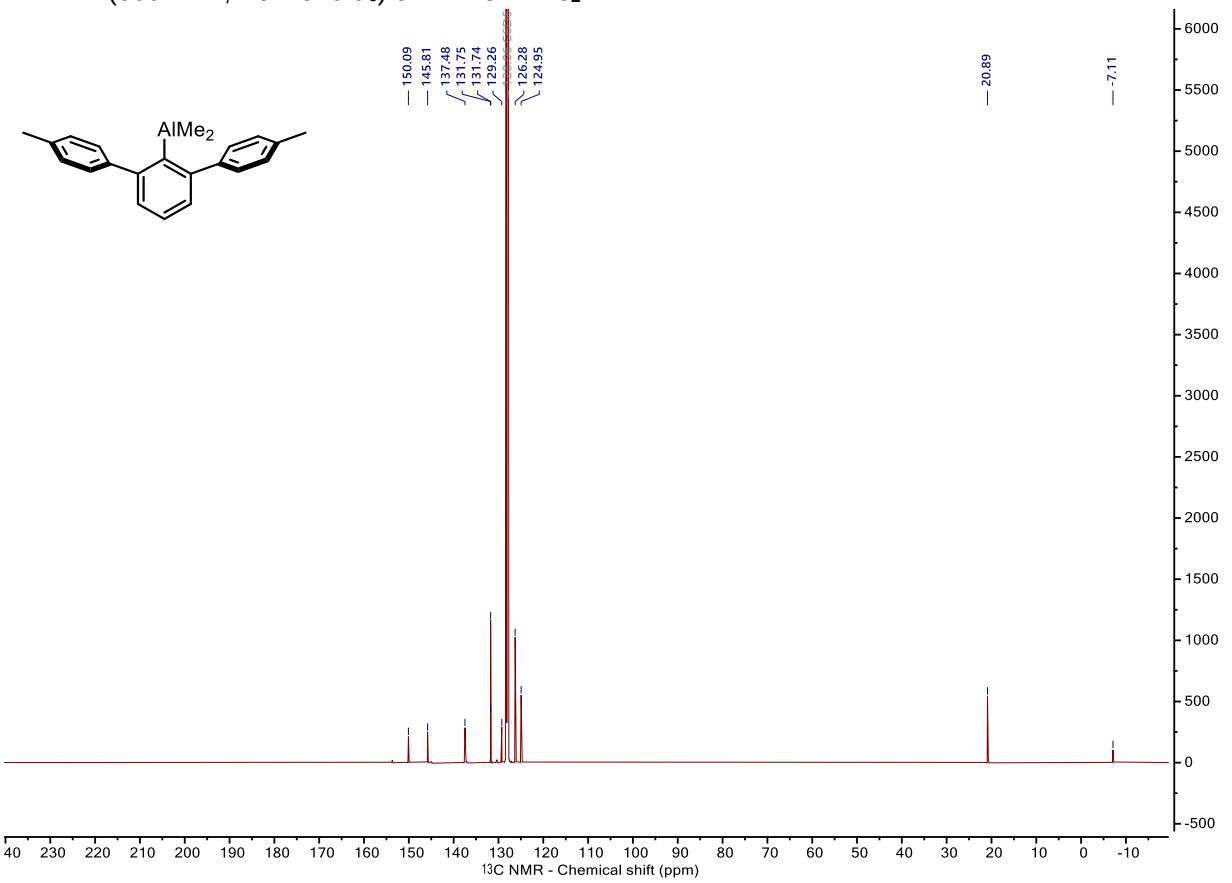

^{13}C {^{1}H} NMR (126 MHz, Benzene-d_6) of **$^{p\text{-Tol}}$TerAlMe$_2$**

$^{p\text{-Tol}}$TerAlMe$_2$•OEt$_2$

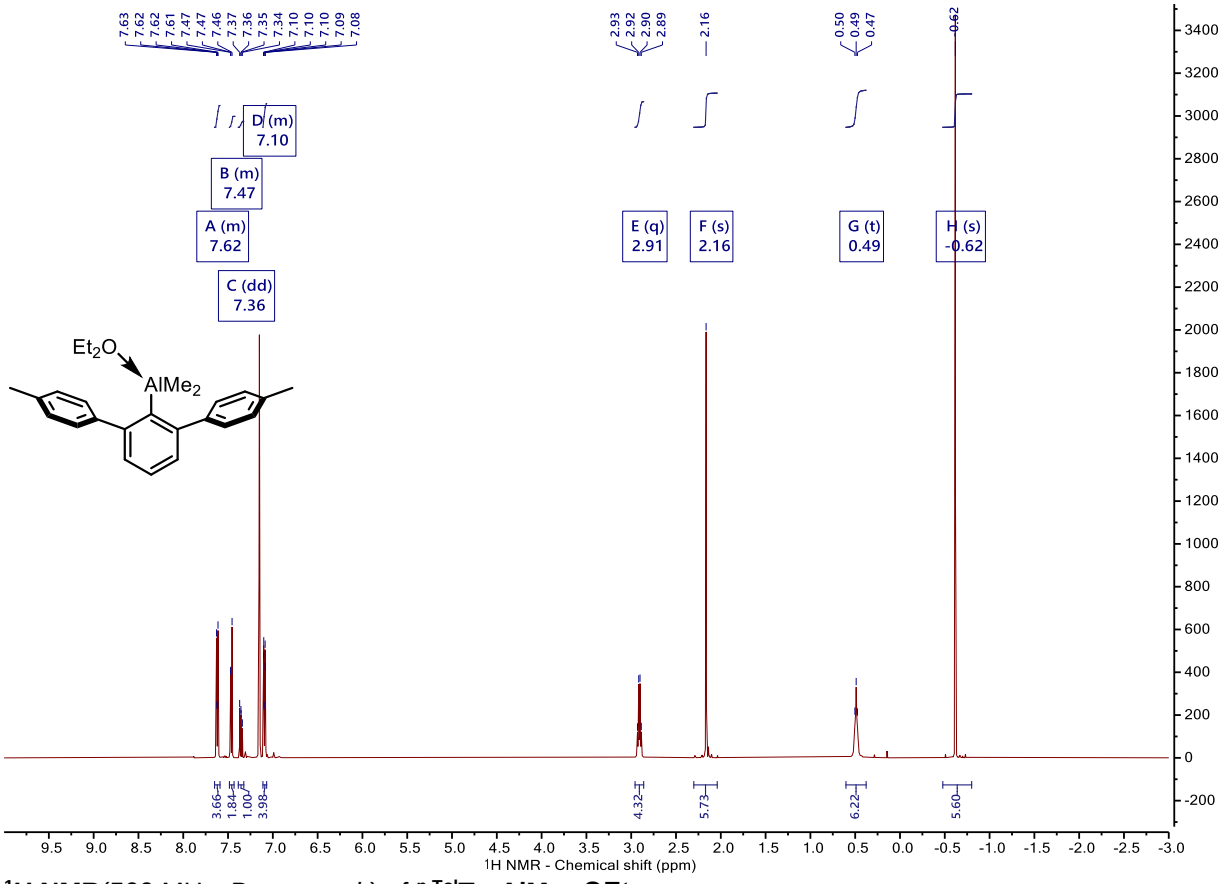

^{1}H NMR(500 MHz, Benzene-d_6) of **$^{p\text{-Tol}}$TerAlMe$_2$•OEt$_2$**

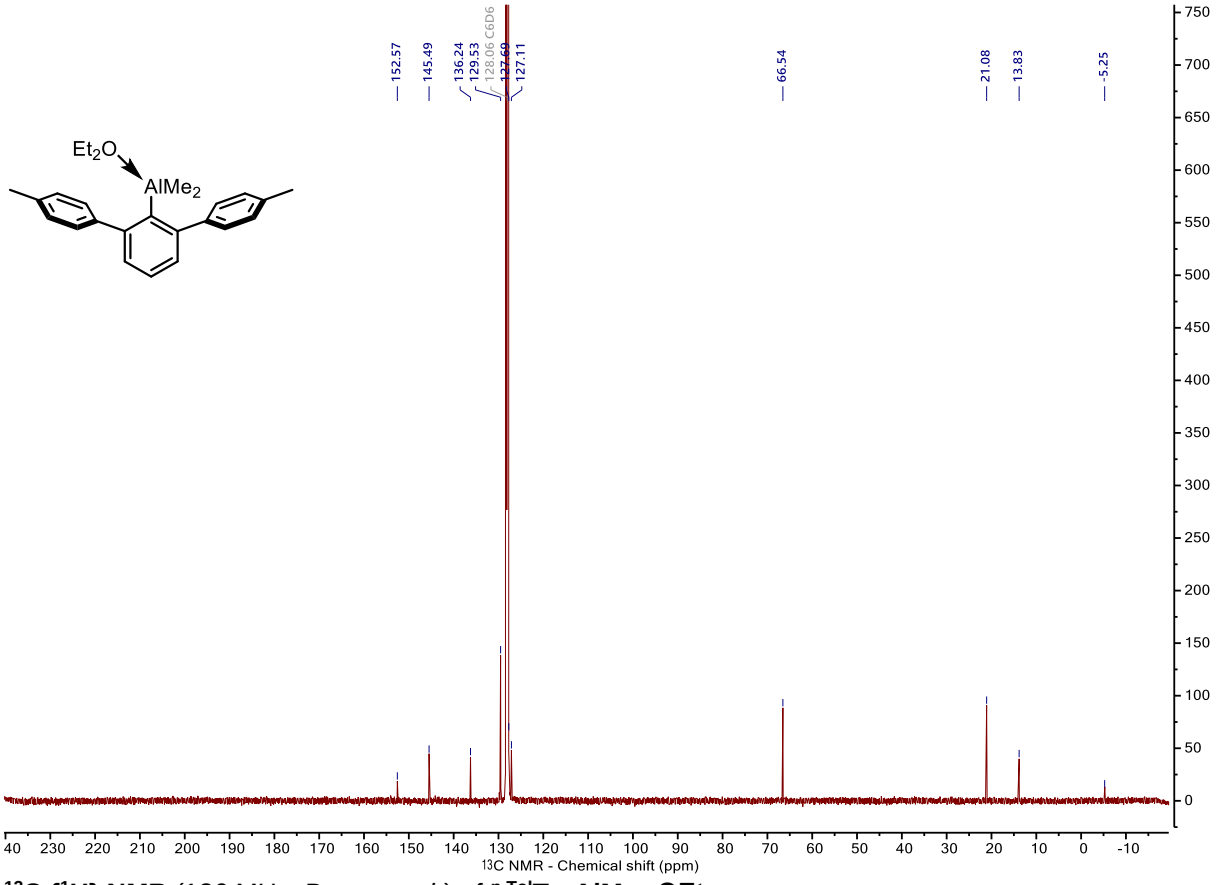

^{13}C {^{1}H} NMR (126 MHz, Benzene-d_6) of **$^{p\text{-Tol}}$TerAlMe$_2$•OEt$_2$**

^{Mes}TerAlH$_2$

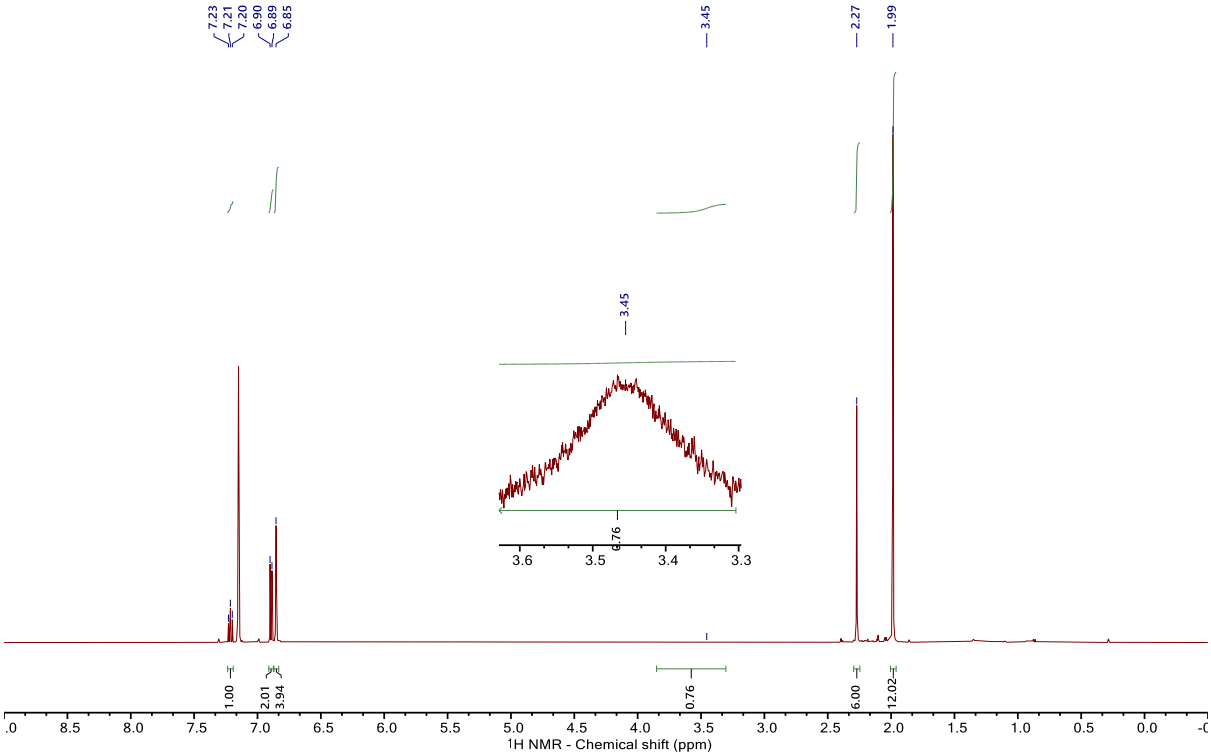

^{1}H NMR (500 MHz, Benzene-d_6) of ^{Mes}TerAlH$_2$

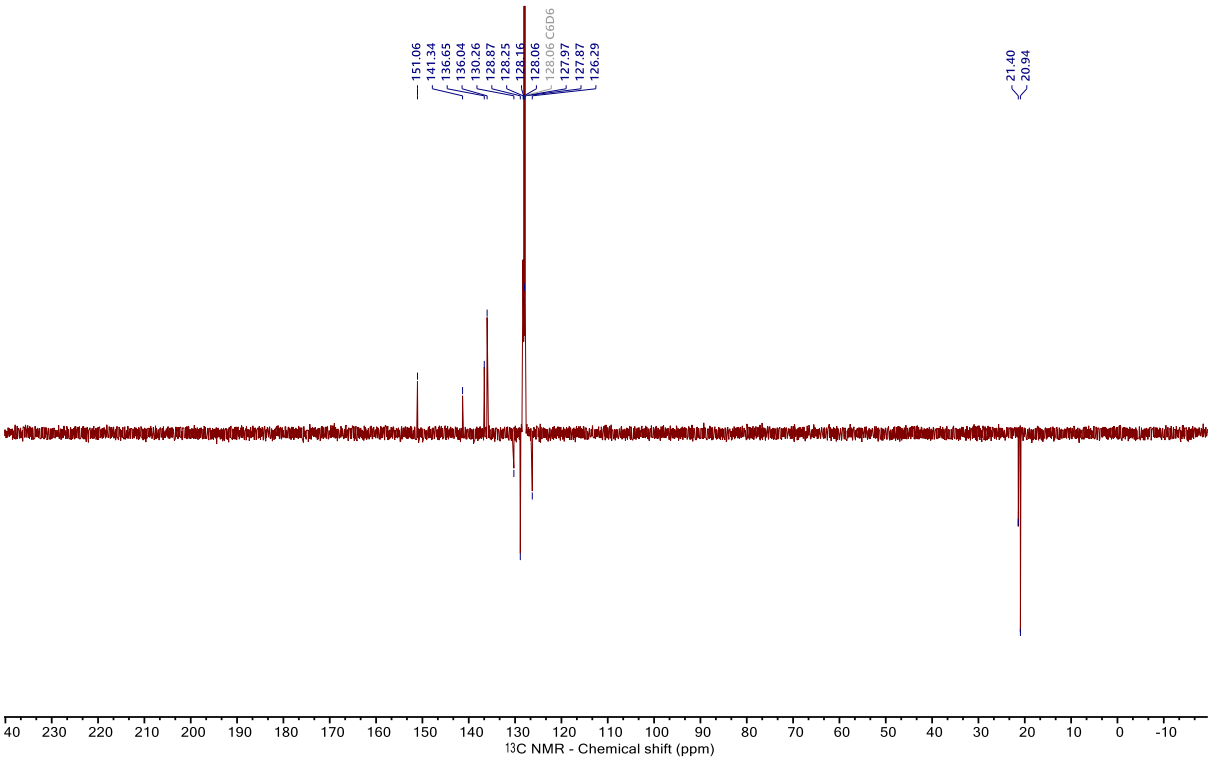

^{13}C {^{1}H} NMR (126 MHz, Benzene-d_6) of ^{Mes}TerAlH$_2$

^{Mes}TerAlMe$_2$

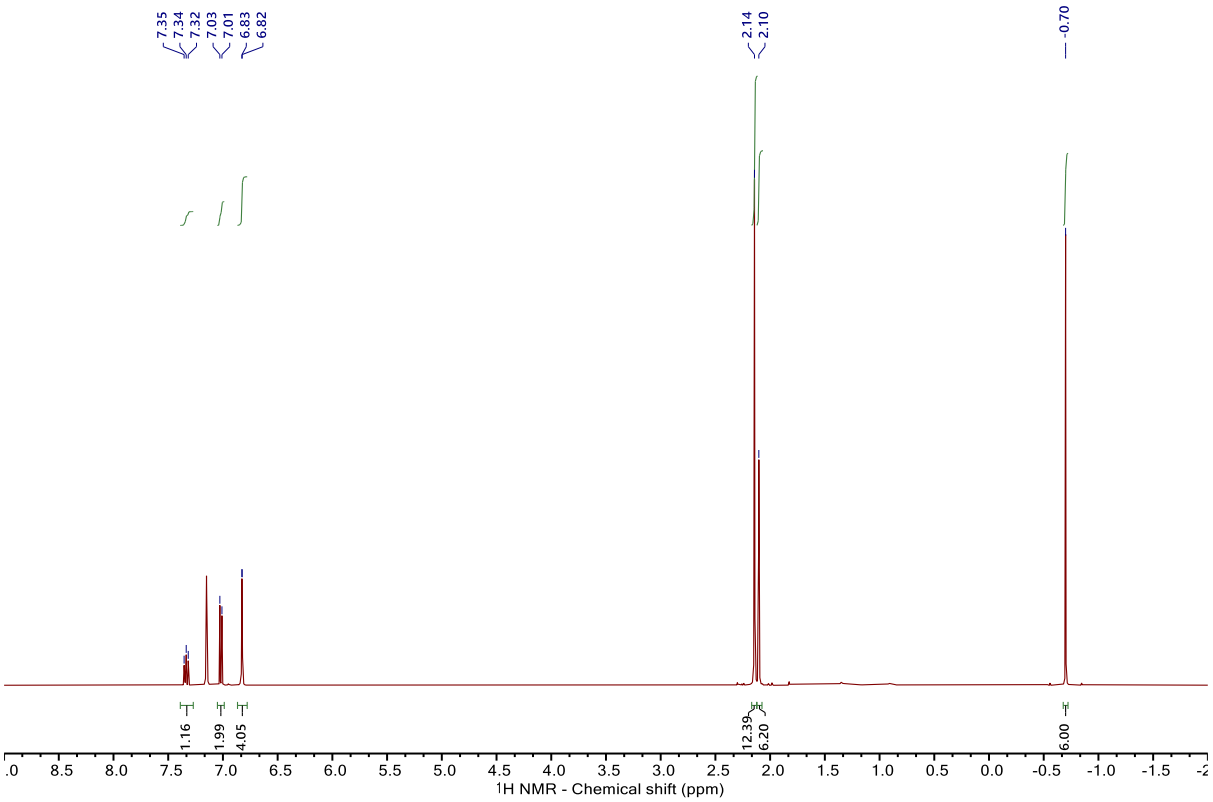

^{1}H NMR (500 MHz, Benzene-d_6) of ^{Mes}TerAlMe$_2$

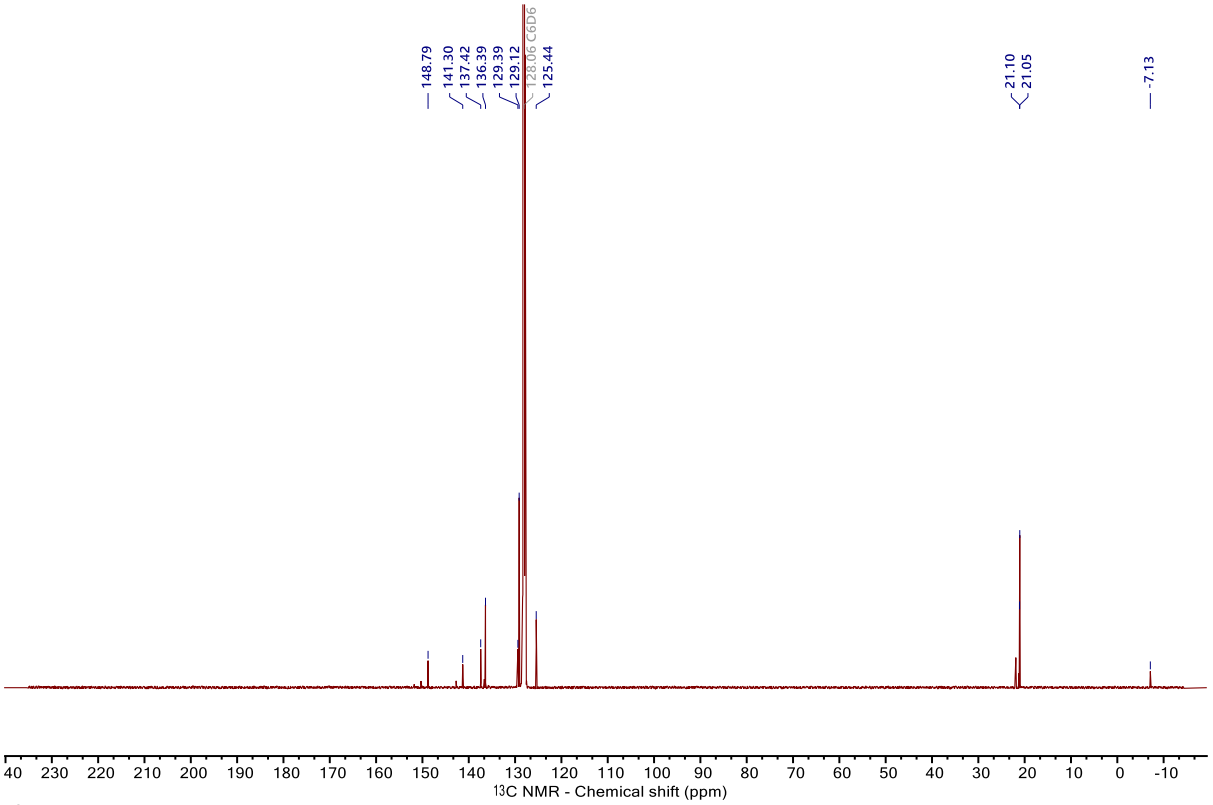

^{13}C {^{1}H} NMR (151 MHz, Benzene-d_6) of ^{Mes}TerAlMe$_2$

^{Mes}TerAlMe$_2$•OEt$_2$

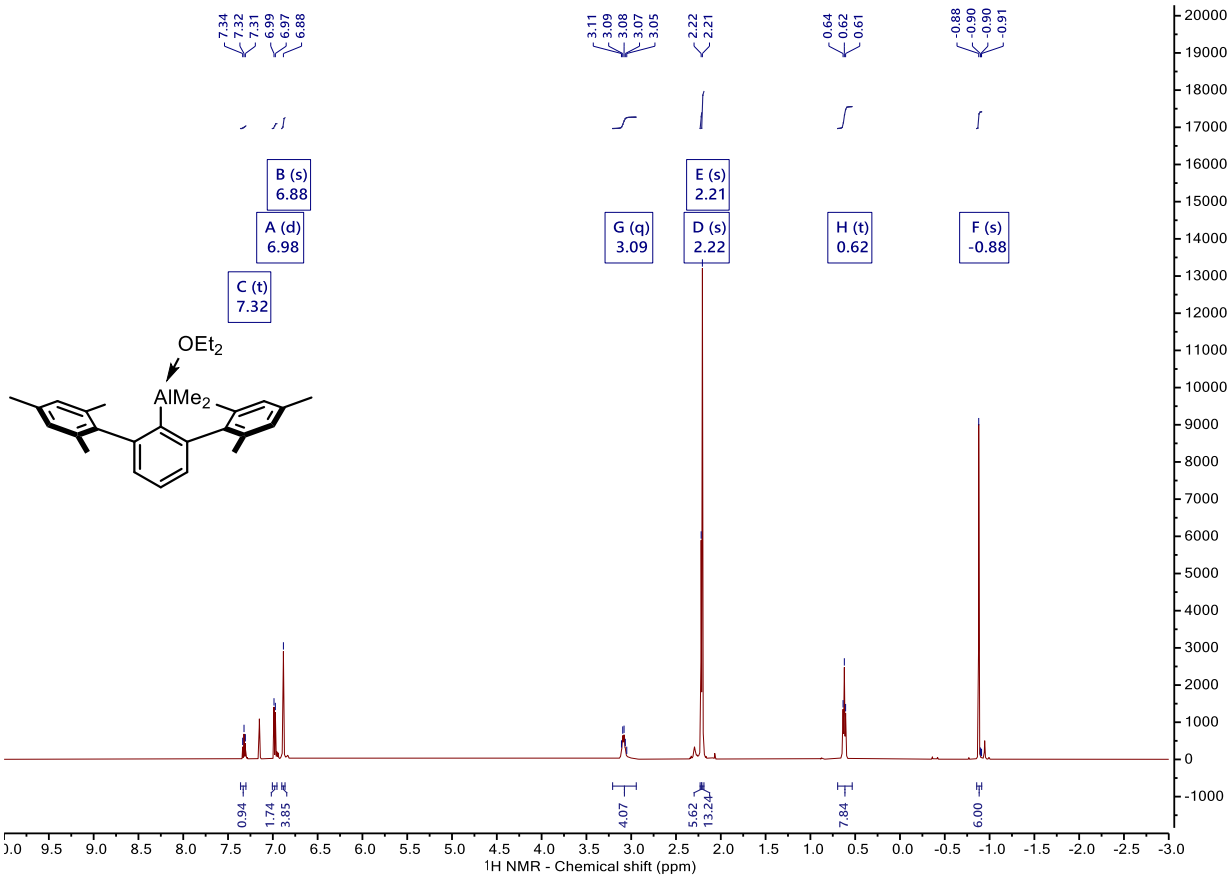

^{1}H NMR (500 MHz, Benzene-d_6) of **^{Mes}TerAlMe$_2$•OEt$_2$**

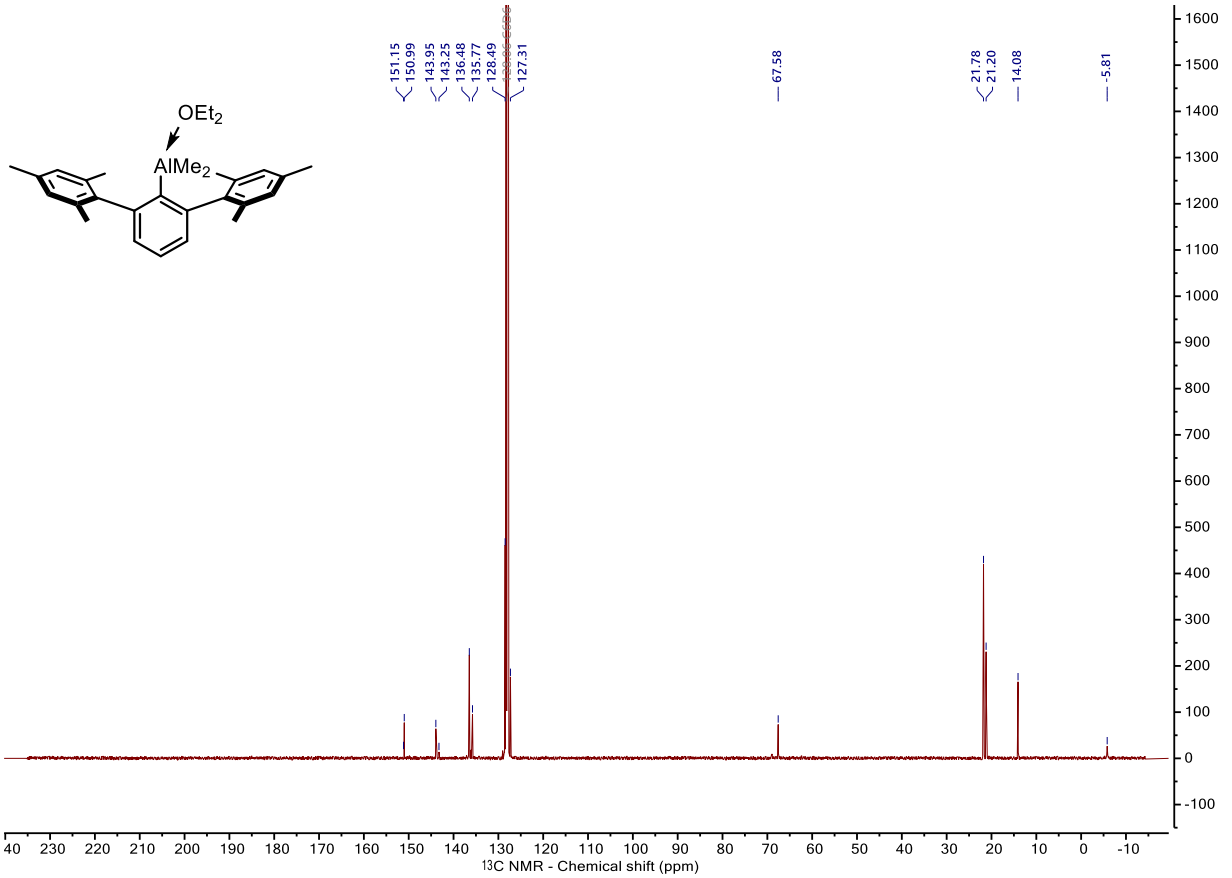

^{13}C {^{1}H} NMR (126 MHz, Benzene-d_6) of **^{Mes}TerAlMe$_2$•OEt$_2$**

^{Mes}TerAl(*i*Bu)$_2$

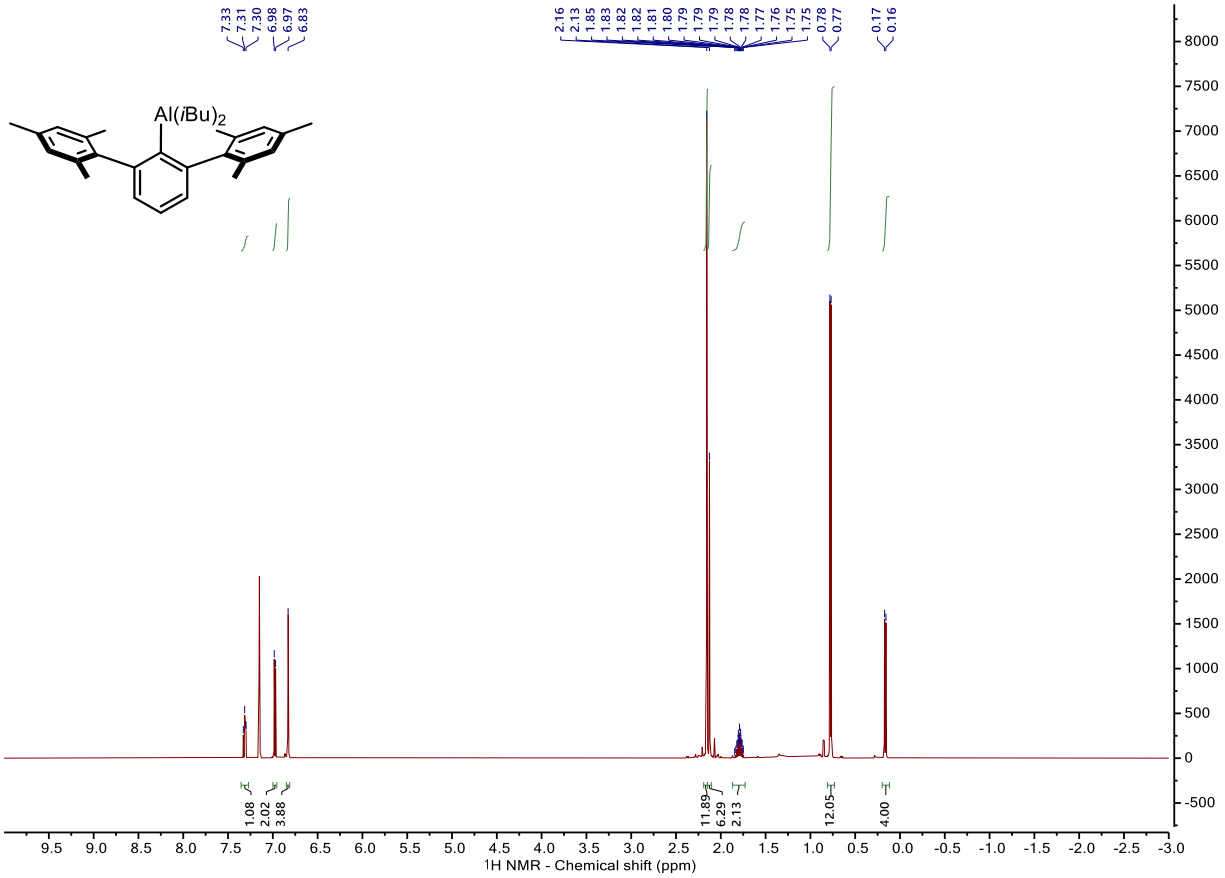

^{1}H NMR (500 MHz, Benzene-d$_6$) of **^{Mes}TerAl(*i*Bu)$_2$**

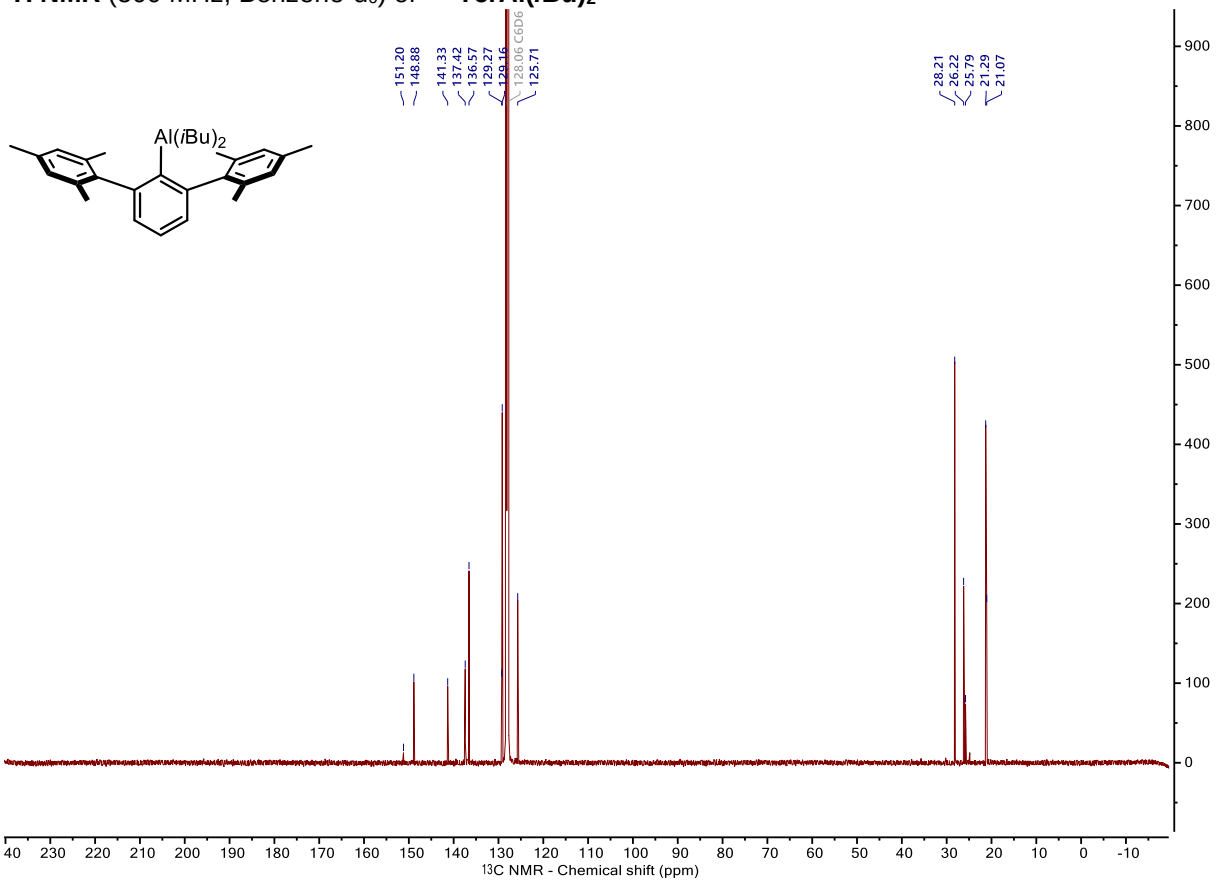

^{13}C {^{1}H} NMR (126 MHz, Benzene-*d*$_6$) of **^{Mes}TerAl(*i*Bu)$_2$**

^{Mes}TerAlEt$_2$

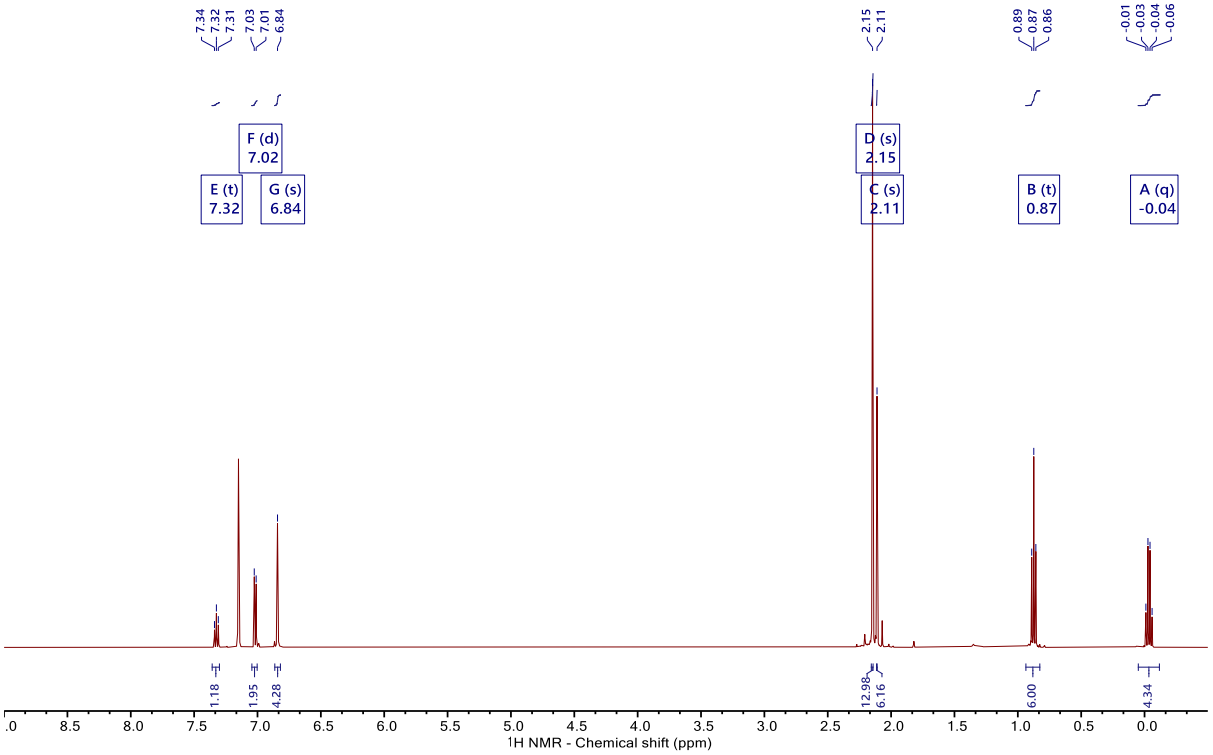

^{1}H NMR (500 MHz, Benzene-d_6) of ^{Mes}TerAlEt$_2$

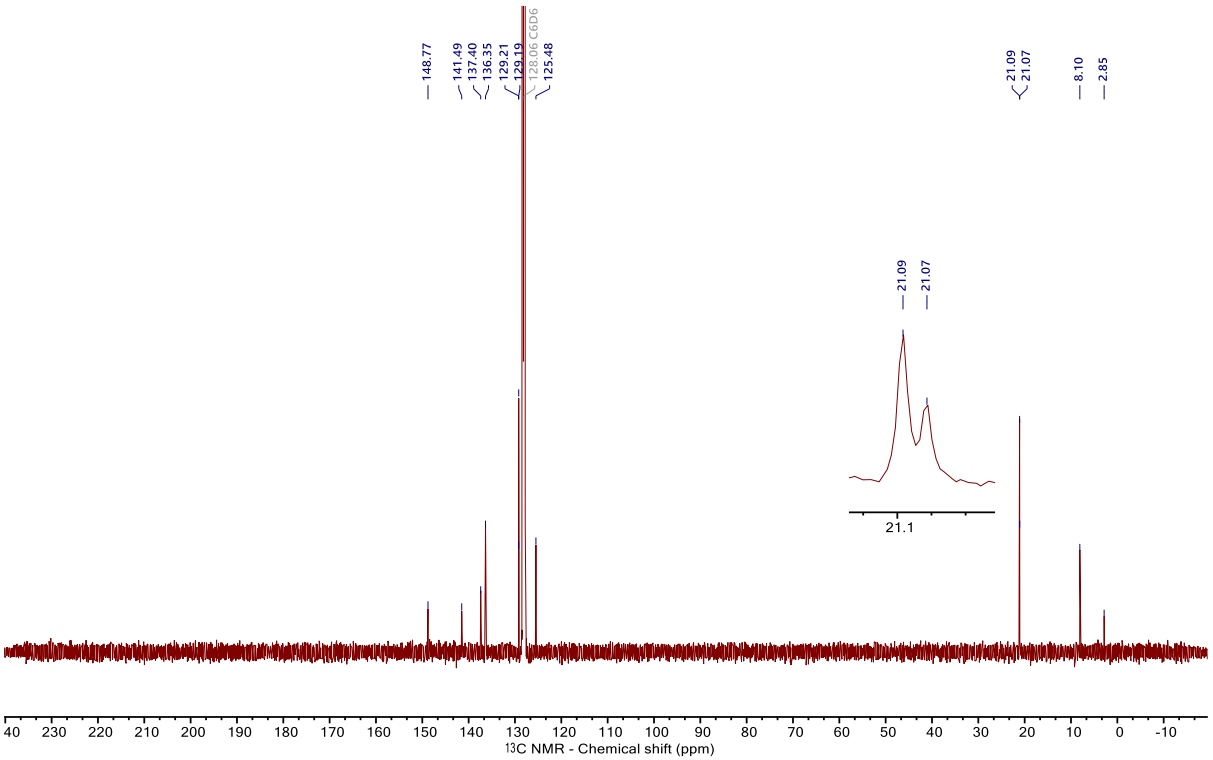

^{13}C {^{1}H} NMR (126 MHz, Benzene-d_6) of ^{Mes}TerAlEt$_2$

^{Mes}TerAl(Et)H

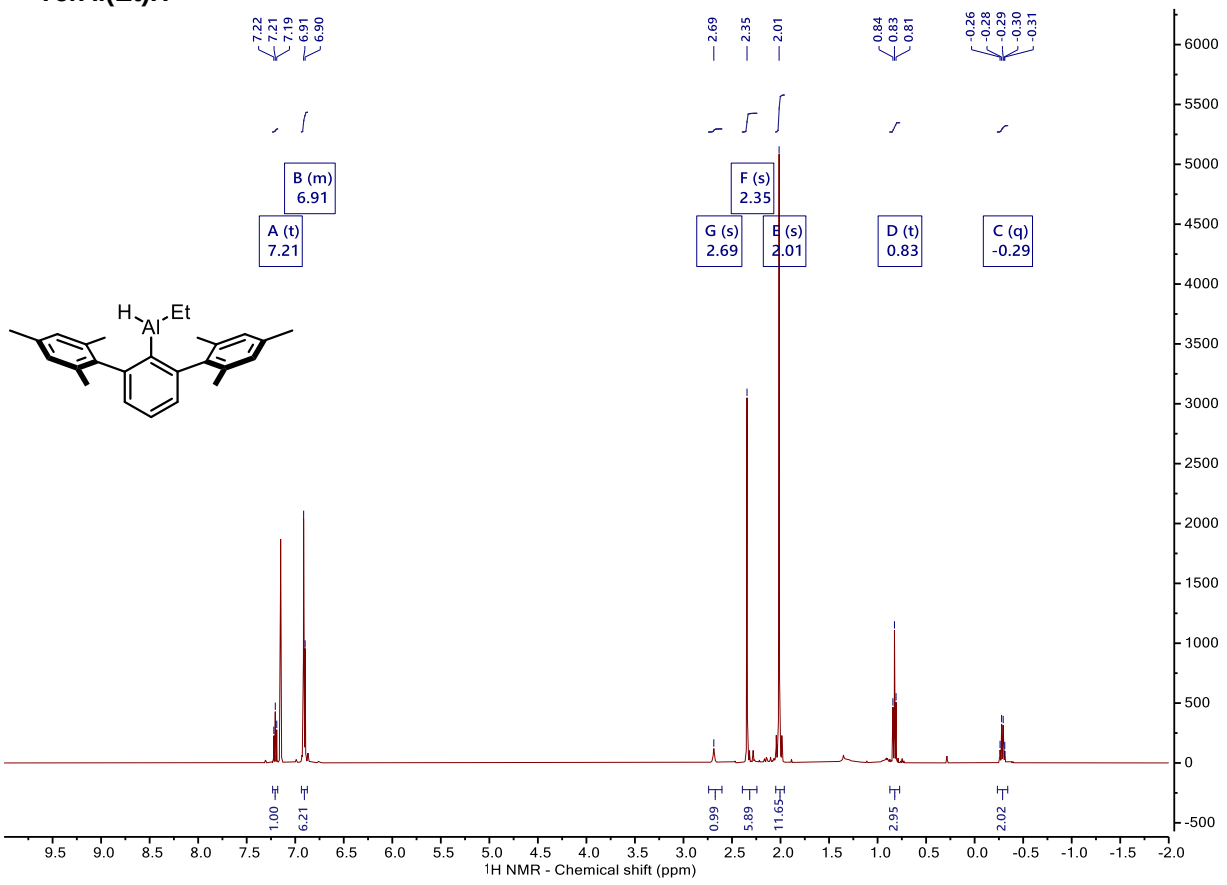

^{1}H NMR (500 MHz, Benzene-d_6) of **^{Mes}TerAl(Et)H**

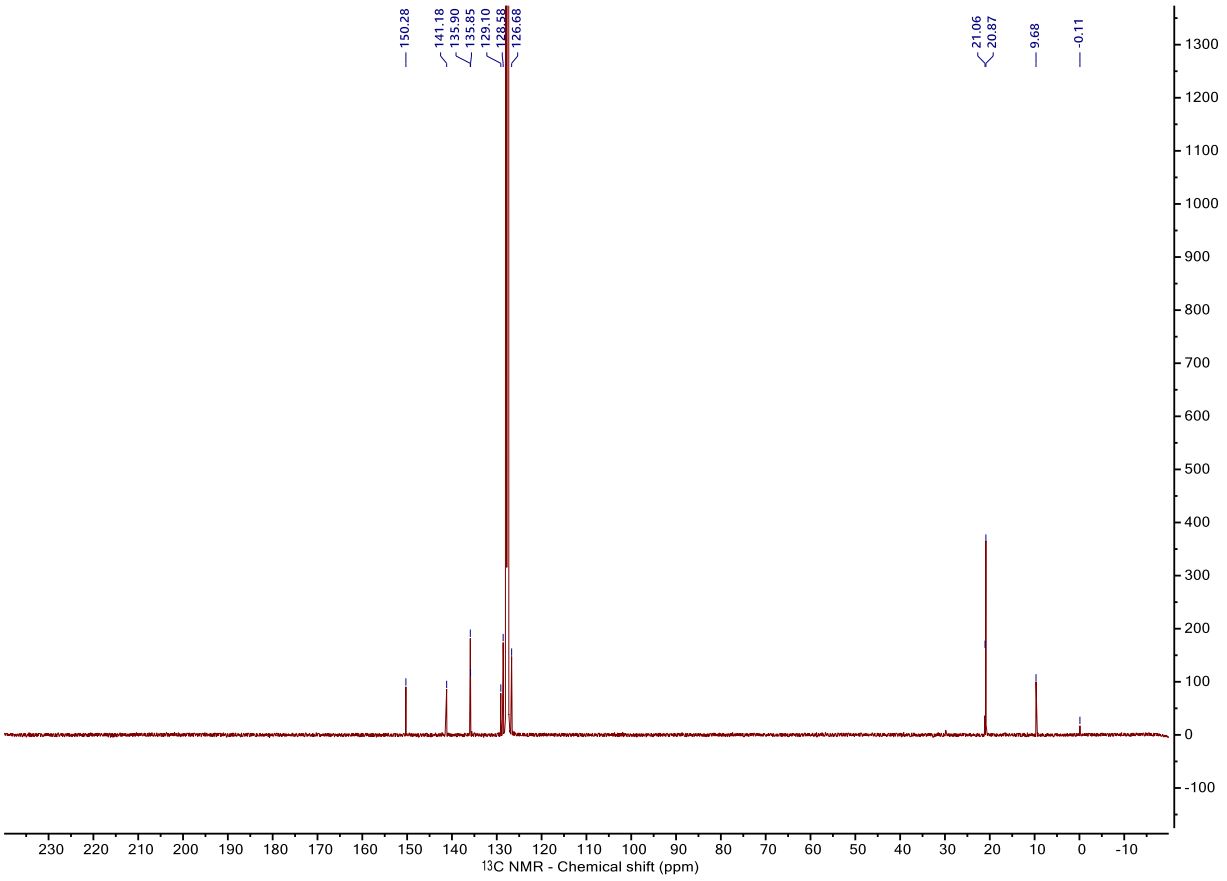

^{13}C {^{1}H} NMR (126 MHz, Benzene-d_6) of **^{Mes}TerAl(Et)H**

^{Tipp}TerAlH$_2$

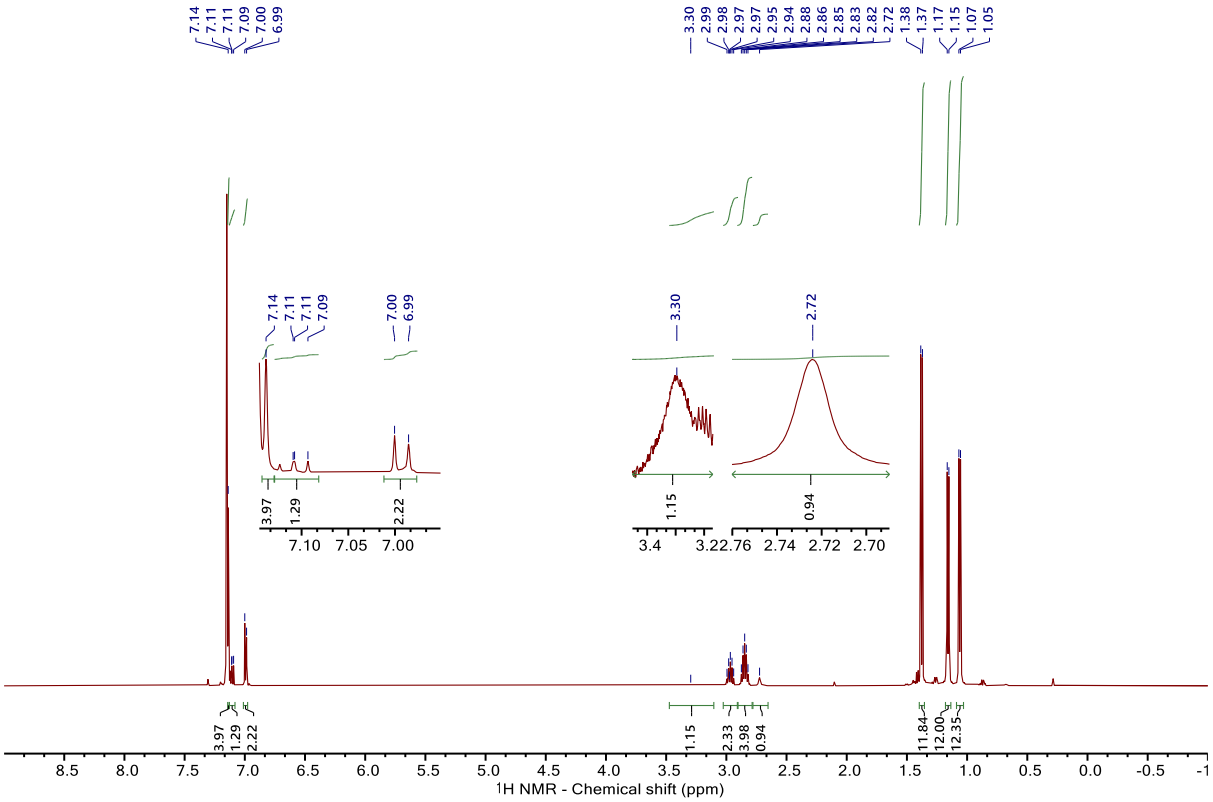

^{1}H NMR (500 MHz, Benzene-d_6) of ^{Tipp}TerAlH$_2$

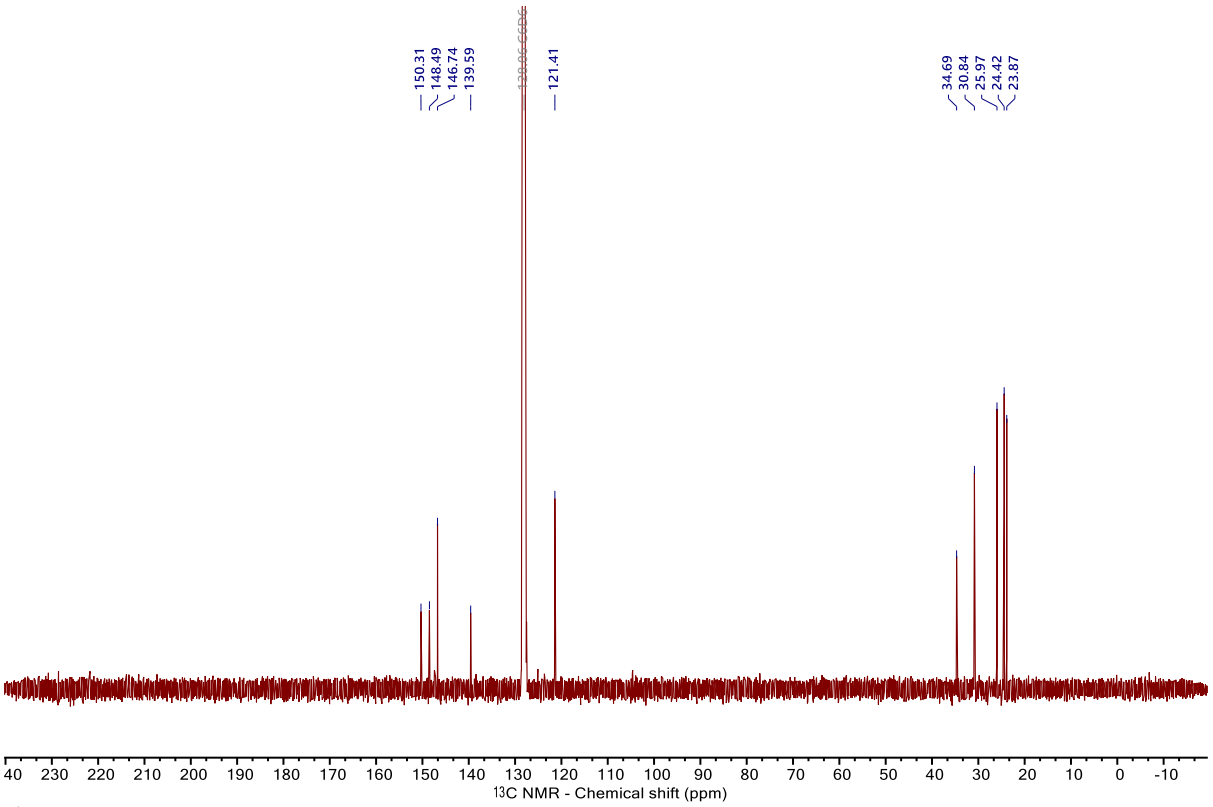

^{13}C {^{1}H} NMR (126 MHz, Benzene-d_6) of ^{Tipp}TerAlH$_2$

^{Tipp}TerAlMe$_2$

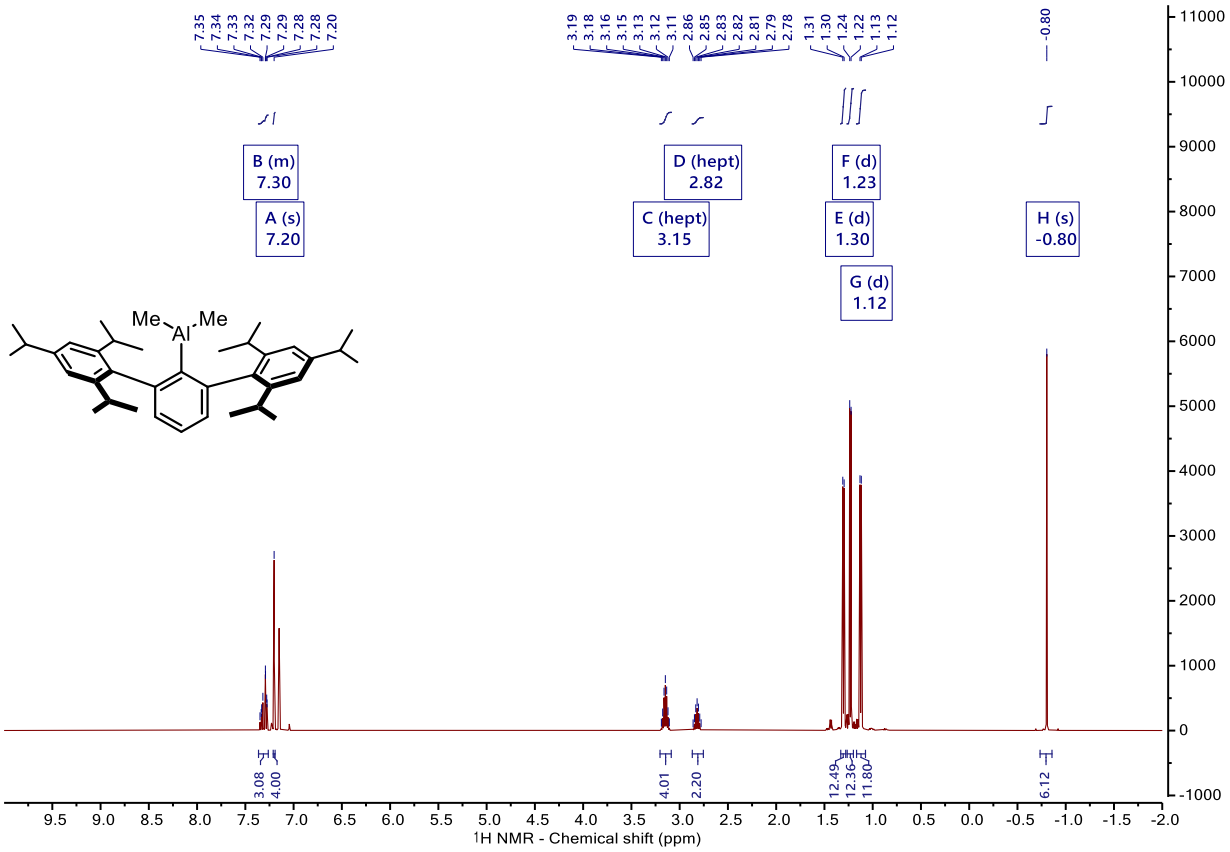

^{1}H NMR (500 MHz, Benzene-d_6) of **^{Tipp}TerAlMe$_2$**

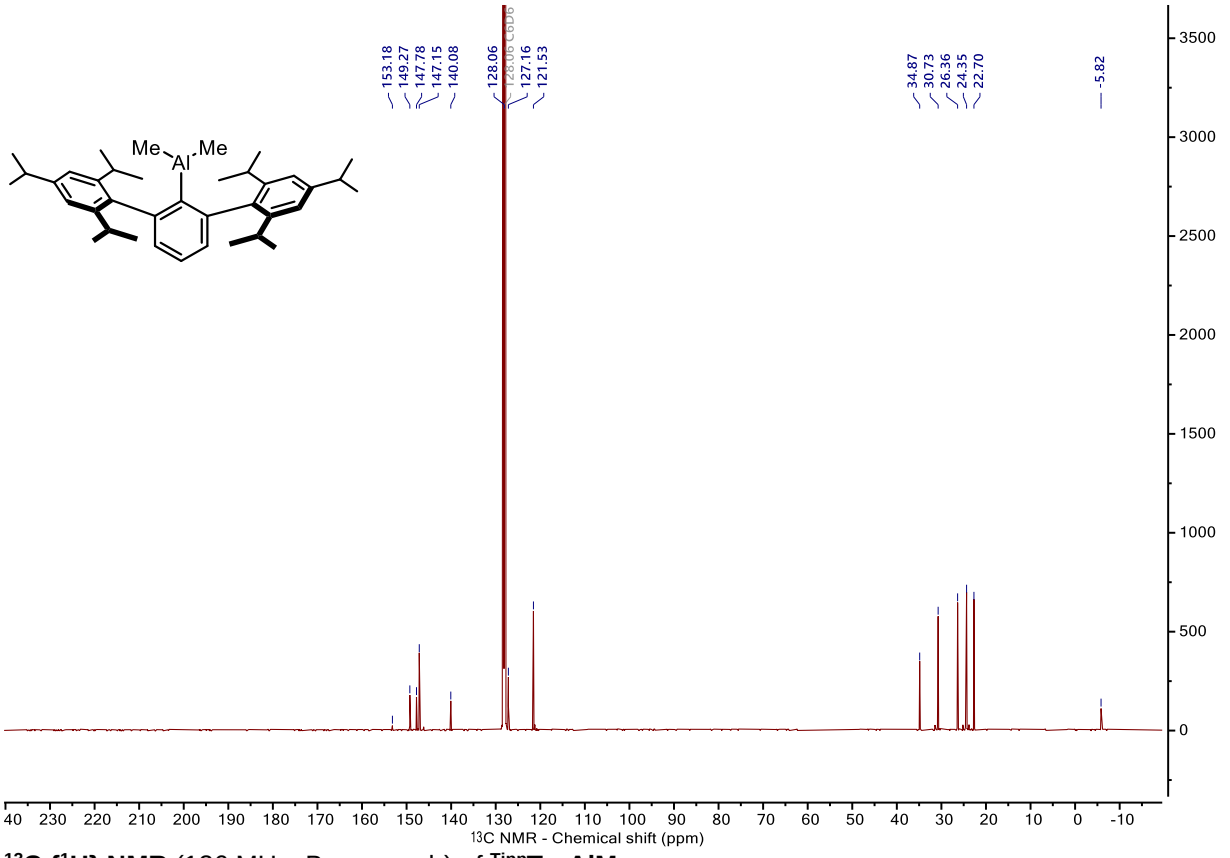

^{13}C {^{1}H} NMR (126 MHz, Benzene-d_6) of **^{Tipp}TerAlMe$_2$**

^{Tipp}TerAlMe$_2$•OEt$_2$

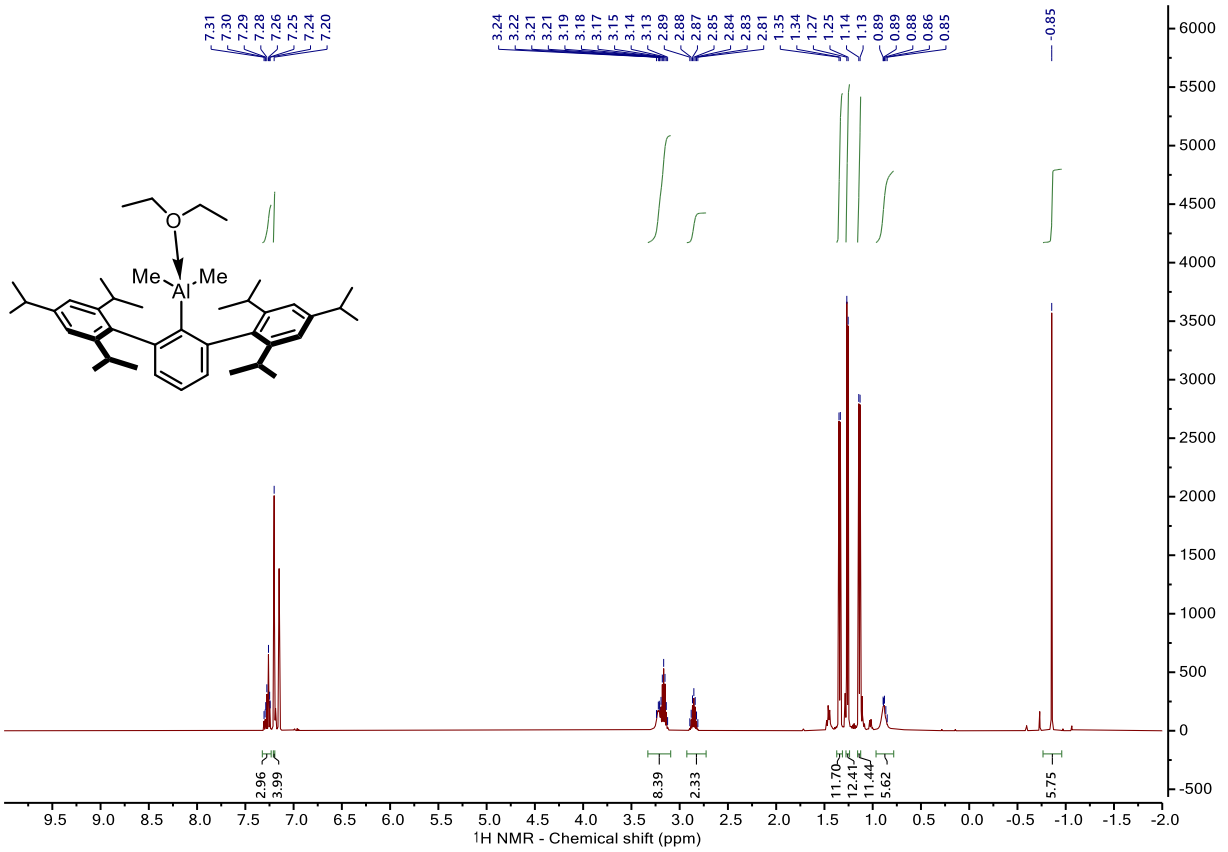

^{1}H NMR (500 MHz, Benzene-d_6) of **^{Tipp}TerAlMe$_2$•OEt$_2$**

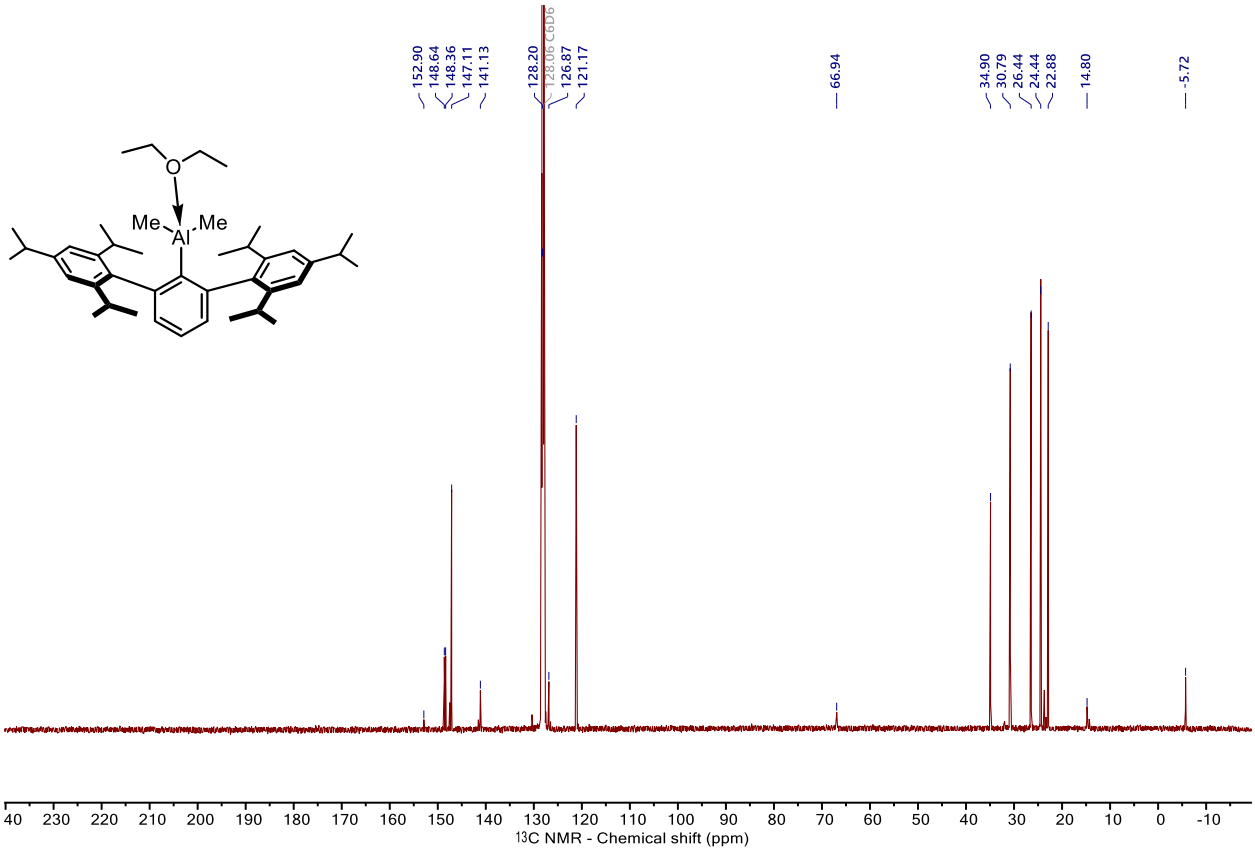

^{13}C {^{1}H} NMR (126 MHz, Benzene-d_6) of **^{Tipp}TerAlMe$_2$•OEt$_2$**

[^{Mes}TerAl(pin)]$_2$ (crude)

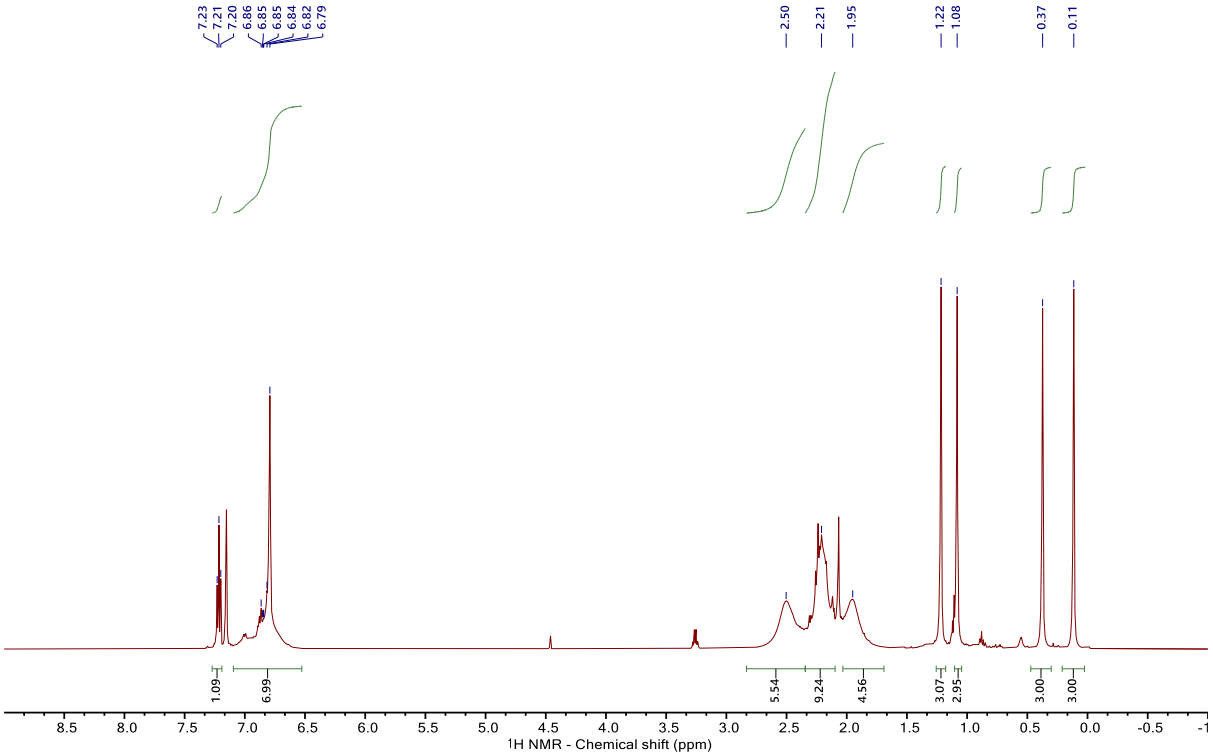

^{1}H NMR (500 MHz, C_6D_6) of the reaction between ^{Mes}TerAlH$_2$ with pinacol (1 equiv.). Major peaks (picked) are [^{Mes}TerAl(pin)]$_2$.

Al–pin

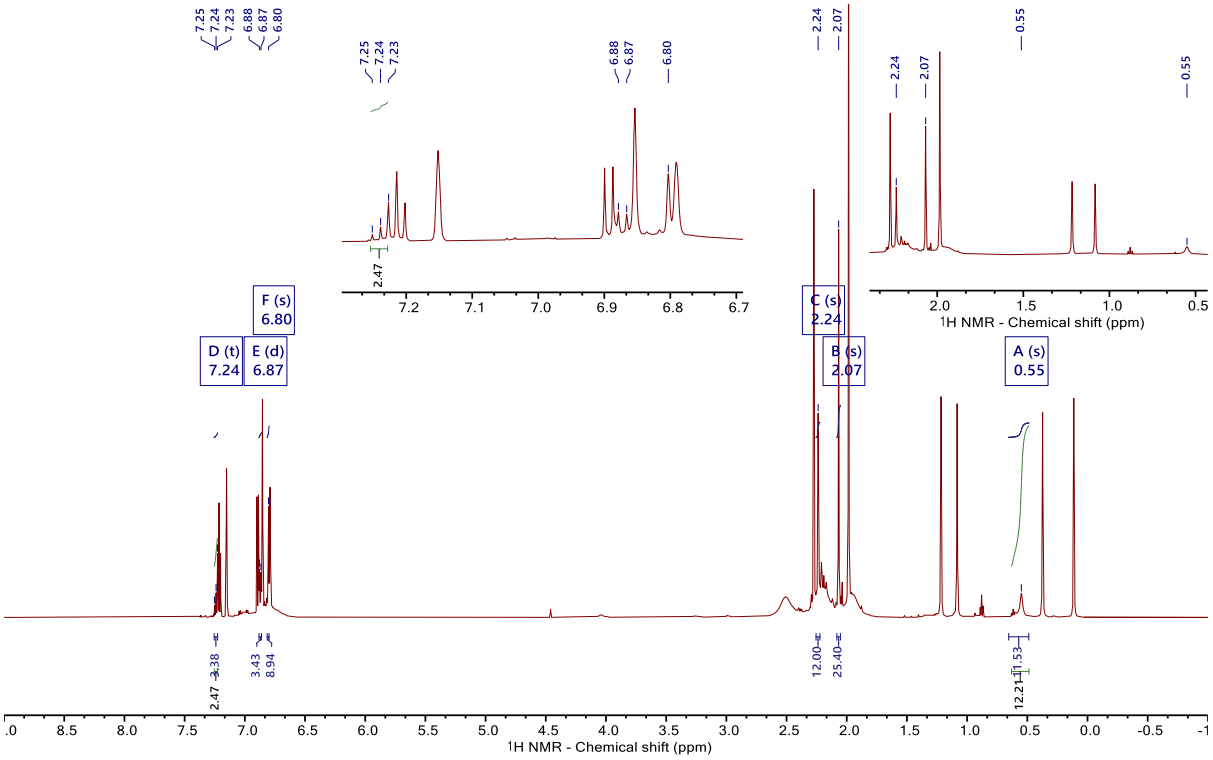

^{1}H NMR (601 MHz, C_6D_6) of the reaction between ^{Mes}TerAlH$_2$ with pinacol (0.5 equiv.). Peaks picked are ***Al–pin***. Obtained as a mixture containing also [^{Mes}TerAl(pin)]$_2$ and [^{Mes}TerAlH$_2$]$_2$.

2. Al–H–B species

3-Mes-1; ^{Mes}TerAl(BH$_4$)$_2$

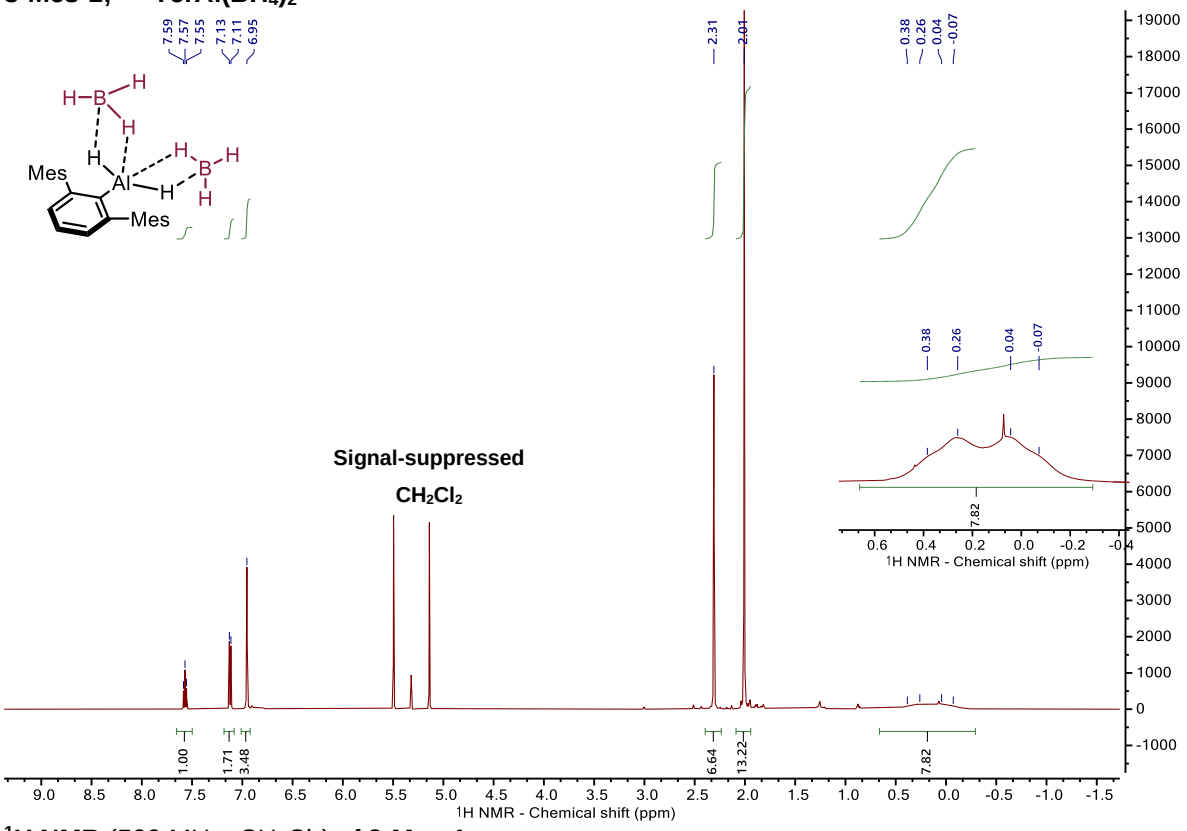

^{1}H NMR (500 MHz, CH_2Cl_2) of **3-Mes-1**

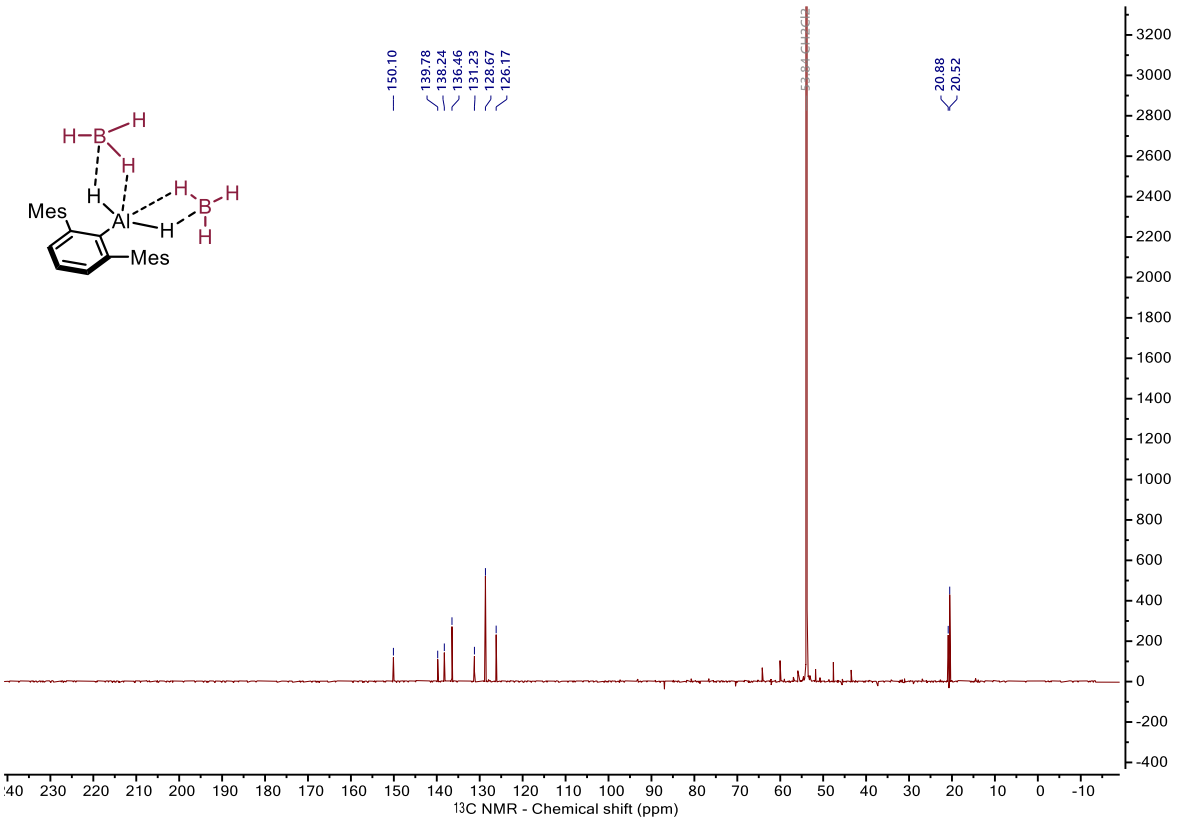

^{13}C {^{1}H} NMR (126 MHz, CH_2Cl_2) of **3-Mes-1**

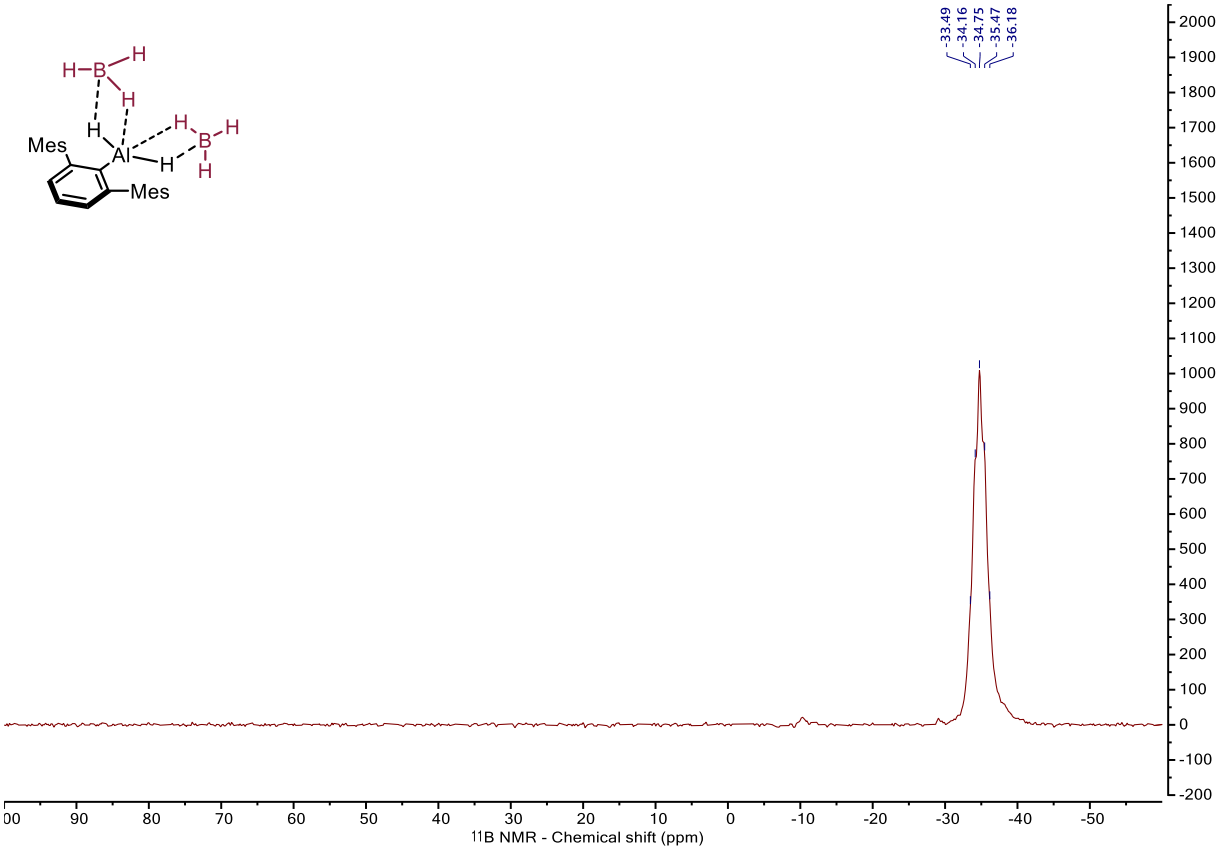

^{11}B NMR (128 MHz, CH_2Cl_2) of **3-Mes-1**

3-Mes-2^{Et}; ^{Mes}TerAl(Et)(BH_4)

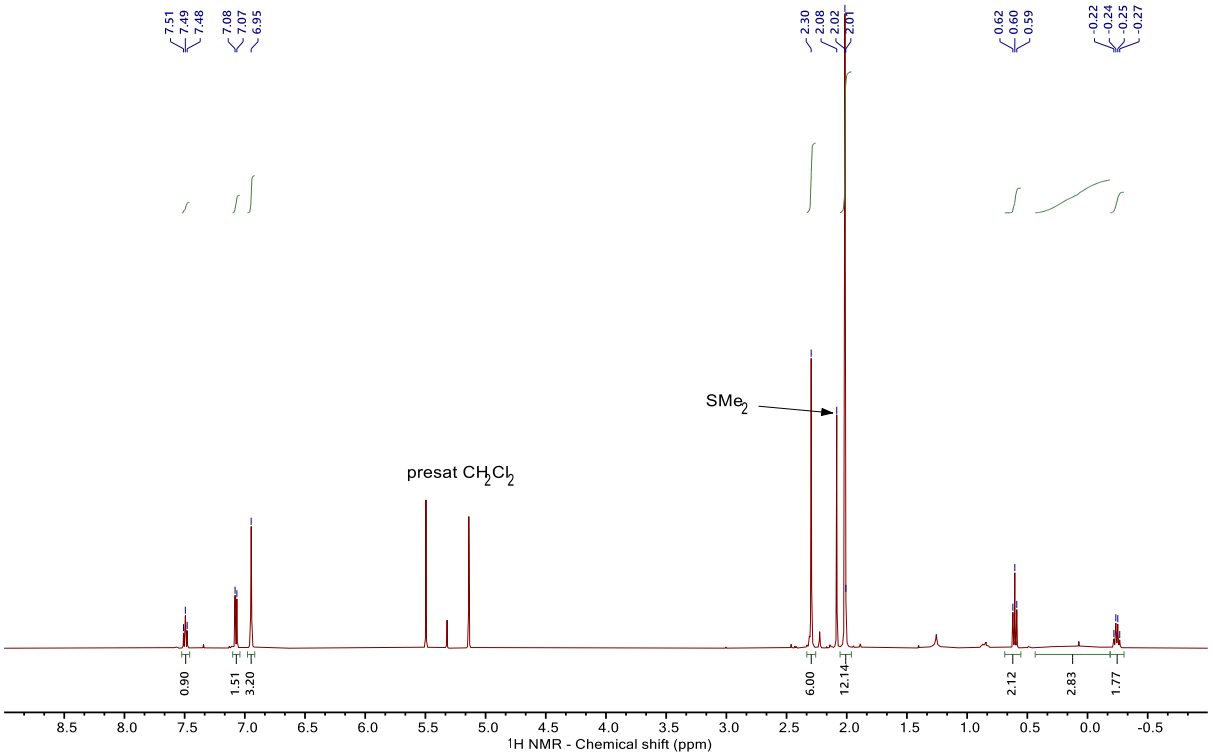

^{1}H NMR (500 MHz, CH_2Cl_2) of 3-Mes-2^{Et} (^{Mes}TerAl(Et)H + Me_2S•BH_3 (1 equiv.))

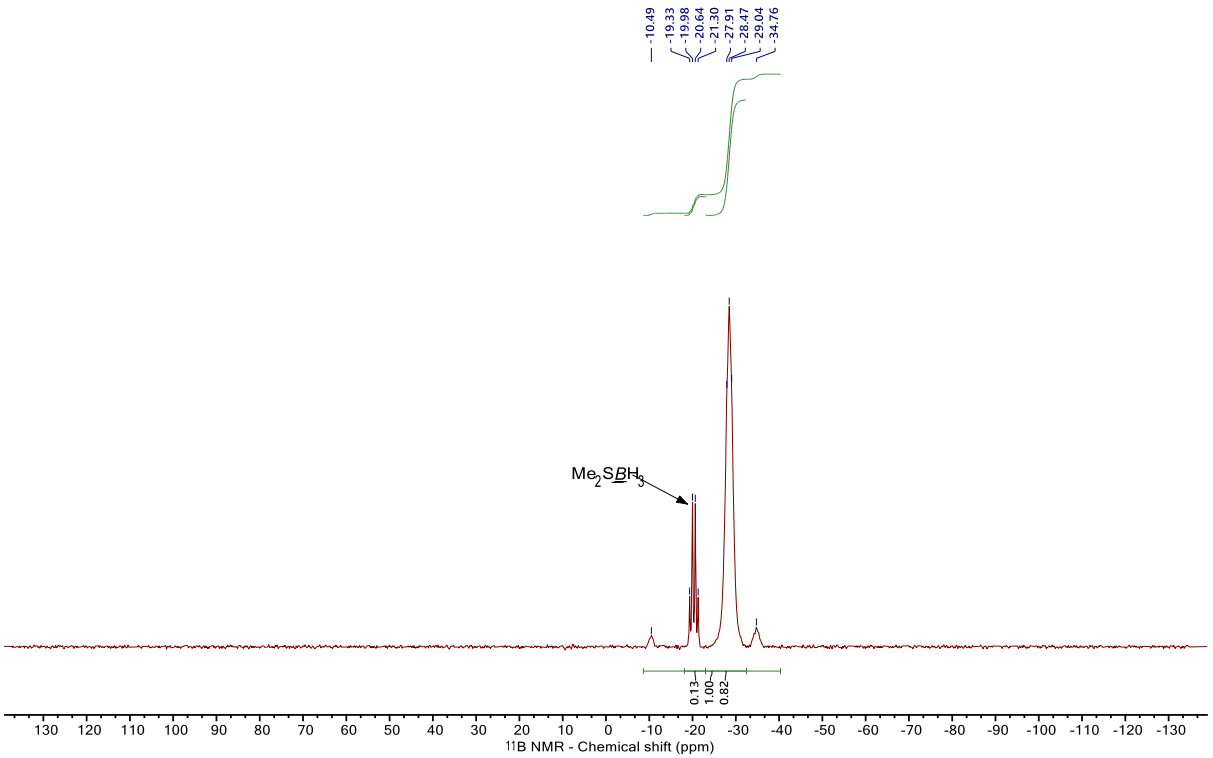

^{11}B NMR (160 MHz, CH_2Cl_2) of 3-Mes-2^{Et} (^{Mes}TerAl(Et)H + Me_2S•BH_3 (1 equiv.))

3-Mes-2^{octyl}; ^{Mes}TerAl(*n*Oct)(BH_4)

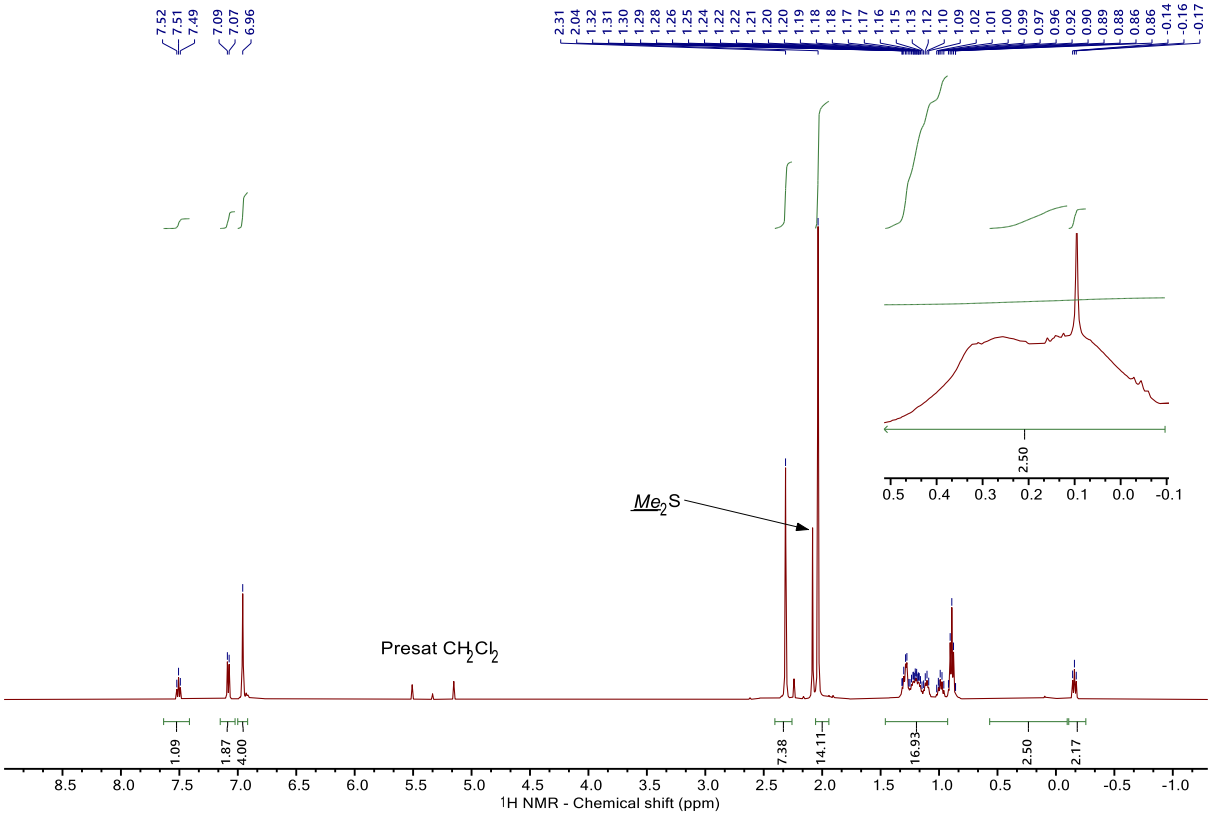

^{1}H NMR (500 MHz, CH_2Cl_2) of **3-Mes-2^{octyl}** (^{Mes}TerAlH_2 + 1-octene (1 equiv.) then Me_2S•BH_3 (1 equiv.))

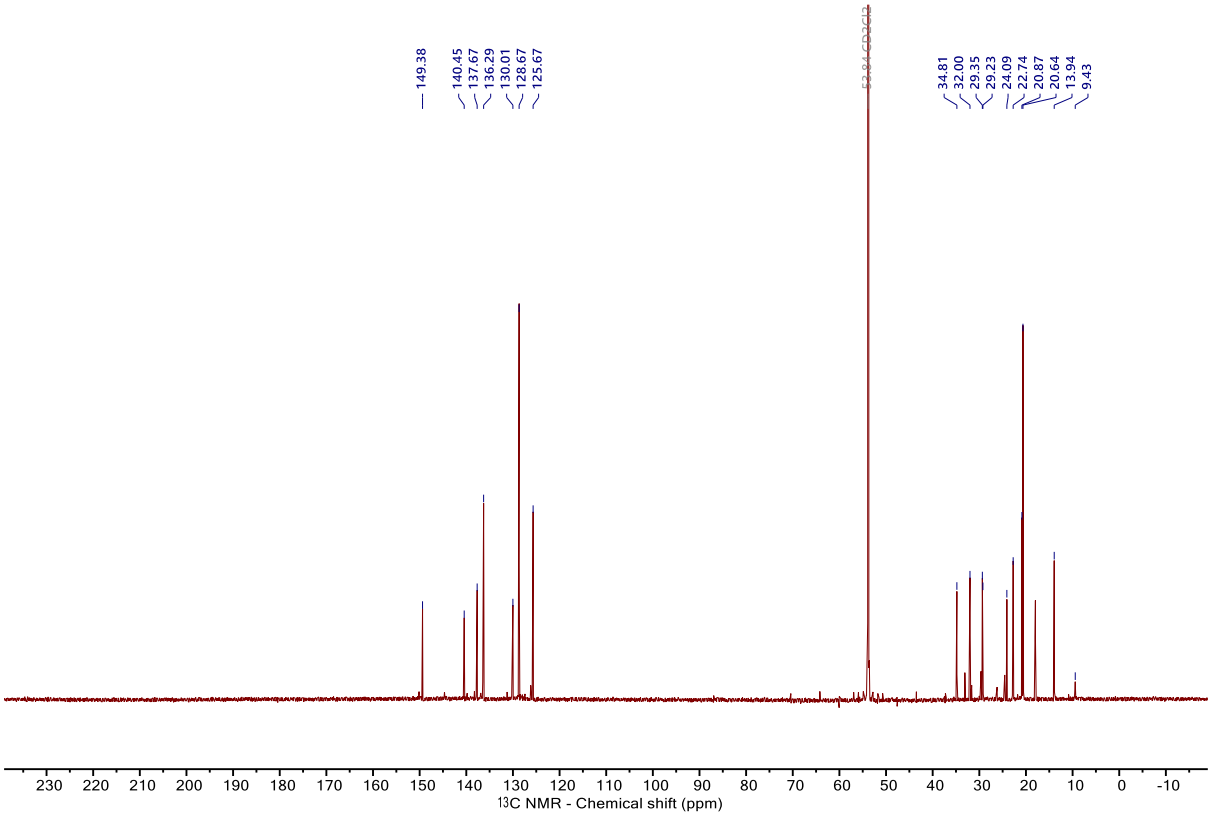

^{13}C {1H} NMR (126 MHz, CH_2Cl_2) of **3-Mes-2^{octyl}** (^{Mes}TerAlH_2 + 1-octene (1 equiv.) then Me_2S•BH_3 (1 equiv.))

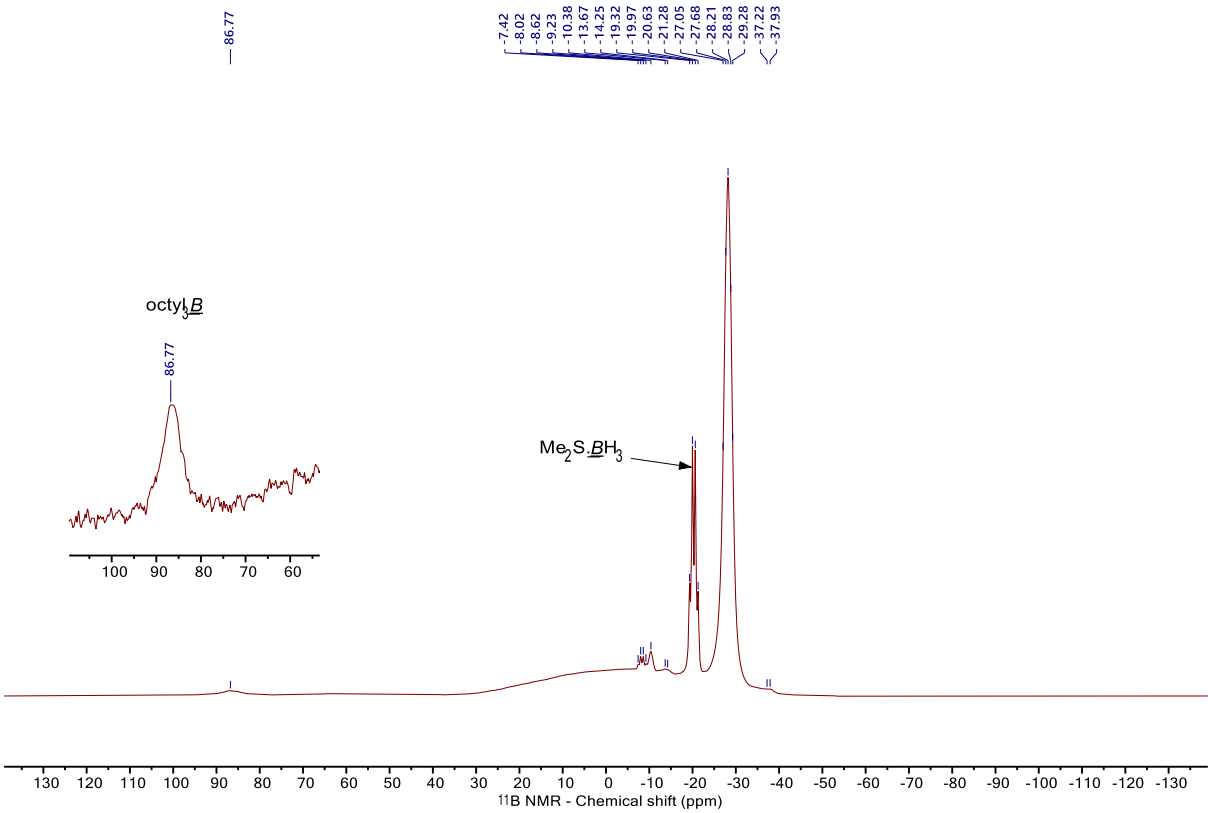

^{11}B NMR (160 MHz, CH_2Cl_2) of **3-Mes-2^{octyl}** (^{Mes}TerAlH_2 + 1-octene (1 equiv.) then Me_2S•BH_3 (1 equiv.))

3-Mes-3^{CH_2CH_2tBu}; ^{Mes}TerAl(*t*BuCH$_2$CH$_2$BH$_3$)$_2$

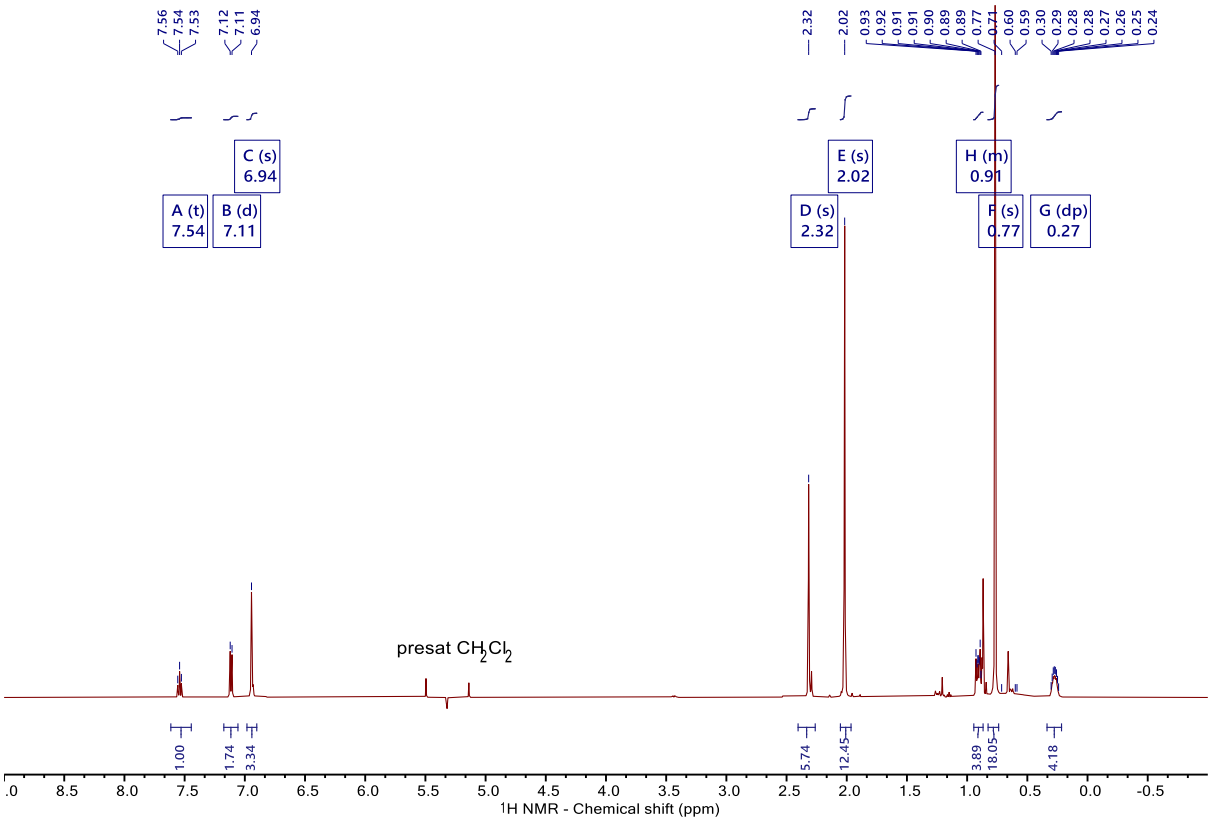

^{1}H NMR (500 MHz, CH_2Cl_2) of **3-Mes-3^{CH_2CH_2tBu}** (^{Mes}TerAlH$_2$ + *t*BuCH$_2$CH$_2$BH$_2$ (1 equiv.))

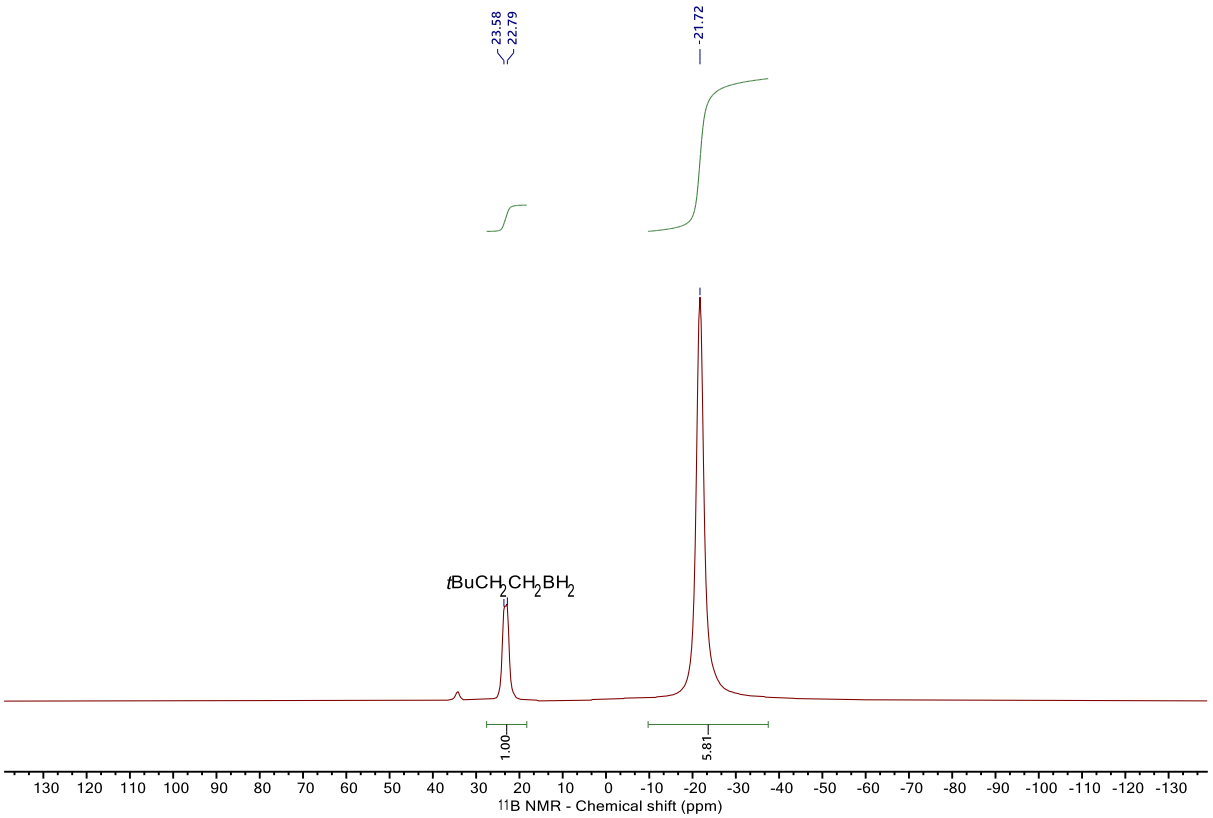

^{11}B NMR (160 MHz, CH_2Cl_2) of **3-Mes-3^{CH_2CH_2tBu}** (^{Mes}TerAlH$_2$ + *t*BuCH$_2$CH$_2$BH$_2$ (1 equiv.))

3-Mes-3^{Mes}; ^{Mes}TerAl(MesBH$_3$)$_2$

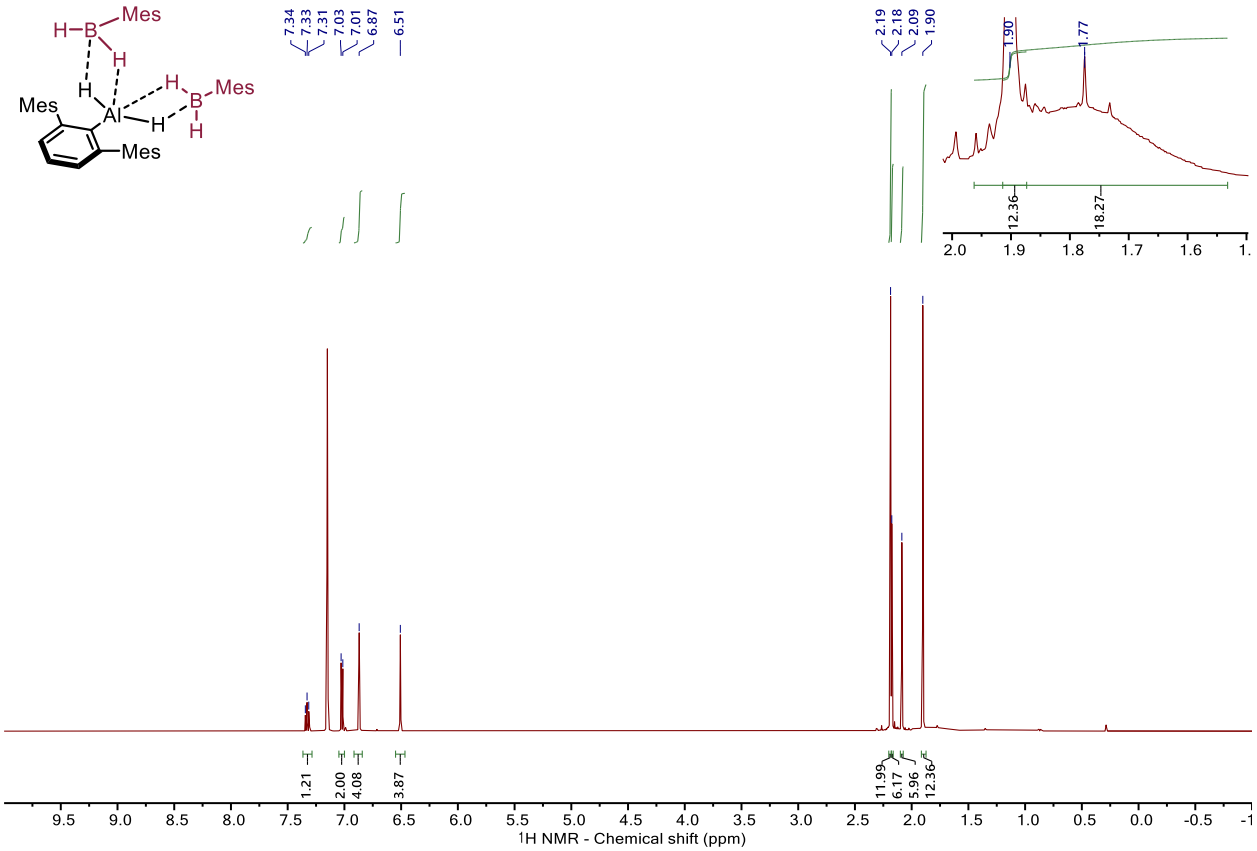

^{1}H NMR (500 MHz, Benzene-d_6) of ABG-0450

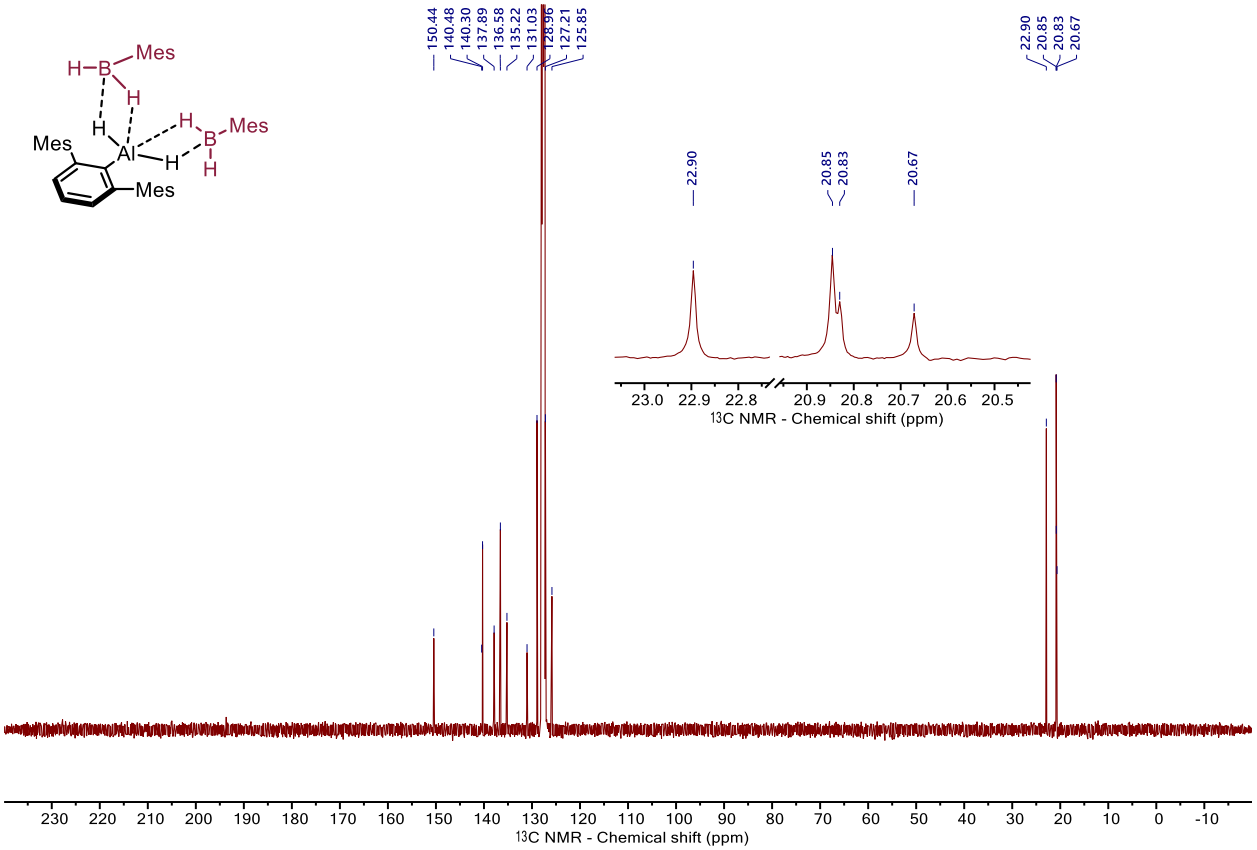

^{13}C {^{1}H} NMR (126 MHz, Benzene-d_6) of ABG-0450

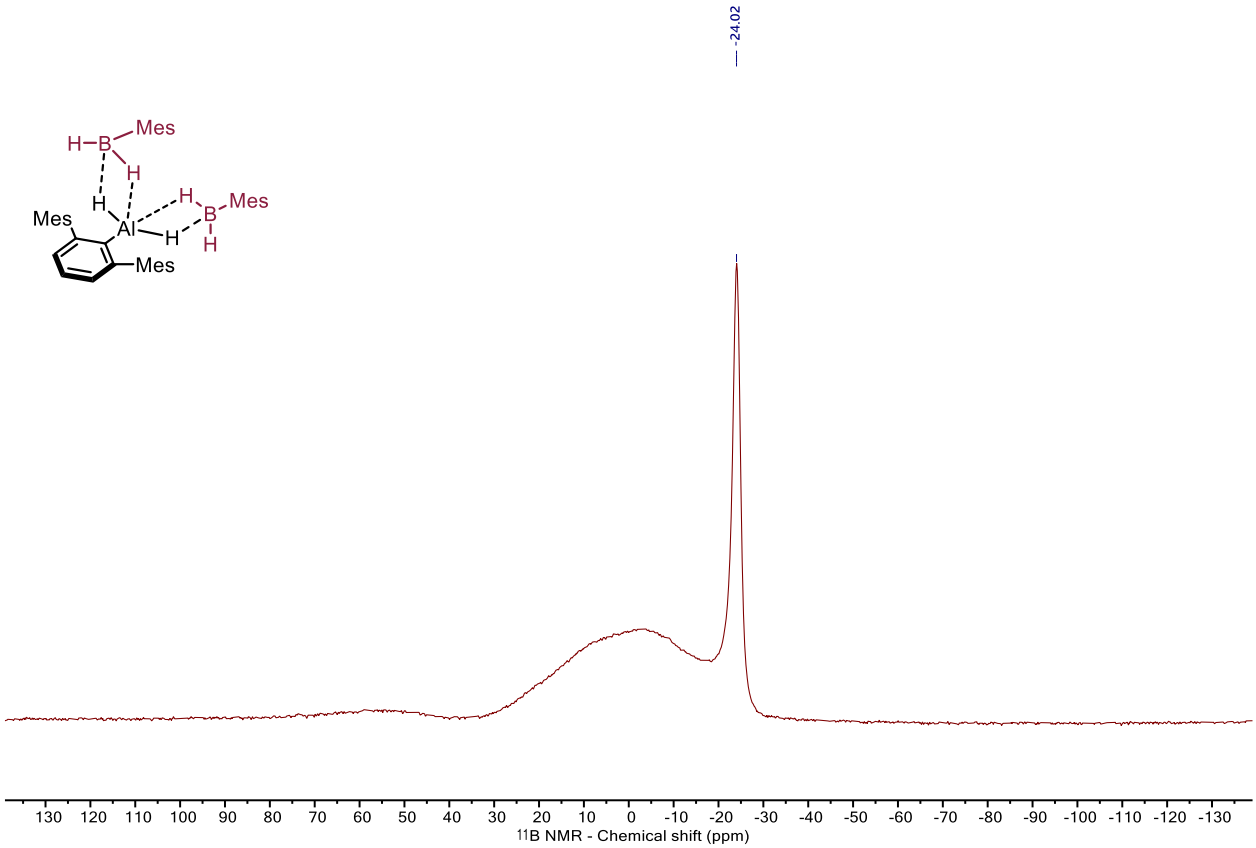

^{11}B NMR (160 MHz, Benzene-d_6) of ABG-0450

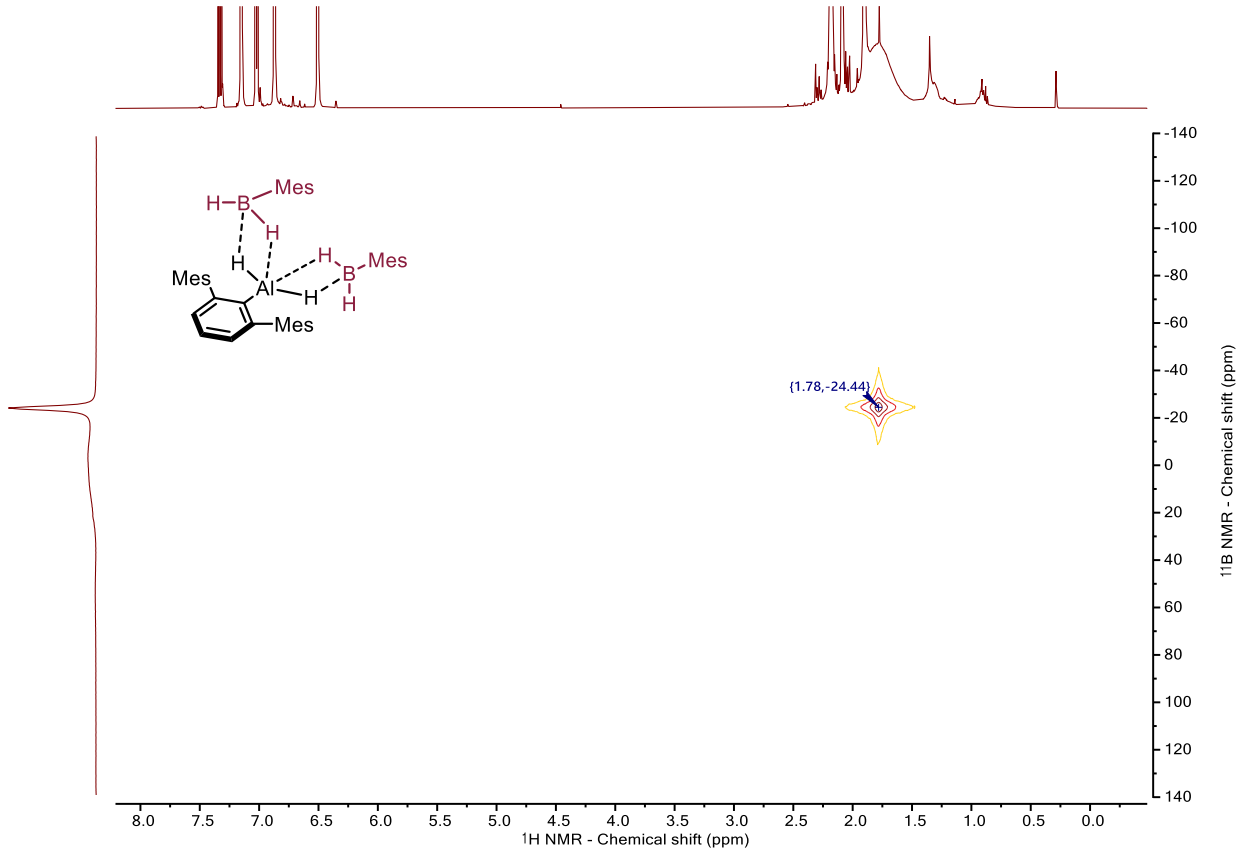

^{1}H-^{11}B HMQC (Benzene-d_6) of ABG-0450

3-Mes-4^{CH_2CH_2tBu,Et} ; ^{Mes}TerAl(Et)(*t*BuCH$_2$CH$_2$BH$_3$)

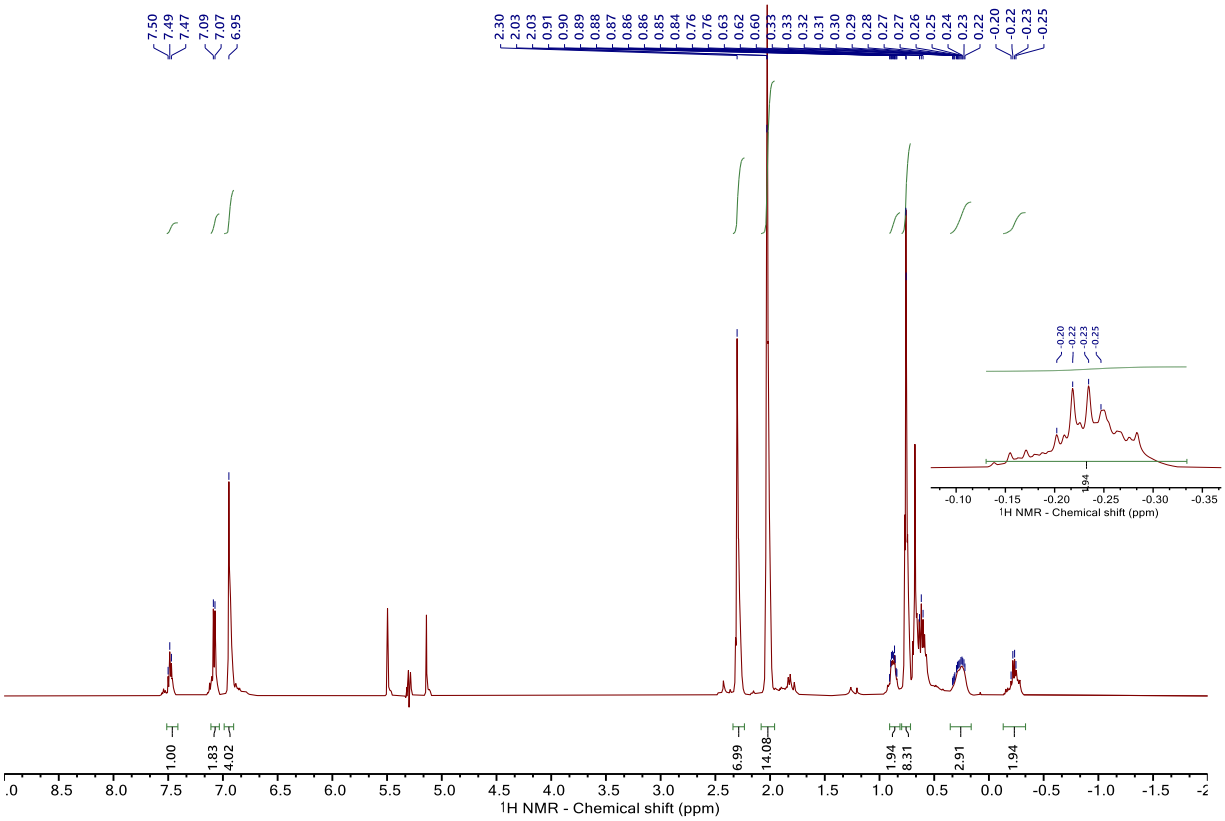

^{1}H NMR (500 MHz, CH_2Cl_2) for **3-Mes-4^{CH2CH2tBu,Et}** (^{Mes}TerAl(Et)H + *t*BuCH$_2$CH$_2$BH$_2$ (1 equiv.))

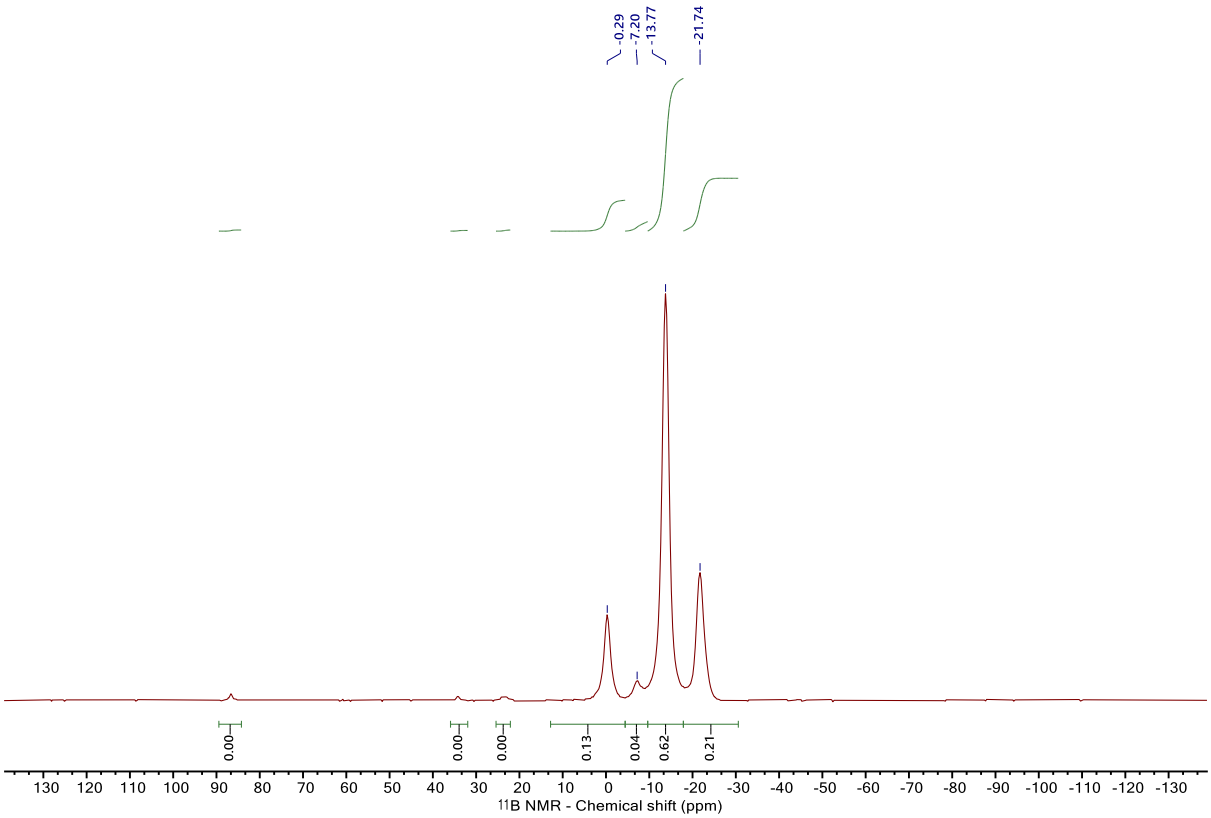

^{11}B NMR (160 MHz, CH_2Cl_2) for **3-Mes-4^{CH2CH2tBu,Et}** (^{Mes}TerAl(Et)H + *t*BuCH$_2$CH$_2$BH$_2$ (1 equiv.))

3-Mes-5^{BBN}; ^{Mes}TerAl(H)(H$_2$-*B*-9-BBN)

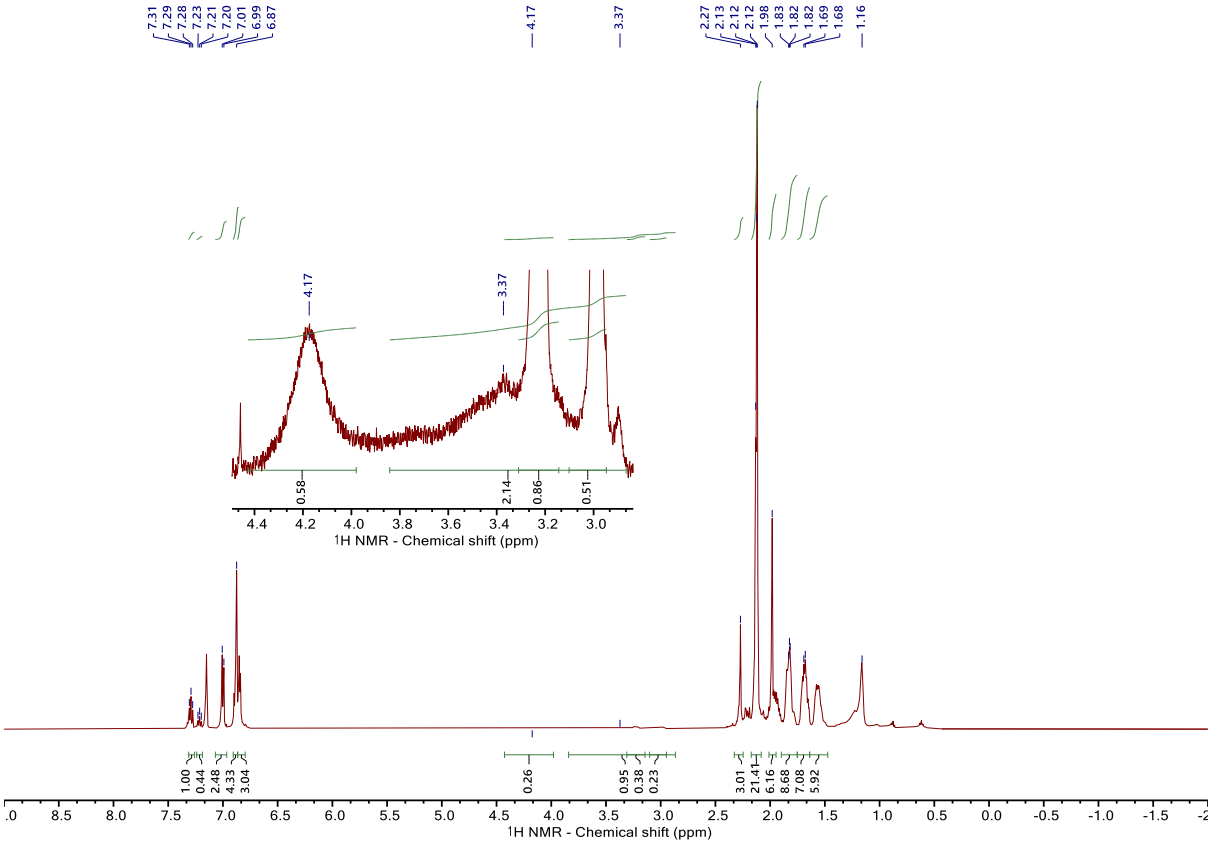

^{1}H NMR (500 MHz, CH_2Cl_2) of **3-Mes-5^{BBN}** (^{Mes}TerAlH$_2$ + H-*B*-9-BBN (1 equiv.))

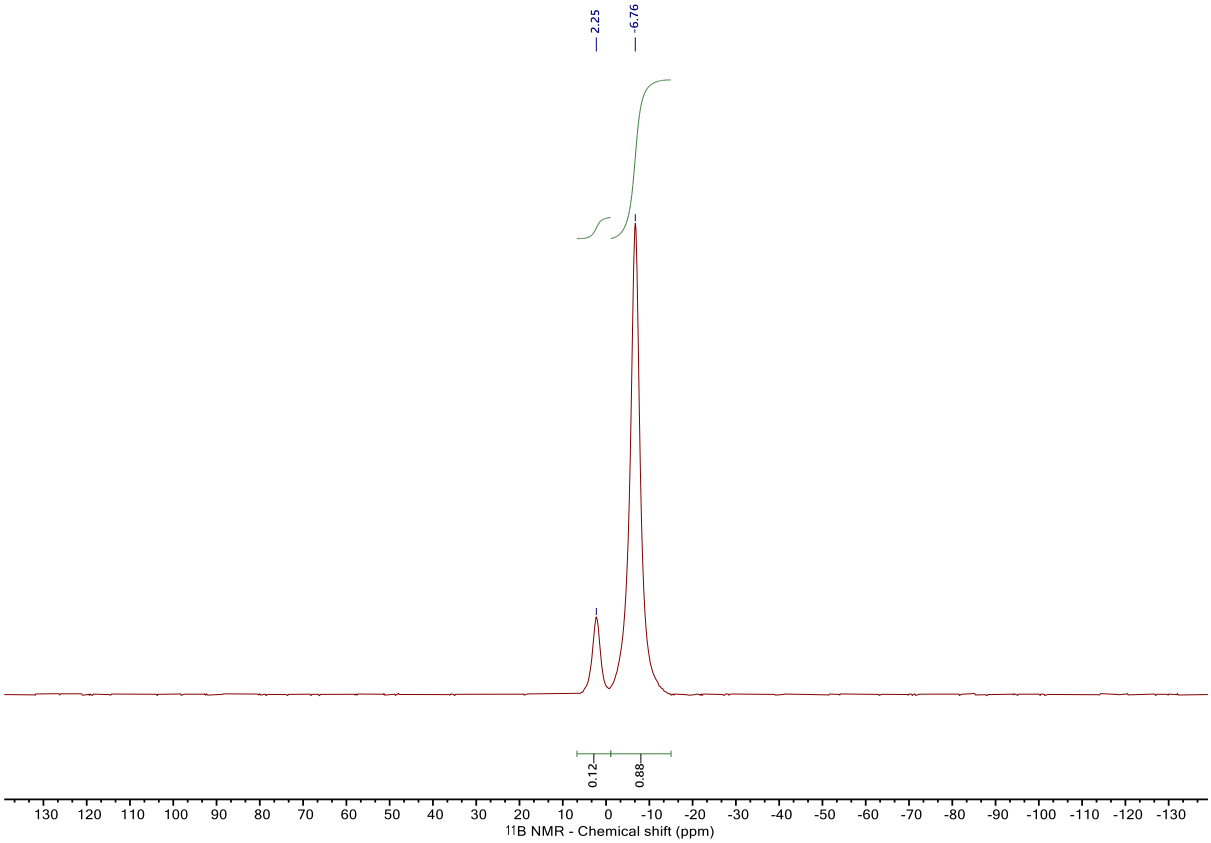

^{11}B NMR (160 MHz, Benzene-d_6) of **3-Mes-5^{BBN}** (^{Mes}TerAlH$_2$ + H-*B*-9-BBN (1 equiv.))

3-Mes-6$^{BBN,Et'}$; ^{Mes}TerAl(Et)(H$_2$-*B*-9-BBN)

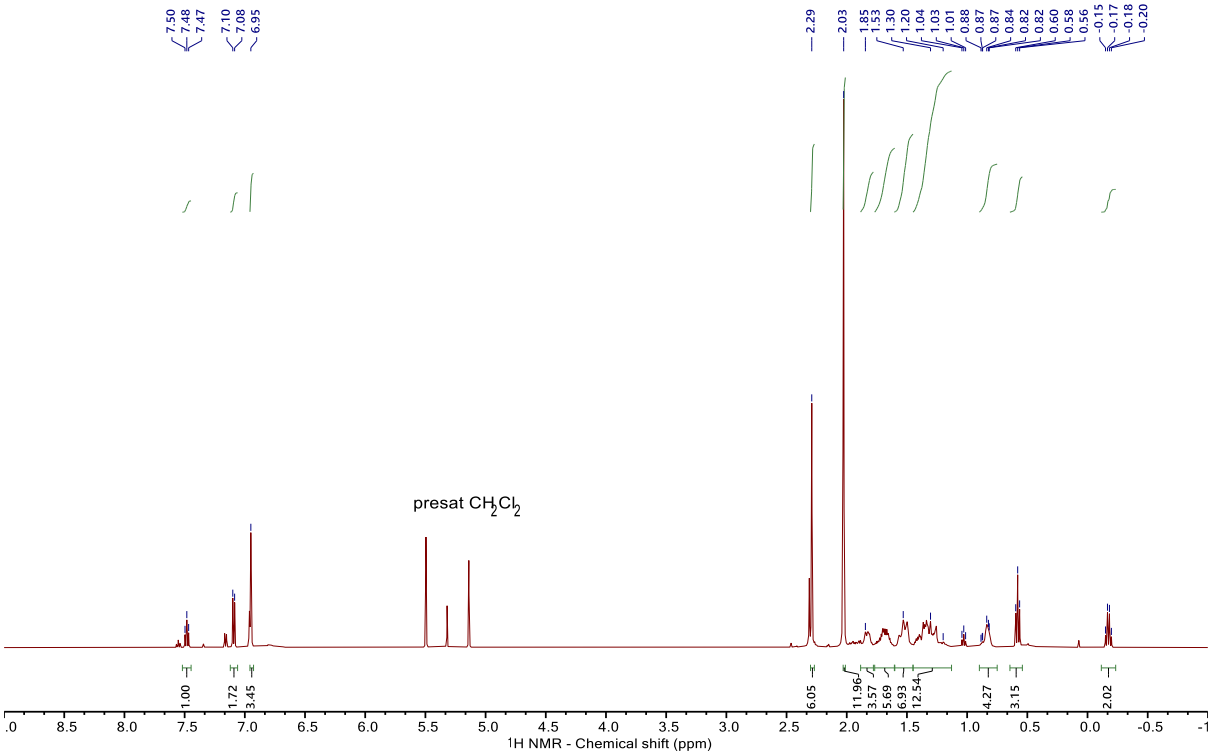

^{1}H NMR (500 MHz, CH_2Cl_2) of **3-Mes-6^{BBN,Et}** (MesTerAl(Et)H + H-B-9-BBN (1 equiv.) – obtained as a mixture also containing **3-Mes-5^{BBN}** (~18%), H-*B*-9-BBN (~16%) and Et-*B*-9-BBN (~13%).

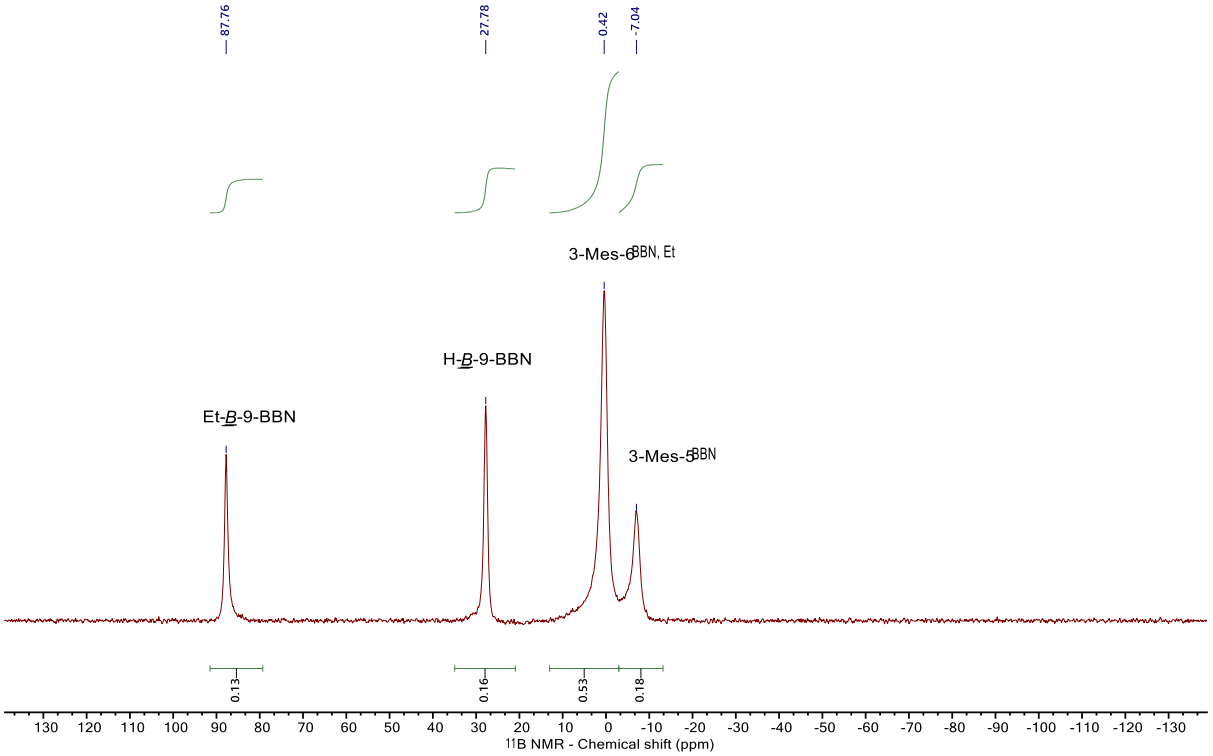

^{11}B NMR (160 MHz, CH_2Cl_2) of **3-Mes-6^{BBN,Et}** (MesTerAl(Et)H + H-B-9-BBN (1 equiv.) – obtained as a mixture also containing **3-Mes-5^{BBN}** (~18%), H-*B*-9-BBN (~16%) and Et-*B*-9-BBN (~13%).

3-Mes-6^{Et}; ^{Mes}TerAl(Et)(H_2BEt_2)

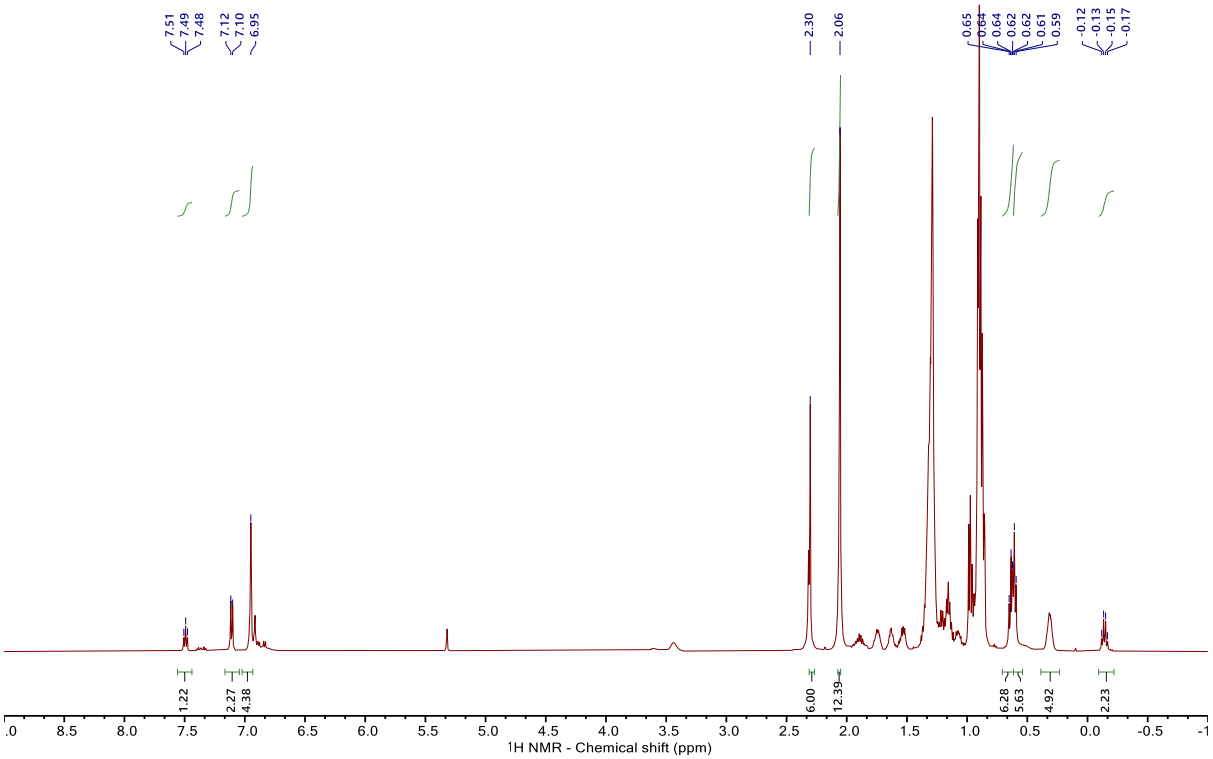

^{1}H NMR (500 MHz, CD_2Cl_2) of **3-Mes-6^{Et}** (^{Mes}TerAlH_2 + Et_3B (1 equiv.)) – contains hexanes.

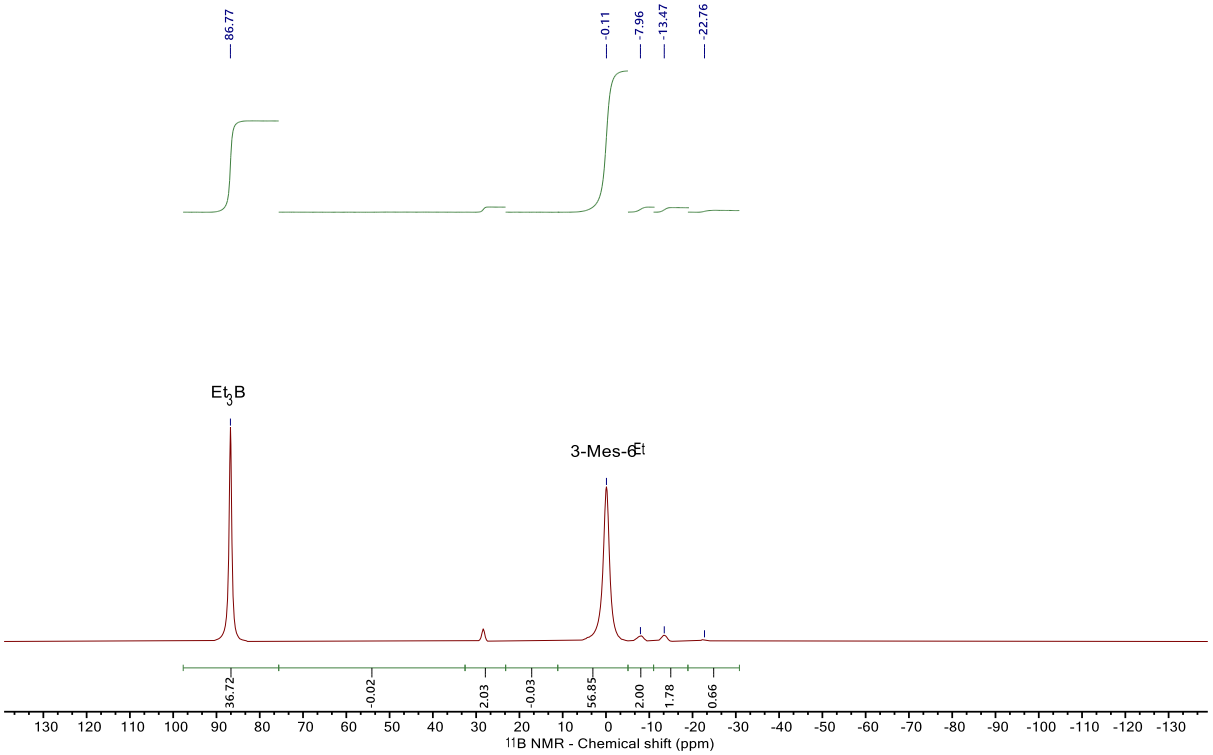

^{11}B NMR (160 MHz, CD_2Cl_2) of **3-Mes-6^{Et}**

3-Mes-7; ^{Mes}TerAl(H)(BH$_4$)

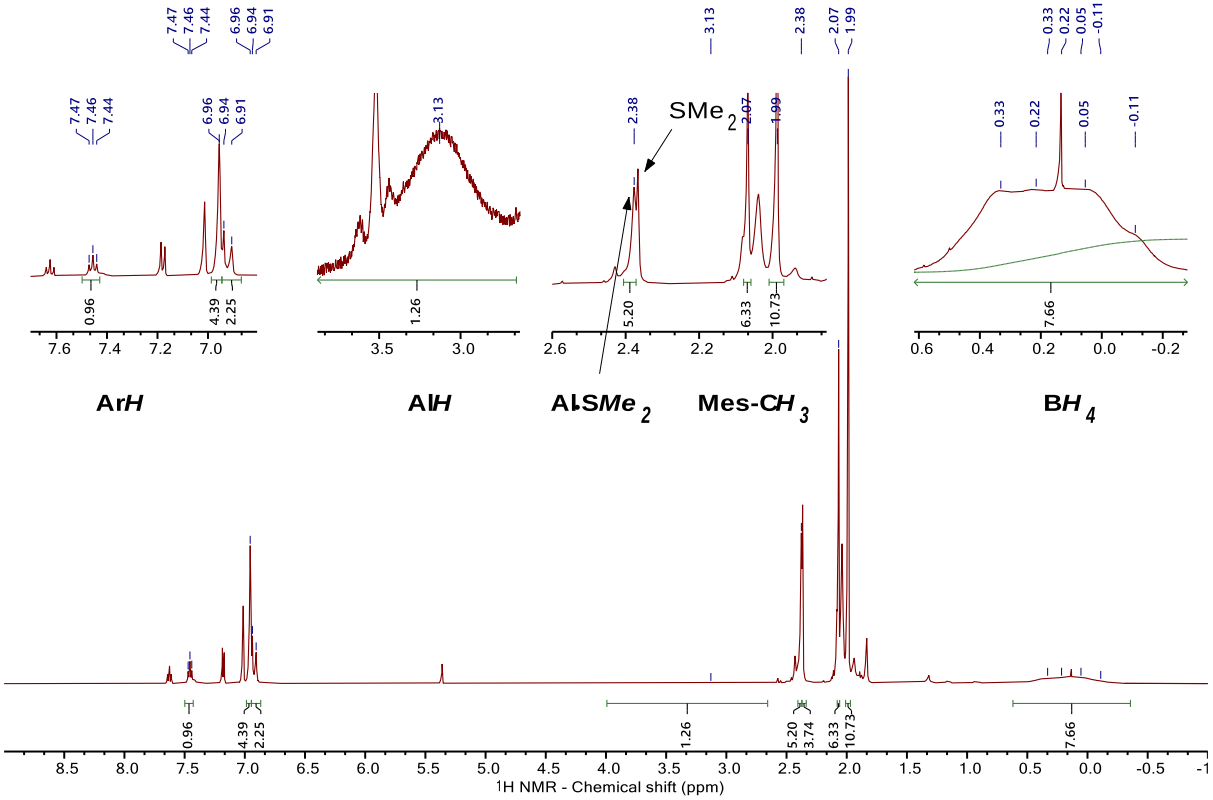

^{1}H NMR spectrum (500 MHz, CD_2Cl_2) of the reaction between ^{Mes}TerAlH$_2$ and $Me_2S{\bullet}BH_3$ (1 equiv.). The peaks picked relate to **3-Mes-7**. Present in a mixture containing also **3-Mes-1** and SMe_2.

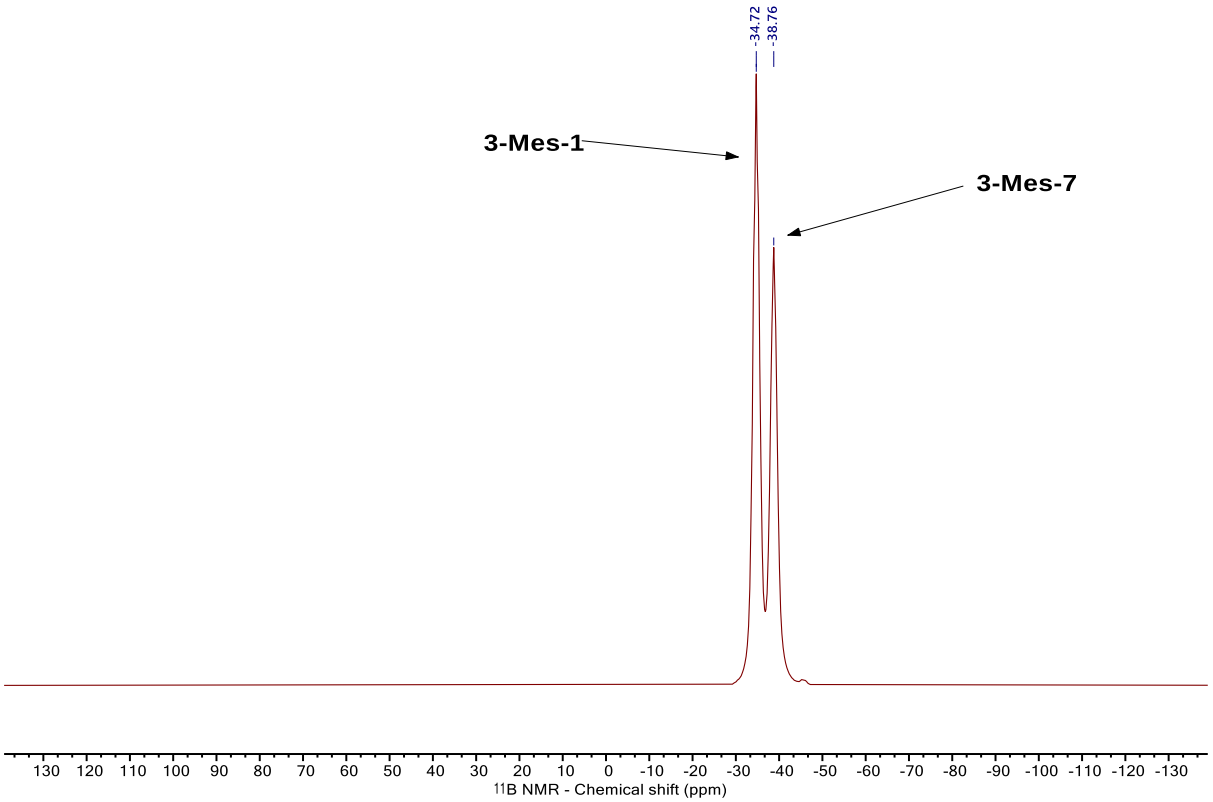

^{11}B NMR spectrum (160 MHz, CD_2Cl_2) of the reaction between ^{Mes}TerAlH$_2$ and $Me_2S{\bullet}BH_3$ (1 equiv.).

3-*p*-Tol-1; $^{p\text{-Tol}}$TerAl(BH$_4$)$_2$

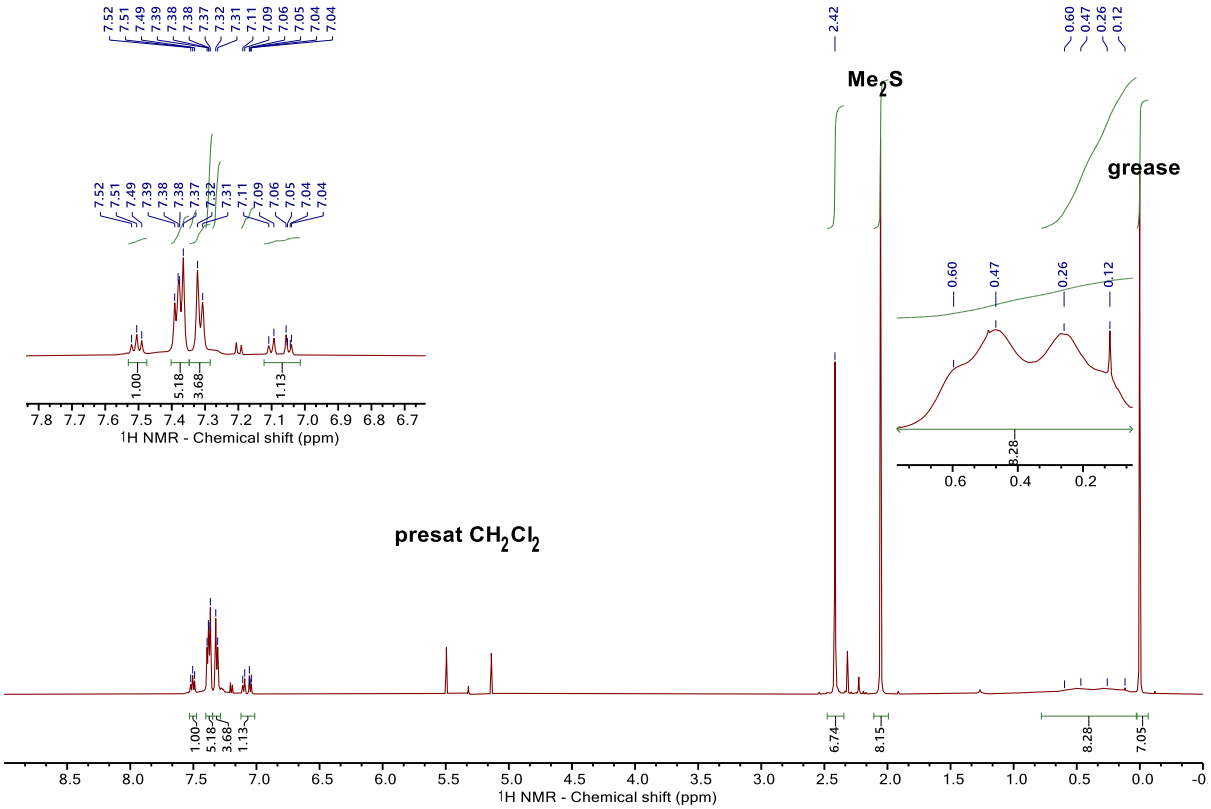

3-Tipp-1; ^{Tipp}TerAl(BH$_4$)$_2$

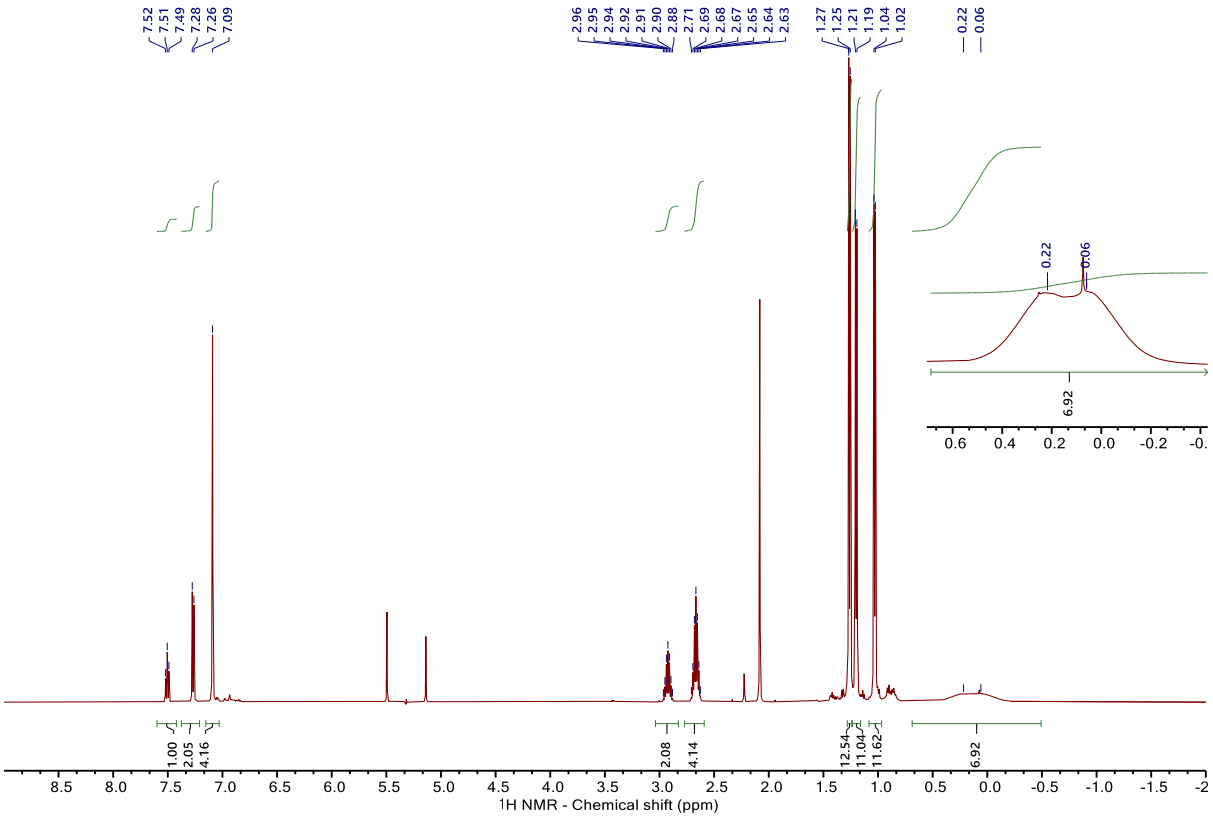

^{1}H NMR (500 MHz, CH_2Cl_2) of **3-Tipp-1** (^{Tipp}TerAlH$_2$ + Me$_2$S•BH$_3$ (2 equiv.)).

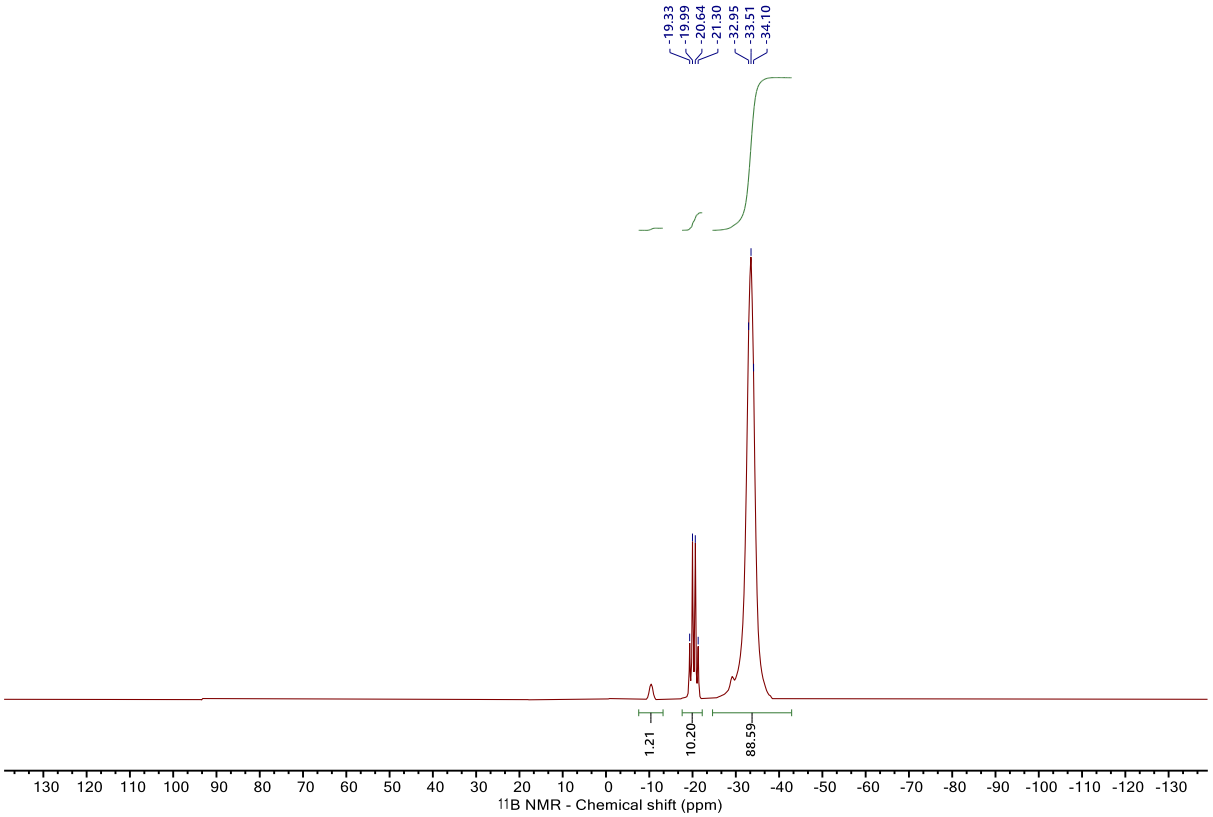

^{11}B NMR (160 MHz, CH_2Cl_2) of **3-Tipp-1** (^{Tipp}TerAlH$_2$ + Me$_2$S•BH$_3$ (2 equiv.)).

3-Tipp-A; ^{Tipp}TerAlH$_2$•HBpin

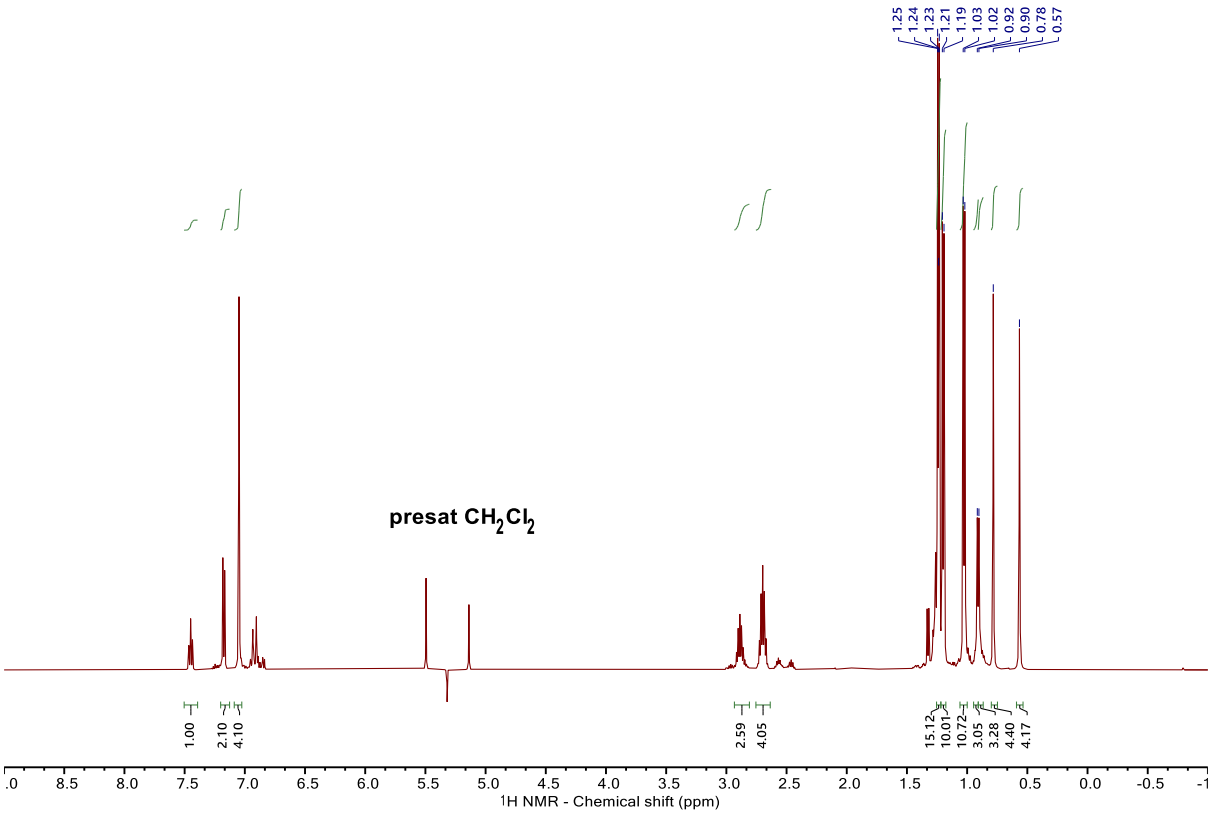

^{1}H NMR (400 MHz, CH_2Cl_2) of **3-Tipp-A** (^{Tipp}TerAlH$_2$ + HBpin (1 equiv.))

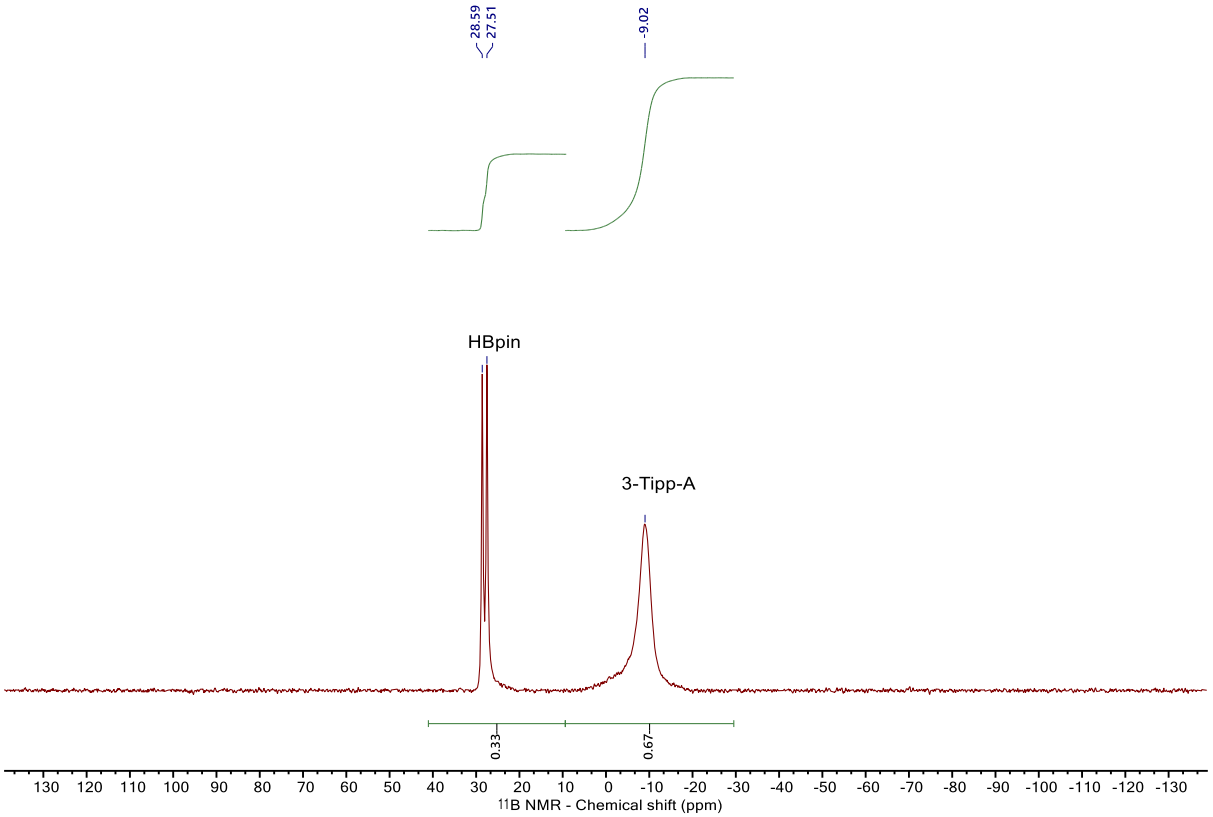

^{11}B NMR (160 MHz, CH_2Cl_2) of **3-Tipp-A** (^{Tipp}TerAlH$_2$ + HBpin (1 equiv.))

***t*BuCH$_2$CH$_2$BH$_2$**

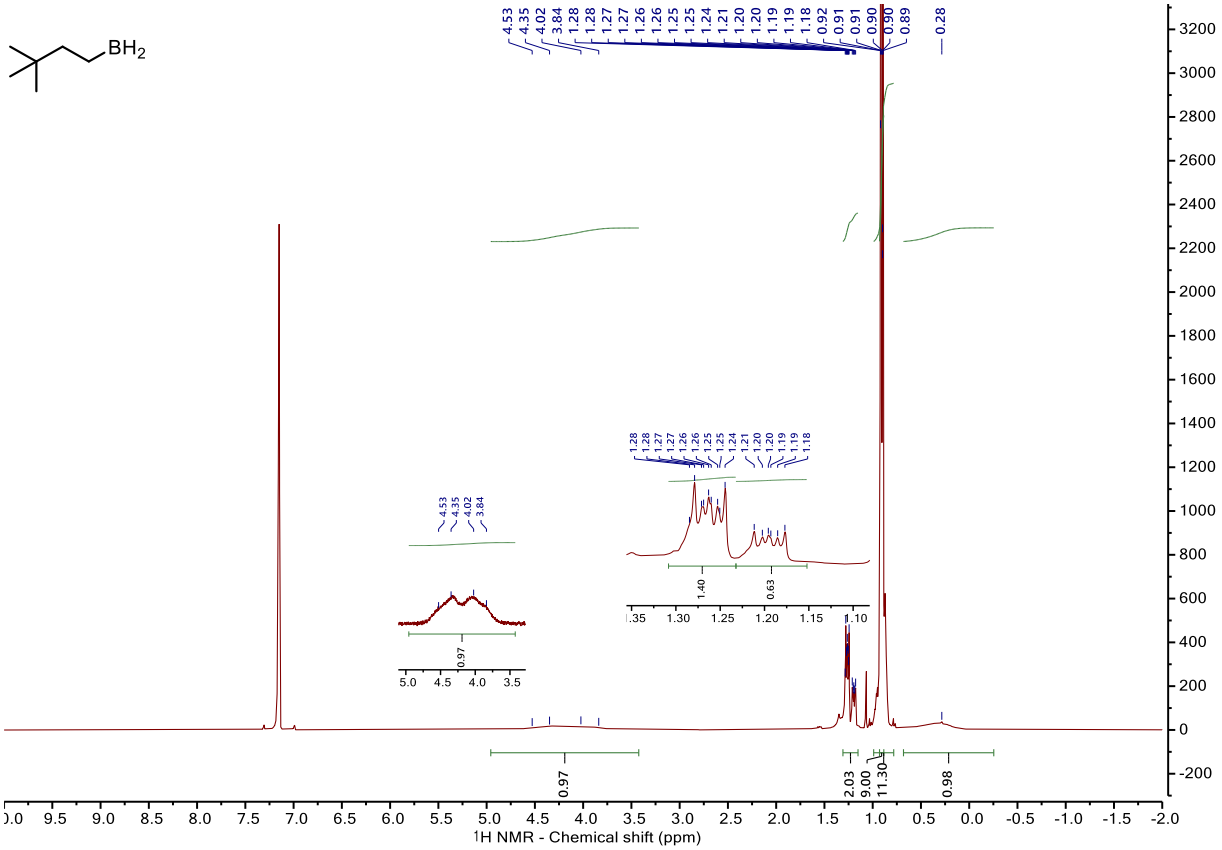

^{1}H NMR (500 MHz, Benzene-d_6) of ABG-0479

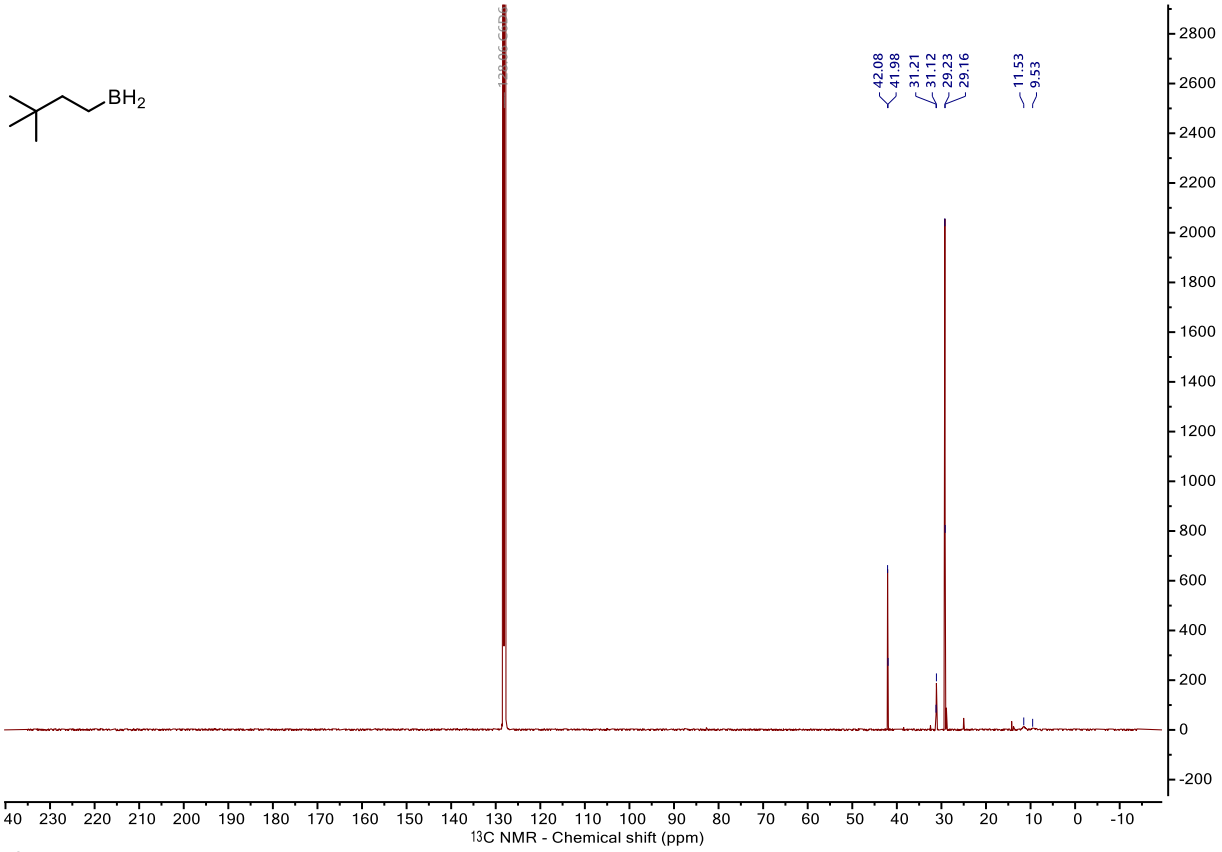

^{13}C {^{1}H} NMR (126 MHz, Benzene-d_6) of ABG-0479

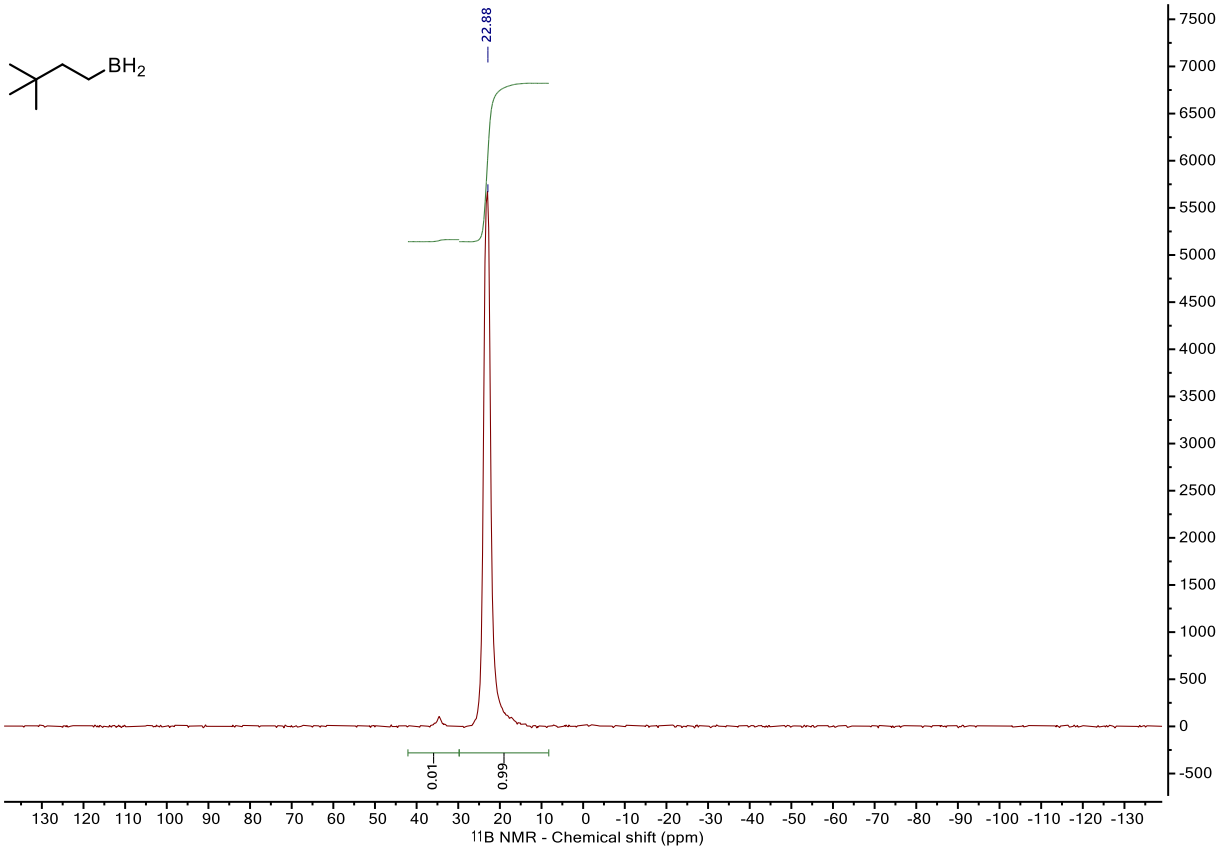

^{11}B NMR (160 MHz, Benzene-d_6) of ABG-0479

3. Boronic esters

2-1a; 4,4,5,5-tetramethyl-2-octyl-1,3,2-dioxaborolane (ABG-0195)

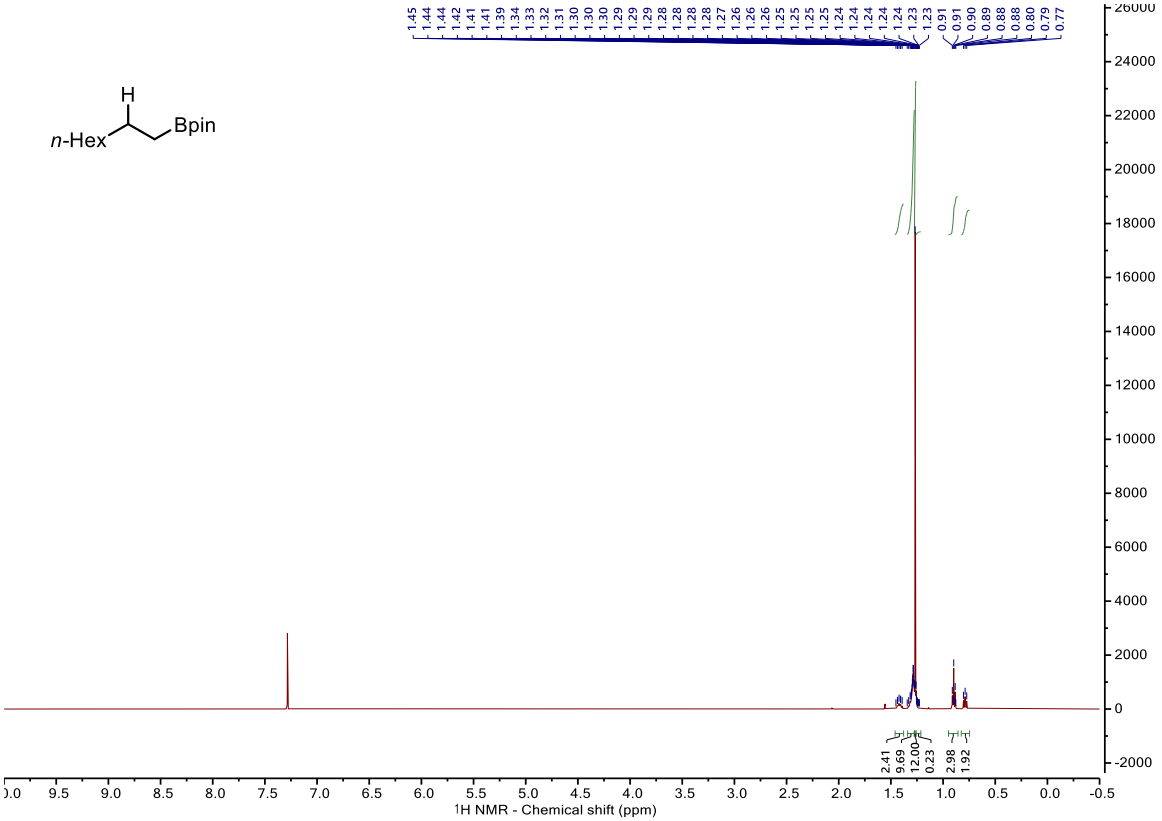

^{1}H NMR (500 MHz, Chloroform-*d*) of **2-1a**

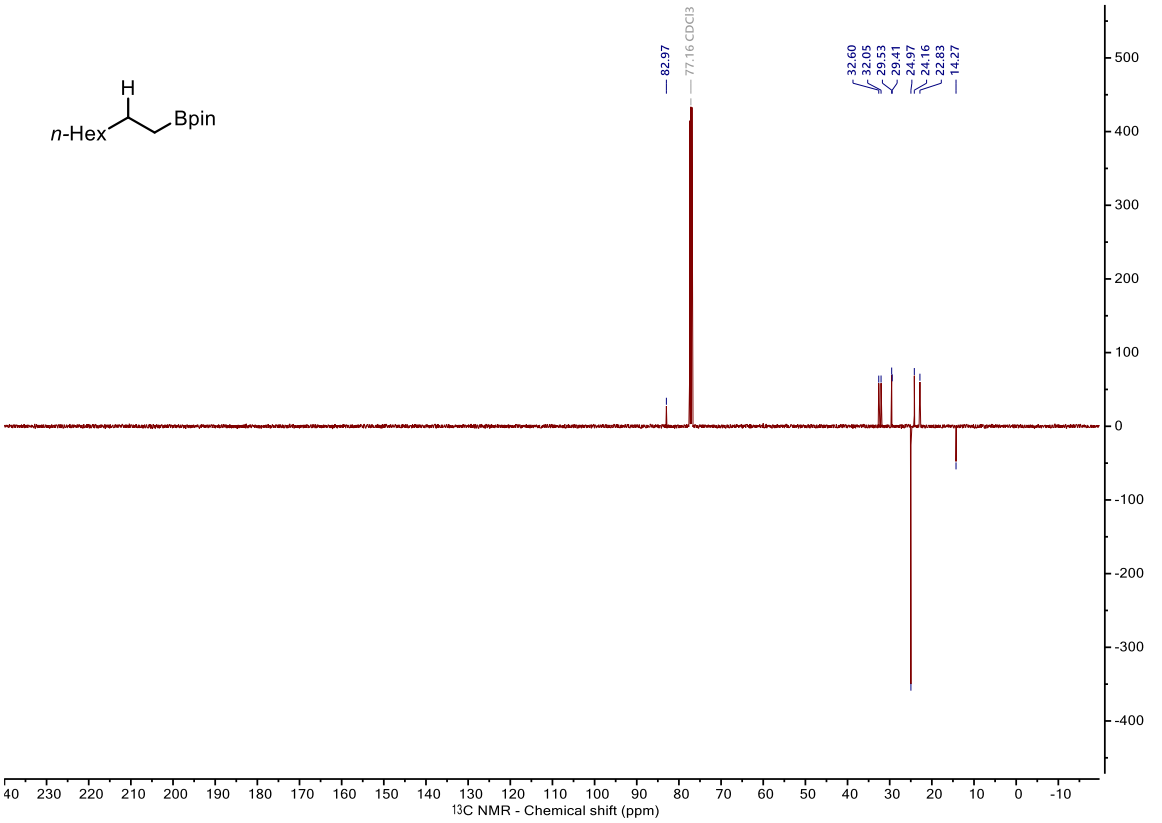

^{13}C {^{1}H} NMR (126 MHz, Chloroform-*d*) of **2-1a**

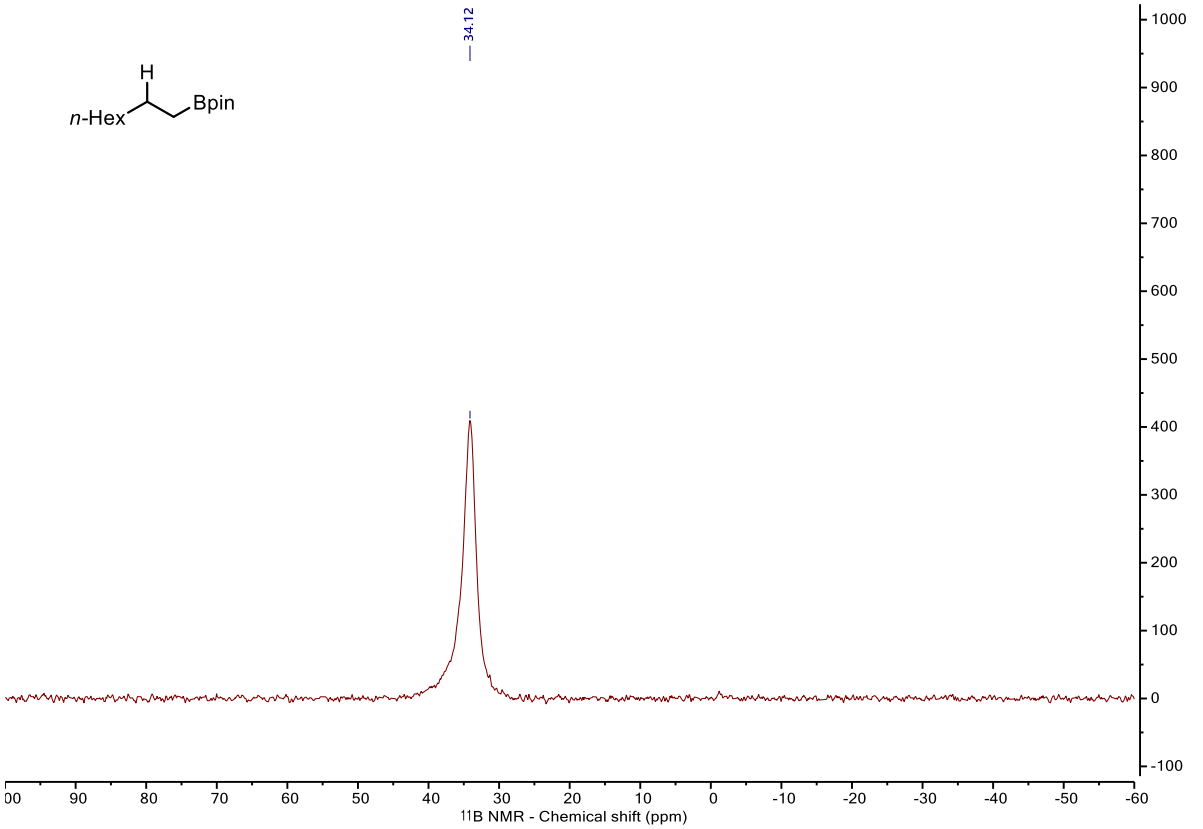

^{11}B NMR (160 MHz, Chloroform-*d*) of **2-1a**

2-1b; 2-cyclohexyl-1-(4,4,5,5-tetramethyl-1,3,2-dioxaborolan-2-yl)ethane (ABG-0334)

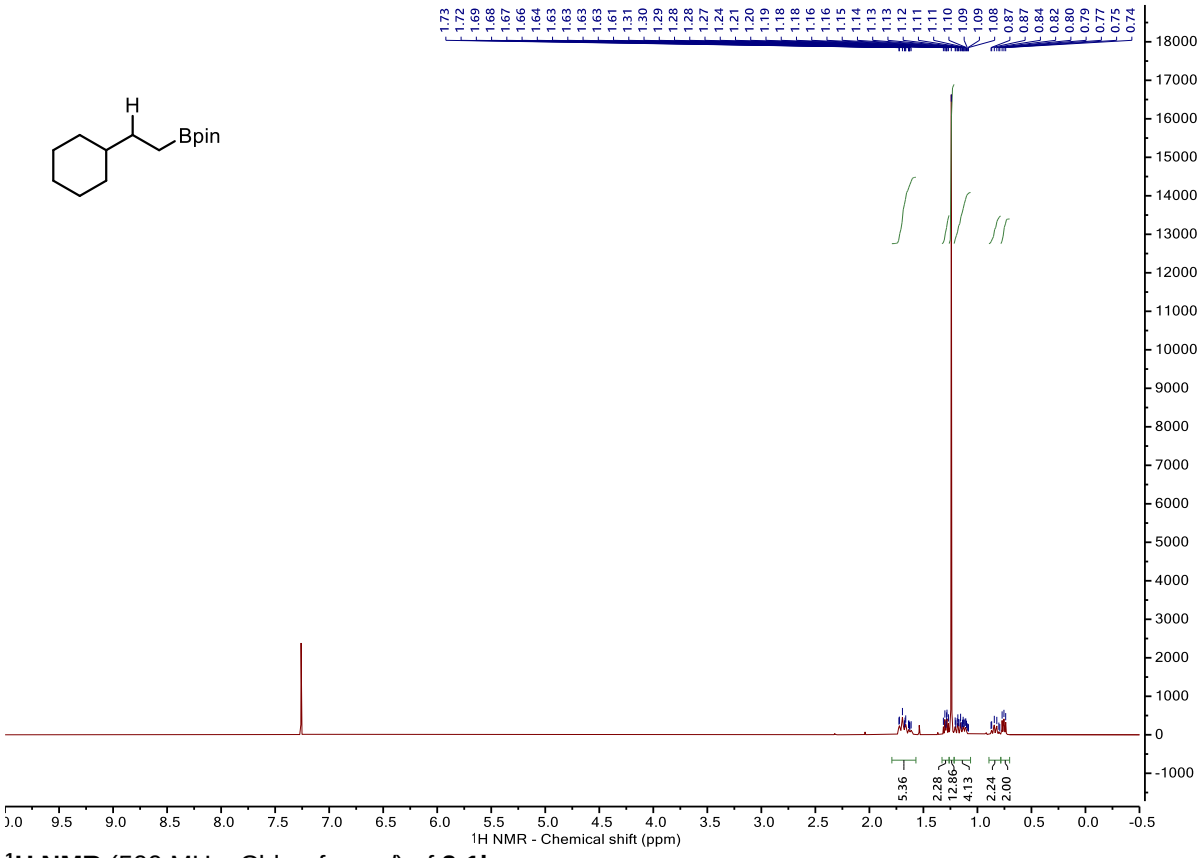

^{1}H NMR (500 MHz, Chloroform-*d*) of **2-1b**

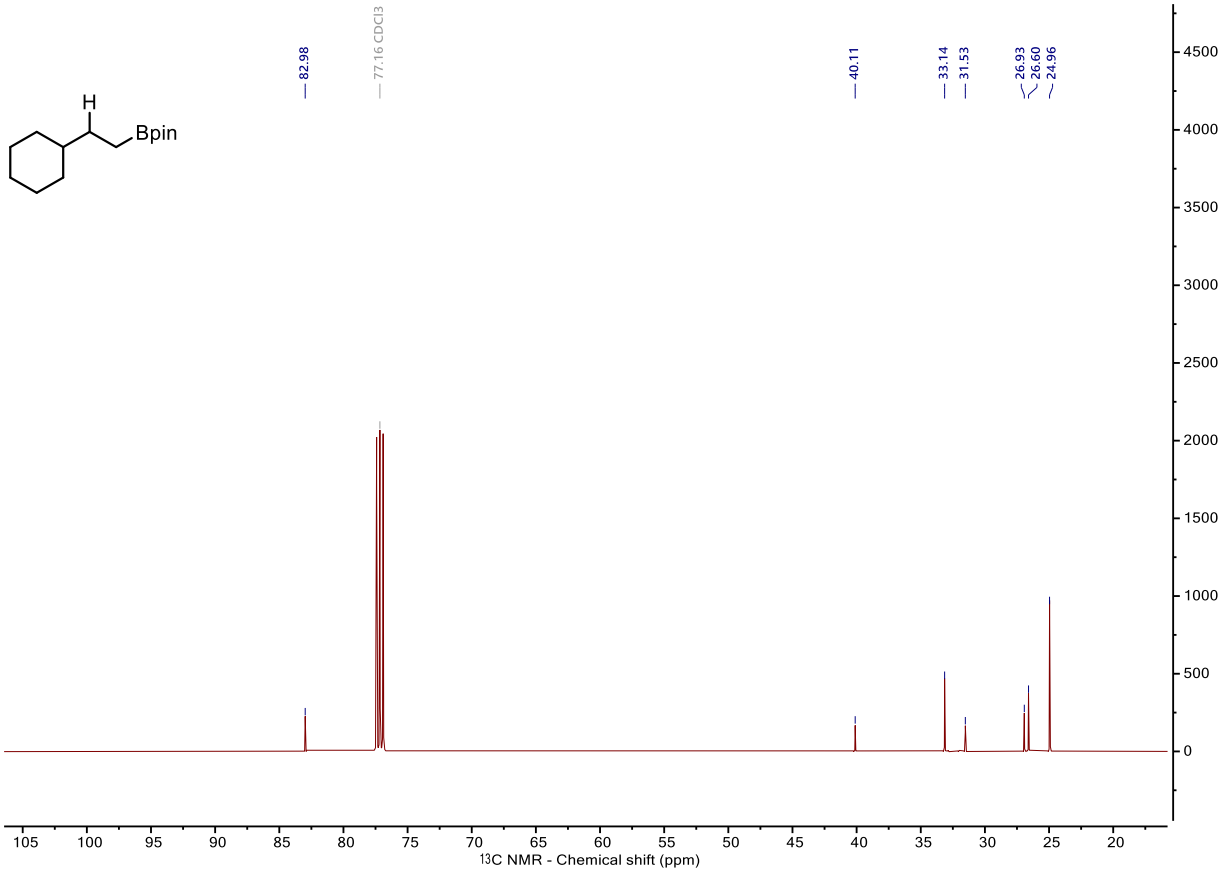

^{13}C {^{1}H} NMR (126 MHz, Chloroform-*d*) of **2-1b**

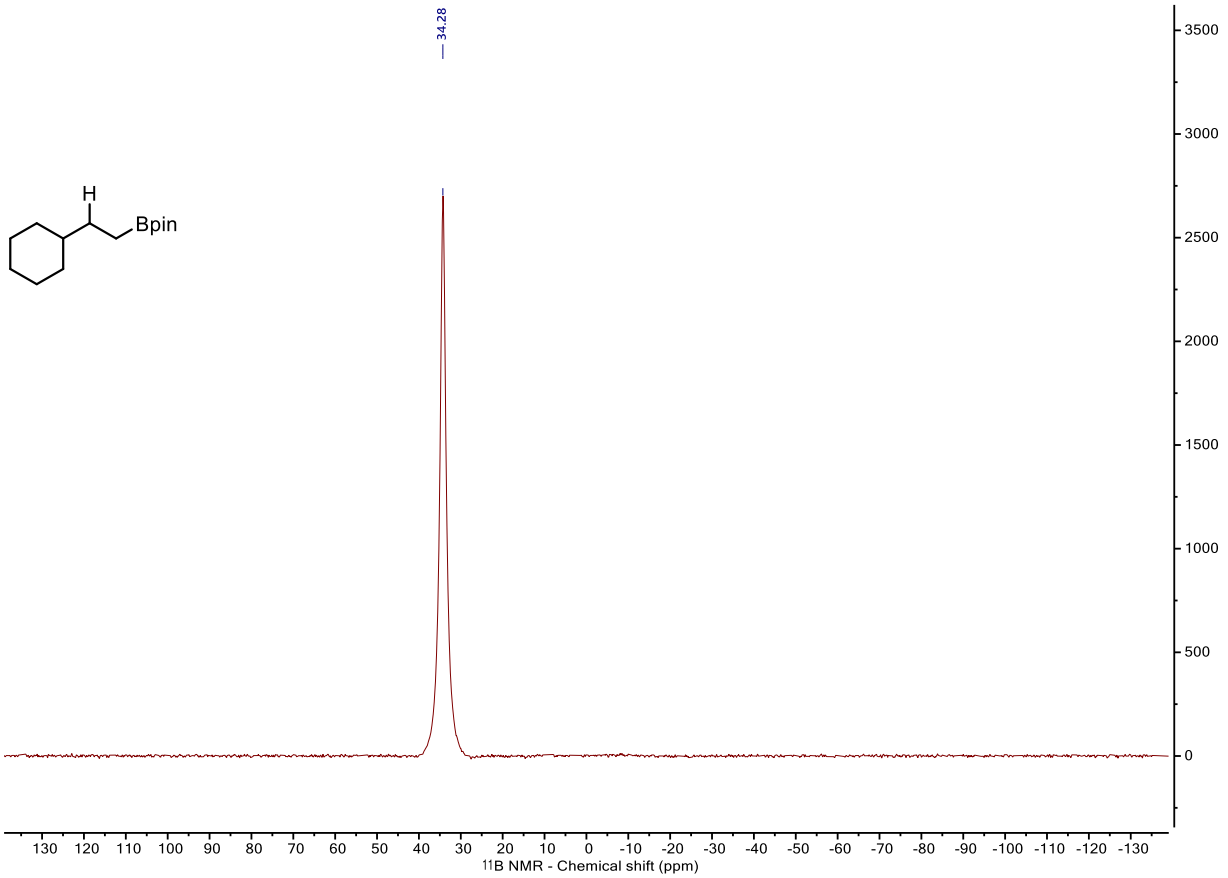

^{11}B NMR (160 MHz, Chloroform-*d*) of **2-1b**

2-1c; 2-(3,3-dimethylbutyl)-4,4,5,5-tetramethyl-1,3,2-dioxaborolane (ABG-0301-A)

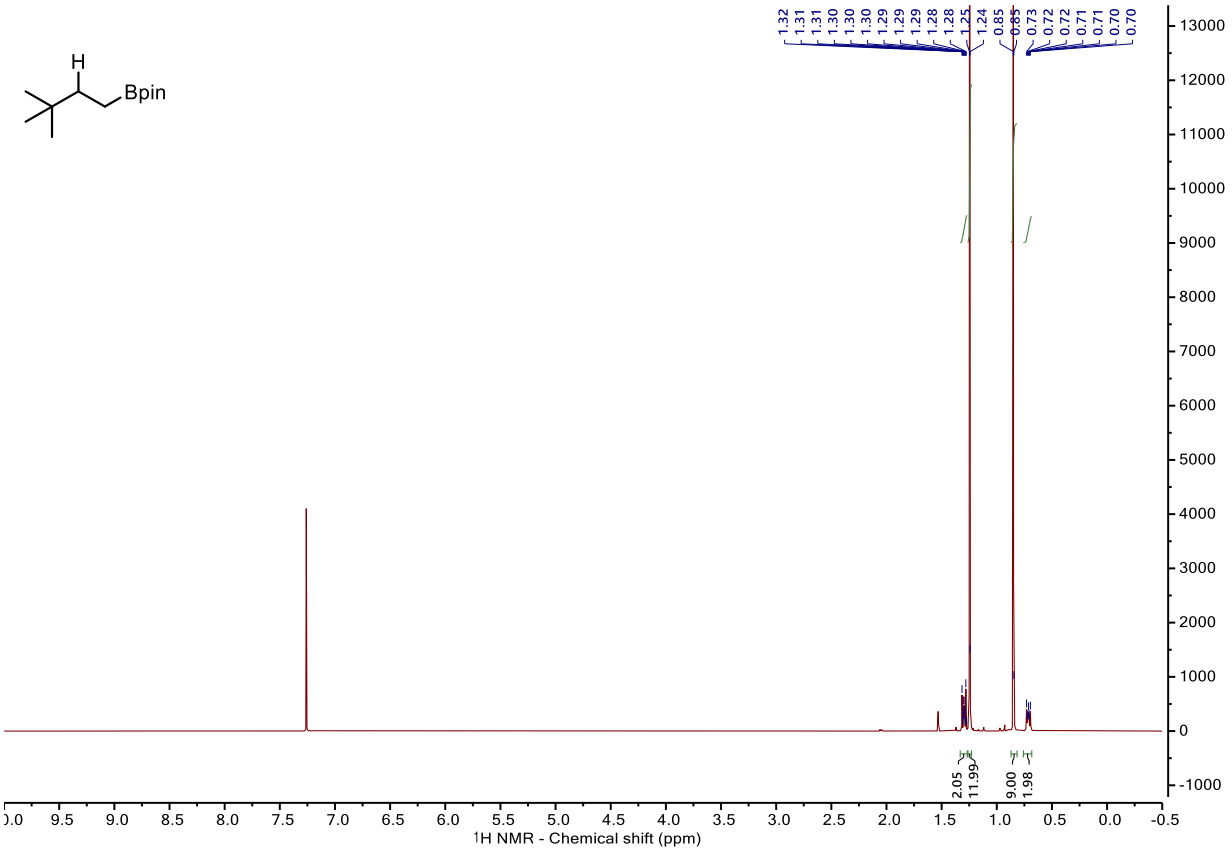

^{1}H NMR (500 MHz, Chloroform-*d*) of **2-1c**

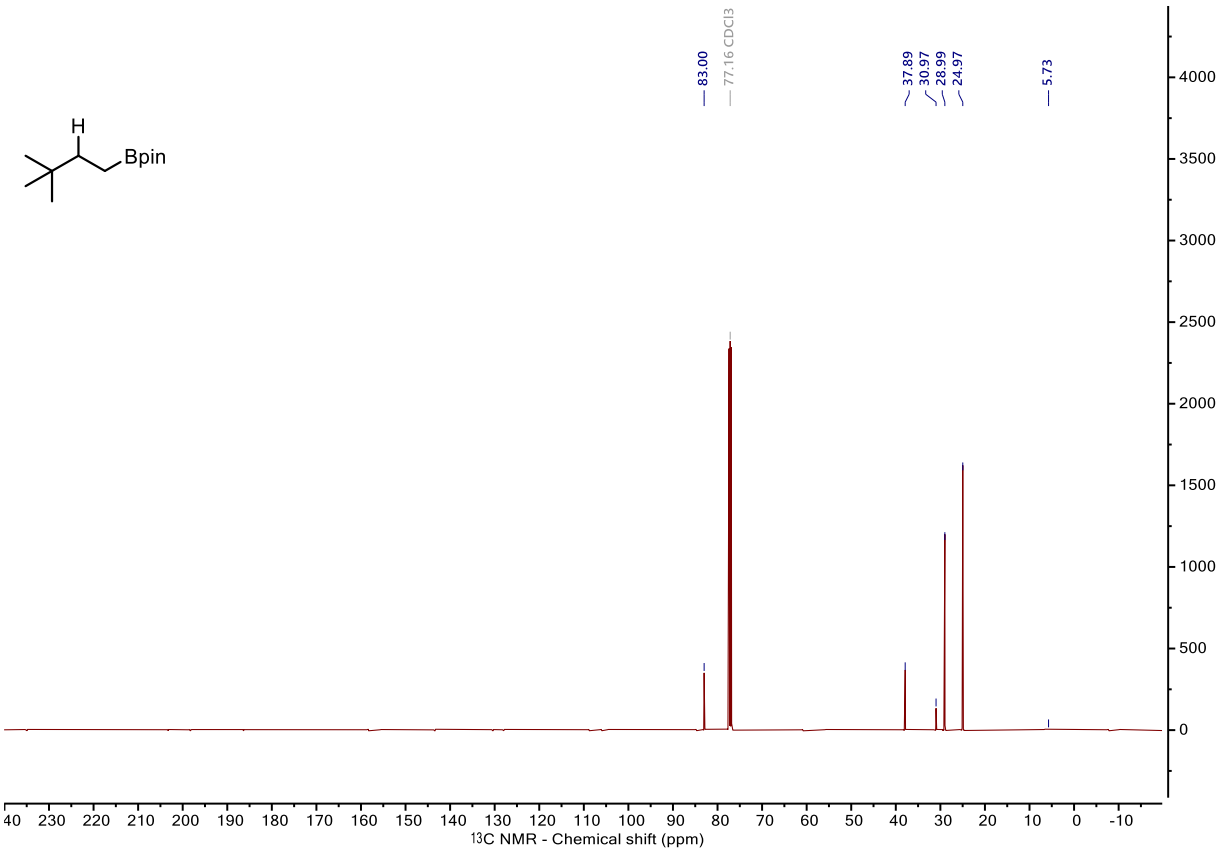

^{13}C {^{1}H} NMR (126 MHz, $CDCl_3$) of **2-1c**

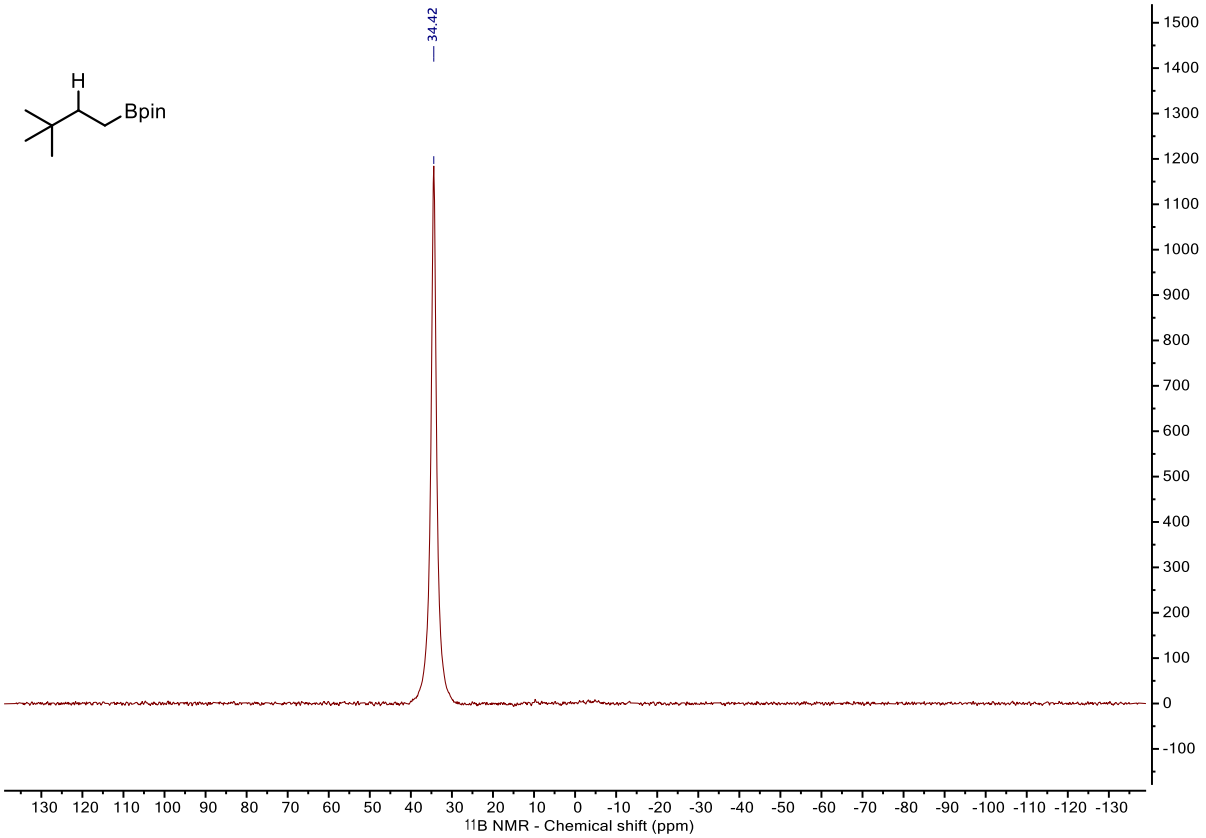

^{11}B NMR (160 MHz, Chloroform-*d*) of **2-1c**

2-1d; 2-(5-bromopentyl)-4,4,5,5-tetramethyl-1,3,2-dioxaborolane (ABG-0324)

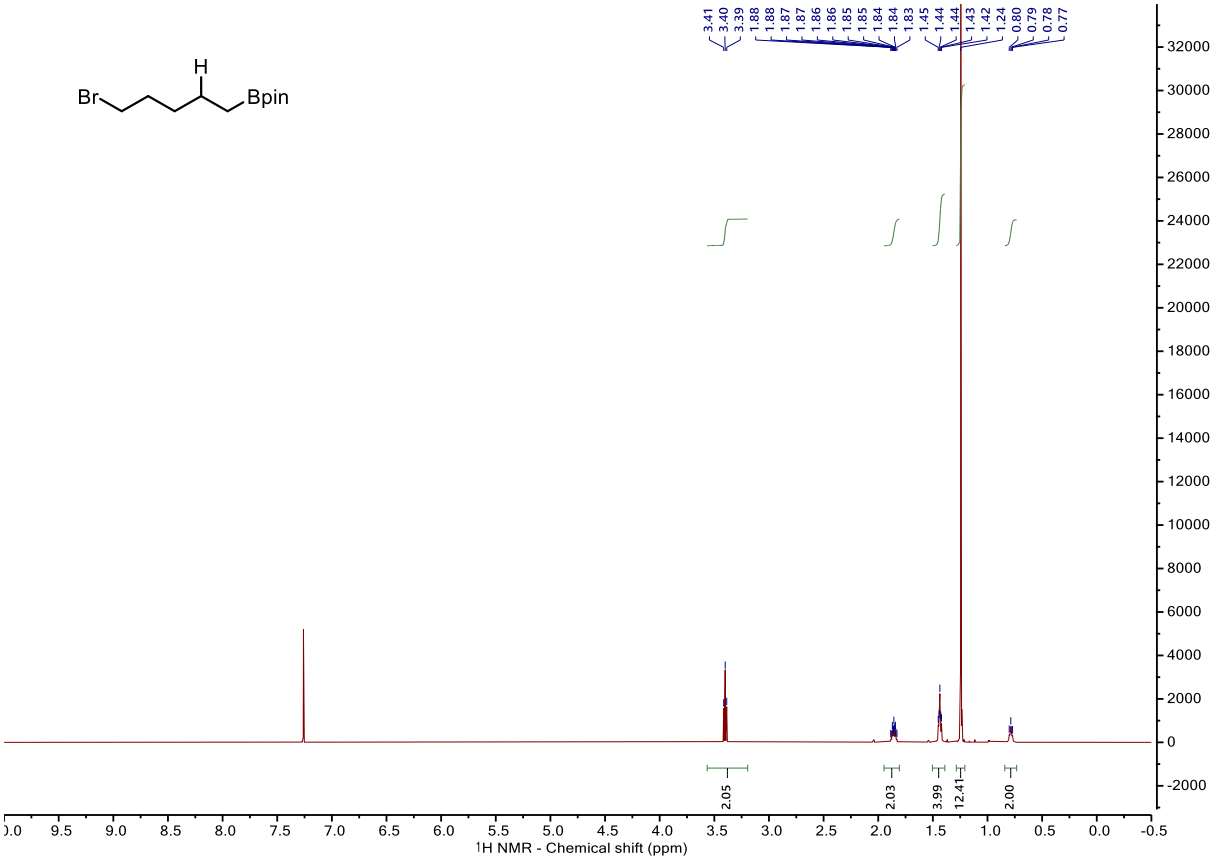

^{1}H NMR (500 MHz, Chloroform-*d*) of **2-1d**

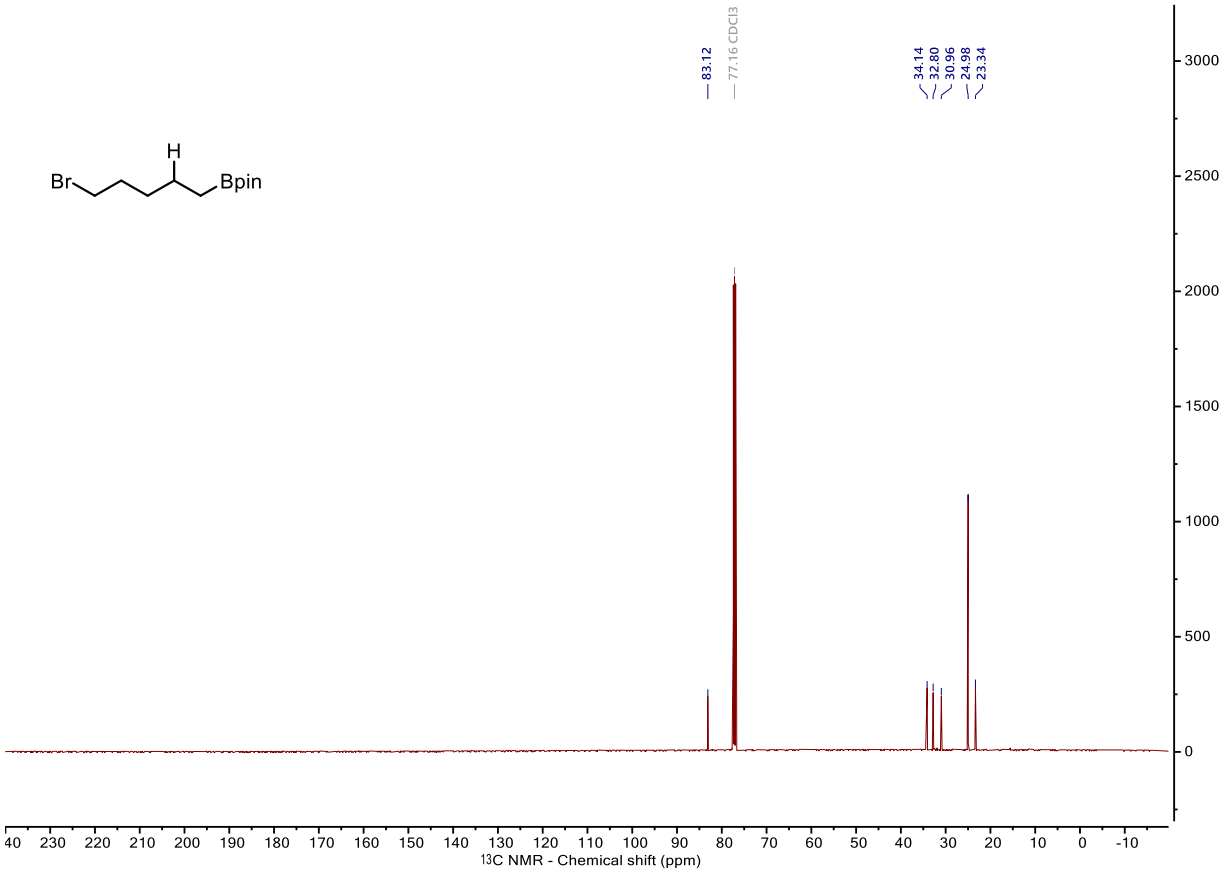

^{13}C {^{1}H} NMR (126 MHz, Chloroform-*d*) of **2-1d**

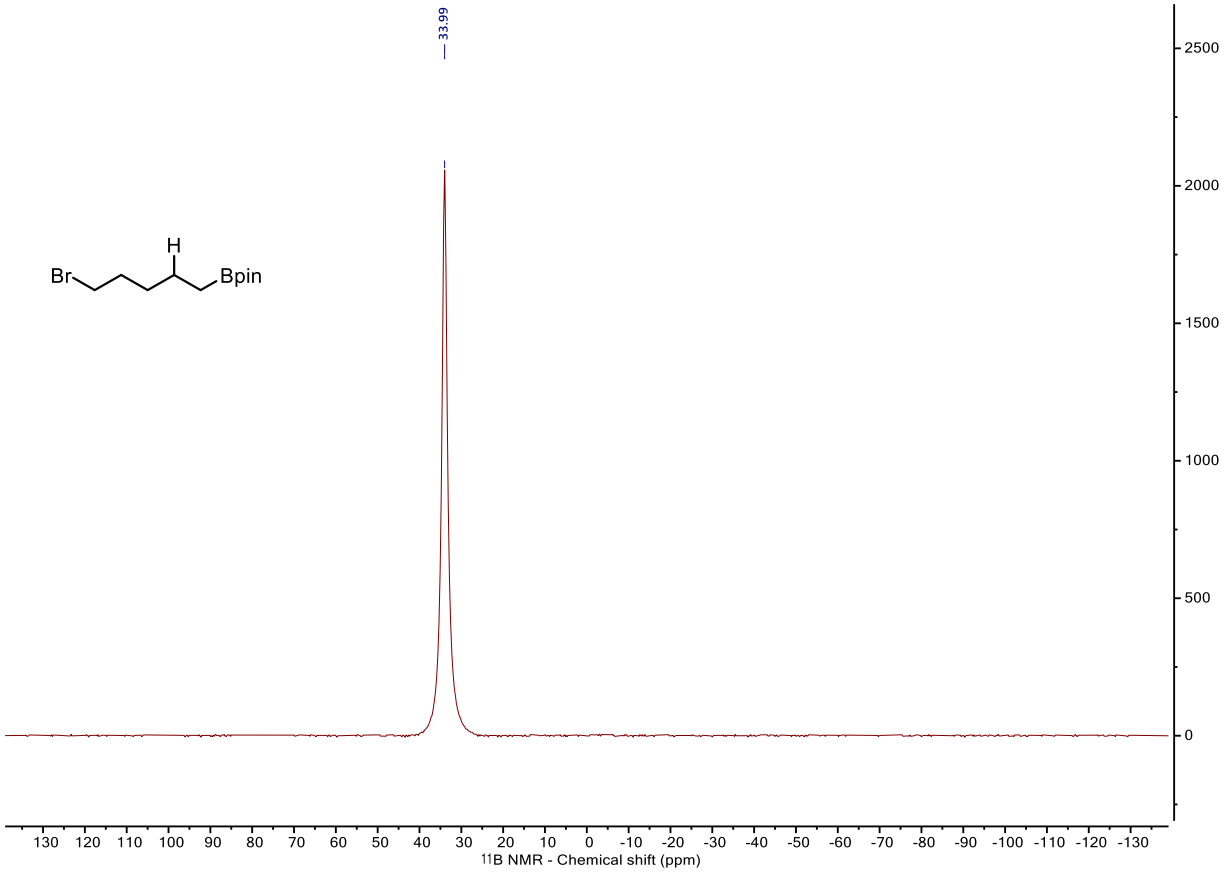

^{11}B NMR (160 MHz, Chloroform-*d*) of **2-1d**

2-1e; Trimethyl(3-(4,4,5,5-tetramethyl-1,3,2-dioxaborolan-2-yl)propyl)silane (ABG-0350/0197-B)

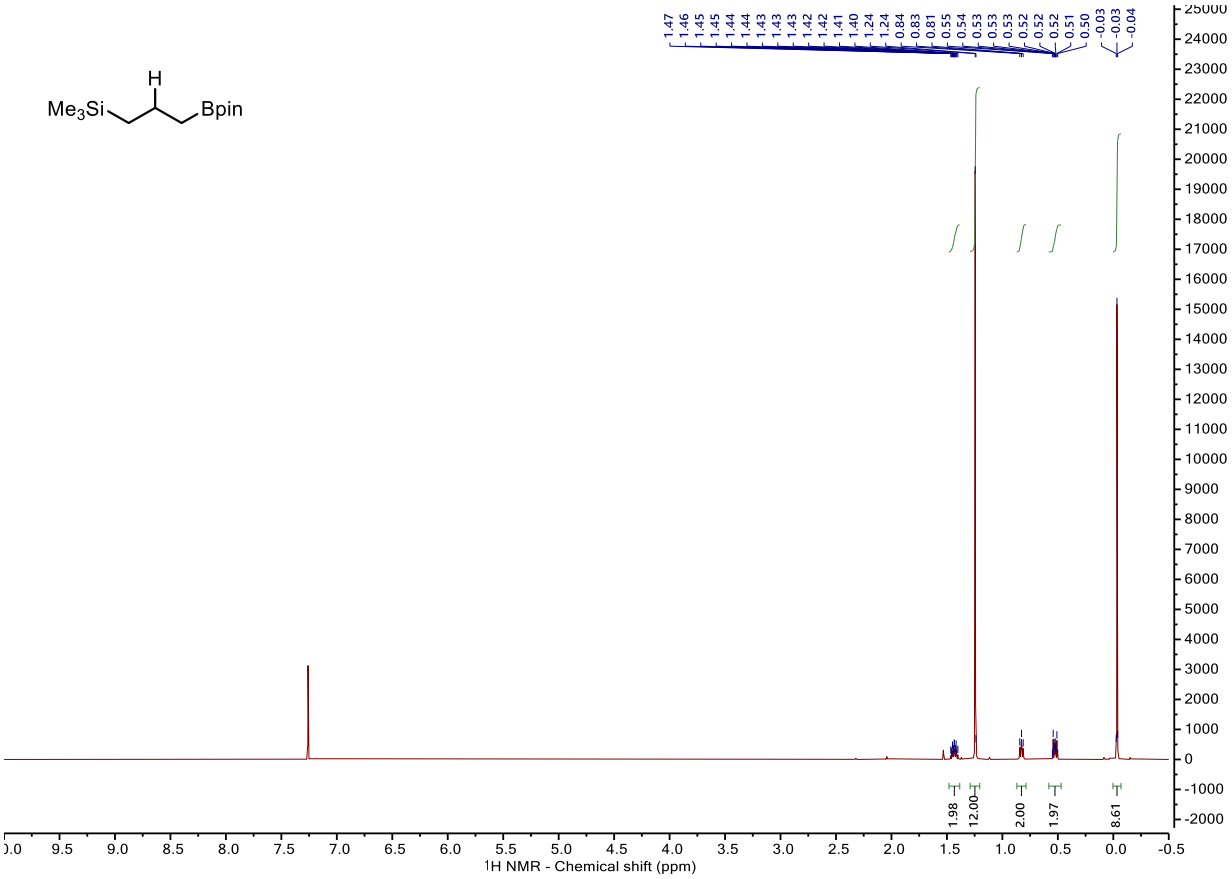

^{1}H NMR (500 MHz, Chloroform-*d*) of **2-1e**

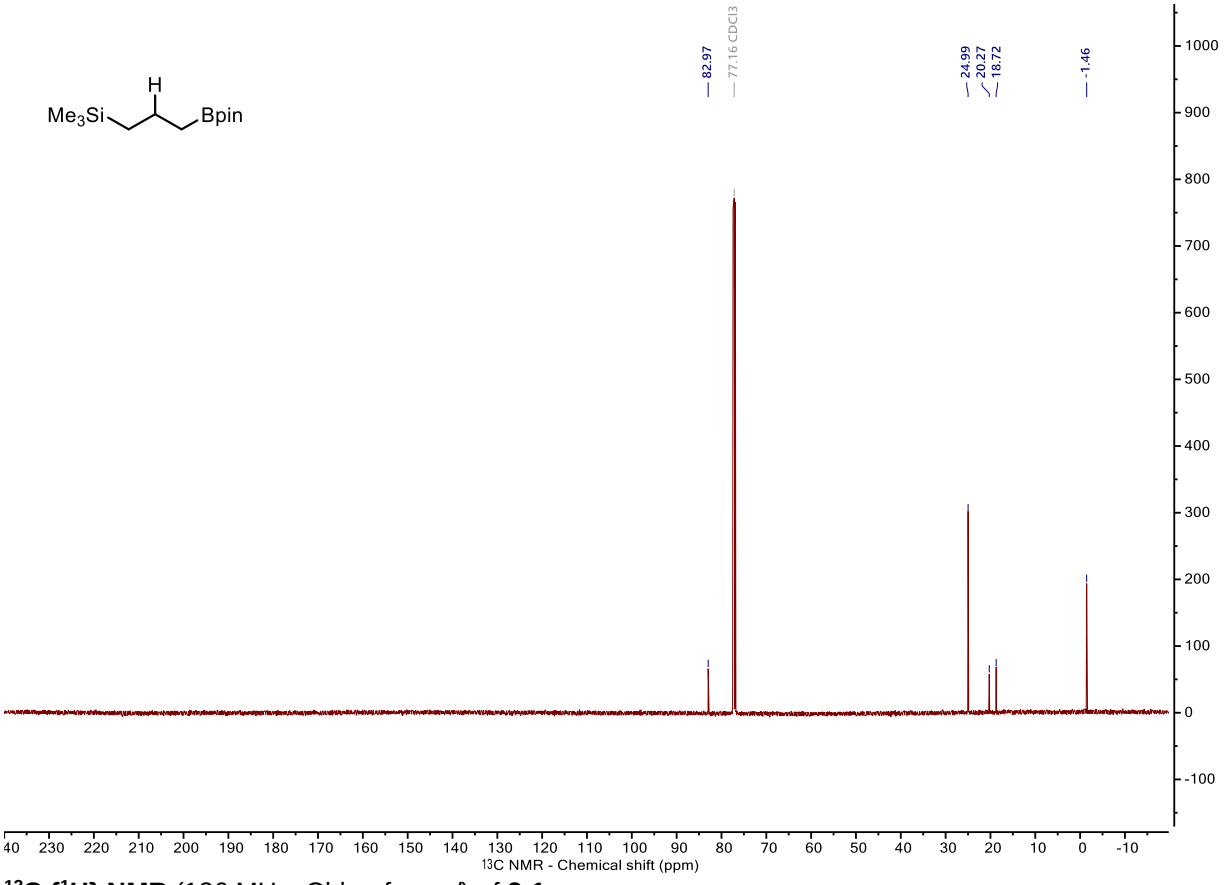

^{13}C {^{1}H} NMR (126 MHz, Chloroform-*d*) of **2-1e**

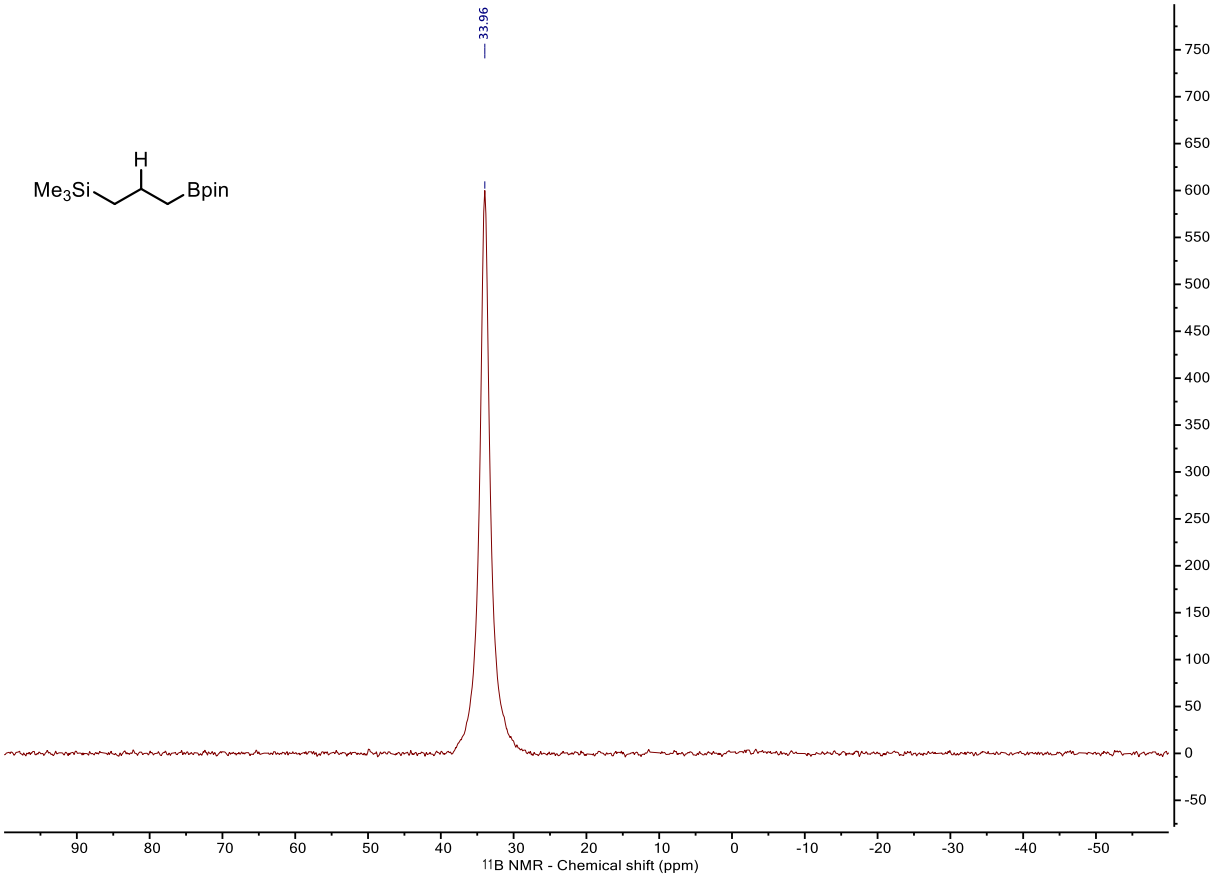

^{11}B NMR (160 MHz, Chloroform-*d*) of **2-1e**

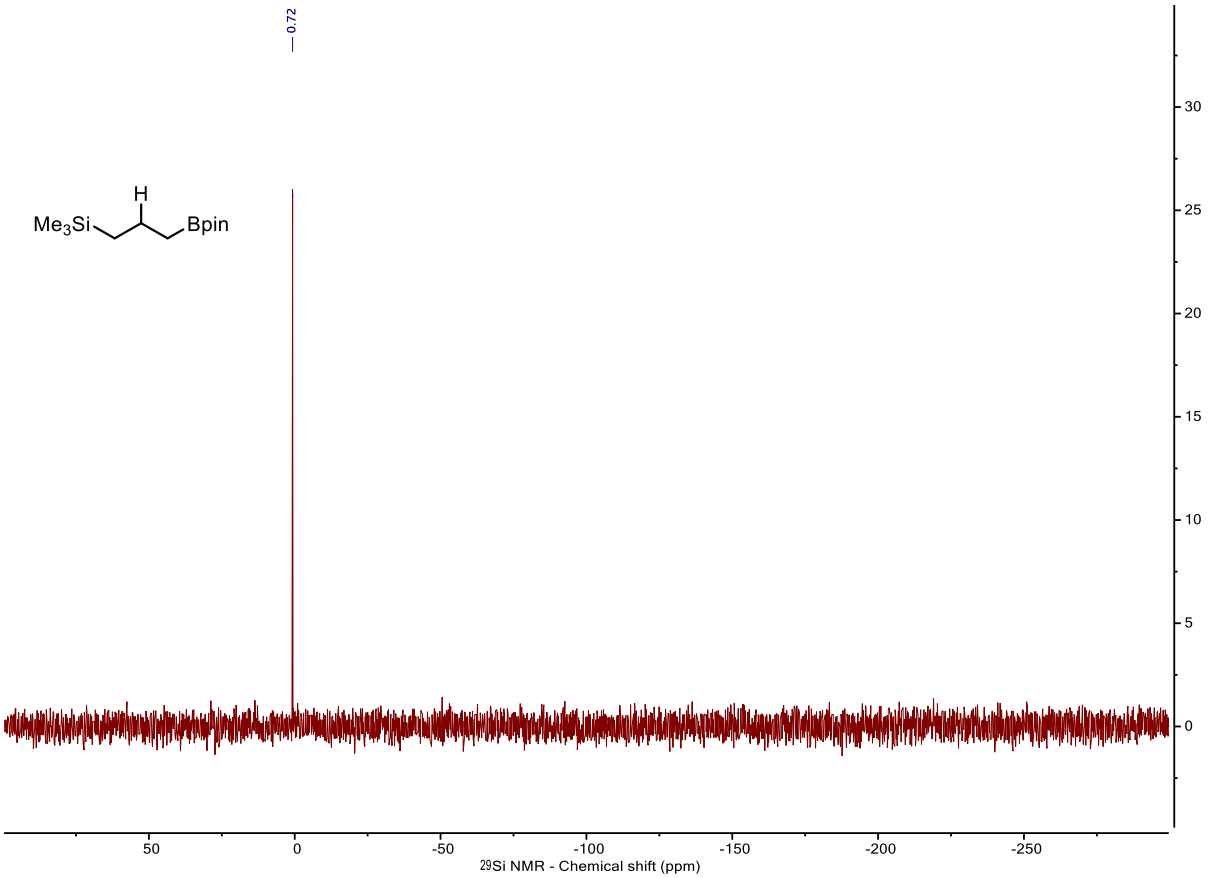

^{29}Si NMR (99 MHz, Chloroform-*d* - INEPT) of **2-1e**

2-1f; 1,3-bis(4,4,5,5-tetramethyl-1,2-oxaborolan-2-yl)propane (ABG-0197-A)

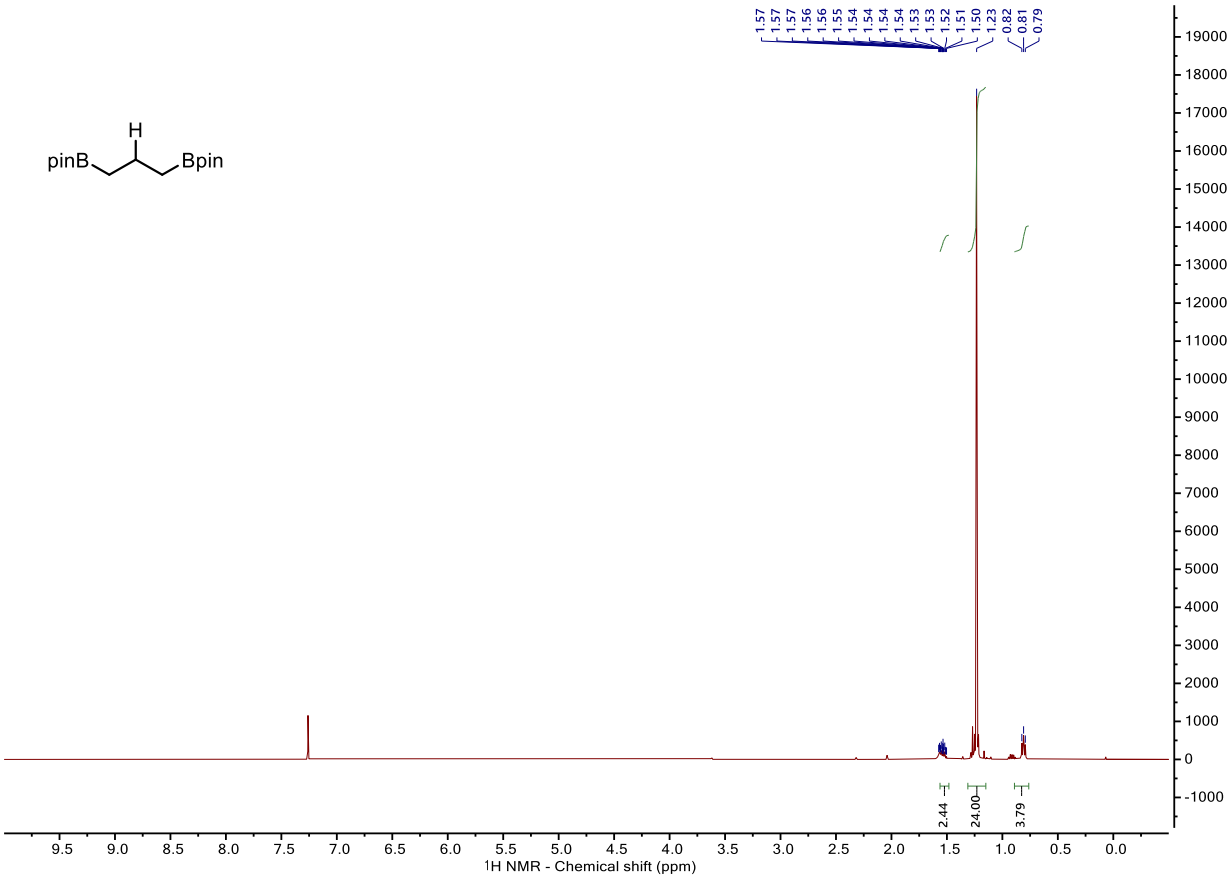

^{1}H NMR (500 MHz, Chloroform-*d*) of **2-1f**

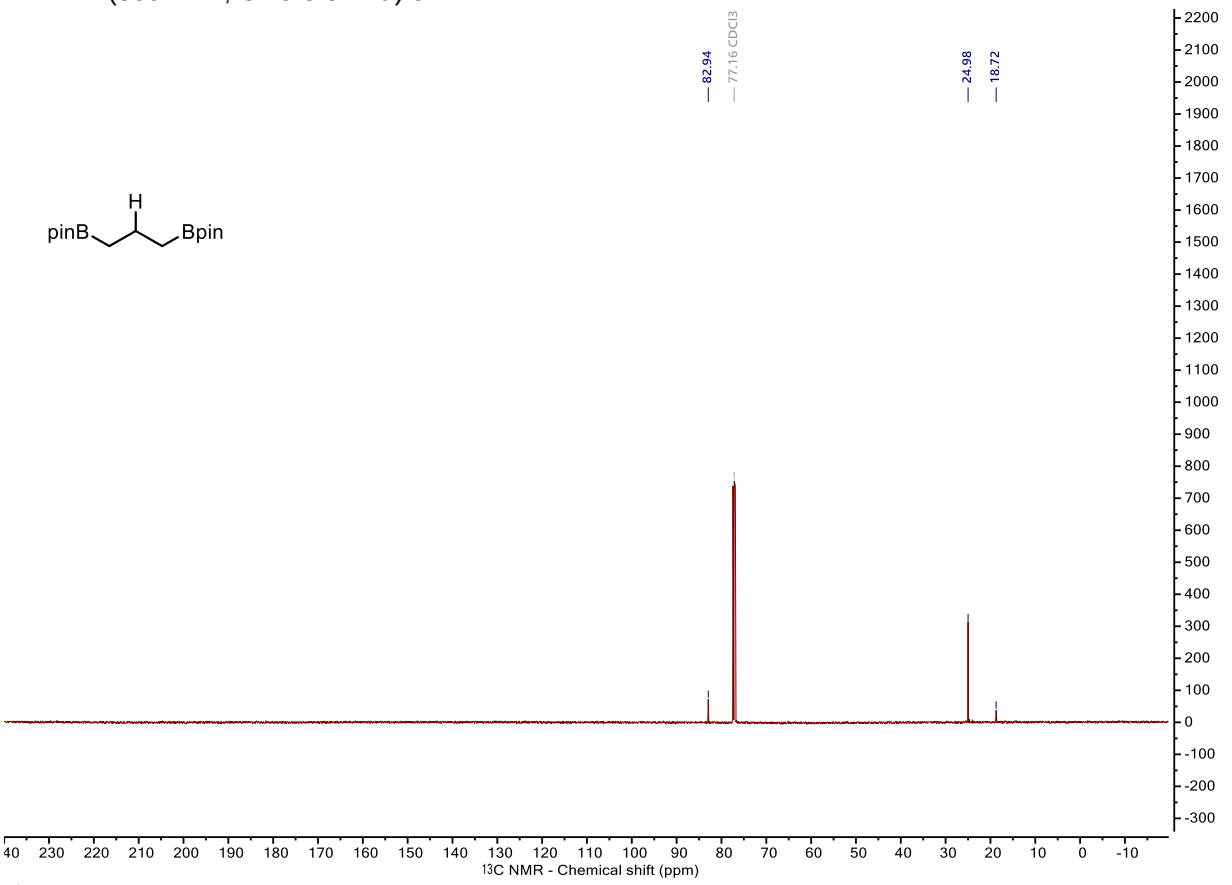

^{13}C {^{1}H} NMR (126 MHz, Chloroform-*d*) of **2-1f**

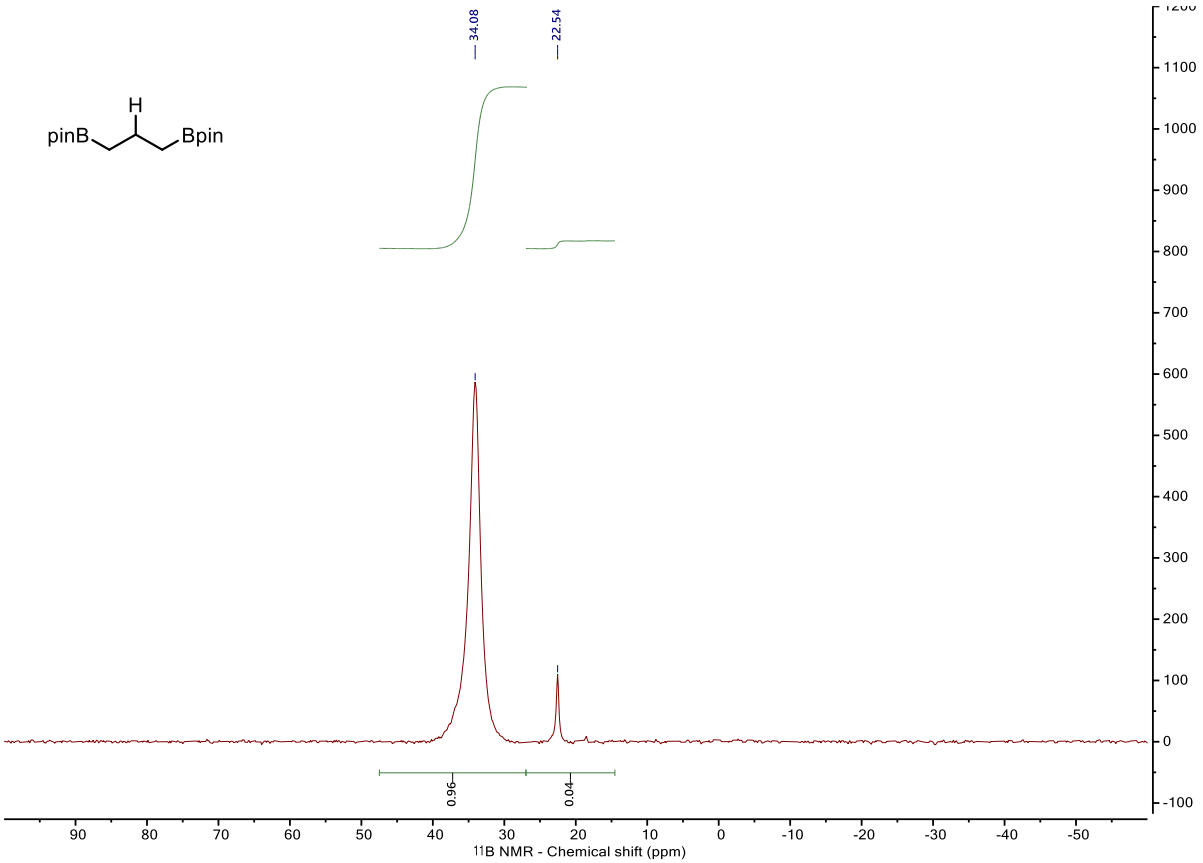

^{11}B NMR (160 MHz, Chloroform-*d*) of **2-1f**

2-1i; 4,4,5,5-tetramethyl-2-phenethyl-1,3,2-dioxaborolane (ABG-0301-B)

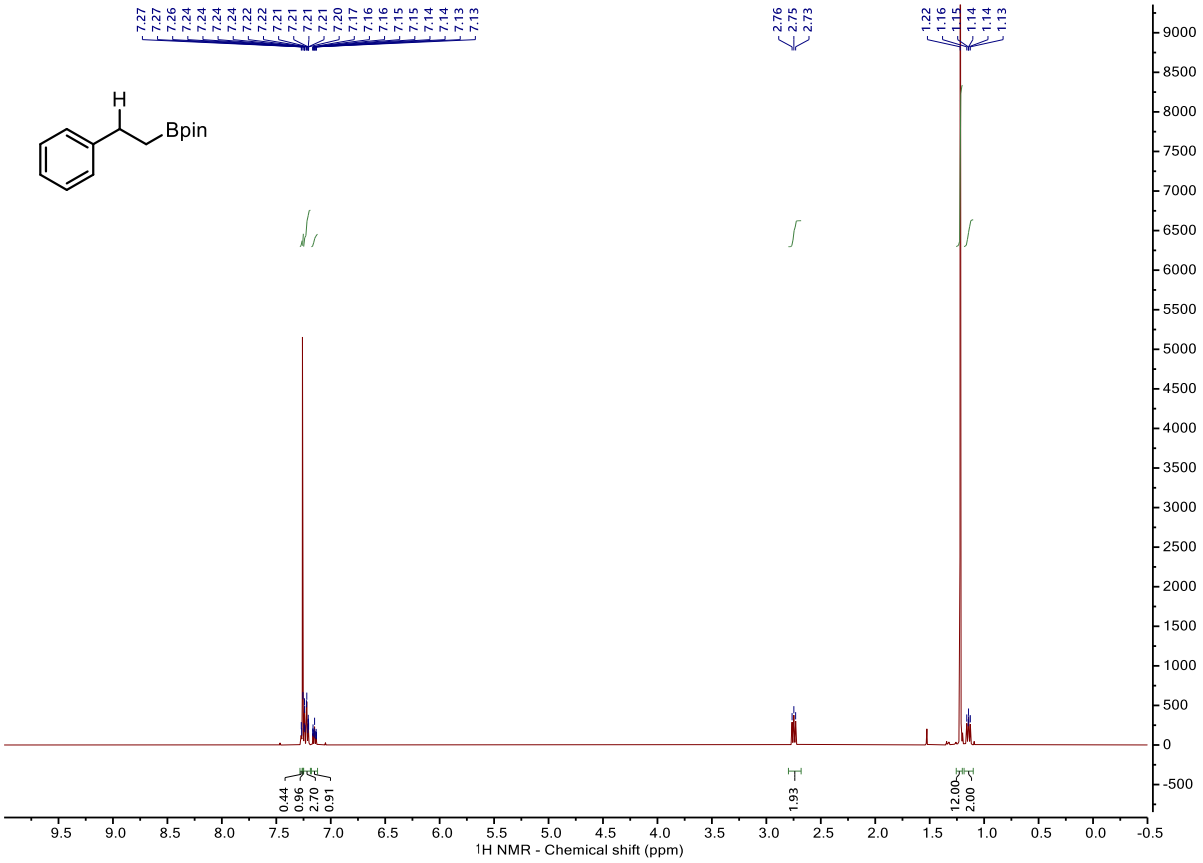

^{1}H NMR (500 MHz, Chloroform-*d*) of **2-1i**

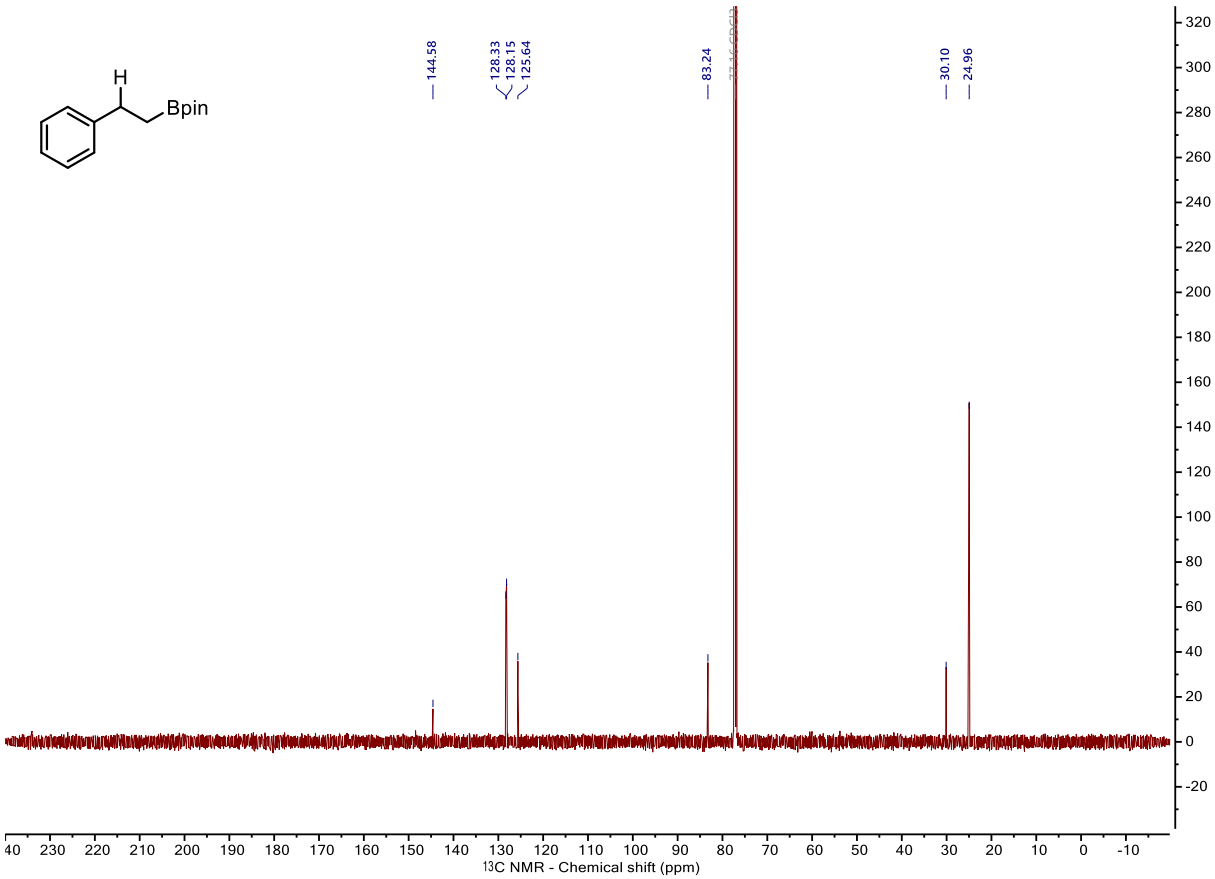

^{13}C {^{1}H} NMR (126 MHz, Chloroform-*d*) of **2-1i**

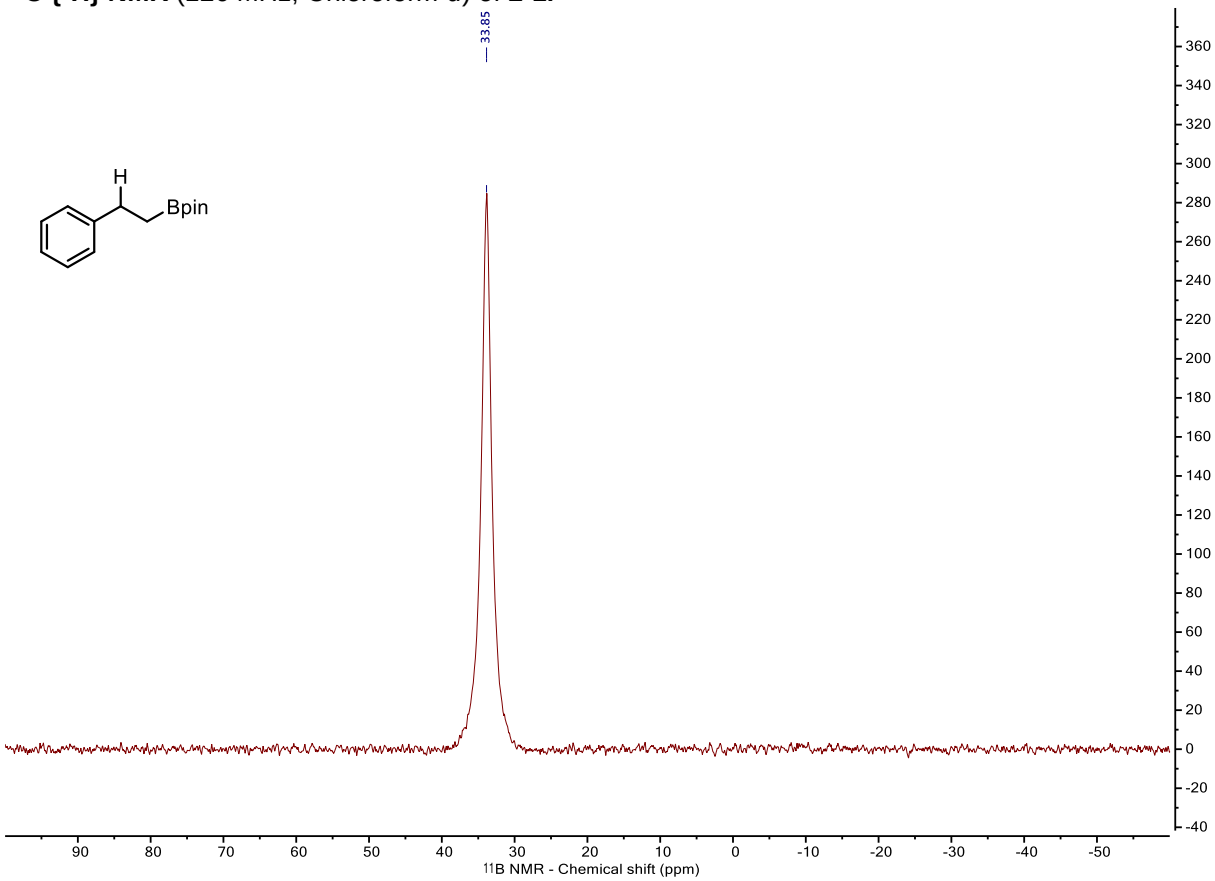

^{11}B NMR (160 MHz, Chloroform-*d*) of **2-1i**

2-1q; 2-(4-fluorophenethyl)-4,4,5,5-tetramethyl-1,3,2-dioxaborolane (ABG-0209-A)

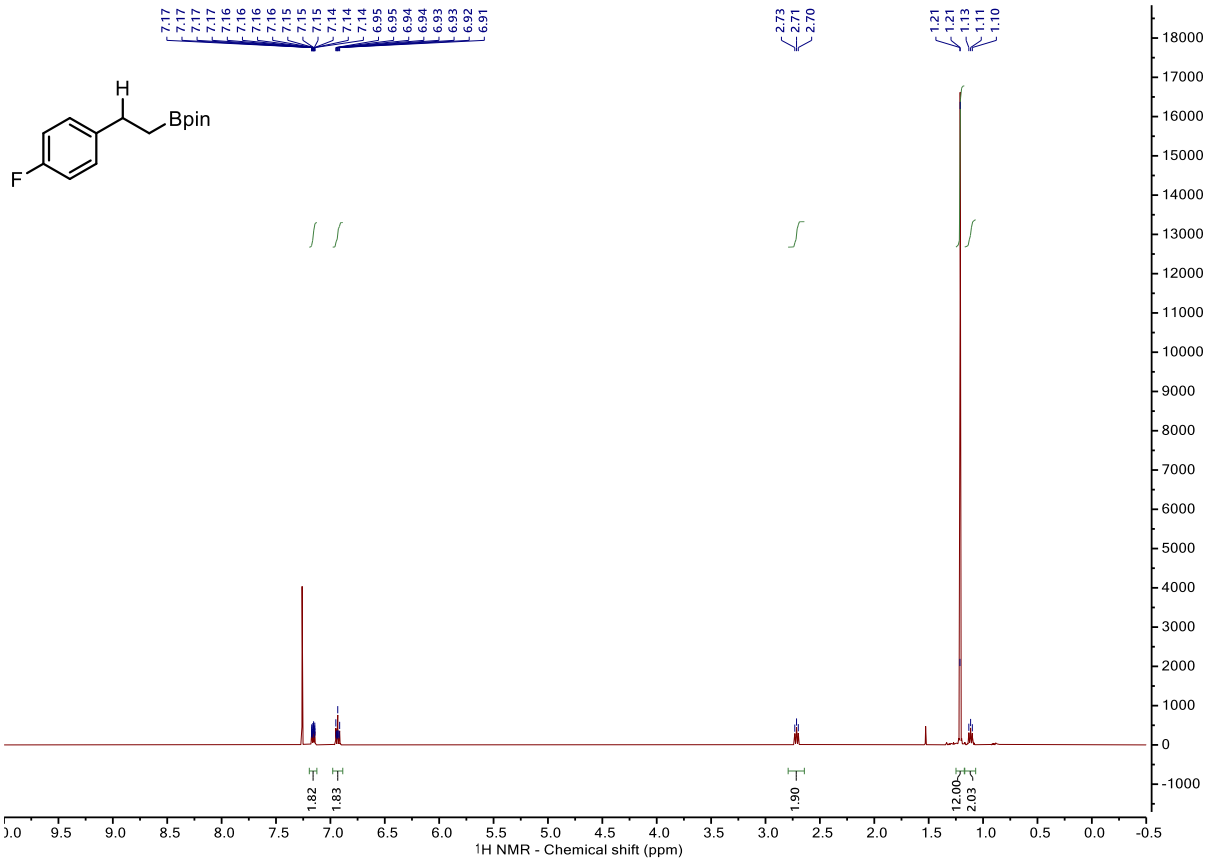

^{1}H NMR (500 MHz, Chloroform-*d*) of **2-1q**

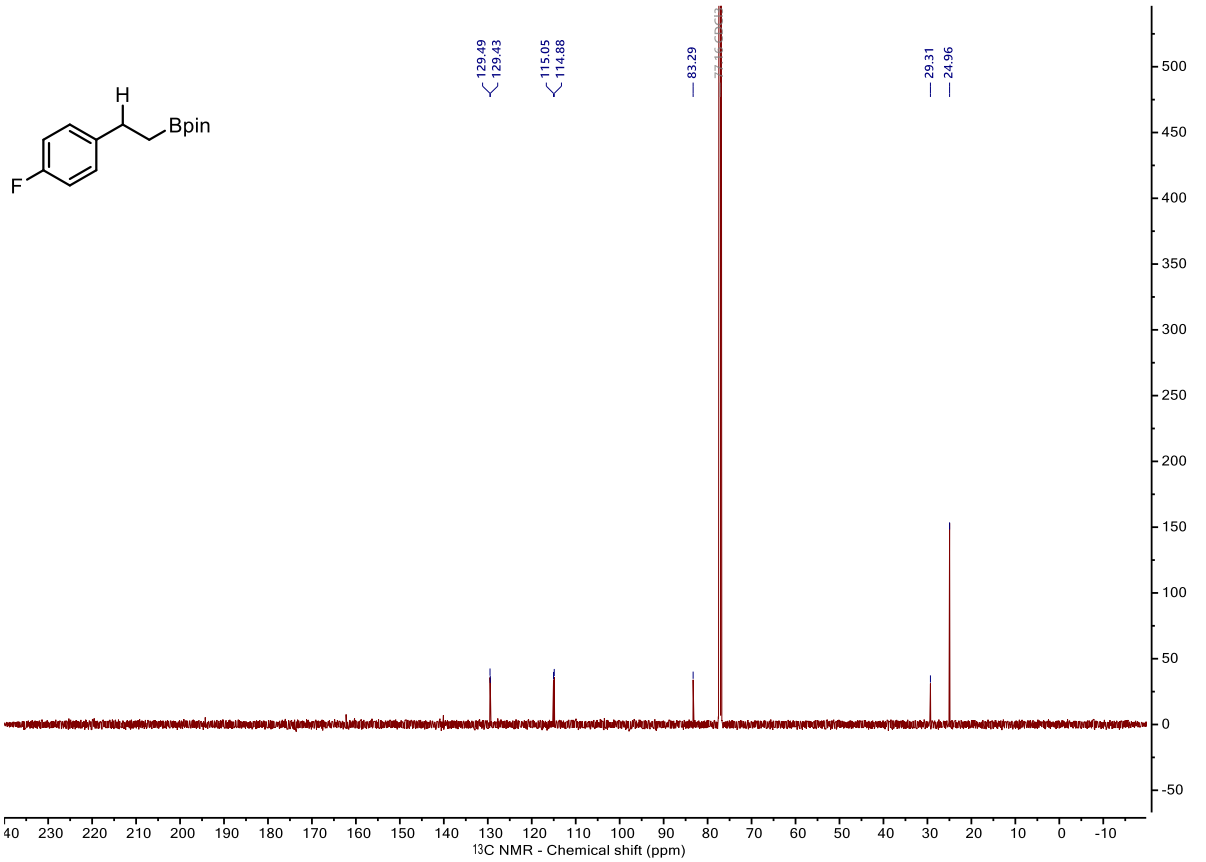

^{13}C {^{1}H} NMR (126 MHz, Chloroform-*d*) of **2-1q**

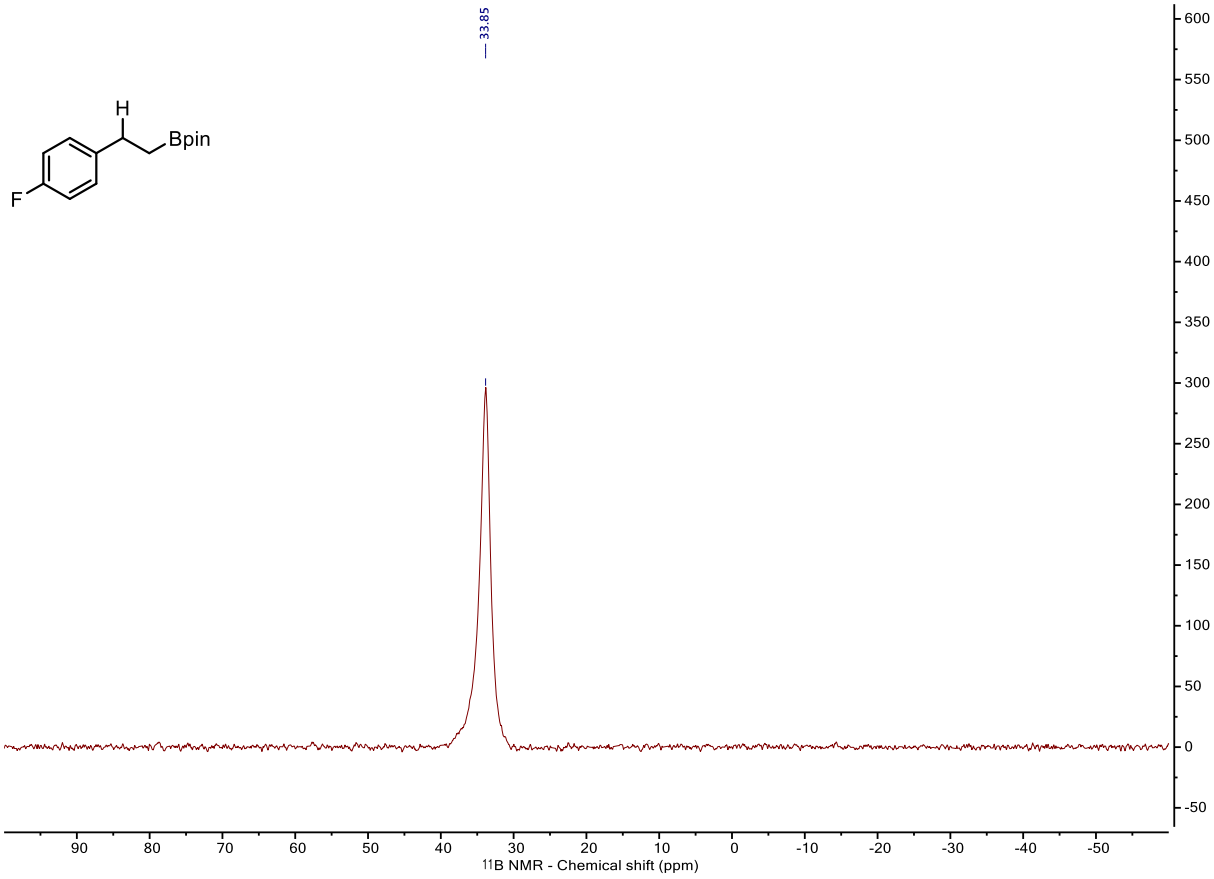

^{11}B NMR (160 MHz, Chloroform-*d*) of **2-1q**

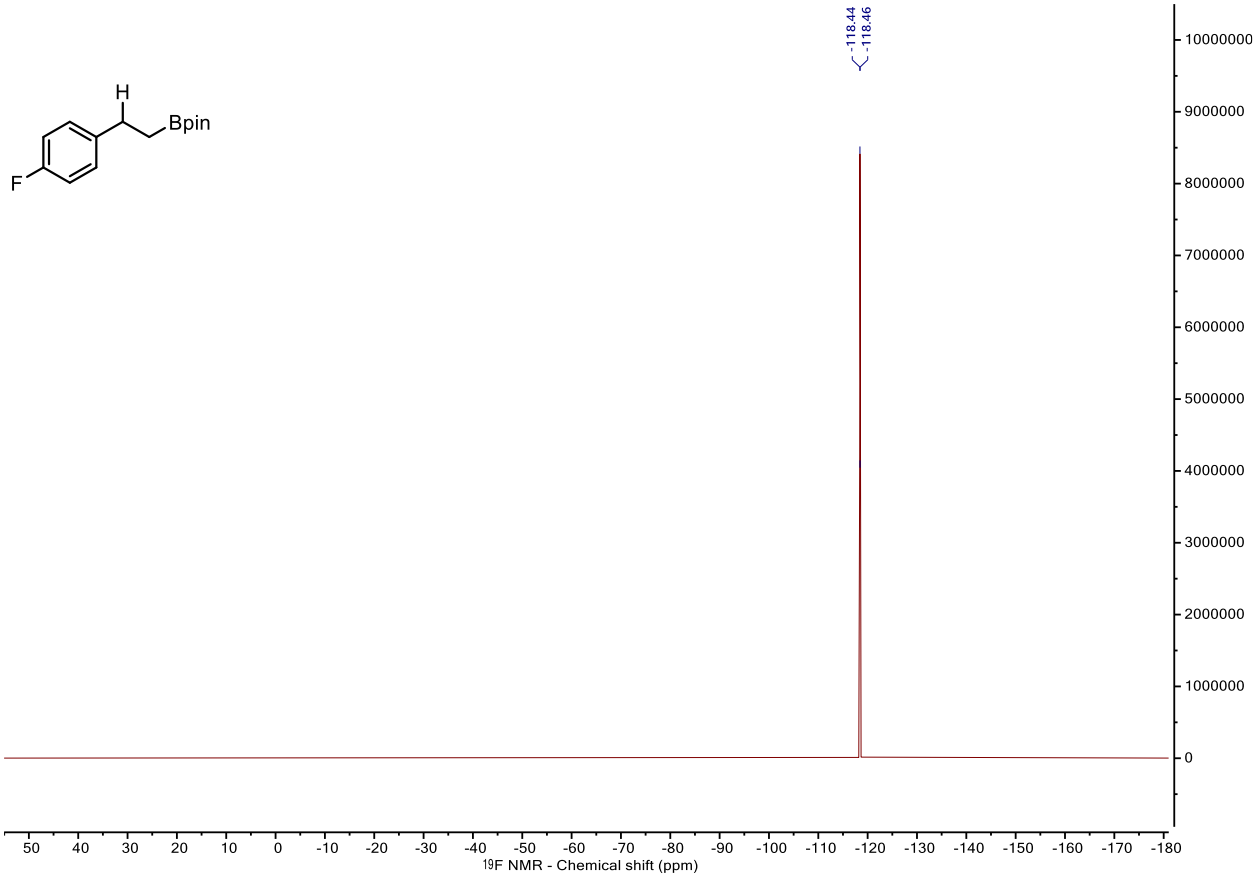

^{19}F NMR (471 MHz, Chloroform-*d*) of **2-1q**

2-1r; 2-(4-chlorophenyl)ethyl)-4,4,5,5-tetramethyl-[1,3,2]-dioxaborolane (ABG-0322)

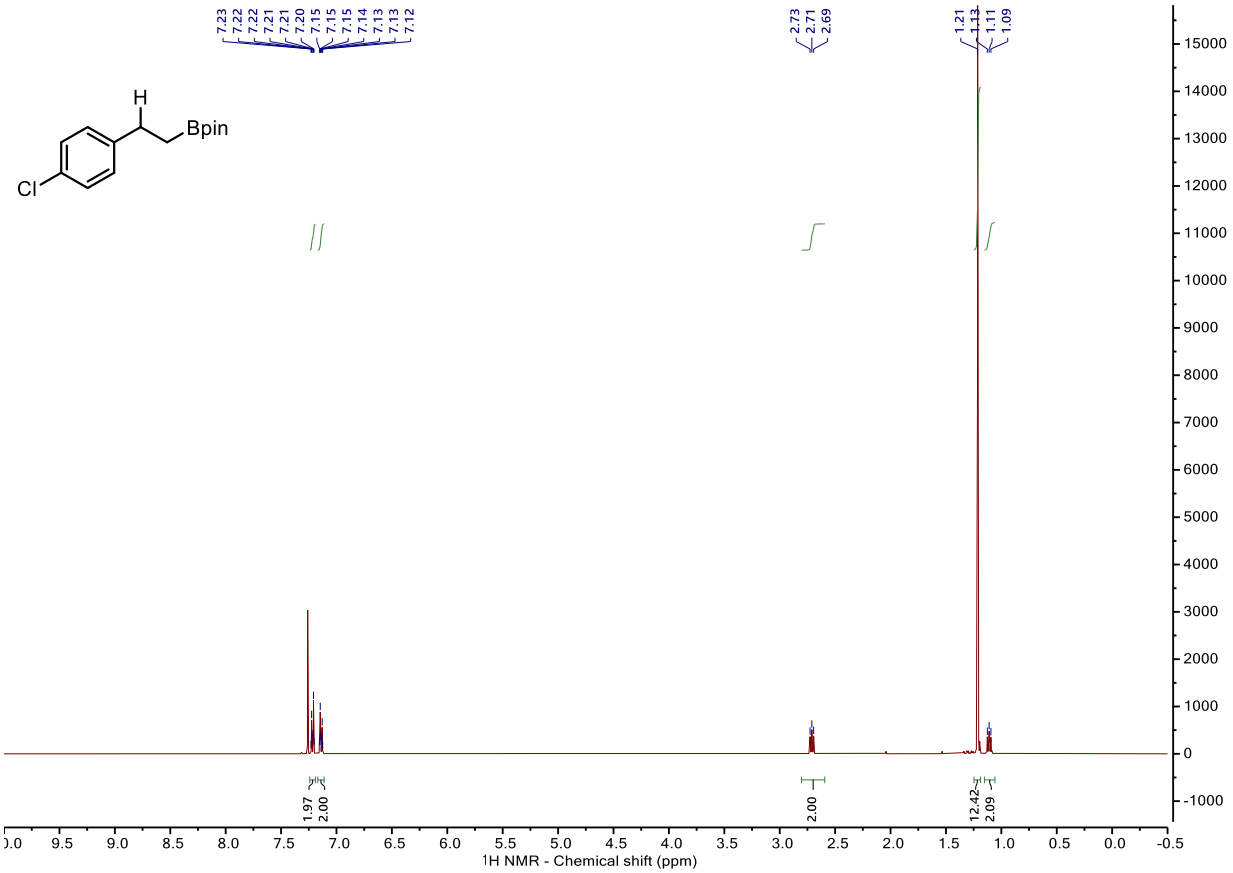

^{1}H NMR (500 MHz, Chloroform-*d*) of **2-1r**

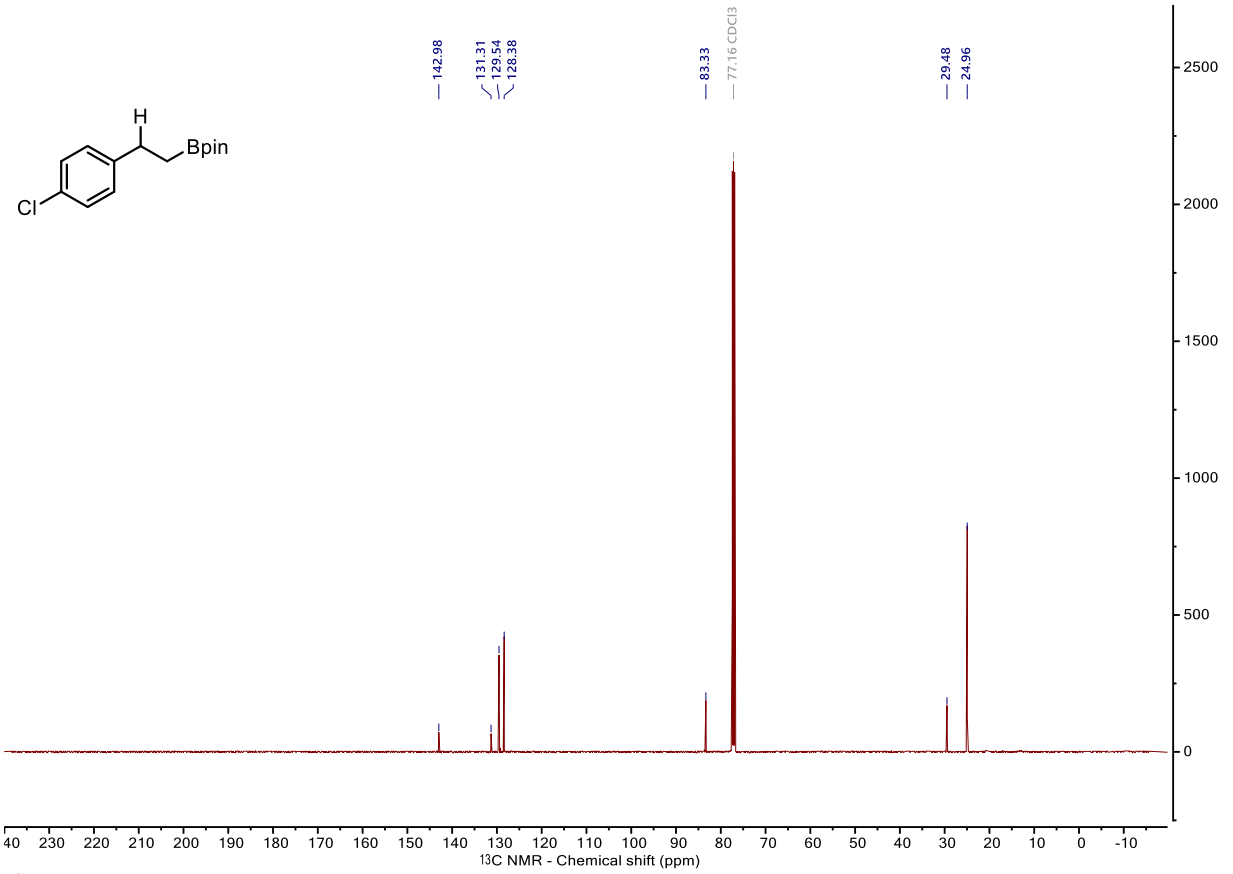

^{13}C {^{1}H} NMR (126 MHz, Chloroform-*d*) of **2-1r**

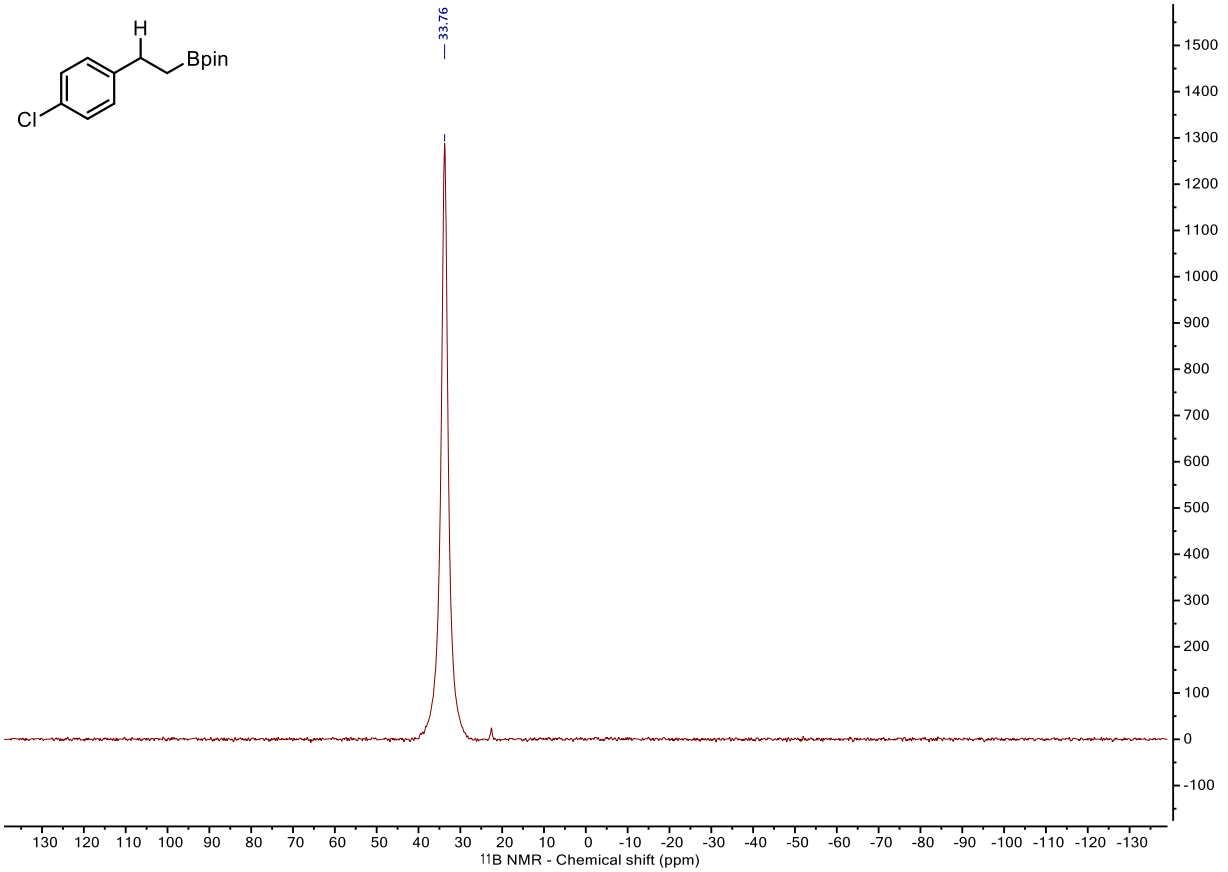

^{11}B NMR (160 MHz, Chloroform-*d*) of **2-1r**

2-1s; 2-(4-bromophenyl)ethyl)-4,4,5,5-tetramethyl-[1,3,2]-dioxaborolane (ABG-0364)

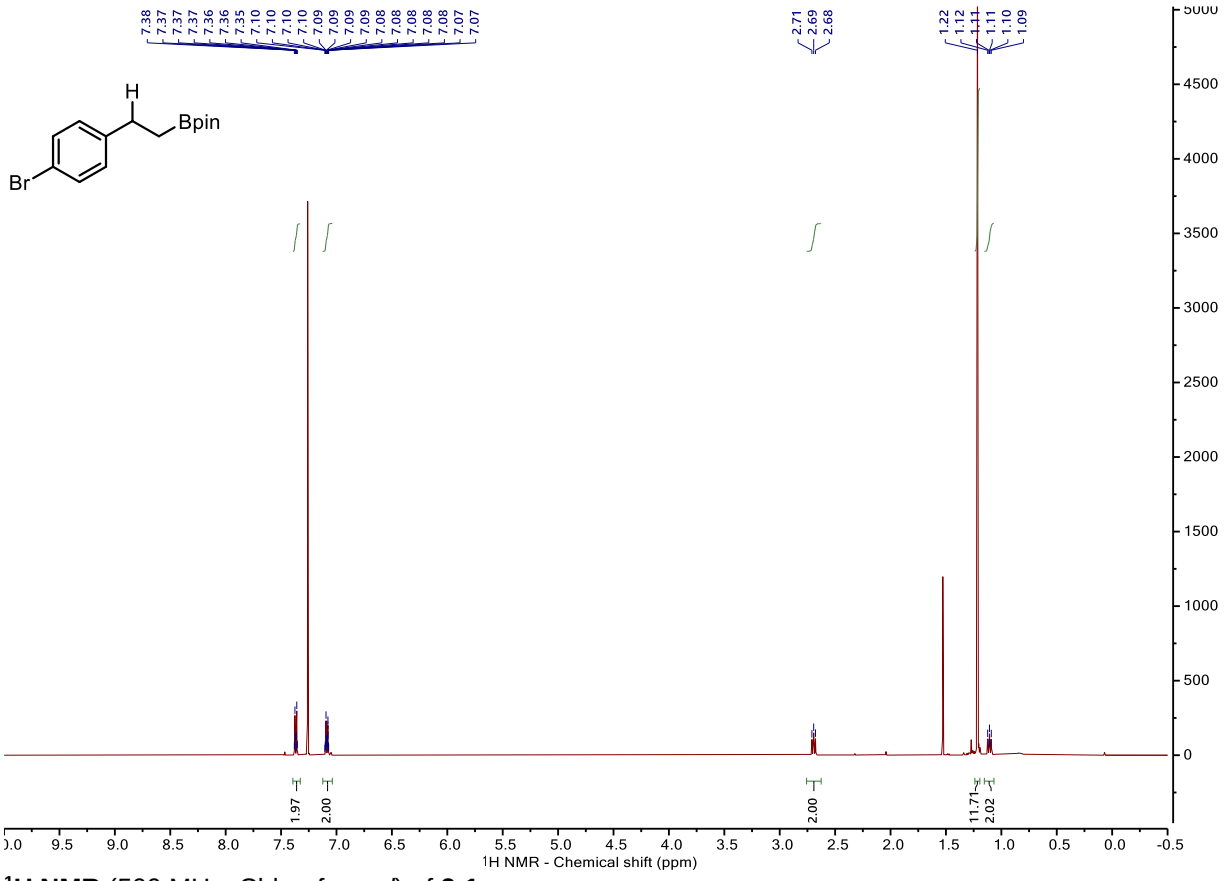

^{1}H NMR (500 MHz, Chloroform-*d*) of **2-1s**

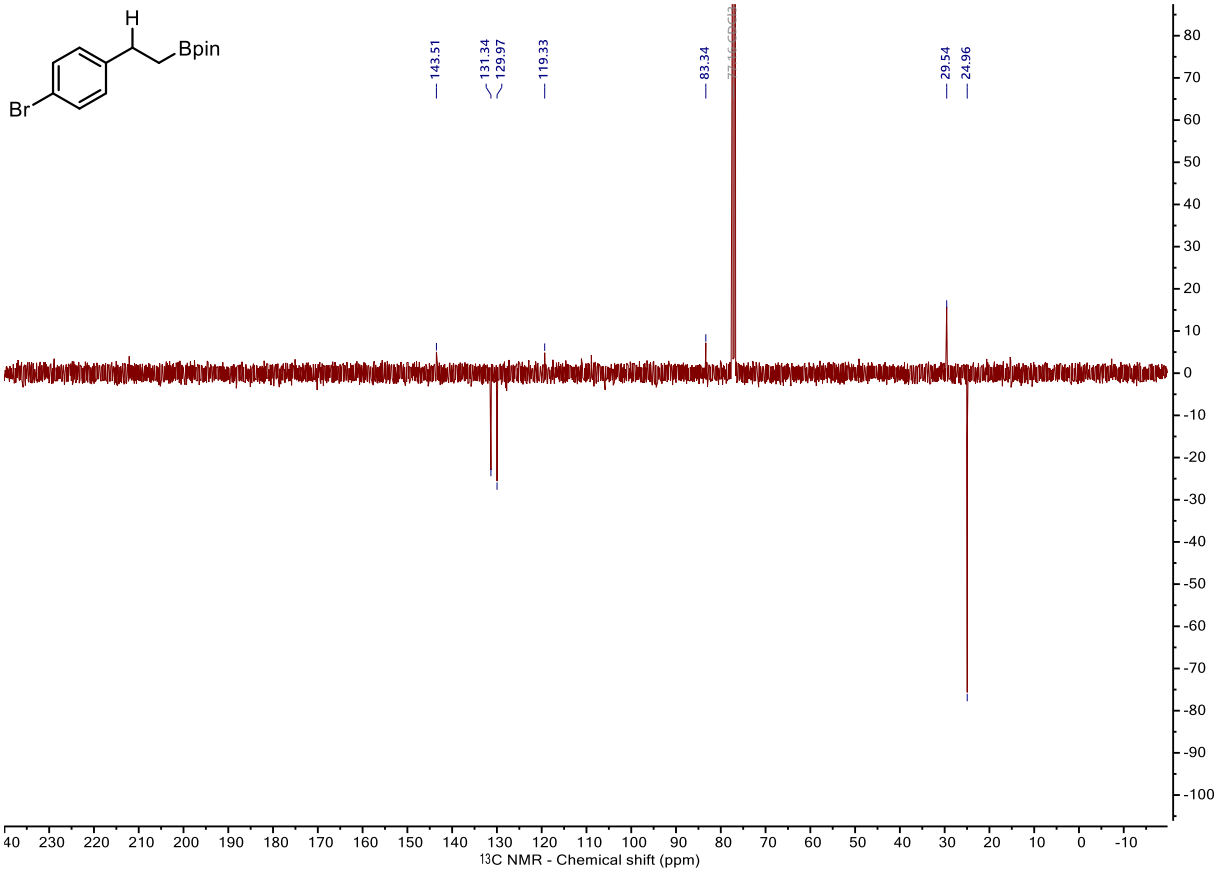

^{13}C {^{1}H} NMR (126 MHz, Chloroform-*d*) of **2-1s**

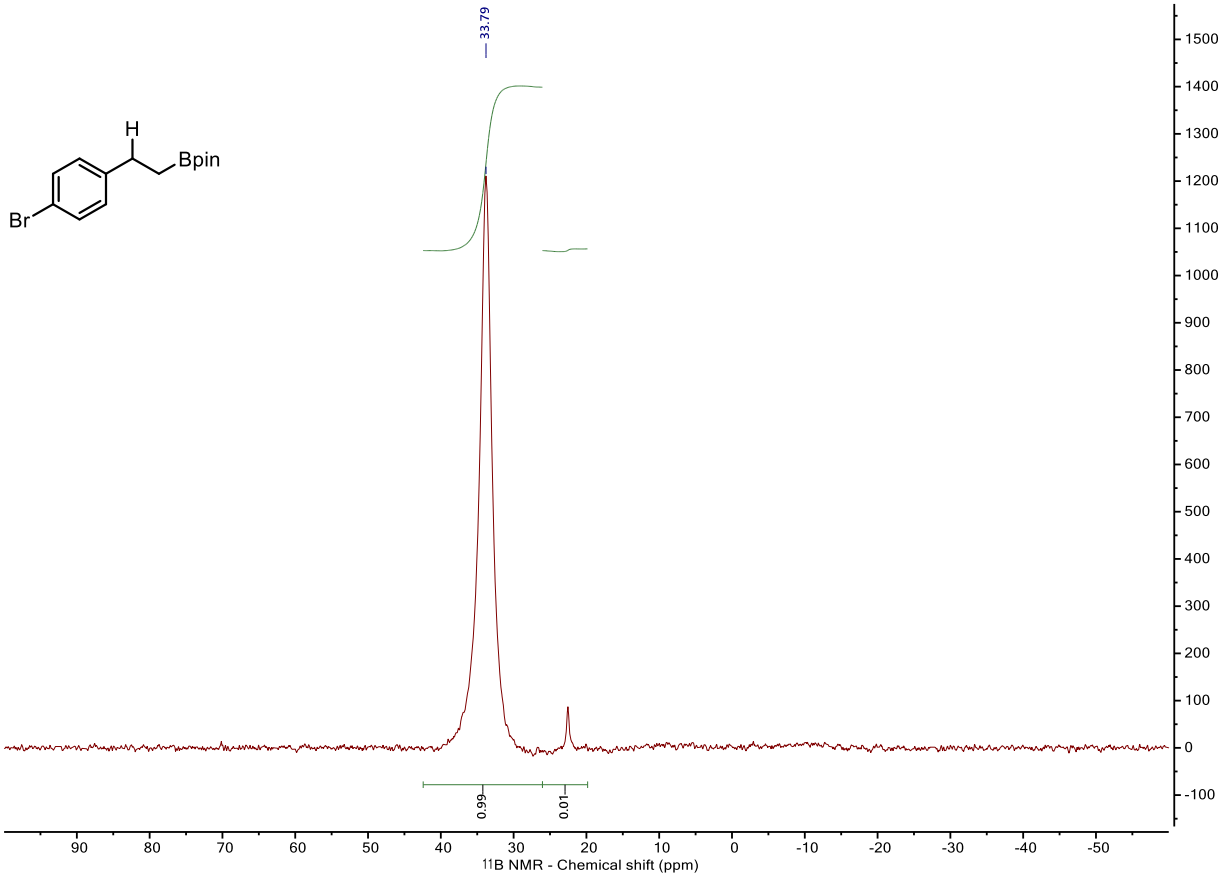

^{11}B NMR (160 MHz, Chloroform-*d*) of **2-1s**

2-1j; 4,4,5,5-tetramethyl-2-(4-methylphenethyl)-1,3,2-dioxaborolane (ABG-0210-C)

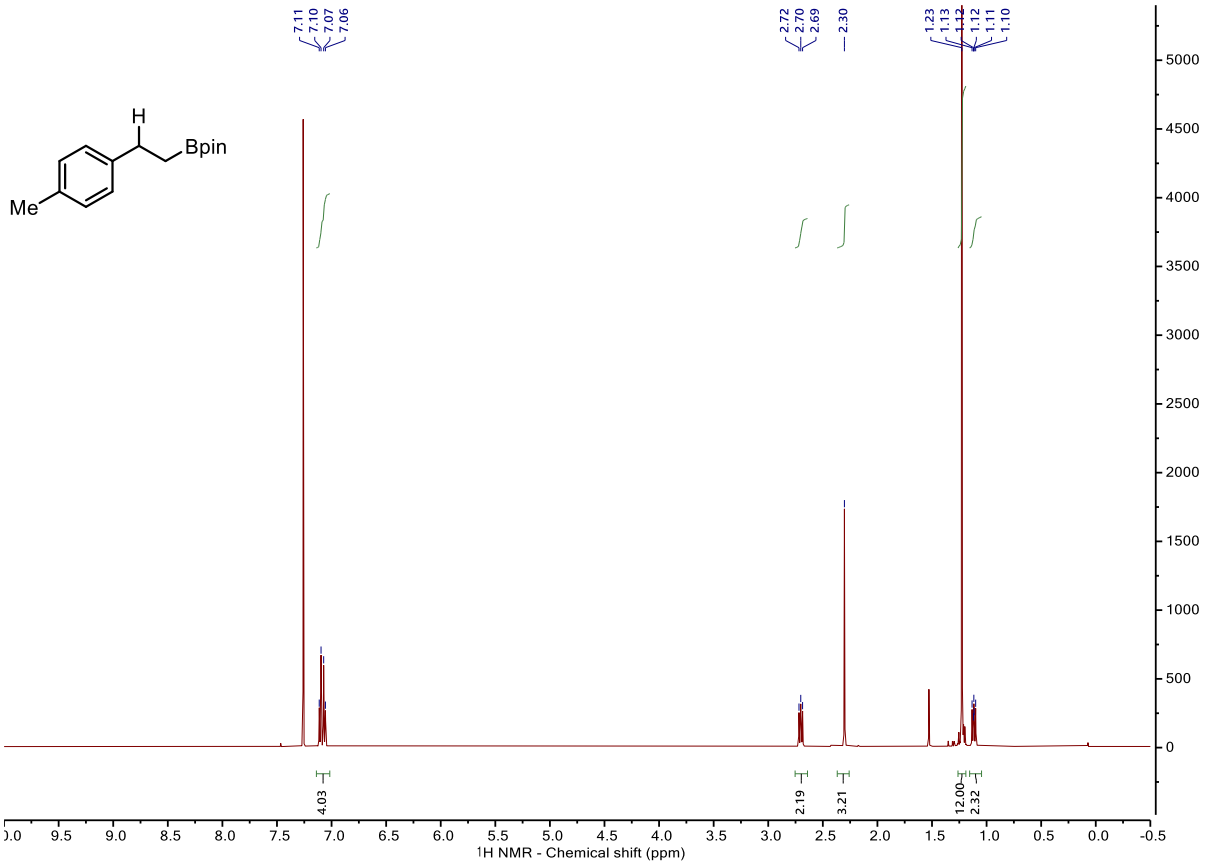

^{1}H NMR (500 MHz, Chloroform-*d*) of **2-1j**

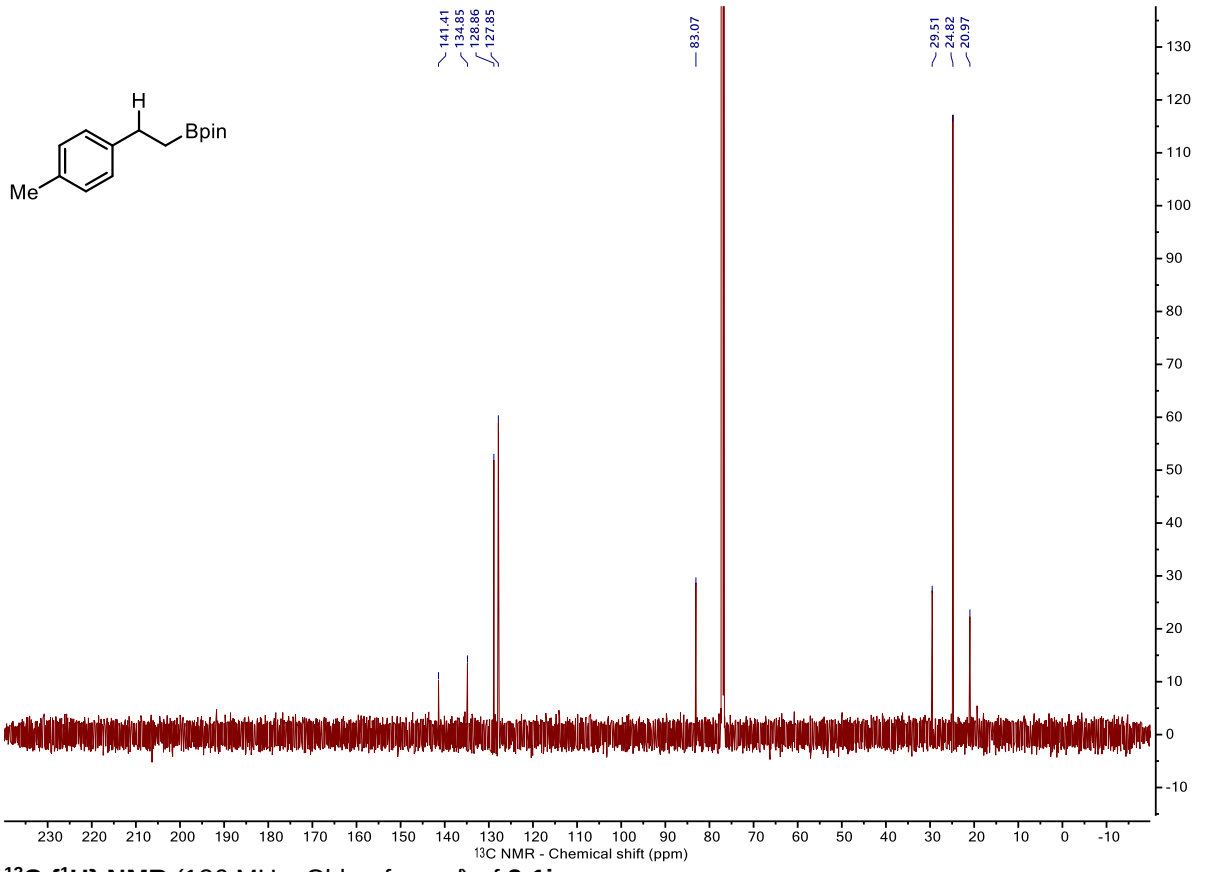

^{13}C {^{1}H} NMR (126 MHz, Chloroform-*d*) of **2-1j**

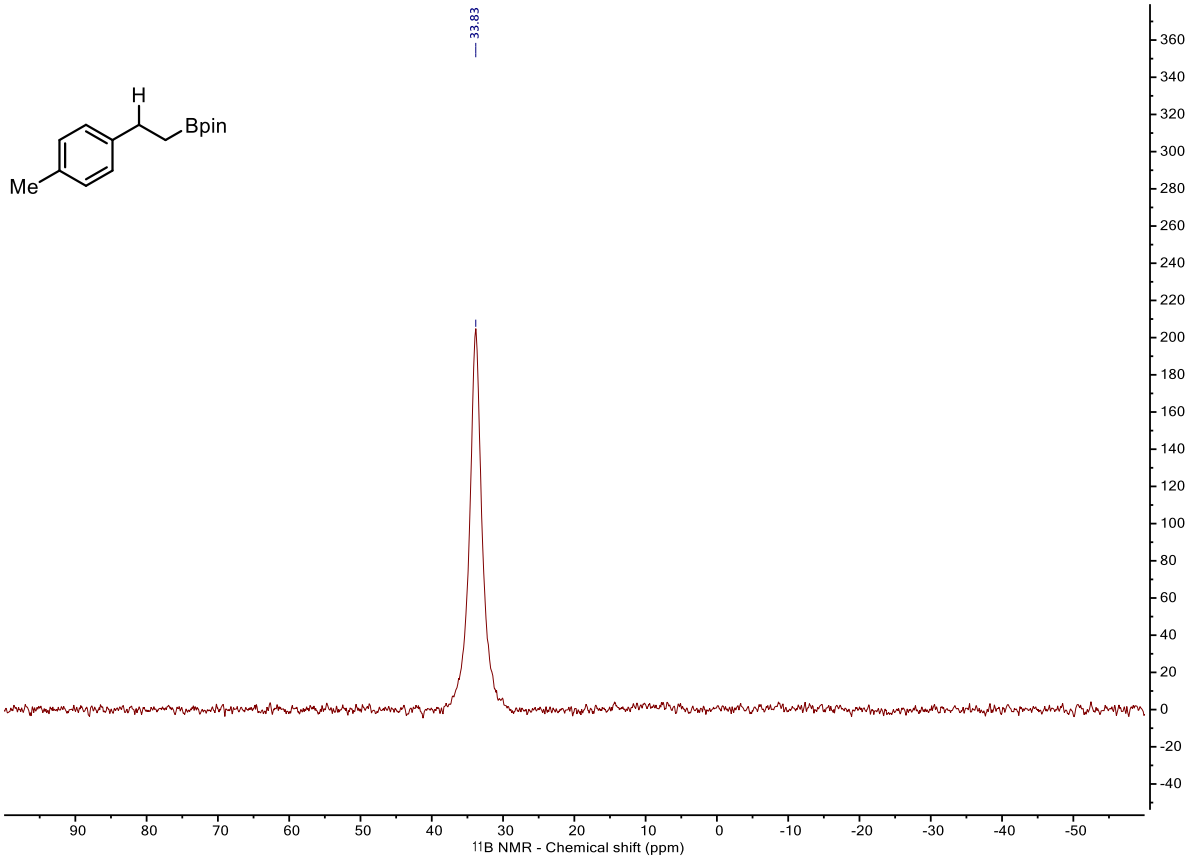

^{11}B NMR (160 MHz, Chloroform-*d*) of **2-1j**

2-1g; 2-(4-(4-chlorophenyl)butyl)-4,4,5,5-tetramethyl-1,3,2-dioxaborolane (ABG-0332)

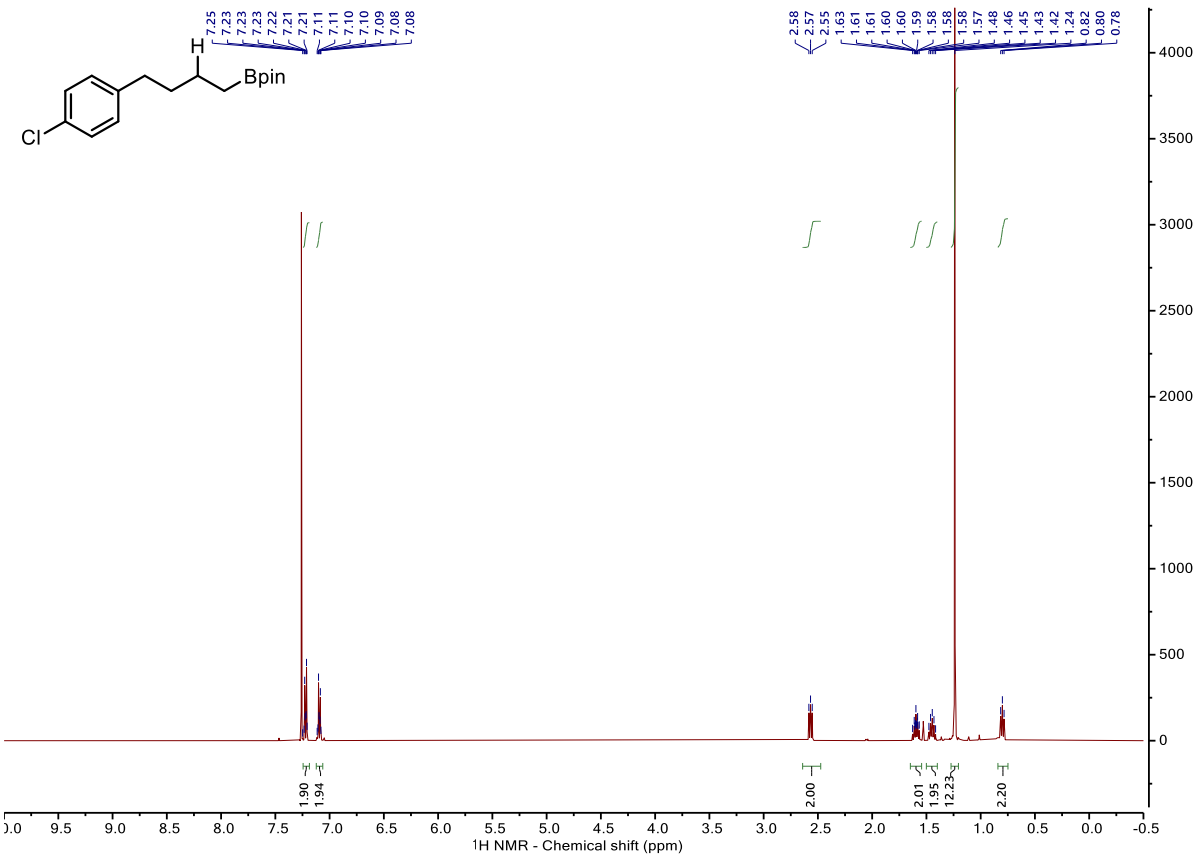

^{1}H NMR (500 MHz, Chloroform-*d*) of **2-1g**

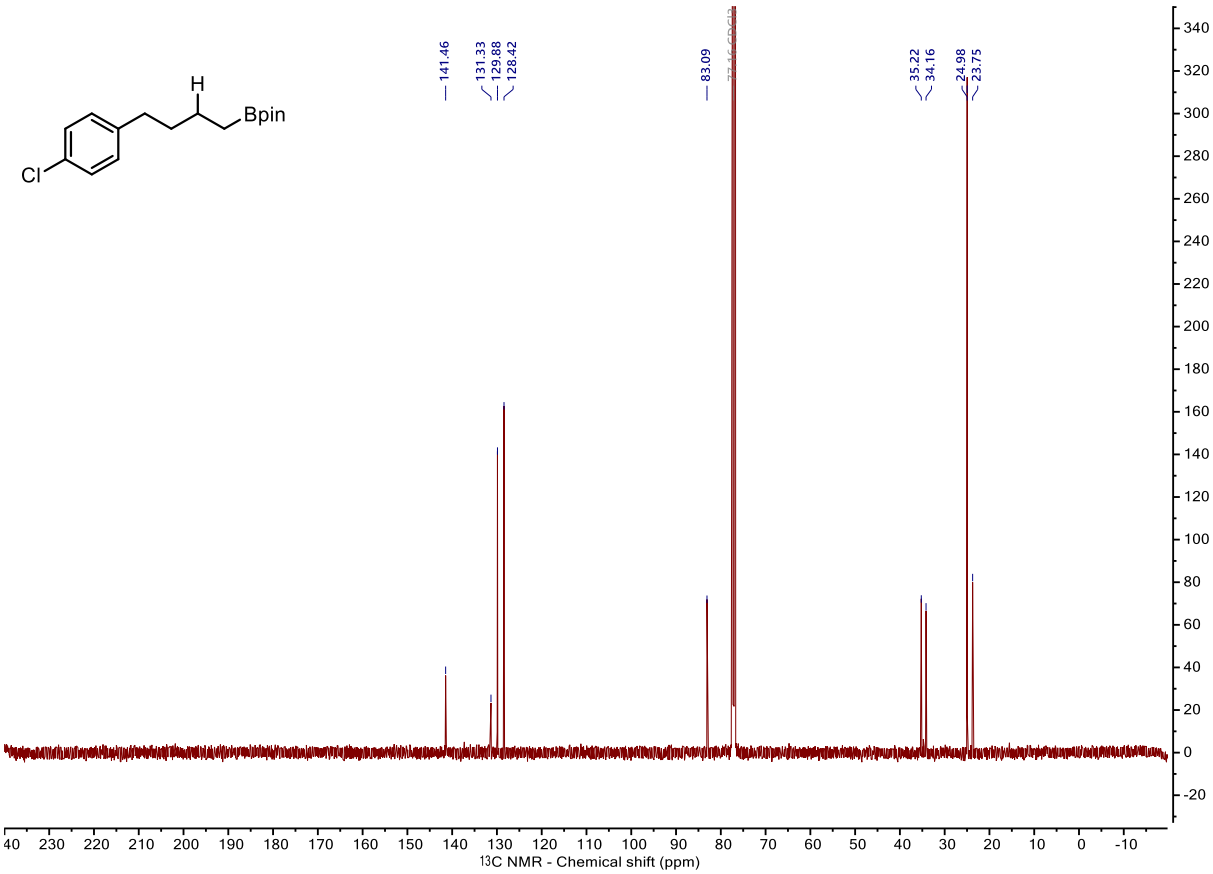

^{13}C {^{1}H} NMR (126 MHz, Chloroform-*d*) of **2-1g**

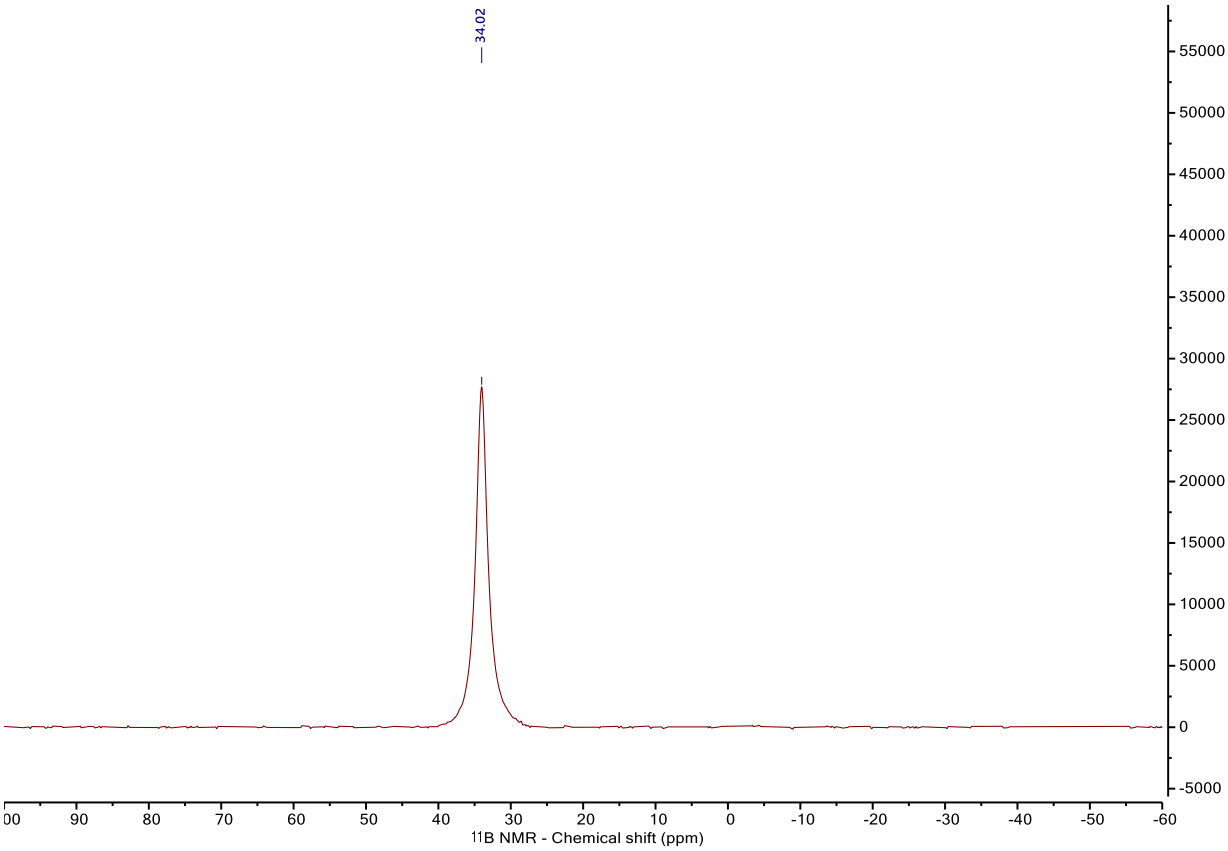

^{11}B NMR (160 MHz, Chloroform-*d*) of **2-1g**

2-1k; 2-(2,4-dimethylphenethyl)-4,4,5,5-tetramethyl-1,3,2-dioxaborolane (ABG-0210-D)

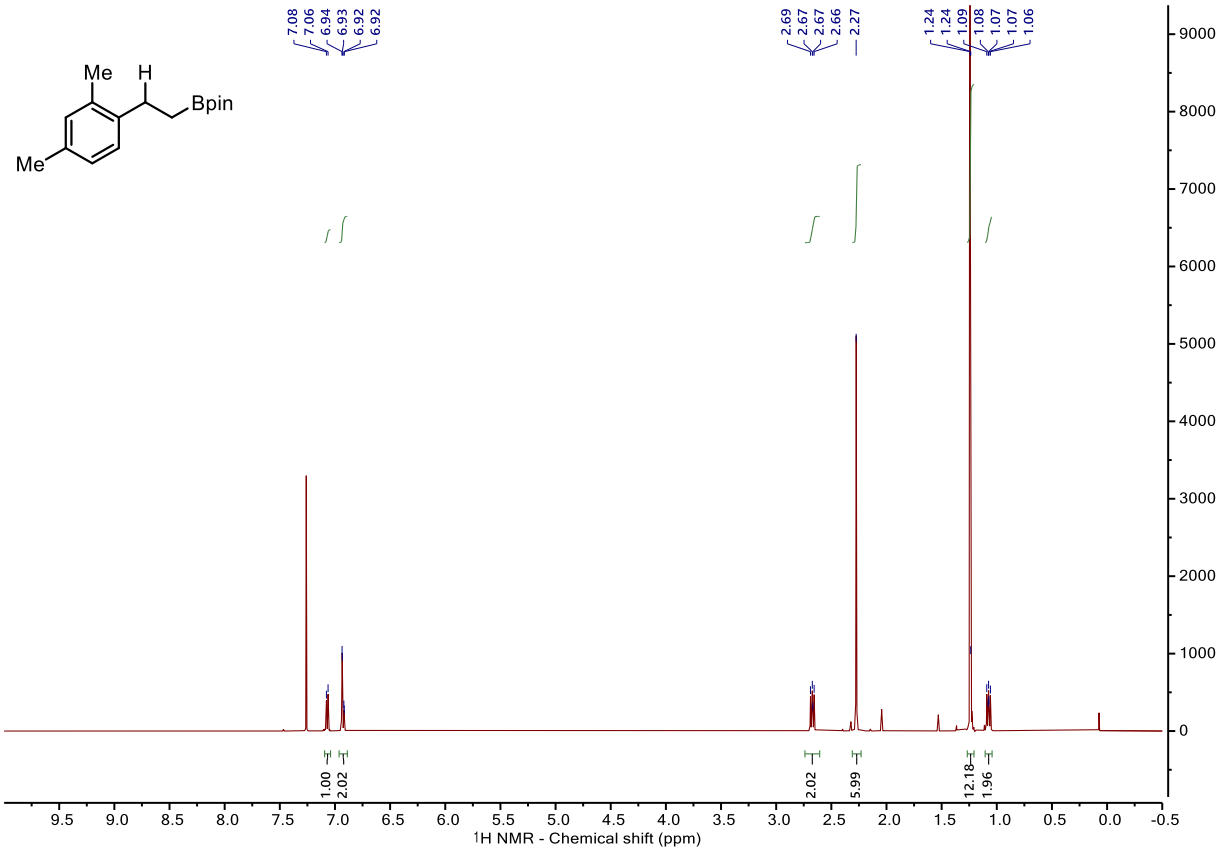

^{1}H NMR (500 MHz, Chloroform-*d*) of **2-1k**

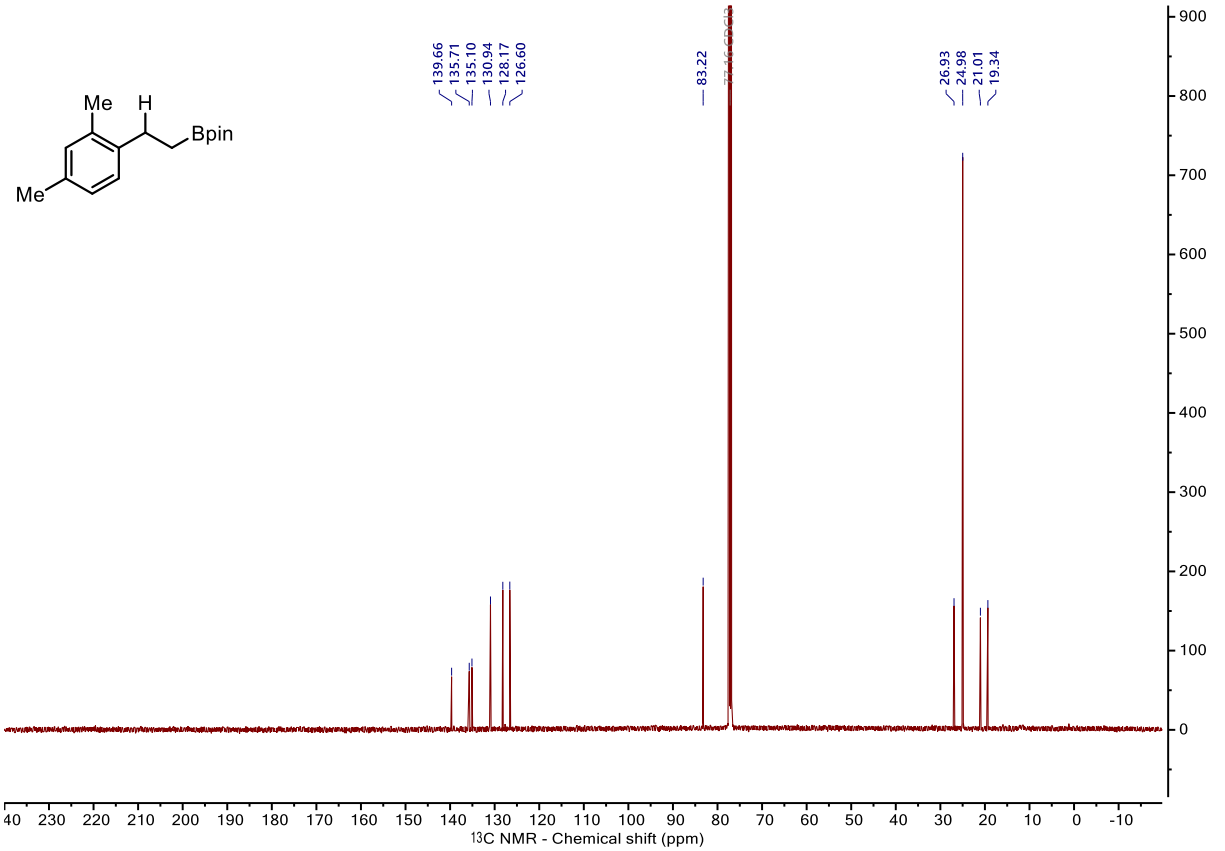

^{13}C {^{1}H} NMR (126 MHz, Chloroform-*d*) of **2-1k**

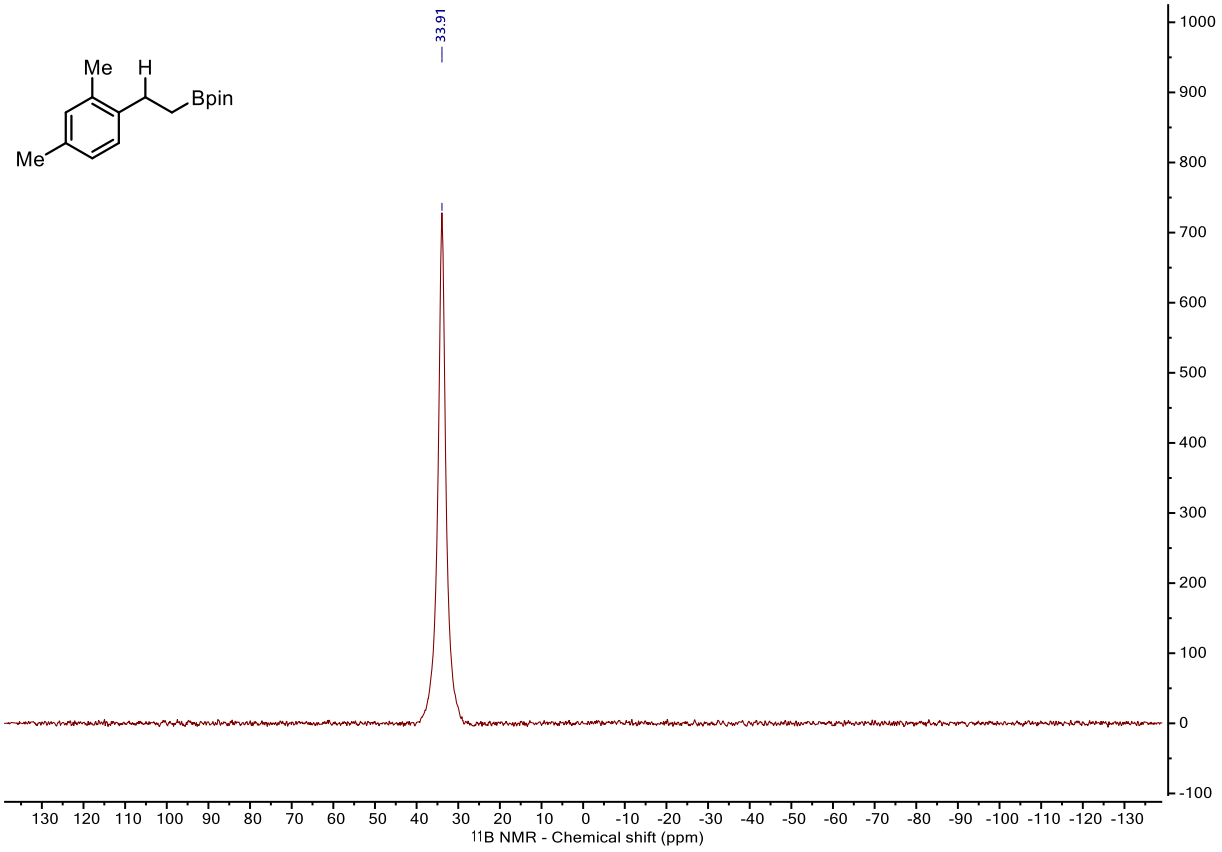

^{11}B NMR (160 MHz, Chloroform-*d*) of **2-1k**

2-1o; 2-(4-methoxyphenethyl)-4,4,5,5-tetramethyl-1,3,2-dioxaborolane (ABG-0363-P)

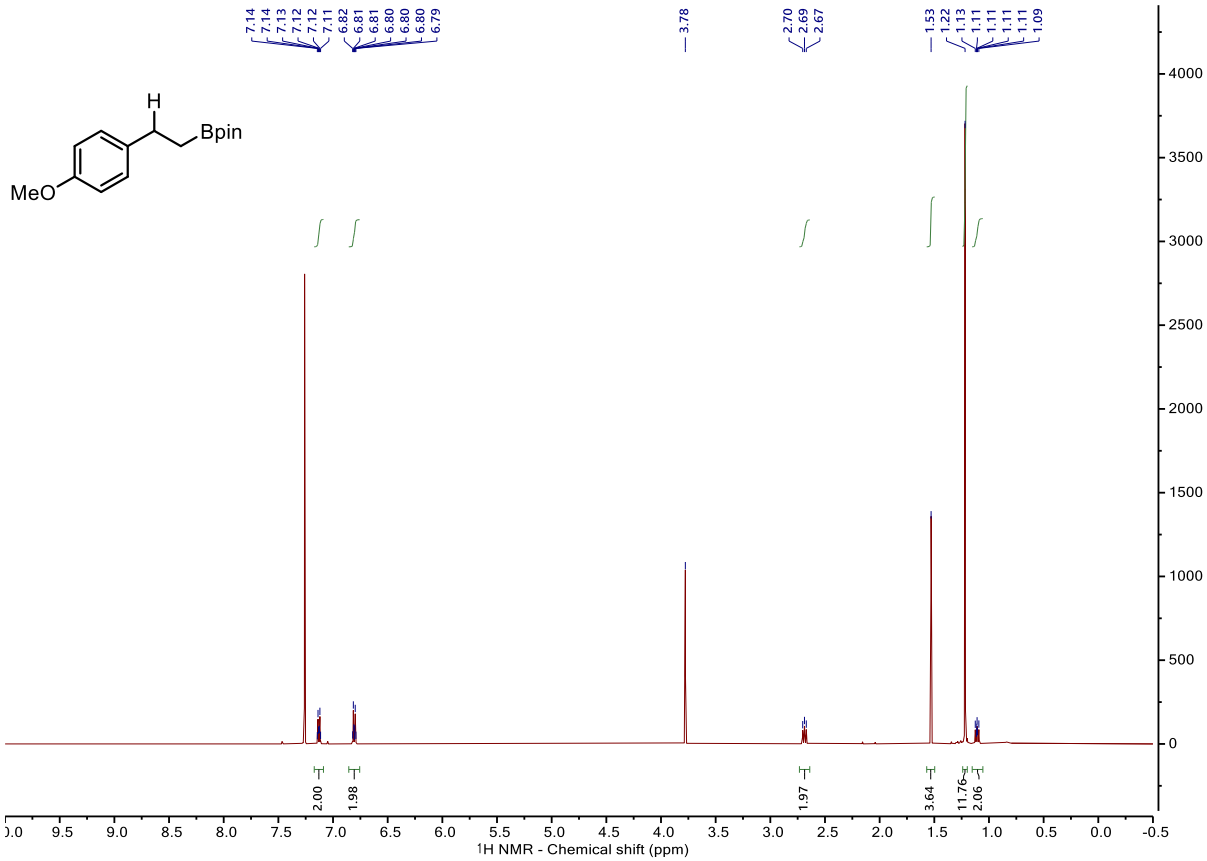

^{1}H NMR (500 MHz, Chloroform-*d*) of **2-1o**

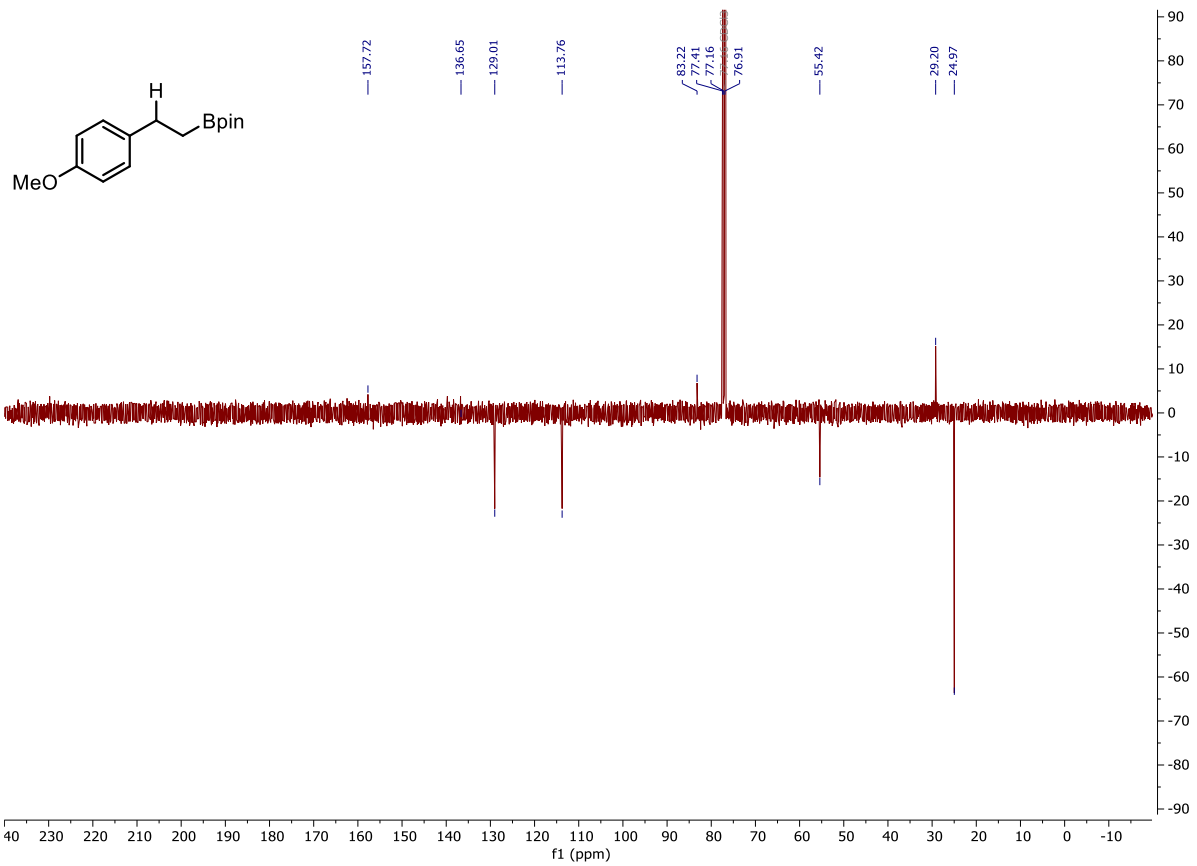

^{13}C {^{1}H} NMR (126 MHz, Chloroform-*d*) of **2-1o**

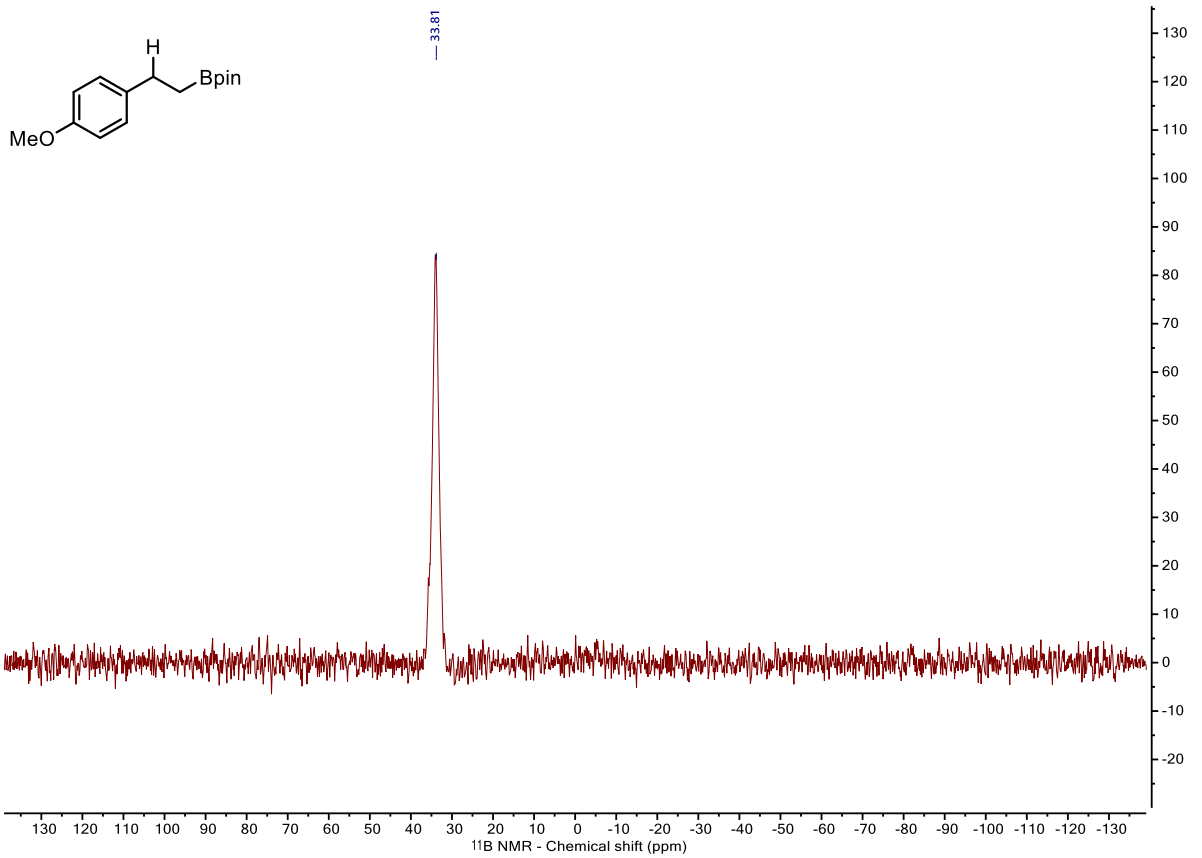

^{11}B NMR (160 MHz, Chloroform-*d*) of **2-1o**

2-1p; *N,N*-dimethyl-4-(2-(4,4,5,5-tetramethyl-1,3,2-dioxaborolan-2-yl)ethyl)aniline (ABG-0297)

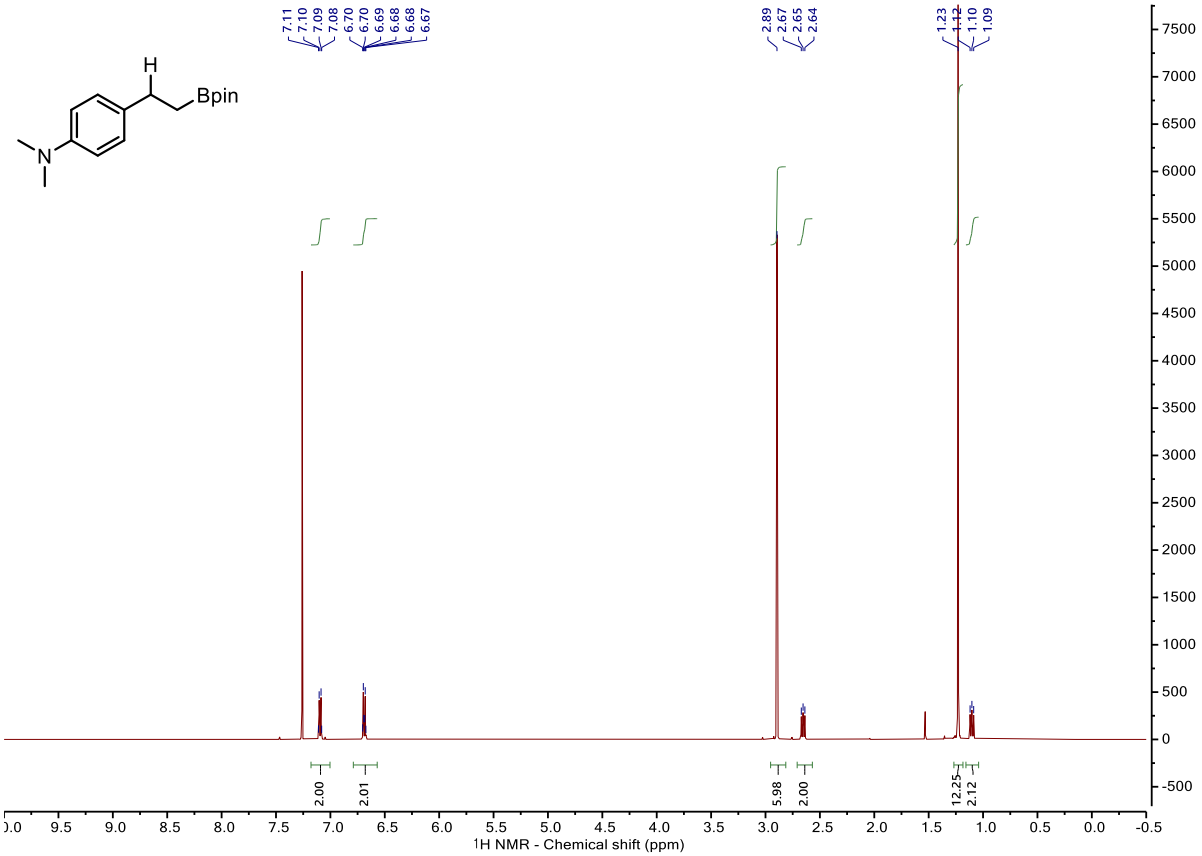

^{1}H NMR (500 MHz, Chloroform-*d*) of **2-1p**

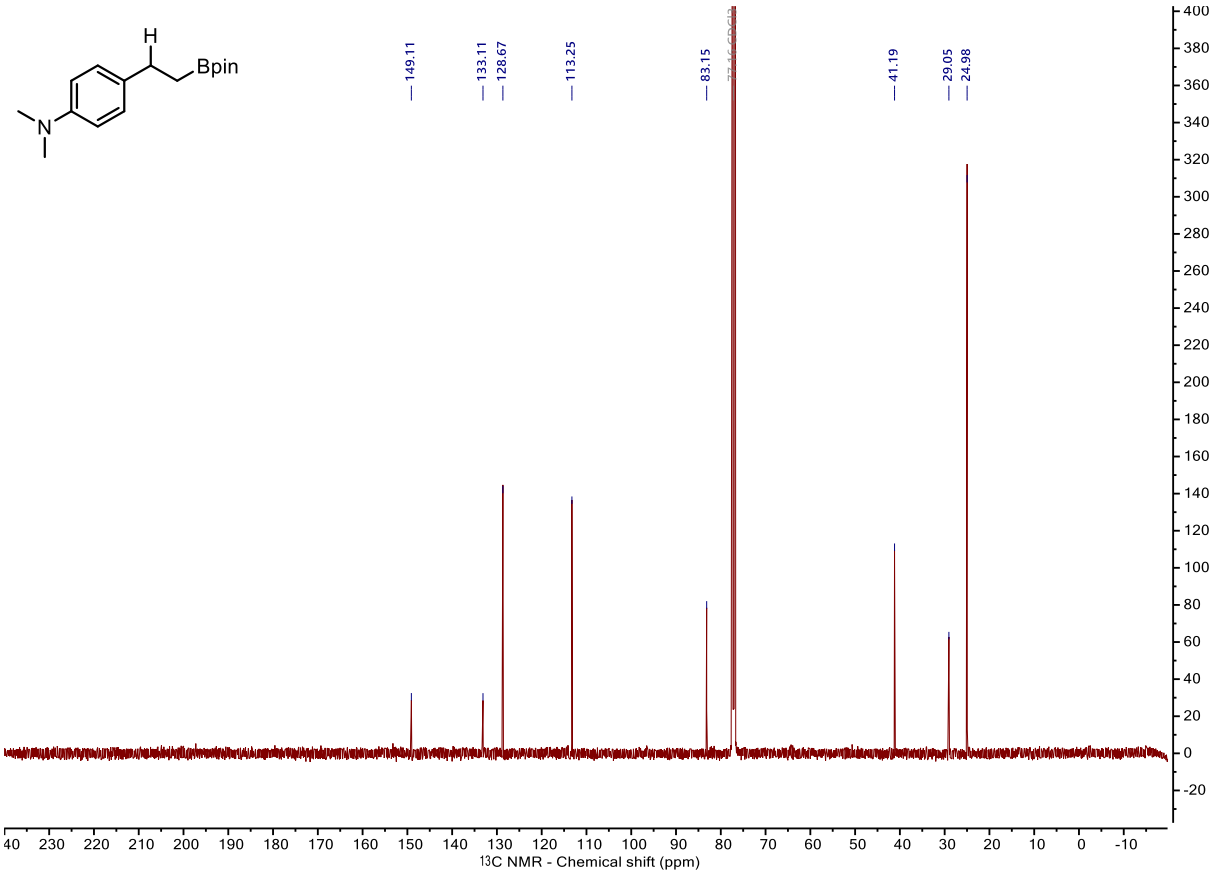

^{13}C {^{1}H} NMR (126 MHz, Chloroform-*d*) of **2-1p**

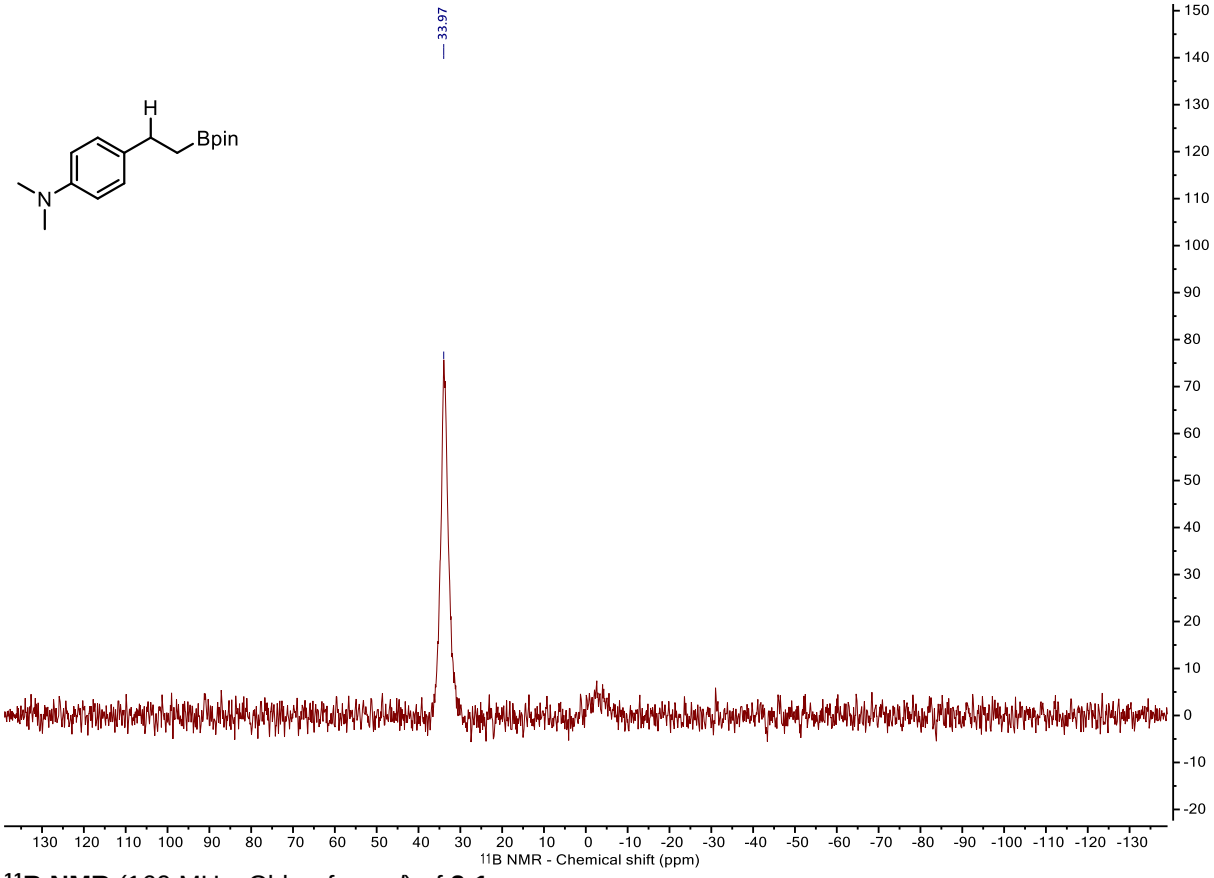

^{11}B NMR (160 MHz, Chloroform-*d*) of **2-1p**

2-1m; 4,4,5,5-tetramethyl-2-(4-tert-butylphenyl-1-ethyl)-1,3,2-dioxaborolane (ABG-0217-D)

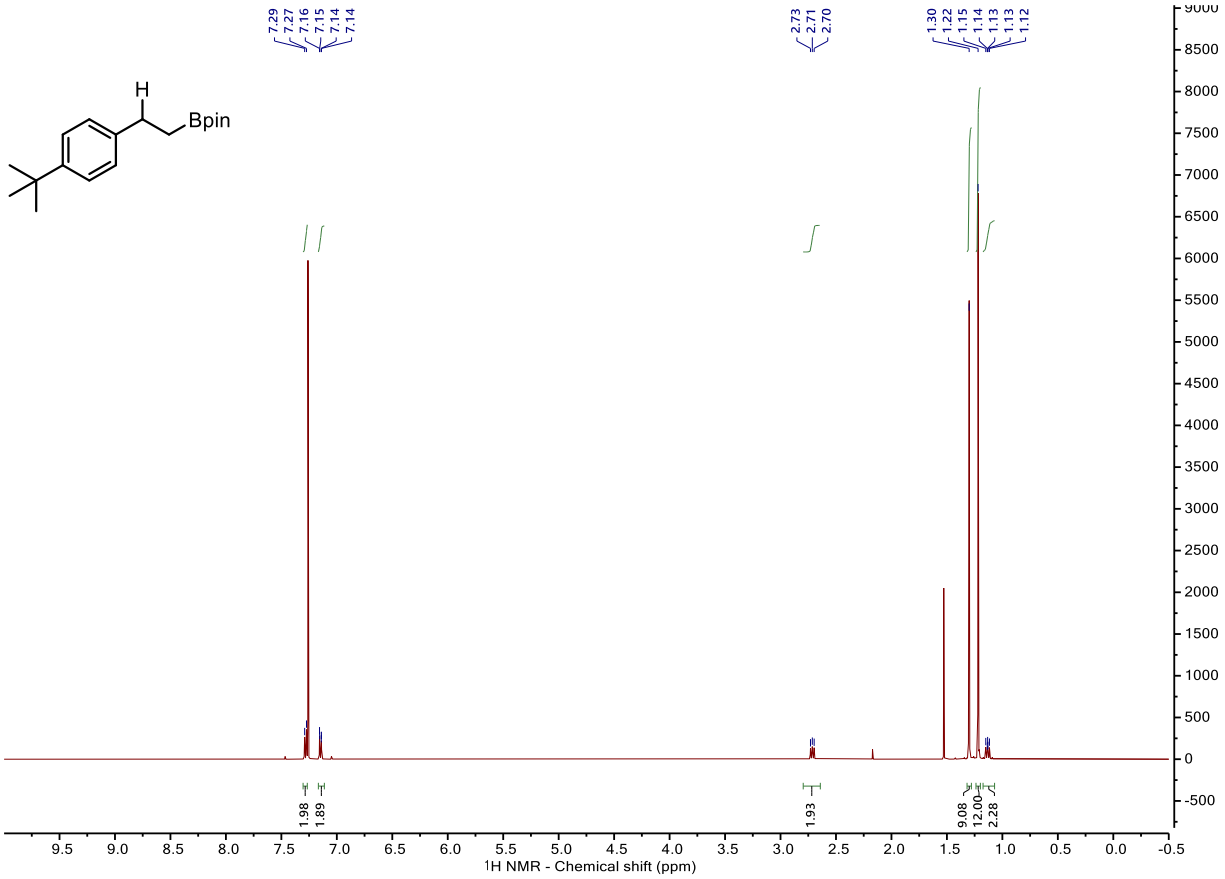

^{1}H NMR (500 MHz, Chloroform-*d*) of **2-1m**

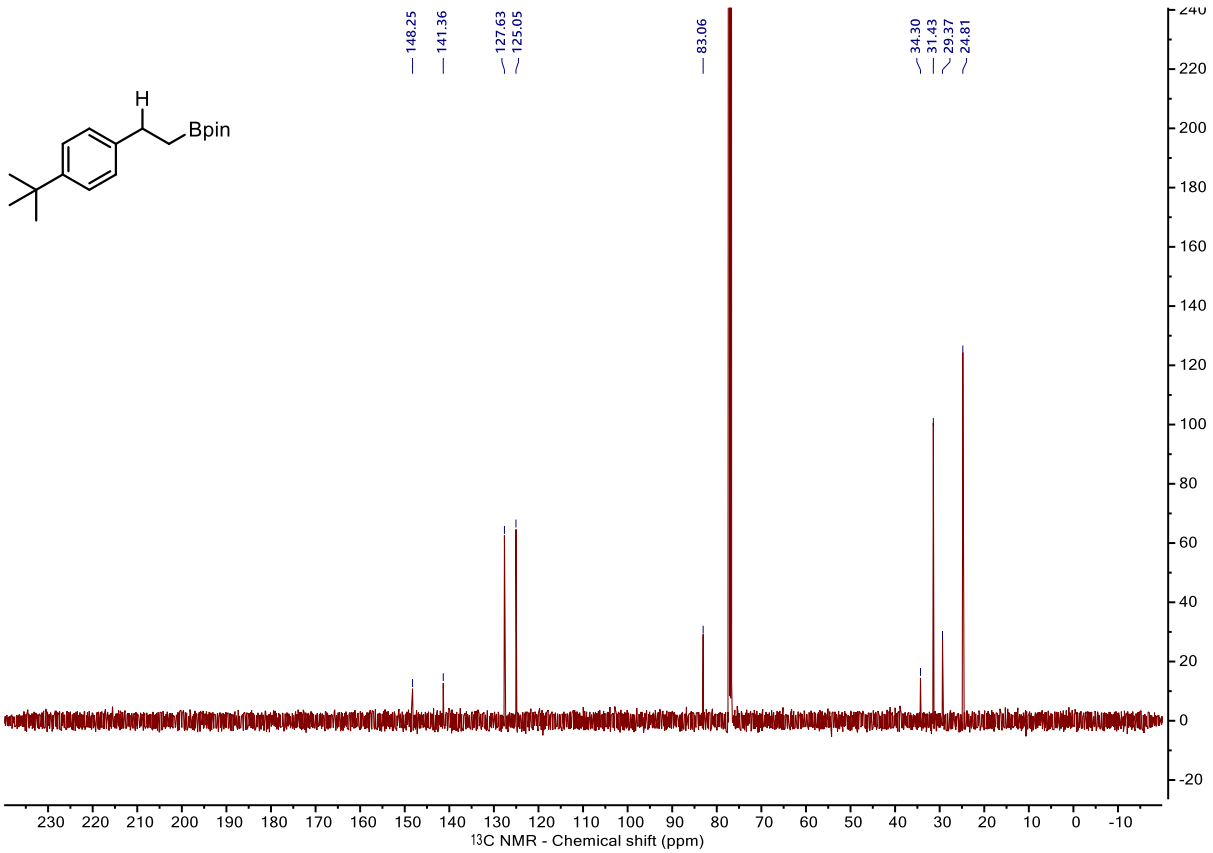

^{13}C {^{1}H} NMR (126 MHz, Chloroform-*d*) of **2-1m**

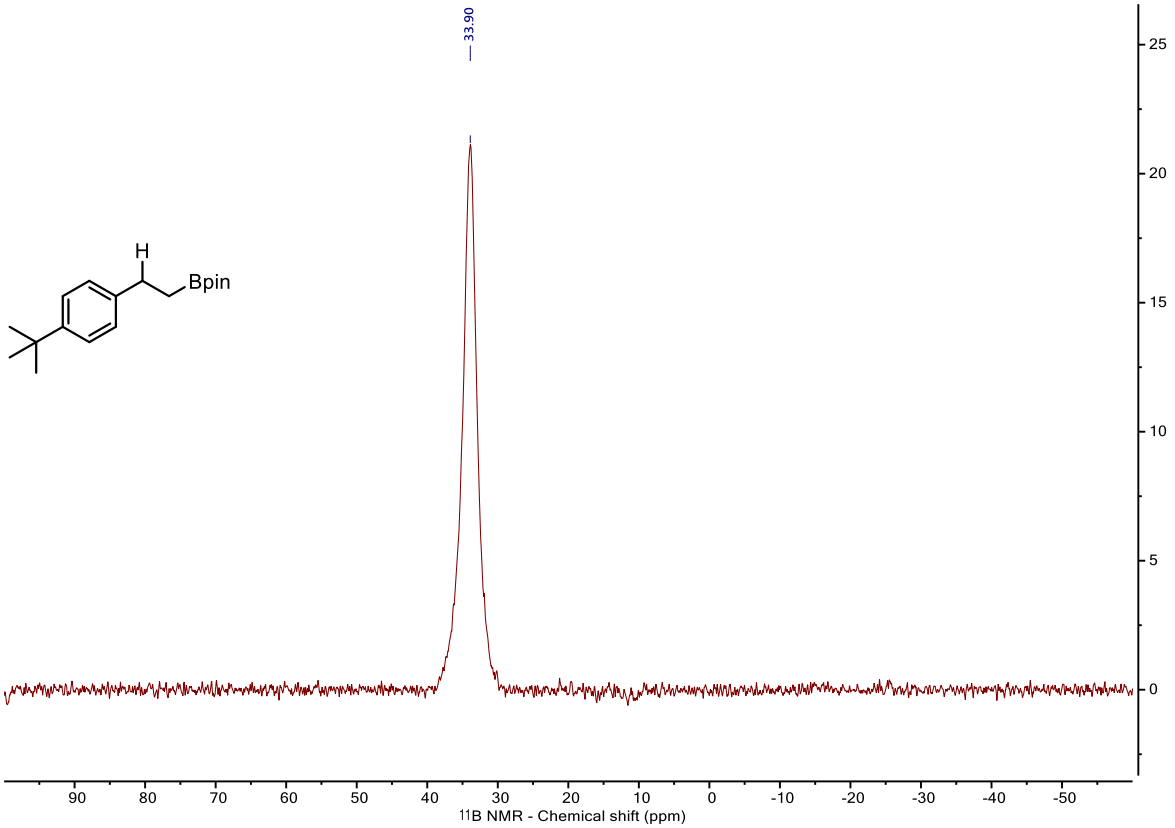

^{11}B NMR (160 MHz, Chloroform-*d*) of **2-1m**

2-1n; 4,4,5,5-tetramethyl-2-(4-*iso*-butylphenyl-1-ethyl)-1,3,2-dioxaborolane (ABG-0333)

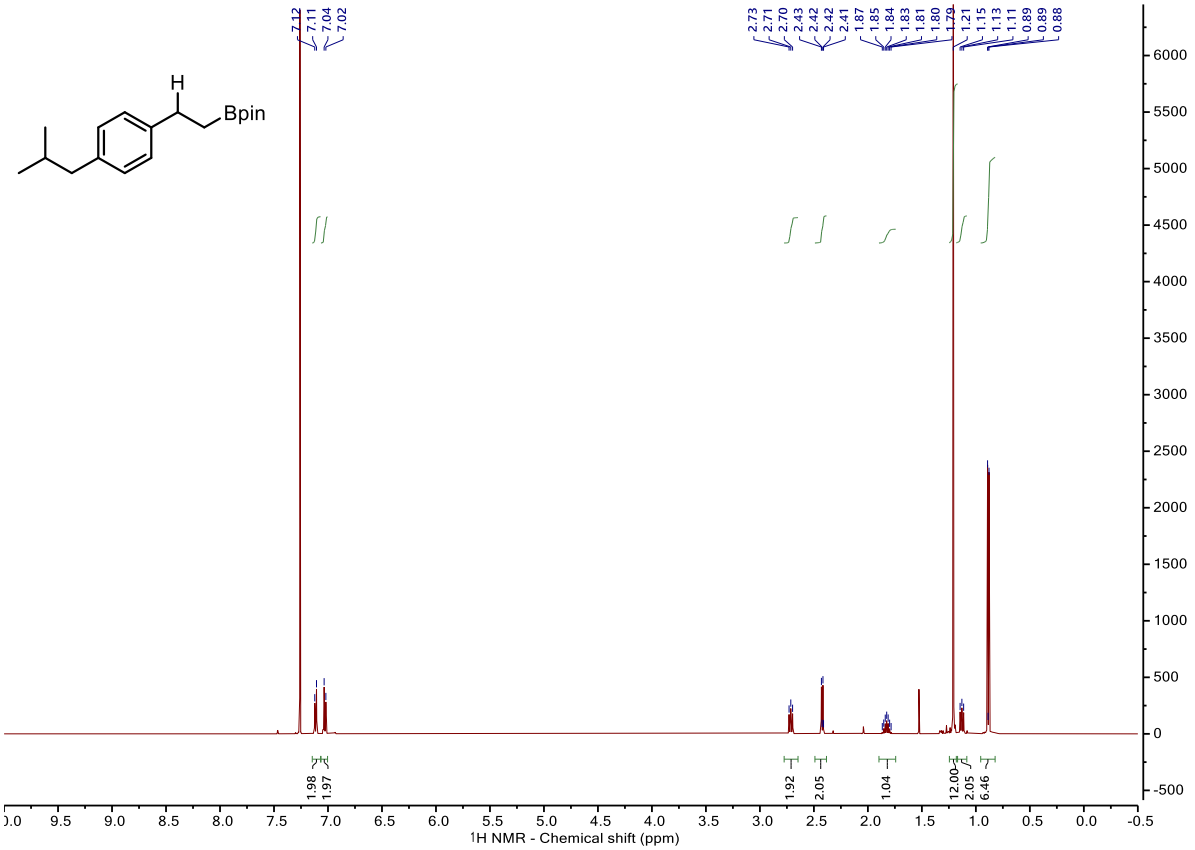

^{1}H NMR (500 MHz, Chloroform-*d*) of **2-1n**

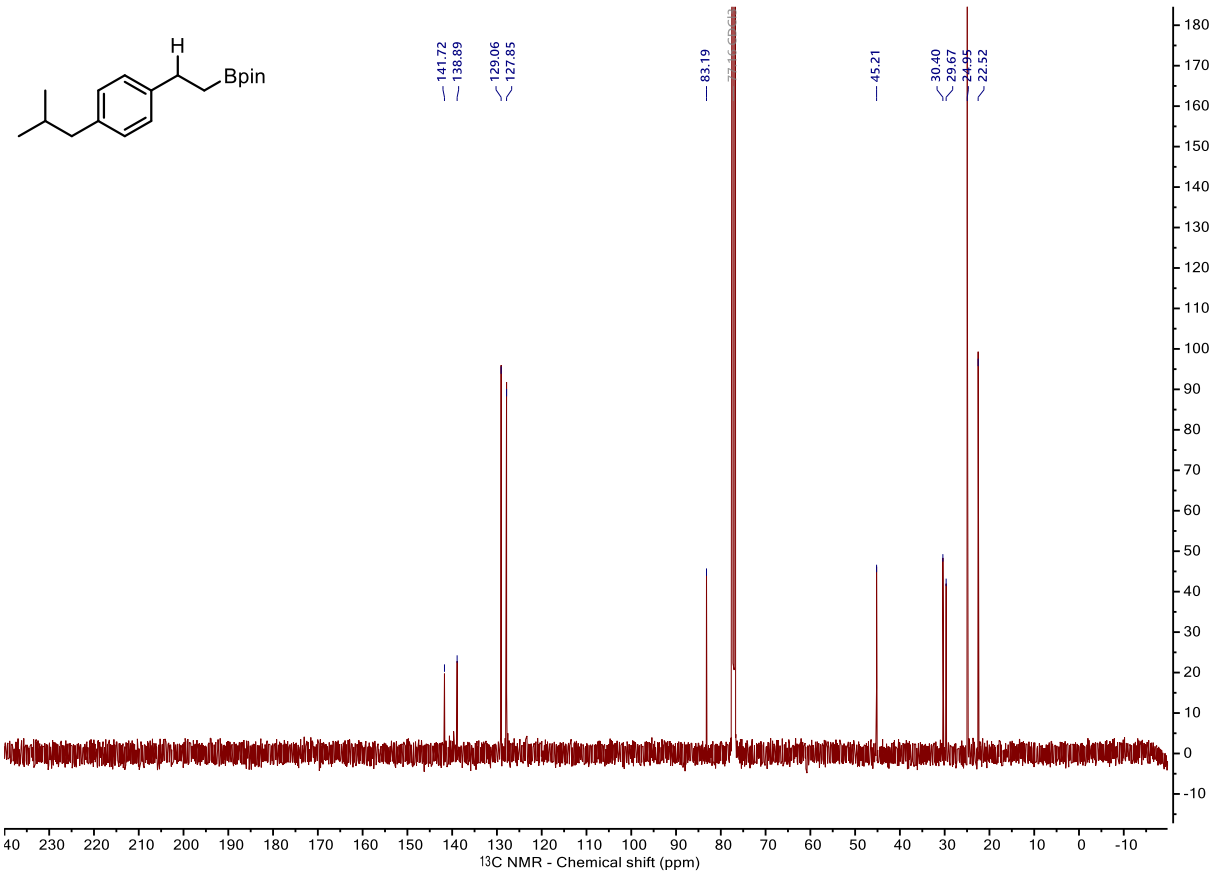

^{13}C {^{1}H} NMR (126 MHz, Chloroform-*d*) of **2-1n**

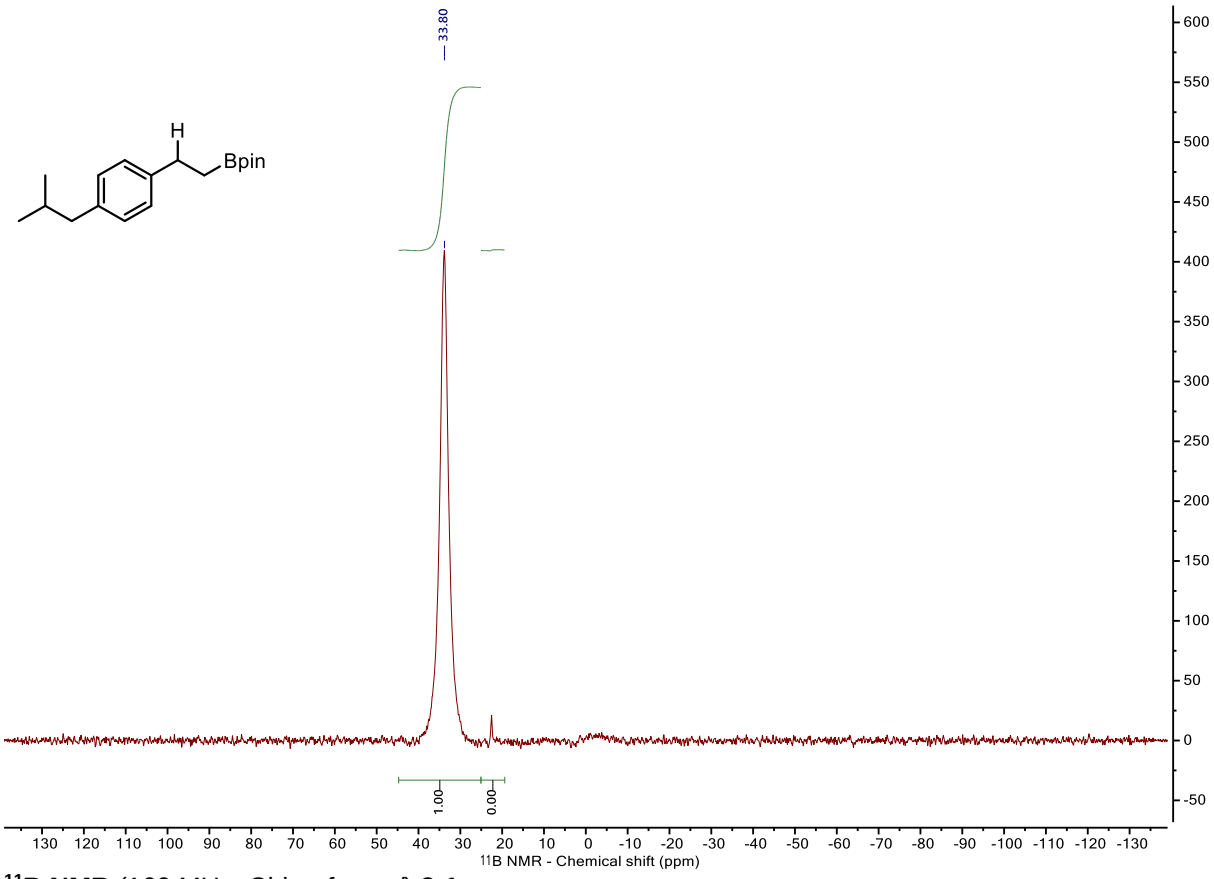

^{11}B NMR (160 MHz, Chloroform-*d*) **2-1n**

2-1h; 2-(3-(Benzo[d][1,3]dioxol-5-yl)propyl)-4,4,5,5-tetramethyl-1,3,2-dioxaborolane (ABG-0368)

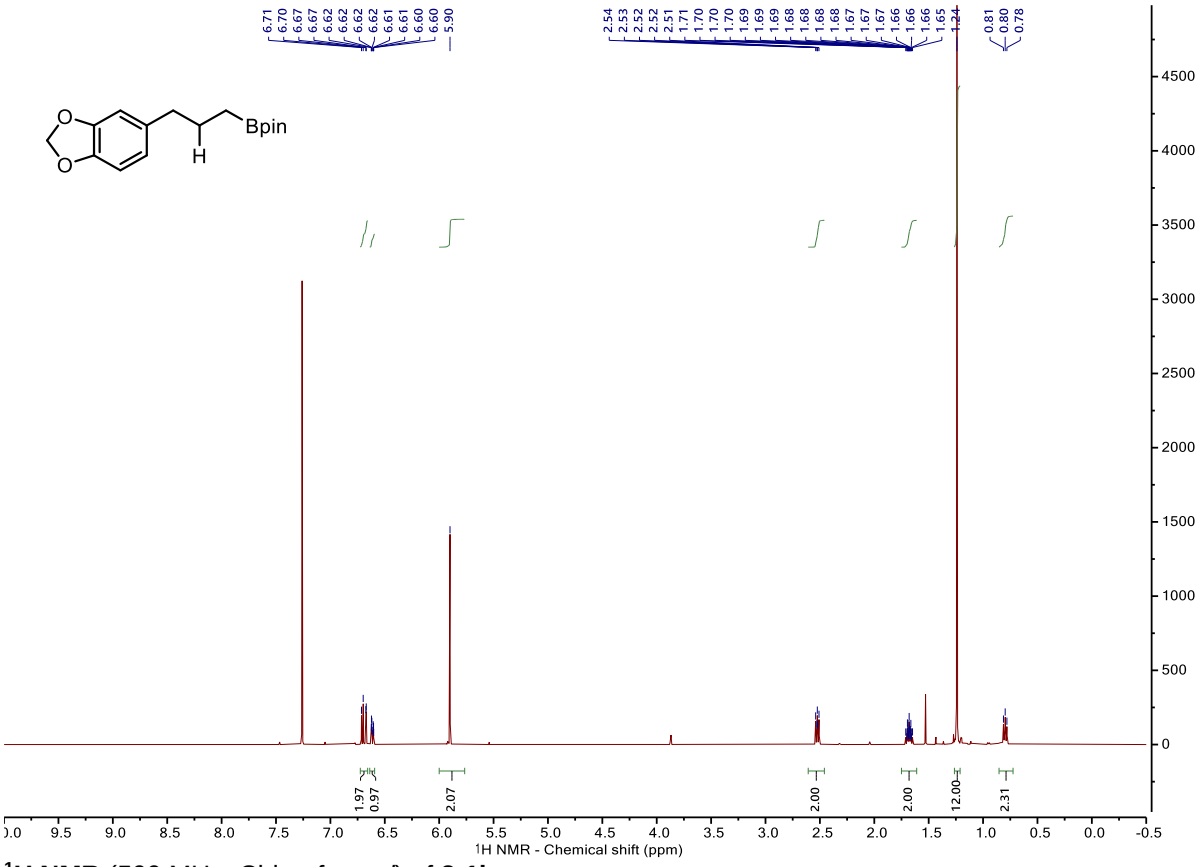

^{1}H NMR (500 MHz, Chloroform-*d*) of **2-1h**

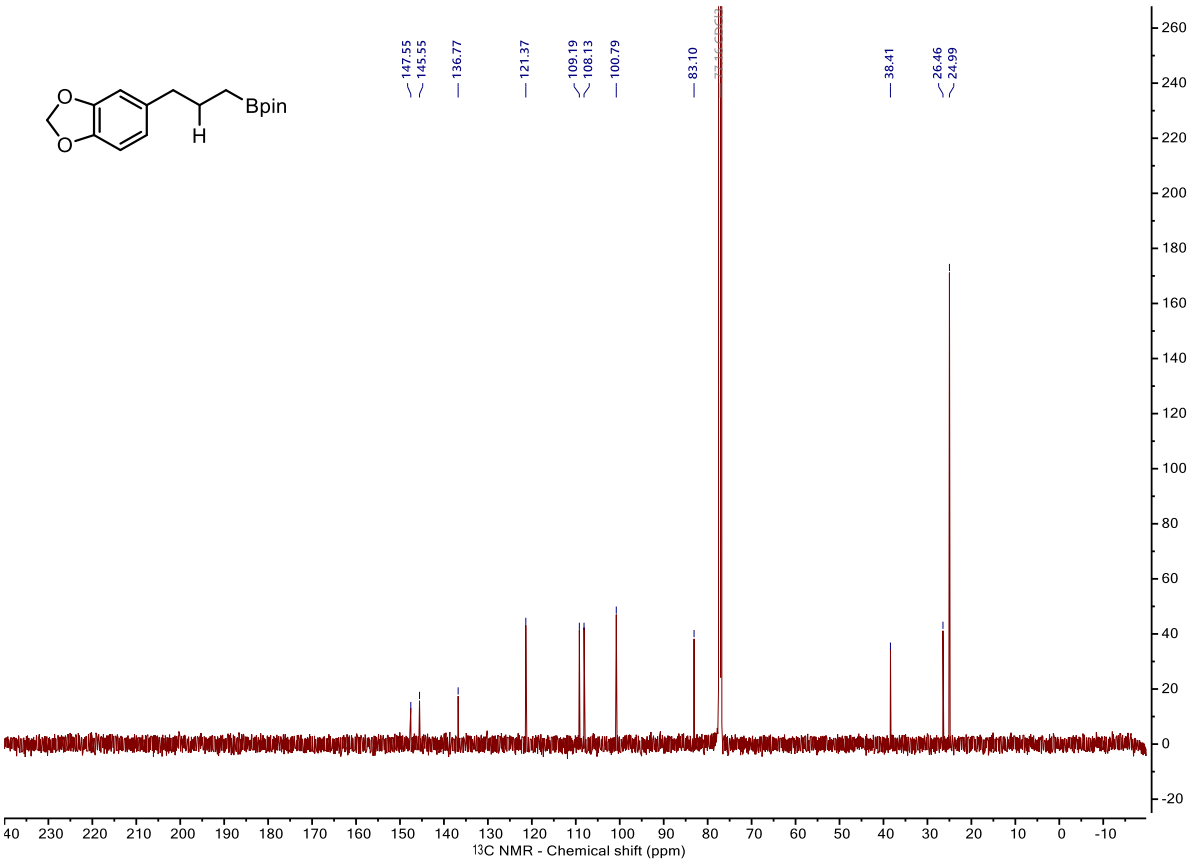

^{13}C {^{1}H} NMR (126 MHz, Chloroform-*d*) of **2-1h**

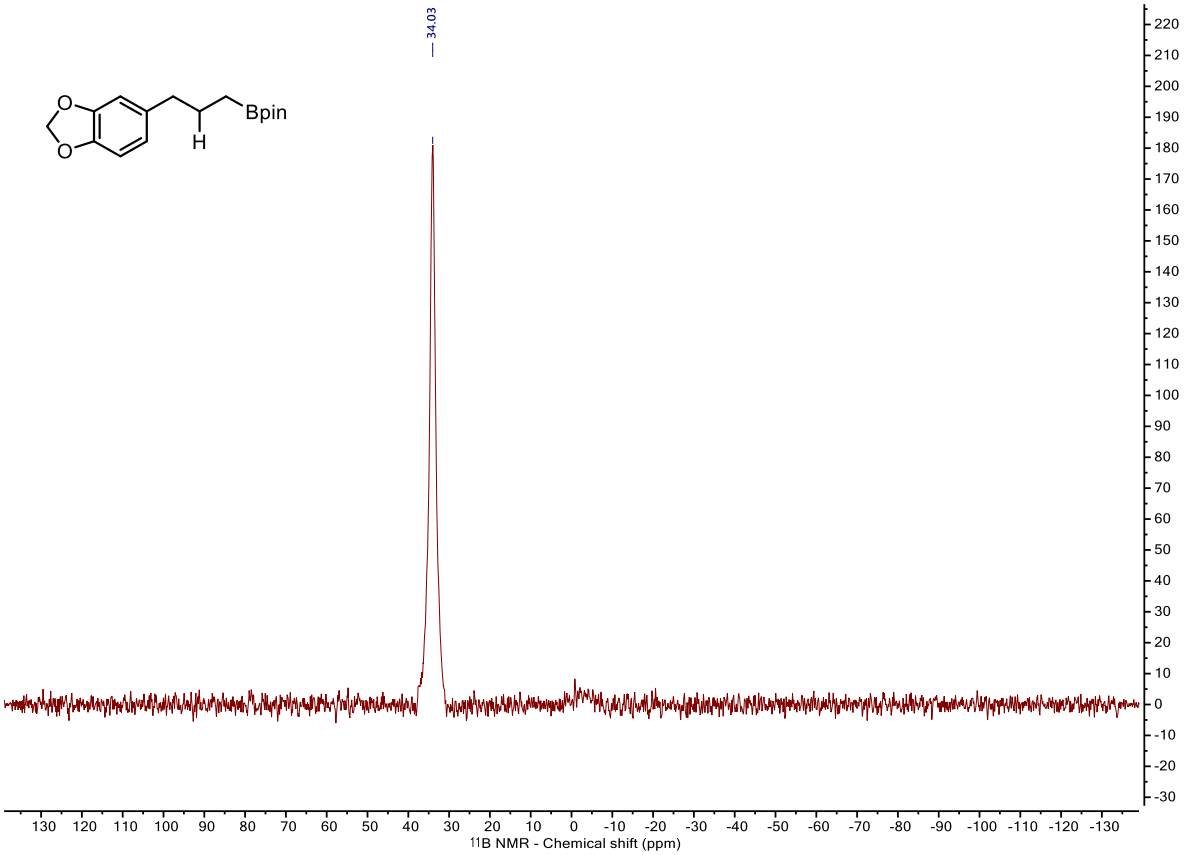

^{11}B NMR (160 MHz, Chloroform-*d*) of **2-1h**

2-1t; 4,4,5,5-tetramethyl-2-(2-methyl-pentyl)-[1,3,2]dioxaborolane (ABG-0335)

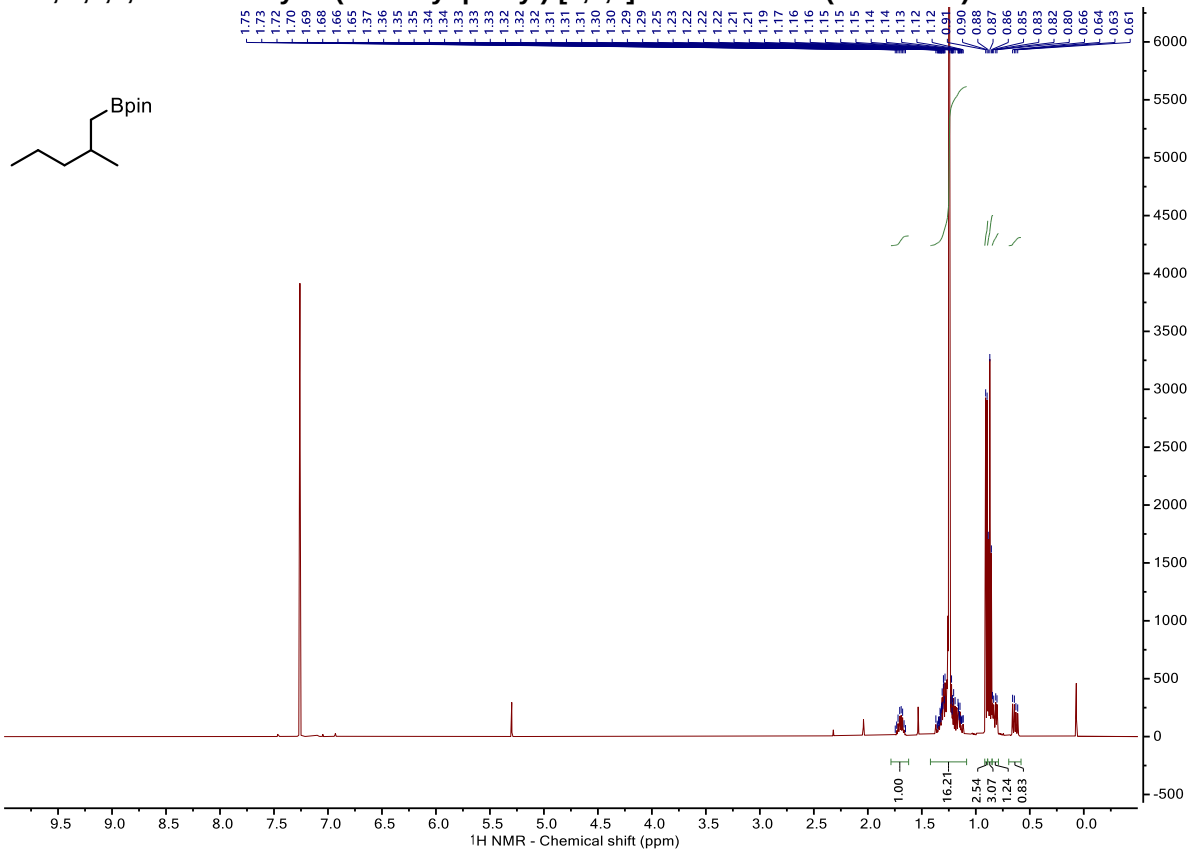

^{1}H NMR (500 MHz, Chloroform-*d*) of **2-1t**

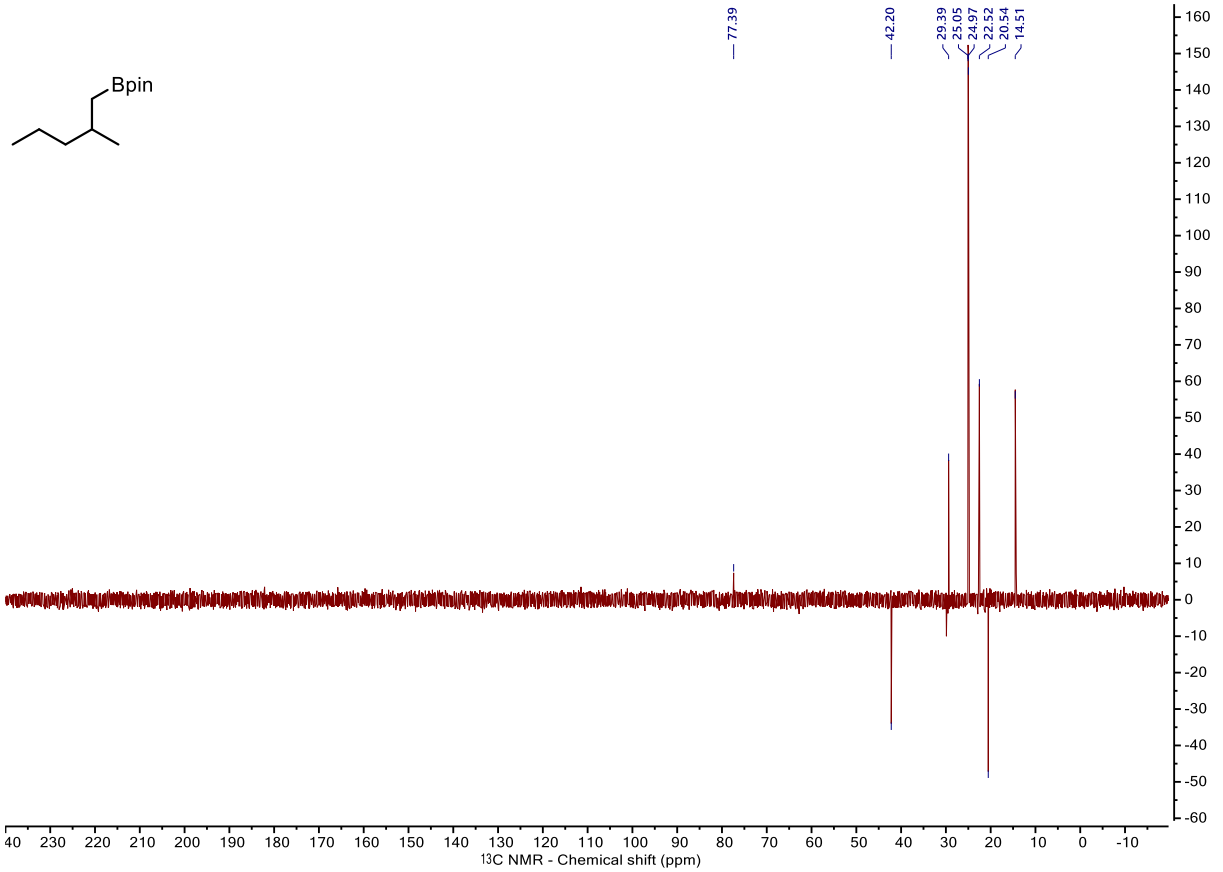

^{13}C {^{1}H} NMR (126 MHz, Chloroform-*d*) of **2-1t**

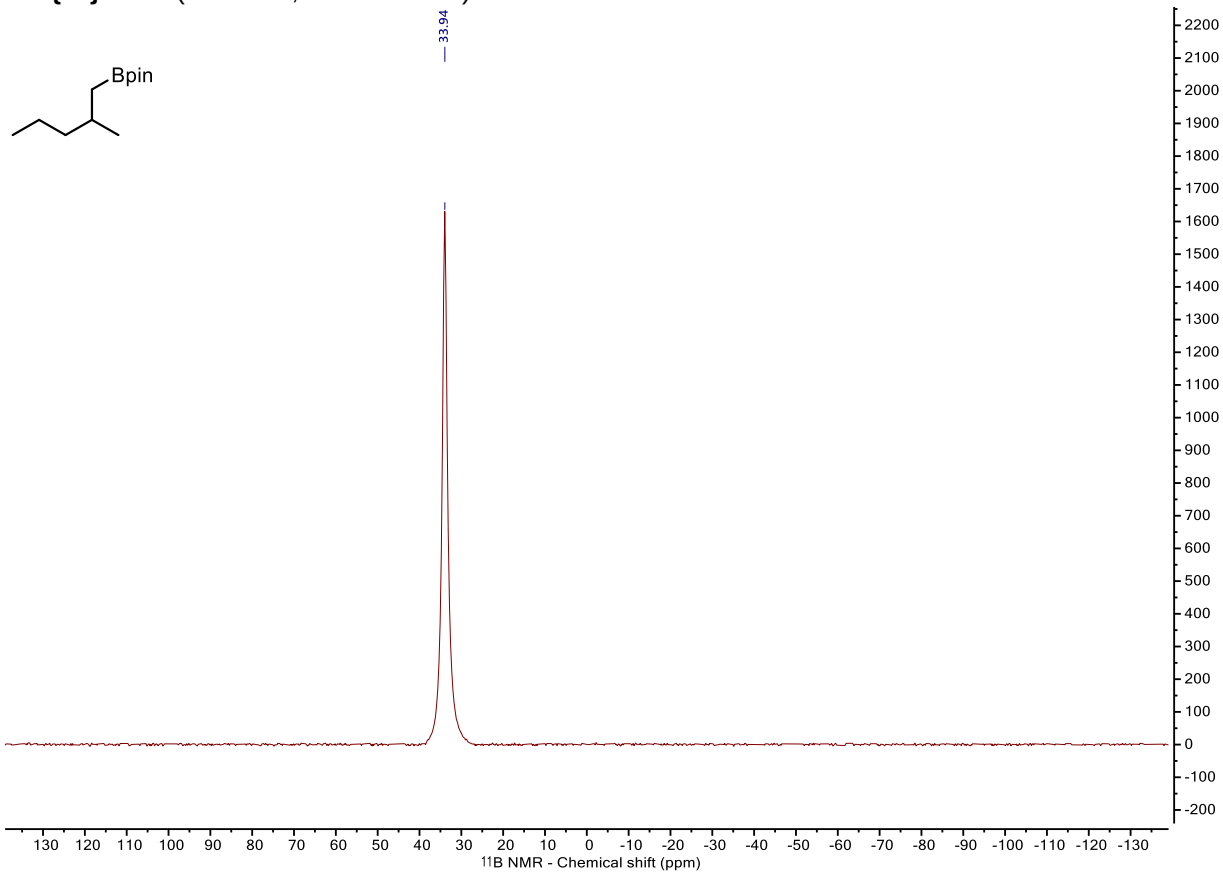

^{11}B NMR (160 MHz, Chloroform-*d*) of **2-1t**

2-1u; (±)2-(2-(4-methylcyclohex-3-en-1-yl)propyl)-4,4,5,5-tetramethyl-1,3,2-dioxaborolane (ABG-0343)

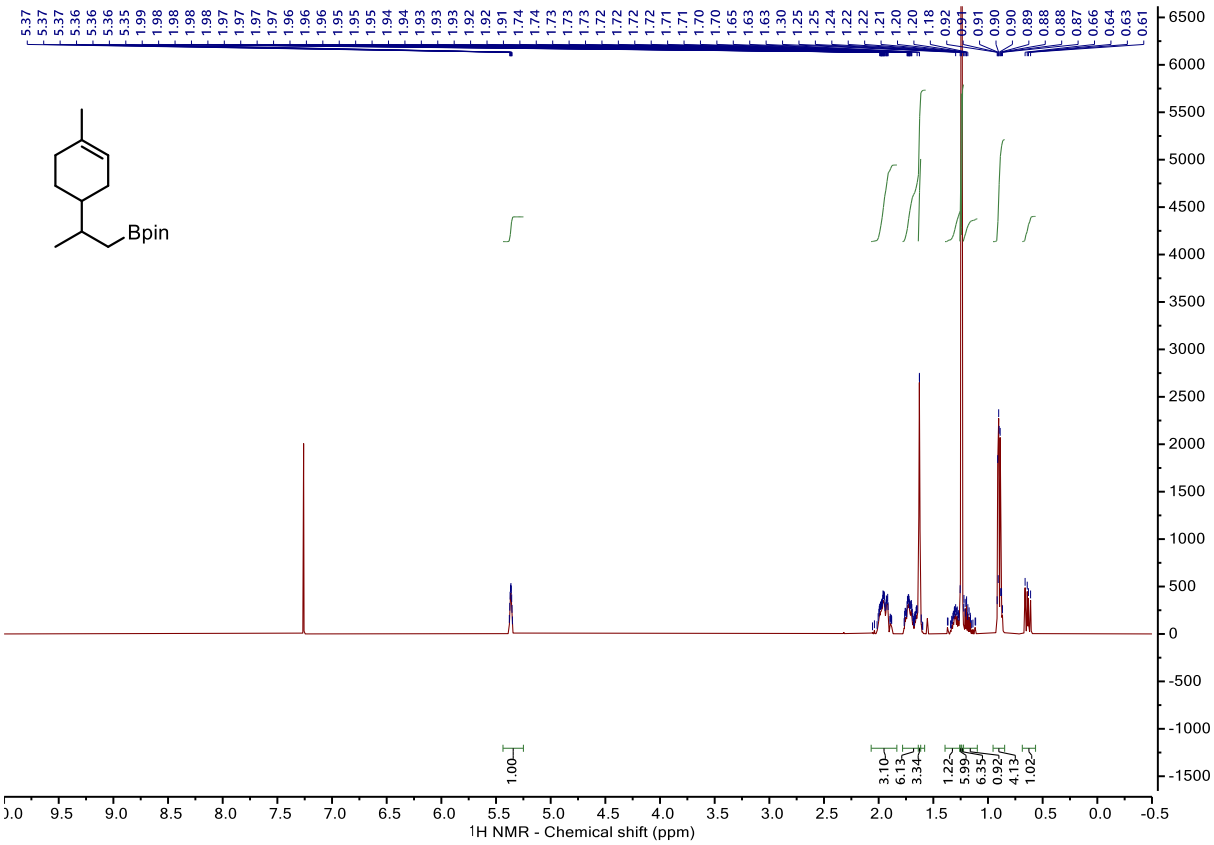

^{1}H NMR (500 MHz, Chloroform-*d*) of **2-1u**

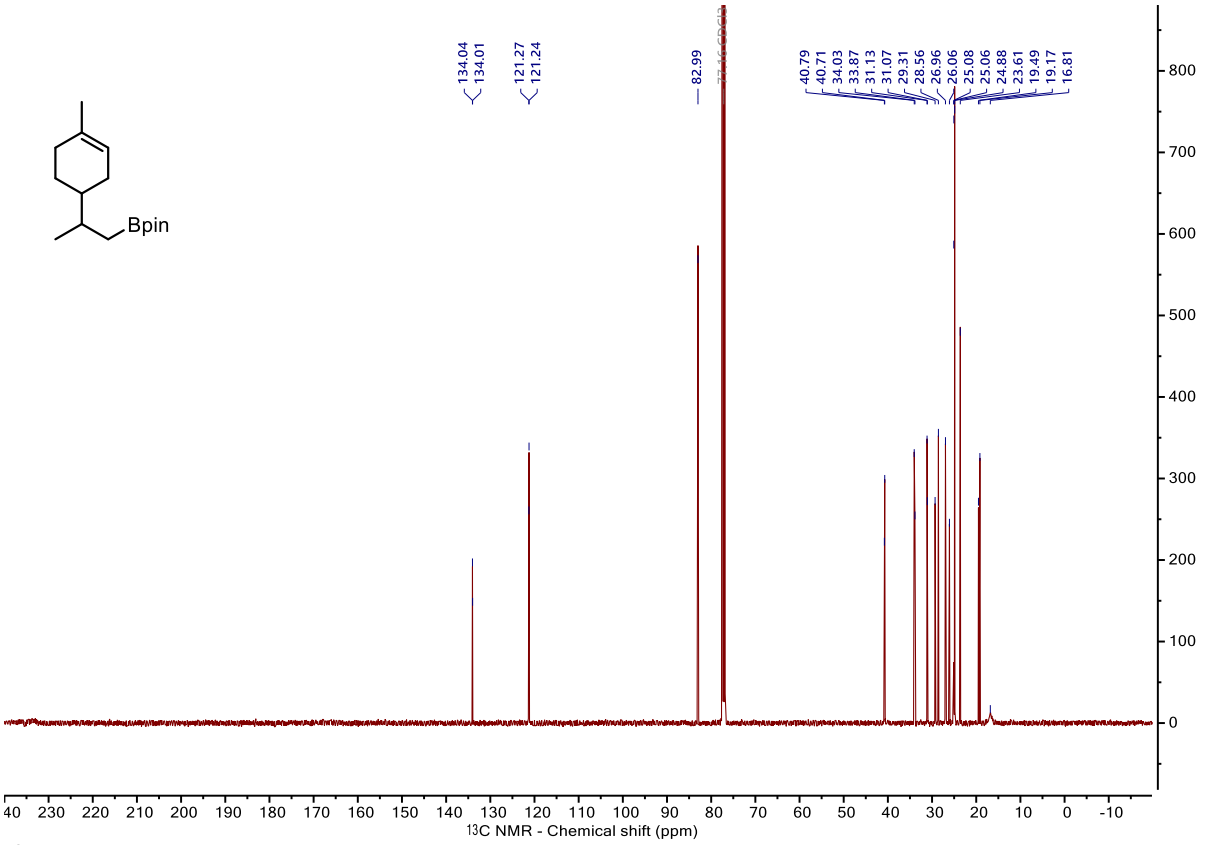

^{13}C {^{1}H} NMR (126 MHz, Chloroform-*d*) of **2-1u**

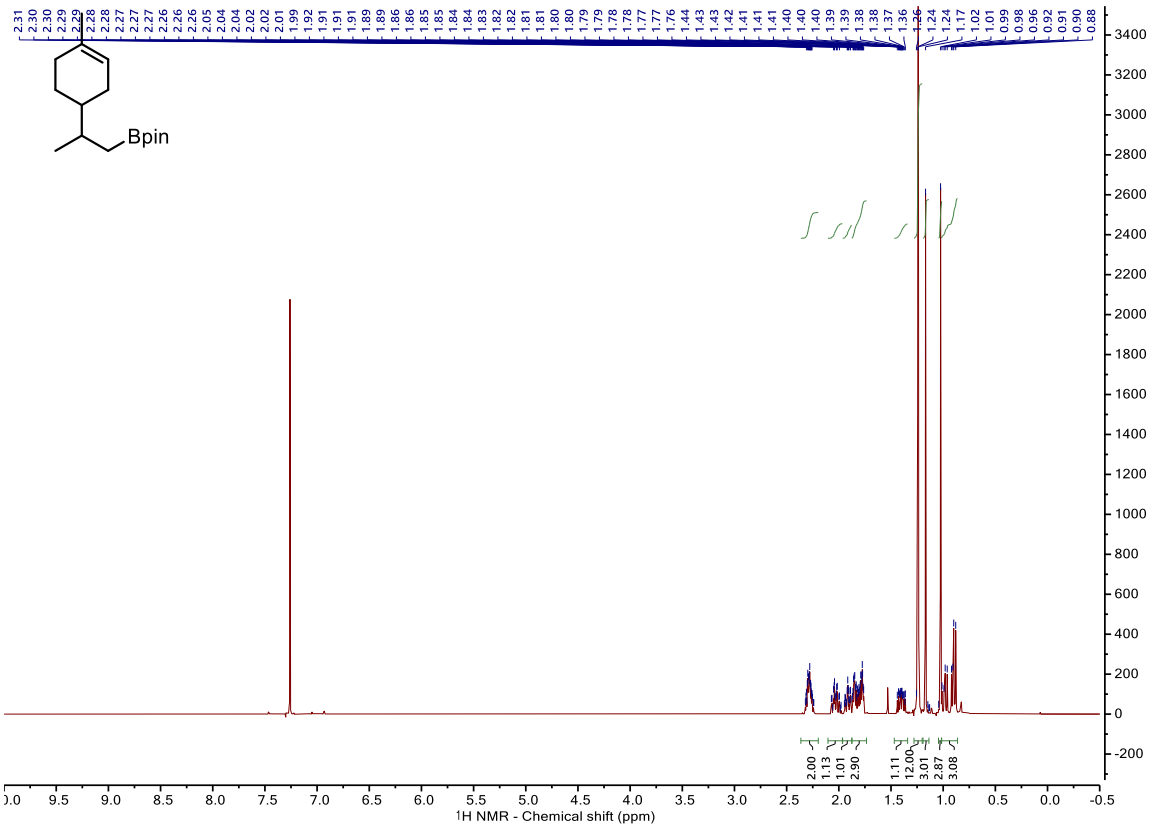

^{11}B NMR (160 MHz, Chloroform-*d*) of **2-1u**

2-1v; 2-(((1S,5S)-6,6-dimethylbicyclo[3.1.1]heptan-2-yl)methyl)-4,4,5,5-tetramethyl-1,3,2-dioxaborolane (ABG-0344)

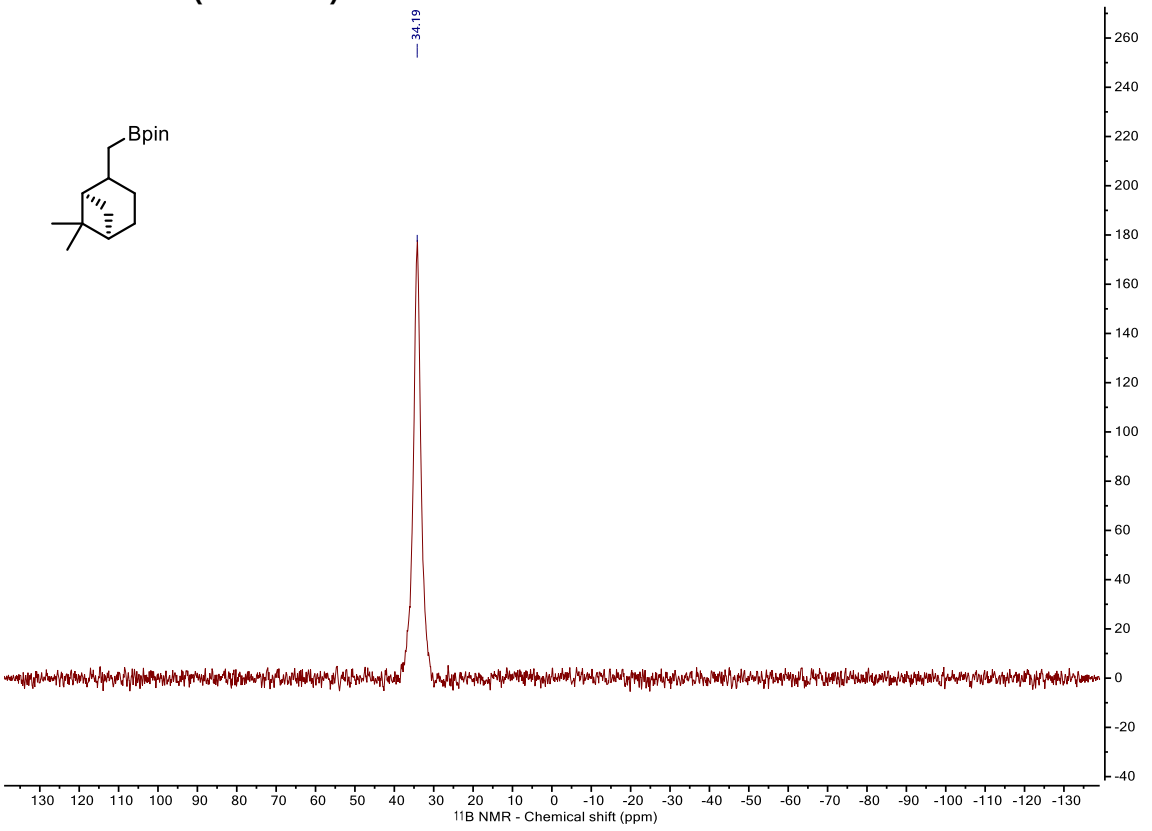

^{1}H NMR (500 MHz, Chloroform-*d* of **2-1v**

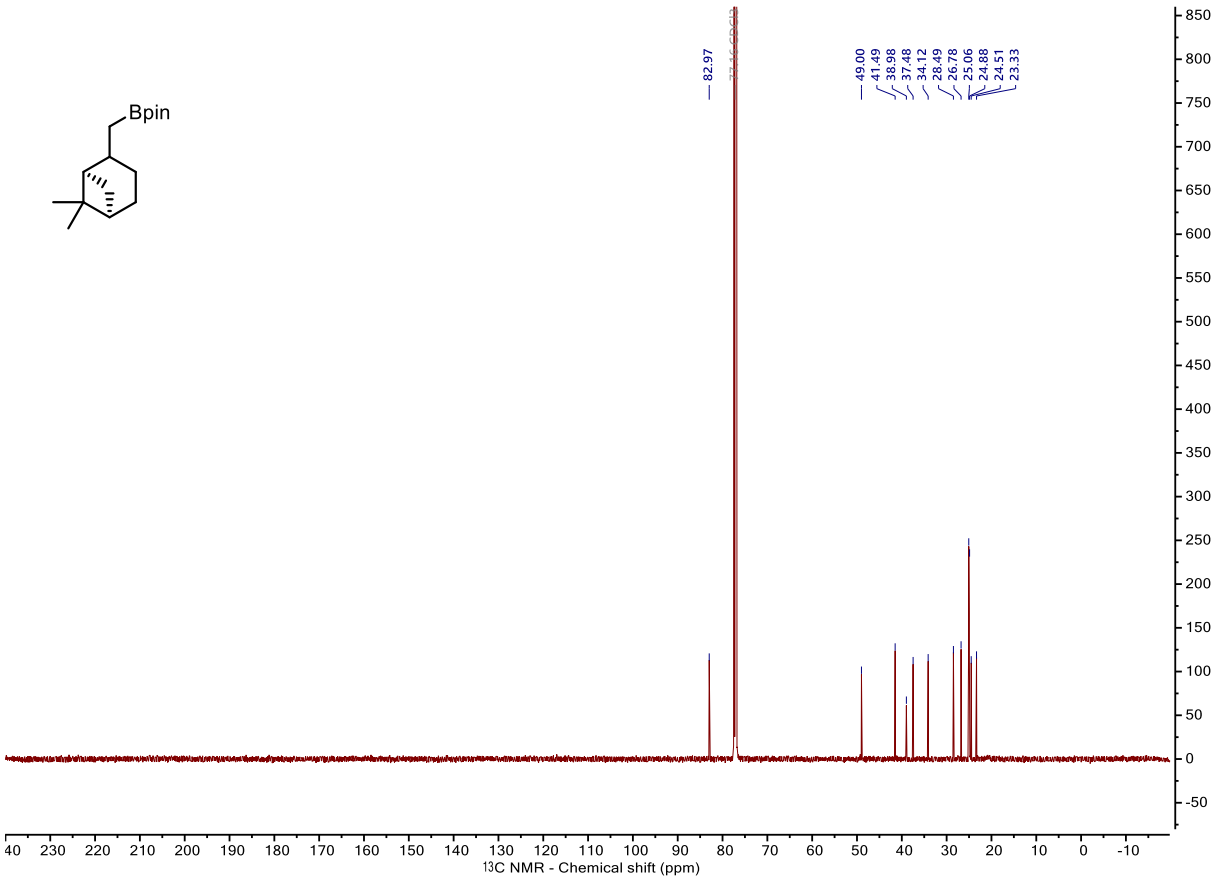

^{13}C {^{1}H} NMR (126 MHz, Chloroform-*d*) of **2-1v**

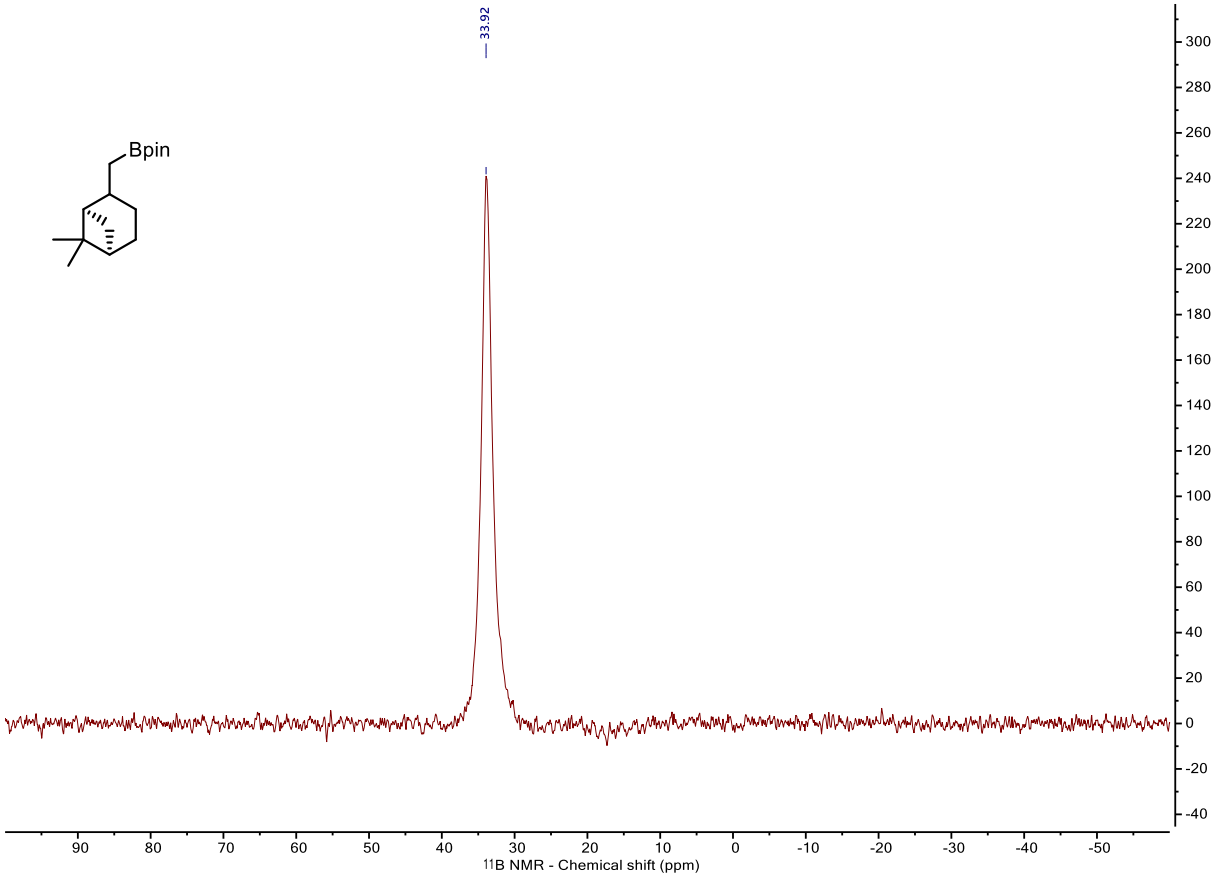

^{11}B NMR (160 MHz, Chloroform-*d*) of **2-1v**

2-1w; 2-((R)-2-((2R,8R,8aS)-8,8a-dimethyl-1,2,3,4,6,7,8,8a-octahydronaphthalen-2-yl)propyl)-4,4,5,5-tetramethyl-1,3,2-dioxaborolane (ABG-0362)

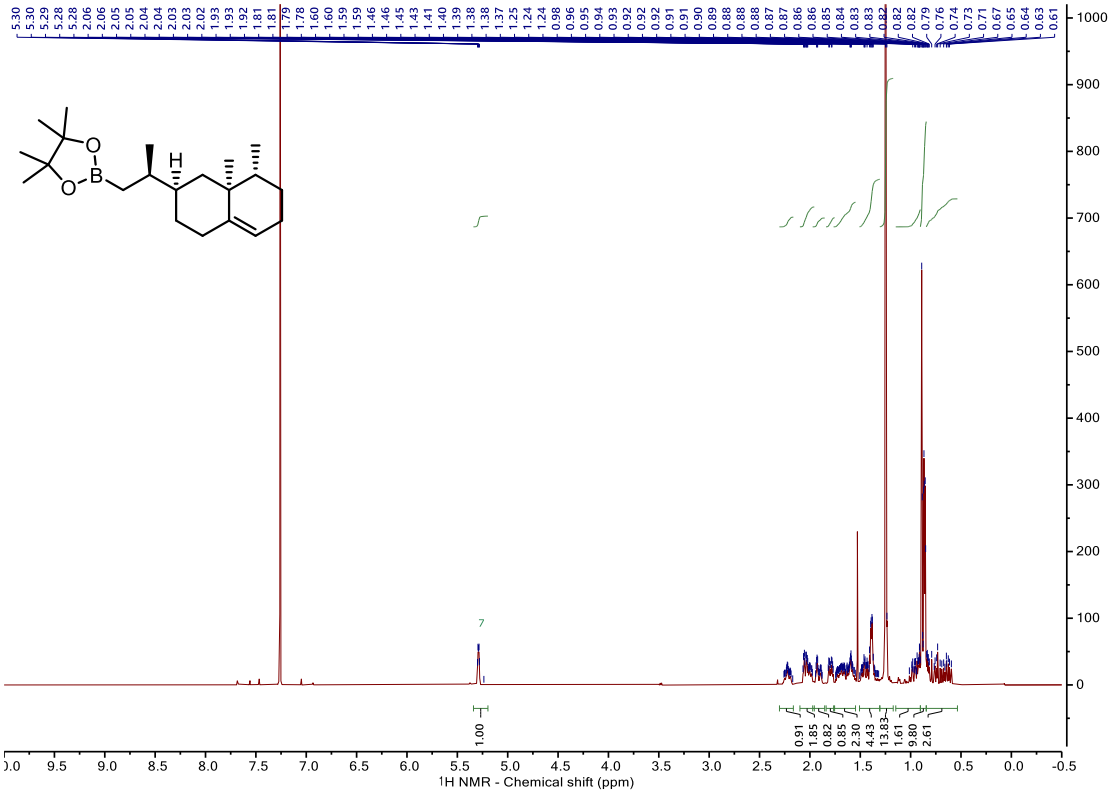

^{1}H NMR (500 MHz, Chloroform-*d*) of **2-1w**

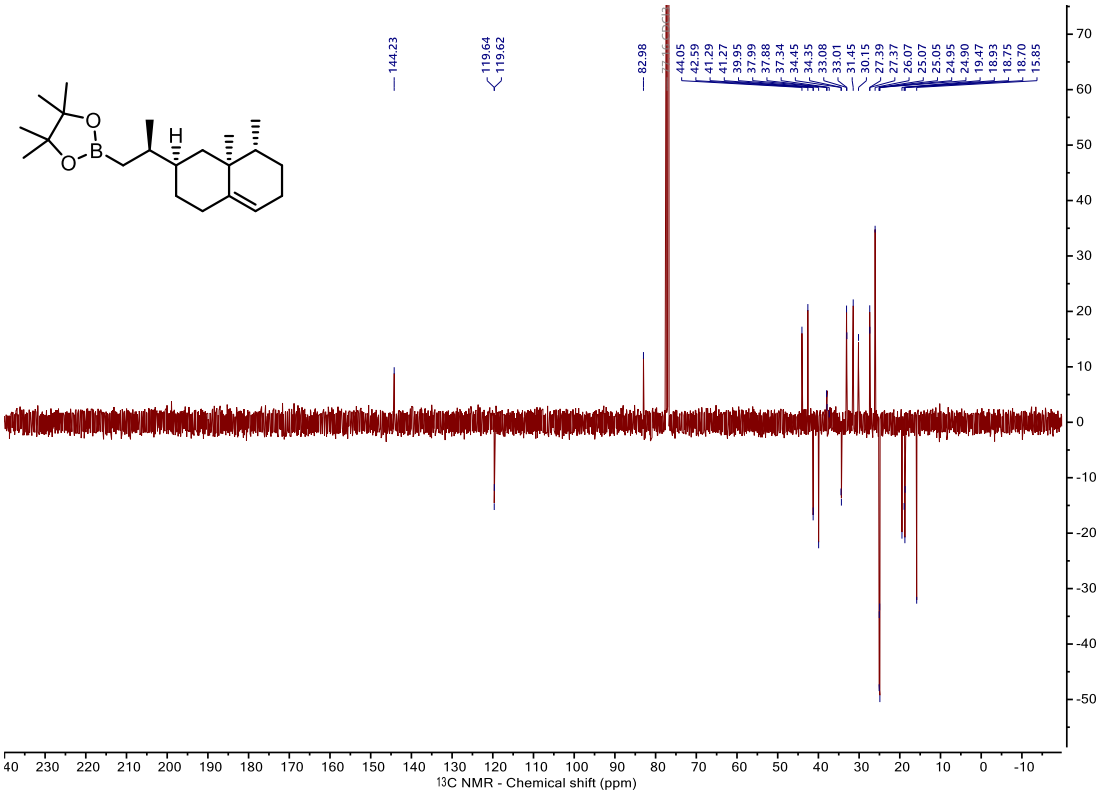

^{13}C {^{1}H} NMR (126 MHz, Chloroform-*d*) of **2-1w**

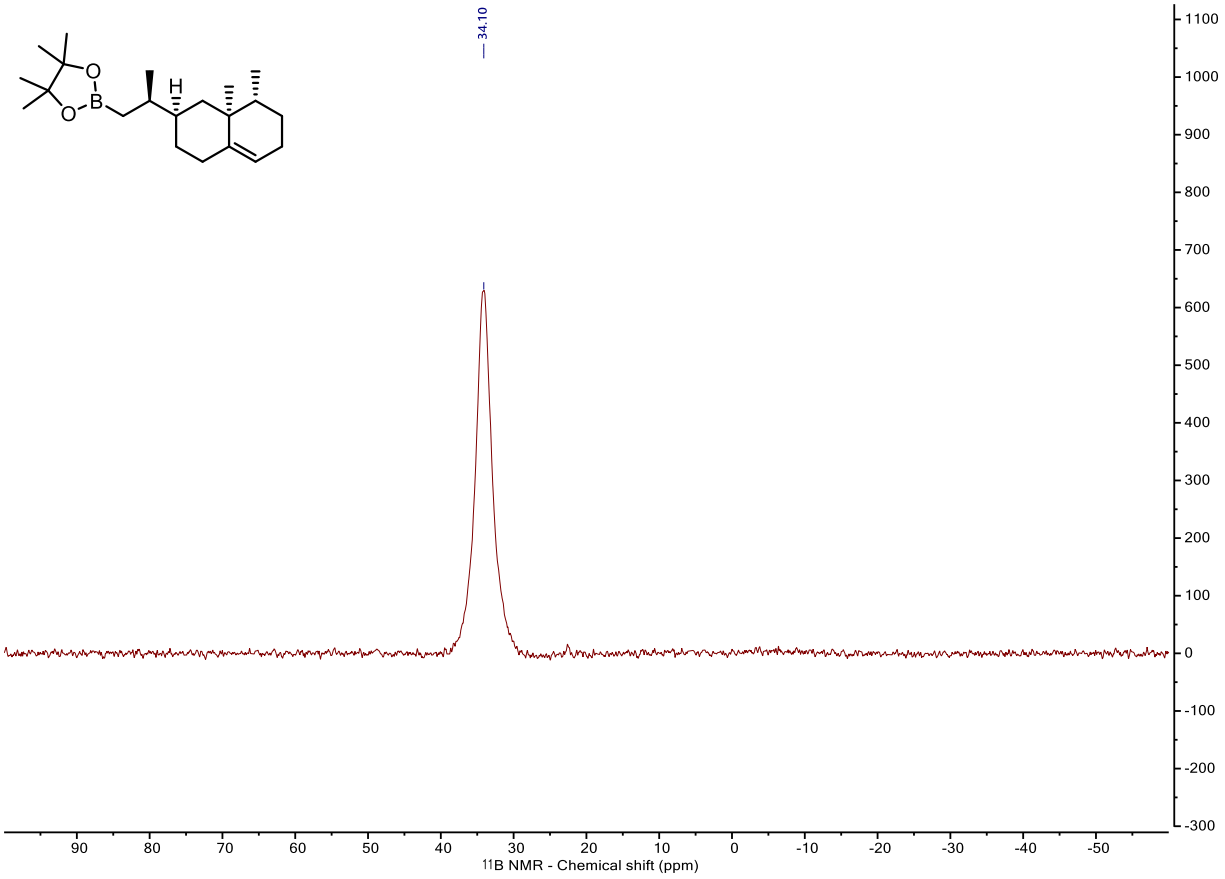

^{11}B NMR (160 MHz, Chloroform-*d*) of **2-1w**

4. RBdan

4-1a; 2-(phenethyl)-2,3-dihydro-1*H*-naphtho[1,8-*de*][1,3,2]diazaborinine (ABG-0550)

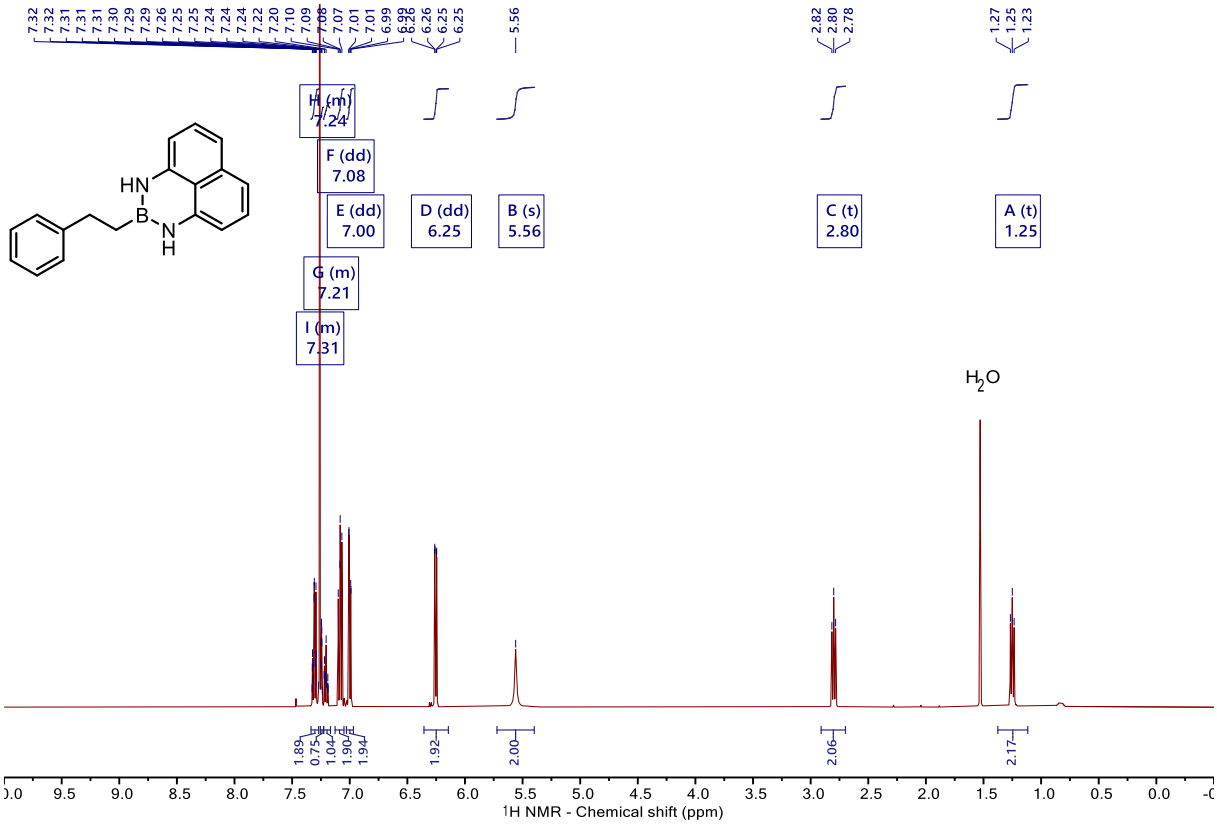

^{1}H NMR (500 MHz, Chloroform-*d*) of **4-1a**

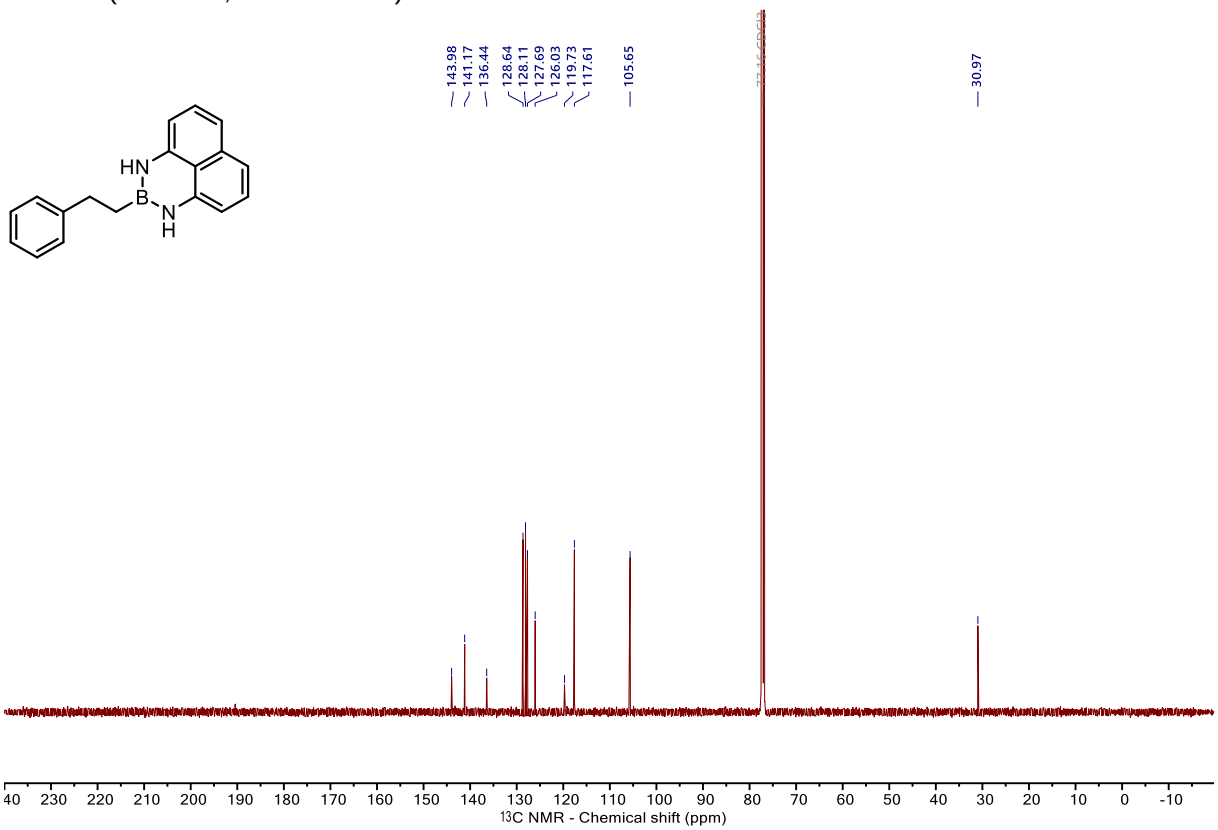

^{13}C {^{1}H} NMR (126 MHz, Chloroform-*d*) of **4-1a**

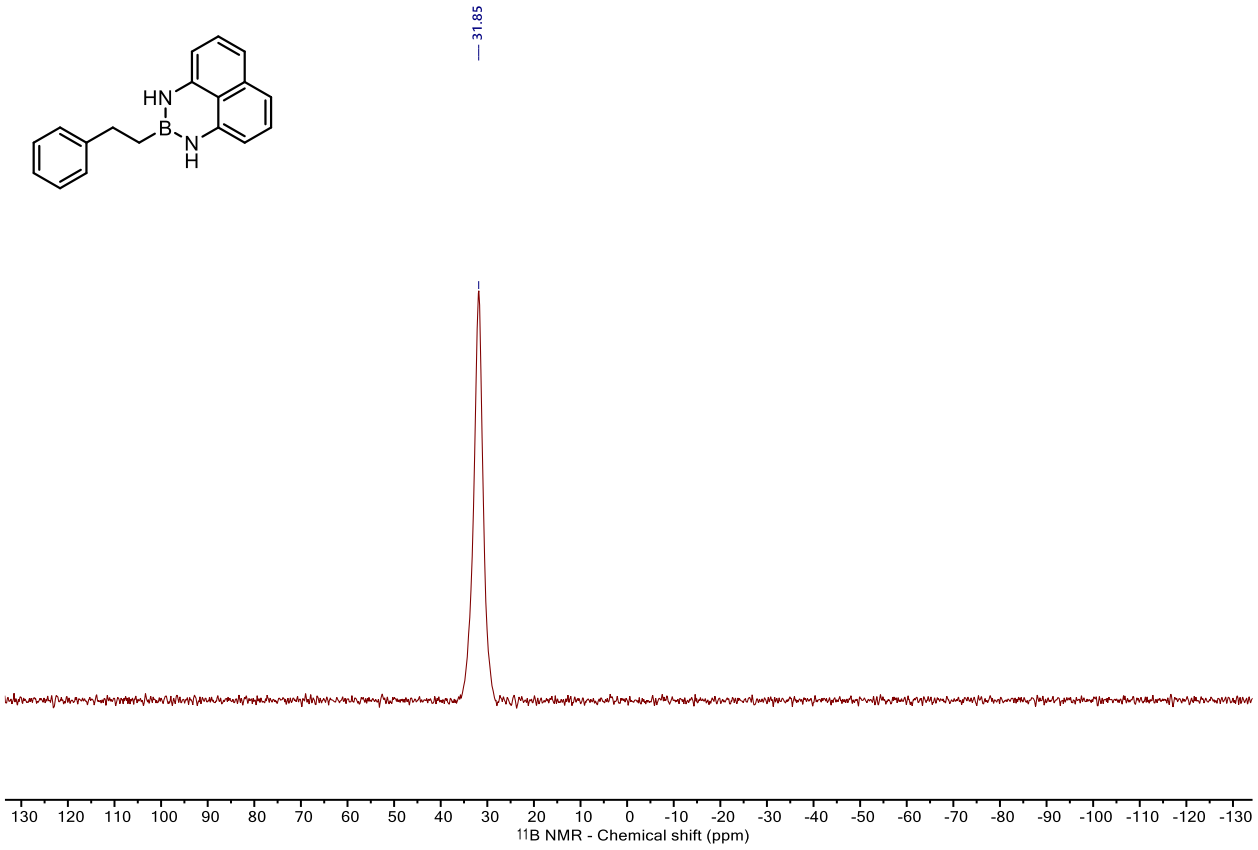

^{11}B NMR (160 MHz, Chloroform-*d*) of **4-1a**

4-1b; 2-(4-(tert-butyl)phenethyl)-2,3-dihydro-1*H*-naphtho[1,8-*de*][1,3,2]diazaborinine (ABG-0384)

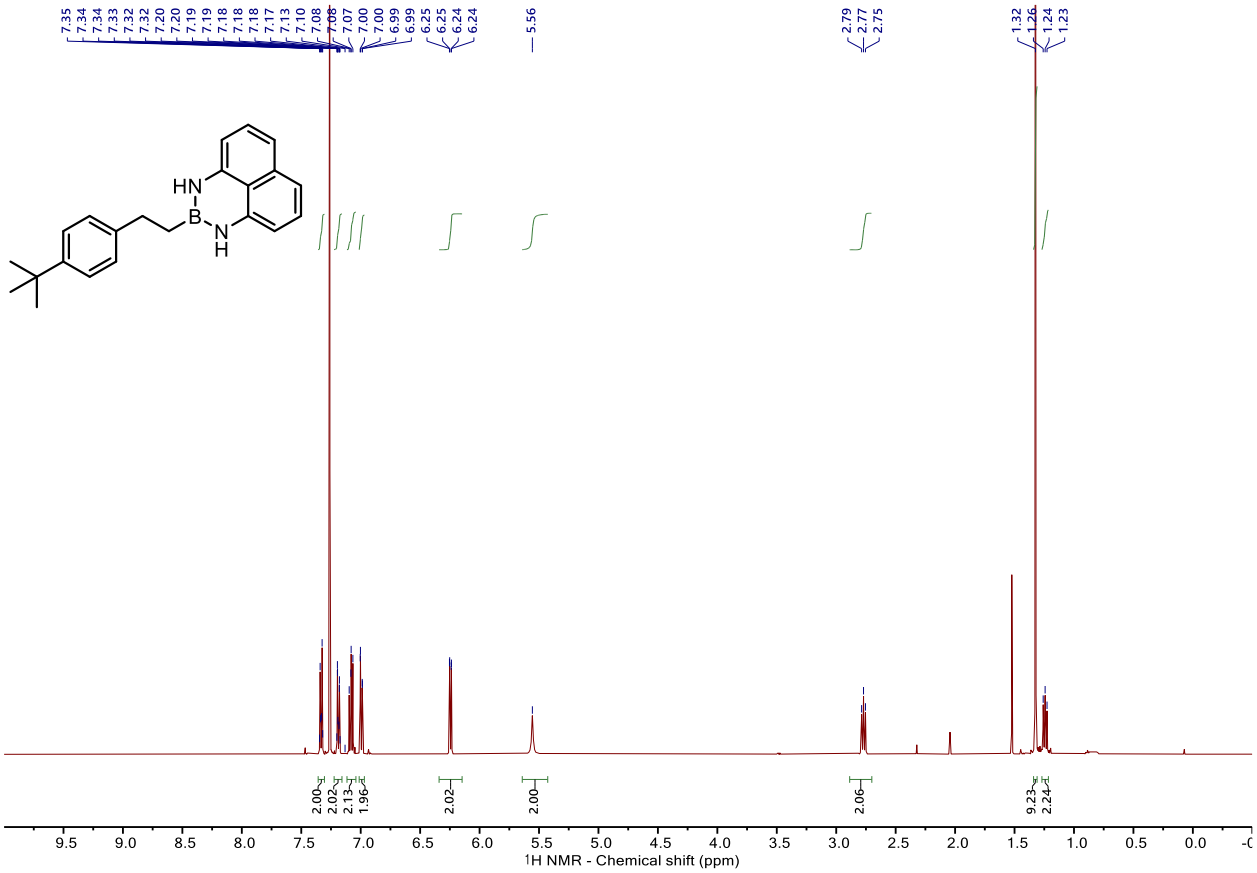

H NMR (500 MHz, Chloroform-*d*) of **4-1b**

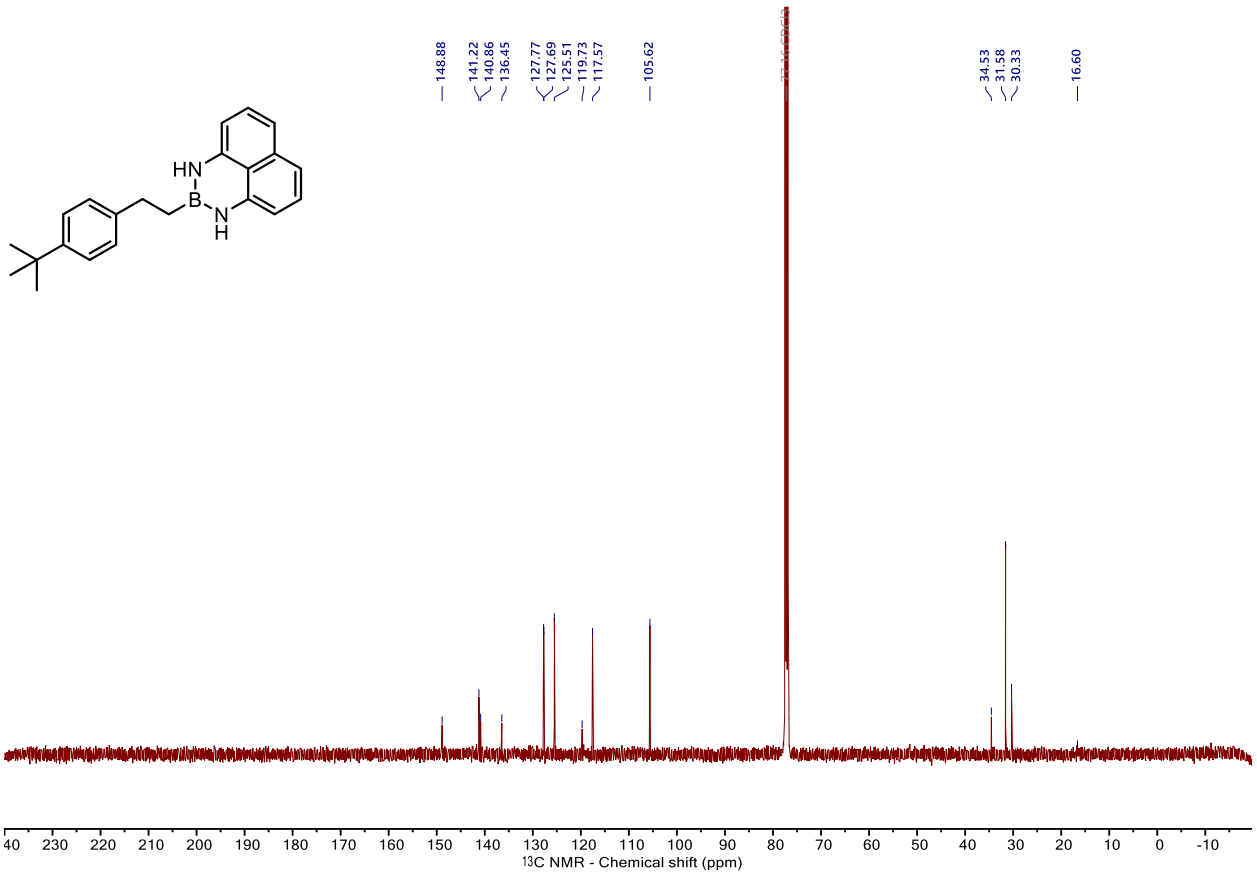

^{13}C {^{1}H} NMR (126 MHz, Chloroform-*d*) of **4-1b**

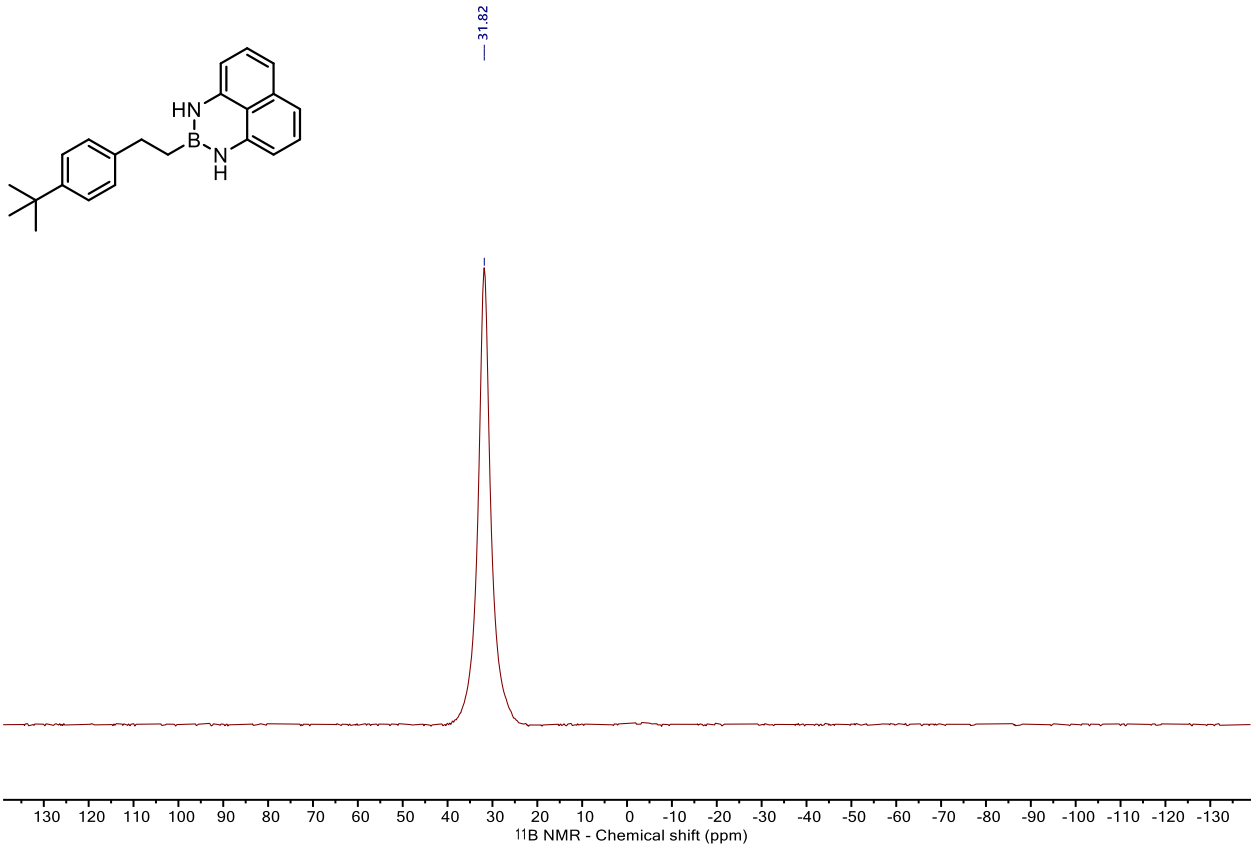

^{11}B NMR (160 MHz, Chloroform-*d*) of **4-1b**

4-1c; 2-(4-isobutylphenethyl)-2,3-dihydro-1*H*-naphtho[1,8-*de*][1,3,2]diazaborinine (ABG-0557)

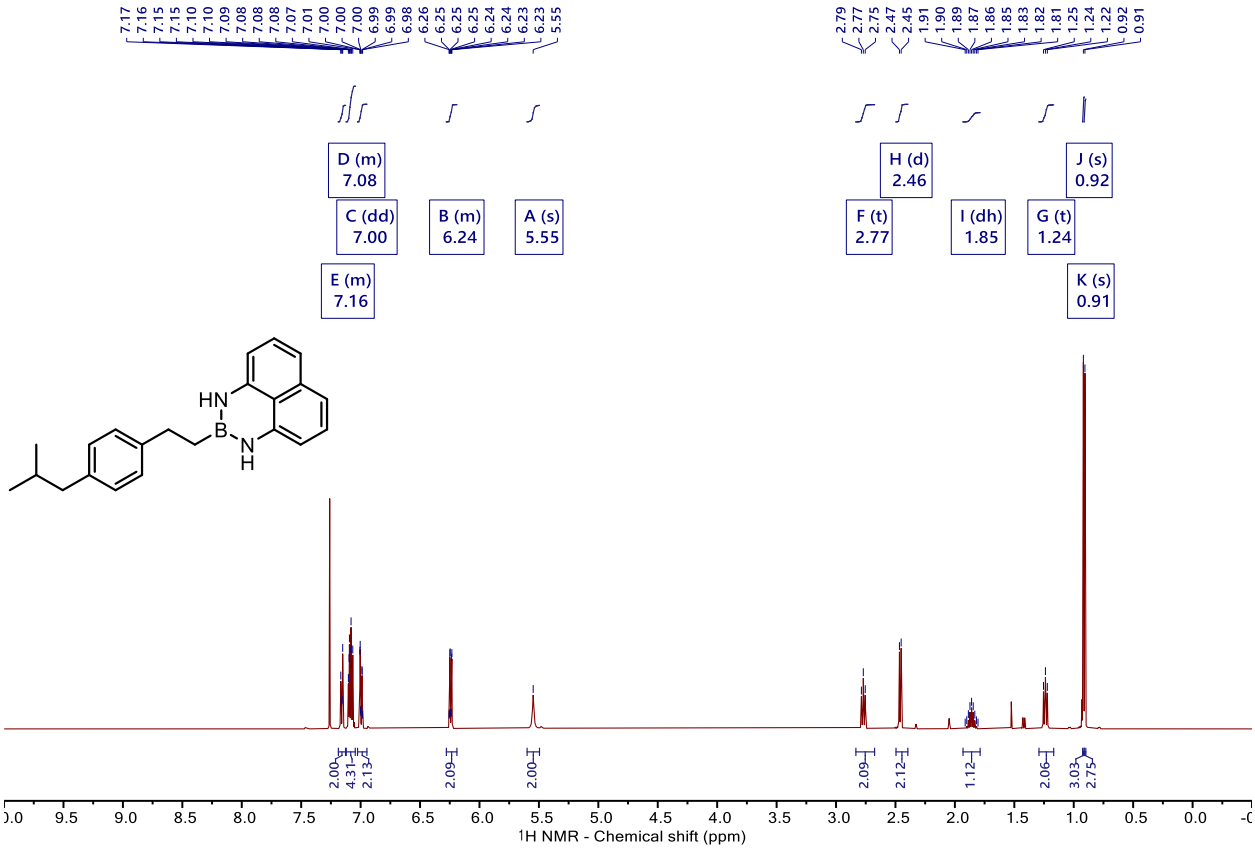

^{1}H NMR (500 MHz, Chloroform-*d*) of **4-1c**

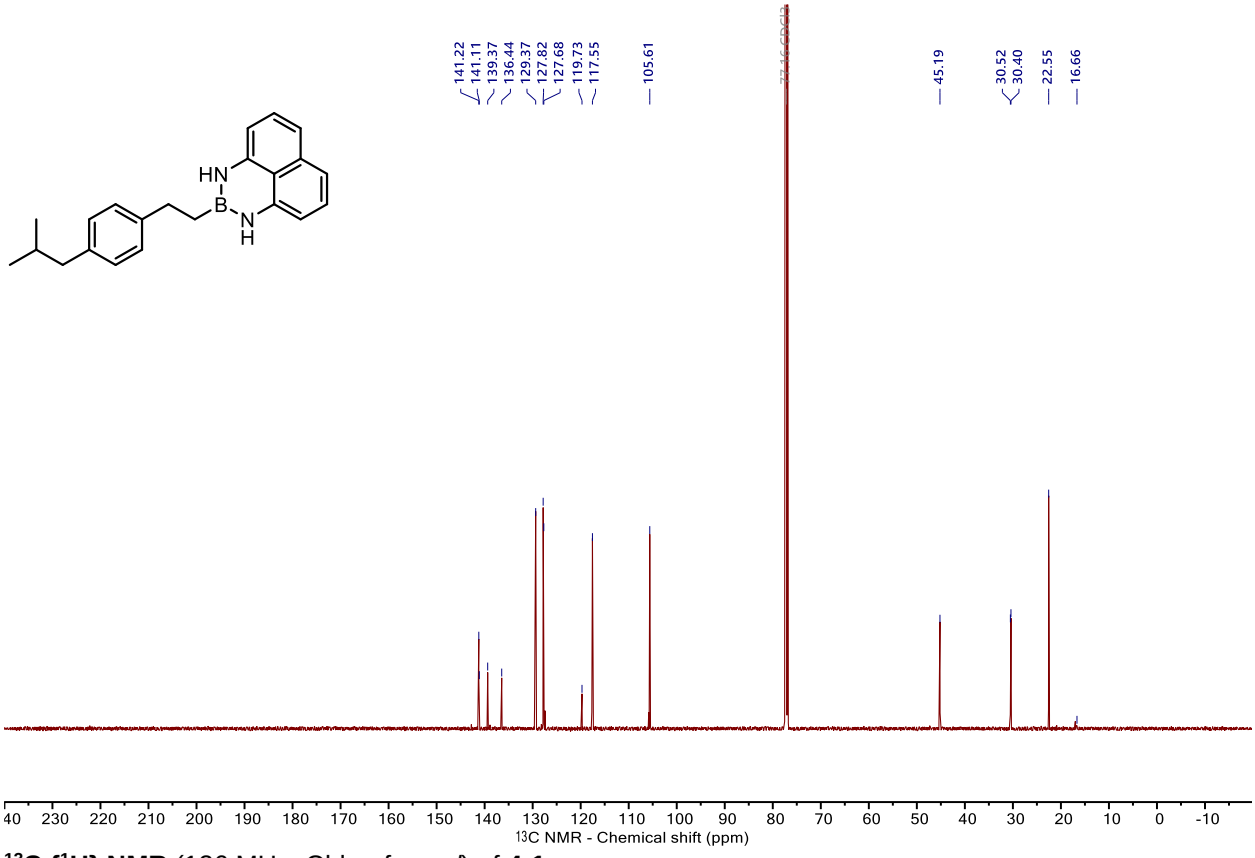

^{13}C {^{1}H} NMR (126 MHz, Chloroform-*d*) of **4-1c**

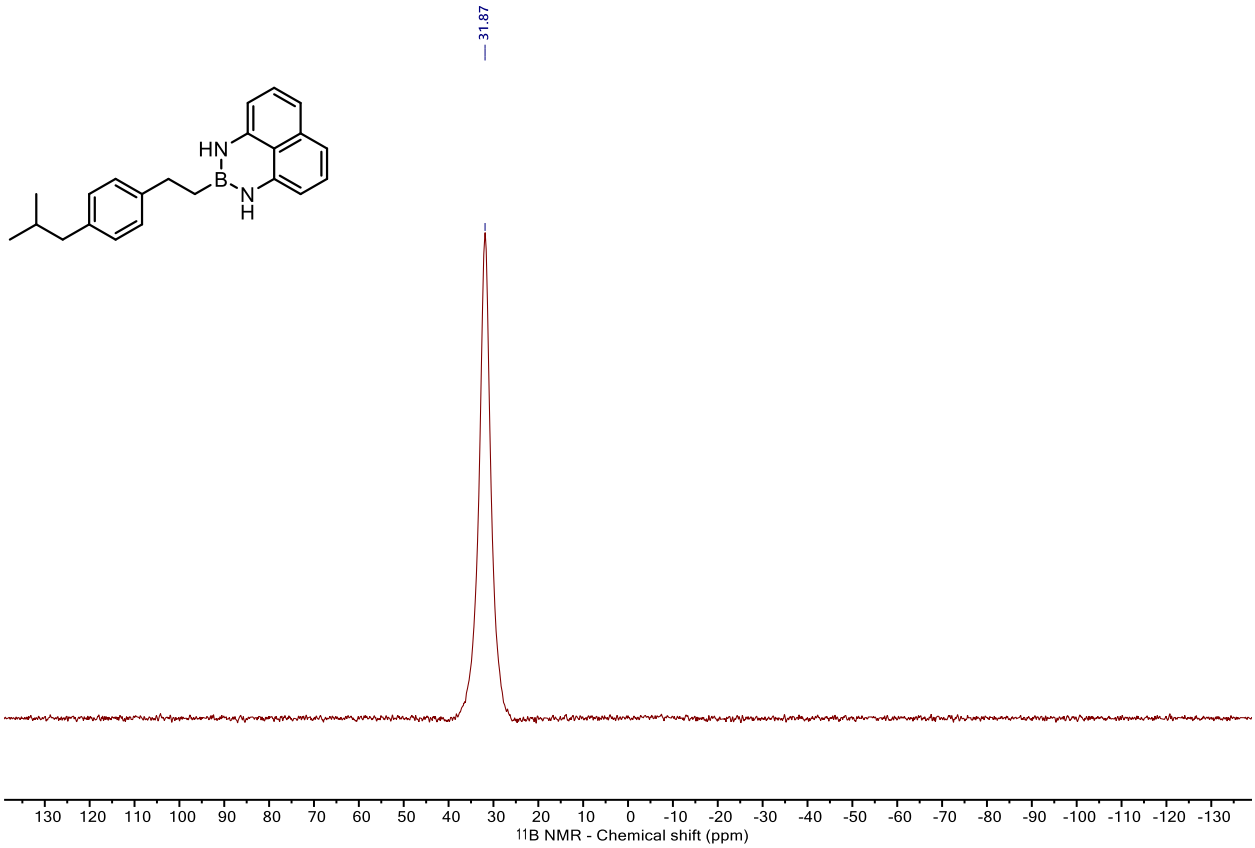

^{11}B NMR (160 MHz, Chloroform-*d*) of **4-1c**

4-1d; 2-(2,4-dimethylphenethyl)-2,3-dihydro-1*H*-naphtho[1,8-*de*][1,3,2]diazaborinine (ABG-0568)

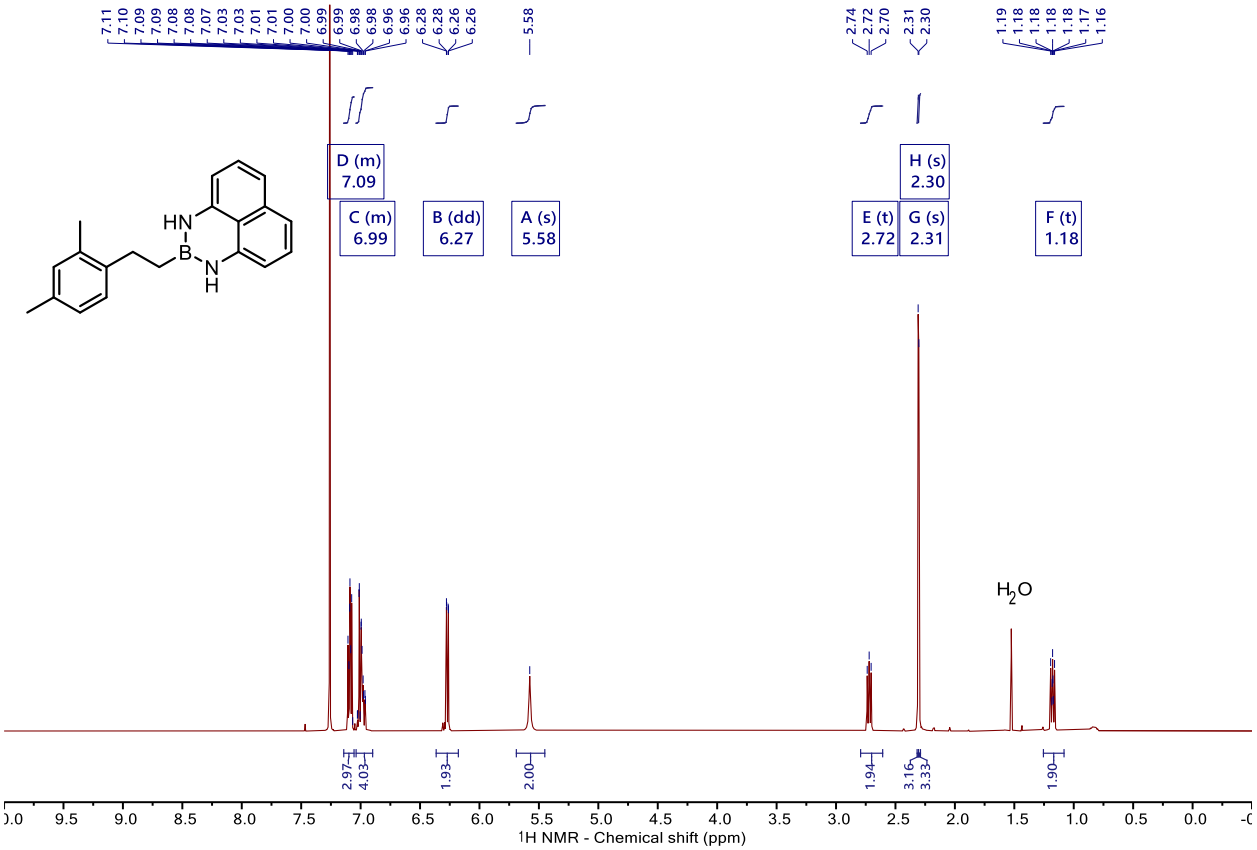

^{1}H NMR (500 MHz, Chloroform-*d*) of **4-1d**

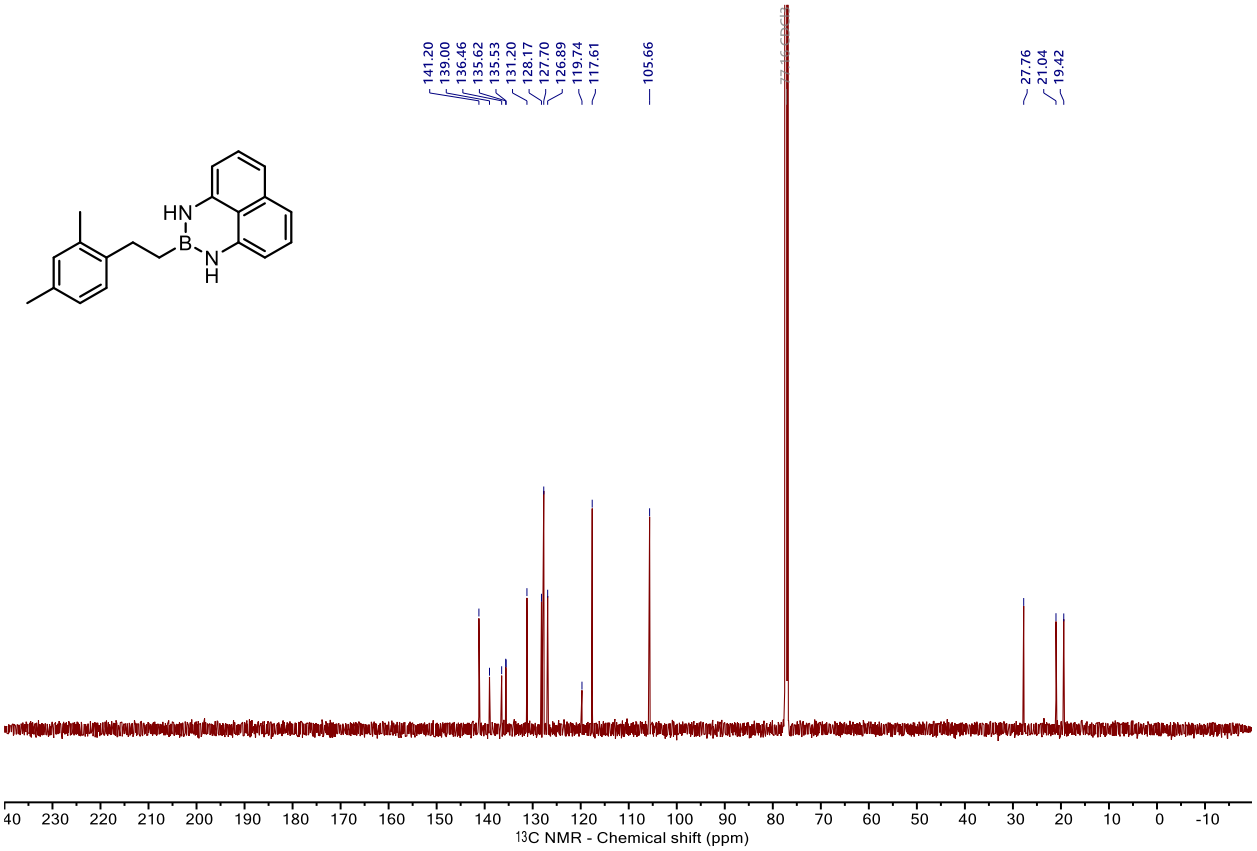

^{13}C {^{1}H} NMR (126 MHz, Chloroform-*d*) of **4-1d**

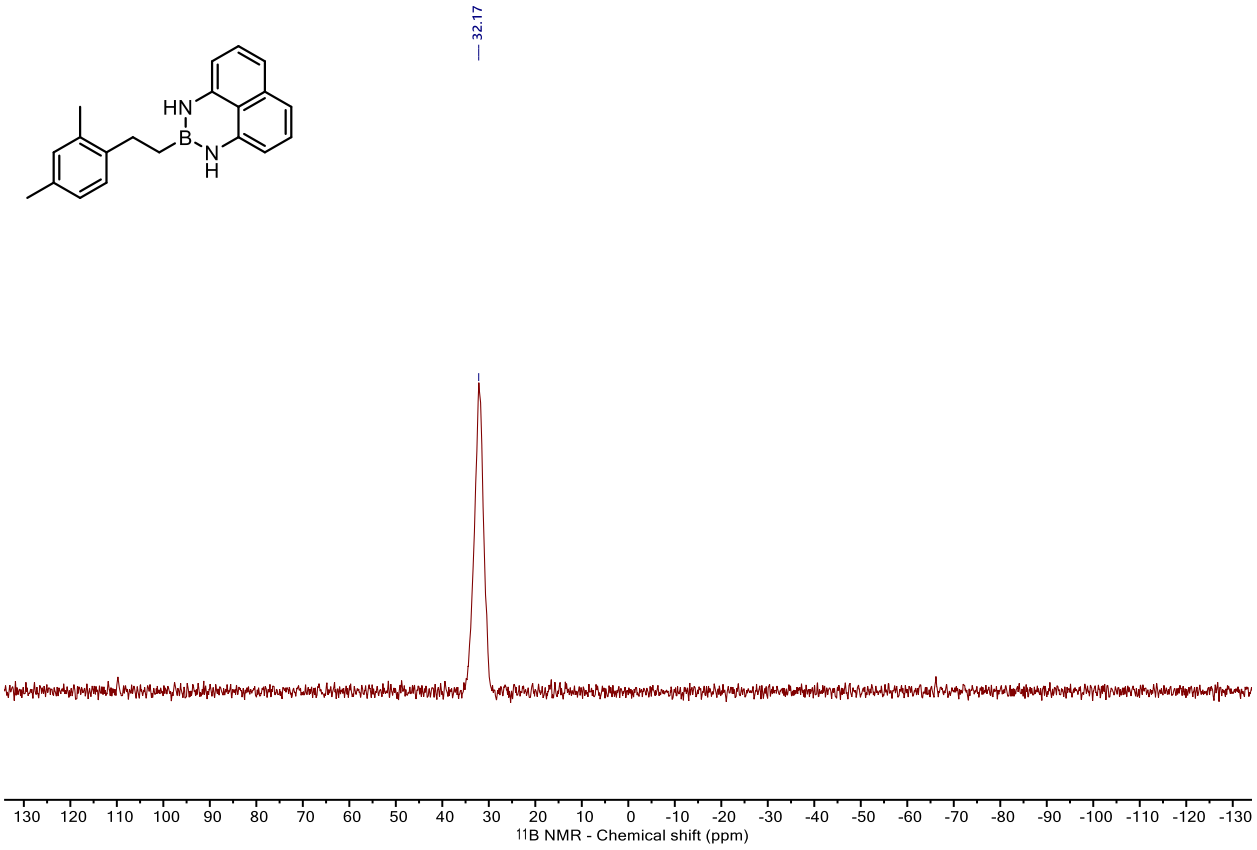

^{11}B NMR (160 MHz, Chloroform-*d*) of **4-1d**

4-1e; 2-(4-methoxyphenethyl)-2,3-dihydro-1*H*-naphtho[1,8-*de*][1,3,2]diazaborinine (ABG-0555)

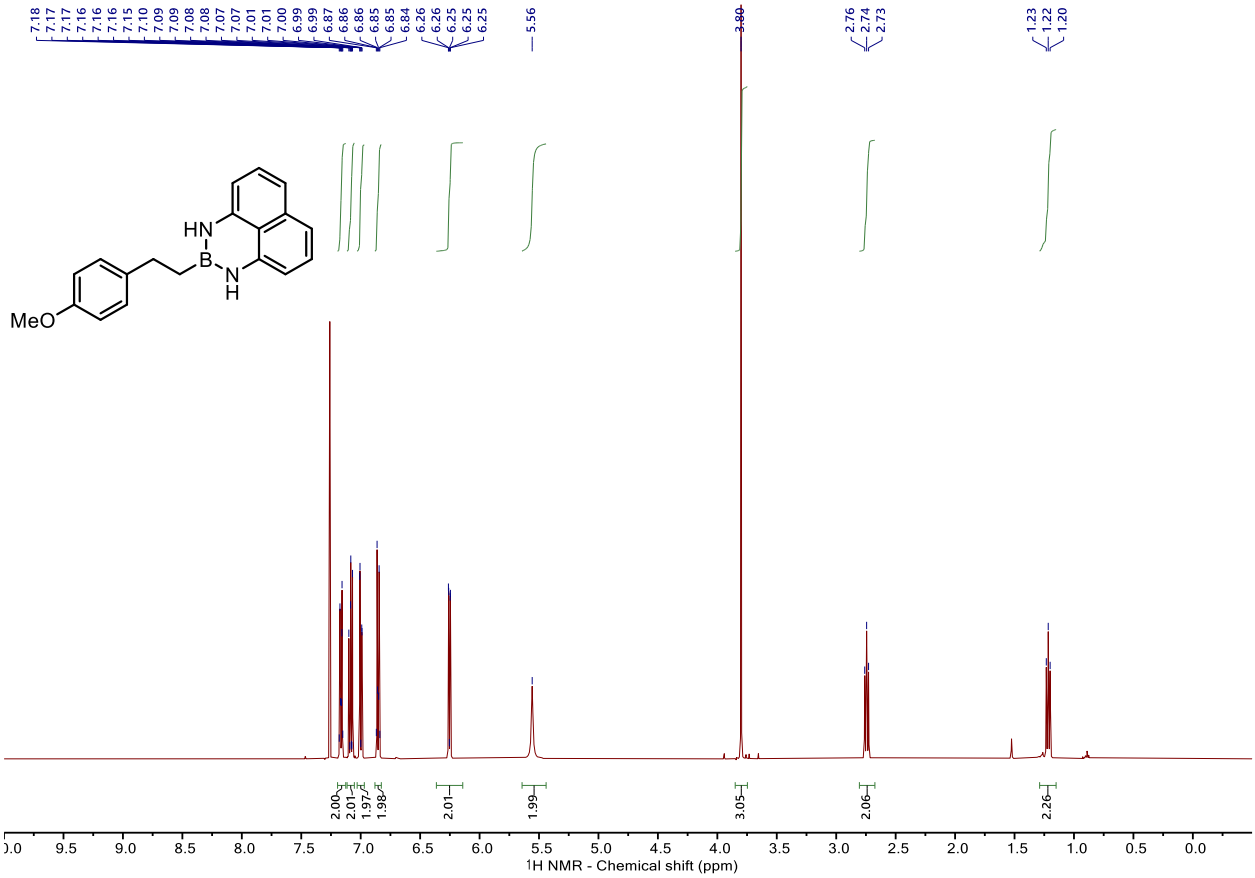

^{1}H NMR (500 MHz, Chloroform-*d*) of **4-1e**

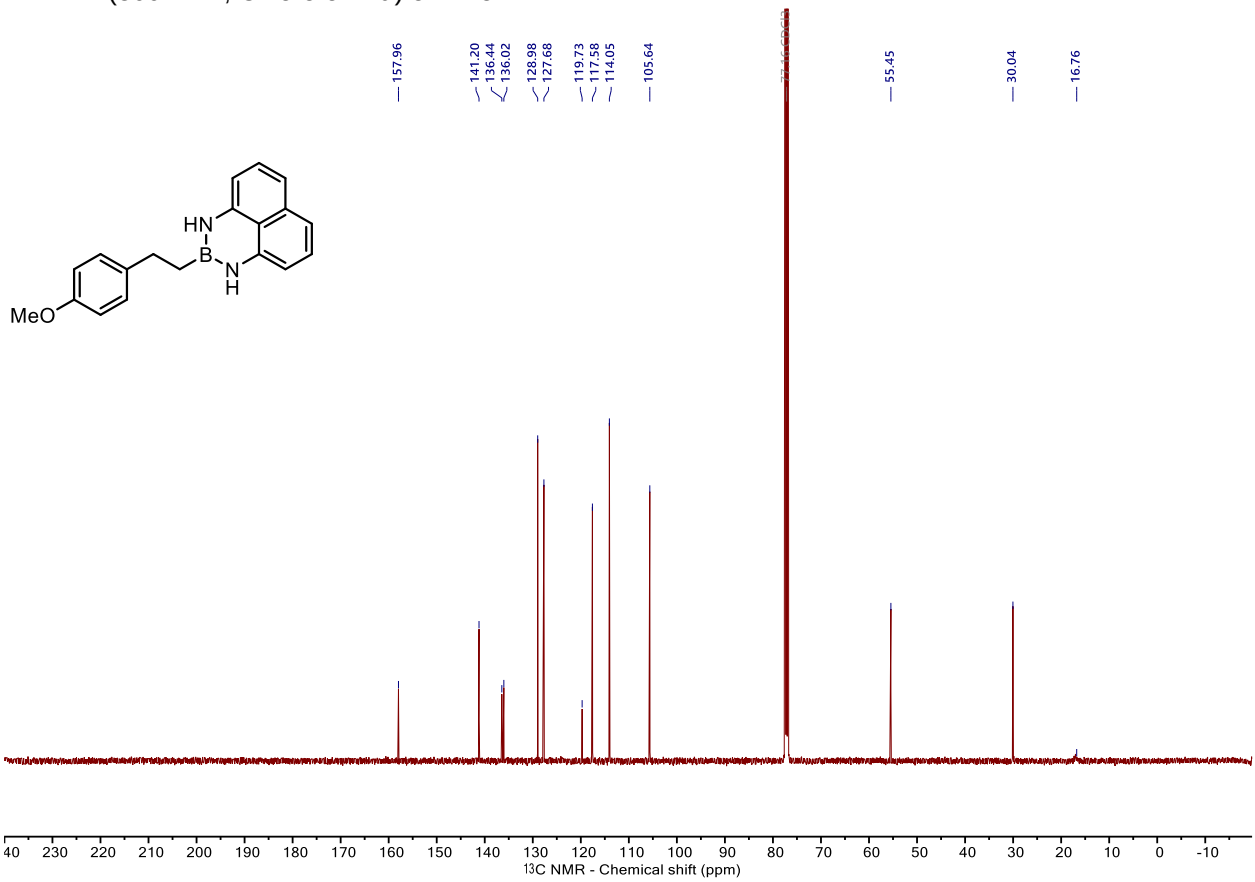

^{13}C {^{1}H} NMR (126 MHz, Chloroform-*d*) of **4-1e**

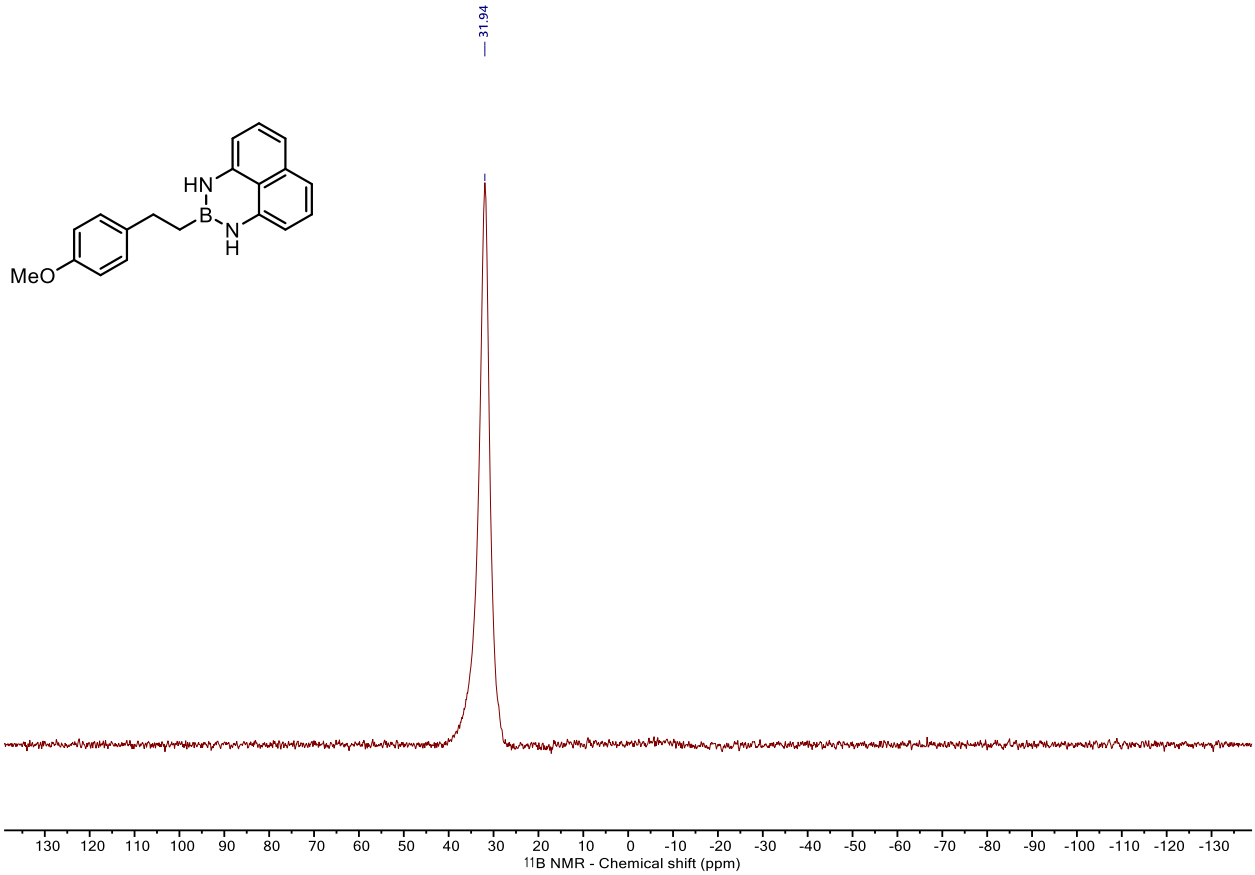

^{11}B NMR (160 MHz, Chloroform-*d*) of **4-1e**

4-1f; 2-(4-fluorophenethyl)-2,3-dihydro-1*H*-naphtho[1,8-*de*][1,3,2]diazaborinine (ABG-0566)

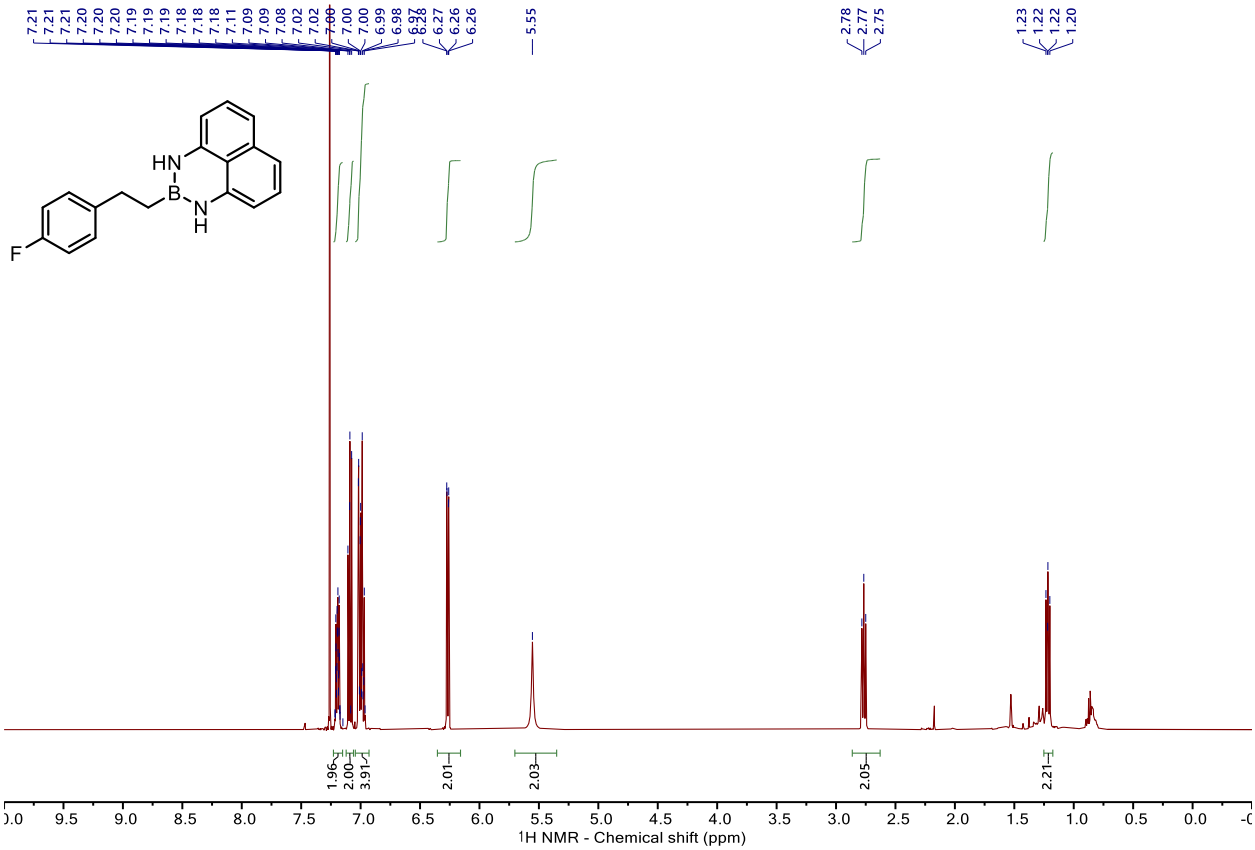

^{1}H NMR (500 MHz, Chloroform-*d*) of **4-1f**

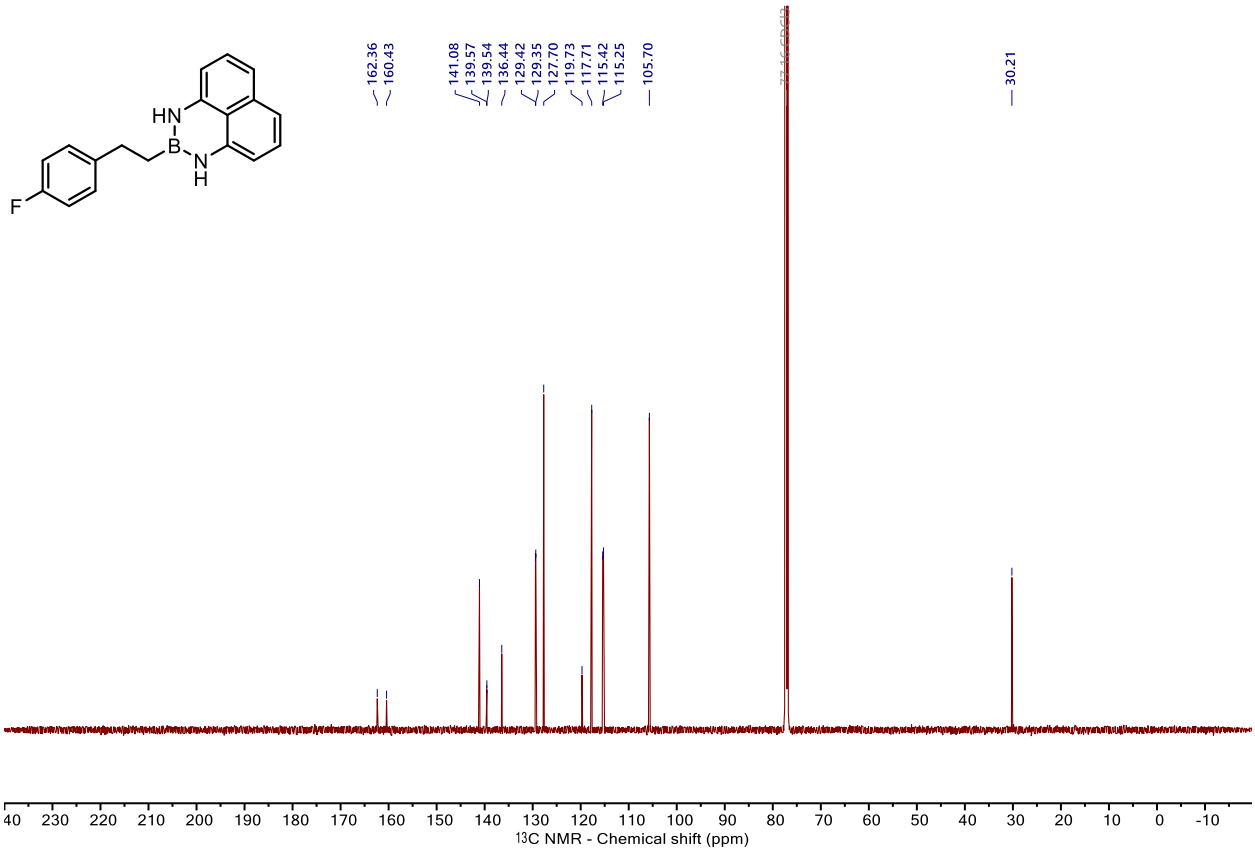

^{13}C {^{1}H} NMR (126 MHz, Chloroform-*d*) of **4-1f**

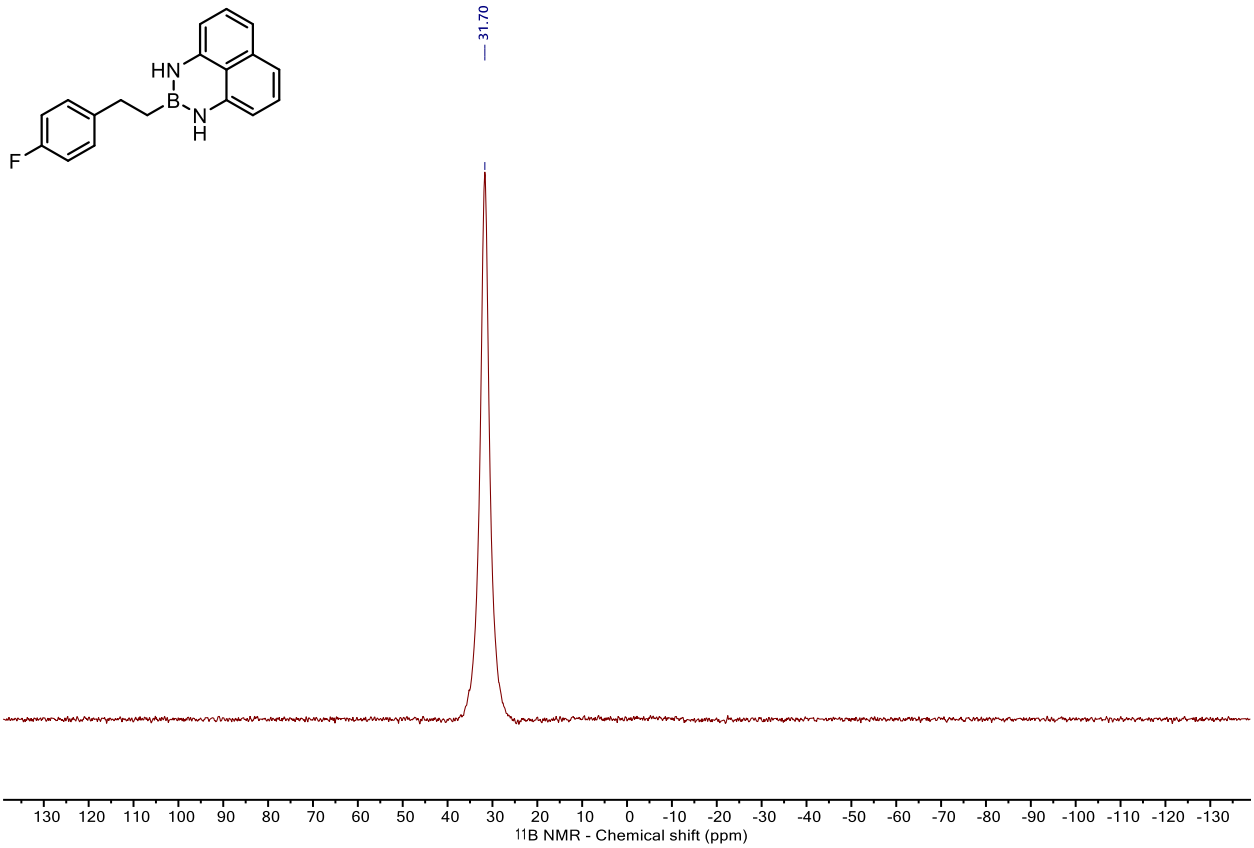

^{11}B NMR (160 MHz, Chloroform-*d*) of **4-1f**

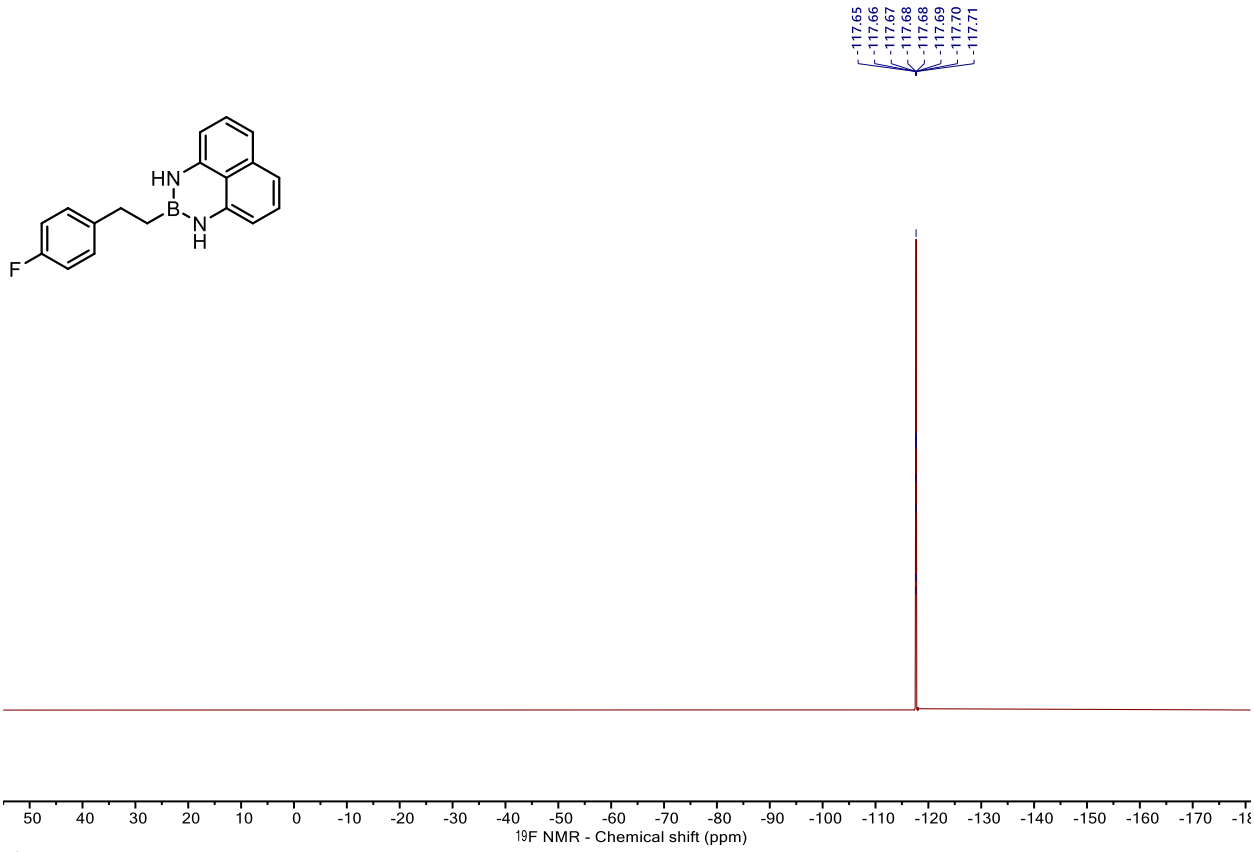

^{19}F NMR (471 MHz, Chloroform-*d*) of **4-1f**

4-1g; 2-(4-chlorophenethyl)-2,3-dihydro-1*H*-naphtho[1,8-*de*][1,3,2]diazaborinine (ABG-0542)

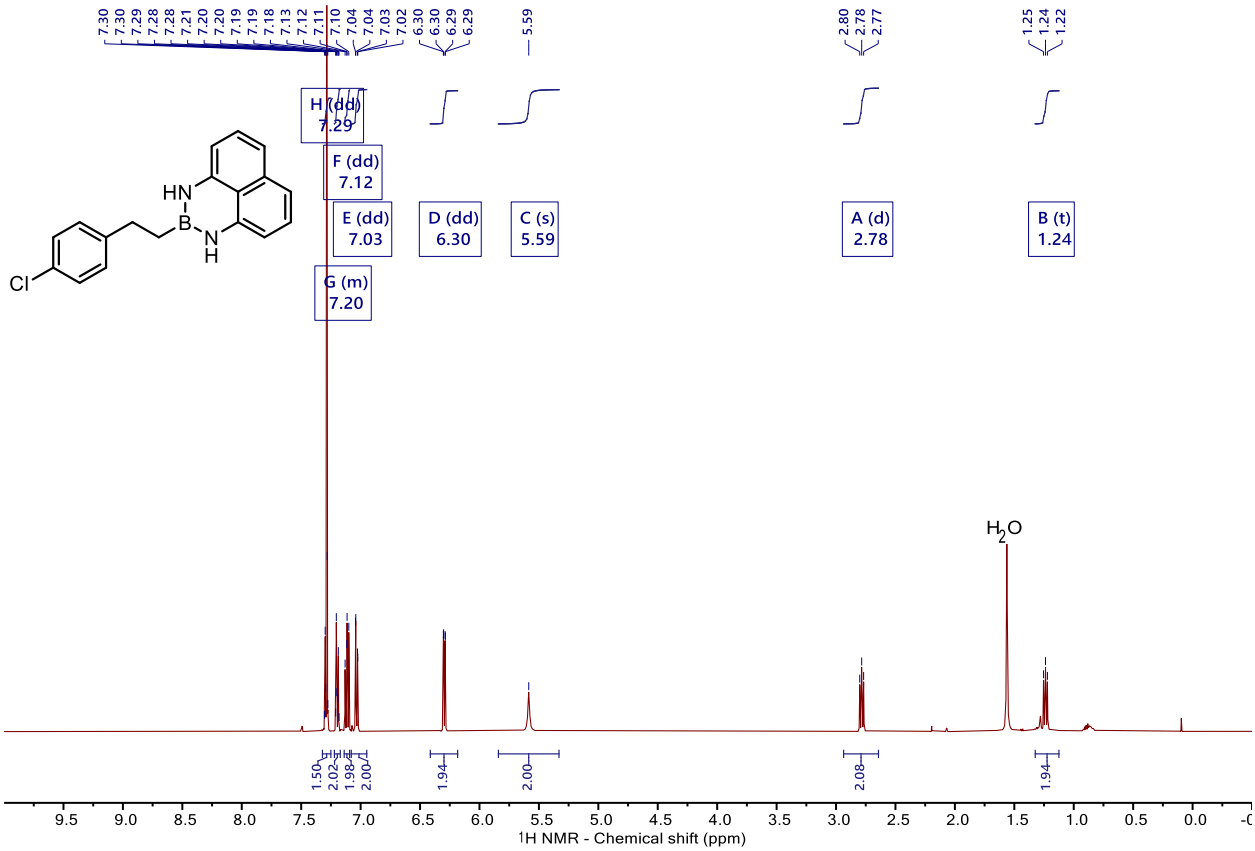

^{1}H NMR (500 MHz, Chloroform-*d*) of **4-1g**

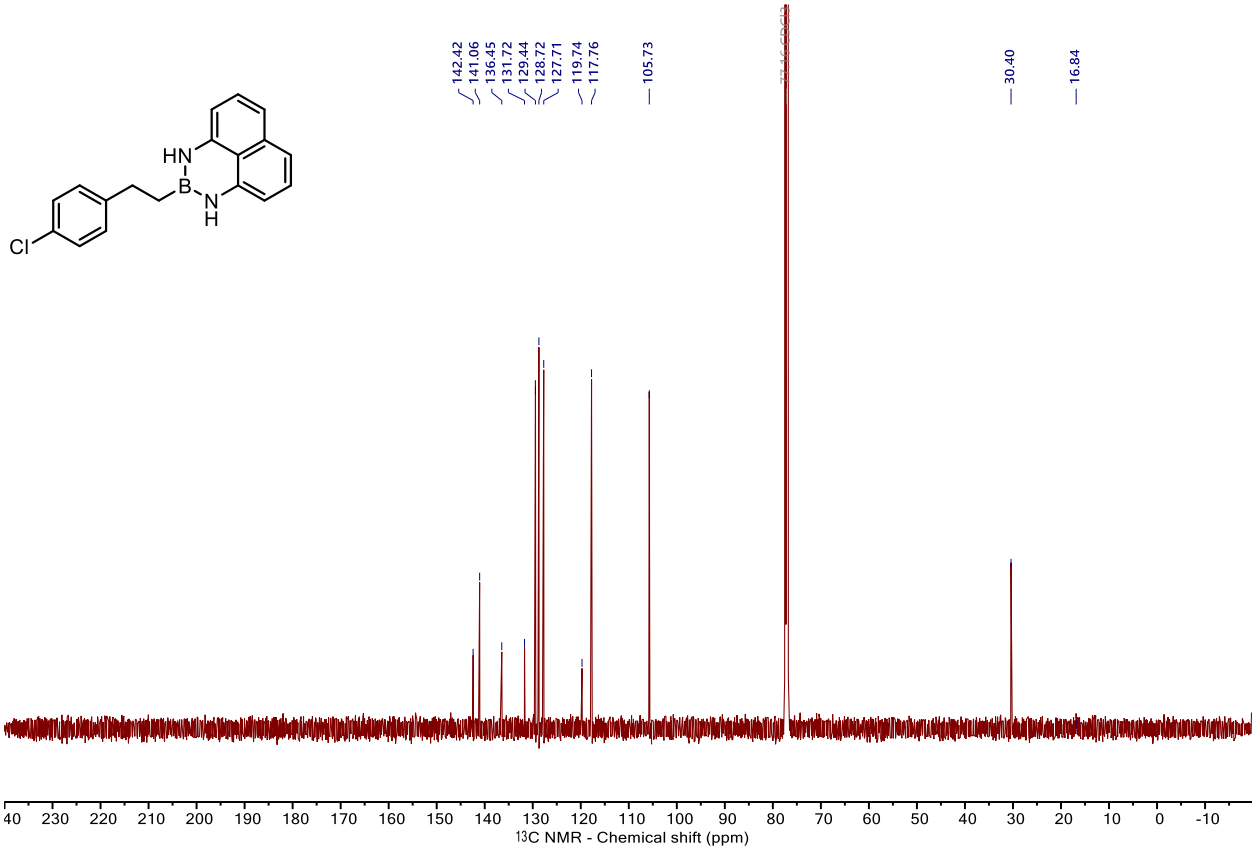

^{13}C {^{1}H} NMR (126 MHz, Chloroform-*d*) of **4-1g**

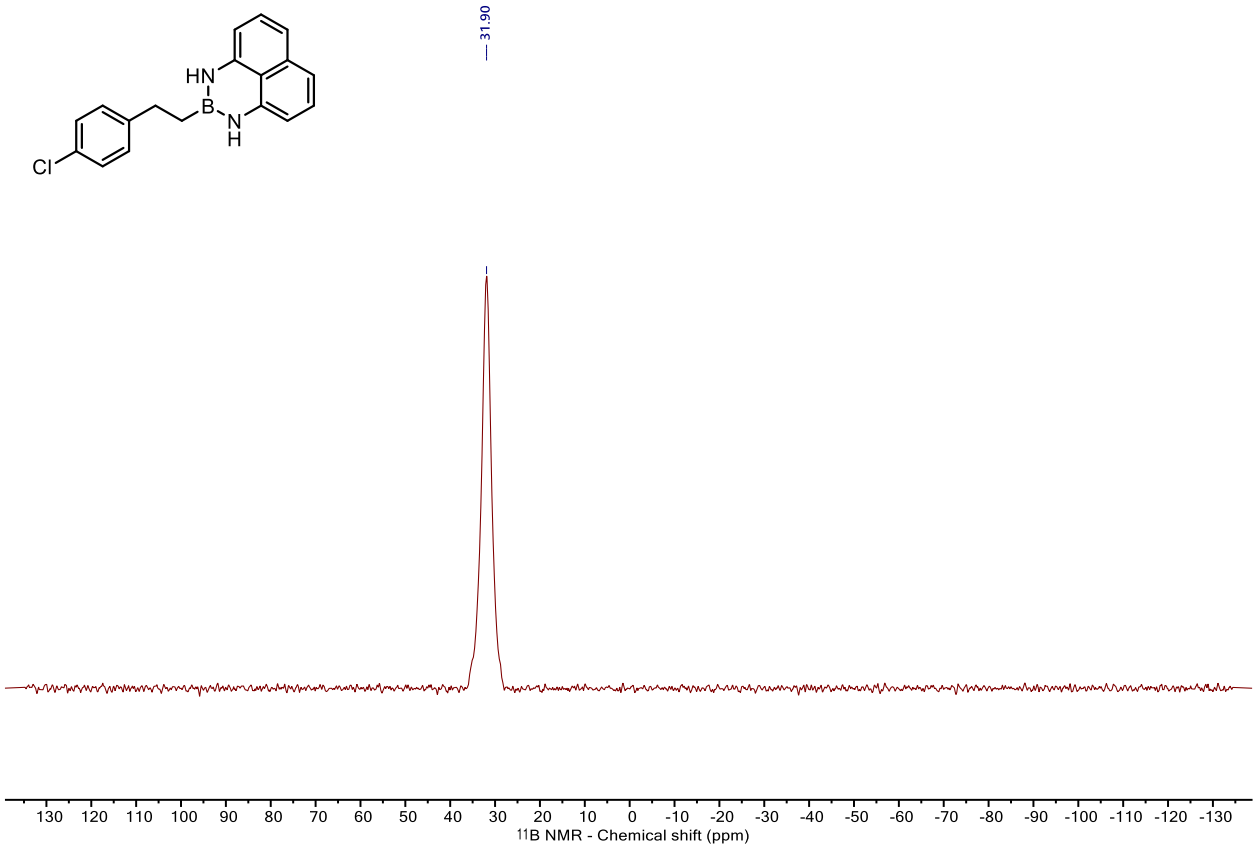

^{11}B NMR (160 MHz, $CDCl_3$) of **4-1g**

4-1h; 2-(4-bromophenethyl)-2,3-dihydro-1*H*-naphtho[1,8-*de*][1,3,2]diazaborinine (ABG-0544)

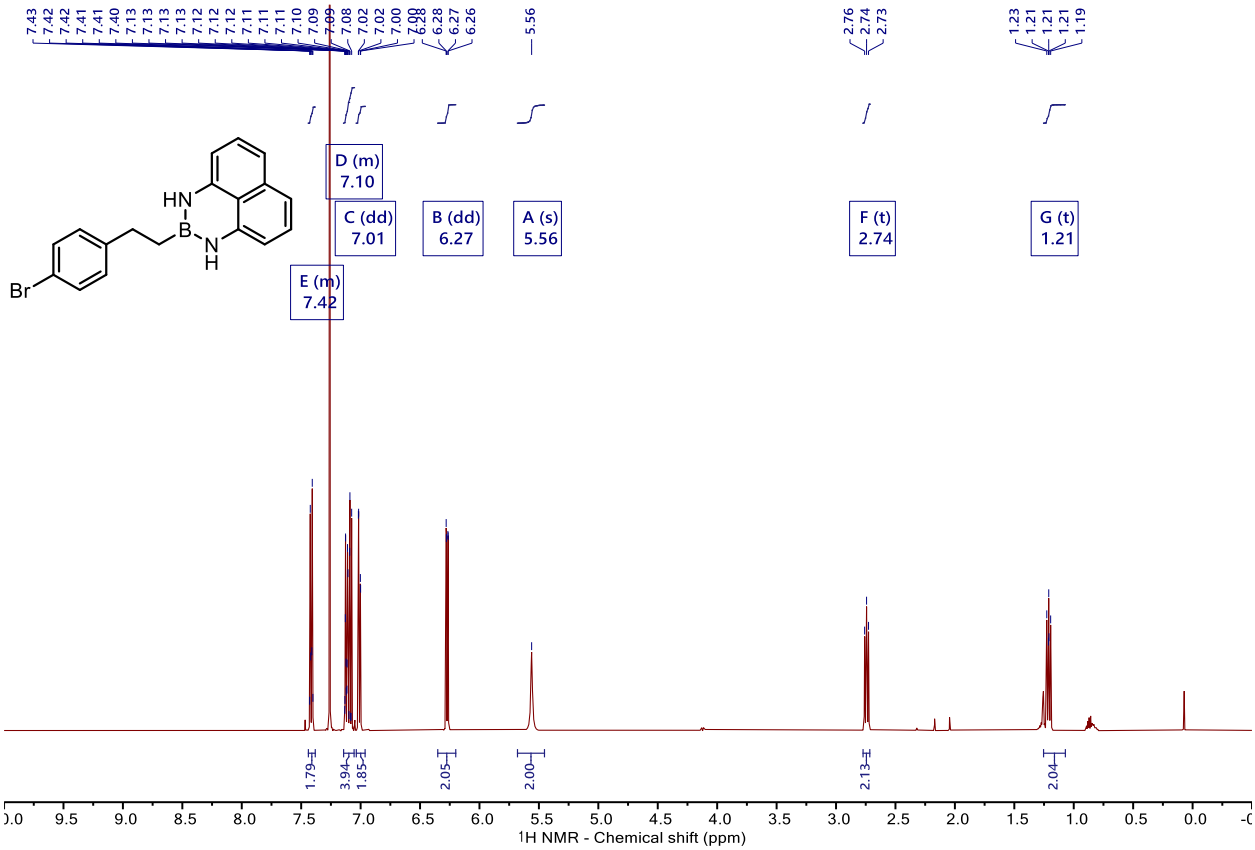

^{1}H NMR (500 MHz, Chloroform-*d*) of **4-1h**

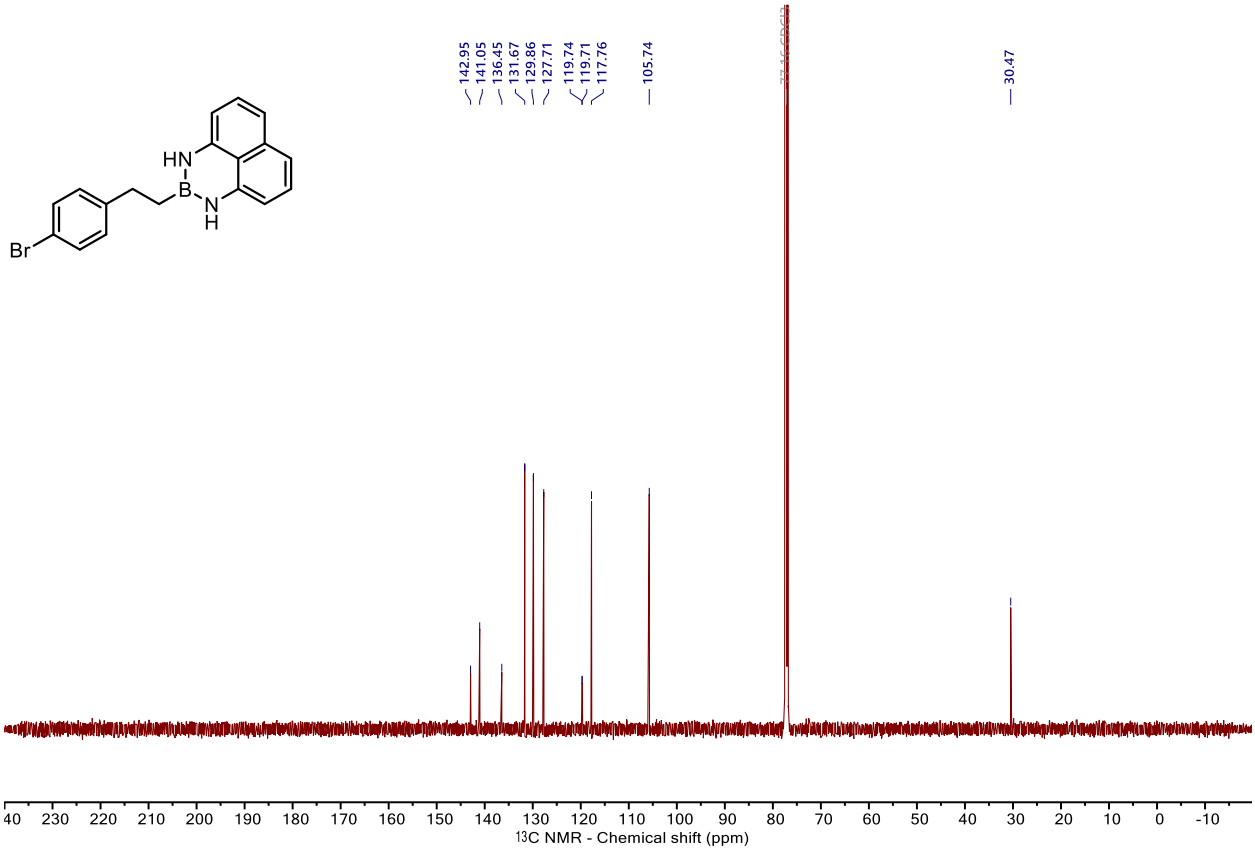

^{13}C {^{1}H} NMR (126 MHz, Chloroform-*d*) of **4-1h**

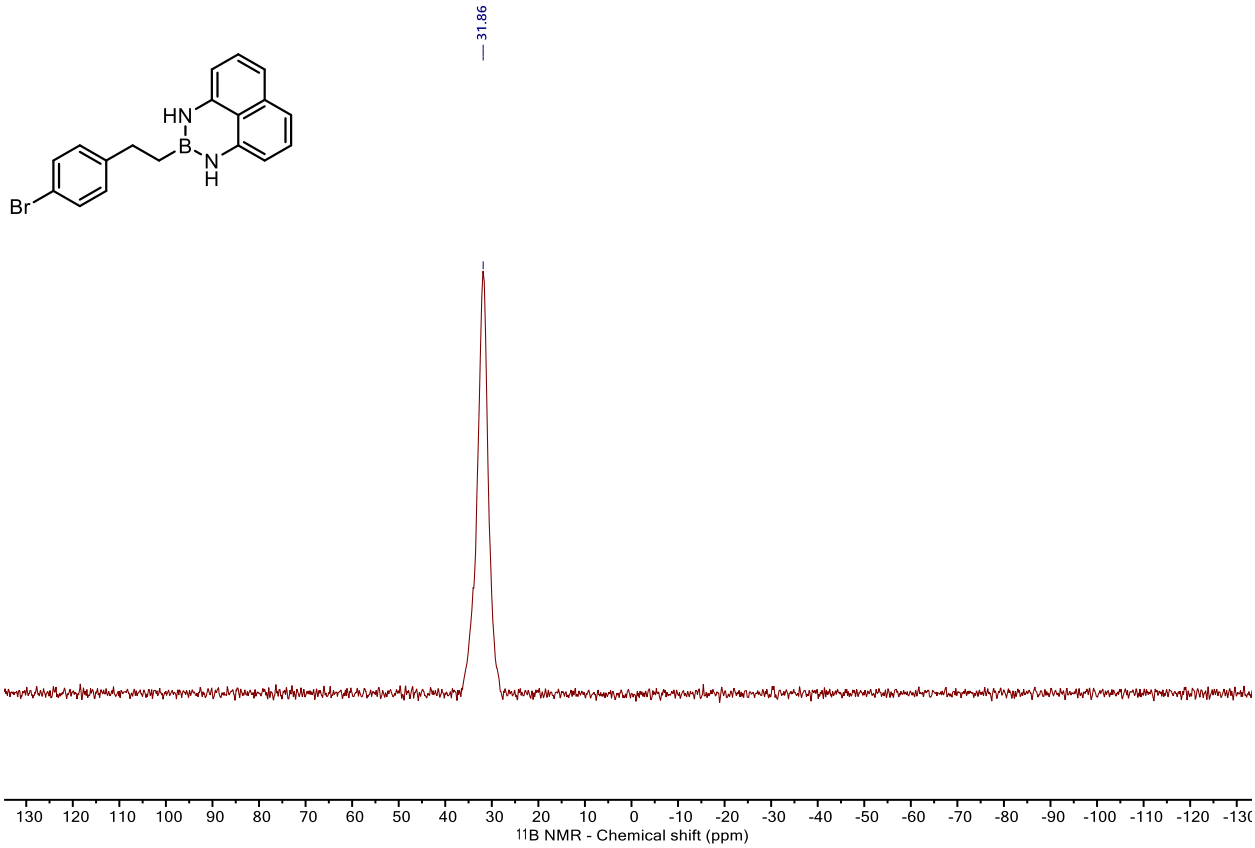

^{11}B NMR (160 MHz, Chloroform-*d*) of **4-1h**

4-1i; 2-octyl-2,3-dihydro-1*H*-naphtho[1,8-*de*][1,3,2]diazaborinine (ABG-0352)

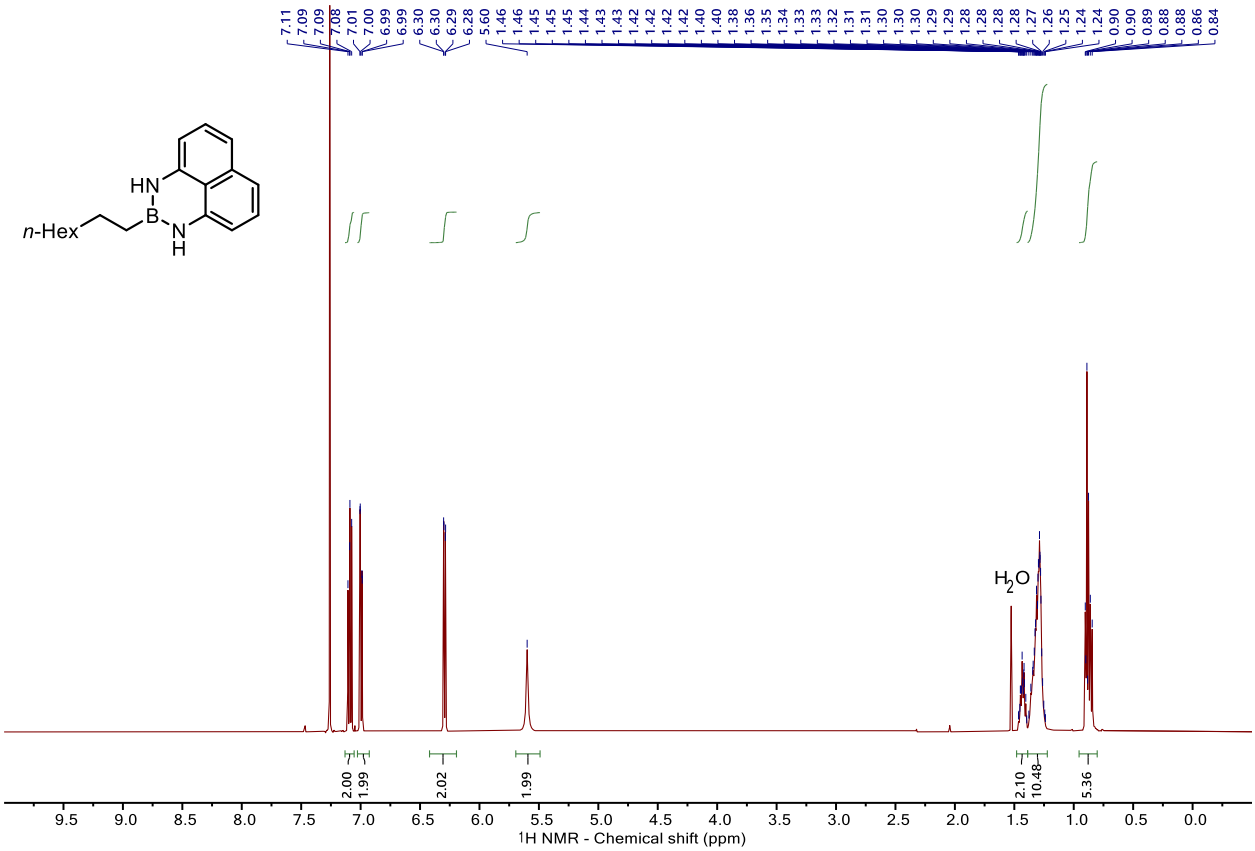

^{1}H NMR (500 MHz, Chloroform-*d*) of **4-1i**

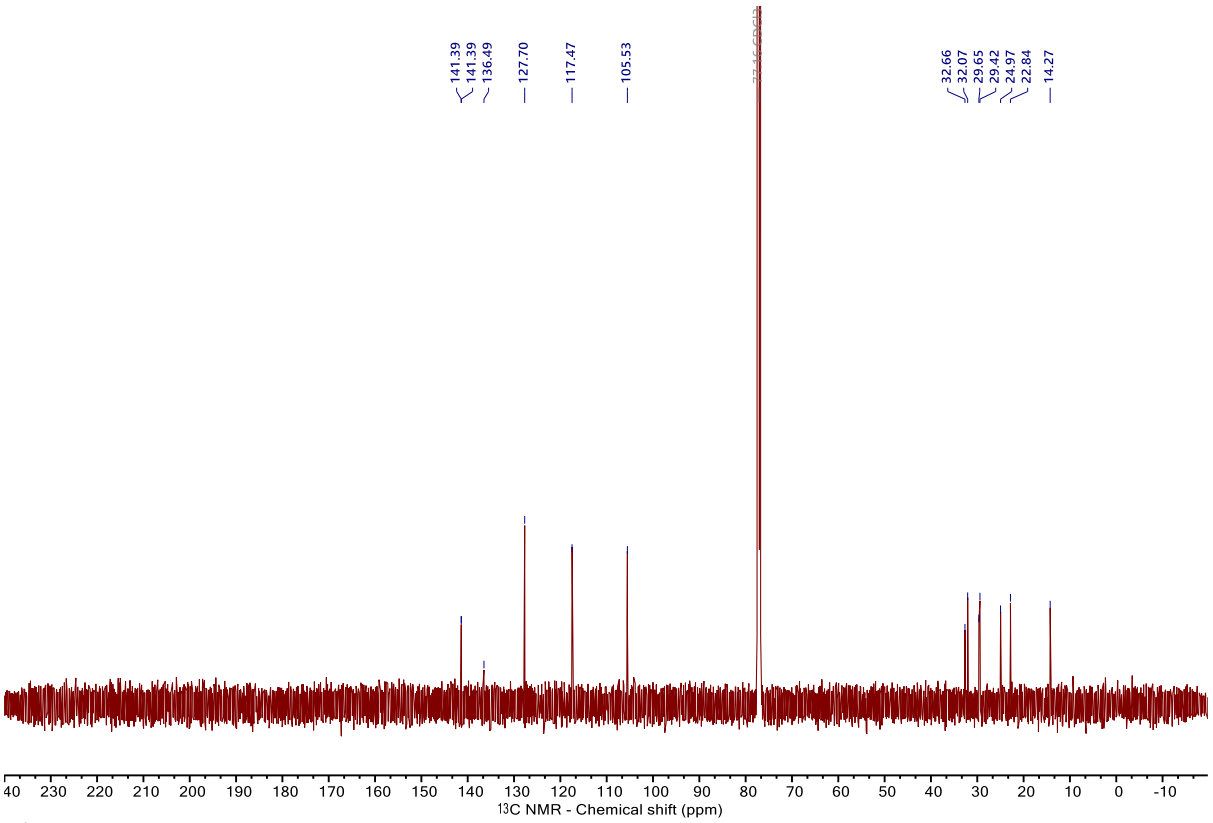

^{13}C {^{1}H} NMR(126 MHz, Chloroform-*d*) of **4-1i**

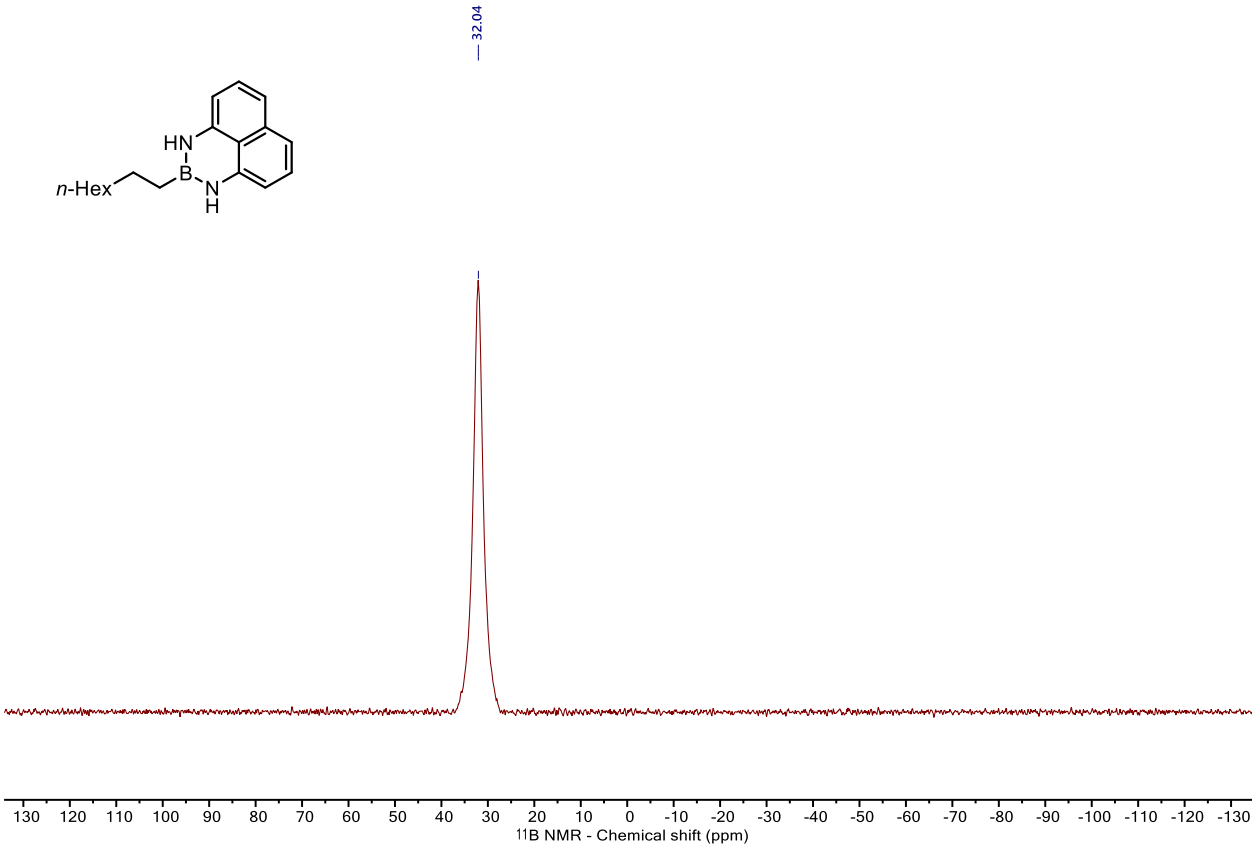

^{11}B NMR (160 MHz, Chloroform-*d*) of **4-1i**

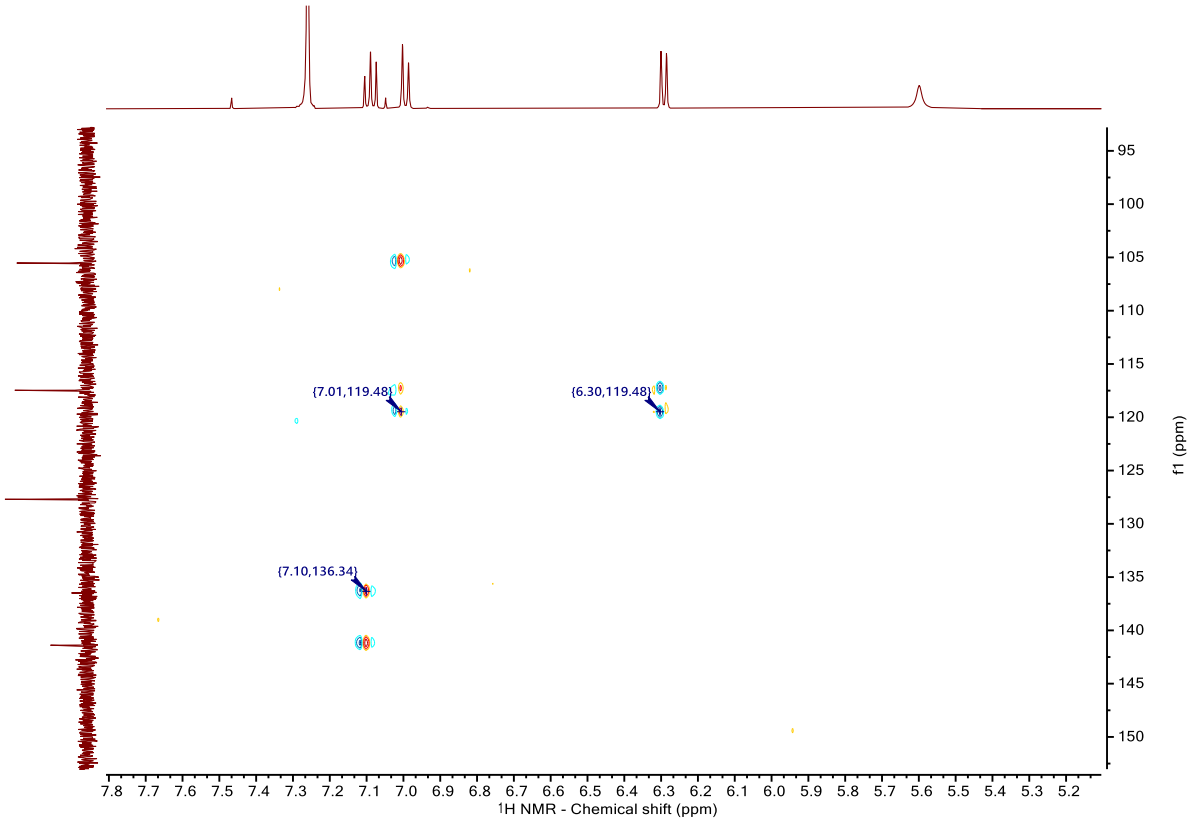

^{1}H-^{13}C HMBC (Chloroform-*d*) of **4-1i** (zoomed in on area of ^{13}C resonances identified by HMBC)

4-1j; 2-(2-cyclohexylethyl)-2,3-dihydro-1*H*-naphtho[1,8-*de*][1,3,2]diazaborinine (ABG-0560)

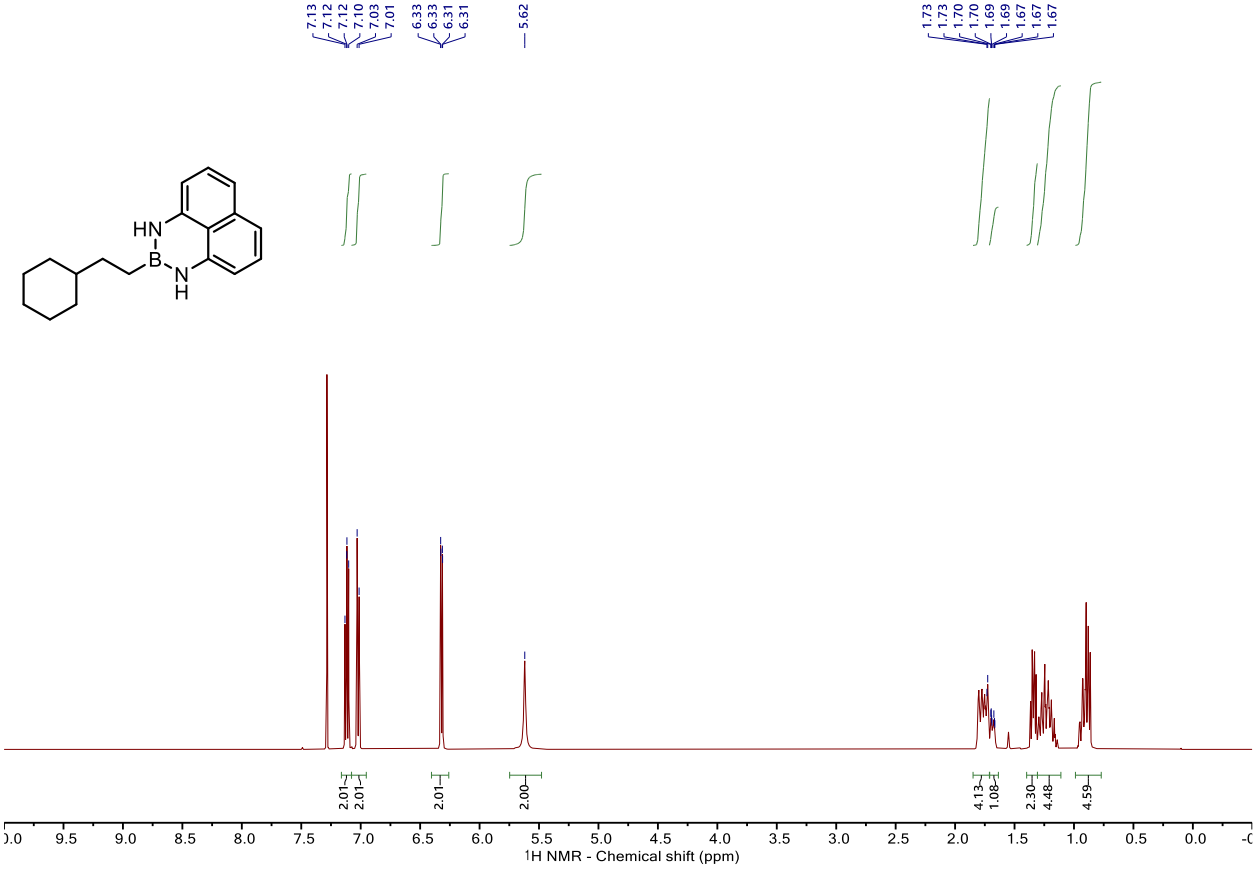

^{1}H NMR (500 MHz, Chloroform-*d*) of **4-1**j

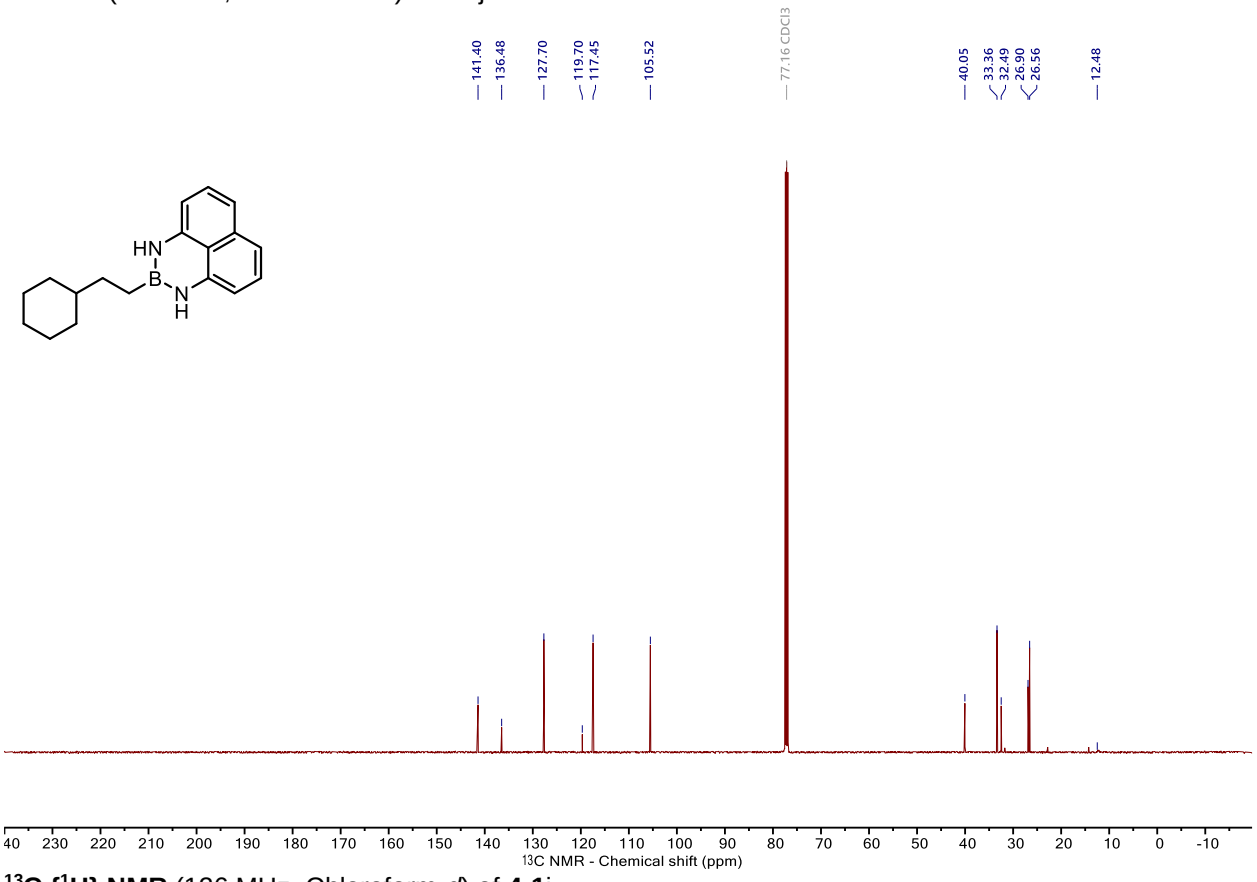

^{13}C {^{1}H} NMR (126 MHz, Chloroform-*d*) of **4-1**j

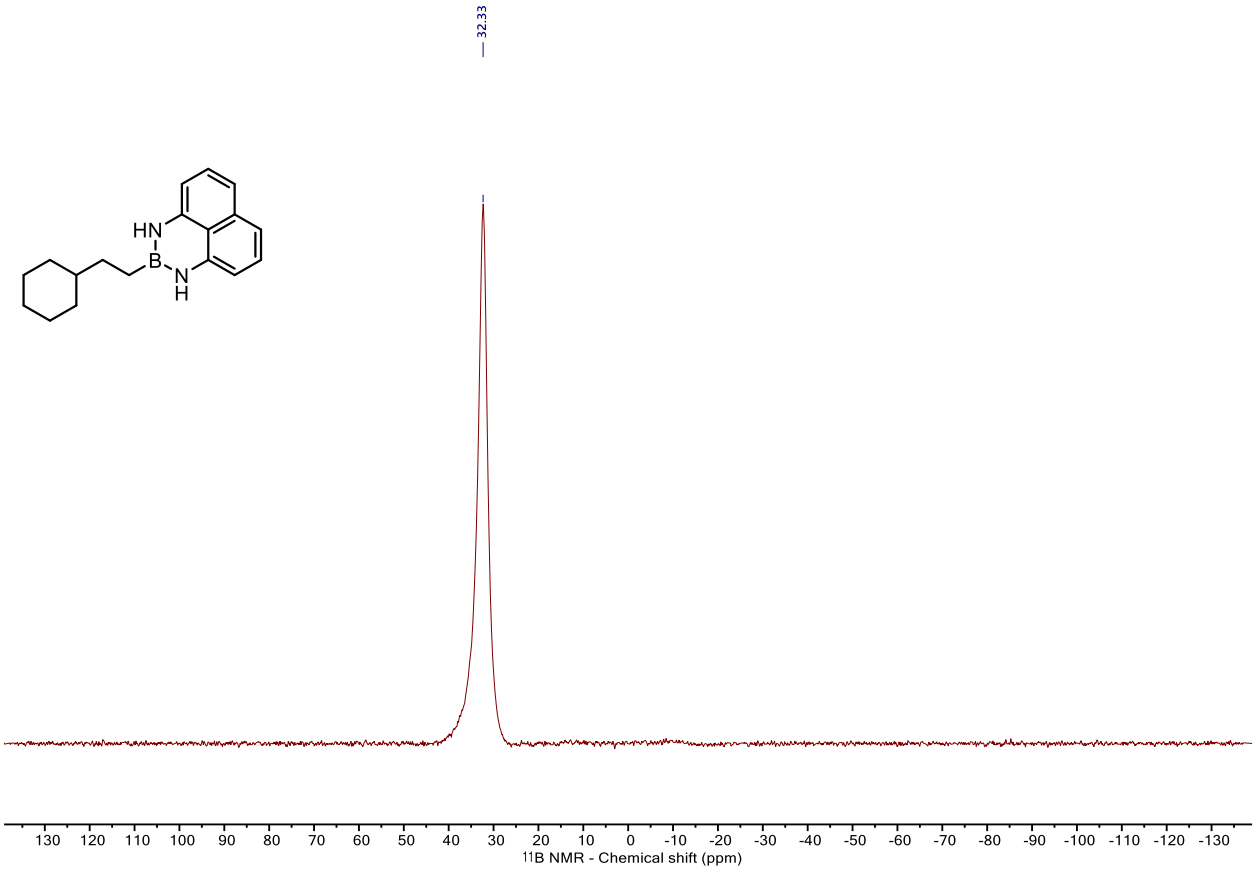

^{11}B NMR (160 MHz, Chloroform-*d*) of **4-1**j

4-1k; 2-(2-(bicyclo[2.2.1]hept-5-en-2-yl)ethyl)-2,3-dihydro-1*H*-naphtho[1,8-*de*][1,3,2]diazaborinin e (ABG-0565)

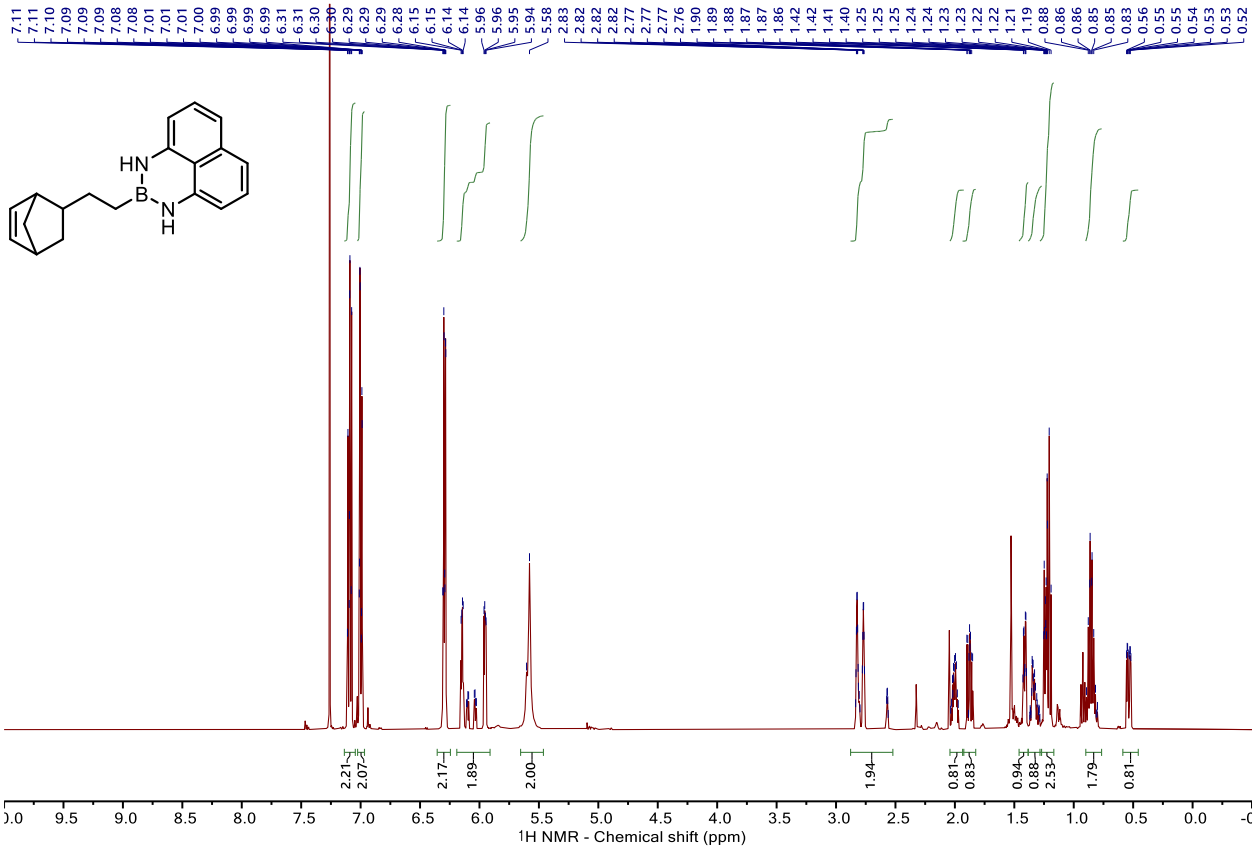

^{1}H NMR (500 MHz, Chloroform-*d*) of **4-1k**

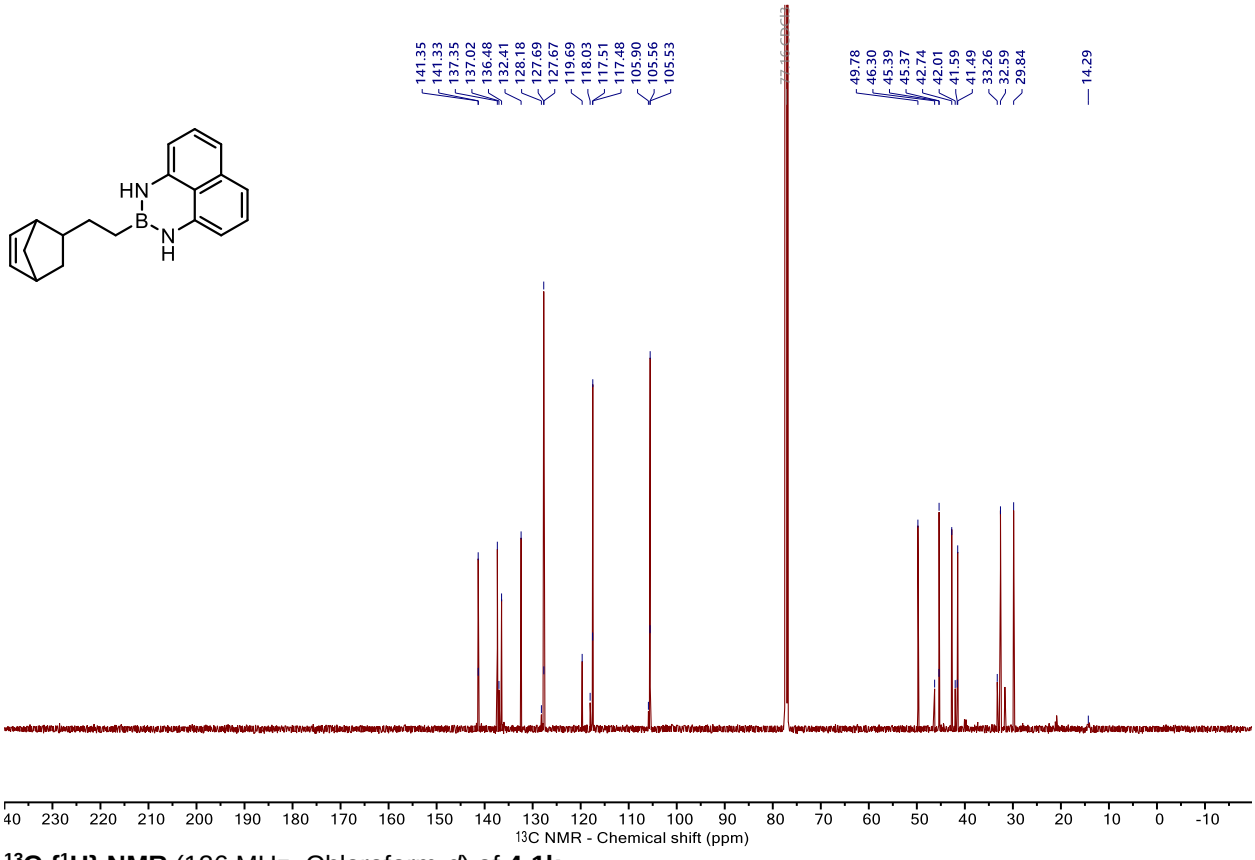

^{13}C {^{1}H} NMR (126 MHz, Chloroform-*d*) of **4-1k**

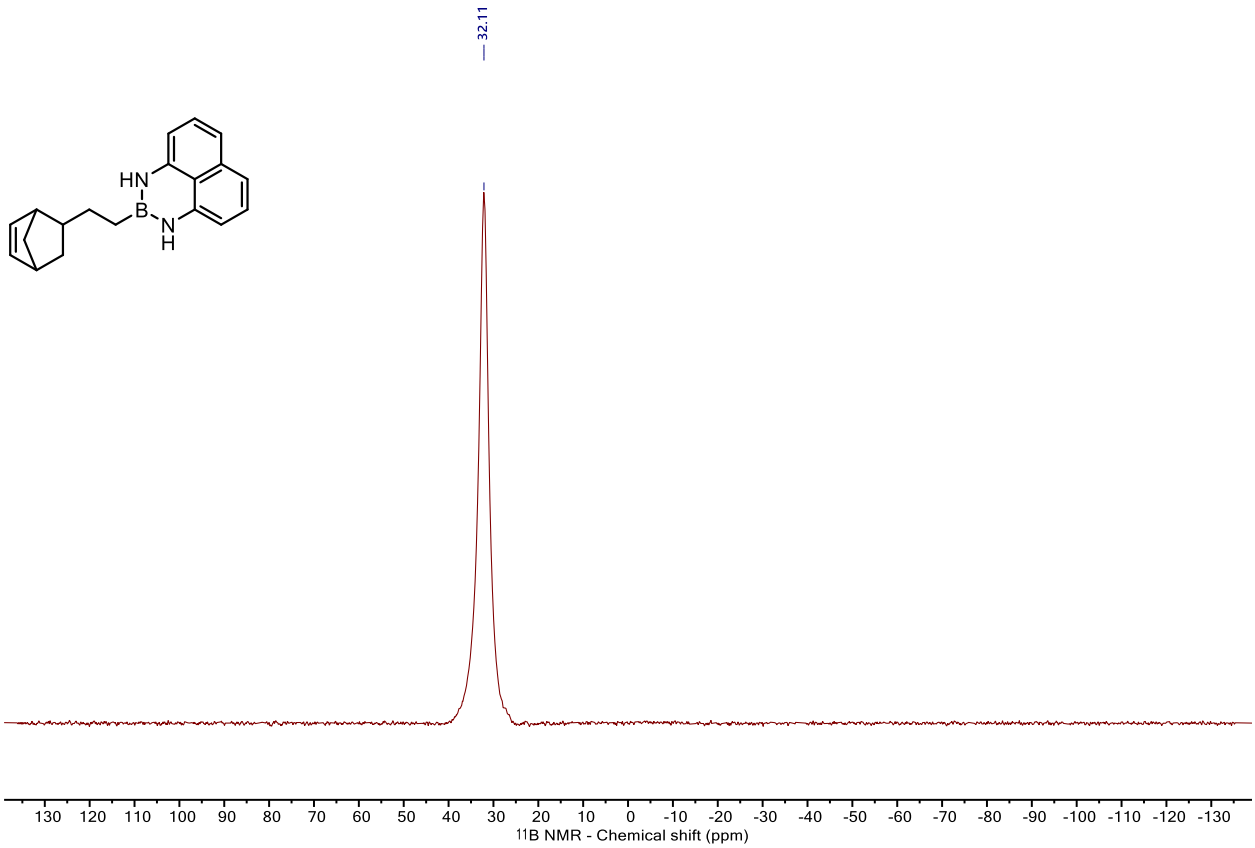

^{11}B NMR (160 MHz, Chloroform-*d*) of **4-1k**

4-1l; 2-(5-((triisopropylsilyl)oxy)pentyl)-2,3-dihydro-1*H*-naphtho[1,8-*de*][1,3,2]diazaborinine (ABG-0589)

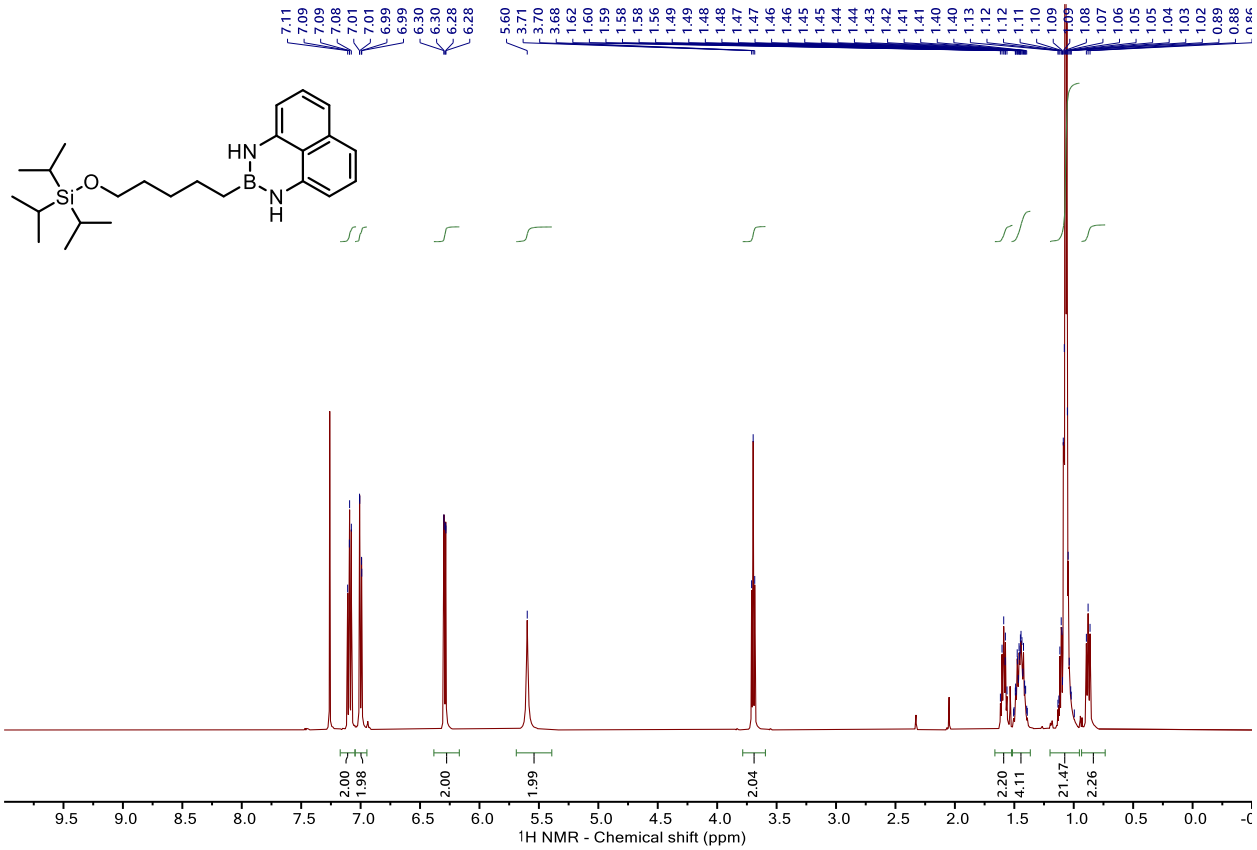

^{1}H NMR (500 MHz, Chloroform-*d*) of **4-1l**

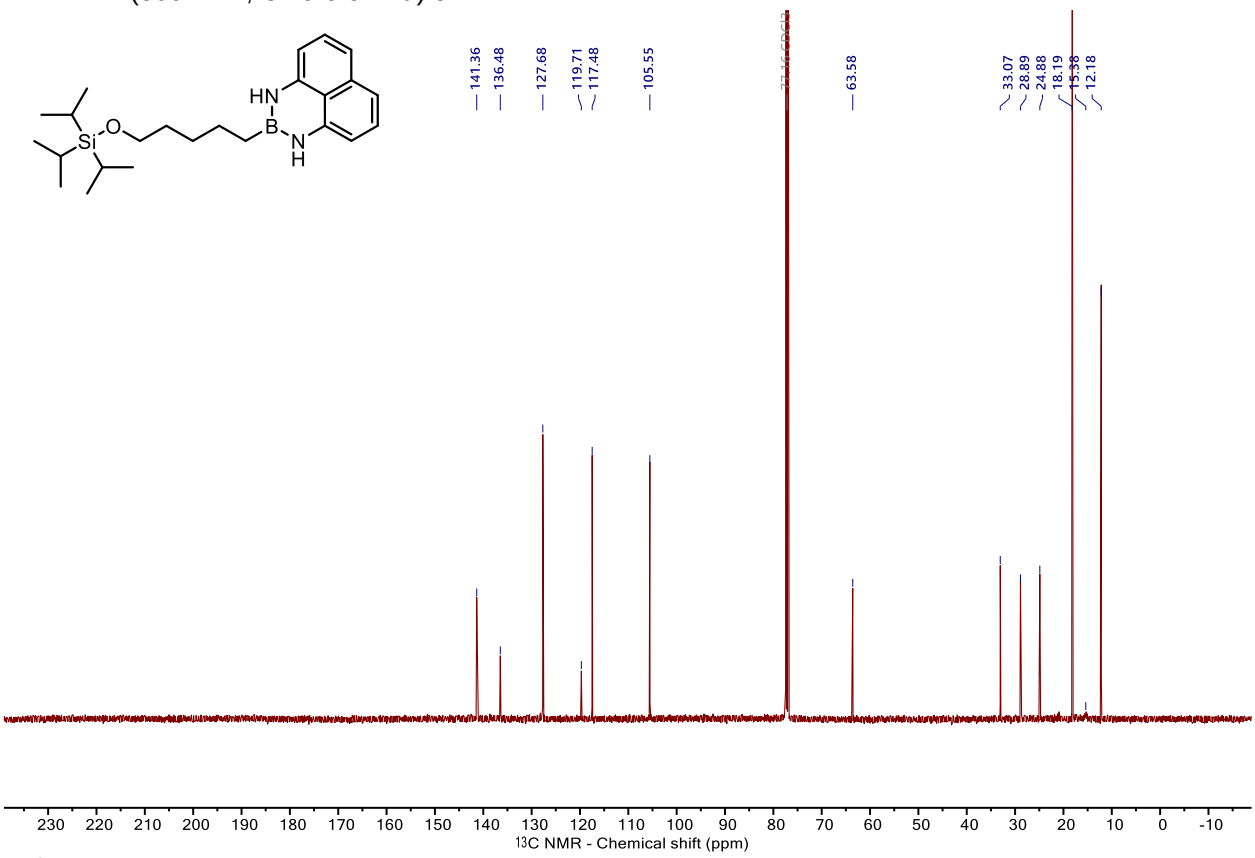

^{13}C {^{1}H} NMR (126 MHz, Chloroform-*d*) of **4-1l**

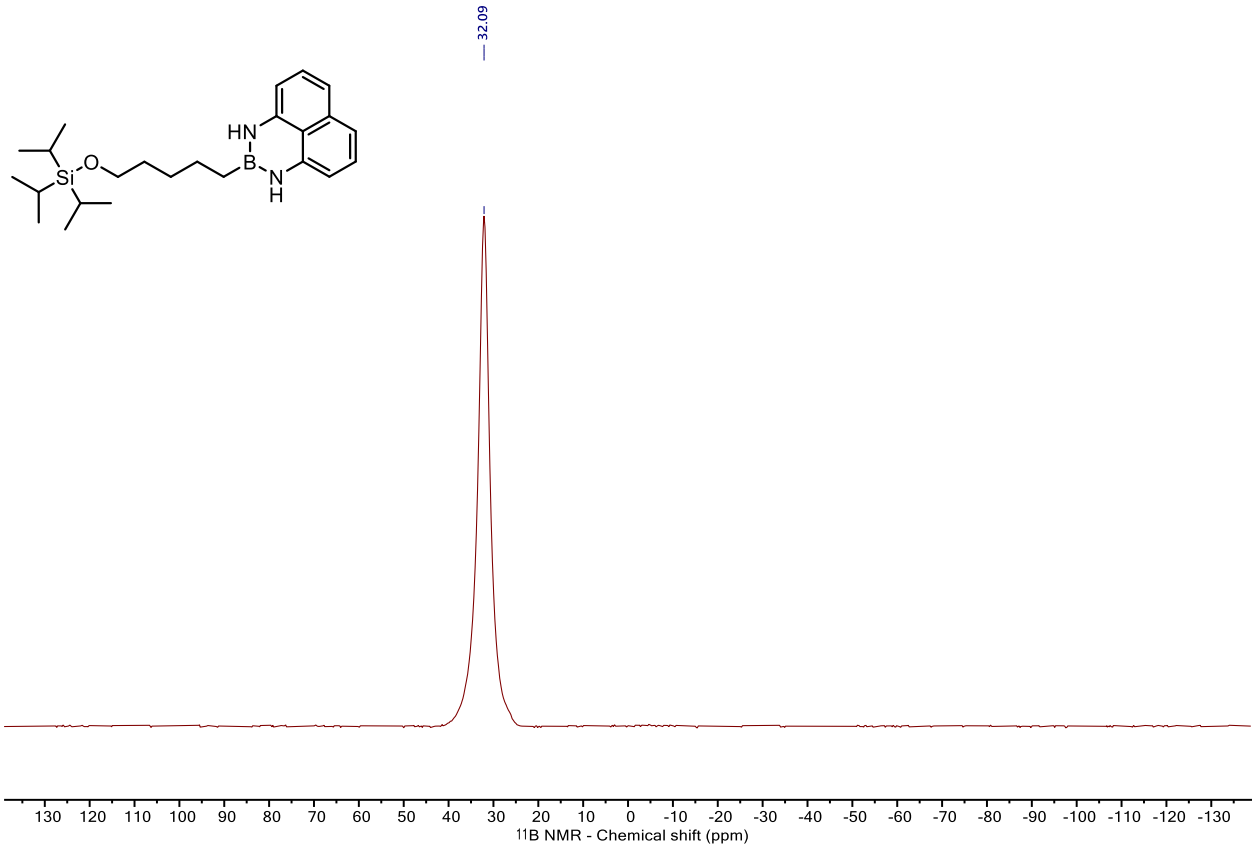

^{11}B NMR (160 MHz, Chloroform-*d*) of **4-1l**

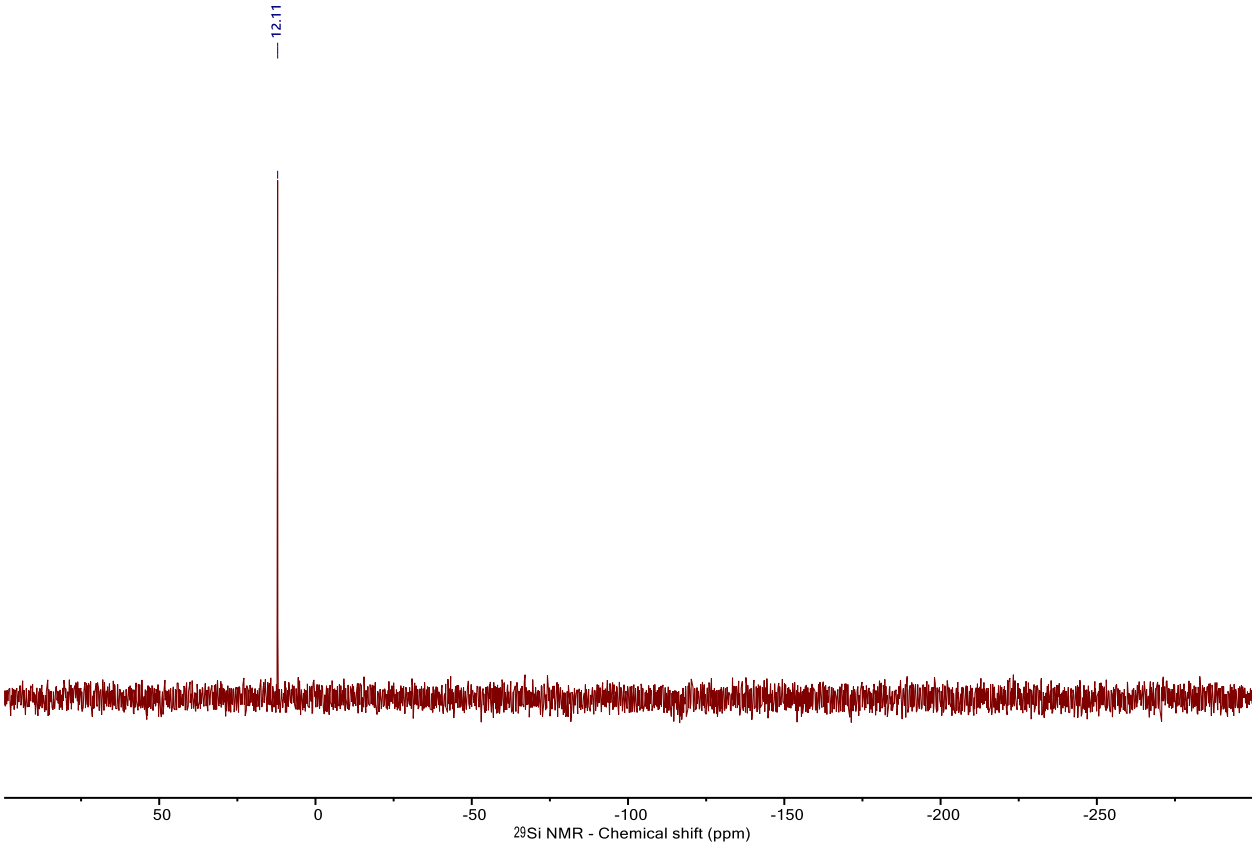

^{29}Si NMR (99 MHz, Chloroform-*d*) of **4-1l**

4-1m; 2-(4-(*p*-tolylthio)butyl)-2,3-dihydro-1*H*-naphtho[1,8-*de*][1,3,2]diazaborinine (ABG-0590)

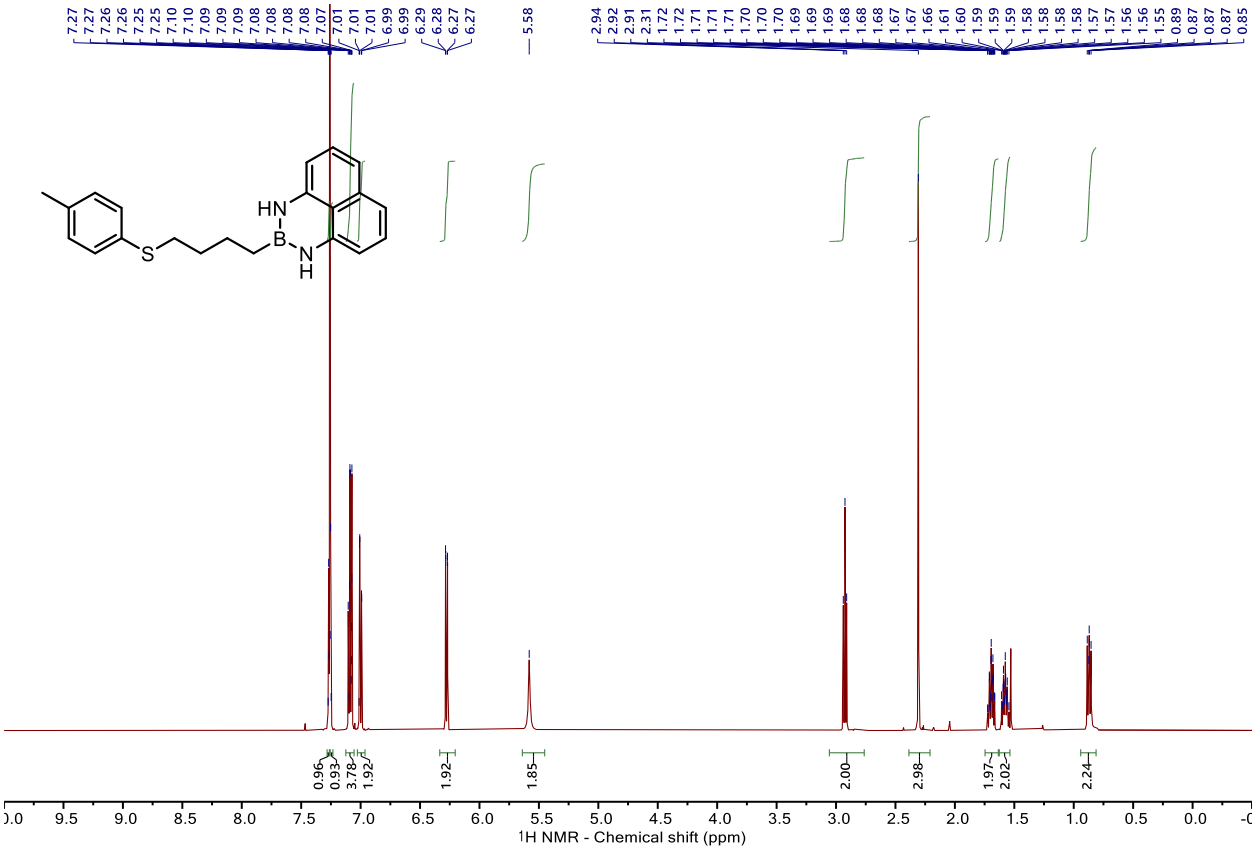

^{1}H NMR (500 MHz, Chloroform-*d*) of **4-1m**

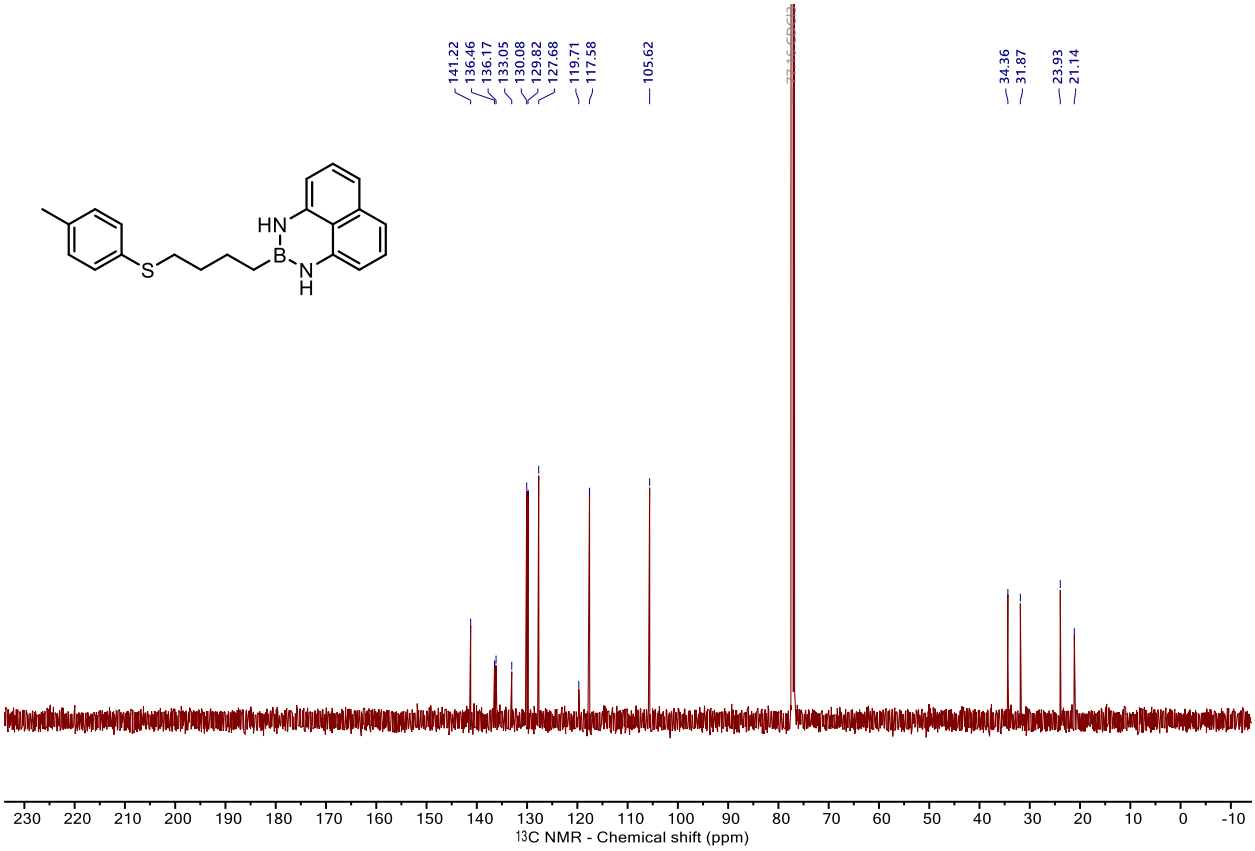

^{13}C {^{1}H} NMR (126 MHz, Chloroform-*d*) of **4-1m**

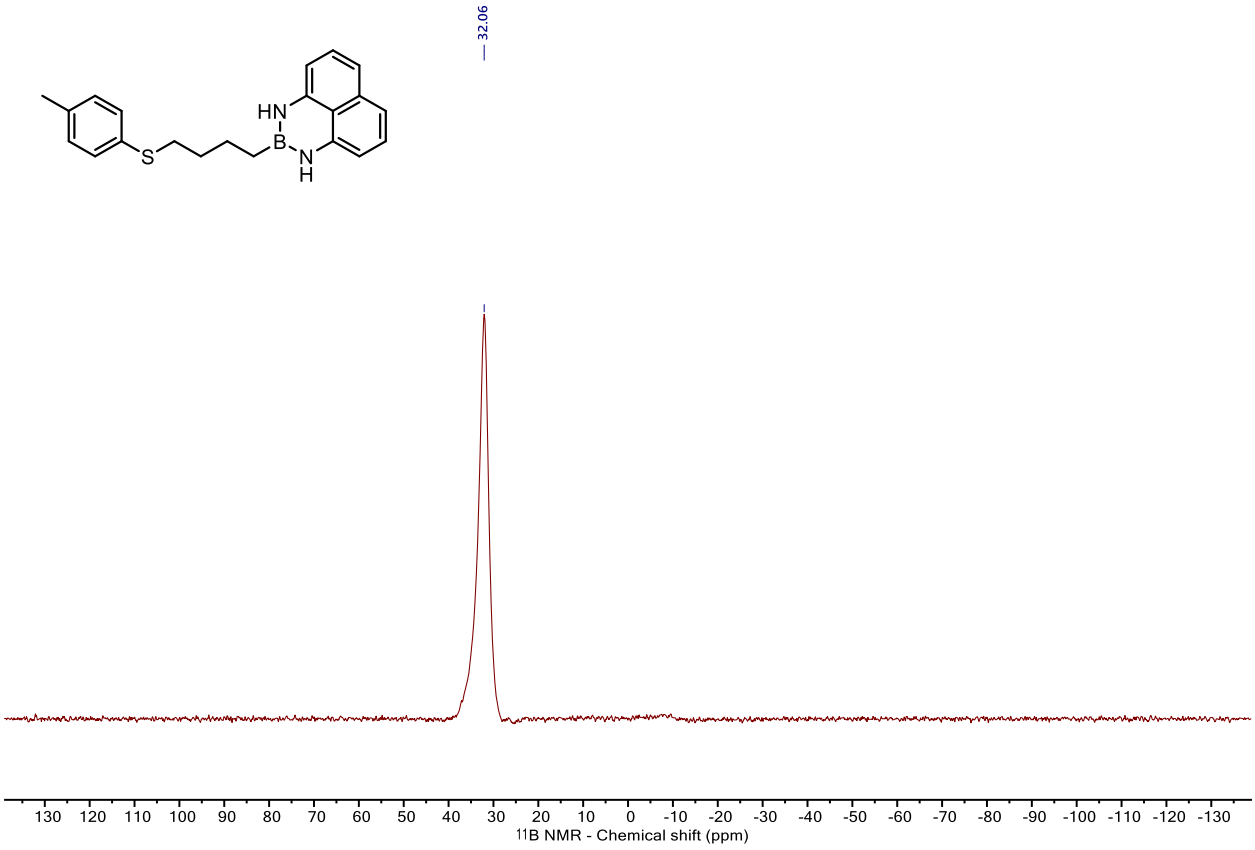

^{11}B NMR (160 MHz, Chloroform-*d*) of **4-1m**

4-1n; 2-(4-bromophenethyl)-2,3-dihydro-1*H*-naphtho[1,8-*de*][1,3,2]diazaborinine (ABG-0594)

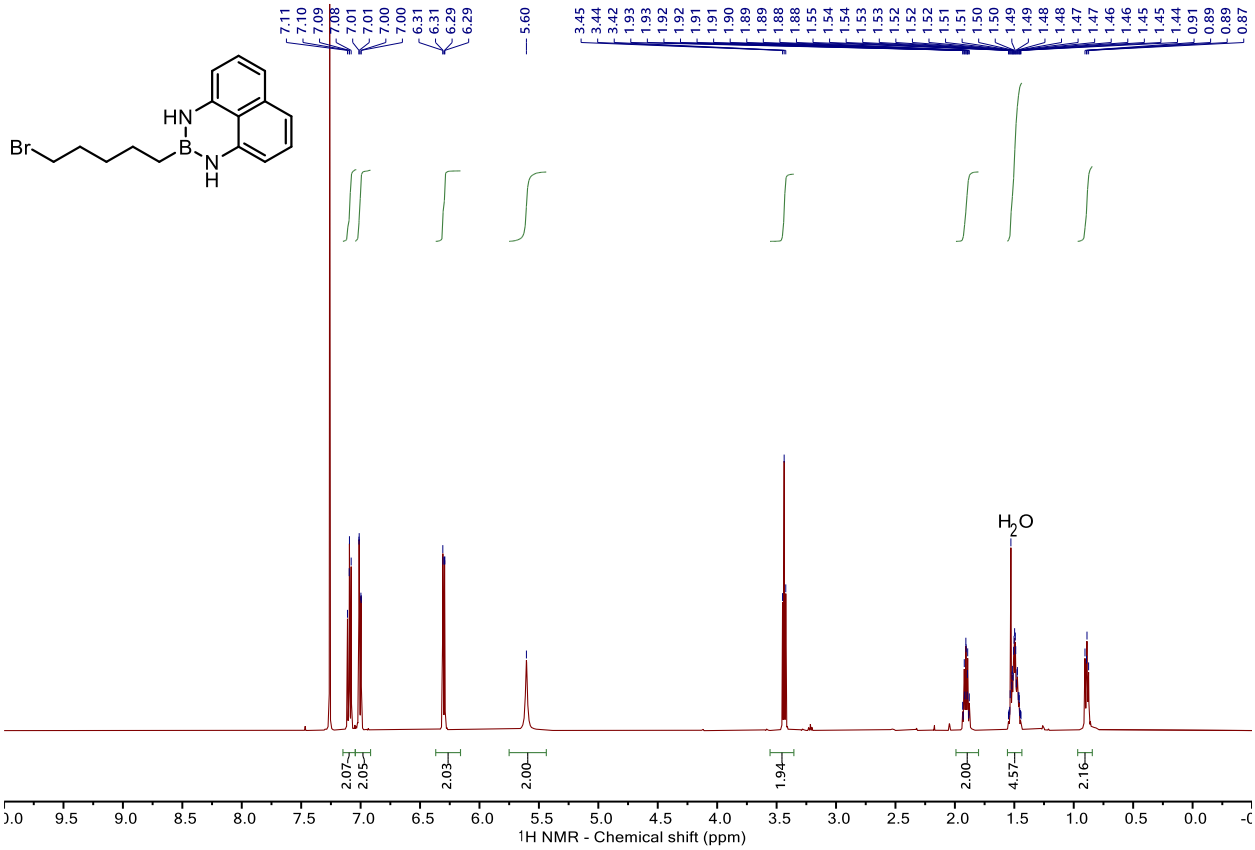

^{1}H NMR (500 MHz, Chloroform-*d*) of **4-1n**

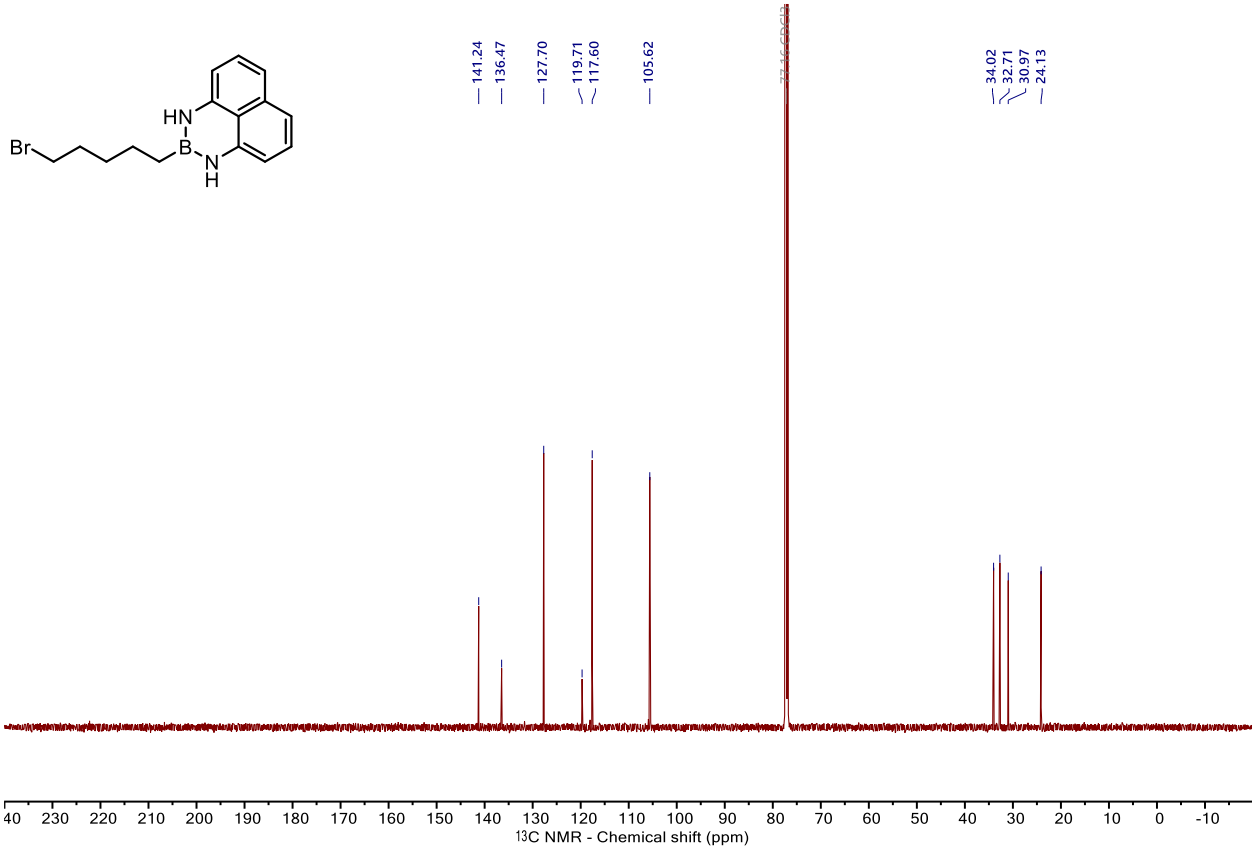

^{13}C {^{1}H} NMR (126 MHz, Chloroform-*d*) of **4-1n**

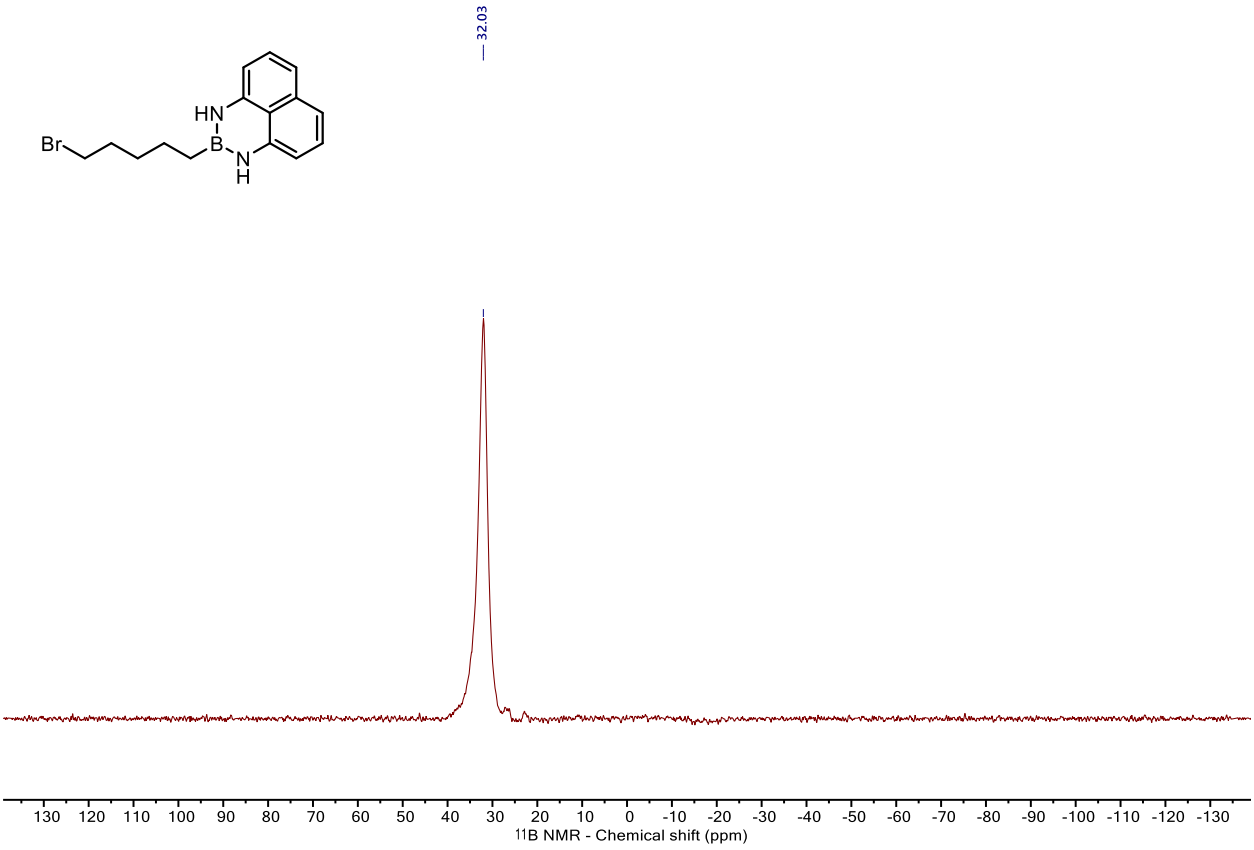

^{11}B NMR (160 MHz, Chloroform-*d*) of **4-1n**

4-1o; 2-(2-methylpentyl)-2,3-dihydro-1*H*-naphtho[1,8-*de*][1,3,2]diazaborinine (ABG-0389)

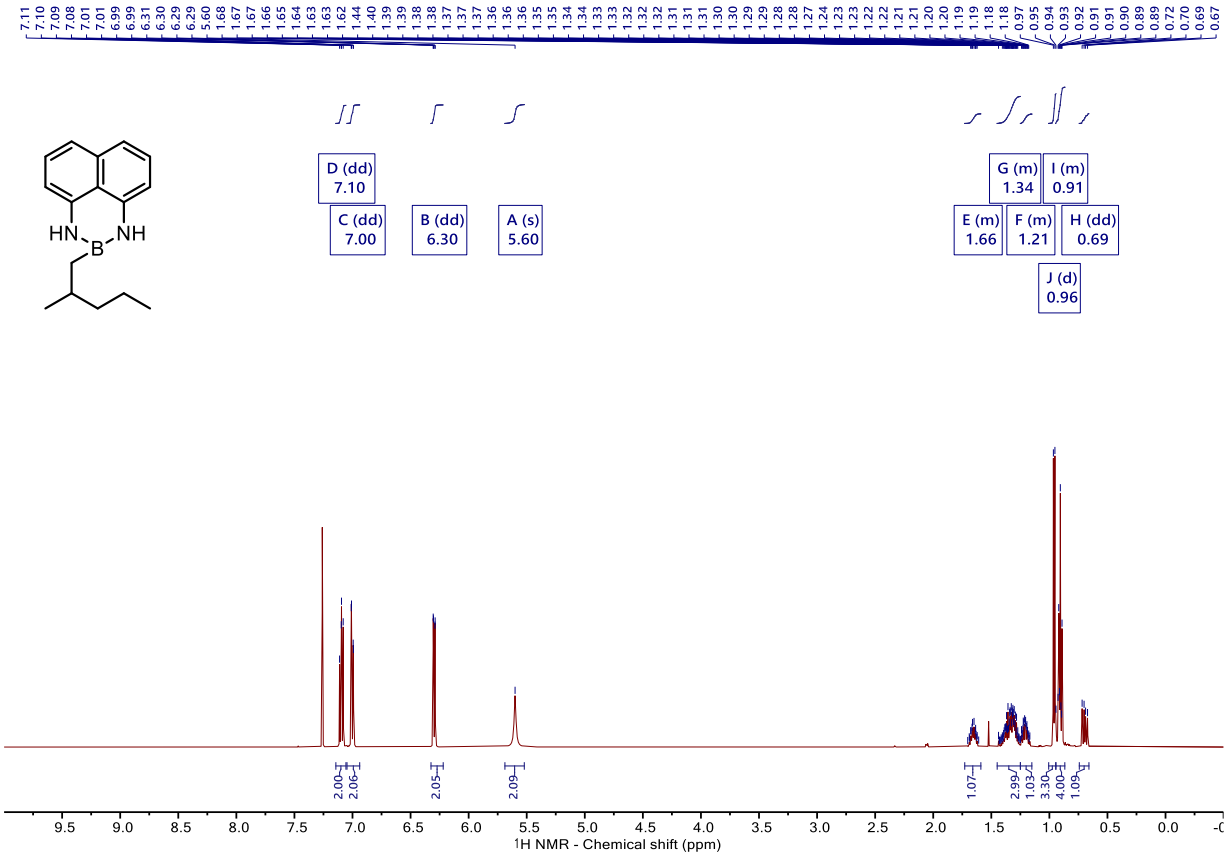

^{1}H NMR (500 MHz, Chloroform-*d*) of **4-1o**

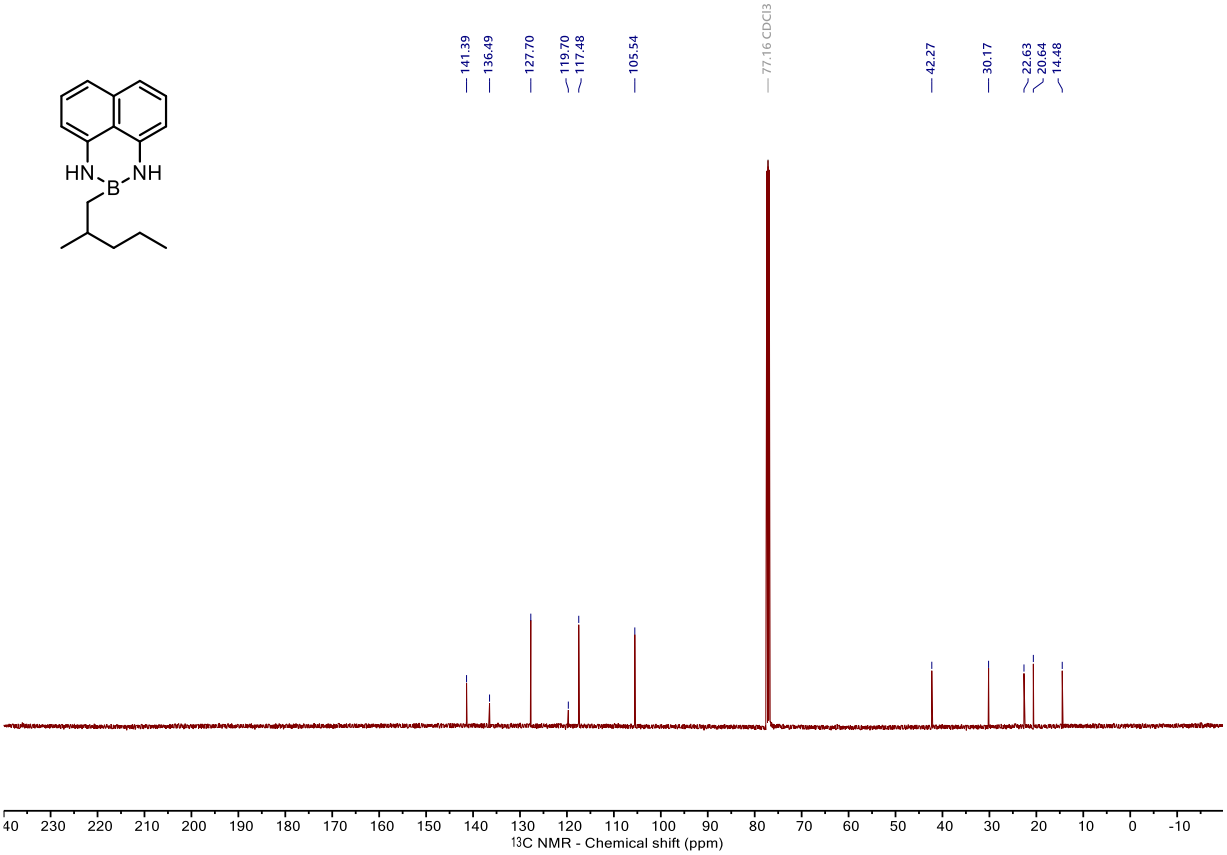

^{13}C {^{1}H} NMR (126 MHz, Chloroform-*d*) of **4-1o**

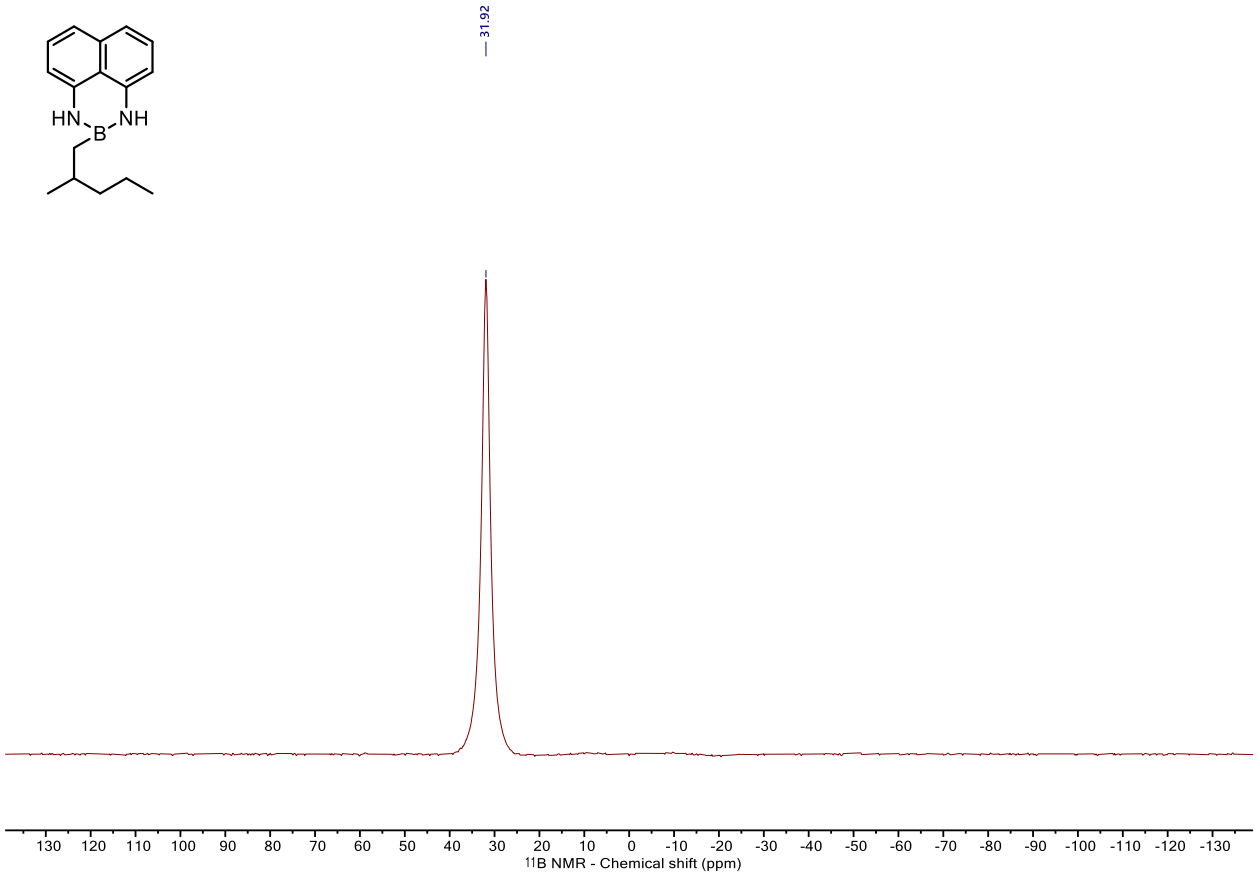

^{11}B NMR (160 MHz, Chloroform-*d*) of **4-1o**

4-1p; 2-(2-(4-methylcyclohex-3-en-1-yl)propyl)-2,3-dihydro-1*H*-naphtho[1,8-*de*][1,3,2]diazaborinine (ABG-0554)

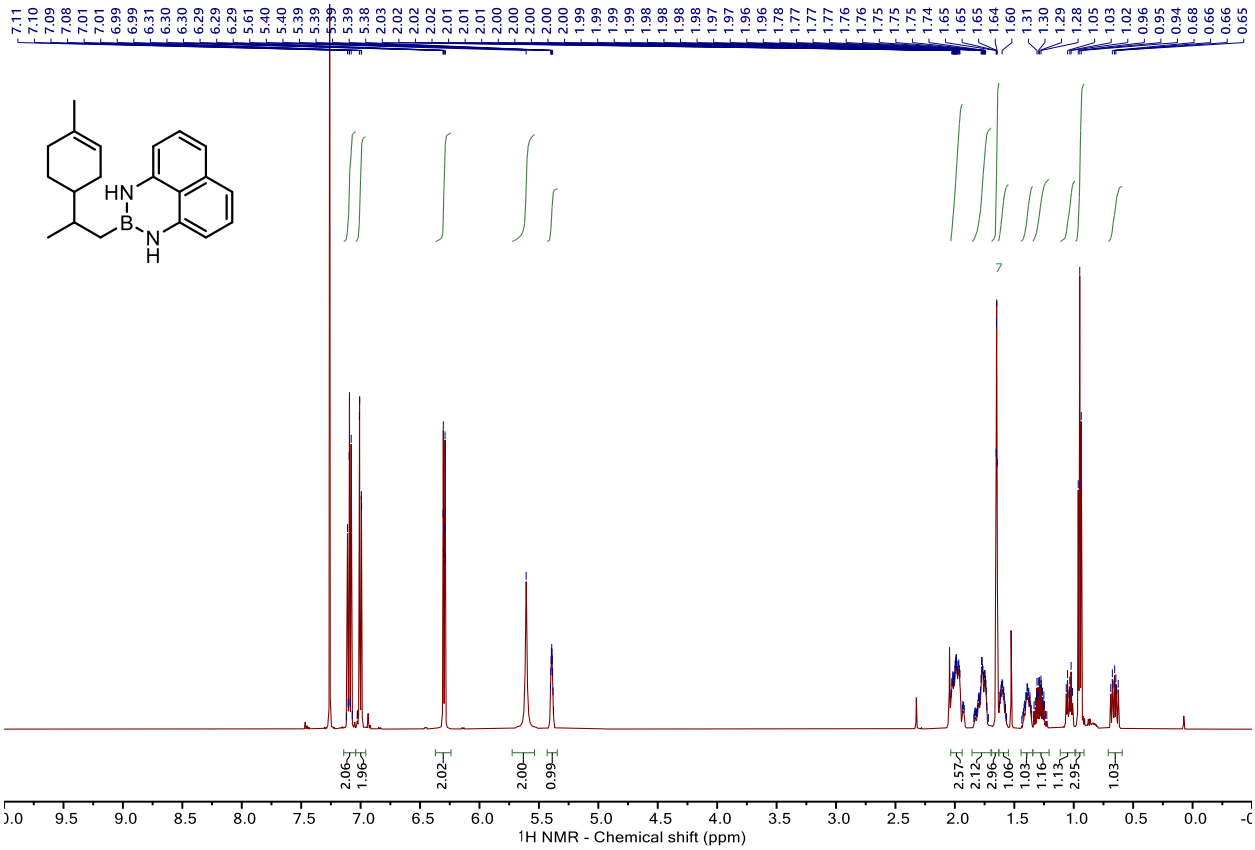

^{1}H NMR (500 MHz, Chloroform-*d*) of **4-1p**

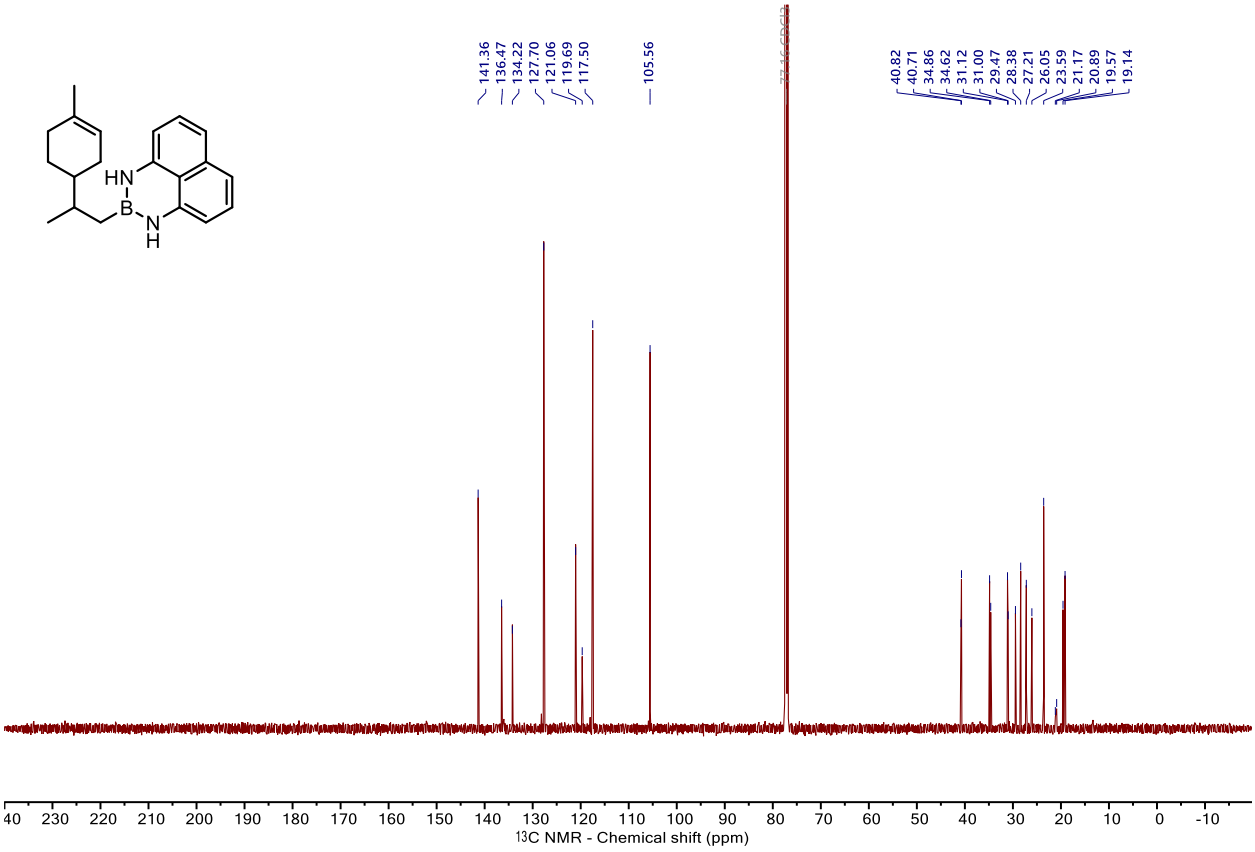

^{13}C {^{1}H} NMR (126 MHz, Chloroform-*d*) of **4-1p**

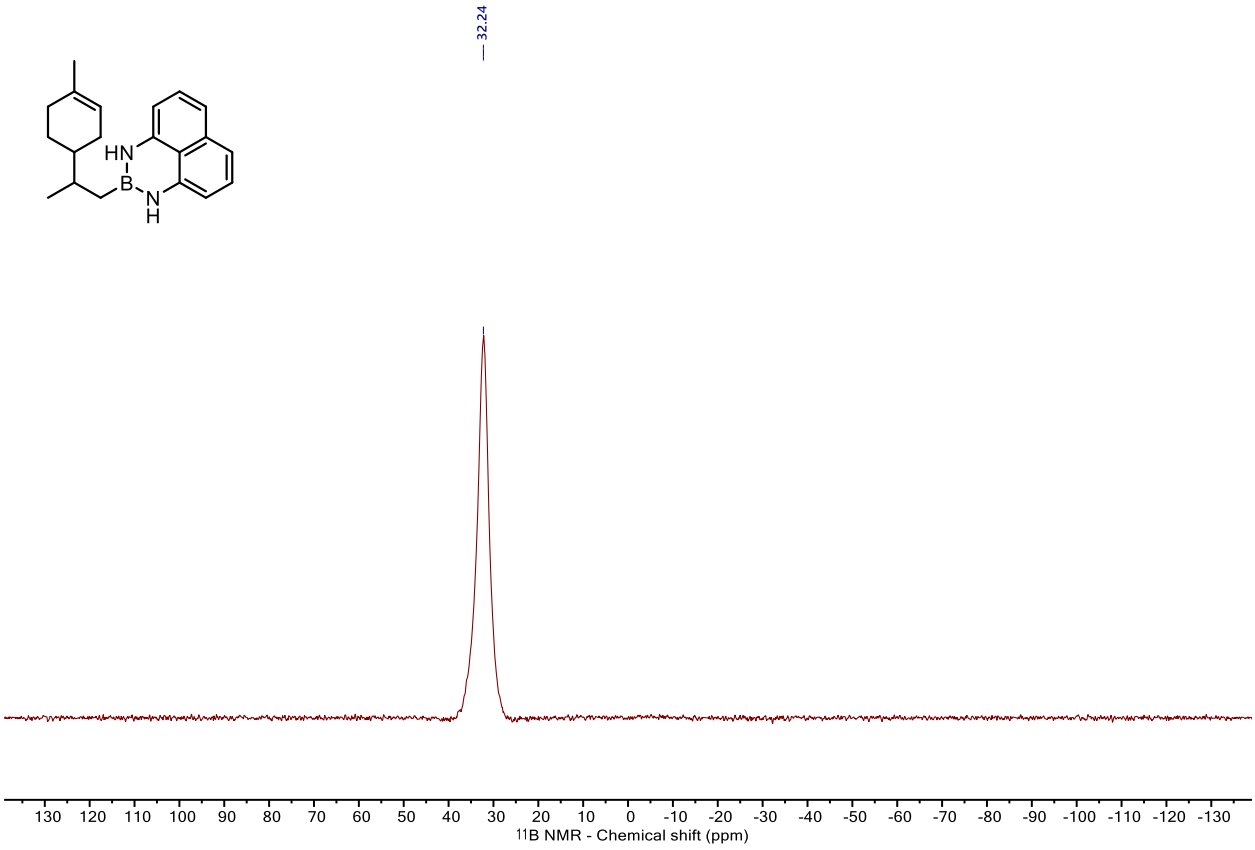

^{11}B NMR (160 MHz, Chloroform-*d*) of **4-1p**

4-1q; 2-(((1*R*,5*R*)-6,6-dimethylbicyclo[3.1.1]heptan-2-yl)methyl)-2,3-dihydro-1*H*-naphtho[1,8-*de*][1,3,2]diazaborinine (ABG-0562)

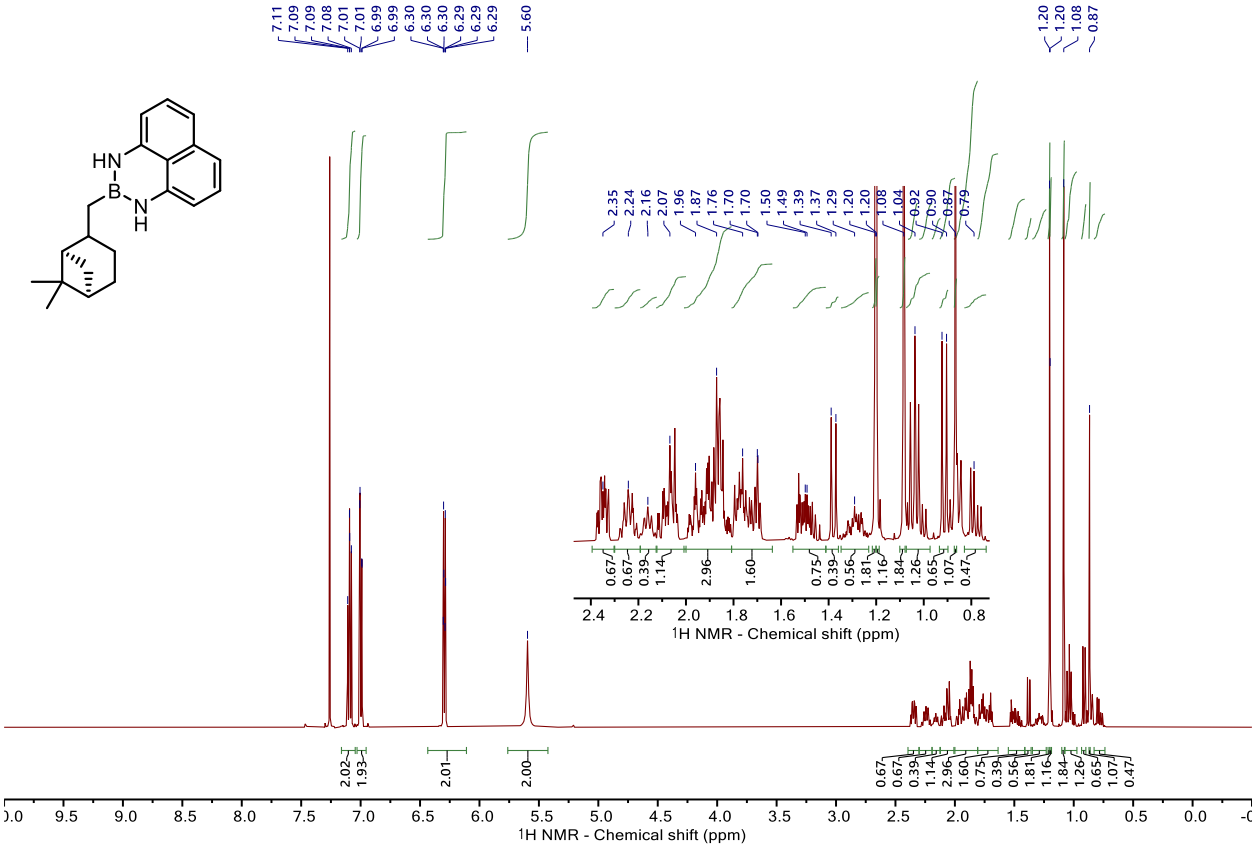

^{1}H NMR (500 MHz, Chloroform-*d*) of **4-1q**

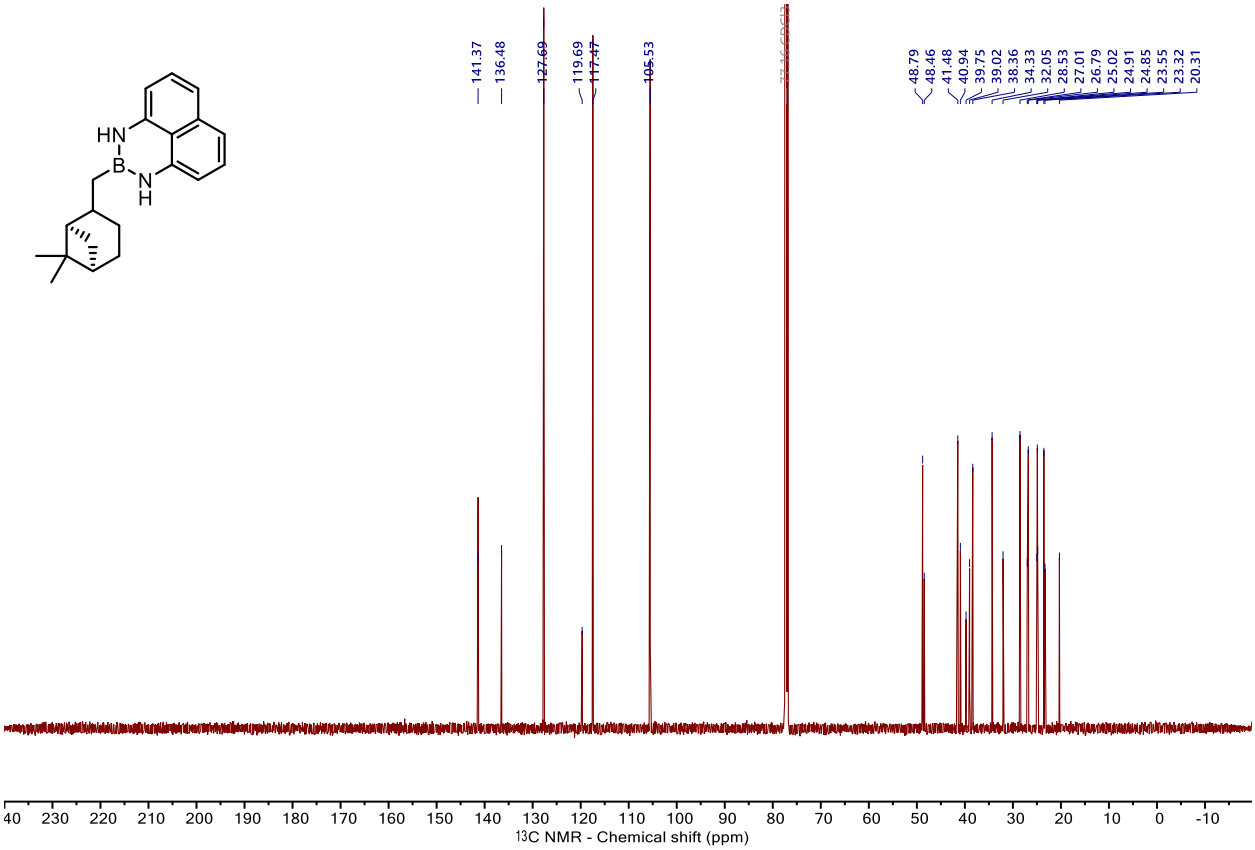

^{13}C {^{1}H} NMR (126 MHz, Chloroform-*d*) of **4-1q**

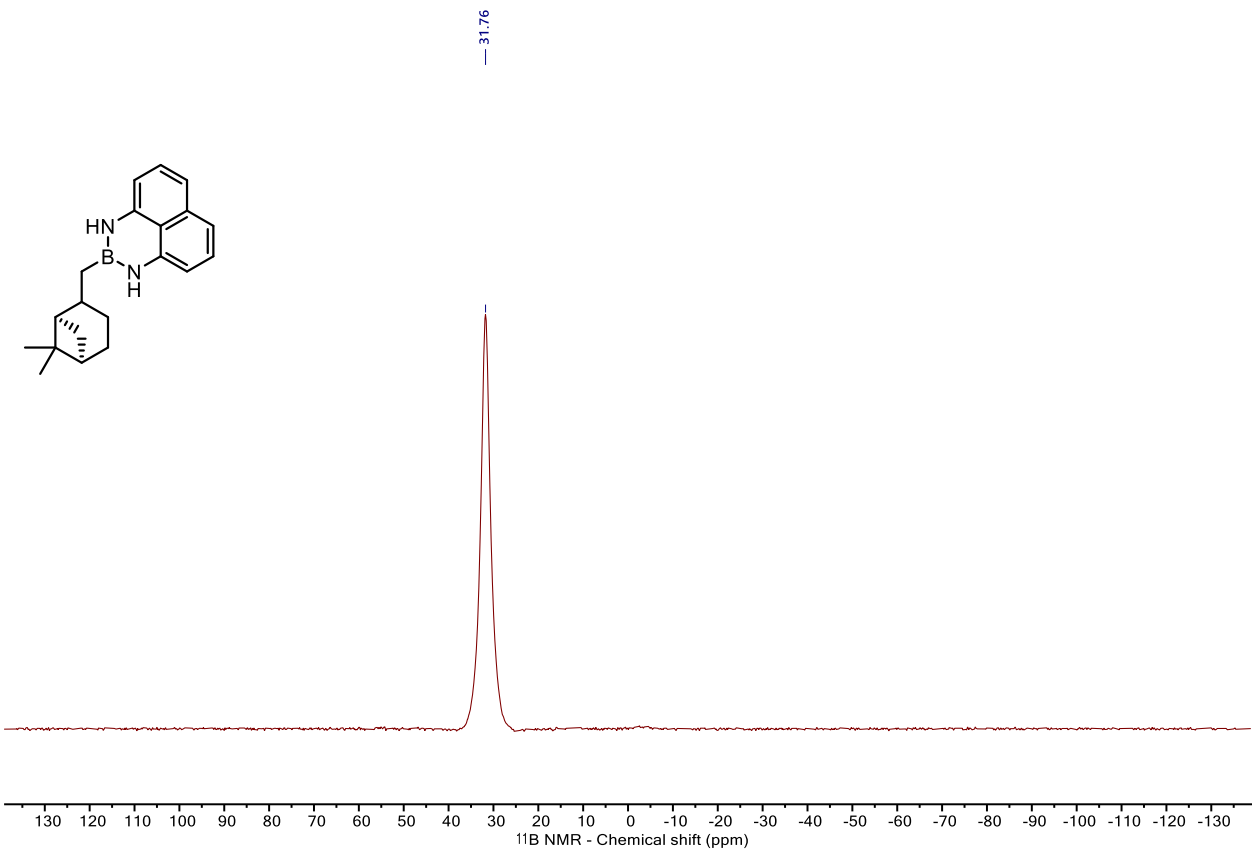

^{11}B NMR (160 MHz, Chloroform-*d*) of **4-1q**

4-1r; 2-((*S*)-2-methyl-4-((1*S*,6*R*)-1,2,6-trimethylcyclohex-2-en-1-yl)butyl)-2,3-dihydro-1*H*-naphtho [1,8-*de*][1,3,2]diazaborinine (ABG-0563)

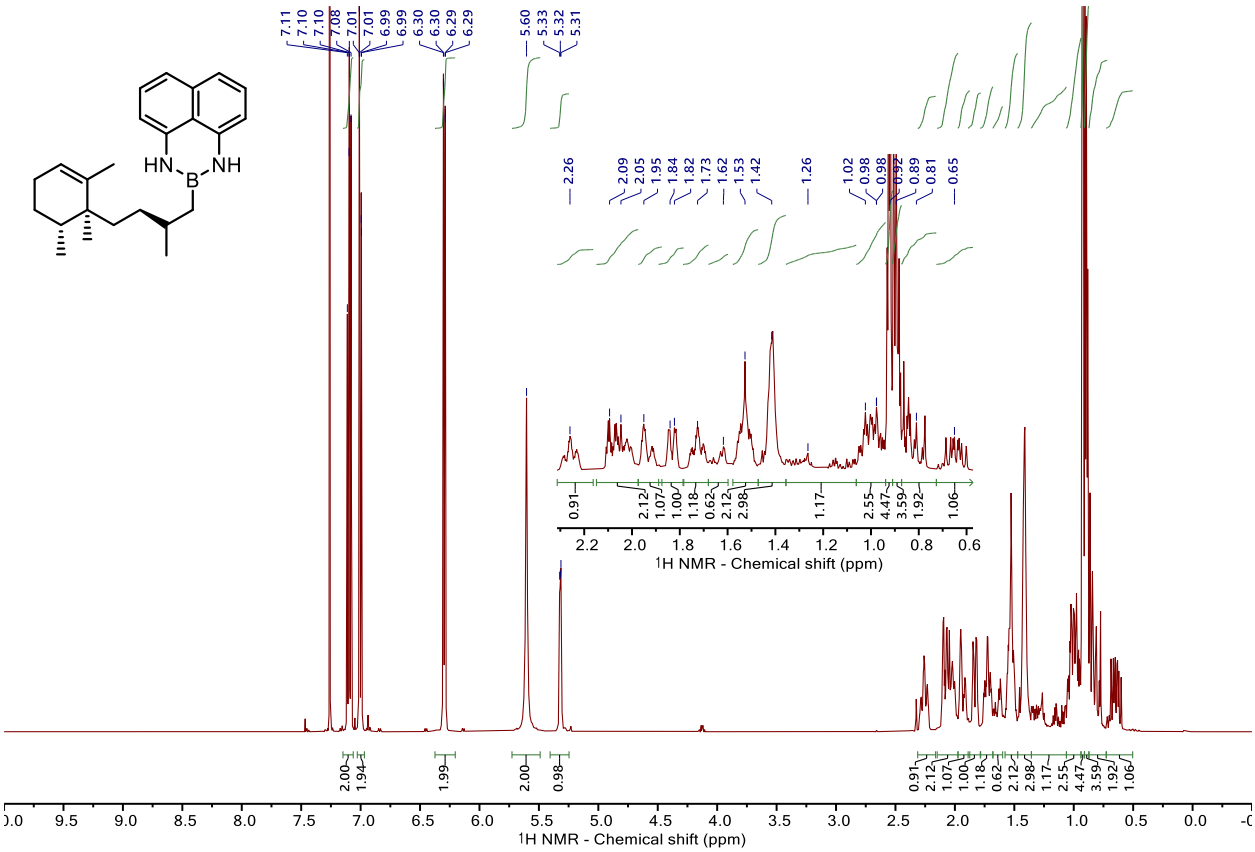

^{1}H NMR (500 MHz, Chloroform-*d*) of **4-1r**

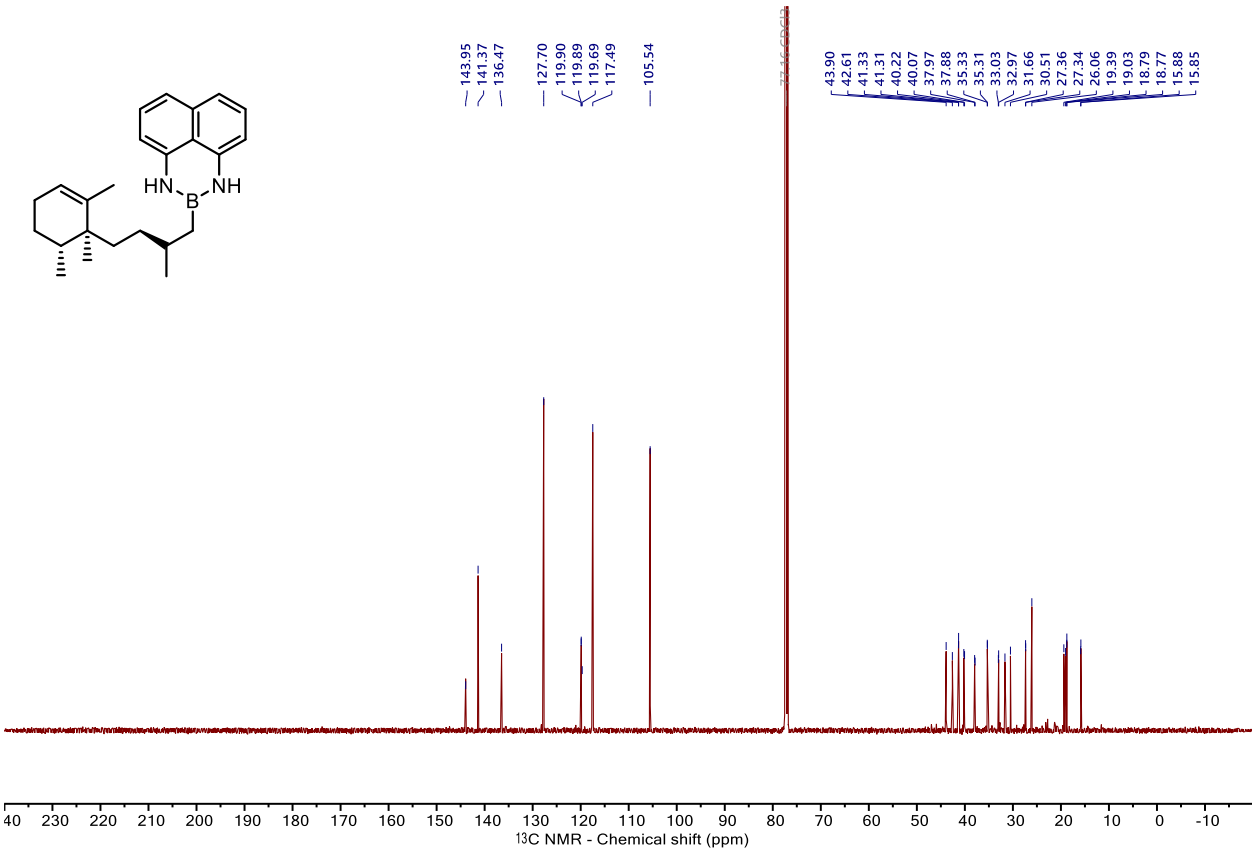

^{13}C {^{1}H} NMR (126 MHz, Chloroform-*d*) of **4-1r**

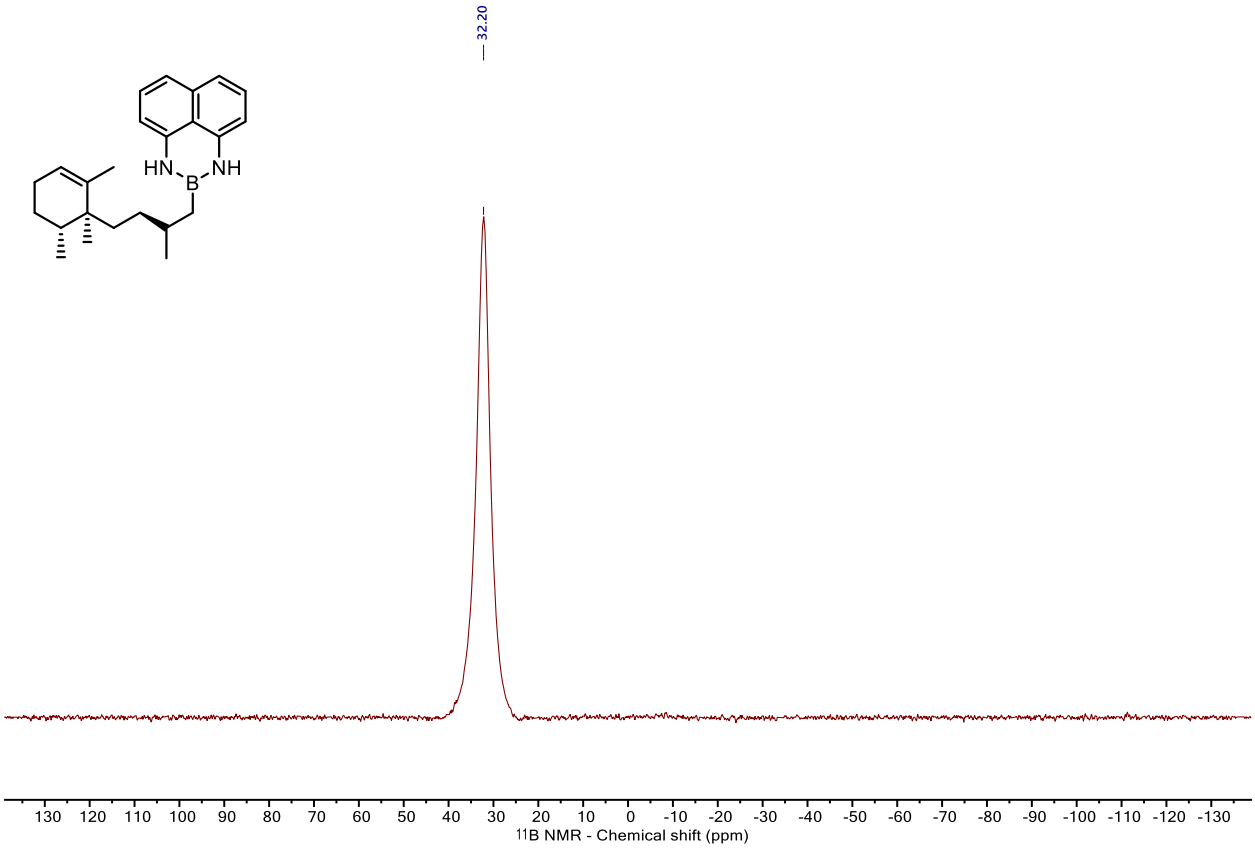

^{11}B NMR (160 MHz, Chloroform-*d*) of **4-1r**

4-3a; 5-(1*H*-naphtho[1,8-*de*][1,3,2]diazaborinin-2(3*H*)-yl)pentan-1-ol (ABG-0592)

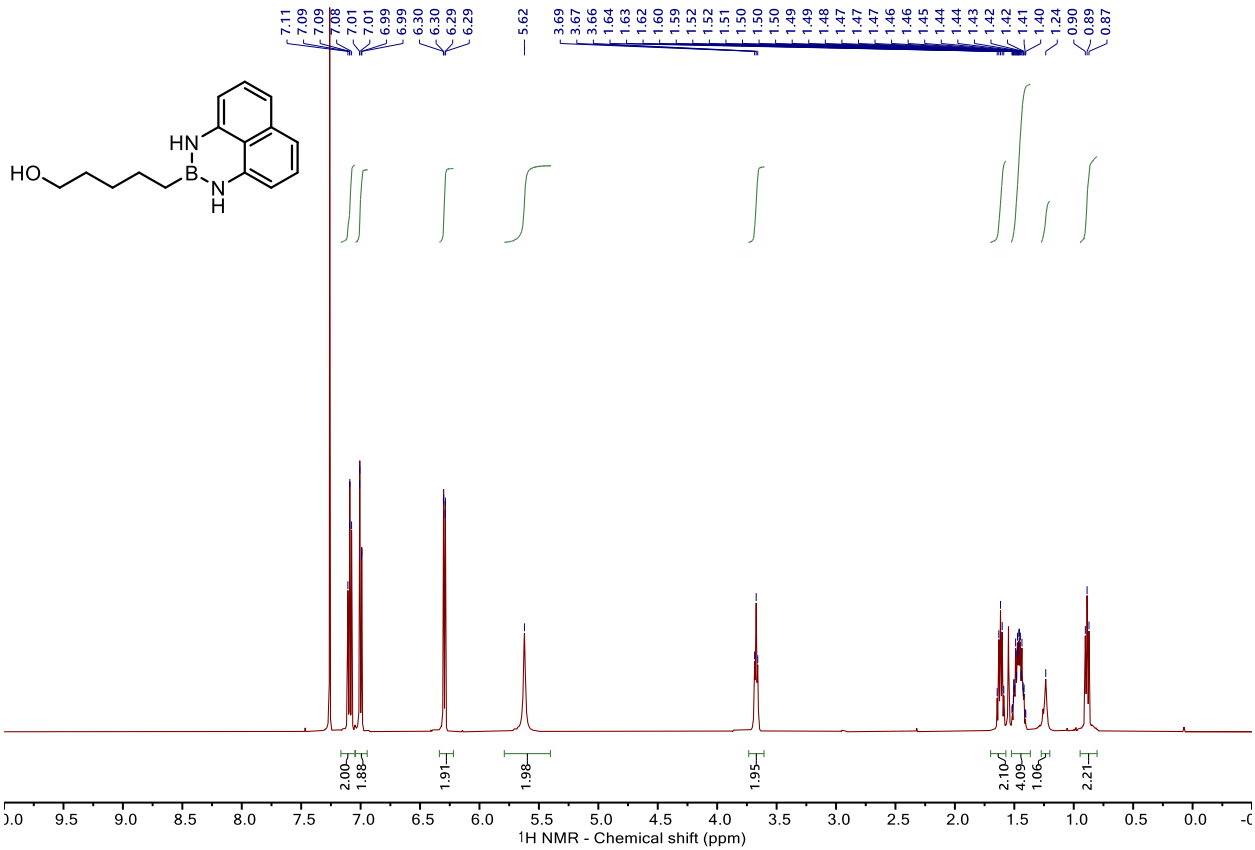

^{1}H NMR (500 MHz, Chloroform-*d*) of **4-3a**

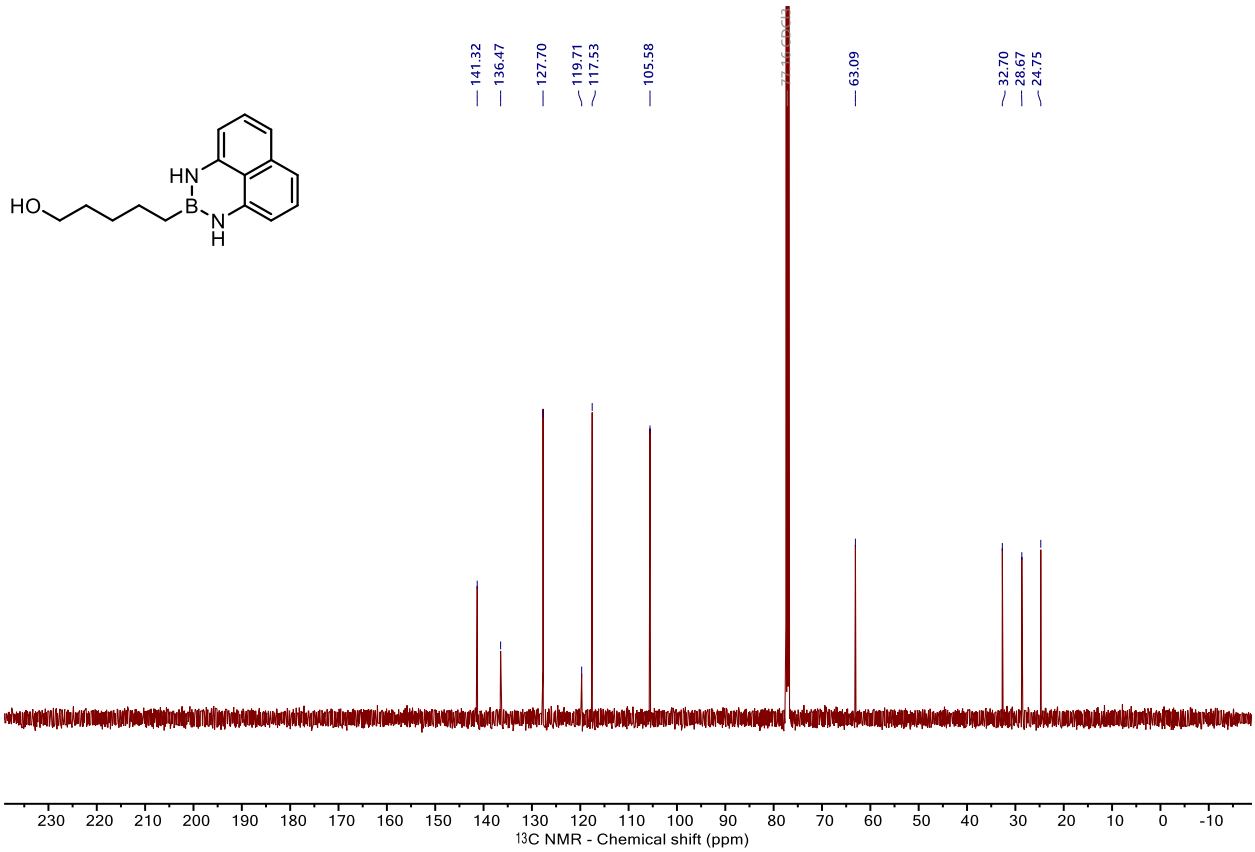

^{13}C {^{1}H} NMR (126 MHz, Chloroform-*d*) of **4-3a**

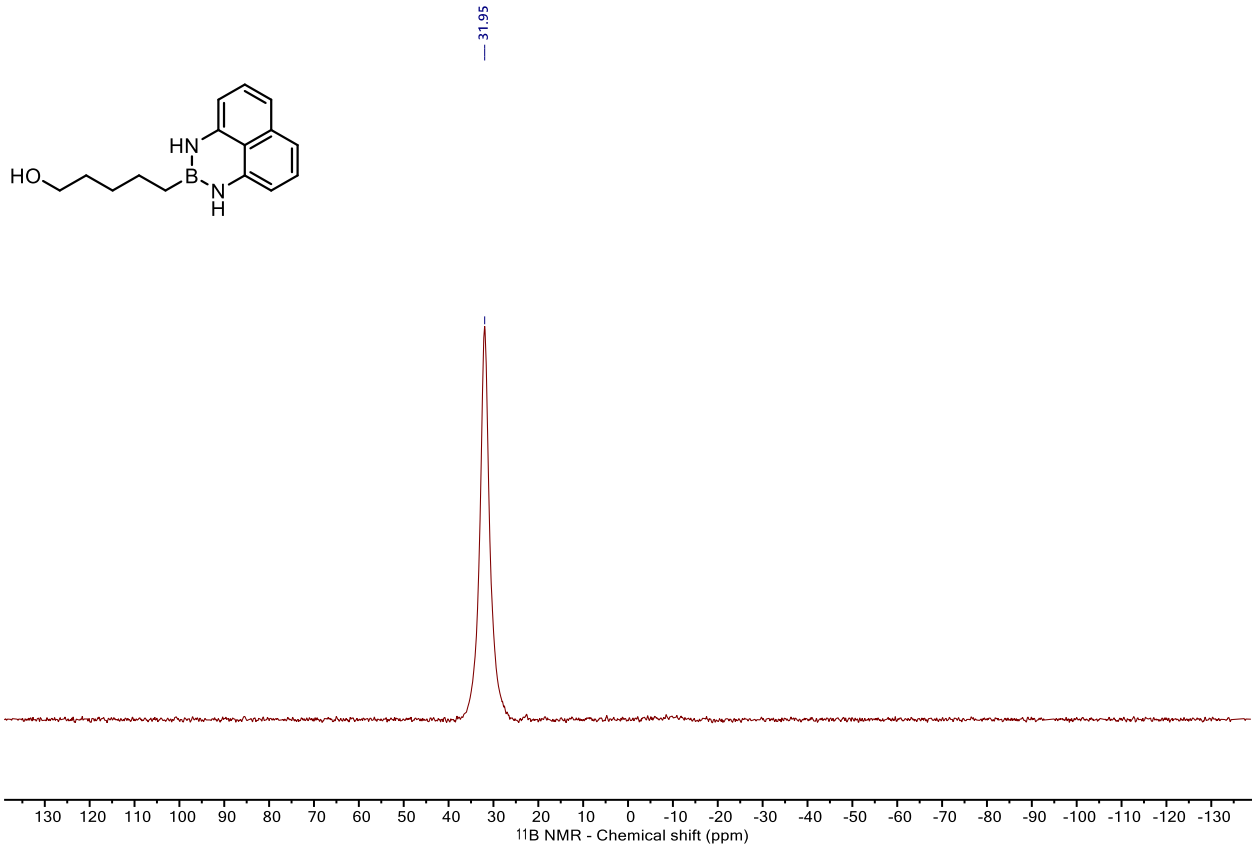

^{11}B NMR (160 MHz, Chloroform-*d*) of **4-3a**

4-3b; 10,11,12,13-tetrahydro-7*H*,9*H*-naphtho[1',8':4,5,6][1,3,2]diazaborinino[1,2-*a*][1,2]azaborepine (ABG-0598-A)

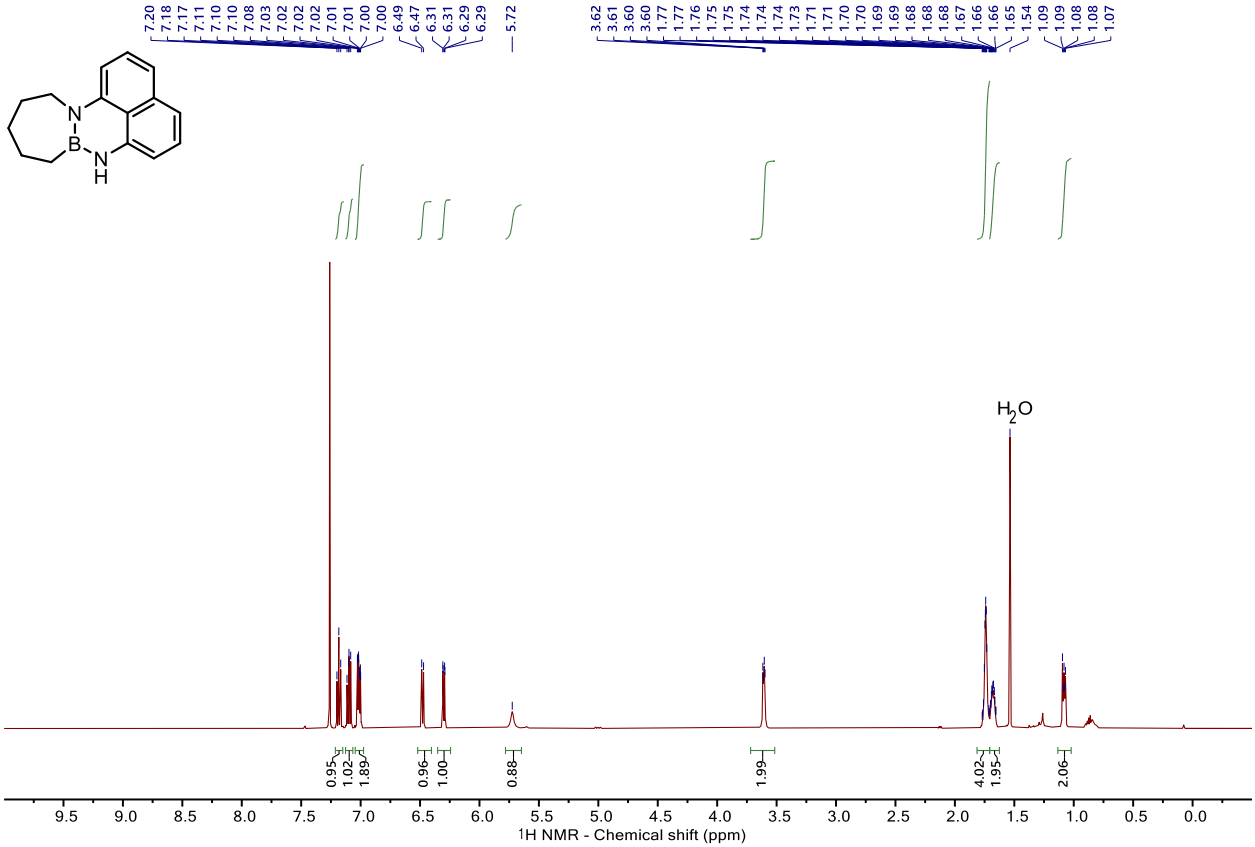

^{1}H NMR (500 MHz, Chloroform-*d*) of **4-3b**

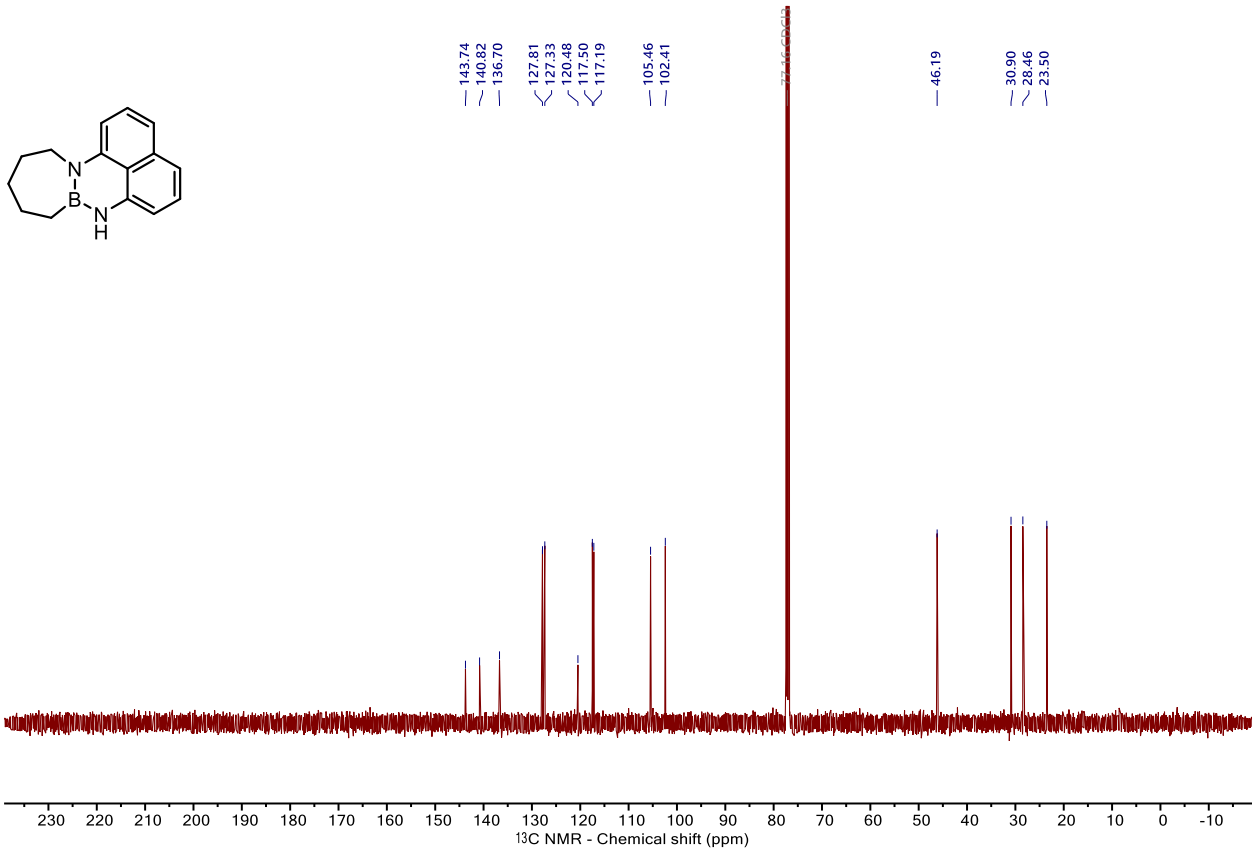

^{13}C {^{1}H} NMR (126 MHz, Chloroform-*d*) of **4-3b**

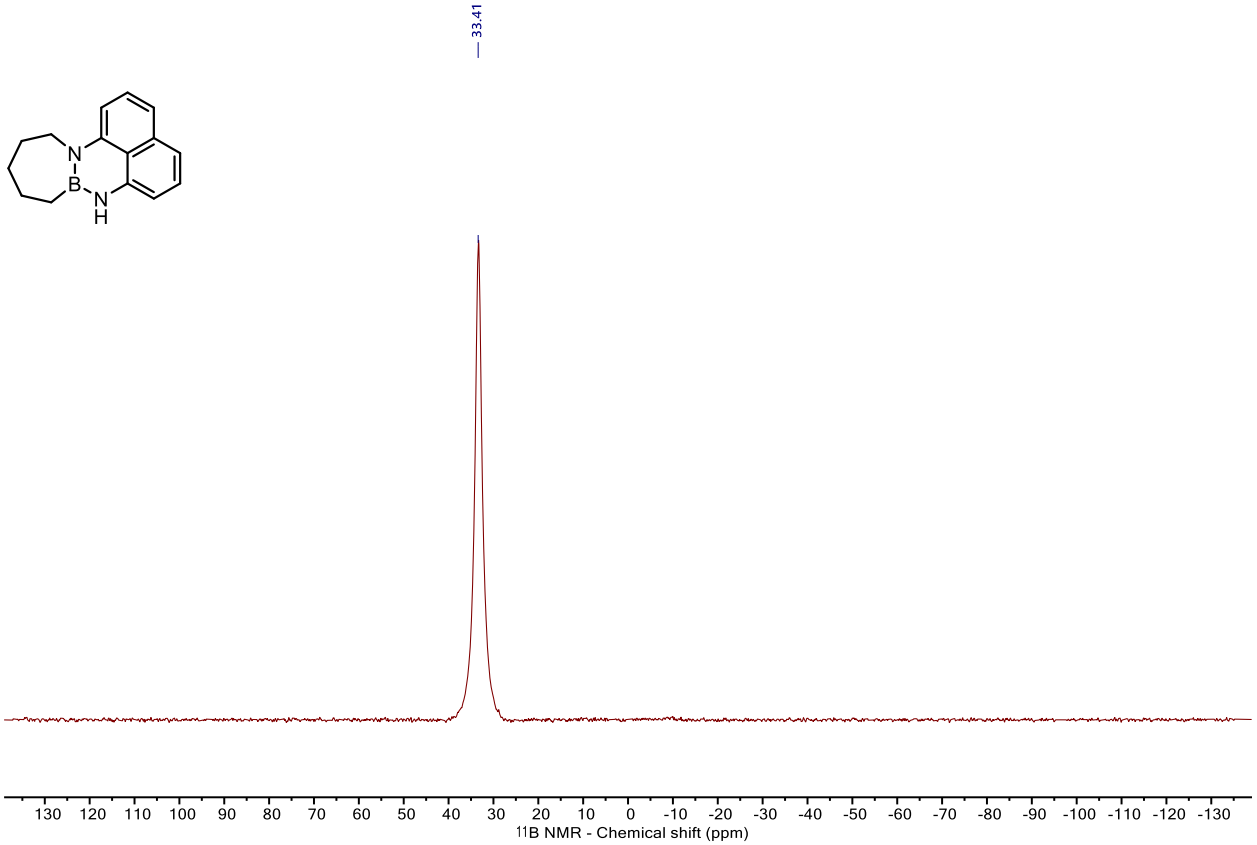

^{11}B NMR (160 MHz, Chloroform-*d*) of **4-3b**

4-3d; 2-(4-(*p*-tolylsulfinyl)butyl)-2,3-dihydro-1*H*-naphtho[1,8-*de*][1,3,2]diazaborinine

(ABG 0601 A)

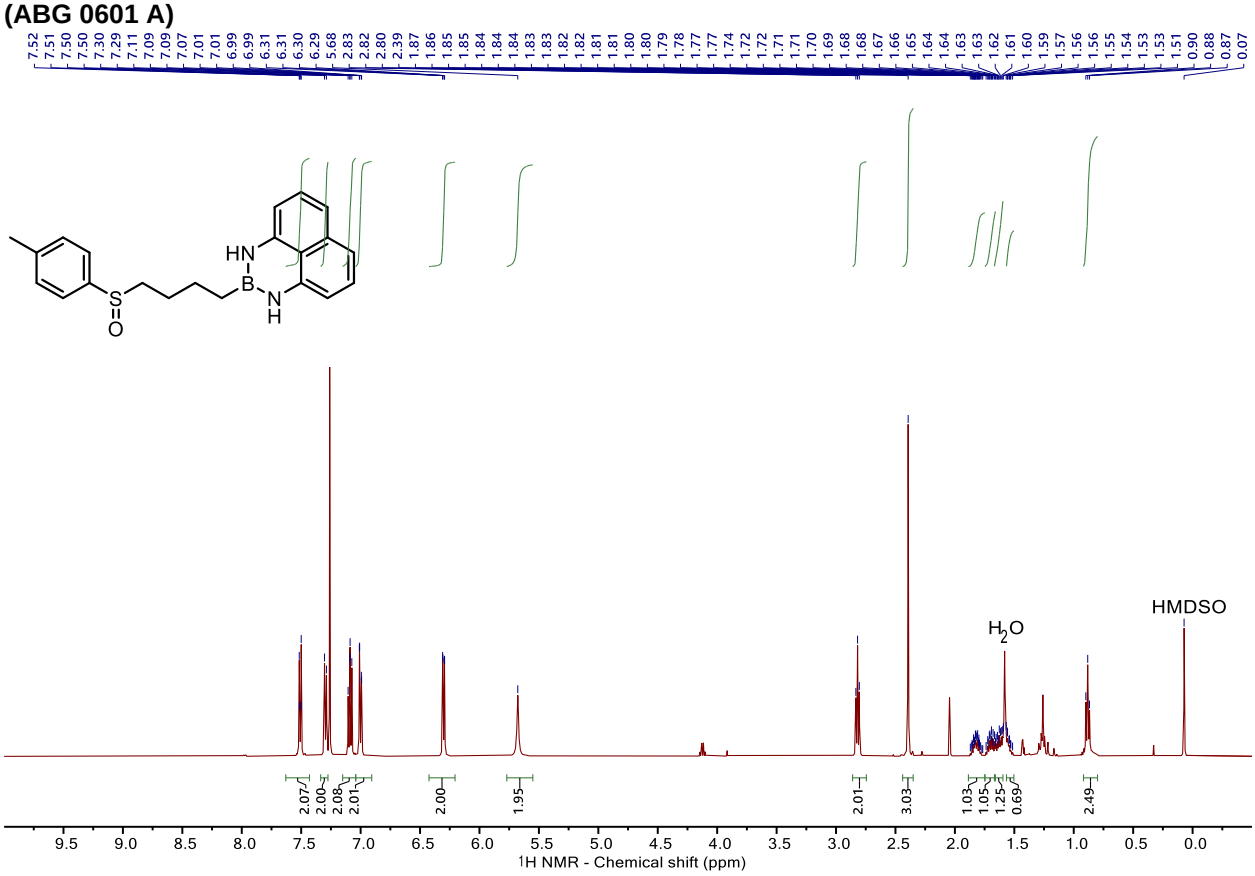

^{1}H NMR (500 MHz, Chloroform-*d*) of **4-3d**

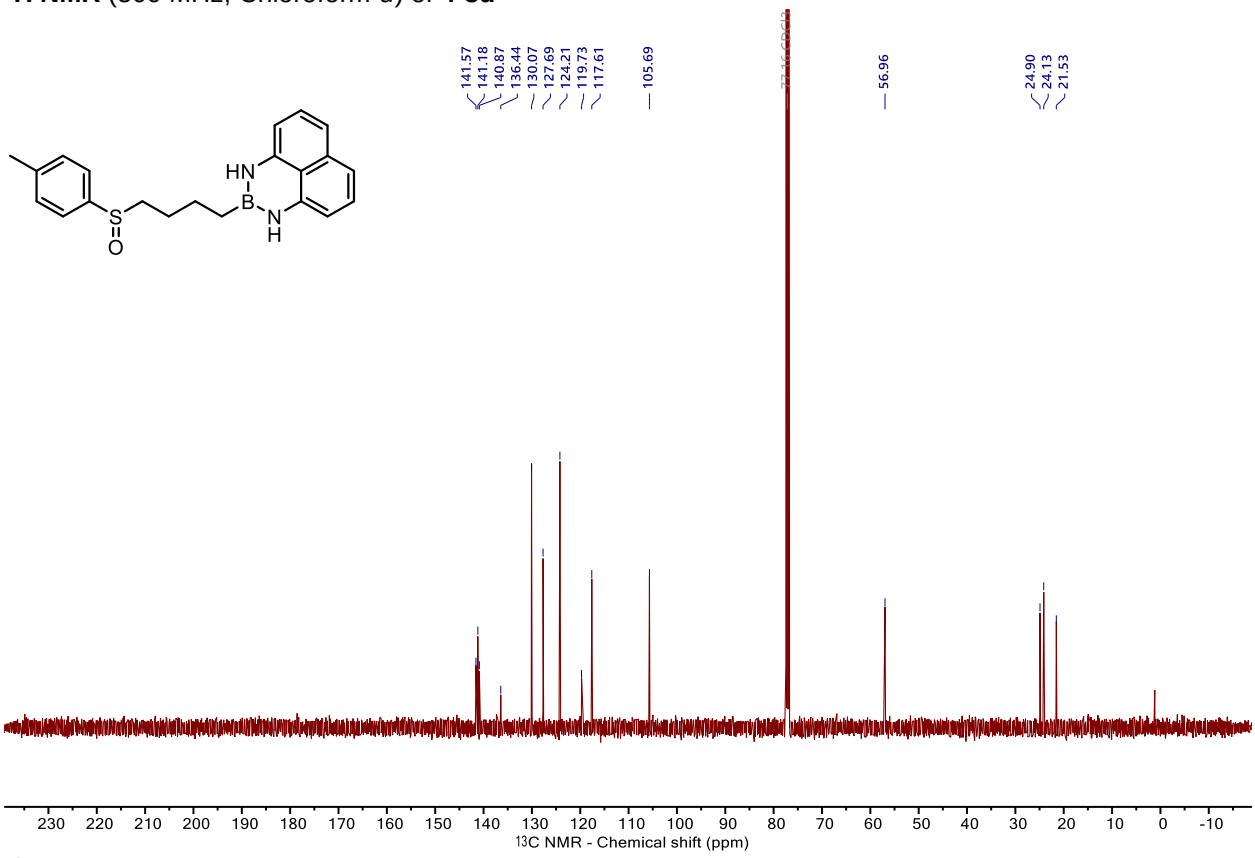

^{13}C {^{1}H} NMR (126 MHz, Chloroform-*d*) of **4-3d**

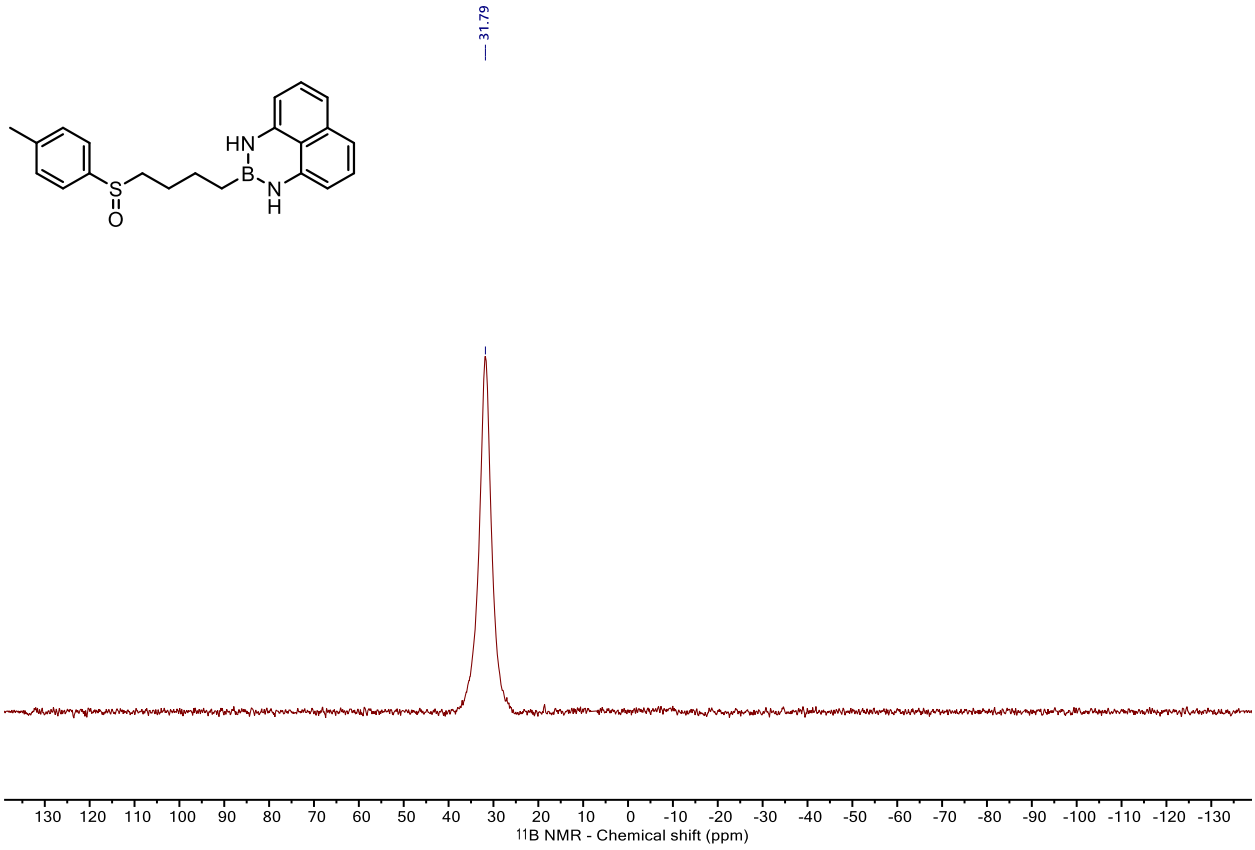

^{11}B NMR (160 MHz, Chloroform-*d*) of **4-3d**

5. Silylalanes

^{Mes}TerAl(Si)$_2$; ^{Mes}TerAl(SiMe$_2$Ph)$_2$ (ABG-0671-Si2)

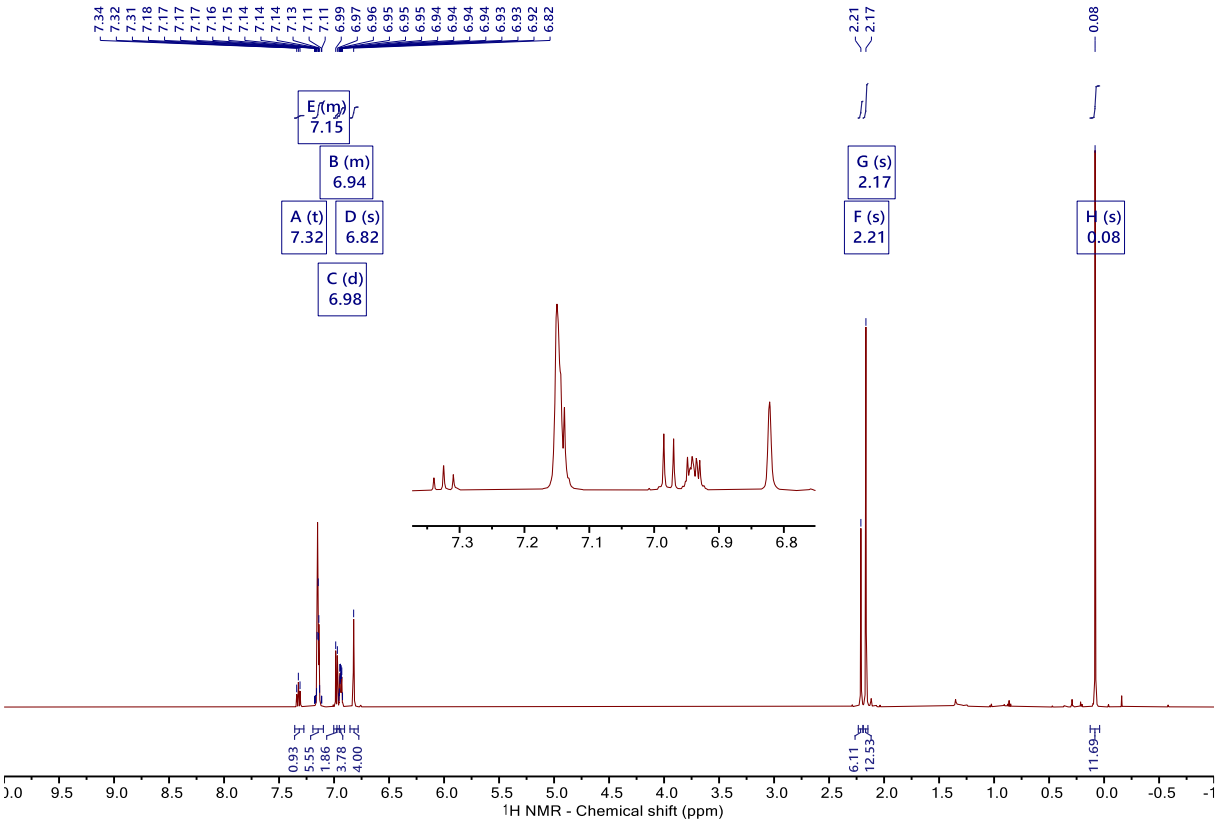

^{1}H NMR (500 MHz, Benzene-d_6) of ^{Mes}TerAl(Si)$_2$

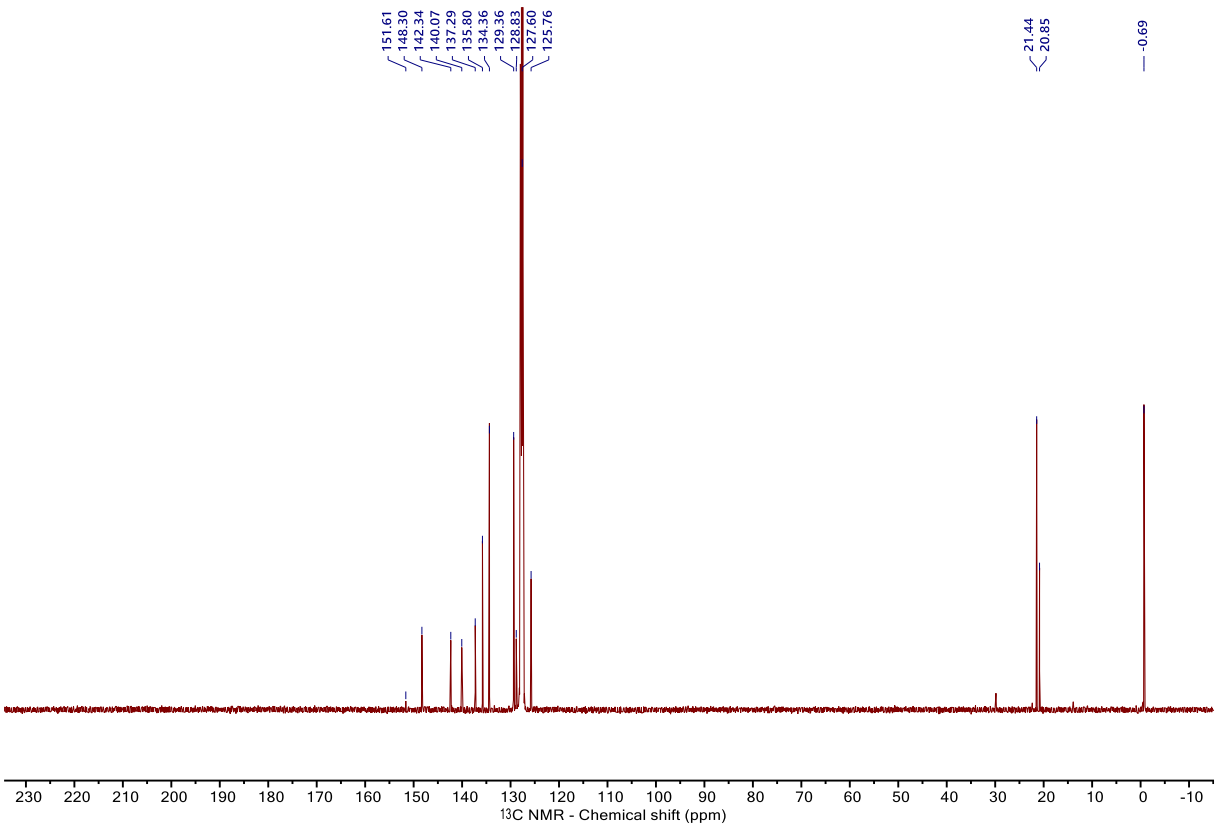

^{13}C {^{1}H} NMR (126 MHz, Benzene-d_6) of ^{Mes}TerAl(Si)$_2$

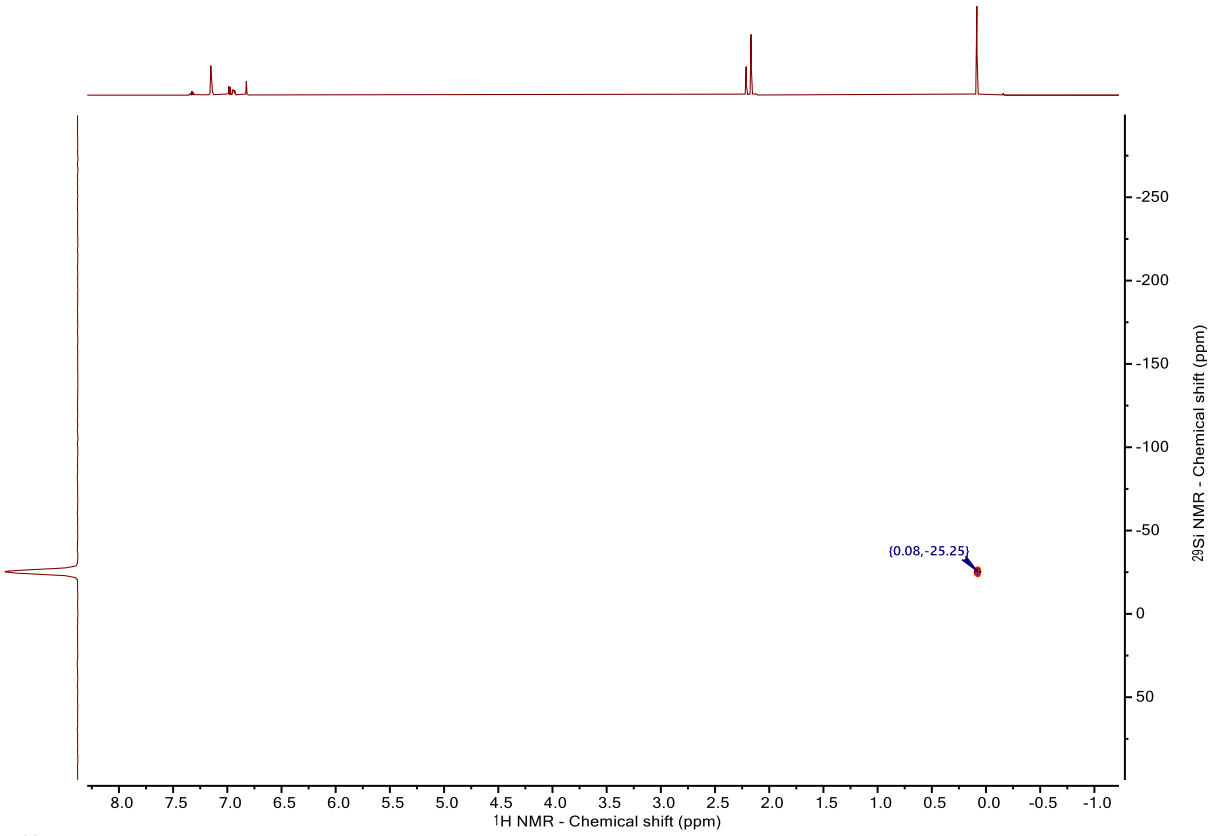

^{1}H-^{29}Si HMBC (Benzene-d_6) of ^{Mes}TerAl(*Si*)$_2$

^{Mes}TerAl(Si)Me; ^{Mes}TerAl(SiMe$_2$Ph)Me (ABG-0671-F3)

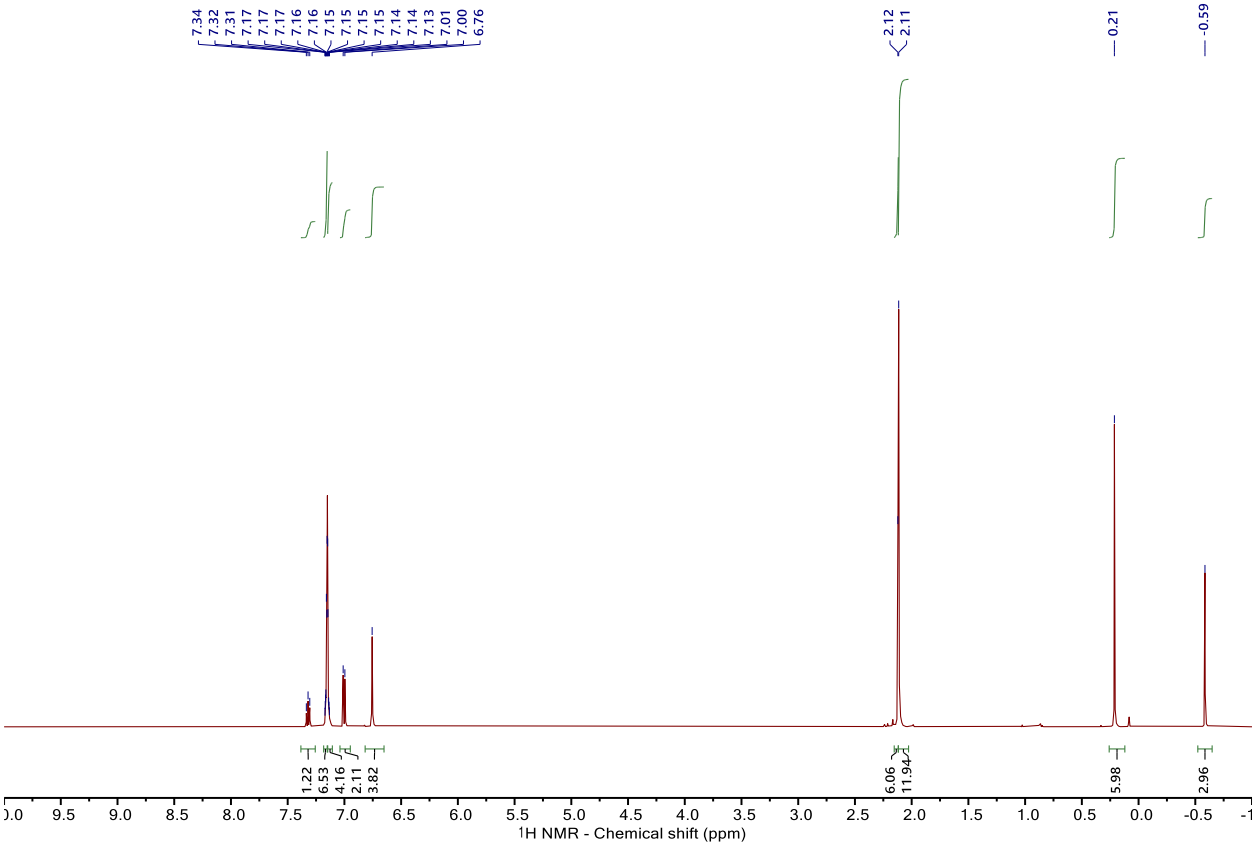

^{1}H NMR (500 MHz, Benzene-d_6) of ^{Mes}TerAl(*Si*)Me

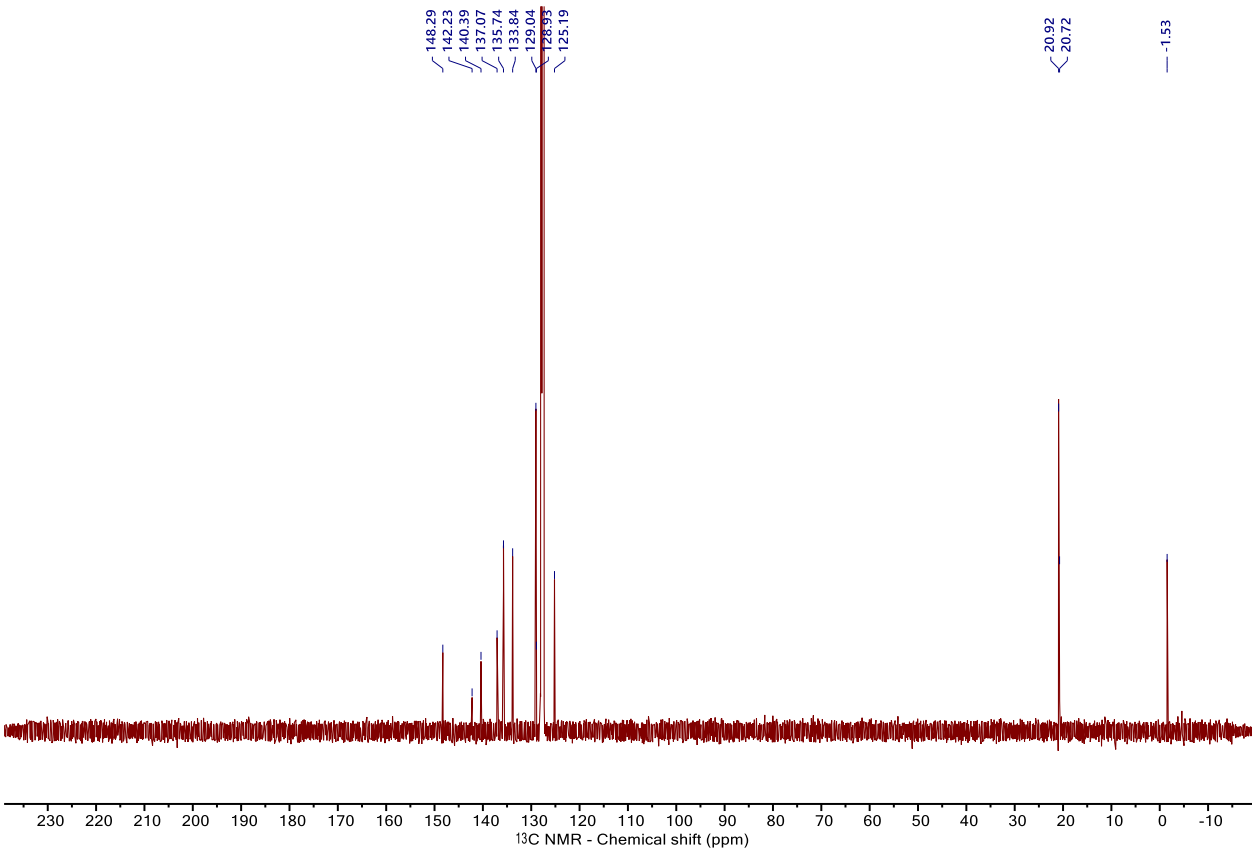

^{13}C {^{1}H} NMR (126 MHz, Benzene-d_6) of ^{Mes}TerAl(*Si*)Me

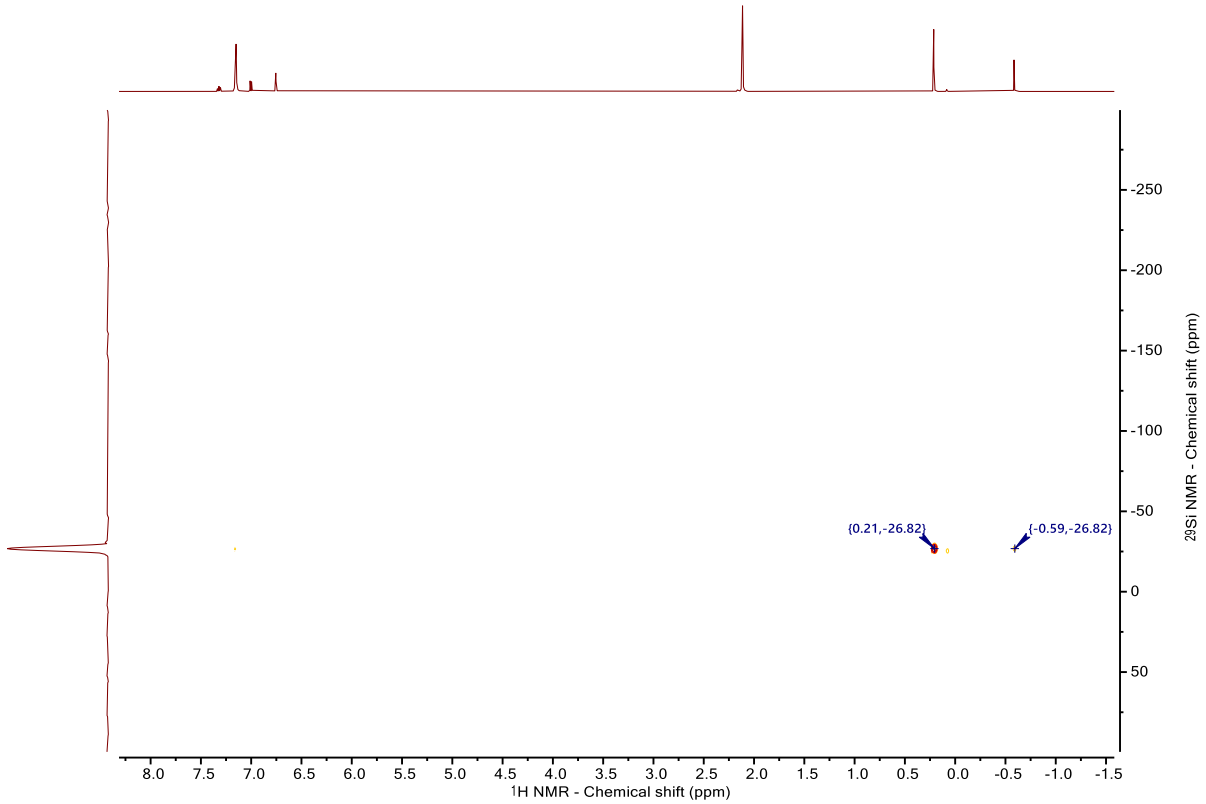

^{1}H-^{29}Si HMBC (Benzene-d_6) of ^{Mes}TerAl(*Si*)Me